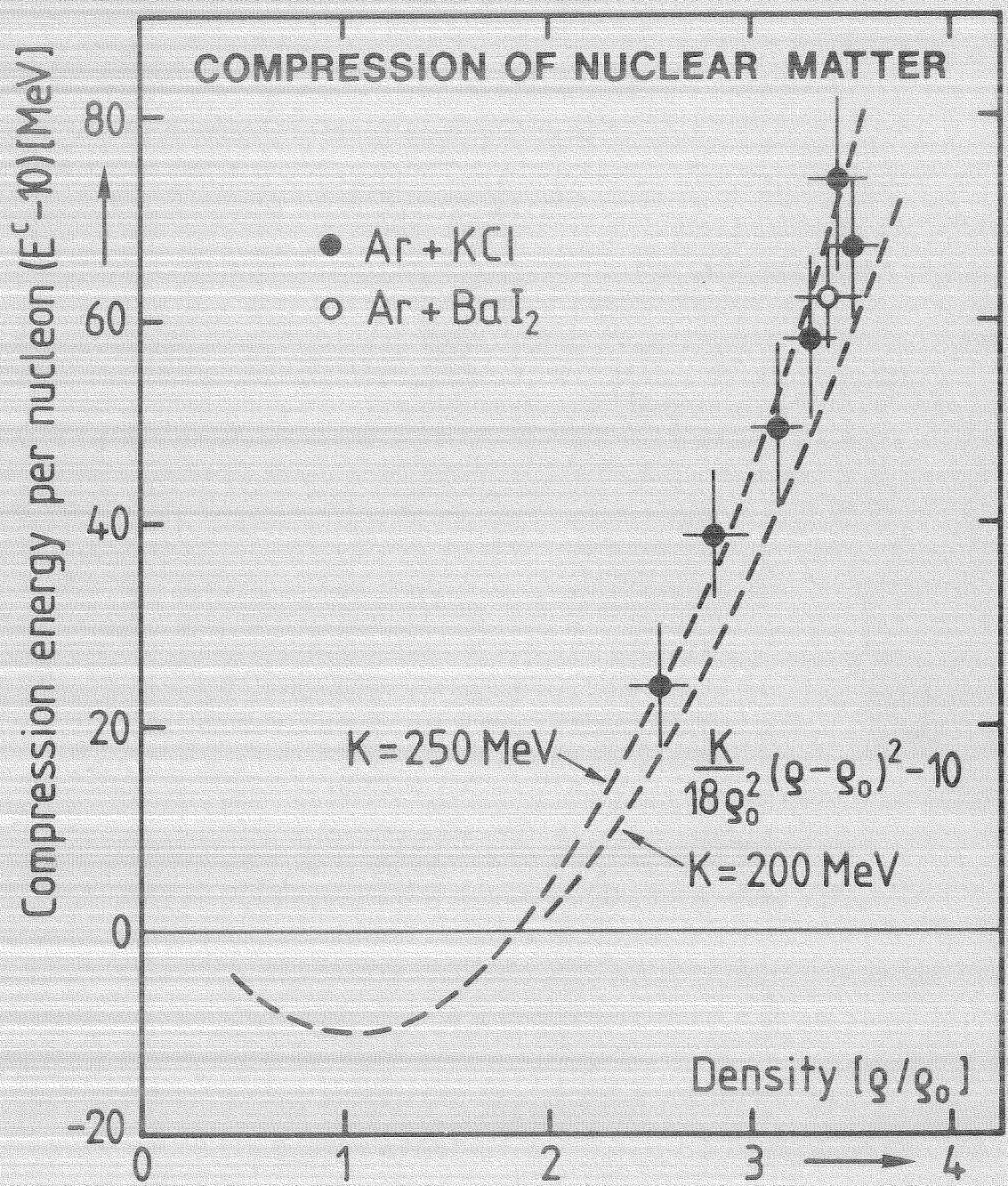
GSI 83-1
MARCH 1983
ISSN 0174-0814

SCIENTIFIC REPORT 1982



GSI GESELLSCHAFT FÜR SCHWERIONENFORSCHUNG
DARMSTADT
MITGLIED DER AGF

Front Cover:

First results for the compression energy per nucleon of nuclear matter, as derived from pion production data in high energy heavy ion collisions. ^{40}Ar projectiles accelerated to energies from 0.4 to 1.8 GeV per nucleon by the Bevalac, LBL Berkeley, and a streamer chamber were used in this study. The compressional energy is shown as a function of the baryon density reached at various incident energies; the density is given in units of ρ_o the density of ground state nuclear matter. The dashed lines represent parabolic energy/density functionals, with two different compressibility constants. The best fit is obtained with K=240 MeV. The derivative of this functional with respect to density is the so called nuclear matter equation of state, i.e. the relation between density and pressure. It is of crucial importance for the understanding of supernova dynamics and neutron star structure. The present results indicate a "hard" equation of state, with no apparent signs of a phase transition.

The corresponding experiments are described on pages 33 and 118 of this report.

S C I E N T I F I C R E P O R T 1982

Herausgeber: Gesellschaft für Schwerionenforschung mbH
Postfach 11 05 41
6100 Darmstadt

Redaktion: G. Siegert

Druck: G. Scheid, Darmstadt-Arheilgen

ISSN 0174-0814

The year of 1982 started with the upgraded UNILAC being operational as planned. In addition to the energy upgrade to 20 MeV/u a considerable improvement of the beam intensity could be achieved. This intensity increase together with numerous improvements along the accelerator may have been the point at issue for some of the experiments described in this report. Such, the UNILAC served as an even more powerful tool for a rich scientific program in the beginning of its second semi decade.

During the year 1982 experiments could be carried out in the energy range of up to 20 MeV/u available now where the picture of stochastic nuclear exchange was found to be valid also. In addition, the beginning of fast processes could be investigated and three body exit channels became increasingly important. In atomic physics, the energy increase resulted in the production of very highly-ionized atoms, e.g. U^{80+} or Xe^{53+}. In this connection it was interesting to see how strong shell effects dominate the ionization of the K-electrons.

As in previous years many experiments have been carried out at projectile energies around the Coulomb barrier. The investigation of rotating nuclear matter could be made for spin states as high as 65 $\hbar$ with the GSI-University of Heidelberg-MPI Heidelberg Crystal Ball. The first case of a well pronounced backbending in the actinides could be found in ^{244}Pu. High precision optical spectra of radioactive In-isotopes obtained by fusion were seen for the first time at the on-line mass separator. Systematic experiments on fusion below the barrier could be reproduced over five orders of magnitude in the cross sections using an average fusion barrier and its fluctuation as parameters. Substantial cross sections for nucleon transfer were found as far as 25 % below the Coulomb barrier. For the first time fusion of heavy ions without particle evaporation (radiative capture) could be observed in the case of two $^{90}_{40}Zr$ nuclei. Systematic measurements of the fusion process and of the extra push needed became available now.

A spectacular highlight in the exotic nuclides research was the discovery of element 109 via a single decay chain separated and detected by the velocity filter SHIP.

In the domain of atomic physics peaks observed in the positron spectra originating from collisions of very heavy nuclei could be confirmed. Further experiments are needed to discriminate between possible explanations of the peaks using different nuclei as projectile or target. Rotational coupling ($2p\pi$-$2p\sigma$) of heavy systems could be studied under circumstances, where the level splitting due to spin orbit interaction was as high as one third of the corresponding binding energy. Furthermore, atomic physics experiments concentrated on the spectroscopy of few electron systems produced either in the beam or by the recoil method. A new type of spectroscopy, the energy gain spectroscopy, showed first results.

The biology program at GSI received increasing interest and support from outside users. It could be shown that the oxygen-effect reappeared when mammalian cells were irradiated with heavy ions. The aberrations of chromosomes showed the same energy dependence as the inactivation process. Systematic measurements of the cross section of mammalian cells for ion irradiation are available now which span over three orders of magnitude in the linear energy transfer.

The application of heavy ions was extended further. Detailed investigations of latent nuclear tracks by small angle neutron scattering and with synchrotron radiation have been carried out. This gave new insight in the production of nuclear tracks. Other technical applications were either improved or newly discovered like e.g. antireflex-coating by heavy ion irradiation. Utilization of a heavy ion punctured membrane for the measurement of the deformability of red blood cells will undergo a field test now.

All the experiments mentioned above were impossible without the efforts made in the support structure of GSI like mechanic and electronic workshops, and the detector and target laboratories. E.g. 11000 targets and stripper foils have been produced by the target laboratory in 1982. Furthermore, it should be mentioned that an off-line mass separator for target production is nearing completion. The computing center increased its computing capability by the installation of a more powerful system now consisting of an IBM 3081-D16 and an IBM 3033-U12. In addition array processors have been attached to the multipurpose computers to make use efficiently of their special capabilities.

A major step was the full development and utilization of a the crystal ball spectrometer. In addition an improved set-up for the detection of neutral pions, a new eight crystal x-ray spectrometer and the electron-positron spectrometer TORI went into operation or are nearing completion. The heavy ion scanning microscope reached a resolution of about 1μm.

Our efforts regarding heavy-ion physics at higher energies showed encouraging results from experiments at the Lawrence Berkeley Laboratory and at CERN.

The Plastic Ball/Wall came fully into operation at the Bevalac in Berkeley. New light could be shed on questions like thermalization, cluster formation and two particle correlations in relativistic heavy-ion collisions. Nuclear temperatures up to 78 MeV were deduced for Nb+Nb collisions. The break-up of residues in central collisions of Ne+Au revealed a new multifragmentation mechanism with a characteristic excitation energy of 20 MeV/u. Another experiment with the Plastic Ball and radio-chemical experiments have contributed to the anomalon question. Both experiments exclude short-lived anomalons.

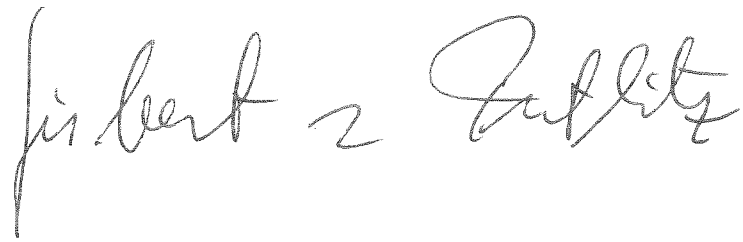
The streamer chamber collaboration at Berkeley investigated the compression energy of nuclear matter via the pion production in high energy Ar+KCl collisions. With ^{40}Ar projectiles of 1.8 GeV/u almost four times the

density of normal nuclear matter at compression energies close to 100 MeV/u could be measured utilizing the pions as probe particles. The results show no sign so far of a phase transition in this energy region.

Experiments at CERN were carried out with ^{12}C and ^{18}O projectiles in the energy-range 60 to 84 MeV/u. The reaction mechanisms including light particle emission were studied. Indications of cooperative effects in nucleus-nucleus collisions were found in the neutral pion production rate.

As far as the future accelerator of GSI is concerned, work towards a two-ring synchrotron facility is continued. The first ring called SIS 12/18 for heavy-ion energies up to 1 GeV/u is in a stage where construction could be started if the project is approved. Regarding the second stage originally designed as SIS 100 for energies up to 10 GeV/u a reduction in size resulting in a final energy for uranium of about 6 GeV/u is anticipated Realization of these accelerators depend not only on sufficient capital funds for the investment but also on the availability of additional personnel for construction and subsequent operation.

The results presented in this Scientific Report have been obtained through the collaborative efforts from scientists of GSI and from universities and other laboratories all over the world. I would like to acknowledge their enormous efforts and the fruitful cooperation with all of them.



Some of the results included here are progress reports of research projects and therefore should be considered preliminary communications.

Several University projects were funded by the BMFT (Federal Ministry for Research and Technology); they are marked with a "B" after the title. In addition GSI supported external groups with certain resources for development of methods and facilities which are of general interest, this is indicated by a "G" in the title.

CONTENTS PAGE

Survey of Experiments at GSI in 1982 XXVII

1. Nuclear Physics/Nuclear Chemistry

1.1 Nuclear Reactions

1.1.1 Reactions near the Coulomb-Barrier

Influence of Collective Surface Motion on the Treshold Behaviour of Nuclear Fusion 2
(W. Reisdorf, F.P. Heßberger, K.D. Hildenbrand, S. Hofmann, G. Münzenberg, J.H.R. Schneider, W.F.W. Schneider, K. Sümmerer, G. Wirth, J.V. Kratz, K. Schlitt)

Evaporation Residue Cross Sections in the Fusion of ^{86}Kr with Ge, Mo, and Ru Isotopes 3
(W. Reisdorf, F.P. Heßberger, K.D. Hildenbrand, S. Hofmann, G. Münzenberg, J.H.R. Schneider, W.F.W. Schneider, K. Sümmerer, G. Wirth, J.V. Kratz, K. Schlitt)

Observation of the γ-deexcitation Channel in the Reaction ^{90}Zr+^{90}Zr->^{180}Hg 4
(J.G. Keller, H.-G. Clerc, K.-H. Schmidt, Y.K. Agarwal, F.P. Heßberger, R. Hingmann, G. Münzenberg, W. Reisdorf, C.-C. Sahm)

Statistical Model Analysis of Neutron Emission in Fusion Reactions of ^{86}Kr with ^{64}Ni and ^{76}Ge 5
(U. Arlt, R. Bass, H. Dittmar, T. Kratz, B. Lohmüller, K. Sapotta, K. Stelzer)

Fusion Cross Sections in ^{40}Ar and ^{50}Ti Induced Heavy Ion Reactions 6
(H.-G. Clerc, J.G. Keller, C.-C. Sahm, K.-H. Schmidt, H. Schulte, D. Vermeulen)

Capture-Fission in the Reaction ^{76}Ge+^{170}Er 7
(K. Lützenkirchen, J.V. Kratz, W. Brüchle, H. Gäggeler, K. Sümmerer, G. Wirth)

An Estimate of the Cross-section for symmetric Fragmentation in the Reaction ^{58}Fe + ^{209}Bi -> ^{267}109 8
(K. Lützenkirchen, J.V. Kratz, W. Brüchle, H. Gäggeler, K. Sümmerer, G. Wirth)

On the Mass Drift in Fast Fission 9
(A. Gobbi, G.-X. Dai, S. Gralla, K.D. Hildenbrand, J. Kuzminski, A. Olmi, W.F.J. Müller, J. Toke)

Studies of Fusion Dynamics in ^{238}U - Induced Reactions 10
(J. Toke, R. Bock, G.-X. Dai, A. Gobbi, S. Gralla, K.D. Hildenbrand, J. Kuzminski, A. Olmi, W.F.J. Müller, S. Bjoernholm)

PAGE

Radiochemical Measurements of Quasielastic, Deep-Inelastic and Fusion Yields in the System ^{132}Xe + ^{nat}Fe 11
(R.A. Esterlund, W. Westmeier, A. Rox, U. Reus, H. Schulte, P. Patzelt)

Capture Processes in the System ^{238}U + ^{nat}Fe 12
(A. Rox, B. Jäckel, R.A. Esterlund, W. Westmeier, U. Reus, H. Schulte, P. Patzelt)

Sub-Coulomb Transfer in Collisions of ^{238}U with ^{238}U 13
(G. Wirth, W. Brüchle, W. Fan, H. Gäggeler, K. Schlitt, K. Sümmerer, J.V. Kratz, M. Lerch, N. Trautmann)

One-particle Transfer in Uranium Induced Reactions at the Coulomb-Barrier 14
(D. Schüll, W.F.W. Schneider, H. Bokemeyer, R. Bock, H. Freiesleben, F. Pühlhofer, D. Bangert, B. Kohlmeyer, M. Marinescu)

Quasi-Elastic Nucleon Transfer Reactions in a Core Excitation Model for ^{48}Ti Incident on ^{42}Ca 15
(C. Brendel, J. Carter, F. Beck, G. Delic, R.H. Lemmer, A. Richter, G. Schrieder, D. Schüll)

Indications of Coherent Nucleon Flow in ^{238}U Induced Deep Inelastic Scattering Near the Coulomb-Barrier 16
(G. Beier, J. Friese, P. Kienle, H.J. Körner, W. Mayer, W.A. Mayer, L. Müller, W. Wagner)

1.1.2 Deep Inelastic Reactions

Mass and Charge Transfer in Heavy Ion Collisions 17
(R. Bass, H. Noll, V. Hartmann, K. Sapotta)

Light Charged Particle Accompanied ^{208}Pb Collisions with ^{26}Mg and ^{58}Fe 18
(P.J. Brülls, H.P. Hollenbach, M. Mutterer, J. Pannicke, J.P. Theobald, K. Weingärtner, H.W. Daues, A. Gobbi)

X-Ray Emission Probabilities and Nuclear Time Delay in the Deep Inelastic Collision U+U at 7.5 MeV/amu 19
(Ch. Stoller, M. Nessi, W. Wölfli, W.E. Meyerhof, J.D. Molitoris, E. Morenzoni, E. Grosse, Ch. Michel)

Measurement of the γ-Ray Circular Polarization in Kr-Induced Reactions at 10 MeV/u 20
(Ch. Schandera, Ch. Lauterbach, J. de Boer, W. Dünnweber, W. Trautmann)

PAGE

Moments of Charge Distributions in the Reaction ^{92}Mo + ^{92}Mo at 14.7 MeV/u 21
(S. Gralla, R. Bock, G.-X. Dai, A. Gobbi, K.D. Hildenbrand, W.F.J. Müller, U. Lynen, A. Olmi, M. Petrovici, H. Stelzer, J. Toke, H.J. Wollersheim)

Two- and Three-body Exit Channels in the Reaction ^{92}Mo + ^{92}Mo at 14.7 MeV/u 22
(S. Gralla, R. Bock, G.-X. Dai, A. Gobbi, K.D. Hildenbrand, W.F.J. Müller, U. Lynen, A. Olmi, M. Petrovici, H. Stelzer, J. Toke, H.J. Wollersheim)

Monte-Carlo Simulation of Ternary Reactions 23
(J. Kuzminski, A. Gobbi, S. Gralla, K.D. Hildenbrand, M. Petrovici)

Nucleon Transfer and Inelastic Excitations in the Reactions of 18 MeV/u ^{86}Kr with ^{208}Pb 24
(H. Sohlbach, H. Freiesleben, B. Kohlmeyer, M. Marinescu, F. Pühlhofer, W.F.W. Schneider, D. Schüll, P. Braun-Munzinger)

Interactions of 16.7 MeV/u ^{238}U with ^{nat}U as Studied with Mica Track Detectors 25
(E.U. Khan, P. Vater, R. Beckmann, R. Brandt)

Multifragment-Emission-Cross-Sections in the Reaction ^{238}U + ^{197}Au for ^{238}U Ion Energies of 10 MeV/n and 16.7 MeV/n 26
(H.A. Khan, R. Brandt, N.A. Khan, K. Jamil, M.A. Sial, G. Hussain)

Evidence of a New Type of Fission within a Solid State Nuclear Detector 27
(M. Debeauvais, J. Ralarosy, J. Tripier, S. Jokic)

1.1.3 Nuclear Reactions at High Energies

Impact Parameter Determination and Event-Types in ^{18}O Induced Reactions at 84 MeV/u 28
(I. Bock, U. Lynen, D. Pelte, U. Winkler, R. Glasow, K.H. Kampert, R. Santo, W.F.J. Müller, A. Gobbi, K.D. Hildenbrand, A. Olmi, H. Sann, H. Stelzer)

Light Particle Emission in Reactions with 84 MeV/u ^{12}C- and ^{18}O-Projectiles 29
(R. Glasow, K.H. Kampert, R. Santo, I. Bock, H. Ho, W. Kühn, U. Lynen, D. Pelte, U. Winkler, A. Gobbi, K.D. Hildenbrand, W.F.J. Müller, A. Olmi, H. Sann, H. Stelzer)

PAGE

Reaction Channels in the Interaction of 84 MeV/u-^{12}C with ^{208}Pb 30
(B. Grabez, R. Beckmann, P. Vater, R. Brandt)

Radiochemical Studies of Transtarget Nuclei in the Reaction Pb(Bi) + 86 MeV/u ^{12}C 31
(T. Lund, D. Molzahn, R. Brandt, E. Hagebo, I. Haldorsen, C.R. Serre)

Cooperative Effects observed in the Neutral Pion Production from Nucleus Nucleus Collisions 32
(H. Noll, H. Dabrowski, E. Grosse, H. Heckwolf, O. Klepper, Ch. Michel, W.F.J. Müller, H. Stelzer, C. Brendel, W. Rösch, P. Braun-Munzinger)

Pion Multiplicity in Relativistic Heavy Ion Collisions as a Probe of Nuclear Compression 33
(R. Stock, R. Bock, R. Brockmann, A. Dacal, J.W. Harris, M. Maier, M.E. Ortiz, H.G. Pugh, R.E. Renfordt, A. Sandoval, L.S. Schroeder, H. Ströbele, K.L. Wolf)

Impact Parameter Selection in Central Ar + KCl Reactions at 1.8 GeV/u 34
(R. Brockmann, J.W. Harris, M. Maier, H.G. Pugh, R.E. Renfordt, A. Sandoval, D. Schall, L.S. Schroeder, R. Stock, H. Ströbele, K. Wolf)

Charged Particle Exclusive Analysis of Central Ar + KCl and Ar + Pb Reactions at 1.8 and 0.8 GeV/u 35
(H. Ströbele, R. Brockmann, J.W. Harris, M. Maier, F. Riess, A. Sandoval, R. Stock, K.L. Wolf, H.G. Pugh, L.S. Schroeder, R.E. Renfordt, D. Schall, K. Tittel)

Charge, Mass and Energy Measured in the Plastic Ball 36
(H.H. Gutbrod, B. Kolb, H. Löhner, B. Ludewigt, A.M. Poskanzer, T. Renner, H. Riedesel, H.G. Ritter, A.I. Warwick, F. Weik, H. Wieman)

The Question of Thermalization within Relativistic Heavy Ion Collisions 37
(H.H. Gutbrod, B. Kolb, H. Löhner, B. Ludewigt, A.M. Poskanzer, T. Renner, H. Riedesel, H.G. Ritter, A.I. Warwick, F. Weik, H. Wieman)

Two-Particle Correlations from the Plastic Ball 38
(H.H. Gutbrod, B. Kolb, H. Löhner, A.M. Poskanzer, T. Renner, H. Riedesel, H.G. Ritter, A.I. Warwick, F. Weik, H. Wieman)

PAGE

Cluster Formation Observed with the Plastic Ball and the Question of Entropy Production in High Energy Nuclear Collisions 39
(H.H. Gutbrod, B. Kolb, H. Löhner, A.M. Poskanzer, T. Renner, H. Riedesel, H.G. Ritter, A.I. Warwick, F. Weik, H. Wieman)

Multifragmentation of Nuclear Residues in Relativistic Nuclear Collisions 40
(A.I. Warwick, H. Wieman, H.H. Gutbrod, M. Maier, J. Peter, H.G. Ritter, F. Weik, H. Stelzer, M. Freedman, D.J. Henderson, S.B. Kaufman, E.P. Steinberg, B.D. Wilkins)

Minimal-Spanning-Tree Analysis of Plastic Ball Events 41
(H. Löhner, H.H. Gutbrod, A.M. Poskanzer, T. Renner, H. Riedesel, H.G. Ritter, A.I. Warwick, H. Wieman)

A Search for Short-lived Anomalons in Projectile Fragmentation 42
(H.A. Gustafsson, H.H. Gutbrod, B. Kolb, B. Ludewigt, A.M. Poskanzer, T. Renner, H. Riedesel, H.G. Ritter, A.I. Warwick, H. Wieman)

Test of Radiochemical Techniques in the Study of Anomalons 43
(G. Dersch, T. Lund, R. Beckmann, R. Brandt, R.M. Weiner, P. McGaughey, E.M. Friedländer, W. Loveland, N. Porile, K. Aleklett)

Comparison of Z=2 Induced Primary and Secondary Interactions in Nuclear Track Emulsion at $\sim$ 2 GeV/u 44
(N. Klein, E. Ganßauge, M. Baagil, U. Bieschke, F. Killinger, R. Kretschmer, A. Laschek, W. Weidner)

1.2 Nuclear Structure

Upper Limit for the Axion Decay of Triplet Positronium 45
(W. Wahl, E. Adelberger, D. Habs, R. Kroth, D. Schwalm, H.J. Specht, V. Metag, R.S. Simon)

Multiple Coulomb Excitation of ^{82}Kr 46
(S. Brüssermann, K.P. Lieb, P. Sona, H. Emling, E. Grosse, J. Stachel)

Alignment in ^{104}Ru 47
(J. Stachel, P. Hill, N. Kaffrell, H. Emling, H. Grein, E. Grosse, Ch. Michel, H.J. Wollersheim, D. Schwalm, S. Brüssermann)

PAGE

Coulomb Excitation of ^{114}Cd and ^{116}Sn 48
(C. Fahlander, A. Bäcklin, L. Hasselgren, V. Mittal, L.E. Svensson, F. Azgui, H. Grein, E. Grosse, R. Kulessa, Ch. Michel, W. Spreng, H.J. Wollersheim, J. Stachel, D. Cline, B. Kotlinski)

Investigation of the Transitional Nucleus ^{152}Gd 49
(P. Hill, N. Kaffrell, J. Stachel, D. Schwalm, F. Azgui, H. Emling, E. Grosse, Ch. Michel, W. Spreng, H.J. Wollersheim)

Collective and Single Particle Configurations at High Spin in ^{154}Dy 50
(F. Azgui, H. Emling, E. Grosse, Ch. Michel, H.J. Wollersheim, D. Schwalm)

Investigation of the Yrast Region in ^{158}Er at High Spins 51
(R. Albrecht, B. Kolb, R.S. Simon, W. Hennerici, H.J. Hennrich, G. Himmele, R. Repnow, D. Habs, K. Helmer, U. v. Helmolt, H.W. Heyng, D. Pelte, D. Schwalm, V. Metag)

Spin Dependence of the High Energy Component in the γ Decay Following Compound Nucleus Reactions 52
(R. Albrecht, B. Kolb, R.S. Simon, W. Hennerici, H.J. Hennrich, G. Himmele, A. Lazzarini, R. Repnow, W. Wahl, D. Habs, U. v. Helmolt, H.W. Heyng, R. Kroth, D. Pelte, D. Schwalm, V. Metag)

Angular Correlationsof γ-Ray Transitions in ^{164}Dy 53
(H.J. Wollersheim, H. Emling, E. Grosse, Ch. Michel, D. Schwalm)

Coulomb Excitation of ^{176}Lu by ^{208}Pb Ions 54
(Th.W. Elze, J. Gerl, Th. Happ, K. Keppler, H. Ower, H.J. Wollersheim)

Study of Deorientation in ^{196}Pt 55
(A. Mauthofer, H. Ower, K. Stelzer, Th.W. Elze, H.J. Wollersheim, H. Emling, E. Grosse, D. Schwalm)

Coulomb Excitation of ^{202}Hg and ^{204}Hg with ^{208}Pb Ions 56
(Y.K. Agarwal, C. Günther, K. Hardt, P. Schüler, J. Stachel, E. Grosse, R. Kulessa, W. Spreng, H.J. Wollersheim)

High Spin States of ^{230}Th Studied in Coulomb Excitations with ^{142}Nd Projectiles 57
(Ch. Lauterbach, J. de Boer, Ch. Mittag, F. Rieß, Ch. Schandera, Ch. Briancon, A. Lefebvre, R.S. Simon)

PAGE

Backbending in ^{242}Pu and ^{244}Pu 58
(W. Spreng, F. Azgui, H. Emling, E. Grosse, R. Kulessa, Ch. Michel, R.S. Simon, H.J. Wollersheim, M. Mutterer, J.P. Theobald, D. Schwalm, M.S. Moore)

1.3 Exotic Nuclides

Laser Spectroscopy at the GSI On-Line Mass Separator 59
(G. Ulm, J. Eberz, G. Huber, D. Kaplan, H. Lochmann, R. Kirchner, O. Klepper, T. Kühl, P.O. Larsson, D. Marx, E. Roeckl, D. Schardt)

Direct Proton Decay of 0.56-s ^{147}Tm and Search for this Decay Mode among very Neutron-Deficient Isotopes with $61 \leq Z \leq 67$ 60
(P.O. Larsson, T. Batsch, R. Kirchner, O. Klepper, W. Kurcewicz, E. Roeckl, D. Schardt, G. Nyman, P. Tidemand-Petersson)

Predictions of Further Proton Radioactivity Near ^{151}Lu 61
(S. Hofmann, Y.K. Agarwal, F.P. Heßberger, G. Münzenberg, W. Reisdorf, J.R.H. Schneider, H.-J. Schött, P. Armbruster)

Neutron-rich Lutetium Isotopes Investigated at the GSI On-Line Mass Separator 62
(R. Kirchner, W. Kurcewicz, E. Roeckl, D. Schardt, N. Kaffrell, P. Peuser, K. Rykaczewski, E. Runte, W.-D. Schmidt-Ott, P. Tidemand-Petersson, K.-L. Gippert, G. Walter, H. Beer)

Alpha Decay of New Neutron Deficient Gold, Mercury, and Thallium Isotopes 63
(J.R.H. Schneider, S. Hofmann, F.P. Heßberger, G. Münzenberg, W. Reisdorf, H.-J. Schött, P. Armbruster)

Alpha Spectroscopy for Nuclei between Fr and U 64
(R. Hingmann, H.-G. Clerc, C.-C. Sahm, D. Vermeulen, K.-H. Schmidt, J.G. Keller)

Decay Properties of Neutron Deficient Isotopes of Element 105 65
(F.P. Heßberger, G. Münzenberg, S. Hofmann, Y.K. Agarwal, P. Armbruster, K. Poppensieker, W. Reisdorf, C.-C. Sahm, K.-H. Schmidt, J.R.H. Schneider, W.F.W. Schneider, H.-J. Schött, D. Vermeulen)

Element 109 66
(G. Münzenberg, Y.K. Agarwal, F.P. Heßberger, S. Hofmann, K. Poppensieker, W. Reisdorf, J.H.R. Schneider, W.F.W. Schneider, K.-H. Schmidt, H.-J. Schött, P. Armbruster, C.-C. Sahm, D. Vermeulen)

PAGE

Heavy Actinide Products from Reactions of ^{18}O and ^{22}Ne with ^{254}Es 67
(M. Schädel, R.W. Lougheed, J.H. Landrum, J.F. Wild, R.J. Dougan, A.D. Hoover, E.K. Hulet, A. Ghiorso, K.J. Moody, G.T. Seaborg)

A New 105-ms Spontaneous Fission Activity Produced in the Reaction ^{18}O with ^{254}Es 68
(L.P. Somerville, M.J. Nurmia, M. Schädel, A. Ghiorso, J.M. Nitschke, R.W. Lougheed, J.H. Landrum, E.K. Hulet)

Recent Searches for Long-Lived Superheavy Elements from the $^{48}Ca + ^{248}Cm$ Reaction 69
(H. Gäggeler, W. Brüchle, M. Brügger, M. Schädel, K. Sümmerer, G. Wirth, A. Ghiorso, K.E. Gregorich, D. Lee, K.J. Moody, G.T. Seaborg, R.B. Welch, P. Wilmarth, G. Herrmann, J.V. Kratz, N. Trautmann, N. Hildebrand, U. Hickmann, C. Frink, N. Greulich, D.C. Hoffmann, M. Fowler, H.R. von Gunten)

The Gas-Filled Separator (SASSY) at LBL Applied to the Production of Heavy Elements via Fusion 70
(A. Ghiorso, M. Leino, S. Yashito, P. Armbruster, J.P. Dufour, S. Hofmann, P. Lemmertz, G. Münzenberg)

Gamma-Ray Catalog 71
(U. Reus, W. Westmeier)

1.4 Theory

1.4.1 Nuclear Structure and Decay

Nuclear Proton Emission Predictions 72
(W.F. Feix, E.R. Hilf)

Analysis of Nuclear Charge Distributions 73
(W.D. Myers, K.-H. Schmidt)

Analysis of the Neutron Excess in the Bulk Region of Finite Nuclei 74
(D. Berdichevsky, U. Mosel)

Influence of Shell Structure and Pairing Correlations on the Nuclear Level Density Including Collective Motions 75
(K.-H. Schmidt, D. Vermeulen, H. Delagrange, J.P. Dufour, N. Carjan, A. Fleury)

Calculation of Energy Averaged Reduced Transition Probabilities (EARTP) 76
(A. Baran, K. Dietrich)

PAGE

Gamma Deexcitation Process of ^{158}Dy and Realistic Level Densities 77
(A. Baran, K. Dietrich)

Yrast Line and g-Factors of ^{158}Er 78
(M. Diebel, U. Mosel, K. Mühlhans)

Alignment Behaviour of Odd-A-Nuclei 79
(E.M. Müller, U. Mosel, K. Neergard)

Improvement of Quasiparticle Levels 80
(U. Mosel, U. Post, E. Wüst)

Multipole Pair Fields at Various Conditions 81
(K. Mühlhans, U. Mosel, E.M. Müller)

How do Nuclei Really Vibrate? 82
(J. Kunz, U. Mosel, A. Schuh, E. Wüst)

On the Existence of Relatively Stable Giant Nuclei around Z = 164-182 83
(N. Abou-el-Naga, W. Greiner)

1.4.2 Nuclear Reactions at Low Energies

Fusion of ^{40}Ar and ^{40}Ca at High Incident Energies - Fusion-Fission and Fusion-Evaporation 84
(J. Carter, H. Feldmeier, C. Brendel, A. Richter, G. Schrieder, W. Bohne, K. Grabisch, H. Lehr, H. Morgenstern)

On Quantal Diffraction in Dissipative Heavy Ion Collisions 85
(H. Spangenberger, F. Beck, H. Feldmeier)

On the Mechanism of Diffusion in Heavy Ion Collisions 86
(H. Feldmeier, H. Spangenberger)

Dissipative Equations of Motion for the One-Body Density 87
(P. Buck, H. Feldmeier, F. Beck)

Unified Description of Statistical Excitations, Deformations and Charge Transfer in a Dynamical Theory of DIC 88
(P. Fröbrich, B. Strack, M. Durand)

Nuclear Transport due to the Stochastical Exchange of Nucleons 89
(D. Bangert, B. Kohlmeyer, M. Marinescu, F. Pühlhofer, F. Busch, D. Schüll, H. Freiesleben)

PAGE

Shell-Structure Affected Stochastic Walk on the (N-Z) Plane 90
(J. Toke, A. Gobbi, T. Matulewicz)

Microscopic Nuclear Dissipation in the Long Mean Free Path Limit 91
(C. Yannouleas)

The Two-Body Collision Term in Dissipative Diabatic Dynamics 92
(S.J. Wang, W. Nörenberg)

On the Role of Memory Effects for Diffusion in Slow Collective Nuclear Motion 93
(W. Cassing, W. Nörenberg)

Study of Time Delay within the Fragmentation Theory 94
(K. Depta, J. Hahn, R. Herrmann, L. Neise, M. Uhlig, K.H. Ziegenhain, J.A. Maruhn, W. Greiner)

Microscopic Calculations of Diabatic Potentials and Mass Parameters 95
(A. Lukasiak, W. Cassing, W. Nörenberg)

On Diabatic Shell-Structure Effects in Heavy-Ion Collisions 96
(A. Lukasiak, W. Nörenberg)

Diabatic Aspects of TDHF 97
(W. Cassing, A.K. Dhar, A. Lukasiak, W. Nörenberg)

On the Energy-Distribution of Diabatically Emitted Neutrons in Heavy-Ion Collisions 98
(W. Cassing, W. Nörenberg)

Comparison of Collective Mass Parameters given by GCM and the Cranking Model 99
(S.J. Wang, W. Cassing, W. Nörenberg)

On the Dynamical Single-Particle Basis in Large Amplitude Collective Motions 100
(S.J. Wang, W. Cassing, W. Nörenberg)

Extension of the Time-Dependent Mean Field Theory within Density Matrix Hierarchy 101
(S.J. Wang)

Potential Energy Surfaces for Ternary Fragmentation 102
(N. Carjan, A. Gobbi, J. Toke)

Potential Pockets in the ^{238}U-^{238}U System and their Possible Consequences 103
(M.J. Rhoades-Brown, V. Oberacker, M. Seiwert, W. Greiner)

PAGE

Polarization Effects for Elastic and Inelastic Scattering with Exact and Approximated Propagators 104
(R. Kaps, J. Makowka, U. Mosel, O. Tanimura, R. Wolf)

The Semiclassical Approximation for Inelastic Scattering 105
(F. Krisztinkovics, J. Reinhardt, B. Müller, W. Greiner)

Contributions to the Theory of Nuclear Molecules Obtained by the Study of the $^{28}Si+^{28}Si$ System 106
(A. Thiel, W. Greiner, R. Könnecke)

1.4.3 Nuclear Reactions at High Energies

Comparison of Hydrodynamical Calculations with Recent CERN $^{12}C(184\ MeV/n)+^{197}Au$ Proton Data 107
(G. Buchwald, G. Graebner, J.A. Maruhn, W. Greiner, J. Theis, H. Stöcker)

Nonrelativistic Neutron-, Proton Fluid Dynamics 108
(J. Theis, G. Buchwald, G. Graebner, J.A. Maruhn, W. Greiner)

Influence of the Deformation of Nuclei on the Cross Section 109
(D. Barthel, G. Buchwald, G. Graebner, J.A. Maruhn, W. Greiner)

Are Solitons already Seen in Heavy Ion Reactions? 110
(S. Raha, R.M. Weiner)

Solitons in Nucleus-Nucleus Collisions near the Speed of Sound 111
(G.N. Fowler, S. Raha, N. Stelte, R.M. Weiner)

Surface Vortex Excitations in Rotating Nuclei 112
(G.N. Fowler, S. Raha, R.M. Weiner)

Subthreshold Pion Production, a Cooperative Process? 113
(J. Knoll, R. Shyam)

Effect of Isobars at Finite Temperature in Pion Condensation in ^{16}O 114
(R.K. Tripathi, A. Faessler)

How Strong is the Rho-Meson Exchange in the N-N Interaction? 115
(W.H. Dickhoff, A. Faessler, H. Müther)

Pion Condensates as Anomalons 116
(G.N. Fowler, S. Raha, R.M. Weiner)

PAGE

The Heavy Ion Potential and the Increasing Transparency at Intermediate Energies 117
(A. Faessler, S.B. Khadkikar, L. Rikus, R. Sartor)

Compression Versus Transparency Effects on the Energy Density in Central Relativistic Heavy Ion Collisions 118
(J.W. Harris, R. Stock)

The Expansion of Hot Nuclear Matter 119
(B. Strack, J. Knoll)

Three Component Fluid Dynamics Applied to Heavy Ion Reactions 120
(A. Rosenhauer, J.A. Maruhn, W. Greiner, L.P. Csernai)

Momentum Distribution of Nuclear Matter in High Energy Heavy-Ion Collisions 121
(A. Rosenhauer, J.A. Maruhn, W. Greiner, L.P. Csernai)

Sensitivity of Collective Nuclear Matter Flow to the Equation of State 122
(G. Buchwald, G. Graebner, M. Uhlig, D. Barthel, J.A. Maruhn, W. Greiner, J. Theis, H. Stöcker)

First Results of a 3-Dimensional Relativistic Nuclear Fluid Dynamical Model 123
(G. Graebner, G. Buchwald, J.A. Maruhn, W. Greiner, H. Stöcker, J. Theis)

Double Shocks in Relativistic Nucleus Nucleus Collisions 124
(G. Graebner, J.A. Maruhn, W. Greiner, H. Stöcker, H. Kruse)

Relativistic Nuclear Fluiddynamics Coupled to Classical Meson Field 125
(J. Theis, G. Graebner, G. Buchwald, J.A. Maruhn, W. Greiner)

Multiparticle Production in Hadron-Nucleus Collisions around 100 GeV 126
(W.Q. Chao, M.K. Hegab, J. Hüfner)

A Model for Multiplicity Distributions in Hadron-Nucleon and α-α Interactions at Very High Energies 127
(H.J. Pirner, W.Q. Chao)

Influence of Isospin Conservation on Particle Spectra 128
(B. Müller, J. Rafelski)

PAGE

Mean Field Theories of Nuclear Matter at Low and Intermediate Temperatures 129
(M. Uhlig, W. Greiner, C.S. Warke)

Entropy Production in Heavy Ion Collisions 130
(M. Uhlig, W. Greiner, C.S. Warke)

Phase Transition of the Nucleon-Antinucleon Plasma in a Relativistic Mean Field Theory 131
(J. Theis, H. Stöcker, J. Polonyi, G. Graebner, G. Buchwald, M. Uhlig, J.A. Maruhn, W. Greiner)

On the Color-Singlet Quark-Glue-Plasma 132
(H.-Th. Elze, W. Greiner, J. Rafelski)

Formation of Quark-Gluon Plasma at Central Rapidity 133
(M. Danos, J. Rafelski)

Particle Radiation by Hot Quark-Gluon Plasma 134
(M. Danos, J. Rafelski)

Quark-Gluon Plasma in $\bar{p}$-Annihilation on Nuclei 135
(J. Rafelski)

Measurement of Baryochemical Potential of Hot Nuclear Matter 136
(P. Koch, J. Rafelski, W. Greiner)

Strangeness as a Signal for Quark-Gluon-Plasma Formation 137
(P. Koch, J. Rafelski, W. Greiner)

High Energy γ's from $s\bar{s}$-Annihilation in Quark-Gluon Plasma 138
(G. Staadt, J. Rafelski, W. Greiner)

Are Glueless M.I.T.Bags Intrinsically Deformed? 139
(D. Vasak, R. Shanker, B. Müller, W. Greiner)

String-Like Quark Bags and Regge-Trajectories 140
(R. Shanker, D. Vasak, W. Greiner, C.S. Warke)

Monte Carlo Simulation of QCD 141
(J. Kuti, J. Polonyi)

Topological Charge of Lattice Field Theories 142
(J. Polonyi)

A New Scheme for Spontaneous-Symmetry-Breaking of Color SU(3) 143
(A. Schäfer, B. Müller, W. Greiner)

Centauros as a Superfluorescence Phenomenon 144
(G.N. Fowler, E.M. Friedländer, R.M. Weiner)

PAGE

2. Atomic Physics

2.1 Superheavy Quasi-Atoms and Inner Shell Excitation Mechanism

Study of Positron-Creation in Overcritical HI-Collision Systems 146
(H. Bokemeyer, H. Folger, H. Grein, Y. Kido, T. Cowan, J.S. Greenberg, J. Schweppe, K. Bethge, A. Gruppe, R. Merten, Th. Odenweller, K.E. Stiebing, D. Schwalm, P. Vincent, N. Trautmann)

Narrow Structure in Positron Spectra from U + U Collisions 147
(E. Berdermann, M. Clemente, P. Kienle, H. Tsertos, W. Wagner, F. Bosch, C. Kozhuharov, W. Koenig)

Positron Production in Peripheral and Close Collisions measured with the New Tori Spectrometer 148
(E. Bozek, U. Gollerthan, E. Kankeleit, G. Klotz, M. Krämer, R. Krieg, U. Meyer, H. Oeschler, P. Senger)

Investigations of the Coherence Betwenn Different Excitation Channels in Heavy Ion-Atom Collisions 149
(A. Warczak, H.D. Dohmann, D. Liesen, B. Liu)

Oscillations in the Inner-Shell Vacancy Production in Heavy Ion-Atom Collisions 150
(B. Liu, H.D. Dohmann, D. Liesen, A. Warczak)

Kinematic Peak in Very Asymmetric Ion-Atom Collisions 151
(D. Maor, Z. Stachura, P.H. Mokler, B. Liu, D. Liesen)

K-Shell Excitation by K- to L-Shell Charge Transfer in Slow Kr^{q+}-Kr and Xe^{q+}-Xe Collisions 152
(R. Schuch, E. Justiniano, R. Hoffmann, W. Schadt, H. Schmidt-Böcking, P.H. Mokler, F. Bosch, W.A. Schönfeldt, Z. Stachura)

Charge Transfer in Atomic Collisions with Highly Ionized, Decelerated Heavy Ions 153
(P.H. Mokler, D.H.H. Hoffmann, W.A. Schönfeldt, Z. Stachura, A. Warczak)

L_3-Subshell Alignment Observed in 1.4 MeV/n Ion - Atom Collisions 154
(Z. Stachura, F. Bosch, D. Maor, P.H. Mokler, W.A. Schönfeldt, H. Wahl, B. Cleff, M. Brüssermann, J. Wigger)

PAGE

2.2 Few Electron Systems, Recoil Ions and Capture Processes

Wavelengths of Transitions in Few Electron Spectra of Titanium 155
(H.D. Dohmann, D. Liesen, E. Pfeng)

Projectile Dependence of Multiple Target Ionization Observed in K Satellite Spectra 156
(H.F. Beyer, R. Mann, F. Folkmann)

Energy Gain Spectroscopy with High Charged Low Velocity Recoil Ions 157
(C.L. Cocke, R. Mann, R. Marrus, M. Prior, A.S. Schlachter)

Production of Highly Charged Recoil Ions and Electron Capture Cross Sections from He Neutrals 158
(R. Mann)

Charge Transfer Involving Multiply Charged Ions 159
(W. Groh, A. Müller, P.C. Kester, I. Wirkner-Bott, A.S. Schlachter, B. Schuch, E. Salzborn)

Pressure Broadening and Pressure Shift of the (λ=410 nm) Indium Line 160
(J. Eberz, G. Huber, G. Ulm, T. Kühl)

Isotope Shift in Two-Photon Transitions of Indium 161
(R. Menges, G. Huber, G. Ulm, T. Kühl)

2.3 Interaction of Heavy Ions with Matter

Charge State Distributions of Ar-, Kr-, Xe-, and U-Ions after Solids at Energies up to 18.7 MeV/u 162
(B. Franzke)

Measurement of Charge Exchange Cross Sections in Atomic Collisions with Highly Ionized, Decelerated Ions 163
(D.H.H. Hoffmann, P.H. Mokler, W.A. Schönfeldt, Z. Stachura, H. Wahl)

Shape of the Convoy Electron Structure and Total Electron Yield in High Energy (882 MeV) Ni -> C and Al Collisions 164
(R. Latz, M. Burkhard, H.J. Frischkorn, D. Hofmann, P. Koschar, J. Schader, K.O. Groeneveld, M. Breinig, S. Berry, I.A. Sellin)

Secondary Ion Emission from Metallic Surfaces Bombarded by Fast Heavy Ions 165
(O. Becker, W. Knippelberg, K. Wien)

Secondary Ion Emission from Phenylalanine as Function of Projectile Charge State 166
(W. Guthier, O. Becker, W. Knippelberg, U. Weickert, K. Wien, Y. Le Beyec, S. Della Negra)

PAGE

2.4 Theory

Interatomic Potentials for Ionized Scattering Systems 167
(H. Hartung, B. Fricke, W.-D. Sepp, W. Schulze)

The Finite-Element Method to Calculate Atomic and Molecular Properties 168
(W. Schulze, D. Kolb)

Solution of the Poisson-Equation for a Di-Atomic Molecular Charge Distribution in Elliptic Hyperbolic Coordinates 169
(W. Sengler, D. Kolb, B. Fricke)

Calculations of Coupling Matrix Elements for Diatomic Systems in an Atomic Basis 170
(W.-D. Sepp)

Additional Couplings of the Innermost Shells in Very Heavy Quasi-Molecular Ion-Atom Collisions 171
(M. Mann, B. Fricke, W.-D. Sepp, H. Hartung, P.H. Mokler, W.A. Schönfeldt)

Solution of the Time-Dependent Hartree-Fock Equation for Atomic Collisions 172
(E. Teubner, N. Grün, W. Scheid)

Use of Ehrenfest's Principle for Inelastic Collisions 173
(M. Kleber, W. Elberfeld)

The Local Representation of the Dirac Equation 174
(P. Schlüter, K.-H. Wietschorke, W. Greiner)

On an Alternative Dirac-Theory 175
(A. Schäfer, J. Rafelski, W. Greiner)

The Dirac Equation for Rotational Symmetric Potentials or Boundary Conditions 176
(K.-H. Wietschorke, P. Schlüter, W. Greiner)

Impact-Parameter Dependence of K-Shell Ionization in Slow Collisions of Near-Symmetric Relativistic Atoms 177
(D.H. Jakubaßa-Amundsen, P.A. Amundsen, K. Aashamar)

Angular Distribuion of δ-Electrons from Slow Heavy-Ion Collisions 178
(D.H. Jakubaßa-Amundsen)

K-Hole Coincident δ-Electron Emission 179
(U. Müller, G. Soff, J. Reinhardt, T. de Reus, B. Müller, W. Greiner)

PAGE

Theoretical Derivation for K-Hole Coincident δ-Electron Emission 180
(U. Müller, G. Soff, J. Reinhardt, T. de Reus, B. Müller, W. Greiner)

Theoretical K-Vacancy Yields in Sm-Pb and Sm-U Collisions 181
(T. de Reus, J. Reinhardt, B. Müller, W. Greiner, G. Soff, U. Müller)

Delta Electron Spectra for Br-Pb and Br-U at 3.88 MeV/u 182
(T. de Reus, J. Reinhardt, B. Müller, W. Greiner, G. Soff, U. Müller)

Positron Spectra Calculated with an SCF Potential 183
(T. de Reus, J. Reinhardt, B. Müller, W. Greiner, G. Soff, U. Müller)

The Effect of a Nuclear Time Delay Distribution on Positron Spectra 184
(U. Müller, G. Soff, J. Reinhardt, T. de Reus, B. Müller, W. Greiner)

Electron Excitation and Positron Emission in Deep-Inelastic Nuclear Collisions 185
(U. Müller, G. Soff, T. de Reus, J. Reinhardt, B. Müller, W. Greiner)

Conversion Processes in Super-Critical Compound Systems 186
(U. Müller, G. Soff, T. de Reus, J. Reinhardt, B. Müller, W. Greiner)

Electronic Transition Times in Supercritical Compound Systems 187
(G. Soff, U. Müller, T. de Reus, J. Reinhardt, P. Schlüter, K.-H. Wietschorke, G. Mehler, B. Müller, W. Greiner)

MO K X-Rays Emitted by Sticking Heavy Quasimolecules 188
(J. Kirsch, B. Müller, W. Greiner)

3. Radiation Effects

3.1 Radiation Effects in Biological Systems

The Radial Dose Distribution of a Heavy Particle Track in a Tissue Equivalent Material 190
(M. Krämer, G. Kraft)

Radiation Induced Strand Breaks in Phage DNA at High Doses 191
(A.M. Kellerer, H. Roos, W.-H. Thomas, F. Zilker)

PAGE

The Induction of Double and Single Strand Breaks Viral DNA in Solution 192
(R. Roots, M. Larsson, G. Kraft)

The Radiation Action of Heavy Ions on Spores of Bacillus Subtilis 193
(M. Schäfer, R. Facius, H. Bücker)

Inhibition of r-RNA Synthesis in Yeast Cells Exposed to Helium-, Carbon- or Fluorine Ions 194
(K.J. Weber, E. Schneider, J. Kiefer, G. Kraft)

The Oxygen Effect in Yeast Cells Exposed to Heavy Ions 195
(F. Schöpfer, E. Schneider, J. Kiefer, S. Rase, G. Lenz)

Interpretation of Heavy-Ion Survival Data 196
(J. Kiefer)

Chromosome Aberrations in Chinese Hamster Cell Cultures Induced by Heavy-Ion Irradiation 197
(W. Müller, H.G. Miltenburger, G. Kraft)

Differences in the Cell Progression Following Heavy-Ion Irradiation 198
(M. Larsson, D. Pollet, G. Kraft)

Inactivation of Mammalian Cells by Light and Heavy-Charged Particles 199
(G. Kraft, H. Meister, M. Schuber, W. Kraft-Weyrather, H.G. Miltenburger)

Modification of Radiosensitivity of Mammalian Cells 200
(W. Kraft-Weyrather, G. Kraft, H. Meister, H.G. Miltenburger, C.A. Tobias)

Micronucleus Induction after Treatment with Ionizing Radiations 201
(U. Bertsche, G. Iliakis, G. Kraft)

3.2 Radiation Effects in Solids

Small Angle Scattering from Latent Nuclear Tracks 202
(D. Albrecht, P. Armbruster, R. Spohr, M. Roth, K. Schaupert, H. Stuhrmann)

Annealing of Heavy Particle Latent Damage Trails in CR-39 (Homalite) Plastic Track Detectors 203
(H.A. Khan, R. Brandt, N.A. Khan, M.A. Sial, K. Jamil)

PAGE

Electrolytical Studies on Tracks of ^{238}U-Ions in Makrofol 204
(J. Krause, W. Enge, R. Beaujean)

Critical Angles of Etching of CR-39 Plastic Track Detectors 205
(H.A. Khan, R. Brandt, N.A. Khan, K. Jamil, M.A. Sial, G. Hussain)

Solid State Nuclear Track Detectors for High Energetic Heavy Ions 206
(K. Schaupert, K. Keiner, G. Fiedler)

A Graded-Index Antireflection Treatment of Optical Surfaces by the Nuclear Track Technique 207
(B.E. Fischer)

Scanning Electron Microscope Investigations of Plastic CR-39 Microfilters 208
(M. Berndt, G. Siegmon, R. Beaujean, W. Enge)

Use of Etched Channels as Charged Particle Collimators 209
(H.A. Khan, R. Brandt, N.A. Khan, K. Jamil, M.A. Sial)

The Single Erythrocyte Rigidometer on the Threshold to a Product 210
(H.G. Roggenkamp, H. Kiesewetter, F. Jung)

Fractionation of Aerosols Using Mica Nuclear Microfilters with Rounded-off Entrance Channels at the NUKEM-Sinteroven 211
(G. Tress, E.U. Khan, H.A. Khan, P. Vater, R. Brandt, M. Kadner, R. Spohr)

Measurements of Aerosol Size Distributions with the Mica Microfilter Cascade Fractionator at the KfK-SASCHA 212
(E.U. Khan, G. Tress, R. Dersch, P. Vater, R. Brandt, H. Wild, H. Albrecht)

A Research Program for Studying the Use of Ion Beam Techniques for Corrosion Protection 213
(J. Dressler, H. Ferber, A. Meger, G. Reiss, G.K. Wolf)

Ion Beam Mixing-A Method for Modifying Catalysts 214
(G.K. Wolf, K. Zucholl, H. Folger)

4. Developments

4.1 Target and Stripper Technology, Chemical Procedures

Survey on the Production of Nuclear Accelerator Targets 216
(H. Folger, W. Hartmann, J. Klemm, W. Thalheimer, U. Glatzel)

PAGE

Operational Conditions of a Duoplasmatron Ion-Source for Sputter Depositions of Nuclear Target Materials 217
(H. Folger, M. Müller)

The Medium-Current Mass Separator 218
(K.H. Behr, A. Brünle, C. Bruske, K. Burkhard, W. Hüller, H.R. Kiesewetter, R. Kirchner, W. Leiser, L. Molnar, F. Nickel, E. Roeckl)

Preparation of Lanthanide and Actinide Samples by Vacuum Evaporation 219
(C. Frink, N. Trautmann, G. Herrmann, M. Schädel)

Chemical Separation of Thorium, Protactinium, Uranium, Neptunium and Plutonium from Complex Heavy Ion Reaction Product Mixtures 220
(M. Lerch, U. de la Chevallerie, D. Gembalies-Datz, W. Kieling, J.V. Kratz, A. Lewening, N. Trautmann, S. Zauner, G. Herrmann)

Rapid Preparation and Gaschromatographic Separation of Carrier-Free Lanthanide Hexafluoracetylacetonates 221
(N. Greulich, N. Trautmann, G. Herrmann)

Hydrogen in Carbon Foils 222
(H. Baumann, K. Bethge, F. Rauch, W. Reeh, H. Wirth)

4.2 Experimental Set-Ups

Performance of the Darmstadt-Heidelberg Crystal Ball 223
(R. Albrecht, B. Kolb, R.S. Simon, H. Gräf, W. Hennerici, H.J. Hennrich, G. Himmele, E. Jaeschke, O. Koschorrek, R. Repnow, W. Wahl, D. Habs, K. Helmer, U. v. Helmolt, H.W. Heyng, H. Krieger, R. Kroth, D. Pelte, D. Schwalm, R.D. Fischer, W. Kühn, V. Metag, R. Mühlhans)

Monte-Carlo Simulation of a HPGe-BGO Compton Suppression Spectrometer 224
(Ch. Michel, F. Azgui, H. Emling, E. Grosse, H.J. Wollersheim)

High-Efficiency Set-up for Binary Reactions Studies 225
(G.-X. Dai, H.W. Daues, S. Gralla, H. Stelzer, J. Toke)

A Lead Glass Cherenkov Hodoscope as Neutral Pion Spectrometer 226
(Ch. Michel, P. Braun-Munzinger, C. Brendel, H. Dabrowski, E. Grosse, H. Heckwolf, O. Klepper, W.F.J. Müller, H. Noll, W. Rosch, H. Stelzer)

PAGE

Improvements to the Plastic Ball 227
(H.H. Gutbrod, B. Kolb, H. Löhner, A.M. Poskanzer, T. Renner, H. Riedesel, H.G. Ritter, A.I. Warwick, F. Weik, H. Wieman)

The Multiple Sampling Ionisation Chamber (MUSIC) 228
(H. Sann, F. Bieser, P. Brady, H. Crawford, B. Christie, D. Greiner, P. Lindstrom, G. Tull, J. Romereo)

Separation and Investigation of Short-Lived Fission Products with the HELIOS Facility 229
(M. Brügger, Th. Karlewski, N. Trautmann, A.K. Mazumdar, H. Wagner, W. Walcher)

Development of an Electron Spectrometer for Contact Time Measurements in Dissipative Heavy-Ion Collisions 230
(H. Backe, R. Barden, M. Begemann)

Status of the Eight Crystal X-Ray Spectrometer ("Octopus") 231
(H.D. Dohmann, U. Kopf, D. Liesen, D. Loos, W. Rösch, H. Wahl)

30° Electrostatic Spectrograph 232
(H.J. Frischkorn, P. Koschar, K.O. Groeneveld)

The Heavy-Ion Scanning Microscope - a Progress Report 233
(B.E. Fischer)

4.3 Detectors

Solar Cells as Detectors for Fragments of Volatile Spontaneously Fissioning Nuclides 234
(N. Hildebrand, W. Kieling, N. Trautmann, G. Herrmann, M. Brügger, H. Gäggeler, K. Sümmerer, W. Weber)

Performance of a Gas-Counter in a Time-of-Flight Set-Up behind SHIP 235
(J.G. Keller, K.-H. Schmidt, H. Stelzer, C.-C. Sahm)

Construction and Performance of a Position-Sensitive Particle Detector with Delay Line Readout 236
(B. Liu, W. Enders, D. Liesen, R. Schulze)

Luminescence Processes in Heavy-Ion Excited Scintillation Gases 237
(P. Grimm, F.-J. Hambsch, M. Mutterer, Chr. Preuss, J.P. Theobald)

PAGE

Liquid-Scintillator Detectors for Neutron Time-of-Flight Measurements 238
(H.-A. Bösser, B. Kohlmeyer, D. Bangert, H.-J. Keim, H. Stege, F. Pühlhofer, W.F.W. Schneider)

Automatic Track measurement on Streamer Chamber Pictures with High Multiplicity Events 239
(D. Schall, H. Ströbele, K. Tittel)

Charge Measurement by a Photometric Method 240
(A. Laschek, W. Weidner, E. Ganßauge, U. Bieschke, N. Klein, R. Kretschmer)

Charge Measurement of Projectile Fragments with $2 \leq Z \leq 6$ in Nuclear Track Emulsion 241
(R. Kretschmer, E. Ganßauge, U. Bieschke, F. Killinger, N. Klein, A. Laschek, W. Weidner)

4.4 Electronics, Computing Center and Workshops

Experimental Electronics Department
(Elektronik/Experimente) 242
(R. Albrecht, J. Dengler, G. Eidmann, A. Fehres, H. Hammal, H. Hardel, J. Hoffmann, H.P. Liebold, H.-G. Martens, W. Meufels, K. Mömerzheim, K. Poppensieker, A. Przybyla, D. Quis, M. Richter, H.-G. Schmidt, G. Schneider, R. Schulze, K. Senft, H. Spieler, E. Sturm, D. Jiao, Y.-Y. Zhou, T. Batsch)

A Flexible Graphic Package for Plotting Experimental and Theoretical Data 245
(K.-H. Schmidt)

Global Analysis with Plastic Ball Data 246
(H.H. Gutbrod, H. Löhner, A.M. Poskanzer, T. Renner, H. Riedesel, H.G. Ritter, A.I. Warwick, F. Weik, H. Wieman)

LISA, an On- and Off-Line Data Analysing Program 247
(B. Kolb)

Computing Center 248
(H. Egger, S. Glückert, H. Hultzsch, J. Lowsky, O. Siart)

Array Processor 253
(H.-J. Lustig)

Experiment Data Processing 254
(F. Busch, H. Göringer, V. Hartmann, J. Lowsky, D. Marinescu, D. Pissowotzki, K. Winkelmann, G. Zaidmann)

EDAS Documentation and Interactive HELP 255
(H. Göringer)

PAGE

Improvements in EDAS Coupled Mode 256
(F. Busch, D. Marinescu, M. Richter)

A Cross Memory Approach for Experimental Data Processing 257
(D. Marinescu)

Optimizing the Data Analysis in SATAN 258
(K. Winkelmann)

Graphics and Numeric Operating Method (GNOM) 259
(I. Giese, W. Kynast, M. Feyerabend, M. Steitz)

GSI Plotfile Interpreter 260
(I. Giese, K. Schwinn, G. Zaidmann)

Engineering and Technology 261
(E. Malwitz, K. Blasche, W. Bleuel, H. Gaiser, C. Hoffmann, K. Illert, H.R. Kiesewetter, U. Kopf, W. Schmidt)

5. Accelerator

5.1 UNILAC Performance and Ameliorations

UNILAC Operation 264
(N. Angert, J. Klabunde, M. Müller, P. Strehl, D. Wilms)

UNILAC Injector 265
(M. Müller, W. Jacoby, M.M. Khaouli, H. Schulte, J. Bossler, H. Emig, N. Hofmann, M. Stork, H.-P. Kurz, H. Krichbaum, K. Schneider, R. Rulfs, K.-D. Leible, G. Jöst)

The "Compact-PIG-Source" 266
(M. Müller, W. Zhao)

ECR Source Development 267
(H. Schulte, B. Wolf, K.-D. Leible)

Operating Modes of the Alvarez Tanks at the UNILAC 268
(J. Klabunde)

Recent Developments at the UNILAC RF 269
(G. Hutter, W. Hartmann, A. Morhardt, W. Vinzenz)

Improvements to the 180 KW/108 MHZ Ampflifiers 270
(G. Hutter, G. Kube, W. Vinzenz)

Time Share Operation of the UNILAC 271
(J. Glatz)

Two Kicker Magnets for the UNILAC Beam Sharing System and the Beam Transfer Line to SIS 272
(W. Bourgeois, K. Küper, B. Langenbeck, G. Moritz, G. Sobainsky, K. Zweig)

PAGE

300 KV Accelerator 274
(P. Spädtke, D. Vogt, B. Wolf)

5.2 Accelerator Projects

SIS - The Two-Stage Synchrotron Facility for Heavy Ions 275
(K. Blasche, D. Böhne, B. Franzke, H. Prange, R. Steiner)

Improved SIS12 Lattice with Variable Optic 277
(B. Franczak)

Variable Transition Energy in SIS12 278
(B. Franczak)

Triplet / Doublet Focussing in SIS12 279
(B. Franczak)

Beam Injection Line to SIS 12 280
(H. Eickhoff, B. Franzke)

Revised Layout for Slow Beam Extraction at SIS 12 281
(H. Eickhoff, B. Franzke)

Measurements on the SIS Prototype Accelerating Station 282
(M. Emmerling, K. Kaspar, K. Sato, A. Gasper)

Status of the Design of SIS Magnet System 283
(W. Bleuel, H. Gaiser, G. Grösch, B. Langenbeck)

Longitudinal Space Charge Limit of SIS 12 Operating in the Micro-Pulse Mode with RF-System II 284
(K. Beckert, R.W. Müller)

6. Inertial Confinement Fusion

System Studies for Heavy-Ion Inertial Confinement Fusion 286
(R.W. Müller, K. Beckert)

SIS for High-Intensity Target Experiments - A Study Report 287
(R.W. Müller)

High-Current Ion Sources Development 288
(R. Keller, F. Nöhmayer, P. Spädtke, M.-H. Schönenberg)

Heavy-Ion RFQ Status Report 289
(R.W. Müller, U. Kopf, L.W. Funk)

High Current Transport Experiments at GSI 290

PAGE

(J. Klabunde, M. Reiser, A. Schönlein, P. Spädtke, J. Struckmeier)

Aspects of Space Charge Compensation in Ion Beams 291
(A. Schönlein, J. Klabunde, M. Reiser)

Envelope Instabilities in FODO - Channels 292
(J. Struckmeier, J. Klabunde, M. Reiser)

Third and Higher Order Instabilities in FODO - Channels for Different Types of Distribution Functions 293
(J. Struckmeier, J. Klabunde, M. Reiser)

KOBRA3 a 3D-Computer Code Solving Vlasov's Equation 294
(N. Schmitt, P. Spädtke)

A High-Current Test Facility for Hollow Beams 295
(P. Krejcik)

Beam-Forming Experiments at the Hollow-Beam Test Stand 296
(P. Krejcik, R. Keller)

Beam Dynamics in the RF Coaxial Accelerator 297
(P. Krejcik)

Experimental Electron Loss Cross Sections for Lowly-Charged Ne-Ions in H_2 and N_2 at 1.4 MeV/u 298
(B. Franzke)

Soft X-Ray Emission in 1.4 MeV/u Pb-Noble Gas Atom Collisions 299
(H. Wahl, H.F. Beyer, P.H. Mokler)

Studies of Rayleigh-Taylor Instabilities - I. Perturbed Surfaces 300
(G. Buchwald, G. Graebner, J.A. Maruhn, W. Greiner, J. Theis, H. Kruse)

Studies of Rayleigh-Taylor Instabilities - II. Growth Rates 301
(G. Buchwald, G. Graebner, J.A. Maruhn, W. Greiner, J. Theis, H. Kruse)

Studies of Rayleigh-Taylor Instabilities - III. Perturbed Foils 302
(G. Buchwald, G. Graebner, J.A. Maruhn, W. Greiner, J. Theis, H. Kruse)

Quantification of the Pellet Irradiation Asymmetry 303
(J.A. Maruhn, J. Theis, G. Buchwald, G. Graebner, W. Greiner)

7. Annex PAGE

7.1 Scientific Activities outside GSI

7.1.1 Publications 306
7.1.2 Conference Contributions 318
7.1.3 Seminars at other Institutes 334
7.1.4 Lectures and Courses 344

7.2 Scientific Activities within GSI

7.2.1 Conferences and Seminars on Research Proposals 345
7.2.2 Seminars at GSI 346
7.2.3 GSI-Preprints 1982 349
7.2.4 GSI-Reports 1982 351
7.2.5 Visiting Groups at GSI 352

7.3 Scientific Committees, Directorate and Personnel 353

7.4 Scientific Cooperation 356

7.5 Author Index 360

S U R V E Y

O F E X P E R I M E N T S A T G S I

I N 1982

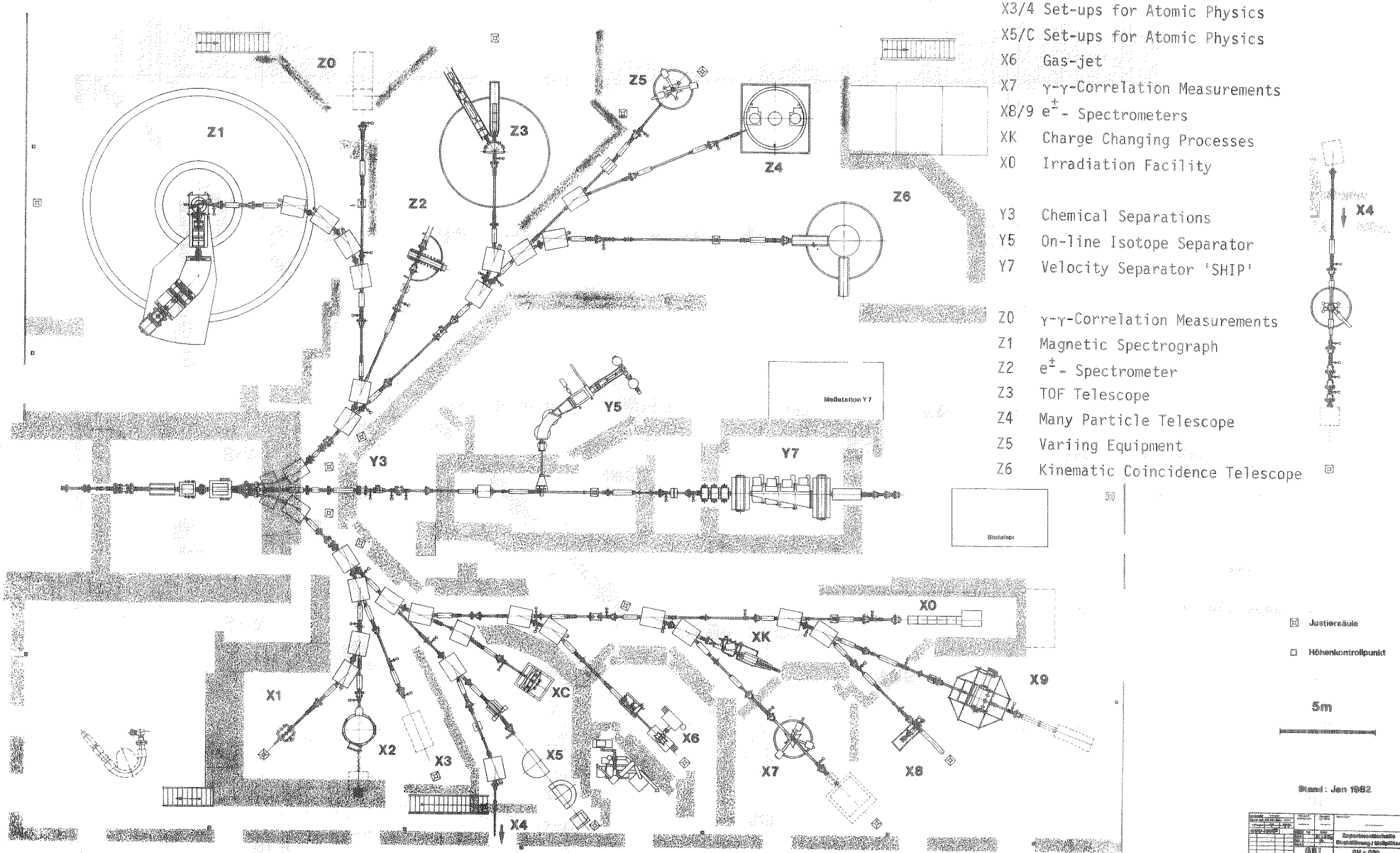
	Exp. Nr.	Authors	Affiliation	Title	Beam-time (d)	Ions	Corresp. Article on Page
Nuclear Physics/ Nuclear Chemistry	4	Gäggeler et al.	GSI,Univ.Mainz	Search for Superheavy Elements	1.7	^{238}U	69, 234
	74	Esterlund,Patzelt, Rajagopalan,Reus, Westmeier	Univ.Marburg	Systematics of Fusion and Deep-Inelastic Transfer in Various Heavy-Ion Systems	0.7	^{132}Xe	11
	101	de Boer,Trautmann, Lauterbach,Schandera, Puchta,Dünnweber, Hering, Graw	Univ.München	Positive and Negative Deflection Angles in Heavy Ion Collisions	2.8	^{86}Kr	20
	114	Arlt,Dittmar, Lohmüller,Kratz, Sapotta,Stelzer	GSI,Univ.Frankfurt	Neutron- and Gamma-emission in Fusion-reactions	2.2	^{86}Kr	5
	144	Becker,Lund,Brandt, Molzahn	Univ. Marburg	Search for Long-Lived Actinides and Superheavy Elements in the Reaction U + Th	1.2	^{208}Pb	-
	147	Kirchner,Klepper, Kurcewicz,Roeckl, Schardt,Grant,Zylicz, Tidemand-Petersson, Płochocki	GSI,Univ.Warsaw, Univ.Göttingen, Univ.Manchester	Studies of Proton and Alpha Emission in the Tin Region	1.2	^{58}Ni	60
	183	Theobald,Gobbi, Hollenbach,Mutterer, Pannicke,Weingärtner, Brülls	GSI,TH Darmstadt	Heavy-Ion Collisions Accompanied by Particles	2.2	^{208}Pb	18
	193	Stachel,Hill,Kaffrell, Emling,Grosse,Michel, Wollersheim,Schwalm	GSI,Univ.Mainz, Univ.Heidelberg	Multiple Coulomb Excitation of ^{104}Ru	1.9	^{104}Ru	47
	194	Lieb,Keinonen,Brüssermann,Wörmann,Emling, Stachel	Univ.Göttingen, GSI,Univ.Mainz	Coulomb Excitation of Krypton Isotopes	1.6	^{82}Kr	46
	201	Huber, Ulm,Klepper, Kühl, Marx	Univ. Mainz,GSI	Laser-Spectroscopy of Fusion Products	3.0	N, Ne	59

	Exp. Nr.	Authos	Affiliation	Title	Beam-time (d)	Ions	Corresp. Article on Page
Nuclear Physics/ Nuclear Chemistry	203	Sikkeland,Gäggeler, Brüchle,Kratz,Schädel, Sümmerer,Weber,Wirth	GSI,Univ.Mainz	Production of Cold Fermium Nuclei	1.0	Xe,Kr,Ti	7
	208	Clerc,Sahm,Vermeulen, Münzenberg,Schmidt	GSI,TH Darmstadt	Cold Fusion	2.1	Kr	4
	216	Beier,Friese,Henning, Kienle,Körner,Mayer, Wagner	TU München	Multi-Nucleon Transfer as a Function of Incident Energy	3.1	^{238}U, ^{208}Pb	16
	218	DeVito,Emling, Grosse,Kulessa, Schwalm,Simon, Briancon,Walen, Elze,Theobald, Moore,Trautmann, Sletten	GSI,Orsay,Univ. Frankfurt,TH Darmstadt,Univ. Mainz,Niels Bohr Inst. Risø	Bandcrossing in the Actinides	2.2	^{208}Pb	58
	221	Gebauer,Bohlen,Gamp, von Oertzen,Busch, Pühlhofer,Schüll	GSI,HMI Berlin, Univ.Marburg	Neutron Transfer between Tin Isotopes	3.0	^{120}Sn, ^{116}Sn	-
	231	Armbruster,Heßberger, Hofmann,Münzenberg, Poppensieker,Reisdorf, J.Schneider,W.Schneider, Schmidt,Sahm,Vermeulen	GSI,TH Darmstadt	Synthesis of Heavy Elements by Fusion	16.7	^{50}Ti, ^{54}Cr, ^{58}Fe	65, 66
	232	de Boer,Mittag,Simon, Zimmermann	GSI,LMU München	Coulomb Excitation of ^{226}Ra	3.4	^{208}Pb	57
	234	Kirchner,Klepper, Kurcewicz,Schardt, Gippert,Runte,Bernas, Schmidt-Ott,Kaffrell, Tidemand-Petersson, Peuser,Dessagne,Lange-vin, Rykaczewski	GSI,Univ.Mainz, Univ.Göttingen, IPN Orsay, Univ. Warsaw	Investigation of Neutron-rich Isotopes of Elements Mn to Cu at the GSI on-line Mass Separa-to	1.4	^{136}Xe, ^{76}Ge, ^{82}Se	62
	237	Batsch,Kirchner, Klepper,Kurcewicz, Roeckl,Schardt, Larsson,Nyman, Tidemand-Petersson	GSI,Chalmers Univ. Göteborg,Univ. Göttingen	Neutron-deficient Lanthanide-Isotopes	4.8	^{58}Ni,Ca	60

	Exp. Nr.	Authors	Affiliation	Title	Beam-time (d)	Ions	Corresp. Article on Page
Nuclear Physics/ Nuclear Chemistry	240	Rox,Esterlund, Patzelt	Univ. Marburg	Investigation of the Symmetric and Deep-Inelastic Components in the System U + Fe	0.3	^{238}U	12
	241	Schädel,Brüchle, Gäggeler,Kratz, Sümmerer,Wirth, Gehmecker,Trautmann	GSI,Univ.Mainz	Effects of the Entrance Channel on the Production of Heavy-Isotopes of Actinides in Damped Heavy-Ion Collisions	1.0	^{238}U	8
	244	Cline,Wu,Hasselgren, Bäcklin,Westerberg, Kavka,Czosnyka, Grosse,Kulessa,Michel, Stachel	Rochester,GSI, Uppsala,Swierk, Univ. Mainz	Shape Coexistence in ^{114}Cd and ^{116}Sn	2.1	^{208}Pb	48
	259	Schneider,Kohlmeyer, Keim,Lehr,Pühlhofer, Freiesleben	GSI,Univ.Marburg, Univ. Bochum	Fusion Reactions at Energies between 10 and 20 MeV/u	0.3	^{48}Ti, ^{84}Kr	-
	261	Dakowski,Gobbi, Gralla,Hildenbrand, Lynen,Müller,Olmi, Pelte,Petrovici,Töke, Rudolf,Stelzer,Wollersheim	GSI,MPI Heidelberg,Univ. Heidelberg,Swierk,CRNS	Fast Dissipative Collisions	5.6	^{86}Kr, ^{98}Mo, ^{238}U	21, 22
	262	Pühlhofer,Freiesleben, Schneider,Schüll	Univ.Marburg, Univ.Bochum,GSI	Nuclear Interaction in the System $^{238}U + ^{238}U$	0.2	^{238}U	14
	263	Emling,Grosse,Michel, Wollersheim,Schwalm Kulessa	GSI,Univ. Heidelberg,Univ.Krakau	Shape Transitions in Nuclei in the Light Rare Earth Region	4.3	$^{132,134}Xe$	50
	264	Wirth,Brüchle,Gäggeler, Kratz,Sümmerer,Lerch, Trautmann	GSI,Univ. Mainz	Sub-Coulomb-Transfer in the System $^{238}U + ^{238}U$	2.3	^{238}U	13
	270	Günther,Agarwal,Hardt, Stachel,Emling,Grosse, Wollersheim	Univ.Bonn,GSI, Univ. Mainz	Measurement of the Multiple Coulomb Excitation of $^{202}Hg + ^{204}Hg$	1.0	^{208}Pb	56

	Exp. Nr.	Authors	Affiliation	Title	Beam-time (d)	Ions	Corresp. Article on Page
Nuclear Physics/ Nuclear Chemistry	271	Wollersheim,Emling, Grosse,Michel,Schwalm, Stachel,Hill	GSI,Univ.Mainz, Univ. Heidelberg	Investigation of the Rotational Alignments by Measurement of B(E2)-values in ^{161}Dy and ^{163}Dy	2.7	^{208}Pb	53
	275	Hill,Kaffrell,Stachel, Emling,Grosse,Michel, Wollersheim,Schwalm	Univ.Mainz, GSI, Univ.Heidelberg	Investigation of the Phase Transition from Spheric to Deformed in ^{152}Gd by Coulomb Excitation with ^{208}Pb	1.9	^{208}Pb	49
	276	Armbruster,Heßberger, Hofmann,Münzenberg, Reisdorf,Schneider	GSI	Search for Further Proton Emitters in the Region of Neutron-deficient Isotopes of the Rare Earth Elements	1.2	^{40}Ca, ^{58}Ni	61
	282	Sohlbach,Schneider, Schüll,Freiesleben, Braun-Munzinger, Kohlmeyer,Marinescu, Pühlhofer	Univ.Bochum,GSI, Stony Brook, Univ.Marburg	Nucleon Transfer and Inelastic Excitations in the System ^{86}Kr + ^{208}Pb at Energies of 8 - 20 MeV/u	1.9	^{86}Kr, ^{208}Pb	24
	283	Bjørnholm,Dai,Gobbi, Hildenbrand,Olmi, Müller	GSI,Niels Bohr Institute Kopenhagen	Dynamic of Fusion	1.0	^{238}U	10
	289	Elze,Gerl,Happ, Keppler,Ower,Wollers-heim	GSI,Univ.Frankfurt	Investigation of the Cosmic Clock ^{176}Lu	0.6	^{208}Pb	54

	Exp. Nr.	Authors	Affiliation	Title	Beam-time (d)	Ions	Corresp. Article on Page
Atomic Physics	175	Balanda,Bokemeyer, Folger,Matsuki, Schwalm,Vincent, Bethge,Gruppe,Kessel, Schulê,Waldschmidt, Greenberg,Schweppe	GSI,Univ. Frankfurt,Univ. Yale	Study of Positron Creation in Superheavy Quasiatomic Systems	2.0	Pb, U	146
	187	Liesen,Schuch,Schmidt-Böcking,Schulê	GSI,Univ. Heidelberg,Univ. Frankfurt	Examination of Multiple Excitation of Inner Shells with X-ray X-ray Coincidences	3.6	Kr,Xe,U	152
	227	Frischkorn,Groeneveld, Latz,Elston,Sellin, Marrus, Gould	Univ.Frankfurt, Oak Ridge,Univ. Calif.Berkeley	Electron Production in High Velocity - Ion/Atom and - Ion/Solid Collisions	0.3	Ar,Ti,Ni	164
	230	Mokler,Schönfeldt, Meyerhof	GSI,Univ.Stanford	Multi-Step Process in Slowly Moving, Highly Ionized Atoms	2.3	Kr,Xe	153, 163
	247	Armbruster,Bosch, Clemente,Kienle,König, Kozhuharov,Martin, Tsertos, Wagner	GSI,TU München, MPI Heidelberg	Spectroscopy of High Energy δ-Electrons	0.7	^{208}Pb	-
	281	Bozek,Gollerthan, Kankeleit,Klotz, Krämer,Krieg,Meyer, Oeschler,Senger	TH Darmstadt	Spectroscopy of Positrons and Electrons after Heavy Ion Collisions	2.6	^{238}U	148
Solid State Physics/ Biology and Applied Heavy Ion Research	var.	Coordinator: Kraft	GSI	Biology	4.2	various	190-201
	var.	Coordinator: Spohr	GSI	Nuclear Tracks	1.4	various	203-212
	248	Albrecht, Armbruster, Roth, Spohr,Stuhrmann	GSI, ILL,DESY	Structure of Latent Nuclear Tracks	0.5	^{136}Xe	202



X1 Irradiation Experiments
X2 Scattering Chamber
X3/4 Set-ups for Atomic Physics
X5/C Set-ups for Atomic Physics
X6 Gas-jet
X7 γ-γ-Correlation Measurements
X8/9 $e^{\pm}$- Spectrometers
XK Charge Changing Processes
X0 Irradiation Facility

Y3 Chemical Separations
Y5 On-line Isotope Separator
Y7 Velocity Separator 'SHIP'

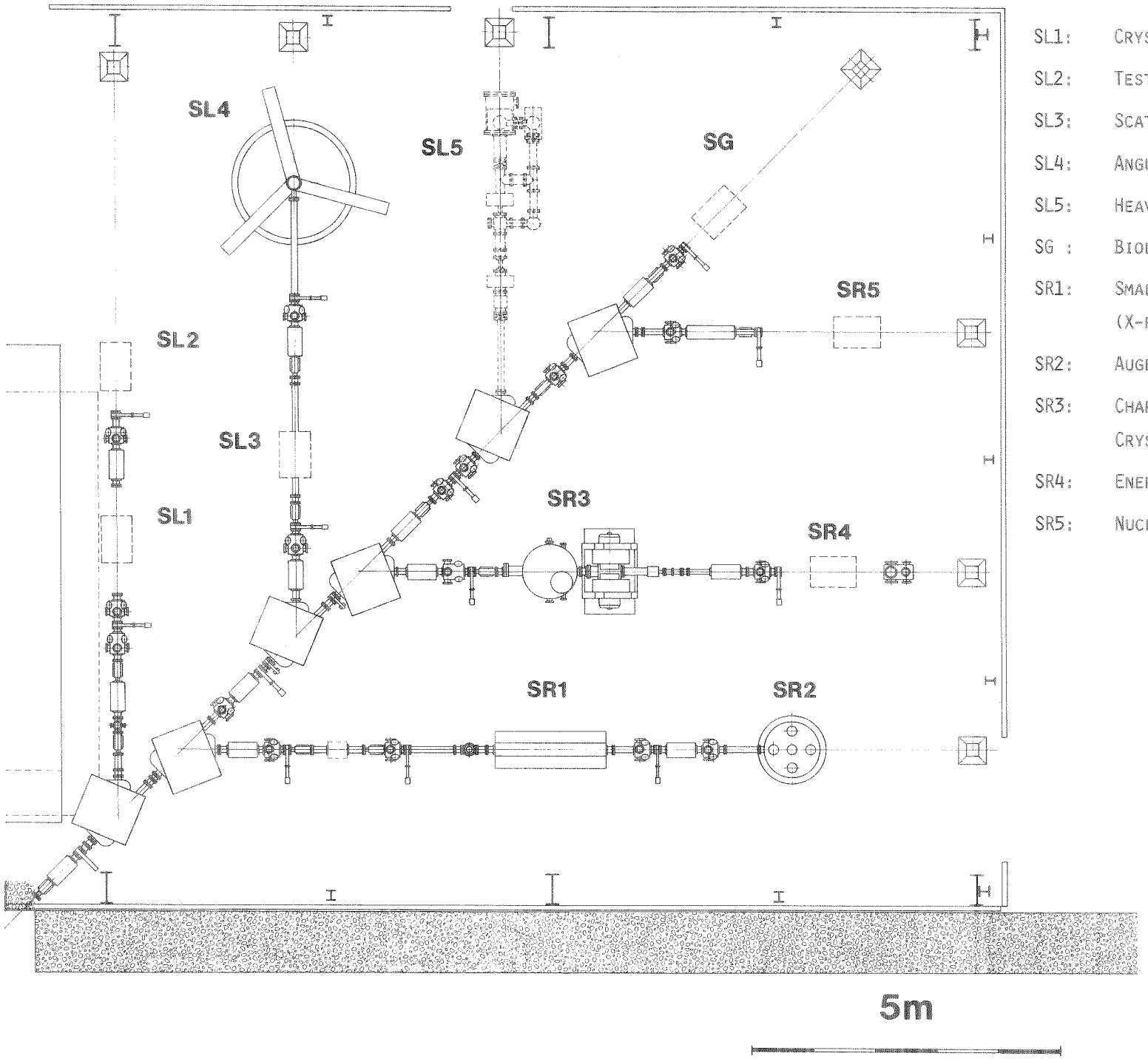
Z0 γ-γ-Correlation Measurements
Z1 Magnetic Spectrograph
Z2 $e^{\pm}$- Spectrometer
Z3 TOF Telescope
Z4 Many Particle Telescope
Z5 Variing Equipment
Z6 Kinematic Coincidence Telescope

Stand: Jan 1982

GSI
DARMSTADT

Experimentierhalle
Strahlführung / Beibehne
GH - 030

IIIXXX



SL1: CRYSTAL SPECTROMETER

SL2: TEST POSITION

SL3: SCATTERING CHAMBER

SL4: ANGULAR CORRELATION

SL5: HEAVY ION MICROPROBE

SG : BIOLOGICAL EXPERIMENTS

SR1: SMALL ANGLE SCATTERING (X-RAY PARTICLE COINCIDENCE)

SR2: AUGER SPECTROMETER

SR3: CHARGE CHANGING COLLISIONS, CRYSTAL SPECTROMETER

SR4: ENERGYLOSS EXPERIMENTS

SR5: NUCLEAR TRACK EXPERIMENTS

ΛΙΧΧΧ

1. Nuclear Physics/Nuclear Chemistry	PAGE
1.1 Nuclear Reactions	2
1.1.1 Reactions near the Coulomb-Barrier	2
1.1.2 Deep Inelastic Reactions	17
1.1.3 Nuclear Reactions at High Energies	28
1.2 Nuclear Structure	45
1.3 Exotic Nuclides	59
1.4 Theory	72
1.4.1 Nuclear Structure and Decay	72
1.4.2 Nuclear Reactions at Low Energies	84
1.4.3 Nuclear Reactions at High Energies	107

Influence of Collective Surface Motion on the Threshold Behaviour of Nuclear Fusion

W. Reisdorf, F.P. Heßberger, K.D. Hildenbrand, S. Hofmann, G. Münzenberg, J.H.R. Schneider,
W.F.W. Schneider, K. Sümmerer, G. Wirth
GSI Darmstadt
J.V. Kratz, K. Schlitt
Institut für Kernchemie, Universität Mainz

Recently measured [1] fusion excitation functions that extend from the μb level up to several 100 mb have been used to test a potential model for fusion that includes a **fluctuation** of the barrier with an amplitude that can be related to known collective nuclear properties.

Typical data, shown in Fig. 1, can be parametrized over the full energy range (full curves) by two parameters only: an average fusion barrier V_B and a standard fluctuation width $\sigma(V_B)$ of the barrier. Table 1 shows a list of parameter values found for a number of systems [1,2].

In the fitting procedure we use a nucleus-nucleus potential of the form $V(s) = V_n R_{12} \exp(-s/d)$ with $s=r-(R_1+R_2)$ and $R_{12} = R_1R_2/(R_1+R_2)$, d = 0.75 fm. The central radii are deduced from published RMS radii, V_n is adjusted to the data and determines the **average** fusion barrier. A Gaussian distribution of fusion barriers is generated by assuming, and adjusting, a Gaussian distribution $\sigma(R_1+R_2)$ (Col. 3 of Table 1) of the sum of radii and calculating the fusion excitation functions by a weighted superposition. Sub-barrier penetration was calculated by a WKB method. The barrier fluctuation can be interpreted as a "vibrational" fluctuation of the surface-to-surface distance originating from the collective vibrational motion of the surfaces[3]. It is then directly correlated to deformation lengths βR determined in inelastic scattering - such as (α,α') - experiments. By an incoherent addition of contributions from low-lying (< 3 MeV) octupole and quadrupole states in both projectile and target nuclei we can estimate the sum-of-radii fluctuation $\sigma_{ZP}(R_1+R_2)$ expected from zero-point surface motion. This is shown in Table 1 and is consistent in detail with the values deduced from the fusion data. The **orientational** part of the fluctuation (^{154}Sm) is not included in Table 1.

In the figure we illustrate for ^{40}Ar+^{122}Sn how the introduction of a barrier fluctuation phenomenon influences the general behaviour of the excitation function. If we first shut off the tunnelling process in the calculation, we obtain the left dotted curve which fails to describe the energy range marked "T" (for tunnelling) below the mb level, but describes well the range above it. If we also shut off the fluctuation (right dotted curve), we can still describe the data in the "classical" range marked "C". The amplitude of the barrier fluctuation is determined rather well from the intermediate range "F", once V_B (or equivalently, V_n) has been fixed by the data in range C. For ^{40}Ar+^{154}Sm we have also plotted a curve showing separately the effect of the "orientational" fluctuations, i.e. the known static deformation (dash-dotted curve). The dashed curves represent the conventional calculation without static deformation and vibrational fluctuation.

Table 1: Parameters deduced from fusion excitation functions[1,2].

System	V_B (MeV)	$\sigma(V_B)$ %	$\sigma(R_1+R_2)$ %	$\sigma_{zp}(R_1+R_2)$ %
^{40}Ar+^{112}Sn	109.1	4.0	4.7	4.85
^{40}Ar+^{116}Sn	108.3	3.9	4.6	4.95
^{40}Ar+^{122}Sn	107.2	3.9	4.5	4.85
^{40}Ar+^{144}Sm	130.2	3.4	3.9	4.4
^{40}Ar+^{148}Sm	129.4	4.3	4.9	5.0
^{40}Ar+^{154}Sm	129.3	3.75	4.2	3.8
^{16}O +^{148}Sm	60.25	2.9	3.6	4.5
^{16}O +^{154}Sm	59.9	2.2	2.8	2.3

[1] W. Reisdorf et al., Phys. Rev. Lett. 49, 1811 (1982)
[2] R.G. Stokstad et al., Phys. Rev. Lett. 47, 465 (1978)
[3] H. Esbensen, Nucl. Phys. 1352, 147 (1981).

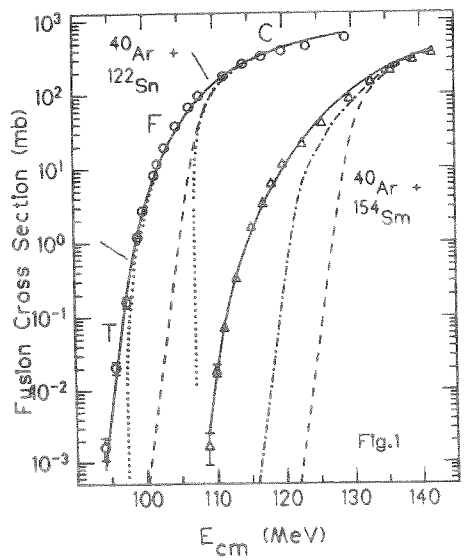


Fig.1

Evaporation Residue Cross Sections in the Fusion of ^{86}Kr with Ge, Mo, and Ru Isotopes

W. Reisdorf, F.P. Heßberger, K.D. Hildenbrand, S. Hofmann, G. Münzenberg, J.H.R. Schneider,
W.F.W. Schneider, K. Sümmerer, G. Wirth
GSI Darmstadt
J.V. Kratz, K. Schlitt
Institut für Kernchemie, Universität Mainz

The analysis of evaporation residue data obtained by combining activation methods with the use of the velocity filter SHIP[1] has been continued with special emphasis on ^{86}Kr induced fusion with ^{70,76}Ge, ^{92,100}Mo, and ^{99,102,104}Ru. On the low-energy side the data extend down to about 10 μb. Three features of the data are illustrated in Figs. 1 and 2.

1) The saturation of the evaporation residue cross sections at high angular momenta, presumably by fission, shows clear-cut isotopic trends. This is stressed by plotting the quantity $l_{max} = (\sigma_{ER}/\pi\lambda^2)^{1/2}$ vs. E_{cm}, where σ_{ER} is the evaporation residue cross section, λ the de Broglie wavelength and E_{cm} the center-of-mass energy (Fig. 1). Whereas the system ^{86}Kr+^{100}Mo → ^{186}Pt saturates at $l_{max} = 35\pm2$, the system ^{86}Kr+^{92}Mo → ^{178}Pt has $l_{max} = 21\pm1$. Similar trends were observed for the Ru targets (leading to Hg compound nuclei). We hope that the data will allow to determine isotopic trends in fissionability and provide long needed information on the stability of excited proton rich nuclei against fission.

2) From a comparison of the slopes of the excitation functions, cf. ^{100}Mo vs. ^{92}Mo in Fig. 1, it is again[1] apparent that the surface properties (^{92}Mo has a closed neutron shell) influence the variation of the fusion cross section below the average fusion barrier.

3) Some of the new data lead to the same compound nuclei as the ^{40}Ar induced fusion data obtained earlier[1]. This allows to study the entrance channel influence on the fusion process. In Fig. 2 we have plotted l_{max} vs. E_{cm} for ^{40}Ar+^{148}Sm and ^{86}Kr+^{102}Ru leading both to the compound nucleus ^{188}Hg. The ^{86}Kr+^{102}Ru data have been rescaled along the E_{cm} axis using the proximity scaling[2]. Whereas this leads to overlapping curves (not shown) for systems involving Er (Z=68) compound nuclei, this is not the case in Fig. 2 Notice that the saturating angular momenta agree approximately as expected from a compound picture. Two possible interpretations for the relative "hindrance" of the ^{86}Kr+^{102}Ru data will be further investigated in the future a) a failure of the proximity scaling b) a possible hindrance to fusion for heavier and symmetric systems. In terms of the barrier fluctuation introduced earlier[1] it could mean that for these systems the full fluctuation width of the zero-point surface- to-surface vibrations is no longer to be found in the fusion channel, but possibly in transfer channels.

[1] W. Reisdorf et al., Phys. Rev. Lett. 49, 1811 (1982)
[2] J. Blocki et al., Ann. Phys. (N.Y.) 105, 427 (1977)

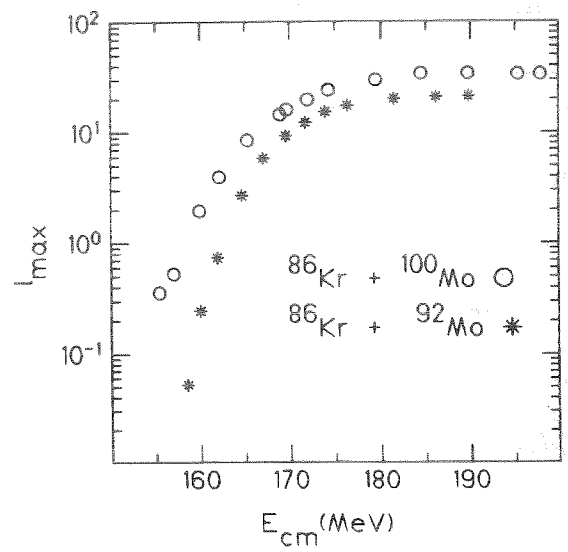


Fig. 1 Excitation functions for $l_{max} = (\sigma_{ER}/\pi\lambda^2)^{1/2}$

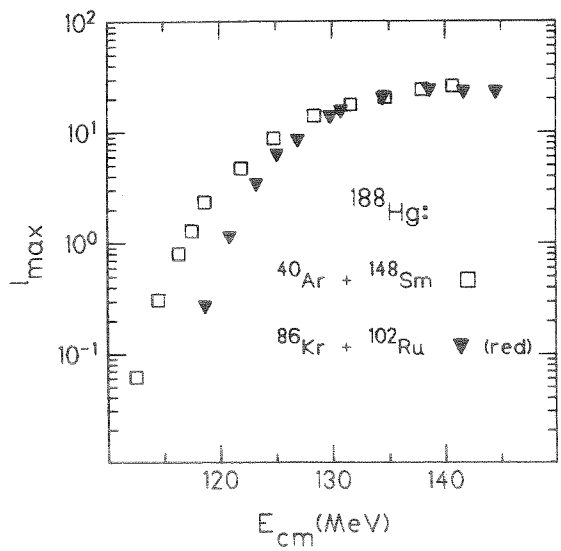


Fig. 2 Same as Fig. 1. The ^{86}Kr+^{102}Ru data have been rescaled along the E_{cm} axis using the proximity scaling.

Observation of the γ-deexcitation Channel in the Reaction $^{90}Zr+^{90}Zr \rightarrow {}^{180}Hg$

B

J.G. Keller*, H.-G. Clerc**, K.-H. Schmidt*, Y.K. Agarwal*, F.P. Heßberger*, R. Hingmann**,
G. Münzenberg*, W. Reisdorf*, C.C. Sahm**
*GSI Darmstadt
**Institut für Kernphysik, TH Darmstadt

In the synthesis of heavy elements by fusion reactions it is important to produce the compound nucleus with an excitation energy as low as possible in order to reduce the fission competition in the deexcitation process. One recipe to achieve low excitation energies in compound nuclei was used by the Dubna group in the production of heavy nuclei: a high binding energy of the reaction partners tends to decrease the Q-value of the reaction. They used targets around the doubly magic nucleus ^{208}Pb, and its shell correction reduces the excitation energy of the compound nucleus by about 13 MeV.

Another way to decrease the Q-value of the fusion reaction of heavy partners is the use of a symmetric projectile - target combination. Just as the fission in symmetric fragments is energetically favoured by liquid drop considerations, the fusion barrier, with respect to the ground state of the compound nucleus, is lowest for a symmetric projectile - target combination.

A further cooling of the compound nucleus may be achieved by fusion below the barrier due to barrier fluctuations[1]. If the system becomes too heavy, however, the extra push concept of Swiatecki[2] predicts that the fusion is severely hindered for systems with roughly $Z_1 \cdot Z_2 > 2000$.

We combined the recipes mentioned above by using the reaction $^{90}Zr+^{90}Zr \rightarrow {}^{180}Hg$. Its calculated Coulomb barrier[3] is expected at 4.15 MeV/u. The system is exactly symmetric and two partners are magic (shell energy about 3 MeV each). This combination is distinctly below the limit where an extra push is expected. Furthermore, the fission barrier of the compound nucleus is about 10 MeV; thus the fission competition - at least for low angular momentum - does not strongly reduce the production cross section for evaporation residues.

The evaporation residues were separated by the velocity filter SHIP and detected by a time-of-flight set-up with a position sensitive double grid avalanche counter [4] and a surface barrier detector in which the reaction products were implanted. The different deexcitation channels were identified by their subsequent α-decay.

Special care was taken to avoid contaminations from neighbouring isotopes in the beam as well as in the targets. The mass spectrum of the beam from the ion source was monitored periodically to ensure a pure ^{90}Zr beam. The targets were especially prepared at the mass separator of the Lab. René Bernas in Orsay. The energy distribution of the UNILAC beam was measured during the whole experiment with a time-of-flight method by use of the beam microstructure and a flight path of about 50 m.

Fig. 1 shows an α-spectrum of the reaction $^{90}Zr+^{90}Zr \rightarrow {}^{180}Hg$ at 3.9 MeV/u. At this energy the excitation energy amounts to (17±2) MeV. The line of ^{180}Hg at 6.12 MeV can only be explained by the deexcitation of the excited compound nucleus exclusively by γ-radiation. The cross section of this channel which is observed here for the first time in a heavy ion fusion reaction with $A_{CN} > 40$, is in the microbarn region.

[1] W. Reisdorf et al., GSI 82-38
[2] J. Swiatecki, Nucl. Phys. A376 (1981) 275-291
[3] R. Bass, Lecture Notes in Physics, Vol. C117, p. 281, Heidelberg 1979
[4] J.G. Keller et al., this report, p. ..

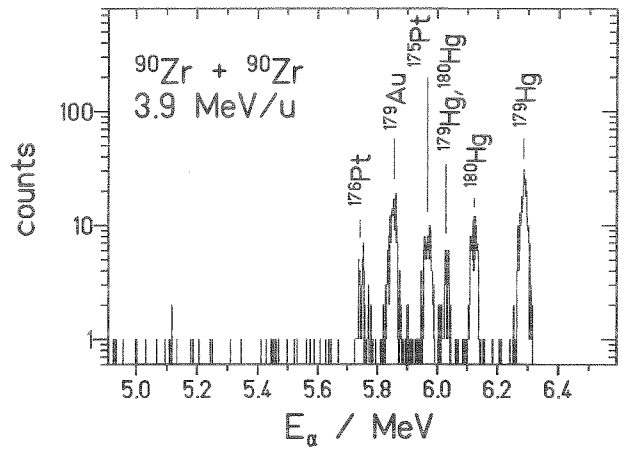


Fig. 1: α-spectrum of evaporation residues produced in the reaction $^{90}Zr+^{90}Zr \rightarrow {}^{180}Hg$ (E* = 17 MeV). A considerable fraction of the fusion cross section leads to the "γ-channel".

Statistical model analysis of neutron emission in fusion reactions of ^{86}Kr with ^{64}Ni and ^{76}Ge [B]

U. Arlt, R. Bass+, H. Dittmar, T. Kratz, B. Lohmüller, K. Sapotta, K. Stelzer
Institut für Kernphysik der J.W. Goethe-Universität Frankfurt a. Main

The analysis of the fusion reactions $^{86}Kr + ^{64}Ni$ and $^{86}Kr + ^{76}Ge$ at 3.8 MeV/u was continued. The aim of this project is to study the decay of the compound nuclei at high angular momentum and high excitation energy by the measurement of neutrons and gamma-rays. The compound nuclei ^{150}Gd and ^{162}Er were formed with an excitation energy E_{ex} = 65 MeV and maximum angular momenta of 70 ħ. The set-up of the multidetector experiment and results of the analysis of the gamma-ray data concerning the distribution of evaporation residues have been reported earlier.[1]

The angular distributions of the neutrons show significant anisotropies in the C.M.system, which can be fitted by $dN/d\Theta = 1+A_2P_2(\cos\Theta)$. The anisotropy parameter A_2 increases with neutron energy.

Theoretical angular distributions were calculated with the semi-classical statistical model of Ericson and Strutinsky.[2] In this model the anisotropy parameter A_2 explicitly depends on the mean squares of the compound nucleus and the neutron angular momenta and on the moment of inertia of the compound nucleus.

The effective angular momentum region in the compound nucleus could be influenced experimentally by neutron- or gamma-coincidence with a NE213-"multiplicity filter"[1], because the neutron- und gamma-multiplicities depend on the angular momentum of the compound nucleus.
Fig. 1 shows the experimental anisotropy parameter A_2 versus neutron energy. The straight line represents the calculated values. Experimental and theoretical values for the dependence of the anisotropy on the mean angular momentum of the compound nucleus are given in tab. 1.

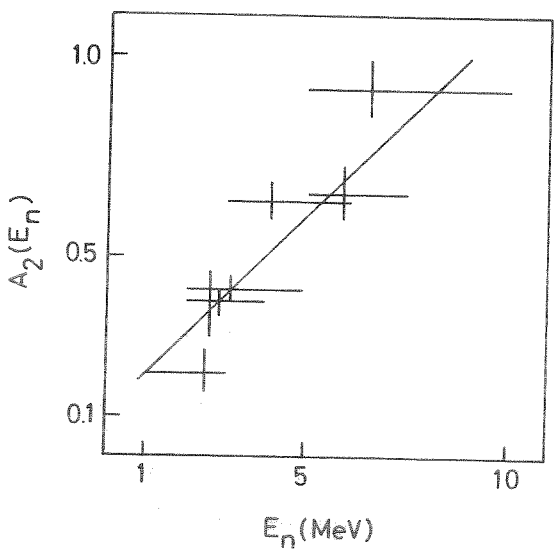


Fig. 1: Energy dependence of the anisotropy parameter $A_2(En)$

measuring modes	angular momentum of comp. nucleus $\langle J(J+1)\rangle$	$\langle J \rangle$	anisotropy parameter A_2 calc.	A_2 exp.
SINGLES	2520	47.3	0.39	0.35 ± 0.03
γ-COINC.	3025	51.8	0.50	0.46 ± 0.05
n-COINC.	2150	43.7	0.34	0.33 ± 0.08

Tab. 1: Dependence of the anisotropy parameter on the angular momentum of the Compound nucleus

The data show that the observed neutron angular distributions can be reproduced by the statistical model including angular momentum coupling, both in their dependence on neutron energy and compound nucleus angular momentum.

The energy dependence of the angular distribution has consequences for the determination of the evaporation temperature. If this effect is not included in the analysis different temperatures (1.4 to 2.1 MeV) are obtained for the different angles of observation. Inclusion of the energy dependence of the angular distribution leads to a common mean temperature of 1.7 MeV for all angles.

The results of the experiments had to be corrected for background neutron contributions from target contaminations with light nuclei. To improve the results, a new experiment for the system $^{86}Kr + ^{64}Ni$ was performed in Dec. 82 with a target essentially free from contamination. In addition neutron energy spectra were measured with two large NE213-detectors (4,5"x2") in coincidence with two Ge(Li)-detectors to determine separate neutron spectra for the different xn-channels and therefore get more specific information on the level densities as a function of angular momentum. The analysis of this experiment is in progress.

[1] U. Arlt et al., GSI Scientific Report 1980, p. 13
U. Arlt et al., GSI Scientific Report 1981, p. 9

[2] T. Ericson, V. Strutinsky, Nucl. Phys. 8 (1958) 284

+ deceased Oct. 2, 1981

Fusion Cross Sections in ^{40}Ar and ^{50}Ti Induced Heavy Ion Reactions [B]

H.-G. Clerc, J.G. Keller*, C.-C. Sahm, K.-H. Schmidt*, H. Schulte**, D. Vermeulen

Institut für Kernphysik der TH Darmstadt, *GSI Darmstadt, **Institut für Kernchemie der Universität Marburg

Cross sections for the symmetric fragmentation in a number of ^{40}Ar and ^{50}Ti induced reactions were determined by using two surface barrier detectors placed at 32° and 58° with respect to the beam axis. The fragment masses were determined by measuring, in addition to the energy, the TOF for the 30 cm flight path from the target to the detector by use of the microstructure of the UNILAC beam. Some preliminary ^{40}Ar-induced fission data were presented previously [1]. Cross sections for compound residues from neutron evaporation were determined by using the velocity filter SHIP. The results are shown in Fig. 1.

The fission cross sections are compared with the fusion cross sections as predicted by the classical formula $\sigma = \pi r_c^2 \frac{1}{E}(E-E_B)$, with parameters from [4]. For the ^{50}Ti-induced reactions, the fission cross sections fall clearly below the classical prediction, in agreement with the results of [4]. However, there is a tendency also for the ^{40}Ar-induced fission cross sections to be smaller than the predicted fusion cross sections. This may indicate a deviation from the classical fusion model for already much lighter systems than considered in the extra-push model [6]. Close to the barrier, the experimental fission cross section is larger than the classical prediction, as is expected from barrier transmission and fluctuation phenomena [7].

For the ^{40}Ar-fission data, a conventional σ vs 1/E analysis in the range 150 mb $\leq \sigma \leq$ 550 mb gives fusion barriers which can be described to a very good approximation by the prescription $E_B = 0{,}96\ E_{\text{proximity barrier}}$ [5].

In all cases shown in Fig. 1 (including ^{50}Ti + ^{208}Pb, ^{209}Bi), the peak in the compound residue cross section, which under certain assumptions can be shown to approximately coincide with the barrier for compound residue production, appears to be very close to the energy given by this prescription. Thus it seems that for the systems considered there (for which the compound residue cross sections span a range of seven orders of magnitude!) the peak of the compound residue section is not shifted to higher energies, even in cases where the fission cross section exhibits an extra-push.

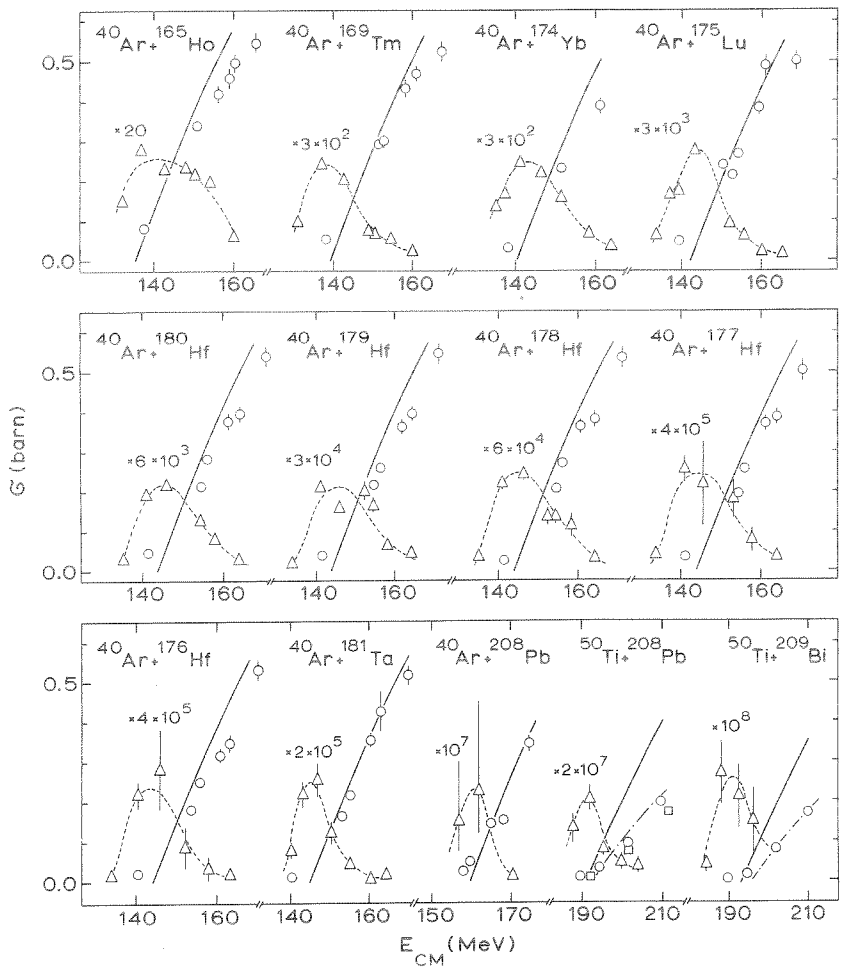


Fig. 1: Fission cross sections and compound residue cross sections versus kinetic energy.
triangles and dashed lines: Measured compound residue cross sections summed over all neutron evaporation channels. Compound residue cross sections for ^{40}Ar + ^{208}Pb from [2], for ^{50}Ti + ^{208}Pb, ^{209}Bi from [3], for all other systems: this work
circles: Measured fission cross sections (this work)
squares: Measured fission cross sections from [4]
solid lines: Standard prediction [4] for the fusion cross section with barrier penetration neglected:
$\sigma = \pi r_c^2 \frac{1}{E}(E-E_B)$, with $E_B = 0.96\ E_{\text{proximity barrier}}$ [5]
$r_c = C_p + C_r + 1.4$ fm, $C = R - \frac{1\text{fm}^2}{R}$,
$R = 1.28\ A^{1/3} - 0.76 + 0.8A^{-1/3}$fm.
dot-dashed lines: Fusion cross section as calculated with the extra-push model [6].

1. H.Schulte et.al.,GSI Scientific Report 1979 (GSI 80-3)
2. G.Münzenberg et.al.,Z.Physik A 302 (1981) 7
3. G.Münzenberg et.al.Proc.Actinide 1981 Conf.,Pacific Grove, Pergamon Press 1982,p.223,and private communication
4. R.Bock et.al., Nucl.Phys.A 388 (1982) 334
5. J.Blocki et.al.,Ann.of Physics 105 (1977) 427
6. W.J.Swiatecki, Physica Scripta 24 (1981) 113
7. W.Reisdorf et.al., Phys. Rev. Letters 49 (1982) 1811

Capture-Fission in the Reaction $^{76}Ge + ^{170}Er$

K.Lützenkirchen and J.V.Kratz, Institut für Kernchemie, Universität Mainz

W.Brüchle, H.Gäggeler, K.Sümmerer and G.Wirth, GSI Darmstadt

Various attempts have recently been made to investigate the dynamical limitations of the fusion of heavy nuclei. A particular class of experiments was the production of ^{246}Fm compound nuclei /1/ through a variety of entrance channels, one of which was $^{76}Ge + ^{170}Er$.

The fusion cross section σ_f was usually determined by measuring the spontaneous fission decay of the (HI,2n) ^{244}Fm evaporation residues. In the case considered here, we found the fusion process to be considerably hindered. To check this result, we decided to measure the fission cross section of the hypothetical compound nucleus $^{246}Fm^*$.

The respective irradiation was performed at the UNILAC accelerator, using a ^{76}Ge-beam (E=5.18 MeV/A), a thick ^{170}Er-target (5.06 mg/cm²) and a total of 3.4×10^{15} incident particles. The products were caught in an aluminum foil stack. Cross sections for individual isotopes were determined via their characteristic γ-ray transitions.

Fig.1 depicts the cross sections σ_c for symmetric fragmentation of one of the catcher foils. A gaussian distribution with FWHM=5.0 amu is well suited to represent the data. The experimentally deduced maxima of the distribution $\langle A \rangle_Z$ for given Z are in accord with calculations based upon minimizing the potential energy and correcting for neutron evaporation. Considering the Z-dependence of $\langle A \rangle_Z$ we were able to construct the mass distribution for each catcher foil and the total element distribution (Fig.2).

Although an excitation energy range of 35 MeV through 65 MeV was covered, we obtained a double humped distribution of fission products. The peak-to-valley ratio turns out to be 2:1 and the average charge asymmetry is about 1:1.3. These facts indicate that the starting point for fission might have been the compound nucleus $^{246}Fm^*$. Nevertheless, processes leading to complete mass equilibration via non-compound reactions (fast-fission) cannot be excluded with certainty.

The thick target cross section deduced from fig.2 is $\sigma_c = 94^{+44}_{-33}$ mb. This result is suitably explained within Swiatecki's Extra-Push model /2/, when we assume an extra-push of $E_x = 10 \pm 5$ MeV over the static fusion barrier B ($B = 0.96 \times B_{prox} = 227.1$ MeV).

Within error limits this value is in agreement with the one deduced from the evaporation residue measurement, which was $E_x = 12^{+\infty}_{-5}$ MeV.

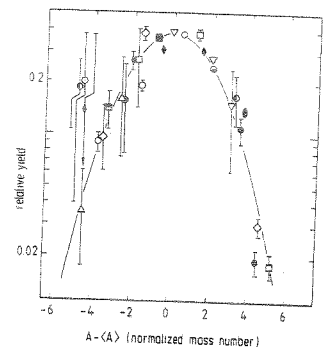


Fig.1. Yields corrected for precursor decay at constant Z versus mass number A normalized with respect to the centroid $\langle A \rangle_Z$ and the element yield P(Z) of each isotope disribution.

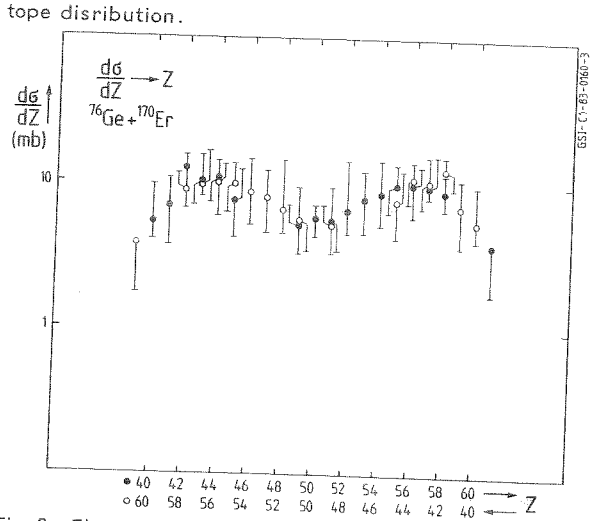


Fig.2. Element distribution for symmetric fragmentation (•) and distribution reflected at Z=50 (○). Cross sections for the elements Z=39,46,47,48,59,60, for which only lower limits exist, are not shown. An estimated portion of the cross section contributed by the deep-inelastic products was subtracted from Z=40-43,61.

/1/ H.Gäggeler et al., Proc.Int. Workshop on Gross Properties of Nuclei and Nuclear Excitations X, Hirschegg 1982,40 (1982)

/2/ W.J.Swiatecki, Nucl.Phys. A376 (1982) 275

An Estimate of the Cross-section for symmetric Fragmentation in the Reaction $^{58}Fe + ^{209}Bi \Longrightarrow ^{267}109$

K.Lützenkirchen and J.V.Kratz, Institut für Kernchemie, Universität Mainz

W.Brüchle, H.Gäggeler, K.Sümmerer and G.Wirth, GSI Darmstadt

During the $^{58}Fe + ^{209}Bi$-experiment, performed at the velocity filter SHIP /1/, we installed an aluminum foil behind the target, suited to catch the fission products. The catcher-foil arrangement covered the angle $\Delta\Omega$=1.6±0.2 sr and allowed the evaporation residues to pass through a hole around 0°. At the two laboratory energies 4.95 MeV/A and 5.15 MeV/A 2×10^{17} and 3×10^{17} particles were accumulated on the target, respectively. An iodine fraction was chemically separated from the rest of the products and was subjected to γ-ray measurements.

Iodine (Z=53) represents the products emerging from symmetric fragmentation. At 4.95 MeV/A we could not detect any iodine isotopes (cross-section limit ≤ 0.3 μb), whereas at 5.15 MeV/A we identified the isotopes ^{123}I, ^{124}I, ^{126}I and ^{130}I (Fig.1). Integration over the resulting gaussian distribution, followed by a second integration over the total Z-distribution, had us arrive at a cross-section for symmetric fragmentation of σ=3.1±1.3 mb at 5.15 MeV/A. The Z-distribution was assumed to be gaussian also with an estimated FWHM of 21 Z-units./2/

For 4.95 MeV/A we obtained an upper limit for the cross-section of $\sigma \leq 0.3^{+0.7}_{-0.2}$ mb. The magnitude of both cross-sections gives good reason to suspect that both energies were close to or below the fusion barrier. Using the equation

$$\sigma_f = (\hbar\omega r_f^2/2E)\times\ln(1+\exp(2\pi(E-B)/\hbar\omega)),$$

which represents the fusion cross-section below the barrier, and the parameters r_f=12.3 fm, $\hbar\omega = 8^{+12}_{-5}$ MeV, E=233.8 MeV, one deducts a barrier of B = 236.5^{+7}_{-2} MeV.

This result implies an extra-push of 11.7^{+7}_{-2} MeV ($0.96\times B_{prox}$ = 224.8 MeV), a value which is consistent with other results concerning the dynamical limitations of the fusion process. (Fig.2 at $x_{eff} \approx 0.8$)

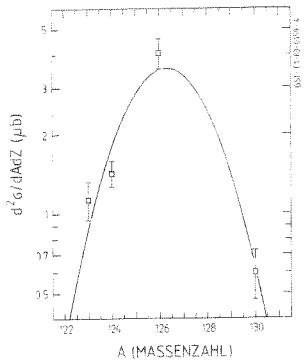


Fig.1. Mass distribution of the iodine isotopes from symmetric fragmentation in the reaction $^{58}Fe + ^{209}Bi$. FWHM equals 4.7, the most probable mass number is $\langle A\rangle_Z$=126.

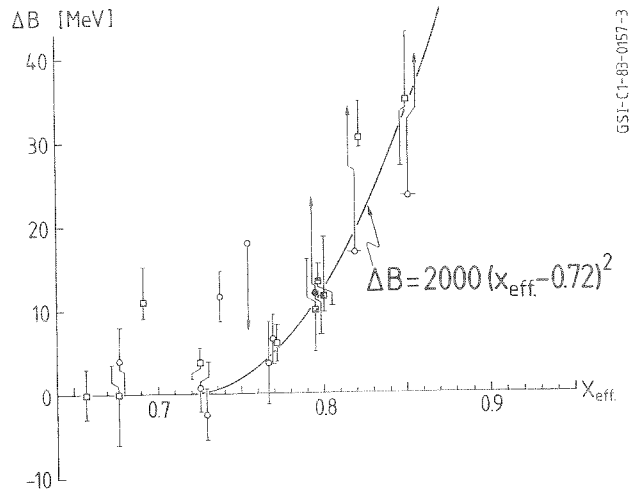


Fig.2. Differences between experimental and calculated fusion barriers ($0.96\times B_{prox}$) as a function of x_{eff} /3,4,5,6/.
$^{58}Fe + ^{209}Bi$, $^{58}Fe + ^{208}Pb$, $^{76}Ge + ^{170}Er$ (sym. fragmentation), $^{76}Ge + ^{170}Er$ (evaporation residues).

/1/ G.Münzenberg et al., Z.Physik A,309,89 (1982)

/2/ C.-C.Sahm et al., Z.Physik A,297,241 (1980)

/3/ H.Gäggeler et al., Proc.Int. Workshop on Gross Properties of Nuclei and Nuclear Excitations X, Hirschegg 1982,40 (1982)

/4/ K.-H.Schmidt et al., Z.Physik,A301,21 (1981)

/5/ G.Münzenberg et al., Z.Physik,A302,7 (1981)

/6/ R.Bock et al., Nucl.Phys.A388,334 (1982)

On the Mass Drift in Fast Fission

A. Gobbi, Dai Guang-Xi[+], S. Gralla, K.D. Hildenbrand, J. Kuźminski[++], A. Olmi, W.F.J. Müller and J. Tõke[+++]
GSI Darmstadt

The reaction $^{56}Fe + ^{208}Pb$, which leads to captured metastable dinuclear configurations, was studied at 6.07 MeV/u; the mass distribution of the light fragments was measured as a function of energy loss and scattering angle. Fig. 1 shows a contour diagram of the dependence of the cross section on element number Z and total kinetic energy TKE^* (energy corrected for Coulomb distortion effects). The products observed at large energy-losses experience a large mass flow from the heavy Pb- to the light Fe-nucleus. A strong net mass transfer in the opposite direction, from the light to the heavy nucleus is not observed. We have investigated to what extent this observation can be ascribed to the increase of the barrier (conditional saddle) height for larger asymmetries, where it inhibits the reseparation of the captured system. For this purpose we have performed potential energy surface calculations as a function of asymmetry η, fragment deformation ε and angular momentum ℓ_{rel}, using the folding potential prescription[1]. In particular we have investigated the limiting conditions for the vanishing of the barrier $B(\eta, \varepsilon, \ell_{rel})=0$. The predictions of such a calculation concerning the ability of the dinuclear system to reseparate (vanishing barrier for large angular momenta and deformations or small asymmetries) have been confronted with the measured cross sections of Fig. 1. We associate the asymmetry η with the measured charge Z; in order to associate average relative angular momenta and deformations at the conditional saddle $\langle\ell_{sa}\rangle$ resp. $\langle\varepsilon_{sa}\rangle$, with the measured total kinetic energy, we have derived the correlation functions ($\langle TKE^*\rangle$ vs. $\langle\ell_{sa}\rangle$) and ($\langle TKE^*\rangle$ vs. $\langle\varepsilon_{sa}\rangle$). The initial angular momenta are deduced from a sharp cut-off integration of the cross section along the TKE^* coordinate; the angular momentum dissipation is calculated according to the diffusion model[2] (Fig. 2). The average deformations $\langle\varepsilon_{sa}\rangle$ are derived from the Coulomb energy of two deformed spheroids (Fig. 3). According to these estimates of η, $\langle\ell_{sa}\rangle$ and $\langle\varepsilon_{sa}\rangle$ we find in Fig. 1 three regions of vanishing barrier: (A) at high TKE^*, mainly because of large angular momenta, (B) at low TKE^*, mainly due to strong deformations and (C) at intermediate TKE^*, because of the joint contribution from moderate deformations and angular momenta. There remains therefore in Fig. 1, at large asymmetry and small TKE^*-values, a region (non-shaded area) where, because of the non vanishing barrier, the captured dinuclear system can not reseparate. This is indeed the region of strongly reduced cross section. We therefore conclude that the observed mass drift, measured as a function of TKE^*, does not necessarily imply the presence of a driving force at large kinetic energy-losses. On the contrary it might well be possible that no drift in the mean mass asymmetry occurs during the interaction and that the final asymmetric distributions reflect only barrier inhibition effects.

[+] A.v.Humboldt-Fellow, IMP, Lanzhou, P. R. of China
[++] on leave from Silesian University, Katowice, Poland
[+++] on leave from Warsaw University, Poland

[1] R. Nix and P. Möller, Nucl.Phys. A281(1977)354.
[2] G. Wolschin and W. Nörenberg, Phys.Rev.Lett.41(1978)691

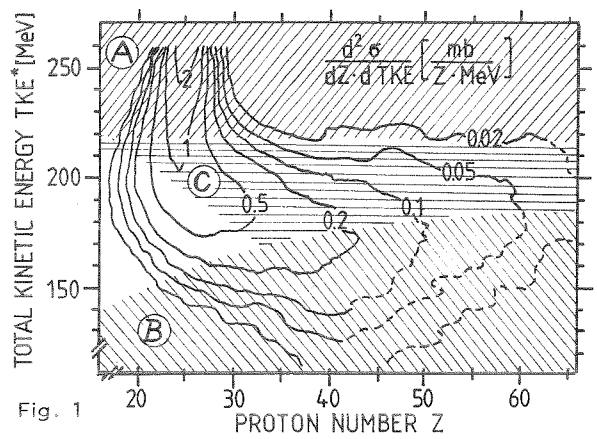


Fig. 1

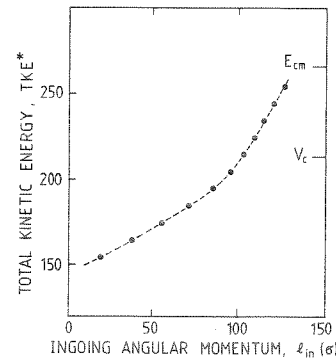


Fig. 2

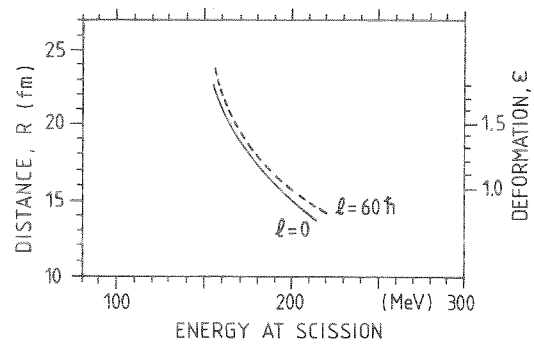


Fig. 3

Studies of fusion dynamics in ^{238}U - induced reactions

J. Tõke[+], R. Bock, Dai Guang-xi[++], A. Gobbi, S. Gralla, K.D. Hildenbrand,
J. Kuźminski[+++], A. Olmi, W.F.J. Müller
GSI Darmstadt
S. Bjørnholm
NBI Copenhagen, Denmark

Earlier systematic studies with Pb-projectiles have been extended by U-reactions induced at 5.5 and 6.0 MeV/u on targets of ^{27}Al, ^{48}Ca, ^{45}Sc, ^{48}Ti, ^{58}Fe and ^{89}Y. The aim is to study the formation and decay of heavier composite systems starting with larger initial asymmetries. The amalgamating dinuclear complex is expected to be rather unstable and to decay with a broad distribution of fragment masses. The collision dynamics is expected to be reflected in the measured angle, energy loss and product mass correlations. The ring counter geometry used in similar previous experiments has been replaced by a device of improved acceptance, selectivity and resolution[1]. The new set-up allows to reach extreme forward and backward scattering angles in the center-of-mass system and to eliminate the three-body background. Figs. 1 to 4 show preliminary results obtained for targets of ^{27}Al and ^{48}Ti at an incident energy of 6.0 MeV/u. The first two figures represent the energy- and angle-integrated yields as a function of the product mass; a drastic difference between the heavier and the lighter target is observed. Figs. 3 and 4 display the detailed dependence of the measured cross section on mass and scattering angle. Again the two systems show striking differences: Whereas in the ^{238}U + ^{27}Al system a clear forward-backward symmetry of the yield persists for a large range of masses centered around the symmetric fragmentation, the mass and angle correlations in the ^{238}U + ^{48}Ti case point to a remembrance of the initial asymmetry.

Comparisons with our previous measurements and with the theoretical predictions are in progress.

[+]on leave from Warsaw University, Poland

[++]A.v.Humboldt-Fellow, IMP, Lanzhou, P. R. of China

[+++]on leave from Silesian University, Katowice, Poland

[1]Dai Guang-xi et al., Contr. to this Annual Report

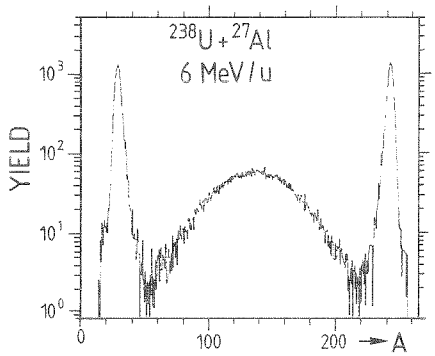


Fig. 1

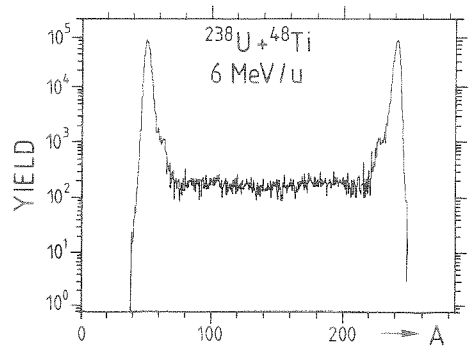


Fig. 2

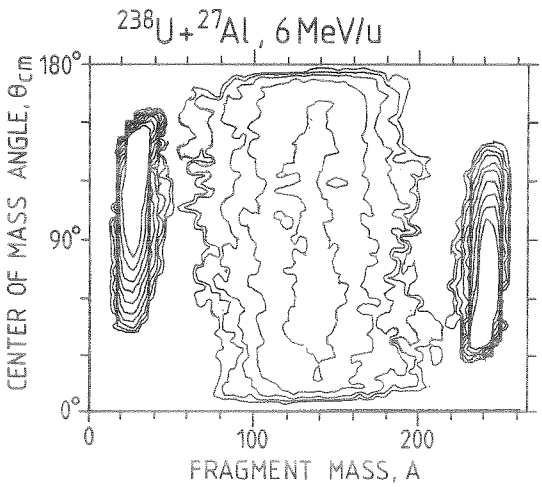


Fig. 3

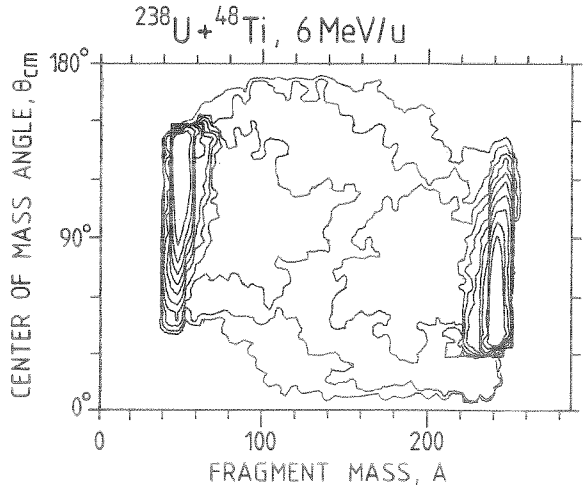


Fig. 4

B

Radiochemical Measurements of Quasielastic, Deep-inelastic and Fusion Yields in the System $^{132}Xe + ^{nat}Fe$

R.A. Esterlund, W. Westmeier, A. Rox, U. Reus, H. Schulte and P. Patzelt
Institut für Kernchemie, Universität Marburg

Thick-target quasielastic yields for this system plotted as a function of the effective energy in the thick target are shown in Fig. 1. A generalized Fresnel model[1] predicts that, for energies sufficiently above the reaction barrier, the ratio of the quasielastic to the total reaction cross section should be constant with bombarding energy and have a value in the range 0.15 - 0.20. The agreement of the line 0.18 x σ_{GEOM} in the figure is good, supporting our method[2] of resolving quasielastic from deep-inelastic yields. Fig. 2 displays experimental deep-inelastic yields in a similar manner. The line in the figure corresponds to the remainder of the geometric cross section after quasielastic (0.18 x σ_{GEOM}) and *theoretical* Capture model[3] fusion cross sections are subtracted. The relatively good agreement of this line with the data indicates the consistency of our analysis and resolution of the corresponding mass-yield curves.

According to Capture model[3] predictions, systems with similar effective fissilities $z(\ell)$ are expected to be dynamically equivalent[4]. Hence, the systems $^{132}Xe + ^{nat}Fe$ (z_e = 32.3) and $^{208}Pb + ^{48}Ca$ (z_e = 31.9) should exhibit similar amounts of extra push in their fusion excitation functions. This can be checked most conveniently via the construction of a rectilinear cross-section

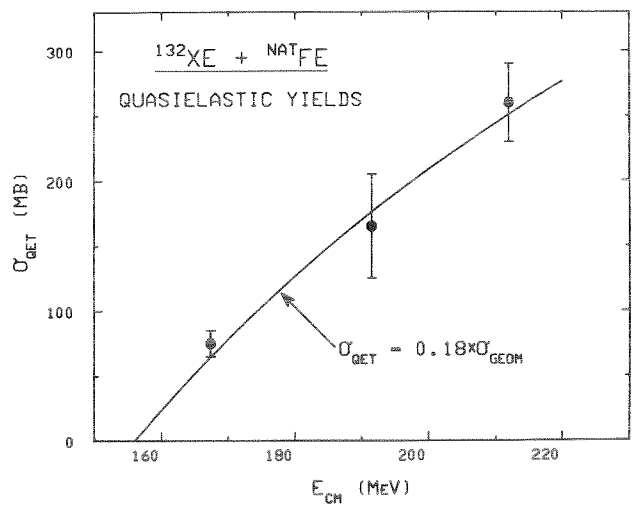


Fig. 1: Excitation function for quasielastic processes.

plot[3], using the measured[4,5] fusion cross sections as a function of energy for the above systems. Such a plot is shown in Fig. 3 with $Y(E,\sigma) = E\sigma/\pi R_c^2$ and $X(E,\sigma) = \sqrt{(E-B-E\sigma/\pi R_c^2)}$, where B is the reaction barrier and R_c is the contact radius. With the exception of B and R_c, such a plot is based on experimental data only, and is hence *model-independent*. It can be shown[3] that $Y(E,\sigma)$ is the orbital energy at contact and that $X(E,\sigma)$ is the square root of the extra push energy. Thus, if two systems exhibit equivalent amounts of extra push with increasing orbital energy, their fusion data points should lie on a common line in such a plot. With the possible exception of the point in brackets <>, corresponding to an experiment which has been only partially evaluated, the agreement of the two systems is good, showing that they are indeed dynamically equivalent.

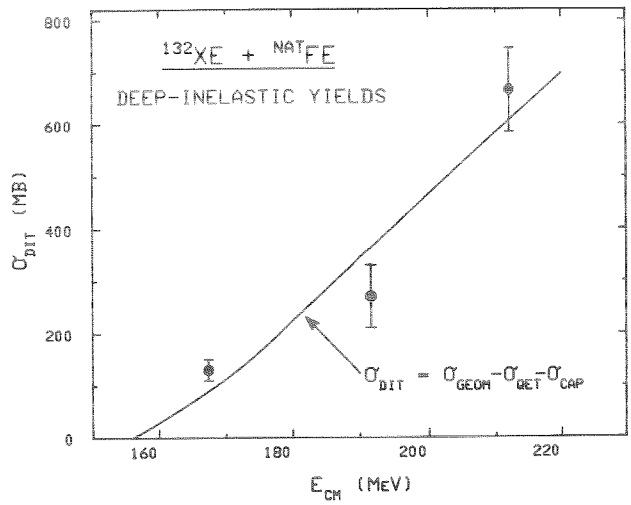


Fig. 2: Same as Fig. 1 for deep-inelastic processes.

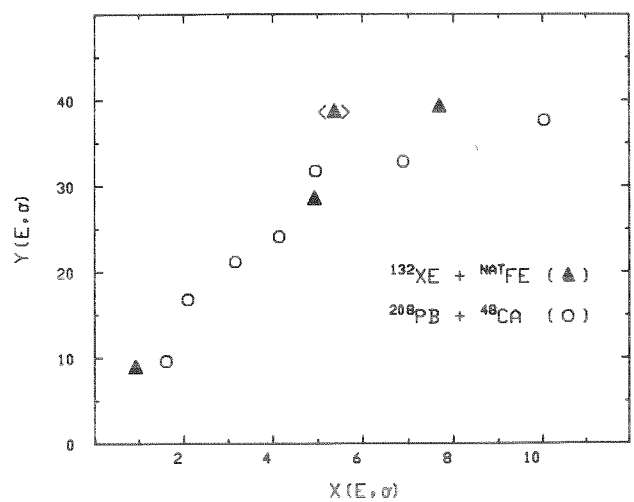


Fig. 3: Rectilinear fusion cross-section plot (see text). The $^{132}Xe + ^{nat}Fe$ points are generated from the differential thick-target cross sections.

[1] W.E. Frahn, Nucl. Phys. A302, 281 (1978).
[2] U. Reus et al., Z. Phys. A301, 363 (1981).
[3] W.J. Swiatecki, Nucl. Phys. A376, 275 (1982); S. Bjørnholm & W.J. Swiatecki, Nucl. Phys. A391, 471 (1982).
[4] W. Westmeier et al., Phys. Lett. 117B, 163 (1982).
[5] R. Bock et al., Nucl. Phys. A388, 334 (1982).

Capture Processes in the System $^{238}U + ^{nat}Fe$ B

A. Rox, B. Jäckel, R.A. Esterlund, W. Westmeier, U. Reus, H. Schulte and P. Patzelt
Institut für Kernchemie, Universität Marburg

In a previous[1] report, it has been shown that the existing fusion data for this system are consistent with Capture model[2] predictions, and exhibit an s-wave fusion barrier shift[3] ("extra push") of 35 ± 8 MeV over and above the reaction barrier. We have performed a further experiment at E_{cm} = 345 MeV in order to obtain an additional point on the fusion excitation function as well as to construct a complete thin-target mass-yield curve.

Thin (0.796 mg/cm^2) natural Fe targets[4] were irradiated with 7.61 MeV/u ^{238}U ions from the GSI UNILAC. A rotating target wheel assembly[5] made possible the utilization of a very high beam intensity. Target thicknesses were monitored via Rutherford scattering into a solid-state detector. The integrated beam intensity was taken from a Faraday-cup measurement. Reaction products were scattered into a circular Al catcher foil which covered laboratory angles to the beam of 2.8 to 26.1°. After irradiation, this catcher foil was chemically processed using a separation scheme similar to one[6] used in other experiments[7] with ^{238}U targets. The resulting three samples were assayed via gamma-spectrometry for a period of ca. 100 d after irradiation. A portion (1/8) of the original unprocessed catcher foil was also counted, in order to obtain some short-lived reaction products as well as to double-check chemical yields determined from tracers.

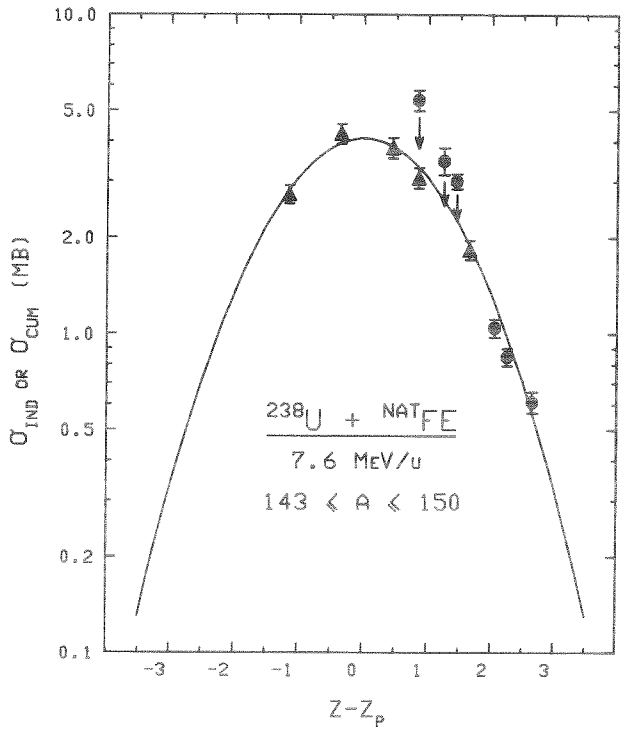


Fig. 1: Independent (triangles) and cumulative (circles) yields for ^{238}U(7.6 MeV/u)+^{nat}Fe, 143 ≤ A ≤ 150.

Although data analysis is not yet completed, a total to date of 243 products in the ranges 47 ≤ A ≤ 240 and 21 ≤ Z ≤ 95 have already been identified and their cross sections evaluated. Data from symmetric fragmentation products are shown in Fig. 1. The agreement with the gaussian is good, reflecting the quality of the data. Similar data from nearby mass ranges show an additional, narrower gaussian with Z_p on the neutron-rich side of beta stability. These products arise from the sequential fission of "uranium-like" few-nucleon transfer species.

It was stated above that the extra push energy at the barrier for this system has been determined to be 35 ± 8 MeV. Fig. 2 displays[8] extra push values derived from both evaporation residues (circles) and symmetric fragmentation (squares) measurements. The solid point at X_{eff} = 0.85 is our value of the extra push ΔB for $^{238}U + ^{nat}Fe$. The scatter of the data is somewhat large, but the evidence is persuasive for the reality and general trend with X_{eff} of the extra push energy.

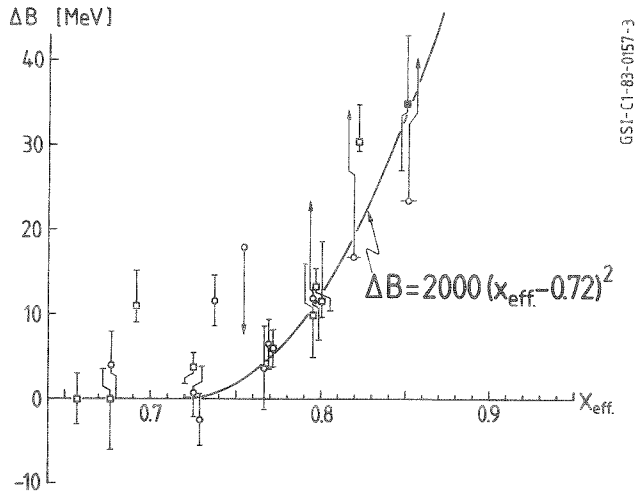


Fig. 2: Extra push energy as a function of the effective fissility. The solid point is $^{238}U + ^{nat}Fe$.

[1] W. Westmeier et al., GSI 82-1, 7 (1982).
[2] W.J. Swiatecki, Nucl. Phys. A376, 275 (1982); S. Bjørnholm & W.J. Swiatecki, Nucl. Phys. A391, 471 (1982).
[3] W. Westmeier et al., Phys. Lett. 117B, 163 (1982).
[4] Prepared by H. Folger & the GSI target laboratory.
[5] Setup kindly lent us by H. Gäggeler & colleagues.
[6] J.V. Kratz et al., Inorg.Nucl.Chem.Lett. 10, 951(1974).
[7] J.V. Kratz et al., Phys. Rev. C13, 2347 (1976).
[8] H. Gäggeler, private communication (1983).

Sub-Coulomb Transfer in Collisions of ^{238}U with ^{238}U B

G. Wirth, W. Brüchle, Fan Wo, H. Gaeggeler, K. Schlitt, K. Sümmerer
GSI Darmstadt
J.V. Kratz, M. Lerch, N. Trautmann Institut für Kernchemie, Universität Mainz

Structures in the positron spectra observed in U-U collisions[1] are discussed as experimental evidence for the process of spontaneous positron production. However, a nuclear background may arise from internal electron-positron pair creation during the decay of excited nuclei, which was determined from the corresponding γ-ray spectrum applying semi-empirical internal pair-conversion coefficients measured in low Z systems. This procedure assumes for different reactions similar multipolarities and may be problematic for γ-transitions from the deexcitation of quasielastic transfer products. Cross sections for quasielastic transfer are known to have a strong dependence on the incident energy of the projectile near the barrier[2]. EO-transitions are completely neglected. Therefore we have measured cross sections radiochemically for several xn, 1pxn and 2pxn transfer channels in the system U + U at incident lab-energies of 5.5, 5.8, 5.9 and 6.1 MeV/u. The targets consisted of 380 µg/cm² Uranium covered with Titanium of 20 µg/cm² respectively 120 µg/cm² on the side opposite to the beam. Catcher foils were placed in the whole angular range from the target to 45°. Following a bombardment the targets and catcher foils were removed and chemically separated. Through γ-ray counting the absolute decay rates and from that cross sections for individual transfer products were determined. Data analysis is still in progress. Some preliminary cross sections are

5.9 MeV/u:	^{239}U	(1n)	95 ± 10 mb
	^{240}U	(2n)	5 ± 1 mb
	^{238}Np	(1p1n)	0.9 ± 0.15 mb
5.8 MeV/u:	^{239}U	(1n)	61 ± 12 mb
	^{237}Pa	(1p)	2.6 ± 0.5 mb
5.5 MeV/u:	^{239}U	(1n)	23 ± 3 mb
	^{237}Pa	(1p)	0.45 ± 0.1 mb

The measurement of the excitation function or angular distributions for ^{239}U (one neutron transfer) at energies below the barrier should give totally equivalent information if the transfer proceeds under semiclassical conditions and the slopes of the angular distributions and of the excitation function should then be determined only by the neutron binding energy in ^{238}U[3]. The peak structure in the positron spectra is most pronounced at ion scattering angles θ_{lab} = 45° and nuclear collisions with a relatively long reaction time as indicated by the width of the positron line[1] could show up in deviations from the expected semiclassical behaviour for quasielastic nucleon transfer assuming pure Rutherford scattering. Therefore we have measured the angular distributions for one neutron transfer at energies near the barrier and well below it and the excitation function for the formation of ^{239}U down to 73 % of the "spherical" Coulomb barrier using an interaction radius $R_{int} = 1.16 \times (A_1^{1/3} + A_2^{1/3} + 2)$ fm. Still at 73 % of the barrier there is a cross section of 0.16 mb for the formation of ^{239}U. The data points of the excitation function plotted in fig. 1 are expected to fall on a straight line with a slope shown by the solid line. Fig. 2 shows the angular distribution of ^{239}U at E_{lab} = 5.7 MeV/u, expected to be backward-peaked. A decrease of the differential cross section at the very backward angles is observed and is also seen at beam energies of 5.9, 5.4 and 5.1 MeV/u. It has to be checked, whether this can be accounted for by Coulomb excitation along the trajectories before and after the neutron transfer and subsequent fission.

1. E. Berdermann et al., GSI Scientific Report 1981, GSI 82-1 (1982) 138
H. Bokemeyer et al., GSI Scientific Report 1981, GSI 82-1 (1982) 139
2. G. Franz et al., Z. Physik A 291, 167 (1979)
3. W. von Oertzen in Nuclear Spectroscopy and Reactions Vol.B ed. J. Cerny (Academic Press) p. 279

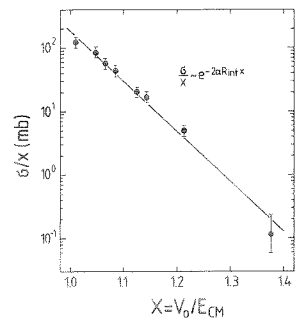


Fig.1:
Excitation function for the formation of ^{239}U in the U+U reaction. The solid line has the semiclassically expected slope whereas the absolute scaling was fitted to the experimental points.
$V_o = e^2 Z_1 Z_2 / R_{int}$;
$R_{int} = 1.16(A_1^{1/3} + A_2^{1/3} + 2)$ fm;
$\alpha = (2mB_n\hbar^{-2})^{1/2}$

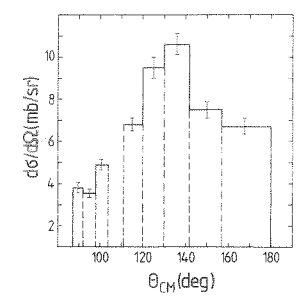


Fig.2:
Angular distribution of ^{239}U from U-U collisions at E_{lab}=5.7 MeV/u.

One-particle transfer in uranium induced reactions at the Coulomb barrier

B

D. Schüll, W.F.W. Schneider, H. Bokemeyer, R. Bock, GSI Darmstadt
H. Freiesleben, Universität Bochum
F. Pühlhofer, D. Bangert, B. Kohlmeyer, M. Marinescu,
Fachbereich Physik der Philipps-Universität Marburg

The identification of line structures in the otherwise smooth e^+-energy spectra[1,2] in U+U collisions at projectile energies close to the Coulomb barrier and the enhanced e^+-production probability might be connected with the formation of a long living dinuclear complex[3]. If it exists, an enhanced transfer cross section and a deviation in the angular dependence compared to a sub-Coulomb transfer mechanism is expected. We therefore intended to study the 1n-transfer cross section in the U+U system with the GSI magnetic spectrometer at otherwise equal experimental conditions as in ref. 1. We selected binary particle events by using a coincidence set-up consisting of the spectrometer for the forward scattered particles and a ΔE-E telescope for the recoil products. We refer also to a similarily motivated experiment of the GSI-Chemists group[4] which, however, avoids the restriction on binary particle events.

The experiment has been carried out at a spectrometer angle Θ_{lab} = 38°at 5.8 MeV/u bombarding energy and Θ_{lab} = 30° and 6.0 MeV/u. The beam divergence and multiple scattering in the rather thick U/C-targets (180 µg/cm² + carbon layer) in conjunction with the large kinematical variation over the aperture angle of the spectrograph caused come loss in energy resolution (ΔE/E = 1.8 %) which could not be compensated in order to reach a mass-resolution of Δm/m=1/380. Asymmetric large tails of several MeV energy loss are observed possibly caused by multiple Coulomb excitation. Fig. 1 shows part of the A/q-spectrum of the U+U collision at Θ_{lab} = 30°. The position of the 1n-transfer according to the mass calibration is indicated by arrows. The sum over all observed charge states reveals an upper limit for the 1n-transfer cross section of $d\sigma/d\Omega(30°) \leq 30$ mb/sr, a value which is consistent with the results of Wirth et al.[4] whose data show no distinct deviation from a sub-Coulomb transfer mechanism in this angular range.

A question discussed in the e^+-experiment[1] is the existence of a distinct atomic charge asymmetry between projectile and targetlike fragments with respect to equilibrium charge. We investigated therefore the atomic charge state distribution of the asymmetric systems U → Au and Pb → Au where the separation was done by the different Z. As can be seen in fig. 2 we find that the Au-recoil and the U-projectile have about the same average charge state of 49^+ in spite of the fact that U is injected with q = 60^+ while Au starts with q=0. The distribution of the Au particles is asymmetric with a long tail to high charge states (q=68^+ has still 1.5 % intensity of the peak value). But the data show a strong target thickness dependence. Especially we find that a 50 µg/cm² target reveals an even higher charge state than the 100 µg/cm² Au-target. This favours the interpretation that the charge state is mainly defined by the quasimolecule existing in close nuclear collisions. The passage through the target reduces this charge state by electron capture, a process which is extremely effective for additional carbon layers of only 20 µg/cm² being enough to symmetrize the distribution completely.

[1] Bokemeyer et al., GSI-Annual report 1981, p. 139
[2] Berdermann et al., GSI-Annual report 1981, p. 138
[3] U. Müller et al., Heavy Ion Collisions Lecture Notes in Physics 168(Springer Berlin 1982)p. 388
[4] Wirth et al., this Annual report

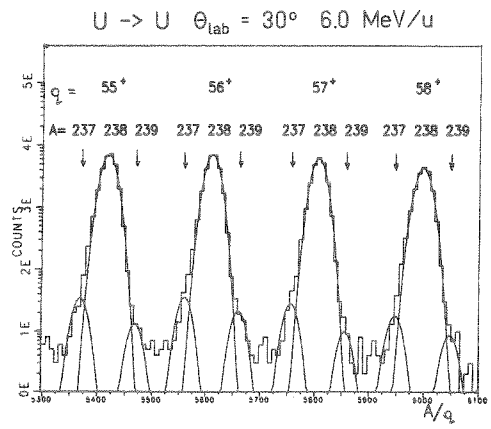


Fig. 1: A/q-spectrum of elastically scattered U-ions and transfer-products

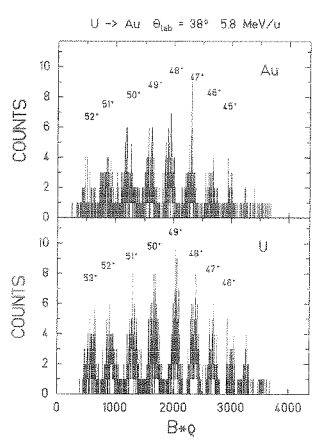


Fig. 2: Atomic charge state distribution for U- and Au-like products.

Quasi-Elastic Nucleon Transfer Reactions in a Core Excitation Model for ^{48}Ti Incident on ^{42}Ca B,G

C. BRENDEL, J. CARTER, F. BECK, G. DELIC*, R.H. LEMMER*,
A. RICHTER and G. SCHRIEDER
Institut für Kernphysik, Technische Hochschule Darmstadt
and D. SCHÜLL, GSI Darmstadt

Quasi-elastic transfer reactions in either direction have been studied extensively for ^{48}Ti on ^{42}Ca at high incident energies using the UNILAC and the magnetic spectrometer at GSI. The measured energy spectra for the many outgoing channels observed[1] have been converted to double-differential cross sections in the centre-of-mass system, $d^2\sigma/d\Omega dE_x$, and include events upto E_x = 50 MeV total excitation energy. The figure shows the resulting spectra for the four single nucleon transfer channels at E_{Lab} = 300 and 385 MeV near the corresponding grazing angle (histogram, 200 keV bin size). The data show in all cases a remarkably broad peak approximately 9 MeV wide located below 12 MeV in excitation energy. Furthermore, besides the transfer of a single nucleon shown, all of the reaction channels display a specific structure which persists both as a function of scattering angle and incident energy. Hithertoo, such spectra have been interpreted as quasi-elastic transfer to continuum states[2] and have been described using a semi-statistical model.[3] Contrary to this approach, however, we have proposed a model involving single particle states in both of the outgoing nuclei.[4] The single nucleon transferred into a particle excited state of the acceptor nucleus may originate either from the valence shell or from within a closed shell of the donor nucleus, thereby inducing core-excitation by creating a hole state. Such hole states have been identified previously in the energy spectra for neutron pick-up with light ions.[5] Consequently, in this one-step direct interaction picture both outgoing nuclei may be excited simultaneously.

The transition matrix elements used to calculate the strength of each individual transition were computed by the full-recoil exact finite-range DWBA code SATURN2 - MARS1.[6] By spreading the resulting strength function using a Breit-Wigner form and suming over all contributions the cross section as a continuous function of energy can be obtained. The cross sections thus calculated are shown in the figure for each transfer channel as a smooth line. The overall normalization parameter, N, determines the absolute magnitude of the predictions and takes into account the approximations used in the DWBA method. A common state-independant spreading width of 1.1 MeV, which includes a contribution from the experimental energy resolution, was found to reproduce the gross structure of the data for all channels. As can be seen, the overall correspondence between the model predictions and the data is very gratifying in all cases. The missing strength at higher excitation energies may be due to more complicated particle-hole excitations and transfer after inelastic excitation which are not included in the model.

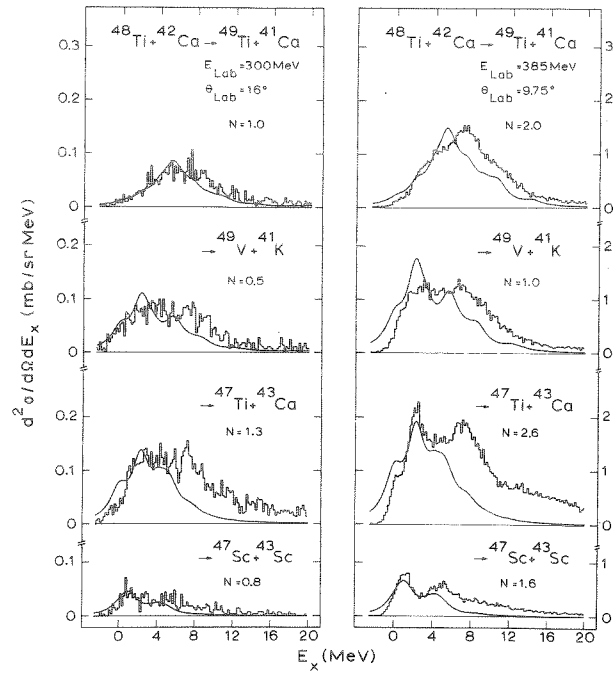


Figure: Double-differential cross sections for the single nucleon transfer channels measured near the grazing angle at E_{Lab} = 6.3 and 8 MeV/amu

The two nucleon transfer and single charge exchange channels have a strength located at somewhat higher excitation energy and are being studied at present within the same framework.

* Department of Physics and Nuclear Physics Research Unit, University of the Witwatersrand, Johannesburg, South Africa

1 C. Brendel, J. Carter, G. Delic, A. Richter, G. Schrieder and D. Schüll, GSI-Report 82-1 (1982) 10; ibid. 11

2 M.C. Mermaz, Phys. Rev. C20 (1979) 1962

3 M.C. Mermaz, Phys. Rev. C21 (1980) 2356

4 C. Brendel, J. Carter, F. Beck, A. Richter, G. Schrieder, D. Schüll, G. Delic and R.H. Lemmer, Phys. Lett. B, submitted for publication

5 S. Gales, Nucl. Phys. A354 (1981) 193c

6 T. Tamura and K.S. Low, CPC 8 (1974) 349; T. Tamura, T. Udagawa, K.E. Wood and H. Amakawa, CPC 18 (1979) 163

Indications of Coherent Nucleon Flow in ^{238}U Induced Deep Inelastic Scattering Near the Coulomb Barrier [B]

G. Beier, J. Friese, P. Kienle, H.J. Körner, Waltraud Mayer, W.A. Mayer, L. Müller, W. Wagner

Physik-Department, TU München

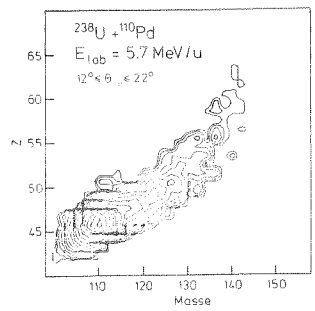
Excitation functions of ^{238}U - induced reactions with ^{110}Pd and ^{124}Sn targets were measured in the bombarding energy range between 5.7 and 6.0 MeV/u in order to study the evolution of the large multinucleon transfer at the Coulomb barrier. Kinematic coincidences using two large area position sensitive parallel plate counters backed with ionization chambers gave resolutions $\Delta A = 1.5$ in mass units and $\Delta Q = 6$ MeV in Q values. With a BCS ionization chamber[1] a charge resolution of $\Delta Z = 1$ was achieved.

Fig. 1 shows the evolution of the multinucleon transfer crossection in the A-Z-plane for binary reactions (-25 MeV $\geq Q \geq -140$ MeV) measured with the ^{110}Pd target. The influence of closed shells is most distinctly seen at the lowest bombarding energy (Fig. 1a). A nucleon flow up to the double magic ^{132}Sn, which shows even an enhanced yield is observed. In addition we find ^{136}Ba and the complementary ^{212}Pb produced with an enhanced crossection. Both final products lie in regions of closed shells. The transfer crossection drops rapidly beyond those. Corresponding data with ^{124}Sn as target show similar shell effects in the nucleon flow. Furthermore a nearly symmetric large neutron flow of up to 10 neutrons between ^{110}Pd and ^{238}U is indicated.

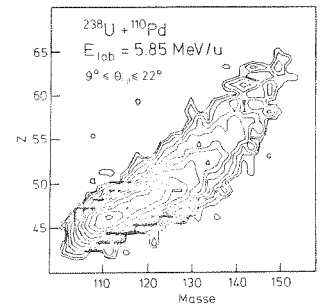
At somewhat higher bombarding energy (Fig. 1b) even more nucleons are transfered. The product yield is rather flat, until the closed shell nuclei are reached and decreases strongly beyond them.

For the next higher bombarding energy (Fig. 1c) the crossection shows a broad maximum in the region, where 8 neutrons and 2 protons are transfered.

a)



b)



c)

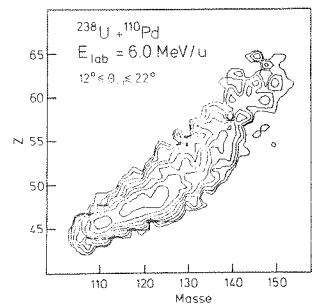


Fig. 1: Contour plots of the reaction cross-section for various bombarding energies

[1] Ch. Schießl et al., Nucl. Instr. and Meth. 192 (1982) 291 - 294

Mass and charge transfer in heavy ion collisions

BG

R. Bass+, H. Noll, V. Hartmann*, K. Sapotta
Institut für Kernphysik der Universität Frankfurt am Main

The analysis of the reactions $^{208}Pb + ^{58}Ni$ (5.9 MeV/u) and $^{208}Pb + ^{64}Ni$ (5.4 MeV/u)[1] measured at the focussing time-of-flight spectrometer was completed. The results agree in most respects with those obtained from the previously investigated system $^{40}Ar + ^{208}Pb$ (5.9 MeV/u)[2]. In the following the results of the three systems are summarized.

1. Elastic scattering.
The long range Coulomb interaction leads to a decrease of the pure elastic scattering cross section below the Rutherford cross section already at deflection angles significantly below the grazing angle, although the nuclei have high excitation energies and small $B(E\lambda)$ values. The sum of the elastic and the Coulomb excitation cross sections shows the well known Fresnel-type diffraction patterns.

2. Quasielastic and deep inelastic reactions.
The mass and charge drift is influenced but not completely determined by the static potential energy surface (PES).

The charge equilibration takes place at an early stage of the reaction, in accordance with the steep slope of the PES in this direction. However, at energy losses (Q^*) up to 40 MeV the mass drift evolves in the direction of mass asymmetry, which is in contrast to the slope of the PES. The trend towards mass asymmetry decreases with decreasing mass asymmetry in the entrance channel. Its dependence on the reaction angle is not uniform within the three reaction systems. In the Ar + Pb system the mass asymmetry has a maximum in the vicinity of the grazing angle, whereas in the Pb + Ni systems it increases at smaller CM angles.

At higher energy losses the expected drift towards mass symmetry is observed.

The variances of the N and Z distributions reflect the fact that the neutron and proton transfer is correlated to the potential energy. The correlation is a consequence of the steep potential valley and the comparatively small energies in the entrance channel ($E_i - E_B$ = 30 - 40 MeV) chosen for our reaction systems. Therefore the variances of the N-Z-distributions in the direction of the potential minimum (σ^2_u) increase monotonically with the energy loss and saturate already at small energy losses ($-Q^*$ = 10-20 MeV) in the direction perpendicular to the potential valley.

In the case of the Ar and the ^{58}Ni reaction the ratio of σ^2_N/σ^2_Z increases from a value near $\bar{N}/\bar{Z}$ at small energy losses to $(dN/dZ)^2$ in the fully relaxed region ($-Q^*$ > 60 MeV), whereas in the case of ^{64}Ni the value of $(dN/dZ)^2$ is reached already at small energy losses ($-Q^*$ = 20 MeV).

Near Q = 0 the ratio of σ^2_N/σ^2_Z is greatly inhanced by a hindering of proton transfer that can be interpreted as a superposition of a Coulomb barrier effect and in the case of the Pb + Ni reactions a shell effect due to the closed proton shells in both target and beam nuclei.

The energy loss rate with σ^2_A is significantly greater than expected for an uncorrelated nucleon transfer as the dominating dissipative mechanism, but can be explained with the assumption of "Pauli blocking".

[1] R. Bass et al., GSI scientific report 1981, GSI 82-1, p. 14

[2] V. Hartmann, Dissertation

+ deceased

* now at GSI

Light Charged Particle Accompanied ^{208}Pb Collisions with ^{26}Mg and ^{58}Fe B

P.J. Brülls, H.P. Hollenbach, M. Mutterer, J. Pannicke,
J.P. Theobald and K. Weingärtner
T.H. Darmstadt
and
H.W. Daues and A. Gobbi
GSI Darmstadt

An experimental set-up has been completed at position Z6a in the experimental hall to measure simultaneously in-plane and out-of-plane yields of light charged particles associated with two-body heavy-ion reactions. The heavy ions are recorded in forward direction by two semi-circular position sensitive parallel plate detectors[2] (below fig. 1), the light charged particles are detected and identified in one plane by three ΔE/E telescopes composed of position sensitive proportional counters as ΔE and semiconductors or a plastic scintillator as E detectors (fig. 1).

Preliminary experiments have been performed with a lead-208 beam of 5,9 MeV/amu bombarding ^{26}Mg, ^{50}Ti, and ^{58}Fe targets. In all three cases protons and alpha-particles have been observed associated as well with deep inelastic as with fusion-fission reactions, Fig. 2 shows for the measurements with ^{26}Mg and ^{58}Fe targets the heavy-ion reaction product yields plotted upon a (θ_{CM}, M) plane[1] i) as singles (si), ii) with alpha- (α), iii) with proton-coincidences (p). The ratio of observed alpha and proton accompanied reactions is 0,25 ± 0,05 for ^{26}Mg and 0,50 ± 0,20 for ^{58}Fe in the range of near symmetric mass products with masses $A = (\frac{208 + A_T}{2} \pm 5\ \%)$, where A_T is the target-nucleus mass, and 0,42 ± 0,05 and 0,29 ± 0,09 resp. outside this mass range.

In the symmetric mass range fusion-fission, outside this range deep inelastic reactions are dominant. A separation of light charged particles originating from entrance- and exit channels has not yet been achieved. The experiments are going on in order to obtain a better statistical accuracy for a detailed evaluation.

1. R.Bock, Y.T.Chu, M. Dakowski, A. Gobbi, E. Grosse, A. Olmi, H. Sann, D. Schwalm, U. Lynen, W. Müller, S. Bjørnholm, H. Esbensen, W. Wölfli and E. Morenzoni, Nucl. Phys. A 388 (1982) 334
2. Y.T. Chu, H.W. Daues and H. Sann, GSI report 80-3 (1980) 182

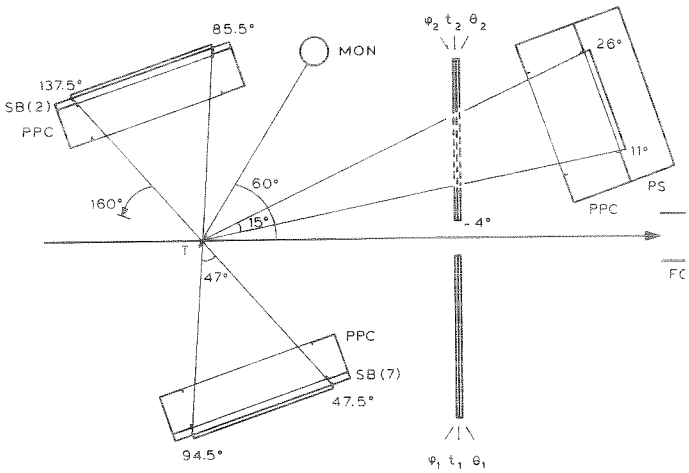


Fig. 1 ↑

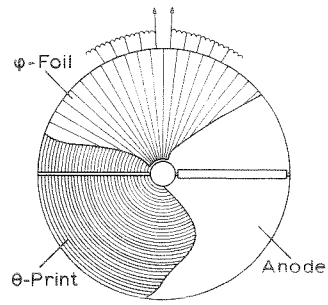
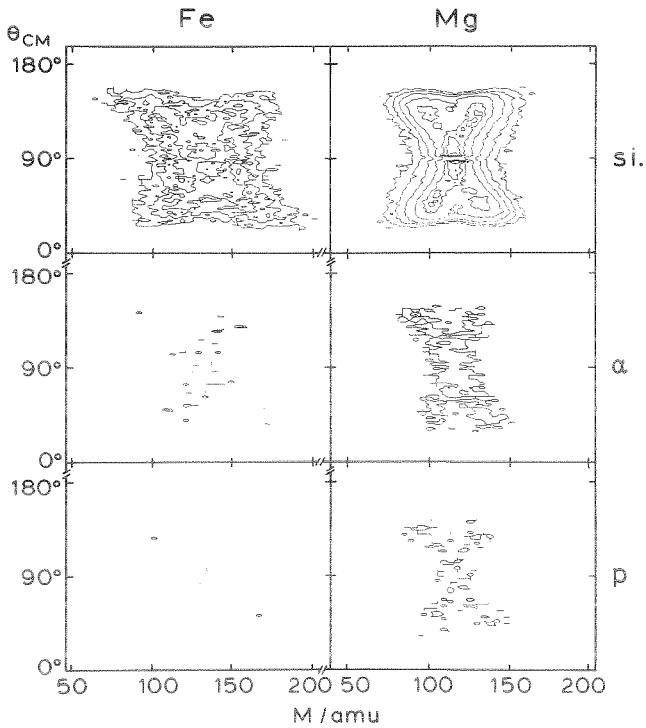


Fig. 2 ↓



X-Ray Emission Probabilities and Nuclear Time Delay in the Deep Inelastic Collision U+U at 7.5 MeV/amu

Ch. Stoller, M. Nessi, W. Wölfli
Laboratorium für Kernphysik, Eidg. Technische Hochschule, CH-8093 Zürich
W.E. Meyerhof, J.D. Molitoris, E. Morenzoni
Standorf University, Standorf, Ca. 94305, USA
E. Grosse, Ch. Michel, GSI Darmstadt, D-6100 Darmstadt

In 1962 Gugelot (1) suggested that the ionization probaliтiy of the atomic inner shells in an atomic collision may be changed if a nuclear reaction takes place which delays the scattered particle. Recent measurements of resonant elastic scattering of protons from various nuclei have confirmed this prediction (2,3). Anholt (4) and U. Müller (5) have suggested that a similar effect should exist in deep inelastic collisions of heavy nuclei. If the ionization probability P_K is measured as a function of the total kinetic energy loss in the reaction -Q, the average time delay associated with a certain Q-value can be deduced.

In a first experiment (6) the reactions Xe+Pb and Xe+Th at 8.6 MeV/amu were investigated without significant results, because in this case the K-shell vacancy formation process is dominated by the internal conversion of γ-rays from the highly excited nuclei. The time delay sensitive 'direct' ionization in the time varying Coulomb field of the scattering nuclei contributes only a small fraction to the total ionization probability.

We therefore chose the U+U system which should exhibit an ionization probability which is at least ten times higher than for Xe-Pb, whereas the internal conversion contribution should be similar to the one of the Xe+Pb and Xe+Th cases. The experimental set up is shown in fig.1. The U beam was directed on a 500 μg/cm² U target. The X- and γ-rays were measured with 2 planar and 1 coax Ge detector and a 3"x3" NaI detector. The particles emerging from the reaction are measured in two parallel-plate-avalanche-detectors (PPAC) positioned symmetrically to the beam axis. The particle detectors were slightly modified: a second plane was added which allowed a better determination of the energy loss ΔE, and the position sensing delay line was equipped with amplifiers on both sides (normally one side is unused and terminated with 50 Ohms). The latter modification allowed us to recognize fission events in which both fission fragments reach the counter. The major part of the events in which one nucleus had undergone fisson was suppressed by requiring that the position deduced from the time signals on both sides of the delay line be the same; this condition is not fulfilled when two fission fragments enter the same detector. The ΔE-counter cannot distinguish between the two types of event since the energy loss of two fission fragments equals the energy loss of one U nucleus at the particle energies of interest.

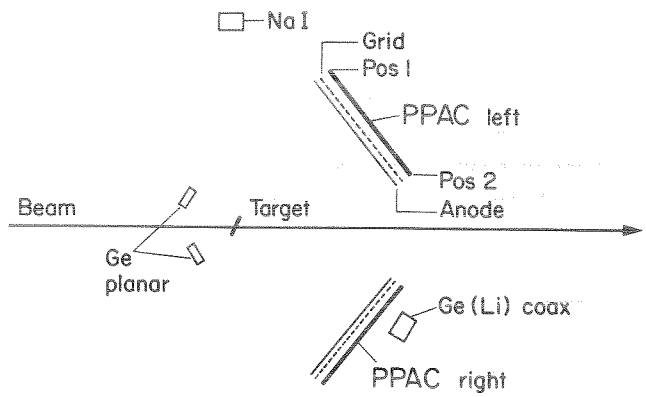


Fig.1. Experimental set up.

Different Q-values were chosen by requiring the corresponding kinematic conditions. The results of the first evaluation averaged over the range of scattering angles are given in fig.2. The contribution from internal conversion (IC) has already been subtracted. The large error bars give the variance obtained by averaging the $P_K(Q)$ obtained at five different scattering angles.

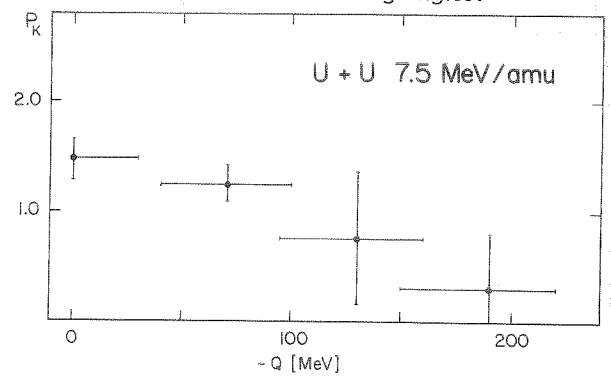


Fig.2. K X-ray emission probability P (-Q). The results have been averaged over the lab scattering angles between 32 and 58°.

One sees that the ionization probability declines as a function of Q. From the calculatons of U. Müller et al. (5) one can infer a delay time of ca 2×10^{-21} s at -Q = 180 MeV. Further evaluation of the data is necessary to confirm these results and to rule out background effects, such as unrecognized fission events, which might influence the observed probability.

1) P.C. Gugelot, in "Direct Interactions and Nuclear Reaction Mechanisms", p.382 (Gordon and Breach, New York, 1962)
2) J.S. Blair et al., Phys. Rev. Lett. 41, 1712 (1978)
3) J.F. Chemin et al., Phys. Rev. A24, 1218 (1981)
4) R. Anholt, Z. Phys. A292, 123 (1979)
5) U. Müller et al., Z. Phys. A297, 357 (1980)

B

Measurement of the γ-Ray Circular Polarization in Kr-Induced Reactions at 10 MeV/u

Ch. Schandera, Ch. Lauterbach, J. de Boer, W. Dünnweber, W. Trautmann
Sektion Physik der Universität München

Much experimental work has been devoted to ^{86}Kr-induced reactions on ^{139}La and ^{166}Er as typical cases of dissipative processes[1]. These data have been the subject of many theoretical studies[2]. Despite these efforts the character of the trajectories is still not understood with respect to the sign of the deflection angle in the deep-inelastic (D.I.) component.

In order to clarify this situation experimentally we have measured the circular polarization of the coincident γ-radiation which carries information on the relative contributions of positive and negative angle scattering. Since the deflection function may depend on the dynamical parameters of the exit channel the polarization was measured as a function of the exit channel energy, the mass asymmetry, and the scattering angle. The experimental set-up and the measuring technique is described in detail elsewhere ([2]and references given there).

The TKE-θ plots (Wilczynsky plots) of the measured γ-coincident doubly differential cross section for ^{86}Kr + ^{139}La at 10 MeV/u is shown in fig.1a. It is noted that events in the quasielastic component (Q ≤ -70 MeV) and events at small forward angles ($\theta_{LAB} \leq 12°$) are not recorded. This is due to the geometrical confinement of the symmetrical kinematic-coincidence set-up. To present the polarization data of the systems 860 MeV ^{86}Kr + ^{139}La and ^{86}Kr + ^{166}Er several regions are chosen in the TKE-θ plane. With the chosen sign convention P_γ is positive for negative scattering angles and negative for positive scattering angles. The values obtained by integration over all masses between A = 58 and A = 105 are given in figs. 1b and 2, respectively, in a schematic representation of the Wilczynsky plots.

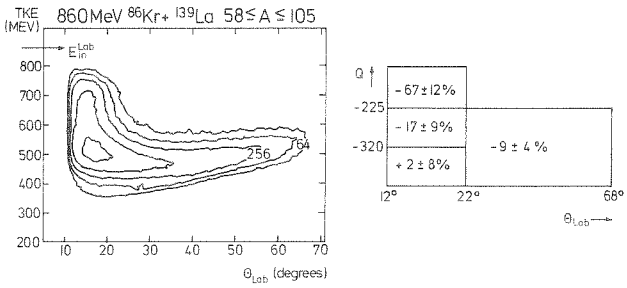


Fig. 1a): Measured γ-coincident mass integrated doubly differential cross section as a function of the scattering angle and the total kinetic energy TKE = $E_1 + E_2$ in the laboratory frame.

Fig. 1b): Measured γ-ray circular polarization for the indicated regions in a schematic representation of the Wilczynsky plot.

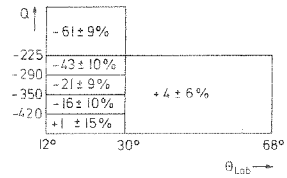


Fig. 2): Same as fig. 1b) but for the reaction 860 MeV ^{86}Kr ^{166}Er.

A clear dominance of positive deflection angles is observed for the partially damped events in both cases. The amount of the polarization varies between 20% and 70% in this group. With increasing energy loss the polarization decreases at forward angles, giving evidence for increasing contributions from negative-angle scattering. For the most negative Q-values and for large scattering angles the value of the polarization is consistent with zero, indicating equal contributions from either side of the interaction region. This means that the fluctuations in the relation between energy loss and scattering angle are larger than has been generally assumed, and it puts in doubt the interpretation of the observed ridge in the Wilczynsky plot at large θ in terms of a simple orbiting picture.

[1]A. Gobbi et al.: Nuclear Structure and Heavy-Ion Collicions, edited by R.A. Broglia, R.A. Ricci and C.H. Dasso (Amsterdam 1981) p.1.
P. Dyer et al.: Phys. Rev. C22, 1509 (1980)
R. Puigh et al.: Nucl. Phys. A336, 279 (1980)

[2]R. Vandenbosch et al.: Phys. Rev. C17, 1672 (1978) and private communication
D.H.E. Gross et al.: Proceedings of the Nuclear Physics Workshop I.T.C.P. (Trieste 1981), p.691
J. Blocki et al.: Phys. Lett. B99, 13 (1981)
K.T.R. Davies et al.: Phys. Rev. C20, 1372 (1979)
R.Y. Cusson et al.: Nucl. Phys. A385, 76 (1982)

[3]Ch. Schandera et al.: Nuclear Structure and Heavy-Ion Collisions, edited by R.A. Ricci and L. Moretto to be published
Ch. Schandera et al.: G.S.I. Scientific Report 1979, p.183

Moments of charge distributions in the reaction $^{92}Mo + ^{92}Mo$ at 14.7 MeV/u.

S. Gralla, R. Bock, Dai Guang-xi[+], A. Gobbi, K.D. Hildenbrand, W.F.J. Müller, U. Lynen, A. Olmi, M. Petrovici[++], H. Stelzer, J. Töke[+++] and H.J. Wollersheim

GSI Darmstadt and MPI Heidelberg

One-particle inclusive, binary and three-body reactions have been studied in the system $^{92}Mo+^{92}Mo$ at 14.7 MeV/u with a set-up consisting of a ionization chamber and 12 position-sensitive parallel-plate avalanche counters[1]. The reaction is overdetermined since in addition to the kinetic energy of one fragment the velocities and angles of both binary partners have been measured; therefore primary quantities can be reconstructed in different ways. For the inclusive data we performed a multi-step iterative correction for evaporation of neutrons, protons, deuterons and α-particles, the multiplicities of which were calculated with the code CASCADE[2], which has been shown to give reliable results in CN reactions up to excitation energies of 100 MeV. The results are displayed in Fig.1 as $d\sigma^2/dTKE.dZ$. Charge distributions for consecutive bins in TKEL (bin size 20 MeV) are shown in Fig.2. The solid lines are Gaussians whose first and second moments are determined by a momentum analysis of the distributions. The first moments exhibit as a function of TKEL only a small net shift towards lighter elements, less than half a Z-unit in the displayed TKEL range. The drift we had postulated after a first inclusive analysis[1] therefore can fully be attributed to sequential evaporation. The second moments as a function of TKEL are displayed as crosses in Fig.3: Horizontal bars just give the bin size in TKEL, vertical bars represent estimated errors caused by the iterative reconstruction. For this estimation assumed primary distributions were subjected to a series of Monte-Carlo simulations of statistical particle evaporation; the resulting secondary distributions were converted back using the procedure which was applied for the measured data and then compared to the input distributions. The solid line in Fig.3 represents calculations based on the theory of Ref.3. Obviously the success of this theory in the description of charge variances in a large variety of systems persists at these higher bombarding energies; this seems to point to the general validity of the assumption of the energy loss being caused by stochastic transitions between single particle states.

[+] A.v.Humboldt-Fellow, IMP, Lanzhou, P. R. of China
[++] on leave from IPNE Bucharest, Romania
[+++] on leave from Warsaw University, Poland

1 M. Petrovici et al., Nucl.Phys. A387(1982)313c
2 Code CASCADE, F. Pühlhofer, Nucl.Phys. A280(1977)267
3 M. Dakowski et. al., Nucl.Phys. A387(1982)189
J. Töke et. al., Contr. to this Annual Report

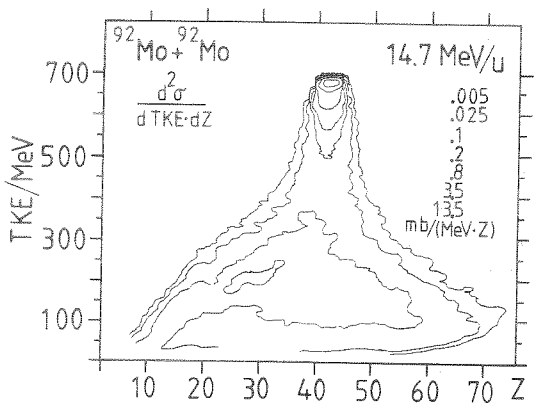


Fig.1: $d^2\sigma/dTKE.dZ$, inclusive results, iteratively corrected for neutron and charged particle emission.

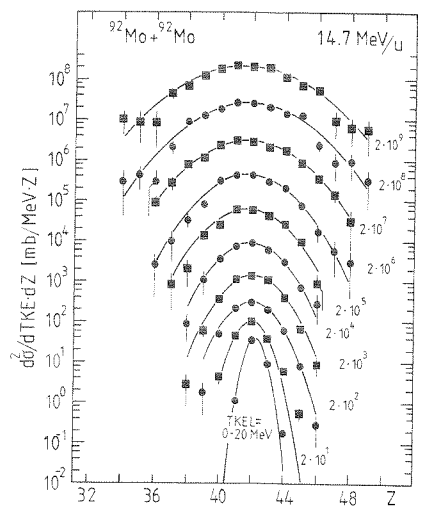


Fig.2: Charge distributions of consecutive bins in TKEL (bin size 20 MeV); the lowest bin represents TKEL=0-20 MeV, the highest TKEL=180-200 MeV. The upper curves have been multiplied by the given factors.

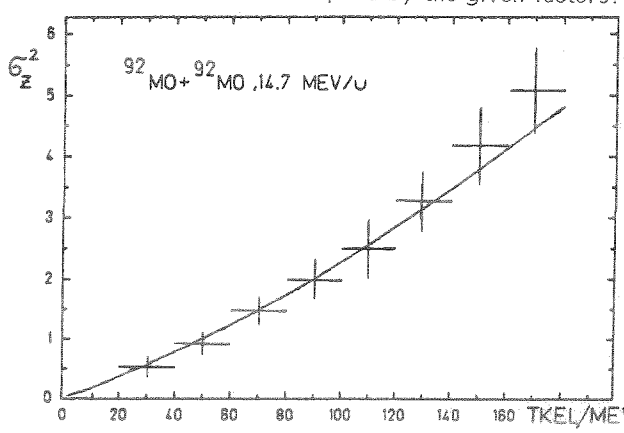


Fig.3: Second moments of the charge distributions as a function of TKEL (crosses); the solid line displays the result of a calculation according to ref. 3.

Two- and three-body exit channels in the reaction $^{92}Mo + ^{92}Mo$ at 14.7 MeV/u.

S. Gralla, R. Bock, Dai Guang-xi[+], A. Gobbi, K.D. Hildenbrand, W.F.J, Müller, U. Lynen, A. Olmi, M. Petrovici[++], H. Stelzer, J. Tõke[+++] and H.J. Wollersheim

GSI Darmstadt and MPI Heidelberg

At higher incident energies the secondary products of dissipative collisions cover a large range both in mass or charge and velocity. Fig. 1a shows as an example an inclusive ΔE-E-matrix measured with an ionization chamber (IC) equipped with a parallel-plate counter (PPC)[1] in front. The element number of events located below the dashed line cannot be determined from this plot since these products are not stopped inside the gas volume of the chamber. Fig. 1b demonstrates that in a plot of ΔE vs. $1/v_{lab}$ the light elements are resolved; thus by a combination of both representations the element number is uniquely determined for all products down to carbon.

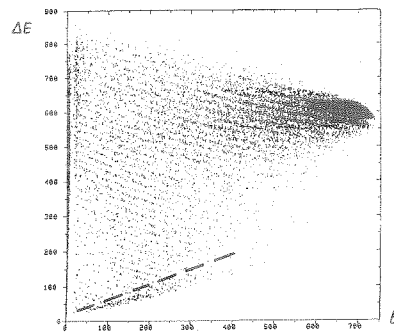
The plots on the left in Fig.2 represent $d^2\sigma/dv_{cm}dZ$ for different trigger conditions. The charge spectra on the right are the projections on the Z-axes. The top row shows inclusive data with a Z-spectrum extending down to carbon. The two-body events can be visualized by selecting coplanar events between IC and an in-plane PPC (center figures): They extend in the contour plot from the elastic region ($Z \approx 42$, $v_{cm} \approx 2.7$ cm/ns) down to the dashed line which denotes the separation velocity of the Viola systematics. The corresponding Z-spectrum still exhibits a skewness since secondary charge values are plotted. Only the tail of the two-body component reaches Viola velocities. Events below this limit represent the remainders of three-body processes, since coplanarity alone is not sufficient to totally suppress this component. They form the scarce extension towards light elements in the Z-spectrum. This is demonstrated by the bottom figures, where three-body events were selected by coincidence with an out-of-plane PPC: They fill the region which is not populated by the two-body products and therefore are located mainly below the Viola line with a broad velocity distribution especially of light elements. Even velocities in excess of the incident velocity are reached, probably by splitting fragments emitted in forward direction in the moving frame of the primary products. The Z-distribution is constant between Mo and C; the light elements produced in ternary reactions are therefore responsible for the strong light component already seen in the inclusive spectrum where their relative yield is even underestimated because of geometrical cuts. In the light of these results one has to assume that the mass (or charge) distribution of the splitting fragments is much broader than expected from earlier measurements.

[+] A.v.Humboldt-Fellow, IMP, Lanzhou, P. R. of China

[++] on leave from IPNE Bucharest, Romania

[+++] on leave from Warsaw University, Poland

[1] S.Gralla et al., preceeding contribution



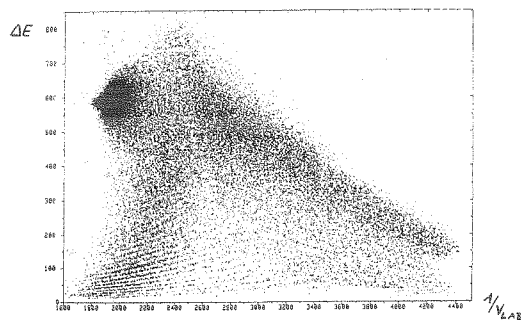


Fig.1: a) ΔE-E-matrix of inclusive products measured with the ionization chamber, b) same products in a ΔE vs. $1/v_{lab}$ representation.

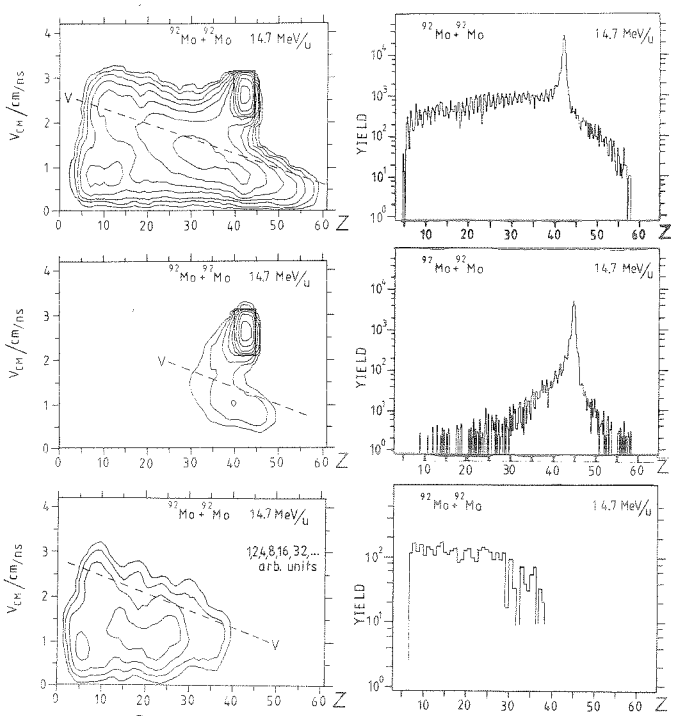


Fig.2: $d^2\sigma/dv.dZ$ for different trigger conditions (left figures). The spectra on the right show the projections on the Z-axes (see text).

Monte-Carlo Simulation of Ternary Reactions

J.Kuźminski[+], A.Gobbi, S.Gralla, K.D.Hildenbrand, and M.Petrovici[++]
GSI Darmstadt

Studies of reaction mechanisms at incident energies of 10-20 MeV/u have demonstrated the presence of ternary reactions which show unexpected characteristics in comparison to the well known sequential-fission process. At present it is still a matter of conjectures whether the new features result from a dynamical mechanism (splitting) or from unknown decay properties of nuclei, at extreme high excitation energies. For a simulation of these processes a Monte-Carlo code has been developed. The code is also used for the determination of the ternary 4π-distributions which have to be reconstructed from the raw data affected by geometrical cuts. The simulation is refined as the results of the calculations are compared with the experimental observations. At present the reaction is assumed to proceed in two steps: after a binary dissipative collision (first step), a massive two-body decay of the excited projectile-like or target-like fragments follows (second step). The dissipative collision is parametrized in terms of first and second moments of the element- and angular-distributions which are functions of the energy loss. Such a parametrization is based on systematics obtained from low-energy measurements and on the binary events observed at an incident energy of 14.7 MeV/u. For the second reaction step we assume a decay probability peaked at large energy losses of the first step. Mass asymmetry and angular distribution of the decay products are assumed to be isotropic. Fig.1a and b show the results of the simulated processes in form of the Wilczynski and diffusion diagrams (reaction ^{92}Mo + ^{92}Mo at 14.7 MeV/u). Simulation takes into account the geometry of the position-sensitive ionization chamber. The experimental data [1] are well reproduced at small energy losses where the yield of the ternary products is negligible. Fig.2 gives the element distribution of the decay products of ternary reactions. Fig. 3 shows the calculated dependence of the velocity on the Z-number of the decay products for the simulated ternary processes (the dashed line corresponds to the Viola energy). This distribution agrees remarkably well with the experimental results (cf. Fig.2 of Ref.1). This is not the case, if a fission-like mass distribution is assumed in the second reaction step.

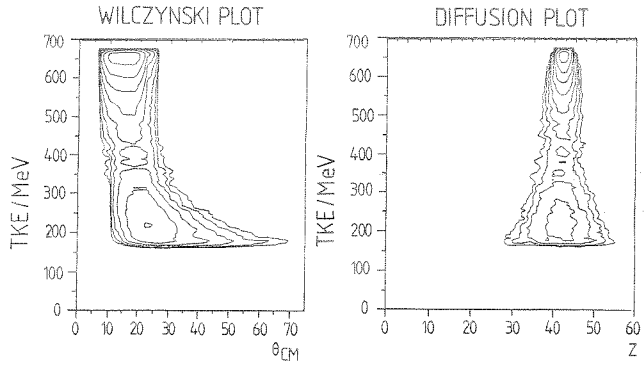


Fig. 1a

Fig. 1b

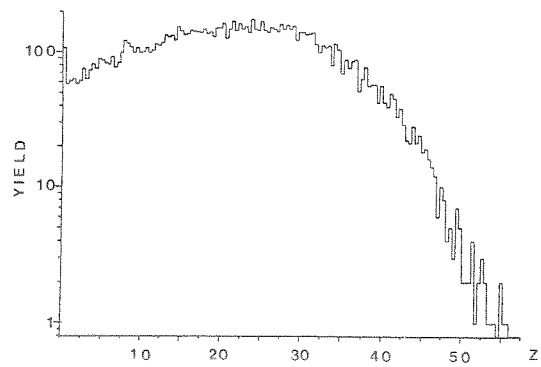


Fig.2

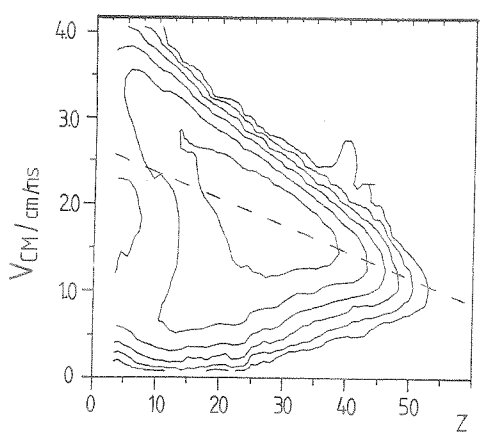


Fig.3

[1] S.Gralla et al., preceeding contribution

[+] on leave from Silesian University, Katowice, Poland

[++] on leave from IPNE Bucharest, Romania

Nucleon Transfer and Inelastic Excitations in the Reactions of 18 MeV/u ^{86}Kr with ^{208}Pb

H. Sohlbach, H. Freiesleben
Institut für Experimentalphysik, Ruhr-Universität Bochum

B. Kohlmeyer, M. Marinescu, F. Pühlhofer
Fachbereich Physik, Universität Marburg

W.F.W. Schneider, D. Schüll
GSI Darmstadt

P. Braun-Munzinger
SUNY, Stony Brook, USA

In this experiment an attempt was made to measure the excitation of giant resonances in ^{208}Pb using a ^{86}Kr beam. The underlying question was, if and to what extend collective excitations contribute to the energy dissipation in reactions between heavy nuclei. After measurements at 10 and 13 MeV/u, the results of which have been reported[1], we continued the investigation with an 18.23 MeV/u beam, hoping that the higher projectile energy would favour the excitation of giant resonances. In addition, the changed kinematical situation would facilitate the identification of sequential decay after transfer. In order to ensure the optimum in energy resolution and nuclide identification, the magnetic spectrometer was used. With ^{208}Pb targets of 500 µg/cm^2 [GSI-target-laboratory] an energy resolution of $\Delta E/E \approx 3 \cdot 10^{-3}$ was obtained, while mass and atomic number resolutions of $\Delta A/A \approx 1/260$ and $\Delta Z/Z \approx 1/80$, respectively, were achieved for ^{86}Kr allowing for unambiguous identification of all reaction products.

The data analysis is presently completed only for one scattering angle out of six. The ^{86}Kr-energy spectra obtained at $\theta_{lab} = 12^{o}$, which is slightly forward of the grazing angle, is displayed in Fig.1 together with spectra at 13 and 10 MeV/u bombarding energy at corresponding angles. One observes a well-developed broad structure at Q = -38 MeV(18MeV/u), similar to those at Q = -28.4 MeV(13 MeV/u) and Q = -22.6 MeV(10 MeV/u). The quoted Q-values were obtained after subtraction of a smooth background and applying two-body kinematics.

The shift of the bump with bombarding energy is compatible with the kinematics expected for the sequential decay of ^{87}Kr formed by the neutron pick-up reaction ^{208}Pb(^{86}Kr, ^{87}Kr)^{207}Pb. Any collective excitation of ^{208}Pb with ^{86}Kr left in a particle-stable state would produce a structure independent of bombarding energy.

Monte Carlo simulations of the sequential decay of ^{87}Kr were performed. The results sensitively depend on the assumption made on the primary ^{87}Kr spectrum. The observed widths of the structure can be reproduced at all energies consistently. However, a rather sharply localized energy distribution above the neutron threshold in ^{87}Kr has to be assumed. The position of the structure can be adjusted if some excitation is given to the recoiling ^{207}Pb nucleus. The energy needed increases from almost zero at 10 MeV/u to about 8 MeV at 18 MeV/u. We conclude that the broad structures in the ^{86}Kr-spectra are mainly due to sequential decay of ^{87}Kr.

1) GSI-Annual Report 1981, p. 26

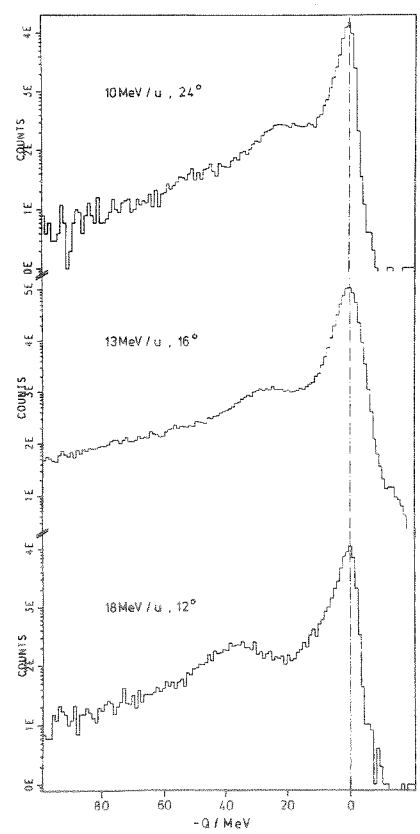


Fig.1: Spectra of ^{86}Kr ions at different bombarding energies and angles slightly forward of grazing

Interactions of 16.7 MeV/u ^{238}U with ^{nat}U as Studied with Mica Track Detectors

B

Ehsan Ullah Khan, P. Vater, R. Beckmann, R. Brandt
Kernchemie, FB 14, Philipps-Universität, 3550 Marburg

Since many years we study the multifragment break-up in interactions of uranium with uranium using mica track detectors. Our technique is particularly well-suited for high-multiplicity events: for example, we can study 5 fission fragments in the exit channel - such a high multiplicity cannot be investigated using electronic counters. Here we report on first results using the highest uranium energy at the GSI; i.e. 16.7 MeV/u ^{238}U irradiations.

We employed the well known 2π-geometry technique[1-3]. All heavy reaction products with m > 30 u focussed into the forward hemisphere have been registered in mica. After scanning about 92 cm^2 area of mica detectors we observed almost 1300 three-, four- and five-pronged events. The total reaction cross-section σ_R as well as reaction cross-section σ_3, σ_4 and σ_5 for three, four and five heavy fragments in the exit channel have been evaluated. Results are shown in the table.

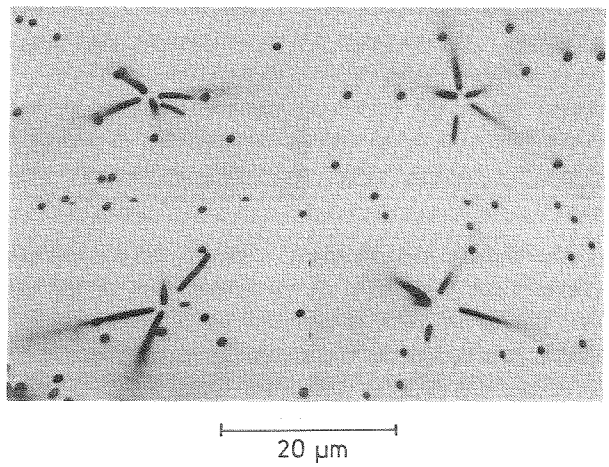


Fig. 1: Typical examples of five-pronged events, quite abundantly observed in the interaction of 16.7 MeV/u ^{238}U + ^{nat}U using mica track detectors.

Most interesting is the observation of 23 five-prong events (fig. 1) yielding σ_5 = 75 ± 45 mb which is about 2 % σ_R. This means, we now have observed a substancial number of five-pronged events. It is also interesting to compare the present U + U reaction with those at the lower energies: 9.03 MeV/u[4] and 7.5 MeV/u (see table).

The next major observation is the total reaction cross-section. The observed value is $\sigma_R > (4220 \pm 580)$ mb.

The theoretical reaction cross-section, calculated using radius parameter r_0 = 1.396 fm is σ_R = 6089 mb which is about 30 % too high as compared to our observed cross-section. Similarly cross-section calculated from the trajectory calculations[5] is again about 33 % higher as compared to our observed one. Our observed cross-section includes only three, four and five prong events. In addition, we observe many two prong events, a number of them appear to be due to inelastic interactions. Therefore, we intend to analyse all observed binary events to look for the cross section of inelastic binaries which may partly then explain the difference between total theoretical and total observed reaction cross-section.

In further studies we will interpret the observation of many-pronged events in terms of the "sequential fission" process, described earlier for the interaction of (10 MeV/u Kr + ^{nat}U)[1,6].

1 P. Vater et al., Phys.Rev.Lett. 39 (1977) 594
2 P.A. Gottschalk et al., Phys.Rev.Lett. 42 (1979) 359
3 R. Brandt et al., NIM 173 (1980) 111
4 P. Vater et al. (in preparation)
5 W. Westmeier (Marburg) Private communication
6 P.A. Gottschalk et al., submitted for publication

Table: Summary of the results in the study of uranium-on-uranium using mica track detectors.

Reaction	Total Reaction Cross-section σ_R/mb Theo.	Exp.	σ_3/mb	σ_4/mb	σ_5/mb	σ_3/σ_R	σ_4/σ_R	σ_5/σ_R	σ_3/σ_4	Number of 5-pronged events*
7.5 MeV/u U + U	1990	> 1775 ±290	918±105	844±101	12 ± 8	∿52 %	∿47 %	∿1 %	1.1	2 (1)
9.03 MeV/u U + U	3250	> 3260 ±780	1280±430	1970±590	14±10	∿39 %	∿60.5%	∿0.5%	0.6	2 (2)
16.72 MeV/u U + U	6089	> 4220 ±580	2620±390	1525±260	75±45	∿62 %	∿36 %	∿2 %	1.7	23 (10)

*(in paranthesis: number of indirect events (Ref. 1))

MULTIFRAGMENT-EMISSION-CROSS-SECTIONS IN THE REACTION "$^{238}U + ^{197}Au$" FOR ^{238}U ION ENERGIES OF 10 MeV/n AND 16.7 MeV/n

HAMEED A. KHAN, REINHARD BRANDT*, NAEEM A. KHAN, KHALID JAMIL,
M. ASLAM SIAL & GULZAR HUSSAIN

Nuclear Engineering Division
Pakistan Institute of Nuclear Science and Technology (PINSTECH)
P.O. Nilore, Rawalpindi, PAKISTAN

The 2 π-geometry technique using mica Solid State Nuclear Track Detectors (SSNTD) has been employed for the determination of multifragment emission cross-sections in heavy ion reactions [1-5]. In the present work, we have used mica and CR-39 plastic track detector for the determination of cross-sections for three-, four- & five-fragment emission in the exit channel of "$^{238}U + ^{192}Au$" for ^{238}U ion energies of 10 MeV/n and 16.7 MeV/n.

The gold target was vacuum deposited on preannealed mica and CR-39 (Homalite) track detectors. These detectors were then irradiated with 10.0 MeV/n and 16.7 MeV/n ^{238}U ions at GSI (Darmstadt). After removing the target coating the mica track detector was etched in 48% HF acid for 8 minutes at room temperature. The CR-39 track detector was etched in 6N NaOH for 30 minutes at 70 ± 1°C. The detectors were scanned for events resulting in the emission of multifragments. In the case of "$^{238}U + ^{197}Au$" reaction for ^{238}U-ion energy of 10.0 MeV/n, the maximum multiplicity of reaction products was observed to be four. However, for 16.7 MeV/n energy, we have observed not only three-and four-fragment events but also a number of five-prong events on mica & CR-39 track detectors. Fig.1 shows one of these five-prong events as observed on CR-39.

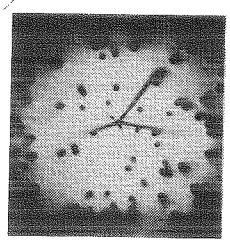


Fig.1

Emission of five heavy reaction products in '16.7 MeV/n $^{238}U+^{197}Au$' reaction

The etching conditions of the detector were such that the latent damage trails due to only heavy particles could be etched in it.

The results have been summarized in Table 1. These cross-sections are slightly under estimated because of the fact that the determination of the contribution of "indirect" events could not yet been finalized. Comparison of the results obtained by using mica and CR-39 track detectors (Table 1) shows relatively higher cross-section values for the emission of four-and five-fragments obtained by using a CR-39 detector. This is due to the fact that the particle registration threshold of CR-39 is lower than that of the mica detector[6].

Table:1

Energy/n (MeV)	Detector	Cross-section (mb)		
		3- Frag-ments.	4-Frag-ments	5-Frag-ments
10	Mica	1811±138	489±72	<11
16.7	Mica	3396±231	363±76	47±27
16.7	CR-39	2786±297	1077±184	253±89

Under the presently employed etching conditions for CR-39, the latent damage trails of low energy ^{16}O ions can be developed in it [6]. On the other hand, the mica detector registers particles only heavier than silicon. The difference in the two sets of the results suggests that quite significant number of low energy fragments having masses between ^{16}O and ^{28}Si are emitted in the above reaction. Table 1 also indicates that, in general, the partial cross-sections for multifragment increases with increasing energy of the projectiles. This is, perhaps, due to the fact that momentum transfer in the forward direction is an increasing function of energy in the present energy range. Further work is under progress.

The authors wish to thank Mr. H. Folger and his colleagues for their help in the preparation of the targets. One of us (HAK) is grateful to Alexander Von Humboldt Foundation for the financial support during his stay at Marburg as AVH-Fellow (1981-82).

REFERENCES

1. P. Vater, H.J-Becker, and R. Brandt: Physics Rev. Letters 39 (1977) 594.
2. R. Brandt, P.A. Gottschalk, and P. Vater: Nuclear Instruments & Methods 173 (1980) 111.
3. P. Vater, H.J. Becker, R. Brandt and H. Freiesteben: Nuclear Instruments & Methods 147 (1977) 271.
4. P. Vater, H.J. Becker, R. Brandt and H. Freiesteben: Physics Rev. Letters 39 (1977) 594.
5. P.A. Gottschalk, P. Vater, H.-J. Becker, R. Brandt, G. Grawert, G. Fiedler, R. Haag and T. Rautenberg, Physics Rev. 42 (1979) 359
6. H.A.Khan, R.Brandt, N.A. Khan, and K. Jamil: Submitted for publication.

* Kernchemie, F.B.14, Philipps Universitat, 3550-Marburg (Lahn), West Germany

Evidence of a new type of fission within a solid state nuclear detector

M. Debeauvais, J. Ralarosy, J. Tripier, S. Jokic
Centre de Recherches Nucléaires, 67037 Strasbourg Cedex, France

Characteristics of the new events

A schematic diagram of the new events is presented in figure 1. In figure 2 is given a photograph of the tracks of these events projected on the plane of the detector. Tracks are identified as follows : number "1" represents the recoil nucleus ; number "2" is the scattered ion before its decay and numbers "3" and "4" are the fragments issuing from the break-up. The characteristics of these correlated tracks are given in table 1.

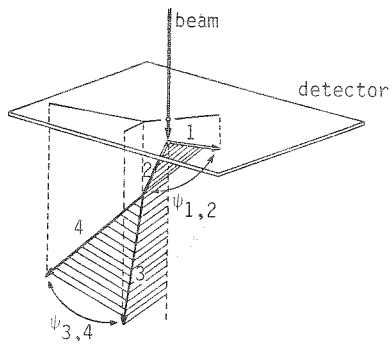


Fig. 1 - Schematic diagram of a typical new event

Table 1 - Characteristics of the 3 correlated tracks of new events

Projectile + target	Range in µm				Lifetime of the scattered nucleus (in s)	Space angle	
	R_1	R_2	R_3	R_4		$\psi_{1,2}$	$\psi_{3,4}$
U + U	15	12	94	88	0.3×10^{-12}	90°	38°
U + Pb	6	32	110	63	0.8×10^{-12}	90°	39°
U + Au	8	45	153	52	1.2×10^{-12}	85°	38°

Discussion

Several tentative suggestions can be advanced to explain these observations :

- that these events be elastic collisions of uranium upon nuclei of the detector. However, this hypothesis is very improbable because MAKROFOL is a polycarbonate and thus collisions would occur with light nuclei only. Oxygen and carbon tracks longer than $\sim$ 12 µm cannot be recorded within this threshold detector in the standard chemical etchings used. Moreover, the angle $\psi_{3,4}$ does not agree with an elastic collision.
- that these events be nuclear reactions of the scattered uranium with a carbon or an oxygen nucleus of the detector, since the cross section is not completely negligible.

Theoretically, the number of nuclear interactions of the scattered uranium with a nucleus of the detector is calculated to be 0.18. In fact, we experimentally found 3 events, or 16 times more. In addition, the decay of of the scattered uranium nuclei occured after path lengths of 12, 32 and 45 µm inside the detector so that the residual energies which eventually would induce fission are close to the fission barriers and thus the probability of forming a compound nucleus is very small.

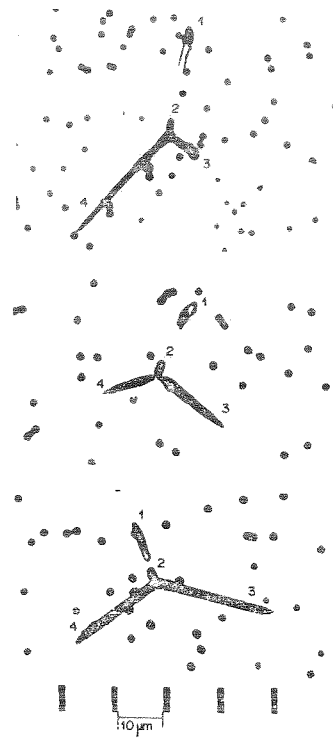


Fig. 2 - Photograph of the three tracks of new events projected on the detector plane.

Since above hypotheses are not totally adequate, we propose that the events can be some type of isomeric fission whose lifetime is of the order of picoseconds. If the branching ratios of these three events relative to that of the prompt fissions is calculated, a value of 3×10^{-3} is found. At first glance, this value seems too high in comparison with that usually given in the literature, which is of the order of 10^{-5}. Nevertheless, when reference is made to the data of P Limkilde et al [1] concerning two isomers of ^{238}Pu it can be pointed out that the branching ratio increases noticeably as the isomer lifetime decreases. The maximum of this ratio is $\sim 2 \times 10^{-5}$ for ^{238}Pu isomer whose lifetime is 0.5×10^{-9} s and 10^{-6} for that whose lifetime is 5×10^{-9} s. Provided that extrapolation of these results is valid, the branching ratio for an isomer whose lifetime is $\sim 10^{-12}$ s would be $\sim 10^{-3}$. This would agree with the values we found and thus is in favour of our proposition.

References

[1] Limkilde P., SLETTEN G., Nucl. Phys. A 199 (1973) 504-512.

Impact Parameter Determination and Event-Types in ^{18}O induced Reactions at 84 MeV/u.

B

I.Bock, U.Lynen, MPI Heidelberg
D.Pelte, U.Winkler, Universität Heidelberg
R.Glasow, K.H.Kampert, R.Santo, Universität Münster
W.F.J.Müller, A.Gobbi, K.D.Hildenbrand, A.Olmi, H.Sann, H.Stelzer, GSI Darmstadt

Reactions induced by ^{12}C and ^{18}O projectiles of 60 to 84 MeV/u on targets between Ni and U have been studied at the CERN synchrocyclotron. The experimental set-up has been improved to allow, as far as possible, the simultaneous measurement of all reaction channels. Especially the detection thresholds have been lowered to improve the sensitivity for light or slow fragments. The plastic scintillator hodoscope is now divided into 20 segments in order to obtain a better multiplicity resolution in central collisions.

In reactions with heavy targets three event-types can be distinguished (the given cross sections refer to ^{12}C + ^{197}Au at 84 MeV/u):

1. no heavy fragment; emission of few p or α (2000 mb)
2. two heavy fission-like fragments (700 mb)
3. one medium-heavy fragment with 10≤A≤40 (300 mb)

Information about the impact parameter can be deduced from the charge of projectile fragments seen close to the beam direction. Fig. 1 shows the distribution of the total charge of projectile fragments found between 1.5° and 10° for the mentioned event-types. In case of type 1 the distributions have been further distinguished according to the multiplicity of light particles (M_{PLA}) emitted from the target.

The steep distribution for type 3 indicates, that medium-heavy fragments are produced in the most central collisions. The relative flat distributions for type 1 show, that those interactions are more peripheral. The high probability at Z=0 (no fragment seen) for M_{PLA} = 1,2 can be explained by the assumption, that in the most peripheral interactions the projectile fragments escape through the beam tube aperture of ±1.5°.

The intermediate behavior for type 2 and the cross sections lead to an average impact-parameter of ~ 5 fm for fission. This corresponds to collisions where the impinging ^{18}O-projectile has full overlap with the Au-target. In more peripheral collisions the incoming orbital angular momentum is much larger, but it is obviously not possible to transfer a sufficient amount to the target nucleus. In the reaction ^{12}C + ^{197}Au the linear momentum transfer is 1.6 GeV/c for the fission component, corresponding to ~ 35% of the beam momentum.

This value is rather small, if we take into account that at an average impact parameter of 5 fm projectile and target have full overlap. This indicates a non-negligible transparency at these energies even for these heavy nuclei.

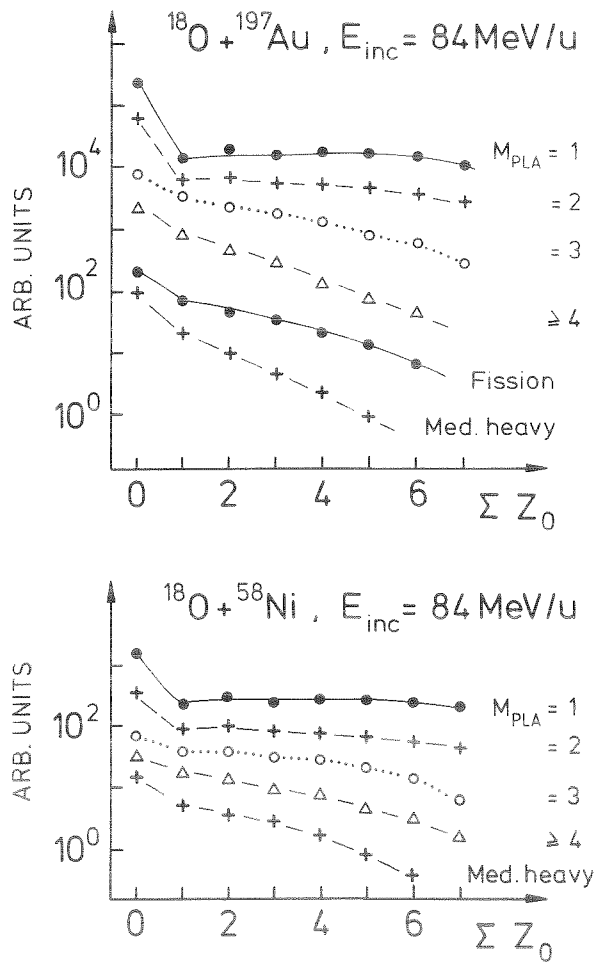


Fig 1: Distribution of the total charge of projectile fragments for different event-types.

Light Particle Emission in Reactions with 84 MeV/u ^{12}C- and ^{18}O-Projectiles

B

R. Glasow, K.H. Kampert, R. Santo
IKP, Universität Münster

I. Bock, H. Ho, W. Kühn, U. Lynen
MPI Heidelberg

D. Pelte, U. Winkler
Universität Heidelberg

A. Gobbi, K.D. Hildenbrand, W.F.J. Müller, A. Olmi, H. Sann, H. Stelzer
GSI Darmstadt

At the CERN-SC, light particle spectra of 84 MeV/u ^{12}C and ^{18}O induced reactions have been investigated by use of 3 detector telescopes, consisting of 2000 µm Si-surface barrier-detectors (ΔE) and 8 cm thick NaJ-scintillation counters (E_{Rest}). The data exhibit the typical behaviour known from relativistic energies: an exponential-like shape of the energy spectra and a forward peaked angular distribution.

In Fig. 1 proton spectra from the reactions $^{12}C+^{58}Ni$ at 84 MeV/u incident energy are shown (symbols). The data are described in the framework of a "moving source" parametrization, assuming three moving sources which emit particles isotropically in their own rest frame according to a Maxwell-Boltzmann distribution[1]. Fits to the data (solid lines) yield the following characteristics:

- a "projectile-like" source moving with about projectile velocity having a temperature between about 10 and 15 MeV,
- an "intermediate" source moving with slightly less than half the projectile velocity having a temperature of about 19 MeV,
- a "target-like" source moving with slightly less than the compound-nucleus velocity having a temperature of about 7 MeV.

The high temperature of the "intermediate" source cannot be explained by compound nucleus evaporation, which would result in much lower values. It rather suggests the emission from a local zone of hot nuclear matter ("hot spot"), which is also supported by a source velocity near to that of the nucleon-nucleon center of mass frame instead of the compound-nucleus velocity.

In Fig. 2 p,d, and t-spectra of ^{12}C and ^{18}O induced reactions on the same target are compared at $\Theta_{Lab}=54°$. In both cases the spectral shapes are nearly identical resulting in similar temperatures. The composite particle to proton ratios, however, are enhanced in reactions with the neutron-rich ^{18}O-beam, as well as of neutron excess targets (see table I).

In order to get a deeper insight into the reaction mechanism, it is useful to classify the light particle production according to the momentum transfer to the target. A promising tool for this purpose is the light-charged-particle multiplicity observed in the "Light-Ion-Hodoscope" (LIH), consisting of 20 plastic-scintillators covering about one half of the total solid angle. Table II exhibits an enhancement of the light particle to proton ratios with increasing multiplicity, suggesting that the composite particles are preferably produced in more violent collisions. A more detailed analysis is in progress.

[1] R. Glasow et al., Phys.Lett. 120B (1983) 71

Table I: Composite particle to proton ratios at $\Theta_{Lab}=54°$

reaction	d/p	t/p	^3He/p	α/p
$^{12}C+^{58}Ni$	0.29	0.060	0.020	0.019
$^{12}C+^{64}Ni$	0.32	0.086	0.018	0.019
$^{18}O+^{58}Ni$	0.30	0.073	0.022	0.025
$^{18}O+^{64}Ni$	0.38	0.12	0.019	0.025

Table II: Composite particle to proton ratios x/p of the reaction $^{12}C+^{58}Ni$ at $\Theta_{Lab}=54°$ as a function of the experimental multiplicity in the LIH.

x/p	0	1	2	3	≥ 4
d	0.24	0.26	0.29	0.31	0.33
t	0.044	0.056	0.070	0.071	0.091
^3He	0.012	0.018	0.018	0.018	0.025
α	0.010	0.013	0.021	0.021	0.023

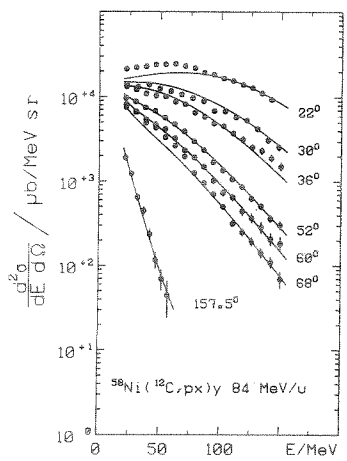


Fig. 1: Proton spectra of the reaction $^{12}C+^{58}Ni$ with "moving source" fits (solid lines)

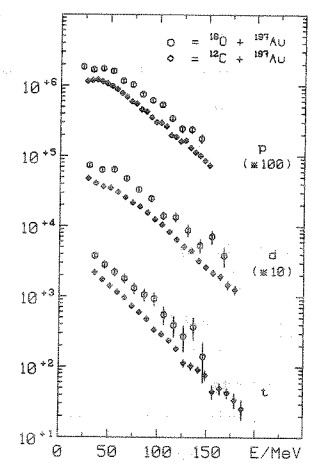


Fig. 2: p-,d- and t-spectra produced by ^{12}C- and ^{18}O beam on a ^{197}Au target

Reaction Channels in the Interaction of 84 MeV/u-^{12}C with ^{208}Pb [B]

B. Grabez, R. Beckmann, P. Vater, R. Brandt
Kernchemie, FB 14, Philipps-Universität, 3550 Marburg

The interaction of 84 MeV/u-^{12}C (from CERN-SC) with ^{208}Pb was investigated using CR-39 plastic track detectors in the 4π-geometry. The identification of target fragments was carried out by measurement onto the finished tracks[1]. Calibration was made with heavy ions ranging from the well-defined ions up to ^{238}U from the GSI and from other accelerators. The available charge resolution in our experiment was: $\Delta Z < 1$ for fragments with $Z < 30$, $\Delta Z \leq 2$ for heavier fragments up to uranium with energy E/A > 0.5 MeV/u and $\Delta Z \leq 4$ for heavy fragments with energy E/A ≤ 0.5 MeV/u.

The main reaction channels are found to be fission (σ_f = 710 ± 30 mb), binary break-up - or fragmentation - characterized by the presence of one fragment with $5 \leq Z \leq 26$ and a heavy fragment ($Z > 50$) in correlation (σ_{fr} = 830 ± 70 mb) and heavy target spallation recoils i.e. only one fragment with $Z \geq 30$ (σ_s = 1650 ± 50 mb). In about 12 % of cases fission is accompanied with a low energy α-particle. The contribution of events with three target fragments having $Z \geq 3$ is less than 1 % of total reaction cross section and comes mainly from double fragmentation or evaporation.

Fig. 1 shows the distribution of energy per nucleon (E/A) integrated over atomic numbers for light fragments with $5 \leq Z \leq 26$. The distribution has a shape typical for fragmentation with the peak near the Coulomb barrier and exponential decrease towards higher energies. The relative small width of the distribution indicates the same production mechanism for fragments in this charge interval. Taking into account also kinematical characteristics of their heavy partners we found that average transfer of longitudinal momentum for this reaction channel was 2270 MeV/c.

The distribution of energy pro nucleon for spallation recoils ($Z \geq 30$) is presented in Fig. 2. Of special interest is that among these target spallation recoils we found nuclei which correspond to a loss of 50 - 100 nucleons from target. Those nuclei have recoil energy between 0.5 - 2.5 MeV/u. The production of such nuclei can't be explained by cascade-evaporation model at our projectile energy. The high recoil energy and big nucleon loss exclude quasi-compound nucleus formation used by Blachot et al.[2] for explanation of some products in 84 MeV/u-^{12}C + Ag interaction. The possible origin of products observed in our experiment is in the small impact parameter collision during which large volume hot zone is formed as supposed in ref. 3. Desintegration of hot zone followed by evaporation from equilibrated cold part leads to high multiplicity of emitted nucleons. We measured cross section of (480 ± 100) mb for spallation recoils having $31 \leq Z \leq 66$. This corresponds to interaction with high multiplicity of emitted nucleons. Further investigations to elucidate reaction mechanism are in progress.

[1] B. Grabez et al., NIM (in print)

[2] J. Blachot et al., Zeitschr. f. Phys. A303, 85 (1981)

[3] A.Q.T. Karvinen et al., Nucl. Phys. A367, 122 (1981)

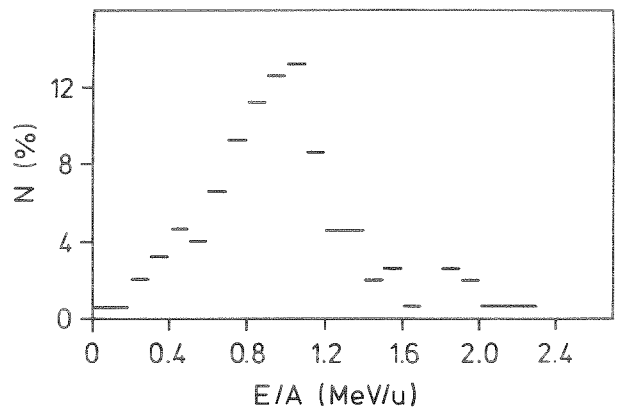


Fig. 1: Distribution of energy-per-nucleon (E/A) for light fragments with $5 \leq Z \leq 26$.

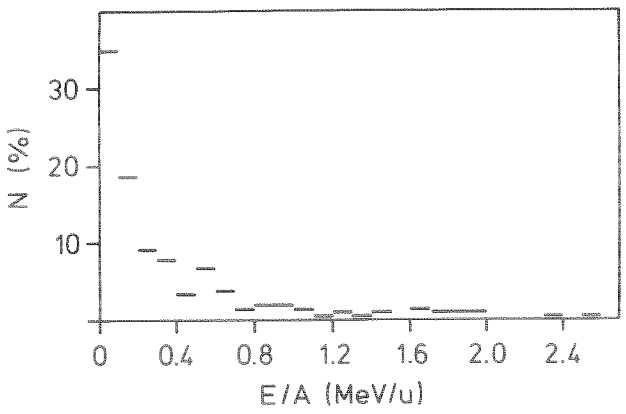


Fig. 2: Distribution of energy-per-nucleon (E/A) for single spallation residuals with $Z \geq 30$.

Radiochemical Studies of Transtarget Nuclei in the Reaction Pb(Bi) + 86 MeV/u ^{12}C B

T. Lund, D. Molzahn, R. Brandt, Kernchemie, FB 14, Philipps-Universität, 3550 Marburg
E. Hagebø, I. Haldorsen, Dept. of Chemistry, University of Oslo
C. R.-Serre, CERN, Genf
and the ISOLDE Collaboration

We present below some results obtained in a radiochemical study of the reactions between lead and bismuth and 86 MeV/u ^{12}C, obtained from the CERN-SC.

The mass yield distribution shows basically two reaction channels, fission and spallation. A third part of the distribution are transtarget (in Z) products, i.e. reactions where one or more projectile protons have been accepted by the target nucleus. To obtain these data we bombarded thin lead or bismuth targets ($\sim$ 100 µg/cm^2) evaporated on Al-backing. The irradiated targets were measured with surface barrier detectors and the alpha-active nuclides of the elements Po, At and Rn were investigated. The measurements could be started about fifteen minutes after end of bombardment. The transtarget nuclides were identified by α-energy and half-life and the end of bombardment activities determined by standard methods. The yields of Bi-nuclides were obtained by γ-measurements of thick targets ($\sim$ 40 mg/cm^2). In both cases the beam was monitored by the reaction $^{27}Al + ^{24}Na$ in order to obtain absolute yields.

The data for +1 Z-transfer products are shown in Fig. 1. For both Pb- and Bi-targets the yield distributions peak at 40 mb. The yields of 2 Z-transfer products (Fig. 2), represented by the data for lead target, are approaching 10 mb at the peak. The yields are substantially higher than found for relativistic heavy ions. Up to 4 Z-transfer products have been observed.[1] In total we measure about 250 mb for transfer products. This equals about 7 % of the total reaction cross section. We have found that the recoil ranges of these products are very short, implying that they are produced in reactions with low excitation energies involved.

This might also be read from the isotopic yield distributions, which are peaking at masses 4 - 5 mass units lighter than the target mass. The low momentum transferred (and the low excitation energies) show that the most likely process is absorption of single protons before deexcitation. Reactions where projectile clusters (α, Li) are involved would leave systems with higher excitation energy and increase the fission probability.

[1] D. Molzahn et al., Radioanal. Chem. (in print)

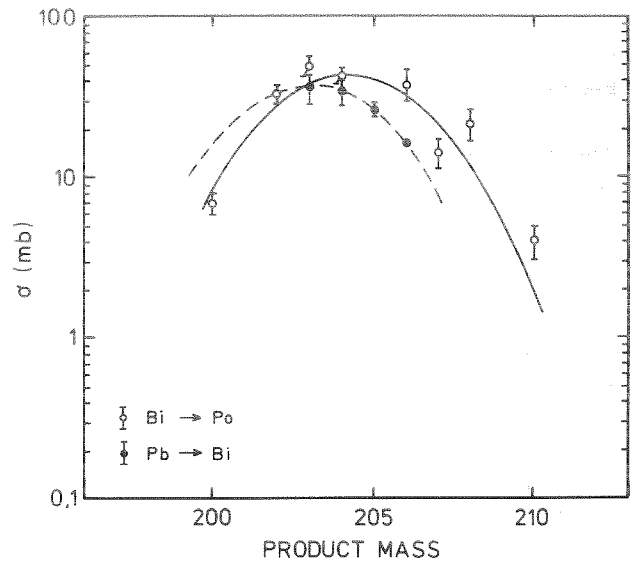


Fig. 1: Yields of 1 Z-transfer products for the reaction between Pb (dashed curve), Bi (full curve) and 86 MeV/u ^{12}C. The curves are fitted Gaussians to data points.

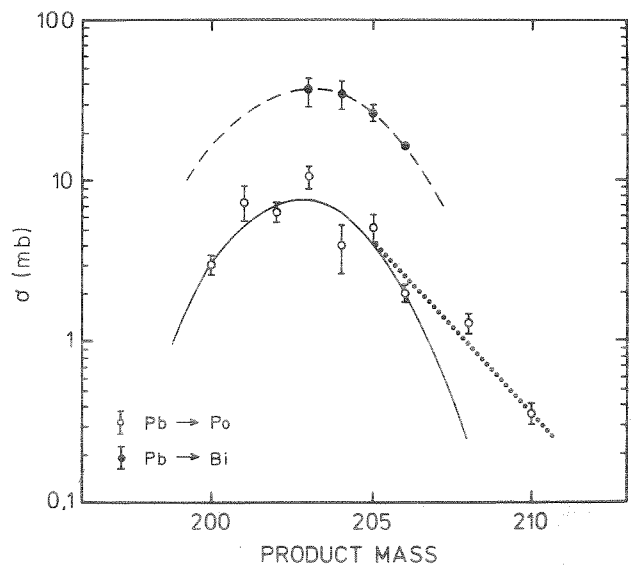


Fig. 2: Yields of +1 Z and +2 Z transfer products in the reaction between Pb and 86 meV/u ^{12}C.

Cooperative Effects observed in the neutral pion production from nucleus nucleus collisions

H. Noll - IKF Universität Frankfurt;
H. Dabrowski, E. Grosse, H. Heckwolf, O. Klepper, C. Michel, W.F.J. Müller, H. Stelzer - GSI
C. Brendel, W. Rösch - TH Darmstadt; P. Braun-Munzinger - SUNY Stony Brook (NY), USA

Pions represent a unique probe for the study of heavy ion reactions at higher energies since they are produced by the participant parts of the colliding nuclei and originate solely from the internuclear collision zone. Neutral pions are especially well suited as probing particles because they do not experience the final state interaction caused by the Coulomb field of the collision fragments. The fast decay of the π^0's into two gamma rays allows their detection independent of their kinetic energy.

With the π^0 spectrometer developed at Darmstadt[1] we took data at the ^{12}C beam of the CERN synchrocyclotron using energies of 60, 74 and 84 MeV/u and targets of C, Al, Ti, Ni, Sn, Ta, Pb and U. The inclusive energy and angle integrated cross sections for π^0 production at 84 MeV/u are plotted in fig. 1 versus the target mass. These data as well as those taken at the other energies show the feature, that , when normalized to the point for A=27, the cross section increases much slower than linearly with target mass; the dotted line proportional to the number[2] of the participant nucleons also overpredicts the cross section at large A considerably. The data are reasonably well reproduced by the lower line representing the nuclear surface $A^{2/3}$, indicating a production by the two nuclei as a whole; the importance of pion reabsorption in heavier mass nuclei - which would strongly influence the A-dependence - is not obvious since the mean free path of such low energy pions is not well known, but probably rather large[3].

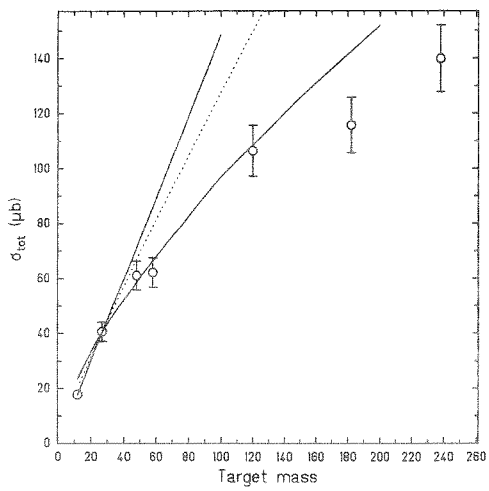


Fig.1: Dependence of the integrated pion production cross section on the target mass

A further indication for a cooperative production of the pions from the two interacting nuclei - as compared to a production in nucleon-nucleon collisions - comes from the π^0 angular distributions as shown in fig. 2 in the form of a dependence of the production yield on the longitudinal and transverse pion momentum. The curves of equal cross section are nearly circles indicating a rather weak emission anisotropy; in the case of C + C they are well centered around the point corresponding to the emission from the center of mass system, as they should be for identical target and projectile. The data obtained in the bombardment of U are rather well described as forward-backward symmetric emission from a source which is only slightly (i.e. by $\Delta\beta \approx 0.04$) faster than the nucleus-nucleus center of mass system; the nucleon-nucleon system is by far too fast ($\Delta\beta \approx 0.14$) to be identified with the emitting source. Since a nearly complete rescattering of the pions in the remnants of the target seems to be unlikely due to their large mean free path (cf. above), we consider the data a proof for the cooperative production of at least most of the pions from the two nuclei as a whole.

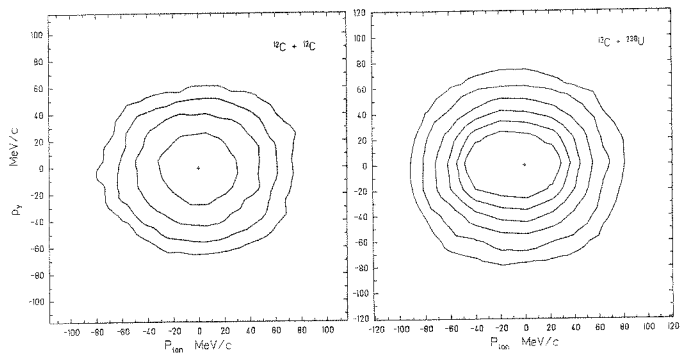


Fig.2: Cross section dependence on logitudinal and transverse momentum of the pion in the N-N-system

The steep fall-off in the spectra suggests a description on the basis of a thermal emission process. A respective analysis[4] allows to determine how much temperature was gained from freezing degreees of freedom in the final state. From our data it is obvious, that the amount of this freezing increases with decreasing beam energy; we thus conclude, that the completely coherent pionic fusion process can be observed more easily at lower bombarding energies. At 60 MeV/u the coherent limit has been missed in the pion spectra by only 50 MeV; to produce pions of the highest energy observed the collaboration of at least half of the target and half of the projectile nucleons is needed. In planned experiments with lower beam energies the sensitivity to cooperative effects should be higher; probably they even allow to observe coherently produced pions at the kinematical limit.

1) Ch. Michel et al., this report
2) J. Hüfner and J. Knoll, Nucl.Phys.A290(77)460
3) K. Nakai et al., Phys.Rev.Lett. 44(79)1446
4) J. Knoll and R. Shyam, this report.

G

Pion Multiplicity in Relativistic Heavy Ion Collisions as a Probe of Nuclear Compression

R Stock[1], R. Bock[1], R. Brockmann[1], A Dacal[2], J.W. Harris[1], M. Maier[3], M.E. Ortiz[2], H.G. Pugh[4], R.E. Renfordt[5], A. Sandoval[1], L.S. Schroeder[4], H. Ströbele[1] and K.L. Wolf[6]

(1) GSI Darmstadt; (2) Instituto de Fisica, UNAM, Mexico City; (3) FB Physik, Univ. Marburg; (4) LBL Berkeley; (5) Institut für Hochenergiephysik, Univ. Heidelberg; (5) Physics-Department, Texas A&M University

Negative pion multiplicities were measured at the Bevalac using a streamer chamber. The systems ^{4}He + KCl, ^{40}Ar + KCl and ^{40}Ar + BaI_2 were studied, both in dependence on the incident energy, ranging from 0.36 to 1.8 GeV/A, and on the impact parameter, as determined from the multiplicity of charged reaction products as measured simultaneously for each event[1]. The total pion yield produced in the state of maximum energy density, is suited for an analysis of the compressional energy. The reason why such a simple variable can be a measure of the compression stage is an interplay of three considerations. Firstly, the primary production yield in nucleon-nucleon collisions in the Bevalac energy range is a rapidly rising function of energy. Secondly, the relative nucleon-nucleon energy in the nucleus-nucleus collision is degraded during the compression state and is low by the time expansion begins. Thus, pion production is heavily weighted towards the compression stage. Finally, even though complex interactions during the expansion stage strongly affect differential pion observables such as angular distributions, spectra, etc., it appears that the total number of pions and delta-resonance, and hence the eventual pion yield, remains approximately constant. This observation is made both in cascade[2] and hadrochemical[3] model calculations. We used the cascade code of Cugnon et al.[2] to compare to our data.

Fig. 1 shows the maximum compression as a function of the incident energy, predicted by the cascade model for Ar + KCl. Also shown is the mean compression, as weighted by the rate of π/Δ production. Compressions from 2.5 to about four times normal nuclear matter density are encountered. Fig. 2 shows a comparison of the predicted and observed negative pion multiplicities, for a "central trigger" experiemnt. The cascade model prediction is systematically too high, with overestimates ranging from a factor of 4 at 360 MeV/A to 1.35 at 1.8 GeV/A. We interpret this failure as an effect of the nuclear medium at high density, not contained in a model incorporating only binary, quasi-free interactions of hadrons. One possible effect, in particular, would be the sharing of the original incident energy between thermal and compressional degrees of freedom. An estimate of the latter fraction of the total c.m. energy per baryon is obtained from Fig. 2, assuming that the cascade model reveals the amount of thermal energy, necessary to produce the observed pion yield at each of the experiment energies. Comparison of the c.m. energies per nucleon at equal $\langle m^{\pi} \rangle$ in experiment and cascade model leads to the compressional energy per nucleon, as given in Fig. 3. This nuclear "equation of state" is of parabolical shape, with K=240 MeV.

This method is now being extended to a wider set of colliding nuclear systems.

[1] R. Stock et al., Phys.Rev.Lett.49(1982)1236
[2] J. Cugnon et al., Nucl.Phys, A379(1982)553
[3] I. Montvay and J. Zimanyi, Nucl.Phys. A316(1979)490.

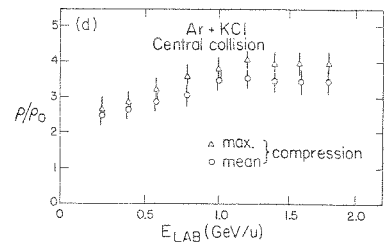


Abb. 1

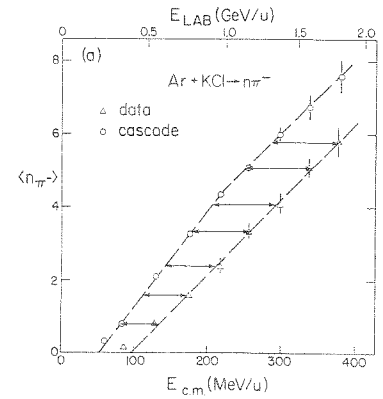


Abb. 2

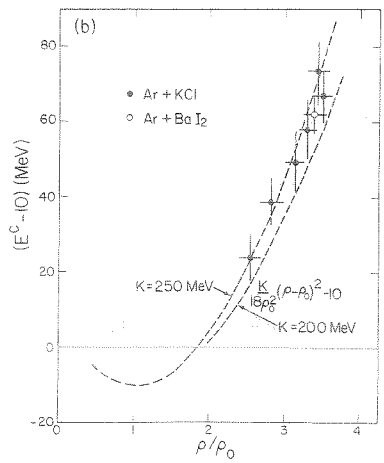


Abb. 3

Impact parameter selection in central Ar + KCl reactions at 1.8 GeV/u [G]

R. Brockmann, J.W. Harris, M. Maier, H.G. Pugh, R.E. Renfordt, A. Sandoval,
D. Schall, L.S. Schroeder, R. Stock, H. Ströbele, K. Wolf
GSI Darmstadt - LBL Berkeley - Universität Heidelberg - Universität Marburg

The correlation between impact parameter and multiparticle observables has been studied for central Ar + KCl collisions at 1.8 GeV/u. Experimental data on this reaction channel are available from a Streamer Chamber exposure to the ^{40}Ar heavy ion beam at the BEVALAC. Central collisions were selected by a hardware trigger which requires the absence of a projectile fragment. A finer selection of impact parameter would provide additional information about reaction volume and number of participant nucleons. Certain multiparticle observables exhibit a direct correlation with the impact parameter providing an indirect measurement of the impact parameter. In order to find those observables which show a strong dependence on impact parameter one has to analyze results of model calculations (which are done for fixed impact parameters).

The intranuclear cascade code by Cugnon et al. was chosen to simulate Ar + KCl collisions, because the overall features of the sample thus generated agree with those of the experimental data. In the simulated event sample the variation of appropriate multiparticle observables with impact parameter was studied. The strongest correlation was found for the total transverse energy carried by all charged particles (n) as given by:

$$E_t = \sum_{i=1}^{n} (\sqrt{M_i^2 + p_i^2} - M_i\delta_i) \qquad \begin{matrix}\delta_i=0 \text{ for pions} \\ \delta_i=1 \text{ for protons}\end{matrix}$$

A further virtue of the quantity E_t is its insensitivity to the experimental biases. Fig. 1 shows the correlation between E_t and the impact parameter. The experimental, "central trigger" E_t distribution ranges from 3 GeV to 9 GeV with the maximum occuring at 6 GeV. The experimental data thus cover the impact parameter interval from 0 to 4 fm with a maximum weight at 1.8 fm.

In fig. 2 some multiparticle observables are plotted as functions of the impact parameter b (derived from E_t) for both the experimental data and the cascade events. It can be seen that the mean transverse pion momentum varies very little with b (fig. 2a) indicating that the degree of thermalization of pions is independent from b. On the other hand, both the mean transverse momentum of "high P_t" protons and the average number of charged pions per event show a clear dependence on the impact parameter, which suggests that not only the number of nucleon-nucleon collisions (governing the production of pions), but also the number of collisions per nucleon (governing the average transverse momentum) increase with decreasing impact parameter.

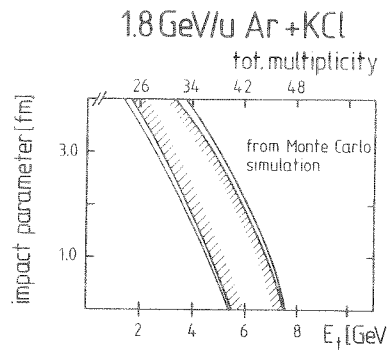


Fig. 1 Correlation between the total transverse energy E_t and the impact parameter b for cascade generated events; the hatched band corresponds to ±σ (rms deviation) of the E_t distribution at a given b.

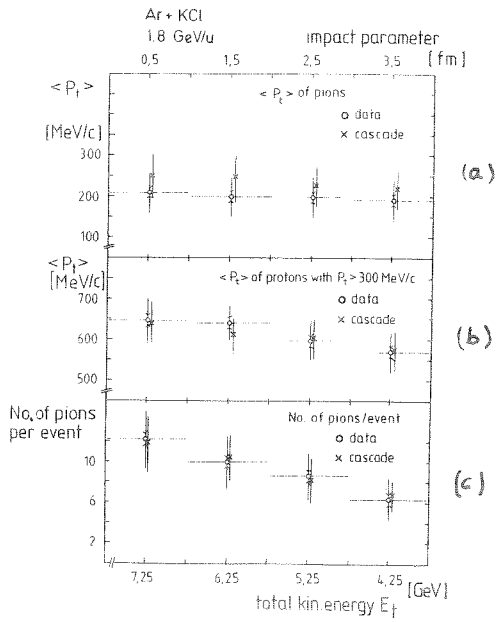


Fig. 2 Mean transverse momentum of pions (a), mean transverse momentum of "high P_t" protons (b) and average number of charged pions per event (c) as function of the impact parameter. The error bars give the rms deviation and the v-marks the error on the position of the maximum of the corresponding distributions.

Charged particle exclusive analysis of central Ar + KCl and Ar + Pb reactions at 1.8 and 0.8 GeV/u

G

H. Ströbele. R. Brockmann, J.W. Harris, M. Maier, F. Riess, A. Sandoval, R. Stock, K.L. Wolf, GSI Darmstadt

H.G. Pugh and L.S. Schroeder

Lawrence Berkeley Laboratory, University of California, Berkeley, California 94720

R.E. Renfordt, D. Schall and K. Tittel,

Institut für Hochenergiephysik, Universität Heidelberg

Our present understanding of the dynamics of relativistic nucleus-nucleus collisions is derived primarily from single particle inclusive measurements. Deeper insight into the interaction may be obtained by a study of multiparticle observables derived from all charged particles produced in these collisions. In this report we present the results of an analysis of charged particle exclusive data in terms of multiparticle variables[1]. Two types of reactions were studied: the near symmetric nuclear system ^{40}Ar + KCl at 1.808 GeV/u and the asymmetric nuclear system ^{40}Ar + Pb at 0.772 GeV/u.

The experiment was carried out using the Streamer Chamber facility at the Bevalac. The Streamer Chamber was triggered whenever a beam particle interacted in the chamber and the net charge of projectile fragments observed in the forward direction (± 8° in the laboratory) was $\Sigma Z_i^2 \leq 4$. In the present analysis 334 Ar + KCl events (~ 12000 tracks) and 102 Ar + Pb events (~ 5000 tracks) were processed by measuring all tracks in three views on film. On line geometrical reconstruction in three dimensions kept measuring losses below 10% of all tracks. Magnetic rigidity, ionization density, and phase space considerations permitted identification of all π^-, 95% of protons, deuterons, and tritons and separation of π^+ from baryons for momenta below 550 MeV/c. Misidentification of π^+ is estimated to be less than 15 %. A detailed analysis of the momentum flux pattern on an event by event basis was performed utilizing the normalized momentum flux tensor,

$$T_{ij} = \left(\sum_\nu p_{\nu i} p_{\nu j} |p_\nu|^{-1}\right)\left(\sum_\nu |p_\nu|\right)^{-1}, \qquad i,j = x,y,z$$

with $p_{\nu i}$ and $p_{\nu j}$ the cartesian components of the c.m. momentum of particle ν and p_ν its total c.m. momentum. The normalized eigenvalues and eigenvectors of T_{ij} define the event shape. Events were classified using the cosine of the angle θ of the main tensor axis with respect to the beam direction.

Fig. 1 shows the cos θ distributions for Ar + KCl and Ar + Pb. The Ar + Pb events are distributed over a broader range of angles. If a further selection is made for small impact parameters (fig. 1b) the experimentally observed distribution is nearly isotropic. Better statistics are needed to decide about the existence of a hydrodynamical sidewards jet, as predicted by Stöcker et al.[2]. The cascade model of Cugnon et al.[3] predicts a forward elongated momentum distribution for this reaction even for zero impact parameter.

The Ar + KCl events are aligned along the beam direction, which implies a forward elongation of the shape of the momentum tensor. The cascade model reproduces the data qualitatively, again with a slight over-estimate of the elongation. Further studies with this model suggest that the observed forward elongation is due primarily to nucleons in the surface "corona" regions of the colliding mass 40 nuclei. Even as b approaches zero these nucleons cause an elongation of the momentum flux tensor along the beam direction. This effect is thus a trivial geometrical transparency.

[1] H. Ströbele et al., to appear in Phys.Rev.C, April 83
[2] H. Stöcker et al., Phys.Rev.C25(1982)1873 [3] J. Cugnon et al., Nucl.Phys.A379(1982)553

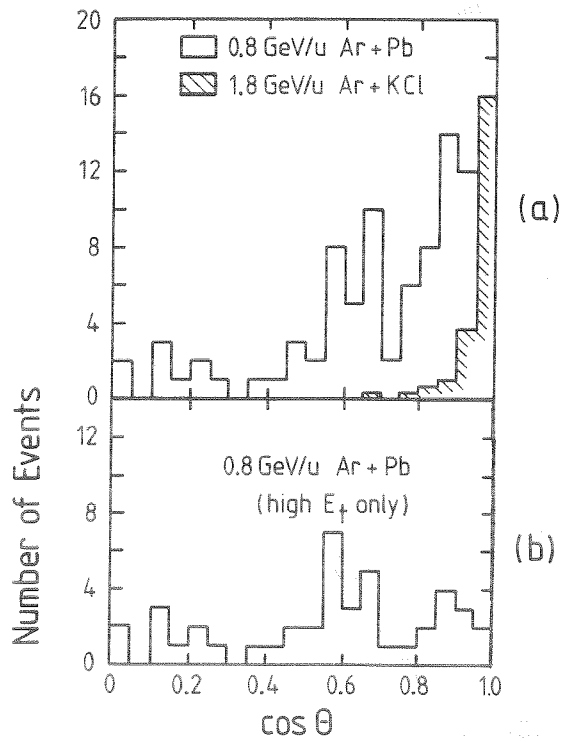


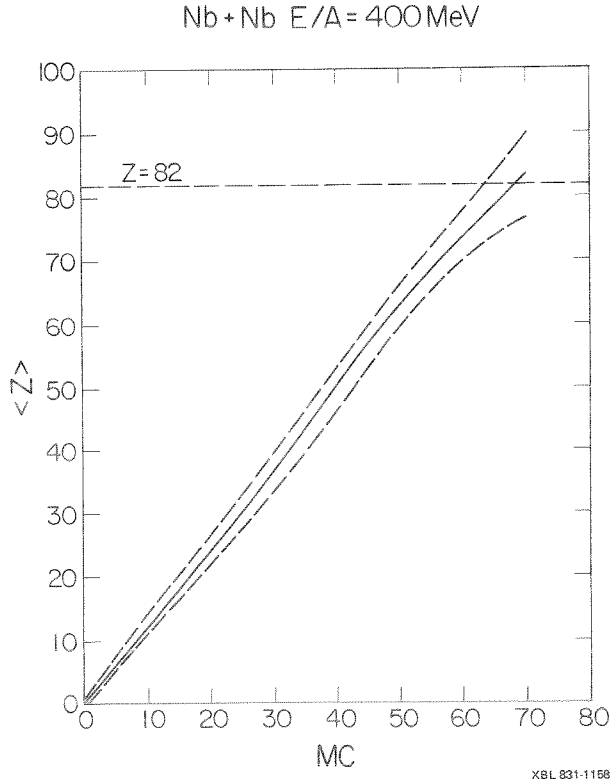
Fig. 1: Distributions of cos θ, with θ being the angle of the main axis of the momentum tensor with respect to the beam direction: (a) For Ar + KCl and Ar + Pb where the Ar + KCl histogram (hatched) is normalized to the last bin of Ar + Pb. (b) For Ar + Pb events selected for small impact parameters.

Charge, Mass and Energy Measured in the Plastic Ball G

H.H. Gutbrod, B. Kolb, H. Löhner, B. Ludewigt, A.M. Poskanzer,
T. Renner, H. Riedesel, H.G. Ritter, A. Warwick, F. Weik, H. Wieman
GSI Darmstadt, LBL Berkeley and Universität Marburg

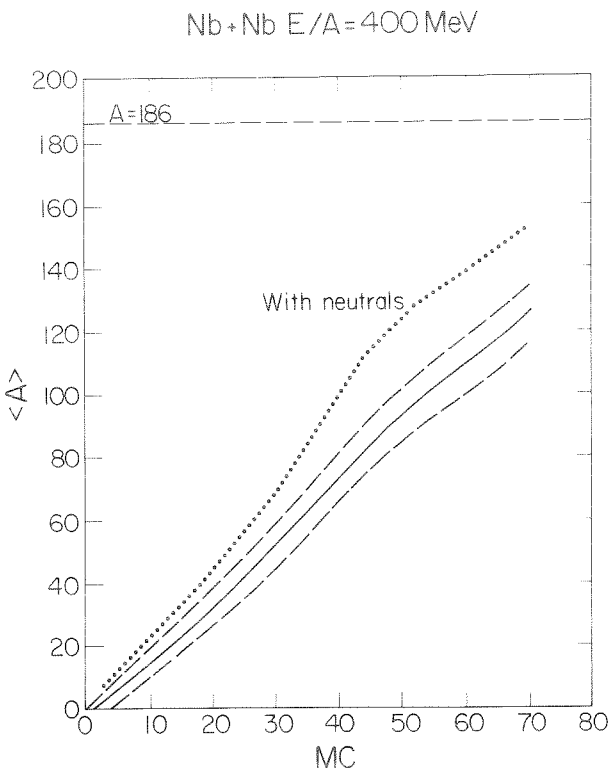
In relativistic nuclear collision the multiplicity of charged particles reflects the violence of the reaction and presumably the impact parameter. Furthermore, the total transverse energy in a collision might be a signature of compression. Both quantities are global features that can be measured in the Plastic Ball. Due to particle identification, the total mass in an event in light charge fragments can be detected (with assumptions made in certain kinematic regions). In addition the neutron detection efficiency is quite high because of the large thickness of the plastic scintillator in the Plastic Ball. In the following several global quantities are given for the reaction of E/A = 400 MeV Nb + Nb.

In Fig. 1 the total charge measured, plotted as a function of charged particle multiplicity (MC), is seen to increase linearly and reaches for some events the initial number of protons in the event (note that the production of a π^- can increase the measured charge by two units). In Fig. 2 the total mass of charged particles is plotted as a function of MC. This curve reaches values of approximately 70 per cent of the initial mass of the system. The dotted line indicates the mass when the neutral particles (which have no DE signal in the Plastic Ball) are added in. The missing masses, especially at lower multiplicities are in fragments that are either not detectable or identifiable with the Plastic Ball/Wall. Figure 3 shows the total kinetic energy and total transverse kinetic energy in the c.m. system as a function of MC. For some events as much as 24 GeV lab kinetic energy or 9 GeV in the c.m. system is detected. Of this as much as two-thirds can go into transverse kinetic energy. It is these events that may be thermalized and for which temperatures can be extracted.



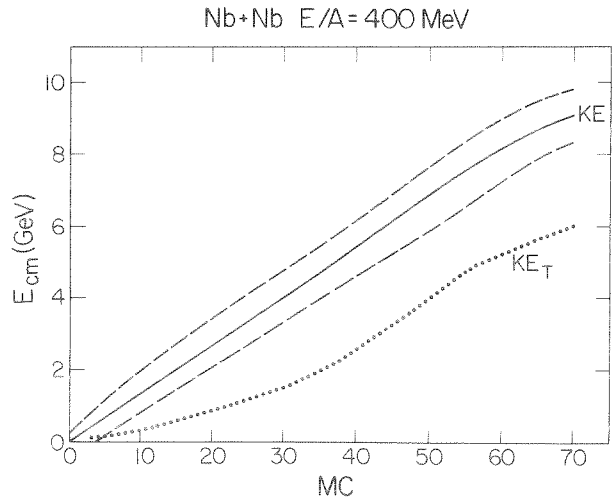
XBL 831-1158

Fig. 1



XBL 831-1159

Fig. 2



XBL 831-1163

Fig. 3

The Question of Thermalization Within Relativistic Heavy Ion Collisions

G

H.H. Gutbrod, B. Kolb, H. Löhner, B. Ludewigt, A.M. Poskanzer, T. Renner,
H. Riedesel, H.G. Ritter, A. Warwick, F. Weik, H. Wieman
GSI Darmstadt, LBL Berkeley, and Universität Marburg

One of the major questions while studying relativistic heavy-ion collisions is whether thermal equilibrium is reached or whether nuclei become transparent in central collisions already at intermediate BEVALAC energies. The appropriate quantities to study are the momentum components perpendicular ($p_\perp$) and parallel ($p_\parallel$) to the beam axis in the center-of-mass frame. The scatter plot (Fig. 1) shows in an event-by-event analysis for Ca on Ca at 400 MeV/A that most of the intensity lies away from the diagonal indicating isotropy. Restricting the data to more central collisions by the trigger and multiplicity selection (Fig. 1, middle part) the maximum of the distribution moves closer to the isotropy line. When larger mass systems are studied the collision of Nb + Nb at 400 MeV/u (Fig. 1, lower part) shows nearly all the intensity lying on the diagonal line. In Fig. 2 the mean value of this ratio is shown for Nb as a function of multiplicity. One sees that only in Nb + Nb at 400 MeV/u the necessary (but not sufficient) criterion for thermalization is reached in the mean event. Cascade calculations with the code of Yariv and Fraenkel show that for the lighter system even a few spectator fragments can deform a spherical event in momentum space to prolate spheroids. However, temperatures were extracted from the proton spectra of events with $2\cdot\langle p_\perp\rangle/\pi\langle p_\parallel\rangle = 1 \pm 0.05$ assuming a Maxwell-Boltzmann distribution. For Ca on Ca at 400 MeV/u the temperature of ~58 MeV is significantly lower than that of ~78 MeV for Nb on Nb.

This clearly states that for light systems not all available kinetic energy is transformed into heat. Thermal models might become more appropriate to describe classes of reactions between high mass nuclei, which stop each other in the center-of-mass frame.

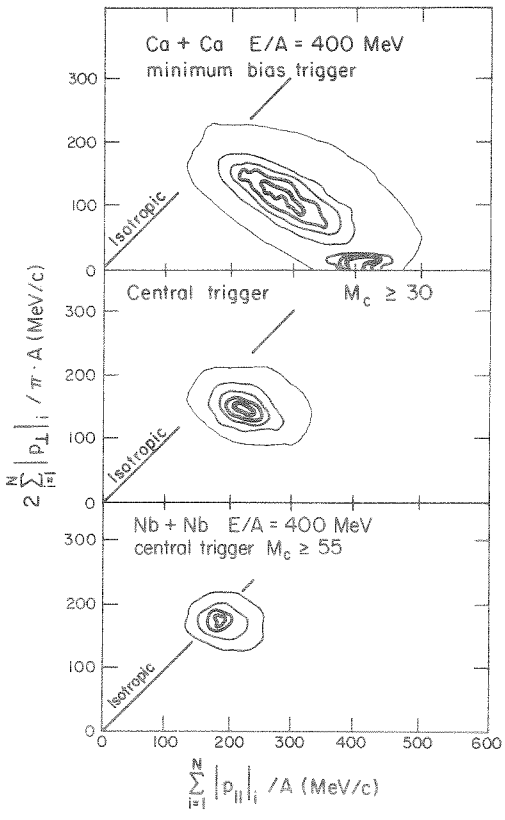


Fig. 1: Scatter plots of $\langle p_\perp/A\rangle$ versus $\langle p_\parallel/A\rangle$ for Ca on Ca at 400 MeV/A for a minimum bias trigger, requesting for the projectile some loss of charge. The middle part shows the same quantity for a central trigger (no beam velocity particle with 2° of the beam) and a charged particle multiplicity cut at 30. The lower part shows the reaction of 400 MeV/u Nb + Nb with a multiplicity cut of 55. The contour lines represent linearly increasing content.

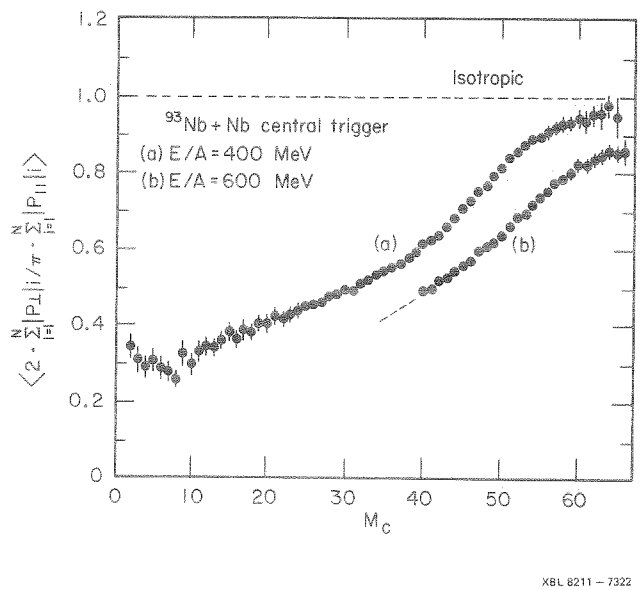


Fig. 2: Ratio of $2\cdot\langle p_\perp\rangle/\pi\ \langle p_\parallel\rangle$ as function of nucleonic charge multiplicity averaged over 50 000 events. A value of 1 for this ratio would correspond to an average spherical shape of the event in momentum space.

Two-Particle Correlations from the Plastic Ball [G]

H.H. Gutbrod, B. Kolb, H. Löhner, A.M. Poskanzer, T. Renner,
H. Riedesel, H.G. Ritter, A. Warwick, F. Weik, H. Wieman
GSI Darmstadt, LBL Berkeley, and Universität Marburg

Using data sets obtained with the Plastic Ball we have been exploring two-particle correlations in relativistic heavy ion collisions. The obvious advantage of the Plastic Ball for such measurements is the large solid angle (4π) and rapid data collection, which allow better statistics than are easily obtained with other devices. On the other hand, the relatively coarse angular resolution (3° to 6°) and limited energy resolution imposes restrictions on the correlations that can be measured. So far our studies have been limited to the possible two-particle combinations of p, d, t, ^{3}He, and ^{4}He with low relative velocities in Ca + Ca at E/A = 400 MeV, the system for which we have the largest data set. These data were recorded using a central collision trigger.

The correlation function F(p) has been generated in a manner similar to that used in two-particle interferometry studies.[1]

$$F(p) = nN_s(p)/N_d(p)$$

where $N_s(p)$ is the number of pairs per unit p taken from the same event and $N_d(p)$ are the number of pairs per unit p constructed from different events. The momentum p is the particle momentum in the center of mass of the pair. The factor n is chosen arbitrarily such that F(p) equals approximately one at large p. Particles included in the analysis were stopped in the Ball (laboratory angle 10° to 160°) where particle type and energy could be determined.

A sample of our results is shown in Fig. 1. The proton-proton correlations (top portion of the figure) have been studied in the past by others[1,2] as a tool for measuring source sizes through interferometry. In our spectrum the correlation has a positive enhancement peaking at ~30 MeV/c. This peak is artificially high because of the minimum relative momentum limit imposed by the detector system. Koonin[1] predicts the peak to lie at 20 MeV/c.

Proton-proton correlations, because of their role in interferometry, have received considerable attention. A number of other two-particle systems, however, have striking correlations, some positive, some negative in the low relative momentum region. The bottom two curves in the figure provide an example of each. The strong positive correlation appearing in the p-^{4}He system at p equal to 50 MeV/c corresponds to the ground state in ^{5}Li. This example is consistent with a trend we see in which positive correlations result when the particle pairs can couple to reach low-lying, widely spaced levels in the composite nucleus. If, on the other hand, the Q value only gives access to closely spaced levels at large excitation, then usually an anti-correlation or no correlation appears. One of the most striking anti-correlations appears in the deuteron-deuteron system (bottom curve in the figure) as a depression extending up to p = 150 MeV/c. This is well beyond the p = 55 MeV/c instrumental cutoff imposed by the angular separation of our detectors in the Plastic Ball. The anti-correlation suggests a coalescence-like final state interaction with the excited ^{4}He (Ex = ~23 MeV) decaying through some other channel.

[1] S.E. Koonin, Phys. Lett. 70B, 43 (1977)
[2] F. Zarbakhsh et al., Phys. Rev. Lett. 46, 1268 (1981)

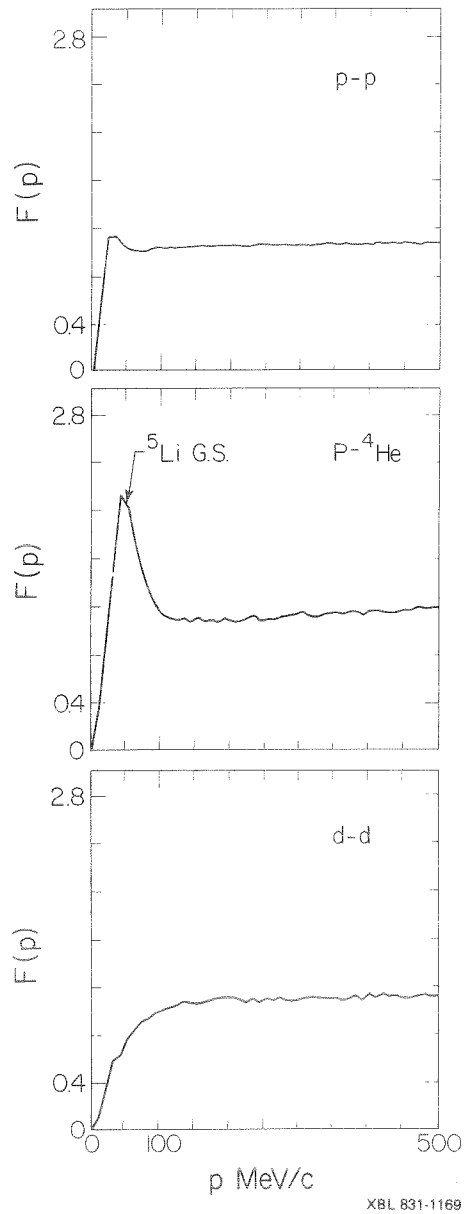


Fig. 1: Two-particle correlations as a function of particle momentum in the center of mass of the pair. Values of F(p) greater than 1 indicate a positive correlation.

Cluster Formation Observed with the Plastic Ball and the Question of Entropy Production in High energy Nuclear Collisions [G]

H.H. Gutbrod, B. Kolb, H. Löhner, A.M. Poskanzer, T. Renner,
H. Riedesel, H.G. Ritter, A. Warwick, F. Weik, and H. Wieman
GSI Darmstadt, LBL Berkeley, and Universität Marburg

With the assumption that relativistic nuclear collisions allow one to study the equation of state of nuclear matter, the hydrodynamical model predicts an increase in entropy for a phase transition at high nuclear density. Recently it was pointed out[1] that entropy can be related to cluster production, in particular to the ratio of deuteron yield to proton yield. This has stimulated a dispute among theorists over whether the information about the early state inherent in this ratio gets lost during the expansion phase or is disturbed only via second order effects, whether the deuteron and proton yields are the proper observables, or whether one should use the quantities deuteron-like and proton-like defined[2] as d-like = d + 1.5 (^{3}He + ^{3}H) + 3 ^{4}He and p-like = p+d+t+2 (^{3}He + ^{4}He). Until now these studies have been limited to single particle inclusive data, which mix together reactions of all impact parameter. With the Plastic Ball/Wall spectrometer for the first time 4π data are available to investigate this subject. Figure 1 shows the ratios averaged over many events as a function of charged particle multiplicity (a,b) and as a scatter plot on an event-by-event basis (c,d). The inclusion of heavier cluster obviously decreases the dispersion in the ratio and supports the choice of these variables in the analysis.

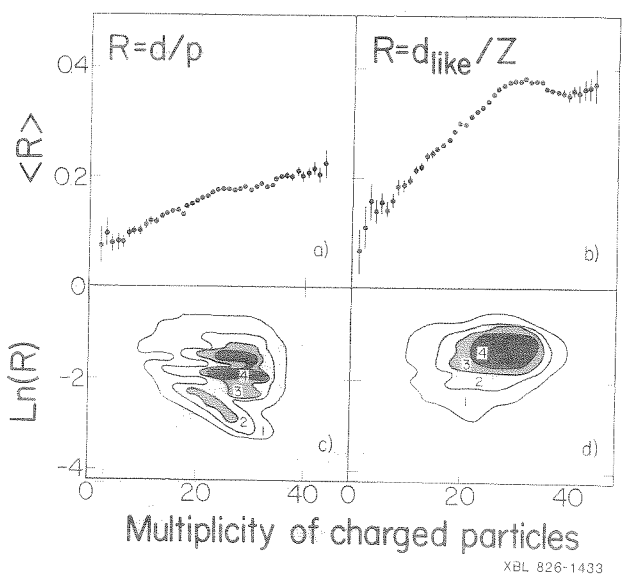


Fig. 1: a,b: Ratio of deuteron to proton production (a) and ratio of deuteron-like to proton-like particles (b) as a function of the total observed charged particle multiplicity for the reaction Ca on Ca at 400 MeV/u. c,d: Corresponding event-by-event contour plots of the logarithm of the ratios versus the charged particle multiplicity. Relative intensities are indicated by the contour lines.

The increase in deuteron production with increasing multiplicity (Fig. 1a,b) can be described by the coalescence model[3] but improved by Sato and Yazaki.[4] It takes now into account both the size of the deuteron and the volume of the participant region. The coalescence radius p_0 in momentum space is related to the deuteron radius r_d and that of the participant volume r_p via $\frac{\text{d-like}}{\text{p-like}^2} = \frac{4\pi}{3}p_0^3 \simeq \frac{1}{(r_d^2+r_p^2)^{3/2}}$, while r_p can be related to the observed charges by $r_p = r_0(2\ \text{p-like})^{1/3}$ with r_0 as a free parameter. Figure 2 shows a fit to the data with $r_d/r_0 = 2.6$.

The analysis of the 400 MeV/u Nb data showed the same cluster production as in 400 MeV/u Ca + Ca when only events with the same number of participants were compared and not the average reaction. The average reaction in both cases is very different because of the larger average numbers of participants in Nb + Nb. Furthermore, a comparison of the cluster production at different bombarding energies but fixed number of participants yields a decrease with increasing energy. It is therefore clear that many conclusions drawn from single-particle inclusive data have to be thoroughly rechecked.

[1] P. Siemens and J. Kapusta, Phys. Rev. Lett. 43, 1486 (1979)
[2] G. Bertsch and J. Cugnon, Phys. Rev. C24, 2514 (1981)
[3] H.H. Gutbrod et al., Phys. Rev. Lett. 37, 667 (1976)
[4] H. Sato and K. Yazaki, Phys. Lett. 98B, 153 (1981)

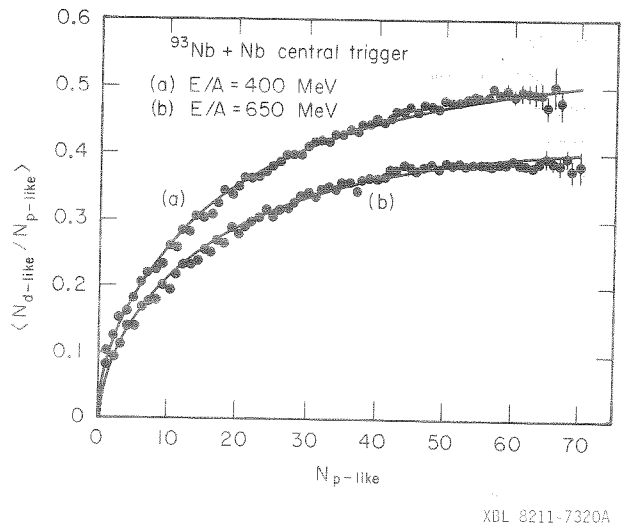


Fig. 2: Ratio of the number of deuteron-like to proton-like particles as a function of the number of proton-like particles. The solid curves represent fits to the data.

Multifragmentation of Nuclear Residues in Relativistic Nuclear Collisions [G]

A.I. Warwick, H.H. Wieman, H.H. Gutbrod, M.R. Maier, J. Péter, H.G. Ritter, H. Stelzer, and F. Weik
G.S.I. Darmstadt, LBL, Berkeley California and Universität Marburg
M. Freedman, D.J. Henderson, S.B. Kaufman, E.P. Steinberg, and B.D. Wilkins
Chemistry Division, Argonne National Laboratory, Argonne, Illinois 60439

In an experiment to study the collisions of Ne + Au at the Berkeley Bevalac we have measured the multiplicities of fast and slow emitted charged particles.[1] In central collisions at 2.1 GeV/u we can approximately account for the entire mass of the target and projectile in the final state, which consists of the light products of an expanding fireball together with the slower, heavier fragments from the breakup of the target nuclear residue.

We address the problem of determining the size and excitation of this residue and its mode of disassembly. In a central collision of Ne + Au at 2.1 GeV/u the multiplicity of fast charged particles indicates a fireball of about 110 nucleons, thus the target residue has a mass number A≈100. We determine the typical breakup mode of the central collision residue by measuring the mean multiplicities of the slow charged particles it emits, as a function of their charge. The results are shown in figure 1, the typical fragmentation produces 3 heliums, 1 lithium and several larger fragments in the range 3<Z<25. Such a multifragmentation process is likely to proceed rapidly, fragments being produced simultaneously and moving apart under their mutual Coulomb repulsion.

We estimate the importance of this late stage Coulomb interaction by a Monte-Carlo calculation of the classical fragment motion, beginning with a Maxwell-Boltzmann ensemble of fragments whose masses satisfy the distribution of figure 1 and whose initial spatial separation and initial thermal energy are variable parameters. With a thermal ensemble of fragments having a temperature T=20 MeV immediately after breakup, before undergoing Coulomb expansion, the calculated asymptotic distribution is close to the observed spectrum (figure 2).

We can relate the ensemble of fragments at T=20 MeV to the excitation of the residue using the statistical considerations of Randrup and Koonin[2]. A residue of excitation E=20 MeV per nucleon undergoing a statistical breakup will lose energy to break binding and redistribute the remaining energy amongst the fewer degrees of freedom of fragment motion, resulting in an ensemble of T≈20 MeV.

Thus the breakup of nuclear residues in central collisions of heavy ions proceeds through a novel multifragmentation mechanism with a characteristic excitation energy of 20 MeV per nucleon.

[1] A.I. Warwick, et al., Phys. Rev. C27, (1983) to be published
[2] J. Randrup and S. Koonin Nucl. Phys. A356, 223 (1981)

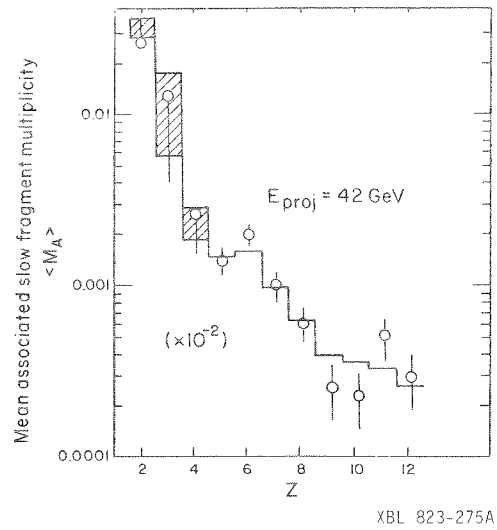


Fig. 1: Open circles show the mean multiplicities of fragments with charge Z associated with a trigger fragment of mass A=20-40 detected at 90° from the reaction Ne + Au. The histogram represents the singles measurement of fragment yield as a function of fragment charge Z, scaled appropriately for comparison to the measured fragment multiplicities.

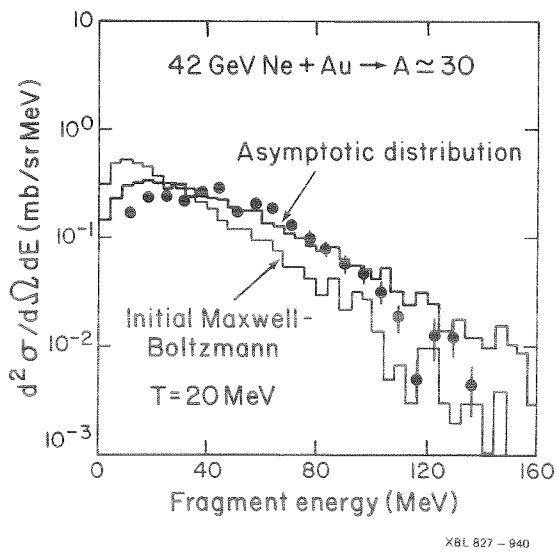


Fig. 2: Results of the Coulomb expansion calculation of the kinetic energy spectra of A = 30 fragments emerging from the Au target residue after a central collision induced by a 42 GeV Ne Projectile.

Minimal-spanning-tree analysis of Plastic Ball events

H. Löhner, H. Gutbrod, A.M. Poskanzer, T. Renner, H. Riedesel
H.G. Ritter, A. Warwick, H. Wiemann
Universität Münster, LBL and GSI Darmstadt

One of the goals of relativistic heavy ion collisions is to study nuclear matter in extreme states of high temperature and compression, which might be reached in the participant region of two colliding nuclei. Spectator matter, however, from target and projectile remnants will mask the emission pattern, so that a clean identification of spectator fragments is desirable. Therefore we have studied the abilities of the cluster algorithm "minimal spanning tree" (MST)[1] by applying it to 4π-exclusive data (Ca+Ca at E/A = 400 MeV) from the Plastic Ball[2]. The following analysis was done in the NN-CM system for symmetry reasons. After extensive tests of the algorithm the analysis should as well be carried out in the lab system and be applied to asymmetric collisions.

The MST algorithm assignes particles of one event to clusters and classifies the event by its cluster number by means of a distance measure d_{ij} between two particles i and j. We took $d_{ij} = \Theta_{ij}/(p_i p_j)$ from ref. 1, where Θ_{ij} is the angle distance between particle i and j and p_i, p_j are the momenta of i and j. This definition favors leading particles by the inverse momentum weighting. After construction of the "tree" it is cut into subtrees (clusters) at edges (connections between 2 tree elements) which are inconsistently long. This cut is defined from the edge distribution showing a long tail which is cut off from the peak at short edges. Other definitions of d_{ij} were tested like inverse energy weighting or euclidic distance in the space of rapidity versus transverse momentum. The resulting edge distributions were rather uniform making a cut definition too ambiguous. Additional parameters are the minimum event multiplicity and the minimum number of particles per cluster which were set to 5 and 2, respectively. A minimum kinetic energy of 500 MeV per cluster was required in order to avoid too many arbitrarily small clusters. The results are qualitatively insensitive to variations of cuts and parameters within certain limits. Two-cluster events in both the minimum-bias and the central trigger mode[2] of the data have been studied in detail.

Fig. 1 shows for minimum-bias data the rapidity distribution for particles of all events (curve a), for particles assigned to a cluster in 2-cluster events (curve b), for unassigned particles in 2-cluster events (curve c) and the rapidity distribution for the resulting two clusters (dashed line). From this a clear separation into target-, projectile-, and participant matter at midrapidity can be seen. 80 % of projectile (target) clusters are found in a cone around the beam axis with opening 18° (33°). The cluster quality is very good with a mean n-ticity (see ref. 1) for n = 2 of 0.88. However, the asymmetric structure of curves b and c and the overlapping of the peaks of curve b at midrapidity indicate that the discriminating power of the MST still needs to be improved by finding a more selective distance measure d_{ij}. Fig. 2 shows in the plane of rapidity versus transverse momentum all unassigned particles of 2-cluster-events. Looking at angles between 30° and 150°, the contour lines resemble an isotropic emission pattern. For small $P_\perp$ the regions at large $|y_{CM}|$ are distorted obviously due to a wrong cluster assignment and to some extent due to experimental thresholds in the target region. Angle integrated proton spectra have been analysed by approximating the invariant cross section: $\sigma_{inv} \sim \exp(-E/E_0)$. A slope parameter of $E_0 = 72$ MeV is found for target and projectile protons. $E_0 = 50$ MeV for participant protons is in agreement with other data[3] analysed at $\Theta_{CM} = 90°$. The same analysis is presently being applied to complete multi fragment events from a statistical model[4] in order to test the discriminating efficiency.

1) J. Dorfan, Z. Phys. C7 (1981) 349
2) A. Baden et al., NIM 203 (1982) 189
3) S. Nagamiya et al., Phys. Rev. C24 (1981) 971
4) J. Randrup and G. Fai, Phys. Lett. 115B (1982) 281

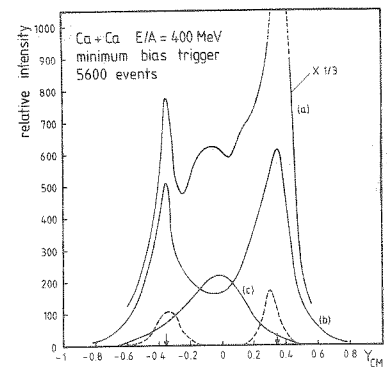


Fig. 1
Rapidity distributions (see text). Arrows indicate the beam and target rapidity in the NN-CM-system.

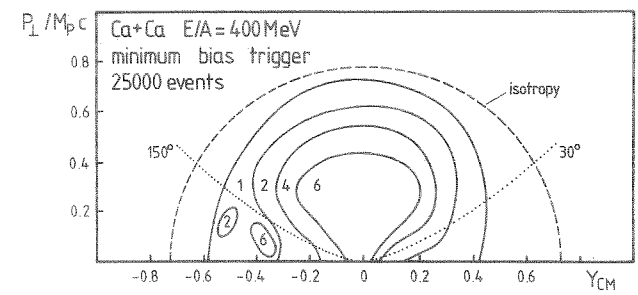


Fig. 2 Rapidity versus normalized transverse momentum for unassigned particles of 2-cluster events. Contour lines are labelled by the relative cross section height.

G

A Search for Short-lived Anomalons in Projectile Fragmentation

H.A. Gustafsson, H.H. Gutbrod, B. Kolb, B. Ludewigt, A.M. Poskanzer,
T. Renner, H. Riedesel, H.G. Ritter, A. Warwick, H. Wieman
GSI Darmstadt, LBL Berkeley, and Universität Marburg

Nuclear emulsion studies[1,2] suggest that fragmentation products from relativistic heavy-ion collisions have anomalously large reaction cross sections and that they disappear over the first few centimeters of their track in emulsions. If these "anomalons" exist, their disappearance could be due to either reactions or decay with a mean lifetime of 10^{-10} seconds. The design of our counter experiment, shown in Fig. 1, was based on the published information from the above-mentioned emulsion studies.

The experiment was performed by bombarding alternately a solid (20 mm thick) and a dilute (ten 2-mm slabs each separated by 20 mm) Cu target with a beam of 1.7 GeV/u ^{56}Fe ions at the Berkeley Bevalac. The produced projectile fragments were detected, within ±3° and 5 mm downstream, in a ΔE plastic detector. An observed difference in the shape of the ΔE spectra measured with the solid and dilute targets would indicate the existence of short-lived "anomalons" ($\tau \simeq 10^{-10}$ s), which decay in the spaces of the dilute target, giving fewer secondary interactions than in the condensed target.

A first analysis of the experimental data, as well as a preliminary Monte Carlo simulation of the experiment, rules out the proposed model[2] in which primary collision produces a fragment of anomalous cross section, subsequently decaying to give the observed "anomalon" mean free path. This means that it should be possible to search for "anomalons" in, for example, a double scattering experiment.

[1] E.M. Friedlander et al., Phys. Rev. Lett. 45, 1084 (1980).
[2] H.B. Barber et al., Phys. Rev. Lett. 48, 856 (1982).

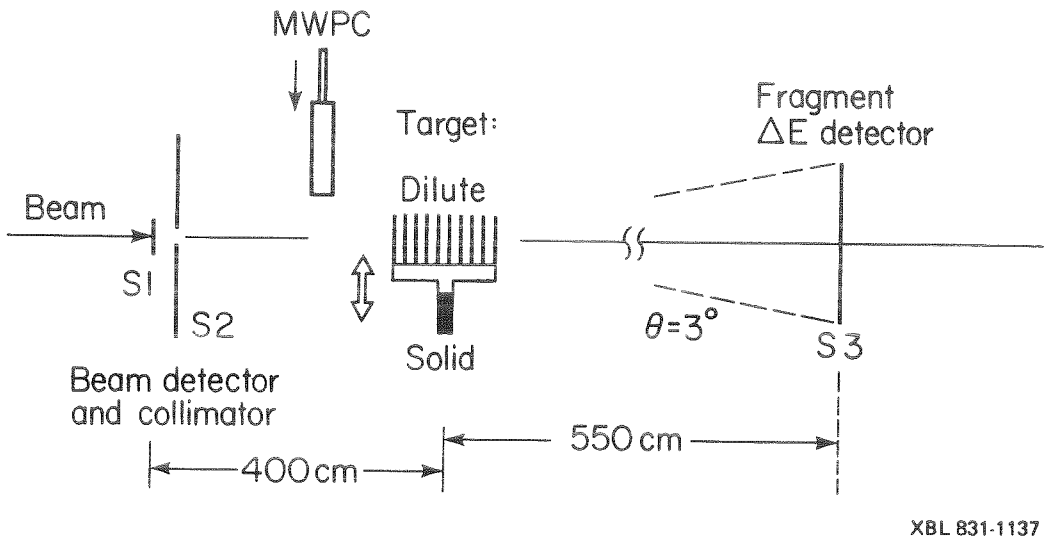


Fig. 1: Schematic view of the experimental layout, S1 and S2 being the beam-defining scintillators. The multiwire chamber MWPC was used for focusing the beam and then retracted. S3 represents the Plastic Wall detectors.

Test of Radiochemical Techniques in the Study of Anomalons [B]

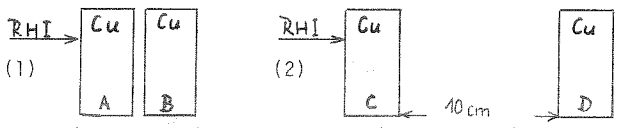
G. Dersch, T. Lund, R. Beckmann, R. Brandt, R. Weiner (Uni Marburg)
P. McGaughey, E. Friedlander (LBL, Berkeley, Calif. USA)
W. Loveland (State University, Corvallis, Oreg. USA)
N. Porile (Purdue University, Lafayette, Ind. USA)
K. Aleklett (Studsvik, Nyköping, Sweden)

The "anomalon" phenomenon was first observed in the study of photographic emulsions exposed to cosmic rays. Several subsequent emulsion experiments were carried out with relativistic heavy ion beams. At energies above 1.8 AGeV this effect, an anomalously short mean free path of projectile fragments in the first few centimeters from their emission point, has also been observed and proven as statistically significant[1,2]. The anomalon effect can be interpreted by two extreme hypotheses (or any combination thereof):

H1: Only about 6 % of all secondary particles are anomalous, however, they have an interaction cross-section enhanced by ∿ 1 order of magnitude as well as a relatively long life-time.

H2: All secondary projectile fragments are anomalous with a cross-section ∿ 2 times normal and are short-lived (∿ 10^{-11} s).

We suggest an independent radiochemical method for the study of anomalons. We need high energy heavy ions (E > 1.7 AGeV) and C, Ar, or Fe projectiles. The proposed technique is simple and has been tested for 24 GeV protons, 0.9 AGeV-^{40}Ar and 400 GeV protons. Two sets of 1 cm-thick Cu-blocks are irradiated, one after the other.



Then we measure the γ-activity of radioactive product nuclei with standard radiochemical techniques and obtain the apparent cross-section for a wide variety of product nuclides in each Cu-block. Of particular interest are deep-spallation products, say ^{24}Na, as one might conjecture, that they are produced in an enhanced manner by anomalons. We obtain cross-section ratios R_I or R_{II} for specific nuclides for set-ups (1) and (2) and the ratio of cross-section ratios R, when we compare result from (1) and (2). $R_{I,II}$ are sensitive to the interaction properties of anomalons, whereas R responds specifically to short life-times (H2). Experimentally, we can determine R within ± 3 % and we hope to improve this accuracy.

During test experiments, we obtained for the production of ^{24}Na in Cu (preliminary values) the ratios:

R (24 GeV p) = 1.02 ± 0.03 (measured)
R (0.9 AGeV-^{40}Ar) = 1.035 ± 0.024 (measured)

This is to be expected, if no anomalons are produced or if they are quasi-stable. For short-lived anomalons we compute a value:

R (> 1.7 AGeV-RHI) ≈ 1.1 – 1.2 (predicted)

Details of this Monte-Carlo calculation will be given in a forthcoming paper.

The qualitative argument is: short-lived anomalons (∿ 10^{-11} s) are produced in (A) and (C). These projectile fragments can interact in the Cu-block (B) and some of them have decayed on the way to Cu-block (D). Thus we have a simple way to estimate the life-time of anomalons by an independent technique.

In case of long-lived anomalons we find as expected, R = 1.00. By comparing the cross-section ratios R_I or R_{II} for different projectiles (protons, heavy ions) at various energies, we can learn how anomalous secondary particles interact with Cu-targets.

The effect of low-energy secondary particles is observable in conventional spallation products close to the target, but as the above-mentioned observed ratios show, it is unimportant for deep-spallation products, as can be seen in Fig. 1.

[1] E.M. Friedlander et al., Phys.Rev.Lett. 45, 1084 (1980)
[2] M.M. Aggrarwal et al., Phys.Lett. 112B, 31 (1982)

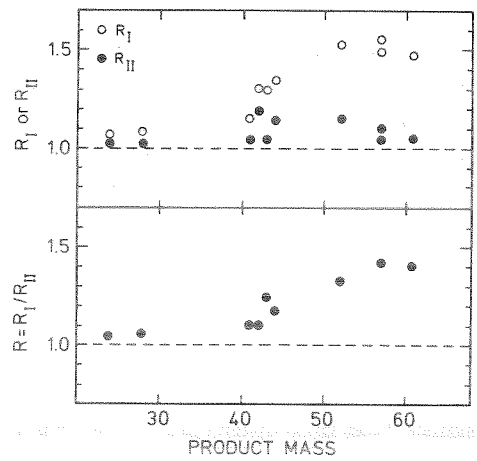


Fig. 1: The observed activity ratios R_I, R_{II}, and R for the reaction (Cu + 0.9 AGeV ^{40}Ar), very similar results are obtained for the reaction (Cu + 24 GeV p).

Comparison of Z=2 induced primary and secondary interactions in nuclear track emulsion at ~2 GeV/u

G

N.Klein, E.Ganßauge, M.Baagil, U.Bieschke, F.Killinger, R.Kretschmer, A.Laschek, and W.Weidner
FB Physik, Philipps-University, AG Exp.High Energy Physics, D 3550 Marburg, Federal Republic of Germany

The geometry of stars induced by primary ^{3}He, ^{4}He and secondary α's was determined [1]. Heavy prongs were identified, their number N_h in each star counted and subdivided into two groups, F and B, the forward and backward cone of the star respectively. From these numbers the asymmetry A, defined by

$$A = (F-B)/(F+B)$$

was calculated for each star.

The data from ^{3}He and ^{4}He beams was combined to "He" in proportion 1:3. Similar to this method used in the case of mean free path measurements[2], the α-data were cutted into two subgroups marked with a lower subscript $\leq$ and $>$ corresponding on whether they were originated inbetween D $\leq$ 3 cm from the emission point or at D $>$ 3 cm. Fig.1 shows the asymmetry distributions for He, $\alpha_>$ and $\alpha_\leq$. While He and $\alpha_>$ seem to behave quite the same, the $\alpha_\leq$ show a shift towards isotropy. The χ^2-test gives a value χ^2=15.8 with 2 degrees of freedom, which corresponds to a probability for the deviation being caused by a statistical fluctuation of less than 1 ‰.

This tendency shows up even more if another cut divides the data into two more subgroups, marked by the upper subscript $\geq$ and $<$ corresponding on whether the multiplicity N_h is ≥ 9 or < 9, see fig.2. This figure gives the asymmetry distributions for larger stars, for only in this case there is a significant difference between $\alpha^{\geq}_{\leq}$ and He$^>$, while the asymmetry distributions for $N_h < 9$ seem to be very much the same.

Tab.1 gives the ratio R of the number of stars with $2 \leq N_h < 9$ and the number of "large" stars with $N_h \geq 9$. From this one sees that the probability to produce a "near" α star is about 1.5 times larger than for He and $\alpha_>$ which are identical within the statistics.

Table 1

projectile	$R = \frac{\#\ (2 \leq N_h < 9)}{\#\ (N_h \geq 9)}$
He	0.80 ± 0.10
α	1.37 ± 0.20
$\alpha_>$	1.04 ± 0.21
$\alpha_\leq$	1.78 ± 0.39

We conclude from this investigation that the behaviour of secondary α's near the emission point differs in a distinct way from that of primary Z=2 stars as well as of secondary α's at longer distances. A connection with the "anomalon" effect [3] seems to be obvious.

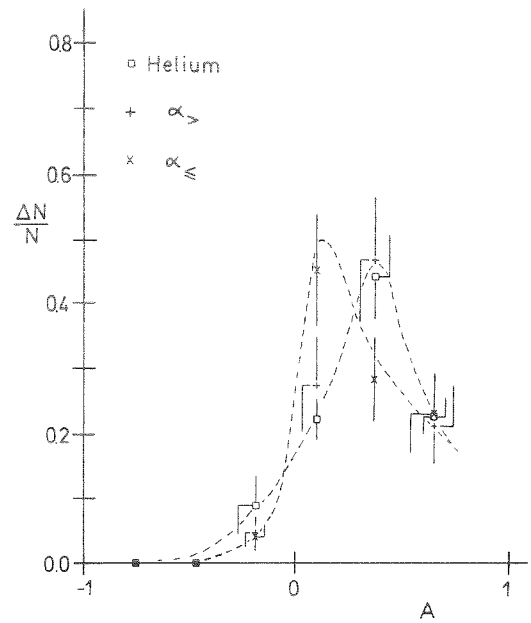


Fig.1: Normalized asymmetry distribution of He, $\alpha_>$, and $\alpha_\leq$. The lines are just eye guides through the experimental points.

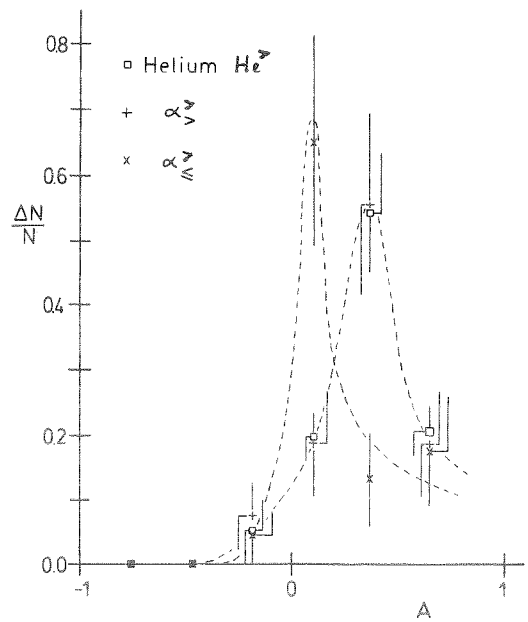


Fig.2: Asymmetry as in fig.1, but for "large" stars only ($N_h \geq 9$)

1. Ganßauge et al., GSI-Scientific report 1981, page 44
2. E.Friedländer et al., Phys.Rev.Lett.45 (1980) 1084
3. Ganßauge et al., GSI-Scientific report 1981, page 43

Upper Limit for the Axion Decay of Triplet Positronium

W. Wahl, E. Adelberger, MPI für Kernphysik Heidelberg
D. Habs, R. Kroth, D. Schwalm, H.J. Specht, Universität Heidelberg
V. Metag, Universität Gießen
R.S. Simon, GSI Darmstadt

Positronium is the bound system of e^+ and e^-. The singlet ($1\,^1S_0$) ground state (τ = 0.125 ns) annihilates into two quanta of 511 keV while the triplet ($1\,^3S_1$) ground state (τ = 142 ns) decays into three γ rays with continuous energies between 0 and 511 keV. In matter the triplet state is usually quenched to the singlet configuration within 1-2 ns.

Theory predicts additional decay modes. One interesting speculation is the decay

$$e^+e^-(1\,^3S_1) \rightarrow a + \gamma \qquad (1)$$

which involves the axion, a hypothetical particle postulated[1] to avoid P and CP violation in the standard model of strong interactions. If the axion mass m_a is smaller than two times the electron mass m_e the decay (1) is allowed energetically. Its intensity relative to the normal 3γ decay is expected[2] to be between 5×10^{-6} and 10^{-11} depending on m_a (see fig.1).

For the axion search we developed a compact source of triplet positronium where the positrons from the decay of ^{68}Ge register in a plastic scintillator and then stop in low density powder of SiO_2. About 10% of all e^+ emitted led to the vacuum decay of the triplet state. As the axion would be only weakly interacting we decided to detect the monoenergetic γ ray instead. Observation of the resulting axion line at $E_\gamma = m_e - m_a^2/4m_e$ in the continuous spectrum of the positronium source should be possible because of the unique signature of the axion which corresponds to the e^+ signal in the scintillator followed by a delayed single γ ray.

The experiment was performed in the Darmstadt-Heidelberg NaI crystal ball. With the positronium source in the center we have an anticoincidence arrangement with a detection probability of 0.98-0.99. This means that the regular triplet rate can be suppressed by three to four orders of magnitude, while the intensity from the prompt singlet decay is excluded by accepting only events which are delayed with respect to the emission of the positron. The 4π geometry for the axion line and the good peak/total ratio guaranteed by the one-module-only condition are two advantages of our all-NaI arrangement.

Shown in fig.2 is a delayed 1γ spectrum corresponding to 7×10^8 triplet decays as accumulated in approximately 10 hours of data taking. The prominent intensity in the spectrum around 511 keV and the corresponding backscatter distribution around 170 keV can be accounted for by conventional decays and probably do not involve the axion. The two modes are quenching to the singlet configuration within the delayed time window or regular 3γ decays involving a photon below the electronic threshold (<70keV). In both cases rejection of the two quanta at or close to 511 keV is impaired. No axion line is observed in the spectrum and from the statistical accuracy of our present data we estimate an upper limit of 5×10^{-7} for the branching ratio relative to the 3γ decay.

1. S.Weinberg, Phys.Rev.Lett. 40 (1978) 223;
F. Wilczek, Phys.Rev.Lett 40 (1978) 279
2. W. Bernreuther and O. Nachtmann, Z.Physik C11 (1981) 235

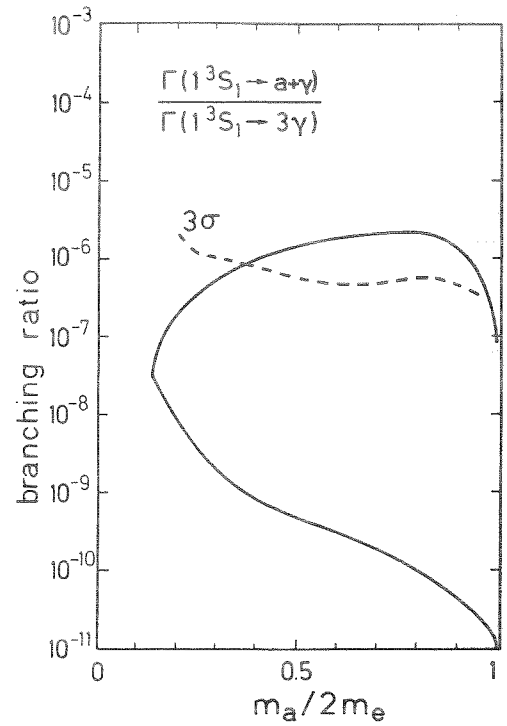


Fig.1 Branching ratio for the axion decay of triplet positronium. The two options as a function of m_a correspond to different couplings between axion and electron. Also shown (dashed line) is the upper limit (3 standard deviations) obtained from the present experiment.

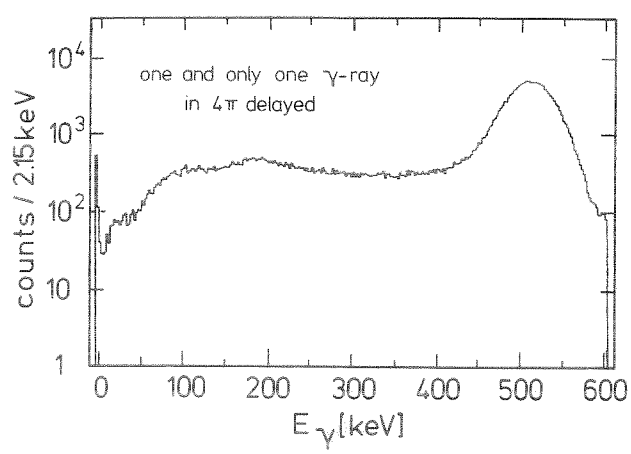


Fig.2 Delayed 1γ spectrum from the positronium source as observed in the NaI modules of the crystal ball.

Multiple Coulomb Excitation of ^{82}Kr [B]

S. Brüssermann, K.P. Lieb, P. Sona
II. Physikalisches Institut, Universität Göttingen
H. Emling, E. Grosse, GSI Darmstadt
J. Stachel, Institut für Kernchemie, Universität Mainz

Recent studies[1] of the level structures of $^{74-82}$Kr have shown that with increasing mass number the nuclear shape changes from a nearly axially symmetric to a triaxial or γ-unstable rotor. The quasi-bands in ^{82}Kr have most recently been investigated in the reactions ^{76}Ge(^{12}C,α2n) (ref. 2) and ^{80}Se(α,2n) (ref. 3) and in the β-decays of ^{82}Rb and ^{82}Br (ref. 4). Previous recoil distance measurements[2,3] did not allow to determine lifetimes of states of the ground and γ-band with sufficient accuray because of the presence of long lived feeder states of 2qp nature.

Therefore, in order to determine transitional and static E2 moments we measured multiple Coulomb projectile excitation by bombarding a 400 μg/cm^2 ^{208}Pb target with the 4.6 MeV/u ^{82}Kr beam of the UNILAC accelerator. The γ-radiation was measured in four Ge detectors positioned at 0°, ± 63° and 180° with respect to the beam axis. The beam was stopped in a 1 mm thick Pb foil mounted on a tungsten cone of 20 mm thickness which shielded the 0° Ge detector against the Pb X-rays. The Ge detectors were operated in coincidence with the backscattered projectiles detected in an annular parallel plate avalanche counter (a similar detector is described in ref. 5 in more detail). The particle counter covered an angular range of $110° \leq \vartheta \leq 167°$, $0° \leq \phi \leq 360°$ corresponding to a solid angle of 4 sr, it was position sensitive in both the ϑ and ϕ coordinates thus allowing to correct for the Doppler broadening of the γ-lines. The polar angle ϑ was determined from the time delay of the cathode signal. The cathode was constructed as a printed circuit of 50 concentric rings, each 2.5 mm wide and separated from its neighbors by 0.5 mm gaps; these rings were connected by LC delays. At a distance of 2.5 mm from the cathode, a thin metalized mylar foil served as anode; it was divided into 20 radial segments thus providing the information on the azimuthal angle ϕ. A second thin mylar foil served to separate the detector volume filled with 13 mbar isobutene from the target chamber. A ring shaped Al frame shielded the detector against particles backscattered from the beam stopper. The experimental arrangement is sketched in fig. 1.

Transitions from levels up to spin $I^\pi = 6^+$ could be observed in the ground state-band as well as in the γ-band although in the transitional nucleus ^{82}Kr the corresponding B(E2) values are fairly small and the transition energies are large. Furthermore, low spin members of several sidebands were excited (see also fig. 2). At present the data are analyzed in order to deduce the relevant E2 matrix elements for the observed levels.

[1] J. Keinonen et al., Nucl.Phys. A376 (1982) 246; K.P. Lieb et al., XX Bormio Meeting (1982) p. 76
[2] L. Funke, XX Bormio Meeting (1982) p. 213
[3] S. Brüssermann et al., Z. Phys. A355 (1982) 335
[4] R.A. Meyer et al., preprint
[5] Y.T. Chu et al., GSI Scientific Report 1979, p. 182 and R. Bock et al., Nucl.Phys. A388 (1982) 334

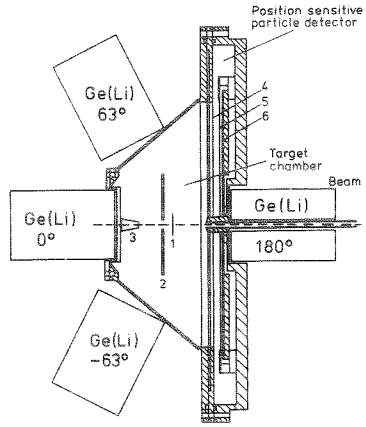


Fig. 1: Experimental set-up
1 = target
2 = Al frame
3 = beam stop
4 = entrance foil
5 = anode
6 = cathode

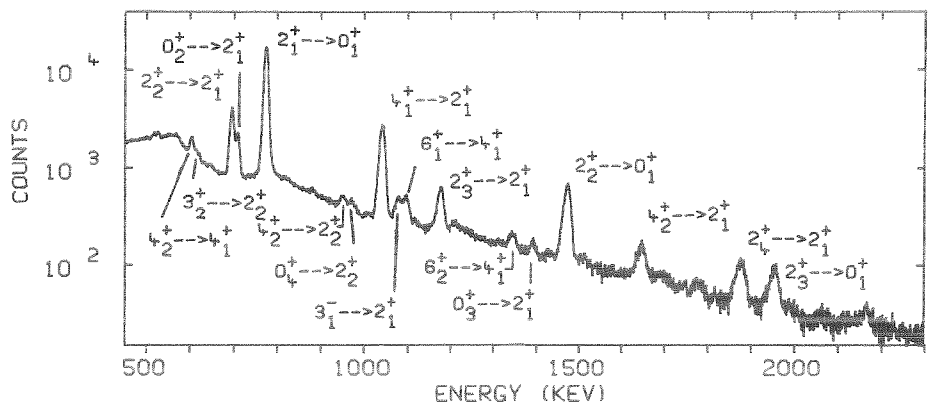


Fig. 2: Doppler corrected γ-spectrum of the Coulomb projectile excitation of ^{82}Kr (ground state band (1), γ-band (2), side bands (3,4))

Alignment in ^{104}Ru [B]

J. Stachel, P. Hill, N. Kaffrell, Institut für Kernchemie der Universität Mainz
H. Emling, H. Grein, E. Grosse, Ch. Michel, H.J. Wollersheim, GSI Darmstadt
D. Schwalm, Universität Heidelberg; S. Brüssermann, Universität Göttingen

Previously[1] we reported on multiple Coulomb excitation experiments ^{208}Pb on ^{104}Ru, which allowed to extract detailed information on the structure of ^{104}Ru. The determined static and transitional E2 moments for the ground state band (gsb) and γ-band gave clear evidence for a mean triaxial ground state deformation of $\gamma \approx 25°$ together with a pronounced softness in γ-direction.

In the energy region extrapolated for the 10→8 gsb transition no unassigned γ-ray had been observed, whereas the B(E2) value for this transition could be estimated from the $8_g \rightarrow 6_g$ intensity at large scattering angles not to be reduced drastically. This means the 10_g state had been excited, but since the continuation of the gsb is energetically not regular, among several candidates no assignment was possible. To clear up the situation and also to insure that no levels had been populated, which would have been important for the analysis but were not included in it we performed an additional Coulex experiment: It aspired at the measurement of particle gamma gamma triple coincidences - and this specially at small impact parameters, where high spin excitations are generally favoured. A ^{104}Ru beam (4.6 MeV/u) was used to bombard a ^{208}Pb target and the backscattered projectiles were detected in coincidence with the deexcitation γ-radiation using a ϑ,ϕ position-sensitive ring avalanche detector and 4 Ge detectors distant 7 and 11 cm from the target[2]. Fig.1 shows p$\gamma\gamma$ coincidence spectra with gates on gsb transitions; together with the measured pγ directional correlation they clearly allow to assign the 791 keV γ-ray (previously thought to be the $8_\gamma \rightarrow 6_\gamma$ transition as the 10→8 gsb transition (a smooth extrapolation of the gsb would lead to ≈ 850 keV); concerning the γ-band, the 8→6 transition can now uniquely be assigned to the 651 keV line, which is 43 keV below the $6_\gamma \rightarrow 4_\gamma$ transition energy. Also shown in Fig. 1 is a spectrum in coincidence with the until now unassigned 964 keV transition; from this coincidence pattern, the high gamma mutliplicity (5-6) and the corresponding particle gamma directional correlation, which is in best agreement with the assumption of a stretched E2 transition, a possible assignment of this 964 keV γ-ray is the decay of a second excited 10^+ state to the 8^+_1 state. In this case the corresponding $10_2 \rightarrow 8_1$ B(E2) value would amount to 36 % of the $10_1 \rightarrow 8_1$ B(E2). Irregularities are expected to occur in this spin and energy region and they are observed in the light Ru isotopes and the neutron rich Pd isotopes. Whereas backbending - typical for a weak interaction - is observed for the gsb's of the N = 58,60 Pd isotopes, in the N = 60 ^{104}Ru isotope the observed upbending at $I^\pi = 10^+$ seems to indicate a strong interaction as observed for ^{110}Pd (N = 64); this nucleus is very similar to ^{104}Ru also concerning the E2 properties of low lying states. On the other hand the observed backbending for the γ-band in ^{104}Ru shows that there - opposit to the gsb - the interaction is weak. If the same aligned configuration is causing the irregularities in the gsb and γ-band of ^{104}Ru the different interaction strength could be explained by the strong influence of the γ-degree of freedom on the alignment process as shown in recent cranking calculations[3].

It should be noted that the previously determined E2 moments[1] are not changed by these new findings but within their error bars.

[1] J. Stachel et al., Nucl. Phys. A383(1982)429
[2] For details see S. Brüssermann et al., this report
[3] S. Frauendorf, F.R. May, Phys. Lett. to be publ.

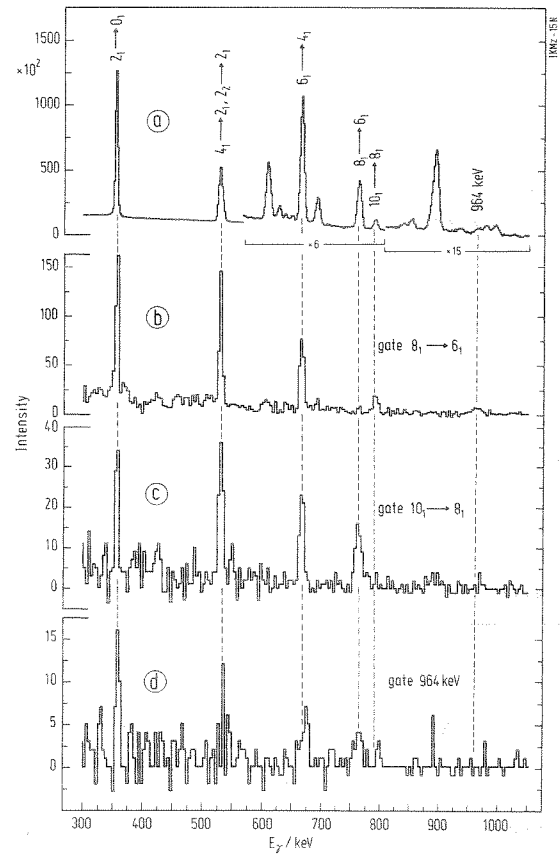


Fig. 1 pγ coincidence spectrum (a) and p$\gamma\gamma$ coincidence spectra (b-d), both integrated over $138° \leq \Theta_{cm} \leq 174°$

Coulomb Excitation of ^{114}Cd and ^{116}Sn

C. Fahlander, A. Bäcklin , L. Hasselgren, V. Mittal, L.E. Svensson
Nuclear Physics Division, Uppsala University, Sweden
F.Azgui, H.Grein, E.Grosse, R.Kulessa+, Ch.Michel, W.Spreng, H.J.Wollersheim, GSI Darmstadt
J. Stachel, Inst. f. Kernchemie der Uni. Mainz
D. Cline, B. Kotlinski, Nuclear Structure Research Laboratory, University of Rochester, USA

+ present address: Jagiellonian University, Kracow, Poland

Low lying band structures associated with a deformed nuclear shape have been observed to co-exist with the normally spherical or less deformed states in the even Sn isotopes[1,2] and in ^{110}Pd[3]. The low lying level structure of some even Cd nuclei like ^{114}Cd may suggest a similar shape co-existence. In order to examine closer these band structures we have performed a Coulomb excitation experiment on ^{114}Cd and ^{116}Sn using 5.0 MeV/u ^{208}Pb ions from the UNILAC. Coincidences were recorded between the scattered projectiles and the recoiling target nuclei and the de-exciting γ-rays. The particles were detected in two large area position sensitive gas counters[4] placed at 15.5 cm from the target and subtending an angle between 17 and 58 degrees with respect to the beam axis. The γ-rays were detected in 3 Ge detectors placed at 30, 150 and 210 degrees with respect to the beam axis. An example of a ^{114}Cd γ-ray spectrum in coincidence with the recoiling target nuclei is shown in fig. 1. The observed transitions and the excited levels are shown in fig. 2. As seen, the spectrum is dominated by low spin states, the highest spin observed being a possible 6^+ state. This is in contrast to e.g. ^{106,108}Pd, in which the states observed in the same process could be grouped[5] into four bands containing levels with spins up to 8. The data are presently being analysed, together with other Coulomb excitation data taken with ^{16}O, ^{40}Ca and ^{58}Ni projectiles at Uppsala, Rochester and Brookhaven respectively, using the recently developed Coulomb excitation code GOSIA[6], which automatically fits the electromagnetic matrix elements to the experimental data using a least squares minimization routine.

The spectrum from ^{116}Sn is dominated by the strong $2_1 \rightarrow 0_1$ transition. Only a few additional transitions could be seen, all with yields of about 2-5 % of that of the $2_1 \rightarrow 0_1$ transition.

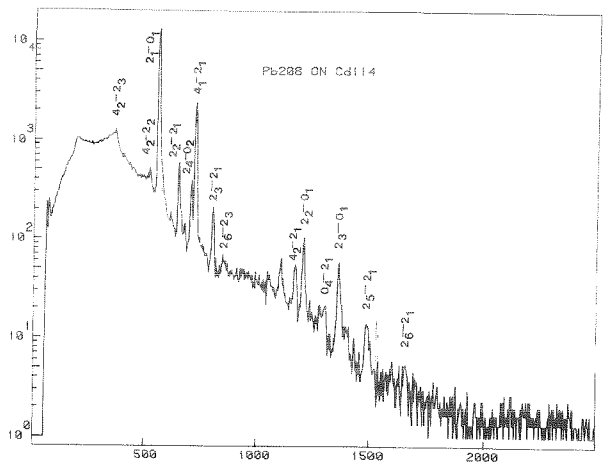


Fig. 1: The Doppler shift corrected γ-ray spectrum observed in Coulomb excitation of ^{114}Cd using ^{208}Pb ions.

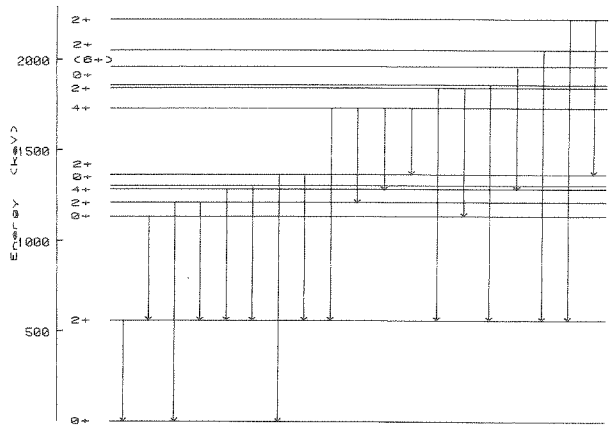


Fig. 2 Levels in ^{114}Cd excited in Coulomb excitation with ^{208}Pb ions.

References

1. J. Bron et al., Nucl.Phys. A 318, 335 (1979)
2. J. Kantele et al., Z.Phys. A289, 157 (1979)
3. L. Hasselgren and D. Cline in Interacting Bose-Fermi Systems in Nuclei, ed. by F. Iachello
4. P. Fuchs et al., to be published
5. L. Hasselgren et al., Ann.Rep. TLU, Uppsala 1982
6. T. Czosnyka et al., to be published

Investigation of the transitional nucleus ^{152}Gd [B]

P.Hill, N.Kaffrell, J.Stachel (Inst.f.Kernchemie, Univ.Mainz)
D.Schwalm (Phys.Inst., Univ.Heidelberg)
F.Azgui, H.Emling, E.Grosse, C.Michel, W.Spreng, H.J.Wollersheim (GSI Darmstadt)

The light lanthanides show a transition from spherical shapes to prolate deformations between neutron numbers N = 88 and N = 90. Due to the influence of the $d_{5/2}$ proton subshell closure this effect should be most pronounced in the Gd isotopes[1]. Moreover, with increasing angular momentum this phase transition is expected to be shifted to more neutron deficient isotopes[2]. This would result in a spin dependent increase of the quadrupole deformation in the yrast sequence of transitional nuclei. If one compares for example the level schemes of the Gd isotopes between N=86 and N=96, the energies of the 8→6 and 10→8 transitions are similar for such different nuclei - as judged from the 2^+ excitation energies - like ^{150}Gd and ^{160}Gd (fig.1). An analysis of these transition energies in terms of the moment of inertia would lead to nearly equal values. Electromagnetic transition probabilities and quadrupole moments are, however, more sensitive to the nuclear structure. They can be used as a tool to investigate the predicted spin dependent deformation change in the soft transitional nucleus ^{152}Gd. Previously measured B(E2) values within the ground state band (up to the 6→4 transition)[3] seem to indicate already an increase of transition quadrupole moments.

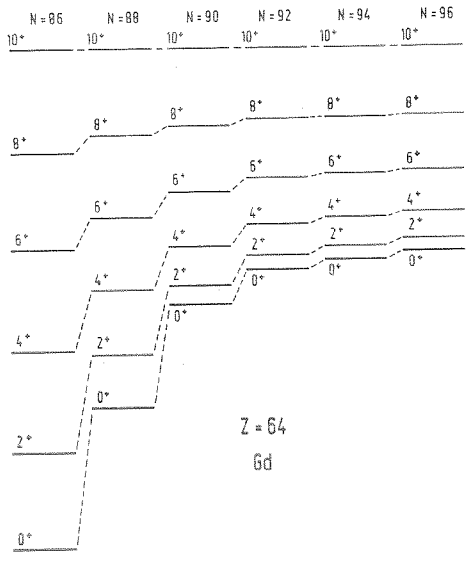


Fig. 1 : Yrast levels of the N=86-96 Gd isotopes normalized to the 10^+ states (energies taken from ref. 5).

To obtain more detailed information about the electromagnetic structure of this nucleus a multiple Coulomb excitation experiment has been performed with a ^{208}Pb beam of the Darmstadt UNILAC accelerator. Projectiles of 3.6 and 4.7 MeV/u incident energy have been used to bombard a target consisting of a 425 µg/cm² ^{152}Gd layer (enriched to more than 90 % isotopic abundance), which was deposited on a 85 µg/cm² carbon foil. A γ-particle coincidence set up[4] has been used to correct γ-spectra for Doppler shift and to measure with three Ge detectors the impact parameter dependence of γ-ray yields, from which B(E2) values can be extracted.

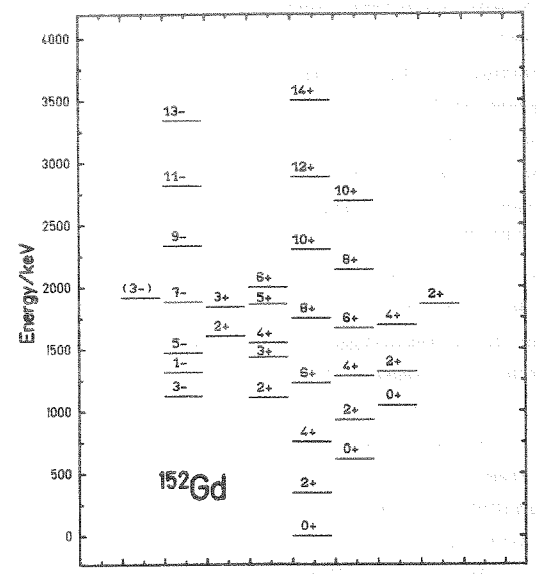


Fig. 2 : Levels populated in multiple Coulomb excitation of ^{152}Gd with a 4.7 MeV/u ^{208}Pb beam.

Beside the ground state band, which was excited up to the 14^+ state, six sidebands have been observed (fig.2) at the higher beam energy (4.7 MeV/u). Some of the ground state band transitions form multiplets with γ-rays depopulating high lying side band levels. These contaminations could be eliminated by an additional measurement at a lower bombarding energy (3.6 MeV/u), where the number of excited levels was drastically reduced. A successive evaluation of electromagnetic transition probabilities for inter and intra band transitions is in progress.

Targets with ^{148}Nd and ^{150}Nd have been shortly exposed to the 4.7 MeV/u ^{208}Pb beam. The 6^+, 8^+ and 10^+ yrast states of ^{148}Nd as well as the 12^+, 14^+ and 16^+ yrast states of ^{150}Nd have been newly identified.

1) R.F.Casten et al., PRL 47, 1433(1981)
2) R.Bengtsson et al., Proc. 4th Conf. on Nuclei far from Stability, Helsingør, CERN 81-09, 509(1981)
3) N.R.Johnson et al., PR C 26, 1104(1982)
4) P.Fuchs et al., GSI-J-1-78, p.195
5) C.M.Lederer and V.S.Shirley (ed.), Table of Isotopes (Wiley, New York, 1978)

Collective and single particle configurations at high spin in ^{154}Dy

F. Azgui, H. Emling, E. Grosse, C. Michel, H.J. Wollersheim
GSI Darmstadt
D. Schwalm, Phys. Institut, Universität Heidelberg

Rare earth nuclei with neutron numbers N = 82 - 86 are spherical in the ground state while the high spin states are formed by the alignment of a few high-j nucleons along a symmetry axis leading to an oblate shape. The heavier isotopes are prolate in the ground state and exhibit highly collective high spin states. The isotope ^{154}Dy with a neutron number N = 88 lies at the borderline between the spherical to prolate shapes. While the properties of the low spin levels of ^{154}Dy indicate a moderate prolate deformation, a transition to an oblate shape at higher spins ($30\hbar \leq I \leq 40\hbar$) via triaxial shapes at intermediate spins has been predicted[1]. The occurence of triaxial shapes was already found for rotation aligned states (s-bands) in the N = 90,92 Dy isotopes[2]. Furthermore, the investigation of the high spin level structure in ^{154}Dy (ref. 3) gave a first indication for a transition from a collective to an aligned particle configuration since above spin 30 the yrast line behaves irregularly. In order to investigate the predicted shape transitions we performed lifetime measurements with the aim to study the evolution of the E2-transition strength between yrast states with increasing spin.

We used the reaction ^{25}Mg (^{134}Xe, 5n) to populate high spin levels in ^{154}Dy and utilized the recoil distance method in measuring their lifetimes. Lifetimes and feeding times could be determined for levels in the positive parity yrast sequence up to spin $I^{\pi} = 28^{+}$ and up to $I^{\pi} = 23^{-}$ in the negative parity band which was also strongly populated. The resulting reduced quadrupole transition moments Q_t (I → I-2) of the yrast states are compared with the corresponding values of ^{156}Dy in fig. 1. Like in ^{156}Dy we observe an enhancement of the E2-transition strength with increasing spin in the ground state band (g-band), however, the Q_t-values of ^{154}Dy are ~ 30 % smaller than in ^{156}Dy on the average. In contrast, we observe similar Q_t-values for both isotopes in the rotation aligned $i_{13/2}$ s-band which forms the yrast line above a critical spin $I_c = 16\hbar$. While the lower Q_t-values in the g-band of ^{154}Dy reflect the transitional character of this isotope, the collective properties of its s-band are similar to that of ^{156}Dy for which a triaxial shape was concluded[2].

Lifetimes of yrast states in ^{154}Dy with $I > 28\hbar$ could not be measured because of their weak population. However, an important information about this spin region was obtained from the feeding times: we observed two components of almost equal intensity in the side feeding into the high spin levels, i.e. a short lived component with a feeding time $.5 \lesssim \tau_F \lesssim 1.$ ps and a long lived component with $\tau_F \sim 10$ ps. In fig. 2 we show a systematics of feeding times for the even N = 88 - 92 Dy isotopes, observed in Mg(Xe, xn) reactions leading to compound nuclei with comparable excitation energies and spins. In these reactions the preyrast γ-decay probes the level structure at spins $30 < I < 40\hbar$. In the N = 90, 92 isotopes only the short lived feeding component appears, indicating the persistence of a basically collective structure. The feeding times of the longlived components in ^{154}Dy (N = 88) are similar to the combined lifetimes and feeding times observed in the N = 86 ^{152}Dy isotope[4] whose high spin states are of single particle nature. Thus, the occurence of long lived feeding components together with the observed[3] fragmentation of the yrastline above spin $30\hbar$ give evidence for a coexistence of collective and single particle type configurations at $I > 30\hbar$.

1. C.G. Andersson et al., Phys. Script. 24 (1981) 266
2. H. Emling et al., Phys. Lett. 98B (1981) 169;
   H. Emling, GSI preprint 82-40
3. A. Pakkanen et al., Phys. Rev. Lett. 48 (1982) 1590
4. B. Haas et al., Phys. Lett. 84B (1979) 178

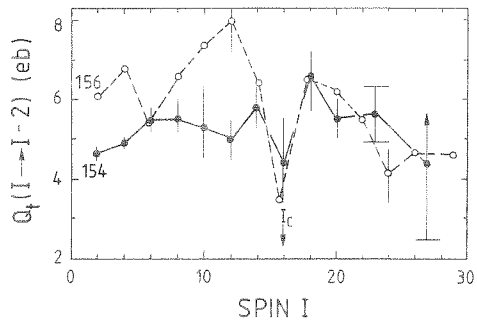


Fig. 1 Reduced quadrupole transition moments Q_t (I → I - 2) of yrast states in ^{154,156}Dy.

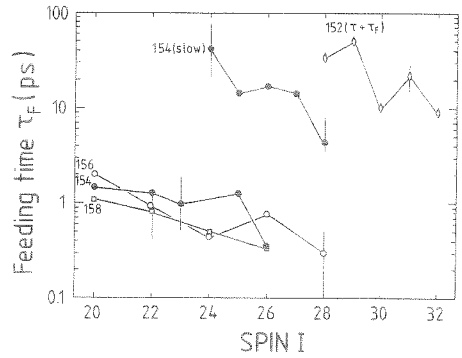


Fig. 2 Feeding times into high spin states of ^{154,156,158}Dy and combined life- and feeding times in ^{152}Dy (see text).

Investigation of the Yrast Region in ^{158}Er at High Spins

B G

R. Albrecht, B. Kolb, R.S. Simon, GSI Darmstadt
W. Hennerici, H.J. Hennrich, G. Himmele, R. Repnow, MPI für Kernphysik, Heidelberg
D. Habs, K. Helmer, U.v. Helmolt, H.W. Heyng, D. Pelte, D. Schwalm, Universität Heidelberg
V. Metag, Universität Gießen

The crystal ball supplemented by high resolution Ge counters is a powerful tool to study the yrast cascades in the evaporation residues from (HI,xn) reactions. The total γ-decay energy and the corresponding γ ray multiplicity from the crystal ball together allow a rather effective selection of nuclei with high angular momentum and low excitation energy. The subsequent γ cascades then can be investigated in detail with the coincident Ge counters or in the individual NaI modules.

For a preliminary experiment we used the $^{128}Te+^{34}S$ reaction at 155 MeV to populate $^{157,158}Er$ nuclei with high spins. The crystal ball, only partially assembled, contained 144 NaI modules and three Ge detectors with relative efficiencies between 10 and 15%. At least two Ge detectors and 30 of the NaI modules were required in coincidence, but due to the limited resolution of the crystal ball no total energy cuts were applied.

Fig. 1. shows a Ge detector spectrum of ^{158}Er. To enhance the yrast sequence above the first backbend we placed gates on the stretched-E2 I→I-2 yrast transitions between the $I^{\pi}=34^{+}$ and $I^{\pi}=16^{+}$ states observed in one of the other two Ge counters. Our spectrum confirms the known transitions up to the 38^{+} level[1] but suggests a different candidate for the 40^{+} state and indicates a steady continuation of the yrast sequence rather than a sharp irregularity.

The marginal energy resolution (6% around 1MeV) is a serious handicap for studying the top of the yrast region in ^{158}Er with the individual NaI modules. Using the crystal ball as a multiple anticompton arrangement, however, one obtains excellent peak/total ratios and it is possible to resolve structures in the transition energy correlations even at NaI resolution. Shown in Fig. 2 is a two-dimensional correlation matrix after unfolding and after corrections for multiple hits have been applied. Cascades in ^{158}Er were selected by gates on the I→I-2 yrast transitions below the 22^{+} level in the coincident Ge counters. One clearly sees the square pattern of horizontal and vertical stripes expected for the first and second backbend. The additional backbends at 1060 and around 1300 keV, however, which have been reported recently from a study of the energy correlations in ^{158}Er with Ge detectors[2] are not observed in our data.

1. J. Burde et al., Phys.Rev.Lett. 48 (1982) 530.
2. C. Ellegaard et al., Phys.Rev.Lett. 48(1982) 670.

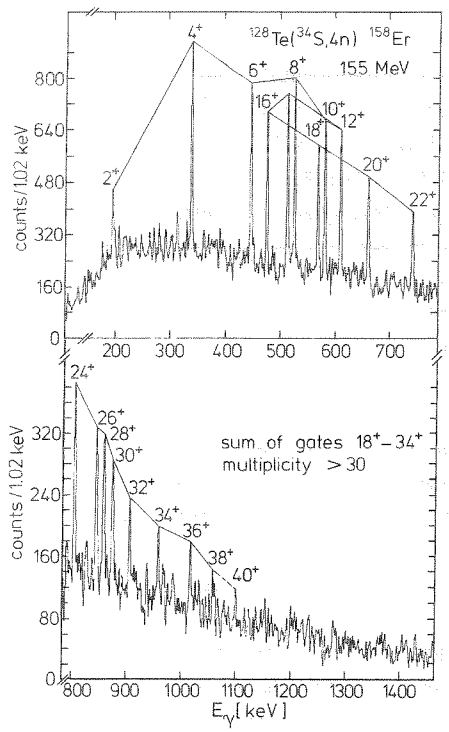


Fig. 1: Ge detector spectrum of the yrast cascade in ^{158}Er.

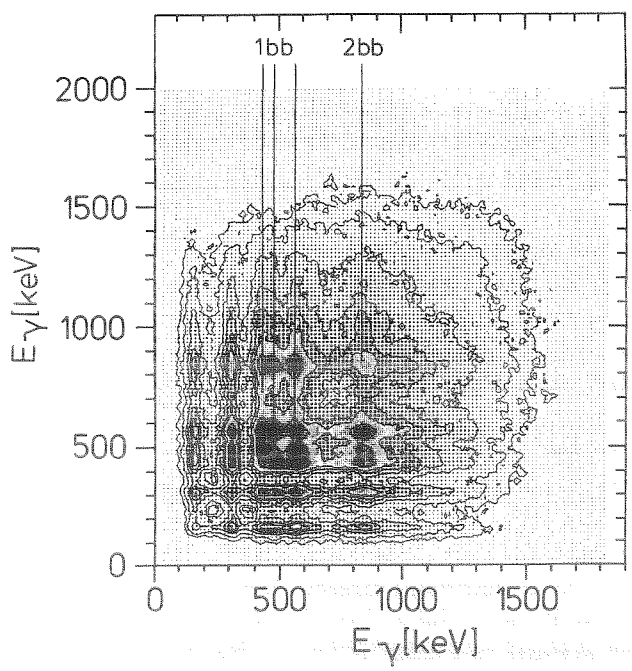


Fig. 2: Transition energy correlations in ^{158}Er as observed with the individual NaI detectors of the crystal ball in anticompton mode.

B G

Spin Dependence of the High Energy Component in the γ Decay Following Compound Nucleus Reactions

R. Albrecht, B. Kolb, R.S. Simon, GSI Darmstadt
W. Hennerici, H.J. Hennrich, G. Himmele, A. Lazzarini, R. Repnow, W. Wahl, MPI für Kernphysik, Heidelberg
D. Habs, U.v. Helmolt, H.W. Heyng, R. Kroth, D. Pelte, D. Schwalm, Universität Heidelberg
V. Metag, Universität Gießen

The γ spectra from compound nucleus reactions usually show an experimentally decreasing continuum above 2MeV which contains the statistical transitions in the deexcitation towards the yrast line. Deviations from the exponential behaviour have been observed recently above 8MeV and were interpreted as evidence for giant dipole transitions between nuclear states of high excitation and large angular momentum[1]. Exploiting the experimental possibilities of the NaI crystal ball spectrometer we have started to investigate this high energy component of the γ decay in detail.

The reaction chosen was $^{128}Te+^{34}S$. Using a pulsed ^{34}S beam of 155 MeV from the tandem postaccelerator in Heidelberg we produced ^{162}Er nuclei with excitation energies around 70 MeV and angular momenta up to 65 ħ. Neutrons and γ rays from the subsequent decay were observed in the closed geometry of the crystal ball. To suppress the random background from cosmic radiation we rejected all events where an individual pulseheight exceeded 30MeV, while prompt background contributions due to light target impurities were eliminated by requiring the characteristic (HI,xn) ratio of neutron to γ multiplicity. Neutron-γ pile-up in a single detector element finally was identified by a pulseshape analysis using the time information from a second threshold at 4.7 MeV in addition to the standard constant fraction timing.

The resulting proper compound nucleus component of the γ radiation is shown in Fig. 1 for 6 different γ multiplicities that cover initial spins from I=10 to I=55. The spectra are corrected for γ-γ pile-up which amounts to 3-10% on the average and they are compared to extrapolations of the statistical intensity assuming a constant Ei strength. The analytical expression used has two terms (see Fig. 2): one describes the γ-n competition in the first steps of the compound nucleus decay at effective temperatures T_{max} while the other, characterized by T_{min}, describes the usual statistical cascades after the emission of the last neutron. The excess of experimental intensity above 8 MeV in Fig. 1 is clearly visible in all cases.

The corresponding strength functions, essentially given as the experimental intensity divided by the statistical estimate, are shown in Fig. 2. They have roughly Lorentzian shape and do support the resonance character suggested for the high energy component. The strength function is centered around 10 MeV at high spins and gradually moves to higher energies with decreasing angular momentum. Over the full range in Fig. 2 the shift amounts to about 1.5 MeV, and even at low spins the center position deviates significantly from the value of 14.6 MeV observed in photoabsorption from the ground state.

1) J.O. Newton et al., Phys.Rev.Lett., 46 (1981) 1383.
2) Handbook of Chemistry and Physics, 46th edition (1965) A-177.

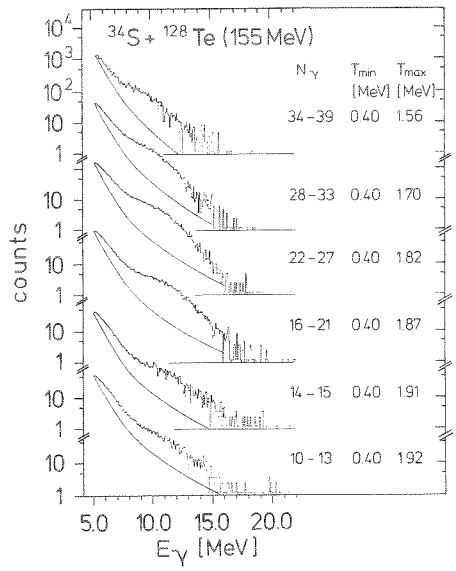


Fig. 1: Spin dependence of the high energy γ component as observed for 6 different multiplicity windows N_γ. The smooth curves show the shape of the statistical intensity estimated for the nuclear temperatures T_{min} and T_{max}.

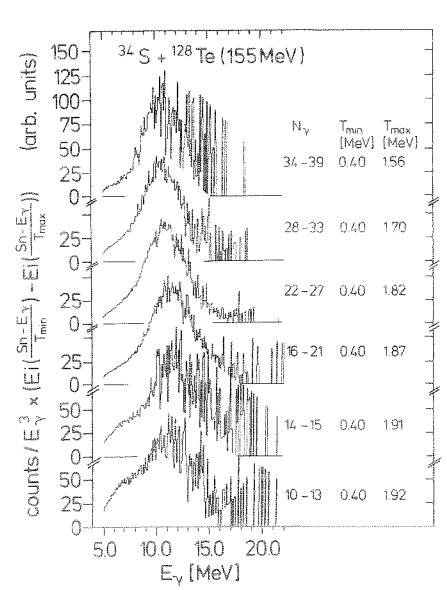


Fig. 2: γ strength functions. The quantity S_n in the argument of the Ei-function[2] is the neutron binding energy in the daughters of ^{162}Er.

Angular Correlations of γ-Ray Transitions in ^{164}Dy

H.J. Wollersheim, H. Emling, E. Grosse, C. Michel and D. Schwalm[1]
GSI, [1]Univ. Heidelberg

Measurements of the cross sections and angular distributions of γ-quanta which are emitted after the Coulomb excitation process can be used to determine the electromagnetic properties of nuclear states. In these experiments the projectile imparts a substantial amount of linear momentum to the nucleus, causing it to recoil out of the thin target foil into vacuum. The recoiling ion is generally in a highly excited atomic state which may produce large hyperfine magnetic fields at the nucleus. If one observes the Coulomb excitation via the yield of subsequent γ-rays it is an important practical question whether the alignment of the nucleus is disturbed by these magnetic fields. As the atomic fields are randomly oriented, the net effect is an attenuation of the anisotropy of the angular correlation.

In a typical Coulomb excitation experiment high spin states in ^{164}Dy have been investigated with a 4.7 MeV/u ^{208}Pb beam using our γ-particle coincidence set-up[1]. Both colliding partners were detected in two position sensitive parallel plate avalanche counters and identified by their time-of-flight differences. The two particle counters were positioned symmetrically with respect to the beam axis at $15° \leq \vartheta_L \leq 58°$, $-28° \leq \phi_L \leq +28°$ and $152° \leq \phi_L \leq 208°$, respectively. The coincident γ-rays were recorded in 4 Ge detectors positioned at $(\theta_\gamma, \phi_\gamma) = (30°, 180°), (30°, 0°), (150°, 0°)$ and $(150°, 180°)$. As the γ-ray angular correlation observed for a given Θ_{cm} scattering angle is symmetric around an axis close to $90°-\Theta_{cm}/2$, i.e. the target-recoil axis, and the relative angle between the recoil direction and Ge positions varies over a wide range due to the large opening angle of the particle detectors a detailed study of the γ-ray directional angular correlations is possible.

In the actual Coulomb excitation experiment the γ-ray angular correlation is not only perturbed but the moving source gives also rise to a distortion of the energy of the observed γ-quanta due to the Doppler shift. Since the change of the solid angle when going from the laboratory to the system where the excited nucleus is at rest is proportional to the square of the Doppler shift, it is possible to transform the γ-ray yields into the rest system using the measured γ-ray energies. Fig. 1 displays the ratio of γ-ray yields transformed in the rest system as a function of the c.m. scattering angle for $\Theta_\gamma = 30°$ and 150°. These yields were obtained by measuring coincidences between a particular γ detector and Dy or Pb ions scattered in the same particle counter and at identical c.m. angles. They measure the γ-ray angular correlation at two angles differing by $\Delta\Theta_\gamma \sim 60°$. The experimental results are compared with theoretical calculations assuming no deorientation $G_2 = G_4 = 1$ (dashed line) while the full drawn line is obtained by fitting the G_2 attenuation coefficients to the data, connecting the G_4 attenuation coefficients to the G_2 values via[2] $G_4 = 3G_2/(10-7G_2)$. The deorientation effect depends strongly on the lifetime of the nuclear state, resulting in an almost isotropic angular correlation for the 4-2 transition and a nearly unperturbed correlation for the decay of the 12^+ state. An average λ_2 parameter of 0.020 (5) ($psec^{-1}$) at a mean velocity $v/c = 6.5$ % has been extracted from the determined G_2 values using the well known Abragam and Pound model[2] for magnetic dipole interaction. This value does not follow the systematic of λ_2 values obtained from other experiments[3]; this is presently not understood assuming reasonable g-factor for the ^{164}Dy states.

[1]P. Fuchs et al., GSI Annual Report 1977, p. 195
[2]A. Abragam, R.V. Pound, Phys.Rev.92(1953), p. 943
[3]C. Michel et al., GSI Annual Report 1981, p. 55

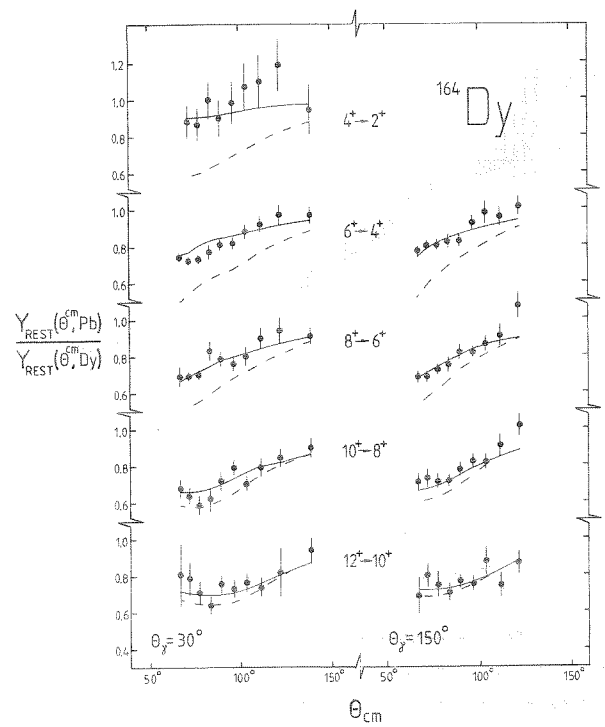


Fig. 1: γ-ray yield ratios (see text) as a function of the c.m. scattering angle.

Coulomb Excitation of ^{176}Lu by ^{208}Pb Ions [B]

Th. W. Elze, J. Gerl, Th. Happ, K. Keppler, H. Ower
Institut für Kernphysik, Universität Frankfurt

H. J. Wollersheim
GSI Darmstadt

The Coulomb excitation of the odd-odd nucleus ^{176}Lu by 4.7 MeV/u ^{208}Pb projectiles was studied employing gamma-particle coincidence techniques. The experimental set-up consisted of 3 Ge-detectors for the gamma rays, two of which were positioned at ±150°, the other at 30° with respect to the beam axis, and two position-sensitive parallel plate gas counters to detect both the scattered projectiles and the recoiling target nuclei. Each particle counter covered an angular range of $17^{\circ} \leq \Theta_L \leq 58^{\circ}$ and $\Delta\phi_L = \pm 28^{\circ}$ in the laboratory frame. The target was prepared in the Karlsruhe isotope separator[1] by depositing ≈1 mg/cm^2 ^{176}Lu on a 0.9 mg/cm^2 Ti foil. The experiment was performed in order to (i) obtain more detailed information on the rotational band built on the $K^{\pi} = 7^-$ ground-state configuration, in particular on the higher-spin states, and (ii) study the properties of collective side bands. These side bands appear to be accessible only via Coulomb excitation since most of the reactions studied so far[2] mainly lead to the excitation of higher-lying two-quasiparticle states.

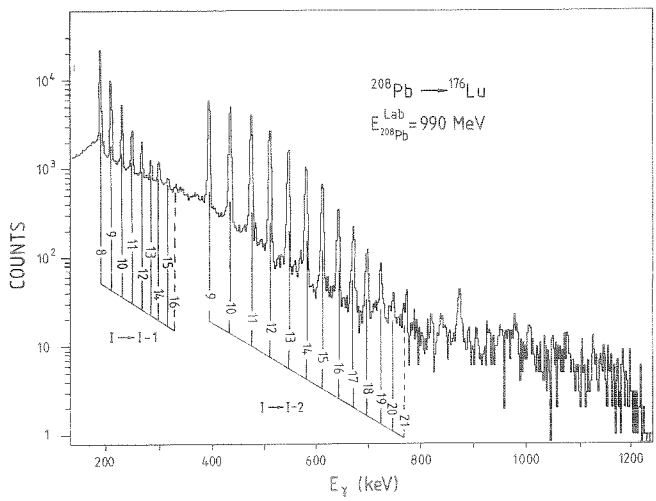


Fig. 1: Particle coincident gamma-ray spectrum resulting from the Coulomb excitation of ^{176}Lu by ^{208}Pb ions.

Fig. 1 shows a gamma-ray spectrum which was accumulated requiring triple coincidences between the gamma rays detected by one of the Ge-detectors at 150°, the scattered projectiles and the recoiling target nuclei. This method allows to distinguish between these two particles and to correct the gamma-ray energies for their strong Doppler shifts. The ground-state rotational band is seen to be excited up to the 20^- (possibly 21^-) level. Additional gamma lines with energies higher than 800 keV may be due to transitions from excited (vibrational) bands into the

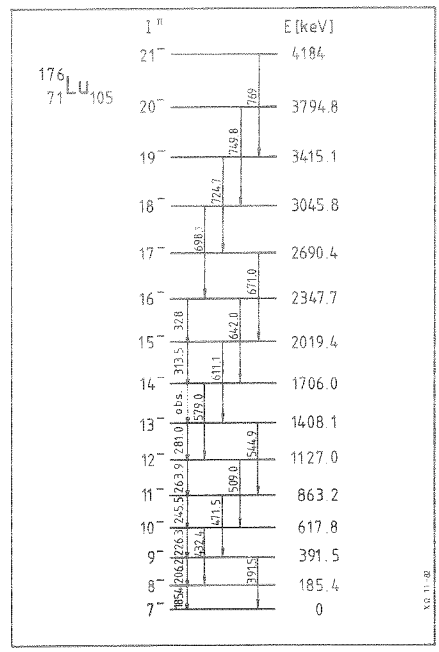


Fig. 2: Ground-state rotational band of ^{176}Lu as deduced from the present experiment.

ground band. The data are presently being analyzed to locate gamma-gamma coincidences in order to identify such transitions. It is also attempted to deduce electromagnetic transition matrix elements from the gamma-ray intensities which were measured as a function of the impact parameter.

Fig. 2 shows a partial level scheme (ground-band levels) of ^{176}Lu based on the gamma transitions identified in the spectrum of Fig. 1. The level energies indicate rotational behavior, but are found to be systematically lower than the values based on the I(I+1) prediction.

[1]The authors wish to thank Dr. A. Hanser for preparing the target.

[2]D. J. Horen and B. Harmatz, Nuclear Data Sheets 19 (1976) 383;
R. A. Dewberry et al., Phys. Rev. C 24 (1981) 1628

Study of Deorientation in $^{196}Pt^{B}$

A. Mauthofer, H. Ower, K. Stelzer, Th. W. Elze
Institut für Kernphysik der Universität Frankfurt am Main
H.J. Wollersheim, H. Emling, E. Grosse und D. Schwalm
GSI Darmstadt

The evaluation of the Coulomb excitation experiments [1] on the shape transitional nucleus ^{196}Pt with ^{208}Pb projectiles of the energy 4.8 MeV/u was continued including the deorientation effect, which had not been taken into consideration in the earlier analysis.

This deorientation is due to hyperfine fields present in the target atoms recoiling into vacuum. The information on the size of this effect could be extracted from the data themselves through the comparison of gammaray yields corresponding to different points of the particle gamma angular correlations.

The γ-spectra always contain two events for each γ-transition. One event, if the recoiling Pt was detected in the position sensitive parallel plate counter (PPC) and the other event, if the Pb projectile was scattered into the PPC. Because no kinematic separation between the nearly equal masses of ^{196}Pt and ^{208}Pb is possible we separated the two events by their different dopplershift and compared spectra belonging to the same c.m. scattering angle, i.e. impact parameter. These two events were used to determine the angular correlation and the deorientation parameters G_2 of states up to $I^{\pi}=6^{+}$ (see [2]). For the χ^2-fit of the G_2-parameters it was assumed that the relation between G_2 and G_4 is given by the theory of Abragam and Pound (A.P.).

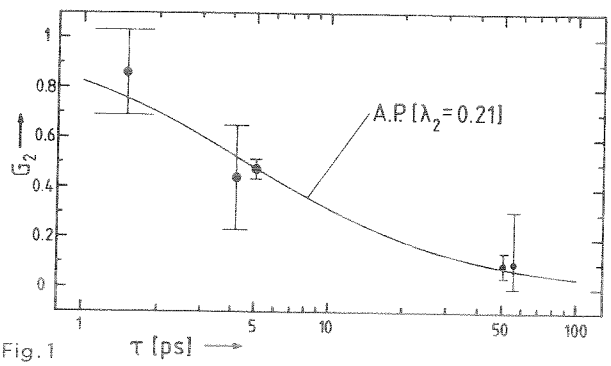


Fig. 1

Figur 1 shows the experimental attenuation factors G_2 and the Abragam and Pound calculation with λ_2=0.21 psec^{-1} plotted versus the meanlives τ of the states taken from Bolotin et al.[3].

With the experimental attenuation factors G_2 and the meanlives of the states we extracted the λ_2-parameters. The results are given in table 1. If we assume a constant g-factor g=0.296 (average from [4]) for I≤6 we obtain an averaged value for λ_2/g^2=2.46±0.37. The velocity of the recoiled nucleus ranged from v/c=0.061 up to v/c=0.086.

Our value for λ_2/g^2 is surprisingly large and exceeds other values in this velocity region [2] which had seemed to indicate an upper limit at λ_2≈0.2 resp. λ_2/g^2≈1. On the other hand good agreement is obtained if the nearly linear trend of the λ_2/g^2-values, observed at lower velocities, is extrapolated.

An analysis of the data to determine E2 matrix elements is in progress.

Tab.1

E(keV)	I^{π}	τ[ps]	G_2	λ_2
355.7	2^+	50.8(22)	0.093(50)	$0.192(^{246}_{74})$
689.0	2^+	55.8(37)	0.10 (21)	$0.16\ (^{27}_{7})$
876.7	4^+	5.05(27)	0.473(40)	$0.26\ (^{5}_{4})$
1293.4	4^+	4.2 (5)	0.44 (21)	$0.30\ (^{50}_{17})$
1526.0	6^+	1.5 (4)	0.86 (17)	$0.109(^{191}_{109})$

References
[1] GSI Scientific Report 1979 p.44
[2] C. Michel et al., GSI Scientific Report 1981 p.55
[3] H. Bolotin et al., Journal of the Phys. Soc. of Japan, Vol. 47, No. 5 (1979) 1397
[4] Nuclear Data Sheets 16 (1979) 521
Phys. Rev. C Vol. 24, No. 5 (1981) p. 2106

Coulomb Excitation of ^{202}Hg and ^{204}Hg with ^{208}Pb Ions

Y.K. Agarwal*, C. Günther, K. Hardt, and P. Schüler
Institut für Strahlen- und Kernphysik, Universität Bonn
J. Stachel
Institut für Kernchemie, Universität Mainz
E. Grosse, R. Kulessa, W. Spreng, H.J. Wollersheim
GSI Darmstadt

The ground state bands in even Hg istopes have been experimentally investigated over a wide mass range. These investigations revealed a very smooth variation of the low spin states ($I \leq 6^+$) for the nuclei with $190 \leq A \leq 198$. This behaviour seems reasonable since the nuclei in the quoted mass range have a small oblate deformation ($\varepsilon \approx -0.15$) which varies only slowly with mass number. For ^{200}Hg one observes a rather sharp discontinuity in the level energies, for which the explanation seems still controversial[1], but for the heavier isotopes ^{202}Hg and ^{204}Hg the 2^+ and 4^+ level energies are again very similar to those of the lighter isotopes. This is rather surprising since for these isotopes one approaches the doubly magic ^{208}Pb, and one would expect a smooth transition from collective to single particle properties. In fact the observed B(E2, $0^+ \rightarrow 2^+$), (see Fig. 2), and Q_{2^+} values indicate[2] a significant decrease of the collectivity from ^{196}Hg to ^{204}Hg.

One problem in the discussion of the properties of heavy Hg nuclei is, that very little information is available on the level schemes of ^{202}Hg and ^{204}Hg. In fact only recently the 4^+ levels of the ground state bands in these nuclei were identified unambiguously in Coulomb excitation experiments[3,4]. We have, therefore, performed multiple Coulomb excitation experiments using a 5 MeV/u ^{208}Pb beam from the UNILAC to bombard thin targets of enriched ^{202}Hg and ^{204}Hg. Particle-gamma coincidences were recorded using the GSI set up[5] to correct for the large Doppler shift and to measure the gamma ray yields as a function of scattering angles. Examples of the measured γ-spectra are shown in Fig. 1. We observe, apart from the known $2^+ \rightarrow 0^+$ and $4^+ \rightarrow 2^+$ transitions, one fairly strong γ-line, which we assign as $6^+ \rightarrow 4^+$ transition on the basis of its impact parameter dependence. In addition a number of weak lines are observed which could so far not be assigned to known levels in ^{202,204}Hg isotopes.

The systematics of the level energies up to the 6^+ states in $^{196\text{-}206}$Hg together with already known B(E2) values is shown in Fig. 2. The increase of the 6^+ level energies from ^{200}Hg to ^{204}Hg again points to the expected transition from collective to single particle excitations.

[1] I. Morrison and R.H. Spear, Phys. Rev. C23, 932 (1981)
[2] M.T. Esat et al., Nucl. Phys. A362, 227 (1981)
[3] A. Bockisch et al., Z. Phys. A291, 245 (1979)
[4] C. Günther et al., Z. Phys. A301, 119 (1981)
[5] P. Fuchs et al., GSI Annual Report 1977, 195
[6] R.H. Spear et al., Nucl. Phys. A345, 252 (1980)

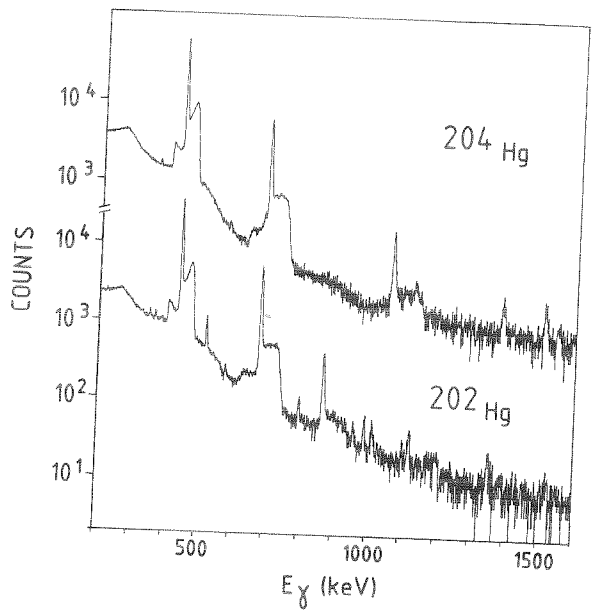


Fig. 1: Doppler shift corrected gamma spectra for ^{202}Hg and ^{204}Hg in coincidence with particle scattered at $64° \leq \theta_{cm} \leq 146°$.

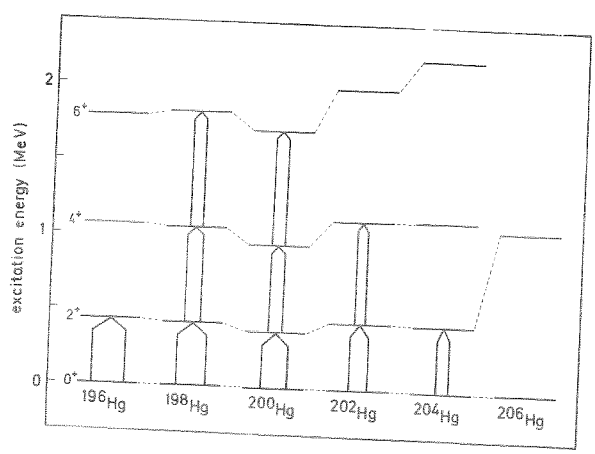


Fig. 2: Level energies and B(E2) systematics for ^{196}Hg-^{206}Hg (size of the arrow indicates the magnitude of the B(E2) value)[2,3,4,6].

Present address: GSI, Darmstadt

B

High Spin States of ^{230}Th studied in Coulomb Excitations with ^{142}Nd Projectiles

Ch. Lauterbach, J. de Boer, Ch. Mittag, F. Rieß, Ch.Schandera, Ludwig-Maximilians-Universität München
Ch. Briançon, A. Lefebvre, CSNSM Orsay
R.S. Simon, GSI Darmstadt

The ground state bands of the even deformed actinides are beautiful examples of nuclear rotation. With increasing angular momentum, however, one finds similar distortions due to the onset of particle alignment as observed in the rotational bands of many rare earth nuclei. Our present experimental information about these alignment effects in the actinides above I=20 is rather limited still, since the measurements only cover the proton numbers from Th to Cm and the neutron numbers from N=142 to N=152. To extend this region we studied Coulomb excitation of ^{230}Th(N=140) with ^{142}Nd projectiles at 4.8 MeV/A.

We used a thin target of Thorium oxide on a thick backing of Be and our method was to stop the excited ^{230}Th nuclei within the first steps of the γ-decay. To confine the recoil directions to a narrow forward cone we identified the backscattered ^{142}Nd projectiles in a parallel plate ring counter. This particle coincidence also helped to suppress the prompt γ-intensity from ^{16}O and ^{9}Be induced nuclear reactions as well as the background radiation from the 5μCi target activity. The target was mounted in the center of a large annular NaI detector which was separated into 6 equal segments of 60°. With one segment displaced by half the detector length the NaI spectrometer allowed to collect the total excitation energy of a given cascade and at the same time provided access for three additional Ge detectors at 0°, 90° and 180° with respect to the beam direction to observe individual γ-transitions with high resolution. To enhance high spin events we required at least multiplicity 3 in the NaI spectrometer and used the total sum energy for further selectivity within this hardware condition.

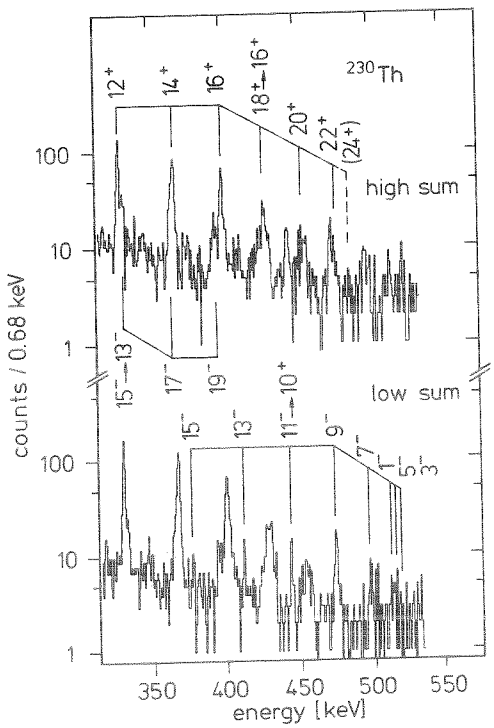


Fig. 1: High spin region of the ^{230}Th γ-spectrum as observed for low and high total decay energy.

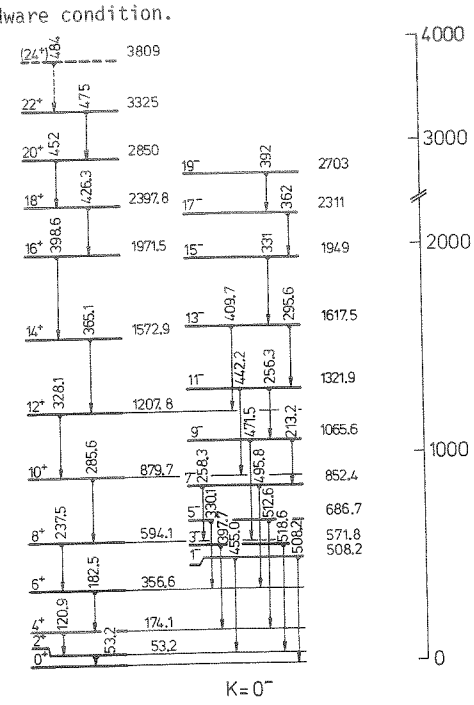


Fig. 2: Partial level scheme of ^{230}Th.

As an example, Fig. 1 shows two 90° spectra. They were accumulated for different sum energies and therefore represent cascades of different length. In both cases the transitions at the top of the γ-cascades are Doppler broadened due to the finite solid angle of the Ge detector, while the subsequent γ-transitions which are emitted from nuclei at rest appear as sharp lines. We assign the additional intensity under the stopped $9^- \rightarrow 8^+$ line in the upper spectrum to the $22^+ \rightarrow 20^+$ transition. Similarly, the surplus intensity observed between 480 and 490 keV probably marks the position of the 24^+ candidate.

A partial level scheme for the yrast and octupole sequence of ^{230}Th is given in Fig. 2. At the top of the yrast sequence the onset of particle alignment is clearly visible from the reduced transition energy spacings. If substantiated, the irregular behaviour of the $24^+ \rightarrow 22^+$ transition would indicate a rather sharp upbend or even backbend of the effective moment of inertia in ^{230}Th at rotational frequencies around 0.25 MeV.

Backbending in ^{242}Pu and ^{244}Pu

W. Spreng, F. Azgui, H. Emling, E. Grosse, R. Kulessa*, Ch. Michel, R.S. Simon,
H.J. Wollersheim (GSI Darmstadt);
M. Mutterer, J.P. Theobald (TH Darmstadt)
D. Schwalm (Univ. Heidelberg); M.S. Moore (Los Alamos SL)

In the region of well deformed actinide nuclei both $i_{(13/2)}$ protons and $j_{(15/2)}$ neutrons are close to the Fermi surface. At rapid rotation these high-j particles will unpair and decouple from the rotating core giving rise to aligned bands (s-bands) that cross the ground-state band. The crossing will cause an irregularity in the yrast sequence and in the case of a weak interaction between the two crossing bands a backbending should be observed. However, the level spacings of the even actinide isotopes studied so far[1,2,3,4] showed only small anomalies at high spins.

The collective bands built on the ground state of ^{242}Pu and ^{244}Pu have been populated via multiple Coulomb excitation using ^{208}Pb ions with 5.6 and 5.8 MeV/u. A γ-particle-particle-coincidence set-up was used to measure the de-excitation γ-rays (see ref. 1 for details of the method). The Doppler corrected γ-spectra for both nuclei are shown in fig.1.

For ^{242}Pu the yrast states have been observed up to spin $I^{\pi}=26^{+}$ and a pronounced upbending was found. In the case of ^{244}Pu we found for the first time an experimental evidence for a well pronounced backbending in the actinide region: the yrast sequence seems to terminate at spin 22^{+}, however, the intensity and the width of the peak at 472 keV indicate an unresolved doublet; it was tentatively assigned to the $22^{+} \rightarrow 20^{+}$ and $24^{+} \rightarrow 22^{+}$ transitions. Moreover, the peak at 458 keV was identified as a transition between high spin states because of its characteristic impact parameter dependence of the γ intensity, and we tentatively assigned it to the $26^{+} \rightarrow 24^{+}$ transition. In order to confirm these assignments a γ-γ coincidence measurement will be performed.

In fig. 2 the experimental results are compared with Hartree-Fock-Bogoliubov calculations[5] which qualitatively reproduce the experimental findings. The calculation suggests an explanation of the observed anomalies as an intersection of the ground state band with an aligned two q.p. $i_{13/2}$ proton band and predicts that the interaction between g-band and s-band is weaker in ^{244}Pu as in ^{242}Pu.

[1] E. Grosse et. al., Physica Scripta(24), 1981, 337
[2] R.B. Piercey et. al., Phys. Rev. Letter(46),1981,415
[3] H. Ower et. al., Nucl.Phys. A388, 1982, 421
[4] R.S. Simon et al., Phys. Letters 108B, 1982, 87
[5] J.L. Egido et al., priv. comm. and to be published
*on leave from Krakow Univ.

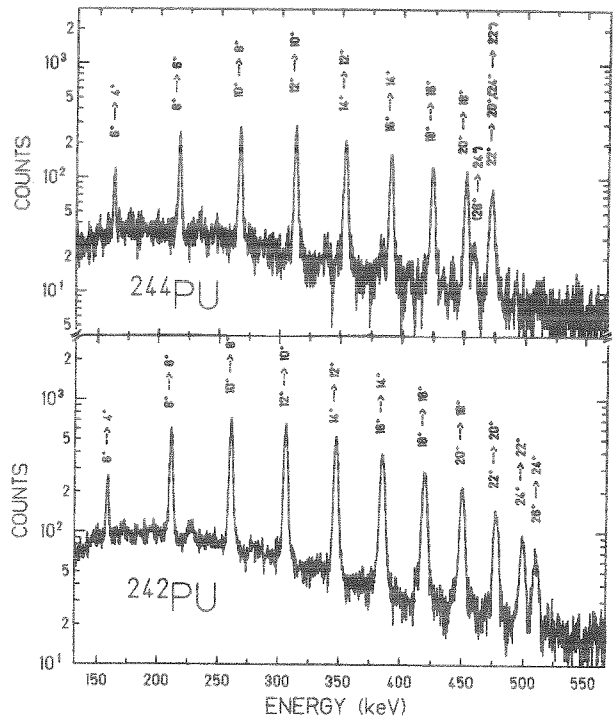


Fig. 1: Dopplershift-corrected gamma spectra for ^{242}Pu and ^{244}Pu.

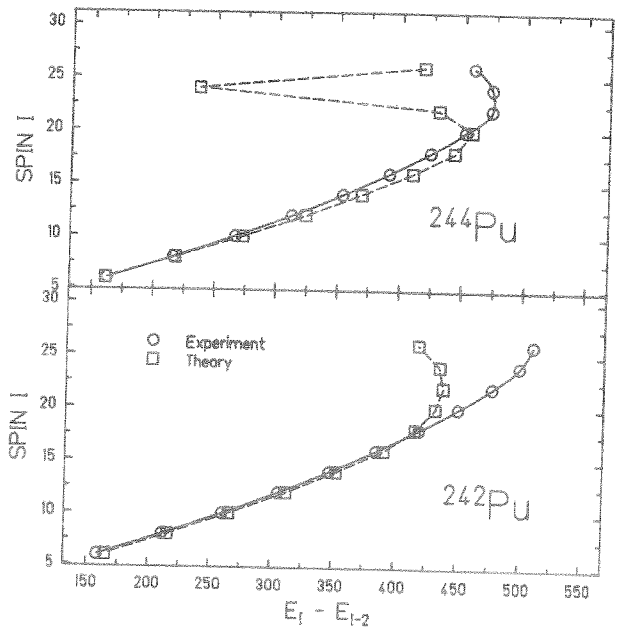


Fig. 2: Comparison of the experimental transition energies with the calculations of ref. 5.

Laser Spectroscopy at the GSI On-Line Mass Separator

G.Ulm, J.Eberz, G.Huber, D.Kaplan and H.Lochmann, Institut für Physik der Universität Mainz,

R.Kirchner, O.Klepper, T.U.Kühl, P.O.Larsson, D.Marx, E.Roeckl and D.Schardt, GSI Darmstadt

A modified version of the fast atomic beam laser spectroscopy set-up[1] is installed at the central beamline of the on-line mass separator (see fig.1). In a first on-line measurement in December 1982, optical spectra of three radioactive isotopes, $^{108,109,110}In$, have been recorded.

Indium isotopes are produced via fusion reaction between ^{14}N and isotopically enriched molybdenum. The target consisting of several molybdenum foils is placed inside a FEBIAD-A plasma ion source[2]. With this modified geometry the yield of mass separated indium isotopes reached 10^7 ions/s at ^{14}N intensities of about 1 particle μA. The mass-separated ion beam is merged with the laser beam by an electrostatic deflector and then neutralized in a sodium charge-exchange cell. Optical fluorescence is detected 30 cm downstream by focusing the light from a large solid angle onto a photomultiplier with an ellipsoidal mirror oriented transverse to the beam. In order to avoid optical pumping in the drift space between charge exchange and observation, the axial magnetic field (240 Gauss) of a long solenoid detunes the resonance of the fast atoms via the Zeeman effect, i.e. the resonance is "Zeeman-quenched". With appropriate magnetic shielding the optical excitation in the observation region takes place at zero field. The resonance is scanned either by tuning the single mode dye laser (Coherent 699) or through a change in the Doppler shift achieved by the application of a decelerating potential at the charge-exchange cell.

Figure 2 shows the spectrum of ^{108}In ($T_{1/2}$ = 58 min) together with the signal from the stable isotope ^{115}In which is fed into the ion source as a reference standard. The hyperfine structure - obviously different for the two isotopes - gives information on the magnetic dipole moment and the electrical quadrupole moment. Due to their different masses the isotopes do not have the same velocity after acceleration in the mass separator, which leads to a relative Doppler shift. This effect is precisely determined by measuring the position of the Doppler shifted lines relative to a catalogued absorption line in Te_2[3]. The remaining (isotope-)shift of the center of gravity of the hfs-multiplets contains information on the change in the mean-square nuclear charge radius.

1) GSI Scientific Report, GSI 82-1, p.234

2) R.Kirchner et al., Nucl. Instr. Meth. 186 (1981), 295

3) Atlas du Spectre d'Absorption de la Molécule de Tellure, J.Cariou, P.Luc, Edition du CNRS (1980)

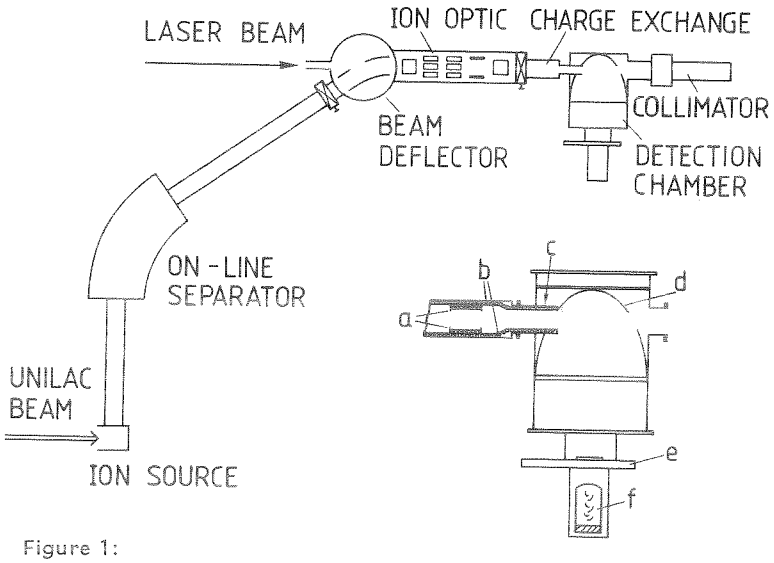


Figure 1:
Schematic view of the on-line laser spectroscopy set-up
a) charge exchange zone, b) solenoid, c) magnetic shielding, d) ellipsoidal mirror, e) filter assembly, f) photomultiplier

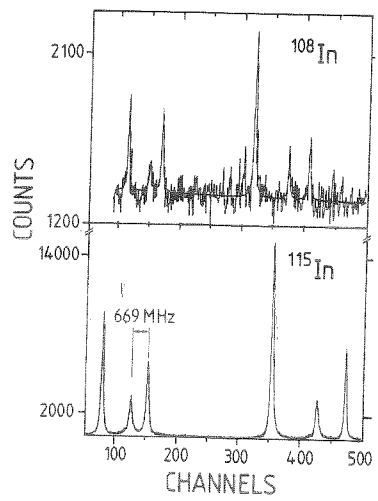


Figure 2:
Hyperfine structure in the 5p $^2P_{3/2}$ - 6s $^2S_{1/2}$ transition (λ = 451 nm) in ^{108}In and ^{115}In

Direct Proton Decay of 0.56-s ^{147}Tm and Search for this Decay Mode Among Very Neutron-Deficient Isotopes with $61 \leq Z \leq 67$

P. O. Larsson, T. Batsch, R. Kirchner, O. Klepper, W. Kurcewicz, E. Roeckl, D. Schardt
GSI, Darmstadt

G. Nyman
Department of Physics, Chalmers University of Technology, S-412 96 Göteborg

P. Tidemand-Petersson
II. Physikalisches Institut, Universität Göttingen, D-3400 Göttingen

Neutron-deficient isotopes with $65 \leq Z \leq 69$, produced in ^{58}Ni + ^{92}Mo and ^{58}Ni + ^{93}Nb reactions, were studied at the GSI on-line mass separator by decay spectroscopy of positrons, protons, γ and X rays. The observed 1055 ± 6 keV proton line at mass number 147, preliminarily assigned to direct proton decay of ^{147}Tm [1], was further investigated by cross bombardment and positron-proton coincidence measurements; the latter showed that the protons do not follow beta decay but are emitted directly. The ^{147}Tm assignment was confirmed, and the half-life was remeasured, with higher precision, to be 0.56 ± 0.04 s [2]. By γ-singles multispectrum analysis and through measured coincidence relations of protons, γ and X rays, the new isotopes ^{147}Er (2.5 ± 0.2 s), ^{149}Er (9.3 ± 0.4 s), and ^{149}Tm (4.5 ± 1 s) were identified.

According to mass formulae, there exist further candidates for direct proton decay among neighbouring lighter odd-Z nuclei in the region $61 \leq Z \leq 67$. Direct proton decay half-lives depend strongly upon available decay energy, which restricts the number of experimentally observable cases. For long proton decay half-lives, β^+/EC decay dominates and for half-lives shorter than 10^{-3} s, detection of the decay mode is hardly possible at a mass separator facility. Calculations on the process [2,3] show that observable intensities can only be expected for proton energies between 0.6 and 1.3 MeV.

Using heavy-ion induced (^{40}Ca, 5 MeV/u) fusion evaporation reactions, we first studied known short-lived isotopes of promethium, europium, terbium, and holmium. From comparisons between observed source strengths and theoretical values for primary production rates (HIVAP code), overall efficiencies for on-line mass separation of these elements were estimated. These measurements were performed for two types of thermal ion sources, Re-TIS(C) and W-TIS(Ta), with graphite and tantalum catchers, respectively, out of which the latter showed the best performance (Table 1) [2]. Employing telescopes of surface barrier detectors, direct proton decay was sought for among very neutron-deficient isotopes of these elements [2]. No evidence for this decay mode was found. Based on estimated overall efficiencies as well as on calculated cross-sections and gross-theory beta decay half-lives, limits for direct proton decay were deduced (Fig. 1).

1) O. Klepper, T. Batsch, S. Hofmann, R. Kirchner, W. Kurcewicz, W. Reisdorf, E. Roeckl, D. Schardt, G. Nyman: Z. Physik A 305,125(1982)

2) P. O. Larsson, T. Batsch, R. Kirchner, O. Klepper, W. Kurcewicz, E. Roeckl, D. Schardt, W. F. Feix, G. Nyman, P. T. Tidemand-Petersson: to be published.

3) W. F. Feix, E. Hilf: Phys. Lett. 120B,14(1983)

Table 1 Overall efficiencies for two thermal ion sources

Isotope	Overall efficiency(%)	
	Re-TIS(C)	W-TIS(Ta)
^{135}Pm(44s)	0.54	5.7
^{140}Eu(1.5s)	0.40	0.41
^{146}Tb(23s)	≤0.046	1.8
^{151}Ho(36s)	0.03	1.5

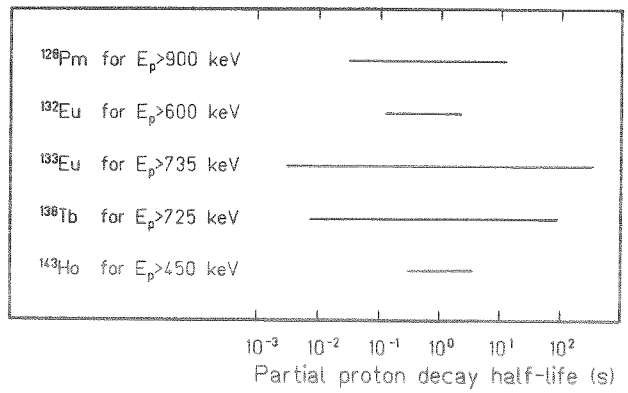


Fig. 1 Observation windows for direct proton decay for isotopes of which at least 10^5 atoms were produced. At low energies, a background of β rays and β-delayed protons was present and the indicated proton-energy limits correspond to a background level of three events observed during the counting time; the observation windows for the half-lives are valid for proton energies higher than these lower limits. The bars show the observation windows for direct proton decay in our experiment and the nonobservations imply that with 90 % probability the real half-lives are outside the intervals. The ranges of the intervals are model-dependent, based on cross-sections calculated with the HIVAP code, proportionality between overall efficiency and half-life, and β decay half-lives predicted by gross-theory.

Predictions of Further Proton Radioactivity Near ^{151}Lu

S. Hofmann, Y.K. Agarwal, F.P. Heßberger, G. Münzenberg, W. Reisdorf, J.R.H. Schneider, H.-J. Schött, P. Armbruster
GSI Darmstadt

Recently many spectroscopic data have been published on nuclei $Z \geq 64$, $N \leq 82$. With the help of these data it was possible to construct level schemes of nuclei around the proton emitter ^{151}Lu by extrapolation (Fig. 1). Characteristic for all the investigated even N nuclei is a level sequence which can be described by application of the seniority scheme to protons in the h 11/2 subshell. Near 3 MeV of excitation energy the s = 2 and s = 3 sequence is closed with a long living (0.1-100 µs) isomer of spin 10^+ and $27/2^-$, respectively. Within the frame of these schemes we discuss the possibility to find further proton radioactive nuclei beside the known p emitters ^{151}Lu[1] and ^{147}Tm[2] in this region of nuclei. A detailed discussion including a list of references has been presented in Ref. 3.

The results of a WKB calculation of partial proton widths are listed in Table 1. Most interesting in ^{151}Lu itself is the decay of the $27/2^-$ isomer to the 2^+ and 4^+ daughter states in ^{150}Yb. Assuming a partial γ half life of 3 µs we calculate proton branches of 0.3 and 0.7 % which are coincident to γ transitions of 620 keV and 860 keV, respectively. The relative position of a low spin state ($\pi d_{3/2}$ or $\pi s_{1/2}$) with respect to the $11/2^-$ state can be investigated in a search experiment for short living proton decays either in ^{151}Lu or ^{153}Lu.

Promising candidates for proton emission are the 10^+ isomeric state in ^{150}Yb and a high spin ground or low lying isomeric state in ^{150}Lu. This high spin state results from the coupling of a $h_{11/2}$ proton and a $d_{3/2}^{-1}$ or $s_{1/2}^{-1}$ neutron hole. If in a proton decay the neutron hole remains unchanged we expect a similar reduced proton width as in case of ^{151}Lu. Experimental hints already exist[3] and demand further experiments. With some restrictions the results are valid also for the proton decay of ^{147}Tm and neighbouring nuclei and ^{155}Ta.

[1] S. Hofmann et al., Z. Phys A - Atom and Nuclei 305, 111-123 (1982)
[2] O. Klepper et al., Z. Phys. A - Atoms and Nuclei 305, 125-130 (1982)
[3] S. Hofmann et al., XI Int. Conf. Gross Prop. of Nuclei and Nucl. Excitations, Hirschegg (1983) to be published
[4] E. Nolte et al., Z. Phys. A - Atoms and Nuclei 306, 223-234 (1982)

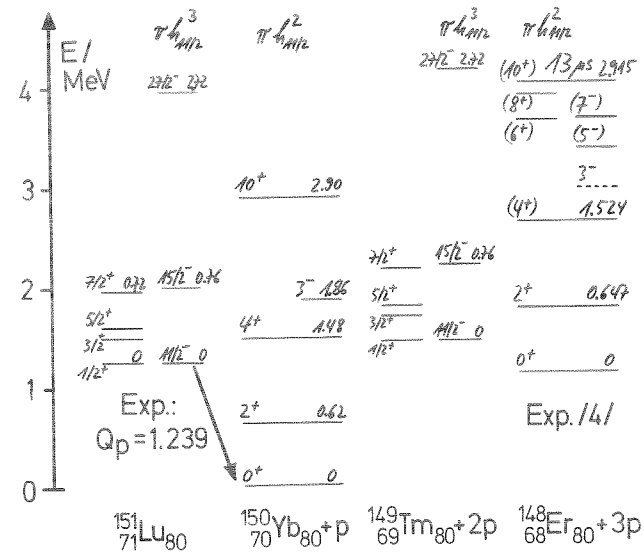


Fig. 1: Levels schemes of ^{151}Lu, ^{150}Yb, and ^{149}Tm which have been obtained by extrapolation of known schemes of $h_{11/2}$ nuclei.

Transition	E_p/MeV	$\Delta l/\hbar$	$T_{1/2,p}$	$(T_{p,i}/T_{p,tot})$/%
^{151}Lu → ^{150}Yb				
$11/2^- \rightarrow 0^+$	1.231	5	81 ms	100
2^+	0.61	3	24 Ms	10^{-7}
$15/2^- \rightarrow 0^+$	1.99	7	70 µs	98
2^+	1.37	5	4 ms	2
$27/2^- \rightarrow 0^+$	3.95	13	110 ms	0.3
2^+	3.33	11	1 ms	28
4^+	2.47	9	400 µs	71
3^-	2.09	10	1 s	0.03
10^+	1.05	3	30 ms	0.9
$1/2^- \rightarrow 0^+$	1.23	0	3 µs	100
^{150}Yb → ^{149}Tm				
$10^+ \rightarrow 11/2^-$	1.47	5	310 µs	100
$15/2^-$	0.71	3	23 ks	10^{-6}
^{150}Lu → ^{149}Yb				
$4^- \rightarrow 3/2^+$	1.26	3	97 µs	100
$5^- \rightarrow 1/2^+$	1.36	5	5 ms	91
$3/2^+$	1.26	5	50 ms	9
$6^- \rightarrow 3/2^+$	1.26	5	50 ms	100
$7^- \rightarrow 1/2^+$	1.36	7	3 s	90
$3/2^+$	1.26	7	27 s	10

Table 1: Calculated partial proton half lives for transitions ^{151}Lu → ^{150}Yb, ^{150}Yb → ^{149}Tm, and ^{150}Lu → ^{149}Yb.

Neutron-Rich Lutetium Isotopes Investigated at the GSI On-Line Mass Separator B

R. Kirchner, W. Kurcewicz, E. Roeckl, D. Schardt, GSI Darmstadt
N. Kaffrell, P. Peuser, Universität Mainz
K. Rykaczewski, University of Warsaw
E. Runte, W.-D. Schmidt-Ott, P. Tidemand-Petersson, K.-L. Gippert, Universität Göttingen
G. Walter, H. Beer, Kernforschungszentrum Karlsruhe

In continuing earlier experiments[1], we studied[2,3] neutron-rich lutetium isotopes produced in multinucleon reactions. Sandwich targets, containing thin natural tantalum and tungsten foils of 10 mg/cm² and 16 mg/cm² total thickness, respectively, were bombarded with 11.7 MeV/u, 10-15 particle•nA ^{136}Xe beams from the UNILAC. On-line mass separated sources were investigated by decay spectroscopy.

We identified[2] the new isotope ^{183}Lu with a half-life of 58(4)s. The decay scheme of ^{183}Lu was constructed on the basis of energy considerations and intensity balances. The levels in ^{183}Hf are interpreted as members of rotational bands based on Nilsson configurations. The most interesting information is connected with a level identified at 1125 keV, which is fed directly by the β-decay of ^{183}Lu with a β-branch of 45 % corresponding to a logft value of 5.4. This logft value indicates that the corresponding β-transition is of the allowed unhindered type. If the ground-state configuration of ^{183}Lu is 7/2+ [404], in analogy to other odd-A lutetium isotopes[4], the state at 1125 keV can be interpreted as a 5/2+ state with a large admixture of the three-quasiparticle configuration π7/2+[404], π9/2-[514], ν7/2-[514], similar to that observed[1] in ^{181}Hf. An alternative ground-state configuration of ^{183}Lu could be 9/2-[514]. Then the allowed unhindered "single particle" β-transition between this and the 7/2-[514] configuration assigned to the 1125 keV state should have a logft value of ~4.5, whereas the measured value is 5.4.

Furthermore, we have investigated[3] ^{180}Lu ($T_{1/2}$=5.7 min) with the aim of measuring the fractional decay branch, f_m^{180}, of ^{180}Lu to the 8⁻ isomeric state ^{180}Hf^m (see fig.1), which is of astrophysical interest. The extremely small solar abundance of ^{180}Ta^m can be explained by small neutron capture and/or β- decay branchings in the common neutron capture nucleosynthesis of the s- and/or r-processes. The s- and r-process paths differ in the way the isomeric state in ^{180}Hf^m is populated (see fig.1). In the s-process, this population is due to neutron capture in ^{179}Hf, the fractional ^{180}Hf^m population being[5] (1.24 ± 0.06)%. Since this does not allow to reproduce the solar ^{180}Ta^m abundance, the post r-process path through ^{180}Lu was investigated. The idea of the present determination[3] of f_m^{180} is to deduce this quantity from a γ-ray measurement on a mass-180 sample and to correct for the part of the ^{180}Hf^m activity, which is not due to ^{180}Lu decay in this sample, but collected as ^{180}Hf^m directly. From preliminary measurements, a f_m^{180} value of 5.7% was estimated, allowing the calculation of the r-process abundance to be 5.95•10^{-6} (Si≡10^6). This result, compared with the solar abundance of ^{180}Ta(2.46x10^{-6}, Si≡10^6), led to the preliminary conclusion that the solar abundance of ^{180}Ta can be explained by predominant r-process production. The present rough estimate of f_m^{180} is based on assumptions concerning production cross-section ratios and separation efficiencies. Experiments are being prepared to remeasure f_m^{180} under improved conditions.

1. R. Kirchner et al., Nucl. Phys. A378 (1982)549
2. K. Rykaczewski et al., Z. Phys. A309 (1983) 273
3. G. Walter et al., KfK 3417 Report, 1982
4. Table of isotopes, 7th ed., eds. C.M. Lederer and V.S. Shirley, New York: Wiley 1978
5. H. Beer, R.L. Macklin, Phys. Rev. C26 (1982) 1404

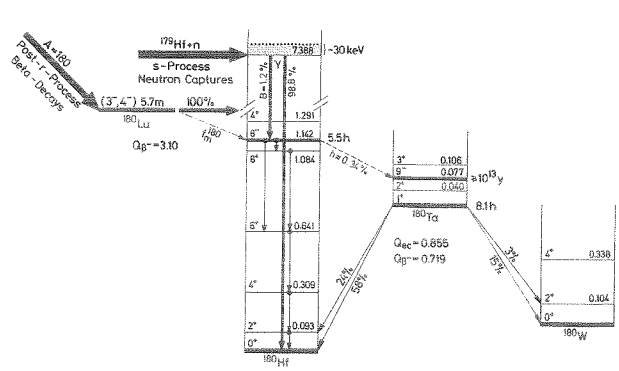


Fig. 1: The nuclear levels along the A=180 isobaric chain of significance to the stellar nucleosynthesis of ^{180}Ta^m ($T_{1/2}$≳10^{13} y)

Alpha Decay of New Neutron Deficient Gold, Mercury, and Thallium Isotopes.

J.R.H. Schneider, S. Hofmann, F.P. Heßberger, G. Münzenberg, W. Reisdorf, H.J. Schött, and P. Armbruster

GSI Darmstadt

At the Velocity Filter SHIP, enriched targets of neutron deficient isotopes between Rb and Mo have been irradiated with a beam of ^{92}Mo ions. The excitation energy of the compound nuclei varied between 32 and 78 MeV. The evaporation residues were implanted into an array of seven position sensitive surface barrier detectors, where their α decay was observed.

New isotopes of the elements Au, Hg, and Tl have been found. The measured decay data are listed in Table 1. The decay of the new isotopes ^{173}Au, ^{175}Hg, ^{176}Hg, and ^{179}Tl could be correlated to the known decays of their daugthers by means of a time and position correlation method, which is described in detail in /1/.

A 6.53 MeV line observed in reactions leading to the compound nucleus ^{177}Au could be assigned to ^{174}Au because this activity was seen to peak at excitation energies (43.5 MeV) intermediate between those of the unambiguously identified isotopes ^{173}Au and ^{175}Au.

Starting from the known masses of ^{148}Dy and ^{146}Gd, α decay chains for the N - Z = 16 and 18 nuclei have been used to determine new masses /2/. In continuation of the N - Z = 16 chain we can add the mass excess value of ^{176}Hg to be (-11.91 ± 0.12) MeV.

A new α line of a comparatively high energy of 7.20 MeV has been observed in reactions leading to the compound system ^{181}Tl (Fig. 1a). Fig. 1b shows a delayed coincidence spectrum taken with a time window of 15 ms and a position window of ± 0.7 mm relative to the implanted evaporation residues. From the time distribution of the 10 correlated events a half-life of (1.4 ± 0.5) ms was deduced for the 7.20 MeV transition.

Observed only at an excitation energy of 37 MeV, it is very likely due to decays of isotopes produced in the 2 nucleon or (α,1 nucleon) evaporation channel. A definite assignment was not possible. But we want to mention that such a transition would fit well into decay properties of an 9/2- isomeric state in ^{179}Tl which can be expected by an energy and half life extrapolation of heavier Tl isotopes with mass numbers from 185 to 205 /4/.

/1/: S. Hofmann et al.: Z. Phys. A291, 53(1979)
/2/: U.J. Schrewe et al.: Phys. Rev. C25, 3091(1982)
/3/: C. Cabot et al.: Nucl. Phys. A241, 341(1975)
/4/: E.F. Zganjar : Future Directions in Studies of Nuclei far from Stability, North Holland (1980), p. 49

Table 1: Decay data of the new isotopes

Isotope	E/MeV	$T_{\frac{1}{2}}$/ms
^{173}Au	6.72 ± 0.02	59^{+45}_{-18}
^{174}Au	6.53 ± 0.02	120 ± 20
^{175}Au /3/	6.44 ± 0.01 /3/	200 ± 22
^{175}Hg	6.86 ± 0.02	20^{+40}_{-13}
^{176}Hg	6.75 ± 0.02	34^{+18}_{-9}
^{179}Tl	6.56 ± 0.02	160^{+90}_{-40}
unidentified Transition	7.20 ± 0.02	1.4 ± 0.5

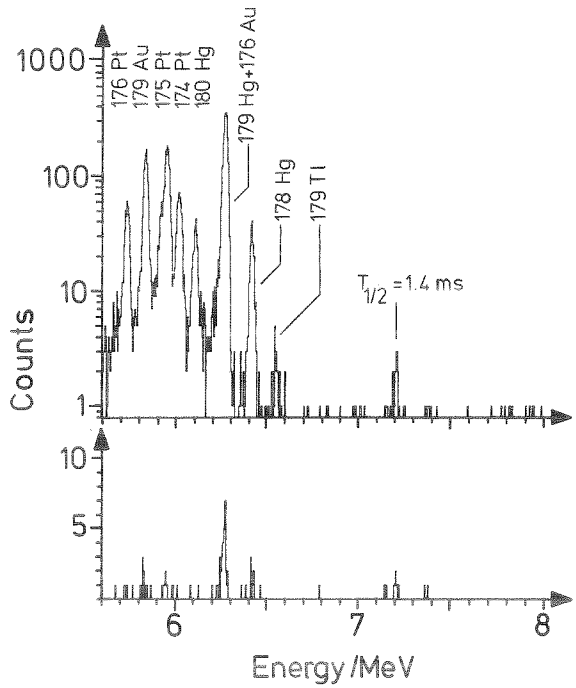


Fig. 1: a) High energy part of the α spectrum measured in the reaction ^{92}Mo + ^{89}Y → ^{181}Tl showing the new isotope ^{179}Tl and the unidentified 7.20 MeV transition; b) spectrum a) correlated to evaporation residues within a time window of 15 ms and a position window of ± 0.7 mm from which the half life of 1.4 ms could be determined.

Alpha Spectroscopy for Nuclei between Fr and U [B]

R. Hingmann, H.-G. Clerc, C.-C. Sahm, D. Vermeulen, K.-H. Schmidt*
and J.G. Keller*
TH Darmstadt, *GSI Darmstadt

In the course of our fusion studies, the alpha decay properties of many heavy evaporation residues were investigated by implantation of these nuclei into a surface barrier detector behind the velocity filter SHIP.

1. The new isotopes ^{222}U (1μs) and ^{221}Pa (6.1μs)

In the reaction ^{186}W(^{40}Ar,4n) ^{222}U at 4.5 MeV/u we observed a total number of three α-cascades which could be attributed to the production of the new isotope ^{222}U. One such cascade, for example, consisted in the advent of an evaporation residue followed after 2.8 μs by an α-decay of 12.08 MeV, which is interpreted as the superposition of the α-decays of ^{222}U and the shortlived daughter ^{218}Th (122 ns), where one or both α's left the detector before they had deposited their full energy. After 1.6 s a 7.16 MeV α-decay was observed, which is assigned to ^{214}Ra. The correlation between the two α-events is certain, since the rate of ^{214}Ra α-decays was extremely low (total number of 12 events during the measuring time of 9 h). From the observed three ^{222}U decays a half-life of $(1.0^{+1.2}_{-0.4})$ μs was deduced.
In the reaction ^{186}W(^{40}Ar,p4n)^{221}Pa at 4.72 MeV/u the new isotope ^{221}Pa was identified in a similar fashion as ^{222}U. From the total number of six decay chains a half-life of $(6.1^{+3.7}_{-2.4})$ μs was determined.

2. A new isomeric state in ^{216}Th (180 μs)

In the reactions ^{40}Ar + ^{178,179,180}Hf, ^{181}Ta and ^{124}Sn + ^{94,96}Zr a new α-line with E_α = (9.912±0.020) MeV was observed. On the basis of the different excitation functions in these cross bombardments, this α-line was assigned to ^{216}Th. The half-life was determined to be (180±40) μs. The excitation energy of this state is 2.028 MeV, if it is assumed that the α-decay proceeds to the g.s. of the daughter nucleus ^{212}Ra. The ratio of the intensity of the new α-line to the intensity of the g.s. α-decay of ^{216}Th is only a few percent; this can be explained by a strong γ-branch with a branching ratio of (0.97±0.01) competing with the isomeric α-decay.

3. Alpha decay of N = 125 isotones

The N = 125 isotones exhibit complex α-spectra. In the past [1,2,3,4] these nuclei were produced in light ion (p, ^{12}C, ^{16}O) induced reactions, and the different α-lines emitted by one N = 125 nucleus have been interpreted as transitions from the ground state to the ground state and to excited states in the corresponding daughter nucleus. However, in the present work we used ^{40}Ar and ^{124}Sn induced fusion reactions (^{40}Ar +$^{176,\ldots,180}$Hf, ^{181}Ta and ^{124}Sn + ^{94,96}Zr), and the relative intensities of the different α-lines were found to be different from the results obtained with light ions. The relative intensities of the two strongest α-lines for each of the nuclei ^{215}Th, ^{214}Ac, ^{213}Ra and ^{212}Fr are strongly dependent on the mass of the projectile, see Fig. 1. Therefore it must be concluded that in addition to the g.s. α-decay the α-decay of at least one isomeric state in each of the N=125 isotonic nuclei is observed.

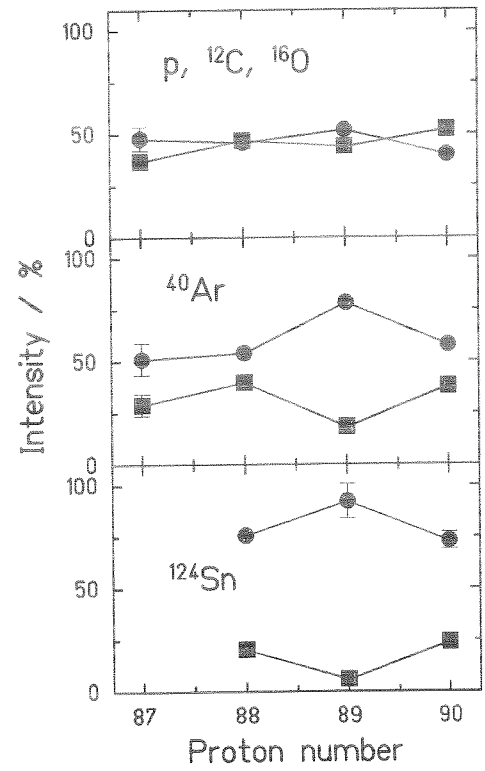


Fig. 1: The intensities of the two strongest α-lines in each of the N=125 nuclei as listed below, plotted for different projectiles as a function of the nuclear charge number of the α-emitting nucleus.

	^{215}Th	^{214}Ac	^{213}Ra	^{212}Fr	symbol
α-energy (MeV)	7.524	7.214	6.731	6.406 + 6.384	●
	7.395	7.082	6.624	6.262	■

The lines 6.406 MeV and 6.384 MeV in ^{212}Fr could not be separated; therefore the sum of their intensities is shown.

References:

1. K.Valli, E. Hyde, Phys. Rev. 176 (1969) 1377
2. K. Valli, W.J. Treytl, E. Hyde, Phys. Rev. 161 (1968) 1094
3. D.G. Raich, H.R. Bowmann, R.E. Eppley, J.O. Rasmussen, Z. Physik A 279 (1976) 301
4. P. Hornshøj, P.G. Hansen, B. Jonson, Nucl. Phys. A 230 (1974) 380

Decay Properties of Neutron Deficient Isotopes of Element 105

F.P.Hessberger, G.Münzenberg, S.Hofmann, Y.K.Agarwal,
P.Armbruster ,K.Poppensieker, W.Reisdorf, C.-C.Sahm*, K.H.Schmidt,
J.R.H.Schneider, W.F.W.Schneider, H.J.Schött, D.Vermeulen*

GSI Darmstadt, *Inst. für Kernphysik TH Darmstadt

Our investigation of the decay properties of neutron deficient isotopes of element 105 have been continued mainly with respect to the isotope ^{258}105. In an irradiation of ^{209}Bi with ^{50}Ti at 4.75 MeV/u with a total projectile dose of ≈1.4x10^{17} particles we collected 27 α-decays of ^{258}105 correlated to ^{254}Lr or ^{254}No (formed by EC of ^{254}Lr) and 3 α-decays of ^{257}105 correlated to ^{253}Lr. The total number of α-decays that can be assigned to element 105 has been 71. The α-energies and halflives of ^{258}105, ^{257}105, ^{254}Lr and ^{253}Lr communicated in the preceeding annual report / 1 / could be reproduced within the errors. The formation cross-section for ER production is listed in table 1. It fits quite well to results obtained in a previous experiment (marked by an asterisk).

Beside α-decay we observed altogether 38 fission events. In the preceeding report / 1 / we supposed that this SF might be ^{258}104, formed by EC of ^{258}105. To confirm this we searched for correlations between x-rays, that accompany EC, and SF. Altogether we found four x-rays, which are followed by a fission event within a time limit of 30 msec (≈3 halflives of ^{258}104), that may fit to expected K-x-ray energies of element 104; the calculated error probability is ≈3%. Therefore this result can only be regarded as an evidence for EC of ^{258}105 and not as a proof.

From the energy distribution (fig.1) of the fission events we calculated the average kinetic energy of the fission fragments. As the range of a fission fragment in the detector exceeds the implantation depth of the ER, the probability that one of the fragments escapes the detector depositioning only part of its energy ΔE is ≈60%. The measured energy E_m is then $E_m < E_{tot}$. Nevertheless E_{tot} might be determined from the upper part (E_m >190 MeV) of the energy distribution. (The lower energies are due to cases where one fission fragment escapes the detector). We determined a value of E_{fiss}=213$^{+}_{-}$13 MeV; yet this value does not include corrections due to neutron emission. Also a second correction must be taken into account; in some cases one of the fission events will escape the detector, but the measured energy still will be larger than our lower cut-off for calculation (190 MeV). Therefore our value for E_{fiss} is somewhat lower than the mean value of the total fission energy. A detailed analysis that needs also asumptions about the mass distribution of the fission fragments as well as about the energy distribution and the range straggling of the ER is still in progress.

/1/ F.P.Heßberger et.al. GSI-Scientific Report 1981 GSI 82-1(1982) p.66

TABLE 1: Measured Formation Cross-Sections for Element 105 in Reactions ^{50}Ti + ^{209}Bi

E_{CM}/MeV	Σα	ΣSF	σ/nb
$188.5^{+3.3}_{-1.5}$	71	38	$3.3^{+}_{-}0.4$
$184.4^{+3.3}_{-1.5}$	0	1	$0.5^{+}_{-}0.3$*
$188.5^{+3.3}_{-1.5}$	10	8	$3.5^{+}_{-}0.8$*
$192.9^{+3.3}_{-1.5}$	6	4	$2.6^{+}_{-}0.8$*
$196.6^{+3.3}_{-1.5}$	8	0	$2.7^{+}_{-}0.9$*

The given errors for the cross-sections include only the statistical errors; systematic errors due to the calculated efficiencies for SHIP and for the detector-system can shift the given values for the cross-sections by a factor of two.

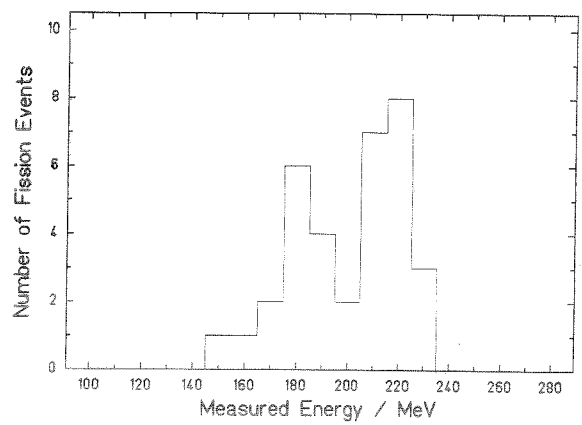


FIG.1 Measured energy distribution of fission fragments observed in the reaction ^{50}Ti + ^{209}Bi at E_p = 4.75 MeV/u

Element 109

G. Münzenberg, Y.K. Agarwal, F.P. Heßberger, S. Hofmann, K. Poppensieker, W. Reisdorf, J.H.R. Schneider, W.F.W. Schneider, K.-H. Schmidt, H.-J. Schött, P. Armbruster
GSI Darmstadt
C.C. Sahm, D. Vermeulen
Technische Hochschule Darmstadt

To produce element 109 we irradiated ^{58}Fe on ^{209}Bi at 4.95 MeV/u, 5.05 MeV/u, and 5.15 MeV/u.[1] The integral projectile doses were between 2×10^{17} and 3×10^{17} per energy step. The total irradiation time was 250 h. For the analysis we accumulated the data of all three irradiations.

With a position window of ± 0.8 mm and a time window of 14 s for decays occuring between the UNILAC beam bursts and 0.04 s for decays during the beam bursts we found about 500 α-decays correlated to recoils (Fig. 1).

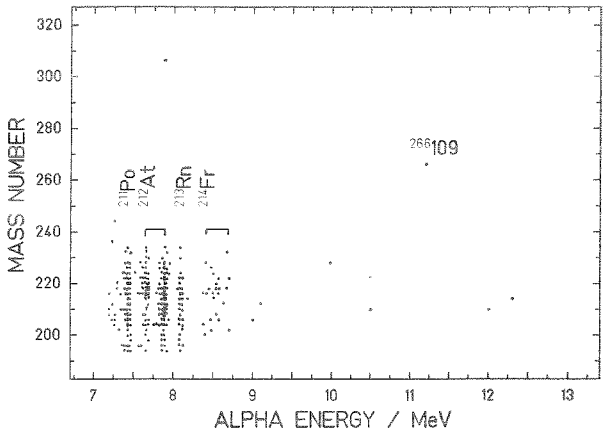


Fig. 1: Identification of the implanted recoils by their α-decays

From time-of-flight and energy we evaluated the masses. As expected, we find a broad distribution around the target mass 209. These recoils are correlated to α-decays in the energy range between 7 MeV and 9 MeV, and can be identified as ^{211}Po, ^{212}At, ^{213}Rn, and ^{214}Fr. The event with mass 305 is found to be correlated to a ^{212}At decay and can be explained as a pile-up of the mother α-decay of ^{216}Fr with 0.7 µs halflife onto the signal of the evaporation residue. Only one event in this two-dimensional plot fulfills the conditions necessary for a heavy fusion product: a high mass and a decay energy above 10 MeV. This event is followed by a decay chain shown in Fig. 2 together with its interpretation.

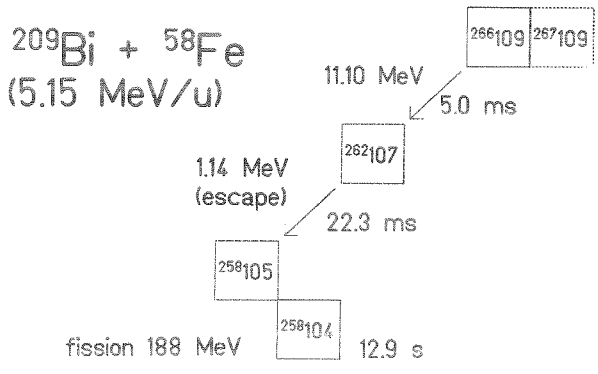


Fig. 2: Observed decay chain.

The chain starts with an impinging nucleus of mass (264±13) u, followed by the (11.10±0.03) MeV α-decay after 5 ms, then after another 22.3 ms an energy signal of (1.14±0.02) MeV, accompanied by a prompt γ of 382.9 keV, follows. This low energy pulse can be understood as due to an α-particle escaping the detector in backward direction. The chain is terminated by the spontaneous fission with an energy signal of 188 MeV after 12.9 s. This is the only spontaneous fission observed during the whole Fe+Bi irradiation.

As one of the fission fragments can escape the detector, the indicated energy may not represent the full total kinetic energy: also the pulse height defect is not taken into account. Fission events with similar energies have been observed in the reaction ^{50}Ti on ^{209}Bi and also for ^{54}Cr on ^{209}Bi. All decays were observed in the pause between the UNILAC beam bursts.

In close analogy to our results on the synthesis of elements 104, 105, and 107 we assign the decay chain to the isotope ^{266}109, which represents the 1n channel in the complete fusion ^{58}Fe and ^{209}Bi. A spontaneous fission preceded by short-lived α-decays is a signature, typical for a trans-actinide element and in view of the high observed mass of the recoil we exclude transfer products. The estimated excitation energy of the compound nucleus is $(21.9^{+3.4}_{-1.7})$ MeV. The preference of the 1n over the 2n decay chain results mainly from a comparison of the time-distance for the fission event with the known halflives of the isotopes ^{258}105 and ^{257}105.

The possible assignment to an evaporation channel involving charged particle emission was also considered. These lead either to even-even istopes with spontaneous fission halflives of the order of 10 ms or less, or to istopes where no or small spontaneous fission branches are known.

[1] G. Münzenberg, P. Armbruster, F.P. Heßberger, S. Hofmann, K. Poppensieker, W. Reisdorf, J.H.R. Schneider, W.F.W. Schneider, K.-H. Schmidt, C.C. Sahm, D. Vermeulen, Z. Phys. A309 (1982) 89

Heavy Actinide Products from Reactions of ^{18}O and ^{22}Ne with ^{254}Es

M. Schädel[+*], R.W. Lougheed[*], J.H. Landrum[*], J.F. Wild[*], R.J.Dougan[*], A.D. Hoover[*], E.K. Hulet[*], A. Ghiorso[&], K.J. Moody[&], and G.T. Seaborg[&]

[+] GSI Darmstadt, [*] LLNL, Livermore CA, [&]LBL, Berkeley CA

We carried out a series of bombardments using ^{254}Es as the target nuclide and ^{18}O and ^{22}Ne as the projectile. In our experiments we used chemical techniques to separate element fractions from a catcher foil after end of bombardment, and measured these fractions to obtain α-energy spectra and count SF events.

Cross sections for the Fm and Md isotopes and ^{259}No from the reactions of 121-MeV ^{22}Ne, 125-MeV ^{22}Ne and 98-MeV ^{18}O with ^{254}Es are shown in Figure 1. Fermium formation cross sections from 97-MeV ^{18}O + ^{248}Cm [1] are shown for comparison.

For the ^{22}Ne + ^{254}Es reaction, we observed only a very slight increase in cross sections with increasing energy. The shape of the isotopic distributions shown do not sift significantly. To determine the most probable mass (Ap), we fitted a gaussian curve to the data and held σ = .977u (FWHM = 2.3u) fixed. For the Fm isotopes, we found Ap = 254.5, and Ap(Md) = 256.0.

More neutron rich products were observed in the ^{18}O + ^{254}Es reaction at 98-MeV incident energy than were found at 121-MeV ^{22}Ne. Ap-values of 255.5 for Fm and 257.1 for Md were determined. This makes the ^{18}O the most favourable projectile for the production of neutron rich heavy actinides when compared to ^{22}Ne. The Fm cross section is enhanced by a factor auf 10^3 and the Md cross section by more than 10^4 when the yields from a ^{254}Es target are compared with a ^{248}Cm target [1].

In the reactions with ^{18}O as a projectile on ^{248}Cm and ^{254}Es targets, we were able to extrapolate (Es^{254},x) cross sections from cross sections measured[1] with a ^{248}Cm target assuming (i) an equal transfer probability for a given number of proton (ΔZ) and neutrons (ΔN), and (ii) no significant shift of the primary fragment distribution by neutron evaporation or fission. This is possible only in these light ion reactions at the barrier where the excitation energies are less than the neutron separation energies and fission barriers, whereas, there are large differences in cross sections for products with the same number of transferred nucleons (ΔZ,ΔN) in reactions with ^{238}U projectiles on ^{238}U and ^{248}Cm targets [2]. Isotope cross sections are in good agreement for two proton transfer products on ^{248}Cm and ^{254}Es as a target and ^{18}O as a projectile, while small differences in cross section for ^{22}Ne may be due to a slightly higher projectile energy with the ^{254}Es target. We used these isotope distributions, and a similar method for three and four proton transfer, to estimate cross section for unknown, neutron-rich heavy actinides. The results are given in Table 1. It is important to note that these estimates still contain large uncertainties because we are not yet able to predict the exact Ap position of the isotope distribution. However, it is fascinating to see that exotic nuclei like ^{261}Md, ^{261}No or ^{262}Lr should be accessible in reactions of ^{18}O with ^{254}Es.

[1] D.Lee et al., Phys.Rev.C25,286(1982)
[2] M.Schädel et al., Phys.Rev.Lett. 48, 852 (1982)

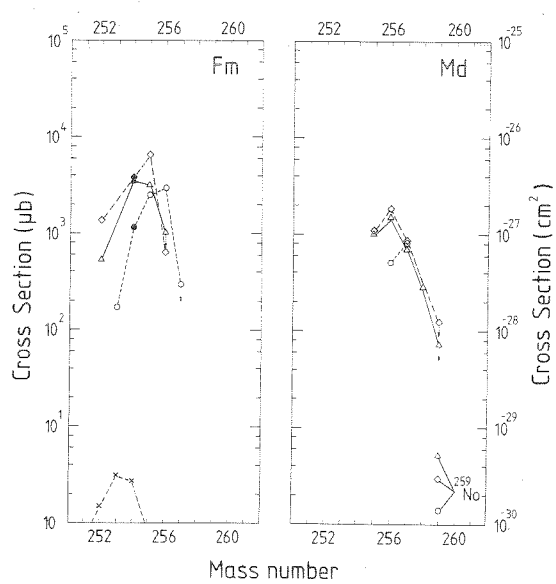


Figure 1:
Cross sections for ^{259}No and Fm and Md isotopes in the reaction 121-MeV ^{22}Ne + ^{254}Es (symbol = Δ), 126-MeV ^{22}Ne + ^{254}Es (symbol = ◇) and 98-MeV ^{18}O + ^{254}Es (symbol = O). Cross sections for Fm isotopes in the reaction 97-MeV ^{18}O + ^{248}Cm from Ref. 1 (symbol = +) are shown for comparison. Open symbols are independent, full symbols are cumulative yields, arrows indicate that these cross sections are upper limits only. The curves are drawn to connect the data point.

TABLE 1: Estimated transfer cross section in μb for unkown neutron-rich actinides

Reaction	Transfer cross section [μb]					
	^{260}Md	^{261}Md	^{260}No	^{261}No	^{261}Lr	^{262}Lr
^{18}O + ^{254}Es	9.	.3	5.	.2	.7	.3
^{22}Ne + ^{254}Es	.3	≲.05	2.	.1	1.	.2

A New 105-ms Spontaneous Fission Activity Produced in the Reaction ^{18}O with ^{254}Es

L. P. Somerville[&], M. J. Nurmia[&], M. Schädel[+*], A. Ghiorso[&], J. M. Nitschke[&], R. W. Lougheed[*], J. H. Landrum[*], E. K. Hulet[*]

[&]LBL, Berkeley CA, [+]GSI Darmstadt, [*]LLNL Livermore CA

Measurements of isotope cross sections and estimate for the production of yet unknown isotopes in the reaction ^{18}O + ^{254}Es have shown that this reaction is exceptionally well suited to investigate the frontier of very heavy neutron-rich nuclei [1].

To search for short-lived spontaneous fission (SF) emitters with half-lives between 10 ms and 5 seconds we used a recoil tape-transport system [2,3]. All heavy recoils from the reaction 99-MeV ^{18}O + ^{254}Es were implanted into a moving stainless steel tape that transported the activity along a series of mica SF-track detectors. Consistent half-lives and cross sections for a new SF-activity were measured from separate experiments with tape speeds of 0.2 ms^{-1} and 0.9 ms^{-1}, respectively. The weighed average half-life from both experiments is (105±7)ms, and the cross section 1.1 μb. The decay curve from one of the experiments (0.2 ms^{-1}) is shown in Figure 1. The long-lived background that is observed in Figure 1 is due primarily to EC-decay of ^{256}Md into the SF-isotope ^{256}Fm also produced in the bombardment [1].

We do not yet know the identity of this 105-ms SF emitter. But the 1 μb cross section for the reaction 99-MeV ^{18}O + ^{254}Es is consistent with the cross section estimates for ^{261}Md (3 μb), $^{260/261}No$ (5.,.2 μb) or $^{261/262}Lr$(.7,.3 μb) [1], extrapolated from similar transfer channels in the reaction ^{18}O with ^{248}Cm. A measured cross-section upper limit of 80 nb in the reaction 125-MeV ^{22}Ne + ^{254}Es is, however, much lower than expected for ^{260}No and ^{261}Lr, but would be consistent with estimates for ^{261}Md. Bearing in mind the large uncertainties in the estimated cross sections, it is premature for an assignment to one specific neutron rich isotopes of elements 101 through 103. An assignment of the 105-ms activity to an isotopes of element Z=104 seem to be not possible, as none of the Z=104 isotopes is expected to be produced with cross sections larger than 50 nb in the reaction of ^{18}O or ^{22}Ne with ^{254}Es.

A 105-ms SF half-life for a new, neutron-rich isotope between $_{101}Md$ and $_{103}Lr$ creates an interesting problem as theoretical estimates for SF half-lives [4,5,6] differ strongly in this very neutron-rich region. For lack of experimental data it is an open question whether the new systematic of half-lives which was observed for isotopes of element 104 [7] can already be observed for neutron-rich $_{102}No$ istopes. An assignment of the 105-ms isotope will be very important and future experiments can yield more information. With a half-life of 105 ms and a relatively high cross section of 1.1 μb it will also be possible to study in detail the decay of this isotope, e.g. total kinetic energy and mass division of fission fragments.

[1] M. Schädel et al., contribution to this report, and Proc. Int. Workshop on Gross Properties of Nuclei and Nuclear Excitations XI, Hirschegg, 1983, in press.

[2] J. M. Nitschke et al., Lawrence Berkeley Laboratory Annual Report, 1977-78, LBL-8151, p. 84, 1979.

[3] L. P. Somerville, Ph. D. thesis, Lawrence Berkeley Laboratory Report LBL-15027, 1982.

[4] A. Baran et al., Nucl. Phys. A361, 83 (1981)

[5] J. Randrup et al., Phys. Rev. C13, 229 (1976)

[6] V. A. Druin et al., Sov. J. Nucl. Phys. 29, 591 (1979)

[7] Yu. Ts. Oganessian et al., Pisma Yh. Eksp. Teor. Fiz.20,580 (1974) [JETP Lett. 20, 265 (1974)]

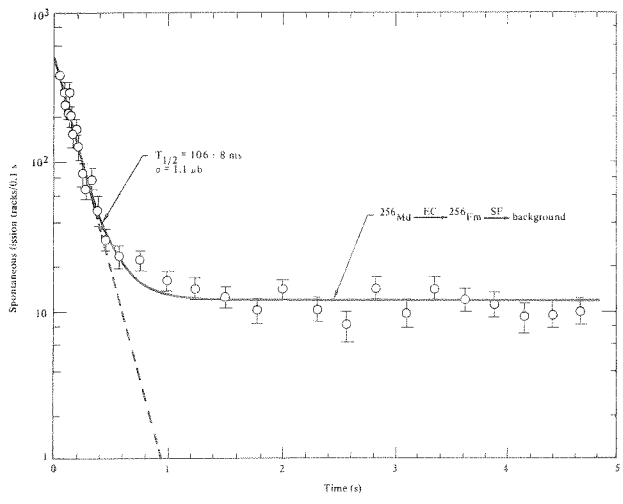


Figure 1:
Decay curve of a new 105 ms SF-activity producted in the 99-MeV ^{18}O + ^{254}Es reaction. The result shown is from one experiment with a tape-speed of 0.2 m/s.

Recent Searches for Long-lived Superheavy Elements from the $^{48}Ca + ^{248}Cm$ Reaction

B

H. Gäggeler, W. Brüchle, M. Brügger, M. Schädel, K. Sümmerer, G. Wirth
GSI Darmstadt
A. Ghiorso, K.E. Gregorich, D. Lee, K.J. Moody, G.T. Seaborg, R.B. Welch, P. Wilmarth
Lawrence Berkeley Laboratory
G. Herrmann, J.V. Kratz, N. Trautmann, N. Hildebrand, U. Hickmann, C. Frink, N. Greulich
Mainz University
D.C. Hoffmann, M. Fowler
Los Alamos Scientific Laboratory
H.R. von Gunten
Bern University

The success in synthesizing elements 107[1] and 109[2] at GSI using cold fusion reactions has much revived the interest in the use of the reaction $^{48}Ca + ^{248}Cm$ to make superheavy elements. In addition, recent theoretical calculations describing the limits of fusion gave optimism to predict that $^{48}Ca + ^{248}Cm$ should fuse without significant hindrance, i.e. without "extra-push"[3]. On the other hand, previous experiments to search for superheavy elements by this reaction gave negative results[4]. These experiments were performed approximately 25 MeV above the barrier resulting in excitation energies of the compound nucleus $^{296}116$ of 40 to 50 MeV. However, the heaviest elements synthesized so far by heavy ion reactions were found to survive at much lower excitation energies of about 20 MeV only[2].

Based on these new insights into cold fusion reactions we restarted to search again for superheavy elements with ^{48}Ca plus ^{248}Cm but at considerably lower excitation energies of the compound nucleus compared to earlier attempts in order to favour low xn-channels.

In a first series of experiments performed in October 82 at LBL off-line chemical techniques were used to search for superheavy elements with half-lives between hours and years. The ^{48}Ca energy entering 1.7 mg/cm² thick ^{248}Cm oxide targets was 239.0 MeV, i.e. 4 MeV above the calculated fusion barrier of 235 MeV (proximity - 4%[3]). The measured energy spread within the target was 16 MeV(lab) which defines a covered excitation energy range for the compound nucleus $^{296}116$ of 16 to 29 MeV. Beam integrals accumulated onto the ^{248}Cm targets were up to 1.0×10^{17} particles. Recoiling reaction products were collected with a copper catcher foil (6.2 mg cm²). After each bombardment this foil was chemically processed with similar procedures used already in earlier attempts to search for superheavy elements by heavy ion reactions at the UNILAC[5]. This chemistry is a combination of a gas-phase separation for gaseous and volatile elements and an aquous procedure aimed to separate bromide complexes from the bulk of reaction products, mainly the actinides[4]. Final samples are presently counted at Mainz University in a low background detection system which registers single and coincident fission fragments, their kinetic energies and the number of neutrons per fission event.

So far, after a counting time of about 3 months, no fission activity was found in any of the superheavy element samples. The cross section limits for the production of spontaneously-fissioning, long-lived superheavy elements 108 through 116 as it results from all experiments performed are plotted in Fig. 1 (solid-line) as a function of an assumed half-life. The calculated curve is based on a counting period of 3 months, an effective target thickness of 4.2×10^{18} ^{248}Cm atoms, a chemical efficiency for the separation procedure of superheavy elements of 80%, a counting efficiency for fission-fragment coincidences of 60% and an assumed count rate of three events, corresponding to a 95% confidence level if no activity was measured.

1. G. Münzenberg et al., Z. Physik, A300, 107 (1981)
2. G. Münzenberg et al., Z. Physik A309. 89 (1982)
3. W.J. Swiatecki, Nucl. Phys. A376, 275 (1982)
4. see e.g. J.V. Kratz, GSI-82-7 (1982) and Radiochim. Acta, in press
5. H. Gäggeler et al., Phys. Rev. Lett. 45, 1824 (1980)

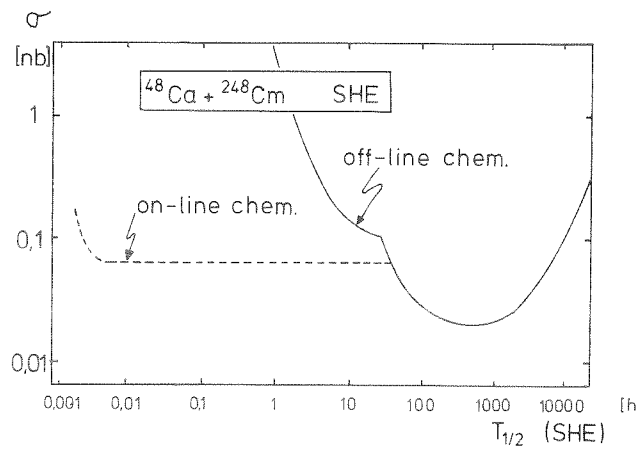


Fig.1: Cross section limits for the production of spontaneously-fissioning superheavy elements as its results after 3 months counting time (solid-line, for details see text). Also shown is the cross section and half-life range to be covered by a future on-line chemistry experiment (dashed line).

The Gas-Filled Separator (SASSY) at LBL Applied to the Production of Heavy Elements via Fusion

A. Ghiorso, M. Leino, S. Yashito
LBL Berkeley
P. Armbruster, J.P. Dufour, S. Hofmann, P. Lemmertz, G. Münzenberg
GSI Darmstadt

A gas-filled separator system has been installed at the Superhilac, Fig. 1[1]. The use of SASSY for the detection of SHE was one out of four experiments planned in an LBL-GSI collaboration to look for SHE in the fusion reaction of ^{48}Ca and ^{248}Cm.

Gas-filled separators until now have been used either for fission product separations or for the separation of heavy ion reaction products at energies well above 0.5 MeV/u. The slow EVR's from very asymmetric fusion reactions, as $^{48}Ca+^{248}Cm$, have velocities equivalent to 0.1 MeV/u. At these small energies the mean ionic charges $\bar{q}$ of EVR's in the gas filled magnetic field are about 6 units. The missing electrons come from outer shells. Their binding energies reflect the chemistry of EVR's. The deflection of EVR's in gas-filled fields is governed by a $\bar{q}$ which increases with increasing atomic number, not monotonically, but in a way reflecting the chemistry of the under-lying elements. For He at 1 mbar at v/c = 1.6 % $\bar{q}$-values have been measured using either EVR's or target recoil atoms under 0°, Fig. 2. Measurements up to Z = 102 exist. Within the 4f and 5f shells a drop of $\bar{q}$ has been observed. An extrapolation to Z = 116 is needed to fix the $B\rho$-values for SHE. This extrapolation is done assuming the electrons of importance for $\bar{q}$ to be taken from the 6d-shell, that is from a rising part of $\bar{q}$ (Z). Not only the absolute value of $B\rho$ depends on Z, but, moreover, the difference in $B\rho$ between neighbouring elements is strongly dependent on Z. Regions of higher resolving power are followed by regions where no separation of elements is possible. Fig. 3 shows the ($B\rho$-E)-plane for the participants of the reaction: ^{48}Ca, ^{248}Cm, and $^{296}116$. At E = 36 MeV and $B\rho$ = 2.2 Ts • m windows are set. The background in these windows finally determines whether SASSY may compete with other separation techniques, as chemistry or velocity selectors. SASSY uses position sensitive parallel plate avalanche counters for TOF-measurement, and an array of position sensitive surface barrier detectors for charged particle detection. As an example the spectrum obtained for ^{208}Pb (^{48}Ca,2n) ^{254}No is given, Fig. 4. The suppression of α-lines from target transfer products is demonstrated. Time-correlations between implanted EVR's, and α-decays, and between successive α-decays have been analyzed. The known half-life for ^{254}No has been reproduced.

^{48}Ca-beams irridated a ^{248}Cm-Target at 4.7 MeV/u. A dose of $7x10^{16}$ particles was put on the target. The data analysis for the experiment is still in progress.

[1] M. Leino, S. Yashito, A. Ghiorso, Phys. Rev. C24, (1981), 2370

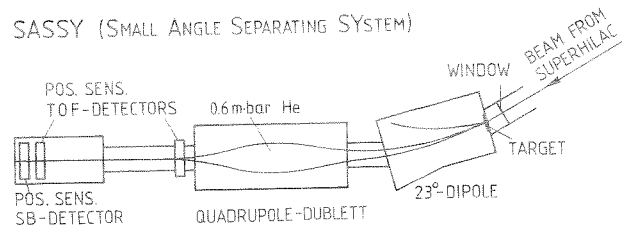


Fig. 1: SASSY - Small Angle Scattering System - is a gas-filled magnetic separator allowing separation of EVR's within 0.5 µs with a total separation efficiency of up to 50 %, /1/.

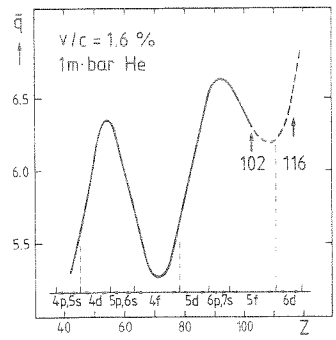


Fig. 2: The mean ionic charge $\bar{q}$ of heavy ions with atomic number Z and v/c = 16 % in He at 1 mbar. The electronic configurations are assumed to be aquivalent to (Z-$\bar{q}$).

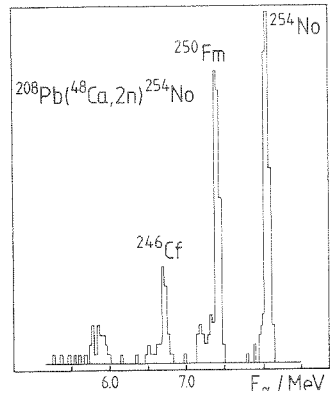


Fig. 3: α-spectrum measured in the focal plane of SASSY. The production cross section of ^{254}No in the bombardment of ^{208}Pb by ^{48}Ca at 4.4 MeV/u amounts to $\sigma \sim 3$ µb. No lines emitted by transfer products are seen in the spectrum.

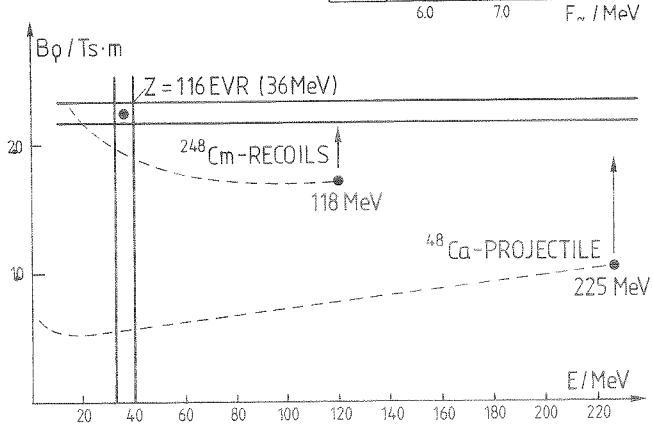


Fig. 4: ($B\rho$-E)-plane for the ^{248}Cm (^{48}Ca,xn) $^{296-xn}116$ reaction at 4.95 MeV/u. In the $B\rho$-window full energy ^{48}Ca-projectiles, slowed-down ^{48}Ca-projectiles, ^{248}Cm-recoils of E < 116 MeV, and EVR's will be found.

Gamma-Ray Catalog G

U. Reus and W. Westmeier

Institut für Kernchemie, Universität Marburg

The objective of this project is the compilation and regular updating of a catalog comprising all available information on gamma-rays from the radioactive decay of nuclides. The catalog is designed for use in the quantitative assay of radionuclides, e.g. cross-section measurements and activation analysis. Information about the structure and layout of the tables has been reported earlier[1,2].

To summarize, Part I of the catalog is a listing of about 32,000 gamma-rays and X-rays ordered by increasing energy and designed as a tool for the identification of photons of unknown origin. Part II of the catalog is ordered by mass number A and nuclear charge Z and contains the complete data sets for 2526 nuclides and isomers i.e., about 42,000 gamma-energies, each data set including all important information on the decay of that nuclide, references, comments etc.

In view of the world-wide demand for the first edition of the catalog (published as GSI-Report 79-2), which by far exceeded the limited number of copies available, we decided in 1980 to publish a second, updated edition of the catalog in a journal. Work on this project has been completed in 1982.

The revised edition includes published experimental results which we received before June 30, 1982. Twenty major journals have been scanned regularly and more than 500 publications have been considered for the revision. In addition, about 100 mass chains have been completely reworked by means of recent evaluations published in Nuclear Data Sheets. A total of about 200 recently discovered nuclides and nuclear isomers have been introduced. The total number of gamma-energies included in the catalog increased by twenty percent. In toto, more than half of all data sets have been revised, the changes made ranging from minor in most cases to major in a few cases.

As reported earlier[1], information on X-rays emitted in radioactive decay has been introduced. Since experimental results for X-ray intensities are rarely reported (why?), most data had to be calculated from the decay schemes, using theoretical values for conversion coefficients, fluorescence yields, EC/β^+ ratios etc. As a result of these calculations, which required great effort, X-ray data are now available for the majority of those nuclides whose decay scheme is well enough established. Also, information on annihilation radiation is included for those nuclides where no strong gamma-rays or X-rays can be measured.

The revised catalog has been accepted for publication in "Atomic Data and Nuclear Data Tables". Due to space requirements, some changes in the printing format (which are currently under discussion) may be necessary. Publication is scheduled in ADNDT for Volume 29, which is to appear in the second half of 1983.

The authors wish to express their gratitude to Prof. P. Patzelt for his support of the project and to A. Merklin for his careful work in transcribing the data.

[1] U. Reus, W. Westmeier, and I. Warnecke, GSI-Report 82-1, 69 (1982) and earlier references therein.

[2] U. Reus, W. Westmeier, and I. Warnecke, IAEA-Report INDC(NDS)-130/G+P (1982), 137.

Nuclear Proton Emission Predictions G

W.F.Feix, E.R.Hilf
Institut für Kernphysik
Technische Hochschule Darmstadt

Following the experimental discovery of direct proton emission from ^{151}Lu and ^{147}Tm [1], we focused our interest upon the prediction of possible candidates for further experimental studies [2]. Nuclear proton emission should be a possible decay mode for all neutron deficient nuclei beyond the proton drip line, $Q_p=0$ [3]. However, the number of observable cases is limited, as competing decay modes, such as α- or β-emission, might strongly dominate the total half-life.

A quantummechanical description of the proton emission may follow the alpha decay theory in close analogy. In the case of lifetimes long compared to typical nuclear times, as it is in our case, the emission width Γ may be determined by solving the quasistationary Schrödinger equation with a complex energy $E_o+i\Gamma/2$, where E_o is the proton energy, predicted from the gross theory of masses (e.g. 3,4).

As the emission half-lives drop about exponentially with proton energies, we have to go beyond the gross theory predictions. Those of ref. 4 are fairly close to known experimental values, but still not to the accuracy needed here. We adopted a local correction to the separation energies of ref. 3,

$$\Delta Q_p^{corr} = C\ p\ (\delta-p)\ A^{-1} \quad ,$$

where p is the number of valence nucleons in the shell ($p_{max}=\delta$). The amplitude C=0.46 MeV was fixed by adjusting to recent known masses. It turned out to be about the same for both proton and neutron separation energies in different regions of the nuclear chart [5]. The additional contribution reflects a new type of corrections to a gross theory of masses. It is cubic in the valence proton or valence neutron number and can be interpreted by interaction between the valence shell and the closed core [6], or via three body interactions [5].

Our analysis results in predictions of half-lives for proton emission from odd(Z,A) nuclei beyond the proton drip line. The lifetimes for 51≤Z≤71 are given in ref. 2. Reasonable agreement with the experimentally determined values of ^{147}Tm and ^{151}Lu is achieved. Taking into account the uncertainties of the model and of the experimental observation windows, the predictions are consistent with recent search experiments at GSI with negative results [7]. Our predictions for 73≤Z≤83 are given in table 1. It can be concluded, that possible next candidates may be ^{155}Ta or ^{165}Ir, where the competing alpha emission is not too strong.

1) S.Hofmann et al., Z.Phys.A305(1982)111 and G.Klepper et al., Z.Phys.A305(1982)125
2) W.F.Feix, E.R.Hilf, Phys.Lett. 120B(1983)14, W.F.Feix, E.R.Hilf, Proc. Int. Workshop on Gross Properties of Nuclei and Nuclear Excitations, Hirschegg (1983) to be published
3) H.v.Groote, E.Hilf, K.Takahashi, ADNDT 17(1976)
4) S.Liran, N.Zeldes, ADNDT 17(1976)
5) W.F.Feix, E.R.Hilf, to be published
6) G.F.Bertsch, Nucl.Phys. 74(1965)234 and T.T.S.Kuo, G.E.Brown, Nucl.Phys. 85(1966) 40
7) P.O.Larsson et al., to be published

Table 1 Calculated half-lives for proton emission from odd(Z,A) nuclei beyond the proton drip line, 73≤Z≤83. The results for two angular momenta of the emitted proton are listed. The corrected Q_p values are given as well.

Parent nucleus	Q_p(MeV)	$t_{1/2}$(p)(s) $j_p^\pi=11/2^-$	$j_p^\pi=3/2^+$
^{183}Bi	1.05	5.5×10^{4}	124.
^{175}Tl	1.23	38.	0.081
^{171}Au	1.13	227.	0.43
^{165}Ir	1.24	2.2	3.9×10^{-3}
^{161}Re	1.07	106.	0.16
^{155}Ta	1.45	1.5×10^{-3}	2.4×10^{-6}

Analysis of Nuclear Charge Distributions

W.D. Myers
Nuclear Science Division, Lawrence Berkeley Laboratory, University of California
K.-H. Schmidt
GSI Darmstadt

The Droplet Model provides a comprehensive description of several macroscopic aspects of nuclei such as the binding energy and the potential energy as a function of the collective coordinates. It also provides a basis for a rather detailed description of both the neutron and proton spatial distributions (1-3). Currently, a large number of excellent measurements of radii and isotope shifts are becoming available and can be compared with the Droplet Model predictions.

The Droplet Model predictions for nuclear density distributions differ from those of the Liquid Drop Model in two important ways. The most important difference is that the equivalent sharp radii of the neutron and proton distributions are determined by minimizing the macroscopic energy of the system. The other difference is the prediction of a small amount of bulk redistribution under the influence of the repulsive Coulomb force. The Droplet Model expressions governing these phenomena have been given previously (1-4).

The most frequently measured quantity, the mean square radius $\langle r^2 \rangle$ can be calculated in the Droplet Model as the sum of several terms:

$$\langle r^2 \rangle = \langle r^2 \rangle_u + \langle r^2 \rangle_r + \langle r^2 \rangle_d,$$

where $\langle r^2 \rangle_u$ is the contribution from the size of the uniform distribution and its shape. The next term, $\langle r^2 \rangle_r$ is the contribution from the redistribution, and its shape dependence. The last term, $\langle r^2 \rangle_d$ is the contribution from the diffuseness.

In Fig. 1, a straight line has been fitted to the experimental RMS charge radii of isotopic sequences and the slope of this line (R_n) is plotted against the Z value for the sequence. The radii were corrected for deformation using the calculations of Möller and Nix[5]. The error bars reflect the errors in the measured RMS values, the lack of linearity in the corrected data, and an estimate of the uncertainty in the calculated deformations that were used. The data are seen to cluster about the solid line representing the Droplet Model prediction. The LDM predictions are off by a factor of about two, and the horizontal line at $R_n = 0$ corresponds to the idea that charge radii depend only on the value of Z, as has sometimes been advocated.

The coefficients of the Droplet Model were determined from fitting only to nuclear masses and fission barriers. Nontheless an excellent agreement is found between the experimental RMS charge radii and the Droplet Model predictions. The accuracy of the Droplet Model seems to be about 0.01 fm, which corresponds to 0.2 % in the RMS radius for a heavy nucleus. This is almost as good as the 0.1 % accuracy (1 MeV out of 1000 MeV) that can be obtained for the binding energy, when the macroscopic approach is supplemented by shell corrections.

[1] W.D. Myers and W.J. Swiatecki, Ann. Phys. (NY) 55 (1969) 395
[2] W.D. Myers and W.J. Swiatecki, Ann. Phys. (NY) 84 (1974) 186
[3] W.D. Myers, Droplet Model of Atomic Nuclei (IFI/Plenum Data Co., New York, 1977)
[4] W.D. Myers and W.J. Swiatecki, Nucl. Phys. A336 (1980) 267
[5] P. Möller and J.R. Nix, At. Data Nucl. Data Tables 26 (1981) 165
und
P. Möller, private communication, March 1982

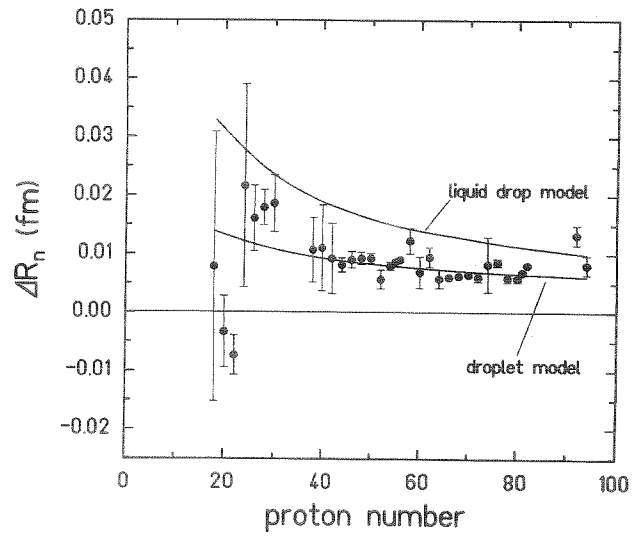


Fig. 1: The slope ΔR_n of the RMS charge radii versus neutron number is plotted against the charge number of the isotopic sequence being considered.

Analysis of the Neutron Excess in the Bulk Region of Finite Nuclei

G

D. Berdichevsky and U. Mosel

Institut für Theoretische Physik, Universität Giessen

A correct description of the neutron excess in the bulk and surface region could be helpful for a better understanding of quasi-elastic and deep-inelastic processes between heavy ions. Also, the failure of the droplet-model (DM) mass formula to predict binding energies of exotic nuclei[1] could be a consequence of an incorrect quantitative description of the neutron excess in the bulk and surface regions of the nucleus[2]. We have, therefore, undertaken to perform Hartree-Fock calculation with Skyrme-type forces for the density distributions.

Our investigation with the forces SIII, SII*, SIV, SV[3], Ka[4], and SKM[5] indicates that the presence of the Coulomb force is responsible for a systematic deviation of the droplet model bulk asymmetry $\delta^m=(\rho_n^m-\rho_p^m)/\rho_A^m$ [$\rho_A^m=\rho_n^m+\rho_p^m$, where $\rho_n^m(\rho_p^m)$ is the neutron (proton) average density in the bulk region] with respect to the result obtained in our HF-calculations (see fig. 1). This deviation is of

7-12/7-12/14-19 %

for the nuclei ^{124}Sn, ^{208}Pb and ^{244}Pu, respectively. For the DM-values we use the corresponding DM-parameters of the corresponding Skyrme force[2,5]. For a quantitative analysis of the average bulk densities ρ_q^m (q=A,n,p) we make use of the following simple geometrical consideration. First we determine the maximum of the function $r^2\rho(r)$. As interesting bulk region we consider only the section between 15/100 and 70/100 of the maximum of $r^2\rho(r)$. This region contains ~80 % of the matter in the bulk region. In fig. 1 we indicate this region with arrows.

Our analysis shows a decrease of the neutron excess δ^m with larger nuclear matter asymmetry coefficient J ($E_{asymm.}=\delta^2 J$[3,6]). The effect is ~15 % in going from SII to SV (see fig. 2). This result indicates that with increasing J a decrease of the neutron excess δ^m in the bulk region and an increase of the neutron skin (nuclei with N>Z), given with $\langle r_n^2\rangle^{1/2}-\langle r_p^2\rangle^{1/2}$ could be energetically more advantageous for the nucleus.

[1] F.K. Wohn and W.L. Talbert, Jr., Phys. Rev. C18, 2328 (1978)
H. Wollnik et al., Phys. Rev. C19, 1504 (1979)

[2] D. Berdichevsky, dissertation Giessen, 1982

[3] M. Beiner et al., Nucl. Phys. A238, 296 (1975)

[4] H. Krivine, I. Treiner and O. Bohigar, Nucl. Phys. A336, 155 (1980)

[5] H.S. Köhler, Nucl. Phys. A258, 301 (1976)

[6] W.D. Myers, in Atomic and Nucl. Data Tables 17, 412 (1976)

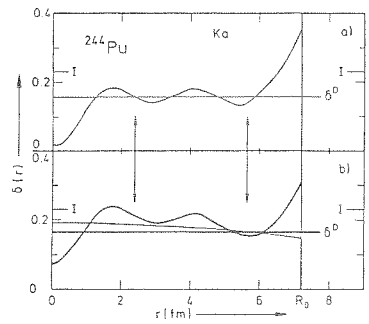


Fig. 1:

Part (a): Without Coulomb-force. The local HF-asymmetry $\delta(r)$ (force Ka) is plotted between the center of the nucleus and the equivalent sharp radius R_0, D is given by the DM-asymmetry formula[6] with the DM-parameter for the force Ka[2,5]. I = (N-Z)/A is the nucleon asymmetry.

Part (b): Same as part (a) but with the Coulomb force. This part includes a plot of the local DM-asymmetry[2] (thin curve).

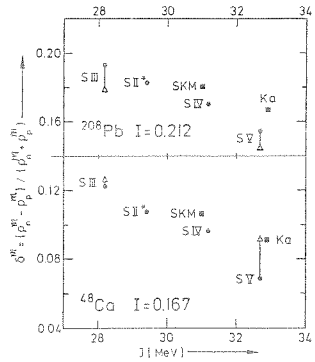


Fig. 2:

Dependence of the matter-asymmetry in the bulk-region as a function of I[3-6]. Full symbols are from HF-calculations and triangles are the results obtained with the DM-formula[6] and the DM-parameters[2,5].

Influence of Shell Structure and Pairing Correlations on the Nuclear Level Density Including Collective Motions

K.-H. Schmidt
GSI Darmstadt
D. Vermeulen
Inst. f. Kernphysik, TH Darmstadt
H. Delagrange, J.P. Dufour, N. Carjan, A. Fleury
Université de Bordeaux I, CEN de Bordeaux-Gradignan

Because of the complexity of microscopic calculations, several efforts have been made to give the nuclear state density including the influence of shell structure and pairing correlations in the form of analytical expressions, whereby several simplifying assumptions were made. We examined the influence of shell structure and pairing on the state densities using microscopic calculations.

The state densities were calculated with the generalized partition function approach similar to the procedures described by Carjan et al.[1]. The single particle energies were calculated in a Cassinoidal- shape diffuse potential[2] with the parameters given by Rost[3]. The pairing strength was normalized as proposed by Strutinsky[4]. The microsopic-macroscopic approach was applied to the ground state energy and to the state density. For this purpose, a temperature smearing method was developed[5].

In the case of equidistant single particle energies, the entropy $\tilde{S}$ as a function of the excitation energy is given by $\tilde{S}^2/4=\tilde{a}E$ with a constant level density parameter $\tilde{a}$. We parametrized the fluctuating part of the entropy which contains the influence of pairing and shell effects by an effective energy shift: $\tilde{S}^2/4=\tilde{a}(E+\delta U+\delta P+\delta E)$, whereby δU represents the ground state shell correction and δP is the pairing condensation energy. For several nuclei, the transition from $\delta E=-(\delta U+\delta P)$ for $E=0$ to $\delta E=0$ for $E\to\infty$ was investigated. It was found that $\delta E=f(E)$ follows closely an exponential function for nuclei in their ground state configuration. (This coincides mostly with an analytical expression of Ignatyuk et al.[6]).

The intrinsic level density represents all levels of a nucleus. Collective motions may, however, lower several levels considerably. This leads to an increase of the level density at low excitation energies. Rotational motions may be included at low excitation energies by superposing a rotational band on each intrinsic level[7]. This "rotational enhancement" is expected to be damped into the intrinsic background at higher energies. Qualitative considerations about this damping are published by Bjørnholm, Bohr, and Mottelson[8]. They discuss that a separation between rotational motion and intrinsic motion can only be preserved at temperatures low enough to ensure a well defined deformation. A limit of $T = 38\ \mathrm{MeV}\ A^{-1/3} \cdot \beta$ is proposed. The dependence of the limiting temperature T on the deformation β causes an interesting interdependence of shell effects and rotational enhancement.

For a qualitative consideration, the rotational enhancement was assumed to be exponentially washed out (in analogy to the influence of shell effects on the level density). As the limiting temperature increases with deformation, the nucleus will be driven to deformation at higher energies because of the gain of rotational levels (see also[9]). Consequently, spherical shell effects will be washed out at much lower excitation energies when the rotational enhancement is included, whereas the influence of deformed shells remains nearly unchanged, as is demonstrated in Fig. 1.

[1] N. Carjan et al., Phys. Rev. C19 (1979) 2267
[2] V.V. Pashkevich, Nucl. Phys. A169 (1971)275
[3] E. Rost, Phys. Lett. 26B (1968) 184
[4] V.M. Strutinsky, Nucl. Phys. A122 (1968) 1
[5] K.-H. Schmidt et al., Z. Phys. A308 (1982) 215
[6] A.V. Ignatyuk et al., Sov. J. Nucl. Phys. 21 (1975) 255
[7] T. Ericson, Nucl. Phys. 6 (1958) 62
[8] S. Bjørnholm et al., Proc. Conf. Phys. a. Chem. of Fission, Rochester 1973, IAEA Vienna 1974, Vol. I, p. 367
[9] Vidgor, H.J. Karwowski, Phys. Rev. C26 (1982) 1068

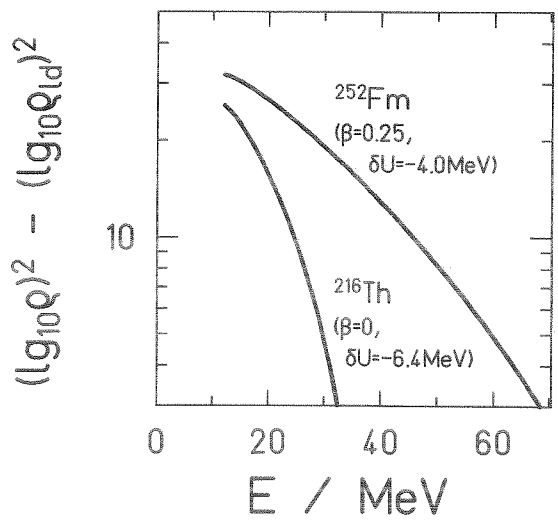


Fig. 1: The influence of the rotational enhancement and the shell effect on the level density of a spherical and a deformed nucleus.

G

Calculation of Energy Averaged Reduced Transition Probabilities (EARTP)

A. Baran, K. Dietrich

Physik-Department TUM Garching and GSI Darmstadt

In statistical codes[1] the competition among different possible gamma transitions is assumed to be described through the following formula for the transition from $|i\rangle = |E_i, I_i\rangle$ to $|f\rangle = |E_f, I_f\rangle$ ($E_{i(f)}, I_{i(f)}$ = initial (final energies, angular momenta)

$$T(O\lambda; i \to f) = C_{O\lambda} (E_i - E_f)^{2\lambda+1} \rho_f / \rho_i \,. \qquad (1)$$

$C_{O\lambda}$ are mode constants referring to the transition operator $O\lambda$ (multipolarity λ). $\rho_{f(i)}$ are the final (initial) level densities.

The parameters $C_{O\lambda}$ are either estimated from the strengths of transitions between low lying states or from the Weisskopf estimates or fitted so that the γ-evaporation theory agrees optimally with experiment. In fact $C_{O\lambda}$ should depend on the angular momenta I_i, I_f and on the energies E_i, E_f as well. We therefore deduce these "constants" from EARTP calculated from a realistic nuclear model which describes the yrast line and the excited states in a simple and satisfactory way.

We use the self consistent cranking model[2]. The ground (yrast) state $|\Phi\rangle$ is a BCS state violating time reversal, particle number and axial symmetry. The wave function $|\Psi\rangle$ in the lab frame can be obtained from $|\Phi\rangle$ by projecting onto a good angular momentum.

Our approximations in this derivation are:

i) For calculating the average transition rates we restrict ourselves to 2qp excitations. The number of 2qp excitations is already so large that we may expect good average values from this sub ensemble.

ii) We use the Kamlah projection technique of zeroth order[2,3] in calculating all the matrix elements of the transition operators.

iii) Calculating the matrix element $\langle 2'qp \| O\lambda \| 2qp\rangle$ we take the same groundstates and the same Bogoliubov representation for the final and initial states.

IV) We use the asymptotic expression for the 3-j symbols in the limit $K \ll I$.

The normalized, angular momentum projected wave function $|\Psi^{IM}\rangle$ is[2]:

$$|\Psi^{IM}\rangle = N_I \sum_K \hat{P}^I_{MK} |2qp\rangle \,. \qquad (2)$$

The $\hat{P}^I_{MK}$ is the "projection" operator and N_I is a normalization constant given by

$$N_I^{-2} = \sum_{KM} \langle n\text{-}qp | \hat{P}^I_{MK} | n\text{-}qp\rangle \,. \qquad (3)$$

The reduced transition matrix element is

$$\langle \Psi^{I'} \| O\lambda \| \Psi^I \rangle = N_I N_{I'} \sum_{KK'\bar{K}\mu} (2I+1) \times \times (-1)^{I'-K'} \begin{pmatrix} I' & \lambda & I \\ -K' & \mu & \bar{K} \end{pmatrix} \langle n'qp | O(\lambda\mu) \hat{P}^I_{\bar{K}K} | n\text{-}qp\rangle \qquad (4)$$

A similar expression can be obtained by using the quantities $\langle n'qp | \hat{P}^{I'}_{K'\bar{K}} O(\lambda\mu) | n\text{-}qp\rangle$. For the approximate evaluation of (4) we take the average of both these expressions[2]. We obtain

$$\langle \Psi^{I'} \| O(\lambda) \| \Psi^I \rangle \approx \sum_\mu F(II'\lambda\mu) \sqrt{2I+1} \times \langle 2'qp | O(\lambda\mu) | 2\text{-}qp\rangle \tfrac{1}{2} [\chi + \chi^{-1}] \qquad (5)$$

The $F(II'\lambda\mu)$ factor originates from the 3-j symbol under assumption iv. In ref.[2] it is shown that $\chi = \chi(II') \equiv N_I (2I+1)^{1/2} / N_{I'} (2I'+1)^{1/2}$ for the off-diagonal matrix elements with $I'=I-2$ is nearly 1 in the case of yrast states. We adopt here the additional approximation that this is true also for our excited states. This leads us to the expression

$$\langle \Psi^{I'} \| O(\lambda) \| \Psi^I \rangle \approx \sum_\mu F(II'\lambda\mu) \langle 2'qp | O(\lambda\mu) | 2\,qp\rangle \qquad (6)$$

Averaging over 2qp states in the interval $I_E = \{E - \frac{\Delta}{2}, E + \frac{\Delta}{2}\}$ around $E_f(E_i)$ we finally end up with the following expressions for EARTP:

$$B(O\lambda; I \to I')_{E \to E' \neq E_{yrast}} = \frac{4}{\Delta^2 \rho \rho'} \sum_{\substack{klm \\ (\epsilon_k + \epsilon_l) \in I_E \\ (\epsilon_m + \epsilon_l) \in I_{E'}}} \left| \sum_\mu F(II'\lambda\mu) O(\lambda\mu)^{11}_{mk} \right|^2 , \qquad (7)$$

$$B(O\lambda; I \to I')_{E \to E_{yrast}} = \frac{1}{\Delta \cdot \rho} \sum_{\substack{kl \\ (\epsilon_k + \epsilon_l) \in I_E}} \left| \sum_\mu F(II'\lambda\mu) O(\lambda\mu)^{20}_{ke} \right|^2 . \qquad (8)$$

ρ and ρ' are 2-qp level densities at E and E' respectively, ϵ_k's are the single qp energies. The transition probability (1) is now to be replaced by the formula

$$T(O\lambda; i \to f) \equiv \bar{C}_\lambda (E_i - E_f)^{2\lambda+1} B(O\lambda; I \to I')_{E \to E'} \qquad (9)$$

where[4] $\bar{C}_\lambda$ is a pure normalization constant and depends only on multipolarity λ of gamma radiation. The energy dependence of $T(O\lambda; i \to f)$ beside the factor $(E_i - E_f)^{2\lambda+1}$ as well as spin dependence are contained in $B(O\lambda; I \to I')_{E \to E'}$. It may be calculated numerically.

[1] M.Wakai, A.Faessler, Nucl.Phys. A307 (1978) 349

[2] P.Ring, A.Hayashi, K.Hara, Phys.Lett. 110B (1982) 423

[3] G.A.Kamlah, Z.Phys. 216 (1968) 52

[4] A.Bohr, B.Mottelson, vol.I (3.145)

Gamma Deexcitation Process of ^{158}Dy and Realistic Level Densities

A. Baran, K. Dietrich
Physik-Department TUM, Garching and GSI Darmstadt

The level densities calculated numerically within the realistic Hartree-Fock Bogoliubov model[1] are used in a Monte-Carlo code generating a set of cascades which consist of E1, M1, E2 and E2 collective (intra band) gamma transitions. Each gamma cascade starts at some entry point which is an intermediate state of the nucleus after particle emission has ceased. We assume a simple triangular spin distribution for this initial ensemble of nuclei and a Gaussian distribution of the energy centred around the single neutron binding energy.

The individual transition is selected on the basis of the calculated partial widths by generating a random number (see e.g. ref.2). The transition rate from an initial state characterized by energy E_i and spin I_i to a final state with E_f and I_f is assumed to be [2,3+]

$$T(\sigma\lambda;\ i\to f) = C_{\sigma\lambda}\,(E_i - E_f)^{2\lambda+2}\,\rho_f/\rho_i\,. \qquad (1)$$

$C_{\sigma\lambda}$ are adjustable parameters which should however have values as obtained in realistic nuclear models. Following ref.2 we take

$$C_{E1} : C_{M1} : C_{E2} = 50 : 25 : 1.$$

The level densities $\rho_i(\rho_f)$ are calculated numerically[1]. At each step of the cascade there is also the possibility of a collective E2-coll transitions ($\Delta I = -2$). The relative width for E2-coll is of the form

$$T(E2\,coll) = C_{E2\,coll}\ E_\gamma^5\,. \qquad (2)$$

The collectivity parameter in the case of ^{158}Dy is chosen to be 8oo.

Gamma spectra obtained from such calculations are displayed in fig.1. The partial (E1,M1,E2, $E2_{coll}$) spectra are also given. As in an experiment we can see the characteristic bump at low energy which is caused by the collective E2-transitions and the flat exponential tail produced mainly through E1 and E2 statistical transitions. The number of cascades is 2ooo.

Fig.2 shows the side feeding population (psf) as a function of angular momentum of the Yrast state. For comparison we plot the experimental results taken from ref.4. We see a qualitative agreement with the experimental data. The two bumps are a natural consequence of the level densities used in the calculations. The difference in the positions of the bumps might be eliminated by application of more realistic transition rates instead of that given in eq.1 (see 5). The average multiplicites of gamma rays are in a fairly good agreement with the experimental data and they are not reported here.

[1] A.Baran,K.Dietrich,GSI report,p.78-79(1981)
[2] M.Wakai,A.Faessler,Nucl.Phys.A3o7(1978)p.349
[3] R.J.Liotta,R.A.Sorensen,Nucl.Phys.A197(1978)136
[4] H. Emling et al.,Phys.Lett.98B(1981)169
[5] A.Baran,K.Dietrich, this report

[+] The theory of elm transitions gives the power $(2\lambda+1)$ and no factor ρ_i.

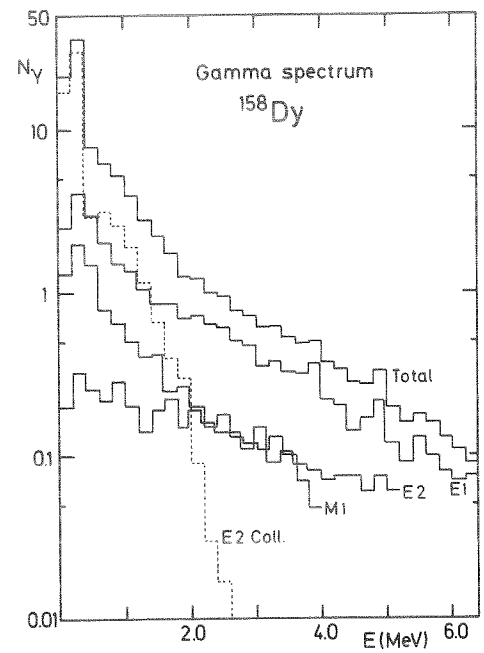


Fig.1 Gamma spectrum of ^{158}Dy (N_γ =number of photons)

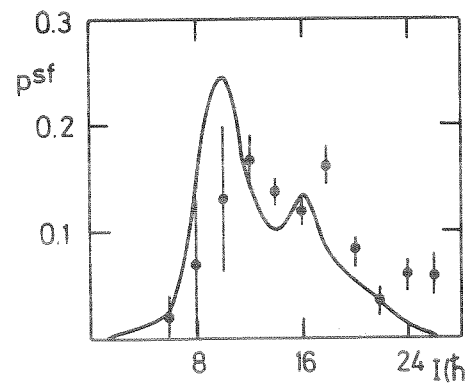


Fig.2 Side feeding population of ^{158}Dy

Yrast Line and g-Factors of ^{158}Er [B G]

M. Diebel, U. Mosel and K. Mühlhans

Institut für Theoretische Physik, Universität Gießen

Motivated by the experiments at the Darmstadt-Heidelberg Crystal-Ball-Spectrometer we have performed HFBC calculations for the nucleus ^{158}Er. The Crystal-Ball makes it possible to study ^{158}Er at spins higher than 38 which is the highest value that has been measured for this nucleus with other methods up to now[1].

The HFBC calculations are carried out in a model using the triaxial Nilsson potential as single particle potential and treating the pair field selfconsistently with a standard monopole pairing force.

The g-factors are then calculated from the HFBC wave functions:

$$g(I) = \frac{Tr\rho^{HFB}(I)(g_l^\tau l_x + g_s^\tau s_x)}{\langle I_x \rangle}$$

$$= \frac{\langle I_x \rangle_p}{\langle I_x \rangle} + \frac{(g_s^p - 1)\langle s_x \rangle_p + g_s^n \langle s_x \rangle_n}{\langle I_x \rangle}$$

Within one band the following relation holds:

$$\frac{\langle I_x \rangle_p}{\langle I_x \rangle} = \frac{J^p}{J^p + J^n}$$

Accordingly g(I) will tend to increase if the proton pairing breaks down faster than the neutron pairing and tend to decrease if the proton pairing breaks down more slowly[2].

Our calculations reproduce all 3 alignments which are seen in the experiment. The first one is the i13/2υ, then h11/2π and at least i13/2ν. The large backbend at I=48 in the theoretical calculation is due to the i13/2π.

The first crossing calculated is seen to appear at a too low spin value, but the nucleus ^{158}Er is supposed not to be a good rotator in its ground state.

In fig. 2 the g-factors are shown. These reflect the various alignments discussed above and are thus a sensitive tool to study single particle effects in rotational bands.

[1] J. Burde et al., Phys. Rev. Lett. 48, 530 (1982)

[2] M. Diebel et al., Nucl. Phys. A345, 72 (1980)

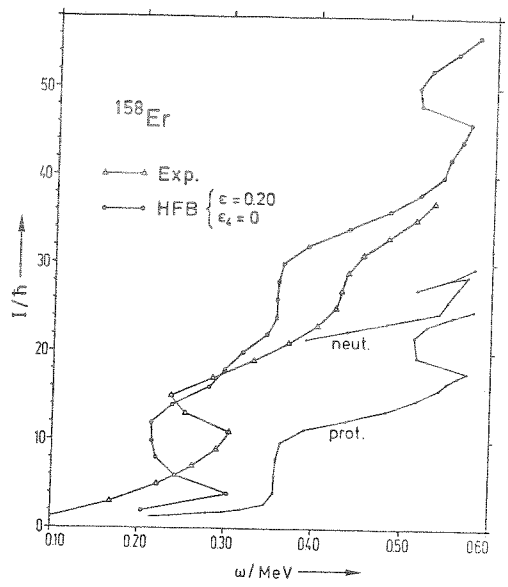


Fig. 1: Experimental (triangles and calculated (circles) yrast line for ^{158}Er. Calculated spin contributions from neutrons and protons are given individually. The experimental data are from ref.[1].

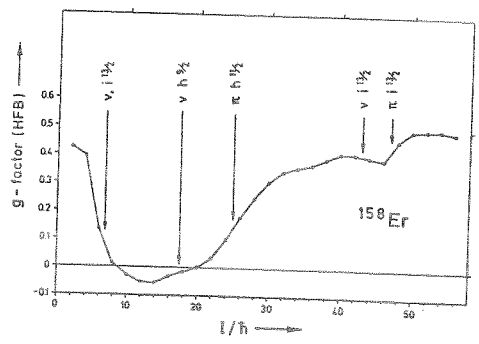


Fig. 2: Calculated spin dependence of the g-factors for ^{158}Er. Arrows indicate spin alignment. The nature of the aligning particles is given on top of them.

Alignment Behaviour of Odd-A-Nuclei B G

E.M. Müller, U. Mosel and K. Neergård

Institut für Theoretische Physik, Universität Gießen

Over the last two years the GSI group has performed quite complete and new experiments concerning the high spin structure of Actinide nuclei[1]. In these studies it was found that the two odd nuclei ^{235}U and ^{237}Np show quite different alignment behaviour which is normally attributed to different blocking features. Since spectra of odd nuclei can often be described quite well by particle rotor models we have performed such calculations for the nuclei mentioned above. In these studies the Coriolis attenuation is achieved by introducing a rotation dependent interaction between the core and the quasiparticle[2].

Fig. 1 shows the quantity $i(\omega)$, defined as the difference between the spin of the odd-A nucleus and the average of the experimentally measured ground state spins of the neighbouring nuclei. For both calculations only one fit parameter α is used, which is nearly equal for both nuclei ($\alpha \approx .6$). This parameter plays a similar role as the usual Coriolis attenuation factor but connects this attenuation with the recoil term (for details see ref. 3).

The QPRM was also tested in the rare-earth region, where good agreement with the experiment was reached, too. For the odd proton nuclei ^{155}Ho and ^{157}Ho the calculations yield to attenuation factors near to unity. The results for ^{155}Ho are shown in fig. 2.

For the ^{161}Yb, ^{163}Yb, ^{165}Yb, ^{167}Yb, and ^{169}Yb isotopes also QPRM calculations are made. It was found that for these nuclei the aligning quasiparticle states ave obviously blocked, while in the neighbouring even-even nuclei a strong backbending takes place due to a crossing of the s-band with the g-band. This blocked situation in the odd-A-nuclei can be simulated by taking the total g-band and not the Yrast band (which is identical with the s-band for high spins) as the core in our model, where only one quasiparticle is moving around the core, thereby implicitly including the blocking mechanism. It can be seen from fig. 3 where, for example, the results for ^{161}Yb are shown, that this procedure leads to a good agreememt with the data.

[1] R.S. Simon, F. Folkmann, C. Briancon, J. Libert J.P. Thibaud, R.J. Walen, and S. Frauendorf, Z. Phys. A298, 121 (1980)

[2] E.M. Müller and K. Neergård, Phys. Lett. Vol 120B, 280 (1983)

[3] K. Neergård, Phys. Lett. Vol 89B, 5 (1979)

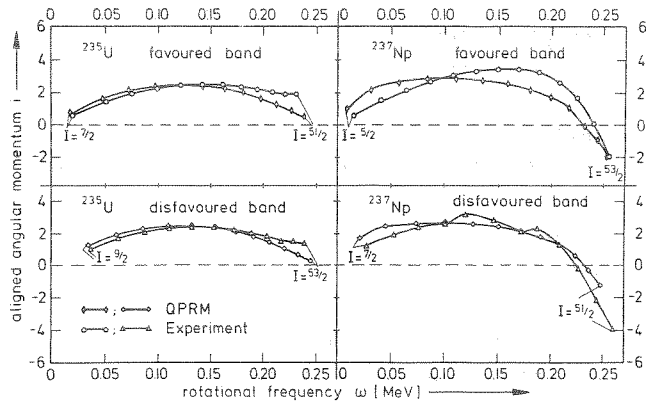


Fig. 1

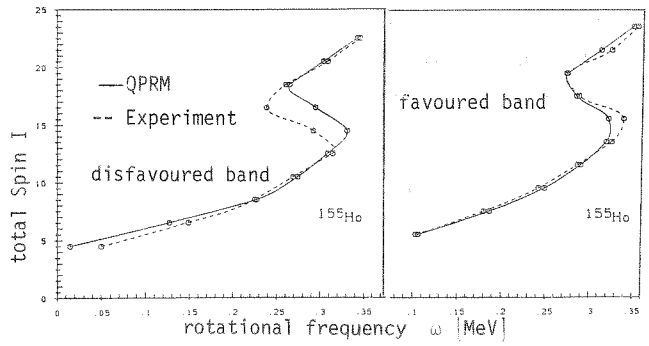


Fig. 2

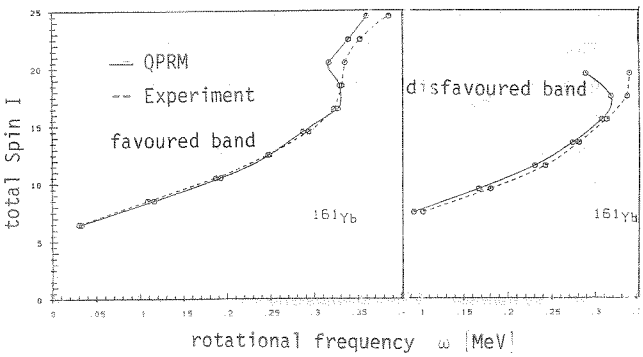


Fig. 3

Improvement of Quasiparticle Levels [G]

U. Mosel, U. Post and E. Wüst

Institut für Theoretische Physik, Universität Giessen

Since the first indication of backbending in the early seventies this effect has been investigated in many experimental and theoretical attempts. Nowadays for many nuclei the yrast line and also the corresponding electromagnetic properties[1] have been measured very exactly with the help of highly developed spectroscopic methods. Even particular pair matrix elements have been determined[2]. Such analyses do depend on a thorough understanding of all other effects, like e.g. deformation changes, coupling to vibrations etc.. In addition to these well discussed effects there could also be new terms in the Hamiltonian that become effective only at high spins. As a guideline for such studies we have chosen the Skyrme forces that lead to the appearance of new terms in the potential for systems with broken time reversal invariance as e.g. in high spin states[3]. It is the purpose of this study to explore the effects of these new terms on quasiparticle spectra and deformation properties of nuclei at high spins.

In our present cranked HFB calculations we substitute the well understood even-even ground-state part of the Skyrme Hamiltonian[4] by a Woods-Saxon single particle potential. The new terms are then calculated from the HFB wavefunctions and the energies are obtained from perturbation theory. Because there are no investigations of Skyrme parameters in time reversal broken systems we use the conventional parameter sets only as guidelines.

First results of our work are shown in fig. 1. There are drawn the lowest quasiparticle energies of the neutron states with positive parity for ^{158}Dy. The diagrams demonstrate that variation of the Skyrme parameters can shift the crossing angular momentum down to lower values.

[1] D. Schwalm, Electromagnetic properties of high spin states; invited talk at Intern. Conf. on Nucl. Structive, Nov. 1982

[2] J.D. Garret et al., Phys. Lett. 118B, 297 (1982)

[3] K.H. Passler and U. Mosel, Nucl. Phys. A257, 253 (1976)

[4] D. Vautherin and D.M. Brink, Phys. Rev. C5, 3 626 (1972)
K.H. Passler and U. Mosel, Nucl. Phys. A257, 242 (1976)
J. Fleckner, U. Mosel, P. Ring and H.-J. Mang, Nucl. Phys. A331, 288 (1979)

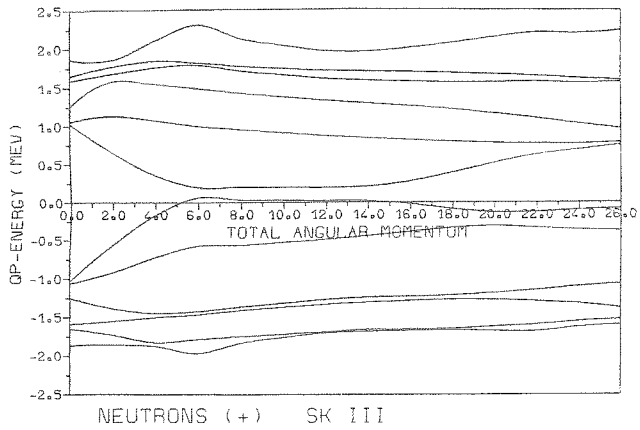


Fig. 1a: Lower quasiparticle levels with Skyrme III parameter set

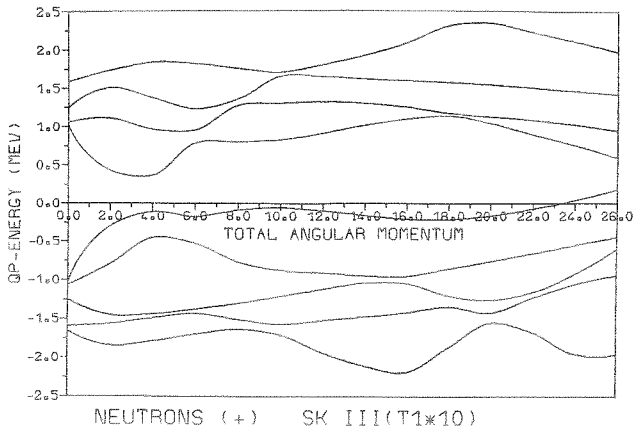


Fig. 1b: Same as a) but t_1 replaced by $10*t_1$

Multipole Pair Fields at Various Conditions [B G]

K. Mühlhans, U. Mosel and E.M. Müller

Institut für Theoretische Physik, Universität Gießen

The GSI-Heidelberg crystal ball makes it possible to study the entry line as well as the yrast line of heavy nuclei with unprecedented accuracy and resolution. It is thus appropriate to study the nuclear structure at temperatures T>0 above the yrast line and to investigate the effects of using more realistic single particle interactions than the standard monopole force.

The breakdown of monopole pairing with increasing angular velocity (CAP) or temperatures[1] is well known. There have also been many investigations in the past (see 2 and refs. therein) about the fact that multipole pairing is more stable against angular momenta than the monopole pair field alone.

Two of the remaining questions are:

(i) Does the amount of multipole pairing compared with monopole pairing depend on the nucleus studied?

(ii) Are higher multipole modes more resistant against increasing the temperature, too?

Our model, consisting of a Nilsson Hamiltonian for the one body part and a Surface Delta Interaction for the selfconsistently treated pair field[2], allows us to answer both of the questions. For the temperature dependent calculation (FTHFBC) we simply have to replace the density ρ and the pair tensor t by[1,3]:

$$\rho = AfA^{+} + B^{*}(1-f)B^{T} \qquad t = AfB^{+} + B^{*}(1-f)A^{T}$$

with

$$f_{ij} = \frac{1}{1+e^{\beta E_i}}\delta_{ij} \quad \text{and} \quad \beta := \frac{1}{k\tau}$$

(E_i : quasiparticle energies)

The result for (i) (fig. 1) displays a decrease of the amount of quadrupole pairing while going from light to heavy rare earth nuclei (fig. 1a) (parameters fixed for ^{162}Er). This could be understood in terms of the decrease of the single particle quadrupole moment of the states closest to the Fermi surface in that region[2].

Fig. 2 shows clearly that higher multipole modes are more stable against increasing the temperature, too, compared with a monopole alone[3] (see dotted line in fig. 1a). T=0 modes behave similar with respect to the temperature (fig. 2a and b).

[1] A.L. Goodman, Nucl. Phys. A352, 30 and 45 (1981)

[2] K. Mühlhans, M. Diebel, K. Neergård, and U. Mosel, Phys. Lett. B120, 44 (1983)

[3] K. Mühlhans, E.M. Müller, U. Mosel, and A.L. Goodman, to be published

Fig. 1:

Multipole composition in a calculation with the oscillator shells 5 and 6 (4 and 5) for neutrons (protons) with G_{JM1} = 0.146 MeV (neutrons) and $G_{JM(-1)}$=0.179 MeV (protons). Dashed line: Δ_{01M_T}. Dotted line: Δ_{21M_T}. Dotted dashed line: Δ_{41M_T}.
a) displays the results for neutrons (Δ_{J11}) and
b) for protons ($\Delta_{J1(-1)}$).

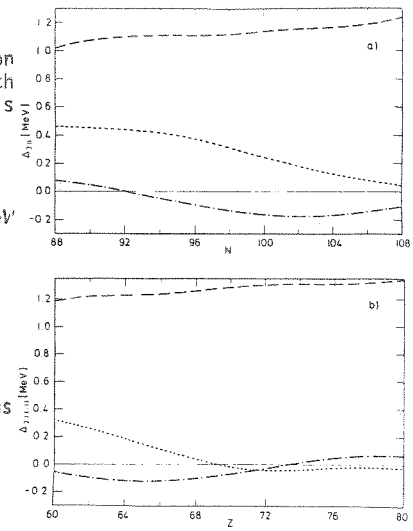
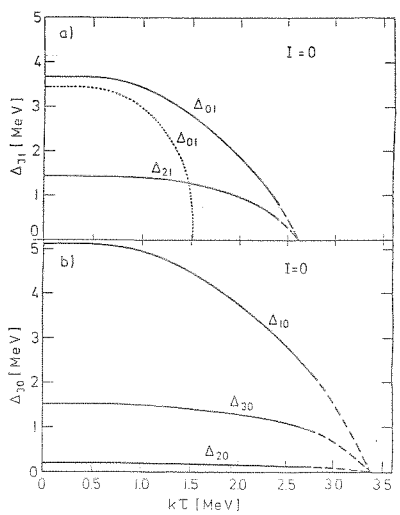


Fig. 2:

Multipole composition for the T=1 (part a) and the T=0 (part b) pair fields with increasing temperature. Solid lines: Result of a calculation with all multipole modes. Multipole modes with J larger than 2 in the T=1 and J larger than 3 in the T=0 case are too small for the scale of the figure. Dashed line: Extrapolation. Dotted line: Result of a calculation with only the monopole pair field included.



How Do Nuclei Really Vibrate?

J. Kunz*, U. Mosel, A. Schuh, and E. Wüst

Institut für Theoretische Physik, Universität Gießen

The question how nuclei really vibrate, i.e. the question for the dynamics of nuclear collective motion, is still largely unanswered. Simple prescriptions like e.g. assumptions of irrotational flow are often employed to calculate mass parameters for collective motion but it should be realized that the only justification for their use is often that the true flow fields are unknown or that irrotational flow is easy to handle.

One of the most well known applications of irrotational flow is the calculation of mass parameters for low-lying collective quadrupole vibrations, a standard textbook example. We have recently performed microscopic calculations of these currents by using the cranking model applied to a deformed Nilsson potential including pairing correlations of the BCS-type[1]. The flow pattern has then been calculated by taking the expectation values of the nuclear current operator in the cranking wave functions. The results of these calculations are shown in figs. 1 and 2 for the low-lying ($\Delta N=0$) and the the high-lying ($\Delta N=2$) quadrupole vibrational states.

It is obvious that the high-lying E2-giant resonance state is described by an irrotational flow pattern, in accordance with current-sum-rule considerations[2]. The low-lying state, on the contrary, that is normally described by irrotational flow shows a strong vortex pattern. The conclusion is thus that macroscopic nuclear models have up to now described the wrong state with irrotational flow dynamics.

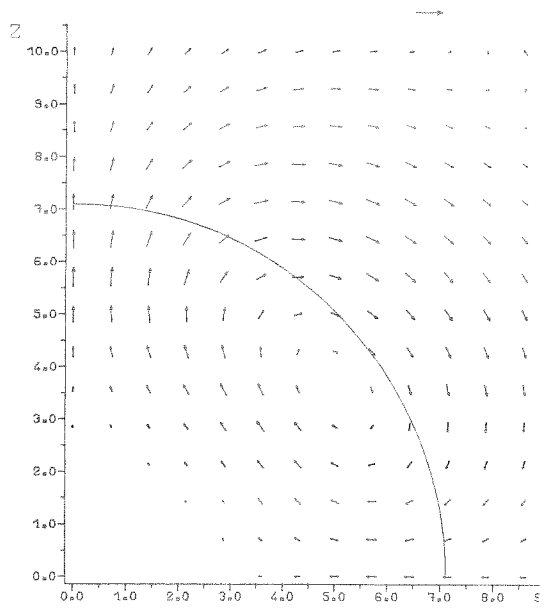


Fig. 1: Velocity distribution for the high lying ($\Delta N=0$) quadrupole state in ^{208}Pb.

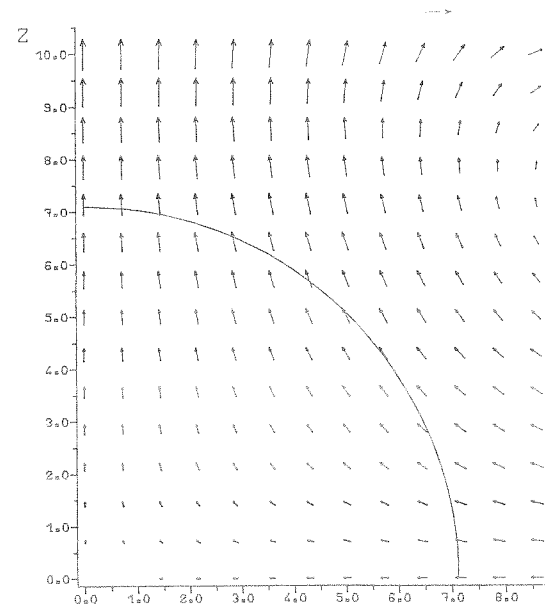


Fig. 2: Velocity distribution for the high lying ($\Delta N=2$) quadrupole state in ^{208}Pb.

[1] A. Schuh et al., Giessen preprint 1982

[2] T. Suzuki and D.J. Rowe, Nucl. Phys. A286, 307 (1977)

* Now at LANL, Los Alamos, USA

On the Existence of Relatively Stable Giant Nuclei around Z = 164-182 [GG]

N. Abou-El-Naga and W. Greiner
Institut für Theoretische Physik der Universität Frankfurt

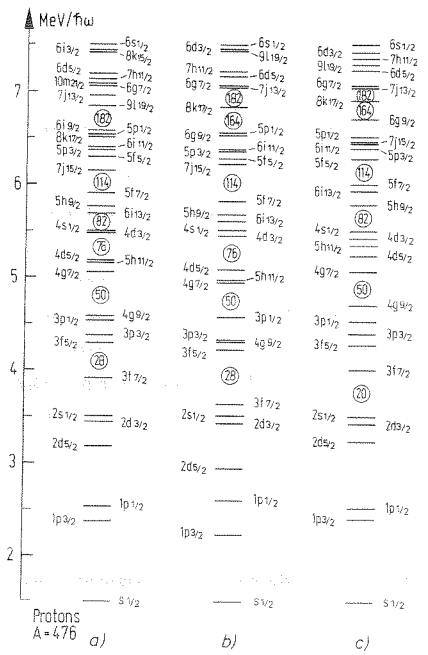
In this investigation we are extrapolating the single particle and the bulk properties of nuclear matter into the region of extremely high numbers of protons and neutrons. The single particle potential is taken as a modified oscillator with the parameters extrapolated to the regions of giant nuclei U+U (Z=184). Such extrapolations are, of course, rather risky and one has to make sure that they are performed in a reasonable way. We have therefore tried various sets of parameters, which are acceptable in ordinary heavy nuclei, and studied their consequences in the domain of the giant nuclei. Fig. 1 shows the proton levels for three different methods of chosing the parameters for the spin-orbit potential. In method (a) the parameters are taken proportional to $A^{1/3}$ [1], in method (b) as a function of the main oscillator quantum number N [2], and in the last one (c) they are proportional to A itself [3]. As shown in Fig. 1 the next magic proton numbers beyond Z=114 are Z=164 and Z=182 in all methods.

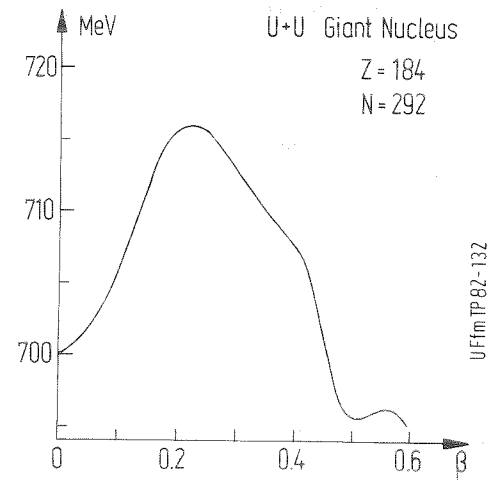
Strutinky's renormalization method is applied to obtain a first systematic survey at the expected stability of giant nuclei of the new island close to Z=164-182. The potential surface of a U+U giant nucleus in Fig.2 shows a spherical minimum with a depth of about ~15 MeV, where the shell correction is calculated with parameters (a). Fig. 3 displays a contour plot for the potential barrier heights for proton numbers Z= 158-190 and neutron numbers N=282-310. The plot contour shows two main islands of relative stability: the first one lies around Z=182 and N=302, while the second occurs at Z=164-168 and the same N=302.

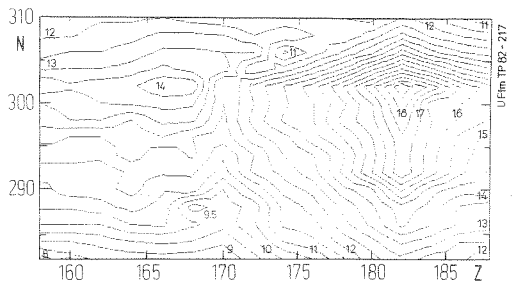
[1] C. Gustafsson, Proc. of the International conference on the properties of nuclei far from the region of beta stability, Lysin, Switzerland, August 31 - September 4, 1970, p. 654

[2] J. Grumann, U. Mosel, B. Fink, and W. Greiner, Z.Physik 228 (1969) 371-386

[3] S.G. Nilsson, C.F. Tsang, A. Sabiczewski, Z. Szymanski, S. Wycech, C. Gustafsson, I.L. Lamm, P. Möller, and B. Nilsson Nucl.Phys. A131 (1969) 1-66







Fusion of ^{40}Ar and ^{40}Ca at High Incident Energies — Fusion-Fission and Fusion-Evaporation

B,G

J. CARTER, H. FELDMEIER, C. BRENDEL, A. RICHTER and G. SCHRIEDER
Institut für Kernphysik, Technische Hochschule Darmstadt
W. BOHNE, K. GRABISCH, H. LEHR and H. MORGENSTERN
Hahn-Meitner Institut, Berlin

The evaporation residue cross sections measured directly for ^{40}Ar + ^{40}Ca at E_{Lab} = 161, 190, 236 and 273 MeV (VICKSI facility, HMI) and the upper limits[1] (UNILAC, GSI) determined by subtracting the deep-inelastic and fusion-fission components from the total reaction cross section (σ_R^{OM} from Optical Model, σ_R^{SOD} from Sum-of-Difference method) are shown in fig. 1. The values obtained by the two different methods are seen to be in good agreement and in order to compare these data with theory the maximum ℓ-value for fusion has to be known, which at high incident energy is limited by a critical angular momentum ℓ_c. For all partial waves below ℓ_c the effective nucleus-nucleus potential is characterized by a potential barrier and a pocket, while for those above ℓ_c the potential pocket disappears and consequently fusion cannot occur. Previously, the determination of ℓ_c for the ^{40}Ar + ^{40}Ca sytem studied was found to be reasonably satisfactory[1] when calculated within the One-Body Window Friction model but was limited to the one-dimensional case. However, during fusion considerable shape distortion may occur resulting in neck formation between the initially spherical nuclei. Therefore, a more realistic dynamical description of the fusion process has been developed by including in a trajectory model a shape degree-of-freedom.[2] This model has been applied to the interaction of ^{40}Ar + ^{40}Ca. By taking the fusion cross section obtained from the trajectory calculations, σ_F^T, and subtracting the liquid-drop model fusion-fission cross section, σ_{FF}^{LD}, the resulting evaporation residue cross sections, σ_{ER}^C (fig. 1, dotted line), can be compared with the measured values. The agreement between the data and the prediction is quite gratifying.

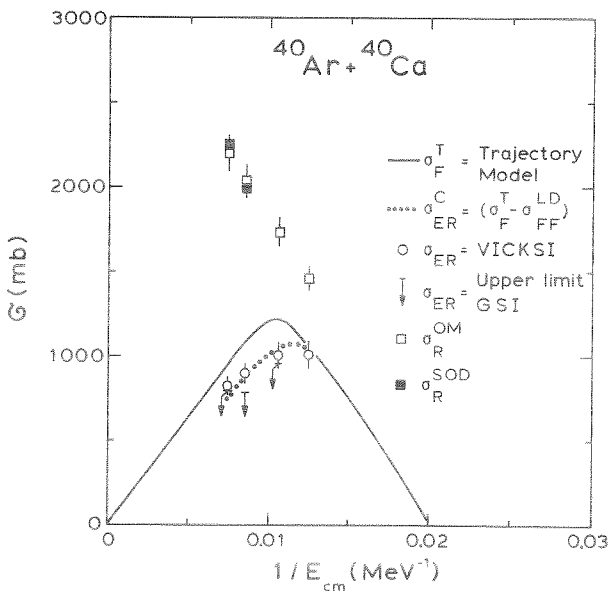


Fig.1: The various cross sections for ^{40}Ar + ^{40}Ca

Figure 2 shows the potential energy landscape for ^{40}Ar + ^{40}Ca calculated with the trajectory model for the critical angular momentum ℓ_c = 62 $\hbar$, where σ is the neck volume as a fraction of the total nuclear volume and s the separation of the nuclear centres. The heavy line depicts the trajectory at E_{Lab} = 273 MeV in time

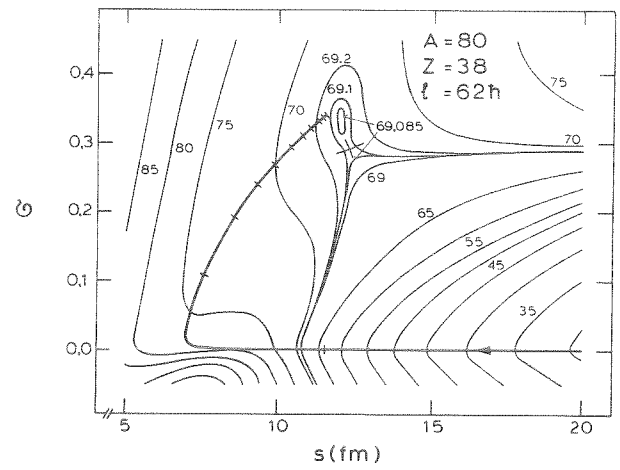


Fig.2: Potential map for ^{40}Ar + ^{40}Ca (contours in Mev)

units of 10^{-21} s, and after a long interaction time fusion occurs in a very shallow pocket behind the saddle point (denoted by a cross). A reliable value for the fission cross section of the compound nucleus, which is very sensitive to the angular momentum possessed by the system, may be calculated then satisfactorily. A somewhat larger evaporation residue cross section is observed at higher incident energies than predicted (see fig. 1) and, therefore, we plan in a future experiment at GSI to investigate this discrepancy further upto 20 MeV/amu.

[1] J. Carter, H. Feldmeier, A. Richter, G. Schrieder and P. Wastyn, Z. Phys. A302(1981)365

[2] H. Feldmeier, Invited Lectures, Int. School of Physics "Enrico Fermi", Varenna (1982)

On Quantal Diffraction in Dissipative Heavy Ion Collisions [G]

H. Spangenberger, F. Beck
Institut für Kernphysik, Technische Hochschule Darmstadt

H. Feldmeier
Max-Planck-Institut für Kernphysik, Heidelberg

The standard diffusion picture utilizing an Einstein relation between friction and diffusion results in a width of the scattering angle which is too narrow compared to measured data. Therefore quantal diffraction effects seem to be important to describe fluctuations for moderate energy losses[1]. However, an improved statistical model which does not assume global thermal equilibrium and thus does not obey an Einstein relation[2,3] results in broad fluctuations comparable to the experimental data. The open questions are: Does the additional quantum diffraction destroy the agreement with the experiment and thus invalidate the particle exchange picture or do quantal effects tend to vanish due to the underlying statistical fluctuations? A semi quantal calculation performed similar to ref. 1) starts with a micro-channel cross section of the form

$$\left(\frac{d\sigma}{d\Omega}\right)_{\alpha\alpha} = \frac{1}{4k_c^2} \sum_{l_1 l_2 l_1' l_2' s' L} G_{l_1 l_2 l_1' l_2' s' L}(\cos\theta) \times$$

$$\times S^{*}_{\alpha' s' l_1' \alpha o l_1} \quad S_{\alpha' s' l_2' \alpha o l_2}$$

where G denotes a geometrical factor. The measured double differential cross section is given by

$$\frac{d^2\sigma}{dE\,d\Omega} = \frac{1}{\Delta E} \sum_{\alpha' \in [E, E+\Delta E]} \left(\frac{d\sigma}{d\Omega}\right)_{\alpha\alpha}$$

Assuming statistical properties for the S-matrix elements we approximate:

$$\sum_{\alpha' \in [E, E+\Delta E]} S^{*}_{\alpha' s' l_1' \alpha o l_1} S_{\alpha' s' l_2' \alpha o l_2} \approx$$

$$\sqrt{F^{C}_{l_1 l_1'}(E)} \sqrt{F^{C}_{l_2 l_2'}(E)} \exp\left\{ i (\Phi_{l_2 l_2'} - \Phi_{l_1 l_1'}) \right\}$$

$F^{C}_{l_1 l_1'}(E)$ are probability distributions resulting from a statistical model[2,3]:

$$F^{C}_{ll'}(E) = \delta(s'-l+l') \frac{\sqrt{\det(\sigma^2)}}{2\pi} \exp\left\{ -\frac{1}{2} [\sigma^2_{ll'}(l)(l'-l_c(l))^2 + \right.$$

$$\left. + 2\,\sigma^2_{l'E}(l)(l'-l_c(l))(E-E_c(l)) + \sigma^2_{EE}(l)(E+E_c(l))^2] \right\}$$

$l_c(l)$, $E_c(l)$ and $\sigma^2_{l'l'}(l)$, $\sigma^2_{l'E}(l)$, $\sigma^2_{EE}(l)$ are the first and second moments of the asymptotic distribution of the final macroscopic variables l' and E, given as a function of the initial angular momentum l. The phases $\phi_{ll'}$ are responsible for the interference effects which we want to take into account. They are calculated by a semiclassical expression[1]. The results of the statistical model without quantal effects are shown in the right hand side of the figure as dashed lines. Including the diffraction effects (full lines) the double differential cross section is modified slightly. There is some more cross section in the shadow region. However, if we artificially use in the statistical model only the temperature contribution to the diffusion, we see (left hand side) big differences between statistical (dashed lines) and statistical + quantal (full lines) cross sections.

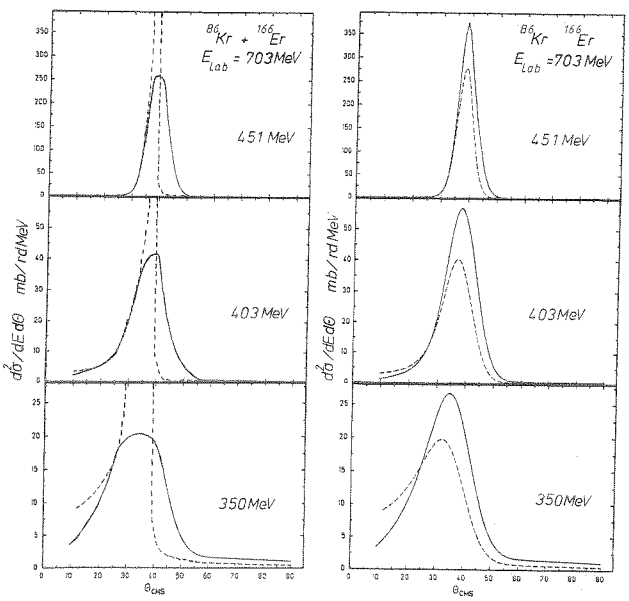


Fig. Double differential cross section for three energies
---- statistical model
——— statistical + quantal model
for temperature diffusion only (left) and full statistical model (right column)

1) W. Cassing, H. Friedrich; Z. Physik, A298 (1980) 129.
2) H. Feldmeier, H. Spangenberger; GSI-Report 1982.
3) H. Feldmeier, International School of Physics "Enrico Fermi", Varenna 1982.

On the mechanism of diffusion in Heavy Ion Collisions [G]

H. Feldmeier
Max-Planck-Institut für Kernphysik, Heidelberg

H. Spangenberger
Institut für Kernphysik, Technische Hochschule Darmstadt

We calculate drift and diffusion coefficients assuming statistical particle transfer between two Fermi gases. We suppose thermal equilibrium in each nucleus separately rather than global thermalization. The temperature parameter $\tau = \sqrt{4E^*/Am}$ is related to the heat produced during the collision. It may be different for the two nuclei if their masses are very different. The second important quantity is the displacement $|\vec{u}_r|$ in velocity space of the two Fermi distributions (cf. fig. 1) given by the relative velocity. It provides a measure how far apart the system is from total equilibrium. Due to the Pauli principle transitions of particles from one nucleus to the other only contribute in the dotted area of velocity-space shown in fig. 1. This in turn is proportional to $|\vec{u}_r|$ if $\tau = 0$ and proportional to τ if $|\vec{u}_r| = 0$, which makes plausible the result of an elaborate calculation which results in a splitting of the momentum diffusion tensor D into a velocity plus a temperature part

$$D = |\vec{u}_r|\, D^u(\alpha) + \tau\, D^\tau\,(\alpha, \tau/|\vec{u}_r|) \qquad (1)$$

D^u and D^τ depend on the angle α between $\vec{u}_r$ and the window-normal $\vec{\sigma}_w$ (fig. 1). The part proportional to $|\vec{u}_r|$ dominates peripheral collisions, whereas the temperature part becomes important for completely relaxed cases ($|\vec{u}_r| \to 0$). Only in this limit we arrive at the Einstein relation between drift and diffusion.

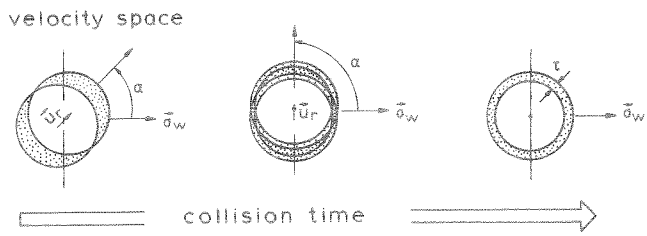


Fig. 1

Within this model we compute double differential cross sections $d^2\sigma/dEd\theta$ via a solution of the moment expansion of the Fokker-Planck equation. The calculation with the diffusion tensor as given in eq. (1) reproduces the large spreading in the scattering angle for moderate energy losses rather well. In the lower part of fig. 2 we artifically set $D^u = 0$ to demonstrate the significance of the nonequilibrium part $|\vec{u}_r| D^u$ in the momentum diffusion. Here we get the type of Wilczynski diagram one is used to for thermal fluctuations.

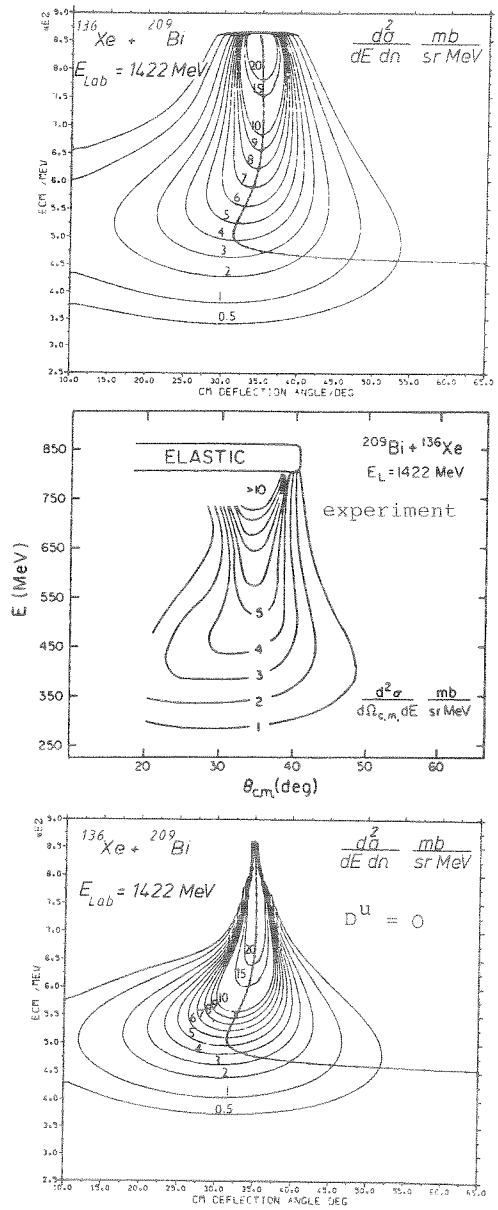


Fig. 2

Dissipative Equations of Motion for the One-Body Density [G]

P. Buck, H. Feldmeier* and F. Beck
Institut für Kernphysik, Technische Hochschule Darmstadt

In former studies we discussed how statistical concepts like equilibration and increase in entropy can be defined even for the time evolution of a pure state describing a closed Fermion system.[1] The salient point is to regard only part of the information contained in the exact many-body wave-function $|\Psi\rangle$. This selected information may be given by a set of operators B_k and their expectation values $\langle B_k \rangle = \langle\Psi|B_k|\Psi\rangle$. Referring only to this information, the best description of the system is to construct a statistical operator R which reproduces the $\langle B_k \rangle$ and maximizes the information-entropy $S = -\mathrm{Tr}(R \ln R)$. R then has the form $R = \exp\{-\sum_k \lambda_k B_k\}$, where the Lagrange multipliers λ_k are to be chosen such that $\mathrm{Tr}(B_k R) = \langle B_k \rangle$ is fulfilled.

Our previous investigations demonstrated the usefulness of the principal of maximum entropy in projecting out unimportant information contained in the exact wavefunction.[1] The one-particle density $\rho^{(1)}_{\alpha\beta}(t) = \langle\Psi(t)|a^+_\beta a_\alpha|\Psi(t)\rangle$ served as the only information to construct R(t). Following Robertson[2] we derive a closed set of dynamical equations for $\rho^{(1)}_{\alpha\beta}(t)$. We define an idempotent time-dependent superoperator P(t) which projects the exact statistical operator $\rho(t) = |\Psi(t)\rangle\langle\Psi(t)|$ onto R(t) which is the maximum entropy statistical operator under the constraints of a given one-body density:

$$\mathcal{P}(t)\,\rho(t) = R(t) \quad \text{and} \quad \mathcal{P}(t)\frac{d}{dt}\rho(t) = \frac{d}{dt}R(t)$$

P(t) is completely determined by $\rho^{(1)}_{\alpha\beta}(t)$ and can be written as

$$\mathcal{P}(t)X := \sum_{\alpha\beta} \frac{\partial R(t)}{\partial \rho^{(1)}_{\alpha\beta}(t)} \cdot \mathrm{Tr}\left(a^+_\beta a_\alpha X\right)$$

Herewith $\rho^{(1)}_{kl}$ fulfills the following exact equation (Robertson equation[2]):

$$\frac{d}{dt}\rho^{(1)}_{kl}(t) = \frac{i}{\hbar}\mathrm{Tr}\left([H, a^+_l a_k]R(t)\right) + \sum_{\alpha\beta}\int_0^t dt'\, K(t,t')_{(k,\alpha\beta}\cdot\lambda_{\alpha\beta)}(t')$$

If h(t) generates the unitary transformation which keeps $\rho^{(1)}$ diagonal, the creation operators $c^+_k(t)$ of the time-dependent basis are defined by

$$i\hbar\frac{d}{dt}c^+_k(t) = \left[h(t), c^+_k(t)\right], \qquad c^+_k(0) = a^+_k$$

The Robertson equation then reads

$$\frac{d}{dt}\rho^{(1)}_{ll}(t) = \frac{i}{\hbar}\mathrm{Tr}\left([H-h(t), c^+_l(t)c_l(t)]R(t)\right) + \sum_{\alpha\alpha}\int_0^t dt'\, K(t,t')_{(l,\alpha\alpha}\cdot\lambda_{\alpha\alpha)}(t')$$

If the principle of maximum entropy is reliable, h(t) should be calculated with the use of R(t) instead of the unknown $\rho(t)$. This yields

$$h(t) = \Pi(t)H,$$

where $\Pi(t)$ is defined by

$$\mathrm{Tr}(XP(t)Y) = \mathrm{Tr}((\Pi(t)X)Y).$$

Writing $H = \Pi(t)H + (1-\Pi(t))H = h(t) + V_r(t)$ and going over to the interaction picture with

$$X' := U_0^{-1}(t,t')\,X\,U_0(t,t'), \qquad i\hbar\frac{\partial}{\partial t'}U_0(t,t') = h(t')U_0(t,t')$$

we get in the weak coupling limit

$$K_{kl,\alpha\alpha}(t,t') =$$

$$-\frac{1}{\hbar^2}\mathrm{Tr}\left\{[V_r(t), c^+_k(t)c_l(t)]\,\overline{(1-\Pi(t))[V'_r(t'), c^+_\alpha(t)c_\alpha(t)]}\,R(t)\right\}$$

Therewith the Robertson equation can be cast into tractable equations for $\rho^{(1)}_{\alpha\beta}(t)$. We would like to emphasize that the statistical assumptions do not depend on a special choice of the single particle basis. Our picture assumes the essential information about the system to be of one-body nature. All other degrees of freedom only serve as a "heat bath". A Hamiltonian H for which $V_r(t) = (1-\Pi(t))H$ is of random nature should provide these properties. Studies on the validity of the dissipative equations for different types of Hamiltonians are under work.

* Max-Planck-Institut für Kernphysik, Heidelberg

1) P. Buck, H. Feldmeier; Lecture Notes in Phys., 171 (1982) 111 and 171 (1982) 384.

2) B. Robertson, in: The Maximum Entropy Formalism; R.D. Levine and M. Tribus, eds. (MIT-Press) 1978.

Unified Description of Statistical Excitations, Deformations and Charge Transfer in a Dynamical Theory of DIC

P.Fröbrich, HMI Berlin West,Germany
B.Strack, GSI Darmstadt,Germany
M.Durand, ISN Grenoble,France

A multi-dimensional Fokker-Planck equation including relative motion, shape deformation and charge transfer was derived[1] by generalizing the Brownian motion theory of ref.2. The equation is given by

$$\left\{\partial_t + \frac{P}{\mu}\partial_R + \frac{\ell}{\mu R^2}\partial_\ell + \partial_R V \partial_P + \sum_i \frac{\pi_i}{D_i}\partial_{\alpha_i} + \sum_i \partial_{\alpha_i} V \partial_{\pi_i}\right\} f =$$

$$= \begin{bmatrix} \partial_P\left[\frac{P}{\mu} + T\partial_P\right] K_{RR} + \sum_i \partial_P\left[\frac{\pi_i}{D_i} + T\partial_{\pi_i}\right] K_{R\alpha_i} + \\ \partial_\ell\left[\frac{\ell - \ell_s}{\mu} + TR^2\partial_\ell\right] K_{\ell\ell} + \\ \sum_i \partial_{\pi_i}\left[\frac{P}{\mu} + T\partial_P\right] K_{\alpha_i R} + \sum_{ij} \partial_{\pi_i}\left[\frac{\pi_j}{D_{ij}} + T\partial_{\pi_j}\right] K_{\alpha_i\alpha_j} + \\ \partial_Z\left[-\partial_Z U(Z) + T\partial_Z\right] K_{ZZ} \end{bmatrix} f$$

The distribution function f depends on the radial distance R, the radial momentum P, angular momentum ℓ and its conjugate variable ℓ_s, amplitudes α_i and momenta π_i of the vibrators (only quadrupole states with nose-to-nose geometry are taken into account in the applications) and the projectile charge Z. The potential consists of a Coulomb term, a centrifugal term, liquid drop potentials for the vibrators and a nuclear part which is obtained from the Gross and Kalinowski[3] potential by including curvature corrections due to deformations. By assuming that friction occurs at the surface[4] the non-diagonal friction coefficients are defined in terms of the radial friction K_{RR}, whose stregth is reduced by 1o% as compared to ref. 3. The intrinsic damping to the vibrators was determined to be $K_{\alpha_i\alpha_j} = 2o\sqrt{C_i D_i}$ (MeVsec)(C_i,D_i are liquid drop stiffness and mass parameters) for all systems.The coefficients $K_{ZZ} = D_{ZZ}/T$ for the charge transfer are those of ref. 5.

The dynamical equation is solved within the quasilinear approximation (moment expansion up to second order).For systems which do not run into fusion and do not show negative angle scattering (as e.g. Xe+Bi) all variances are sufficiently small during the collision process and themoment expansion does not loose its validity as in ref. 6.

Calculations for avariety of systems[7] have been performed. The universal parametrisation discussed above reproduces at least the rough features of Coulomb-like, focusing and orbiting systems as well as fusion excitation functions throughout the periodic table[8].

Because of lack of space we give here only as a representative example the calculated $d^2\sigma/dEdz$ cross sections for $^{136}Xe + ^{2o9}Bi$ at E_L=94o,113o,1422 MeV in comparison with the experimental data[9].

[1] Durand,Fröbrich , Fizika 13(1981)74
[2] D.H.E. Gross , Z.Physik A291(1979)145
[3] Gross,Kalinowski ,Phys.Rep. 45(1978)175
[4] D.H.E. Gross et al, Z.Phys. A299(1981)63
[5] S.Ayik et al , Z.Phys. A286(1978)271
[6] Yadav,Nörenberg , Pyhs.Let. B115(1982)179
Brosa,Cassing ,Z.Phys. A3o7(1982)167
[7] H.Siekmann et al , Z.Phys.A3o7(1982)113
Fröbrich,Strack,Durand; HMI-Bericht (1981)16;
Proc.Int.Conf.on Nucl. Coll., Michigan,1982,p.43 and to be publ.
[8] P.Fröbrich (accepted for publication in Phys.Let.)
[9] H.J.Wollersheim et al, Phys.Rev. C24(1981)2114

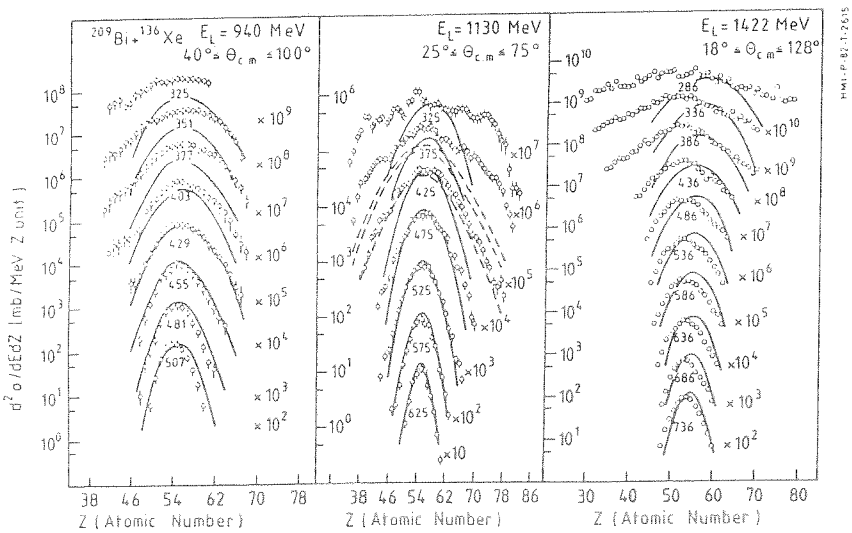


Fig. left: Double differential cross section $d^2\sigma/dEdZ$ at three different final energies. For the 113o MeV case of the $^{136}Xe + ^{2o9}Bi$ reaction the results for endenergies of 325,375,425MeV are indicated by dashed lines.

Nuclear transport due to the stochastical exchange of nucleons[B]

D. Bangert, B. Kohlmeyer, M. Marinescu, F. Pühlhofer, Fachbereich Physik, Universität Marburg

F. Busch, D. Schüll, GSI Darmstadt

H. Freiesleben, Institut für Experimentalphysik, Ruhr-Universität Bochum

Recently, a systematic study of dissipative heavy-ion reactions was carried out using the magnetic spectrometer at GSI [1]. For a number of systems drift and variances of the nuclide distributions were determined as a function of the dissipated energy with high resolution in mass, charge and energy. Due to the particular choice of the entrance channel, mass and N/Z-equilibration could be observed independently. The data cover the range from quasielastic to deep inelastic reactions where models based on the interaction of two undeformed reaction partners should be approximately valid. These experimental results therefore lend themselves to a detailed test of theories for dissipative heavy-ion collisions, and they have indeed been used for this purpose by other authors also [2,3].

One result, which one can read off directly from the data, is the dominant role of the PES of the dinuclear complex on the evolution of the system. This suggests that a stochastical exchange of nucleons is the underlying mechanism for both the N/Z and the mass asymmetry relaxation. Since each transferred nucleon dissipates kinetic energy from the relative motion of the reaction partners, there is a coupling between mass exchange and energy loss. However, other non-exchange modes like collective excitations might contribute to the energy dissipation also.

Starting from these ideas we have formulated a quantitative model. The four modes of single-nucleon transfer form the basis for a random-walk calculation for the evolution of the dinuclear system during contact. An additional non-exchange energy loss mode with adjustable strength was added. The relative transition probabilities were taken to be proportional to the level density of the dinuclear system. Two limiting cases were tested. In a strong-coupling limit the total level density is the relevant quantity, whereas for a pertubative treatment the single-particle level density should be inserted.

The comparison of model calculations with the experimental results for the reactions $^{129,132}Xe+^{56}Fe$, $^{116,124}Sn$ at 5.9 MeV/u shows that the data can consistently be described using the total level density as determining the available phase space for the evolution and assuming only a minor contribution ($\leq 20\%$) of energy loss without particle exchange. Figs. 1 and 2 give one example for the excellent agreement between calculation and experiment.

If, on the other hand, the single-particle transition probability is used in the model, an approximate fit to the data can only be obtained assuming that at least 2/3 of the energy dissipation are due to non-exchange excitations. Even then the model fails to describe the drift in the N-Z plane for systems like $^{136}Xe + ^{56}Fe$. This is mainly due to the fact that the dependence of the transition probability on the PES is far less strong in this case.

We conclude that nucleon exchange is the dominant mechanism for energy damping for the dissipative heavy-ion reactions studied here.

1.) D. Schüll et al., Phys. Lett. 102 B (1981) 116
2.) D. Gross and K. Hartmann, Phys. Rev.C 24 (1981)2526
3.) J. Tõke and A. Gobbi, Scientific Report 1981, GSI 82-1, p. 91

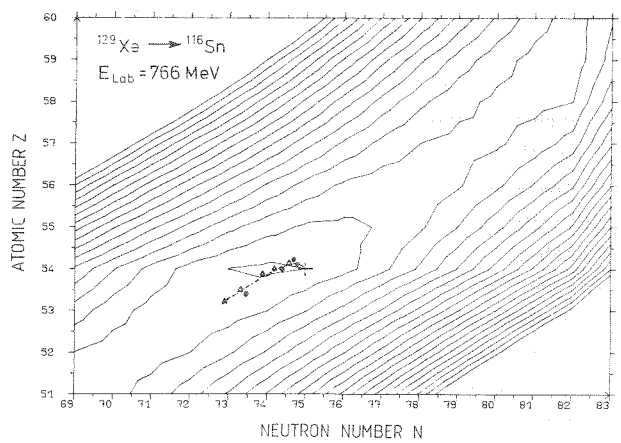


Fig. 1: Experimental (●) and calculated (▲) drift path as a function of excitation energy in steps of 20 MeV together with a contour plot of the PES (1 MeV per line). The injection point is indicated by an arrow.

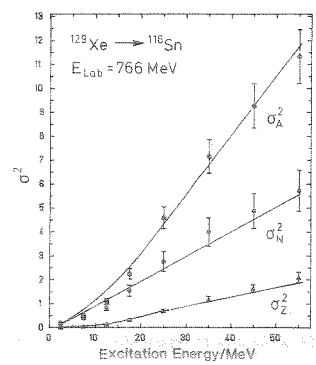


Fig. 2: Experimental and calculated variances as a function of excitation energy.

Shell-Structure Affected Stochastic Walk on the (N-Z) Plane

J.Tõke*, A.Gobbi, GSI Darmstadt and T.Matulewicz, Warsaw University, Poland

It has been shown in the past that the evolution of a dinuclear system during a dissipative collision can be to a large extent understood in terms of discrete random-walk calculations on the (N-Z) plane [1-3]. Such calculations reproduce routinely the σ_A^2 vs. TKEL correlations when proper kinetic energy loss rate is assumed. The quantities which are sensitive to the details of the model (specifically to the response of the branching ratios to the structure of the potential energy surface) are σ_Z^2 values at constant A and σ_A^2 values at constant Z.

In the approach we adopted in ref.3, at each point on the (N-Z) plane the branching ratios corresponding to the five possible steps (including the no-move inelastic exitation) are determined by the relative displacements of Fermi levels, single particle level densities and their occupancy probabilities and certain momentum conservation considerations. Recently we undertook an attempt to account in such calculations additionally for the shell effects since it has been shown in ref.4 that such effects are important. In the evaluation of the branching ratios and energy loss rates we follow essentially the formulation of ref.4 except for the treatment of the single particle level schemes. Those schemes we generate accordingly to the Myers and Swiatecki level bunching recipe [5] for all the nuclei involved (separately for protons and neutrons). They reproduce essentially the results of ref.4 (obtained with discrete Nilsson level diagrams) when fed into the code of ref.4.

One effect of the level bunching is that the kinetic energy loss rate is modified by a structure-related term (ref.4.) which for closed shell nuclei leads to some narrowing of the mass (charge) distributions. There is, however, also another effect which could not be accounted for in the simple "one-dimensional" approach of ref.4. Namely, now the Fermi level displacements and thus the acting driving force acquire in a natural way a temperature dependent contribution due to the level bunching (shell effects). This results in additional correlations acting considerably also along the bottom of the valley in PES and thus breaking the otherwise valid approximation $\sigma_A^2 = N_{exch}$.

1. J.J.Griffin et al., Nucl.Phys.A369(1981)181 and Nucl.Phys.A382(1982)159.
2. D.Schüll et al., Phys.Lett.102B(1981)116.
3. J.Tõke and A.Gobbi, GSI Scientific Rep.(1981)91.
4. M.Dakowski, A.Gobbi, W.Nörenberg, Nucl.Phys.A378(1982)189.
5. W.D.Myers and W.Swiatecki, Nucl.Phys.81(1966)1.

* On leave from Warsaw University, Poland.

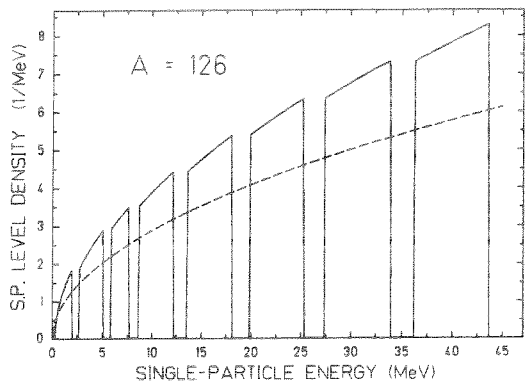


Fig. 1: An example of the bunched single-particle level density for the system of 126 nucleons. Dashed line represents the standard Fermi-gas model result.

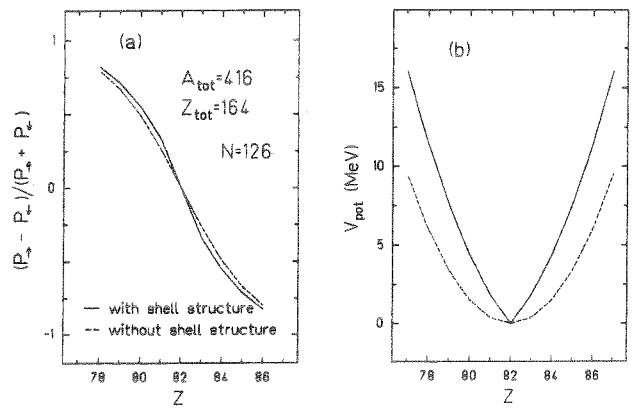


Fig. 2: (a) - Response of the branching asymmetry (for rightwards and leftwards moves along the PES profile shown in (b)) to the structure of the PES. Notice the relatively weak response to the shell-effect caused alteration of the profile.

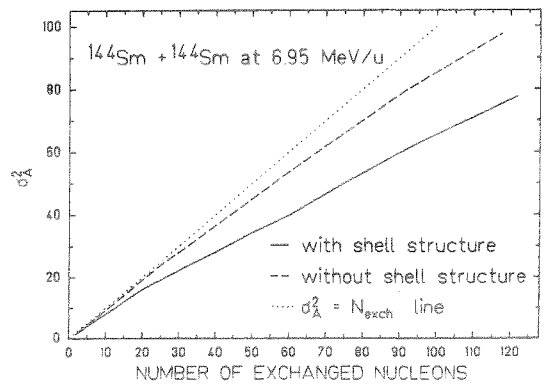


Fig. 3: Random-walk model prediction for the dependence of the mass variance on the number of exchanged nucleons for the ^{144}Sm+^{144}Sm collision.

Microscopic Nuclear Dissipation in the Long Mean Free Path Limit

C. Yannouleas
GSI, Darmstadt

A microscopic, nonperturbative, time reversible model, which exhibits a dissipative decay of collective motion for times short compared to the system's Poincare time, has been formulated[1-3]. The model assumes an RPA approximate description of the initial collective state within a restricted subspace, then traces its time evolution when an additional subspace is coupled to the restricted subspace. It invokes no statistical assumptions. The damping of the collective motion occurs via real transitions from the collective state to other more complicated nuclear states of the same energy. It corresponds therefore to the so-called "one-body" long mean free path limit of nuclear dissipation when the collective state describes a surface vibration.

When the simplest RPA is used, this process associates the dissipation with the escape width for direct particle emission to the continuum. When the more detailed Second RPA is used, it associates the dissipation with the spreading width for transitions to the 2p-2h components of the nuclear compound states as well. The energy loss rate for sharp n-phonon initial states is proportional to the total collective energy, unlike the dissipation of a classical damped oscillator, where it is proportional to the kinetic energy only. However, for coherent multiphonon packets, which explicitly describe the time-dependent oscillations of the mean field, dissipation proportional only to the kinetic energy is obtained.

Canonical coordinates for the collective degree of freedom are explicitly introduced and a nonlinear frictional Hamiltonian to describe such systems is specified.

Within this description, a specific set of assumptions is shown to reduce the RPA result precisely to that given by the Wall Formula[4].

Currently, this model is expanded so that

1. it describes dissipation in the case of large amplitude collective motion. To this purpose the coupled cluster approximation[5] is used.
2. it applies to the dinuclear system.
3. it incorporates superfluidic effects. To this purpose the Hartree-Fock-Bogoliubov theory is used.
4. it incorporates dissipative effects analogous to those of Navier-Stokes hydrodynamics. To this purpose the renormalized RPA[6] is utilized.

References:

1) C. Yannouleas, Ph. D. Thesis (1982) U. of Md., College Park
2) C. Yannouleas et al., Nucl. Phys. A379 (1982) 256
3) C. Yannouleas et al., Nucl. Phys. A397 (1983) 239
4) J. Blocki et al., Ann. of Phys. 113 (1978) 330
5) P. Hoodbhoy and J.W. Negele, Phys. Rev. C18 (1978) 2380
6) D.J. Rowe, Rev. Mod. Phys. 40 (1968) 153

The two-body collision term in dissipative diabatic dynamics[1]

S.J. Wang* and W. Nörenberg
GSI, Darmstadt

A general transport theory based on the diabatic single-particle motion has been formulated recently[2]. In the derivation of transport equations time averaging has been introduced as a natural procedure to apply on the macroscopic or collective motion which by definition should be the slow modes of the system. In connection with the time dependence of the diabatic single-particle levels the time average introduces irreversibility in the equations of macroscopic motions and justifies the use of the weak-coupling and the Markov approximation in the basic collision terms. These collision terms conserve not only the total occupation probability (i.e. conservation of total mass and charge) but also the total energy (i.e. sum of single - particle energies). This time-dependent shell-model theory with residual interactions can be regarded as a simplified version of extended TDHF theories. However, apart from two-body collisions, we also describe some couplings of the one-body type by irreversible collision terms. At the cost of selfconsistency and with the constraint to a few collective degrees of freedom, the formulation looks more transparent and can easily supply transport coefficients which may be used in transport equations. Thus this shell-model approach to the transport theory of large amplitude collective motion of nuclei seems to be promising for future applications.

In ref.[2] the two-body collision term was obtained diagrammatically in analogy to the one-body expression (cf. Fig. 1). In order to complete the general formulation of dissipative diabatic dynamics, we have now added the analytical derivation of the two-body collision term: We start from the diabatic basis states

$$|\alpha(q,t)> = |\alpha(q)> \exp[-i\int^{t} \varepsilon_\alpha(t')\,dt'] \quad (1)$$

where q and $\varepsilon_\alpha(t)$ denote the collective variable and the time-dependent single-particle energies. Neglecting three-body correlations we obtain up to second order in the residual interaction v for the one-body matrix

$$\dot{\rho}_{\alpha\beta}(t) = \sum_{\gamma\delta} L_{\alpha\beta,\gamma\delta}(t)\ \rho_{\gamma\delta}(t) - \frac{i}{2}\sum_{\lambda\mu\nu}[v_{\lambda\mu\beta\nu}(t)\ c_{\alpha\nu\mu\lambda}(t) - v_{\alpha\nu\mu\lambda}(t)\ c_{\lambda\mu\beta\nu}(t)] \quad (2)$$

where the two-body correlations are given by

$$c_{\alpha\beta\gamma\delta} = i\int_{t'}^{t} dt' \sum_{\lambda\mu\nu\sigma} v_{\lambda\mu\nu\sigma}(t')\,[(1-\rho)_{\alpha\lambda}(1-\rho)_{\beta\mu}\,\rho_{\sigma\gamma}\rho_{\nu\delta} - \text{exch.}]_{t'} \quad (3)$$

and L denotes the Liouville operator of the one-body coupling. Eliminating from (2) the non-diagonal elements of the one-body density matrix and averaging the diagonal part $\rho_{\alpha\alpha} = n_\alpha(t)$ (occupation probabilities of diabatic states) over a time interval θ we find

$$\frac{\partial n_\alpha}{\partial t} = \sum_\beta W_{\alpha\beta}(n_\beta - n_\alpha) + \sum_{\beta\gamma\delta} W_{\alpha\beta\gamma\delta}[(1-n_\alpha)(1-n_\gamma)\,n_\beta n_\delta - \text{exch.}] \quad (4)$$

with $W_{\alpha\beta}$ as derived in ref.[2]. The two-body transition probability is given by

$$W_{\alpha\beta\gamma\delta} = 2Re\int_0^\infty d\tau\ [\overline{V_{\alpha\gamma\beta\delta}(t)\ V_{\beta\delta\alpha\gamma}(t-\tau)} - \text{exch}]\ \exp[-i\omega_{\delta\gamma\beta\alpha}\tau - \Gamma_{\delta\gamma\beta\alpha}\tau] \quad (5)$$

with $\omega_{\delta\gamma\beta\alpha} = \varepsilon_\beta + \varepsilon_\delta - \varepsilon_\alpha - \varepsilon_\gamma$ and $\Gamma_{\delta\gamma\beta\alpha} = |\dot{\omega}_{\delta\gamma\beta\alpha}|\,\theta$. The matrix elements V in (5) are smooth functions of the time since the phase factors have been treated explicitly in the time average giving rise to the decay factor. The correlation time Γ^{-1} becomes small because of the strong time dependence of the diabatic levels. This justifies the weak-coupling limit (only second order in v) and the Markov approximation in (4).

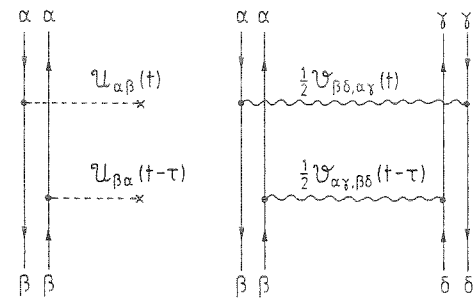


Fig. 1.: Graphs of the one- and two-body collision terms. The pair of lines denote a diabatic state (↑) and a conjugate diabatic state (↓). The time average allows significant contributions only from τ-values not much larger than the correlation time of the matrix elements.

*On leave from the University of Lanzhou, China

References:

1) S.J.Wang, W. Nörenberg, in preparation

2) S. Ayik, W. Nörenberg, Z. Phys. A 309, 121 (1982)

3) W. Nörenberg, Nucl. Phys.A (in press)

On the Role of Memory Effects for Diffusion in Slow Collective Nuclear Motion

W. Cassing, W. Nörenberg
GSI Darmstadt

Diabatic single-particle motion in heavy-ion collisions, nuclear vibration or fission leads to memory effects in the equation of motion [1] for the mean collective variable κ. In this approach it is assumed that the stochastic properties of the process are determined by residual two-body collisions which induce stochastic transitions between Slater determinants. For a more complete description of the process we also need the evolution of the spreading in the collective degree of freedom.

According to the above assumptions the system is described at any time by a statistical mixture (ensemble) of Slater determinants $\Phi_i(t)$ which stochastically change the single-particle states $\phi_\alpha^i(t)$. In other words, the single-particle occupation numbers $n_\alpha^i(t)$ of an ensemble member i change between 0 and 1. This induces a stochastic variation of the forces

$$F_i(\kappa,t) = -\sum_\alpha \frac{\partial \eta_\alpha}{\partial \kappa}\, n_\alpha^{(i)}(t) \quad , \qquad (1)$$

which essentially are nothing but the mean slopes of the diabatic s.p. levels η_α [1]. We introduce the stochastic variable $F_s(\kappa,t)$ which satisfies the Langevin-type equation

$$\frac{\partial F_s}{\partial t}(\kappa,t) = -\tau_{loc}^{-1}\,[F_s(\kappa,t)-\bar{F}(\kappa,T)] + G(\kappa,t) \quad . \qquad (2)$$

Here $\bar{F}(\kappa,T)$ denotes the force in local equilibrium [1] (T: nuclear temperature); τ_{loc} corresponds to the local equilibration time and $G(\kappa,t)$ is an irregular function in time with zero mean and a white spectrum (δ-functions in time) in analogy to the irregular force in Brownian motion theory [2]. Employing Newtons equation and restricting to small fluctuations in the variable κ we obtain the time evolution for the fluctuations in the collective velocity $\dot{\kappa}$, i.e. $\sigma_{\dot\kappa}^2 = \langle\dot\kappa^2\rangle - \langle\dot\kappa\rangle^2$,

$$\frac{d^2}{dt^2}\,\sigma_{\dot\kappa}^2 = 2B^{-2}\sigma_F^2 + 2B^{-1}\langle\frac{\partial F}{\partial\kappa}\rangle\sigma_{\dot\kappa}^2 - \tau_{loc}^{-1}\frac{d}{dt}\,\sigma_{\dot\kappa}^2 \quad , \qquad (3)$$

In eq.(3) the quantity B denotes the collective mass-parameter in the diabatic cranking approximation. As the source for fluctuations in $\dot\kappa$ the variance σ_F^2 in the force enters which can be calculated directly from the ensemble average << >>:

$$\sigma_F^2 = \langle\langle F_i^2\rangle\rangle - \langle\langle F_i\rangle\rangle^2 = \sum_{\alpha,\beta}\frac{\partial\eta_\alpha}{\partial\kappa}\frac{\partial\eta_\beta}{\partial\kappa}\{\langle\langle n_\alpha^{(i)} n_\beta^{(i)}\rangle\rangle - n_\alpha n_\beta\} \qquad (4)$$

$$\approx \sum_\alpha \left(\frac{\partial\eta_\alpha}{\partial\kappa}\right)^2 n_\alpha(1-n_\alpha) \, .$$

Thus the variance of the force is directly related to the variance of the occupation probabilities.

We have solved eq.(3) for nuclear quadrupole motion in a 3-dim. deformed harmonic osicllator basis [1] (full line in fig. 1) and compared the result for $\sigma_{\dot\kappa}(t)$ with the corresponding quantitiy derived from a Fokker-Planck equation where drift and diffusion are related via the Einstein relation [1] (dashed line in fig. 1).

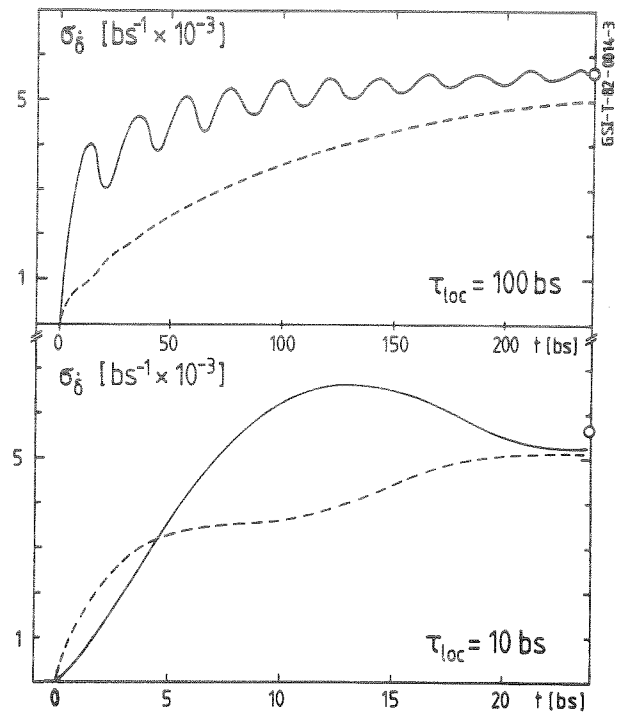


fig. 1

While for $t \to \infty$ the solutions for $\sigma_{\dot\delta}$ ($\kappa \equiv \delta$; $\sigma_{\dot\delta}(\infty)$: open circle in fig. 1) in both cases are the same according to the equipartition theorem the time evolutions for $t < \tau_{loc}$ are significantly different and sensitively depend on the value of the local equilibration time τ_{loc}(1bs = 10^{-23} s). Thus for fixed asymptotic $\sigma_{\dot\delta}(\infty)$ the initial slope of $\sigma_{\dot\delta}(t)$ might yield some information about local equilibration times in large amplitude collective nuclear motion.

References

1) W. Cassing, W. Nörenberg: Preprint GSI-82-33, Nucl. Phys. A(in press)
2) R. Becker, Theorie der Wärme (Springer-Verlag, 1978) p.272

Study of Time Delay within the Fragmentation Theory [B G]

K. Depta, J. Hahn, R. Herrmann, L. Neise, M. Uhlig, K.H. Ziegenhain, J.A. Maruhn, and W. Greiner

Institut für Theoretische Physik der Universität Frankfurt

We treat the mass transfer in heavy-ion collisions within the framework of the fragmentation theory[1] by solving a time-dependent Schrödinger equation for the mass asymmetry degree of freedom $\eta = (A_1-A_2)/(A_1+A_2)$ along a classical trajectory R(t). For the potential energy we assume:

$$V(R,\eta,T) = V_{LDM}(R,\eta) + \delta U(R,\eta,T=0)\cdot e^{-\left(\frac{T}{T_0}\right)^2}$$

i.e. the nuclear shell structure is damped by temperature T which depends on the excitation energy and the energy loss $\tilde{E}$ via the relations

$$E^* = \left(\frac{A}{10\,MeV}\right) T^2 \quad \text{and} \quad E^*(t) = f\,\tilde{E}(t-\tau)\,.$$

The parameter f gives the part of the energy loss $\tilde{E}$, which after a delay time τ goes into heat. This simulates the storing of energy in collective excitations that will not destroy the shell structure. The influence of the delay time and the sharing parameter f on the charge distribution was studied for the system $^{86}Kr + {}^{166}Er$.

In Figs. 1 and 2 we show the results for the final charge distribution $d\sigma / dZ_1$, which is assumed to be the mass distribution times (Z/A). The case f=0 implies the conservation of the shell structure during the collision and therefore the initial wave packet is focused around the initial distribution, whereas for f=1 and τ=0 (Fig. 1) the shell effects are smoothed out from the beginning and the wave packet can spreed quickly. Increasing the delay time τ (Fig. 2) we restore the shell structure for a longer time and focus the final distribution. The effect of the delay time is the same for $\tau \to \infty$ as the case of a sharing parameter f=0.

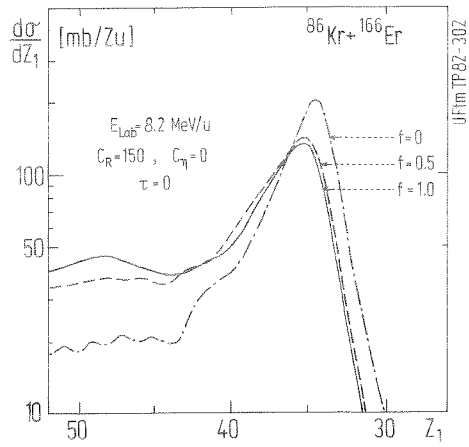


Fig. 1.

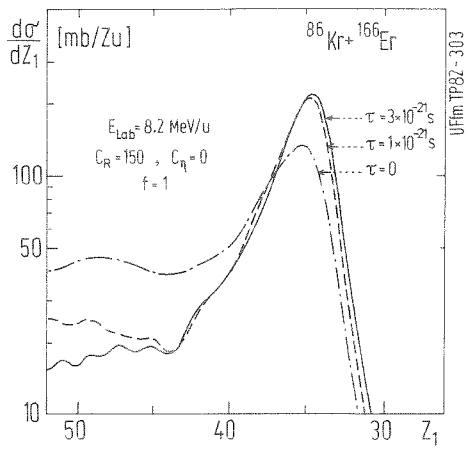


Fig. 2.

[1] J.A. Maruhn, W. Greiner, and W. Scheid, Heavy Ion Collisions, Vol.II, ed. R. Bock, North Holland Publ. Comp., Amsterdam 1980

Microscopic Calculations of Diabatic Potentials and Mass Parameters[1]

A. Lukasiak*, W. Cassing and W. Nörenberg
GSI, Darmstadt

A main element in dissipative diabatic dynamics (DDD)[2] is the diabatic single-particle motion which is considered as the dominant coherent aspect of large amplitude collective nuclear motion. Two methods for the construction of diabatic states have been considered[3]. (a) The method of maximum overlap reconstructs the diabatic level crossings from the quasi-crossings of adiabatic levels. (b) The method of maximum symmetry starts from basis states obtained from a Hamiltonian which separates in the three spatial coordinates. The diabatic states are then constructed by the expansion in terms of these basis states, the expansion coefficients defined by the expansion of the true single-particle states for the separated nuclei. This method preserves the nodal structure of diabatic states.

We have studied the diabatic potential ΔV_{diab} produced by the diabatic particle-hole excitations within a two-center shell-model. The single-particle potential of the system of two interacting nuclei is described by two oscillator potentials with a center- to-center distance Δz and a deformation (ω_z/ω_ρ). An inverted oscillator potential defines the neck between the nuclei. The corresponding family of shapes is illustrated in Fig. 1.

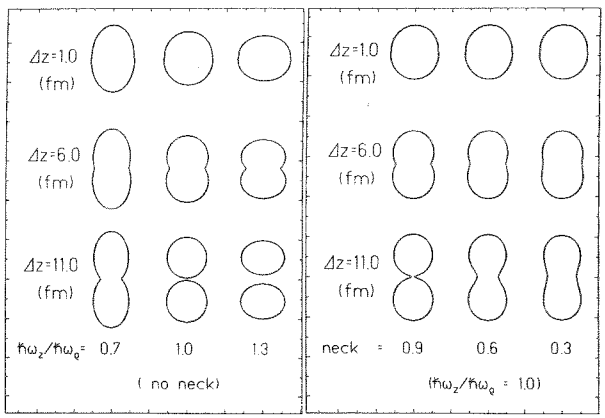


Fig. 1

The diabatic potential landscape for the symmetric system $^{92}Mo + ^{92}Mo$ is displayed in Fig. 2 as function of the distance R_{cm} between the mass centers and the deformation parameter ω_z/ω_ρ. In the region of overlap where the diabatic potential becomes important for the dynamical behaviour of the system, ΔV_{diab} depends essentially only on R_{cm} and only slightly on deformation.

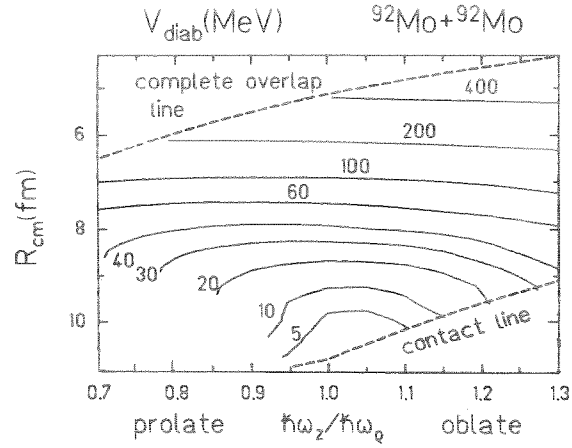


Fig. 2

We have also studied the mass tensor within the cranking approximation for the three collective variables R_{cm}, ω_z/ω_ρ and neck. Figure 3 shows the radial mass parameter as function of R_{cm}. This mass turns out to be less than 20% larger than its irrotational flow value and approaches the reduced mass within 10%. In contrast to the adiabatic mass parameters all diabatic mass parameters are smooth functions of the collective variables.

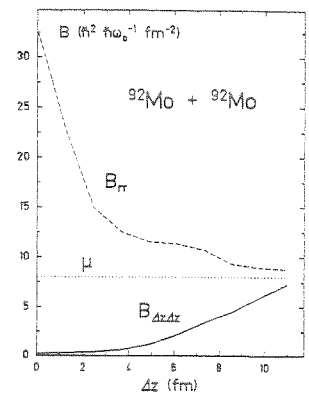


Fig. 3

*On leave from the Institute for Nuclear Research, Warsaw, Poland

References:

1) A. Lukasiak, W. Cassing and W. Nörenberg, in preparation

2) W. Nörenberg, Dissipative Diabatic Dynamics, GSI-Preprint- 82-36 , Nucl. Phys. A (in press)

3) A. Lukasiak, W. Cassing and W. Nörenberg, GSI Scientific Report 1981 p. 94

On Diabatic Shell-Structure Effects in Heavy-Ion Collisions

A. Lukasiak* and W. Nörenberg
GSI, Darmstadt

The properties of the diabatic potential depend both on the single- particle occupation probabilities and on the two-center properties of occupied diabatic states. One can distinguish repulsive and attractive states according to the number of nodes n_z along the collision axis z and the number of nodes n_ρ along the perpendicular axis ρ. In a heavy-ion collision the occupation of the diabatic states is determined by the ground-state configuration of the approaching nuclei. Thus the corresponding numbers of repulsive and attractive states exhibit shell effects.

In our study of these diabatic shell effects we use a simplified diabatic two-center shell model where only the z-components $l_z s_z$ and l_z^2 of the spin-orbit coupling and the l^2-term are retained.

Fig. 1 shows the neutron part of the diabatic potential versus the center-to-center distance for three different values of the neutron number. The shell effect is exhibited by the fact, that the curve for N=72 lies between the curves for N=40 and N=56. The neutron numbers in Fig. 1 (N=40) and (N=72) correspond to the two minima of the number of nodes n_z (see Fig. 2(a)). The third number N=56 in Fig. 1 corresponds to the middle of the bump of repulsive states. From Fig. 2(b) one sees that the fluctuations of the central value of the diabatic potential are of the order of 100 MeV over a distance of 10 units in the number of neutrons. Also the curvature (stiffness) of the diabatic potential shows shell effects. Fig. 2(c) displays the stiffness coefficient during the initial stage of the collision. A result of these shell effects in the stiffness is that the distance of closest approach shows variations of the order of ± 1 fm for fixed initial kinetic energy.

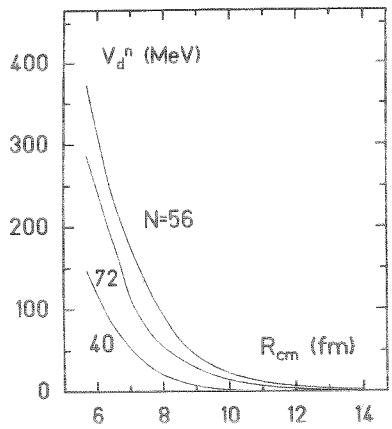


Fig. 1: The neutron part of the diabatic potential for a symmetric colliding system versus the distance R_{cm} between the mass centers.

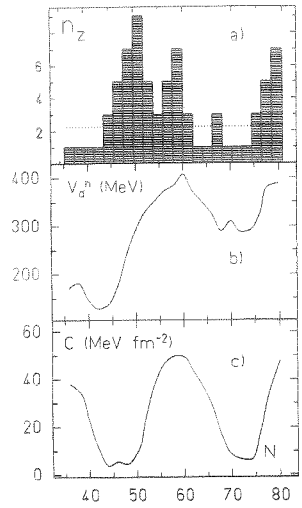


Fig. 2(a): The number of nodes n_z in z direction for the highest occupied state versus the number of neutrons N (N/2 is the number of states). States with $n_z > 2.25$ (<2.25) are repulsive (attractive); (b) The neutron part of the diabatic potential versus the number of neutrons N when the composite system is spherical (cf. Fig. 1); (c) The stiffness of the diabatic potential versus the neutron number N.

Fig. 3 illustrates the importance of the spin-orbit coupling. While the gross qualitative features are comparable with and without spin-orbit coupling, minima and maxima of the corresponding diabatic potentials are shifted considerably relative to each other. These shell effects are expected to have observable effects on the pre-equilibrium emission of neutrons. Effects of the diabatic shell structure may also be relevant in fusion reactions (shell effects in "extra-push").

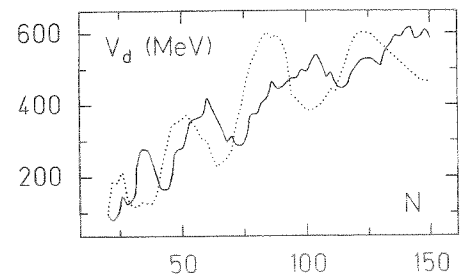


Fig. 3: Solid line displays the same as Fig. 2(b) however over a larger range of neutron numbers for symmetric systems selected along the beta stability line. The dotted and solid curves correspond to the diabatic potentials with and without spin-orbit coupling, respectively.

References

1) J.B. Delos, Rev. Mod. Phys. 53 (1981)287
2) W. Nörenberg, Nucl. Phys. A (in press)

*On leave from the Institute for Nuclear Research, Warsaw, Poland

Diabatic Aspets of TDHF

W. Cassing, A.K. Dhar+, A. Lukasiak, W. Nörenberg
GSI Darmstadt
+Daresbury Laboratory

Within the concept of dissipative diabatic dynamics (DDD)[1,2] the initial phase of a heavy-ion collision is assumed to proceed via coherent particle-hole excitations which yield a conservative potential with respect to the relative motion. The underlying idea of this approach is that for sufficiently fast collective nuclear motion the intrinsic single-particle motion follows the changes of the mean-field except close to quasi-crossings of the adiabatic levels where the nucleon likes to jump to the higher unoccupied level (Landau-Zener transition probability ≈ 1). This type of diabatic s.p. motion is time-reversible as long as residual two-body collisions can be neglected and in case of heavy-ion collisions several MeV/u above the Coulomb barrier should be valid for times up to $1.5 \cdot 10^{-22}$s from nuclear contact[2]. In order to check the idea of diabatic s.p. motion for the short times considered we performed TDHF calculations[3] for head on collisons of ^{86}Kr on ^{166}Er at three bombarding energies of 8.2, 15 and 20 MeV/u. Calculating as a function time the relative distance R(t), velocity $\dot{R}(t)$, time dependent s.p. energies $\varepsilon_\nu(t) = \langle \Psi_\nu(t) | i\hbar \frac{\delta}{\delta t} | \Psi_\nu(t) \rangle$ (mass asymmetry fixed) and transforming into the moving frames of each nucleus we obtain approximately quasi- stationary levels

$$\bar{\varepsilon}_\nu(R(t),\dot{R}(t)) := \varepsilon_\nu(R(t)) - \frac{m}{2}\left(\frac{A_{1/2}}{A_1+A_2}\right)^2 \dot{R}(R(t))^2 . \quad (1)$$

The quantities (1) for fixed level ν agree within an accuracy of 5% for various TDHF calculations at 8.2, 15 and 20 MeV/u and show that the assumption of quasi-static s.p. levels seems to be valid approximately in the energy region of interest. This can in addition be seen from a comparison of the corresponding 'TDHF potentials'

$$V_{TDHF}(R) := E_{cm} - \frac{\mu}{2}\dot{R}(R)^2 \quad (2)$$

$$\approx \frac{2}{3}\sum_\nu \{\bar{\varepsilon}_\nu(R) - \bar{\varepsilon}_\nu(\infty)\} \quad (3)$$

which is shown in fig. 1 for 20 MeV/u (dashed line) and 15 MeV/u (dotted line). In eq. (2) E_{CM} denotes the relative energy in the center of mass system and μ corresponds to the reduced mass. The equivalence of (2) and (3) holds within an accuracy of 1%(factor 2/3 adjusted). The differences between the two curves are probably due to a different coupling to further collective degrees of freedom. Nevertheless we like to interpret fig. 1 in the sense that the dynamical behaviour during the initial phase of a heavy-ion collision is governed by a stiff conservative potential.

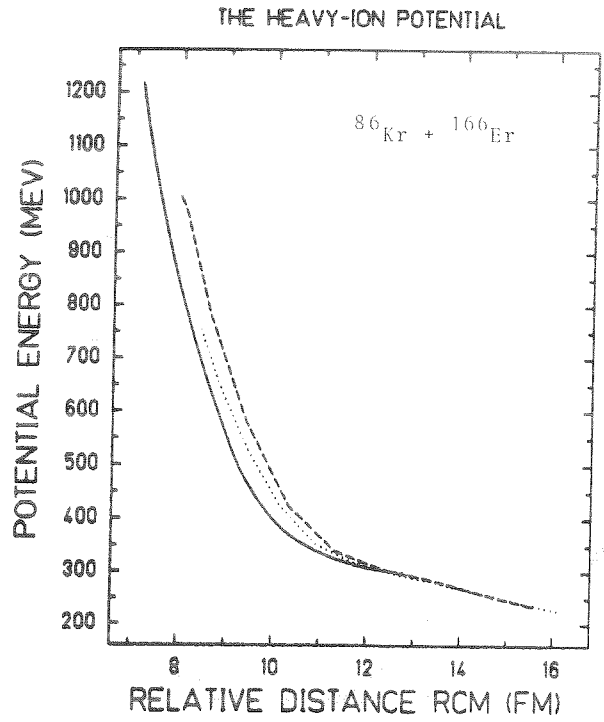


fig. 1

According to the preceeding discussion the potential V_{TDHF} (2) may be compared to the conservative heavy-ion potential of the diabatic two-center shell-model[4]. This quantity is shown in fig. 1(full line) and reasonably coincides with the corresponding TDHF potentials for 20 MeV/u (dashed line) and 15 MeV/u (dotted line). From this quantitative comparison as well as qualitative behaviour of the quasi-static TDHF levels (1) we conclude that TDHF is close to diabatic s.p. motion in the initial phase of a heavy-ion collision.

References

1) W. Nörenberg, Phys. Lett. 104B,107(1981)
2) W. Cassing, W. Nörenberg, Preprint GSI/82/33 and Nucl. Phys. A, in press
3) A.K.Dhar et al., Nucl. Phys. A364,105(1981)
4) A. Lukasiak, W. Cassing, W. Nörenberg, this Annual Report and to be published

On the Energy-Distribution of Diabatically Emitted Neutrons in Heavy-Ion Collisions

W. Cassing, W. Nörenberg
GSI Darmstadt

Diabatic single-particle motion in heavy-ion collisions induces highly excited s.p. states due to the direct coupling of the s.p. states to the collective motion[1]. For illustration the corresponding s.p. levels (full lines) are plotted in fig. 1 for $^{86}Kr + ^{166}Er$ as a function of the distance between the center of masses of the two nuclei together with the local Fermi-level indicated by □. These highly excited states decay due to residual two-body collisions with width $\Gamma_{\nu}{}^{\downarrow}$ or due to the coupling to the continuum with width $\Gamma_{\nu}{}^{\uparrow}$. The latter process is attributed to diabatic emission of protons or neutrons. In order to learn some features about the energy distribution of these light particles the width $\Gamma_{\nu}{}^{\uparrow}(\varepsilon_{\nu} - \varepsilon_F)$ (which is a function of the s.p. energy ε_{ν} above the Fermi-energy ε_F) was adopted from Ref.[2].

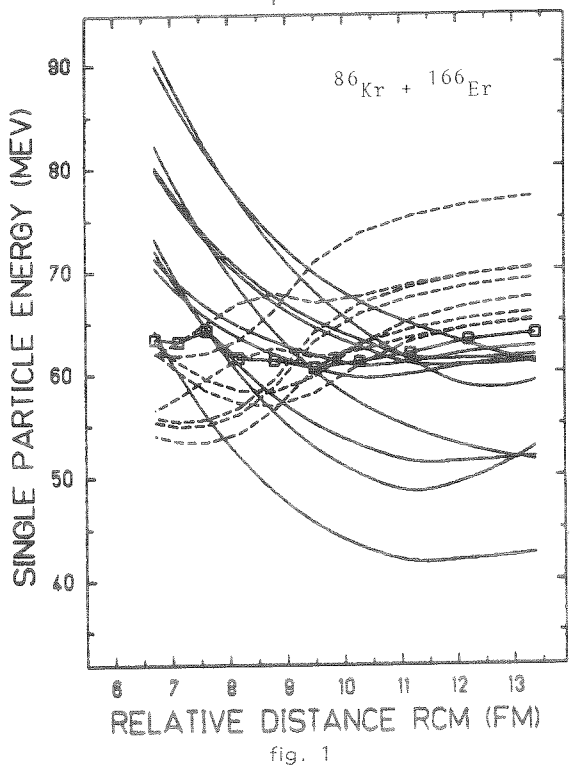


fig. 1

The width $\Gamma_{\nu}{}^{\uparrow}(\varepsilon_{\nu} - \varepsilon_F - \varepsilon_{\nu}^{s})$, which in addition depends on the experimental separation energy ε_{ν}^{s}, was calculated in a two dimensional box model which generated s.p. states of the same nodal struture as the highly excited states in the diabatic two-center shell-model. The energy distribution (multiplicity M per energy unit) was calculated according to

$$\frac{dM}{dE} = \sum_{\nu} \int_{0}^{\infty} dt' \; \frac{\Gamma_{\nu}(t')}{\hbar} \; f(E, \varepsilon_{\nu}(t'), \Gamma_{\nu}(t')) \; n_{\nu}(t')$$

with $\Gamma_{\nu} = \Gamma_{\nu}{}^{\uparrow} + \Gamma_{\nu}{}^{\downarrow}$ and $f(E, \varepsilon_{\nu}, \Gamma_{\nu})$ given by a Gaussian with mean ε_{ν} and width Γ_{ν}. The explicit time dependence of $\varepsilon_{\nu}(t)$, $\Gamma_{\nu}(t)$ results from the solution of the effective equation of motion for the collective degree of relative motion in the framework of DDD[3].

The preequilibrium neutron multiplicity for central collisions of $^{86}Kr + ^{166}Er$ at 10MeV/u (full line), 15MeV/u (dashed line) and 20MeV/u (dashed-dotted line) is displayed in fig.2 . The spectra are very close to the preequilibrium neutron spectra in the reaction $^{20}Ne + ^{165}Ho$ at 11,14.6 and 20MeV/u[4], which have been parametrized by a moving hot spot model with temperatures of 5.9, 6.3 and 7.9 MeV respectively. We like to conclude that diabatic neutron emission yields an alternative explana tion of experimental preequilibrium neutron spectra.

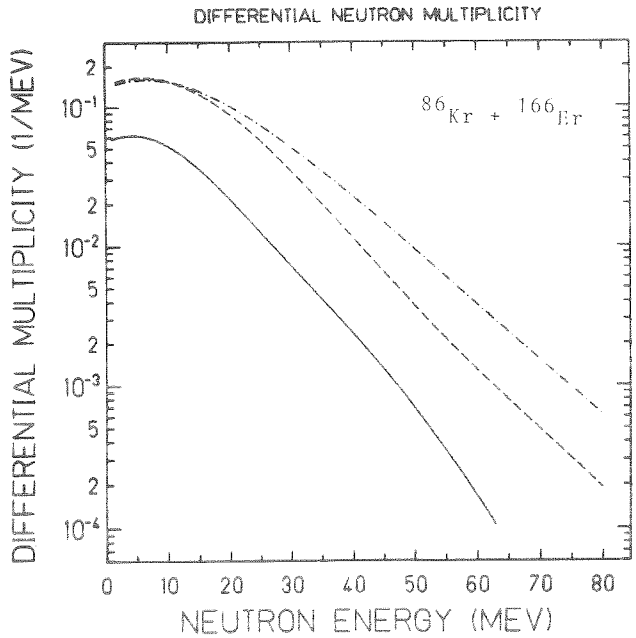


fig. 2

References

1) A. Lukasiak, W. Cassing, W. Nörenberg, Proceedings of the International Workshop on Gross Properties of Nuclei and Nuclear Excitations X, Hirschegg, Jan. 82, p. 80-84
2) P. Morel, P. Nozières, Phys. Rev. 126 (1962) 1909
3) W. Cassing, W. Nörenberg, Preprint GSI-82-33, Nucl. Phys. A (in press)
4) E. Holub, D. Hilscher et al., Preprint HMI 82/9R

Comparison of Collective Mass Parameters given by GCM and the Cranking Model

S.J.Wang, W. Cassing, W. Nörenberg
GSI Darmstadt

The expression for a collective mass parameter within the generator coordinate method (GCM)[1]

$$B_{GCM} = 2\hbar^2 \frac{[\sum_n |\langle\phi_n|\hat{p}|\phi_o\rangle|^2]^2}{\sum_n (E_n - E_o)\,|\langle\phi_n|\hat{p}|\phi_o\rangle|^2} \qquad (1)$$

is compared with the corresponding quantity in the Cranking model (CM)

$$B_{CM} = 2\hbar^2 \sum_{n\neq o} \frac{|\langle\phi_n|\hat{p}|\phi_o\rangle|^2}{E_n - E_o} \quad . \qquad (2)$$

In eqs. (1,2) $\hat{p}$ denotes the infinitesimal generator for the collective variable under consideration. Without any specification of $\hat{p}$ the inequality

$$B_{CM} \geq B_{GCM} \qquad (3)$$

can be proved for the groundstate band.[2] Equality only holds if $(E_n - E_0)$ are constant.

To get a more specific feeling about the quantitative aspects of B_{GCM} we apply formulae (1) and (2) to quadrupole motion and rotation in the deformed harmonic oscillator model. For quadrupole motion, the mass paramters are given by simple expressions[2] which essentially depend on the total number of oscillator quanta $N_{x,y,z}$ in x,y,z direction. Some care, however, has to be attributed in fixing N_x, N_y, N_z as a function of q. In the diabatic limit[3] the s.p. wavefunctions do not change their quantum numbers as a function of q, thus

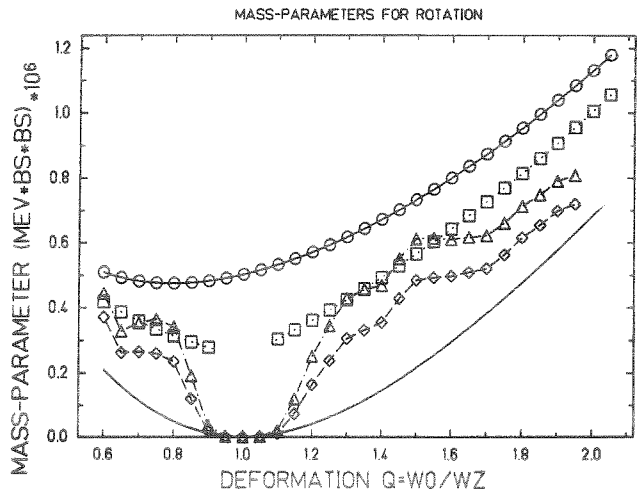
$$N_x = N_y = N_z = N_o \qquad (4)$$

are constant. The other limit which can easily be evaluated corresponds to the limit of a system with infinite particle number (no shell effects) at zero excitation energy[4], i.e.

$$\omega_x N_x = \omega_y N_y = \omega_z N_z . \qquad (5)$$

In both cases (4),(5) B_{GCM} and B_{CM} coincide within an accuracy of 10% which is even slightly better if we include pairing correlations.[2]. For vibrations B_{CM} is identical with the mass parameter for irrotational flow B_{irr} if B_{irr} is calculated for the corresponding microscopic density.

In case of collective rotation however the situation changes drastically. In the continuum limit (5) B_{CM} yields the rigid rotor limit[4] (open circles in fig. 1 for a nucleus of mass number 224) while B_{GCM} (open squares in fig. 1) is significantly lower and closer to experimental values. For spherical nuclei (Q = q = 1) B_{GCM} is not defined. Implying the condition (4), which physically is only legal for nuclei close to spherical shape where the symmetries of the wavefunctions are approximately conserved due to a degeneracy of the s.p. spectrum, we obtain $B_{CM} = B_{GCM} = B_{irr}$ (full line in fig. 1). It thus corresponds to the lowest limit, the irrotational flow limit B_{irr}. Taking into account pairing correlations (gap parameter Δ = 0.7MeV), we obtain approximately irrotational moments of inertia for nuclei close to sphercal shape (B_{GCM}: ◇ fig. 1, B_{CM}: Δ in fig. 1). For larger deformations however the mass parameters are both well in between the limits of a rigid rotor and B_{irr}. From our studies we conclude that the quantal mass parameter B_{GCM} coincides approximately with the semi-classical mass parameter B_{CM} for nuclear vibration but yields more reasonable moments of inertia in case of collective rotation.



References

1) G.O.Xu, S.J. Wang; The Inertia Parameter of Nuclear Collective Excitations, to be published
2) S.J. Wang, W. Cassing, W. Nörenberg; to be published
3) W. Nörenberg; Phys. Lett. 104B(1981)107
4) P. Ring, P. Schuck; The Nuclear Many-Body Problem (Springer, 1980)

On the Dynamical Single-Particle Basis in Large Amplitude Collective Motions

S.J. Wang, W. Cassing, W. Nörenberg
GSI, Darmstadt

We aim at describing large amplitude collective nuclear motion in a dynamical single-particle basis which is the most reasonable approximation to the time-dependent single-particle Schroedinger equation

$$i\hbar \frac{\partial}{\partial t} \psi_\alpha = h(x,q)\psi_\alpha \qquad (1)$$

in which q denotes a collective parameter. Eq.(1) usually is solved within the adiabatic representation $|\phi_n\rangle$

$$h(x,q)\,|\phi_n(x,q)\rangle = \varepsilon_n(q)\,|\phi_n(x,q)\rangle \qquad (2)$$

which, however, is only applicable for small collective velocities ($\dot q \to 0$) and if no quasicrossings of the adiabatic levels $\varepsilon_n(q)$ occur[1]. Assuming q(t) to be a given function of time eq. (1) can be written as

$$h(x,q) - i\hbar\dot q \frac{\partial}{\partial q}\,|\bar\psi_\alpha(x,q)\rangle = 0 \qquad (3)$$

which allows further interesting approximations with respect to a static basis.

For small $\dot q$ an optimal representation of $\psi_\alpha(q)$ is given by

$$|\bar\psi_\alpha\rangle = \sum_n \bar C_{\alpha n}|\phi_n\rangle \quad , \qquad (4)$$

where the coefficients $\bar c_{\alpha n}$ are determined by the eigenvalue equation

$$\sum_n \langle\phi_m|h - i\hbar\dot q \frac{\partial}{\partial q}\,|\phi_n\rangle \bar C_{\alpha n} = E_\alpha \bar C_{\alpha m} \; . \qquad (5)$$

Returning to the initial value problem (1) and expanding

$$|\psi_\alpha\rangle = \sum_\beta d_{\alpha\beta}|\bar\psi_\beta\rangle \exp\{-i/\hbar \int_0^t E_\beta(t')dt'\} \qquad (6)$$

we find that the time evolution of the expansion coefficients $d_{\alpha\beta}$ is proportional to $\dot q^2$ (instead of $\dot q$ in the CM) which shows an improvement with respect to the cranking model (CM).

For somewhat larger collective velocities $\dot q$, i.e. within the range of collective kinetic energy per nucleon of

$$1/40 \text{ MeV} \lesssim E_{coll}/A \ll 40 \text{ MeV}, \qquad (7)$$

a diabatic basis is more appropriate[2] because in the vicinity of quasicrossings it includes jump probabilities close to 1 in a nonperturbative way. The diabatic basis e.g. can be obtained by retaining only terms of h(q) which keep the symmetries of the collective motion. In case of quadrupole motion this implies a neglect of the coupling between spin $\vec s$ and angular momentum $\vec l$ and a term $\sim l^2$ in the Nilsson Hamiltonian. The diabatic Hamiltonian h_o for a 3-dim. deformed oscillator problem then reads

$$h_o(q) = -\frac{\hbar^2}{2m}\Delta + \frac{m}{2}\omega_o^2\{q(x^2+y^2) + q^{-2}z^2\} \qquad (8)$$

and eq. (3) with h substituted by h_o can be solved analytically within a boson representation[3]

$$h_o(q) - i\hbar\dot q \frac{\partial}{\partial q} = \sum_{i=x,y,z} \hbar\Omega_i(b_i^+b_i^+ + \tfrac{1}{2}) \; . \qquad (9)$$

We obtain

$$\bar\psi_n(q,\dot q) = N_n \underbrace{e^{-(a_x^2x^2 + a_y^2y^2 + a_z^2z^2)}}_{\bar H_n(x,y,z)} \exp(-i\frac{m}{\hbar}\Phi) \qquad (10)$$

with $a_i^2 = m\frac{\Omega_i}{\hbar}$

and

$$\Phi(x,y,z;q,\dot q) = \frac{\dot q}{8q}(x^2+y^2-2z^2) \; . \qquad (11)$$

In eq. (10) $\bar H_n$ is a polynomial of order n with complex coefficients and does not contain significant phases as a function of $\dot q$, $\dot q^2$ ... . The essential phase is given by the velocity potential Φ and implies incompressible irrotational flow. The mass parameter for quadropule motion

$$B(q,\dot q) = \frac{\hbar}{4} \sum_{i=x,y,z} \frac{K_i^2 N_i}{\Omega_i}$$

$$\text{with } K_x = K_y = \frac{1}{2q} \; , \; K_z = -\frac{1}{q} \qquad (12)$$

$$\text{and } N_i = \sum_{j=1}^{A} \langle|b_i^+b_i^+ + \frac{1}{2}|\rangle_j$$

reduces to the cranking formula for $\dot q = 0$. The variation of B with q is less than 5% for

$$\dot q/\omega_o \lesssim 0.5 \qquad (13)$$

in the physically interesting range of deformations $0.5 \lesssim q = \omega_o/\omega_z \lesssim 2.5$.

We conclude from this study that the diabatic cranking model, i.e. solutions of eq. (9) up to first order in $\dot q$, works well in the energy range (7) for nuclear quadrupole motion up to collective velocities $\dot q \cdot R$ which are half of the typical s.p. velocity $\omega_o \cdot R$ (R = nuclear radius). The mass parameter in the diabatic cranking approximation turns out to be a smooth function of q in contrast to the adiabatic cranking model.

References:

1) V.M. Strutinsky, Z. Phys. A280(1977)99
2) W. Nörenberg, Phys. Lett. 104B(1981)107
3) J. Kunz and U. Mosel, Relation Between Current and Inertial Parameter in the Cranking Model, Preprint Univ. Gießen 1982

Extension of the time-dependent mean field theory within density matrix hierarchy

S.J. Wang
GSI Darmstadt

The behavior of a closed system is described by its complete many-body density matrix $\rho_A(t)$ evolving according to the von Neumann equation

$$ih\dot{\rho}_A = [H,\rho_A] \ . \qquad (1)$$

The A-body Hamiltonian H can be divided into a mean-field part H_o and a residual interaction V with

$$H_o = \sum_i h_o(i) \qquad (2)$$

From (1) we can derive a set of coupled equations of motion for density matrices of lower rank[1].

$$ih\dot{\rho}_1(1,1') = [h_o,\rho_1]_{1,1'} + \mathop{\mathrm{Tr}}_{(2)}[V,\rho_2]_{12,1'2} \qquad (3a)$$

$$ih\dot{\rho}_2(12,1'2') = [h_o(1)+h_o(2),\rho_2]_{12,1'2'} + [V,\rho_2]_{12,1'2'} + \mathop{\mathrm{Tr}}_{(3)}[V(13)+V(23),\rho_3(123)]_{123,1'2'3'} \qquad (3b)$$

The reduced density matrices can be separated as follows

$$\rho_2(12,1'2') = \rho_{2o}(12,1'2') - C(12,1'2') \qquad (4a)$$

$$\rho_3(123,1'2'3') = A[\rho_1(11')\rho_1(22')\rho_1(33')] - C(123,1'2'3') - A[\rho_1(11')C(23,2'3') + \rho_1(22')C(13,1'3') + \rho_1(33')C(12,1'2')] \qquad (4b)$$

Here $\rho_{2o}(12,1'2') = A[\rho_1(11')\rho_1(22')]$ and A is an antisymmetrizing operator. If we assume that the three-body correlations vanish, the hierarchy (3) is cut down at the second rank. Eq. (3a) then reads

$$ih\dot{\rho}_1(1,1') = [h,\rho_1]_{11'} - \mathop{\mathrm{Tr}}_{(2)}[V(12)-V(1'2')]\times C(12,1'2') \qquad (5a)$$

with $h_o = h_o + \mathop{\mathrm{Tr}}_{(2)}(V\rho_{2o})$ and (3b) turns to be

$$\begin{aligned} ih\dot{C}(12,1'2') = &-[V(12)-V(1'2')]\times[\rho_{2o}(12,1'2')-C(12,1'2')] \\ &+ [h_o(1)+h_o(2)-h_o(1')-h_o(2')]C(12,1'2') \\ &+ \mathop{\mathrm{Tr}}_{(3)}\{[V(13)\rho_{2o}(13,1'2')\rho_1(23)+(V(23)\rho_1(12')\times\rho_1(31')-ex(1'2')\rho_1(23) \\ &+ (V(13)-V(1'3'))C(23,2'3')\rho_1(11') \\ &- (V(13)-V(2'3'))C(23,1'3')\rho_1(12') \\ &+ \{V(13)+V(23)-V(1'3)-V(2'3)\}C(23,1'2')\rho_1(13)]-ex(12)\} \\ &+ \mathop{\mathrm{Tr}}_{(3)}\{[V(13)+V(23)-V(1'3)-V(2'3)][C(12,1'2')\rho_1(33) \\ &- C(12,32')\rho_1(31')-C(12,1'3)\rho_1(32')]\} \end{aligned} \qquad (5b)$$

These equations represent an extension of TDHF theory to the inclusion of the two-body correlations. If the residual interaction is weak, (5b) can be solved by perturbation. In the first order approximation, we obtain

$$\begin{aligned} C(12,1'2') = &\frac{i}{h}\int_{-\infty}^{t} d\tau \int d\bar{x}_1 d\bar{x}_2 V(\bar{x}_1,\bar{x}_2) \\ &\cdot\{[\delta(x_1-\bar{x}_1)-\rho_1(x_1,\bar{x}_1)]\cdot[\delta(x_2-\bar{x}_2)-\rho_1(x_2\bar{x}_2)]\times \\ &\times A[\rho_1(\bar{x}_1x_1')\rho_1(\bar{x}_2x_2')] \\ &-\rho_1(x_1\bar{x}_1)\rho_1(x_2\bar{x}_2)A[(\delta(\bar{x}_1-x_1')-\rho_1(\bar{x}_1x_1'))\times \\ &\times(\delta(\bar{x}_2-x_2')-\rho_1(\bar{x}_2x_2'))]\}_\tau \end{aligned} \qquad (6)$$

This result coincides with the corresponding result of the Martin-Schwinger hierachy[2] in the equal time green-function limit.

References:

1) W.C. Schieve, Lecture Notes in physics 28. "Lectures in Statistical Physics" (1974)

2) C.Y. Wong and H.H.K. Tang, Phys. Rev. Lett. 40(1978)1070.

Potential Energy Surfaces for Ternary Fragmentation

N. Carjan, Centre d' Etudes Nucleaires de Bordeaux-Gradignan, 33170 Gradignan
A. Gobbi and J. Tõke[+], GSI Darmstadt

The aim of these calculations is to study the underlying potential surfaces for a projectile splitting in a 10-20 MeV/u heavy ion collision and to search for the energetically most favorable configuration in a three-body decay. The splitting (instantaneous fission) of a ^{100}Mo projectile in the field of a ^{100}Mo target was chosen as numerical example. A convenient set of parameters able to describe our system is represented in Fig. 1: Z and ρ describe the position of the center of mass of the recoil nucleus relative to the fissioning nucleus (measured from the center of mass of the latter); D is the distance between the center of mass of the fission fragments; A_3, A_1 and A_2 are the masses of the recoil nucleus and of the fission fragments, respectively. The nuclear shapes occuring during projectile splitting were described by a series of asymmetric Cassinian ovals whereas the target nucleus was considered to be spherical. The (z,ρ)-plot in Fig. 2 shows the potential seen by a spherical ^{100}Mo in the vicinity of a symmetrically (A_1=A_2) scissioning ^{100}Mo, the half density surface of which is defined by the solid curve. For the nuclear part a generalization of a Woods-Saxon potential for Cassinian shaped axially-symmetric nuclei has been used[1]. The parameters V_o=100 MeV, a=0.8 fm and r_o=1.13[$A_3^{1/3}$ + (A_1+A_2)$^{1/3}$] were chosen to reproduce the unified nuclear potential[2]. For the Coulomb part a radius R_o=1.225(A_1+A_2)$^{1/3}$ has been used. Comparing the values of the ridge of the interaction potential one sees that a collinear configuraton lies about 90 MeV lower in energy than a trefoil configuration. Since collinear configuration are energetically favoured, ρ will be kept zero in the following examples. The (Z,D) plot in Fig. 3 shows how the presence of the recoil nucleus influences the fission of the projectile. It is a striking feature of these results that for Z-values between -30 and -25 fm the fission is slowed down and even pushed back (the re-fusion between A_3-A_1 is energetically favoured). In addition we have investigated, also for collinear configurations, the energetically most favourable mass-asymmetries of a ternary decay. For this purpose we used spherical touching configurations with liquid drop masses and proximity forces. As it can be seen from Fig. 4 a small central mass A_1, confined between two equally large lateral masses A_2 and A_3 gives the most favorable configuration. The calculation also indicates a preference for the formation of neutron rich central masses A_1.

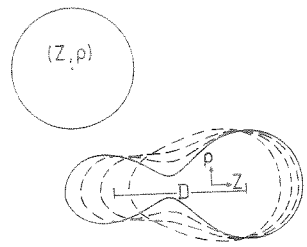


Fig. 1

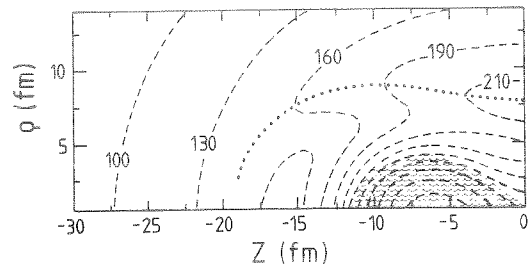


Fig. 2

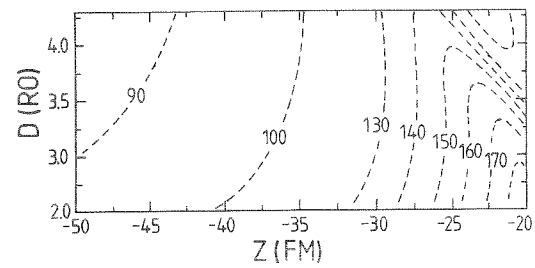


Fig. 3

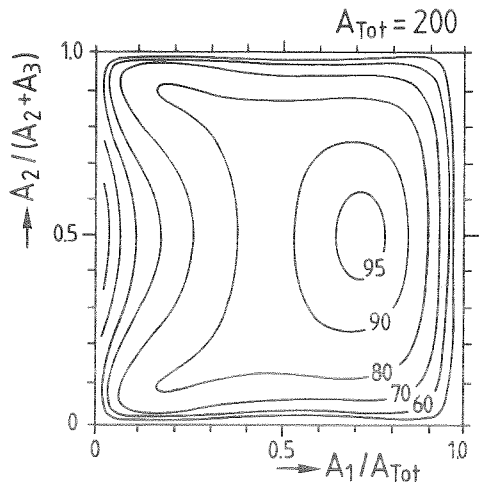


Fig. 4

[+] on leave from Warsaw University, Poland

[1] N. Carjan and B. Leroux, Phys.Rev. C22(1980)2008 and references therein

[2] H.J. Krappe, J.R.Nix and A.J.Sierk, Phys.Rev. C20(1979)992

Potential Pockets in the ^{238}U-^{238}U System and their Possible Consequences [B G]

M.J. Rhoades-Brown
Oak Ridge National Laboratory, Oak Ridge, TN, US
Volker Oberacker
Vanderbilt University, Nashville, TN, USA
M. Seiwert and W. Greiner
Institut für Theoretische Physik der Universität Frankfurt

In the last year, we reported the results of a calculation of the total nuclear potential of the U-U system in terms of the proximity approach[1]. Minima occured for such orientations, where two flat surface parts due to the hexadecupole deformation face each other. We study now such deformation and orientation effects for the ^{238}U+^{238}U system within the context of the double-folding model and test the idea of possible potential pockets leading to large reaction times. Using this model to calculate the real component of the potential energy V involves averaging a nucleon-nucleon interaction over the static matter distributions of the two ions. For this calculation we use as the N-N interaction the M3Y-force based on G-matrix elements constructed from the Reid soft-core potential[2]:

$$V(r) = 7999\,\frac{\exp(-4r)}{4r} - 2134\,\frac{\exp(-2.5r)}{2.5r} - 262\,\delta(r)$$

We assumed the intrinsic charge and matter distribution can be described in the form $\varrho = \varrho((r-R)/a)$ (i.e., a Fermi form) and that the nuclear radius parameter R is parametrized in the usual way,

$$R(\theta') = R_0\left[1 + \delta_2 Y_{20}(\theta') + \delta_4 Y_{40}(\theta')\right].$$

We used the recent experimentally determined results[3], δ_2=.261, δ_4=.087, R_0=6.8054 fm, a=.6049 fm, $B(E2,0^+\rightarrow 2^+) = 11.70\ e^2b^2$ and $B(E4,0^+\rightarrow 4^+)=1.20e^2b^4$. To study shape-dependent effects, δ_4 only was artifically increased to the value δ_4 = .12 resulting in $B(E2,0^+\rightarrow 2^+) = 12.78e^2b^2$ and $B(E4,0^+\rightarrow 4^+) = 1.41\ e^2b^4$.

To evaluate the double-folded potential of the form

$$U(\vec{r}) = \int d^3r_1 \int d^3r_2\ \varrho(\vec{r}_1)\ v(\vec{r}_{12} = \vec{r} + \vec{r}_2 - \vec{r}_1)\ \varrho(\vec{r}_2) \qquad (1)$$

we use a momentum space method. If the Fourier transform of a function f(x) is denoted by $\tilde{f}(k)$, the following relations hold:

$$f(\vec{x}) = (2\pi)^{-3} \int d^3k\ \tilde{f}(\vec{k})\ \exp(-i\vec{k}\cdot\vec{x})$$

$$\tilde{f}(\vec{k}) = \int d^3x\ \exp(i\vec{k}\cdot\vec{x})\ f(\vec{x})$$

Inserting the Fourier transformation of the N-N interaction $v(\vec{r} + \vec{r}_2 - \vec{r}_1)$ into eq.(1), we find for the folded potential

$$U(\vec{r}) = (2\pi)^{-3} \int d^3k\ \exp(-i\vec{k}\cdot\vec{r})\ \tilde{v}(\vec{k})\ \tilde{\varrho}_1(\vec{k})\ \tilde{\varrho}_2(-\vec{k})$$

i.e., the Fourier transformed heavy-ion potential reduces to a product of the Fourier transforms of the two densities and the effective N-N interaction. The remaining integrals are solved numerically using the Gaussian method. In figs. 1 and 2 the total nuclear plus Coulomb potential is plotted for a selection of relative orientation angles. Fig. 1 corresponds to the experimental values for δ_2 and δ_4, while fig. 2 is for the artifically larger δ_4 value. In these figures we have indicated the range of the experimental beam energies and the radial position of the half-density overlap for the appropriate orientation angles. Both parameter sets show the largest probability of averaging the Coulomb barrier for orientation angles $\beta_1=\beta_2=0^o$. As the quantity $\beta_1+\beta_2$ increases a systematic increase in the magnitude of the Coulomb barrier was observed together with a systematic decrease in the radial position of this barrier. Obviously these results are in contrast to the proximity calculations. A comprehensive comparison between these models is in progress.

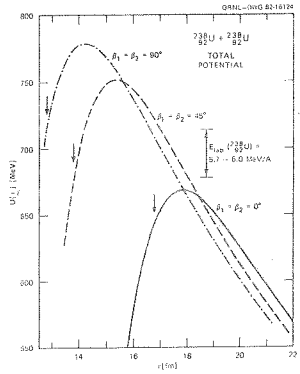


Fig. 1:

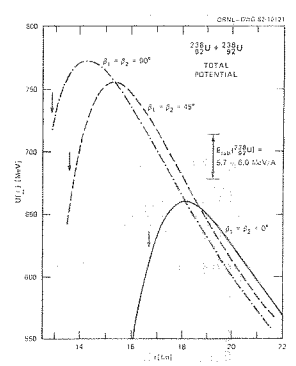


Fig. 2:

[1] GSI report 1981: M. Seiwert et al., p. 83
[2] G.R. Satchler, et al., Phys.Rep.55, 183 (1979)
[3] T. Cooper et al., Phys.Rev. C13, 1083 (1976)

Polarization Effects for Elastic and Inelastic Scattering with exact and approximated propagators B G

R. Kaps, J. Makowka, U. Mosel, O. Tanimura, and R. Wolf

Institut für Theoretische Physik, Universität Gießen

In fusion and deep-inelastic reactions of heavy nuclei shape changes and polarization effects are of considerable importance. For example, the strong enhancements of fusion cross sections, measured e.g. at GSI by Reisdorf et al.[1], at low energies may have their origin in such effects. A complete - though often impractical - theoretical framework for the description of such effects is provided by the coupled channels method. Starting from this method we have, in a first step of our investigation of polarization effects, looked for their importance in inelastic heavy ion scattering.

For this purpose we reduce the full coupled system by Feshbach's projection method to two main channels: The elastic one is denoted by P, whereas $Q_{\alpha i}$ specifies a subchannel i of the inelastic state α in the Q(=1-P) space. Within this formalism we get the following Schrödinger equation for $Q_{\alpha i}$

$$\left[E-H_{Q_{\alpha i}Q_{\alpha i}}-V_{Q_{\alpha i}\bar{Q}_{\alpha i}}\frac{1}{E^{(+)}-H_{\bar{Q}_{\alpha i}\bar{Q}_{\alpha i}}}V_{\bar{Q}_{\alpha i}Q_{\alpha i}}\right]\Psi^{(+)}_{Q_{\alpha i}}=$$

$$\left[H_{Q_{\alpha i}P}+V_{Q_{\alpha i}\bar{Q}_{\alpha i}}\frac{1}{E^{(+)}-H_{\bar{Q}_{\alpha i}\bar{Q}_{\alpha i}}}V_{\bar{Q}_{\alpha i}P}\right]\Psi^{(+)}_{P} \quad (1)$$

where $\bar{Q}_{\alpha i}$ is defined by $Q-Q_{\alpha i}$. If we write the square bracket on the right hand side as $V^{eff}_{Q_{\alpha i}P}$, the T-matrix of the conventional DWBA is given by

$$T_{Q_{\alpha i}P} = \langle \Psi'^{(+)}_{Q_{\alpha i}} | V^{eff}_{Q_{\alpha i}P} | \Psi^{(+)}_{P} \rangle \quad (2)$$

with the homogeneous solution $\Psi'^{(+)}_{Q_{\alpha i}}$ of (1). This $T_{Q_{\alpha i}P}$ is exactly equal to the full coupled channel T-matrix. The "optical potential" in the $Q_{\alpha i}$ channel is in general not the same as the elastic optical potential, which was also stressed by Seglie et al.[2] for the case of $^{40}Ca+^{16}O$ inelastic scattering.

It is now important to compare the exact polarization effects on the bare interactions with approximations for the propagator in (1), because such approximations - if valid - allow significantly simplified calculations.

In an adiabatic formulation of the scattering process, e.g., we derive perturbation theoretical expressions for the exact propagator that describe the deformations induced in one nucleus by the close presence of the other one. They lead to prominent shifts of the excitation energy in the diagonal terms and to changes of the transition probability in the nondiagonal elements.

As an example we choose a vibrational model for $^{16}O+^{16}O$ with a standard Woods-Saxon derivative coupling potential up to second order. The (3^-, 6.13 MeV) state is regarded as first excited level of an octupole phonon spectrum. When we restrict the Q-space to two phonon couplings, the energy shifts for typical interaction strengths look like fig. 1. Of course the correction terms become the more important the closer the nuclei approach each other.

The third term on the right hand side of eq. 1 contains all effects of zero point motion and polarization in it. For the ground channel it corresponds to an energy-dependent correction to the heavy ion potential that should thus be equivalent to the empirical prescription used in ref. 1. The analyses described above are, therefore, presently performed for the fusion channels where, in particular close to the barrier, quantum mechanical effects are important[3].

[1] W. Reisdorf et al., Phys. Rev. Lett. 49, 1811 (1982)
[2] R.J. Ascuitto et al., Phys. Rev. Lett. 41, 1159 (1978)
[3] G. Münzenberg et al., Z. Phys. A300, 107 (1981)
G. Münzenberg et al., Z. Phys. A309, 89 (1982)

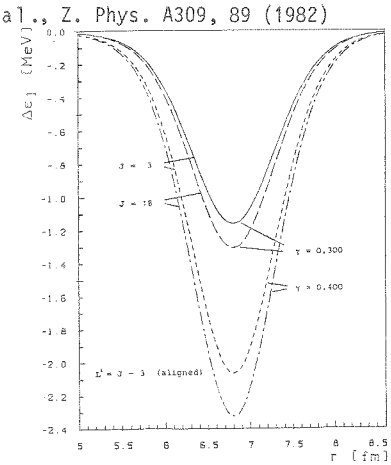


Figure 1:
Energy shift of the (3^-,6.13 MeV)-level in ^{16}O

The Semiclassical Approximation for Inelastic Scattering [BG]

F. Krisztinkovics, J. Reinhardt, B. Müller, and W. Greiner
Institut für Theoretische Physik der Universität Frankfurt

The method of path integrals provides an elegant framework to derive the semiclassical approximation in inelastic scattering processes. Following the formulation of Pechukas[1] we have studied the influence of internal quantum excitations of the colliding particles on their relative motion which is described by a classical but state-dependent trajectory.

The system under consideration is described by a Hamiltonian $\mathcal{H} = T_{rel} + H(\vec{r},x)$ consisting of the kinetic energy of relative motion and the internal and interaction energies which depend on the relative distance $\vec{r}$ and the internal coordinates x.

The propagator for scattering accompanied by a transition between the internal states is given by the path integral

$$K_{\beta\alpha}(\vec{r}',t'|\vec{r}'',t'') = \int_{\vec{r}'',t''}^{\vec{r}',t'} d\vec{r}(t)\, e^{\frac{i}{\hbar}S_0[\vec{r}(t)]}\, T_{\beta\alpha}[\vec{r}(t)] \qquad (1)$$

where S_0 is the action for the relative motion and $T_{\beta\alpha}$ is the transition amplitude which are both functionals of the path $\vec{r}(t)$. The stationary phase approximation for (1) reads

$$\delta\left\{ S_0[\vec{r}(t)] + \hbar\, \mathrm{Im}\, \ln T_{\beta\alpha}[\vec{r}(t)] \right\} = 0. \qquad (2)$$

This leads to a classical equation of motion for the trajectory $\vec{r}(t)$:

$$\mu \ddot{\vec{r}}(t) = -\vec{\nabla} \left\{ \mathrm{Re} \left(\frac{\langle \Psi_\beta^-(t) | H(\vec{r}(t),x) | \Psi_\alpha^+(t) \rangle}{\langle \Psi_\beta^-(t) | \Psi_\alpha^+(t) \rangle} \right) \right\}_{\vec{r}=\vec{r}(t)} \qquad (3)$$

$\Psi_\alpha^+(t), \Psi_\beta^-(t)$ describe solutions of the time dependent Schrödinger equation for the internal state

$$\left(i\hbar \frac{\partial}{\partial t} - H(\vec{r}(t),x) \right) \begin{pmatrix} \Psi_\alpha^+(t) \\ \Psi_\beta^-(t) \end{pmatrix} = 0 \qquad (4)$$

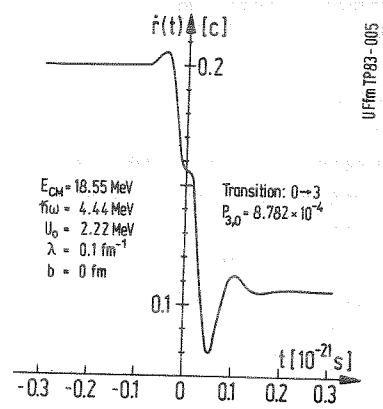
with boundary conditions prescribed before/after the collision. We have studied the influence of the quantum mechanical force term on the relative motion in a simple one-dimensional harmonic oscillator model with a linear perturbing potential

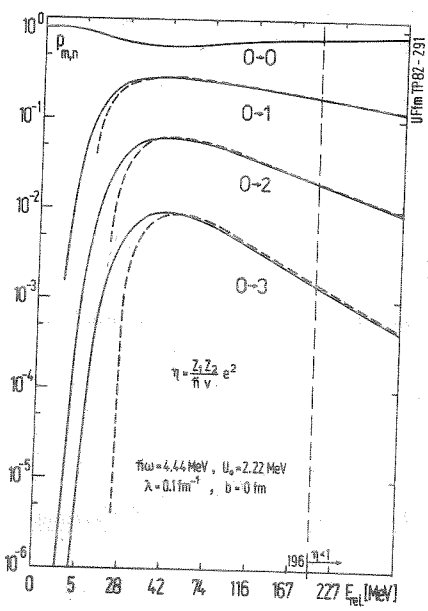
$$H(\vec{r},x) = \frac{p_r^2}{2\mu} + \frac{p_x^2}{2m} + \frac{m^2\omega^2}{2}x^2 + \left(\frac{2m\omega}{\hbar}\right)^{\frac{1}{2}} x \cdot U_0 \left(\cosh \lambda r\right)^{-1} \qquad (5)$$

Here the transition amplitudes can be reduced to a simple quadrature. Eqs. (3) and (5) have been solved iteratively to obtain a trajectory $r(t)$ which includes the effect of the quantum transition in a selfconsistent way.

Fig. 1 shows the selfconsistent velocity $\dot{\vec{r}}$ for the example of a 0→3 transition for protons incident on a heavy nucleus with oscillator quantum $\hbar\omega$ = 4.44 MeV. The chosen values of E_{kin}, λ, b and the transition probability $P_{30} = |T_{30}|^2$ are indicated in the figure. The effects of selfconsistence are most prominent near threshold, where a large fraction of the kinetic energy is taken up by the internal excitation. This is demonstrated in Fig. 2 which shows the transition probabilities P_{mn} calculated with the unperturbed trajectory $r^{(0)}(t)$ (full lines) and the selfconsistent trajectories $\bar{r}(t)$ (broken lines) as a function of initial kinetic energy.

[1] P. Pechukas, Phys.Rev.181 (1969) 166 and 174





Contributions to the Theory of Nuclear Molecules Obtained by the Study of the $^{28}Si+^{28}Si$ System [B]

A. Thiel and W. Greiner
Institut für Theoretische Physik der Universität Frankfurt
R. Könnecke
GSI Darmstadt

We investigate the $^{28}Si+^{28}Si$ system measured by Betts et al.[1] in the framework of a coupled channel calculation based on the adiabatic coupling model[2].
The first requirement to be fulfilled was the reproduction of the five resonances, Betts could assign to angular momenta of 34-42 $\hbar$, by the corresponding grazing resonances in the real potential $V^{elastic} + V_L^{angul.mom.}$. These generate the gross structure of the elastic excitation function (s.Table 1).
In the statistical model for the imaginary potential[3], the radial dependence of the matrix element $|\langle\Psi_{comp}|V_{int}|\Psi_{el}\rangle|^2$ was approximated by the surplus number of nucleons in the overlap region of two Gaussian density distributed nuclei (adapted to the measured charge density distribution of ^{28}Si [4]).
The calculated elastic cross-section (without coupling) shows the gross structure generating effect of the grazing resonances (five bumps between 50 and 64 MeV).
With the calculated coupling potentials we shall consider the coupling of inelastic channels $((2^+,0^+),(2^+,2^+),(4^+,2^+))$ to the virtual resonances via the double resonance mechanism.

L [$\hbar$]	E_{CM}^{Theory} [MeV]	$E_{CM}^{Exp.}$ [MeV]	Δ [MeV]
34	50.75	50.5	.25
36	53.25	53.0	.25
38	56.25	55.5	.75
40	59.25	59.	.25
42	62.75	64.	1.25

Table 1
Comparison of the energies of the first virtual state ($\delta_l = \frac{\pi}{2}$) just above the Coulombbarrier of the effective potential $V^{elastic}+V_L$ ($V^{imag}=0$) to the measured resonances

[1] R.R. Betts, S.B. DiCenzo, and J.F. Petersen, Phys.Rev.Lett. 43, 253, (1979); Phys.Lett. 100B, 117, (1981); R.R. Betts, H.-G. Clerc, B.B. Back, I. Ahmad, K.L. Wolf, B.G. Glagola, Phys.Rev.Lett. 46, 313, (1981) R.R. Betts, B.B. Back, B.G. Glagola, Phys.Rev.Lett. 47, 23, (1981)
[2] R. Könnecke, J. Guirguis, W. Greiner, W. Scheid J.Phys.G:Nucl.Phys. 8, 535, (1982) R. Könnecke, Dissertation 1982
[3] H.-J. Fink, W. Scheid, W. Greiner Nucl.Phys. A188, 259, (1972); R. Könnecke, W. Greiner, W. Scheid, J.Phys. G: Nucl.Phys. 8, L11 (1982)
[4] R. Hofstadter, Rev.Mod.Phys. 28, 214 (1956)

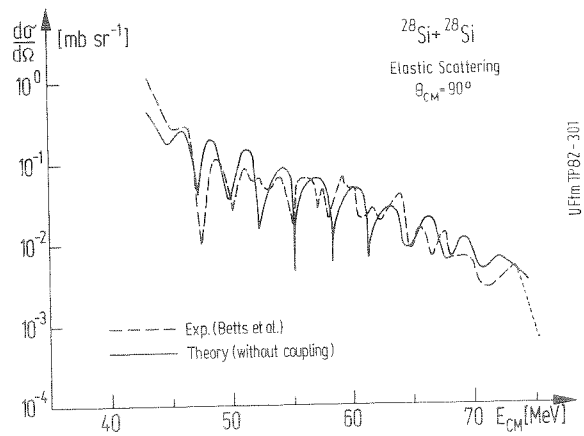


Fig. 1: Comparison between the experimental and calculated 90° cross-section for elastic ^{28}Si-^{28}Si scattering. The theoretical curve was obtained by an optical model calculation without the coupling of inelastic channels.

Comparison of Hydrodynamical Calculations with Recent CERN $^{12}C(184\ MeV/n)+^{197}Au$ Proton Data [B]

G. Buchwald, G. Graebner, J.A. Maruhn, and W. Greiner
Institut für Theoretische Physik der Universität Frankfurt
J. Theis
GSI Darmstadt
H. Stöcker
Nat. Supercond. Cycl. Lab., East Lansing, Michigan, USA

Viscous three dimensional fluid dynamical calculations are performed for the reaction $^{12}C+^{197}Au$ at 84 MeV/n. In order to obtain inclusive cross sections which can be compared with experimental data, fluid dynamical calculations are made for impact parameters b=1;3;5;7 fm. Subsequently a subroutine asuming local thermal and local chemical equilibrium is attached[1] to each run. The resulting cross sections are averaged over all impact parameters.

Fig. 1 shows the fluid dynamical results compared with the data of Jakobsson et al.[2]. The calculations are in qualitative agreement with the data. There are two points , however, which require further discussion. First the experimental data seem to indicate a dip at energies around 50 MeV which does not occure in the calculations. But comparison with other data[3] seems to show that this point is not settled experimentally. Second the absolute value of the calculational result is a factor 5-6 too small. Most of this is due to the fact that the chemical equilibrium model used here does not take into account the decay of excited reaction products into protons. The additional amount of protons stemming from this mechanism can be estimated to shift our results by a factor 4-5[4]. Thus improved calculations now in progress promise to yield much better agreement between data and theory. Selecting to central events the fluid dynamical model predicts a strong forward suppression of the cross section. This can be seen most impressively in the α cross section (Fig. 2) because the α's are formed preferentially in the colder reaction zones[1]. Therefore their cross section is smeared out least by thermal motion and retaining a large amount of collective flow information.

[1] G. Buchwald, G. Graebner, P.R. Subramanian, L.P. Csernai, J. Theis, J. A. Maruhn, W.Greiner and H. Stöcker, Proceedings of the XX.Int. Winter Meeting on Nuclear Physics, Bormio, Italy 25-30 Jan. 1982, p. 734 and all refs. therein
[2] B. Jakobsson et al., Phys.Lett. 102B, 121 and Univ. of Lund, preprint LUIP 8208, June 1982
[3] R. Glasow et al., GSI report 82-1, p. 35
[4] H. Stöcker privat discussion and G. Buchwald et al., UFTP preprint 95/1982, to be published

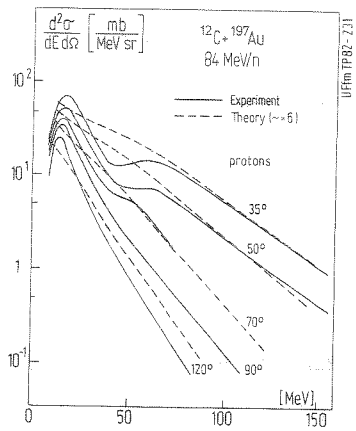


Fig. 1: Inclusive proton cross section for the reaction $^{12}C+^{197}Au$ at E_{Lab}=84 MeV/n.

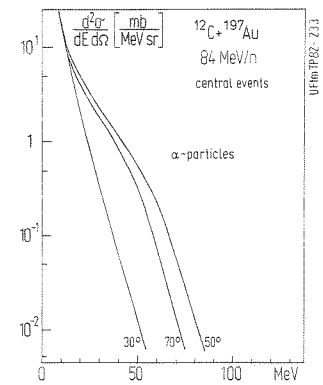


Fig. 2: The central selected α-cross section for the same reaction as above is predicted as showing strong forward suppression, i.e. the 50° cross section is much larger than that for 30°.

Nonrelastivistic Neutron-, Proton Fluid Dynamics

J. Theis*, G. Buchwald, G. Graebner, J.A. Maruhn, and W. Greiner

*GSI Darmstadt

Inst. f. Theor. Physik, Johann-Wolfgang Goethe Universitität Frankfurt

The subject of this investigation is the dynamics of a nuclear fluid involving neutron and proton degrees of freedom. Measurements of different neutron and proton distributions in static nuclear density profiles and collective oscillations of the giant resonant type indicate that this degree of freedom is important for nuclei. Here we investigate the situtation in a collision of heavy ions. We have already examined [1] how fluid dynamical equations governing these degrees of freedom can be derived from a microscopic theory. We start with the time dependent Hartree-Fock (TDHF) equations:

$$i\hbar \frac{\partial \psi_i}{\partial t} = \frac{\hat{p}^2}{2M}\psi_i + tr_2\left\{\hat{v}(1,2)\left[1-P(1,2)\right]\hat{\rho}(2)\right\}\psi_i - 4\pi\beta\phi\psi_i$$

Here the single particle states ψ_i are treated as 2-component objects posessing isospin degree of freedom and $\hat{v}(1,2)$ stands for the two-body potential.

$$\hat{v}(1,2) = \left[t_0(1+x_0P_\sigma) + (t_3/6)(1+P_\sigma)(\rho_n+\rho_p)\right]\delta(\vec{r}_1-\vec{r}_2) + (t_1/2)\left[\delta(\vec{r}_1-\vec{r}_2)k^2 + k'^2\delta(\vec{r}_1-\vec{r}_2)\right] + t_2\vec{k}'\delta(\vec{r}_1-\vec{r}_2)\vec{k}$$

The spin-orbit force is neglected and P_σ denotes the spin exchange operator. The t_3-contribution provides a simple phenomenological representation of many-body effects, and describes the interaction between two nucleons in the presence of other nucleons. The t_1- and t_2-contribution stands for the momentum-dependent part of the interaction.

A hydrodynamical approximation is made to the complex nonrelativistic TDHF equations coupled to a dynamical meson-field ϕ. This yields a system of non-linear coupled equations for the matter- (sum-) density $\rho_0 = \rho_n + \rho_p$ and the fluctuation- (excess-) density $\rho_\tau = \rho_n - \rho_p$, the respective currents $\vec{j}_0$, $\vec{j}_\tau$ and the meson field:

$$\partial_t \rho_0 + \vec{\nabla}\vec{j}_0 = 0 \quad ; \quad \partial_t \rho_\tau + \vec{\nabla}\vec{j}_\tau = 0$$

$$\partial_t \vec{j}_0 + \vec{\nabla}\cdot(\vec{j}_0\vec{v}_0) = -\vec{\nabla}(\vec{j}_\tau\vec{v}_\tau) - \vec{\nabla}P/M - \rho_0 4\pi\beta\vec{\nabla}\phi/M$$

$$\partial_t \vec{j}_\tau + \vec{\nabla}\cdot(\vec{j}_\tau\vec{v}_0) = -\vec{\nabla}\cdot(\vec{j}_0\vec{v}_\tau) - \rho_\tau\vec{\nabla}U_0/M - \rho_0\vec{\nabla}U_\tau/M - \rho_\tau 4\pi\beta\vec{\nabla}\phi/M$$

$$\partial_t \mathcal{H} + \vec{\nabla}(\vec{v}_0\mathcal{H}) = -\vec{\nabla}(\vec{v}_0 P) - \vec{j}_0 4\pi\beta\vec{\nabla}\phi + -\vec{\nabla}\left(\vec{v}_\tau\left[\rho_\tau U_0 + \rho_0 U_\tau\right]\right) - \frac{\hbar^2}{2}\vec{\nabla}\left(\vec{v}_\tau\left[\vec{j}_0\vec{\nabla}\vec{v}_\tau + \vec{j}_\tau\vec{\nabla}\vec{v}_\tau\right]\right)$$

The solution of the complete set of coupled equations has to be done numerically in one dimension. Integrating our set of equations with the initial conditions of two static slabs moving with uniform velocity towards each other leads to fusion, oscillating compound nuclei and fission depending on the incident energy per particle. For the numerical integration we have used the SHASTA flux corrected transport algortihm[2]. Preliminary results are shown in figure 1. Initially both slabs move with uniform velocity v=0.4c towards each other. A long-range meson-field, dynamically described by the Klein-Gordon equation

$$\left\{-\partial_t^2 + \vec{\nabla}^2 - \alpha^2\right\}\phi = -4\pi\beta\rho_0$$

is computed together with the fluid equations. Apparently large deviations from the initial neutron and proton distribution are created, while the total neutron and proton number is conserved. This first result may show the non-negligible effect of the fluctuation densities on nuclear fluid dynamics. The extension of the model to 2- and 3- dimensions is in progress.

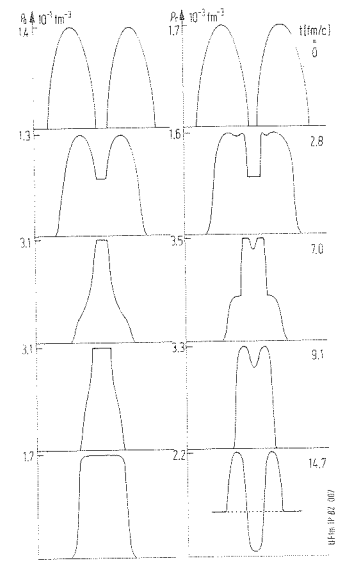


Fig. 1: The mass density $\rho_0 = \rho_n + \rho_p$ and the neutron excess density $\rho_\tau = \rho_n - \rho_p$ are plotted as a function of the space coordinate for different collision times.

References:

[1] J. Theis et al., Bormio Conf. proceedings, Suppl. 25 752, 1982

[2] J. P. Boris et al., J. Comp. Phys. 11, 38, 1973

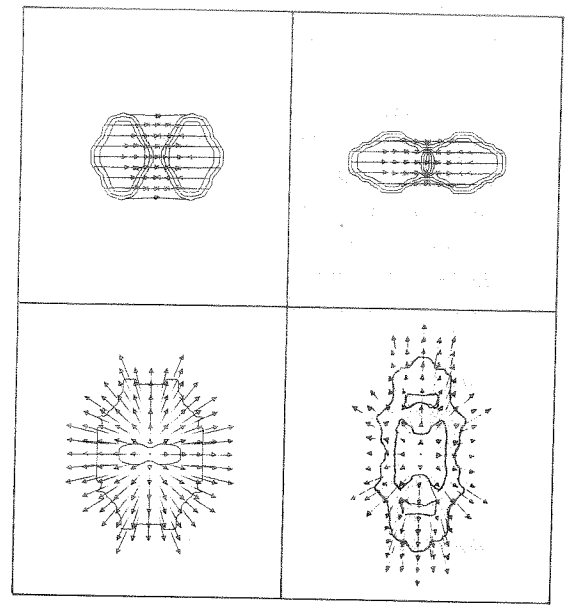
Influence of the Deformation of Nuclei on the Cross Section

B G

D. Barthel, G. Buchwald, G. Graebner, J.A. Maruhn, and W. Greiner
Institut für Theoretische Physik, Universität Frankfurt

Up to now the hydrodynamical calculations of heavy ion collisions[1-2] took only spherically symmetric nuclei into account. If the deformation of the nuclei is included, differences in the resulting matter flow show up in two-dimensional test calculations for different orientations of the nuclei. By taking the average over all possible orientations, however, we expect, that the predicted forward suppression in the cross section can still be observed.

Figure 1 shows contour plots of the density distribution of an $^{238}U + ^{238}U$ collision at 300 MeV/u. The arrows indicate the flow velocity in the equal speed system. In the upper line the initial situation is shown and in the lower line the system after the collision can be seen. It is clearly visible, that the results of the two cases differ strongly in the velocity flow. Thus a considerable difference in the cross sections is expected when doing full 3D-calculations being in preparation now.



[1] G. Buchwald, L.P. Csernai, J.A. Maruhn, W. Greiner, H. Stöcker, Phys.Rev. C24, 135 (1981);
[2] H. Stöcker, L.P. Csernai, G. Graebner, G. Buchwald, H. Kruse, R.Y. Cusson, J.A. Maruhn, W. Greiner, Phys.Rev.C25, 1873 (1982)

Fig.1: Density distribution with flow velocity (indicated by arrows) of $^{238}U + ^{238}U$ (300 MeV/u). On the left side the angle between main axis of symmetry and beam direction is 90° both for target and projectile. On the right side this angle is 0°.

G

Are Solitons Already Seen In Heavy Ion Reactions?

S.Raha and R.M.Weiner
Fachbereich Physik, Universität Marburg

In a recent article[1], Galin et al. have reported their determination of linear momentum transfers in heavy ion reactions with 1 GeV C^{12} beams. They conclude that the amount of linear momentum transfer is limited and from an extrapolation to low energy data, it is found that this limitation effect is reached above a bombarding energy of about 15 MeV/nucleon. So far, no explanation of this very interesting finding has been put forward. We propose that this effect is a consequence of solitary wave formation, an effect predicted very recently[2] to occur exactly in this energy regime i.e. that corresponding to the velocity of sound in nuclear matter.

When a small projectile nucleus hits a large target nucleus, one expects density oscillations to be set up in the target matter. Treating the process in the hydrodynamic scenario, we were able to show in ref.2 that under suitable conditions expected to be met in the nuclear reactions we are discussing here, the dispersive nature of the nuclear fluid plays an important role and when the amount of ordered velocity of the nuclear fluid exceeds the local velocity of sound, a stable pulse of higher density (a soliton) is formed which propagates along the longitudinal direction. The velocity of the solitary wave is bigger than the velocity of sound in nuclear matter and smaller than twice the velocity of sound. Because of the solitary nature of this density pulse, it is expected to be remarkably stable.

Starting from this, the observation of Galin et al.[1] can be easily understood. When the small projectile impinges on the target, it starts slowing down within the target until it is finally stopped. This happens before the projectile has traversed the whole target, because in the energy range below 100 MeV/nucleon, the momentum decay length as discussed by Sobel et al.[3] is of the order of 1.5 fm. Therefore, during the slowdown, there comes a time when the conditions of ref.2 are fulfilled and a soliton is formed. Because of the stability property of the soliton, the flow velocity associated with the soliton would not be thermalized or randomized in any other way. The amount of linear momentum $\Delta p_{\parallel}$ still available is taken over by the soliton and this explains the limitation of $\Delta p_{\parallel}$. The rest of the linear momentum is taken over by the fast emitted particles. Thus, the linear momentum associated with the fast particles must increase with beam energy. Indeed, the independent experiment of Jakobsson et al[4] verifies this expectation.

The observation that the limiting behavior starts at a bombarding energy of about 15 MeV/nucleon is already a strong indication for a hydrodynamic scenario, since it corresponds to a velocity in the range where the velocity of sound in nuclear matter is expected to lie[3]. The facts that (a) hydrodynamics predicted the emergence of solitary waves in this energy region, (b) these waves can apparently explain the effect in discussion and (c) there is no other obvious explanation available, make it very plausible that we are witnessing a soliton event in heavy ion reactions in the intermediate energy range. It follows from this interpretation of the result of ref.1 and from the estimates of the momentum decay lengths of ref.3 that as long as the small projectile - large target combination is used, the limiting behavior should persist upto energies of about 1 GeV/nucleon. For large projectile - large target combinations, hoever, the possibility of strong shock formation[5] must be considered and the role of solitons there, if any, is yet unclear.

Thus, it becomes very important to study theoretically the details of the soliton dynamics with the hope of a better understanding of such nuclear collisions processes. Also, experiments in the sensitive area of 15 MeV/nucleon are clearly necessary in order to check the extrapolation into the lower energy domain of the results of ref.1. Not only would this bring new insight into the important phenomenon of solitons in nuclear matter, but it might also provide much more stringent bounds on the velocity of sound in nuclear matter than those in existence.

This work was supported in part by GSI-Darmstadt.

References

1) J.Galin et al.,Phys.Rev.Lett.48,1787 (1982)
2) G.N.Fowler et al.,Phys.Lett.115B,286 (1982)
3) M.I.Sobel,P.J.Siemens,J.P.Bondorf and H.A.Bethe, Nucl.Phys.A251,502 (1975)
4) B.Jakobsson et al.,Phys.Lett.102B,121 (1981)
5) A.M.Gleeson and S.Raha,Phys.Rev.C21,1065 (1980); Phys.Rev.C26,1521 (1982)

Solitons in Nucleus-Nucleus Collisions near the Speed of Sound

G.N.Fowler
Physics Department, University of Exeter
S.Raha, N.Stelte, R.M.Weiner
Fachbereich Physik, Universität Marburg.

In this work, we investigate a solution of the hydrodynamic equations under conditions which might arise in nuclear collisions at energies close to the speed of sound. At such low energies, a non-relativistic approximation is quite adequate. We follow closely the approach of Glassgold et al[1]. But for a light heavy ion impinging on a heavy target the basic assumption of ref.1, namely that the change in density is of first order of smallness is no longer valid. Here we investigate the ramifications of this very feature and find that under certain circumstances, a new type of motion might be expected consisting of a soliton.

The collision process, in the fluid dynamical framework is described by the following well-known set of equations:

$$\frac{\partial \rho}{\partial t} + \vec{\nabla}\cdot(\rho\vec{v}) = 0 \qquad (1)$$

and

$$\frac{d\vec{v}}{dt} \equiv \frac{\partial \vec{v}}{\partial t} + (\vec{v}\cdot\vec{\nabla})\vec{v} = -\vec{\nabla}\phi \qquad (2)$$

where ϕ is a potential, playing the role of heat function. ρ is the local number density and $\vec{v}$ is the local velocity field.

From ref.1,

$$\phi = \frac{1}{\rho_0}\left[c_1\rho' + c_2\nabla^2\rho' + \cdots\right] \qquad (3)$$

where $\rho' = \rho - \rho_0$ with ρ_0 the equilibrium density. $\sqrt{c_1}$ may be interpreted as the velocity of sound in nuclear matter.

With the change of variables:
$\hat{\rho} = \frac{\rho}{\rho_0}$, $x_i' = \frac{x_i}{c_1}$, $v_i' = \frac{v_i}{\sqrt{c_1}}$, $t' = \frac{t}{\sqrt{c_1}}$ and $C = \frac{c_2}{c_1^3}$,
and dropping the primes, we get

$$\frac{\partial \hat{\rho}}{\partial t} + \frac{\partial(\hat{\rho}v_i)}{\partial x_i} = 0 \qquad (4)$$

$$\frac{\partial v_i}{\partial t} + v_j\frac{\partial v_i}{\partial x_j} = -\frac{\partial \hat{\rho}}{\partial x_i} - C\frac{\partial}{\partial x_i}\frac{\partial}{\partial x_j}\frac{\partial \hat{\rho}}{\partial x_j} \qquad (5)$$

Clearly, we are faced with a preferred direction of flow along the beam axis. Denoting this direction as the x-axis, we may define the following scaling variables

$$\xi = \sqrt{\varepsilon}(x-t),\ y = y,\ z = z \text{ and } \tau = \varepsilon^{3/2}t$$

so that the ξ frame is the slowly varying frame in the x-direction. The higher order derivatives in all directions other than ξ may then be neglected.

We now expand $\hat{\rho}$ and v_i around their equilibrium values:

$$\hat{\rho} = 1 + \varepsilon\hat{\rho}_1 + \varepsilon^2\hat{\rho}_2 + \cdots \qquad (6)$$

$$v_i \equiv v^i = \varepsilon v_1^i + \varepsilon^2 v_2^i + \cdots \qquad (7)$$

After some straight forward algebra, we get[2]

$$v_1^x = \hat{\rho}_1 \qquad (8)$$

and

$$\frac{\partial \hat{\rho}_1}{\partial \tau} + \frac{3}{2}\hat{\rho}_1\frac{\partial \hat{\rho}_1}{\partial \xi} + \frac{C}{2}\frac{\partial^3 \hat{\rho}_1}{\partial \xi^3} = 0 \qquad (9)$$

Equation (9) is the Korteweg-DeVries (KdV) equation which has a solution of the form:

$$\hat{\rho}_1(\xi,\tau) \propto \operatorname{sech}^2\left[\frac{\sqrt{b}}{2}(\xi - b\tau)\right],\ b>0 \qquad (10)$$

Physically, this corresponds to a localized pulse of higher density. This brings to mind the phenomenological picture of nuclear hot spots[3] where the incoming energy might be localized within a small spatial volume. There might also be other signatures. In any case, it should have an energy threshold intimately connected with the velocity of sound in nuclear matter. To see this, one should rewrite eqn.(10) in the x-t variables[2]. Then one finds that if the velocity u of the pulse is less than or equal to $\sqrt{c_1}$, the pulse disappears (width becomes infinite at $u=\sqrt{c_1}$). On the other hand, if $u >> \sqrt{c_1}$, the expansions (6)-(7) break down. Thus the criterion that the effects of a soliton should be concentrated in a certain energy range is characteristic of such solutions.

This work was supported in part by GSI-Darmstadt, BMFT and DFG.

References

1) A.E.Glassgold et al., Ann.Phys.(N.Y.) 6, 1 (1959)
2) G.N.Fowler et al., Phys.Lett.115B, 286 (1982)
3) R.M.Weiner and M.Weström, Nucl.Phys.A286, 282 (1977).

G

Surface Vortex Excitations In Rotating Nuclei

G.N.Fowler
Physics Department, University of Exeter
S.Raha, R.M.Weiner
Fachbereich Physik, Universität Marburg

Local excitations in nuclear matter (hot spots) have been a subject of high current interest[1]. Here we look at the hot spots (h.s.) expected to be generated in reactions induced in heavy ion collisions at intermediate energies where the reaction partners rotate rapidly after separation. The relative stability of h.s. suggest a possible connection with soliton solutions. In the field of planetary physics, the great red spot (GRS) of Jupiter has been explained[2] in terms of Rossby waves[3] in the jovian atmosphere as a consequence of its rotation. We show that even after considering the quantum nature of the nuclear system, this anology persists and leads to the prediction of a new type of nuclear excitation.

We consider rotating nuclei as consisting of a core together with additional nucleons which we refer to as the "atmospheric" nucleons. This leads to the equation for the total angular momentum

$$\vec{L}_{tot} = \vec{L}_{core} + \vec{L}_{at} \qquad (1)$$

The conserved quantity is $\vec{L}_{tot}$; $\vec{L}_{core}$ and $\vec{L}_{at}$ need not be separately conserved. We shall treat $\vec{L}_{core}$ classically, replacing it by its expectation value. Thus we write

$$\tilde{L}_{at,z} = L_{tot,z} - \tilde{L}_{core,z} \qquad (2)$$

where $\tilde{L}_{core,z}$ is no longer quantized.
Then the nuclear atmosphere may be described by going to a rotating coordinate frome with angular velocity ω and using a hydrodynamical description of the Schrödinger equation. The Schrödinger equation for a single nucleon is

$$\left\{\frac{1}{2m}\left[\frac{\hbar}{i}\vec{\nabla} - m\vec{\omega}\times\vec{r}\right]^2 - \frac{1}{2}m(\vec{\omega}\times\vec{r})^2 + \Phi(r)\right\}\Psi = \frac{\hbar}{i}\frac{\partial\Psi}{\partial t} \qquad (3)$$

where $\Phi(r)$ is the nuclear potential. The hydrodynamical description gives

$$\frac{\partial\rho}{\partial t} + \vec{\nabla}\cdot(\rho\vec{v}) = 0 \qquad (4)$$

$$\frac{\partial\vec{v}}{\partial t} + (\vec{v}\cdot\vec{\nabla})\vec{v} = 2\vec{v}\times\vec{\omega} - \frac{\vec{\nabla}}{m}\left[\Phi(r) - \frac{1}{2}m(\vec{\omega}\times\vec{r})^2\right] + \frac{\hbar^2}{2m^2}\left(\vec{\nabla}\frac{\nabla^2\rho^{1/2}}{\rho^{1/2}}\right) \qquad (5)$$

with $\Psi = Re^{i\chi}$, $\rho = R^2$ and $\vec{v} = \frac{\hbar\vec{\nabla}\chi}{m} - \vec{\omega}\times\vec{r}$

The quantum constraint condition is

$$m\oint\vec{v}\cdot d\vec{l} + m\oint(\vec{\omega}\times\vec{r})\cdot d\vec{l} + \tilde{\mathcal{L}}_{core,z} = \alpha_z \qquad (6)$$

with α_z quantized and the contour of integration is in a plane normal to the z-axis. As $\tilde{L}_{core,z}$ need not have integer values, χ cannot be represented by the usual scalar function. There exists a vector $\vec{A}$ such that

$$\Psi = R\exp\left[\frac{i}{\hbar}\int_{\vec{r}_0}^{\vec{r}}\vec{\nabla}\Phi\cdot d\vec{l} + \frac{i}{\hbar}\int_{\vec{r}_0}^{\vec{r}}\vec{A}\cdot d\vec{l}\right] \qquad (7)$$

The second term in χ implies that Ψ depends on the chosen path. (6) and (7) yield

$$m\oint\vec{A}\cdot d\vec{l} + \tilde{\mathcal{L}}_{core,z} = \alpha_z \qquad (8)$$

This quantum problem in the hydrodynamical framework may be solved in the same manner as in the classical problem of the atmosphere of a rotating planet.Under certain circumstances, when the scale of vertical disturbance (z-direction) is small, $\vec{v}$ has components only in the xy plane and may be decomposed into an irrotational and a rotational part:

$$\vec{v}(x,y) = \hat{k}\times\vec{\nabla}\psi(x,y) + \vec{\nabla}\phi(x,y) \qquad (9)$$

$\hat{k}$ is the unit vector in z-direction. Since we are interested only in the rotational part of the velocity, we can set ϕ =0 and obtain the equation

$$\left\{\frac{\partial}{\partial t} + \frac{\partial\psi}{\partial y}\frac{\partial}{\partial x} - \frac{\partial\psi}{\partial x}\frac{\partial}{\partial y}\right\}\left(\frac{\partial^2}{\partial x^2} + \frac{\partial^2}{\partial y^2}\right)\psi + \beta\frac{\partial\psi}{\partial x} = 0 \qquad (10)$$

where $\beta = \frac{2\omega\cos\theta_0}{R_0}$ with θ_0 a mean angle of latitude and R_0 the corresponding radius of curvature. Equation (10) has a plane wave solution $\psi = \psi_0\exp[-i\omega t + i\vec{k}\vec{r}]$ with the dispersion relation $\omega = \frac{\beta k_x}{k^2}$ known as Rossby waves[3]. Thus, we have a solution for $\vec{A}$.

In deep inelastic reactions of heavy ions, the separated nuclei will rotate and there will appear a local velocity on their surface. For certain velocity distributions, we can find soliton-like solutions for ψ moving in the x-direction with a velocity depending on ω and other quantities. This may be the origin of surface h.s. in nuclei. Experimental signatures of these new nuclear excitations could be looked for by investigating the angular and momentum distributions of particles emitted from the surface h.s. If the surface h.s. have vortex lines, the emitted particles should have a non-vanishing velocity in the vortex plane.

This work was supported in part by GSI Darmstadt.

References

1) D.K.Scott,Nucl.Phys.A354,375c (1981)
2) T.Maxworthy and L.G.Redekopp,Nature 260,509 (1976)
3) J.Pedlosky,Geophysical Fluid Dynamics,Lectures in Applied Mathematics,Vol.13,American Mathematical Society, Providence,1971.

Subthreshold pion production, a cooperative process?

J. Knoll, R. Shyam
GSI, Darmstadt

The production of pions or strange particles at beam energies per nucleon below the corresponding nucleon-nucleon threshold are a particularily interesting tool to study cooperative i.e. genuine multi-nucleon effects. In a way these processes are very sensitive to any possible source of energy, be it: i) the initial Fermi motion, ii) the interaction contact among many nucleons which allows the share of a larger amount of energy or iii) the freezing of degrees of freedom in the final state i.e. the production of composite nuclei rather than nucleons.

The suggested single step mechanism (first chance) exploits only the possibility (i) the Fermi motion. It leads to spectra which besides an overall normalization factor are insensitive on the masses A and B of the colliding nuclear system. Recent data, however, show a move of the centroid of the distribution for asymmetric systems[1]. Further on, the model presented in the literature, suffers from an improper energy prescription in the initial state.

Here helps the second mechanism. The more nucleons are in interaction contact to share their energy the more they have a chance to produce a pion, in addition this mechanism shows the desired dependence on the nuclear masses. Further on, the lower the beam energy the more nucleons are required for the production process until close to the absolute threshold the whole nuclei act coherently.

The last mechanism, the final state interaction is a non-negligible source of energy as the freezing a final degrees of freedom implies so to say a heating of the system. This mechanism however requires a coupling of the produced particle with the final configuration. It should reflect itself in the apparent 'temperature' of the spectra and in a correlation between the rate of pion production and the abundancy of composite particles.

All three alternatives can be studied without too much input with respect to special dynamical effects in the nuclear phase space model[2]. The initial aim is to understand the systematics of the data and to establish cross correlations among the various observables prior to a sophisticated microscopic understanding of the reaction mechanism.

Preliminary results of our calculation (Fig. 1) indicate that all three effects discussed above are vital to understand the shape of the pion spectra. The Fermi-motion is seen to be not sufficient to approach the quite flat slopes observed, rather a freezing of degrees of freedom in the final state by about a factor of two gives a good reproduction of the data. Also the dominant contributions come from cases where about four incident nucleons or more share their collision energy in order to produce a pion.

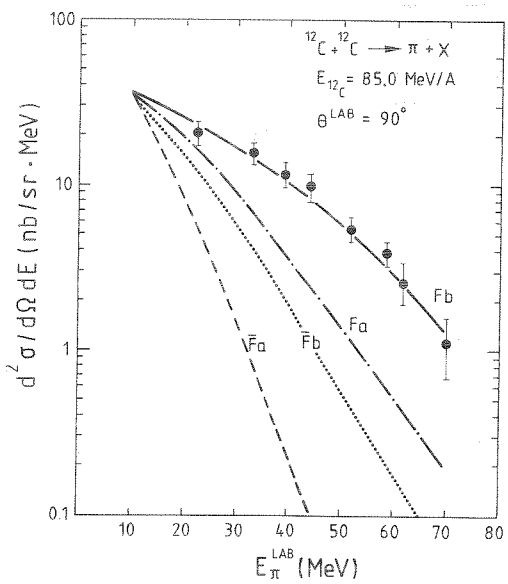


Fig. 1) Pion spectra at 90° laboratory angle as a function of the pion kinetic energy. Data from ref. [32]. The few calculations shown are with (F) and without (F) Fermi folding and a) all nucleons are released as free nucleons, b) the nucleons are frozen to composites such that the kinetic degrees of freedom are reduced by about a factor two.

References:

1) H. Noll et al., contribution to this report

2) J. Knoll, Phys. Rev. C20 (1979)773, S. Bohrmann and J. Knoll, Nucl. Phys. A356 (1981)498

3) B. Jakobsson, Proc. Nordic meeting on Nucl. Physics. Fuglso, Denmark (1982)

G

Effect of Isobars at Finite Temperature in Pion Condensation in ^{16}O

R.K. Tripathi, A. Faessler
Institut für Theoretische Physik, Universität Tübingen

If one wants to observe a possible phase transition to pion condensation in the laboratory e.g. by means of heavy ion reactions, one has to keep in mind, that in such experiments this phase transition will occur in small regions of nuclear matter only and, since the colliding nuclei at such high energies will not remain in their ground states, at a temperature which is different from zero. The effects of finite size and temperature may lead to different critical parameters for the phase transition. It is the aim of this investigation, to perform a self-consistent analysis for the phase transition which takes these effects into account and which treats isobar degrees of freedom, which are an important ingredient for the phase transition explicitly. The quantity of interest in the case finite temperature T is the free energy,

$$F = E - T \cdot S \qquad (1)$$

where E is the energy and S the entropy. The free energy is calculated for the finite nucleus ^{16}O in the normal phase. This means that the nucleons are assumed to occupy the single-particle states of a spherical harmonic oscillator with an occupation probability for the level $|\alpha>$,

$$f_\alpha = \{1 + \exp[(\varepsilon_\alpha - \mu)/kT]\}^{-1} \qquad (2)$$

where the chemical potential is chosen in such a way, that the total number of nucleons $N=\Sigma_\alpha f_\alpha$ .. The single-particle energies ε_α are calculated in the Hartree-Fock approximation assuming π and ρ-meson exchange for the residual interaction. For the condensed phase we allow configurations in a deformed harmonic oscillator in which all protons have spin-up and all neutrons have spin-down[1,2]. In this case we also allow an admixture of Δ-isobar by taking the generalized single-particle state

$$|\alpha> = \{|N_\alpha> + A|\Delta_\alpha>\}/(1+A^2)^{1/2} \qquad (3)$$

where A is the mixing amplitude for the Δ-isobar, which is assumed to be the same for each single-particle state α. For a given density ρ and temperature T we vary A to obtain a minimum for the free energy of the condensed phase F_C minus the free energy of the normal state F_N. For each value of temperature there is a density ρ_C beyond $F_C<F_N$ and the nucleus undergoes phase transition to pion condensed phase. The phase diagram is shown in the figure, where the solid line (line 2) and the dashed line (line 1) represents the results of calculations with and without inclusion of isobar excitations. It should be remarked that for systems which show a small level density at the Fermi surface in the normal phase, a small temperature assists in condensation. In order to observe the thermally assisted pion condensation one should select a nucleus like ^{16}O where the level density at T=0 is low for normal phase but it is high for the condensed phase. The critical density predicted in this calculation should be interpreted with some care, since more realistic residual interactions may lead to much higher critical density[3].

[1] G. Do Dang, Phys. Rev. Lett. 43, 1708 (1979)
[2] R.K. Tripathi, A. Faessler, K. Shimizu, Z. Physik A297, 275 (1980)
A.L. Goodman, R.K. Tripathi, A. Faessler, Phys. Lett. B107, 341 (1981)
[3] W.H. Dickhoff, A. Faessler, J. Meyer-ter-Vehn, H. Müther, Nucl. Phys. A368, 445 (1981

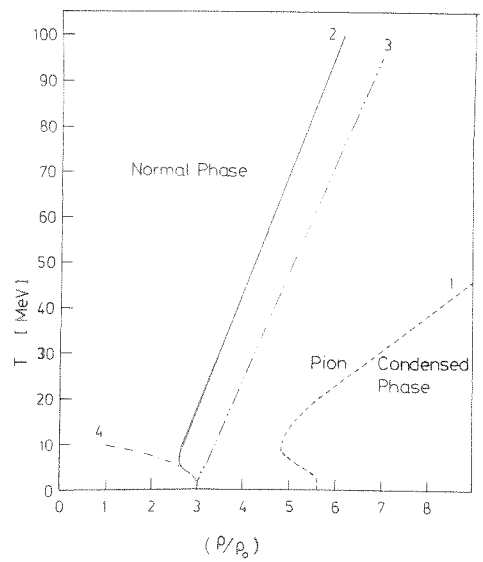


Fig. 1: Phase diagram of ^{16}O. Solid line (line 2) with Δ isobar excitations and dotted line (line 1) for nucleons only.

How strong is the rho-meson exchange in the N-N interaction?

W.H. Dickhoff, A. Faessler, H. Müther
Institut für Theoretische Physik, Universität Tübingen

The possibility of a phase transition to pion condensation in nuclear matter at a density, which is only slightly higher than the normal density, has been discussed in the literature now for some years already[1]. This would mean, that particle-hole states with quantum numbers of the π-meson (T=1, S=1, M=0) would form a collective state which comes down to zero energy[2]. Investigations of screening effects for the renormalization of the effective particle-hole interaction, however, imply that the critical density is probably much higher[3]. Recently it has been suggested[4], that nuclei might be close to rho-meson condensation, which would mean, that a similar phenomenon occurs for ph-states with quantum numbers of the rho meson (T=1, S=1, M=±1). For this investigation it was assumed, that the driving force, the direct ρ-exchange, can be approximated by

$$G_\rho^{ph}(q) = f_\rho^{(q)} \vec{\sigma}_1 \times \vec{q} \cdot \vec{\sigma}_2 \times \vec{q} \vec{\tau}_1 \cdot \vec{\tau}_2 + g' \vec{\sigma}_1 \cdot \vec{\sigma}_2 \vec{\tau}_1 \cdot \vec{\tau}_2 \qquad (1)$$

The coupling constant f_ρ can be related to the $N\bar{N} \to 2\pi$ isovector helicity amplitude, which leads to the so-called strong ρ-coupling. The constant g' is used to simulate exchange terms and short-range correlations. In contrast to this method, we derive the ph-interaction from a realistic NN-interaction which fits the NN-phase shifts[2]. The effects of isobar excitations are taken into account. Using such realistic interactions we do not obtain a phase transition to rho-meson condensation, even if we neglect the screening effect in the ph-interaction[5]. The reason of this discrepancy to the results of ref. 4 can be seen in the figure, where we display the form of $f_\rho(q)$ (see eq. 1) as a function of the transferred momentum q. Results are given for the "strong" rho-exchange (denoted by Höhler-Pietarinen) and for this function as it can be obtained by realistic NN-interactions. One can see that realistic interactions lead to a much weaker f_ρ, even if a one boson-exchange potential with a large ρ-coupling constant or the Paris potential is used. It seems, that NN-phase shifts determine $f_\rho(q)$ quite uniquely to a magnitude which does not allow a rho-meson condensation.

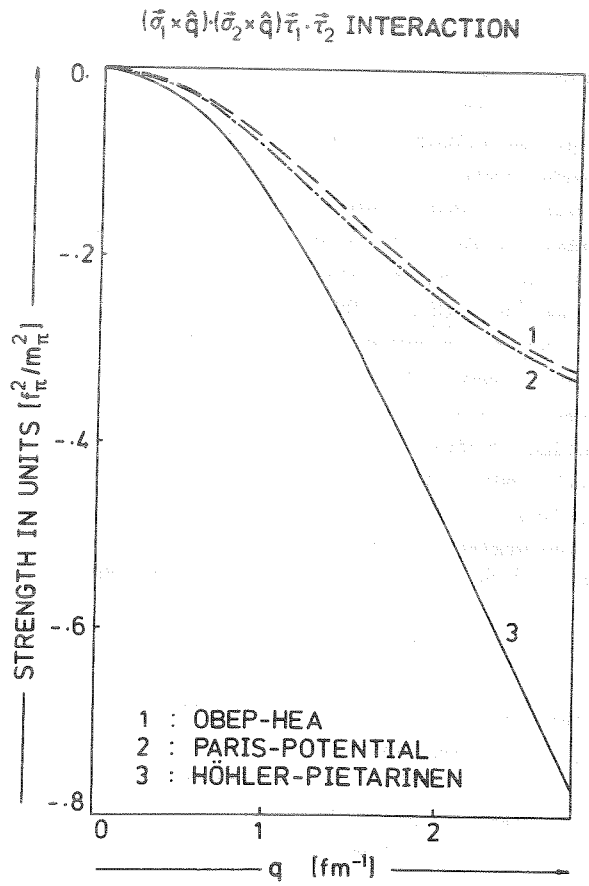


Fig. 1: Strength of effective ρ-meson exchange in nuclear matter as a function of the momentum transfer. While for the curve 3, the strong ρ-exchange was deduced from realistic NN interactions.

[1] G.E. Brown, W. Weise, Phys. Rep. 27C, 1 (1976)
[2] W.H. Dickhoff, A. Faessler, H.J. Meyer-ter-Vehn, H. Müther, Phys. Rev. C23, 1154 (1981)
[3] W.H. Dickhoff, A. Faessler, J. Meyer-ter-Vehn, H. Müther, Nucl. Phys. A368, 445 (1981)
[4] H. Toki, J.R. Comfort, Phys. Rev. Lett. 47, 1716 (1981)
[5] W.H. Dickhoff, A. Faessler, H. Müther, Phys. Rev. Lett. to be published

G

Pion Condensates As Anomalons

G.N.Fowler
Physics Department, University of Exeter
S.Raha, R.M.Weiner
Fachbereich Physik, Universität Marburg

To date, the theoretical explanations of "anomalons" tend to be exotic. In this note, we propose a scenario where the anomalon phenomenon is tied intimately to another property of nuclear matter - namely pion condensate for which there is good theoretical support. Indeed the fact that relativistic heavy ion collisions have not already produced them is in itself curious. We attribute this to the ambiguities associated with the possible signatures of a pion condensate and suggest a common solution to both features. The essential idea is the realization that the pion field outside a nucleus in which a pion condensate exists can have a much longer range than the pion field outside a normal nucleus. This is due to the change in the vacuum state characteristic of nuclei with pion condensates extends up to some distance outside the nucleus.

Outside the nucleus, the pion field π is well described by the chiral symmetric σ model with a spontaneous symmetry breaking through $\langle vac|\sigma|vac\rangle \neq 0$, where σ is a scalar field. Inside the nucleus with a pion-condensate, we have, on the contrary, $\langle vac|\sigma|vac\rangle = 0$ and $\langle vac|\vec{\pi}|vac\rangle \neq 0$. The quantity $\langle vac|\sigma|vac\rangle \equiv v$ must therefore change from inside to outside nuclear matter, so that we must think of v as a function of the space coordinates.

Starting from the σ-model lagrangian (with the usual symmetry breaking term)

$$\mathcal{L} = \frac{1}{2}\left\{\left(\frac{\partial\sigma}{\partial x_\mu}\right)^2 + \left(\frac{\partial\vec{\pi}}{\partial x_\mu}\right)^2\right\} + \frac{\mu^2}{2}\left\{\sigma^2+\vec{\pi}^2\right\} - \frac{\lambda^2}{4}\left\{\sigma^2+\vec{\pi}^2\right\}^2 + c\sigma \qquad (1)$$

we obtain the equation of motion for the σ-field:

$$\frac{\partial^2\sigma}{\partial x_\mu^2} - \mu^2\sigma + \lambda^2\sigma^3 + \lambda^2\sigma\vec{\pi}^2 - c = 0 \qquad (2)$$

Treating σ as classical, we have

$$\frac{\partial^2 v}{\partial x_\mu^2} - \mu^2 v + \lambda^2 v + \lambda^2 v\langle vac|\vec{\pi}^2|vac\rangle - c = 0 \qquad (3)$$

We solve this equation in two different approximations.

(a) In the chiral symmetric σ-model at large γ or in the limit of M_σ, λ large, one has

$v^2 + \langle vac|\vec{\pi}^2|vac\rangle \approx f_\pi^2$ where f_π is the usual pion decay constant. Since this same relation holds also within the nucleus, we assume that this is true everywhere. Then $c = v(-\mu^2 + \lambda^2 v^2)$ and equation (3), in the static limit, becomes

$$\nabla^2 v - \lambda^2 f_\pi^2 v + \lambda^2 v^3 = 0 \qquad (4)$$

(b) The second case is a more conservative one which assumes $\langle vac|\vec{\pi}^2|vac\rangle = 0$ and then $c = v(-\mu^2 + \lambda^2 f_\pi^2)$ In that case equation (3) becomes, again in the static limit

$$\nabla^2 v + \lambda^2 f_\pi^2 v - \lambda^2 v^3 = 0 \qquad (5)$$

Equations (4) and (5) are solved numerically with the appropriate boundary condition, namely $v(R)=0$ where R is the radius of the condensed state nucleus. The other boundary condition is $v \to f_\pi$ as $r \to \infty$. The values for λ^2 and f_π are taken from $\pi\pi$ phase-shift data. Figure 1 shows the solutions for an anomalon of radius $R = 1.75\ m^{-1}$ with $\lambda^2 = 5.63$ and $f_\pi = 125$ MeV. It is seen that in both cases (a) and (b), an appreciable enhancement in the range is obtained which, in principle, can explain the anomalon effect. These considerations explain the larger cross-section. Another property, the metastability, follows automatically since we are faced with a (meta)stable thermodynamic phase. Lastly, the "memory" effect is also easily understood. To produce the condensate phase, a higher than normal density is necessary. Once this is achieved in the first collision, the probability to observe an anomalon in successive reactions is enhanced due to two factors: (1) a higher than normal density already exists and (2) the primary anomalon can survive.

References

(1) For a detailed version, see G.N.Fowler et al., University of Marburg preprint, 1982

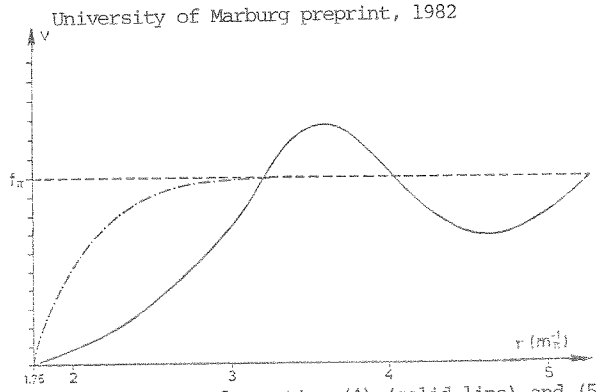


Fig.1. Solutions of equation (4) (solid line) and (5) (dash-dotted line). The curve starts at r=R.

The Heavy Ion Potential and the Increasing Transparency at Intermediate Energies

B G

A. Faessler, S.B. Khadkikar, L. Rikus, R. Sartor
Institut für Theoretische Physik, Universität Tübingen

Collisions between two heavy ions at higher energies between 20 to 200 MeV/A show a reduction of the total reaction cross section with increasing energy[1,2].

The purpose of our work is to explain this reduction of the total reaction cross section starting from a realistic nucleon-nucleon interaction like the Reid soft core potential. We start from the collision of two infinite nuclear matters[3-7]. The two Fermi momenta k_{F_1} and k_{F_2} define the two densities and the two Fermi spheres. The distance of the two Fermi spheres is the average momentum per nucleon K_r. The solution of the Bethe-Goldstone eq. yields a complex reaction matrix $\langle k_1 k_2 | G(W, k_{F_1}, k_{F_2}, K_r | k_3 k_4 \rangle$ which depends on the starting energy, the densities of the two heavy ions $\rho_i(\vec{r}) \alpha k_{F_i}^3(\vec{r})$ and the relative average momentum per nucleon K_r. The energy density $e(k_{F_1}, k_{F_2}; K_r)$ in infinite nuclear matter yields the volume part of the optical potential with real and imaginary part by the local density approximation.

$$U_{Opt}^{Vol.}(R) = E(R;K_r) - E(\infty;K_r)$$
$$E(R;K_r) = \int d^3r\, e(k_{F_1}(\vec{r}), k_{F_2}(\vec{r}); K_r) \qquad (1)$$

The surface contribution has to be calculated in the finite nuclei using the Feshbach expression with collective intermediate states $|\lambda\rangle$.

We use the standard vibrational model formfactor for the giant resonances and the low lying collective vibrations α_μ^λ. The optical potential is then localized and used in a Lippmann-Schwinger equation to describe the heavy ion collision. Fig. 1 shows the energy dependence of the total reaction cross section (square: total potential; crosses: volume part only). The maximum in the reaction cross section found between 10 and 30 MeV per nucleon is essentially due to the surface contribution. The increasing transparency at higher energy is due to a drastic decrease of the real part of the volume potential. At the surface it even becomes slightly repulsive and diverts the relative wave function away from the imaginary part which is increasing with energy. The final reason for the reduction of the total reaction cross section is the decrease of the nucleon-nucleon cross section at higher energies. This is built into the Reid soft core interaction which is the starting point of all our investigations.

[1] R.M. de Vries, J.C. Peng, Phys. Rev. C 22, 1055 (1980)
[2] M. Buenerd et al., Phys. Lett. 102 B, 242 (1981)
[3] T. Izumoto, S. Krewald, A. Faessler, Nucl. Phys. A 341, 319 (1980) and A 357, 471 (1981)
[4] S.B. Khadkikar, L. Rikus, A. Faessler, R. Sartor, Nucl. Phys. A 369, 495 (1981)
[5] A. Faessler, T. Izumoto, R. Sartor, Nucl. Phys. A 359, 509 (1981)
[6] R. Sartor, A. Faessler, S.B. Khadkikar, S. Krewald, Nucl. Phys. A 359, 467 (1981)
[7] R. Sartor, A. Faessler, Nucl. Phys. A 376, 263 (1982)
A. Faessler, L. Rikus, R. Sartor, to be published in Comp. Phys. Comm.

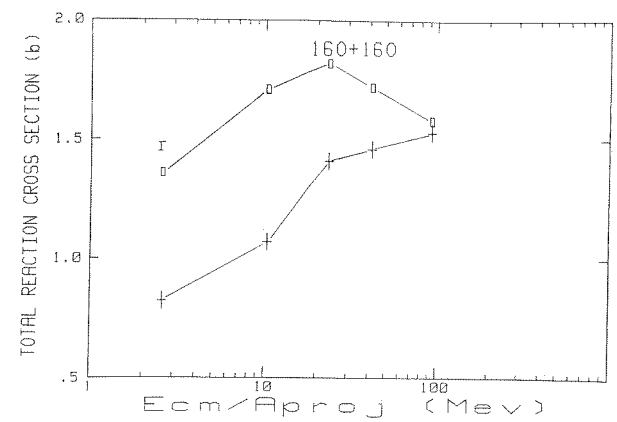


Fig. 1: Energy dependence of the total reaction cross section $^{16}O + ^{16}O$ for the total (squares) and the volume part of the potential.

Compression versus Transparency Effects on the Energy Density in Central Relativistic Heavy Ion Collisions

J.W. Harris and R. Stock
GSI Darmstadt

We used the multinucleon cascade code, developed by J. Cugnon et al.[1], to investigate maximum compressions, energy densities, and the extent of thermalization in symmetric collisions of mass 40 + 40 and 238 + 238. Fig. 1 shows the reaction dynamics for the ^{40}Ar + KCl reaction at 977 MeV/A: the compression ρ/ρ_o, as determined in a sphere of 3 fm diameter about the origin of the cm coordinate system[2], reaches a broad plateau of ca. 2 x 10^{-23}s duration, at about 7 fm/c of elapsed time which corresponds to the end of the interpenetration time for A=40 nuclei. About half of the binary baryon collisions have occured until this time. Fig. 2 gives the compressions for Ca + Ca and U + U as a function of the energy, and also the minimum compression $\rho/\rho_o = 2\,\gamma_{cm}$, expected for an extremely hard equation of state. Obviously the cascade model predicts higher ρ/ρ_o, due to a dynamical pile-up of baryons at mid-rapidity. Compressions rise steeply up to 2 GeV/A reaching values of about 5 for U + U.

The total energy density per fm³ at mid-rapidity is also shown in Fig. 2. It rises steeper than γ^2 up to ca. 2 GeV/A, because of the combined effect of increasing compression and cm energy. Above 2 GeV/A, E ~ γ in the cascade model because of the observed saturation in the compression.

In order to test the applicability of thermodynamical models to the volume of nuclear matter piled up near mid-rapidity, the extent of momentum equilibration was analyzed using the ratio R = $\pi/2$ (mean $|p_{\parallel}|$ per baryon)(mean $|p_{\perp}|$ per baryon)$^{-1}$ for each event studied. <R> → 1 for an equilibrium distribution[3]. Values close to unity were in fact found for the matter inside the high density "core" of the events, at the time of maximum compression, for all energies studied: there is no transparency effect, diluting the midrapidity energy density, predicted by the cascade code up to 5 GeV/A. For the momenta of all the nucleons in the final state, on the other hand, R = 2.0 and 2.65, for U + U at 2 and 5 GeV/A, respectively. It has been shown[3] that this is caused by the surface "corona" part of the intersecting nuclear densities. Even at b → 0 a significant fraction of the nucleons interacts less often than twice; their momenta remain forward-backward enhanced and stay near the fragmentation domains of phase space. The relative effect of this trivial but unavoidable surface transparency goes down like $A^{-1/3}$, towards heavy nuclei. For the interior of the fireball, however, the onset of true transparency should be at E/A ≳ 10 GeV for central U + U collisions.

[1] J. Cugnon et al., Nucl.Phys. A379(1982)553
[2] R. Stock et al., Phys.Rev.Lett. 49(1982)1236
[3] H. Ströbele et al., Phys.Rev. C, April 1983

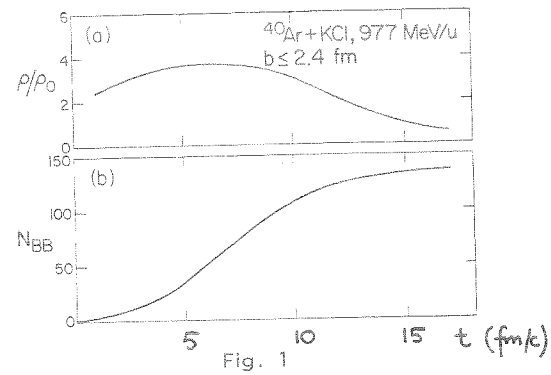


Fig. 1

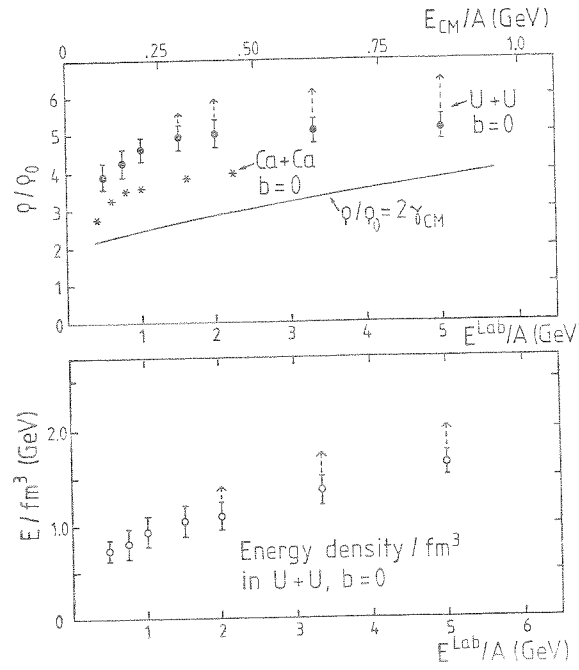


Fig. 2

The Expansion of Hot Nuclear Matter

B. Strack, J. Knoll
GSI, Darmstadt

We discuss the expansion phase of a highly excited and compressed nuclear system as e.g. formed in a high energy heavy-ion reaction. How does such a system disassemble into the various stable nuclei? While temporarily disregarded, the interest in this question has grown recently. Does the abundancy of light fragments like deuterons or alpha particles tell us something about the entropy attained during the reaction or about the nuclear phase diagramm at densities lower than the normal saturation density, i.e. the coexistence of nuclear vapor (nuclei) and nuclear fluid (nuclear matter) and/or about the tensile strength of nuclear matter?

To settle these questions we first reexamined concepts that have been employed so far: these are the chemical equilibrium model[1] and the coalescence model[2]. While initially these models were certainly an aid to understand the systematics of the data we do not see them to allow quantitative predictions. The reasons being manifold. Firstly, they are static concepts, that is they do not include relaxation phenomena and secondly they are only valid in the dilute density limit. However, during the whole expansion the internucleonic distance is smaller than the range of nuclear 'bonds'. Thus, a description in terms of rate equations between nucleons and and light nuclei or their coalesce within a certain momentum sphere gives no explanation of the intrinsic interaction mechanism nor new insight into the reaction dynamics. In terms of quantum mechanics: The different physical channels (N_p, N_n, N_d, ...), as characterized by the number of 'free' protons, neutrons, deuterons ... have a sizeable overlap and are therefore indistinguishable to a high degree! That is to say, during the whole expansion the system is in strong interaction contact and only ultimately it has to examine its tensile strength at each point. Since nuclear binding is of genuine quantum nature, it seems appropriate to study the evolution of the disassembly process by a method that includes wave mechanical effects.

We therefore study the following model scenario: The intital and compression phase (≤to) is supposed to be described by an appropriate model (e.g. cascade model). When the expansion begins (to), the high entropy is generated, we assume the situation to be described by an ensemble of corresponding slater determinants. From thereon (t'to) the expansion of each individual state is described by its one-body evolution (Hartree-Fock) in its own one-body field until it fragments into 'stable' pieces of matter. As compared to ordinary mean field theories at finite temperature which treat the whole statistical ensemble in a single common mean field, here each individual state evolves in its proper one body field. That is to say we account for fluctuations in the one body field, which in turn generates the various forms the system can granulate. Our picture implies that the evolution for t 'to is isentropic and results at the very end of the interactions in strong density fluctuations of the outgoing events.

In our time dependent model we use a saturating Skyrme nucleon-nucleon interaction. Yet we neglect finite nuclear size effects as Coulomb or surface energy and study the behaviour of the one-body wavefunctions while the hot nuclear system is granulating.

The extraction of e.g. d/p ratios are under progress and hopefully can give some insight into the entropy puzzle[3] by learning what phase-space occupation is needed to get reasonable ratios.

Beyond that, we focus our interest on the following question: In which way does the possible coexistence of nuclear vapour and/or fluid give us hints for constructing an equation of state? Taking a fluctuating field description may overcome the unability of a mean field approach in producing an equation of state in the expansion or coexistence phase.[5].

Cluster formation (and further: particle production) at given temperature and pressure up to relativistic energies[4] as well as the phase stability of hot nuclear matter (T≈20 MeV) are native questions of intermediate energy physics.

References:

1) A.Z. Mekjian, Phys. Rev. Lett. 38(1977)640, Phys. Rev. C 17(1978) 1051
2) H. Gutbrod et al., Phys. Rev. Lett. 37(1976)667
H. Sato, K. Yazaki, Phys. Lett. 98B (1981)153
3) P.J. Siemens, J.I. Kapusta, Phys. Rev.Lett. 43 (1979)1487
J. Knoll, L. Muenchow, G. Roepke, H. Schulz, Phys. Lett. 112B (1982)13
4) G. Roepke, L. Muenchow, H. Schulz and M. Schmidt, Phys. Lett. 110B (1982) 21, Phys. Lett. 119B (1982)13
5) P. Bonche, D. Vautherin, Nucl. Phys. A372 (1981) 496

Three Component Fluid Dynamics Applied to Heavy Ion Reactions [BG]

A. Rosenhauer, J.A. Maruhn, and W. Greiner
Institut für Theoretische Physik der Universität Frankfurt
L.P. Csernai
Central Research Institute, Budapest, Hungary

Hydrodynamical models turned out to be able to reveal collective effects occuring in heavy ion reactions, which have been observed in experiment. However, the assumption of immediate local equilibration requiring a short mean free path is only partly fulfilled, whereas most models based on kinetic theory forecast a complete thermalization in the course of the collision as long as the beam energy is not too large. This aspect is taken into consideration in a three component hydrodynamical model[1] by introducing a separate component for thermally excited matter, which is populated by collisions of nucleons belonging to target and projectile component previously.

Under the assumption that the total distribution function can be decomposed into a sum of three thermal distributions and that all nucleons going into the thermalized matter component carry all their momentum and energy with them, a set of hydrodynamical equations is obtained from Boltzmann transport theory.

In fig. 1 the maximum density (full lines) and that of the third component (dashed lines) as a function of the total N-N cross section are plotted at different beam energies. A non-vanishing difference of n_{MAX} and n_{3MAX} indicates that a certain number of nucleons of target and projectile component survive the reaction without having participated in collisions. Thus the limiting case $n_{3MAX}=0$ for $\sigma_{tot} \longrightarrow 0$ corresponds to two noninteracting fluids, while at $n_{MAX}=n_{3MAX}$ a completethermalization has been reached during the reaction, but one should note that n_{MAX} and n_{3MAX} are found at different times as long as the cross section is not too large ($\sigma_{tot} > 60$ mb). Increasing the cross section to infinity the transition from the three component system to conventional hydrodynamics can be observed. For an averaged N-N cross section of 25mb at 0.2 GeV/n, n_{MAX} and n_{3MAX} do not differ essentially, but in contrary to onefluid calculations the maximum density is lowered indicating that the compression stage is governed by a different pressure balance. Fig. 2 shows the time t^* which is necessary to convert 90 % of the nucleons in a central region of the reaction into the thermalized matter component. In contrast to kinetic models, t^* decreases with increasing beam energy for E_{LAB} 0.2 GeV/n, but it has been pointed out[2] that in the one GeV/n energy range the assumption of a thermal distribution for the third component does not apply.

[1] L.P. Csernai et al., Phys.Rev. C26, 149 (1982)
[2] A. Rosenhauer, et al., Nuov.Cim. A71, 215 (1982).

Fig. 1

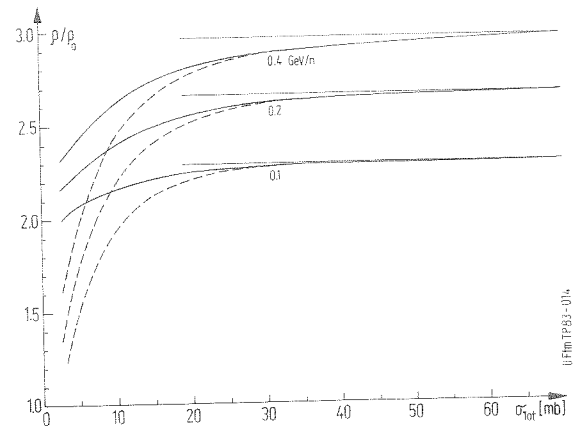
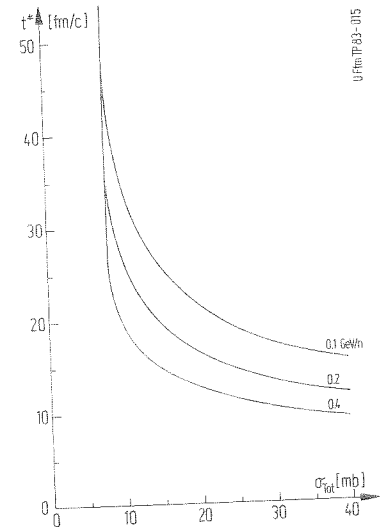


Fig. 2



Momentum Distribution of Nuclear Matter in High Energy Heavy-Ion Collisions

B G

A. Rosenhauer, J.A. Maruhn, W. Greiner
Institut für Theoretische Physik, Universität Frankfurt
L.P. Csernai
Central Research Institute for Physics, Budapest

In this model the process of thermalization is studied in a three-component kinetic approach[1-2]. The reaction of two colliding heavy-ions is described by the development of three momentum distribution functions. Two of those distributions represent the nucleons of target and projectile, while a third component is introduced to take into account the formation of thermalized nuclear matter in the course of the reaction. One may assume that collisions of nucleons belonging to target and projectile component populate the thermalized one. Then, the momentum distribution function of the singly collided nucleons belonging previously to two different Maxwell-Boltzmann distributions can be calculated. This is achieved by computing the partial differential collision numbers:

$$Z_{ik}(v_e) = \int d^3r_1\, d^3r_2\, d\Omega\, |v_1 - v_2|\sigma(\Omega) \times f_i(v_1) f_k(v_2) \times \\ \times 2/[\pi(v_1 - v_2)^2] \times \delta(|v_e - \tfrac{1}{2}(v_1 + v_2)| - \tfrac{1}{2}|v_1 - v_2|) \qquad (1),$$

with the normalization property

$$\int d^3r_e \; 2/[\pi(v_1 - v_2)^2] \times \delta(|v_e - \tfrac{1}{2}(v_1 + v_2)| - \tfrac{1}{2}|v_1 - v_2|) = 2 .$$

The delta function used in (1) reflects the kinematics of elastic scattering, which is assumed to be isotropic in the 0.1 - 1.0 GeV/n energy range. Fig. 1 shows the distribution $Z_{12}(v_e)$ of singly collided nucleons at different beam energies. Up to a few hundred MeV/n the resulting momentum distributions are very close to thermal ones of T = 50-70 MeV. At energies above 0.4 GeV/n a hole in the central region of momentum space indicates that the assumption of immediate equilibration becomes worse. After the reaction has started, the thermal component is rapidly built up. If we consider collisions of nucleons belonging to all three components, the differential collision numbers are given by the sum

$$Z(v_e) = Z_{12}(v_e) + Z_{13}(v_e) + Z_{23}(v_e) \qquad (2).$$

Fig. 2 shows the beam directed and orthogonal momentum distributions computed from (2). The typical features of a symmetric heavy-ion reaction are reproduced in the 0.4 GeV/n energy range. At foreward angles we obtain the characteristic 'shoulder arm' spectrum shape, which means that the invariant cross-sections decrease rather slowly with increasing momenta, while at higher momenta the slope is steep and has an exponential shape. At θ=90 this 'shoulder-arm' behaviour is not observed.

Fig.1

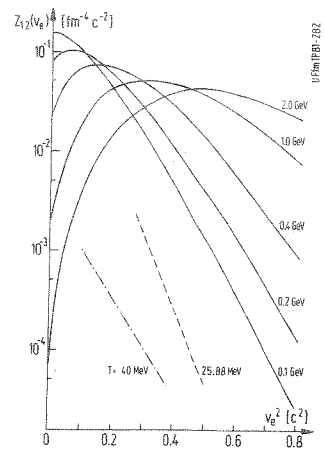


Fig. 1. – Momentum distribution of singly collided nucleons for different beam energies. The straight lines are plotted Maxwell-Boltzmann distributions at temperatures of – – – 25.88 and —·—·— 40.00 MeV, respectively, with arbitrary densities.

Fig.2

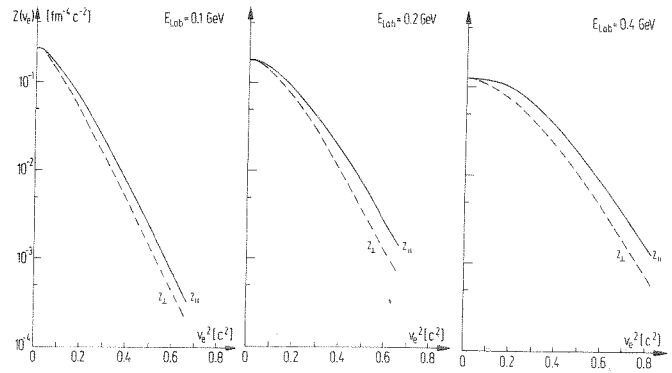


Fig. 2. – Beam directed and orthogonal momentum distribution in the late stage when the third component already exists.

[1] A. Rosenhauer, L.P. Csernai, J.A. Maruhn, W. Greiner; Nuovo Cimento 71A, 215 (1982).
[2] L.P. Csernai, I. Lovas, J.A. Maruhn, A. Rosenhauer, J. Zimanyi, W. Greiner; Phys.Rev. C26, 149 (1982).

Sensitivity of Collective Nuclear Matter Flow to the Equation of State [B]

G. Buchwald, G. Graebner, M. Uhlig, D. Barthel, J.A. Maruhn, W. Greiner
Institut für Theoretische Physik der Universität Frankfurt
J. Theis
GSI Darmstadt
H. Stöcker
Nat. Supercond. Cycl. Lab., East Lansing, Michigan, USA

Nuclear collisions at high energy offer the unique opportunity to explore properties of excited matter. In particular they allow the investigation of the nuclear equation of state $E_c(\varrho)$. One tool for doing this is the analysis of the collective nuclear matter flow resulting from a high energy heavy ion collision. This "global" momentum tensor analysis[1] can be done in 4π detector systems like emulsions, streamer chambers, or the plastic ball. The basic idea is to measure on an event-by-event basis simultaneously all particles and all the associated momenta. Once this information is available, one can transform the physical quantities into the center-of-momentum frame and determine the direction of maximum momentum and energy flow by performing a principal axis transformation. One possible concept proposed to analyze nuclear collisions is the kinetic flow tensor[1]:

$$F_{ij} = \frac{1}{N} \sum_{\nu} \frac{p_i(\nu)\, p_j(\nu)}{2m(\nu)} \qquad (1)$$

which gives the principal axes of the kinetic energy flow.

The most important observables from this analysis are the flow angle $\theta = \arccos([Q_3]_z/Q_3)$ and flow ratio $R_{1/3}=Q_1/Q_3$ with $Q_1>Q_2>Q_3$ the principal values of the flow tensor.

We have calculated the flow tensor resulting from hydrodynamical model calculations at b=o and found a strong dependence of the flow ratio ($R_{1/3}$) excitation function on the nuclear equation of state. Fig. 1 shows a strong enhancement of $R_{1/3}$ at intermediate and low energies $E_{Lab}<300$ MeV/n, where the reaction becomes more sensitive to the collision dynamics. Here, owing to lower temperatures thermal effects are weeker and therefore collective flow effects resulting from nuclear properties and reflecting the equation of state become more important.

For the compression constant K=200 MeV (full line) and $E_c(\varrho) \sim \varrho$ for $\varrho \gg \varrho_o$ $R_{1/3}$ is approximately constant for $E_{Lab} \gtrsim 400$ MeV, whereas for $E_{Lab}<400$ MeV a drastic increase with decreasing E_{Lab} can be observed. K=400 MeV (broken line) yields the same limit for high E_{Lab}, but the enhancement for low energies is even greater than for K=200. This is reasonable because at higher compressibility nuclear matter is pressed to the side much more strongly, resulting in a larger $R_{1/3}$. With K=400 and $E_c(\varrho) \sim \varrho^2$ for $\varrho \gg \varrho_o$ this feature is even more pronounced and further the limiting $R_{1/3}$ for high E_{Lab} is larger than in the previous two cases. Thus Fig. 1 shows that it seems to be possible to obtain information about the nuclear equation of state by measuring the $R_{1/3}$ excitation function at energies below $E_{Lab} \sim$ 600 MeV/n.

[1] M. Gyulassy, K. Frankel, H. Stöcker, Phys.Lett. 110B (1982), H. Stöcker, G. Buchwald, C.P. Csernai, G. Graebner, J.A. Maruhn, and W. Greiner, Nuclear Physics A387 (1982) 205c

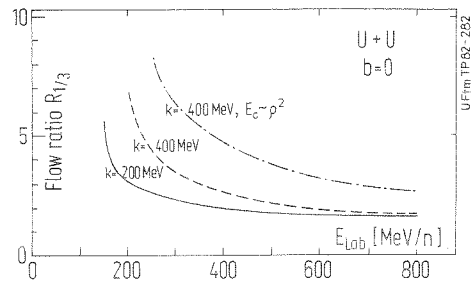


Fig. 1: Dependence of the $R_{1/3}$ excitation function on the shape of the nuclear equation of state.

First Results of a 3-Dimensional Relativistic Nuclear Fluid Dynamical Model [B]

G. Graebner, G. Buchwald, J.A. Maruhn, and W. Greiner
Institut für Theoretische Physik der Universität Frankfurt
H. Stöcker
Nat. Supercond. Cycl. Lab., East Lansing, Michigan, USA
J. Theis
GSI Darmstadt

Energetic heavy ion collisions provide a unique tool for investigating nuclear matter at high densities and temperatures. The nuclear fluid dynamical model describing such collisions has the equation of state (E.O.S.) which describes these properties, as a direct input. This allows the examination of the E.O.S. and its effects on reaction dynamics[1]. At high energies where exotic phenomena such as density isomers and quark matter may be present, it is necessary to do the calculations relativistically.
We have solved the relativistic fluid dynamic equations numerically in 3-dimensions using a modification of the FCT-SHASTA algorithm[2]. Particular care must be taken to ensure numerical stability even at velocities near the speed of light. Further care is required in defining particle and energy densities. In the reference frame used for the calculations ("Lab" frame), matter in motion exhibits an apparent kinematic compression proportional to the local Lorentz-γ. The density of physical interest is the "proper" density, as measured in the local rest frame. It is a non-trivial numerical problem to determine the local rest frame of each calculational fluid cell.
Fig. 1 shows first results for U-U collisions at b=0. The proper density in the collision plane is shown for lab energies of 0.4, 0.8, 1.2 and 2 GeV/n. Since the calculations are performed in the equal speed frame, both target and projectile appear Lorentz contracted in the beam direction. The extent of the kinematic compression is evident in Fig. 2, which shows the proper density and the lab density for E=1.2 GeV/n at an intermediate time. Note that the matter in the compressed region in the middle is at rest, and hence shows no difference between lab and proper densities. The third part of Fig. 2 shows the nuclear surface at this time. Note that it is as yet undisturbed by the compression zone.
Densities attained in the compressed region in the 3-D calculations are somewhat lower than those determined from the Rankine-Hugoniot equations, largely because of the additional spatial degrees at freedom. Temperature values are comparable.
Since density and temperature distributions are not directly observable in experiment, it is necessary to calculate quantities such as spectra or kinetic flow tensors.
These calculations are in progress.

[1] J.A. Maruhn, W. Greiner, "Relativistic Collisions: Theoretical Models", Heavy Ion Science Vol.2, Ed.D.E.Bromley in press
[2] J.P. Boris and D.L. Book, J.Comp.Phys. 11 (1973) 38

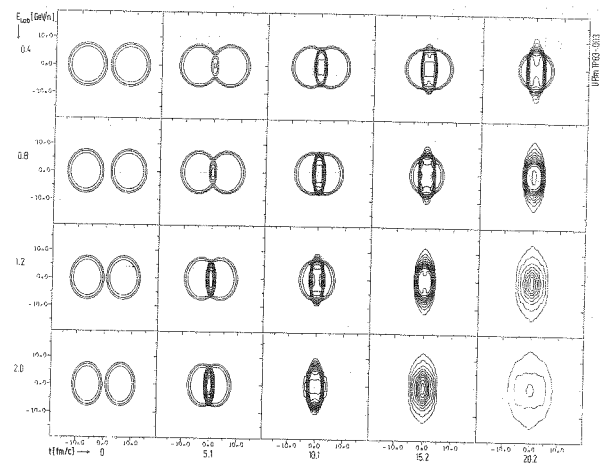


Fig. 1: Time development of reaction plane density for $^{238}U+^{238}U$ at E=0.4,0.8, 1.2, and 2.0 GeV/n and b=0.

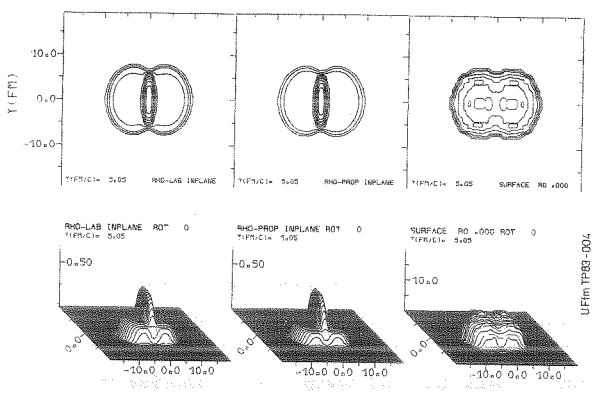


Fig. 2: Reaction plane densities and nuclear surface for $^{238}U+^{238}U$ at E=1.2 GeV/n, t=5,05 fm/c.

B G

Double Shocks in Relativistic Nucleus Nucleus Collisions

C. Graebner, J.A. Maruhn, and W. Greiner
Institut für Theoretische Physik der Universität Frankfurt
H. Stöcker, and H. Kruse
Nat. Supercond. Cyclotron Lab., East Lansing, Michigan, USA

Although the existence of shock waves in the region of a phase transition in nuclear matter has been discussed a number of times[1-4], there are still interesting aspects to be investigated. In particular, the question arises whether a density isomer in nuclear matter reveals a characteristic signature in the behaviour of shock waves, e.g. the appearence of double shocks.

We have investigated a schematic equation of state (EOS) for nuclear matter (Fig.1) with a second minimum at relatively high density. The thermal energy is taken to be that of a non-relativistic fermi gas. In the schematic shock model, a slab symmetry is assumed for two colliding nuclei and the relativistic Rankine-Hugoniot equation is solved for the state variables behind the shock front(s).

The density and temperature behind a single shock wave are shown as a function of bombarding energy by the solid lines in Fig.2.

In the region indicated by the arrows, a single shock wave is not stable because the shock velocity, β_s, decreases as a function of density. Here one finds two shock waves[5]. The first compresses the matter to the state corresponding to the local β_s maximum, indicated by the lower dashed line in Fig. 2, and is followed by a second shock wave which compresses the matter from this intermediate state to the isomeric state indicated by the upper dashed line. For a given bombarding energy, this double shock condiguration is stable, with growing spatial regions of intermediate as well as isomeric density, if the second shock does not overtake the first. Note that such a double shock exists as well if the Maxwell construction is used in the phase transition region because β_s still decreases with ρ

In addition to the schematic shock model, the relativistic fluid dynamical equations were solved numerically in one dimension for this EOS. The values of ρ and T behind the shock front are in excellent agreement with the shock model, as indicated in Fig. 2. In particular, the double shock configuration, with growing regions of both densities, is found in an appropriate energy region.

The density and temperature behind the second shock front are considerably higher than behind the first. However the doubly shocked zone represents only a fraction of the matter present so that the experimental manifestation of the double shock will be a smearing out of threshol phenomena, e.g. pion emission, associated with density isomer.

[1] J. Hofmann, H. Stöcker, U. Heinz, W. Scheid, and W. Greiner, Phys.Rev.Lett.36 (1976) 88
[2] V.M. Galitskii, and I.N. Mishustin, Phys.Lett. 72B (1978) 285
[3] J. Hofmann, B. Müller, W. Greiner, Phys.Lett. 82B (1979) 195
[4] H. Kruse, W.T. Pinkston, W. Greiner, J.Phys.G8 (1982) 567
[5] G.E. Duvall and R.A. Graham, Rev.Mod.Phys. 49 (1977) 523

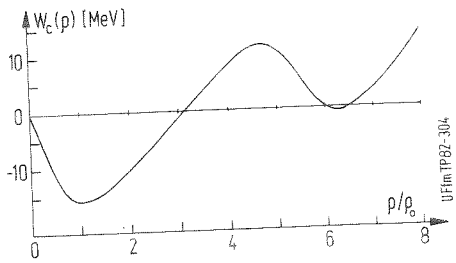


Fig. 1: Compressional energy per particle as a function of density

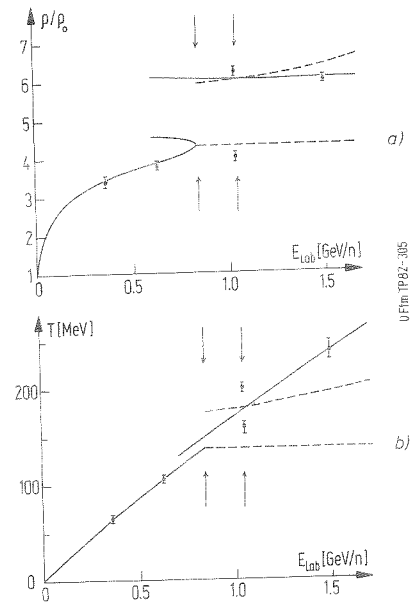


Fig. 2: Density (a) and temperature (b) after single shock (solid line) and double shock (dashed line). Arrows delimit double shock region and points are fluid dynamical solutions

Relativistic Nuclear Fluiddynamics Coupled to Classical Meson Field

J. Theis[+], G. Graebner, G. Buchwald, J. Maruhn and W. Greiner
[+]GSI Darmstadt
Inst. für Theor. Physik, Johann-Wolfgang-Goethe Universität, Frankfurt

For the purpose of studying relativistic heavy-ion collision we already developed a theory of relativistic nuclear fluid dynamics coupled to classical meson fields[1]. The equations of motion simply correspond to baryon conservation and the equations for baryon momentum and energy, respectively:

$$\partial_t(\gamma\rho) + \vec{\nabla}(\vec{u}\gamma\rho) = 0$$

$$\partial_t\vec{H} + \vec{\nabla}\cdot(\vec{u}\vec{H}) = -\vec{\nabla}(P_n + P_{therm}) - g_v\gamma\rho\vec{\nabla}V_0' + g_v\vec{u}\gamma\rho\vec{\nabla}\vec{V}' + m_s^2\bar{\phi}\vec{\nabla}\phi'$$

$$\partial_t h + \vec{\nabla}(\vec{u}h) = g_v\partial_t(V_0'\gamma\rho) - m_s^2\bar{\phi}\partial_t\phi' - g_v\vec{u}\gamma\rho\partial_t\vec{V}' - g_v\vec{u}\gamma\rho\vec{\nabla}V_0' + g_v\gamma\rho\vec{\nabla}\vec{V}' - \vec{\nabla}(\vec{u}P_{therm}) \qquad (1)$$

In addition we have the Klein-Gordon equations governing the time evolution of the meson fields:

$$(-\partial_t^2 + \vec{\nabla}^2 - m_s^2)\,\phi' = -m_s^2\bar{\phi}(\rho)$$

$$(-\partial_t^2 + \vec{\nabla}^2 - m_v^2)\,V_\mu' = -m_v^2(1,\gamma\vec{u})\bar{V}_0(\rho) \qquad (2)$$

For the first we only consider the mean meson fields. The temperature dependence is incorporated within the thermal pressure, taken from a nonrelativistic Fermigas model:

$$P_{therm} = \alpha E_{therm} \quad ; \quad \alpha = 2/3 \qquad (3)$$

Integrating numerically the equations of motion (1) with initial conditions of two static slabs moving with uniform velocity towards each other leads to fusion, oscillating compound nuclei and fission depending on the incident energy per particle. Fig. 1 shows the essential features of the model for colliding slabs. The reaction typifies a deep inelastic process in which the system is so much heatched up in the shock region that it will not form larger clusters after the collision process, but expands as a dilute Fermigas. The maximum compression $\rho/\rho_{eq} \sim 3.7$ is relatively small since the model yields a stiff equation of state ($\kappa \approx 540$ MeV). Table 1 shows the maximum compression and thermal energy for different collision processes; these results are in agreement to shock calculations.

Table 1

System	v/c	$(\rho/\rho_{eq})_{max}$	$(E_{therm})_{max}$ [MeV]
Ne-U	0.6	2.62	86.
Pb-U	0.6	2.66	85.
U -U	0.6	2.71	85.9
Ne-U	0.8	3.72	325.
Pb-U	0.8	3.67	329.
U-U	0.8	3.74	330.

A more consistent treatment of the temperature dependence can be obtained from Walecka's mean field theory[2], yielding α (eq. 3) as a function of density ρ and temperature T (see Fig. 1). The extension of the numerical calculations to this $\alpha(\rho,T)$ is in progress.

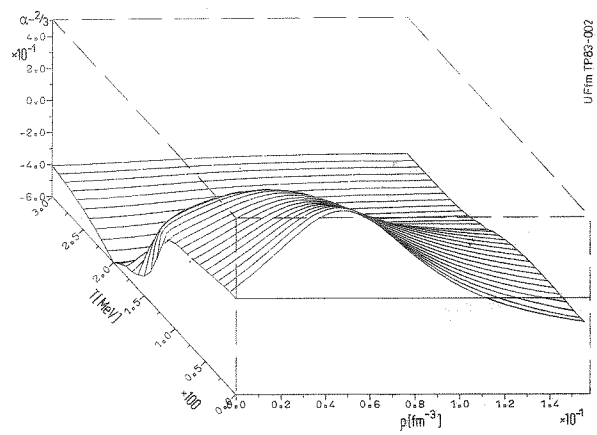


Fig. 1: The density $\rho(t,z)$ is shown for a P-U slab collision with $\beta = 8$.

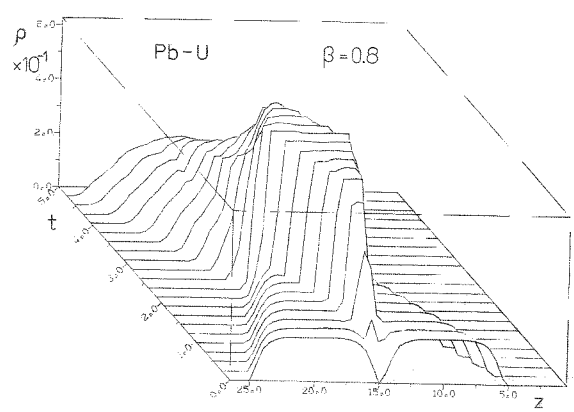


Fig. 2: $\alpha = P_{therm}/E_{therm}^{-2/3}$ is shown as a function of density ρ and temperature T.

References:

[1] J. Theis et al., Bormio Conf. proceedings, Suppl. 25,752, 1982
[2] J.D. Walecka, Phys. Lett. 59B, 109, 1975

Multiparticle Production in Hadron-Nucleus Collisions Around 100 GeV

G

W. Q. Chao, M. K. Hegab and J. Hüfner

Institut für Theoretische Physik, Universität Heidelberg

How does an excited hadron interact with a nucleon? The answer can only be found in hadron-nucleus collisions: Because of relativistic time dilatation the projectile hadron, which has been excited after colliding with one nucleon, does not decay before it scatters by another nucleon of the same target nucleus. Quite a number of experiments have been done and a number of theories proposed. The present work is a kind of review. We analyse data from different experiments under the same conditions and evaluate various theories with the same input data.

The number n of shower particles ($\beta = v/c > 0.7$) and their rapidity distribution are investigated as a function of the type of incident hadron (p, π, K, $\bar{p}$) its energy E and as a function of the number ν of struck nucleons. We propose parametrizations, e.g. for the mean multiplicity $\bar{n}^{hA}(E, \nu)$ of shower particles for hadron-nucleus (hA) collisions a linear one

$$\bar{n}^{hA}(E,\nu) = n(E)\left(1 + \alpha(\nu-1)\right)$$

and for their mean rapidity a logarithmic dependence

$$\bar{\eta}^{hA}(E,\nu) = \eta_0(E) - \beta \ln \nu .$$

The parameters α, β (and several more) which describe the effects of multiple scattering are found to be independent of the type of hadron and the energy E. Fig. 1 shows a typical result. It exhibits well the linear dependence in ν. But different experiments give different values for the slopes. We conclude $\alpha = 0.5 \pm 2$. We don't understand these large experimental discrepancies. The value β in eq. (2) is found to be $\beta = 0.7 \pm 0.2$.

Although the theoretical approaches are based on very different assumptions (like hydrodynamics, partons or valence quarks), they often predict the same functional dependence in ν. Therefore at the moment the situation in multiparticle production is unclear. We are even not sure about the correct physics. A few basic assumptions common to most approaches seem to suffice to reproduce experiments.

As an example we discuss the predictions of two extreme approaches: In the collective tube model, the "tube" of ν target nucleons are assumed to act as one massive nucleon. The properties of this collision with incident energy E are equivalent to hadron-nucleon collisions at the energy νE. This theory predicts $\alpha \simeq 0.12$ and $\beta = 0.5$ and is probably excluded by experiment. At the other extreme one has the two-fireball model: Hadron-proton collision leads to two fireballs, which decay into mesons. The collision between a hadron and ν target nucleons leads to one projectile-like fireball and ν target-like fireballs. The decay properties of all fireballs are the same as in the hadron-nucleon case. This theory predicts $\alpha = \beta = 0.5$ and is compatible with present day experiment.

An interesting property may be worth mentioning. The inelasticity coefficient $\varepsilon(\nu)$, i.e. the fraction of the total energy which is contained in the produced particles is nearly independent of the number ν of collisions. To say it simply: The projectile hadron cannot be multiply excited.

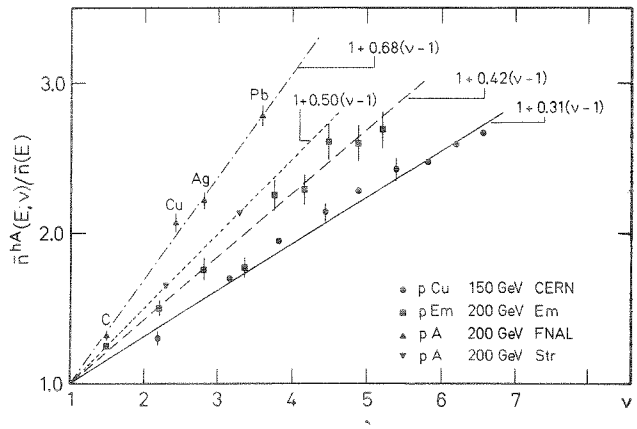


Fig. 1: The normalized mean multiplicity as a function of ν for proton nucleus collisions at 150 and 200 GeV. The results of four different experiments are displayed.

A Model for Multiplicity Distributions in Hadron-Nucleon and α-α Interactions at Very High Energies

H. J. Pirner and W. Q. Chao
Institut für Theoretische Physik, Universität Heidelberg
and
Max-Planck-Institut für Kernphysik, Heidelberg

The recent data on He^4-He^4 collisions at a c.m. energy of 125 GeV or $S_{NN} \approx 31$ GeV[1] have advanced a new step in multiparticle production phenomena. Can theoretical models which agree with hadron-nucleon data explain the nuclear data[2]. We assume that for h-N collisions two color polarized superclusters form and break up into final state hadrons. We emphasize the importance of a microscopic model in order to assess whether a quark gluon plasma can be formed. The model constructed in ref. 2 gives a constant ratio, $d/\langle n\rangle$, of the dispersion over the mean $\langle n\rangle$ of the multiplicity distribution which is an essential feature of multiparticle production. We obtain

$$d/\langle n\rangle \rightarrow \frac{1}{\sqrt{2}}\sqrt{(1-p)/1+p)}$$

with p as the probability that one $(q\bar{q})$ cluster breaks up into two subclusters by the creation of quarks. The so obtained probability p = 0.25 is consistent with QCD estimates for the $p_\perp$ distribution of hadrons.

In α-α collisions the average number of produced superclusters is bigger than in hadron-proton collisions. It equals the number of wounded nucleons in the α-α interaction. As a simple approximation we then assume that the final pion multiplicity distribution results from the independent decay of the formed superclusters. Depending on the impact parameter of the two nuclei different physical situations are possible (Fig. 1):
a) a single nucleon collides with a row of nucleons,
b) two or more independent collinear collisions take place and c) many (≥ 2) projectile nucleons collide with many (≥ 2) target nucleons in one row ("high density" events). The probabilities for these different events are calculated.

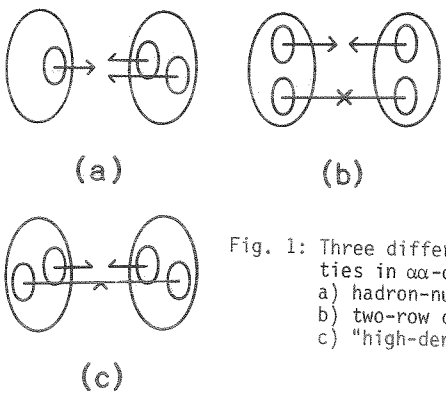


Fig. 1: Three different possibilities in αα-collisions:
a) hadron-nucleus type,
b) two-row contributions,
c) "high-density" events.

We get for $\pi R^2(NN) = \sigma_{NN}^{in} = 30$ mb.
a) N-α $w_a = 60\%$
b) 2 row: $w_b = 30\%$
c) "high density": $w_c = 10\%$

So 40% of the reaction cross section are of different origin than N-α collisions. Corresponding to a geometrical picture of NN-scattering we take the minimal separation of the two rows equal to their diameter 2R. Therefore, two-row events will be also dynamically independent if nothing unusual happens to color-color correlations. We are left with 10% of the cross section where a new domain of hadronic matter may be investigated. Clearly larger nuclei are needed to investigate this problem more deeply.

On the average we find the mean number of participants

$$\bar{N}_{\alpha\alpha} = \sum_{\nu\,\mu}(\nu+\mu)W(\nu,\mu) = 3.1$$

which is compatible with the number given by the traditional model $\bar{N}_{\alpha\alpha} = 8 \cdot \sigma_{p\alpha}/\sigma_{\alpha\alpha}^{in} = 3.2$. Due to the independent decay of the formed superclusters as in h-p collisions we obtain the negative particle multiplicity.

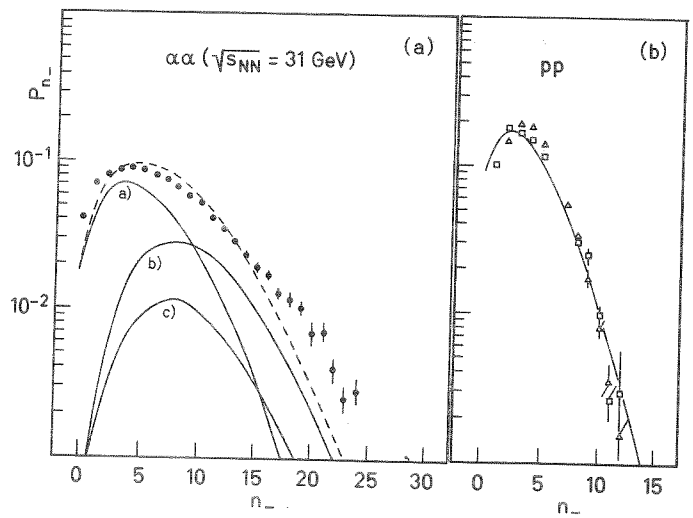


Fig. 2: Negative multiplicity distribution in αα and pp collisions (a, b, c as in Fig. 1)

The contribution from two independent rows is much wider than the N-α contribution, which explains the big difference between pp and αα distributions. Comparing the total theoretical α-α multiplicity distribution with the data, the agreement is rather satisfactory, which supports the multiple collision model.

[1] CERN-Heidelberg-Lund Collaboration, CERN-EP/81-61
[2] W.Q.Chao and H.J.Pirner, Z. Phys. C Particles and Fields 14 (1982) 165-169

Influence of Isospin Conservation on Particle Spectra [B G]

B. Müller and J. Rafelski
Institut für Theoretische Physik der Universität Frankfurt

Isospin conservation influences the form of quantum spectra as well as the abundance of pions produced in highly energetic reactions. We have quantitatively illustrated this influence on a fireball model of $\bar{p}p$-annihilation at moderate energies. Quite surprising agreement with experiment is found. We note that similar effects may be important in particle emission from relativistic nuclear reactions.

Our interest in the proton-antiproton system, and its annihilation channel in particular, is motivated by the observation that the annihilation provides a "central" trigger for the $\bar{p}p$-reaction, and we may assume that all primary particles originate in a finite common volume. Furthermore, the known exponential behaviour of the particle spectra from $\bar{p}p$-annihilations suggests the use of the canonical ensemble for the description of the central fireball. We implement total energy and momentum conservation only on average while isospin will be conserved exactly.

In order to correlate the reaction volume of a hypothetical annihilation fireball with the centre-of-mass energy, $\sqrt{s}$, we assume a constant energy density $4B = s/V$, where the bag constant, $B = 59.5$ MeV/fm^3, is taken from fits to hadronic spectra.

The particle spectra are obtained by considering the quantity

$$n_k^i = -\frac{\partial}{\partial(\beta\omega_k^i)} \ln\left(\mathrm{Tr}_{I,E}\, e^{-\beta H}\right) = -T\frac{\partial}{\partial\omega_k^i} \ln Z_I^E$$

to be the average number of particles of sort i, energy $\omega_k(m_i)$ in a system coupled to total isospin I and omitting the one-particle states (indicated by the index "E"). The trace over all states of given isospin symmetry is performed by a projection formalism in the SU(2)-isospin group space[1].

In the Figure we show the effective primary pion temperature (i.e. the slope parameter from a local fit to the spectrum) as a function of the pion energy. Without isospin projection, the Bose-Einstein (B-E) distribution function fits almost exactly and would lead to a slope of 160 MeV, the input temperature at which the pions are produced. After isospin projection, the spectra are found to deviate strongly from the Bose distribution. In particular, we do not find the "condensation" enhancement at low energies. This leads to a high apparent temperature at low pion energies in agreement with experimental findings in several exclusive channels.

By taking a Maxwell-Boltzmann (M-B) distribution function for the temperature fit (i.e. taking the logaritmic derivative of the spectrum) a systematically lower temperature is found when isospin is conserved. This indicates that some contribution from the condensation terms survives the isospin projection. The average temperature, after weighting the temperature function with the spectrum, turns out to be about 145 MeV. This is again in qualitative agreement with experiments that single out the annihilation channel in $\bar{p}p$-reactions.

[1] B. Müller and J. Rafelski, Phys.Lett. 116B, 274 (1982)

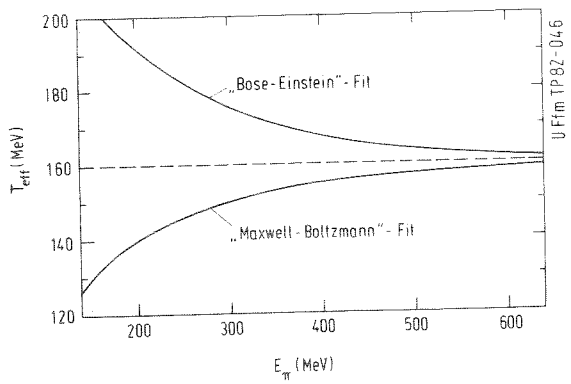


Fig.: Slope parameter (temperature) of primary pions as function of pion energy assuming Bose-Einstein (B-E) or Maxwell-Boltzmann (M-B) spectral forms for isospin projected spectra. Without projection the slope parameter is 160 MeV for the Bose-Einstein form.

Mean Field Theories of Nuclear Matter at Low and Intermediate Temperatures

B G

M. Uhlig and W. Greiner
Institut für Theoretische Physik, Universität Frankfurt
C.S. Warke
Tata Institute for Fundamental Research, Bombay

The recent field theoretic models are used to compute the thermodynamic quantities energy density, pressure and entropy in the temperature and density range of interest to relativistic heavy ion reactions (RHIC).
The basic Lagrangian has the form:

$$L = -\bar{\Psi}\,(\gamma_\lambda \partial_\lambda + M)\,\Psi - 1/2*\left[(\partial_\lambda \phi)^2 + m_s^2 \phi^2\right]$$

$$- 1/4\, F_{\lambda\mu} F_{\lambda\mu} - m_v^2\, V_\lambda V_\lambda + i g_v\, \bar{\Psi}\gamma_\lambda \Psi\, V_\lambda$$

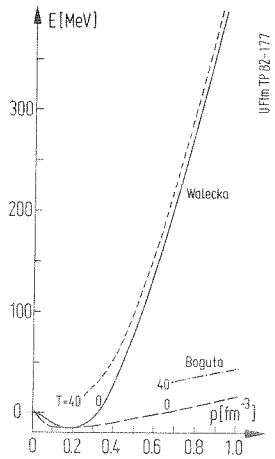
$$- 2 g_s\, \bar{\Psi}\Psi\, \phi - (B/3\, \phi^3 + C/4\, \phi^4)$$

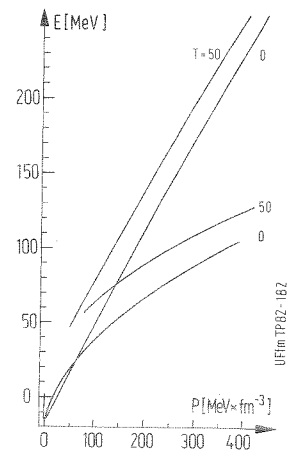
with $F_{\lambda\mu} = \partial_\lambda V_\mu - \partial_\mu V_\lambda$ and $\hbar = c = 1$.

Ψ is the nucleon field, ϕ the self-interacting scalar field and V_λ represents a neutral vector field ; M is the nucleon mass, m_s, g_s the scalar mass and coupling constant, m_v, g_v the vector mass and coupling strength. If one switches off the self-interaction of the scalar mesons (B = C = 0) and uses $c_s = m_s/g_s = 16.34$ and $c_v = m_v/g_v = 13.99$ one gets the Walecka model[1]. If one considers the self-interaction one has to readjust the coupling to the nucleon fields to produce the proper bulk properties of nuclear matter. To take $B/Mg_s^3 = 0.471$, $C/g_s^4 = 9.1$ and c_s=8, c_v=2 was one choice of Boguta and Bodmer[2].
The fields that interact with the nucleons, a system of Dirac particles, are treated classically. The theoretical formalism is based on the variational ansatz for the Gibb's free energy. The final expressions of the thermodynamic quantities are identical to those derived from the finite temperature field theoretic propagator method[3].
In order to gain insight into the parametrization of these quantities with the view to use them in hydrodynamic model calculations of RHIC, we studied the low temperature limit and expanded the Fermi-integrals. The limiting criterion of the expansion can be expressed to the following: for a given density ρ the temperature T must be smaller than a critical T (hence low-T expansion) or for a given T ρ must be larger than a critical ρ. In effect, the plots of the thermodynamic quantities for higher T begin only at a certain ρ and cannot be continued to smaller ρ.
With the two adjustable parameters of the Walecka model c_s , c_v it is only possible to fit the binding energy $E_{Bind}(\rho_0)$. The compressibility of nuclear matter turns out to be much too large (≈550 MeV). Using the additional parameters of the Boguta model the compressibility can be adjusted to 150 - 250 MeV and another surface property can be fitted. Due to the strong difference in the bulk modulus $E_{Bind}(\rho)$ looks quite different for the two models (Fig. 1). The same holds for the pressure $p(\rho)$ or $E(p)$, which is given in Fig. 2. The Boguta equation of state is much softer.

[1] J.D. Walecka, Ann.Phys. 83, 491 (1974)
[2] J. Boguta, A.R. Bodmer, Nucl.Phys. A292, 413 (1977)
[3] J.D. Walecka, Phys.Lett. 59B, 109 (1975)
S.A. Chin, Ann.Phys. 108, 301 (1977)
R.L. Bowers et al., Phys. Rev. D15, 2125 (1977)
R.A. Freedman, Phys. Lett. 71B, 369 (1977)

Fig.1: Binding energy versus density in the Walecka and Boguta model. Temperatures in MeV.
Fig.2: Binding energy versus pressure in the Walecka (upper) and Boguta model (lower curves).





Entropy Production in Heavy Ion Collisions

B G

M. Uhlig and W. Greiner
Institut für Theoretische Physik, Universität Frankfurt
C.S. Warke
Tata Institute for Fundamental Research, Bombay

The low temperature expansion of the equation of state[1] is used to calculate thermodynamic quantities in a temperature and density region of interest to relativistic heavy ion collisions (RHIC).

The theoretical framework can be used to study two points: the difference between the Walecka and Boguta equation of state and the temperature dependence of both models.

The differences in all thermodynamic quantities are found to be considerably. Especially that the amount of entropy produced in a RHIC depends on the equation of state is an interesting result. Because of the softer equation of state (compare[1]), the Boguta model predicts larger values of specific entropy (Fig. 1). In that context it will be interesting to compare with the values one tries to extract from the proton to deuteron ratio. There is a vivid discussion[2] about the experimental determination of entropy values. At the moment the associated uncertainties do not allow to favour the Walecka or Boguta values.

Fig. 2 shows curves of constant specific entropy in a ρ-T diagramm. These curves offer information on the expansion path of a HIC, because the time development of the system in the expansion stage is believed to follow lines of constant entropy. The full lines are the results for the Walecka model. The dash-dotted lines give T(ρ) for a nonrelativistic noninteracting Fermigas in a low-T expansion, whereas the dashed curves are the ultrarelativistic noninteracting Fermigas results in low-T expansion. Comparing the different limiting cases with the Walecka model, one can see that for higher densities the Walecka model behaves like an ultrarelativistic noninteracting Fermigas, whereas for $\rho < \rho_0/2$ it tends towards a nonrelativistic Fermigas, which is understandable because the effective nucleon mass $M^* \to M$ for $\rho \to 0$ and $M^* \to 0$ for $\rho \to \infty$.

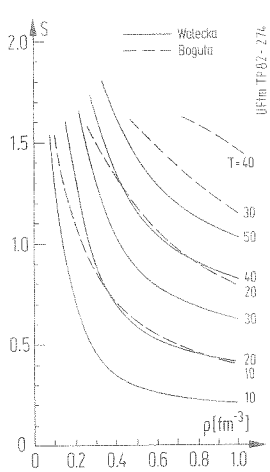
The same conclusion can be drawn if one studies the ratio $p_{therm}/\varepsilon_{therm}$ (Fig.3), which gives 2/3 in the nonrelativistic limit and 1/3 in the ultrarelativistic case. The Walecka curve quickly approaches the ultrarelativistic value 1/3 for $\rho \geq 5\rho_0$, where on the other hand a compression of $10\rho_0$ is necessary to get to the same value in the Boguta model. The low density limit of both models is the nonrelativistic noninteracting Fermigas. However, only for the Boguta model the value 2/3 is a good estimate in the low density range. Because the high density asymptotic value of 1/3 is approached so slowly, the Boguta model behaves like a nonrelativistic noninteracting Fermigas in the whole density range of 0 to $10\rho_0$. That is supported by an effective nucleon mass M^* very close to M in that region.

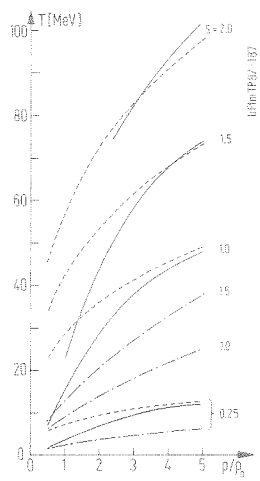
Taking the results together: temperature effects are found to be more pronounced in the Boguta model and the Boguta equation of state produces clearer signatures such as higher compression.

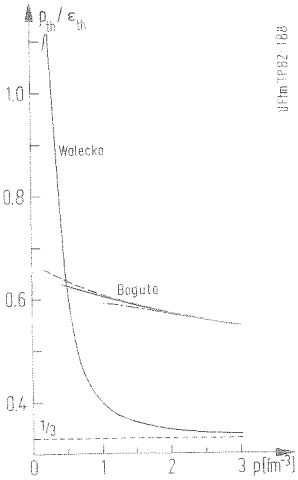
[1] M. Uhlig et al., GSI Scientific Report 82
UFTP Preprint 89/1982

[2] P. Siemens et al., Phys. Rev. Lett. 43, 1486 (1979)
J.I. Kapusta et al., Phys. Rev. 23C, 1282 (1981)
I.M. Mishustin et al., Phys. Lett. 95B, 361 (1981)
H. Stöcker et al., Phys. Lett. B103, 269 (1981)

Fig.1: Specific entropy versus density for the Walecka and Boguta model. Temperatures in MeV.
Fig.2: Lines of constant entropy in the temperature-density plane: Walecka (full), ultrarelativistic (dashed), nonrel. Fermigas (dash-dotted).
Fig.3: Ratio of thermal pressure to thermal energy.







Phase Transition of the Nucleon-Antinucleon Plasma in a Relativistic Mean Field Theory [B]

J. Theis, H. Stöcker, J. Polonyi
GSI Darmstadt
G. Graebner, G. Buchwald, M. Uhlig, J.A. Maruhn, and W. Greiner
Institut für Theoretische Physik der Universität Frankfurt

We study Walecka's mean field theory[1] with the following results: i) We can reproduce the observed binding energy and density of nuclear matter within experimental precision in an area characterized by a line in the coupling plane (Fig. 1). The coupling constant values proposed by Walecka represent a point close to the end of this line. ii) We have found that a part of this line defines systems which exhibit a phase transition around $T_c \sim 200$ MeV for zero baryon density. The rest of this line corresponds to such systems where the phase transition is absent but there is a peak in the specific heat around T~200 MeV.

Phase structure:

We explore the phase structure for the effective Lagrangian

$$\mathcal{L} = \mathcal{L}_{Dirac}^{free} + \mathcal{L}_{\phi}^{free} + \mathcal{L}_{V_\mu}^{free} + g_s\phi\bar{\psi}\psi + ig_v V^\mu\bar{\psi}\gamma_\mu\psi$$

at vanishing chemical potential μ and vector density ρ. In constrast to $\mu \neq 0$, the Fermi integration can be done analytically yielding for the total energy density

$$\varepsilon = \frac{1}{2C_s^2}(1-x)^2 + \frac{\gamma\theta x^3}{\pi^2}\sum_{n=1}^{\infty}\frac{(-1)^{n-1}}{n}\left\{K_1(nx/\theta) + \frac{3\theta}{nx}K_2(nx/\theta)\right\} \qquad (1)$$

for the pressure

$$p = -\frac{1}{2C_s^2}(1-x)^2 + \frac{\gamma\theta x^2}{\pi^2}\sum_{n=1}^{\infty}\frac{(-1)^{n-1}}{n^2}K_2(nx/\theta) \qquad (2)$$

and for the effective mass

$$x = \left[1 + \frac{\gamma C_s^2\theta x}{\pi^2}\sum_{n=1}^{\infty}K_2(nx/\theta)\frac{(-1)^{n-1}}{n}\right]^{-1} \qquad (3)$$

here γ is the degeneracy factor .0 defines the dimensionless temperature $\theta = T/Mc^2$. K_1 and K_2 stand for the modified Bessel-functions of first and second order, respectively. Fig. 2 contains the solution x of the self consistency equation (3) as a function of the temperature. The general trend of the function $x(\theta)$ can be understood as follows: The scalar density, which appears as a source for the scalar meson field ϕ, increases with increasing temperature. This leads to an increase of the mean field value of ϕ. Since the scalar meson describes an attractive interaction of the nucleons, these will be bound more strongly, and thus the effective mass is reduced. This mechanism is reinforced by the fact that a decrease of the effective mass increases the scalar density again. The most striking feature is the sudden drop in x at temperature T~200 MeV where the transition from x=.7 to x=.3 occurs in an intervall of $\Delta T \sim 3$ MeV only.

We calculated the thermodynamical quantities for the various coupling constants of the region shown in Fig. 1. For $C_s^2 > 342$ we found a phase transition of first order. For $C_s^2 < 342$ the thermodynamical behaviour is smooth in the temperature but a peak of finite width is found in the specific heat. For $C_2^2 = 342$ there is a phase transition of second order. Thus we have an effective theory in which the order of the phase transition directly depends on the strenght of the coupling constant.

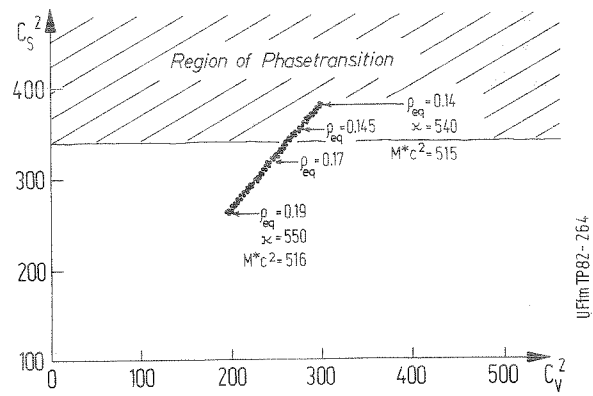


Fig. 1: The coupling constant plane is shown.

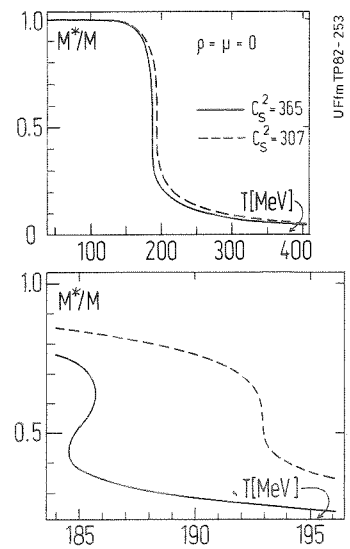


Fig. 2: The effective mass is shown as a function of temperature for different C_s^2-values.

References:

[1] J.D. Walecka, Phys. Lett. 59B, 109, 79

On the Color-Singlet Quark-Glue-Plasma [B G]

H.-Th. Elze, W. Greiner, and J. Rafelski
Institut für Theoretische Physik der Universität Frankfurt

We study in a semi-phenomenological way the so-called (color) confinement phenomenon[1]. While it is not yet fully understood in the framework of QCD, why colored quarks or gluons cannot exist as free particles, it is presently believed that all physical states behave as singlets under $SU_c(3)$ gauge transformations. Assuming the colorless character of all (many-particle) states as a starting-point, we ask for its influence on a statistical description of an ideal quark-glue-plasma: all other corrections due to (perturbative) QCD interactions are neglected for the moment which, however, is correct only in the asymptotically free region of high temperature or high baryon density in the plasma. - We are left with the task to calculate the partition function of an ideal quantum gas with an exact inner symmetry. This can be achieved by following a group theoretical projection technique formulated by Redlich and Turko for the general case of a compact semi-simple Lie-group[2]. One obtains for the partition function of color singlets a projection integral which uses a generating partition function.

We neglect the masses of the light quarks and work in the continuum approximation for the single-particle energy levels. The integrals can be evaluated in the limits $VT^3 \ll 1$ and $VT^3 \gg 1$ analytically, but for the transition region $TV^{1/3} \approx 1.5$ we have to use numerical procedures. However, by a direct calculation one gets the ultrarelativistic equation of state for massless particles, without doing the integrals.

Fig. 1 shows the corrections $E^{(1)}/T$ and $S^{(1)}$ to the energy over T and entropy as a function of $TV^{1/3}$. The behaviour of our results and of the free Stephan-Boltzmann-like contributions $E^{(0)}/T$ and $S^{(0)}$ is illustrated in the inset for comparison. We observe that the dip in both curves in the transition region $TV^{1/3} \approx 1.5$ does not change the monotonically rising character of the color singlet $E_{(0,0)}/T$ and $S_{(0,0)}$ as functions of $TV^{1/3}$ although the corrections amount to 50 % sometimes.

The physical effect can be understood from fig.2, where the effective degeneracy D_{eff} of single-particle energy levels is plotted against $TV^{1/3}$, which measures the deviation from the Stephan-Boltzmann-ideal-gas-like behaviour. We see that in the transition region already mentioned there occurs a rapid decrease of the number of internal (color) degrees of freedom of the quark-glue-plasma. One may call this a "phase transformation" of the system. The consideration of the internal $SU_c(3)$-symmetry in an idealized model of the QCD plasma phase thus leads us to the observation of a gradual "freezing" of the internal color degrees of freedom. The constant solid line corresponds to the perturbative effect in order $_s$, choosing $_s=1/2$. Interestingly, also perturbative corrections reduce the number of degrees of freedom. We note that the correlation effects are more relevant for $V^{1/3} \approx 1.5/T$ than the perturbative effects in the plasma. In nuclear collisions relatively small plasma regions will be formed just of the order of $\hbar/T \approx 2.5$ fm and our calculations show the relevance of color confinement effects for such experiments.

[1] H.-Th. Elze, et al., On the Color-Singlet Quark-Glue-Plasma, UFTP-preprint 98/83
[2] K. Redlich, et al., Z.Phys. C5 (1980) 201

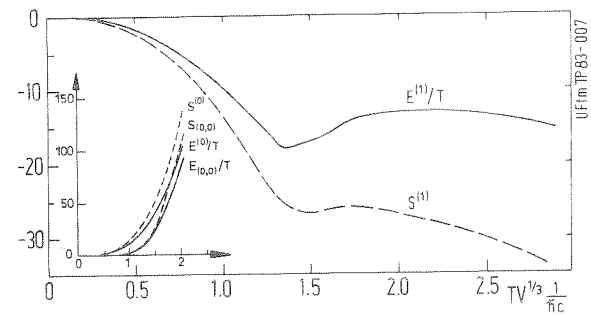


Fig. 1: The corrections $E^{(1)}/T$ and $S^{(1)}$ to the Stephan-Boltzmann-limit energy $E^{(0)}/T$ and entropy $S^{(0)}$ as functions of $TV^{1/3}$.

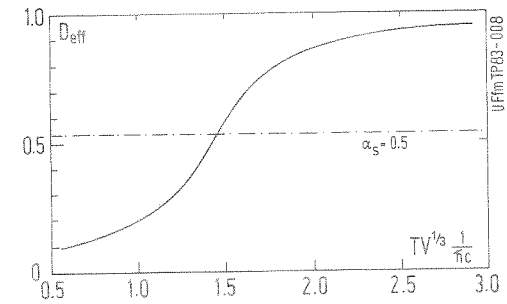


Fig. 2: The effective degeneracy D_{eff} of single-particle energy levels as a function of $TV^{1/3}$.

Formation of Quark-Gluon Plasma at Central Rapidity [B G]

Michael Danos
National Bureau of Standards, Washington, USA
Johann Rafelski
Institut für Theoretische Physik der Universität Frankfurt

Not all head-on nuclear collisions will lead to the formation of the quark-gluon plasma state, even if the kinematical requirements are fulfilled. A lower limit on the reaction cross section is deduced from preliminary cosmic ray data[1] which suggest that very high particle multiplicity events are seen with a frequency of above 1% of all hard collisions.

Our intention[2] was to discuss kinematic and geometric constraints for the plasma formation in the central rapidity region. We assume that a plasma seed must have been formed by a statistical fluctuation before the quark gluon plasma can begin to grow by capture of the trailing nucleons of the colliding nuclei. In such events the baryon number content of the plasma would be appreciable for large nuclei, peaking for events in the central repidity region. In order to obtain the conditions on the plasma ignition in the CM-frame (central repidity region) we must balance energy gain a loss terms of a plasma seed: the energy lost by the particle radiation from the plasma[3] must be less than that supplied by the incoming nucleons from the projectile and target nuclei. We note that the balance of loss (radiation) and gain (nucleon influx) terms involve the actual size of the plasma mainly in an energy absorption coefficient which controls the probability of energy deposition in the plasma by high energy particles.

In fig. 1 we show the minimum size a plasma seed must have in order for it to grow, i.e., the minimum seed size for plasma ignition, as a function of projectile energy for a selection of plasma ignition temperatures, T_I, computed taking $\mu/T=2$. Since the mean free path λ in a low density plasma is about 1.5-2 fm one sees that for the case T_I 150-160 MeV, beam energies of 20-50 GeV/nucleon should suffice to lead to plasma ignition with $R/\lambda \sim 1$.

Once the plasma has ignited the temperature of the plasma will grow until the nuclear collision terminates or until the temperature has risen to a level at which the pion radiation overwhelms energies influx. This maximum achievable temperature is shown in fig. 2 for a few choices of the pion turn-around coefficient η, as a function of projectile beam energy. Here we have used $R/\lambda = 5$, $\mu/T=1$. As one can see the maximal temperature achievable in the collision does not depend too sensitively on the choice of the parameters and reaches for 50 GeV a value around 200-250 MeV. Hence, once a plasma has ignited, one can expect that a full-fledged quark-gluon plasma event will take place, with energy density reaching several GeV/fm^3. However, we note that underlying this scenario is the requirement that collisions of quite heavy nuclei are considered with $R \sim 5\lambda \sim 5$ fm.

[1] G.B. Yodh, Rev. of Recent Developments in Cosmic Ray Experiments at Very High Energies, Maryland Preprint, to be published

[2] M. Danos and J. Rafelski, Formation of Quark-Gluon Plasma at Central Rapidity, UFTP 94/1982 and to be published

[3] M. Danos and J. Rafelski, Particle Radiation by Hot Quark-Gluon Plasma, NBS-Preprint 1982 and to be published

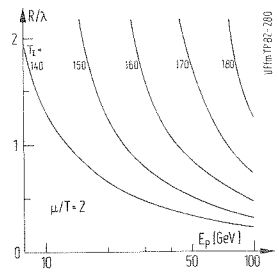


Fig. 1:
Minimal size of the quark-gluon plasma seed required to lead to plasma ignition. T_I is the assumed plasma ignition temperature.

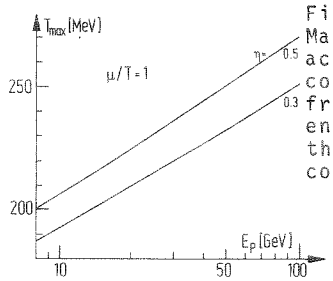


Fig. 2:
Maximal temperature achievable in nuclear collisions. η is the fraction of the radiated energy swept back into the plasma by the colliding nuclei.

B G

Particle Radiation by Hot Quark-Gluon Plasma

M. Danos
National Bureau of Standards, Washington
J. Rafelski
Institut für Theoretische Physik, Universität Frankfurt

While it is widely accepted that a new form of hadronic matter - quark-gluon plasma- is created in high energy nuclear collisions so far little attention has been paid to the time-development of such a quark-gluon plasma state. As this time-development is of crucial importance for the prediction of experimentally observable effects we address this question here. We see two main physical mechanisms: The spatial expansion of the compressed hadronic matter, and the evaporation of mesons from the surface. Our main effort concerns this latter effect which,as we have shown, is probably the dominant process for the cooling of the plasma[1].

We consider an approximately spherical region of the perturbative QCD vacuum, filled with quarks, antiquarks, and gluons. The particle densities are assumed to be reasonably well described by local thermal and chemical equlibrium distributions.

For an impenetrable surface between the perturbative and true vacuum states the inside thermal and degeneracy pressure would lead to an expansion until either pressure equilibrium or a phase transition into individual hadrons is reached; the posibility of break-up into several droplets does not significantly influence our line of arguments. However, if the surface is penetrable, i.e., if it allows transmission of momentum and energy (but not color) from the inside, then this can lead to a substantial internal energy and pressure loss -- the pressure acting on the surface is reduced as not all the momentum impinging on the surface is reflected. The microscopic mechanism for this transmission arises in the following manner. When a fast quark (antiquark) hits the boundary, it can form a jet-like structure filled with color field flux, i.e., a fluxtube. For sufficiently high quark momentum this tube instead of retracting splits by qq pair creation. The leading particle associates with the antiparticle of the pair to form a meson, usually a pion, while the remaining pair particle may retract into the plasma.

We developed a quantitative model suitable for surface temperatures of about 160 - 220 MeV and moderate baryon densities, such that the particle density is less than ≈ 10 particles/fm^3. Under these circumstances surface collisions involving more than one particle per fm^2 are rare. Hence we have limited ourselves to consider sequential one-particle events. In order for the surface collision to lead to pion emission the particle momentum normal to the surface must exceed a certain threshold. This momentum has to be larger than the normal momentum of the emitted pion. We take this threshold momentum to be of the order of 1/4 GeV/c; our results are quite insensitive to this choice,as well as to the actual shape of the threshold function θ describing the probability of pion emission. From these considerations we obtain the generalized Stefan-Boltzman law:

$$\frac{d^3E}{d^2A\,dt} = \bar{f}\,\frac{g}{2\pi^2}\cosh(\mu/T)\;T^4\;3e^{-p_M/T}\left(\frac{1}{3}\left(\frac{p_M}{T}\right)^2+\left(\frac{p_M}{T}\right)+1\right)$$

In figure 1 we show the cooling rate calculated for several choices of p_M as a function of the surface temperature T, choosing $\mu/T = 1$. (For $\mu \approx 0$ the values are lower by about 30 %.) We see that precise value of p_M does not matter.

To appreciate these results we now discuss the rate of energy loss through a surface. For example, through the surface of a sphere with a radius of 4 fm the energy loss per $\Delta t = 2 \times 10^{-23}$ sec at T = 180 MeV is 260 GeV. This shows that during the minimum estimated lifetime of the plasma almost the entire avalable energy can be radiated by the surface.

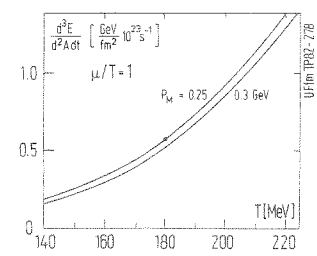
In order for this radiation to actually participate actively in the time evolution of the plasma a sufficiently large plasma heat conductivity is required. Since the plasma consists of rather free particles the naive expectation is that a sufficently high conductivity obtains. In our example, the required temperature gradient following from typical QCD interaction length is about 9 MeV.

Particle radiation relieves some of the internal pressure and only about 60 % of the internal pressure is actually felt by the plasma surface.

The physical distinction between the cooling by pion radiation and by expansion resides in the reduction of the temperature without a significant increase of the plasma volume.

[1] M. Danos, J. Rafelski, NBS preprint 1982, Phys. Rev. D (1983) (in print).

Fig. 1: Surface brightness of a quark-gluon plasma as function of the temperature for several cutoffs p_M at fixed $\mu/T = 1$. The dot indicates the parameters of our numerical example.



Quark-Gluon Plasma in $\bar{p}$-Annihilation on Nuclei [B G]

Johann Rafelski
Institut für Theoretische Physik der Universität Frankfurt

In a fraction of $\bar{p}$-nucleus annihilations the annihilation energy will be transfered to nuclear fragments[1] allowing a study of highly excited forms of nuclear matter. More recently[2] arguments leading to the conclusion that quark-gluon droplets may be created in such reactions have been made. We recall that these droplets are internally excited multibaryon numer, large quark bags. Quark and gluons form inside the blob a (perturbative) Fermi-Bose liquid. When a slow antiprotons penetrate into a nucleus, the first step in the annihilation process can be the formation of a baryonnumber = zero fireball, filled with coloured gluons and quark -anti-quarks pairs. As it turns out, this picture allows to describe satisfactorily π-multiplicities in annihilations[3]. In $\bar{p}$N reactions such a state would than break up into several mesons - a process that may last sufficiently long to allow (sometimes) the fireball to collide with one of the nearby nucleons before hand. This can lead to the absorbtion of this nucleon into the fireball - continuing the argument we find that yet unspecified number A of nucleons could be absorbed into the fireball. In this process the baryon density of the blob remains similar to that of the normal nuclear matter. The quark droplet will desintegrate into A-1 baryons and several mesons. The understanding of this process is still poor but some properties of emerging particles can none the less be estimated. First we observe that inside the low density droplet temperature of the order of about 160 MeV (A=1) prevails, actually a value which is slightly A-dependent but which will even for large A, due to the low baryon density will be about 140 MeV. Particles originating from the desintegration of the blob will (in the event-ensemble) show a momentum distribution with this characteristic slope (1/T). More characteristic feature of the quark blob is the relative enhancement of strangness production. There are two reasons: a) The increased hadronic volume suppresses the volume quenching factor[4] and b) those events in which quark blobs are formed will, on average, live longer allowing for the $q\bar{q}\to s\bar{s}$, $gg\to s\bar{s}$ processes to continue for longer[5]. I expect strange particles yield to be enhanced at least by a factor 5 in the quark blobs created in $\bar{p}$-nucleus annihilations.

Aparently, an experiment to observe a quark-blob would consist of using a strangness trigger and to measure the momentum distribution of high-momentum so called spectator protons or pions. Indeed, such an experiment has been carried out for the lightest of all nuclei. In Fig. 1 I show the results of the p-d annihilation taken from Ref. 6.

[1] J. Rafelski, Phys.Lett. 91B (1980) 281
[2] J. Rafelski, "Quark-Gluon Plasma in $\bar{p}$-Annihilation on Nuclei", to be publ. in proc. of the Workshop "Physic at Lear", Erice/Itali, 82
[3] B. Müller and J. Rafelski, Phys.Lett. 116B, (1982) 274
[4] J. Rafelski and M. Danos, Phys.Lett. 97B (1980) 279
[5] J. Rafelski and B. Müller, Phys.Rev.Lett. 48 (1982) 1066
[6] B.Y. Oh et al., Nucl.Phys. B51 (1973) 57

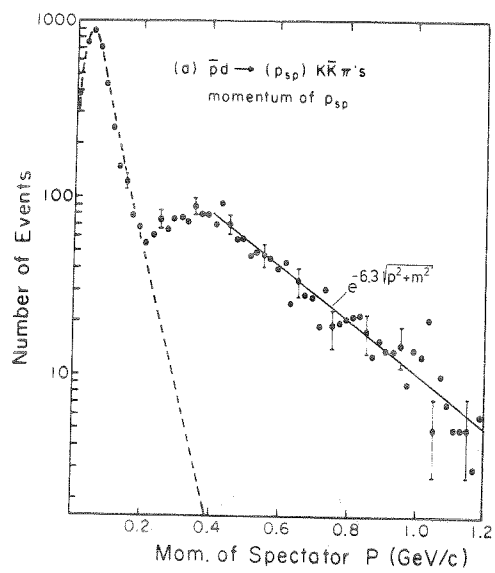


Fig.1: Proton spectrum from $\bar{p}$-d annihilation; KK̄ trigger. Dashed line - deutron-wave-function. Full line - eyeball fit, T=160 MeV.

Measurement of Baryochemical Potential of Hot Nuclear Matter [BG]

P. Koch, J. Rafelski, and W. Greiner
Institut für Theoretische Physik der Universität Frankfurt

We consider the production of light strange particles from highly excited nuclear matter[1] consisting of individual hadrons under the asumption of thermal equilibrium among all hadrons, baryochemical equilibrium between strange and non-strange hadrons and relative strangeness equilibration among particles containing s or $\bar{s}$ quarks. It turns out, that to use these equilibrium conditions only the large strangeness exchange cross-sections known experimentally are needed. Strange particle abundances are primarily influenced by the following reactions

a) $p+p \rightleftarrows K^+ + \bar{K} + p + p$ (pair production)

b) $\pi^0 + p \rightleftarrows K^+ + \Lambda$ (associated production)

c) $\bar{K} + p \rightleftarrows \Lambda + \pi^0$ (exchange reaktion)

Here we notice the influence of the baryonnumber on the production of K-mesons and we see, that K^+ is more likely produced through the associated production than together with a K^- in direct pair-production. For this reason we expect the ratio of K^+/K^- to contain information about the baryon-density of the hot and dense phase of nuclear matter. Starting from the grand canonical partition function:
$\ln Z^{strange}(T,V,\lambda_s,\lambda_q)$ where λ_s, λ_q counting the strangeness - and respectively, the quark-baryonnumber, we can impose explicitly a detailed balance condition through

$$\langle n_s - n_{\bar{s}} \rangle = \lambda_s \frac{\partial}{\partial \lambda_s} \ln Z^{strange}(T,V,\lambda_s,\lambda_q) = 0 \qquad (1)$$

to arrive at the following expression for the K^+/K^- ratio (Fig. 1).

$$\frac{\langle n_{K^-} \rangle}{\langle n_{K^+} \rangle} = \left\{ \frac{W(x_K) + \lambda_B^{-1}[W(x_\Lambda) + 3W(x_\Sigma)]}{W(x_K) + \lambda_B[W(x_\Lambda) + 3W(x_\Sigma)]} \right\} \qquad (2)$$

with $W(X_i) = X_i^2 K_2(X_i)$ and

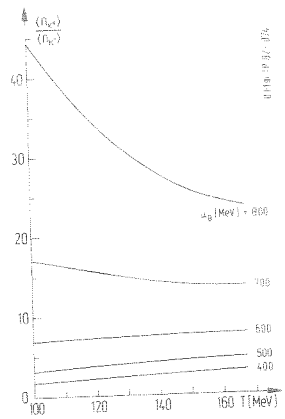


Fig. 1: The particle ratio K^+/K^- as a function of temperature T for several μ_B

where $\lambda_B = e^{\mu_B/T} = \lambda_q^3$
We record that this particular particle ratio is a good measure of the baryochemical potential when temperatures are approximately known. Comparison of K^- differential crossection as measured in the reaction $^{28}Si + ^{28}Si$ at 2.1 GeV/n at K^- momentum of 1 GeV/c and 0^{o2} with K^+ differential crossection[3] at same momentum and angle but different collision systems lead to $K^+/K^- \sim 24$
Comparing this value with Fig. 1 we estimate, that the baryon chemical potential was about 750 MeV, at T ~ 120 MeV,

[1] P. Koch, J. Rafelski, and W. Greiner; UFTP-Preprint UFTP-82-77, Phys.Letters in print
[2] A. Shor, et al., Proc. 5th High Energy Heavy Ion Study, LBL-12652, 1981, p. 470
[3] S. Schnetzer et al., Proc. Intern. Conf. on Nuclear Physics, Berkeley, Aug. 1980, p. 619
S. Schnetzer, Ph. D. Thesis, unpublished

Strangeness as a Signal for Quark-Gluon-Plasma Formation [BG]

P. Koch, J. Rafelski, and W. Greiner
Institut für Theoretische Physik der Universität Frankfurt

In order to establish the relevance of a strangeness signal for diagnosis of a possible formation of quark gluon plasma in heavy ion collisions we must look for the strange channels of highly excited hadronic matter, to be able to distinguish them from those of the quark phase. In the case of the hadronic gas phase we are dealing with a grandcanonical partition function $Z^{strange}(V,T,\lambda_s,\lambda_q)$ from which we obtain, as in ref.[1], the strange antiparticle component to be

$$\langle w_{\bar{s}} \rangle_{nucl.mat.} = \left(\frac{VT^3}{\pi^2}\right)\left\{W(x_K) + \lambda_B^{-1}\left[W(x_\Delta) + 3W(x_\Sigma)\right]\right\}\cdot\gamma^{-1} \quad (1)$$

with

$$\gamma^{-1} = \lambda_B^{-4/3}\left\{\frac{W(x_K) + \lambda_B\left[W(x_\Delta) + 3W(x_\Sigma)\right]}{W(x_K) + \lambda_B^{-1}\left[W(x_\Delta) + 3W(x_\Sigma)\right]}\right\}^{1/2} \quad (2)$$

The expression (1) is now compared to

$$\langle \bar{s} \rangle_q = 6\int\frac{d^3p}{(2\pi)^3}\frac{1}{e^{\sqrt{p^2+m_s^2}/T}+1} \approx 3\left(\frac{VT^3}{\pi^2}\right)\left(\frac{m_s}{T}\right)^2 K_2\left(\frac{m_s}{T}\right)$$

the mean number of s-quarks in the quark plasma.

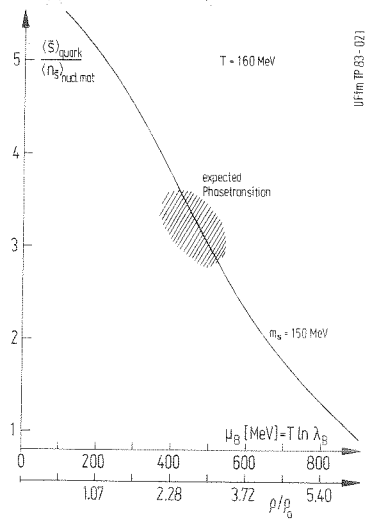


Fig. 1: The ratio of $\langle\bar{s}\rangle/\langle w_{\bar{s}}\rangle$ as a function of μ_B for fixed T=160

In Fig. 1 we have displayed the ratio $\langle\bar{s}\rangle/\langle w_{\bar{s}}\rangle$ and we notice an enhancement factor of about (3-4) for the antistrangeness coming from the quark plasma phase.

If now quark matter is produced and decays into hadrons, some of the $\bar{s}$ -quarks may, instead of being bound in a $(q,\bar{s})$ Kaon enter into a $(\bar{q}\bar{q}\bar{s})$ or $(\bar{q}\bar{s}\bar{s})$ antibaryon and inparticular, a $\bar{\Lambda}$, $\bar{\Sigma}$ or may be also in a heavier multistrange antibaryon. Now it seems, that the production of this $\bar{s}$ carrying hadrons will be comparable to the one of the s carrying baryons. Noteworthy about this is, that the strange antibaryons conventionally can only be produced indirect pair production mechanisms which are up to high energies suppressed by energy momentum conservation and phase space considerations. So we turn our interest rightaway to one of the rarest of all simply strange particles, and show in Fig. 2 the upper limit of the ratio $\langle w_{\bar{\Lambda}}\rangle/\langle w_{\bar{\Delta}}\rangle$ as we expect it for the hadronic gas phase[1].

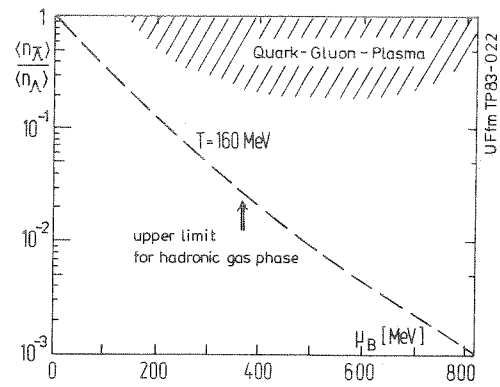


Fig. 2: The upper limit curve of the ratio $\langle w_{\bar{\Lambda}}\rangle/\langle w_{\bar{\Delta}}\rangle$ as expected for the hadronic gas phase and naive expectation for the quark-phase.

We notice for $\bar{\Lambda}$'s coming from the hadronic gas phase a maximal abundance of 10^{-3}-10^{-2}, whereas our estimates for $\bar{\Lambda}$'s coming from the quark-phase, based on flavour content, are one-two orders of magnitude higher.

[1] P. Koch, J. Rafelski, and W. Greiner; UFTP-preprint, UFTP-82-77, Phys.Lett. B (1983) in print

High Energy γ's from $s\bar{s}$-Annihilation in Quark-Gluon Plasma [BG]

G. Staadt, J. Rafelski, and W. Greiner
Institut für Theoretische Physik der Universität Frankfurt

Given the present knowledge about strong interaction one has to assume that in collisions of heavy nuclei with sufficiently high kinetic energy such a high energy density can occur that the hadrons dissolve into their constituents, i.e. into a quark-gluon plasma. The quark-gluon plasma represents a new physical phase. In order to test the correctness of this concept one has to investigate such processes, which could give a hint on the existence of the plasma. Here we are interested in processes leading to high energy photons, as these leave the plasma without further interaction. We intend to calculate the spectrum of such photons, in particular when they originate from the annihilation of a strange and an antistrange quark into a gluon and a photon. This process is particularly interesting, because relatively many s and $\bar{s}$ quarks have been created in the plasma, and because these quarks have a great mass. Therefore we expect relatively high energy photons with a low energy cutoff.
First we compute $|\mathcal{M}|^2$ ($\mathcal{M}$ =invariant amplitude) of the process $s\bar{s}\to\gamma G$ as function of the invariant Mandelstam-variables s and t. For that purpose we use the lowest order perturbative QCD. This means that we evaluate the Feynman diagrams, shown in the figure.

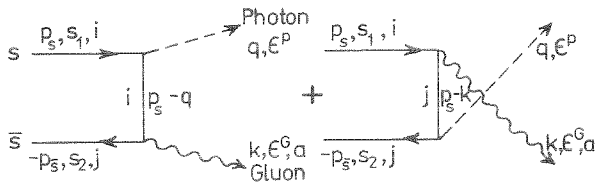


Fig.: $s\bar{s}\to\gamma G$ in 1. order $\alpha_s\alpha$
Here the symbols are $p_s, p_{\bar{s}}, k, q$= four-momentum of the particle, s_1, s_2= spin of the quarks, i,j= quark colour, a=gluon colour, ϵ^P, ϵ^G = polarization vektor.
We find that the propagator of the virtual quark is not dependent on the presence of the other plasma particles, because the chemical potential of the strange quarks is zero. We obtain:

$$\sum|\mathcal{M}|^2 = \frac{8}{9}\frac{e^2 g^2}{m^2}\left[\frac{(m^2-t)}{(s+t-m^2)} + \frac{(s+t-m^2)}{(m^2-t)} - \frac{4m^2(-s+2m^2)}{(m^2-t)(s+t-m^2)} - \frac{4m^4}{(m^2-t)^2} - \frac{4m^4}{(s+t-m^2)^2}\right].$$

'Σ' means the sum over the spin/colour quanten numbers of all particles. Because the created gluon is a Bose-particle, the presence of the other gluons, which exist in the plasma, yield an additional stimulation factor. We calculate the number of photons, which are emitted in a momentum interval d^3q per unit time and volume; d^3A. Then, $E_q\frac{d^3A}{d^3q}$ is a Lorentz-invariant quantity that we calculate in the rest frame of the plasma.

$$E_q\frac{d^3A}{d^3q} = \int d^3p_s\, d^3p_{\bar{s}}\, d^3k\, \frac{m^2}{(2\pi)^8\, 4E_sE_{\bar{s}}E_k}\, g(p_s)g(p_{\bar{s}})\left[1+g(k)\right]\delta^4(p_s+p_{\bar{s}}-k-q)\sum|\mathcal{M}|^2.$$

$g(K)$, $g(p_s)$, $g(p_{\bar{s}})$ are the distribution functions of the corresponding particles. For the quarks we use Fermi-functions, and for the gluons we use the Bose-function.
The spectrum of the photons is proportional to $E_q\frac{d^3A}{d^3q}$. We expect a peaking structure in the spectrum to result from further numerical calculations. The form of the photon spectrum depends only on the temperature of the plasma and not on the baryon chemical potential. Also, the number of photons is proportional to the volume of the plasma and is strongly dependent on the short lifetime of the plasma. Hence the form of the spectrum is a measure of the mean plasma temperature, while the strength is a measure of the size and lifetime of the plasma state.

Are Glueless M.I.T. Bags Intrinsically Deformed? [B G]

D. Vasak, R. Shanker, B. Müller, and W. Greiner
Institut für Theoretische Physik der Universität Frankfurt

In this work we go beyond the spherical approximation for the description of baryons used in the original M.I.T. bag model[1,2], but neglect the contributions of the gauge fields, thus being complementary to previous calculations which considered either only free gluons[3] or did not take quark dynamics into account[4-6]. To find the stationary solution of the free Dirac equation inside a given stationary cavity (with reflection and axial symmetries), supplemented by the linear M.I.T. boundary condition on it's surface, we expand the wave function to given energy, E, fixed parity, π, and fixed z-component of the angular momentum, μ, in terms of the spherical basis, and then adjust the expansion coefficients and the energy to fulfill the boundary condition[7]. For massless quarks there is only one dimensional parameter present, namely the scale parameter r_0 in the expansion

$$r(\theta) = r_0 \left(1 + \alpha_2 P_2(\cos\theta) + \alpha_4 P_4(\cos\theta) + \cdots\right)$$

of the cavity shape. Thus $r_0 E$ is independent of r_0. In Fig. 1 we present the "Nilsson-levels" $(r_0 E)_n$ for pure quadrupole deformations ($\alpha_{2n} = 0, n>1$). The proper shape of a hadron should be adjusted to balance the pressure on the bag surface. We do not use the proper M.I.T. pressure balance condition, but a weaker one which for spherical bags is equivalent[1]. We minimize the total hadron energy

$$E_{HAD}(r_0, \alpha_2) = \frac{1}{r_0} \sum_i (r_0 E)_i(\alpha_2) + B V_{BAG}(r_0, \alpha_2)$$

with respect to shape parameters r_0, α_2. Here $B=(120\ \mathrm{MeV})^4$ is the vacuum pressure[8], V_{BAG} the bag valume and the sum runs over the occupied quark modes in the hadron. In Fig. 2 we present the masses of different baryonic resonancies, already minimized with respect to r_0, as function of α_2. The energy minima for baryons with quarks excited to higher modes lie off the spherical point $\alpha_2 = 0$.

[1] A. Chodos et al., Phys. Rev. D9, 3471 (1974)
A. Chodos et al., Phys.Rev.D10, 2599 (1974)
[2] T.A. de Grand and R.L. Jaffe, Ann.Phys. 100, 425 (1976)
T.A. de Grand, Ann.Phys. 101, 496 (1976)
[3] P. Gnädig et al., Phys.Lett. 64B, 62 (1976)
[4] P.J. Mulder et al., Phys.Rev. D19, 2635 (1979)
A.T. Aerts et al., Phys.Rev. D21, 1370 (1980)
P.J. Mulders et al., Phys.Rev. D21, 2653 (1980)
[5] Wang Gia-Zhan et al., Phys.Lett. 107B, 381 (1981)
[6] D. Robson, Z.Phys. C3, 199 (1980)
[7] D. Vasak, R. Shanker, B. Müller, W. Greiner: Deformed solutions of the M.I.T. bag, 1982, to be published
[8] P. Hasenfratz, and J. Kuti, Phys.Rep. 40, 75 (1978)

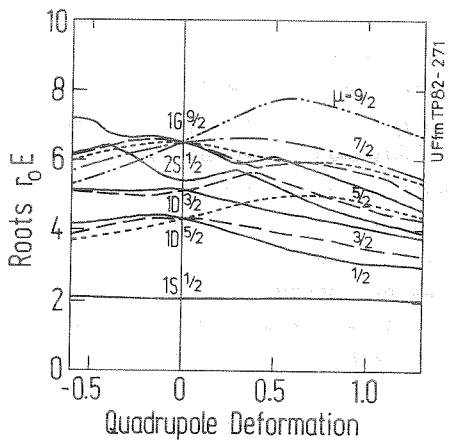


Fig. 1: The energy eigenvalues $r_0 E$ for $\pi=+1$ up to the "G 9/2"-level as a function of the quadrupole deformation α_2. The spectroscopic names S1/2, D5/2, D3/2, 2S1/2, 1G9/2, well defined in the spherical case, label the whole curve. The calculated points (at α_2 = -0.6,-0.5, -0.4,..., 1.3) are connected by straight lines. Since we do not expect having some additional symmetry in the problem, the levels with equal quantum numbers, μ and π, will not cross.

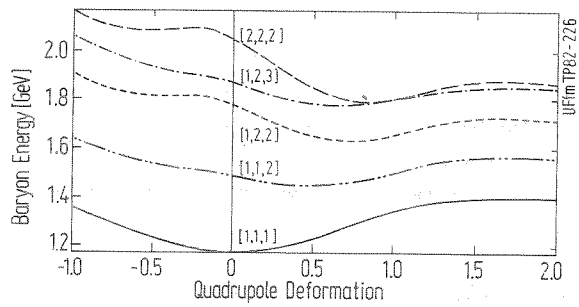


Fig. 2: The total energies of different baryon resonances as function of the deformation parameter α_2. Since there is no interaction, each of the states is degenerate with respect to isospin and spin. The occupied quark modes have the quantum numbers $n=1, \pi=+1, \mu=1/2$. The numbers [1,1,2] indicate that the first and the second quarks are in the S1/2-mode and the third one in the D5/2-mode (this is the $(1S1/2)^2$ D5/2-state). Number 3 corresponds to the D3/2-mode.

String-like quark bags and Regge-trajectories

B G

R. Shanker, D. Vasak, W. Greiner, B. Müller
Institut für Theoretische Physik, Universität Frankfurt
C.S. Warke
Tata Institute for Fundamental Research, Bombay

With the string picture in mind, we study quark bags of a simple fixed geometry: cylindrical. It is shown that the Dirac boundary value problem $i\not{n}\psi=\psi$ of the M.I.T. bag model[1] has no solutions, if this quark confinement condition is applied simultaneously on the radial walls as well as on the edges of the cylinder. By introducing a cruder condition, $\bar{\Phi}\phi=0$, instead, but now only on the side walls, we calculate properties of non-strange baryons. A justification for the use of this cruder condition on the side walls, instead of the proper M.I.T. condition, is then provided by showing that the M.I.T. "cylindrical" bag with smooth rounded corners gives essentially the same result, while being computationally more involved[2]. Notwithstanding this departure from the M.I.T. confinement condition on the side walls, we find the following curious results: for high excitations, this bag attains string-like shapes. (see Fig.1.) The sequence of baryonic states corresponding to pure single quark excitations fall on a linear Regge trajectory (see Fig. 2) with a slope of 0.85 (GeV^{-2}). These trajectories hold at low-angular momenta.

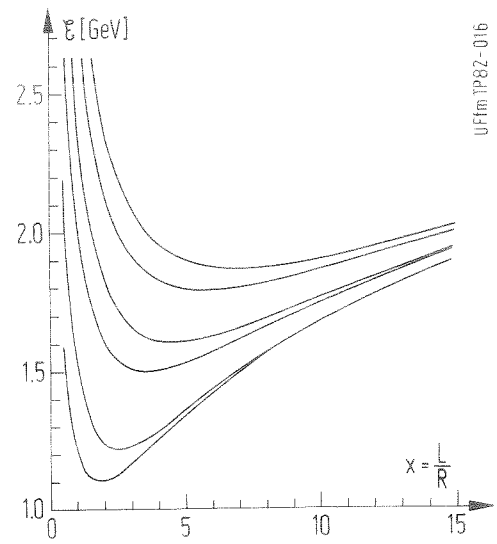


Fig. 1

[1] A. Chodos, R.L. Jaffe, K. Johnson, C.B. Thorn, V.F. Weisskopf; Phys.Rev. D10 (1974), 2599
[2] D. Vasak, R.Shanker, B. Müller, W. Greiner; Deformed solutions of the M.I.T. quark bag model, 1982, to be published
[3] Particle Data Group; Phys.Lett. 75D (1978)
[4] R. Shanker, D. Vasak, B. Müller, W. Greiner; String-like solutions and Regge trajectories in a cylindrically deformed quark bag model, 1982, to be published

Fig.1: Energies of the even-parity non-strange baryonic configurations corresponding to different quark occupancies of the bag modes. The ground state (the cylinder length = twice the cylinder radius) is optimally spherical. The excited states are obtained by single-quark excitations of the ground state.

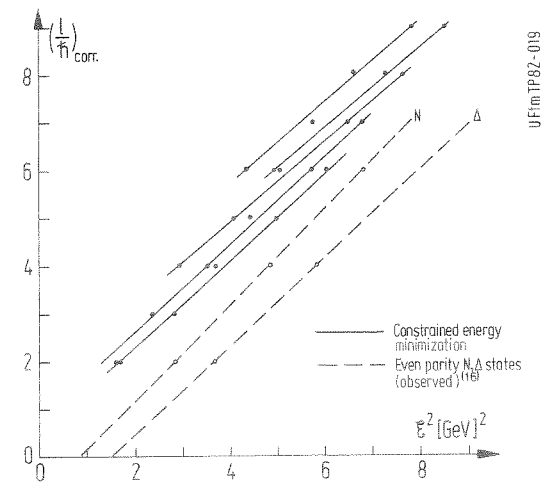


Fig. 2

Fig.2: Regge trajectories of the even-parity lowest band ($(\mu R)^{+}_{01}$ =1.435, m_q=o, $J_z=\hbar/2$) baryons, as calculated by the method of constrained minimization[4] of bag energy. The slope is found to be 0.85 GeV^{-2}. Experimental data is from Ref.[3].

Monte Carlo Simulation of QCD

J. Kuti
Institute for Theoretical Physics, Univerity of California, Santa Barbara, California
93106

J. Polonyi
GSI Darmstadt

An unexpected succes has been achieved in quantum field theory during the last years. The quarkless QCD has been solved numerically in a few fm sized four dimensional hypercube. In addition it has been proved that this theory undergoes a quark deliberating phase transition at high temperature. In these calculations a finite mesh was introduced in spac-time and the quantum field theory was transformed into a four dimensional classical system. The vacuum expectation value of an observable O(A) is given by

$$\langle O(A)\rangle = \frac{\int D[A(X)]\exp(-S\{A\})\ O(A)}{\int D[A(X)]\exp(-S\{A\})} \qquad (1)$$

where S{A} is the action functional of the field A. Such kind of integrals can be evaluated by means of Monte Carlo method where the factor exp(-S{A}) is interpreted as the Gibbs factor exp(-βH{A}) of a four dimensional calssial system.

This method proved to be extremely powerful in studying bosonic theories because the integral measure exp(-S) is a local positive functional of the field A. This situation gets worst including dynamical fermions in the theory. Because of the spin statistical theorem one has to use anticommuting c-numbers to describe the path of a fermion. The only way to get rid of these unconvenient anticommuting objects is to integrate them out from the action. Suppose that the action is given by $s\{A,\psi,\psi,\} = S_\alpha\{A\}=\psi K\{A\}\psi$. Then the vacuum expectation value of a bosonic operator O(A) reads as

$$\langle O(A)\rangle = \frac{\int D[A(X)]\det K\{A\}\exp(-S_A\{A\})\ O(A)}{\int D[A(X)]\det K\{A\}\exp(-S_A\{A\})} = \frac{\int D[A(X)]\exp(-S_{eff}\{A\})\ O(A)}{\int D[A(X)]\exp(-S_{eff}\{A\})} \qquad (2)$$

The determinant of the quadratic form K{A} is a complicated nonlocal quantity (the index space of K is the space-time so Dim(K) is the number of mesh points). The usual Monte Carlo method becomes very unefficient in calculations such type of integrals.

An almost forgot idea of von Neumann and Ulam offers a possible way out from this situation. They remarked that an individual matrix element of $1/(1-V)=\Sigma V^n$ is the sum of terms corresponding to walks in the index space of the matrix V (the length of a walks in the n-th order is n). Dividing the matrix elements V_{ij} into positive normalisable part and the rest one can define a random walk in the space of index in such a way that the expectation value of a functional of the walks gives the correct inverse matrix elements.

The application of this idea in the QCD consist of expanding the fermion determinant in the integrand[1]. As a result one arrives to an effective action $S_{eff}\{A\}$ which is the sum of terms corresponding to closed loops in space-time. The convergence of this expansion is helped by the phenomenon of confinement which states that quark loops with large area are suppressed by the fluctuation of the gauge field A. In the Metropolis type Monte Carlo method the decision step requires the ratio of the integrand of the trial and the original configuration. We initiate a secondary Monte Carlo procedure at the decision step to calculate the difference of the effective action. The advantage of this procedure is that the number of instruction of an update of the gauge field configuration is proportional with N^4 (N is the number of mesh points in one dirction in the space-time) in contrast to other exciting approaches where this number increases as N^8. The disadvantageo us feature of the proposed method is that since te decision process contains the statistical fluctuation of the integrand (the effective action) in a nonlinear way we have no theoretical control over the fluctuation of the end results at the present.

We calculated the free energy of a static charge in QCD at finite temperature. This quantity is the order parameter of the quark deconfining phase transition. We found that in the presence of dynamical quarks there is a well pronounced crossover between the confining and the free behaviour. It is possible to define the temperature where the quarks become free as this happens quite abruptly. Although the precise determination of this temperature requires more computer time, our present results suggest that this temperature may be considerably smaller than the corresponding quarkless of value T = 180MeV.

References

1) J. Kuti, J. Polonyi, Some appliations of a new stochastic method in lattice theories, in the proceedings of th John Hoyking Meeting of Theoretical Particle Physics, Maryland, 1982 and GSI-preprint GSI-82-22

Topological Charge of Lattice Field Theories

J. Polony
GSI Darmstadt

We know two sufficiently general nonperturbative methods to study the ground state structure of an asymptotically free theory. One is the saddle point approximation which leads to the "instanton" structure of the vacuum and the other is the Monte Carlo method in the lattice formulation of the theory. The first gives a transparent explanation of some nonperturbative phenomena in terms of the saddle point instanton configurations. The disadvantage is that this approximation is not a systematic expansion of the path integral. The Monte Carlo method gives in principle the exact result however through an intransparent numerics only. In fact we can not learn physics directly from configuration sequence generated by a computer. It is natural to ask whether one cannot connect both methods above. In the case of the two dimensional CP^n model (where the saddle point approximation was developed first) I was able to define the set of dominant configurations on the lattice and to show the relevance of the topological structure[1]. A similar approach is in progress in the case of the four dimensional lattice QCD.

The result of the study of the CP^n model is the following.

1. The lattice version of the CP^n model involves an n-component complex field $z(n)$ of unit length and a U(1) gauge field $U_\mu(n)$. In the continuum theory the study of the field at the space-time infinity led us to recognize the relevance of the topology in the path integral. In the lattice case the study of the vicinity of a space- time point gives the corresponding result. In fact I defined the dominant subset of configurations showing that the path integral is dominated by configurations where the relative phase $\phi_\mu(n)$ of the neighbouring z values takes such values that $\mathrm{curl}\,\phi \sim 2\pi p_n$. The phenomenon was confirmed by Monte Carlo calculation.

2. $q_n = \mathrm{curl}\phi \pmod{2\pi}$ is gauge invariant and gives back the correct topological charge density of the CP^n theory in the classical continuum limit.

3. I introduced the topolocial charge of a periodic lattice configuration $Q = 1/(2\pi)\ \tau_m\, q_n = \tau_m\, P_n$ which is a gauge invariant integer. In addition it is impossible to change Q whithout leaving the subset of dominant configurations. The Monte Carlo calculation of the topological susceptibility $\chi = \langle Q^2\rangle/\mathrm{volume}$ gave a finite result in the quantum continuum limit. In such a way this is the first example where the topological structure persists the quantum continuum limit on the lattice.

4. I pointed out that the usual weak coupling expansion is singular at $g^2 = 0$ in the gauge variant sector even in the presence of a complete gauge fixing term. This is caused by a family of configurations which represents the vortices of finite energy in the continuum theory but becomes gauge equivalent with the trivial vacuum in the lattice case. This shows that an important role of the gauge invariance is to select the observables having regular g behaviour according to the asymptotical free character of the CP^n theory. In addition the existence of this lattice mode forbids the use of fractional charged particles in the lattice gauge theories.

The topological charge concept was also extended to the four dimensional lattice QCD. The first nontrivial question in defining this quantity is the notion of the topological charge of the continuum theory defined in a finite periodic box. Since the topological charge $Q = \int d^4x\ \partial_\mu J_\mu$ is a surface quantity it vanishes on smooth periodic configurations. But it turned out that the known instanton solutions become singular forcing the periodic boundary condition. In this case the space-time integral defining the topological charge is not uniquly defined. A reasonable extension of the definition is that if there is a gauge transformation which converts the instanton solution regular (the singularity at the center of the instanton is a pure gauge one) then the integral is to be evaluated in that gauge. Since Q is formally gauge invariant this procedure assignes a unique value to the integral. The application of this idea led to an expression of the topological charge which involves the thermal Wilson line, the free energy of a static quark. The classical action of the continuum gauge theory involves no dimensional parameter so the instanton solution have a zero mode, the dilatation transformation. On the lattice one deals with the regularised action which contains the lattice spacing as dimensional cut-off. It is a central question for the application of the saddle point approximation in lattice theories to clarify the effect of the dilatation transformation on the saddle point configuration. The study of the CP^n model showed that in case the usual instanton configurations become instable on the lattice and the minimal action configuration in a given Q sector is at the boundary of that sector (in other words only point-like instantons are stable in the lattice CP^n model). The study of this question and the Monte Carlo calculation of the topological charge in the four dimensional QCD is running. I hope to learn a more comprehensive picture of the dynamics of nonabelian gauge theories from these studies.

References

1) J. Polonyi, Topological charge of the lattice CP^n model, submitted to Nucl. Phys. B.

A New Scheme for Spontaneous-Symmetry-Breaking of Color SU(3) B C

A. Schäfer, B. Müller, and W. Greiner
Institut für Theoretische Physik der Universität Frankfurt

Various attempts have been made to describe quark-confinement as a mechanism that is analogous to superconductivity. This parallel is realized either phenomenologically, by introducing spontaneous-symmetry-breaking (SSB), which is equivalent to the phenomenological description of superconductivity by the Landau-Cinzburg theory; or on a more fundamental level by dynamical symmetry breaking copying the BCS-theory. We propose[1] a new phenomenological model using a modified scheme of SSB. Our Lagrangian is:

$$\mathcal{L}(x) = :\Big[-\tfrac{1}{4} A^a_{\mu\nu} A_a^{\mu\nu} + \sum_{i=u,d,\dots} \bar{\psi}_i (\not{\partial} + g T^a \not{A}_a - m_i)\psi_i + |\bar{\chi}(\partial_\mu - i g T^a A^\mu_a)\chi|^2 + \mu^2 |\bar{\chi}\chi|^2 - \lambda |\bar{\chi}\chi|^4 \quad (1)$$
$$- \sum_i f_i \bar{\psi}_i \psi_i \bar{\chi}\chi \qquad \{+\mathcal{L}_\chi\} \Big] :$$

The term $\alpha(x)\rho(x) := -\langle vac| \sum_i f_i \bar{\psi}_i \psi_i \bar{\chi}\chi |vac\rangle$ gives rise to an additional potential because the quarks are already initially massive in contrast to e.g. the Glashow-Salam-Weinberg-Model (Fig. 1). Thus the presence of quarks inhibits SSB and a quark-bag is formed. (Fig. 2). Another consequence of our SSB-scheme is that the A^8_μ-gluon (or the gauge equivalent gluon) gets massive. Following the arguments of de Rujula, Giles and Jaffe[2] we conclude that massive Q^8-charged bags are possible. These bags are not colored but have a kind of "color-polarization" which is particular in SU(3). Furthermore in contrast to ref. 2 quarks are still confined. As the volume of the Q^8-charged bag is made large by the gluons there are many unoccupied, low-energy quark states in it. Therefore a color-charged bag can reduce its mass by "swallowing" normal nucleons, gaining about one BV(nucl) per nucleon (i.e. the volume-energy per nucleon bag) in the process. Hence such charged bags should be produced most easily in a nuclear surrounding, i.e. in high-energy heavy-ion collisions. In fact there are several puzzeling experiments stating a reduced mean free path for secondaries produced in heavy ion collisions[3] and one experiment claiming the excistence of two temperatures[4] which can be explained qualitatively by our model.

[1] UFTP-preprint 97/1982
[2] A. de Rujula, R.C. Giles, R.L. Jaffe, Phys.Rev. D17, 285 (78)
[3] E.M. Friedlander, R.W. Gimpel, H.H. Heckmann, Y.J. Karant, B. Judek, E. Canssauge, Phys.Rev.Lett. 45, 1084 (80)
P.L. Jain, G. Das, Phys.Rev.Lett. 48, 305 (82)
H.B. Barber, P.S. Freier, C.J. Waddington, Phys.Rev.Lett. 48, 856 (82)
W. Heinrich et al., to appear in Nucl.Phys. A
[4] H.G. Baumgardt, E.M. Friedlander, E. Schopper, J.Phys. G7, L175 (81)

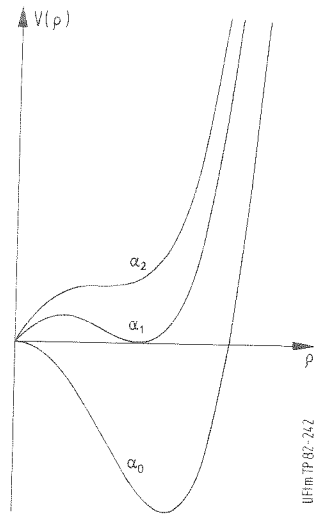


Fig. 1: The VEV of the Higgs-potential as a function of p for different values of α.
$\alpha_0 = 0$; $\alpha_1 = \left(\frac{2}{3}\right)^{3/2} \frac{\mu^3}{2\sqrt{\lambda}}$; $\alpha_2 = 2\alpha_1$

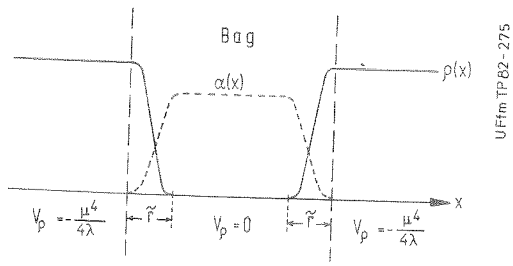


Fig. 2: The creation of quark bags by the prevention of SSB ($\tilde{r}$ denotes the width of the transition-region).

Centauros As A Superfluorescence Phenomenon G

G.N.Fowler
Physics Department, University of Exeter
E.M.Friedländer
Lawrence Berkeley Laboratory,University of California
R.M.Weiner
Fachbereich Physik, Universität Marburg

One of the recent challenges of cosmic ray high energy physics is the observation of Centauro events. In this work[1], we suggest that present knowledge might be sufficient to explain Centauros provided this knowledge is not restricted to the narrow domain of usual "theoretical high energy physics" and includes some recent advances in atomic physics. We connect the Centauro events with the phenomenon of superfluorescence and with the peculiar energy threshold for photons in the measuring device.

In order to understand the "abnormal" behaviour characteristic for Centauros, it is necessary to reconsider the explanation of the "normal" events characterized by the dominance of low p_T pions. Heavy particles constitute a small percentage of particles and high p_T particles an even smaller fraction. A simple explanation for these facts is given by the Pomeranchuk-Landau model. In the present model, we are, however, faced with a system in preequilibrium - a succession of equilibrium states characterized by a time dependent temperature T(t). To each value of T(t) corresponds an equilibrium configuration of different particle species governed by the statistical function

$$f \sim g_i p_i^2 / \exp\left(\frac{\sqrt{m_i^2 + p_i^2}}{T} \pm 1\right) \qquad (1)$$

where g_i is the statistical weight factor for species i and m_i the respective mass. Then it follows that the higher T(t) the more important the contribution of large masses to the spectrum of produced particles at the moment t.

An inspection of the particle tables shows that at energies (and hence temperatures) large enough for all known particles to be in equilibrium, pions have to complete with 36 kinds of mesons and 47 kinds of baryons. Most of these particles have pions as decay products but these secondary pions have energies lower by factors ranging from 2 to 6 than primary pions. It turns out that at initial temperatures large enough for all known resonances to be in equilibrium, the relative weight of primary pions is at most $^3/_{762}$ with our present knowledge of "elementary" particles.

In the high energy limit, the secondary pions, in spite of their larger weight, are suppressed by the Boltzmann factor and this the more so, the higher their weight. From this argument, it follows that if one could inhibit in a few events the expansion and let the system decay completely at an early stage of its history, at the very high energies where Centauros are found, no pions (and a fortiori photons) with energies exceeding the experimental threshold of 2000 GeV in the laboratory frame could be seen. Furthermore, because of the higher decay temperature the average p_T of particles produced would be much higher than in "normal" events. Such a precocious decay can be understood in analogy with the optical superfluorescence phenomenon[2]. It consists in the cooperative emission of particles from a coherently excited system. For a superfluorescence decay, the coherence length L_c must exceed the characteristic dimension L of system: $L_c \gg L$.
Also, the superfluorescent decay time τ_c should be smaller than any time scale of competing decay processes (lifetime of an isolated emitter): $\tau_c \ll \tau_0$.
For a system described by a Dicke-type hamiltonian, these two conditions may be met if the number of sources N is large: $N \gg 1$. At energies relevant for Centauro events, thus, the expectation that superfluorescence effects might occur in the decay of the hadronic fireball is not far-fetched.

If our interpretation of Centauro events as a "precocious" decay of the fireball due to superfluorescence is correct, it follows that contrary to what has been assumed so far, Centauro events do contain pions, but only low energetic ones. This prediction could be checked both at the CERN $\bar{p}$-p collider where mini-Centauros are expected and in cosmic rays. On the other hand, within this approach the frequency of Centauro events may not be predictable since the initial polarization from which the pulse begins is intrinsically random in character[2].

This work was supported in part by USDOE, DFG and GSI Darmstadt.

References

1) For details, see G.N.Fowler et al.,Phys.Lett.116B, 203 (1982)
2) B.Bonifacio and L.A.Lugiato,Phys.Rev.A11,1507 (1974); F.Haake et al.,Phys.Rev.A20,2047 (1979).

2. Atomic Physics

		PAGE
2.1	Superheavy Quasi-Atoms and Inner Shell Excitation Mechanism	146
2.2	Few Electron Systems, Recoil Ions and Capture Processes	155
2.3	Interaction of Heavy Ions with Matter	162
2.4	Theory	167

Study of positron-creation in overcritical HI-collision systems [B]

H. Bokemeyer, H. Folger, H. Grein, Y. Kido (GSI, Darmstadt);
T. Cowan, J.S. Greenberg, J. Schweppe (Yale U.);
K. Bethge, A. Gruppe, R. Merten, Th. Odenweller, K.E. Stiebing (Univ. Frankfurt);
D. Schwalm (Univ. Heidelberg); P. Vincent (Rutgers U.); N. Trautmann (Univ. Mainz)

We report the recent results of our investigations of e^+ production in $^{238}U+^{208}Pb$, $^{238}U+^{238}U$, and $^{238}U+^{248}Cm$ collisions at bombarding energies near the Coulomb barrier, as performed with the e^+-solenoid spectrometer EPOS[1].

The overall features of the e^+-production cross section as observed in the e^+-energy spectra (Fig. 1) and particle angular distributions are in good agreement with the theoretically proposed dynamic mechanisms of quasiatomic e^+-production involving Coulomb trajectories only[2]. Agreement over the whole measured range is also seen for the impact parameter dependence of e^+-production in the subcritical U+Pb system, where we have separated close from distant collisions.

In addition to the bell-shaped energy distributions identified with dynamic e^+-production processes, structures have been observed in the U+U and U+Cm collision systems for specific kinematic conditions[1]. In particular, a well defined peak has been observed in the U+Cm collision system[3] centered at 320 keV with a width of ~80 keV. The intensity of the peak seems to be correlated with events which overlap the angles of backward elastic scattering ($100° \lesssim \theta_{cm} \lesssim 130°$) and the peak appears to be absent for forward elastic scattering angles and $\theta_{cm} \approx 90°$. Partial kinematic separation in this nearly symmetric collision system was demonstrated by the γ-ray emission ($E_\gamma > 1$MeV), which exhibits a pronounced asymmetry between forward and backward scattering.

The observed width of the line is largely due to Doppler broadening and implies that the emitting system lives for more than 10^{-20} sec. Among the possible known sources for this peak structure are both nuclear and electrodynamic processes. A principle nuclear process to be considered is internal pair-conversion in one of the two residual nuclei. In order to explain the observed width, however, the transition must occur in the U-like fragment and must be accompanied by the unlikely capture of the electron, preferentially into the atomic K-shell. The exclusion of such nuclear processes by experiments in progress would then open up for serious consideration the possibility that spontaneous positron emmision is being observed associated with the formation of metastable giant nuclear complexes[2].

1) H.Bokemeyer et al., NASI, Lahnstein, 1981, ed. W.Greiner, (Plenum Press, New York 1982)
and in J.S.Greenberg, Proc. X-82, Eugene, 1982, ed. B.Crasemann (AIP, New York 1982) p. 173

2) U.Müller et al., HI Coll. Lect. Notes in Phys. 168 (Springer Verlag, Berlin 1982) p. 388
and T.de Reus et al., to be published

3) J.S.Greenberg & W.Greiner, Phys. Today 35:8(1982)24

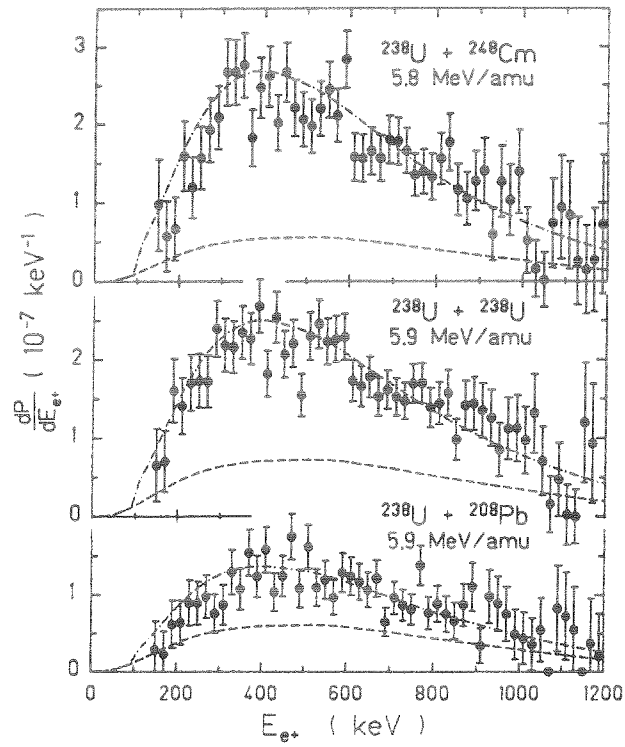


Fig. 1: e^+-energy spectra for particle scattering angles of $25° < \theta_{Lab} < 65°$. The data are compared with the sum (dashed-dotted line) of the theoretical e^+-distribution[2] and the e^+-contribution originating from nuclear transitions (dashed line).

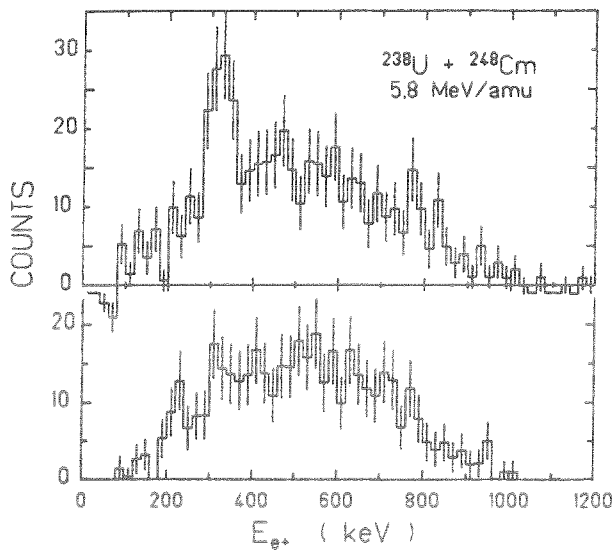


Fig. 2: e^+-energy spectra for the U+Cm collision system - not corrected for the spectrometer efficiency - when selecting HI scattering angles corresponding to close (upper part) and distant (lower part) collisions (see text) in the particle scattering angular region $27.5° < \theta_{Lab} < 40°$.

Narrow Structure in Positron Spectra from U + U Collisions [B]

E.Berdermann, M. Clemente, P. Kienle, H. Tsertos, W. Wagner (TU München)
F. Bosch, C. Kozhuharov (GSI)
W. Koenig (MPI Heidelberg)

In previous Scientific Reports[1] a sample of representative results of our studies of e^+-production has been presented: e^+-spectra, exhibiting a pronounced and narrow peak structure, superimposed over the broad distribution of the dynamically induced positrons. The position and the width of the structure as well as its dependence on particle scattering angle and on the incident energy of the U-beam conspicuously coincide with the speculation about spontaneous positron emission from the combined U+U collision system, if the latter undergoes a nuclear reaction with a rather long ($> 10^{-20}$ sec) reaction time[2,3].

In our present investigations we addressed ourselves to the question whether a detailed analysis of the measured strong dependence on the particle scattering angle and on the bombarding energy in the vicinity of the Coulomb barrier may corroborate the above conception and - combined with studies of the γ- and δ-ray spectra - may point to or rule out other possible explanations.

Fig. 1 and Fig. 2 show as illustrative example spectra of positrons, measured at different bombarding energies (Fig. 1: 5.7 MeV/u and Fig. 2: 6.2 MeV/u) and associated with particles scattered between 38° and 52° (Fig. 1) and between 29° and 32° (Fig. 2) respectively. The solid curves represent the results of least square fits to the data, using spectral distributions for the dynamically induced e^+-emission[4] and superimposed a line from the spontaneous positron decay of a K-vacancy in the field of two U-nuclei in contact[2] with the resonance energy and the nuclear contact time as parameters. Reasonable agreement with the experimental points is achieved for resonance energies of 310 keV and of 270 keV and contact time values as large as $(6.0 \pm 0.5).10^{-20}$ sec and $(4.6 \pm 1.0).10^{-20}$ sec for the spectra in Fig. 1 and Fig. 2 respectively.

Fig. 3 displays the cross section for the narrow structure as a function of the particle scattering angle at three bombarding energies. For the lowest 5.7 MeV/u incident energy the effect is apparently peaked at 82° with a minimum at 90° c.m., whereas the highest bombarding energy leads to the largest enhancement with a rather flat angular distribution.

[1] GSI-Sc.Rep.1980, p. 128 & 1981, p. 138
[2] J. Rafelski et al. Z.Phys.A285(1978)49
[3] J. Reinhardt et al. Z.Phys.A303(1981)173
[4] U. Müller - private communication

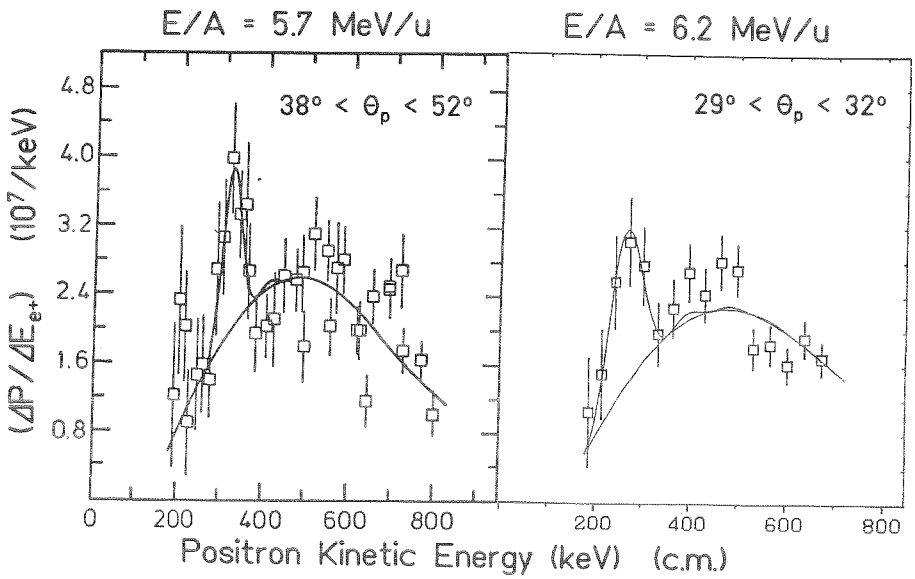


Fig. 1: (left) and Fig. 2: (center) e^+-spectra at different bombarding energies and for particle scattering angles as indicated. The solid curves represent a fit to the data using results of theoretical calculations

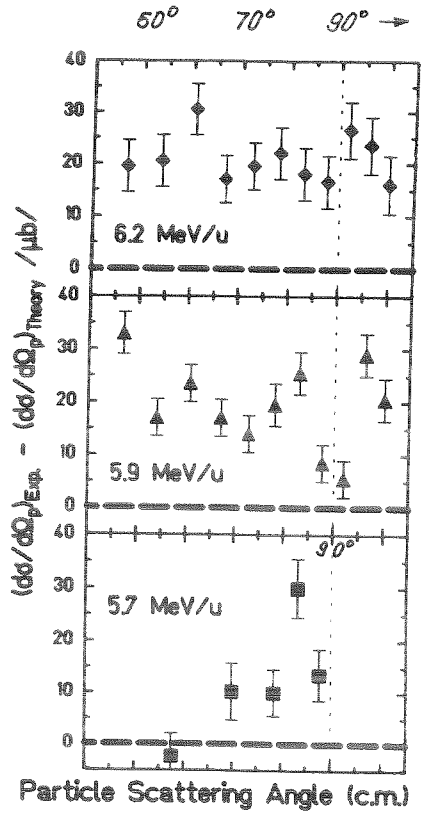


Fig. 3 : Peak area (excess over the dynamical theory) as a function of the scattering angle

Positron Production in Peripheral and Close Collisions measured with the New Tori Spectrometer

E. Bozek, U. Gollerthan, E. Kankeleit, G. Klotz, M. Krämer
R. Krieg, U. Meyer, H. Oeschler, P. Senger
Institut für Kernphysik der TH Darmstadt

On the new Tori spectrometer[1]), installed at beam position X8, several detailed test and calibration experiments were carried out and a first production experiment studying positrons emitted in heavy ion collisions was performed in october 82.

The Tori spectrometer[1]) combines a high positron transmission (80 %) with an excellent suppression of electrons. Figure 1 shows the fraction of electrons reaching the positron detector in dependence of the diaphragm position in the middle plane of the instrument. For a position of 2 mm towards the positron side as used in the runs there are only scattered electrons reaching the positron detector. This allows excellent measurement of the positrons being produced with a probability of about 10^4 times less.

Our experimental program is devoted to the study of time-delay effects due to nuclear contact in heavy ion collisions. The spectral distribution of the positrons emitted from the quasi atom reflects the dynamics of the collision process[2]). Compared to elastic or quasi-elastic reactions, the collision time increases for damped reactions which leads to a different slope in the high-energy tail of the positron spectra[2]). In the case of U + U, the deep-inelastic collisions are identified by their subsequent fission decay.

We studied the reaction U + U at 7.5 and 8.4 MeV/u. The detected positrons are grouped into two classes of collision types; those are determined by two parallel-plate avalanche counters and figure 2 represents a 2-dimensional plot of the polar angles of two emitted fragments. Elastic scattering is clearly separated from inelastic collisions as the subsequent fission decay destroys a unique angular correlation. Figure 3 shows the first positron spectra measured simultaneously in coincidence to peripheral (elastic) and close (inelastic) collisions. In order to obtain the nuclear origin positrons the U + Pd and U + Ta systems has been studied. Analysis is in progress to deduce the high energy positron tail by unfolding the spectra and substracting nuclear positrons. Because of the statistical quality of the high energy region of the spectra valuable information should be obtained concerning the time delay of the deep inelastic reaction.

1. E. Kankeleit et al., GSI Scientific Report 1981; and to be published in Nucl. Instr. and Meth.
2. E. Kankeleit, Nukleonika 25,253(1980); H. Backe et al.; to be published.

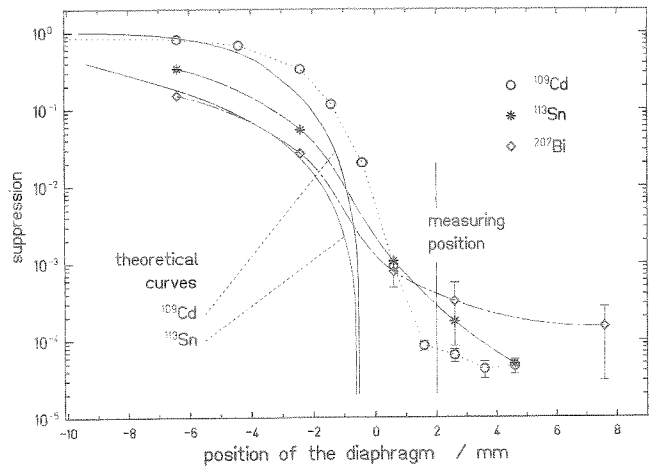


Fig.1: Electron suppression as function of diaphragm position

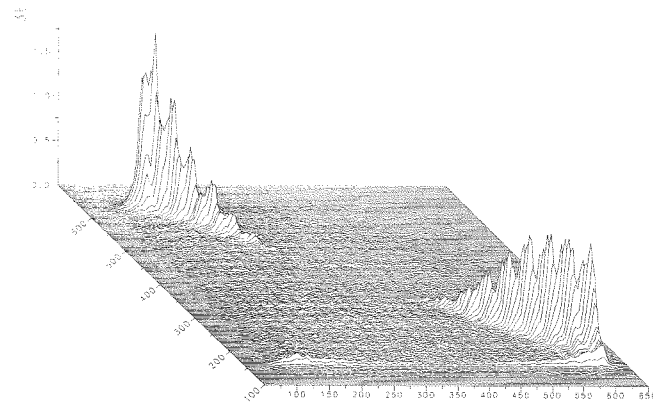


Fig.2: U + U 8.4 MeV/u: Angular correlation between the emitted fragments exhibiting the two classes: elastic scattering and deep-inelastic collisions observed by their fission decay.

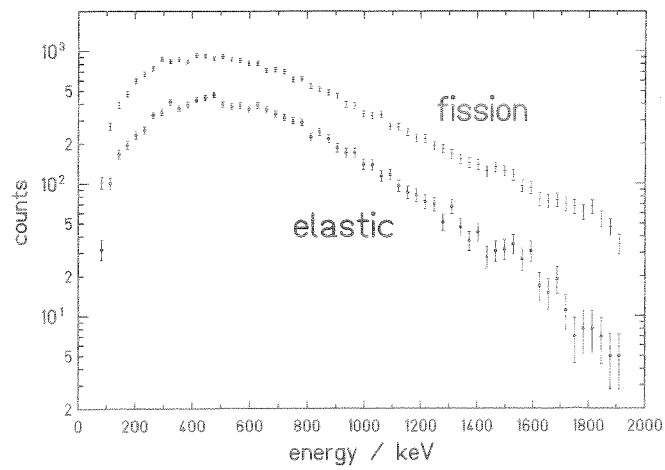


Fig.3: Positron spectra in coincicence to the two reaction processes indicated in figure 2.

Investigations of the Coherence Between Different Excitation Channels in Heavy Ion-Atom Collisions

A. Warczak*, H.D. Dohmann, D. Liesen, B. Liu**
GSI Darmstadt
*permanent address: Jagellonian University, Cracow, Poland
**permanent address: Institute of Modern Physics, Academia Sinica, Lanzhou, China

In order to verify our suggestions in respect to possible coherence between different excitation channels in adiabatic ion-atom collisions[1], the impact parameter dependence of K- and L-vacancy production has been measured using targets with different thickness in U+Sn and Kr+U collisions at 1.4 MeV/N energy.

The excitation processes responsible for K- and L-vacancy production are found to be dependent on the outer-shell structure of the combined Z_1+Z_2 system, especially in very asymmetric collisions, indicating the increasing role of multistep excitation.

Therefore, we expected for targets of different thickness and thus, for different outer-shell configurations of the projectiles (solid state effects), a possible change in the coherence conditions leading to variations of phase and amplitude in the oscillations observed in the excitation curves[1].

The scattered ions, registered by a position sensitive avalanche detector[2], were recorded in coincidence with characteristic X-rays yielding the excitation curves shown in Figs. 1, 2 for U+Sn collisions.

Both, U-L and Sn-K vacancy production depends on the target thickness in the impact parameter range under consideration. The $3d\sigma$ excitation, dominating the U-L vacancy production depends on the target thickness and thus, on the outer-shell structure of the combined atom (Z_1+Z_2=142). The peak at small impact parameters (Fig. 1), produced probably due to the rotational $3d\delta$-$3d\pi$-$3d\sigma$ coupling, seems to be not sensitive to the target thickness.

The Sn-K vacancy production (Fig. 2) is well described by an exponential function characterizing the direct excitation of the $2p_{3/2}\sigma$ MO. This excitation increases by almost a factor of 2 for a 40 µg/cm² target in comparison to a 5 µg/cm² target. At impact parameters between 70 and 150 fm both curves (Fig. 2) exhibit an oscillating structure.

We interprete these oscillations as interference between $2p_{3/2}\sigma$ and $2p_{1/2}\sigma$ excitation. As expected, as well the amplitude, as the phase are influenced by the target thickness.

In Fig. 3 similar but more significant phase shifts due to target thickness variations are shown for Kr+U collisions.

Further investigations on this subject are in progress.

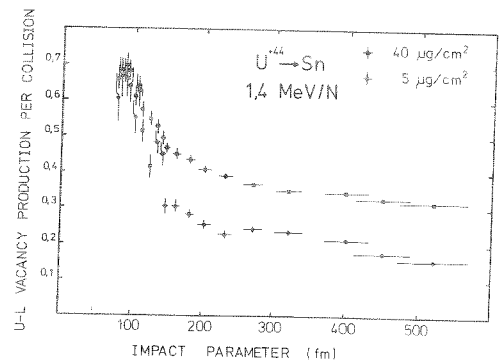


Fig. 1

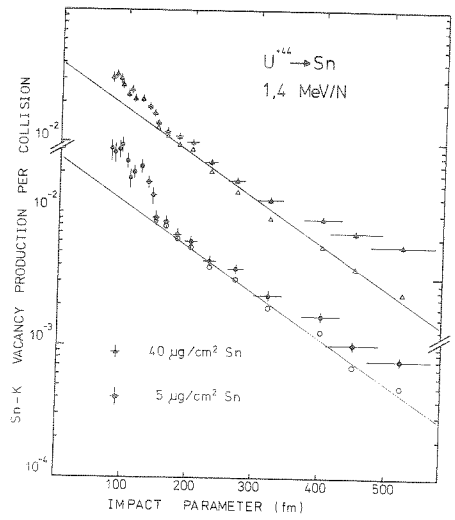


Fig. 2

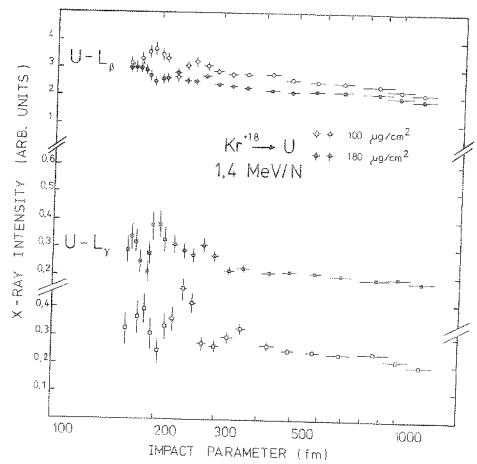


Fig. 3

[1] B. Liu et al., this issue
[2] B. Liu et al., this issue

Oscillations in the Inner-Shell Vacancy Production in Heavy Ion-Atom Collisions

B. Liu*, H.D. Dohmann, D. Liesen, A. Warczak**
GSI Darmstadt
*permanent address: Institute of Modern Physics, Academia Sinica, Lanzhou, China
**permanent address: Jagellonian University, Cracow, Poland

The general features of the impact parameter dependence of the inner-shell vacancy production probability in adiabatic ion-atom collisions seem to be reasonably well understood nowadays. Extensive experimental and theoretical investigations revealed the characteristics of the dominant excitation mechanisms, the direct ("Coulomb") and the molecular excitation.

The direct process shows a pure exponential dependence on the impact parameter b. The molecular process exhibits for a rotational coupling a typical double-peak structure ("the adiabatic peak at large b and the kinematic peak at small b"), and for a radial coupling in most cases a smooth dependence on b, usually a decreasing excitation probability with increasing b.

The measurements of the vacancy production probabiltiy P(b) proceed mostly via the observation of the characteristic x rays which are emitted with the decay of the excited states. Thereby, only the final states are fixed, while the many initially excited states can not be separated. Thus, the coherent superposition of all these excitation channels which lead to the same final state, may result in structures in the impact parameter dependence which should be observable in favourable cases.

Using an especially designed position sensitive particle detector with delay-line read-out[1] experiments at 1.4 MeV/N projectile energy have been performed in order to find such structures. The results are plotted in Figs. 1-3 which show L- and K-shell vacancies per collision as a function of the impact parameter for three different collision systems. Obviously, oscillations show up with increasing amplitudes at small impact parameters. For Xe+Ni and Zr+Pb collisions these osciallations are in phase for the L- and the K-shells, respectively, while they are out of phase for Kr+U collisions. Additionally, the phase of the oscillations depends for a given collision system on the thickness of the target[2]. Therefore, gas target experiments are planned in order to find a possible systematic.

For a theoretical analysis of the data the usually applied two-state models have to be replaced by coupled-channel calculations based on realistic correlation diagrams. Thus, steps towards a spectroscopy of inner-shell molecular orbitals may be possible.

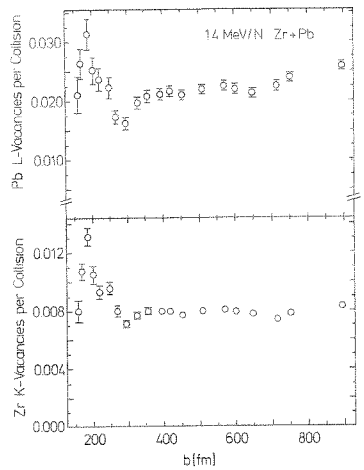


Fig. 1

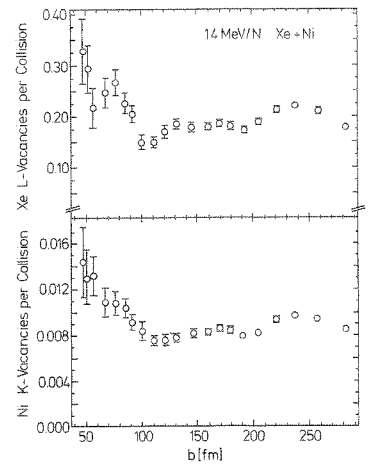


Fig. 2

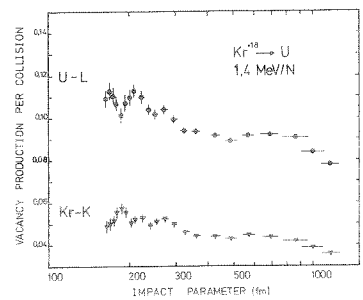


Fig. 3

[1] B. Liu et al., this issue

[2] A. Warczak et al., this issue

Kinematic peak in Very Asymmetric Ion-Atom Collisions

D. Maor
Department of Physics, Technion, Haifa, Israel
Z. Stachura*, P.H. Mokler, B. Liu**, D. Liesen
GSI Darmstadt

In almost symmetric ion-atom collisions, vacancy production in shells for which the orbital velocity u is higher than the collision velocity v is considered to be due to electron promotion, mainly via the $2p\pi$-$2p\sigma$ rotational coupling. In more asymmetric collisions, the adiabatic peak in the vacancy production probability as a function of impact parameter P(b) disappears and the main mechanism there is direct ionization from the molecular orbitals, near the united atom limit[1].

In the present experiment, P(b) measurements for asymmetric systems ($Z_2/Z_1 \geq 1.8$) were extended to very small impact parameters, where a second, kinematic peak is expected due to rotational coupling. This peak has been measured for near-symmetric I - Ag collisions by Anholt et al.[2]. The consideration for looking for this peak here was that in the sudden approximation the kinematic peak is a geometrical effect which requires only that the electrons follow the molecular orbitals.

P(b) was determined by coincidences between K x-rays of the lighter collision partner and scattered particles. The heavier collision partner was chosen as projectile. Thus, more $2p\pi$ vacancies are introduced into the collision by the double-collision mechanism and the effect should be larger. Also, large center-of-mass angles (ϑ_{cm}) can be measured at moderate lab. angles (ϑ_{lab}) and, due to the dual kinematics, up to three impact parameters can be measured at the same ϑ_{lab}. ^{136}Xe and ^{120}Sn ion beams, at 1.4 MeV/u impinged upon thin Ni and Cu targets, respectively. The x rays were recorded by two Si(Li) detectors on both sides of the target and at 90° to the beam. The particles were detected by one annular, or by an array of several normal surface barrier detectors.

Fig. 1 displays P(b) for the Cu K-shell. For larger b, these data agree well with our previous work[1]. At the lowest b values, a prominent peak appears, its maximum being at $\vartheta_{cm} = 90°$, exactly where it should be for the kinematic peak. The solid curve in the figure is $A\sin^2\vartheta_{cm}+B$ with the parameters, A and B, fitted to the data. B is the assumed constant contribution of the direct ionization. An asymmetry of the data compared to the calculated shape can be seen. This cannot stem from the change in the shape of the wavefunctions due to relativistic effects[3].

However, the peak is probably due to the kinematic effect. No other mechanism is supposed to cause such a shape in a region corresponding to distances of closest approach from 65 fm to 36 fm, when the K-shell radius of the united atom is ≈ 600 fm.

It seems therefore that the kinematic peak appears even in asymmetric systems, provided the MO model is still applicable and one might even consider using it as an adiabaticity test.

*Permanent address: Institute of Nuclear Physics, Cracow, Poland
**Permanent address: Institute of Modern Physics, Academia Sinica, Lanzhou, China

[1] D. Maor et al., Phys. Rev. A, in press
[2] R. Anholt et al., J. Phys. B: At. Molec. Phys. 13, 3807 (1981)
[3] B. Fricke, private communication

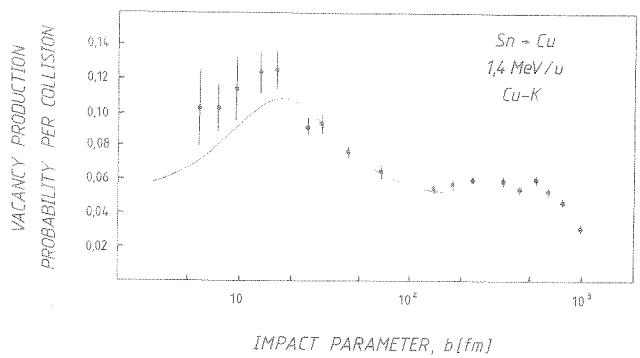


Fig. 1: Vacancy production probability for Cu-K excitation in 1.4 MeV/u Sn-Cu collisions. The solid line gives the expected shape for the kinematic peak of the $2p\pi$-$2p\sigma$ coupling.

B

K-Shell Excitation by K- to L-shell Charge Transfer in Slow Kr^{q+}-Kr and Xe^{q+}-Xe Collisions

R. Schuch, E. Justiniano, R. Hoffmann
Physikalisches Institut, Universität Heidelberg

W. Schadt and H. Schmidt-Böcking
Institut für Kernphysik, Universität Frankfurt

P.H. Mokler, F. Bosch, W.A. Schönfeldt, Z. Stachura
G S I Darmstadt

In collisions of slow highly charged ions with atoms vacancies in the inner atomic shells are predominantly produced by charge transfer instead of ionization. We investigated in this work the mechanism for capture of K-electrons into projectile L-vacancy states for heavy collision systems ($Z_1+Z_2 \simeq 70$-110). From measurements of impact parameter dependent K-vacancy probabilities ($P_K(b)$) for light symmetric collision systems it is well known that this transfer process occurs with a high probability ($\simeq 10\%$ per projectile L-vacancy) by rotational coupling between $2p\pi$, $2p\sigma$ quasimolecular states.

Because of the increasing fine structure splitting with increasing Z, it is not clear whether $2p\pi$-$2p\sigma$ rotational coupling is still the predominant L- to K-shell vacancy transfer mechanism in heavy collision systems. Calculations[1] have shown that in very heavy collision systems radial coupling between states of equal parity is predominant. A sensitive tool to determine the charge transfer mechanism is the measurement of $P_K(b)$ with slow highly charged projectiles incident upon a gas target. Such a measurement did not exist to date in the region of heavy collision systems.

The projectiles of 2.8 MeV/u Kr^{q+} (q=16,26,29-33) and 3.6 MeV/u Xe^{q+} (q=43,45,47), respectively were obtained by the Unilac accelerator by poststripping at 5.9 MeV/u and 8.6 MeV/u, respectively and deceleration to low velocities. A thin Kr and Xe gas target, respectively was used in order to have single collision conditions. The $P_K(b)$ for Kr on Kr (fig.1) shows for q=16 and 26 (no L-vacancy) a flat behaviour at small b and a strong decrease at b > 2000 fm. This can be understood as ionization of the $2p\sigma$ state as shown by the SCA prediction (dashed line). The shape of $P_K(b)$ changes drastically as soon as L-vacancies are brought into the collision. In this case one observes a clear peak at about 1300 fm which increases with increasing q and reaches a saturation at an empty 2p-shell. The full line represents the calculation[2] of the $2p\pi$-$2p\sigma$ rotational coupling for q=29. The agreement is good especially when considering that in this calculation a nonrelativistic description of the states is used. A better agreement of the $P_K(b)$ data with calculations[3] done with relativistic quasimolecular 2p wavefunctions is obtained for the Xe-Xe collision system. These data are plotted in fig.2 in comparison with a nonrelativistic[2] (full line) and relativistic[3] (dashed line) description of the K- to L-shell charge-transfer process.

References

1 Soff, G., Greiner, W., Betz, W., Müller, B., GSI Report VT-5-78
2 Taulbjerg, K., Briggs, J.S., Vaaben, J., F. Phys. B19, 1451, 1976
3 Jakubassa D.H., Taulbjerg, K., J. Phys. B13, 757, 1980 and Jakubassa, D.H., private communication

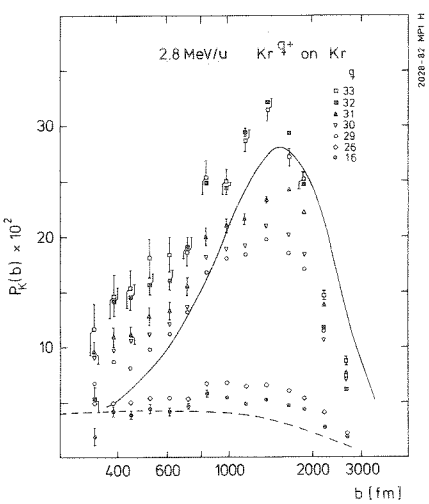


Fig.1: K-vacancy production probability as function of impact parameter and projectile charge state.

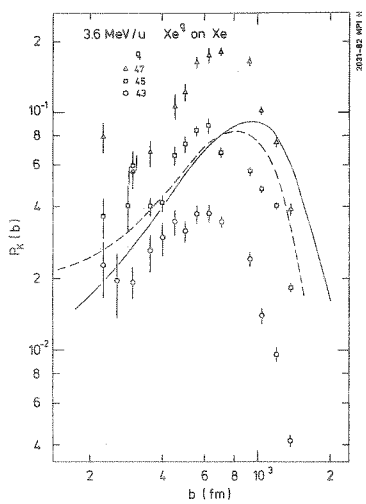


Fig.2: Same as fig.1.

Charge Transfer in Atomic Collisions with Highly Ionized, Decelerated Heavy Ions

P.H. Mokler, D.H.H. Hoffmann, W.A. Schönfeldt
GSI Darmstadt
Z. Stachura and A. Warczak
Inst. Nucl. Physics and Jagellonian University, Cracow, Poland

For Xe^{q+}-Xe collisions the charge transfer in the various atomic shells has been studied using the acceleration-stripping-deceleration method[1]. 3.6 MeV/u Xe^{q+} ions with charge states up to q=47 - i.e. up to 3 vacancies in the projectile L shell - have been provided by the UNILAC.

Considering the corresponding correlation diagram, we can deduce from the increase in K x-ray emission with q for an opened incoming projectile L shell the vacancy transfer, see Fig. 1. The measured L-K vacancy cross section agrees roughly with the calculated $2p\pi$-$2p\sigma$ transfer cross sections given in 10^3 barn in the table:

MeV/u	exp.	TBV[2]	AMS[3]	JT[4]
2.2	2.5±0.3	5.6	5.8	4.4
3.6	2.9±0.1	7.1	6.6	5.4

For the theoretical values a statistical factor of 1/6 has been applied. Using a factor of 1/8, i.e. considering all L-shell states a better agreement is yielded. This agreement is remarkable as for the collision system investigated the spin-orbit splitting in the united atom L shell of 9 keV is already 30 % of the binding energy.

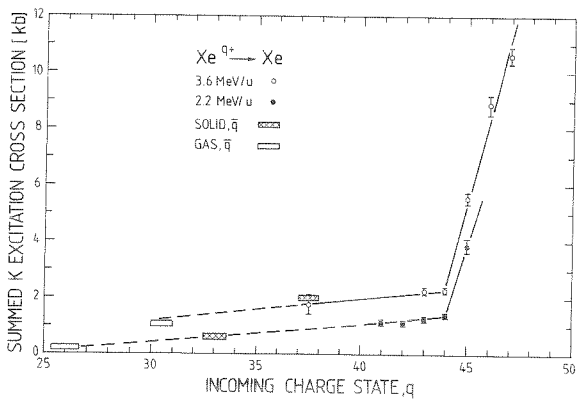


Fig. 1: Variation of the K excitation cross section with projectile charge state q. The data exhibit a pronounced rise with the opening of the projectile L shell.

Vacancy transfer to higher lying projectile shells (M,N,...) has been studied via L x-ray emission. After opening of the projectile L shell a captured M,N,... electron has a chance to decay radiatively to the projectile L shell. Hence, a drastic increase in L x-ray emission is observed after opening of the projectile L shell[1]. Surprisingly, a drastic intensity variation of the various L x-ray components is observed, see Fig. 2: For one projectile L vacancy the normally weak M_1-L_3 transition dominates, for three

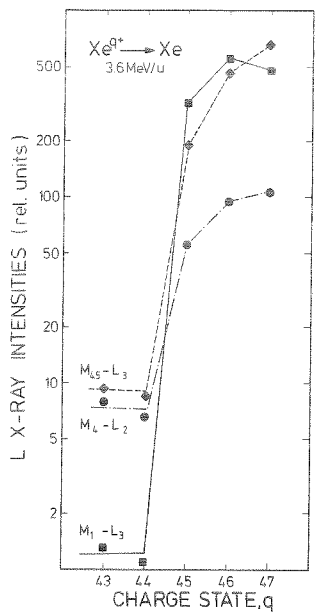


Fig. 2: L xray intensities showing a different behaviour for various transitions to the projectile L shell. At charge state q=45 the M_1-L_3 transition dominates the L x-ray spectrum.

incoming vacancies the normal $M_{4,5}$-L_3 transitions gains again.

The total charge transfer into the projectile was determined by observing the L x-ray emission as a function of the traversed target thickness by a position sensitve proportional counter. From the variation of L x-ray emssion with gas target thickness, see Fig. 3, total capture cross sections in the region of almost 10^{-16} cm^2 have been found. An appreciable amount of electrons are not captured to the projectile ground state.

[1] P.H. Mokler et al., in annual report GSI 82-1, p. 143
[2] K. Taulbjerg et al., J. Phys. B9 (1976) 1351
[3] R. Anholt et al., Phys. Rev. A16 (1977) 951
[4] D. Jakubassa, K. Taulbjerg, J. Phys. B13 (1980) 757

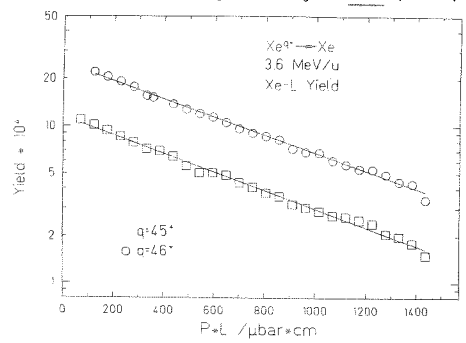


Fig. 3: Total x-ray yield as a function of increasing target thickness.

L_3-Subshell Alignment Observed in 1.4 MeV/N Ion - Atom Collisions

Z. Stachura*, F. Bosch, D. Maor**, P.H. Mokler, W.A. Schönfeldt, H. Wahl
GSI Darmstadt
B. Cleff, M. Brüssermann, J. Wigger
University of Münster

We continued the systematic investigation of a collisionally induced L_3-subshell alignment in collisions of heavy ions with atoms. In systems with $Z_{projectile} \approx Z_{target}$ a quasimolecular type of inner shell excitations dominates over a direct Coulomb excitation mechanism. We bombarded thin (30-200 $\mu g/cm^2$) targets of various elements with 1.4 MeV/N ions of U, Pb, Xe, Kr, Cu, and Ca. As in our previous studies[1], the alignment values, A_{20}, are derived from the measured anisotropy of the L_ℓ line distribution with respect to the beam axis. In a region of K-L level matching an analysis of angular distribution is impeded by a proximity of K- and L-transitions, with a relative energy difference being angle dependent because of a different Doppler shift for projectile and target radiation. In order to overcome this difficulty, a value for the alignment in Xe + Ti collisions has been deduced from a linear polarization measurement of the L_ℓ transition in xenon. In the experiment a polarimeter of the University of Münster was used.

The A_{20} values derived in the experiment have been corrected for Coster-Kronig transitions using experimental Coster-Kronig transitions rates obtained by Schönfeldt[2]. The corrections are negligible except for very asymmetric collision systems. Corrected values for the alignment, together with the results of our previous experiment[1] are shown in Fig. 1 and are compared with the data obtained by Jitschin et al.[3] for collisions of Au atoms with light ions.

In the present experiment the reduced projectile velocity, $v_r = v/v_{L_3}$ varies betwwen 0.21 and 0.24 for collisions with U and Pb particles, respectively. For the comparison with the data from Ref. 3 we selected a reduced velocity of $v_r \approx 0.22$. As can be seen in Fig. 1 for very asymmetric collision systems (before K-L level matching) the alignment is negative (and depends on the reduced collision velocity). Around the K-L level matching itself the alignment varies strongly. Beyond the K-L level matching the alignment vanishes. This general behaviour may result from a competition between direct and quasimolecular excitation. For very asymmetric collision systems the direct excitation mechanism overwhelms yielding negative A_{20} values. Beyond the K-L level matching the quasimolecular excitation - mainly via the $3d\sigma$ level - dominates and all the L sublevels may interact with each other resulting in a vanishing alignment.

The authors are indebted to Dr. H. Folger and his Group for providing numerous targets used in the experiment.

*Permanent address: Institute of Nucl. Physics, Cracow, Poland
**Permanent address: Dept. of Physics, Technion, Haifa, Israel

[1] Z. Stachura et al., GSI Scientific Report 1981, p. 144
[2] W.A. Schönfeldt, GSI Report, GSI-81-7
[3] W. Jitschin, private communication and Proceedings, Energiereiche Atomare Stöße (EAS-3), Schönau, January, 1982

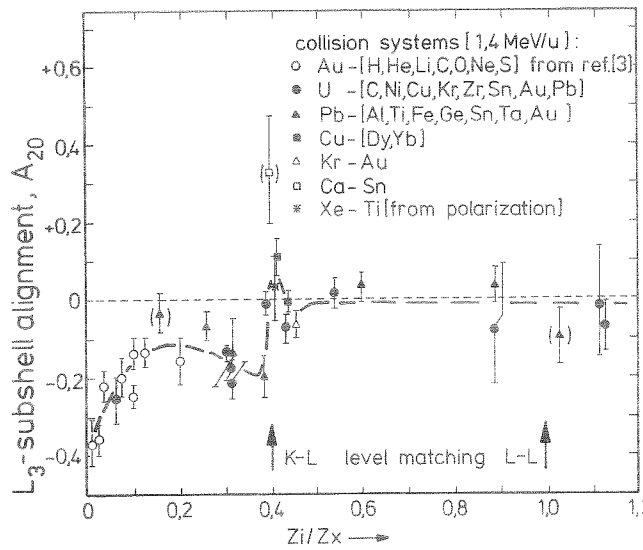


Fig. 1: L_3-subshell alignment (A_{20} of ions with atomic number Z_2 plotted as a function of the asymmetry of the collision (Z_i/Z_x), where Z_i is the atomic number of the other collision partner. The solid line is just an eye guide.

Wavelengths of Transitions in Few Electron Spectra of Titanium

H.D. Dohmann, D. Liesen, E. Pfeng
GSI Darmstadt

Using the beam foil technique, Ti-ions with specific energies of 3.6 and 4.8 MeV/N were excited by C-foils (110 $\mu g/cm^2$). Prompt and delayed emitted K x-rays have been studied with a flat-crystal spectrometer ($\lambda/\Delta\lambda \approx 1200$ FWHM). Fig. 1 shows the prompt emitted spectrum taken at 4.8 MeV/N projectile energy in the wavelength region between 2.45 and 2.70 Å. At this specific beam energy, the emission from He-like Ti ions with one K-vacancy is dominant. Therefore, at λ = 2.6105 Å we find the He-like resonance line which is separated from the decay of Li like configurations $1s2s2p$, $1s2s^2$, and $1s2p^2$ (marked by bars in Fig. 1 between 2.62 and 2.7 Å).

In the lower wavelength region between 2.48 and 2.50 Å Fig. 1 shows the clearly resolved Lyman-α splitting. A detailed analysis of the spectrum (Fig. 2) which takes the resolution function of the spectrometer into account, reveals that the wavelength of the transitions can only be calibrated properly if the influence of spectator electrons with principal quantum number n = 3 is considered. By measurements of every line at two known beam velocities, the influence of the linear and quadratic Doppler effect on the accuracy of the absolute wavelength was drastically reduced.

A preliminary comparison of experimental and theoretical wavelengths is shown in Table 1. Within the absolute error bar of the experiment $\Delta\lambda = \pm 0.0003$ Å most theoretical data agree with the experimental result[1].

The aim of further experiments is the precise measurement of the fine structure splitting and of the Quantum Electrodynamics (QED) effects.

[1] H.D. Dohmann et al., to be published

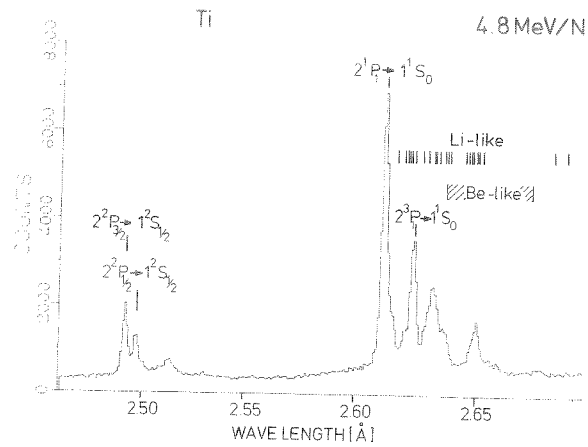


Fig. 1: Few-electron x-ray spectrum of a Ti beam with 4.8 MeV/N specific energy.

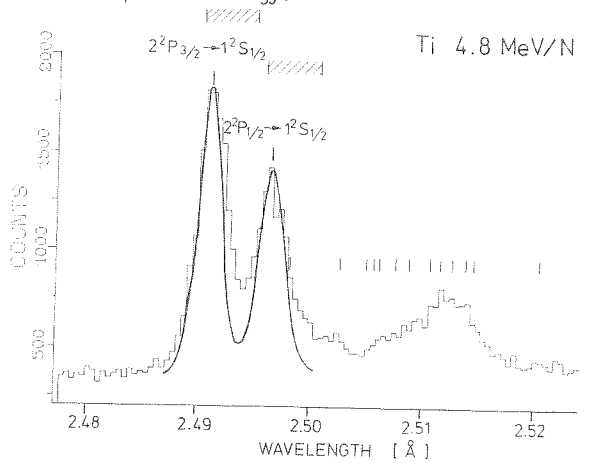


Fig. 2: Lyman-α lines of Ti. The position of the $2p2s,p \rightarrow 1s2s,p$ transition is marked by bars and the region of the $2p3s,p,d \rightarrow 1s3s,p,d$ wavelength is hatched. These transitions with an spectator electron in n=3 result in the observed asymmetry of the Lyman-α lines.

Table 1

Comparison of experimental λ_{exp} and theoretical wavelengths λ_{the} in H-, He-, and Li-like Ti ions.

Charge State	Transition	λ_{exp} [Å]	λ_{the} [Å] Ref. 9	Ref. 21	Ref. 11	Ref. 12	Ref. 13	Ref. 14	Ref. 15	Ref. 16
H-like	$2^2P_{3/2} \rightarrow 1^2S_{1/2}$	2.4911	2.4912$_2$	2.4911$_7$		2.4903		2.4900$_4$		
	$2^2P_{1/2} \rightarrow 1^2S_{1/2}$	2.4966	2.4966$_4$	2.4965$_9$		2.4956		2.4954$_5$		
He-like	$(1s2p)^1P_1 \rightarrow (1s^2)^1S_0$	2.6105			2.6104$_5$	2.6097	2.6098	2.6102		
	$(1s2p)^3P_2 \rightarrow (1s^2)^1S_0$	2.6186			2.6191$_3$	2.6183	2.6186	2.6189		
	$(1s2p)^3P_1 \rightarrow (1s^2)^1S_0$	2.6229			2.6228$_8$	2.6221	2.6224	2.6227		
Li-like	$1s2s2p^4P_{5/2} \rightarrow 1s^22s^2S_{1/2}$	2.6439				2.6436	2.6437		2.6476	2.6438

Projectile Dependence of Multiple Target Ionization Observed in K Satellite Spectra

H.F. Beyer, R. Mann
GSI Darmstadt
F. Folkmann
University of Aarhus, Aarhus Denmark

The production of highly charged slow target ions by bombardment with highly stripped ion beams has been studied systematically by observation of K x rays and Auger electrons in high resolution. It is of great interest to know how multiple target ionization depends on beam parameters such as projectile charge and velocity. This affects the efficiency of high-charge recoil ion sources employed either in situ for spectroscopic studies or in extraction mode for secondary collision studies. Previously we have studied the neon x-ray spectra[1] after bombardment with heavy ions. The data revealed a systematic trend with the probability for L-shell electron removal (in K-shell ionizing collisions) to lie on a universal curve when plotted as a function of projectile velocity devided by ionic charge. Nearly all of those data were obtained with projectiles which were in their equilibrium charge states. We have now extended[2] these studies to a broader range of projectile velocities and also to different charge states at constant velocity. Beams were employed of Ar up to U of charges from 10+ to 70+ and energies 1-9 MeV/amu from the UNILAC and Cl and Br beams of charge 4+ to 12+ and of energies 0.3-0.9 MeV/amu from the 6-MV tandem Van de Graaff accelerator in Aarhus.

Representative spectra are given in Figs. 1 and 2. Fig. 1 shows the uranium projectile charge-state dependence in the relative population of Ne^{7+} and Ne^{8+}. For comparison is given the spectrum induced by Ar^{12+} which has a similar charge state as U^{10+}. It is interesting to note that the high-Z projectile produces a higher degree of target ionization than the low-Z projectile of comparable ionic charge. This fact leads to substantial deviations from the "universal curve" found earlier for projectiles of equilibrium charge states. Similar deviations are found in the data extracted from the spectra of Fig. 2 where the decrease in multiple ionization is shown going from 0.4 MeV/amu Br^{15+} up to 8.0 MeV/amu Kr^{16+}. It can be summarized that highly stripped projectiles with ionic charges being at least as high as the equilibrium charges behave like point charges. However, the electron cloud of a heavy projectile in considerably lower charge state does not completely screen the projectile nucleus during the collision. Therefore, the effective charge to be taken into account is somewhat higher than the ionic charge.

[1] H.F. Beyer, R. Mann, and F. Folkmann, GSI Scientific Report 1980

[2] cf. F. Folkmann, R. Mann, and H.F. Beyer, Physica Scripta, in press

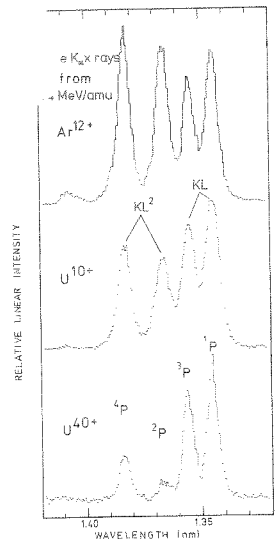


Fig. 1

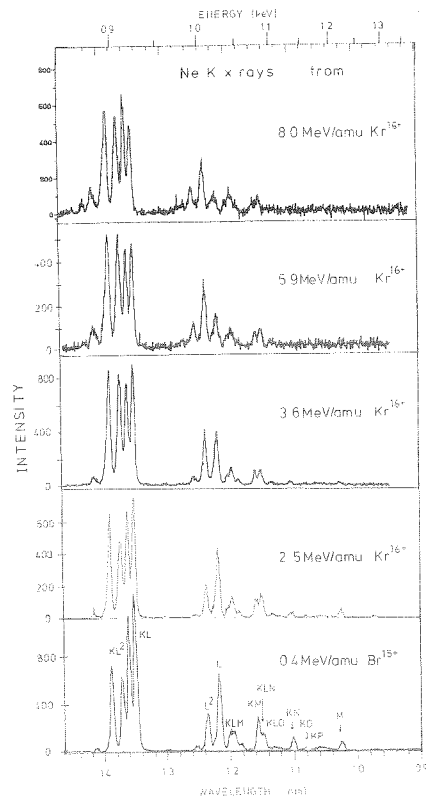


Fig. 2

Energy Gain Spectroscopy with High Charged Low Velocity Recoil Ions

C.L. Cocke, R. Mann*, R. Marrus**, M. Prior**, A.S. Schlachter**
J.R. MacDonald Laboratory, Kansas State University, Manhattan KS 66506
*GSI Darmstadt
**Lawrence Berkeley Laboratory, Berkeley, CA 94720

Experiments with highly charged ($2 \leq q \leq 15$) but slow ($v < 10^7$ cm/s) recoil ions (HQLV) have gained increasing attraction in recent years since different sources of ion production became available. Most interest was focused on charge transfer reactions between HQLV recoil ions and neutrals as this concerns fundamental questions in plasma physics and astrophysics and it touches a heretofore relatively unstudied area in atomic collisions. Although some pioneering work was done recently[1,2] where the charge states of both the low velocity projectile ions and the secondary target ions were analyzed after capture collisions, a detailed exploration of the charge transfer mechanisms and the final state populations was still outstanding. Therefore, we have started to measure the kinetic energy distributions of the outgoing projectile ions revealing the energy defects of different capture reactions which, in most cases, can be attributed definitely to the final states populated.

Ne^{q+} (q=10,9) recoils were produced by a 4.6 MeV/u Au $^{56+}$ beam impinging on a thin gas target. The ions were extracted from the target by an electric field and charge state analyzed by a 180° magnet. After passing through a gas cell the kinetic energy of the ions was measured using a hemispherical electrostatic 180° analyzer combined with a retardation field at the entrance[3]. Total single electron capture cross sections σ_1 were obtained from the relative intensities of q+ and (q-1)+ ions distinguished by their penetration through a retardation field before detection by a channeltron multiplier.

Figure 1 shows examples of energy spectra of Ne^{9+} and Ne^{10+} ions after collisions with He, Ne, Ar, and Xe atoms. Besides a strong peak from the throughpassing ions of initial charge q pronounced peaks of ions with charges (q-1) indicate a dominance of single electron capture reactions for all targets. From the energy gains of the exoergic capture processes (where the scales in Fig. 1 refer to) $\Delta E = E_b - I_p$ ($E_b = (q-1)^2/2n^2$ = final and I_p = initial electron binding energies) it follows, that a single , or at most two, principal quantum numbers n are populated which are associated with the energy balance of the electronic levels according to a quasi-reasonance over-barrier transition (CB-model). The values n_c as predicted by the classical model are inserted in each figure. Further structures at higher energy gains are supposed to result from double electron capture and transfer ionization channels[1].

Based on a pure Coulombic trajectory for the separating charge exchange particles, the crossing distance for electron capture $R_c = q-1/\Delta E$ (a.u.) was obtained. Comparing the geometrical cross section πR_c^2 with the measured values σ_1 it is noticed that the one electron transition probability (averaged over all impact parameters) is quite dependent on the particular collision system and is found to be < 0.5 for all present cases[3].

[1] C.L. Cocke, R. DuBois, T.J. Gray, E. Justiniano and C. Can, Phys. Rev. Lett. 46, 1671 (1981)
[2] E. Justiniano, C.L. Cocke, T.J. Gray, R.D. DuBois and C. Can, Phys. Rev. A24 2953 (1981)
[3] R. Mann, C.L. Cocke, A.S. Schlachter, M. Prior and R. Marrus, Phys. Rev. Lett. 49 1329 (1982)

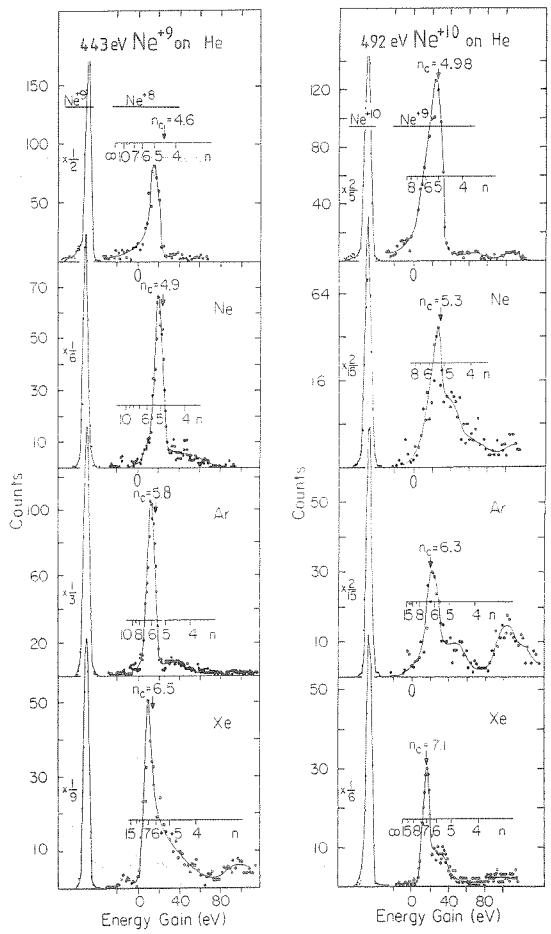


Fig. 1: Energy spectra from Ne^{10+} and Ne^{q+} recoil ions passing through different gas targets. The energy gain-scales refers to one electron captures into main quantum numbers n.

Production of Highly Charged Recoil Ions and Electron Capture Cross Sections from He Neutrals

R. Mann
GSI Darmstadt

Charge state distributions of rare gas recoil ions were measured in coincidence with the magnetically analyzed outgoing projectile charge states, using a time of flight spectrometer, similar as in Ref. 1. Pronounced shifts to higher charge states q are found (Fig. 1) when i = 1 to 4 electrons are captured from Xe into U^{45+} projectiles. The strong change of q for i = 0 to i = 1 can be explained by a stronger interaction at smaller impact parameters where electron capture (most likely from the Xe M-shell) into U^{45+} occurs, as also demonstrated by T. Gray et al.[2] for lighter projectiles. A further increase of the mean charge states q for $i \geq 2$ as $q(i) \sim q(i=1) + 2i$ may suggest that electron evaporation via Auger decays of the induced vacancies is important which is also in the framework of the energy deposition (ED)-model[3].

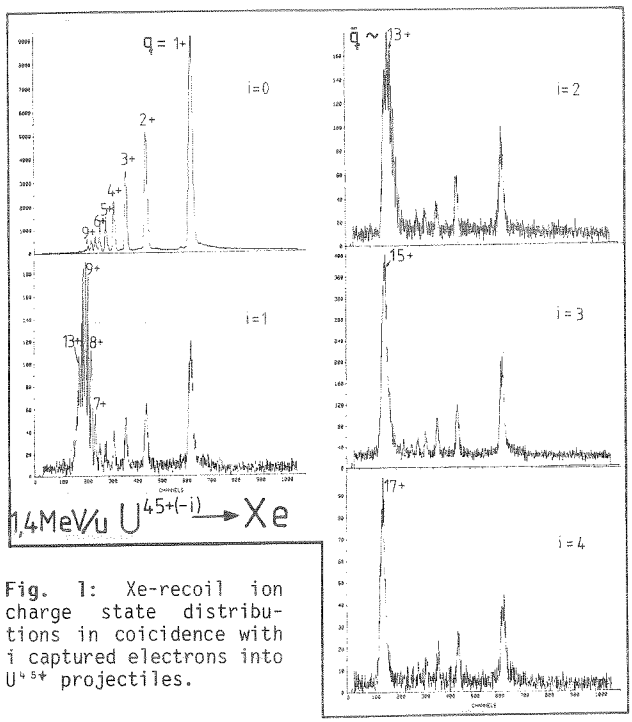


Fig. 1: Xe-recoil ion charge state distributions in coicidence with i captured electrons into U^{45+} projectiles.

In a second experiment the upper limit of q where slow recoil ions still can be sufficiently produced and isolated from the target region for secondary experiments was tested. Bombarding HJ molecules with 1.4 MeV/u U^{45+} projectiles iodine recoils up to q = 25+ were extracted (Fig. 2) by an extracting voltage of 200 V and subsequently charge state analyzed by a 180° magnetic selector as described in Ref. 4. The HJ gas used has the advantage of an isotopic free target giving uniquely analyzed q/M ratios (M = recoil mass) in contrast to Xe. In addition, the kinetic energy distribution of J^{q+} due to the molecular Coulomb explosion is negligibly small as most energy goes into H^+, so it does not affect much the extractibility of J^{q+}. In a first secondary experiment total one electron capture cross sections σ_1 from He atoms into 200 eV/q J^{q+} were measured for $12 \leq q \leq 20$ and compared with the classical barrier (CB)-model calculations in Fig. 3.

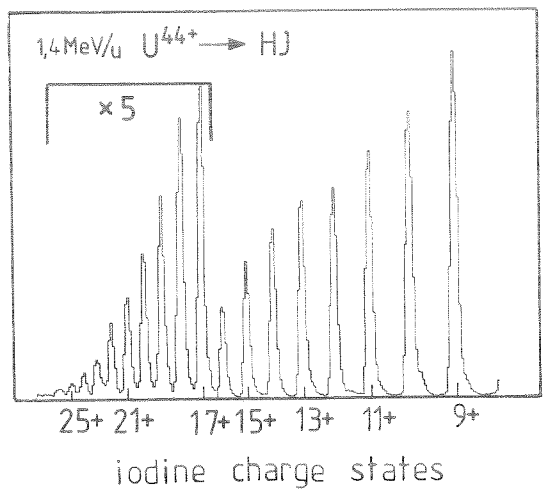


Fig. 2

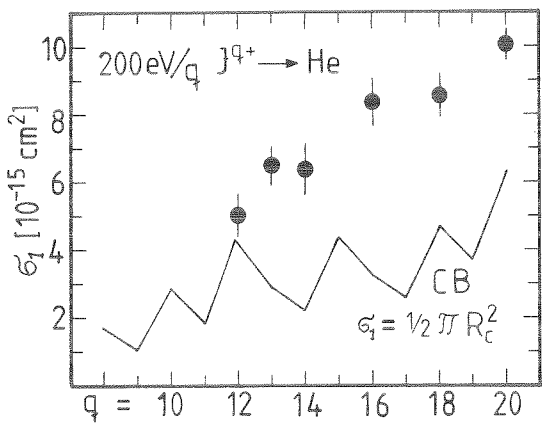


Fig. 3: Total single electron capture cross sections from He into J^{q+} recoils

[1] A.S. Schlachter, W. Groh, A. Müller, H.F. Beyer, R. Mann, and R.E. Olson, Phys. Rev. A26 (1982) 1373
[2] T.J. Gray, C.L. Cocke, and E. Justiniano, Phys. Rev. A22 (1980) 849
[3] C.L. Cocke, Phys. Rev. A20 (1979) 749
[4] R. Mann, C.L. Cocke, A.S. Schlachter, M. Prior, and R. Marrus, Phys. Rev. Lett. 49 (1982) 1329

Charge transfer involving multiply charged ions G

W. Groh, A. Müller, P.C. Kester, I. Wirkner-Bott, A.S. Schlachter, B. Schuch, E. Salzborn
Institut für Kernphysik, Universität Giessen

Our research program on charge transfer processes involving multiply charged ions included several topics:

1. Transfer-ionization in highly charged many-electron systems at low collision energies

By using a time-of-flight coincidence method[1] we performed a systematic investigation of processes

$$A^{q+} + B \rightarrow A^{(q-k)+} + B^{i+} + (i-k)e \qquad (1)$$

where A,B are the rare gas atoms, q is the charge state of the projectile ions (up to q=15 for Xe ions), and k the number of electrons captured in a single collision (k=1,2,3). Projectile energies are in the range 10 to 150 keV depending on the ion charge state. We determined relative charge-state fractions F_i of ions B^{i+} created for a given number of electrons captured in a process of type (1). Using the results of earlier experiments[2] it is possible then to evaluate absolute partial cross sections for transfer-ionization processes.

The main results of the present experiments are the following: a) in the investigated energy range the fractions F_i are constant for exoergic collisions of many-electron systems; b) the maximum potential energy available in an electron-capture process determines the charge-state spectrum of the recoil ions. This energy increases with the charge state of the incident ions and the number of electrons captured. Hence, for example, for the capture of 2 electrons from Xe atoms by 120 keV Kr^{12+} ions ($v \approx 5 \cdot 10^7$ cm/s) we could observe an average recoil-ion charge state $\langle i \rangle = 5$ and even Xe^{7+} ions are produced with a probability of nearly 8%.

A statistical model of transfer-ionization processes was developed which allows to calculate the observed charge state fractions of recoil ions. The theory is based on the assumption that the available potential energy is distributed statistically among the target electrons which can "boil off" if their energy is high enough.

2. Transfer-ionization in slow collisions of He^{2+} ions in rare gases

He^{2+} ions at velocities less than $v=6.6 \cdot 10^7$ cm/s changing to He^{1+} in an Ar gas target are found to produce more Ar^{2+} than Ar^{1+} recoil ions. Different from the observations described in section 1. the charge state fractions F_2 and F_1 strongly depend on the projectile energy. A similar phenomenon has been found also for Kr target atoms at still lower He^{2+} velocities (the functions $F_1(v)$ and $F_2(v)$ cross at $v \approx 4 \cdot 10^7$ cm/s with a strong increase of F_2 at smaller v). For Ne and Xe targets F_1 and F_2 are nearly constant with $F_1 >> F_2$.

It is possible to obtain a qualitative understanding of the experimental results[3] by constructing simple potential energy curves for the colliding particles based on the energy levels at infinite separation and considering that at low energies the probability for endothermal transitions decreases with decreasing collision energy and that potential-curve crossing distances R_c between $3a_o$ and $10a_o$ are preferred in electron capture reactions.

3. Electron capture with ionization at intermediate velocities

While at low relative velocities (see 1.) the charge state fractions of recoil ions are only determined by the potential energy available in the electron capture process, at higher projectile velocities also endothermal reaction channels are opened.

Using a new recoil-ion spectrometer which is able to resolve even the isotopes of natural Xenon the intermediate velocity range is investigated for singly and doubly charged ions. With the electron capture by $2 \cdot 10^8$ cm/s He^+ ions from Xe atoms recoil ion charge states up to i=5 can be observed which is only possible by making use of kinetic collision energy. These measurements are extended to UNILAC energies and ion charge states.

[1] W.Groh, A.Müller, Ch.Achenbach, A.S.Schlachter and E.Salzborn; Phys.Lett. 85A, 77 (1981)

[2] A.Müller and E.Salzborn; Phys.Lett.62A,391(1977)

[3] W.Groh, A.S.Schlachter, A.Müller and E.Salzborn; J.Phys.B 15, L207 (1982)

Pressure Broadening and Pressure Shift of the (λ= 410 nm) Indium Line

J.Eberz, G.Huber and G.Ulm, Institut für Physik der Universität Mainz
T.Kühl, GSI Darmstadt

In completion of our earlier results[1] pressure broadening and pressure shift of the $5p\ ^2P_{1/2}$ - $6s\ ^2S_{1/2}$ indium line (λ = 410 nm) in the noble gases He, Ne, Ar, Kr and Xe and the molecular gases H_2 and N_2 have been measured. Information on the dependence of broadening and shift of the observed transition on the foreign gas pressure was obtained by fitting a Voigt profile, i.e. the convolution of a Lorentzian and a Gaussian distribution, to the measured Doppler and pressure broadened indium resonance lines. Figure 1 depicts the experimental broadening and shift parameters for all noble gases. In order to prevent confusion the results for the molecular gases are not included.

Since accurate interaction potentials for the indium - foreign gas system are not available, we have attempted to interpret our results in terms of the semi-classical impact theory by assuming an empirical modified Lennard-Jones potential (C_6-C_8-C_{12}) to describe the interaction potential V(R) between the perturbing atom positioned at the distance R from the radiating atom :

$V(R) = \hbar C_{12} R^{-12} - \hbar C_6 R^{-6} - \hbar C_8 R^{-8}$

Here C_6, C_8 and C_{12} are the interaction constants. Calculations for the interaction constants have been performed by using the non relativistic Hartree-Fock wave functions evaluated by the computer program given by Froese-Fischer[2].

In accordance to the procedure of Hindmarsh et al.[3] theoretical values of the broadening and shift rates can be calculated and compared with the experiment. This comparison between measured and calculated broadening constants shows that the chosen interaction potential can adequately describe the broadening and shift of the (λ= 410 nm) line perturbed by foreign gases.

1) GSI Scientific Report 1981, GSI 2-82, p.157
2) Ch.Froese Fischer, Comp.Phys.Comm. 14, 145(1978)
3) W.R.Hindmarsh et al., J.Phys. B3, L5 (1970)

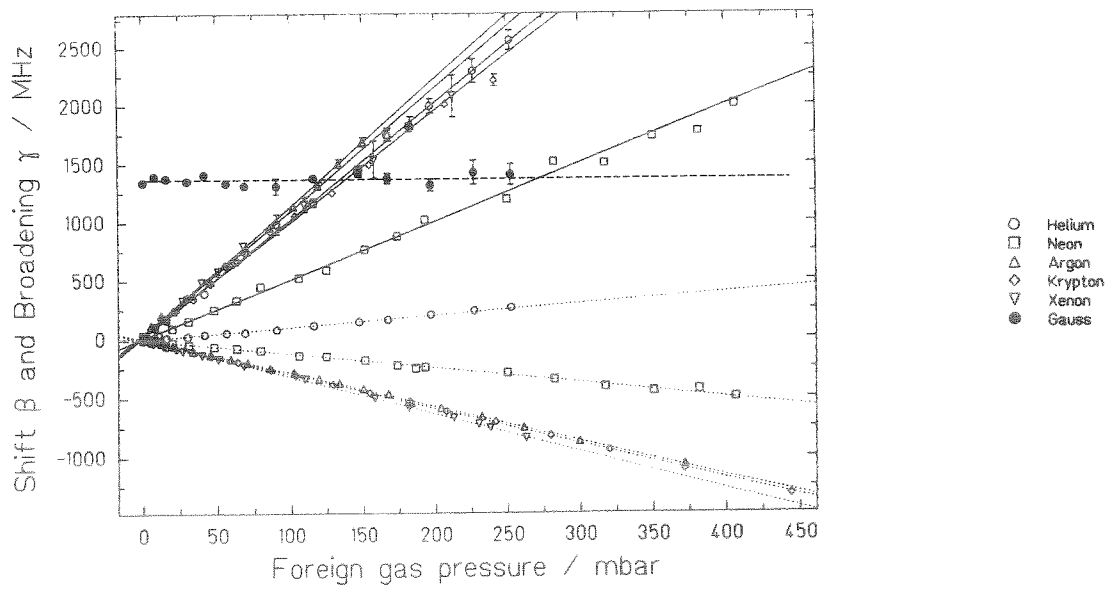


Figure 1:
Broadening parameter γ (full lines) and shift parameter β (dotted lines) for the (λ = 410 nm) indium line, plotted against the foreign gas pressure. The negative sign of β indicates a red shift. The constant width of the Gaussian component (helium as perturber is chosen as example), depicted by a dashed line, reproduces the correct value for the Doppler broadening due to the cell temperature, which was kept constant during the experiment. The broadening parameters are quoted for the full width at half maximum (FWHM).

Isotope Shift in Two-Photon Transitions of Indium

R.Menges, G.Huber and G.Ulm, Institut für Physik der Universität Mainz

T.Kühl, GSI Darmstadt

The fine structure (fs) of several $5s^2np\ ^2P_{1/2,3/2}$ - Rydberg states of ^{113}In and ^{115}In has been observed by Doppler-free two-photon spectroscopy in an indium heatpipe[1] using cw dye laser excitation and thermionic detection. The fs - splitting was measured for n = 27 - 35. It shows the expected $(n^*)^3$ - dependence (fig.1) indicating that irregularities - like configuration mixing - do not occur in these Rydberg states. Moreover it could be observed that the isotope shift between ^{113}In and ^{115}In in the $5s^25p$ - $5s^2np$ transition is independent of the principle quantum number in the given range. We conclude that there is no contribution from the Rydberg state to these isotope shifts and that the measured values are exclusively caused by the term shift of the $5s^25p\ ^2P_{3/2}$ - ground state relative to the ionisation limit.

Together with the literature values for the isotope shift in transitions between the lower levels, our results then allow the evaluation of the individual shift of the $5s^26s$ and $5s^27s$ levels with respect to the ionisation limit. This made possible a detailed analysis of the specific mass effect and the nuclear volume effect in these states by using non-relativistic Hartree-Fock screening corrections[2] and semi-empirical values for the electron density at the nucleus.

The results (fig.2) postulate an extremely large volume effect for the 5p - electron, which is due to the screening of the $5s^2$ core electrons, and a specific mass shift up to nine times larger than the normal mass effect.

1) GSI Scientific Report 1981, GSI 82-1, p.156

2) P.Aufmuth, priv.comm.

3) J.Neijzen, A.Dönszelmann, Physica 111c, 127(1981)
J.Neijzen, A.Dönszelmann, Physica 114c, 241(1982)

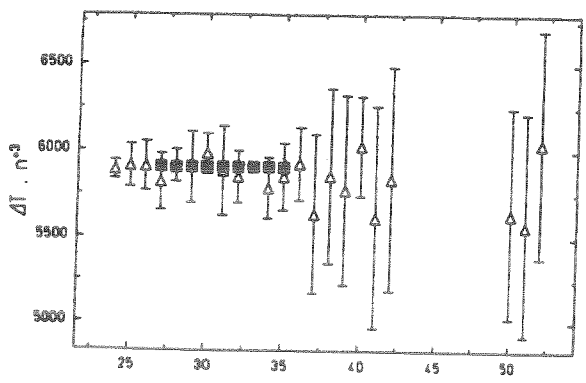
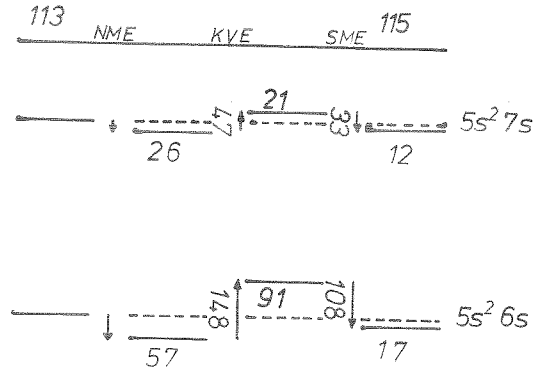


Figure 1:
$(n^*)^3$ dependence of the fine structure splitting ΔT on the principal quantum number n.

■ This work

Δ Reference 3)



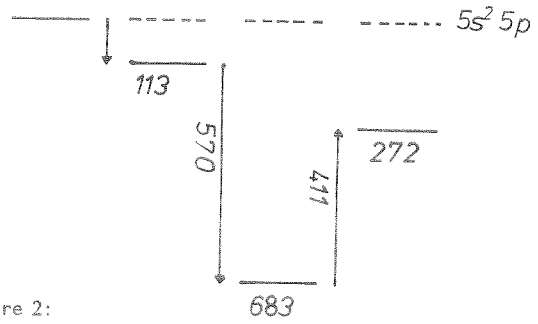


Figure 2:
Contributions (in MHz) to the isotope shift of the lowest atomic levels in indium : The total shift of the level position between ^{113}In (left side) and ^{115}In (right side) is determined by the Rydberg measurements. Calculations give the quoted values for the normal mass effect (NME), the nuclear volume effect (KVE) and the specific mass effect (SME).

Charge State Distributions of Ar-, Kr-, Xe-, and U-Ions After Solids at Energies up to 18.7 MeV/u

B. Franzke
GSI Darmstadt

Coinciding with the completion of the UNILAC up-staging in 1982 there was a marked increase in interest in experimental charge state distributions. Among others, the main questions were:

- Optimal choice of material and thickness for the second stripper in the UNILAC at 11.5 MeV/u.
- Charge state and intensity yield after stripping at 11.5 MeV/u and the highest energies available at the UNILAC. From this data the maximum beam intensities and energies attainable with the heavy ion synchrotron SIS 12 are determined.
- Yields for fully stripped or H- and He-like ions as functions of atomic number and energy of the ions. Experimental data would allow better estimation of beam time for spectroscopic investigations of heavy, few-electron ions.

As part of accelerator development experiments more than 200 charge state spectra of Ar-, Kr-, Xe-, and U-Ions were accumulated using the target materials C, Al, Ni, Y, Ag, and Au with thicknesses varying from 10 up to 500 µg/cm². The specific ion energies were 11.5 MeV/u (Ar, Kr, Xe, U), 16.3 MeV/u (U), and 18.7 MeV/u (Ar, Kr). The experimental set-up is described in a previous report[1].

A brief summary of the large amount of experimental observations gives some answers to the most important questions:

Optimal target material:
Equilibrium charge state distributions with the highest average charges and the smallest widths are produced by C-foils. For a given ion species and energy the average charge decreases and the width increases with increasing atomic number Z_T of the target material. This is shown in Fig. 1 by means of a plot of charge state distributions for U-ions at 16.3 MeV/u after various target materials. Compared to the Au-target, the centre of the distribution after the C-target is shifted by 9 units of charge to 78+, and the intensity maximum is elevated from 17.6 % to 25 %.

Optimal target thickness:
The higher the atomic number of the target material the more massive the target has to be to reach equilibrium. Whereas, for instance, Ag- or Au-foils of 200 µg/cm² are sufficient to equilibrate 18.7 MeV/u Ar-ions, more than 500 µg/cm² are necessary using C- or Al-foils. There is no single case in this experiment, where C-foils of 490 µg/cm², the maximum available thickness for C-foils, would have led to equilibrium.

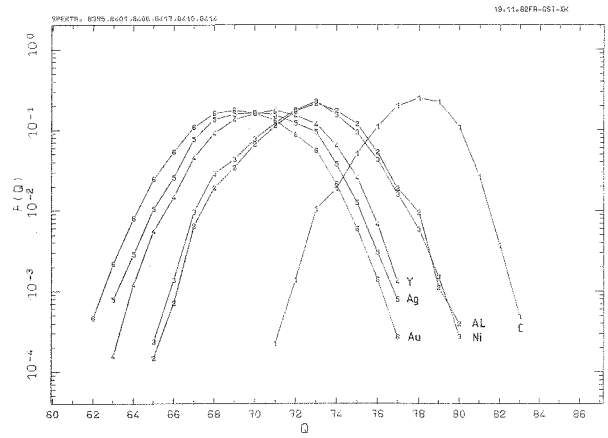


Fig. 1: Charge state distributions of uranium ions at 16.3 MeV/u after passage through different target materials of about 500 µg/cm².

Yields for fully stripped ions:
Using 490 µg/cm² carbon foils, the intensity fractions of fully stripped or H-like ions are the following:

Argon	17+	18+
11.60 MeV/u	0.216	0.768
18.70 MeV/u	0.105	0.893
Krypton	**35+**	**36+**
11.59 MeV/u	0.044	0.0018
18.66 MeV/u	0.136	0.0077
Xenon	**53+**	**54+**
11.49 MeV/u	2.6×10^{-4} ±35%	-

The observation of H-like Xe at 11.5 MeV/u is somewhat unexpected, although the fraction seems to be not very attractive for high resolution atomic spectroscopy.

Reference

[1] B. Franzke, Ann. of Isr. Phys. Soc. 4, 111 (1981)

Measurement of Charge Exchange Cross Sections in Atomic Collisions with Highly Ionized, Decelerated Ions

D.H.H. Hoffmann, P.H. Mokler, W.A. Schönfeldt, Z. Stachura*, and H. Wahl
GSI Darmstadt

Charge changing collisions between highly ionized heavy ions and atoms that involve electron capture processes have recently gained increasing interest in problems related to inertial confinement fusion with heavy ions [1]. Therefore, we have measured the total charge transfer into Xe^{q+}-projectiles in Xe^{q+}-Xe collisions at 3.6 MeV/u. Charge states q = 44, 45, 46, and 47 were selected to study the influence of a rising number of vacancies in the L-shell of the projectile. At q = 44 the L-shell is still filled with electrons, whereas at q = 45,46,47 one,two,three L-shell vacancies are present, respectively.

In order to produce highly charged Xe^{q+} ions, the particles were first accelerated to 8.6 MeV/u, then stripped in a foil to high charge states, and finally decelerated to 3.6 MeV/u [2]. The charge state selected Xe^{q+} ions hit a 12 cm long gas cell which is schematically shown in Fig. 1. Target thicknesses used were of the order of 100 - 1000 µbar·cm. The target region is viewed by a Si(Li) detector and a position sensitive proportional counter. Soller slits were used to minimize Doppler shift effects for the projectile emitted x radiation. Rutherford scattering in a thin gold target at the exit of the gas cell was used for particle normalization.

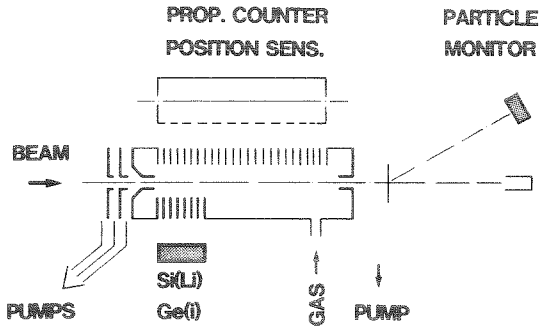


Fig. 1

For single collision conditions we observe with the Si(Li) a small, almost charge state independent L x-ray emission for $q \leq 44$; beyond q = 44 a dramatic yield increase is observed[2]. As for 3.6 MeV/u the average charge state in a gas target is $q \approx 30$, an appreciable yield decrease with target thickness is expected for $q \geq 45$. In Fig. 2, the normalized total x-ray yield observed with the position sensitive proportional counter is displayed as a function of increasing target thickness for charge states q = 44 up to q = 47. The data show an exponential decay of the measured yield for q = 45-47, which correspond to 1, 2, and 3 L-shell vacancies, whereas the q = 44 data are practically constant over the observed range of target thickness.

The full lines in Fig. 2 represent decay functions of the form

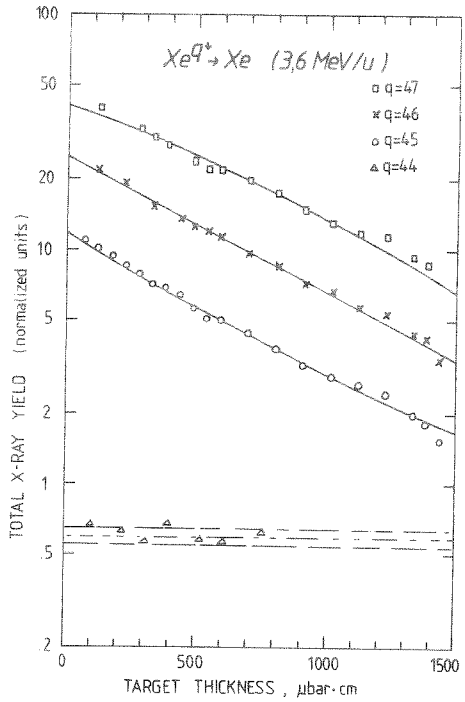


Fig. 2

$$Y_i(x) = \sum_{j=1}^{i} a_{ij} \exp(-\lambda_j x) \qquad (1)$$

which were fitted to the background corrected data, where $Y_i(x)$ (with i = 1, 2, 3) is the x-ray yield corresponding to the number i of the L-shell vacancies, x is the target thickness, a_{ij} are weight factors and $\lambda_j (j=1,\ldots,i)$ are the decay constants which are proportional to the charge exchange cross sections.

This representation was chosen under the assumption that one-electron capture is the dominating charge exchange process. From this fitting procedure total capture cross sections have been deduced. The results are shown in Fig. 3 as a function of the projectile charge state q. These results are compared to an empirical formula [3] for capture cross sections shown as a full line.

*Permanent address: Inst. Nucl. Phys., Cracow, Poland

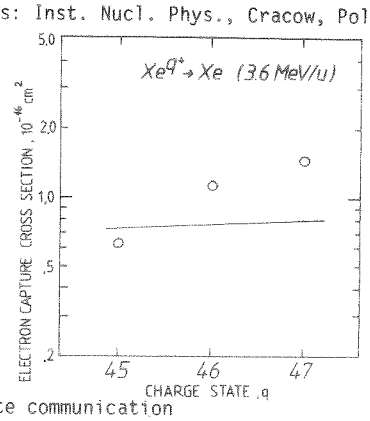


Fig. 3

[1] M. Reiser, private communication
[2] P.H. Mokler et al., annual report GSI 82-1, p. 143
[3] W. Erb, GSI-Bericht p-7-78

Shape of the Convoy electron structure and total electron yield in high energy (882 MeV) Ni → C and Al collisions.

R. Latz, M. Burkhard, H.J. Frischkorn, D. Hofmann, P. Koschar, J. Schader, K.O. Groeneveld
J.W. Goethe Universität, 6000 Frankfurt/Main, Germany
M. Breinig, S. Berry, I.A. Sellin
Univ. of Tenn. and Oak Ridge Nat.Lab., Oak Ridge TN, USA

Recent studies[1] of the zero degree electron emission (i.e. convoy electrons) with heavy ions on gaseous targets at high projectile velocities $v_p > 3.8 \cdot 10^9$ cm/s revealed a strong asymetry of the cusped shaped convoy electrons at electron energies $v_e \approx v_p$. This asymetry was explained theoretically as a result of a double collision of the electrons which is described in Born approximation by terms of high order.[2] These higher order terms are expected 1) to become increasingly important with higher v_p and 2) to depend strongly on the initial charge q_i of the projectile.

To elucidate these phenomena we measured the shape of the convoy electron structure. We chose as collision system Ni^{+q_i} (882 MeV) → C or Al (ρx = 3 to 500 µg/cm^2) with q_i = 24 and 26. The zero degree convoy electron momentum spectra were recorded with a magnetic analyzer.[3] Fig. 1 presents a result of such a measurement. The background has been substracted; the solid line is a fit to the data using the approach by Meckbach et al.[4]

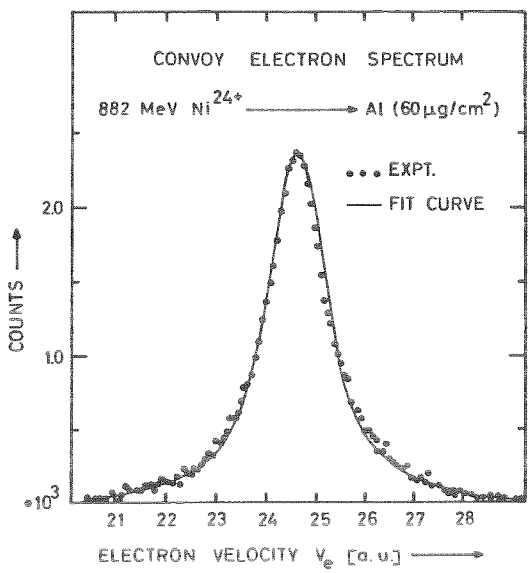


Fig. 1: Convoy electron spectrum from Ni^{+24} → C collisions.

Two results of these measurements can be stated:
1. Under the present experimental condition with $v_p = 5 \cdot 10^9$ cm/s no significant asymetry of the convoy electron structure has been observed for all measured target atomic numbers Z_t and for all target thicknesses ρx.
2. Within the experimental uncertainties no significant asymetry has been found for the two initial charge states q_i of the projectile.

In addition to the measurement of the convoy electrons we recorded simultaneously the total yield of electrons per projectile γ by a method described in ref.[5]. The convoy electron yield Y_c, the yield of ionisation electrons Y_I and γ were found to depend on the target thickness ρx in a similar way:

1. At $\rho x < 10$ µg/cm^2: Y_c, Y_I and γ increase slowly.
2. At $10 < \rho x < 200$ µg/cm^2: All three quantities increase more rapidly.
3. At $\rho x > 400$ µg/cm^2: Y_I saturates independent of q_i.
4. At $\rho x > 200$ µg/cm^2: Both Y_c and γ saturate with γ_∞(C) = 95 ± 10 and γ_∞ (Al) = 105 ± 10 independent of q_i.

The observed γ_∞-values are in quantitative agreement with the lineare dependence of the electronic stopping power.[6]

*Supported by BMFT/Bonn, GSI/Darmstadt, NSF/Washington, DFG/Bonn

References

1 M. Breinig, S. Elston, I.A. Sellin, C. Liljeby, R.Thoe, Phys. Rev. Lett. 45, 1689 (1980)

2 R. Shakeshaft, L. Spruch, Rev. Mod. Phys. 51, 369 (1974).

3 R. Latz, G. Astner, H.J. Frischkorn, P. Koschar, J. Pfennig, J. Schader, K.O. Groeneveld, Nucl. Inst. and Meth. 194, 315 (1982)

4 W. Meckbach, I.B. Nemirovsky, C.R. Ganbotti, Phys. Rev. A24, 1795 (1981)

5 J. Schader, B. Kolb, K.D.Sevier, K.O. Groeneveld Nucl. Inst. and Meth. 151, 563 (1978)

6 H.J. Frischkorn, P. Koschar, R. Latz, J. Schader, M. Burkhard, D. Hofmann, K.O. Groeneveld, IEEE Transactions NS (1983) to be published.

Secondary Ion Emission from Metallic Surfaces Bombarded by Fast Heavy Ions

O. Becker, W. Knippelberg, K. Wien
Institut für Kernphysik, TH Darmstadt

Sputtering of solid metals by heavy ions is generated via atomic collision processes - even at bombarding energies of ca. 1 MeV/N where the energy loss is dominated by electronic excitation. Emission of charged metallic particles represents only a small part of the sputtering yield. The few approaches to describe ionization are still in a preliminary state[1,2]. The aim of our experiments on secondary ions emitted from metals is to determine ionization probabilities as function of projectile velocity using measured ion yields and theoretical sputter yields[3].

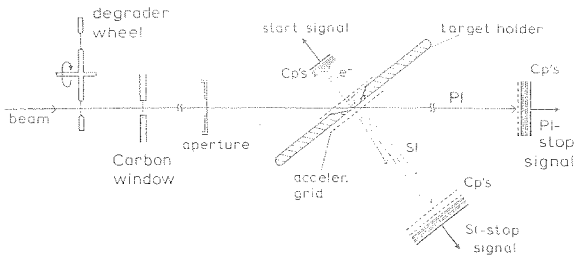


Fig. 1 Experimental setup of the spectrometer

The experiments were performed in the stripper hall. Foils of Al, Sc, Y, Ta and Pt were bombarded with ^{58}Ni, ^{132}Xe and ^{238}U ions of different energies. As illustrated in Fig. 1 the projectile velocity as well as mass spectra of secondary ions emerging from the target were measured by time-of-flight techniques. By means of low energy ion etching the target surfaces were cleaned removing at least 300 monolayers from Al, Sc, Y and 150 from Ta and Pt. The partial pressures of H_2, O_2, H_2O and other reactive gases were kept below 10^{-10} mbar. In order to reduce a background produced by succeeding beam bursts, the beam intensity was restricted to ca. 100 ions per second.

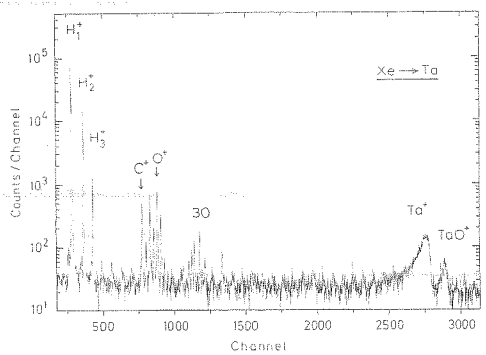


Fig. 2 A time-of-flight mass spectrum of ions emitted from a Ta surface

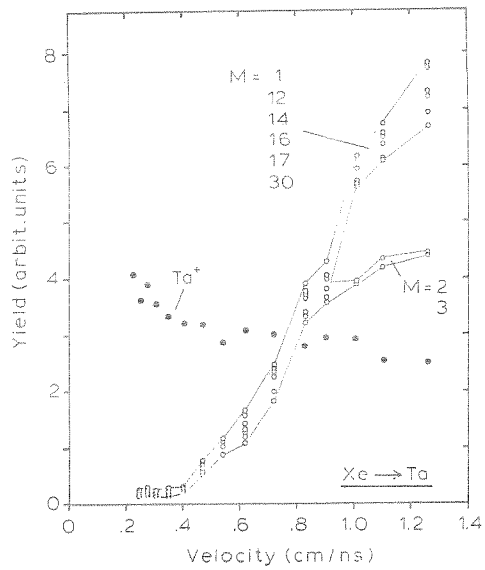


Fig. 3 Comparison of ion yields measured as function of projectile velocity. The yields of impurity ions are comprehended to one area by normalization.

A typical mass spectrum is presented in Fig. 2. Besides the expected metal ions also a distinct pattern of ions due to a residual surface contamination appears. The mass lines of metal ions are considerably broadened by the recoil energy of atomic collisions. In agreement to sputter theory their yield (in the order of 1%) decreases with rising projectile velocity (see Fig. 3).

We expected the yield curves of impurity ions to be alike the curves of metal ions. Actually as shown in Fig. 3 their yields increase with rising projectile velocity. Additionally their mass lines have a narrow width compared to that of metal ions. We conclude that the emission of impurity ions is related to the electronic energy loss in spite of the fact, that the emission occurs from a metallic surface. One suggestion is that this kind of ion emission is performed by the decay of individual excited states near the surface.

[1] B.J. Garrison, N. Winograd and D.E. Harrison, Jr., Phys. Rev. B18, 6000 (1978).
[2] Z. Šroubek, Phys. Rev. B, Rapid Comm., 25, 6046 (1982).
[3] P. Sigmund, Phys. Rev. 184, 383 (1969).

The authors wish to thank the target laboratory of the GSI for preparation of metal foils.

Secondary Ion Emission from Phenylalanine as Function of Projectile Charge State

W. Guthier, O. Becker, W. Knippelberg, U. Weikert, K. Wien
Institut für Kernphysik, TH Darmstadt
Y. Le Beyec, S. Della Negra
Institut de Physique Nucléaire, Université Paris Sud, Orsay

Above projectile energies of 20 keV/N sputtering of condensed gases[1,2] and UF_4[3] as well as secondary ion emission of organic materials[4] increase drastically with rising energy. This enhancement is obviously related to the electronic energy loss or to one of its derivatives (primary ionization etc.). In any case a strong dependence of sputter- or ion emission-yields on the projectile charge should be present. Since inside the material the charge state q approaches rapidly an equilibrium distribution, the variation of yields with q is smeared out, if processes inside the bulk contribute considerably to desorption.

Up to q = 8+ the q-dependence of secondary ion emission has been already measured by two groups[4] using a ^{16}O beam. Instead of using the rather unreliable electrosprayed targets we evaporated in vacuum films of Phenylalanine (2000 Å) onto metal foils. These targets were irradiated by ^{14}N and ^{238}U ions having charge states of q = 2+ to 7+ and q = 26+ to 49+ respectively and a fixed energy of 1.4 MeV/N · q was varied by help of a gas stripper. Time-of-flight mass spectra were taken using the same apparatus as shown in Fig.1 of the proceeding article, but turning round target and start- and stop-detectors by 180°. The Carbon window and the degraders were removed.

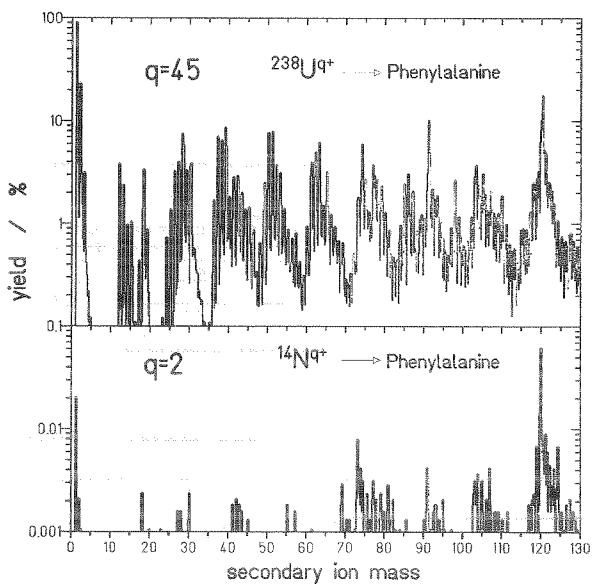


Fig. 1: Time-of-flight mass spectra of ions emitted from a Phenylalanine film.

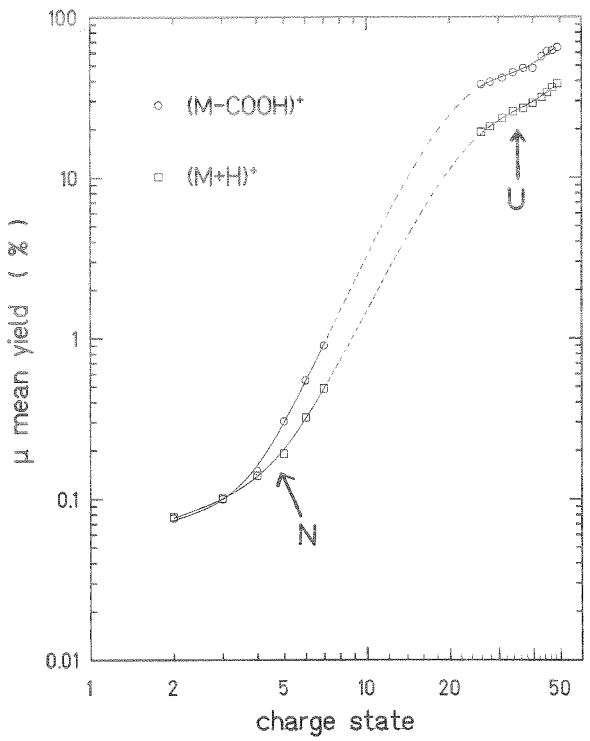


Fig. 2: Measured yields of two Phenylalanine ions as function of the charge state.

Two mass spectra, one for q = 2+ and one for q = 45+, are presented in Fig. 1. For q = 45+ a remarkable fragmentation is observed. In this case chemical reactions during desorption certainly complicate the ion emission process. In Fig. 2 the yields of the two most prominent ions of Phenylalanine (M = 165) are presented as function of q (the yields are not corrected for detection efficiency). A unique answer about a q^n-dependence of yields is hardly possible. Depending on the secondary ion we observed exponents n between 0.8 and 4.3. In case of ^{238}U the mean total ion yield can be as high as 15 per projectile. An unexpected result is, that the relative ion yields remain unchanged for different ion multiplicities.

[1] W.L. Brown, W.M. Augustyniak, L.J. Lanzerotti, R.E. Johnson and R. Evatt, Phys. Rev. Lett. 45, 1632 (1980)
[2] F. Besenbacher, J. Bøttiger, O. Graversen and J.L. Hansen, Nucl. Instrum. and Methods 191, 221 (1981)
[3] J.E. Griffith, R.A. Weller, L.E. Seiberling and T.A. Tombrello, Rad. Eff. 51, 223 (1980)
[4] see Nucl. Instrum. and Methods, Vol. 198/1 (1982)

Interatomic Potentials for Ionized Scattering Systems

G

H. Hartung, B. Fricke, W.-D. Sepp, and W. Schulze
Physics Department, University of Kassel

For heavy ion scattering experiments it is interesting to get information about the influence of the projectile charge state on the elastic scattering process. The usual description by Coulomb trajectories is very rough because the electron screening, which depends on the charge states of the scattering partners, is ignored completely. Within a statistical model[1] we calculated the interatomic potential of the system I^{n+}-I with different charge states n. The electron density ρ was taken to be the sum of the separated ion and atom densities which we obtained from atomic Dirac-Fock-Slater calculations. For the exchange energy we used Slater's term:

$$E_x = -\kappa_a \int \rho^{4/3}\, d^3r$$

with

$$\kappa_a = \alpha_x \cdot \frac{3}{2} \left(\frac{3}{\pi}\right)^{1/3}$$

and the Slater-exchange parameter $\alpha_x = 0.7$.

The interatomic potential curves are shown in Fig.1 in a scaled plot. The quantity $(V-V_{LJ})\cdot R$ is drawn as function of the internuclear distance R. V is the calculated interatomic potential, V_{LJ} is the average Lenz-Jensen[2] potential as suggested by Loftager et al.[3]. The ionized particles with n = 7+, 17+, 25+ are assumed to be in the ground state.

In Fig.1 potential structures show up in the region between 0.1 and 2.0 atomic units. These structures result from the electronic shell structure of the atomic electron systems. The minima at 0.02 a.u. are due to the analytic form of the Lenz-Jensen potential.

With increasing ionization the electron screening is reduced, resulting in a repulsive rising of the potential in the whole range of electron shell overlap. The peak structures are varying slightly in height, due to the different outer shell population, and in position, due to the shrinking of the ionized partner's wavefunction with increasing n.

For these interatomic potentials we calculated classical elastic differential scattering cross-sections for centre-of-mass impact energies from 25 to 400 keV, which are shown in Fig.2. The axes have a dimensionless LNS-scaling[4].

The cross-sections for n = 7 can be compared to the measurement of the system Xe^+-Xe by Loftager et al.[3]. The agreement is quite good except for the peak at $s = 2\cdot10^{-3}$ which is smeared out by inelastic processes during the collision.

For highly ionized systems we predict a general increase of the scattering cross-section while the peak structure will change only slightly to higher s-values as shown for n = 17 and n = 25.

[1] P. Gombas, Handb.d.Phys., ed. D. Flügge (Springer, Berlin 1956), vol. 36, p.109

[2] W. Lenz, Z.Phys. 77, 713 (1932); H. Jensen, ibid. 77, 722 (1932)

[3] P. Loftager et al., Phys.Rev. A20, 1443 (1979)

[4] J. Lindhard et al., K.Dan.Vid.Selsk.Mat.-Fys. Medd. 36, no. 10 (1968)

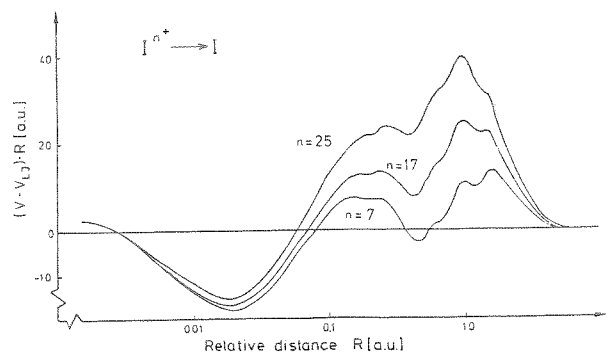


Fig.1: Relative interatomic potentials for I^{n+}-I

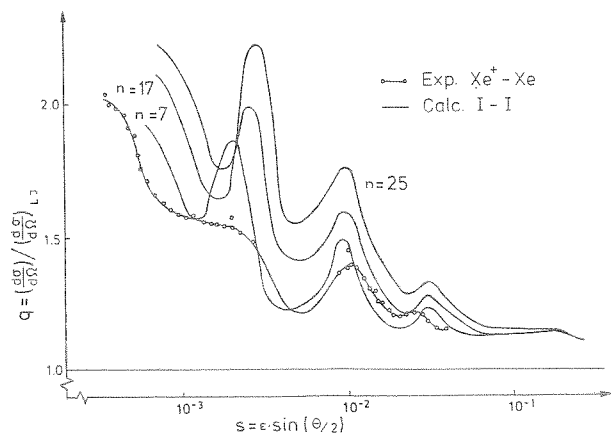


Fig.2: Calculated differential scattering cross-sections and experimental data from ref.3

The Finite-Element Method to calculate Atomic and Molecular Properties [G]

W. Schulze and D. Kolb
Department of Physics, University of Kassel

In the description of atomic ion-ion collisions by coupled-channel calculations particularly good convergence is expected, if one takes adiabatic energies as well as rotational and radial coupling matrix elements from self-consistent calculations. This, however, requires to calculate correlation diagrams and the corresponding wavefunctions rather accurately, a requirement which is only partly met by basis function expansions, where at least the angular part consists of a given set of functions.

More promising are finite-element methods. In the case of axial symmetric molecules or quasi-molecules the φ-coordinate may be separated. The remaining 2-dimensional problem can be solved by finite-element methods. In first calculations we treated non-relativistic cases in cylindrical coordinates. The total energy then takes the form:

$$2\pi \int \left[\left(\frac{\partial \Psi}{\partial \rho}\right)^2 + \frac{m^2}{\rho^2} \Psi^2 + \left(\frac{\partial \Psi}{\partial z}\right)^2 + V\Psi^2 \right] \rho d\rho dz$$

This has to be minimized under the subsidiary condition that the particle number $N = 2\pi \int |\Psi|^2 \rho d\rho dz$ is conserved. This leads to the eigenvalue equation

$$KU = \varepsilon MU$$

where K is the energy matrix and M the norm matrix. K and M have to be elvaluated by integration over the finite-elements. In particular M contains integrals

$$I_{om} = \int_{\text{Element}} FF^T \rho d\rho dz$$

with $F^T = (f_1(\rho,z), \ldots, f_n(\rho,z))$.

For our test the functional set $\{f_i\}$ consists of powers of ρ and z:

$$\rho^{\alpha_{ij}}, z^{\beta_{ij}}, \text{ with } \alpha_{ij} = a_{2i-1} + a_{2j-1} + 1,$$

and $\beta_{ij} = a_{2i} + a_{2j}$,

where $\underline{a} = (0,0,1,0,0,1,2,0,1,1,0,2,\ldots)$.

In this case I_{om} takes the explicit form

$$(I_{om})_{ij} = \frac{1}{\beta_{ij}} \sum_{k=0}^{\beta_{ij}} \binom{\beta_{ij}}{k} (\Delta m)^{\delta_{ijk}} (\Delta b)^k \frac{1}{\gamma_{ijk}} \left(x_2^{\gamma_{ijk}} - x_1^{\gamma_{ijk}}\right)$$

with $\gamma_{ijk} = \alpha_{ij} + \beta_{ij} - k + 3$

$$\delta_{ijk} = \beta_{ij} - k + 2.$$

The finite-elements where chosen to be triangles having three nodal points, thus $\underline{a} = (0,0,1,0,0,1)$ and the convergence order is $\mathcal{O}(h^2)$. We tested in cylindrical coordinates non-relativisticly for the three analytically solvable potentials: V = const, the harmonic oscillator $V(|r|) = \frac{\kappa}{2}(\rho^2+z^2)$ and the point Coulomb potential $V(|r|) = \frac{e^2}{\sqrt{\rho^2+z^2}}$.

Since the norm matrix in general is non-diagonal we used a modified lumped mass representation leading to a diagonal norm matrix. It is worth to mention that already by local rather than a global diagonalization the norm matrix M can always be brought into diagonal form. Typical accuracies for the eigenvalues ε, using 200 nodal points, are of order 1%, the further improvement being linear in the number of points. At the boundaries one observes Gibbs oscillations which, fortunately, are considerable only in regions where the wavefunctions are small, thus not disturbing the physical quantities of interest.

Highly accelerated convergence ($\mathcal{O}(h^6)$) is expected from quintic elements [1], where one demands that in addition to the functional values itself also all first and second order partial derivatives be continuous at the nodal points. This work is in progress together with relativistic extensions.

1) G. Strang, G.J. Fix, An Analysis of the Finite-Element Method. 1973 by Prentice-Hall, Inc., Englewood Cliffs, N.Y.

Solution of the Poisson-Equation for a Di-Atomic Molecular Charge Distribution in Elliptic Hyperbolic Coordinates [G]

W. Sengler, D. Kolb, and B. Fricke

Physics Department, University of Kassel

In numerical Hartree-Fock-Slater calculations it is necessary to calculate the potential from a given charge distribution. The correct way to do this is to solve the Poisson-equation:

$$\Delta\phi = -4\pi\rho \tag{1}$$

To be consistent with the whole numerical procedure used in our Hartree-Fock-Slater calculations we try to solve this equation numerically. To obtain an accuracy of $1o^{-6}$ in the total energy it is necessary to calculate the potential at least to the order of $1o^{-5}$ because all other numerical procedures in such a Hartree-Fock-Slater calculation are of the same accuracy.

Elliptic hyperbolic coordinates prove to be well adapted to the geometry for a di-atomic molecule and thus the Poisson-equation has to be solved within these coordinates. The corresponding transformations are:

$$\begin{aligned} x &= a \sinh\eta \sin\theta \cos\Psi \\ y &= a \sinh\eta \sin\theta \sin\Psi \\ z &= a \cosh\eta \cos\theta \end{aligned} \tag{2}$$

with $o < \eta < \infty$, $o < \theta < \pi$, $o < \Psi < \pi$.

Due to the cylinder symmetry of the di-atomic molecule the problem is reduced to 2 dimensions ($\Psi = o$). Thus the Poisson-equation takes the form:

$$\frac{\partial^2\phi}{\partial\eta^2} + \cosh\eta\,\frac{\partial\phi}{\partial\eta} + \frac{\partial^2\phi}{\partial\theta^2} + \cos\theta\,\frac{\partial\phi}{\partial\theta} = -a^2\,(\sinh^2\eta + \sin^2\theta)\cdot 4\pi\rho. \tag{3}$$

This equation can be solved by discretisation where the resulting difference equation reduces the solution of the differential equation (3) to an algebraic problem[1].

The boundary conditions are of Neumann type with $\frac{\partial\phi}{\partial\eta} = o$ at $\eta = o$ and $\theta = o, \infty$. For large η we have boundary conditions of Dirichlet type which can be determined by multipole expansion of the density for large distances.

To test the accuracy of the numerical solution we used a sum of charge distributions of the form:

$$\rho(r) = c\,\left(\frac{\alpha}{\pi}\right)^{3/2} e^{-\alpha r^2}$$

$$\rho(r) = \frac{de^{ar}}{(1+e^{ar})^2} \tag{4}$$

where the potentials can be calculated analytically. Due to the singularities in equation (3) we have to introduce transformations with the following properties:

$$u \simeq \begin{cases} \alpha_1\eta^2+\beta_1; & \eta\to o \\ e^{\delta\eta} & \eta\to\infty \end{cases} \qquad v \simeq \begin{cases} \alpha_2\theta^2+\beta_2 & \theta\to o \\ \alpha_2(\theta-\pi)^2+\beta_2; & \theta\to\pi \end{cases} \tag{5}$$

This allows to get rid of the singularities and to adapt the distribution of the numerical points even more to the physical problem.

In addition the Mullikan charge density was used as a test as well. For a system like Ni^{2+}-Ni^{2+}, at a distance of 1.5 a.u. and using 1oo x 1oo mesh points, an accuracy of $5\cdot1o^{-5}$ in the potential and $2\cdot1o^{-5}$ in the total energy has already been reached.

A further increase in accuracy can be obtained by use of the Mullikan charge density as a zero-order approximation so that only the difference between the real density and the Mullikan charge density (which is in the order of 1% only) has to be treated. So probably the accuracy can be brought down to the order of $1o^{-5}$. To demonstrate the smoothing power of our transformations we show in Fig.1 a contour diagram of the potential in the transformed coordinates. This shows that the potential in these new coordinaes is rather linear over wide regions.

1) P.N. Swarztrauber, and R.A. Sweet, ACM Trans. Math. Software 5, 352 (1979)

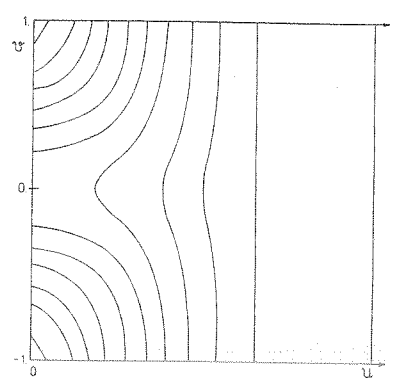


Fig.1: Contour diagram of the potential

Calculations of Coupling Matrix Elements for Diatomic Systems in an Atomic Basis [G]

W.D. Sepp
Department of Physics, University of Kassel

During the last year the relativistic molecular program, which calculates energy eigenvalues and molecular wavefunctions, has been further optimized. The processing time has been reduced by a factor of 2 to 3. In addition the diophantine method to calculate the 2-dimensional integrals was changed to a combined Gauß-Laguerre integration which uses less points but is better up to a factor of 1000. Since rotational and radial coupling matrix elements are needed for coupled channel calculations, we started to calculate them within our program.

The dynamic coupling matrix element between two adiabatic molecular orbitals $|\Psi_i\rangle$ and $|\Psi_j\rangle$ is given by

$$\langle\Psi_i|\frac{\partial}{\partial t}|\Psi_j\rangle = \dot{R}\langle\Psi_i|\frac{\partial}{\partial R}|\Psi_j\rangle + \frac{i}{\hbar}\dot{\varphi}\langle\Psi_i|j_y^{CM}|\Psi_j\rangle = M_{ij}^{Rad} + M_{ij}^{Rot} \quad (1)$$

where $\dot{R}$ is the radial velocity between the two nuclei, $\dot{\varphi}$ the angular velocity of the internuclear axis, and j_y^{CM} the y-component of the electronic angular momentum operator in the CM system.

The MO-wavefunctions $|\Psi_i\rangle$ are expanded in atomic wavefunctions $|\varphi_\mu\rangle$, centered at the nuclei

$$|\Psi_j\rangle = \sum_\mu c_{j\mu}|\varphi_\mu\rangle \quad (2)$$

The expansion coefficients $c_{j\mu}$ depend only on the internuclear distance R, whereas the atomic states $|\varphi_\mu\rangle$ depend on the coordinates of the nuclei as well as on the orientation of the internuclear axis which is used as quantization axis for the atomic states. Inserting (2) in (1), the radial coupling matrix may be written as

$$M_{ij}^{Rad} = M_{ij}^{MO} + M_{ij}^{kin} \quad (3)$$

where the MO-part of the coupling is given by

$$M_{ij}^{MO} = \dot{R}\sum_{\mu\nu} c_{i\nu}^* \left(\frac{\partial}{\partial R}c_{j\mu}\right)\cdot S_{\nu\mu}^{AO} \quad (4)$$

with the atomic overlap matrix

$$S_{\nu\mu}^{AO} = \langle\varphi_\nu|\varphi_\mu\rangle \quad (5)$$

and the kinematic part is given by

$$M_{ij}^{kin} = \dot{R}\sum_{\mu\nu} c_{i\nu}^* c_{j\mu}\cdot\langle\varphi_\nu|\frac{\partial}{\partial R}|\varphi_\mu\rangle. \quad (6)$$

Equ.(4) is calculated by numerical interpolation and differentiation of the transformation coefficients. Equ.(6) can be further reduced since the atomic state $|\Psi_\mu\rangle$ depends only on the coordinates X^A or X^B of one of the nuclei A or B. Therefore, the differential operator $\frac{\partial}{\partial R}$ can be replaced by the linear momentum operator p and we get

$$M_{ij}^{kin} = \dot{R}\sum_{\mu\nu} c_{i\nu}^* c_{j\mu}\cdot\frac{M_{I(\mu)}}{M_A+M_B}\cdot\frac{i}{\hbar}\langle\varphi_\nu|p_z|\varphi_\mu\rangle \quad (7)$$

where $M_{I(\mu)}$ is M_A or $-M_B$ if the atomic state $|\Psi_\mu\rangle$ is centered at the nucleus A or B, respectively. The resulting p_z-matrix element is calculated without any numerical differentiation using the identity

$$p_k = \frac{1}{2}\left[\alpha_k(\vec{\alpha}\vec{p}) + (\vec{\alpha}\vec{p})\alpha_k\right],\ k = x,y,z \quad (8)$$

and the DF-equation for the atomic basis states

$$(\vec{\alpha}\vec{p} + (\beta-1)m + V_{Atom})|\varphi_\mu\rangle = \varepsilon_\mu^{AO}|\varphi_\mu\rangle\ . \quad (9)$$

Since the MO-coefficients $c_{j\mu}$ are independent of the orientation of the colliding system, the rotational coupling matrix element is given by

$$M_{ij}^{Rot} = \frac{i}{\hbar}\dot{\varphi}\sum_{\mu\nu} c_{i\nu}^* c_{j\mu}\langle\varphi_\nu|j_y^{CM}|\varphi_\mu\rangle.$$

Shifting the origin of the angular momentum operator from the center of mass to the center of the atom I(μ)

$$j_y^{CM} = j_y^{I(\mu)} + [\underline{p}\times\underline{X}^{I(\mu)}]_y \quad (11)$$

we get two contributions to the rotational coupling matrix element

$$M_{ij}^{Rot} = M_{ij}^{Orient.} + M_{ij}^{Displ.} \quad (12)$$

where the orientation part is given by

$$M_{ij}^{Orient.} = \frac{i}{\hbar}\dot{\varphi}\sum_{\mu\nu} c_{i\nu}^* c_{j\mu}\langle\varphi_\nu|j_y^{I(\mu)}|\varphi_\mu\rangle \quad (13)$$

and the displacement part by

$$M_{ij}^{Displ.} = -\frac{i}{\hbar}\dot{\varphi}\sum_{\mu\nu} c_{i\nu}^* c_{j\mu} X_z^{I(\mu)}\cdot\langle\varphi_\nu|p_x|\varphi_\mu\rangle. \quad (14)$$

Inserting a complete set of states $|\varphi_\lambda^{I(\mu)}\rangle$ of the atom I(μ) in the orientation matrix element

$$\langle\varphi_\nu|j_y^{I(\mu)}|\varphi_\mu\rangle = \sum_\lambda\langle\varphi_\nu|\varphi_\lambda^{I(\mu)}\rangle\langle\varphi_\lambda^{I(\mu)}|j_y^{I(\mu)}|\varphi_\mu\rangle \quad (15)$$

the calculation of (13) is reduced to a normal one-center angular momentum matrix element and a two-center overlap matrix element $\langle\varphi_\nu|\varphi_\lambda\rangle$. The displacement part (14) is calculated using equ.(8) and (9). The advantage of the method is that all calculations except (4) can be done at a fixed internuclear distance R avoiding numerical differentiation. Up to now no translational factors are included in the coupling matrix elements. These are expected to modify mainly the kinematic part of the radial coupling.

Additional Couplings of the Innermost Shells in Very Heavy Quasi-Molecular Ion-Atom Collisions

M. Mann, B. Fricke, W.-D. Sepp, H. Hartung
Fachbereich Physik, Gesamthochschule Kassel
P.H. Mokler, W.A. Schönfeldt
GSI Darmstadt

In very heavy collision systems the most interesting molecular orbitals are the most strongly bound ones, the $1s\sigma$ and $2p\sigma$ levels more precisely called the $1s_{1/2\ 1/2}$ and $2p_{1/2\ 1/2}$ levels. Due to the tremendous spin orbit splitting around $Z \approx 164$, the $3s_{1/2}$ and the $3p_{1/2}$ levels from the UA M-shell approach the $2p_{3/2}$ levels of the UA L-shell, see the SCF-DFS multi electron correlation diagrams in Fig. 1. This is in clear contrast to lighter collision systems. Hence, for such heavy collision systems around $Z_1+Z_2 \approx 164$ preformed, steady-state vacancies from the projectile M-shell may have a chance to be transferred in the collision molecule at small internuclear distances to the $2p_{3/2}$-MO levels (i.e. $2p_{3/2\ 3/2}$ and $2p_{3/2\ 1/2}$ - see box 1 in Fig. 1). On the outgoing part of the collision the original projectile M-shell vacancy finally may end up as a $2p_{1/2\ 1/2}$ vacancy for those heavy systems - cf. box 2 in Fig. 1.

For lighter collision systems ($Z_1+Z_2 \lesssim 140$) a vacancy transfer via box 1 is hindered; for heavier systems ($Z_1+Z_2 \gtrsim 178$) the vacancy transfer probability in box 2 may be reduced. Hence, the observed total $2p_{1/2\ 1/2}$ cross section enhancement around $Z_1+Z_2 \approx 164$ - see literature values summarized in Fig. 2 (cf. Ref. 1) - may partially be caused by this projectile M vacancy transfer (via boxes 1 and 2). Coupled channel calculations support this interpretation. In how far a less Z dependent, possible vacancy transfer of projectile L vacancies via the crossings in box 2 alone to the $2p_{1/2\ 1/2}$ level contribute to the cross section enhancement is not clear. The relevance of an initial M vacancy transfer compared to other effects [2,3] should be tested experimentally.

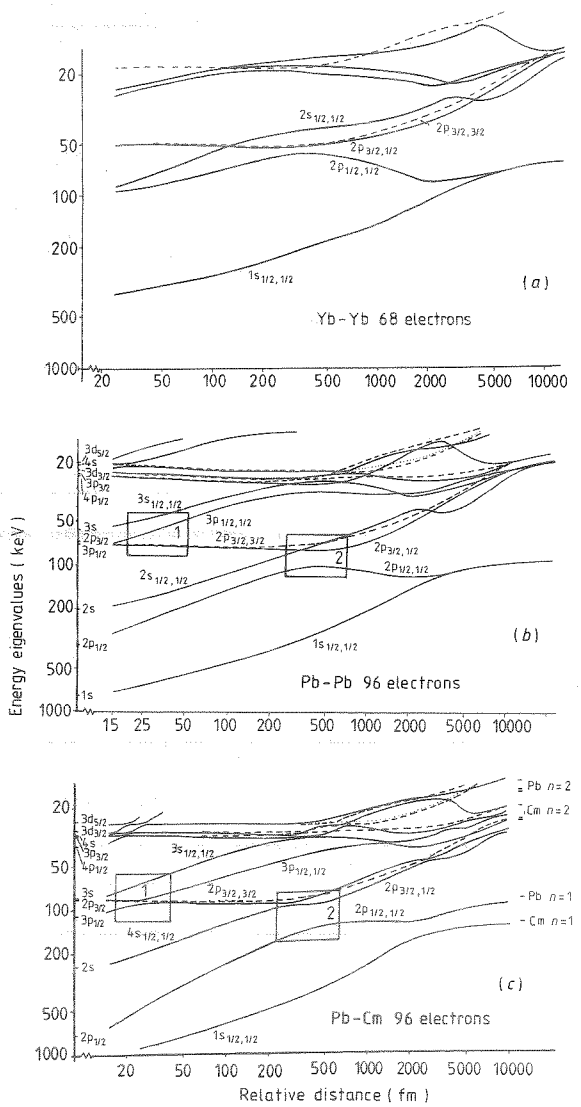


Fig. 1: Calculated SCF-DFS multielectron correlation diagrams with Z_1+Z_2 = 140, 164, and 178.

[1] M. Mann et al., J. Phys. B15 (1982) 4199
[2] G. Soff et al., Fizika 9 Suppl. 4 (1977) 721
[3] G. Soff et al. Z. Phys. A294 (1980) 37

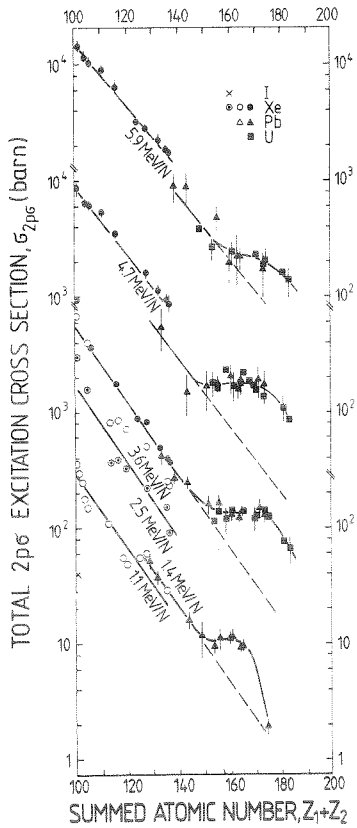


Fig. 2: Summary of experimental $2p_{1/2\ 1/2}$ excitation cross sections for superheavy collision systems with $Z_1+Z_2 \gtrsim 100$ for 1 to 6 MeV/u (cf. Ref. 1).

Solution of the time-dependent Hartree-Fock equation for atomic collisions

G

Eberhard Teubner, Norbert Grün and Werner Scheid

Institut für Theoretische Physik der Justus-Liebig-Universität Giessen

In order to treat the problem of a collision of atomic shells with many electrons we assume that each electron moves in the Coulomb fields of the two nuclei and in the self-consistent field generated by the other electrons. The motion of the electrons is approximately described by the one-body density matrix $\rho(\vec{r},\vec{r}',t)$ solving the time-dependent Hartree-Fock equation:

$$(-\frac{\hbar^2}{2m}(\vec{\nabla}^2-\vec{\nabla}'^2)+V(\vec{r},t)-V(\vec{r}',t)-i\hbar\frac{\partial}{\partial t})\rho(\vec{r},\vec{r}',t)$$
$$-e^2\int(\frac{1}{|\vec{r}-\vec{x}|}-\frac{1}{|\vec{r}'-\vec{x}|})\rho(\vec{r},\vec{x},t)\rho(\vec{x},\vec{r}',t)d^3\vec{x}=0, \quad (1)$$

where $V(\vec{r},t)=-\frac{Z_1e^2}{|\vec{r}-\vec{R}_1(t)|}-\frac{Z_2e^2}{|\vec{r}-\vec{R}_2(t)|}-e\varphi(\vec{r},t)$ (2)

$$\Delta\varphi = 4\pi e\rho(\vec{r},\vec{r},t) \quad (3)$$

In this report we outline a new method for solving Eq.(1), which is based on the procedure of Heller[1,2], who expanded wave functions into semi-classically moving Gaussian wave packets with time-dependent widths and applied this formalism to problems of molecular physics.

First we introduce the Wigner transformed function of the density matrix defined by

$$F(\vec{r},\vec{p},t)=\frac{1}{(2\pi\hbar)^3}\int\rho(\vec{r}+\frac{\vec{x}}{2},\vec{r}-\frac{\vec{x}}{2},t)\exp(-\frac{i}{\hbar}\vec{p}\vec{x})d^3\vec{x}. \quad (4)$$

This function is expanded into Gaussian wave packets with time-dependent parameters determined later:

$$F(\vec{r},\vec{p},t) = \sum_{n=1}^{N} A_n(t)f_n(\vec{r},\vec{p},t), \quad (5)$$

$$f_n(\vec{r},\vec{p},t)=\exp[-\{(\vec{r}-\vec{r}_n(t))^T\alpha_n(t)(\vec{r}-\vec{r}_n(t))$$
$$+2(\vec{r}-\vec{r}_n(t))^T\beta_n(t)(\vec{p}-\vec{p}_n(t)) \quad (6)$$
$$+(\vec{p}-\vec{p}_n(t))^T\gamma_n(t)(\vec{p}-\vec{p}_n(t))\}],$$

where $\alpha_n(t)$, $\beta_n(t)$ and $\gamma_n(t)$ are real 3x3 matrices with $\alpha_n^T=\alpha_n$ and $\gamma_n^T=\gamma_n$.

The functions $f_n(\vec{r},\vec{p},t)$ are chosen as solutions of the Liouville equation for a potential $V_n(\vec{r},t)$, which is the Taylor expansion of the Hartree potential $V(\vec{r},t)$ defined in Eq.(2) about $\vec{r}=\vec{r}_n(t)$ up to quadratic terms:

$$V_n(\vec{r},t)=V(\vec{r}_n(t),t)+(\vec{r}-\vec{r}_n(t))(\vec{\nabla}V(\vec{r},t))_{\vec{r}=\vec{r}_n(t)}$$
$$+\frac{1}{2}(\vec{r}-\vec{r}_n(t))^TV_n''(\vec{r}_n(t),t)(\vec{r}-\vec{r}_n(t)) \quad (7)$$

Here, V_n'' denotes the symmetric 3x3 matrix formed by the second partial derivatives of V with respect to the coordinates. Since the potential (7) is of oscillator type, Liouville's equation is identical with the quantum mechanical equation of motion for the Wigner function f_n:

$$(\frac{\partial}{\partial t}+\frac{\vec{p}}{m}\vec{\nabla}_r-\vec{\nabla}V_n\vec{\nabla}_p)f_n = 0 \quad (8)$$

With the condition that f_n fulfills Eq.(8), we obtain equations for the parameters:

$$\dot{\vec{r}}_n=\frac{1}{m}\vec{p}_n, \quad \dot{\vec{p}}_n=-\vec{\nabla}V|_{\vec{r}=\vec{r}_n(t)} \quad (9)$$

$$\dot{\alpha}_n=\beta_nV_n''+V_n''\beta_n^T, \quad \dot{\beta}_n=V_n''\gamma_n-\frac{\alpha_n}{m}, \quad \dot{\gamma}_n=-\frac{1}{m}(\beta_n+\beta_n^T) \quad (10)$$

Hence the evolution of the packets f_n is equivalent to the motion of a pseudo-particle with coordinate $\vec{r}_n(t)$ and momentum $\vec{p}_n(t)$ in the potential $V(\vec{r},t)$. Next we transform the Wigner function back into the density matrix:

$$\rho(\vec{r},\vec{r}',t) = \sum_{n=1}^{N} A_n(t)\rho_n(\frac{\vec{r}+\vec{r}'}{2},\vec{r}-\vec{r}',t) \quad (11)$$

$$\rho_n(\vec{s},\vec{q},t) = \int f_n(\vec{s},\vec{p},t)\exp(\frac{i}{\hbar}\vec{p}\vec{q})d^3\vec{p} \quad (12)$$

The functions ρ_n fulfill Eq.(1) with the potential V_n defined in Eq.(7), but without the exchange terms. The coefficients $A_n(t)$ are obtained by solving the following set of equations:

$$\sum_{k=1}^{N}[S_{nk}\dot{A}_k(t)-M_{nk}A_k(t)]=0, \quad n=1,\ldots N, \quad (13)$$

where $S_{nk}=i\hbar\int\rho_n^*(\vec{s},\vec{q},t)\rho_k(\vec{s},\vec{q},t)d^3\vec{s}d^3\vec{q}$, (14)

$$M_{nk}=\int\rho_n^*(\vec{s},\vec{q},t)(V(\vec{r},t)-V(\vec{r}',t)-V_k(\vec{r},t)+V_k(\vec{r}',t))$$
$$\cdot\rho_k(\vec{s},\vec{q},t)d^3\vec{s}d^3\vec{q} + \text{exchange terms} \quad (15)$$

with $\vec{r}=\vec{s}+\vec{q}/2$, $\vec{r}'=\vec{s}-\vec{q}/2$

The time variation of the coefficients $A_n(t)$ is small if the potential $V(\vec{r},t)$ is well approximated by an oscillator potential inside the width of a Gaussian wave packet.

This method allows to solve the TDHF equation (1) on the basis of a finite number of Gaussian wave packets, which move on self-consistent classical trajectories. When we have developed analytical approximations for the matrix elements (15), we will obtain a fast computational procedure for solving the TDHF-equation for problems in atomic or nuclear physics.

[1] E.J. Heller, J.Chem.Phys. 62 (1975) 1544

[2] S.Y. Lee and E.J. Heller, J.Chem.Phys. 76 (1982) 3035

Use of Ehrenfest's Principle for Inelastic Collisions

B G

M. Kleber and W. Elberfeld
Physik-Department
Technische Universität München

In a recent study[1] we showed

1) how to put Ehrenfest's principle into action for heavy particle impact;
2) how to determine transition probabilities in a unique way from trajectories.

We investigated the Landau-Teller model[2] for the collinear atom-diatomic molecule collision. In this model a harmonic oscillator CB is exposed to an exponential potential acting between A and B. We found excellent agreement between the results of the optimized Ehrenfest method and those of an exact semiclassical coupled channel calculation. In the following example the Ehrenfest results cannot be distinquished from exact coupled channel results.

The reaction dynamics is depicted in Figs.1-2. These show the deformation of the oscillator in configuration and momentum space as a function of time. Also shown is the time dependence of the uncertainty Δx^2. We have chosen a heavy scaled reduced mass (m=3.737) and a deep molecular potential width (α=0.5584) which approximately represents the collision HBr+He with Br being atom C. $\tilde{E}=E/\hbar\omega + 0.5$ is the sum of impact energy and ground state energy of the oscillator ($\tilde{E}$=6 in Fig.1). Fig. 3 shows energy transfer, excitation probability and the Cauchy-Schwarz lower bounds for the squared overlap between exact wave function $|\psi(t)\rangle$ (coupled channels) and the approximate wave function $|\phi(t)\rangle$ (Ehrenfest method)

$$|\langle\psi(\infty)|\phi(\infty)\rangle|^2 \geq 1 - \sin^2 \min \{ \int_{-\infty}^{\infty} dt' \langle\varepsilon(t')|\varepsilon(t')\rangle^{1/2} \}^{\pi/2} \quad (1)$$

with $|\varepsilon(t)\rangle = (H - i\hbar\partial_t)|\phi(t)\rangle$. This lower bound is an extremely pessimistic estimate in view of $|\langle\psi(\infty)|\phi(\infty)\rangle|^2 \geq 0.999$ in the whole range of impact energies. In part b of Fig. 3 we compared for illustrative purposes various approximations to a complete quantal calculation in which the relative atom-molecule motion has been treated quantally. Fig. 3 warns us not to believe too faithfully in semiclassical methods for head-on collisions.

Fig.1: Average displacement (in units of the oscillator length d) and momentum (in units of $\hbar$/d) of the harmonic oscillator in a collinear collision. Starting point t=-∞, turning point t=0.

Fig.2: Change of the collision induced fluctuation Δx^2. Length and time are in units of d and ω^{-1} respectively. Trajectory starts with Δx^2=0.5.

Fig.3: a) Energy transfer ΔE in units of $\hbar\omega$. A is the classical result, B the result of the Ehrenfest method. C are the r.h.s. values of Eq.(1).
b) Vibrational transition probabilities for the 0→1 transition. Compared are various methods: complete quantal calculation by Clark and Dickinson (D), Ehrenfest method (E), classical (F), first order distorted wave (G).

[1] W. Elberfeld and M. Kleber, preprint (1982)

[2] A.P. Clark and A.S. Dickinson, J.Phys. B6, 164 (1973)

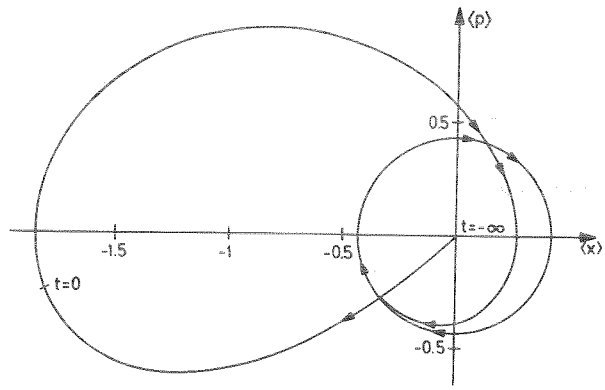


Fig. 1

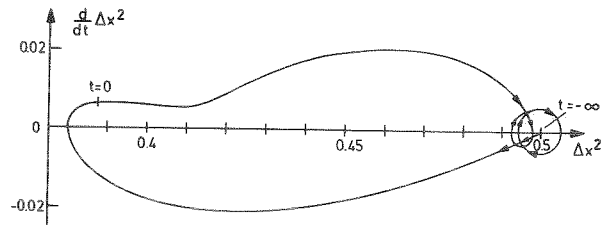


Fig. 2

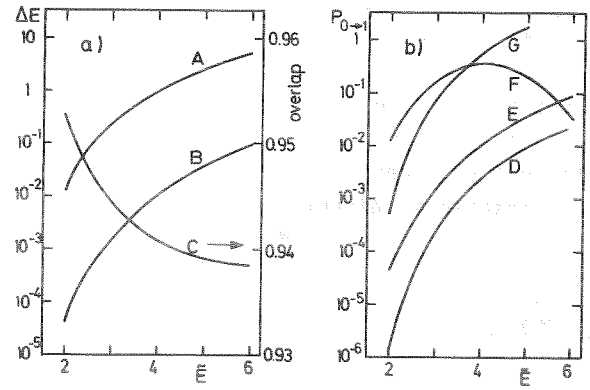


Fig. 3

The Local Representation of the Dirac Equation [B G]

P. Schlüter, K.-H. Wietschorke and W. Greiner
Institut für Theoretische Physik der Universität Frankfurt

The theoretical treatment of relativistic fermions in an external potential or in the presence of boundary conditions becomes simpler and more transparent by the use of a well-suited set of coordinates. Examples are given by the two-centre problem or the study of non-spherical bags.
The straightforward introduction of those non-cartesian coordinates leads to a rather complicated partial differential equation for the wave function ψ_c. To simplify this we established a space-dependent ("local") representation of the Dirac matrices

$$\bar{\gamma}^\mu = e^{B(\vec{r})}\, U(\vec{r})\, \gamma^\mu \left(e^{B(\vec{r})}\, U(\vec{r})\right)^{-1} \qquad (1)$$

with a unitary matrix $U(\vec{r})$ and a scalar-valued function $B(\vec{r})$ depending on the coordinate system. This corresponds to a wave function ψ, given by

$$\psi_c(\vec{r},t) = e^{B(\vec{r})}\, U(\vec{r})\, \psi(\vec{r},t). \qquad (2)$$

The function B, which influences the volume element, connects also the covariantly formulated Dirac equation with the solution ψ_r with ψ by

$$\psi_r(\vec{r},t) = e^{B(\vec{r})}\, \psi(\vec{r},t). \qquad (3)$$

A first advantage of the Dirac equation in this form is the minimization of the space dependence of the Hamiltonian, and so far less expense for a numerical treatment can be expected. Also analytical investigations become more lucid, e.g. the $\hat{K}$-operator in the spherical case can be derived easily. Moreover, the study of the asymptotic behaviour is simplified.
As a example we will look for the well known spherical hydrogen problem in the different representations. Direct introduction of the spherical coordinates r,ϑ,φ leads to

$$\left[-i\left\{\gamma^0\frac{\partial}{\partial t} + \frac{1}{r}\left(\bar{\gamma}^1\frac{\partial}{\partial\vartheta} + \bar{\gamma}^2\frac{1}{\sin\vartheta}\frac{\partial}{\partial\varphi}\right) + \bar{\gamma}^3\frac{\partial}{\partial r}\right\} + 1 - \frac{2d}{r}\gamma^0\right]\psi_c = 0 \qquad (4a)$$

with

$$\begin{aligned}\bar{\gamma}^1 &= \cos\vartheta\,(\cos\varphi\,\gamma^1 + \sin\varphi\,\gamma^2) - \sin\vartheta\,\gamma^3,\\ \bar{\gamma}^2 &= -\sin\varphi\,\gamma^1 + \cos\varphi\,\gamma^2,\\ \bar{\gamma}^3 &= \sin\vartheta\,(\cos\varphi\,\gamma^1 + \sin\varphi\,\gamma^2) + \cos\vartheta\,\gamma^3.\end{aligned} \qquad (4b)$$

The equation for ψ_r is

$$\left[-i\left\{\gamma^0\frac{\partial}{\partial t} + \frac{1}{r}\left(\gamma^1\frac{\partial}{\partial\vartheta} + \gamma^2\frac{1}{\sin\vartheta}\frac{\partial}{\partial\varphi}\right) + \gamma^3\frac{\partial}{\partial r}\right\} + 1 - \frac{2d}{r}\gamma^0 - i\left\{\frac{\cot\vartheta}{2r}\gamma^1 + \frac{1}{r}\gamma^3\right\}\right]\psi_c = 0, \qquad (5)$$

while ψ fulfills

$$\left[-i\left\{\gamma^0\frac{\partial}{\partial t} + \frac{1}{r}\left(\gamma^1\frac{\partial}{\partial\vartheta} + \gamma^2\frac{1}{\sin\vartheta}\frac{\partial}{\partial\varphi}\right) + \gamma^3\frac{\partial}{\partial r}\right\} + 1 - \frac{2d}{r}\gamma^0\right]\psi = 0. \qquad (6)$$

The functions B and U are given by

$$e^B = \frac{1}{r\sqrt{\sin\vartheta}}, \qquad U = e^{-i\frac{\varphi}{2}\Sigma_3}\, e^{-i\frac{\vartheta}{2}\Sigma_2}. \qquad (7)$$

In the local representation $\hat{K}$ and the z-component of the angular momentum are simply

$$\begin{aligned}\hat{J}_z &= -i\frac{\partial}{\partial\varphi},\\ \hat{K} &= \gamma^0\gamma^3\left(\gamma^1\frac{\partial}{\partial\vartheta} + \frac{1}{\sin\vartheta}\gamma^2\frac{\partial}{\partial\varphi}\right).\end{aligned} \qquad (8)$$

Such a local representation can be given for all practically used orthogonal coordinate systems. The only restriction is implied by the requirement that the coordinate transformation can be decomposed in steps of two dimensional ones, each induced by a conformal mapping.

[1] P. Schlüter, K.-H. Wietschorke, and W. Greiner; The Dirac Equation in Orthogonal Coordinate Systems, I. The Local Representation, to be publ. in Journal of Physics A
[2] K.-H. Wietschorke, P. Schlüter, and W. Greiner; The Dirac Equation in Orthogonal Coordinate Systems, II. The Two Centre Dirac Equation, to be publ. in Journal of Physics A

On an Alternative Dirac-Theory [BC]

A. Schäfer, J. Rafelski, and W. Greiner
Institut für Theoretische Physik der Universität Frankfurt

The main aim of some atomic physics experiments is to test QED under hitherto inaccessible conditions, namely for very strong electromagnetic fields. Therefore it is interesting to know which kind of derivations from QED is at all consistent and imaginable from the theoretical point of view. In our work[1] we considered possible alternatives to the Dirac-equation. We didn't want to introduce ad hoc modifications. Instead we proposed a new interpretation of the Dirac-theory which leads us quite naturally to alternative equations of motion. The basic ingredient of this interpretation is the generalization of the Dirac-equation to five dimensions introducing a forth space-coordinate. The mass in the ordinary Dirac equation can then be interpreted as the eigenvalue of the additional momentum-operator.
We can write the five-dim. Dirac-equation as

$$\hat{p}_\alpha \tilde{\gamma}^\alpha \chi(x_\beta) = i\gamma_5(\gamma_\mu \hat{p}^\mu - \hat{p}_5)\chi(x_\beta) = 0 \qquad (1)$$

Eq.(1) is invariant under five-dim. Lorentz-transformations (i.e. the group O(1,4)). We determine the Lagrangian leading to(1), obtain the plain wave solutions and quantize this five-dim. Dirac-theory. Finally, the propagator in coordinate space is found to be

$$S(x_\beta) = \frac{3}{8\pi^2} \frac{x^\alpha \tilde{\gamma}_\alpha}{(-x_\alpha x^\alpha + i\eta)^{5/2}} \qquad (2)$$

So far this new interpretation of the Dirac-equation has no observable consequences. If however you change the properties of the additional dimension, e.g. discretize it, a projection onto the Minkowski-space gives new physics. Defining our theory by(2) and setting

$$x_5 = \ell\lambda \qquad \ell = \ldots,-2,-1,0,1,2,\ldots \qquad (3)$$

we get for the propagator in momentum space the surprisingly simple form

$$S_{discr.}(p_\mu, p_5) = \frac{\lambda}{2} \frac{1}{\cot g[\frac{\lambda}{2}(\not{p} - p_5)]} \qquad (4)$$

Thus, if the fifth dimension is descretized, the equation of motion of a Dirac-particle in the ordinary Minkowski-space becomes[2]

$$\frac{2}{\lambda} \cot g[\tfrac{\lambda}{2}(\not{\hat{p}} - p_5)]\, \psi(x_\mu; p_5) = 0 \qquad (5)$$

The continuum-limit $\lim$ leads to the ordinary Dirac-equation. However for $\lambda \neq 0$ eq.(5) predicts derivations of the order λ^2. We think that the proposed way to look for alternatives to the Dirac-eq. is attractive as it attempts to relate possible derivations from QED to a fundamentally new interpretation of the underlying space-time structure.

[1] A. Schäfer, J. Rafelski, and W. Greiner, UFTP-preprint 84/82, to be published in Annals of Physics
[2] M. Danos, W. Greiner, and J. Rafelski Phys.Rev. D6 (1972) 3476

The Dirac Equation for Rotational Symmetric Potentials or Boundary Conditions [B G]

K.-H. Wietschorke, P. Schlüter and W. Greiner
Institut für Theoretische Physik der Universität Frankfurt

The consideration of fermions in a potential induced by two pointlike or extended particles each with charge Ze becomes difficult because then the Dirac equation does not separate in any known coordinate system. Nevertheless there exists a well suited coordinate system for the treatment of the problem in the form of a two dimensional partial differential equation. The equipotential and field lines of two equal point charges in two dimensional electrodynamics lead to coordinates ω, δ, φ similar to the Cassini coordinates described in the book of Moon and Spencer[1]. They are related to the cylindrical coordinates z, ρ by

$$\log \omega + i\delta = \frac{1}{2} \log \frac{(z+i\rho)^2 - a^2}{a^2},$$

$$0 < \omega < \infty, \quad 0 < \delta < \pi, \quad 0 < \varphi < 2\pi.$$

In the standard formulation the Dirac equation looks then rather complicated. Here we can use the idea of the local representation of the Clifford Algebra in a very effective way[2,3]. We are left with a relatively simple equation for the symmetric two centre problem in the coordinates ω, δ, φ

$$\left[-i\gamma^0 \frac{\partial}{\partial t} + \frac{\sqrt{D}}{a\omega}\left(\gamma^3 \frac{\partial}{\partial \omega} + \frac{1}{\omega}\gamma^1 \frac{\partial}{\partial \delta}\right) + \frac{1}{\rho}\gamma^2 \frac{\partial}{\partial \varphi} + 1 + V\right] \psi = 0$$

with the abbreviations

$$D = \omega^4 + 2\omega^2 \cos 2\delta + 1,$$

$$\rho = \frac{a}{\sqrt{2}} \sqrt{\sqrt{D} - 1 - \omega^2 \cos 2\delta},$$

$$V = -\frac{2\alpha\sqrt{2}}{a\omega^2} \sqrt{\sqrt{D} + 1 + \omega^2}.$$

The two centre distance is 2a. In both asymptotic cases of large and small ω this equation reduces to the Dirac equation in spherical coordinates. Also the examination of the asymptotic behaviour near the remaining boundaries, necessary for a numerical treatment is technically simple. As a commendable procedure to solve a partial differential equation we mention the semidiscrete Galerkin method or method of lines[4]. For the bound states a very effective matching method can be used to find the eigen energies. We are able to reproduce the known energy correlation diagrams over a large range of two centre distances.

Another problem, which has gained increased attention in the last time, has been treated with the same method: the description of deformed hadrons by the MIT bag model. If the bag surface coincides with a coordinate plane it is straightforward to implement the above mentioned method to find eigen energies and eigensolutions. For prolate-elliptical bags we found eigen energies, which agree with those of D. Vasak et al. within 5 decimal places.

[1] P. Moon and D.E. Spencer, Field Theory Handbook, Berlin, Springer-Verlag 1961
[2] P. Schlüter, K.-H. Wietschorke, and W. Greiner, The Dirac Equation in Orthogonal Coordinate Systems, I. the Local Representation, to be publ. in Journal of Physics A
[3] K.-H. Wietschorke, P. Schlüter and W. Greiner, The Dirac Equation in Orthogonal Coordinate Systems, II. The Two Centre Dirac Equation, to be published in Journal of Physics A
[4] M.H. Schultz, Spline Analysis, Englewood Cliffs, Prentice Hall, 1973
[5] D. Vasak, R. Shanker, B. Müller, and W. Greiner, Deformed Solutions of the M.I.T. Bag Model, to be published

D.H.Jakubaßa-Amundsen, P.A.Amundsen
Physik-Department, Technische Universität München
K.Aashamar
Institute of Physics, University of Oslo

K-vacancy creation in slow collisions is well described by the rotational coupling of the $2p\pi$ and $2p\sigma$ molecular orbitals[1] if a $2p\pi$-vacancy is brought into the collision. However, for heavier collision systems the experiments show a substantial deviation from this theory, especially at small impact parameters[2,3].

If the projectile has no L-shell vacancy, two different processes are possible. The L-vacancy may be created in one collision and, provided its lifetime is long enough, be transferred to the K-shell in a second collision. The probability for this double-collision process is given by[4]

$$P(b)\frac{d\vec{b}}{d\Omega} = c_0 \int d\Omega_1 \left(P_L(b_1)\frac{d\vec{b}_1}{d\Omega_1} \right)\left(P_C(b_2)\frac{d\vec{b}_2}{d\Omega_2} \right) \qquad (1)$$

where $P_L(b_1)$ is the probability for creation of a L-vacancy at scattering angle Ω_1 (impact parameter b_1), and $P_C(b_2)$ is the probability for $2p\pi$ - $2p\sigma$ coupling at scattering angle Ω_2 (impact parameter b_2). This process dominates the K-vacancy creation at medium and large impact parameters. The impact-parameter dependence of (1) for large b differs appreciably from $P_C(b)$ due to the strong b-dependence of P_L (see Fig.1).

The second possibility to create a K-hole is the production of the L-vacancy and the transfer to the $2p\sigma$ orbital in a single collision. In the case of relativistic systems, where a strong spin-orbit splitting suppresses the coupling between the $2p\pi$ and $2p\sigma$ orbitals at small internuclear distances R, a separation in time of the L-vacancy production and the $2p\pi$-$2p\sigma$ coupling is possible. The L-vacancy is created via direct ionisation at very small R provided the velocity is low enough, with an amplitude approximated by[5,6]

$$A_{fi}(\tau) = \frac{1}{i\hbar}\int_{-\infty}^{\tau} dt \,\langle \psi_f | -\frac{Z_1 e^2}{|\vec{r}-\alpha\vec{R}|} - \frac{Z_2 e^2}{|\vec{r}+\beta\vec{R}|} | \psi_i \rangle \, e^{i/\hbar (E_f - E_i)t} \qquad (2)$$

with $\alpha = 1-\beta = Z_2/(Z_1+Z_2)$, and the wavefunctions and energies are time-independent united-atom functions.

The amplitudes $A_{fi}(\tau)$ which determine the number of vacancies in the state i, are taken as initial conditions for the system of equations coupling the states i[7]:

$$\frac{dc_i(t)}{dt} = \frac{1}{i\hbar} c_i(t)\varepsilon_i(t) - \sum_k \langle \chi_i | \dot{R}\frac{\partial}{\partial R} + \dot{\theta}\frac{\partial}{\partial \theta} | \chi_k \rangle c_k(t)$$

$$c_i(\tau) = A_{fi}(\tau) \qquad (3)$$

where the χ_i are time-dependent, adiabatic wavefunctions with energy $\varepsilon_i(t)$. In relativistic systems, both radial and rotational couplings are present. We have found that the ionisation process is essentially finished when the coupling becomes large, if the condition holds

$$v/v_L \ll 1/4 \qquad (4)$$

where v_L is the united-atom L-shell velocity, and that the replacement of the initial condition by $c_i(\tau=0) = A_{fi}(\tau=\infty)$ is a good approximation.

As seen from Fig.1, this single-collision process is important at small impact parameters. Together with the double-collision process, the experimental b-dependence over the whole range of impact parameters is well described.

[1] K.Taulbjerg, J.S.Briggs, J.Vaaben, J.Phys.B9, 1351 (1976)
[2] E.Morenzoni, M.Nessi, P.Bürgy, Ch.Stoller, W.Wölfli, X82 Conference, Eugene, Oregon, Contrib. Paper (1982)
[3] R.Anholt, Ch.Stoller, W.E.Meyerhof, J.Phys.B13, 3807 (1980)
[4] R.Anholt, Nucl. Instr. Meth. 198, 567 (1982)
[5] J.S.Briggs, J.Phys.B8, L485 (1975)
[6] P.A.Amundsen, J.Phys. B11, L737 (1978)
[7] D.H.Jakubaßa, K.Taulbjerg, J.Phys.B13, 757 (1980)

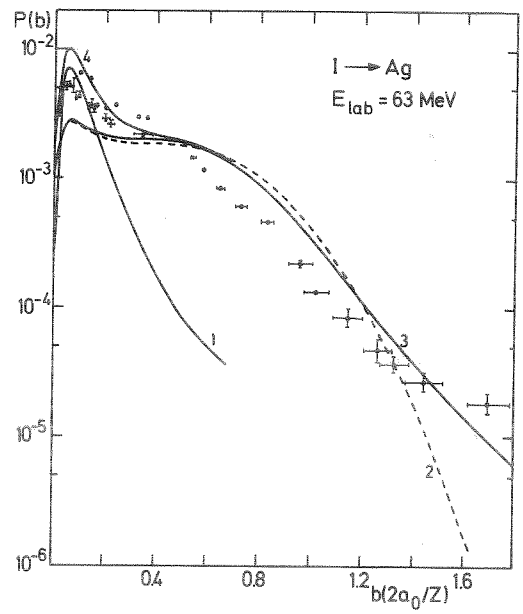


Fig.1 K-vacancy production in 63 MeV I+Ag collisions. Curve 1 is the single-collision, curve 3 the double-collision contribution to the K-vacancy production, curve 4. The dashed line is the normalised $P_C(b)$. The data are from Ref. 2 and 3

D.H.Jakubaßa-Amundsen

Physik-Department, Technische Universität München

The spectroscopy of high-energy electrons emitted in heavy-ion collisions serves as a tool to study the energy and the momentum distribution of the inner-shell electrons in quasi-atomic systems. An additional study of the angular distribution of the electrons yields a direct information on the transition amplitudes and thus on the relative phases.

In slow collisions, the ionisation amplitude can be calculated in the adiabatic perturbation theory by means of[1]

$$a_{fi} = \frac{1}{i\hbar}\int_{-\infty}^{\infty} dt \left\langle \psi_f \left| -\frac{Z_1 e^2}{|\vec{r}-\alpha\vec{R}|} - \frac{Z_2 e^2}{|\vec{r}+\beta\vec{R}|} \right| \psi_i \right\rangle e^{i/\hbar (E_f - E_i)t} \qquad (1)$$

with $\alpha = 1-\beta = Z_2/Z_{ua}$ where $Z_{ua} = Z_1 + Z_2$ is the combined charge of the system. The wavefunctions and energies are taken at a fixed internuclear distance R (and thus time-independent). For strongly asymmetric systems one may take R=0, but otherwise $R=R_o$ with R_o the impact-parameter dependent distance of closest approach is more appropriate[2].

An expansion of the perturbing field and the final state into partial waves

$$\psi_f(\vec{r}) = \sum_{j\ell m} \left(\vec{e}\, Y^*_{j\ell m}(\hat{k}_f)\right) i^{\ell} e^{-i\delta_{j\ell}}\, f_{\ell}(k_f r)\, Y_{j\ell m}(\hat{r}) \qquad (2)$$

where f_l is the radial part, δ_{jl} the phase shift and $\vec{e}$ the polarisation direction of the electron, enables one to write the differential cross section in terms of a multipole expansion with respect to the direction of the emitted electron[2,3]

$$\frac{d^2\sigma}{d\Omega_f dE_f} = 2\pi \frac{m k_f}{\hbar^2} \int_0^{\infty} b\,db \sum_{\vec{e}} |a_{fi}|^2 = \sum_{\lambda\mu} A_{\lambda\mu}(k_f)\, Y_{\lambda\mu}(\hat{k}_f) \qquad (3)$$

For large momentum transfer $(E_f - E_i)/\hbar v \gg 1$, only the lowest multipoles ($\lambda \lesssim 1$) contribute. In the asymmetric C+Pb system (Fig.1) the dependence on ϑ_f is rather strong, but decreases when Z_1 approaches Z_2.

It is interesting that for certain values of Z_{ua} or electron energy E_f the dipole term for L-subshell ionisation attains a negative sign, due to the behaviour of the wavefunction (for the $2p_{1/2}$-state) or the phase shifts. This means that more electrons are emitted in the backward direction.

If in addition to the electron, the angles Θ and Φ of the scattered projectile are measured, the dependence on the electronic azimuthal angle can be obtained. Including only dipole terms, the transition probability may be written in analogy to (3)

$$\frac{d^2P(b)}{d\Omega_f dE_f} = M + D\cos\vartheta_f + A\sin\vartheta_f \cos\varphi_f \qquad (4)$$

The dependence of the probabilities M, D and A on impact parameter is shown in Fig.2 for K-shell ionisation.

[1] J.S.Briggs, J.Phys.B8, L485 (1975)

[2] D.H.Jakubaßa-Amundsen, Physica Scripta 26, 319 (1982)

[3] M.Pauli, F.Rösel, D.Trautmann, J.Phys.B11, 2511 (1978)

[4] W.Koenig, priv. com.; Güttner et al, Z.Phys. A304, 207 (1982)

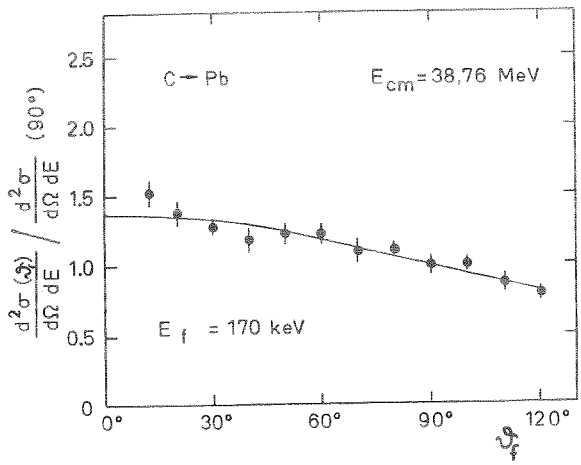


Fig.1 Differential cross section for electron emission in C+Pb collisions. The theory includes K- and L-shell contributions, the data are from Ref. 4

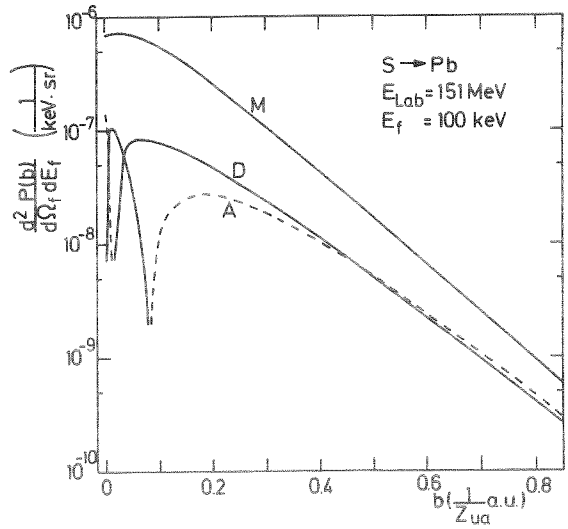


Fig.2 Probability for electron emission in S+Pb collisions. For the symbols, see text. Dashed curves denote a negative sign

K-Hole Coincident δ-Electron Emission [B]

U. Müller and G. Soff
GSI Darmstadt
J. Reinhardt, T. de Reus, B. Müller, and W. Greiner
Institut für Theoretische Physik der Universität Frankfurt

To describe electron excitations in heavy ion collisions rigorously, one has to solve the time-dependent two-centre Dirac equation or, equivalently, a set of coupled channel equations for the excitation amplitudes $a_{ij}(t)$. The number of correlated particle-hole pairs can be deduced from the single-particle amplitudes[1]

$$N_{p,q} = 4 N_p \cdot N_q + 2 \left| \sum_{k<F} a^*_{kp}(\infty)\, a_{kq}(\infty) \right|^2 . \qquad (1)$$

The first term describes accidental coincidences, whereas the second one is the real correlation term. Eq.(1) contains a summation over spin orientations.

For K-hole-electron coincidences further terms arise, if it is impossible to distinguish between $1s\sigma$ - and $2p_{1/2}\sigma$-vacancy formation as is the case in symmetric colliding systems, like U+U. Here the vacancy sharing process produces asymptotically atomic K-vacancies resulting from both $1s\sigma$ - and $2p_{1/2}\sigma$-excitation. Also the origin of the emitted δ-electrons can not be detected. Thus one obtains[1] for the number of δ-electrons with energy E (p=E) measured in coincidence with a K-vacancy ($q=K=1s_{1/2}$)

$$N^{tot}_{E,K} = \left(N_{Es\sigma,\,1s\sigma} + 4\, N_{Ep_{1/2}\sigma} \cdot N_{1s\sigma} \right) + \left(N_{Ep_{1/2}\sigma,\,2p_{1/2}\sigma} + 4\, N_{Es\sigma} \cdot N_{2p_{1/2}\sigma} \right). \qquad (2)$$

Considering slightly asymmetric systems the second term in eq.(2) has to be weighted due to the vacancy sharing process[2].

Within the schematic trajectory model[3] we calculated K-hole coincident δ-electron spectra in the head-on heavy-ion collision U+U (E_{lab}=6.2 MeV/u), where the nuclei stick together for, e.g., T=0 (pure Rutherford scattering, Fig. 1a) and $T=10^{-20}$s (Fig.1b). The dashed-dotted and the short-dashed lines represent the accidental coincidence term and the correlation term without of consideration for spin orientations. Their sum is denoted by full lines. The oscillatory pattern in part b is caused by the real correlation term. The incoherent term produces only a smooth distribution, reflecting the fact that the measurement of δ-electron spectra alone in very high - Z systems will not be sufficient to measure long reaction times.

However, taking into account different spin orientations (eq.(1), long-dashed lines) and both parities (eq.(2), upper full lines), the oscillatory structures diminish[4]. Thus one would expect, if at all, observable oscillatory structures in coincident δ-electron spectra only for asymmetric collision systems.

[1] G. Soff et al., Z.Phys.A294, 137 (1980);
U. Müller et al., Contribution to this GSI Scientific Report
[2] W. Meyerhof, Phys.Rev.Lett. 31, 1341 (1973)
[3] J. Reinhardt et al., Z.Phys. A303, 173 (1981)
[4] U. Müller et al., to be published
[5] T. de Reus et al., to be published

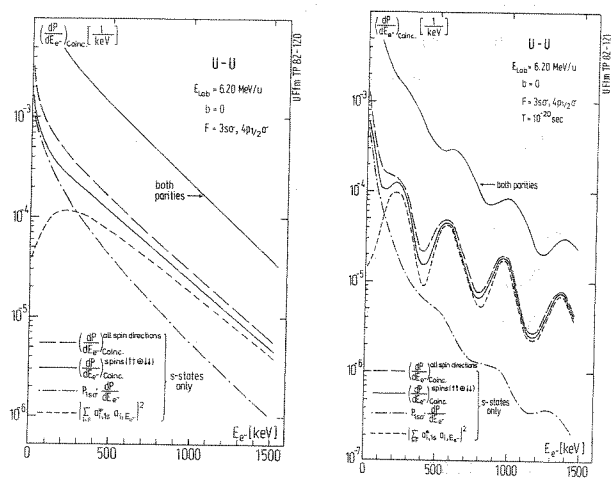


Fig. 1: Spectra of K-hole coincident δ-electrons for the system U+U at E_{lab}=6.2 MeV/u and b=0 (a) No nuclear sticking time, (b) $T = 10^{-20}$s. Electron shielding effects[5] are neglected.

Theoretical Derivation for K-Hole Coincident δ-Electron Emission [B]

U. Müller and G. Soff
GSI Darmstadt
J. Reinhardt, T. de Reus, B. Müller, and W. Greiner
Institut für Theoretische Physik der Universität Frankfurt

An expression for the probability to measure a particle, e.g. a δ-electron, in coincidence with a hole, e.g. a K-vacancy, for heavy ion collisions is derived[1]. It is assumed that there is no experimental discrimination between states with spin up and those with spin down, and no distinction for the final atomic 1s-state, whether it was formed as a molecular $1s\sigma$ - or $2p_{1/2}\sigma$ -vacancy.

Consider $N_{\alpha\beta\gamma\delta,\,\kappa\lambda\mu\nu}$ as a probability for pair-hole coincidences. The indices $\alpha\beta\gamma\delta$ are related to particles, $\kappa\lambda\mu\nu$ are those for holes. They have possible values 0 and 1 for detecting no or just one particle (hole) in the gives state. The indices are associated with the properties: $s\uparrow, s\downarrow, p\uparrow$, and $p\downarrow$. In this convention, e.g., $\alpha=1$ indicates that one can detect a particle in the $s\uparrow$-state, $\mu=0$ that there is no hole in the $p\downarrow$-state recognized.

Because in our calculations these four properties are independent, $N_{\alpha\beta\gamma\delta,\,\kappa\lambda\mu\nu}$ factorizes in $N_{\alpha\kappa}\cdot N_{\beta\lambda}\cdot N_{\gamma\mu}\cdot N_{\delta\nu}$.

Thus a sum $\sum N_{\alpha\beta\gamma\delta,\,\kappa\lambda\mu\nu}$ can be written as

$$\sum N_{\alpha\beta\gamma\delta,\kappa\lambda\mu\nu} = \left(\sum N_{\alpha\kappa}\right)\left(\sum N_{\beta\lambda}\right)\left(\sum N_{\gamma\mu}\right)\left(\sum N_{\delta\nu}\right) \quad (1)$$

Each term $N_{\alpha\kappa}$ can take on four possible values: N_{00}, N_{10}, N_{01}, and N_{11} with expressions[2]

$$\begin{aligned} N_{11} &= N_{pq} = N_p\,N_q + \Big|\sum_{i\in F} a_{ip}^{*}\,a_{iq}\Big|^2 , \\ N_{10} &= N_p - N_{pq},\quad N_{01} = N_q - N_{pq}, \\ N_{00} &= 1 - N_p - N_q + N_{pq}. \end{aligned} \quad (2)$$

We are interested is those terms $N_{\alpha\beta\gamma\delta,\,\kappa\lambda\mu\nu}$, where at least one of the first sequence of indices is 1 and at least one of the second sequence

$$N_{(1),(1)} = 1 - \tilde{\sum} N_{\alpha\beta\gamma\delta,\,\kappa\lambda\mu\nu} , \quad (3)$$

where $\tilde{\sum}$ represents the terms where either no particles or no holes can be detected

$$\begin{aligned} \tilde{\sum} N_{\alpha\beta\gamma\delta,\,\kappa\lambda\mu\nu} &= \sum N_{\alpha\beta\gamma\delta,\,0000} \\ &\quad + \sum N_{0000,\,\kappa\lambda\mu\nu} - N_{0000,\,0000} . \end{aligned} \quad (4)$$

If we consider that in our calculations there is no difference between the excitation rates of states with spin up and those with spin down, we arrive finally[1] at

$$\begin{aligned} N_{(1),(1)} = 1 &- (1-N_\kappa)^2(1-N_\mu)^2 \\ &- (1-N_\alpha)^2(1-N_\gamma)^2 \\ &+ (1-N_\alpha-N_\kappa+N_{\alpha,\kappa})^2 \\ &\quad (1-N_\gamma-N_\mu+N_{\gamma,\mu})^2 . \end{aligned} \quad (5)$$

All terms in eq. (5) have to be understood as measurable quantities within (for continuum states) a certain energy range ΔE_i and solid angular windows $\Delta\Omega_i$. For the theoretically interesting limit $\Delta E_i, \Delta\Omega_i \to 0$ one can easily achieve at

$$N_{pq}^{tot} = N_{E,1s\sigma} + N_{E,2p_{1/2}\sigma} , \quad (6)$$

with

$$\begin{aligned} N_{E,1s\sigma} &= 2\,(N_{Es\sigma,1s\sigma} + N_{Es\sigma}\cdot N_{1s\sigma}) \\ &\quad + 4\,N_{Ep_{1/2}\sigma}\cdot N_{1s\sigma} , \\ N_{E,2p_{1/2}\sigma} &= 2\,(N_{Ep_{1/2}\sigma,2p_{1/2}\sigma} + N_{Ep_{1/2}\sigma}\cdot N_{2p_{1/2}\sigma}) \\ &\quad + 4\,N_{Es\sigma}\cdot N_{2p_{1/2}\sigma} . \end{aligned}$$

The formalism can be easily extended to include the detector efficiency ε_i as other experimental quantities[1]. Considering slightly asymmetric systems the second term in eq.(6) has to be weighted due to the vacancy sharing process[3].

[1] U. Müller et al., to be published
[2] G. Soff et al., Z.Phys. A294, 137 (1980)
[3] W. Meyerhof, Phys.Rev.Lett. 31, 1341 (1973)

Theoretical K-Vacancy Yields in Sm-Pb and Sm-U Collisions [B]

T. de Reus, J. Reinhardt, B. Müller, and W. Greiner
Institut für Theoretische Physik der Universität Frankfurt
G. Soff and U. Müller
GSI Darmstadt

Inner shell vacancy formation was measured for the systems Sm-Pb(Z_{tot}=144) and Sm-U (Z_{tot}=154) at E_{Lab}=3.6, 4.75, and 5.9 MeV/u at the GSI-UNILAC by P. Mokler, D. Liesen, and coworkers[1]. For the charges $Z_{tot} \gtrsim 137$, it is necessary to consider relativistic effects for the electron motion. The nuclei are assumed to follow classical trajectories (semiclassical approximation). Furthermore we perform a multipole expansion of the two centre potential, taking into account only the $V_{l=0}(R,r)$-term (monopole approximation).

In contrast to former calculations, electron-electron interactions in the framework of the relativistic selfconsistent field method are included[2] now:

$$\left(\vec{\alpha}\cdot\vec{p} + \beta m_e + V_{l=0}(R,r)\right)\varphi_i(\vec{r},\vec{R}) + \int \frac{\varrho(\vec{r}')\,d\vec{r}'}{|\vec{r}-\vec{r}'|}\varphi_i(\vec{r},\vec{R}) - \frac{3}{2}\left(\frac{3}{8\pi}\right)^{4/3}(\varrho(\vec{r}))^{4/3}\varphi_i(\vec{r},\vec{R}) = E_i\,\varphi_i(\vec{r},\vec{R}). \quad (1)$$

The states $\varphi_i(\vec{r},\vec{R})$ are used as a basis for the expansion of the time dependent wavefunction. The expansion amplitudes are obtained by numerical coupled channel calculations. The number of holes[3] N_q in the level q is obtained by means of the expansion coefficients

$$N_q = \sum_{i>F} |a_{iq}|^2. \quad (2)$$

In Fig. 1 K-vacancy formation in the system Sm-Pb is investigated. The full lines represent coupled channel results using the Hartree Fock Slater potential, whereas the dashed curves neglect screening effects. Apart from deviations in the 3.6 MeV/u data between b=10 and b=50 fm, a general improvement is achieved by the inclusion of electron screening. The same holds true for the system Sm-U (Fig. 2) except for the 3.6 MeV/u data, where the experimental data still are somewhat underestimated.

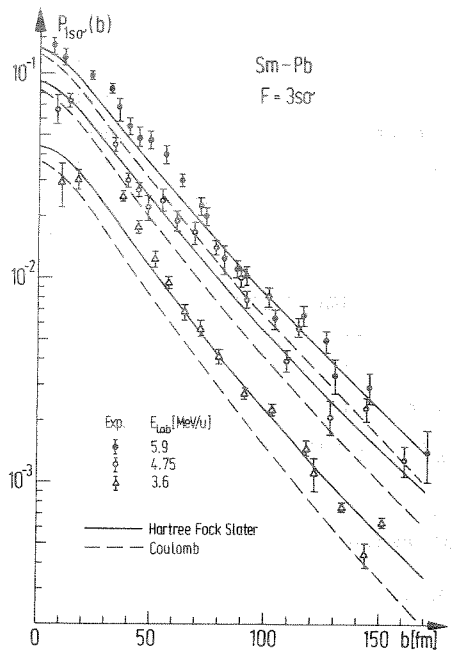


Fig. 1: 1sσ-vacancy probability ($P_{1s\sigma}$(b)) as a function of the impact parameter b for the system Sm-Pb at different bombarding energies E_{Lab}=3.6,4.75,5.9 MeV/u in comparison with experiment[1]. Full lines include electron screening, broken lines do not.

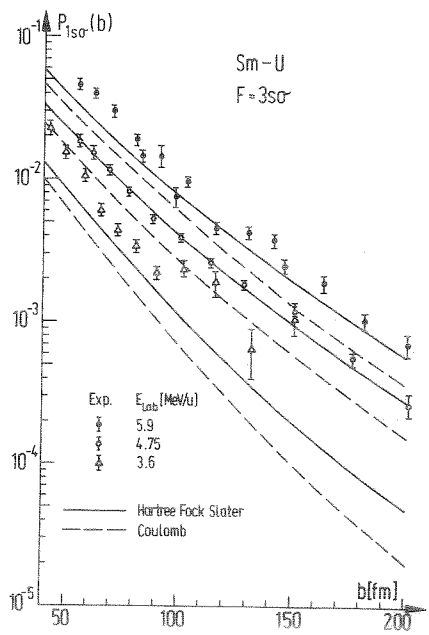


Fig. 2: The same as in Fig. 1 for the system Sm-U.

[1] P.H. Mokler and D. Liesen, "X-Rays From Superheavy Collision Systems", GSI-81, Nov. 1981
[2] D.A. Liberman, D.T. Cromer, and J.T. Waber, Comp.Phys.Comm. 2, 107 (1971)
[3] J. Reinhardt, U. Müller, B. Müller, and W. Greiner, Z.Physik A303, 173 (1981)

Delta Electron Spectra for Br-Pb and Br-U at 3.88 MeV/u [B]

T. de Reus, J. Reinhardt, B. Müller, and W. Greiner
Institut für Theoretische Physik der Universität Frankfurt
G. Soff and U. Müller
GSI Darmstadt

The spectra of electrons ionized in heavy ion collisions (δ-electrons) were detected for the systems Br-Pb and Br-U by W. König and coworkers[1]. At a bombarding energy of 3.88 MeV/u the total number of δ-electrons and of those emitted in coincidence with a K-hole were measured by this group.

Solving the time dependent two centre Dirac equation in the monopole approximation under use of a Hartree Fock Slater potential[2], the number of δ-electrons with energy E results as[3,4]

$$N_E^{tot} = 2\left(\sum_{i<F} |a_{i\,1s\sigma,\,Es\sigma}|^2 + \sum_{j<F} |a_{j\,p_{1/2}\sigma,\,Ep_{1/2}\sigma})|^2\right) \quad (1)$$

For δ-electrons in coincidence with a 1sσ-hole the following expression is obtained

$$N^{tot}_{E,\,1s\sigma} = 2\left(N_{Es\sigma,\,1s\sigma} + N_{Es\sigma}\cdot N_{1s\sigma}\right) + 4\,N_{Ep_{1/2}\sigma}\cdot N_{1s\sigma} \quad (2)$$

where

$$N_{Es\sigma,\,1s\sigma} = N_{Es\sigma}\cdot N_{1s\sigma} + \left|\sum_{i<k} a^{*}_{i1s\sigma,\,Es\sigma}\, a_{Es\sigma,\,1s\sigma}\right|^2 \quad (3)$$

Products $N_{Es\sigma}\cdot N_{1s\sigma}$ represent accidental coincidences; real coincidences, however, originate from the second term in eq.(3). Since there is no experimental distinction between an $E_{s\sigma}$- and an $E_{p1/2\sigma}$- δ-electron, accidental coincidences between an 1sσ-hole and $E_{p1/2\sigma}$ δ-electrons become possible. This is taken into account by the third term in eq.(2).

In Fig. 1 we compare coupled channel calculations for the double differential δ-electron cross section at E_{Lab}=3.88 MeV/u in the system Br-Pb (Z_{tot}=117) with experiments of the Heidelberg group[1]. Remarkable agreement is achieved for the total and 1sσ-coincident spectrum. The bump around 500 keV originates from a nuclear transition in Br. Fig. 2 displays the same for the system Br-U(Z_{tot}=127). Here the total cross section is slightly underestimated. Superimposed upon 1sσ-coincident data, Doppler-broadened conversion lines from U-Coulomb excitations arise as indicated. Further investigations will have to clarify the slight difference between theory and experiment concerning the slopes.

[1] W. König et al., private communication, publ. in this report
[2] T. de Reus et al., Theoretical K-vacancy yields in Sm-Pb and Sm-U Collisions, in this report
[3] G. Soff, J. Reinhardt, B. Müller, and W.Greiner Z.Phys. A294, 137 (1980)
[4] J. Reinhardt, B. Müller, and W. Greiner Phys.Rev. A24, 103 (1981)

We are grateful to W. König and coworkers for making their data available to us prior to publication.

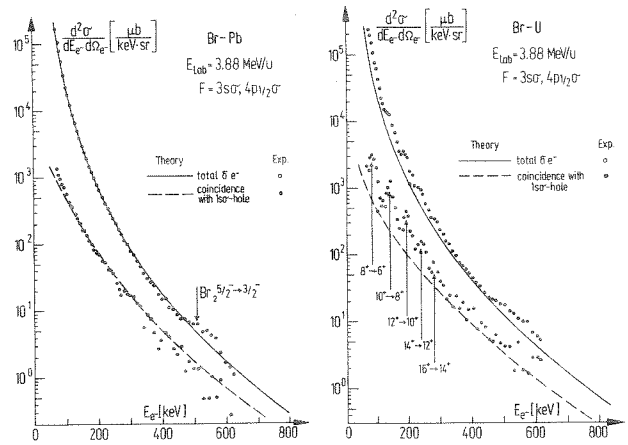


Fig. 1: Double differential cross sections for δ-electrons in the system Br-Pb at E_{Lab}=3.88 MeV/u. Experimental data[1] (open and full circles) for the total and 1sσ-coincident yield is compared with coupled channel results including electron screening (full and broken lines).

Fig. 2: The same as in Fig. 1 for the system Br-U.

Positron Spectra Calculated with an SCF Potential B

T. de Reus, J. Reinhardt, B. Müller, and W. Greiner
Institut für Theoretische Physik der Universität Frankfurt
G. Soff and U. Müller
GSI Darmstadt

In previous reports[1,2] we presented the spectra of positrons emitted in Pb-U and U-U collisions including electron screening in the framework of a modified Thomas-Fermi (TF) potential. Meanwhile improved calculations are available, based on the monopole approximation to the two-centre-potential plus the electron-electron interaction and exchange term, as briefly indicated in Ref.3. In contrast to former calculations, the time-dependent wave-function is expanded in a basis of selfconsistent states $\varphi(\vec{r},\vec{R})$, which already include electron interaction effects.
In agreement with earlier calculations, maxima of positron emission probabilities are found to shift towards smaller kinetic positron energies by $\sim$ 50 keV. The absolute values at the maxima, however, decrease throughout, when compared with results neglecting electron screening. For reasons, explained in more detail in Ref.4, this is in contrast to earlier TF calculations. Coupled channel results including a Hartree-Fock Slater (HFS) potential are compared with evaluations, neglecting electron-electron interaction, in Fig. 1 for different combined charges (Z=182,184,188). The positron yields at $(dP(E_e+)/dE_e+)_{max}$ reduce by 16 % (U-Th), 11 % (U-U), and 5 % (U-Cm) when compared with results, where only a Coulomb potential was used. As an effect of the relative increasing $1s\sigma$- and $2p_{1/2\sigma}$-hole formation with growing Z (in comparison with former calculations), this behaviour becomes plausible, since positron production rates depend sensitively on the number of $1s\sigma$ and $2p_{1/2\sigma}$-holes.

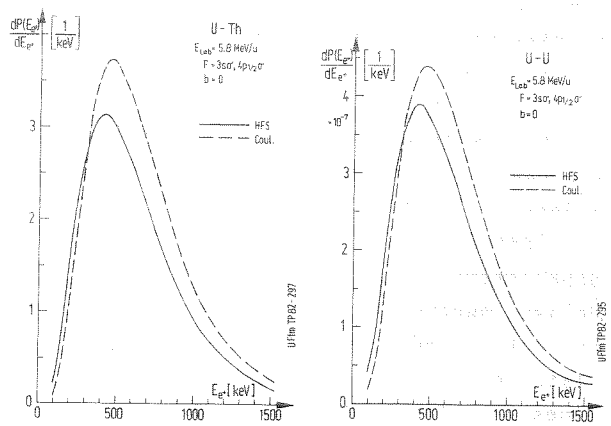
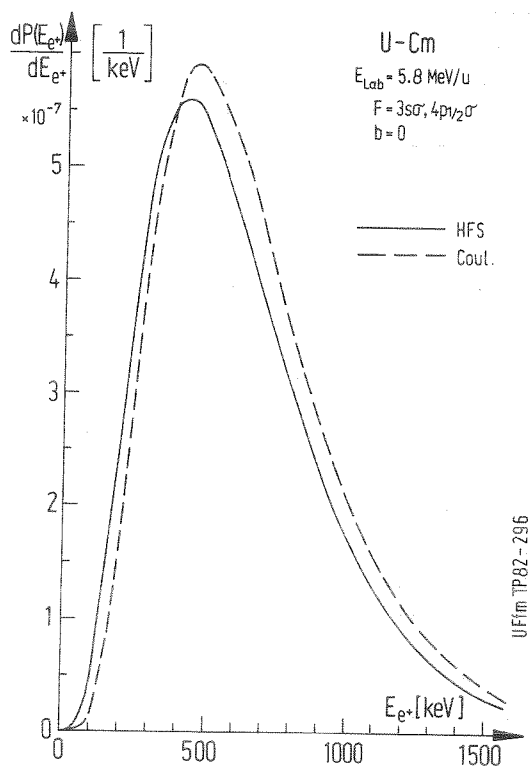


Fig. 1: Differential production rates for positrons versus their kinetic energy at E_{Lab}=5.8 MeV/u and b=0fm. Full and broken curves indicate calculations using HFS and Coulomb potentials, resp. for U-Th, U-U, and U-Cm.



[1] T. de Reus et al., GSI Scientific Report 1980, p. 151
[2] T. de Reus et al., GSI Scientific Report 1981, p. 172
[3] T. de Reus et al., Theoretical K-vacancy yields in Sm-Pb and Sm-U collisions, in this report
[4] T. de Reus et al., to be publ.

The Effect of a Nuclear Time Delay Distribution on Positron Spectra [B]

U. Müller and G. Soff
GSI Darmstadt
J. Reinhardt, T. de Reus, B. Müller, and W. Greiner
Institut für Theoretische Physik der Universität Frankfurt

A nuclear delay time T should provide a handle to distinguish supercritical systems[1]. In subcritical collision systems ($Z_T+Z_p \lesssim 173$) a delay time causes modulations in the positron spectrum with a width $\Delta E=h/T$. The modulations are due to interferences between atomic excitations on the incoming and the outgoing path. In addition to the interference patterns an enhancement of positron production in time-delayed supercritical collisions is observed, where the binding energy of the lowest bound states exceeds the value $2mc^2$. For long delay times a distinct peak in the positron spectrum is found at the location of the supercritical bound state resonance (binding energy minus $2mc^2$) due to the spontaneous pair-creation mechanism. With increasing delay time the position of the maximum drifts slowly from the kinematic maximum to the "resonance energy". However, for any chosen set of experimental parameters, the nuclear reaction time T will not be sharp but distributed over a certain range with a time distribution function f(T). As an assumption we took a Gaussian centered at $\bar{T}$

$$f(T) = \frac{1}{\sqrt{2\pi}\tau} \exp\left(-\frac{(T-\bar{T})^2}{2\tau^2}\right). \qquad (1)$$

The resulting positron spectra[2] for parameters $\bar{T} = 16\cdot10^{-21}$ s and $\tau = 0$ or $\tau = 2\cdot10^{-21}$ s are displayed in Fig. 1 for a head-on U+U collision at $E_{lab} = 5.9$ MeV/u. If we consider the "subcritical" p-states only (part a) we observe that the oscillations disappear already for $\tau = 2\cdot10^{-21}$ s. Thus we conclude that the appearance of several oscillations in the spectrum can be expected only for sufficiently sharp nuclear reaction times if the system is subcritical.
Also in the total spectrum (part b) the oscillations are damped out for increasing τ. But most striking is the invariance of the dominant nonvanishing first peak, which originates from the spontaneous part of the positron production mechanisms.
However, a distribution of the nuclear delay time, f(T), is equivalent to nuclear resonance scattering with the corresponding, Fourier transformed energy width.

[1] J. Reinhardt et al., Z.Phys. A303, 173 (1981)
[2] U. Müller et al., to be published

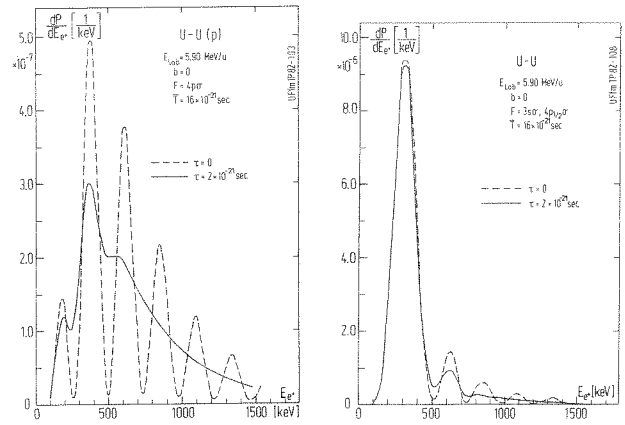


Fig. 1: Differential positron production probability versus kinetic positron energy E_{e^+} in a central U+U collision at $E_{lab} = 5.9$ MeV/u, assuming a Gaussian nuclear reaction time distribution centered at $\bar{T}$ with a width τ. (a) p-states only, representing a subcritical system, (b) including also the contribution of the s-states. Most striking is the appearance of the first pronounced peak which originates from spontaneous positron production.

Electron Excitation and Positron Emission in Deep-Inelastic Nuclear Collisions [B]

U. Müller and G. Soff
GSI Darmstadt
T. de Reus, J. Reinhardt, B. Müller, and W. Greiner
Institut für Theoretische Physik der Universität Frankfurt

We will discuss in the following the positron emission in deep inelastic nuclear collisions[1,2]. To analyse a given experiment the employed nuclear trajectories should be consistent with the elastic and inelastic heavy-ion scattering data. Many reaction models with different degrees of refinement have been discussed in the literature. We have calculated trajectories with the macroscopic friction model of Schmidt et al.[3], which includes nuclear neck formation. Strong deviations from Coulomb trajectories are found and an energy loss up to ≈30 % (for b≈0 and E_{lab} = 7.5 MeV/u) can be obtained. The corresponding positron spectra show a gradual enhancement at E_{e^+} = 500 keV due to the occurence of the spontaneous positron production in the s-channel. On the other hand the change in kinematics causes a drift to lower kinetic energies in the $P_{1/2}$-partial wave spectra due to destructive interferences between atomic excitations on the incoming and outgoing paths[1]. Both effects taken together lead to an enhancement of the maximum and a drift towards lower energies also in the total spectrum. Measurements by Backe et al.[4] seem to indicate such tendencies: In U+U and U+Cm collisions at energies above the Coulomb barrier, positron spectra have been measured in coincidence with fission fragments in order to get a signature for close nuclear contact. The analysis shows an enhancement of dP/dE_{e^+} at lower kinetic energies. For a quantitative comparison one has to integrate the theoretical impact parameter-dependent positron spectra over all values of b which lead to a nuclear reaction, weighted by the corresponding probability w(b) to induce nuclear fission. Performing the integration with a weight factor w(b) = 1 for $b<b_{gr}$ and w(b) = 0 elsewhere, there remains an energy shift of ≈50 keV in the experimental data in comparison with the theoretical curves, which is due to electron screening effects[5]. Furthermore, the theoretical values have to be reduced by an overall factor ≈2/3 (or ≈.8 when including electron shielding). Fig. 1 shows the experimental data for U+U collisions at E_{lab} = 5.9 MeV/u, 7.5 MeV/u, and 8.4 MeV/u, in comparison with theoretical results excluding electron screening, but reduced by the factor mentioned above. Dashed lines indicate pure Rutherford scattering trajectories, whereas the solid lines display spectra calculated with the modified trajectories. For an even better agreement longer delay times ΔT (≈$2\cdot10^{-21}$s) may be needed.

For the same collisions the δ-electron distribution (Fig. 2) has been calculated. Compared with calculations for the elastic Rutherford trajectory it is most striking that due to the modified interferences between the excitations on the two branches of the trajectory in deep inelastic nuclear collisions, the spectrum decreases considerably and falls off steeper.
Further investigations along these lines seem to be very promising, both to establish the mechanism of positron production and to deduce the nuclear reaction time scale.

[1] J. Reinhardt et al., Z.Phys. A303, 173 (1981)
[2] U. Müller et al., GSI Scientific Report 1981, GSI 82-1, p. 171
[3] R. Schmidt et al., Nucl.Phys. A311, 247 (1978)
[4] H. Backe et al., GSI Scientific Report 1981, GSI 82-1, p. 140
[5] T. de Reus et al., to be published

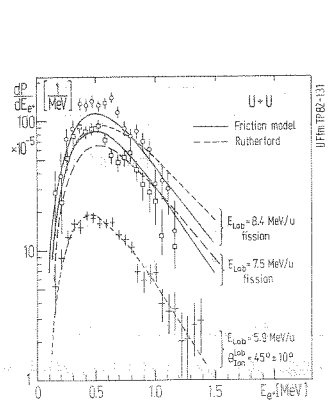


Fig. 1

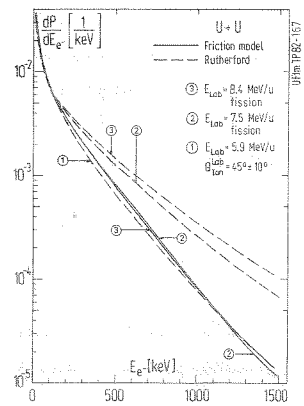


Fig. 2

Positron and δ-electron spectra in deep inelastic U+U collisions.

Conversion Processes in Super-Critical Compound Systems [B]

U. Müller and G. Soff
GSI Darmstadt
T. de Reus, J. Reinhardt, B. Müller, and W. Greiner
Institut für Theoretische Physik der Universität Frankfurt

A superheavy nuclear compound system very likely is not a static object. Its internal dynamics may influence the spectrum of emitted positrons. Clearly, a rigorous treatment of such effects cannot be based on the semiclassical approximation, but requires a fully quantum mechanical reaction theory for the nuclear scattering. While we are working on such an extension, we have attempted to understand possible consequences in the framework of a very simple (and probably oversimplified) model[1].

Let us imagine a classical picture for a nuclear excitation of the supercritical compound system in the spirit of the correspondence principle. The "internuclear separation" R(t), or better: the quadrupole deformation of the dinuclear system, is supposed to oscillate around the distance of closest approach R_0 of the Coulomb trajectory for a fixed duration T

$$R = R_0 \{1 - \alpha_0 \sin(2\pi\nu t)\}, \qquad (1)$$

where $h\nu$ is the quantum mechanical oscillator energy.

In Fig. 1 positron spectra are plotted for a central U+U collision at E_{lab} = 6.2 MeV/u. In order to demonstrate the qualitative effect we have restricted the calculations to couplings between s-states only. The parameters in eq.(1) are fixed by α_0 = .25 and $\nu = .125 \cdot 10^{21} s^{-1}$ corresponding to an oscillator energy $h\nu$ = 517 keV. Various sticking periods between T=0 and $T=108 \cdot 10^{-21}$s are considered in Fig. 1. In addition to the dominant "spontaneous peak" we find a second pronounced peak at about E_{e^+} = 800 keV. This reflects the fact that part of the vibrational energy of the dinuclear system is transferred to the emitted positron.

This is nothing but the classical analogue of a pair conversion process in the supercritical nuclear compound system. If the nuclear system is vibrationally excited, it may decay to the ground state transferring its excitation energy to an electron-positron pair. The electron occupies the vacant 1s-state and the positron carries the energy balance. I.e., if the nuclear de-excitation takes place, the positron line is shifted by the nuclear excitation energy, while without it would simply be the spontaneous positron production process.

In ordinary stable nuclei the conversion process is rather slow, having transition times in the order of $> 10^{-12}$s (corresponding to partial decay widths $\Gamma_{conv} < 10^{-3}$eV). The contraction of bound and continuum wavefunctions in superheavy atoms strongly enhances this process. This is most prominent in electric monopole (E0-) conversion, where Γ_{conv} (E0) increases by more than five orders of magnitude when going from a single U nucleus to the combined Z=184-system, assuming constant ζ. Depending on the strength of the nuclear matrix element this means that the width of the conversion process can approach the spontaneous decay width within one or two orders of magnitude[2,3].

[1] U. Müller et al., to be published
[2] J. Reinhardt et al., Z.Phys. A303, 173 (1981)
[3] G. Soff and W. Greiner, J.Phys. B15, L681 (1982)

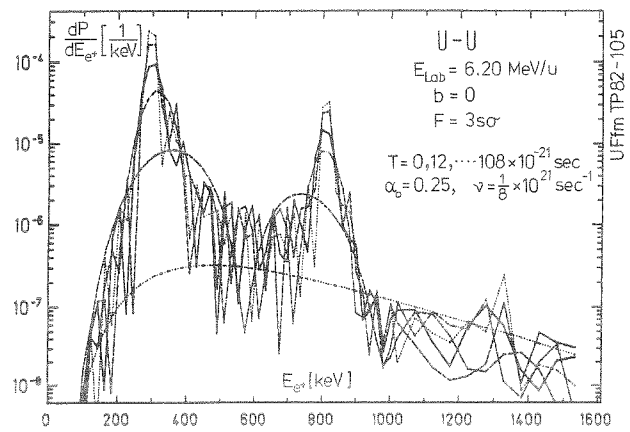


Fig. 1: Positron spectra. Nuclear reaction times T = 0, 12, 36, 60, 84, and $108 \cdot 10^{-21}$s are considered. The longest duration T corresponds to the most pronounced "spontaneous peak", etc.

Electronic Transition Times in Supercritical Compound Systems

G. Soff and U. Müller
GSI Darmstadt
T. de Reus, J. Reinhardt, P. Schlüter, K.-H. Wietschorke, G. Mehler, B. Müller and W. Greiner
Institut für Theoretische Physik, J.W. Goethe-Universität, Frankfurt

Positron production has been observed in quasi-molecular collisions of very heavy ions such as $_{92}U + _{96}Cm$ with a combined charge $Z=Z_1+Z_2=188$. For specific ion scattering angles the measured energy distribution of the emitted positrons exhibits distinct structure[1,2]. According to the ideas of ref.[3] the projectile and target may come into nuclear contact even for bombarding energies slightly below the nuclear Coulomb barrier. It is assumed that for a period of $T\sim4\cdot10^{-20}$s a superheavy compound system is produced. This long sticking time causes phaseshifts in the complex electron excitation amplitude leaving as an observable effect structures in the positron spectra. In the superheavy system Z=188 the electron K shell is imbedded as a resonance in the negative energy continuum. A vacant K shell thus may lead to spontaneous positron production. A pronounced peak in the positron spectra is predicted due to the spontaneous part of the positron production mechanism thereby indicating the energetical location of the $1s_{1/2}$ resonance in the negative energy continuum[3].

In this connection we considered the question whether a created K vacancy may also decay by radiative transitions during the sticking period.

The initial step in the theoretical determination of transition rates is the calculation of electron binding energies and wavefunctions. For levels in the discrete spectrum and for the continuum this is easily achieved by solving the radial Dirac equation. For the nucleus we assumed a homogeneously charged sphere with a radius $R=1.2A^{1/3}$ and $A=A_1+A_2=486$. In the system Z=188 the $1s_{1/2}$ and the $2p_{1/2}$ states are both inbedded as resonances in the negative energy continuum. The energy eigenvalue E_r of the resonance has been evaluated by the methods presented in ref.[3]. In the figure we show the binding energies of various bound states. The arrows indicate the considered radiative transitions to the $1s_{1/2}$ state. In our calculations we neglected radiative transitions from electron states of the Dirac sea to the vacant resonance state which is equivalent to positron bremsstrahlung in the strong Coulomb field of the nucleus.

For the projection of the bound state out of the continuum we applied the formalism of Reinhardt et al.[4].

For the evaluation of the various radiative decay widths Γ and equivalently for the transition times $\tau = \hbar/\Gamma$ we employed the formulae of refs.[5] and [6]. For the total decay width we found Γ= 746 eV which corresponds to $\tau = 8.8\cdot10^{-19}$s. This radiative transition time is about a factor 20 larger than the assumed nuclear sticking time by Reinhardt et al.[3] and may also safely be neglected in the positron production mechanism. A striking feature is the dominance of the $2s_{1/2}$-$1s_{1/2}$ transition of multipolarity M1 which yields about one-half of the total decay width.

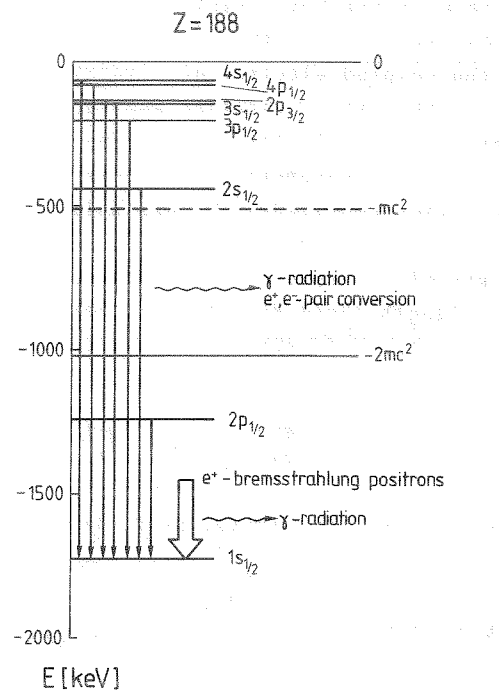


Fig.: Binding energies of various electron states in the superheavy atom Z=188. The arrows indicate the considered radiative transitions to the vacant $1s_{1/2}$ resonance state. Additional radiative transitions from electron states of the Dirac sea to the K shell are depicted qualitatively by the large arrow.

References:

[1] E. Berdermann, F. Bosch, M. Clemente, F. Güttner, P. Kienle, W. Koenig, Ch. Kozhuharov, B. Martin, B. Povh, H. Tsertos, W. Wagner and T. Walcher, 1981 GSI Scientific Report 1980,GSI 81-2,p 128

[2] H. Bokemeyer, H. Folger, H. Grein, S. Ito, D. Schwalm, P. Vincent, K. Bethge, A. Gruppe, R. Schulé, M. Waldschmidt, J.S. Greenberg, J. Schweppe and N. Trautmann, 1981 GSI Scientific Report 1980, GSI 81-2, p. 127

[3] J. Reinhardt,U. Müller, B. Müller and W. Greiner, Z. Phys. A303 (1981) 173

[4] J. Reinhardt, B. Müller and W. Greiner, Phys. Rev. A24 (1981) 103

[5] R. Anholt and J.O. Rasmussen, Phys. Rev. A9 (1974) 585

[6] G. Soff and B. Müller, Z. Phys. A280 (1977) 243

MO K X-Rays Emitted by Sticking Heavy Quasimolecules B G

J. Kirsch
Battelle Institut e.V., Frankfurt
B. Müller and W. Greiner
Institut für Theoretische Physik der Universität Frankfurt

As consequence of the formation of long-lived composite nuclear states, a pronounced structure in the molecular orbital (MO) X-ray spectra should be observed[1].
To investigate heavy systems as Pb+Pb, a formalism based on the second quantized version of the coupled electron and radiation field is used, where the excitation and radiative matrix elements are calculated employing relativistic two center wavefunctions Φ_l. The electronic transition amplitudes $a_{jl}^{(in)}$ are solutions of the coupled channel equations[2].
An essential approximation made is the long wave length limit for photons. For symmetric systems the differential radiation spectrum is given by

$$\frac{dP}{d\omega} = \frac{e^2\omega}{6\pi^2} \sum_{k=1}^{3} \sum_{\substack{i>F \\ j<F}} \left| T_k^{ij} \right|^2 \qquad (1)$$

denoting the Fermi-level by F. In case of head-on collisions T_k^{ij} takes the form

$$T_k^{ij} = \int_{-\infty}^{\infty} dt\, e^{i\omega t} \sum_{l,l'} a_{il}^{(in)*} a_{jl'}^{(in)}\, e^{i\int^t dt'(\omega_l - \omega_{l'})} (\omega_l - \omega_{l'}) \langle \phi_l | r_k | \phi_{l'} \rangle . \qquad (2)$$

Assuming a time delay T_s caused by a nuclear reaction and parametrizing the nuclear path correspondingly[3], the time integral in eq.(2) can be performed. The contribution to T_k^{ij}, originating from sticking of both nuclei, is given by

$$-\sum_{l,l'} \frac{a_{nl}^{(in)}(0)^*\, a_{ml'}^{(in)}(0)\, D_k^{ll'}(0)}{\omega_l(0) - \omega_{l'}(0) + \omega}\, e^{i(\omega_l(0) - \omega_{l'}(0))T_s} \cdot \left[e^{i(\omega_l(0) - \omega_{l'}(0) + \omega)T_s} - 1 \right]. \qquad (3)$$

Our calculations are based on a model including the 18 lowest two center bound states. The result for a Pb+Pb head-on collision with projectile energy E_{lab}=5.8 MeV/u is shown in fig. 1 for various values of the delay time. About at the united atom $K\alpha_1$-energy a line appears, which becomes sharper with increasing T_s. A second smaller line can be seen at 432 KeV due to the $K\alpha_2$-transition. Its ratio to the $K\alpha_1$-line agrees with the squared ratio of the according radiative transition matrix elements.

[1] R. Anholt, Z.Physik A292, 123 (1979)
[2] J. Kirsch et al., Z.Naturforsch. 35a, 579 (1980)
[3] J. Reinhardt et al., Z.Physik A303, 173 (1981)

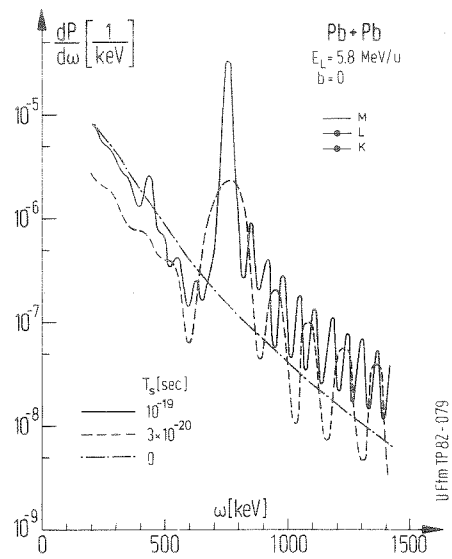


Fig. 1.

3. Radiation Effects

PAGE

3.1 Radiation Effects in Biological Systems 190

3.2 Radiation Effects in Solids 202

The radial dose distribution of a heavy particle track in a tissue equivalent material

M. Krämer[+], G. Kraft[*]
[+]TH Darmstadt [*]GSI Darmstadt

In order to obtain an estimation of the radiation effects of moving heavy ions on biological material the spatial dose distribution around a particle track has been calculated. This distribution can be characterized by two terms :

- a source term representing the initial delta electron spectrum produced by the HI along its path. This is a distribution double differential in electron energy and emission angle against the ion's path.
- a dissipation term describing the spatial displacement and energy loss and deposition of the delta electrons.

For the calculation of the initial distribution the binary encounter approximation (BEA) was used. This theory assumes pure coulomb interaction between a moving charged projectile impinging on electrons bound in a carbon atom in the K- and L- shell for which an isotropic 1s-velocity distribution was assumed [1),2)]. The energy spectrum of the ejected electronshows a "kinematic peak" at the energy $T_p = 4\, m_0\, \varepsilon \cos^2 \theta$ where ε is the specific projectile energy and m_0 the electron rest mass and θ the electron emission angle (Fig. 1).

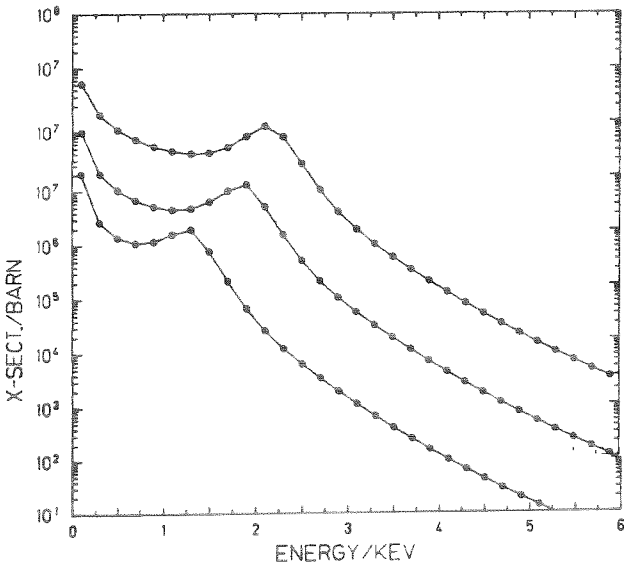


Figure 1. Electron spectra at 0, 20 and 40 degr. to the beam axis: for 1 MeV/u protons

To get the second term a monte carlo procedure was developed which follows the path of the ejected electrons individually and record its spatial energy deposition in water as tissue equivalent. An electron history is made up of about 150 steps on the average. This method groups together a large number of single interactions to one step in which multiple scattering laws can be applied [3)].

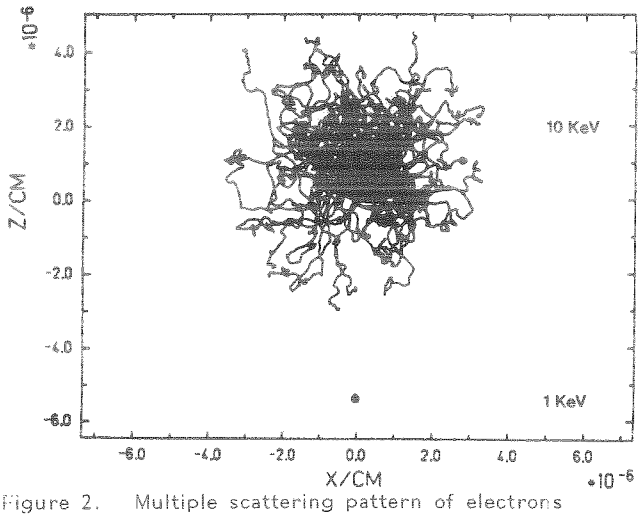


Figure 2. Multiple scattering pattern of electrons in water:: 1 kev (bottom), 10 kev (top)

A semiempirical range-energy relation is used to transform energy loss into pathlength and vice versa each step [4)]. To evaluate the multiple scattering probability distribution, the Moliere theory [5)] with the Bethe correction [6)] was used. Fig. 2 shows 100 electron tracks calculated with this monte carlo procedure projected onto the x-z-plane.

Fig. 3 shows the radial dose distribution for 1 MeV protons on carbon integrated over the z-axis which represents the ion's path. It exhibits the $1/r^2$ dependence reported in literature [7)]. An extension of the procedure to heavy particles with higher specific energies is under way.

1) Bonsen,Vries, Physica 47 (1970) 307
2) I. Hasselmann, Dipl.-Arbeit Marburg 1977
3) M. Berger, Meth. Comp. Phys. 1 (1963) 135
4) C. Feldman, Phys. Rev. 117 (1960) 455
5) H. A. Bethe,Phys. Rev. 89 (1953) 1256
6) G. Moliere, Z. Naturforschung 3a (1948) 78
7) H. Paretzke, Advances in Rad. Prot. and Dosimetry in Medicine, Publish. Corp.,New York

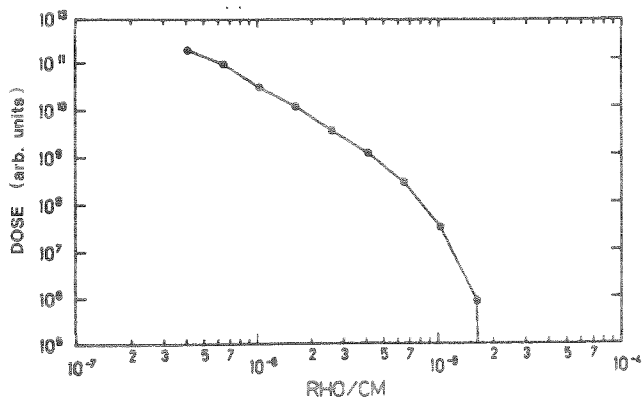


Figure 3. Radial dose distribution of 1 MeV/u proton in water:

Radiation Induced Strand Breaks in Phage DNA at High Doses G

A. M. Kellerer, H. Roos, W.-H. Thomas, F. Zilker . Institut für Med.Strahlenkunde der Universität Würzburg

This project is aimed at the determination of DNA-strand breaks in bacteriophage PM2 exposed to densely ionizing radiations and to sparsely ionizing radiations. The intent is to assess the yields of double- and single strand breaks and their influence on the relative biological effectiveness of different radiations.

Undamaged PM2 phages (NATIVE) have a supercoiled, circular closed DNA with approximately 50 supernumerary turns per molecule and a molecular weight of 6.3×10^6 dalton. Exposed to ionizing radiations the phages can suffer single- and double-strand breaks. After removal of their protein coat the phages with single strand break (SSB) assume circular uncoiled form, the phages with double strand break (DSB) linear form. These conformations can be separated by gel electrophoresis and their mass contribution can be determined by fluorescent measurements.

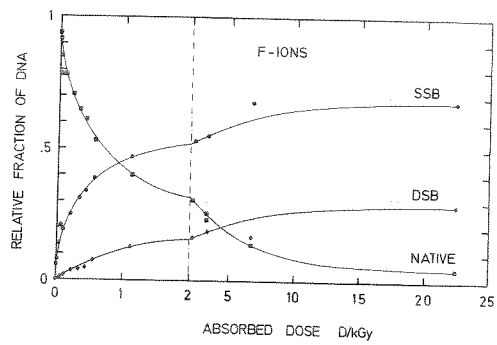


Fig. 1

In Fig.1 the dose dependence of the various DNA conformations is shown for PM2 phages irradiated by F-ions of 11 MeV/amu. For high doses one would expect to find all DNA in the linear form (DSB). However, fragments with multiple DSBs are in a continuum band in the gel electrophoresis rather than in the discrete band of linear molecules with one DSB. This explains that in Fig.1 the curve for DSB tends towards a plateau.

It is of particular interest whether densely ionizing radiations, such as heavy ions, produce clusters of double-strand breaks in DNA molecules, which would admit little if any repair in higher cells. The evaluation of the fragments with multiple DSBs is therefore a central problem in our studies. We have developed techniques for performing this analysis by utilizing a barrier containing ion exchange cellulose in the gel, in order to stop and collect the small DNA fragments in the continuum band that migrate faster than the entire molecules. Fig.2 indicates schematically the method. In its present form the technique for the analysis of the small fragments requires relatively large DNA samples that can not be obtained with the small ranges of heavy ions available at the Unilac. We have therefore performed the initial experiments with x-rays and fission neutrons. Fig.3 and 4 show the results that are then obtained with the small fragments included. We are now attempting to develop the method further so that it can also be applied to the heavy ion experiments.

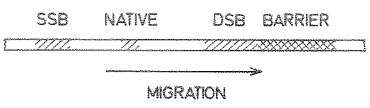


Fig. 2

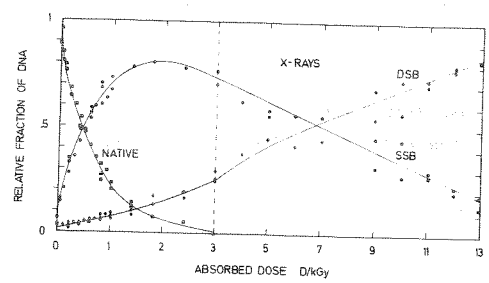


Fig. 3

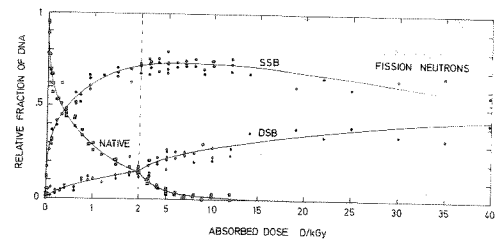


Fig. 4

The dosimetric work with heavy ion track etching that is required for this and the other biological projects is being continued; an automatic self-focusing optical analyzer connected to a microcomputer has been built for this work. The theoretical problem of the edge and overlap corrections in these dosimetric studies have led to a result that is also of interest to other problems of geometric probability (Ref.: On the Number of Clumps Resulting from the Overlap of Randomly Placed Figures in a Plane, A.M.Kellerer, J.of Appl.Probl., to appear March 1983).

The induction of double and single strand breaks viral DNA in solution

R. Roots[+], M. Larsson[*], G. Kraft[*],

[+]LBL, Berkeley, *GSI Darmstadt

In the inactiviation measurements of mamalian cells by heavy charged particles, a variation of the radiation response is observed even for the very heavy ions[1]. This finding is in a strict contradiction with the widely used assumption, that for a high linear energy transfer (LET) the molecular damage of the DNA in the cell nucleus is much greater than necessary for cell killing (over kill-effect). If this would be the case, a variation in LET between 10 000 and 15 000 keV/µm which corresponds to a dose of 10 to 15 Gy, respectively per particle traversing the cell nucleus, should not have any consequences for the cell survival. But in the experiments with mamalian cells as well as with yeast cells and bacteria spores drastic variations have been observed. Therefore, it is necessary to prove the assumption, whether the induction of single and double strand breaks (which are believed to be the biologically most relevant events) is proportional to the energy deposition of heavy charged particles.

For the experiment double stranded supercoiled SV40-DNA was purchased from Bethesda Research Laboratories. The stock solution was diluted with a 0.5 m M Tris, 0.1 mM $MgCl_2$ solution (pH 7.9) to a DNA content of 20 µg/ml. Aliquots of 20 µl DNA solution were irradiated as a 50 µm thick film between a 19 µm thick Mylar foil and a gold backing. After irradiation the induction of single and double strand breaks were measured by separating the fractions of supercoiled, circular and linear DNA through gel electrophoresis techniques.

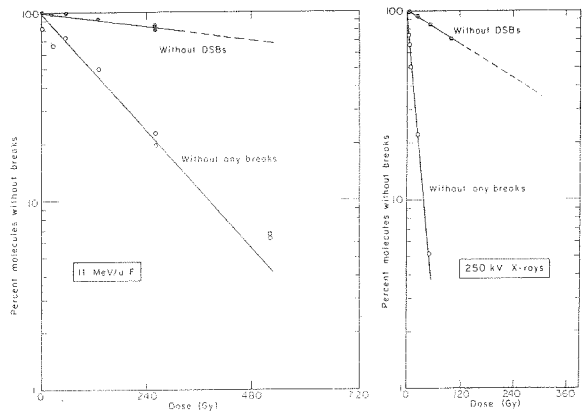


Fig.1: Induction of single and double strand breaks as a function of dose.

In Fig.1 first results from DNA experiments using a 11 MeV/u fluorine beam are compared with the corresponding x-ray data. In these panels the induction of single strand breaks, which correspond to the decrease of the amount of native DNA is much faster in the x-ray experiment than in the fluorine experiment. The same holds for the induction of double strand breaks except at very high doses where, in the x-ray experiment, a high number of DNA fragments induced by two or more double strand breaks are present. breaks are plotted as a function of dose. In both cases the x-rays yield a steeper slope than the particle radiation and also for the very heavy particles like uranium, the efficiency for strand break induction increases much slower than the LET. From these data which are in general agreement with comparable data obtained with ϕ × 174 DNA7[2], we may conclude that the so-called overkill process and the decrease in the relative biological effectiveness of the high LET radiation, is caused by diminished strand break efficiency rather than by an accumulation of too many lethal events in the cell nucleus.

1.) G. Kraft et al., Proceeding of the 8th Conference on on Microdosimetry Jülich 1982 in print.

2.) R. C. Christensen et al., Int. J. Radiat. Biol. 1972 vol 22 no.5 457-477.

The Radiation Action of Heavy Ions on Spores of Bacillus Subtilis

M. Schäfer, R. Facius, H. Bücker

DFVLR - Flugmedizin, Köln 90

The irradiation experiments with spores of Bacillus subtilis are continued and extented to higher particle energies of up to about 18 MeV/u. The experimental procedures and methods were described earlier[1,2]. Inactivation cross sections have been determined from the slope of the survival curves, which seem to be exponential within the errors of measurement also for the higher energies. In addition to the experiments with such high initial energies some experiments with reduced energies are performed using absorber foils. It is therefore possible to test the agreement between these and earlier measurements with low energies. Comparison of the data shows that with few exceptions and within the dosimetric errors the agreement of the experimental results can be accepted.

The inactivation cross sections are presented in Fig. 1. Some values of the cross sections should be considered as preliminary data until the final results of the dosimetric measurement have been obtained which were made by counting etch pits of a series of glass plates irradiated during the beam time. This is important in the case of argon irradiation at 18 MeV/u to decide between the two extreme different cross section values. Despite the small number of experimental data above 10 MeV/u it is possible to describe the general trend of the inactivation cross sections as a function of the energy. Obviously the cross sections increase with increasing energies reaching a maximum value and decreases for further increasing energies above certain energy values. These energies are dependent on the type of the particle and are higher for higher atomic numbers.

The inactivation cross sections for the higher energies deviate from the linear dependence of the cross sections as a function of the square of effective charge[3] found for energies up to about 10 MeV/u. One of the reasons to explain the decrease in the cross sections beyond its maximum value is that the increase in the effective charge is retarded at higher energies where the effective charge approaches asymptotically its maximum value.

1 GSI Report 1979, p.150
2 GSI Report 1980, p.158
3 M. Schäfer, R. Facius, H. Bücker
Proc. 8th Symp. on Microdosimetry
Jülich, 1982, in press.

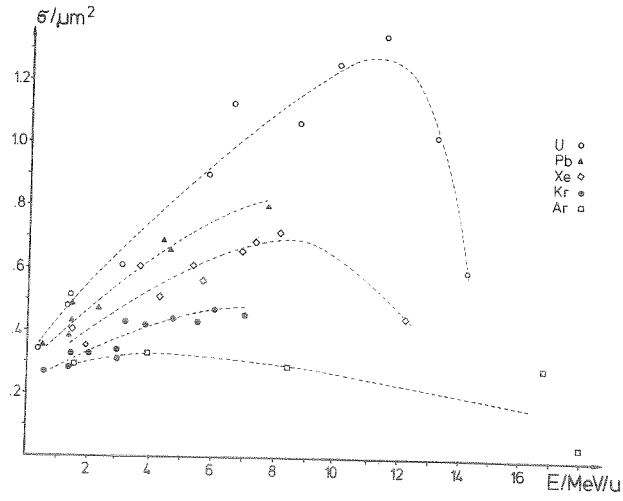


Fig. 1 Inactivation cross sections as a function of the specific energy of the particles

Inhibition of r-RNA synthesis in yeast cells exposed to Helium-, Carbon- or Fluorine ions G

K.J. Weber, E. Schneider, J. Kiefer
Strahlenzentrum der Justus-Liebig-Universität Giessen
G. Kraft
GSI Darmstadt

Heavy ion induced inactivation of small cellular structures can be mainly attributed to delta-electrons produced by heavy particle collisions. This had been tested in yeast cells by measuring the inhition of transcriptional activity of genes coding for ribosomal RNA[1,2] or the enzyme arginase[3]. Quantitative verification of experimentally determined inactivation cross-sections with theoretical predictions for the inactivation of small targets[4], however, failed. The basic assumption of concept is that the response to heavy ion exposure is predictable from the known sensitivity to X-rays alone. In contrasts, experimental results quoted above showed distinct differences in their response to charged particle irradiation, despite of their nearly identical sensitivity to X-rays. This may be due to differences in target structure. In fact, r-RNA genes in yeast cells are grouped in one single cluster[5] (~ 100/haploid genome) whereas arginase is coded by a single gene. If a mechanism exists that a direct hit by one particle inactivates the whole r-RNA cluster with high probability and local dose from secondary electrons in the "penumbra" of the charged particle track is too low to contribute (small Z_{eff}^2/β^2), the experimental cross-sections should be solely determined by the geometrical section of this structure. Experiments with charged particles that exhibited Z_{eff}^2/β^2 low enough to test the above assumption were performed at the MPI für Kernforschung Heidelberg (see table)

Ion	specific energy MeV/u	$\frac{Z_{eff}^2}{\beta^2}/10^3$	inactivation cross-section 10^{-10} cm^2
^{241}Am-α	0.65	2.8	1.25 ± 0.15
^{4}He	8.9	0.21	1.2 ± 0.6
^{12}C	6.5	2.5	2.0 ± 0.2
^{19}F	5.6	6.2	5.0 ± 0.3

The measured inactivation cross sections (σ) for relative r-RNA synthesis are summarized in table 1. The high error values result mainly from the great uncertainty in fluence determination.
Together with the data from previous experiments[1,2,3] they are plotted in the figure as a function of Z_{eff}^2/β^2 of the charged particles. It is seen that for He-ions σ is independent of Z_{eff}^2/β^2 indicating a true single hit inactivation by track core interaction.
The measured cross-section is compatible with the geometrical extensions of the r-DNA gene cluster.
Furthermore, it has to be amended that inactivation probability depends also on the local density of energy deposition. Curve 1 represents a simple mathematical formulation for σ based on the assumption of interaction processes in the production of inactivating lesions in the "penumbra".
$\sigma_1 = K'(1-w \cdot \exp(-K, \cdot Z_{eff}^2/\beta^2)) \cdot Z_{eff}^2/\beta^2$
where K', K,w are adjustable parameters. This phenomenon should saturate for high Z_{eff}^2/β^2 (linear component). The upper plot (2) is the superposition of σ_0, the estimate of the geometrical cross section of the r-RNA gene-cluster $\sigma_1 : \sigma_2 = \sigma_1 + \sigma_0$.
Thus, the experimental data available so far, and the simple hypothesis outlined above, are in fair agreement, supporting

(i) the importance of gene-cluster inactivation by charged particles
(ii) the idea, that sensitivity to low LET radiation is not a sufficient parameter to predict effectiveness of heavy ions exposure but the energy density plays also an important role.

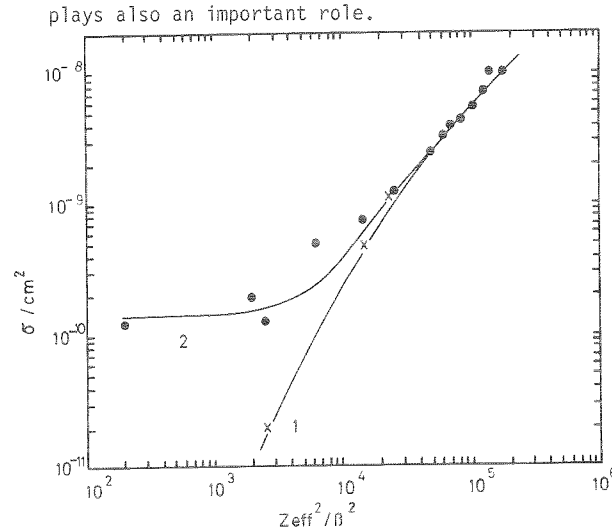


figure: Inactivation cross sections (σ) for relative r-RNA (o) or arginase (x) synthesis in yeast cells after exposure to accelerated heavy charged particles as a function of Z_{eff}^2/β^2 of the ions used (explanation see text).

[1] K.J. Weber GSI Scientific Report 1979, p. 148
[2] K.J. Weber GSI Scientific Report 1980, p. 161
[3] K.J. Weber GSI Scientific Report 1981, p. 185
[4] J.J. Butts and R. Katz, Radiat.Res. 30, 855 (1967)
[5] T.D. Petes, J.Bateriol. 138 (1), 185 (1979)

The oxygen effect in yeast cells exposed to heavy ions

G

F. Schöpfer, E. Schneider, J. Kiefer, S. Rase
Strahlenzentrum der Justus-Liebig-Universität Giessen

G. Lenz
GSI Darmstadt

The radiosensitization of a biological system, called oxygen effect, was studied in the yeast cell system in a wide range of particles with stopping powers up to approximately 140000 MeV·cm²/g. Preliminary results were reported earlier[1].

The survival of 3 strains of the yeast Saccharomyces cerevisiae after exposure to accelerated ions was investigated: a wild type diploid strain (211), the haploid strain (211-1a) and a radiation sensitive mutant double strand breaks. A linear energy transfer range from about 1000 keV/µm to 13000 keV/µm in water was covered using beams of argon, krypton, xenon, samarium, lead and uranium ions accelerated up to about 14% of the light velocity.

With ions of a specific energy of less than 1.6 MeV/u ($\beta<0.06$) the oxygen enhancement ratio (OER) did not exceed the value of 1.2. With faster ions ($\beta>0.06$, E/m>2 MeV/u) the OER was found to increase with increasing E/m to values about equal to that of low LET radiation (table 1).

The results may be explained by the microscopic dose distribution in the path of a particle penetrating a cell. The extension of the secondary electron penumbra around the core of an ion path depends upon the specific energy of the primary particle. The maximum range of a secondary electron emitted from the core of a 9 MeV/u ion is approx. 2000 nm. The total amount of energy deposited in the penumbra mainly depends upon the intensity of the high energetic electrons. Ions with high mass number produce much more secondary electrons than light ions do, regarding the same specific energy.

Thus, very heavy ions of high velocity deposit a remarkable part of their total energy outside the core. This fact leads to a much larger inactivation cross section compared with light ions. Since the δ-electrons are low LET radiation the OER also increases the more energy is deposited by these long ranging secondary particles.

A graph in which the OER is plotted versus the inactivation cross section σ demonstrates this correlation (fig. 1): Very heavy ions (Xe, Pb) of high energy (7-8 MeV/u) cause large inactivation cross sections (7 to 9 µm²) and a high OER (ca. 1.8) in the sensitive strain whereas light particles as α-particles from an Am-241 source and argon ions cause low inactivation cross sections and an OER close to 1.

Radiation (MeV/u)	Strain 211 σ/µm²	OER	211-1a σ/µm²	OER	rad 52 σ/µm²	OER
80kV-X-rays		2.0				1.9
α 0.65	0.2	1.1	0.42		0.48	
Ar 9.5	(0.45)	(1)			(1.16)	(1.35)
Kr 7.0	1.48	1.27	3.3		3.9	
Kr 4.4	1.29	1.23	2.6		3.1	1.7
Xe 7.3	1.67	1.67	2.76	1.34	6.5	1.83
Xe 1.6	1.16	1.2	1.17		1.77	1.02
Sm 0.3	0.68	1.16				
Pb 7.7	3.67	1.63			9.4	1.8
U 3.5			2.4	1.2		
Xe ~ 10			4.3	1.6		
U ~ 14			4.7	1.7		

Table 1: Inactivation cross sections and OER values of the 3 yeast strains. Results in brackets are preliminary.

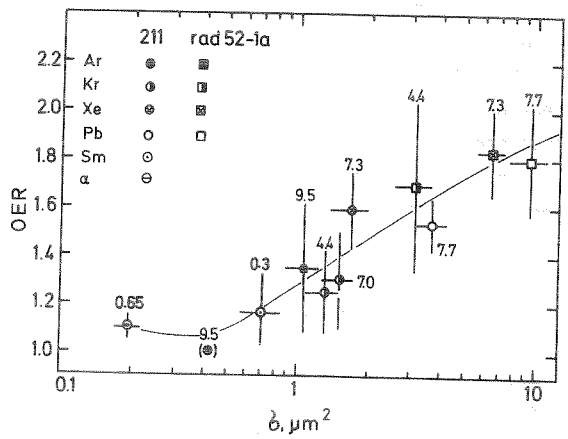


Figure 1: OER values of strain 211 and the rad 52 mutant versus inactivation cross section for Am, Sm, Kr, Xe, Pb ions and α-particles. The numbers indicate the specific energy in MeV/u. The error bars represent standard errors.

[1] GSI - Scientific Report 1980, p. 160
GSI - Scientific Report 1981, p. 184

Interpretation of heavy ion survival data

J. Kiefer
Strahlenzentrum der Justus-Liebig-Universität Giessen

Energy deposition by heavy ions is highly inhomogeneous in space. It may be operationally divided into the contributions of the track core and the penumbra which is created by high energy δ-electrons and whose extension depends on the ion's specific energy. Dose quantifying the average energy absorbed per mass in macroscopic volumes is not an appropriate parameter to describe this situation. If one deals with microscopic sites, e.g. cell nuclei, the microdosimetric quantity z, the "specific energy", has to be used which is defined as energy absorbed per mass in small, but not infinitesimally small volumes. Because of the stochastic nature of energy deposition z is not single-valued but follows a statistical distribution f(z)dz. Biological effectiveness, however, may not only depend on the total energy absorbed in a sensitive site but also on the spatial pattern of its deposition. This may be characterized by the "energy density" or "local dose" ρ defined as the ratio energy absorbed per unit mass in infinitesimally small volumes. Theoretical calculations[1,2] and few measurements[3] show that for heavy ions ρ in the penumbra region depends on the distance x from the track center according to

$$\rho(x) = C \cdot a/x^2 \qquad (1)$$

where C is a function of the absorbing medium and a is related to ion speed and effective charge. ρ(x) is zero for x>R, R being the penumbra radius. If ρ(x) and the dimensions of the sensitive site are known f(z) can be calculated. If $f_1(z)$ is the distribution of z for hits by a single ion the respective function for ν hit is given by the ν-fold convolution:

$$f_\nu(z) = f_1(z)^{*\nu} \qquad (2)$$

Cell survival curves after X- or γ-ray exposure can be described by the expression

$$y = 1-(1-e^{-kD})^n \qquad (3)$$

where y is fractional survival, D dose, k and n parameters typical for the cell line and experimental conditions. In the case of n=1 equation (3) reduces to a mere exponential dependency. If one assumes that the same relation as in equation (3) holds with D being replaced by z the survival behaviour can be evaluated:

$$y = 1 - \sum_{\nu=0}^{\infty} e^{-\sigma\phi} \frac{(\sigma\phi)^\nu}{\nu} f_1(z)^{*\nu} \sum_{l=1}^{n} \binom{n}{l} e^{-\nu l k z} \qquad (4)$$

σ is here the effective cross section and ϕ ion fluence. Using the formalism of Le-Place transforms for the convolution integrals one finds

$$y = 1 - \sum_{l=1}^{n} \binom{n}{l} \exp\left(-\sigma\phi\left(1 - \int_0^\infty f_1(z) e^{-lKz}\, dz\right)\right) \qquad (5)$$

Equation (5) shows that even with very heavy ions non-exponential survival curves may be found. This is contrary to the theoretical treatment by Katz and coworkers[4] but agrees with experimental results[5,6]. The survival of diploid yeast was analyzed using the formalism of equation (5); details of the procedures will be published elsewhere. An example is shown in figure 1 demonstrating a fair agreement. A more refinement will have to take into account that the inactivation constant may depend on energy density ρ as suggested by various investigations[7,8,9].

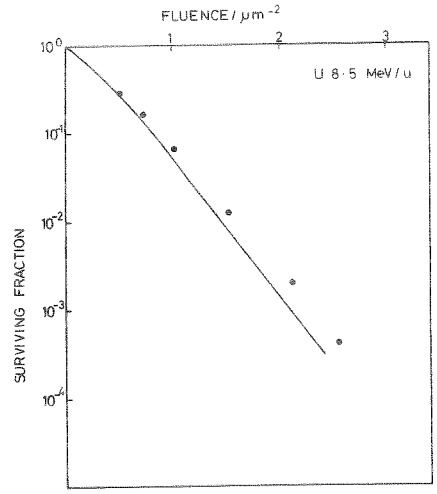


Figure 1: Comparison of theoretically expected (line) and experimentally found (points) survival of diploid yeast after exposure to Uranium ions. Data were taken from[6].

References:
[1] J.J. Butts, R. Katz, Radiat.Res. 30, 855 (1967)
[2] A. Chatterjee, H.J. Schaefer, Radiat.Env.Biophys. 13, 215 (1976)
[3] M.N. Varma et al., Radiat.Res. 62, 1 (1975)
[4] R. Katz et al., Radiat.Res. 47, 402 (1971)
[5] H. Liesem, R. Katz, GSI Scientific Report 1981, p. 187
[6] F. Schöpfer et al., Radiat.Res. 92, 30 (1982)
[7] E.L. Powers et al., Int.J.Radiat.Biol. 14, 131 (1968)
[8] J.A. Sayeg et al., Radiat.Res. 10, 449 (1959)
[9] T.A. Manney et al., Radiat.Res. 18, 374 (1963)

Chromosome aberrations in Chinese hamster cell cultures induced by heavy ion irradiation G

W. Müller, H. G. Miltenburger
TH Darmstadt
G. Kraft
GSI Darmstadt

The induction of chromosome aberration was measured at the linear accelerator UNILAC in Darmstadt. Beams of heavy ions from argon to uranium having an energy range between 1 and 20 MeV/u were used to irradiate exponentially growing monolayers of V 79 Chinese hamster cells. After exposure the cells were incubated at 37° C and accumulated in metaphase by colcemid treatment. Chromosomes were prepared by standard procedures. The introduction of chromosome aberrations was measured at different time intervals after irradiation as a function of particle dose. 150 metaphases were scored for each experimental point and the types of chromosomal aberrations were specified as breaks, deletions, fragments, exchanges, dicentrics and disintegrations [Fig. 2] (gaps were recorded separately).

The percentage of metaphases with chromosomal aberrations (excluding gaps) is given as a function of particle dose in Fig. 1. At low particle dose a steep increase in aberration induction is observed wich exhibits a saturation effect at higher particle dose as expected.

Fig. 1 indicates that the effectiveness for aberration induction increase with the increasing atomic number. Also, the curves may support the assumption that the increase of the percentage of cells with aberrations is not proportional to the increase of the linear energy transfer.

However, this possibility has still to be verified because these may be interfering selection processes with regard to the elimination of cells carrying different types of damages after irradiation with different LET's. The metaphases from cell populations irradiated with 4,7 MeV/u uranium ions show increasing chromosomal disintegrations with increasing fluence. This effect is not observed in cells irradiated with 13,0 MeV/u argon ions [Fig. 2] as there are only a few heavily damaged cells even after high particle fluences.

Therefore, further experiments are under way to exclude the possibility that samples of cells with quantitatively and qualitatively different chromosomal damages and consequently different survival capacity are counted together as in the experiments presented here.

In addition, these experiments with different heavy charged particles will gain further microdosimetric information on the energy deposition of heavy ions.

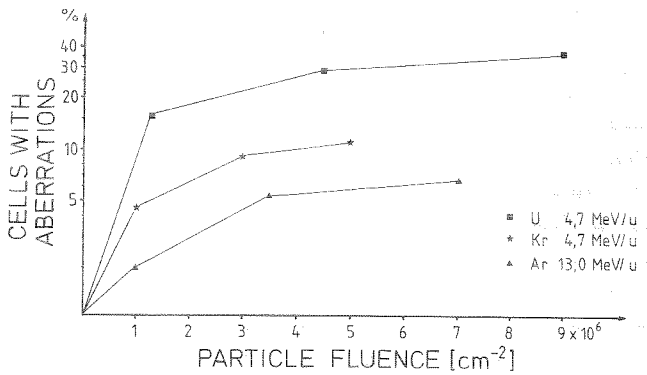


Fig. 1: Percentage of cells with aberrations accumulated 4 hours after irradiation as a function of particle dose

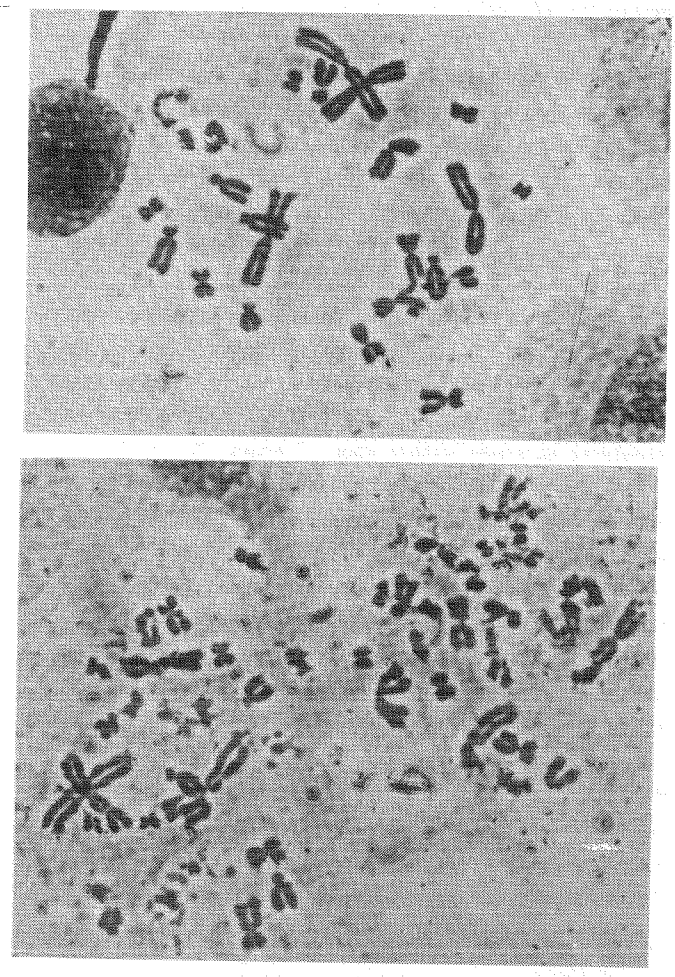


Fig. 2: Metaphases with typical aberrations by irradiation with 13.0 MeV/u Ar ions [top], and 4.7 MeV/u U ions [bottom].

Differences in the cell progression following heavy ion irradiation

M. Larsson, D. Pollet, G. Kraft
GSI Darmstadt

The interaction process of heavy charged particles with living material as mammalian cells exhibit remarkable differences in comparison to the action of Xrays. The high local energy deposition produces a small but severe damaged region in the cell nucleus which may result in a letal event to the cell.

Because there are only a few hits of the cell nucleus required for cell killing the question raises whether the overwhelming part of the undamaged cell and the cell nucleus remains function ing and whether the cells progress in the course of the cell cycle more or less undisturbed or whether even these spots of high local damage would also result in the same delay in the cell cycle progression as measured with Xrays.

In the experiment V79 chinese hamster cells has been prepared 24 hours before irradiating by seeding approximately 200 000 cells in a petri dish and incubating at 37^{0} C. The samples are irradiated either by 250 kVp Xrays or by mono-energetic heavy ions. After exposure the cells are incubated again for time intervalls from 1 to 24 hours. After this incubation time cells are stained with Hoechst dye and the DNA content was measured in a cyto fluorometer (Phywe ICP 22). In fig. 1 the DNA spectra as a function of incubation time after irradiation is plotted for Xray and 5,9 MeV/u at uranium exposure, which both correspond to a survival level of about 1 %. In the Xray spectra, the well known block of cells in S phase starts at about 4 hours after irradiation and the compartment of S cells move slowly to G_2 phase within about 7 hours. The cells which have been irradiated by low energetic uranium ions do not exhibit the same pattern in the DNA distribution. A pronounced S block can not be observed even for longer time intervalls and the cells seem to proceed at least within the first 24 hours nearly undisturbed through the cell cycle. But it should be noted that this behaviour may be changed by an exposure to higher energetic particles, where the diameter of the particle track becomes much larger than the cell nucleus. There may be also differences in the effectiveness to lighter particles like α-particles, where the energy deposition is much lower and much more similar to the Xrays as reported in the literature.[1]

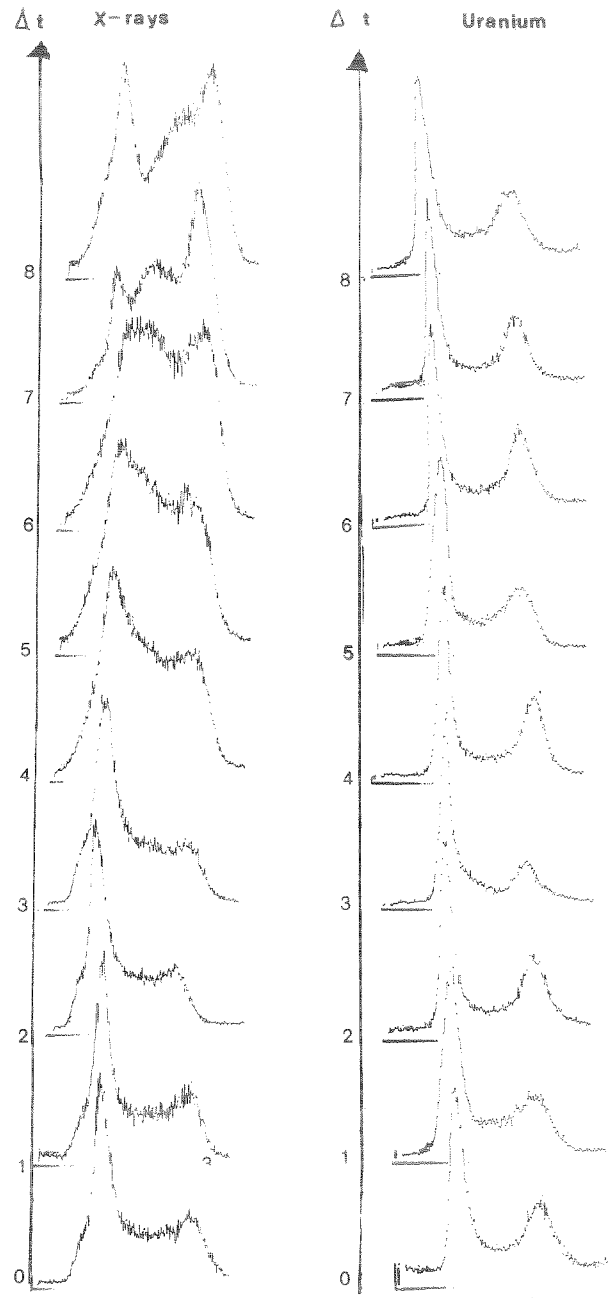


Fig. 1: DNA distribution of exponentially growing cells 0 - 8 hours after Xray and uranium exposure.

1.) H. Schlag et al. Int. J. Radiat.Biol. (1981) 1 75-85
M.R.Raju Rad. Res. 84(1980) 16-24

Inactivation of mammalian cells by light and heavy charged particles

G. Kraft, H. Meister, M. Schuber
GSI Darmstadt

W. Kraft-Weyrather, H.G. Miltenburger
TH Darmstadt

To study the radiation response of mammalian cells to charged particles over a large range of atomic numbers and linear energy transfers (LET) we irradiated chinese hamster cells at the UNILAC Darmstadt and at the Tandem van de Graaf Heidelberg with heavy ion beams from α particles to uranium in the energy range between 1 and 20 MeV/u. This particle and energy spectrum covers an LET range between 10 and 15 000 keV/µm and a radius of the particle tracks between 0.2 and 2 µm. The cell survival as a function of particle dose is plotted for various ions at comparable energies (fig. 1). With increasing atomic number an increase of killing efficiency is observed. This effect is greater for the lighter ions (for example between Helium and Carbon) and it is a small effect for the heavier particles.

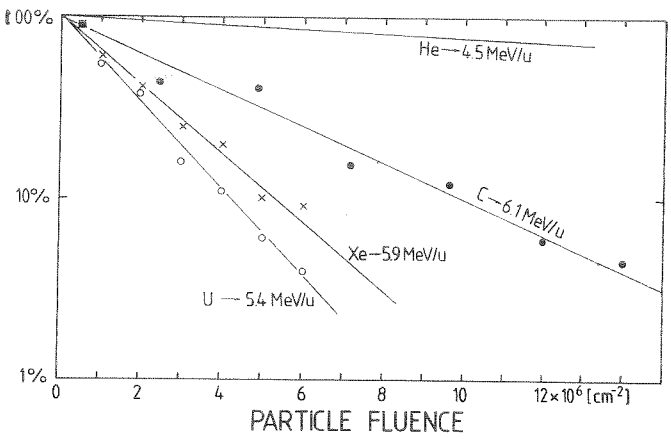


Fig. 1: Cell survival as a function of particle fluence for various ions having comparable velocity.

These changes in effectiveness are more pronounced in a plot of the corresponding cross sections, extracted from the survival curves and plotted versus LET. For low LET values (LET $\lesssim$200 keV/µ) the cross sections obtained with different ions show a common curve while for the higher LET values deviations from this curve can be observed which indicate a saturation effect. But the saturation of the carbon and fluorine data points occurs at lower LET values than in the argon experiments; also, the maximum value, which is obtained, is different in each case (45 µm^2 and 60 µm^2, respectively). These values are far below the geometrical cross sections of about 110 µm^2, which were measured under the same condition as in the heavy ion experiment using light miscrocopy. For the heavier ions only the decreasing branch of the cross section curve can be observed, because there is no heavy

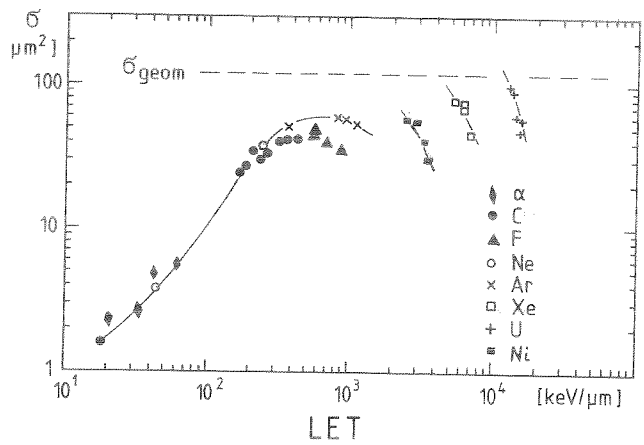


Fig. 2: Inactivation cross section as a function of linear energy transfer for various particles.

ion machine able to generate ion beams of the required energies. Nevertheless it is evident from this curve that even for the high LET values the same trend as for the lighter ions is continued and a variation of the cross section exist which is independent from LET.

This finding can only be explained by assuming that in the high LET region the track structure of the particle track becomes more important than the overall energy deposition. This assumption is supported by the fact that for the heavy particles the increase of the measured cross section is direct proportional to the increase of the track diameter which is proportional to the specific energy.

Therefore, reaching a certain level of local damage the size of the damaged site is more important than the intensity of the damage in these spots. This finding is in good agreement with heavy ion experiments using other biological test systems like bacteria[1] spores and yeast cells[2].

[1] M. Schäfer et al., GSI Report 1980, p. 158

[2] F. Schöpfer et al., Rad. Res. 92, 30-46(1982).

Modification of Radiosensitivity of Mammalian Cells [G]

W. Kraft-Weyrather[x], G. Kraft[+], H. Meister[+], H.G. Miltenburger[x], C.A. Tobias[*]
[x]TH Darmstadt, [+] GSI Darmstadt, [*] LBL Berkeley

Experiments with sparsely ionizing radiation show that the radiation sensitivity of cells can be influenced by several factors as e.g. temperature, chemicals and espcially the presence of oxygen, which leads to a decreased survival (oxygen effect). These effects decrease with increasing LET. Barendsen[1] showed that the oxygen effect with α-particles disappeared at an LET above 100 keV/µm. Mammalian cells (V79) irradiated with heavy ions from Ar to U and an energy below 15 MeV/u do not show any oxygen effect. But first experiments with energies above 15 MeV/u indicate a reappearance of the OER with higher energies. In fig. 1 the survival of V79 cells irradiated with 250 kV x rays and with a ^{56}Fe beam of 18.7 MeV/u is plotted as a function of particle fluence. The survival curve exhibits a small difference in sensitivity which yields an OER of 1.16. Similar results have been found with 18.5 MeV/u Argon ions. Using yeast cells the reappearance of the oxygen effect at much lower energies has been reported by Schöpfer et al.[2].

The reappearance of the oxygen effect indicates that some other effects wich are typical for less dense ionizing radiation can be expected, too. There were no recovery or repair effects of mammalian cells found for heavy ions with energies below 10 MeV/u [3]. As the influence of a hyperthermic treatment on the radiation sensitivity of cells or tissues is mainly caused by a repair inhibition, an increase of the repair capacity would lead to an increased hyperthermic sensitization. First experiments with uraium ions with an energy of 15 MeV/u and a 20 minutes treatment at 43°C after irradiation give indication that this effect will start here, too.

Another possibility to influence the repair capacity is changing the dose rate, when always the same total dose is given. This was dicussed by Tobias[4], who claimed an influence on the survival when the time of irradiation reaches the half-time for repair of a certain dammage. V79 cells, irradiated with 250 KVp x-rays show an increased survival when the total dose is given in times longer than 45 minutes. Whether there is another very short repair time (2-7 minutes) has to be studied in some further experiments.

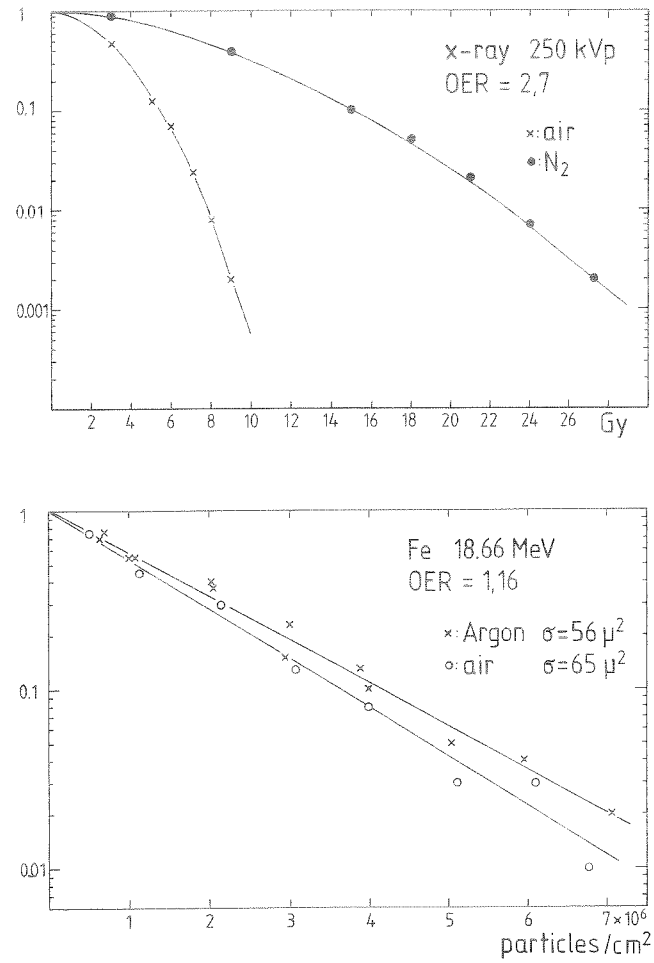


Fig. 1: Survival of V79 cells in presence or absence of oxygen.
a) Irradiated with 250 kV x-rays.
b) Irradiated with ^{56}Fe ions of 18 MeV/u.

References:

[1] G.N. Barendsen, in: Current Topics in Radiation Research, Vol. IV, p. 293, Amsterdam 1968.
[2] GSI-Scientific Report 1980, p. 160.
[3] GSI-Scientific Report 1981, p. 189.
[4] C.A. Tobias, E.A. Blakely, F.Q.H. Ngo, and T.C.H. Yang, The Repair-Misrepair Model of Cell Survival, in: Radiation Biology in Cancer Research, p. 195-230, New York, 1980.

Micronucleus induction after treatment with ionizing radiations

U. Bertsche and G. Iliakis
Gesellschaft für Strahlen-und Umweltforschung, Frankfurt

G. Kraft

GSI Darmstadt

It has been shown before that irradiation of mammalian cells in culture using heavy ions from the UNILAC resulted in an exponential or near exponential dose response, whereas no reparable component of the damage to colony forming ability (CFA abbrev.)was observed, i.e. all damage induced by the radiation was found irrepairable under non-growth conditions (1).

Detailed knowledge about the irrepairable events on the molecular and supramolecular level which lead to cell killing (loss of CFA) is absent up to now; however, it is generally accepted that damage to the nuclear DNA plays a crucial role. It was suggested also that further events include chromosome and chromatid aberrations and repair on higher conformations of DNA (2).

To get more information into some of these important aspects of radiobiology, i.e. into the chain of events from the molecular target to the cellular endpoint (CFA-loss), a study was initiated to assess chromosome and cellular damage after treatment with ionizing radiations by the detection of micronucleated and multinucleated cells. The ocurrence of a micronucleus beside the main nucleus in a cell is mainly due to chromosome fragmentation: the fragments lag behind the normal movement of the chromosomes to the spindle poles at anaphase (3). The ocurrence of bi-and multinucleated cells, on the other hand, probably arises from damage to the mitotic apparatus responsible for cell division and may be caused also by other events as those which impair the DNA integrity.

In detailed studies with X-and alpha-particle irradiated mammalian cells it was found that most events which lead to loss of CFA were mediated by micronucleation and a minor part by multinucleation and formation of giant cells. These morphological features can be detected easily with a fluorescence device: the cells were stained after irradiation and incubation (to allow for mitotic activity which is a prerequisite of the formation of aberrants)with a fluorescent dye of the DNA (Hoechst 33258). Micronucleated and binucleated cells appear

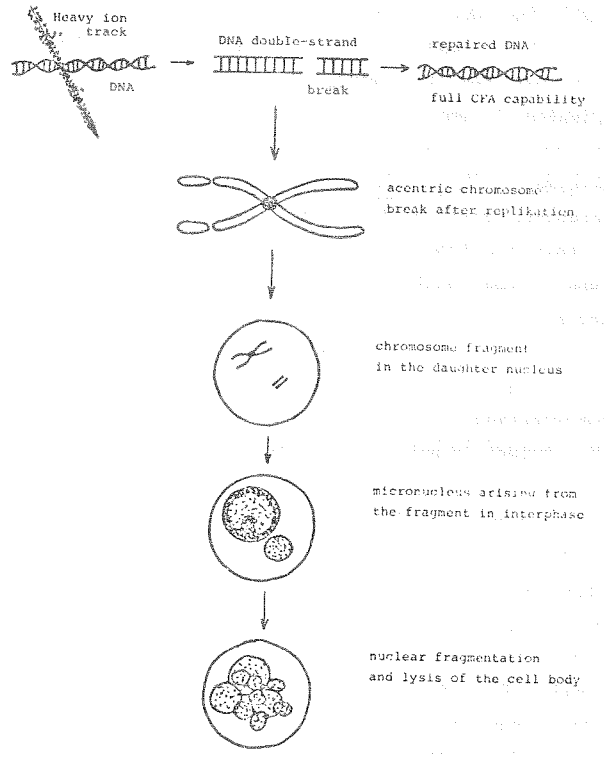


Fig.1. Proposed link between DNA damage by heavy ion impact and loss of colony forming ability (in more than 50 % of all CFA-loss events).

also in unirradiated controls, however, with a rather low frequency. It could be shown that the repair of potentially lethal damage normally observed on the CFA-level is likewise apparent on the micronucleus level. This and other results let suggest that loss of CFA after impact of ionizing radiation is mainly due to acentric fragmentation of the chromosomes (fig.1). Further studies with heavy ions at high Linear Energy Transfer should cover the time sequence of micronucleus formation after irradiation; the repair of PLD on the micronucleus level and a detailed search for other morphological features which could characterize the high energy input of the heavy ion into a small, localised area of the cell nucleus.

[1] U.Bertsche, G.Iliakis and G.Kraft; GSI-Scientific Rep. 1981, p.

[2] M.A.Bender, H.G.Griggs and J.S.Bedford; Mutat. Res. 23, 197 (1974).

[3] W.Schmid; Mutat. Res. 31, 9 (1975).

Small Angle Scattering From Latent Nuclear Tracks G

D. Albrecht, P. Armbruster, R. Spohr / GSI Darmstadt
M. Roth / ILL Grenoble
K. Schaupert / Zweites Physikalisches Institut, Univ. Gießen
H. Stuhrmann / Institut für Physikalische Chemie, Univ. Mainz

By calculating the pair correlation for molecules in fluids Zernike and Prins (1927) did the first step to small angle scattering. Since this time small angle scattering has developed to a well approved method of research in physics, chemistry and biology. Standard solutions for the analysis are available for **not oriented** systems, consisting of scatterers with spherical shape or nonspherical scatterers without favored alignment. Both give similar, isotropic scattered intensity distributions. Only few strongly **oriented** systems are known, for example, flux-line lattices in type-II superconducters and the latent nuclear tracks, where the scattering centers are well aligned. The flux lines are periodically arranged. Therefore, the observed scattered intensity contains grating like contributions.

The latent tracks have, due to their statistical position distribution, a vanishing distance correlation. Therefore, the scattered intensity is calculated to be the incoherent sum of the scattering contributions of the single tracks. We measure an integral value: the folding of the size distribution of all tracks and of the density variations in the single tracks. For the irradiation ions of well defined mass and energy are used at GSI. If we assume a small variance of the size distribution and the density variation for all tracks, we obtain as result the picture or model of an average track.

Because of the sample properties mentioned above, the scattered intensity distributions observed on the detector are unsymmetrical and depend strongly on the angle α between the beam and the surface normal of the foil. For different angles the longitudinal- and the radial density distribution give contributions of different weight to the observed intensity. This property helps to separate the length and radial distribution and also to discriminate different models. The measurements show that the form of the defects in mica and Hostaphan should be quite similar. In both cases we have a Gaussian radial density variation.

The simple model of a cylinder gives the best agreement for the longitudinal distribution in mica. For Hostaphan this cylinder shows additionally an axial modulation. This periodicity produces the "wings" (or side maxima) on the scattered intensity distributions. All numerical values for the parameters depend on the ion, its energy and the foil material.

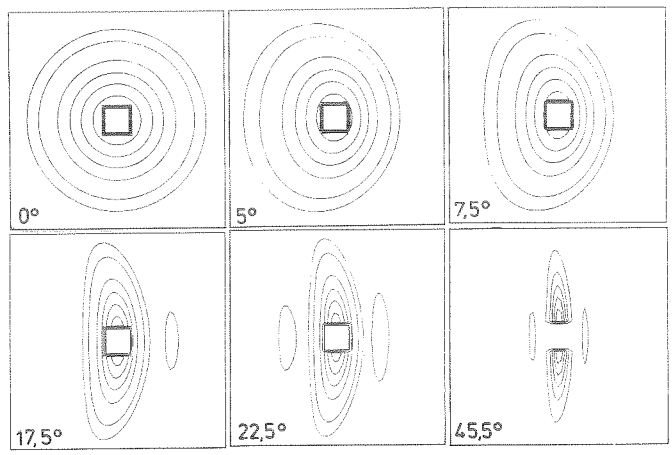


Fig. 1: Model calculation for Hostaphan: Contours of the calculated intensity distribution on the detector area as a function of angle α (see Fig. 2).

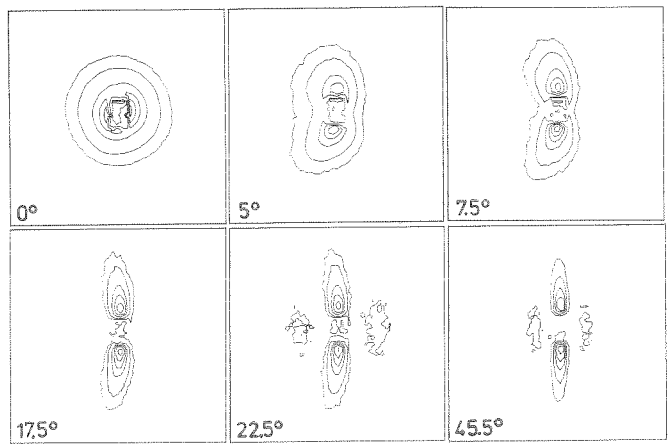


Fig. 2: Measured intensity distributions for Hostaphan irradiated with Uranium (8.6 MeV/u) as function of α.

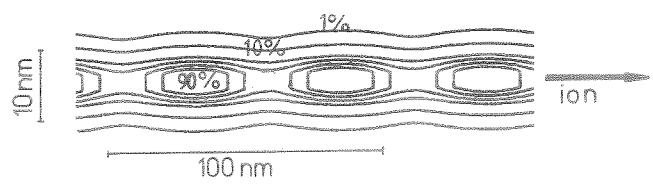


Fig. 3: Model of an average track in configuration-space: Density variation normalized to the maximal density variation in the latent track of Hostaphan (Kalle, FRG).

ANNEALING OF HEAVY PARTICLE LATENT DAMAGE TRAILS IN CR-39 (HOMALITE) PLASTIC TRACK DETECTORS

HAMEED A. KHAN, REINHARD BRANDT*, NAEEM A. KHAN, M. ASLAM SIAL
and
KHALID JAMIL

Nuclear Engineering Division
Pakistan Institute of Nuclear Science and Technology (PINSTECH)
P.O. Nilore, Rawalpindi, PAKISTAN

CR-39 plastic detector is the latest member of the Solid State Nuclear Track Detection family [1]. The detector has been found to possess some unique track registration properties. It is highly suitable for registration of lightly ionizing particles such as energetic protons and alpha particles.

In many situations, one needs to employ this detector at elevated temperatures. Experience with the conventional track detectors operated at high temperature shows that post-exposure annealing affects the stability of latent damage trails [2,3]. The present paper summarizes the results of annealing experiments carried out by us in studying the thermal stabilty of latent damage trails in CR-39 (Homalite) plastic track detectors.

Small strips of CR-39 were exposed to 16.7 MeV/n ^{238}U ions at an angle of 30° with respect to the detector surface. The strips were annealed at various temperatures in the temperature range of 50° - 300 °C for ten minutes each. The detectors were then etched simultaneously in 6N solution of NaOH kept at 70±1 °C for one hour.

Figure 1 is a set of photomicrographs showing the etched versions of the latent damage trails annealed at various temperatures. Results of the systematic studies of the variation of etched-channel-dimensions can be summarized as follows:

1. The shape of the etched channels is transformed from "needle-like" to "funnel-like" ;
2. The length of the "funnel" is a gradually decreasing function of the anealing temperature. A sudden decrease appears around a temperature of 180 °C ;
3. The major and minor axes of the elleptic etch pit opening increase, at first gradually, and then abruptly ;
4. The overall thickness of the stem of the funnel increases significantly beyond annealing temperatures of 240 °C. ;
5. It appears as if the annealing process, at first, affects the top surface of the detector and then creeps inside its body.

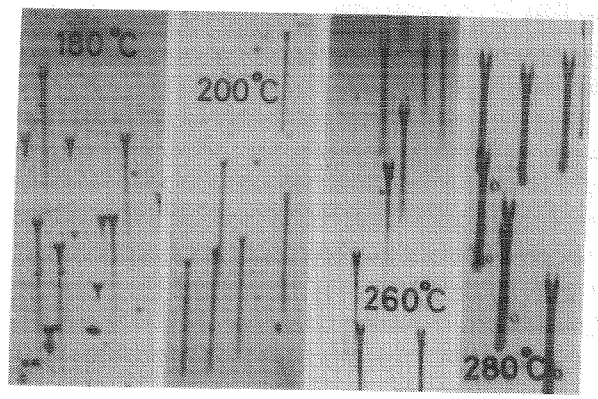


Figure 1 : Set of photomicrographs showing the etched channels in CR-39 plastic detector obtained after annealing the latent damage trails at 180, 200, 260, and 280 °C before etching.

It is our pleasure to thank Dr. M.C. Scott and Mr. T. Cartwright for exposures at Nuffield Cyclotron, Birmingham University. Financial support to one of us (HAK) by the Alexander Von Humboldt (AVH) Foundation is also gratefully acknowledged. We thank Dr. R. Spohr (GSI) for carrying out the irradiations with ^{238}U.

REFERENCES

1. B.G. Cartwright, E.K. Shirk, and P.B. Price: Nuclear Instruments and Methods 153 (1978) 457.
2. R.L. Fleischer, P.B. Price, and R.M. Walker: Nuclear Tracks in Solids : Principles & Applications (University of California Press, Berkeley, 1975).
3. H.A. Khan: Nuclear Instruments and Methods 173 (1980) 55.

* Kernchemie, F.B. 14, Philipps Universitat, 3550-Marburg(Lahn), West Germany

ELECTROLYTICAL STUDIES ON TRACKS OF ^{238}U-IONS IN MAKROFOL

J.Krause, W.Enge and R.Beaujean

Institut für Reine und Angewandte Kernphysik, Universität Kiel, D-2300 Kiel, 1982

Plastic-Nuclear-Track-Detectors can be used to measure heavy Cosmic-Ray ions. The ions can be identified according to their energy loss-range relationship. The energy loss dE/dx is usually determined by measuring the etch cone length at a known range of the ion after a fixed time of etching at constant etching conditions.

A new potential technique for the determination of dE/dx is to measure the time needed to etch through a detector foil along a track section of a fixed length at a known range of the ion. While in the old conventional method the etch cone length supplies the information on dE/dx here the etch through time takes care of it.

Experimentally the problem is solved by using 6 n-NaOH simultaneously as etchant and as electrolyte. The following setup is used. An etching chamber is divided into two parts by an isolating detector foil which carries the latent tracks to be analysed. The detector foil is aluminized on one surface (see [1]). One part of the chamber is filled with 6 n-NaOH the other with dieseloil which is a very good dielectric liquid. The dieseloil is touching the Al-surface, furthermore the dieseloil is under higher pressure than the NaOH. The Al-layer and the NaOH are the two electrodes of the electrolyte chamber. 25 Volts DC are used.

Many polycarbonat-foils (Makrofol KG of Bayer, FRG) with a thickness of 60 µm were irradiated by the GSI each with only one ^{238}U-ion (5.9 MeV/u). Lateron the foils were aluminized in our institute with an Al-layer of 300-1000 Å. 50 of the foils were etched at 30°C in 6 n-NaOH with 0.05 % Benax surfactant (Dow Chemical).

As long as there are no etched through tracks in the dividing detector foil no electric current is flowing in the electrolyte chamber. In the moment of the first break through the electric current increases by 5 orders of magnitude within about 20 seconds.[2]

If there is more than one track in the detector foil the current has to be stopped after each break through to allow the measurement of the break through time of each single track. The Al-layer which is immediately etched away around the track cylinder (maybe only with negative Al, see later) by the penetrating NaOH together with the dieseloil isolating this circle area of missing Al around the track cylinder make a self-stopping-system for the current.

Depending on the polarity of the Al-layer there are two different effects to be observed for one single track:

a) With positive Al-layer a well defined first current peak is observed which is, however, followed by many other peaks in random order. Furthermore no visible cycle area of missing Al could be found.

b) With negative Al-layer only one current peak (see fig.1) is obtained and there are definitely no further disturbing peaks. The circle area of missing Al-layer (fig.2) has a diameter of about 80 µm and can be well detected with unaided eye.

The following results were obtained up to now: An average break through time of (83.3 ± 4.5) min. could be measured from 48 tracks. In 6 of 50 foils there were no tracks at all, which is astonishing but consistent with the irradiation electronic of the GSI. In two foils there were two tracks (fig.1 and fig.2) and in one foil there were three tracks.[2]

Summarizing our first results this new technique looks very promising. First, very high ratios of track to bulk etching rates can be easily measured. Usually those values are very badly measurable by the conventional method of microscope measurements. Second, the energy loss is already now measurable with an improved accuracy of 0.6 % as known from other data obtained with the same technique.[2]

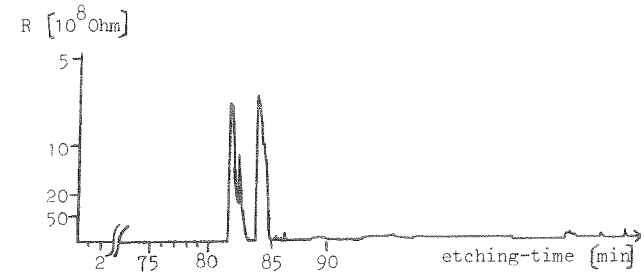


Fig.1: Current peaks of two individual tracks (converted to foil resistance)

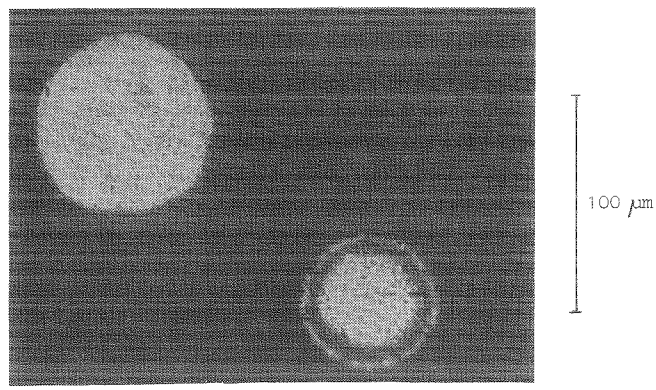


Fig.2: Micrograph showing the detector foil used for the measurement of fig.1. The tracks in the centre of the circle area of missing Al-layer are not resolved.

Acknowledgements-The authors like to thank Dr. R. Spohr, Dr. P. Vater and Dipl. Phys. K. Schaupert for the irradiation at the GSI.

[1] L. Tommasino, G. Zapparoli and F. Caiazzo, Solid State Nuclear Track Detektors, 211 - 219, Pergamon Press Ltd, Oxford, England (1982)

[2] J. Krause, Diplomarbeit der mathematisch-naturwissenschaftlichen Fakultät, Universität Kiel (1983)

CRITICAL ANGLES OF ETCHING OF CR-39 PLASTIC TRACK DETECTORS

HAMEED A. KHAN, REINHARD BRANDT*, NAEEM A. KHAN, KHALID JAMIL, M. ASLAM SIAL, & GULZAR HUSSAIN

Nuclear Engineering Division
Pakistan Institute of Nuclear Science and Technology (PINSTECH)
P.O. Nilore, Rawalpindi - PAKISTAN

The critical angle of etching (Θ_c) is an important parameter in the field of Solid State Nuclear Track Detection [1-3]. It is of immense use when one is dealing with the emission of different types of charged particles in nuclear reactions and/or the determination of reaction rates and cross-sections.

CR-39 the newly introduced track detector has been found to be very sensitive for both heavy and light charged particles. In this report we give a summary of the work carried out by us to find the critical angles of etching of this extremely useful detector for a variety of charged particles.

Two different approaches were made for the determination of critical angles:

In the first approach, direct measurement of Θ_c was performed. Here, pieces of CR-39 were positioned on an aluminium backing so that the faces of the detectors were subtending different angles with respect to the incoming beam of varying energy charged particles. The exposed detectors were etched in 6N solution of NaOH kept at 70 ± 1 °C. The angular interval in which the tracks failed to produce etchable latent damage trails were located and then finally narrowed down so that to determine the exact critical angles of etching.

In the second approach, both light and heavy charged particles were allowed to fall perpendicular to the surfaces of CR-39 detectors. The exposed detectors were etched and the etch pit channels were broken apart in such a way that their profiles could be seen using Scanning Electron Microscope (SEM). Using this technique the cone angles of the etched channels and the critical angles of etching were determined.

The cone angles and the critical angles of etching for various energy protons are given in Table 1.

TABLE-I

CONE ANGLES, CRITICAL ANGLES OF ETCHING AND TRACK REGISTRATION EFFICIENCIES OF CR-39 FOR DIFFERENT ENERGY PROTONS

ENERGY (MeV)	CONE ANGLES† (DEGREES)	CRITICAL ANGLES OF ETCHING (DEGREES)	EFFICIENCY FOR 2π - EXPOSURES (%)
10.0	122	61	12.5
7.6	114	57	16.1
5.1	104	52	21.2
3.9	96	48	25.7
1.8	72	36	41.2
1.2	54	27	54.6

† Etching Conditions: 6N NaOH, 70 ± 1 °C, 12h

The results for six different energies of alpha particles have been summarized in Table 2.

The critical angles obtained for ^{16}O and ^{12}C have been shown in Figure 1 and 2.

TABLE-2

CRITICAL ANGLES OF ETCHING OF CR-39 FOR DIFFERENT ENERGY ALPHA PARTICLES

ENERGY (MeV)	CRITICAL ANGLE OF ETCHING (DEGREES)	EFFICIENCY FOR 2π - EXPOSURES (%)
40.0	28.4	52.4
20.2	26.4	55.6
6.5	25.7	56.7
4.3	24.6	58.3
2.1	15.7	73.0
0.9	6.4	88.9

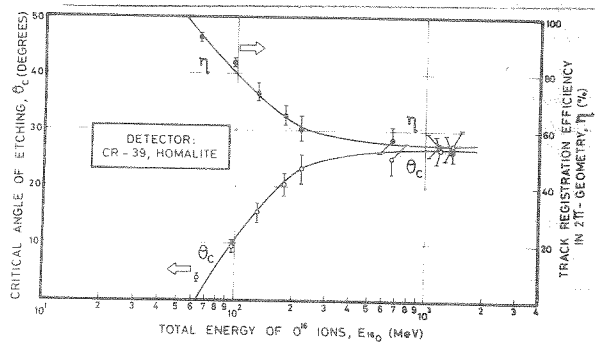


Fig.1

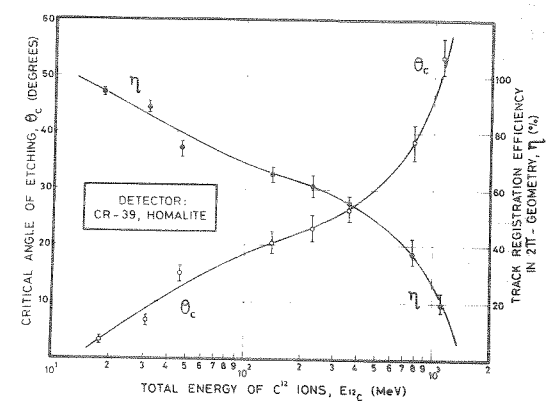


Fig.2

1. R.L. Fleischer, P.B. Price, and R.M. Walker: Nuclear Tracks in Solids (University of California Press, Berkeley, 1975

2. H.A. Khan: Nuclear Instruments & Methods 173 (1980) 43

3. C.S. Johnson, E.V. Benton, R.M. Cassou, R.P. Henke and D.J. Hildebrand: Proceedings of 10th International Conference on SSNTD, pp. 303-310 (July 1979).

* Kernchemie, F.B. 14, Philipps Universitat, 3550 - Marburg (Lahn), West Germany.

Solid State Nuclear Track Detectors for High Energetic Heavy Ions G

K. Schaupert, K. Keiner, G. Fiedler
II. Physikalisches Institut, Universität Giessen

Concluding our studies on the borate glass MSKP33 as a detector for heavy ions [1] we evaluated ionisation density curves. This was done by determining the detector-specific constant K in the Bethe-Bloch-Formula [2], using experimentally obtained track data. Fig.1 shows the resulting ionisation density in this glass for ions with kinetic energies up to 14MeV/u.[3] The value $(dJ/dx)_{crit}$ is the critical ionisation density below which no track etching occurs. As can be seen, ions lighter than Sodium are not recorded in this detector.

In accordance with our observations is the fact that - above 2 MeV/u - increasing kinetic energy of an ion results in decreasing damage in the detector. Finally the critical ionisation density is reached and no track etching takes place at the detector surface. For energies beyond this threshold the etchable part of the track is buried and only revealed after the top layer is dissolved with the bulk etch rate v_b. For ionisiation densities higher than the critical value, the track etch rate v_t rises above the bulk etch rate v_b and reaches $v_t = 4\ v_b$ for Krypton ions below 2 MeV/u.

In addition to our measurements on glasses we began a study on gamma-irradiated CR 39 plastic as a nuclear track detector. The aim of this work is the development of a detector for heavy ions with a variable critical ionisation density. By irradiating the material with gamma rays we achieve a higher bulk etch rate, thus suppressing tracks of particles with low ionisation densities. An irradiation with 1.5 MRad increases the bulk etch rate v_b by 20%, a dose of 5 MRad results in an increase by a factor of four.

However, as shown in fig. 2, v_b of gamma irradiated CR 39 is decreasing to the value in the unirradiated material in a depth of 7 µm. This has to be taken into account while applying this detector.

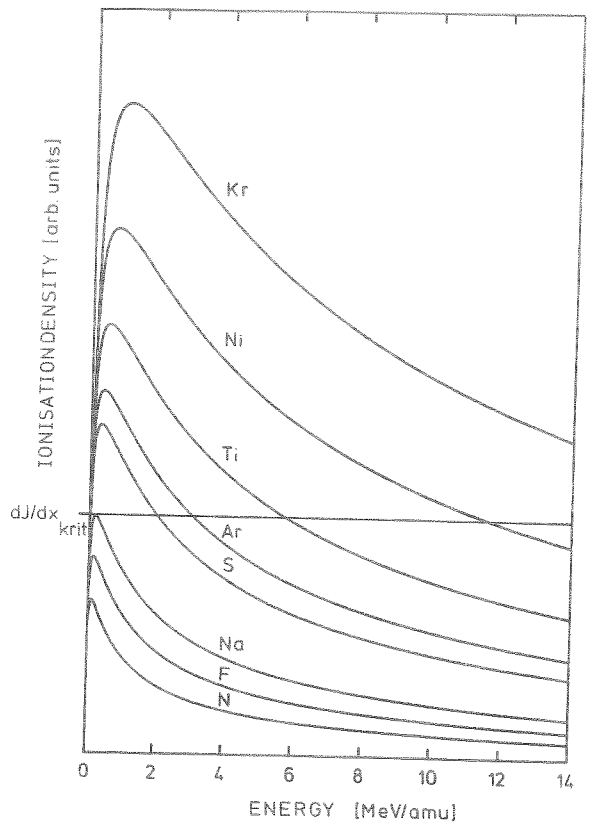


Fig.1 Ionisation density vs specific ion energy for borate glass

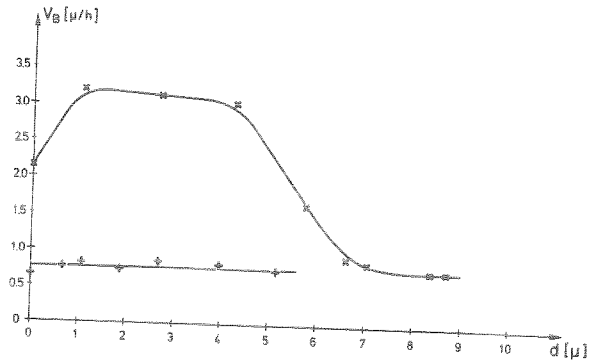


Fig.2 Bulk etch rate vs depth in CR 39
+ unirradiated ×5 MRad gamma radiation

[1] Schaupert, Keiner and Fiedler, GSI Scientific Report 82-1, p 247
[2] Fleischer, Price and Walker: Nuclear Tracks in Solids, Univ. of Calif. Press (1975), pp 29-31
[3] K. Keiner, Diplomarbeit 1983 ,2.Phys. Inst., Univ. Giessen

A graded-index antireflection treatment of optical surfaces by the nuclear track technique

B.E. Fischer, GSI Darmstadt

Today the standard method to reduce light reflection from optical surfaces is vacuum deposition of thin films of intermediate refractive index. In a search for highly damage resistant antireflection coatings for high power lasers Lowdermik and Milam[1] revived an old technique producing a continuous transition of the refractive index. The method depends on a special molten glass with two finely dispersed components, one of which is easily dissolved in an etchant. If the surface of such a glass is exposed to an etchant, a microporous surface layer results, the pore size of which is decreasing with depth (because at larger depth the material is exposed to the etchant for a shorter time). If these pores are made small enough (100-1000 Å), there should be no visible light scattering and the porous surface layer should only appear to have a continuous transition of the refractive index from 1 to that of the bulk material. Such a graded index surface reflects no light if its thickness is $\lambda/2$. For larger thicknesses the antireflection effect is still very strong. Therefore a given graded index surface is effective over a large range of wavelengths and incident angles.

As the latent track of a heavy ion manifests itself as a region of increased solubility in a region of 50 to 100 Å around the ion's path, irradiation of normal optical materials with heavy ions should produce a quasi two-component material with exactly the required properties for graded index surfaces. The production of such surfaces would then proceed as indicated in fig. 1.

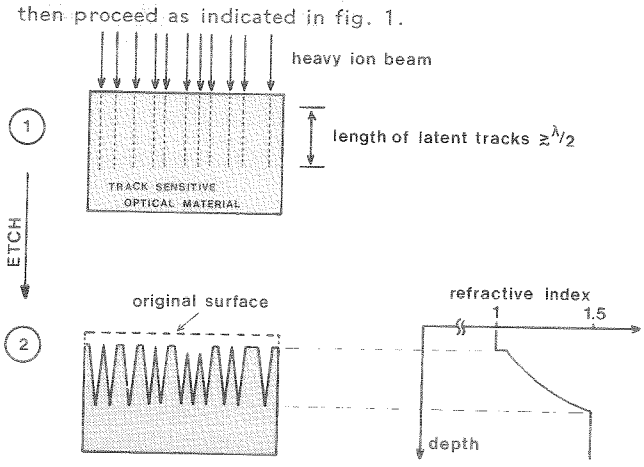


Fig. 1: Production scheme for graded index surfaces

For an experimental test of the idea a plastic material called CR-39 was chosen in which tracks can be etched already at very low energies. Thin sheets of that material have been irradiated on both sides with argon ions of 750 keV and etched in 6.25 n NaOH at 40° C. The remaining transmission losses after etching are shown in the lable below.

Sample No.	treatment		transmission loss [%] at wavelength				
	fluence	etch time	400 nm	500 nm	600 nm	700 nm	800 nm
1	$3*10^{12}$ cm^{-2}	6 min	15.5	8	5.8	5	5
2	$1.8*10^{12}$ cm^{-2}	6 min	12.2	6.5	5	4.5	5
3	$6.25*10^{11}$ cm^{-2}	6 min	6.8	3.3	2.2	1.5	1.3
4	$1.25*10^{11}$ cm^{-2}	6 min	8.5	5.3	4.5	4.5	4.5
5	$6*10^{10}$ cm^{-2}	5 min	8	5.9	5.7	5.3	5.5
6	"	6 min	6	5	4.7	4.5	4.7
7	"	8 min	12	7	5	4	4
8	"	10 min	13	7	5	3.8	3.8
	untreated controls		7.8	7.4	7.4	7.3	7.7
	bulk absorption only		0.78	0.35	0.30	0.28	0.27

As the transmission loss is the loss due to reflection and scattering the effect of scattering has been checked indirectly by measuring the reflectivity alone for sample No. 3. The measured reflectivities have been 0.55 % for a He-Ne-laser (633 nm) at 10° angle of incidence and 0.38 % for an extended light spectrum around 550 nm at an angle of 22.5°. So the measured transmission losses seem to be largely due to scattering at least at small wave lengths. (Unfortunately the lack of suitable equipment prevented a more comprehensive measurement of light scattering and reflection for all wavelengths and all samples.)

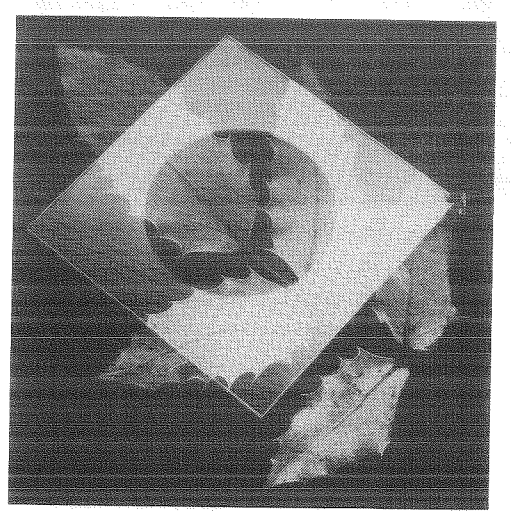


Fig. 2: Photography of a graded-index surface.

The circular central area has been irradiated with 1.6 x 10^{11} neon ions per cm² on both sides and etched for 23 min. in 6.25 n NaOH at 40° C.

[1] W. Howard Lowdermilk and David Milam, Graded-index surfaces to limit reflection, Laser Focus, Dec. 1980, pp 64-70.

SCANNING ELECTRON MICROSCOPE INVESTIGATIONS OF PLASTIC CR-39 MICROFILTERS

M. Berndt, G. Siegmon, R. Beaujean and W. Enge

Institut für Reine und Angewandte Kernphysik, Universität Kiel, D-2300 Kiel (FRG), 1982

Nuclear track filters are used in more and more fields of science and technology. This paper presents a nuclear track filter of Plastic CR-39 (manufactured by PERSHORE MOULDINGS LTD.; Pershore, Worcestershire, England), a material not used for that purpose up to now.

Laboratory specimens were obtained by irradiating 70-100 µm thick Plastic CR-39 discs with 5 cm diameter and an irradiated area of 4 cm diameter in their centre. The irradiations were carried out by the GSI, Darmstadt (FRG), with ^{238}U-ions (10^6 ions/cm^2) having a specific energy of 14.2 MeV/nucleon. Using the well-known track etching technique (6n-NaOH as etchant, 70°C, 120 min) we got a microfilter with pore diameters of 5 µm.

The following scanning electron micrographs are showing interesting details of the surface structure in the pores:

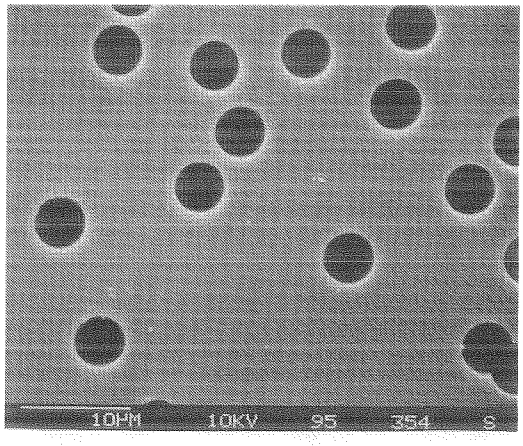


Fig.1

The surface of the Plastic CR-39 filter can be seen with extremely circular pores of 5 µm diameter and no roughness of the surface in spite of an etching time of 120 minutes.

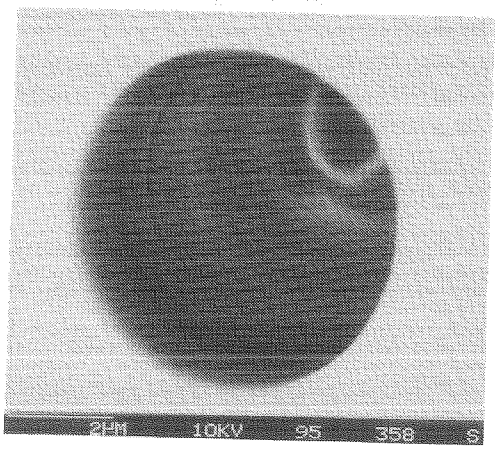


Fig.2a

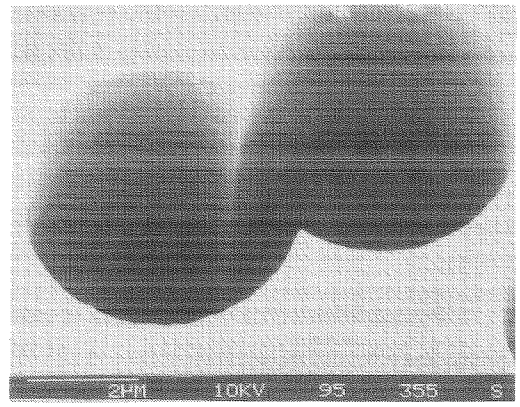


Fig.2b

These figures are showing the inner walls of a single (2a) and of two joined pores (2b) . In both cases no roughness of the pore walls can be observed. That is a very important fact for theoretical studies of the laminar air flow through the pores of a nuclear microfilter.

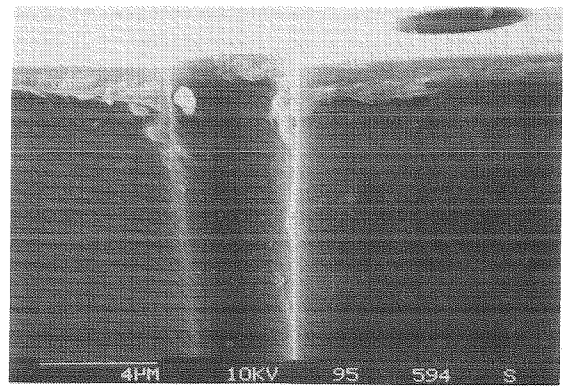


Fig.3

This is a micrograph of the edge of a Plastic CR-39 filter which shows the homogenous bulk structure of this material This edge cuts a pore and again no roughness or pits as in Makrofol-polycarbonate, Kodak-cellulosenitrate[1] or LAVSAN-polyester nuclear track filters[2] can be seen.

Plastic CR-39 seems to be a very suitable material for nuclear track filters because of its extremely homogenous surface and bulk structure even after a long etching time. Further more the optical properties of Plastic CR-39 (high transparency) together with its surface quality are very promising for optical investigations on aerosols collected with this nuclear microfilter.

Acknowledgements-The authors like to thank Dr. C. Samtleben and the technician Mr W. Reimann, Geologisch-Paläontologisches Institut und Museum, Universität Kiel, for the assistance with the SEM Cambridge S 150 and Dr. R. Spohr and Dipl.Phys. K.Schaupert for the performance of the exposure at the GSI.

[1] Röll I. Staatsexamensarbeit der mathematisch-naturwissenschaftlichen Fakultät, Universität Kiel (1981) .

[2] Hoppe J. and Rauschenbach B. Nucl. Tracks, 4,161-169, (1981)

USE OF ETCHED CHANNELS AS CHARGED PARTICLE COLLIMATORS

HAMEED A. KHAN, REINHARD BRANDT*, NAEEM A. KHAN, KHALID JAMIL, & M. ASLAM SIAL

Nuclear Engineering Division
Pakistan Institute of Nuclear Science and Technology (PINSTECH)
P.O. Nilore, Rawalpindi - PAKISTAN

In many situations, a collimating system occupying small space and/or having a high degree of collimation is required. To this end, we need to have a collimator with minimum possible length. This, in turn, restricts the cross sectional area (or diameter) of the collimating channel. The smallest possible hole size of a mechanically drilled channel is believed to be of the order of 0.1 mm [1]. On the other hand, the minimum size of the "hole" produced by the passage of a charged particle in insulating media (such as plastics, glasses, and crystals) can be as small as 100 ^{o}A [2]. The size can be, of course, easily increased to a few microns if the latent damage trails are enlarged through chemical etching (Figure 1). Therefore, the etched channels in insulating media can be used as micron sized collimators. This is particularly useful when one needs to channelize low energy light charged particles like alpha particles or medium energy heavy charged particles such as fission fragments, emitted in spontaneous or induced fission of heavy elements.

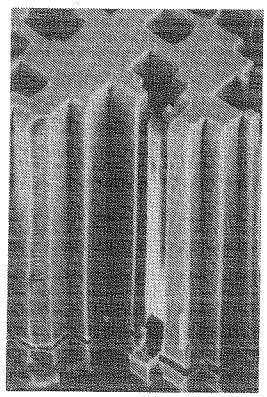


Fig.1

SEM-Photomicrograph of channels in an Etched-Channel-Collimator

A mica Solid State Nuclear Track Detector (SSNTD) has been successfully used as a particle filter [3,4]. We have studied the collimating properties of uniformly shaped etched channels in a mica track detector. The mica sheets were exposed to energetic heavy ions at UNILAC (GSI, Darmstadt). The exposed mica track detectors were etched in 48% HF. The etched channel size is a function of the etching time and the porosity of the filter is controlled by the flux of heavy ions.

Mica filters having channel length of 50 μm and a channel density of about $5 \times 10^{5}/cm^{2}$ were used in the present studies. The transmission (number of fragments transmitted through the collimator as a fraction of the total emission in 2π-geometry) of mica filters for fission fragments (emitted by a spontaneous fission source of ^{252}Cf in 2π-geometry) has been studied as a function of the size of the etched channels. The transmission increases linearly with (a) increasing exposure time, and (b) increasing hole size. The variation of percent transmission as a function of hole size has been given in Table-I.

TABLE-I

HOLE SIZE (μm)	SOURCE-STRENGTH IN 2π-GEOMETRY (# /cm^2/hr)	TRANSMISSION (%)
3.0	8.8	5.8×10^{-4}
4.9	3.5×10^{1}	2.3×10^{-3}
∞ (No collimator)	1.5×10^{6}	100

These preliminary results show that the etched channels in a mica track detector can be successfully applied in achieving a high-degree-collimation of charged particles like alphas and fission fragments. The space occupied by an Etched-Channel-Collimator is only a few microns. Further work on the optimization of the parameters of this new type of charged particle collimator is under progress.

The authors are grateful to Dr. R. Spohr (GSI) for his help in carrying out the heavy charged particle exposures and for many fruitful discussions. One of us (HAK) is grateful to the Alexander Von Humboldt (AVH) Stiftung for the financial help during his stay at Marburg as AVH-Fellow (1981-82).

REFERENCES

1. R. Spohr:
GSI patent number P 2951 376.6 (1981-1)

2. R.L. Fleischer, P.B. Price, and R.M. Walker:
Nuclear Tracks in Solids: Principles and Applications.
University of California Press, Berkeley (1975)

3. P. Vater, G. Tress, R. Brandt, B. Genswürger, and R. Spohr:
Nuclear Instruments & Methods 173 (1980) 205

4. R. Spohr:
Nuclear Instruments & Methods 173 (1980) 229

* Kernchemie, F.B. 14, Philipps Universitat, 3550-Marburg (Lahn), West Germany.

The single erythrocyte rigidometer on the threshold to a product

H.G. Roggenkamp, H. Kiesewetter, F. Jung
Abt. Physiologie des Klinikums der RWTH Aachen

The ability of the erythrocyte to deform themself is an important hemorheological parameter since the deformability of the red blood cell is the limitating factor for passing the smallest vessels of the circulation. The diameter of the capillaries is about 3 - 7 µm, whereas the resting diameter of an erythrocyte is about 7.5 µm. So the erythrocyte has to reduce his diameter to values of about 2.9 µm (Fig.1).

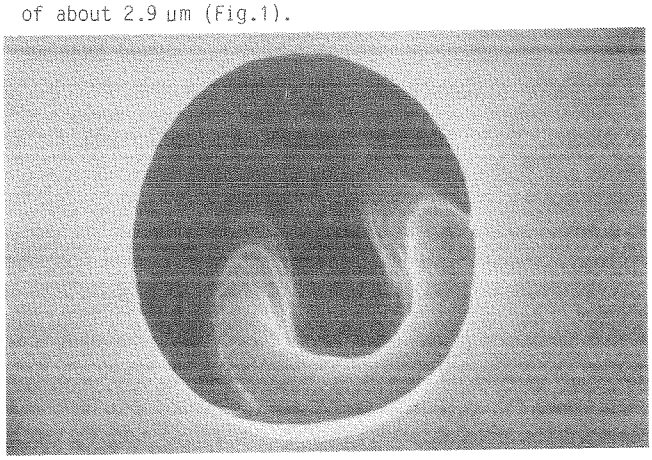


Fig.1: The passage of an erythrocyte through a pore with a diameter smaller than the resting diameter of the erythrocyte

In the Scientific Report 1979 an optoelectronical device was presented which determines the passage time of erythrocytes through a single pore membrane as a dimension for the deformability of erythrocytes. The measurement was realized with a single pore membran to simulate the physiological conditions as well as possible. The received dates (mean passage time of erythrocytes t_M and number of relative rheological occlusions RRO) permit not only a classification of the measured erythrocyte population compared to a normal population, but also detailed statements about the behaviour of single groups of erythrocytes.

The measurement with the 1979 introduced apparatus, however, needs a very high time spent, a great technical effort (a microscope with great working distance, a special microcope table and a photomultiplier; an external pressure system, a microprocessor with a printer), a trained operator and constant peripheral conditions. Therefore the single erythrocyte rigidometer (SER) was developed to a routine apparatus which can be handled very simply. The construction of the measuring chamber, the generation of the pressure and the measurement of the passage times had to be varied. Figure 2 shows a provisional version of the developed device, the single erythroyte rigidometer (SER).

The principle item of this method is still the single pore membrane. The measurement of the passage time of an erythrocyte through this single pore membrane is not determined optically as in the past, but electrically by the alteration of the resistance of the fluid-filled pore.

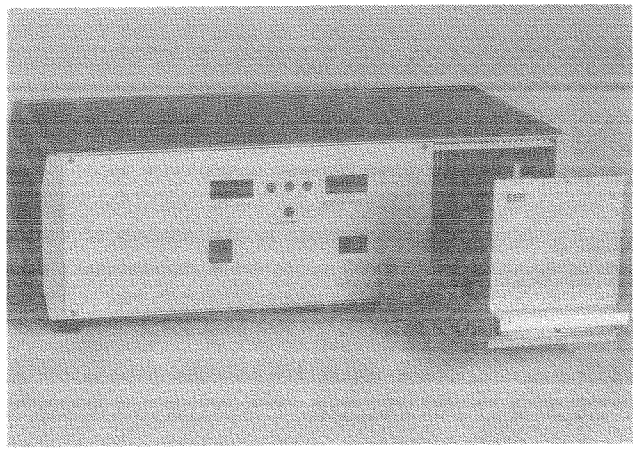


Fig. 2: The single erythrocyte rigidometer (SER)

This routine instrument (SER) is supported at present by an important industrial enterprice and will soon be marketable. A greater number (10) of experimental types will be tested in this year by some well-known scien - tists

Fractionation of Aerosols Using Mica Nuclear Microfilters with Rounded-off Entrance Channels at the NUKEM-Sinteroven B

G. Tress, E.U. Khan, H.A. Khan, P. Vater, R. Brandt, Kernchemie, Uni Marburg
M. Kadner, NUKEM GmbH, Hanau
R. Spohr, GSI, Darmstadt

During the last year we improved our mica nuclear microfilters considerably by rounding-off the entrance and exit channels. With these new micropores we have a much smoother air-flow in the system, resulting in an improved fractionation of particles. This is obtained by a two-step etching: at first, HF-etching results in well-known sharp-etched entrance channels; a second etching for 10 to 100 h etching in boiling 10 n NaOH results in rounded off entrance channels as shown in Fig. 1.[1]

The mica nuclear microfilters arranged as a cascade (3 to 9 filters, 25 µm > k > 0.1 µm; areal density D: $10^4 < D < 10^9$ cm^{-2}) and used for filtration of hot, radioactive aerosols from a sinter-oven at the NUKEM GmbH, Hanau, allow simultaneously the quantitative separation of 99,99 % of the particles and their fractionation according to the size and shape. Additionally, 99,5 % of α - and β -activity was filtered out. The rest activity has its origin in small ^{222}Rn accounts emanated from the sinter-material and the walls of the oven[2].

The principle and the effects of particle separation and fractionation in filtration of aerosols using micafilters in a cascade particle fractionator has been described in another contribution.[3]

Analytical evaluations of loaded filters using a microprobe at the REM show the potential of this system. On tiny aerosols we could identify the following elements (Figs. 2 and 3): besides K, Al, Si (mica constituents): W, U, Fe, Ti, Ca, S.

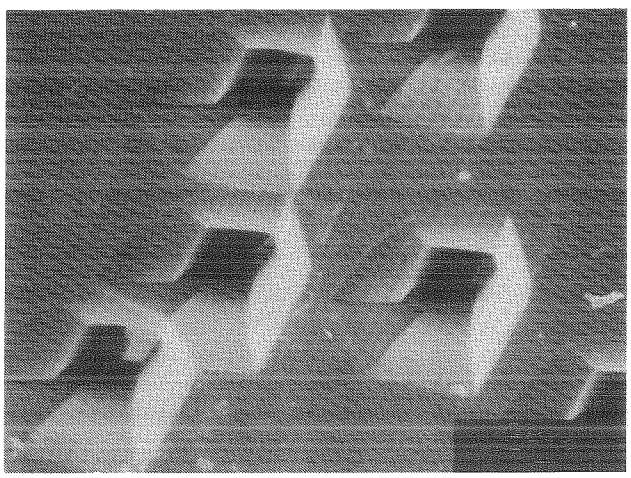


Fig. 1: Mica track microfilters with "rounded-off" entrance and exit channels.

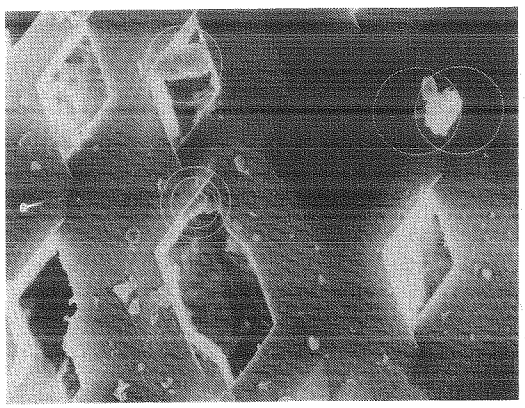


Fig. 2: Microphotograph of three different aerosol particles found on one mica microfilter. Their analysis is shown in Fig. 3.

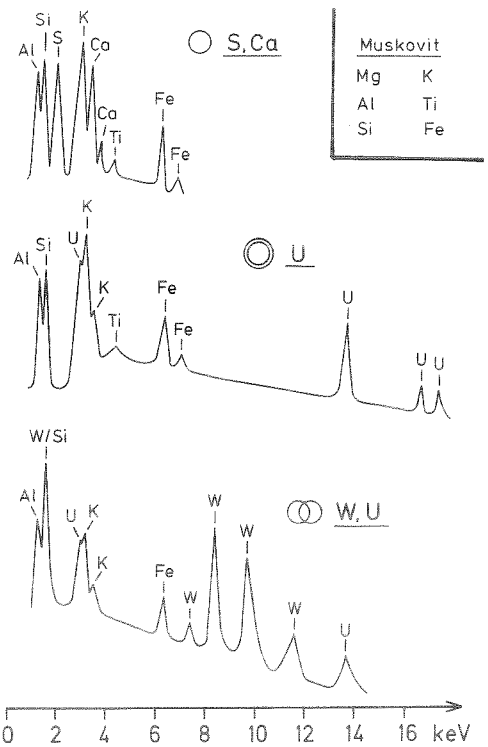


Fig. 3: X-ray fluorescence spectra of three different aerosol particles shown on Fig. 2 (a microprobe analysis).

[1] H.A. Khan et al., GSI Report 1980, p. 210
[2] G. Tress et al., Nuclear Tracks, 6 (1982) p. 87 - 97
[3] E.U. Khan et al. - this report -

B

Measurements of Aerosol Size Distributions with the Mica Microfilter Cascade Fractionator at the KfK-SASCHA

Ehsan Ullah Khan, G. Tress, R. Dersch, P. Vater, R. Brandt, Kernchemie, FB 14, Uni Marburg
H. Wild, H. Albrecht, KfK-Karlsruhe, Institut für Radiochemie

The KfK-SASCHA apparatus at the KfK, Karlsruhe, was developed for the determination of activity release and of aerosol characteristics under realistic light water core melting conditions. It is composed of a high-frequency induction furnace, a ThO_2 crucible system and an aerosol collection apparatus.[1] At Marburg a Mica Microfilter Cascade Fractionator has been developed[2] and has been tested at the above-mentioned apparatus. The aerosols were produced by melting at app. 1800° an artificial material "Corium" (150 g steel, 10 g Zircaloy, 30 g "Fissium", a material composed of uranium and inactive elements found among fission products - details are given in Ref. 1). The resulting aerosols were cooled down to T < 100 °C and send through our Cascade Fractionator, having four mica filters (F1 - F4). The average pore size k decreased from F1 to F4, all pores had rounded-off entrance channels, as described in ref. 3. The filters are characterized in the table.

The aerosols on each filter were photographed with the help of SEM. Typical pictures are shown in Fig. 1,2. The aerosol sizes were determined by fitting the best suited circles of known diameters to the aerosols such that both the areas of circle and aerosols were almost equal. Only those aerosols have been chosen for the size determination which lie on the planar mica surface (Fig. 1, 2) and not on the holes since in later case they can form clusters during the filtration process itself and thus we don't obtain the primary aerosol size distribution.

The entire aerosol size distribution is shown in Fig. 3. The mean value decreases from F1 down to F4, also the width of the distribution decreases. This clearly demonstrates that our Mica Microfilter Cascade Fractionator allows a useful analysis of aerosol size distributions. How this system compares with other systems has to be seen in the future.

Tabele:

Filter	k/µm	holes/cm²	porosity/%	load/mg
F 1	16.9	2.8×10^4	8.0	0.245
F 2	5.34	2.0×10^5	5.7	0.253
F 3	1.68	1.8×10^6	5.08	0.203
F 4	0.47	2.3×10^7	5.08	0.014

[1] H. Albrecht et al., Nuclear Technology 40 (1978) 278
[2] G. Tress et al., Nuclear Tracks 6 (1982) 87
[3] G. Tress et al. (this Annual GSI-report)

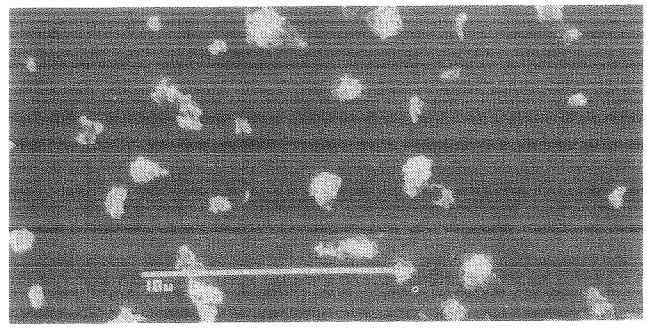


Fig. 1: The aerosoles on filter F 1.

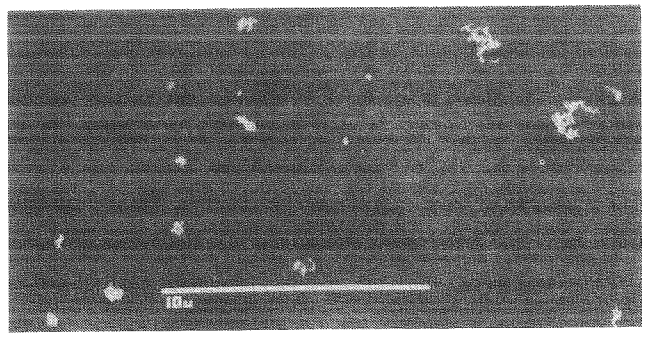


Fig. 2: The aerosoles on filter F 2.

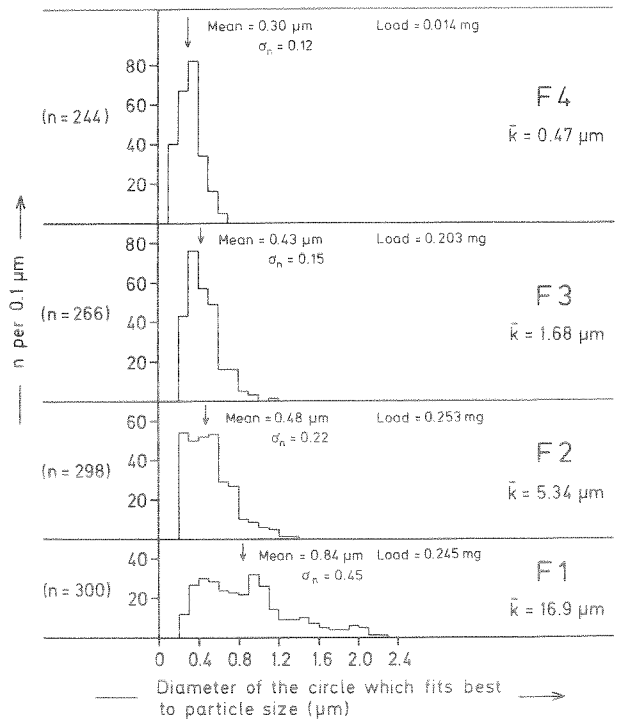


Fig. 3: Distribution of aerosole sizes on the four filters

A Research Program for Studying the Use of Ion Beam Techniques for Corrosion Protection

J. Dressler, H. Ferber, A. Meger, G. Reiss, G.K. Wolf. Physikalisch-Chemisches Institut der Universität Heidelberg

We started 1981 a program for testing potential applications of ion implantation and ion beam mixing in the field of corrosion. It is coordinated by the DECHEMA and funded by BMFT. We collaborate with corrosion departments of the companies Bayer and Krupp and with the Institut für Werkstoff-Forschung of DFVLR,Köln. A major part of the ion irradiations is done with the 300 keV accelerator at GSI. The following problems are under study:

1. Titanium/Palladium Alloys

Titanium, alloyed with 0,2% palladium, is commercially used for work pieces which are in contact with sulfuric acid. Pure titanium may lose its passivity in strong acids ($pH \ll 1$). Because of the high price of the bulk alloy, we studied the possibility of replacing it by surface alloys prepared by means of ion implantation or ion beam mixing. It could be shown that not only the implanted or mixed samples maintain their passivity, even in 20% H_2SO_4, but, have a dissolution rate lower by a factor of 10 than passive titanium without implanted palladium. The majority of samples stayed passive for nearly half a year in 20% H_2SO_4. The dissolution rates were determined by neutron activation analysis. From the results we calculated a lifetime of the passive layers in 1n H_2SO_4 of more than one year. The thermal and mechanical stability of the surface layers produced by ion irradiation is studied at present.

2. Stress Corrosion Cracking of Aluminum Alloys

Many aluminum alloys which are used for parts of aircrafts may undergo severe stress corrosion cracking. The initiation of cracks can be impeded by altering the texture of the near surface region of the metal. We investigate the potential of ion implantation for obtaining such effects. After a preliminary series of experiments it looks as if suitable implanted metals would have a beneficial effect on the time to failure when the tests are done under constant load, but not under constant strain rate. The experiments are continuing in order to get a more consistent picture of the mechanism.

3. Aqueous Corrosion of Iron and Steel

The corrosion properties of iron in aqueous neutral solutions can be improved in direction to the performance of stainless steel. Implantation of high doses of chromium or tantalum cause spontaneous passivation of the iron surface. Molybdenum ions have a beneficial effect on the pitting resistence of the material. Carbon steel is more difficult to alloy because of its carbon content leading to the formation of carbides. In addition to the improvement of the passivation of the metal one is also able to inhibit the active corrosion considerably. Implantation of elements with a low activity for the hydrogen redox reaction as lead or mercury may lower the active dissolution rate by more than one order of magnitude. Presently the long term behaviour of these iron surface alloys is under investigation.

Ion Beam Mixing-A Method for Modifying Catalysts

G.K. Wolf, K.Zucholl, Physikalisch-Chemisches Institut,der Universität Heidelberg

H. Folger, GSI Darmstadt

Recently we could show that ion implantation is a useful technique for preparing or modifying catalysts. Metals[1] as well as non-metals[2] have been used as substrates, noble metals as implant and the electrochemical oxidation of HCOOH, CH_3OH and reduction of H^+, O_2 as test reactions.

With implanted catalysts it is a problem to obtain a high enough concentration of the catalytically active element in the outermost monolayers of the substrate. The major part of the implanted ions penetrates into the bulk of the underlying material. In order to overcome this difficulty we started to test the potential of the ion beam mixing technique for this purpose. The principle of the method is to evaporate or sputter a thin layer of catalytically active material onto a suitable substrate and to intermix the two phases subsequently with an inert ion beam.

The method was studied with a Pt layer on a RuO_2 substrate, a system the performance of which we know very well from our former implantation work[2]. 1μm thick films of RuO_2 on tantalum foils were covered with 20 nm of platinum. Afterwork the phase intermixing was done with 10^{14}-$5x10^{16}$ Kr^+ ions of 150 keV from the GSI 300 kV accelerator. The electrochemical oxidation of formic acid and methanol in $HCLO_4$ was used for comparing the catalytic activity of the resulting surface alloys. In order to account for platinum losses from the surface, either by sputtering or by injection into the bulk of the substrate, the platinum concentration on the outermost layers was determined experimentally by a standardized reaction namely the oxidation of CO to CO_2.

The activity of the samples was determined by recording the potentiodynamic current/potential curves for the reactions mentioned above. All curves showed maxima in a certain potential region dependent on the individual reaction. The maximum values were normalized to the standard surface area and plotted as function of the ion dose applied for the mixing procedure. The results are plotted in figure 1.

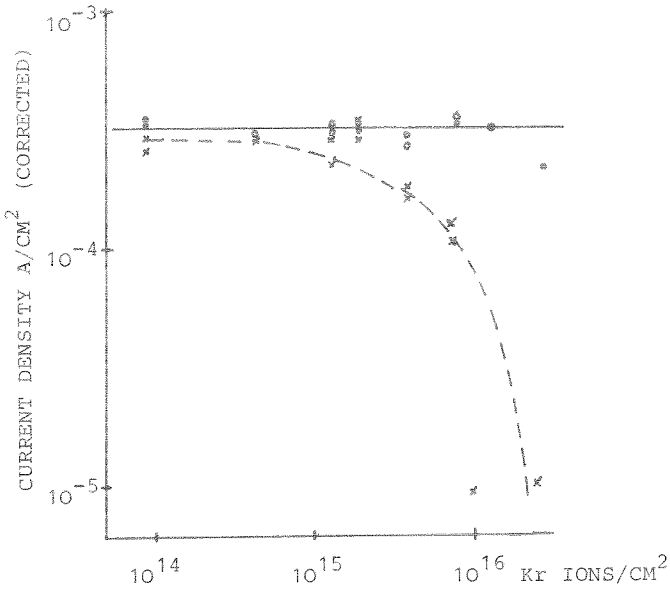


Fig.1: Current density maximum for the electrochemical oxidation of HCOOH (—o—) and CH_3OH (-*-) as function of the Kr ion dose used for intermixing a 20 nm thick Pt-layer with the RuO_2 substrate. The values are corrected for a standard surface area.

The formic acid oxidation is nearly independent on the degree of intermixing. The pure original Pt layer acts in the same way as the intermixed surface. The only difference is an increased mechanical stability of the mixed samples. However, the activity of the methanol oxidation decreases dramatically with increasing degree of intermixing, and approaches the very low values measured earlier[2] for implanted samples. This finding is consistent with the interpretation given already in [2]: HCOOH adsorbs at smooth platinum as well as at very small particles or even single atoms. Methanol adsorbs only at Pt particles above a certain minimum size. The exact dimensions above which the oxidation starts to take place are presently unknown.

[1] H.Kasten,G.K.Wolf, Electrochim. Acta 25 (1980) 1581

[2] G.K.Wolf, W.E. O'Grady, GSI-82-1 (1982) 201

[3] G.K.Wolf, K.Zucholl,H.Folger, W.E.O'Grady, IBMM-Conference,Grenoble 1982 (to be published in Nucl. Instr. Meth. 1983)

4. Developments

		PAGE
4.1	Target and Stripper Technology, Chemical Procedures	216
4.2	Experimental Set-Ups	223
4.3	Detectors	234
4.4	Electronics, Computing Center and Workshops	242

Survey on the Production of Nuclear Accelerator Targets G

H. Folger, W. Hartmann, J. Klemm and W. Thalheimer, GSI Darmstadt

U. Glatzel, Institut für Kernchemie, Universität Mainz

A wide variety of nuclear accelerator targets, target systems, backings, stripper foils, beam monitors, and thin conductive or protective layers has been prepared from various chemical elements, chemical compounds, as well as from stable enriched isotopes, and from the radioisotopes ^{232}Th and ^{238}U. Layers of thicknesses from 0.001 to 300 mg/cm^2, that is a variation of more than 6 orders of magnitude, were fabricated as self-supported foils or as thin films on appropriate backings. The number of requested targets increased promptly by a factor of about two after the up-grading of the UNILAC in 1981. The high intensity of the heavy-ion beam often destroyed targets, so that more and more target wheels were utilized successfully to reduce radiation damages; this increased, however, the number of targets to be prepared, as can be seen from a comparision of target requests in the last 3 years. (Standard targets are about 20x20 mm in size; larger dimensions are taken into account on this basis.)

Target Preparation Procedure	Number of Targets in: 1980	1981	1982
Cold rollings	2 400	1 220	3 101
Carbon sublimation-condensations	1 961	2 190	4 292
Focused ion-beam sputterings	120	110	90
Vacuum evaporation-condensations	2 020	1 810	3 517
Total numbers of targets	6 501	5 290	11 000

Cold rolling between stainless steel sheets is very efficient in the preparation of metallic layers of more than 1 mg/cm^2. Among others, milligram-amounts of oxides of dysprosium isotopes have been reduced with Hf in a high-vacuum reduction-distillation process before being rolled under argon in a glove box. The different materials rolled in 1982 are listed below:
Ag, ^{109}Ag, Al, Au, ^{48}Ca, Cd, ^{106}Cd, Cu, ^{63,65}Cu, Dy, ^{160,161,162,163,164}Dy, Fe, ^{56,58}Fe, Gd, Ho, Li, Lu, ^{24,25}Mg, Mo, ^{92,94,96,98,100}Mo, Nb, Ni, ^{58,64}Ni, ^{64}Ni/Pb, Pb, ^{208}Pb, Pb/Cu, Pd, ^{102,108,110}Pd, Ni/Pr/Ni, Rh, Sc, ^{147,154}Sm, Sn, ^{116}Sn, Ta, Th, Ti, U, Ni/U/Ni, V, W, Y, ^{64,68}Zn, Zr.

A substrate fixture for carbon sublimation-condensations was enlarged and improved to hold 8 substrate plates of 100x100 mm in the preparation of more than 4000 target backings, degraders, stripper foils, etc. of 0.003 to 0.1 mg/cm^2 in 1982.

Sputter deposition[1] with a focused beam of 1 mA Ar$^+$ at 10 kV has been used in the preparation of some special targets, as for instance self-supported Ta and ^{184}W. Other target systems were: Ag/C, Cr/C, Nd_2O_3/C, ^{64}Ni/Pb, ^{108,110}Pd, ^{96}Ru/C, Ta/Al, ^{90,94}Zr/C.

Numerous high-vacuum evaporation-condensations have been performed, applying resistive heating as well as direct or indirect electron bombardment in the evaporation of target materials. In one case only 10 mg of $^{130}BaF_2$ were available to prepare 3 targets of 1.3 mg/cm^2. Also a new procedure has been developed to prepare large amounts of 5x1 cm layers of Bi on C for the use on target wheels (fig.1). All target materials evaporated in 1982 were:
Ag, Ag/C, Al, Au, Au/C, Au/CR39, Au/mica, Au/Ti, BaF_2/C, $^{130,132}BaF_2$/C, Bi, Bi/C, C/Bi/C, CaF_2/C, Cd, ^{106,112,116}Cd, Co, Cr, Cr/st-steel, C/CsJ/C, Cu, Dy/C, Eu/C, Fe, Fe/Al, Ge/C, ^{74}Ge/C, Hf/Al, Ho/C, In, KBr/C, LaF_3/C, LiF/C, Lu, ^{25}Mg/Au, Ni, ^{58}Ni, Ni/C, Pb, ^{206,207,208}Pb, C/^{207}Pb/C, C/^{208}Pb/C, Pb/Cu, Pb/CR39, Pb/glass, Pd, Pd/Ni, Pd/Ti, Pt/RuO_2/Ta, Pt/Ta, ^{87}RbCl/C, Sc/C, ^{144,147}Sm, ^{154}Sm/C, Sn, ^{116}Sn, Ta, Ti, C/U/C, C/Ti/U/C, Ti/U/Ti, glass/Ni/U/Ni V, V/C, W, Y/C, Zr, st-steel/steel, st-steel/glass.

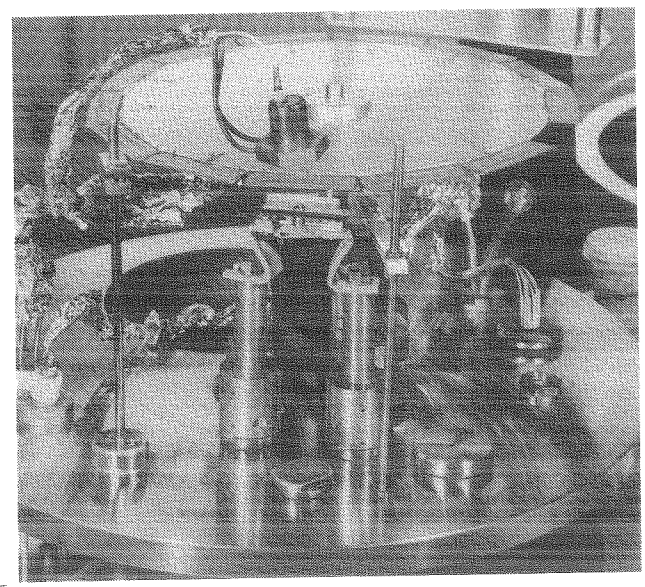


Fig. 1: Quartz controlled high-vacuum vapor deposition of homogeneous Bi layers to C backings on a rotating target-substrate fixture[2].

[1] H.Folger, J. Klemm and M. Müller, IEEE Trans. Nucl. Sci. Vol. NS 30, 1983.

[2] H. Folger, J. Klemm and W. Thalheimer, 11th Conf. of the International Nuclear Target Development Society, Seattle, Washington, USA, Oct. 1983.

Operational Conditions of a Duoplasmatron Ion-Source for Sputter Depositions of Nuclear Target Materials

H. Folger and M. Müller, GSI Darmstadt

The preparation of nuclear targets by sputter depositions with heavy ions strongly depends on the quality of the ion beam. Therefore, a duoplasmatron ion-source with einzellens extraction from a sputtering apparatus of the Sletten-type[1] was investigated at an ion-source test bench normally used for PIG-source experiments[2]. There, the source has to be operated at high positive potential; the ions are transported through a magnetic quadrupole doublet to a 77°5 analyzer magnet of a bending radius of 34 cm and of a maximum magnetic field strength of 0.7 tesla. A big aperture Faraday cup is placed in the focal point in the deflection plane for e/m-spectra recordings. A seperate cup is used for measurements of total extracted ion currents versus extraction voltages. As parameters the arc current, the gas pressure, and the filament current had been varied for beams of Ar ions of up to 30 kV and 1 mA DC.

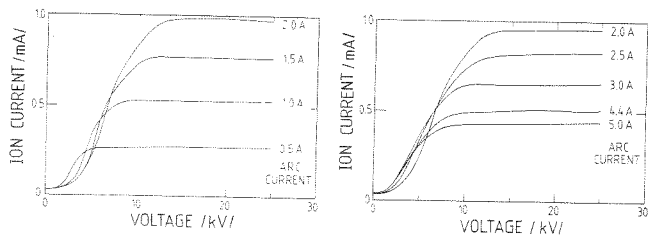


Fig. 1: Ion current vs. voltage diagrams for arc currents of 0.5 to 2.0 A (left) and 2.0 to 5.0 A (right).

Optimal ion-source discharge conditions at 20 kV extraction voltage have been derived from ion current versus voltage curves as shown for different arc currents in fig.1. The functional correlations between extracted ion current and arc current, gas pressure, or filament current, respectively, are given in fig.s 2 to 4.

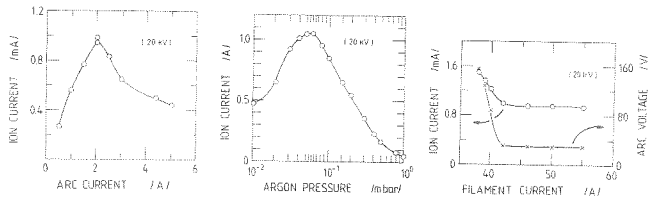


Fig. 2: Ion current as a function of arc current (left).

Fig. 3: Ion current in dependence of the Ar pressure in the ion source (center).

Fig. 4: Ion current (left scale) and arc voltage (right scale) as a function of the filament current of a Ta-wire of 8 mm in diameter (right).

An e/m-analysis of the ion-beam using a 77°5 magnet gives information on the charge states of the sputter-gas ions and on the relative amount of contaminations from extraneous source materials. - The Ar^+ charge-state predominates in all mass spectra. Particular discharge conditions corresponding to high parameter values produce growing ion-currents of Ar^{2+} and of impurities of light ions (C^+, H^+, H_2^+, etc.) in the beam. In the mass range between 50 and 180 AMUs only Fe^+ can be tentatively identified as possible contaminant of less than 2% of the Ar^+ current; heavier masses are not present down to about 10^{-3}% of the Ar^+ intensity. Differential ion currents derived from mass spectra are shown in fig.5 as a function of the arc current to demonstrate this general behaviour.

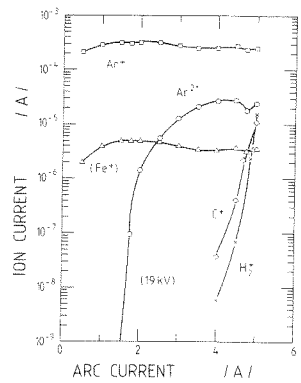


Fig. 5: Differential ion currents of the main components of an Ar^+-beam as a function of the arc current.

As a result from measuring the total currents in dependence of extraction voltages and from analyzing mass spectra obtained in different experiments the following optimum conditions for using the duoplasmatron ion-source in the preparation of nuclear targets by focused ion-beam sputtering[3] were derived: The extraction voltage should be higher than 12 kV, an arc current of 2 A is recommended which can be achieved at an argon gas pressure of 5.10^{-2} mbar and a filament current of more than 42 A using 0.8 mm diameter tantalum wires.

[1] G. Sletten and P. Knudsen, Nucl. Instr. and Meth. 102, 459 (1972).

[2] M. Müller, IEEE Trans. Nucl. Sci. Vol. 30, 1983.

[3] H. Folger, J. Klemm and M. Müller, IEEE Trans. Nucl. Sci. Vol. NS 30, 1983.

The Medium-Current Mass Separator

K.H. Behr, A. Brünle, C. Bruske, K. Burkard, W. Hüller, H. Kiesewetter,
R. Kirchner, W. Leiser, L. Molnar, F. Nickel, E. Roeckl
GSI Darmstadt

In 1982, the mounting of the medium-current mass separator [1] has been started in the experimental hall (see fig. 1). This separator will be used for the direct production of thin (~ mg/cm²) targets with high isotopic enrichment (> 99%)[2].

The housing for the Bernas-Nier ion sources is installed in a position which might allow a future on-line connection to UNILAC beams. The vacuum of the source region and the new ion source magnet was tested. The extraction chamber with the movable slit system, the collimator and the beam diagnosis region are completed. The double-focussing (n=0.5) 135°-magnet had been excited by the magnetic current supply (280 V, 100 A) to a field of approximately 0.6 T in the center of the 15 cm gap. In order to be able to correct the ion optics of the inhomogeneous magnetic field, so-called α- and β-coils[3] have been built and mounted to the pole faces of the magnet. A measurement of the magnetic fields from these coils proved that the first (~ 0.5) and second (~ 0.25) field index of the large magnet can be corrected satisfactorily within ± 10% (see fig. 2).

The vacuum chamber in the magnet region, the following focal plane chamber and the beam line region with the target position have been leak-tested. At the end of the beam line system, with an electrostatic quadrupole doublet followed by a deflection and retardation section, a target wheel is installed. This wheel is connected to the high voltage and can be wobbled mechanically in two directions; the mechanics of the wobbling system were tested in a long-time test under vacuum.

The vacuum system with 5 diffusion pumps, 5 roughing pumps, 20 valves and 11 vacuum gauges is controlled and regulated by an electronic unit being placed at the control console. An additional electronic system allows a specified control of the whole separator by a continuous registration of all relevant operation parameters.

Operation of the high voltage power supply (60 kV/100 mA) has been started, the stabilization up to a level of $2 \cdot 10^{-5}$ has however not been tested yet under working conditions with the ion source. The ion source power supplies are connected to the high voltage through insulating transformers and can directly be regulated from the console with the aid of an electronic interface system using fiber optic links.

1. K.H. Behr et al., GSI Scientific Report 1981, p.212
2. R. Meunier et al., Nucl. Instr. and Meth. 186(1981)7
3. J. Camplan et al., Nucl. Instr. and Meth. 186(1981)445

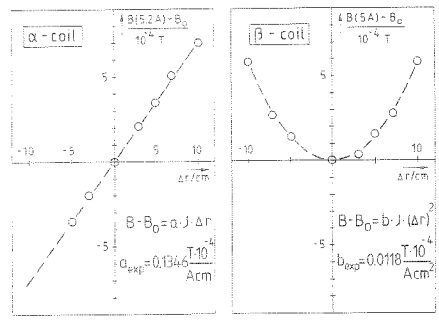


Fig. 2: The measured magnetic induction $B-B_0$ of the α- and β-coils (B_0 is the remanent induction of the magnet) as a function of the distance Δr from mean radius of the magnet and the current J of the exciting coil.

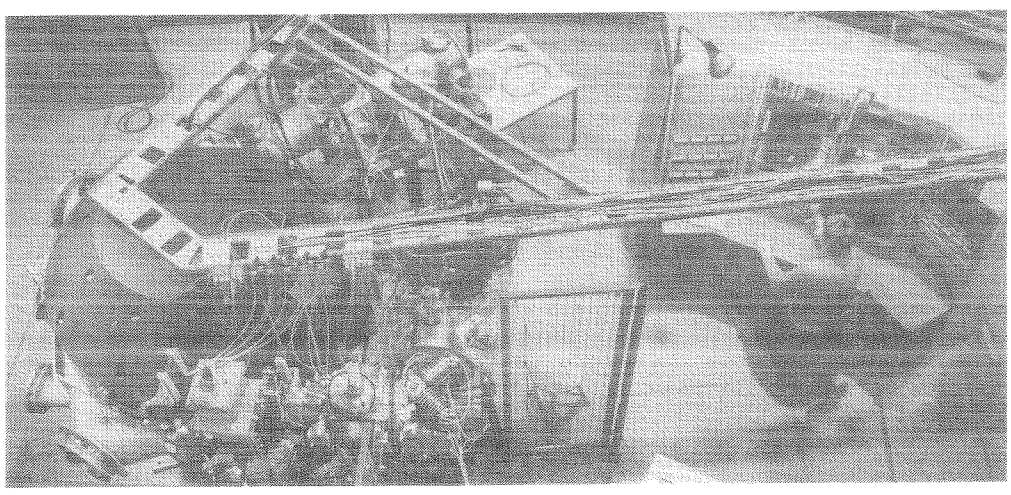


Fig. 1: General view of the separator

Preparation of Lanthanide and Actinide Samples by Vacuum Evaporation G

C. Frink, N. Trautmann, G. Herrmann
Institut für Kernchemie, Universität Mainz

M. Schädel
GSI, Darmstadt

For α- and spontaneous fission measurements of actinides and superheavy elements carrier free and homogenous sources are needed. Such sources can be prepared by various techniques[1], most of them are time consuming and, therefore, investigations of short lived nuclides are hampered. For lanthanides and actinides with low evaporation heat samples can be prepared within short times by reduction on a metallic surface with subsequent evaporation and deposition on a cold catcher.

The reducing material must be a thermic stable metal with low adsorption energy such as titanium or zirconium[2].

In this work experiments with Eu-152, Sm-155 and Am-241 as representatives for lanthanides and actinides were performed in order to determine the optimum evaporation and deposition conditions. The lanthanide activities were produced by neutron irradiations in the Mainz reactor. All the experiments were carried out in a vacuum system as shown in Fig. 1.

In each case 10 µl of a nitrate solution was transfered to a titanium crucible and evaporated to dryness converting the nitrate to the oxide. Then the crucible was fixed between two copper holders in the recipient of the vacuum system and the catcher was placed in a distance of some millimeters above the crucible. At a pressure of 2×10^{-5} mbar the crucible was heated by resistance heating for a predetermined time. The temperature of the crucible was measured with a pyrometer. The evaporation and deposition yields were determined after the end of the experiment by γ-spectroscopic measurements of the crucible and the catcher.

The investigated nuclides have been evaporated with a yield of 60-72 % at a temperature of 1000 °C and with 93-95 % at 1070 °C or higher temperatures. The shape of the crucible and the distance between crucible-catcher have great influence on the deposition yields. Crucibles with a large aperture deliver only 20-30 % of the original activity to the collector. If the distance between crucible and catcher is varied from 3 to 10 mm the deposition yield decreases from 85 % (3 mm) to 54 % (10 mm) for Eu-152. This can be explained by the fact that the evaporated activity is not completely collected on an aluminum catcher of 28 mm x 37 mm as shown by audioradiography. At a distance of 3 mm homogenous samples of 12 mm diameter were obtained while at 10 mm the spot smeared out. The evaporization of the investigated nuclides at a temperature of 1070 °C takes 40-60 s. At higher temperatures (1140 °C) the time is reduced to about 20 s.

The adaption of this technique to a fast automatic high performance liquid chromatography system[3] requires a cylindric crucible with a hole of 6 mm and a volume of about 1 ml. Evaporation rates of ∿ 85 % (1150 °C) and deposition yields of ∿ 70 % were obtained with this type of crucible at a crucible-catcher distance of 4 mm and an evaporation time of 60-80 s.

The good quality of the samples obtained with this method was checked with Am-241 samples and α-spectromeric measurements with a surface barrier detector yielding a FWHM of 32 keV compared to a FWHM of 37 keV achieved with samples prepared by molecular plating .

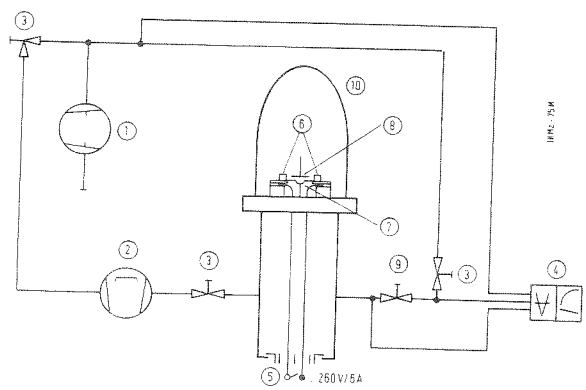


Fig. 1: Schematic diagram of the evaporation system ① ② pumps; ③ ⑨ valves; ④ vacuummeter; ⑤ ⑥ resistance heating; ⑦ crucible; ⑧ catcher; ⑩ quartz bell

1 W. van der Eijk et al, Nucl. Instr. Meth. 112, 343 (1978)

2 E. Rhede et al., Zentralinstitut für Kernforschung Rossendorf ZfK 367 (1978) S. 23

3 W. Schorstein et al. GSI Scientific Report 82-1, 220 (1981)

Chemical Separation of Thorium, Protactinium, Uranium, Neptunium and Plutonium from Complex Heavy Ion Reaction Product Mixtures [G]

M. Lerch, U. de la Chevallerie, D. Gembalies-Datz, W. Kieling, J.-V. Kratz, A. Lewening, N. Trautmann, S. Zauner, G. Herrmann

Institut für Kernchemie, Universität Mainz

A method for the separation of Th, Pa, U, Np and Pu from heavy ion reaction product mixtures was developed for i) the measurement of cross-sections for sub-Coulomb transfer in collisions of ^{238}U with ^{238}U and ii) the radiochemical determination of actinide cross-sections in the $^{48}Ca+^{248}Cm$ reaction. The separation is based on differences in the ion exchange behaviour of these elements from hydrochloric and nitric acid solutions.

Pa, U, Np and Pu form strong chloro-complexes which can be adsorbed from 8 N HCl on an anion exchange column whereas Th and the transplutonium elements (TPE) pass through. Th is adsorbed from 8 N HNO_3 on a second anion exchange column while the transplutonium elements are not retained. Desorbents for the subsequent elution of Th, Pa, U, Np and Pu are summarized in Table 1.

Table 1

Separation of Th, Pa, U, Np and Pu on anion exchange columns (BioRad AG 1x8, -400 mesh)

	element	desorption with
1st anion exchange column; adsorption from 8 N HCl	Th + TPE	8 N HCl
	Pa	8 N HCl/0.05 N HF
	Pu	8 N HCl/NH_2OH·HCl/NH_4I
	Np	4 N HCl/0.05 N HF
	U	0.5 N HCl
2nd anion exchange column; adsorption from 8 N HNO_3	TPE	8 N HNO_3
	Th	2 N HCl

In the $^{238}U+^{238}U$ experiments[1], targets and recoil product catchers were processed separately, since the initial dissolution steps are different for the uranium targets and the gold catcher foils.

The uranium targets on titanium backings were dissolved in hot 10 N HCl/0.01 N HF. With H_3BO_3 the fluoride complexes were destroyed and with a few drops of conc. HNO_3, Pu(III) was oxidized to Pu(IV) before column injection. The gold catcher foils after segmentation into bins of laboratory angles were dissolved in aqua regia and Au was removed by extraction with diethyl ether. After evaporation and dissolution in 8 N HCl, the aqueous phase was submitted to column separation.

Counting sources of Pa and Np for γ-spectroscopic measurements were prepared by coprecipitation of these elements with $Fe(OH)_3$. U from the target processing was precipitated as $(NH_4)_2U_2O_7$. Th, Pu and U from the catcher treatment were electrodeposited on tantalum foils for α-particle spectroscopy. Before electrolysis traces of iodine had to be removed from the plutonium fraction. Therefore, Pu was coprecipitated with $Zr(OH)_4$, the precipitate dissolved in 0.5 N HCl/0.025 N HF and, after reduction of Pu with NH_2OH·HCl, transferred to a small cation exchange column. The fluoro-complex of Zr passed through while Pu was adsorbed and could be eluted with 4 N HCl.

For the measurement of cross-sections for relatively short-lived transfer products (e.g. 37 min ^{236}Th, 8.7 min ^{237}Pa etc.) in the $^{238}U+^{238}U$ system[1] chemical separations and the preparation of suitable counting samples had to be accomplished rapidly. Separate processing of the targets and the catcher foils - in these experiments Cu was used as catcher material - was necessary.

The targets were dissolved in a HCl/HF mixture. The copper catcher foils were dissolved in a hot mixture of conc. HCl and HNO_3 (3:8) and the actinides were coprecipitated with $La(OH)_3$ using ammonia. In this step Cu was removed as the diamine complex. Pa was isolated from the feed solutions resulting from the dissolution of the targets and the $La(OH)_3$ precipitate by extraction chromatography with di-isobutylcarbinol (DIBC). Then Th and U were separated by ion exchange (see Tab.1).

Sources for γ-ray spectroscopy were prepared by coprecipitation of Th, Pa and U with $Fe(OH)_3$. In the target processing U was precipitated as $(NH_4)_2U_2O_7$.

In the $^{48}Ca+^{248}Cm$ experiment[2] the reaction products were stopped in a copper catcher foil. After removal of volatile elements by a gas-phase chemistry the catcher was dissolved in dilute HBr and this solution passed through a cation exchange column. With 0.1 N and 0.8 N HBr the SHE fraction was eluted. Then U and Cu were eluted with 2.5 N HCl containing a few drops of bromine, the actinides were desorbed with 6 N HCl, and finally Th with oxalic acid. The actinide and the U/Cu fractions - after removal of Cu as the diamine complex in a $La(OH)_3$ precipitation step - were treated as described in Table 1. The thorium fraction after conversion to the nitrate system was injected onto an anion exchange column.

Th, Pa and U were electrodeposited directly from the effluents of the anion exchange columns. The plutonium fraction had to be purified prior to electrolysis as described before.

[1] G. Wirth et al., this report

[2] H. Gäggeler et al., this report

Rapid Preparation and Gaschromatographic Separation of Carrier-Free Lanthanide Hexafluoracetylacetonates [G]

N. Greulich, N. Trautmann, G. Herrmann
Institut für Kernchemie, Universität Mainz

The investigation of neutron-rich or neutron-deficient actinide nuclides produced in heavy-ion reactions requires fast procedures for their isolation. For unravelling actinide or lanthanide mixtures, multistep processes have to be applied. Gaschromatography is one powerful tool for the fast separation of small quantities, because the mobile phase can be operated with a high flow-rate without losses in separation efficiency. A prerequisite for rapid performance is the fast preparation or formation of volatile compounds with subsequent separation in a gaschromatograph. Due to their similar chemical properties homologous lanthanide elements can be used to study the applicability of gaschromatographic methods for the isolation of actinides.

Carrier-free lanthanide isotopes were produced by neutron induced fission of ^{235}U and were transported continuously with a KCl/N_2-gasjet out of the target chamber. The KCl-clusters, together with the attached fission-products, were trapped in two glass-fiber filters. After 30 min of irradiation time, they were dissolved in an aqueous solution of NaH_2PO_2. A reducing agent is required for quantitative extraction of lanthanides at moderate pH-values. The lanthanides, together with some other fission products, are extracted within 10 s with a mixture of 0.05 M hexafluoracetylacetone (HHFA) / 0.035 M tri-n-butylphosphate (TBP) in cyclohexane[1]. The distribution coefficients for some lanthanides and other fission products from various aqueous phases into a 0.05 M HHFA/ 0.035 M TBP cyclohexane solution are given in table 1. Obviously, a reducing aqueous medium gives the best extraction yields for yttrium and the lanthanides and the lowest values for undesired accompanying fission products.

For the gaschromatographic separation of yttrium and the lanthanides, 0.1 ml of the organic phase is syringed into the injector of a gaschromatograph[2]. With a carrier-gas (70 ml/min N_2) loaded with HHFA passing the N_2 through HHFA at 40°C, a decomposition of the β-diketonates in the column (2 m long, glass, 2.4 mm inner diameter, 1% PPE 20 on Chromosorb G 80-100 mesh) is prevented. The injection temperature was kept at 250°C, the column temperature was increased from 150°C to 250°C with a rate of 10 °C/min. Fig. 1 shows a chromatogram obtained under these conditions, together with the temperature gradient. Iodine, which is partly extracted, appears first in the eluate, then yttrium followed by the individual lanthanides according to their decreasing ionic radii of the threevalent states. The gap between yttrium and the lighter lanthanides can be explained by its relatively large radius of 0.89 Å which corresponds to that of Ho^{3+}. Total retention times between 3.5 (Y) and 12.5 min (La) were measured. The alkaline earth elements also extracted into the organic phase (see table 1) are not volatilized. The described method should also allow the separation of individual actinide elements within a few minutes.

1 W.C. Butts and C.V. Banks, Anal. Chem. 42, 133 (1970)
2 N. Greulich, N. Trautmann and G. Herrmann, GSI Scientific Report 82-1, 219 (1981)

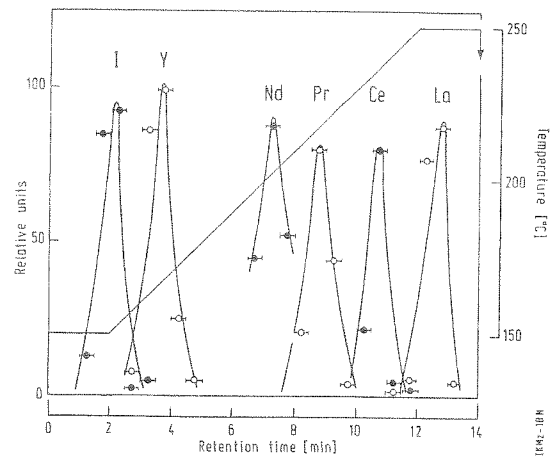


Fig. 1 Separation of lanthanide hexafluoracetylacetonates by temperature-programmed gaschromatography

Table 1
Distribution coefficients for the extraction of lanthanides and some other fission products from various aqueous phases with 0.05 M HHFA/0.035 M TBP in cyclohexane

Element	aqueous phase		
	0.3 m Na_2PO_2	H_2O	0.3 m H_2O_2
Y	141	74	1.9
La	∞	52	1.1
Ce	41	66	3.5
Pr	68	75	2.0
Nd	∞	∞	2.1
Mo	3.10^{-3}	3.10^{-3}	0
Tc	0	4.10^{-3}	0
Rb	0	0.012	-
Cs	0	0.011	0.03
Sr	1.47	1.73	1.39
Ba	1.32	1.10	1.25
Te	0.38	0.52	0.49
I	0.72	0.91	0.57

0 = not detectable in the organic phase
∞ = not detectable in the aqueous phase

Performance of the Darmstadt-Heidelberg Crystal Ball

B G

R. Albrecht, B. Kolb, R.S. Simon, GSI Darmstadt
H. Gräf, W. Hennerici, H.J. Hennrich, G. Himmele, E. Jaeschke, O. Koschorrek, R. Repnow, W. Wahl
MPI für Kernphysik Heidelberg
D. Habs, K. Helmer, U.v. Helmolt, H.W. Heyng, H. Krieger, R. Kroth, D. Pelte, D. Schwalm, Universität Heidelberg
R.D. Fischer, W. Kühn, V. Metag, R. Mühlhans, Universität Gießen

The crystal ball is a modularized NaI detector for γ-radiation. The detector comprises 162 individual elements of equal solid angle that from a complete spherical shell of scintillator material which is 20 cm thick and which has an inner free diameter of 50 cm. A joint project of GSI Darmstadt, the Max-Planck-Institute and the University of Heidelberg, the crystal ball and its specially designed data acquisition system have gone into operation at the tandem laboratory in Heidelberg.

The crystal ball offers unique possibilities to investigate the complex γ decay chains typical for in-beam experiments: Its 4π geometry allows to register the full γ cascade of a given event; its modular structure provides enough spatial resolution to distinguish the individual γ transitions; its overall size finally is sufficient to separate γ rays and reaction neutrons by time of flight. In the following we briefly discuss the relevant detector parameters which are summarized in Table 1.

The most important observables in the crystal ball are the total γ decay energy and the corresponding γ ray multiplicity. They are determined from the pulseheights of the responding modules and from their number, respectively, and reflect the nuclear excitation and the initial angular momentum at the start of the γ cascade. Energy and multiplicity resolution both depend on the detection probabilities for the individual γ rays. In addition details of the detector response enter, like the actual energy deposited per γ quantum in the energy measurement or the competition between crosstalk and multiple hits in the determination of the multiplicity. By successively folding single γ events from calibration sources we are able to simulate the detection of long γ cascades experimentally.

The γ cascades following compound nucleus formation often are dominated by stretched-E2 transitions and the $(1-\cos^4\theta)$ distribution of this component may be exploited to determine the direction of the nuclear spin in addition to its magnitude. Thus the crystal ball provides the possibility to study angular correlation effects relative to the spin rather than to the beam direction and to take advantage of the larger anisotropies expected there.

Each crystal ball element and its next neighbours represent an anticompton arrangement. Isolated hits with their favourable peak/total ratios most likely show full energies and provide a rather direct view of the transition energy spectrum at NaI resolution. In the $^{128}Te+^{34}S$ reaction at 155 MeV for example we observe 6-7 isolated hits per cascade on the average and one may combine their pulseheights into pairs or triplets to investigate the transition energy correlations in the γ decay.

The efficiency of the crystal ball to neutrons is comparable to its γ ray efficiency. In the $^{128}Te+^{34}S$ example we find a clear correlation between neutron and γ multiplicity: more γ rays in this compound nucleus reaction mean fewer neutrons as expected from the different angular momentum bins of the 4n and 5n channel. Taken together the two multiplicities may help to suppress prompt background radiation from reactions with light target impurities where the neutron/γ ratio is different.

The crystal ball may be combined with high resolution Ge detectors by exchanging a few of its NaI modules or it can be supplemented by particle detectors that are installed within the NaI shell. Our present experiments that cover in-beam γ ray spectroscopy as well as the study of rare decay modes with radioactive sources already show the broad range of applications for the new spectrometer.

Table 1: Parameters of the crystal ball[a)]

individual γ (example 1.17 MeV):	
total efficiency	0.968
energy resolution (fwhm)	5.9 %
average energy depos. (full CB)	1.04 MeV
peak/total (anticompton)	0.72
time resolution (fwhm)	2.8ns
direction	±7 degree
γ cascade (example 30 x 1.17 MeV):	
sum energy	30.3 ± 2.7 MeV
responding modules	35.7 ± 4.2
isolated hits	5 ± 2
n cascade (example $^{128}Te(^{34}S, 4n)^{158}Er$, 155 MeV)	
sum energy deposited	7 ± 5 MeV
responding modules	6.5 ± 4.0

[a)] electronic threshold for individual detector module < 70 keV

Monte-Carlo simulation of a HPGe-BGO Compton Suppression Spectrometer

C. Michel, F. Azgui, H. Emling, E. Grosse, H.J. Wollersheim, GSI Darmstadt

The use of arrays of Compton Suppression Spectrometers (CSS) in in-beam γ-ray spectroscopy has been proposed in many laboratories. Nowadays compact arrays can be built using Bismuth Germanate (BGO) crystals. As this material remains rather expensive, careful design studies should be undertaken in order to optimize the CSS characteristics. We have investigated the performance of CSS set-ups consisting of HPGe detectors coupled to BGO scintillators in various configurations using the EGS (Electron Gamma Shower) code system[1] whose use is now generalized in high energy physics.

The reliability of such Monte-Carlo type calculations was tested by comparing them with absolute Germanium peak-efficiencies measured for γ-ray energies up to 12 MeV. Full Energy (FE), Single Escape(SE) and Double Escape (DE) peak-efficiencies or their various ratios R=DE/SE, R'=SE/FE and R''=DE/FE have been measured by Seyfarth et al.[2] for a 38 cc coaxial Ge(Li). The experimental ratios are shown in fig.1 while fig.2 displays the results of our EGS calculations. As can be seen, the agreement is excellent; the R function is independent of energy and solid angle but is sensitive to the active volume of the crystal; the absolute FE peak-efficiency can be reproduced acurately only when the active volume and the solid angle of the detector are well known. Such calculations take into account the presence of an inert core, the dead layer and aluminium housing of the Germanium detector.

The properties of several CSS's have been calculated for various symmetric and asymmetric configurations, simulating single γ-ray sources and γ-ray cascades with high multiplicities; the influence of factors such as the dimensions, shielding, dead layer thickness of the Germanium and summing effects have been studied. The results of these investigations will be detailed in a forthcoming publication. Here we will show only a few results of such calculations in order to illustrate the power of the method. The upper part of fig.3 displays ^{60}Co spectra calculated with and without anti-Compton veto in the geometry proposed for the OSIRIS CSS array.[3] The geometry is shown in the insert and is characterised by two parameters, A and B, which define the size of the crystal; for this particular case, they were fixed to 30 and 100 mm respectively. The lower part of fig.3 shows the corresponding Compton suppression factor (CSF). Several calculations were carried out by selecting various sets of values for the parameters A and B and choosing different γ-ray sources to optimize the performance/cost ratio of this CSS. Similarily any other geometry can be studied and we are presently performing an optimization for a CSS to be used in Coulomb excitation and (heavy ion,xn) reactions at the UNILAC.

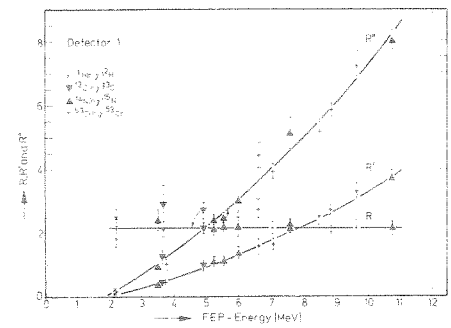


fig.1: Peak-efficiency ratios versus γ-ray energy as measured for a 38 cc coaxial Ge(Li).[1] (R,R' and R'' are defined in the text)

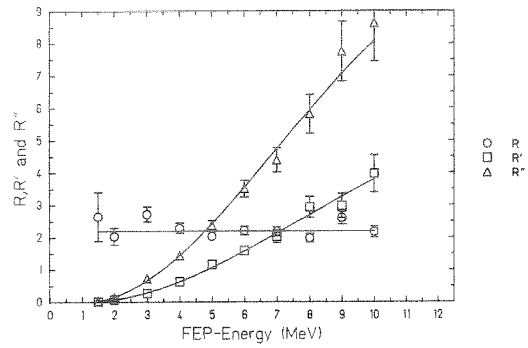


fig.2: Peak-efficiency ratios as calculated with EGS. As in fig.1, the drawn lines are a polynomial fit to guide the eye.

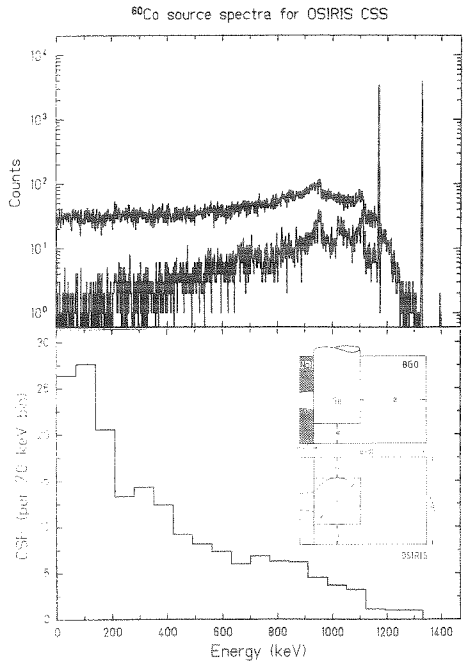


fig.3: The upper part displays calculated ^{60}Co spectra with and without anti-Compton veto for the OSIRIS ACS shown in the insert. The lower part shows the corresponding Compton Suppression Factor.

References

1) R.L.Ford and W.R.Nelson, The EGS code system SLAC Report-210 Stanford
2) H.Seyfarth et al.,Nucl.Instr.and Meth. 105(1972)301
3) R.M.Lieder, private communication

High-Efficiency Set-up for Binary Reactions Studies

Dai Guang-xi*, H. Daues, S. Gralla, H. Stelzer and J. Tōke+
GSI Darmstadt

Studies of the formation and decay of metastable heavy nuclear complexes (Z_{tot}≈100-115) require the observation of the differential reaction cross section over a broad range of masses and over the full range of center of mass scattering angles. In earlier experiments a ring counter set-up has been successfully used, which allowed to reconstruct the reaction kinematics from the measured velocity vectors. Based on essentially the same ideas a new set-up has now been devised which again exploits the advantages of the inverted kinematics (concentration of the binary producs in the forward laboratory hemisphere) but which at the same time is free from some important limitations of the old ring counter set-up. The new set-up consists of 4 rectangular parallel-plate counters each of which has an active area of 20 x 30 cm^2 and measures the position in x and y with a precision of 4 mm and the time with a resolution of about 1 ns. The angular range covered by these counters can be inferred from the scatter plot of the measured events shown in Fig. 1. (Angles ϑ and ϕ refer to the polar coordinate system oriented with the z-axis along the beam direction and the x-axis along the vertical direction).

The new set-up offers the following advantages with respect to the old one: (i) It covers a larger range of laboratory angles (2° to 65°) and thus allows to extend the center-of-mass angular range to the extreme forward and backward angles which are of particular interest, (ii) it allows longer flight paths (~60 cm at forward angles for counters A and B, and ~35 cm at larger angles for counters C and D) and thus a more accurate measurement of the velocity vectors, (iii) it provides energy-loss information which is important for a reliable elimination of the random coincidences between the two small-angle counters (see Fig. 2), (iv) it can also register elastic and quasielastic products with a rate which can be properly reduced in order not to undermine the recording of the other, lower cross section events. In contrast to the ring counter the new set-up has an azimuthal acceptance, which for binary events is a function of the two scattering angles. This is taken into account in the data analysis by weighting the yields appropriately on the event-by-event basis. Figs. 1 to 3 present results of the reaction $^{238}U + ^{27}Al$ at 6 MeV/u, which demonstrate the performance of the set-up.

*A.v.Humboldt-Fellow, IMP, Lanzhou, P. R. of China
++on leave from Warsaw University, Poland

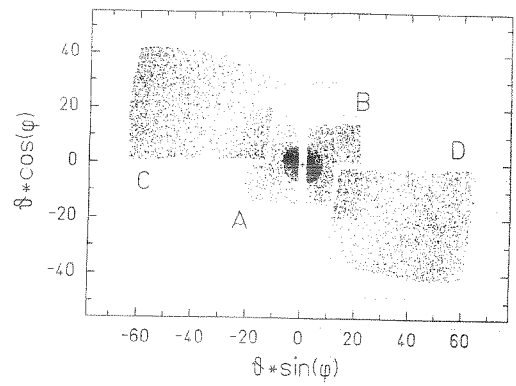


Fig. 1: Scatter plot of the registered events.

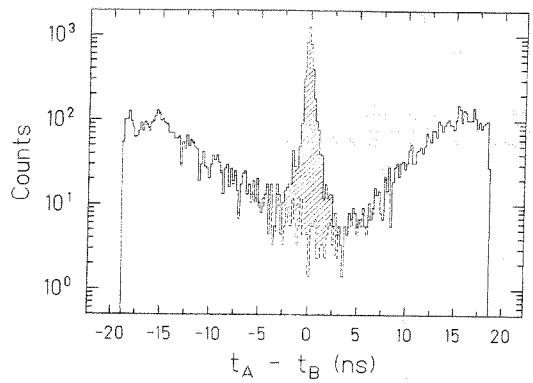


Fig. 2: Quality of the elimination of random coincidences: Shown is the spectrum of the time difference between counters A and B; hatched area represents the yield corresponding to the events which are rejected based on a combined time-difference, energy-loss and lab.-angle condition.

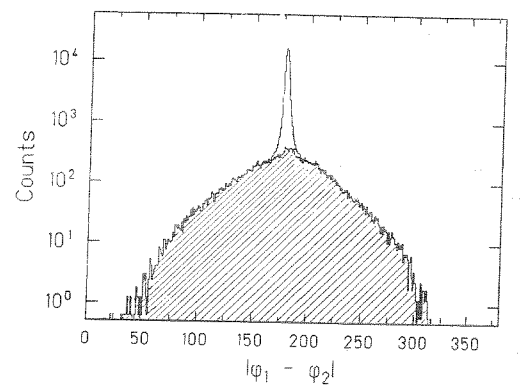


Fig. 3: Quality of the selection of binary events: Shown is the spectrum of the difference in azimuthal angle for coincident ejectiles; the hatched area represents the yield corresponding to the events which were rejected based on the collinearity (in c.m.) condition.

A lead glass Cherenkov hodoscope as neutral pion spectrometer

C.Michel, P.Braun-Munzinger[1], C.Brendel[2], H.Dabrowski[+],
E.Grosse, H.Heckwolf, O.Klepper, W.F.J.Mueller,
H.Noll[3], W.Rosch[2], H.Stelzer
GSI Darmstadt, [1]SUNY Stony Brook, [2]TH Darmstadt, [3]IKF Frankfurt
[+] on leave of absence from INP Cracow

The π^0 produced in subthreshold heavy-ion collisions[1] are detected via their decay into two γ-rays in a Cherenkov detector hodoscope. This detector consists of two concentric lead glass (LG) rings with an intermediate layer of multiwire proportional chambers (MWPC). Such a Cherenkov type detector was choosen for its high proton threshold (about 230 MeV) and its rather low efficiency for neutron and proton detection.[2] We select the SF5 lead glass for its rather high lead contents. The inner ring acts as an active γ-ray converter; it is 1.9 χ_0 thick (1 radiation length χ_0 is 2.34 cm) and consists out of 10 pieces covering 30° each. The outer ring has 6.4 χ_0 and absorbs most of the energy of the shower created by the γ-rays; it is subdivided into 20 pieces of 15° each. In the vertical direction the opening angle is 30°. The centroid of the lepton distribution emerging from the converters is localized in the MWPC's. The spatial resolution of the chambers can be obtained combining their intrinsic resolution (2 mm) to the shower spread which depends on the γ-ray energy. Each of the 10 chambers has an active surface of 7 X 9 cm^2. The MWPC's are read out by delay lines for each coordinate. A schematic layout of the set-up is shown in fig.1.

A π^0 is registered when a valid γ-ray signal is seen in at least 2 cells of the hodoscope and a γ-ray is accepted in one cell when the converter is coincident with at least one of the absorbers of the same cell. The MWPC are not taking part in the trigger logic and are only read when at least one LG in a cell is flagged (read trigger).

The detection efficiency for photons as function of their energy was calculated by Monte Carlo techniques using the EGS (Electron Gamma Shower) system code[3]. The Cherenkov light transport inside the LG and the collection efficiency of the photomultipliers were adjusted to reproduce experimental spectra for the $\pi^- + p \rightarrow \pi^0 + n$ charge exchange reaction. The observed signals correspond to approximately 0.6 photoelectron/MeV. The γ-ray energy resolution in the Cherenkov detectors, the MWPC efficiencies (the probability to have at least one lepton coming out of the converter) and the contribution to the spatial resolution of the MWPC due to the shower propagation were also calculated using the EGS system code.

The π^0 detection efficiency, their energy and angular resolutions can be calculated combining the π^0-decay kinematics with the γ-ray detection efficiency. These functions depend simultaneously on the γ-ray energy and angular resolutions. As the γ-ray angular information can be obtained either from the MWPC's or from the natural segmentation of the hodoscope, two π^0 detection efficiencies can be defined; the one calculated with the natural segmentation is shown in fig.2 as a function of the π^0 kinetic energy and the emission angle in the laboratory system. As can be seen, such a set-up is able to measure complete energy and angular distributions with an efficiency of about 1%. This hodoscope can easily detect π^0 up to 210 MeV kinetic energy. For higher energies, the efficiency is reduced since the symmetric π^0-decay leads to angles between the two γ-rays smaller than 45° and in this range the hodoscope segmentation is not good enough to discriminate a good π^0 event from a shower spread over neighbouring cells. The π^0 invariant mass spectra as measured from the $^{12}C + ^{12}C$ reaction at 84 MeV/u at the Cern SC is shown in fig.3; the invariant mass resolution is about 50% and is mainly governed by the γ-ray resolution. As can be seen, the π^0 signal can clearly be separated from the background. The sensitivity we obtained is about 100 pb/MeV. We hope to gain a factor of 10 by shielding the hodoscope against cosmic radiation.

1) H. Noll et al., this report
2) M. Lebrun et al., Nucl.Instr.Meth. 166(1979)151
3) R.L. Ford and W.R. Nelson, The EGS Code System, SLAC Report 210 Stanford(CA)

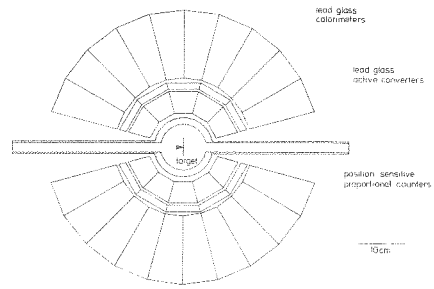


Fig.1: Lay-out of the π^0 spectrometer

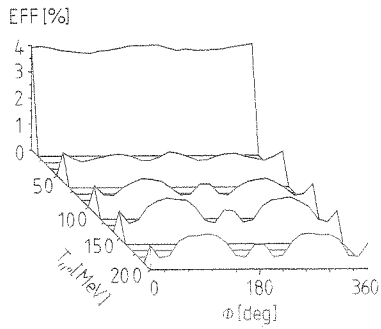


Fig.2: Pion detection efficiency in the lab. frame plotted versus the pion angle at five kinetic energies 1,50,100,150 and 200 MeV.

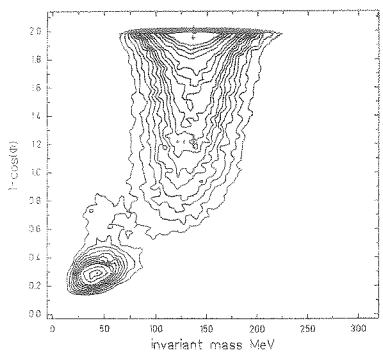


Fig.3: Invariant mass plot for π^0 produced in the C + C collision at 84 MeV/u. The pion yield is displayed versus the invariant mass and (1-cos ϕ) where ϕ is the angle between the two γ-rays.

Improvements to the Plastic Ball [G]

H.H. Gutbrod, B. Kolb, H. Löhner, A.M. Poskanzer, T. Renner,
H. Riedesel, H.G. Ritter, A. Warwick, F. Weik, H. Wieman
GSI Darmstadt, LBL Berkeley, and Universität Marburg

After the first round of experiments in 1981, several hardware modifications were made to the Plastic Ball[1] to improve its performance or to facilitate calibration procedures.

Several photomultiplier tubes, which all were glued to the lucite lightguide, broke off, resulting in a reduced light collection efficiency of ~50%. A new springmount was built to prevent this breakage for each photomultiplier and installed before the new round of experiments in 1982.

For the pulse-shape analysis a fully passive 50Ω 4-way split has been introduced, which helped improve the efficiency for π^+ detection. Furthermore, the early AMP-multiconnectors for the 25-fold coaxial ribbon cables had to be modified to prevent the pins from being pushed back. The electronic "Ball boxes" were modified to allow the use of a delayed multiplicity trigger, which will be used in the 1983 experiments.

For the Plastic Wall it became clear that the LED pulser system with its slowly rising pulses was not convenient for an on-line time calibration. Therefore, a N_2-Laser system was built that supplies all Wall modules with short pulses of light monitored by a pin diode. Thus, the Wall stability in the ADC- as well as in the TDC-channels can be checked on-line. Figure 1 shows the layout of the Laser system. An overall intensity variation is obtained via the Laser-light aperture, whereas an individual light intensity variation in each fiber optics channel is made possible by polarisation filters.

To improve the on- and off-line analysis, the computer system was largely expanded by the addition of a VAX 11/780 computer. This computer replaces in the on-line mode the PDP 11-44, which in turn replaces the PDP 11/50, increasing the speed of the front end.

A further improvement was achieved by integrating into the CAMAC system the CERN-Romulus Processor, which controls all fast LRS 2228A and LRS 2229 TDCs. This added intelligence in the CAMAC reduced the readout time by about 500 μsec.

For the off-line use the VAX 11/780 is coupled via DECNET to most of the LBL computers. Whereas the big processing of the raw data tapes is still done at the LBL CDC-7600 these newly generated tapes are then played into the large disk space at the VAX for further analysis. The GSI streamer chamber group is the other user of the VAX.

[1] A. Baden et al., Nucl. Instr. Meth. 203, 189 (1982).

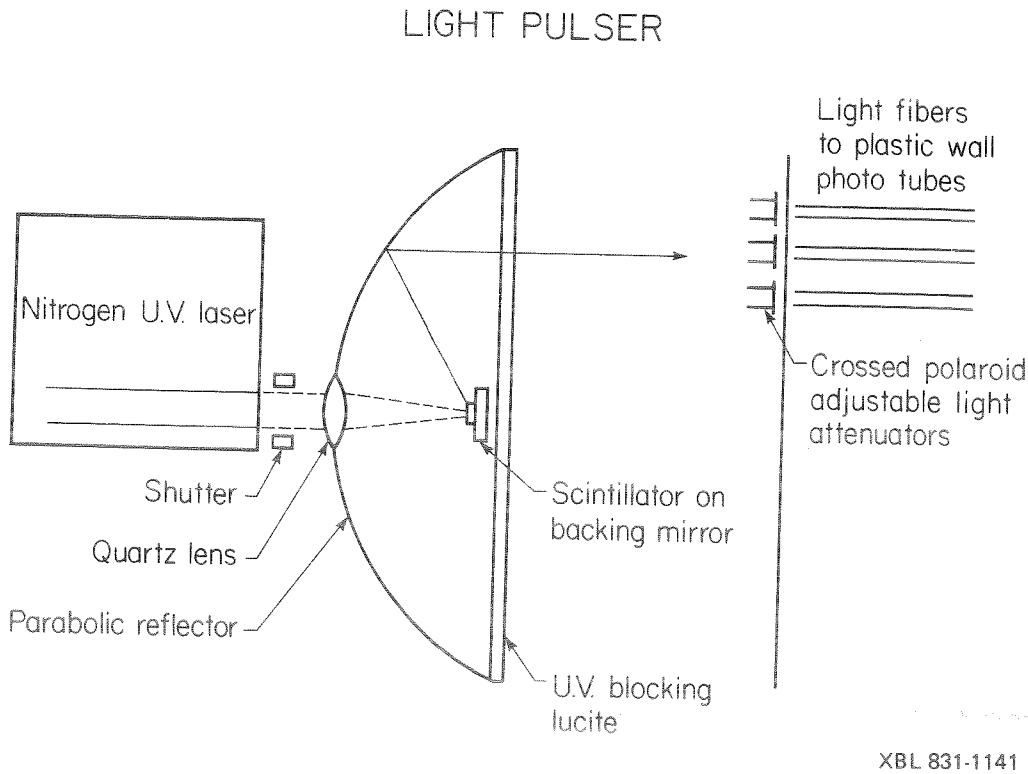


Fig. 1: Schematic view of the Laser-Calibration system.

The MUltiple Sampling Ionisation Chamber (MUSIC)

H.Sann, F. Bieser[1], P. Brady[2], H. Crawford[1], B. Christie[2], D. Greiner[1], P. Lindstrom[1], G. Tull[2], J. Romereo[2]

GSI Darmstadt, LBL Berkeley[1], UC-Davis[2]

In order to determine the element numbers (Z>6) of the projectile fragments at the Bevalac HISS spectrometer, an ionisation chamber with an active area of 1x2m² was built. The detector measures the energy loss of the minimum ionizing relativistic heavy ions up to 64 times. So the energy loss parent distribution for each detected particle can be reconstructed, whose most probable value determines the fragment charge to a very high accuracy. Even for Uranium the resolution is calculated to be well below one charge unit.

The detector consists of a stainless steel barrel with a diameter of 3.2m and a length of 2m. In order to reach the required gas purities, the vessel is evacuated before filling it with the detector gas.

The entrance and exit window for the particles consist of two mylar-copper-mylar foils, which are separated by a 1.5cm gas gap. In order to maintain the gas purity in the detector a clean gas is purged through this gap. The sensitive volume has a size of 1x2x1.7m³. The field cage consists of a Mylar foil onto which horizontal copper stripes are evaporated. They are connected by a 20 MΩ/cm resistor chain. So the negative cathode voltage (<80kV) is divided down to the grounded Frisch grid (Fig.1).

The anode structure is mounted 2cm below the Frisch grid and operated at a positive voltage. The anode configuration consists of two symmetric parts with 64 dE divisions, in order to be prepared for the big dynamic range of the signals expected in relativistic heavy ion collisions. The preamplifiers are mounted outside the tank, so that the number and size of the samples can be adapted to the experiment. In the low charge range (6<Z<15), a small number of bigger samples is necessary, because for these fragments the charge resolution is noise limited, whereas the resolution for the heavy fragments improves with the square root of the number of samples.

In order to be able to record multiple tracks (<20) in the detector, the history of the amplitudes of all anode signals has to be recorded for 20µsec after a trigger has occured. During that time the amplitudes of the anode signals are measured every 100nsec, and then stored in an analog storage (CCD) before they are digitized and written to tape. This readout system was derived from the LBL-TPC detector. Fig.2 shows the reconstructed amplifier signals for the pulser and an Fe particle.

In the final configuration the detector was tested with a Ne beam. The resolution for a single energy loss measurement was 29%. By sampling the energy loss 16 times, the distribution for the most probable value improved by a factor 2.7. Fig.3 shows the Ne fragmentation charge spectrum measured with the MUSIC detector. The resolution is dZ/Z≈0.6 charge units for Neon.

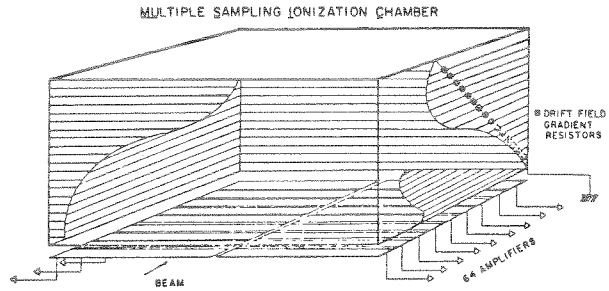


Fig.1: MUSIC detector configuration. The active volume of the detector is 1x2x1.7m³.

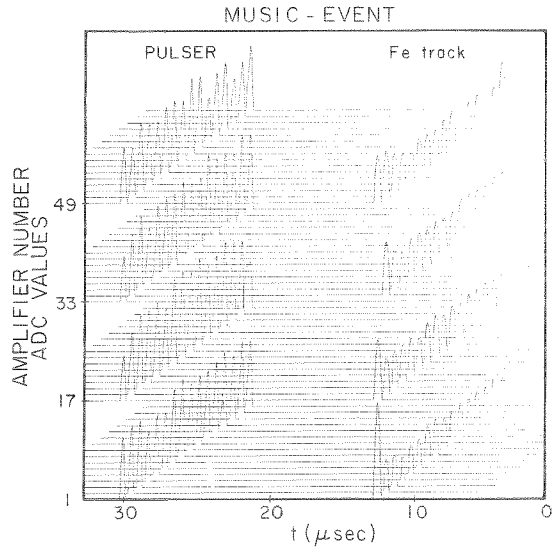


Fig.2: The MUSIC response to a pulser and a Fe particle

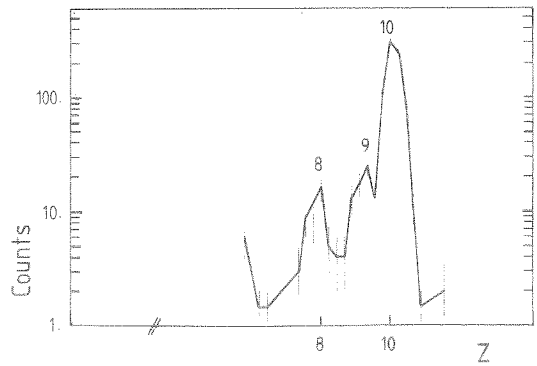


Fig.3: The charge spectrum measured for Neon fragmentation. Charges Z<7 are below the digitizer thresholds.

M.Brügger, Th. Karlewski, N. Trautmann
Institut für Kernchemie, Universität Mainz
A.K. Mazumdar, H. Wagner, W. Walcher
FB Physik, Philipps-Universität Marburg

For studies on short lived lanthanide nuclides the heliumjet on-line isotope separator HELIOS[1] has been equipped with a fast tape transport system. This tape transport system consists of a high vacuum chamber, diffusion slits and the drive electronics. The vacuum of $1x10^{-5}$ mbar in the separator beamline as well as in the high vacuum chamber is obtained by means of a 3000 l/s diffusion pump. By differential pumping through the diffusion slits the atmospheric pressure is reduced stepwise. The mass separated ion beam is implanted into the transport tape (computer tape) at an energy of 20 keV. After collecting the activity it is transported through the diffusion slits to the detector station, where γ-singles, γ,γ,t-coincidence and γ,γ,t-angular correlation measurements can be performed. The tape is driven by a stepping motor and the velocity is controlled by a microprocessor system. The maximum speed of the tape is 10 m/s in the continuous mode and 6 m/s in a start-stop mode obtaining a stopping accuracy of ±1 mm. With this tape unit γ-singles, γ,γ,t-coinicidence and γ,γ,t-angular correlation measurements on 2.3 min ^{148}Pr and 6.2 s ^{150}Pr were performed using a 6.5 mg/cm^2 ^{235}U target in the gasjet system and the high temperature surface ionization source[2]. Several new γ-lines could be assigned to the decay of these transitional nuclides and partial decay schemes were established.

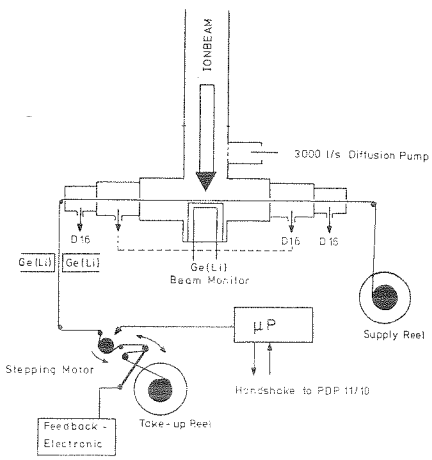


Fig. 1: Schematic drawing of the HELIOS tape system

Furthermore, the optimal operating conditions for the integrated plasma ion source of the HELIOS system[3] with respect to the ionization of light fission products (mass number 83 - 85) were explored. Since the fission yields for arsenic and selenium in the mass region 83 - 85 are rather low the optimization experiments were performed with their homologues, for which the efficiency measurements of the He/KCl-jet plasma ion source have already been made[4]. In Table 1 efficiency values of antimony and tellurium isotopes yielding from measurements behind the ion source with two different cluster materials are summarized. With $PbCl_2$ an enhancement by a factor of 2 compared to KCl could be observed[2].

Table 1

Efficiency values for the HELIOS system using two different cluster materials

Nuclide	Efficiency/%	Clustermaterial
^{131}Sb	0.82	$PbCl_2$
	0.46	KCl
^{133}Te	0.46	$PbCl_2$
	0.27	KCl
^{134}Te	1.06	$PbCl_2$
	0.60	KCl

In Table 2 the overall efficiency values of the HELIOS system for ^{84}As, ^{84}Se and ^{85}Se under optimum conditions using $PbCl_2$ as cluster material in the gasjet are given.

Table 2

Overall efficiency values for the HELIOS system

Nuclide	Efficiency / %
^{84}As	$0.5x10^{-2}$
^{84}Se	$1.0x10^{-2}$
^{85}Se	$1.5x10^{-2}$

1/ A.K. Mazumdar et al., Nucl. Instr. and Meth., 174 183 (1980)
2/ M. Brügger et al.,GSI Scientific Report 1981, 82-1 , p. 225
3/ A.K. Mazumdar et al., Nucl. Instr. and Meth., 139 319 (1976)
4/ W.Ziegert et al., Jahresbericht,Inst. f. Kernchemie Mainz, 1980,p.22

Development of an Electron Spectrometer for Contact Time Measurements in Dissipative Heavy Ion Collissions

G

H.Backe, R.Barden, M.Begemann
Institut für Physik, Universität Mainz

Experimental results gained from detection of δ-ray-, positron- and characteristic x-ray radiation in close Coulombic heavy-ion collisions (like U+U at 5.9MeV/u) reflect the dynamical aspects of the collision process. The nearly exponentially decreasing high energy part of the δ-ray spectra, e.g., can simply be explained in first order adiabatic perturbation theory by the Fourier transform of the transition matrix element. If the colliding nuclei come close enough together that nuclear forces become important, the Rutherford trajectories will be perturbed. This results in a change of the Fourier frequency spectrum and, consequently, in an alteration of the energy distribution of the emitted δ-rays[1]. As recent δ-ray and positron experiments show[2], a smooth slope change is observed which indicates a contact time of about 10^{-21}s.

In order to systematically investigate such effects of a nuclear contact time, an electron spectrometer is presently being developed which can be used in connection with the large area position sensitive particle counters of the Z4 experimental set-up[3]. With these detectors, the dissipated energy, which is related to the nuclear contact time, can still be determined from four body kinematics. Such events which originate from a fission process of both interacting nuclei produce, presumedly, the lowest conversion electron background (Z^3 dependence!). Since this background is a serious experimental problem, it seems to be appropriate to complement a state of the art particle detection system by an electron spetrometer rather than to equip an existing electron spectrometer with highly sophisticated particle counters. The spectrometer is shown in Fig. 1. Basically, it is a solenoidal transport system with two Si(Li) - detectors as energy resolving elements. The magnetic field is produced by two packs of "pancake" coils powered by a current of 1500 A. The Si(Li) detectors are mounted as shown in Fig. 2. The separation between the detectors of 8mm excludes the very intense low energy electron background from detection and at the same time allows the heavy ion beam to enter the solenoid on the symmetry axis. The target position compromises between high electron detection efficiency and minimum deflection of the charged reaction products in the magnetic stray field. A broad band detection efficiency as shown in Fig. 2 is expected from trajectory calculations. The main technical problem in the construction of this spectrometer arises from the fact that the magnetic field coils also have to be included into the vacuum chamber of the particle counters.

[1] G.Soff et al., Phys.Rev.Let. 43, 1981 (1979)

[2] H.Backe et al., GSI Sci. Rep. 82-1, 140 (1982)

[3] B.Martin et al., GSI - J - 1, 148 (1977)

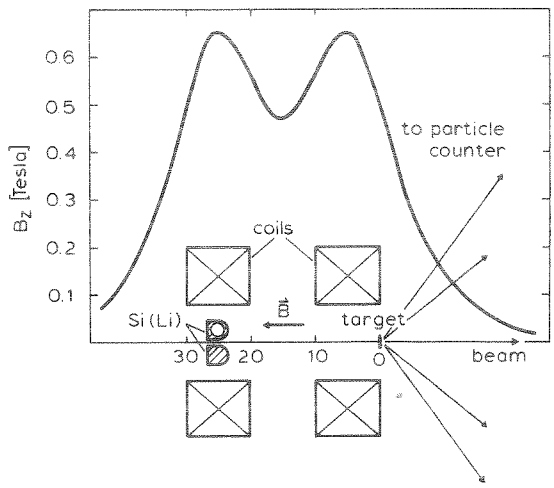


Fig. 1: Experimental set-up with the calculated magnetic field on axis of the solenoid. The Si(Li) detectors have an active area of 500 mm² and a thickness of 5 mm. Numbers on the abzissa are given in centimeters.

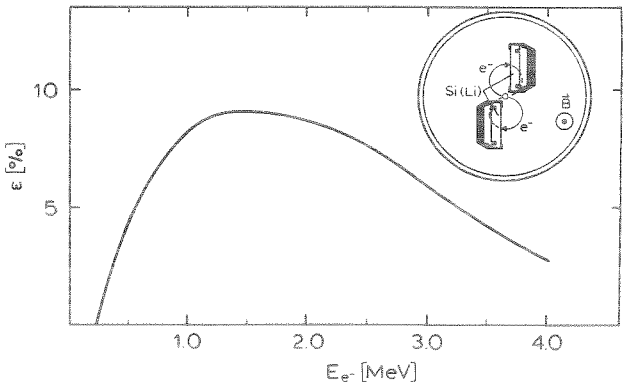


Fig. 2: Calculated electron detection efficiency ε for the experimental configuration shown in Fig. 1. The insert shows a cut perpendicular to the solenoid axis at z = 25 cm.

Status of the Eight Crystal X-Ray Spectrometer ("Octopus")

H.D. Dohmann, U. Kopf, D. Liesen, D. Loos, W. Rösch, H. Wahl
GSI Darmstadt

In order to perform lifetime- and wavelength-measurements with rather high efficiency and precision an eight-fold flat crystal spectrometer ("Octopus") has been designed. Based on the large total solid angle, the precise Doppler corrections due to always two simultaneous measurements at azimuth angles 0° and 180°, and the possibility to determine the scattering angles of projectile and recoil particle, high-precision spectroscopic data even on weak lines (e.g. the forbidden $2s_{1/2}$-$1s_{1/2}$ transition) should be available in the next future.

In the course of the last year the mechanical parts of the Octopus-spectrometer have been completed so that the spectrometer is now ready to be flanged to the beam-line in the Stripperhalle for test experiments. The Octopus is shown in Fig. 1; the picture was taken in the Stripperhalle.

The x rays are detected by 8 three-chamber proportional counters (not yet mounted) so that in a beam-foil experiment the x-ray intensity can be measured simultaneously at three different positions behind the foil. These counters were built in such a way that no mutual influence of the three chambers could be observed in measurements with 5.9 keV x rays from an Fe55 source.

Eight twofold gears have been mounted to guarantee an independent motion of the eight crystals and detectors and to fulfill the ϑ-2ϑ condition for each crystal-detector pair. The actual position of all the pairs can be controlled by an especially developed read-out unit. Special care was taken to achieve a geometrical adjustment as good as possible for the experiments to be performed. On an extremely parallel base plate ($\sim 10^{-5}$) 8 Soller slits were mounted and adjusted to a precision better than 10^{-4} (the telescope for the adjustment of the slits and the crystals can be seen). After primary test runs with x rays induced by electron impact (the electron gun is not shown in Fig. 1), the set-up will be mounted to the beam- line at SL2 in the Stripperhalle for first on-line experiments.

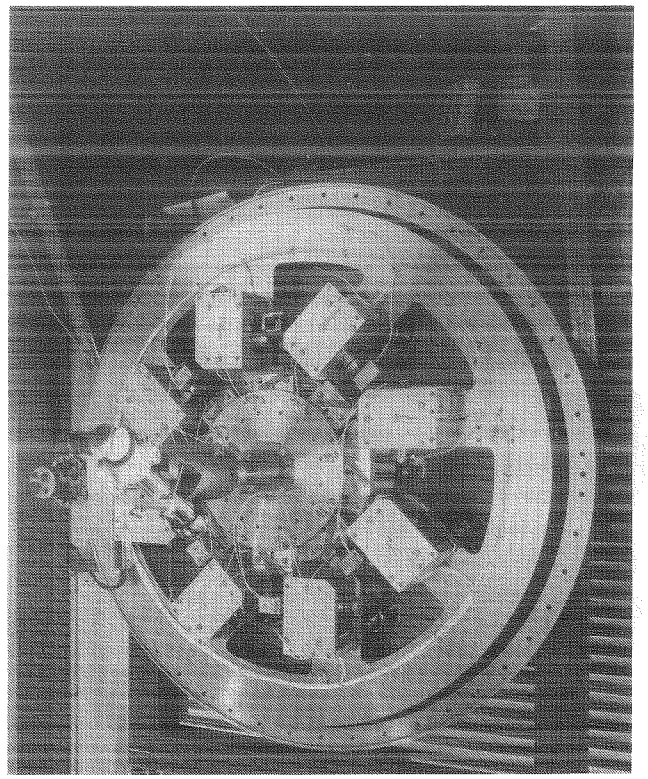


Fig. 1: Octopus-spectrometer in the Stripperhalle. With the telescope fixed in front of the spectrometer the 8 Soller-slits which are mounted on a solid base plate, are adjusted.

30^0 Electrostatic Spectrograph [G]

H.J. Frischkorn, P. Koschar, K.O. Groeneveld
Inst. für Kernphysik, J.W. Goethe Universität, 6000 Frankfurt/M.

Previously we reported on a set-up of a 45^0-electron spectrograph with a position sensitive electron detector[1]. The analyzer consists of 1) a focussing and retarding element ("retarding lens"), 2) an electrostatic parallel plate analyzer and 3) a position sensitive electron detector (Chevron plate).

The 45^0-parallel plate analyzer did not have the minimum angular abberation[2]. The angular abberation can be minimized, however, by changing the entrance angle of the analyzer to 30^0. Here, the angular abberation in the focal plane of the analyzer approaches zero[2]. For an entrance angle of 30^0 the focal plane of the analyzer is turned $10,9^0$ with respect to the exit plane of the inner analyzer plate. The size of the spectrograph is 7 cm x 13,5 cm. The plate distance is 2.5 cm and the mean distance between entrance and exit of the analyzer amounts to 5 cm. The exit slit in front of the positron sensitive electron detector is 1,9 cm long.

An example for the properties of the focussing lens is shown in fig. 1

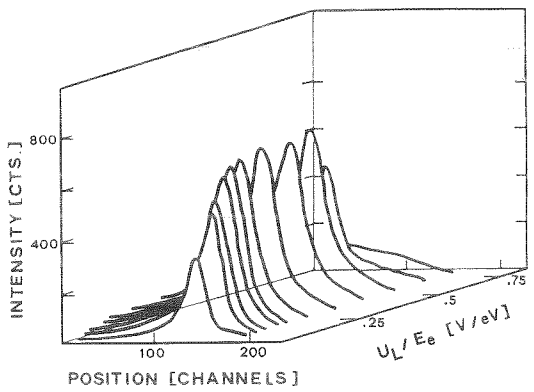


Fig.1: Position spectrum of monoenergetic electrons (E_e = 400 eV) at different focussing voltages.

The position spectrum of a diffuse electron beam (mean energy E_e = 400 eV) is presented as a function of the focussing voltage U_L. The intensity of the peak in the position spectrum is a measure for the transmission of the lens. In the range $0.2 \leq U_L/E_e \leq 0.6$ V/eV the transmission is constant within 5%. Yet, this range may be increased by further adjustment of the focus of the lens with respect to the entrance in the analyzer. Fig. 2 illustrates the linearity of this instrument. The position x of electrons with E_e = 300 eV is shown as a function of the analyzer voltage U_A. At present the position resolution of the position sensitive detector is 0.15 mm. The deviation of the experimental points from a linear relationship is < 0.5%. This also indicates the correct position of the detector in the focal plane.

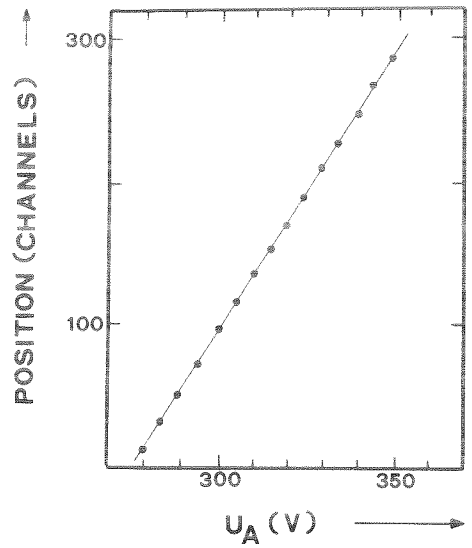


Fig.2: Position of 300 eV electrons as a function of the analyzer voltage

The mean spectrometer factor of the analyzer has been measured to be $U_A/\bar{E}_e$ = 1.05 V/eV. The measured relative energy range is $\Delta E/\bar{E}_e$ = 0.23. This range $\Delta E/\bar{E}_e$ can be measured simultaneously with the position sensitive detector. The values are also expected from the geometry of the spectrometer.

This instrument will be especially useful in measurements of electron energy spectra under various experimental condition with parameters as angle, projectile Z etc. The time needed to accumulate one spectrum is reduced by a factor of at least 100 because of the focussing property of the lens and the simultaneous measurement of the whole energy range with good energy resolution.

References:

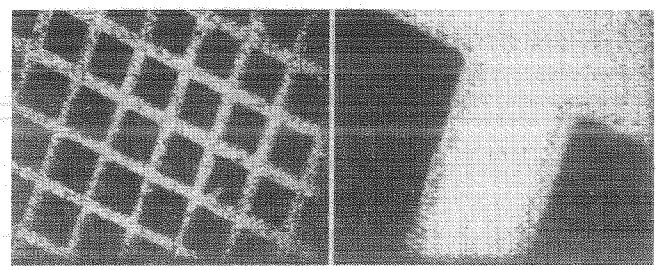
[1] H.J. Frischkorn, P. Koschar, K.O. Groeneveld, GSI Annual Report, 232 (1981)

[2] G.A. Proca, T.S. Green, Rev. Sci.Instr. 41, 1778 (1970) and 41, 1409 (1970)

B.E. Fischer, GSI Darmstadt

In spring 1982 the instrument (described in annual report 1981, p. 237-238) was moved from the 300 kV dc-accelerator to the stripper hall (1.4 MeV/u fixed energy for all ions; pulsed beam).

Though we achieved a considerable improvement in resolution to about 1 µm (see fig. 1) most of the time was spent to cope with a seemingly trivial feature of the accelerator, the pulsed beam:



a) b)

Fig. 1: a) Heavy ion micrograph of a nickel grid with 100 µm grid spacing. The brightness of the image is determined by the number of secondary electrons set free by the ion beam. The "image noise" is due to the pulsed beam.
b) Part of fig. 1a at higher magnification. The edges between front and back side of the 5 µm thick grid are clearly visible.

At ion microprobes connected to DC-accelerators life is much easier, because, as the microbeam scans over the target, any change in the reaction rate reflects a change in target structure. (In the worst case there is a slowly variing beam current, which can be easily measured by intercepting the beam from time to time.)

At a RF-accelerator the current of reaction products mainly reflects the pulse structure of the beam and target structures appear as tiny modulations on top of this signal. Therefore the time structure of the beam must be accurately known at any time, before one can hope to get information about the target structure.

As in most cases the current of the microbeam is to small to be measured by a current amplifier connected to the target, two indirect methods have been tried to measure the current of the microbeam.

1) For thin transparent targets the standard nuclear physics method is to catch the beam in a Faraday-cup after passage through the target.
As we tried this method we found the current in the Faraday-cup to be distinctively higher, when the microbeam was scanned over thicker parts of the target where the ions were stripped to higher charge states.

Though this method failed to measure the microbeam current it is a first experimental indication for the usefulness of charge state measurement for heavy ion microscopy, which has been predicted as one of the gentlest ways of gaining microscopic information by Martin[1].

2) For thick targets we tried to measure the current of the microbeam halo falling on the entrance aperture of the lens and we found it to be very different from the true microbeam current (Fig. 2).

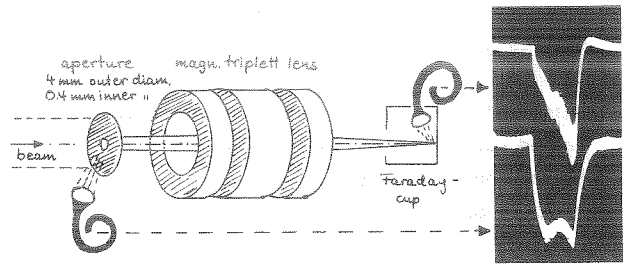


Fig. 2: Set-up for the current measurement at the micro beam. Part of the micro beam is intercepted at the entrance aperture and its intensity is measured by collecting secondary electrons from the aperture. The part of the microbeam normally falling on the target is measured in a Faraday-cup by another channeltron detector.

Though the shape of these two signals can be influenced to some extent by beam tuning it was never possible to get similar signal shapes. So it is still not clear if this method will ever work satisfactorily.

There have also been a number of electronic developments mainly to cope with the pulsed beam of the UNILAC.

- A pulsed beam simulator together with a pulsed electron source for detector and electronic tests.
- An analog division unit to normalize the detector outputs to the microbeam current (for fast scanning).
- A digital unit for the same purpose (for slow scanning)
- A two channel 1000 x (max) dc-coupled amplifier for small signals on a large dc-offset, with automatic offset nulling and the capability of various arithmetic operations.
- A new beam scanning electronic which adjusts the scanning speed so that every part of the target gets the same fluence (provided the beam current can be measured accurately). Together with a newly developed fast beam switch and the capability to aim at any part of the target under computer control the heavy ion microscope can be expected to be a versatile instrument for microanalysis, micromachining and radiation biology.

[1] F.W. Martin, Is a Scanning Ion Microscope Feasible? Science, Vol. 179(1973), pp 173-174.

Solar Cells as Detectors for Fragments of Volatile Spontaneously Fissioning Nuclides G

N. Hildebrand, W. Kieling, N. Trautmann, G. Herrmann
Institut für Kernchemie, Universität Mainz

M. Brügger, H. Gäggeler, K. Summerer, W. Weber
GSI, Darmstadt

In the search for superheavy elements detection of spontaneous fission activity provides the most sensitive method. From the predicted chemical and physical properties some superheavy elements such as 112 and 114 are expected to be volatile at room temperature. So far such species could be measured only in 2-π-geometry by a surface barrier detector (ring detector) through which the gases were transported and condensed on a cooled copper-surface placed opposite to the detector. By the application of thin photovoltaic cells, cooled from the backside by a cryogenic pump and acting both as a condensing surface (down to 70 K) and as a fission fragment detector[1] it is possible to perform 4π-measurements under coincidence conditions. The energy resolution for fission fragments of monocrystalline as well as polycrystalline solar cells from different suppliers was determined with a ^{248}Cm-source using conventional electronics and applying no bias voltage. The best results with respect to temperature and energy resolution were obtained with a monocrystalline cell from AEG with 100 µm thickness and ≈200 mm^2 active surface. Fig. 1 shows the energy spectrum of ^{248}Cm-fission fragments obtained with such a photovoltaic cell demonstrating a peak-to-valley ratio of 2:1.

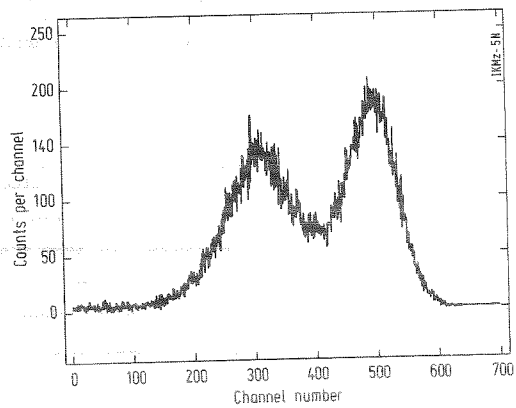


Fig. 1: Energy spectrum of ^{248}Cm fission fragments measured with a solar cell

Furthermore coincidence measurements were made with the solar cell and a surface barrier detector (ring detector) to define the optimal coincidence conditions. The tests with a ^{248}Cm source on a thin carbon foil demonstrated that the total kinetic energy of the fission fragments can be determined with a FWHM of 23 MeV.

In the next step the solar cell was fixed to the cold head of a cryo pump and the energy spectrum was measured at 70 K. No drastic decrease in the energy resolution was observed. In the set-up modelling the final experimental conditions, an annular surface barrier detector was positioned opposite to the solar cell in the cryogenic chamber (Fig. 2). A capillary through which

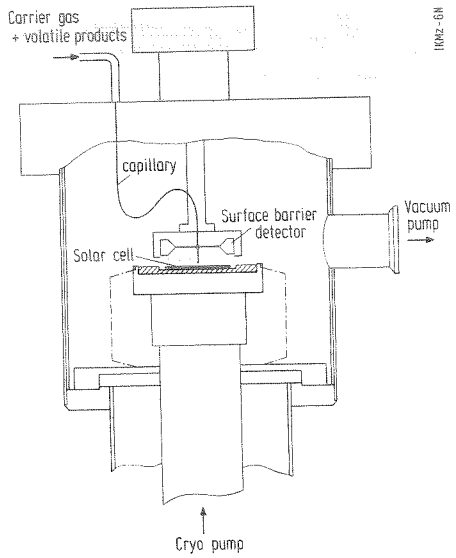


Fig. 2: Schematic diagram of the cryogenic chamber with an annular surface barrier detector and a solar cell for measurement of volatile spontaneously fissioning nuclides under 4π geometry and coincidence conditions.

the volatile products are transported by means of a carrier gas (argon) is passed through the hole of the surface barrier detector ending 1 mm above the solar cell. This arrangement allows to measure E_1/E_2 coincidences from gaseous spontaneously fissioning nuclides.

The condensation efficiency of the set-up was investigated with radon isotopes (4.0-s ^{219}Rn, 56-s ^{220}Rn, 3.8-d ^{222}Rn) liberated from ^{227}Ac-, ^{228}Th- and ^{226}Ra-sources and transported with argon as carrier gas through the capillary. A temperature of 70 K on the cold head of the cryo pump can be maintained for a carrier gas flow rate of up to 150 ml/min. The condensation yield for radon was determined by α-spectroscopy with the ring detector. The cryogenic chamber with the solar cell was for the first time applied in a search for gaseous superheavy elements in the ^{48}Ca+^{248}Cm experiment[2] performed in October 1982.

[1] G. Siegert, Nucl. Instr. Meth. 164, 437 (1979)
[2] H. Gäggeler et al, this report, p.

Performance of a Gas-counter in a Time-of-flight Set-up behind SHIP

J.G. Keller, K.H. Schmidt, H. Stelzer, GSI Darmstadt
C.C. Sahm, Institut für Kernphysik, TH Darmstadt

The velocity filter SHIP efficiently separates the evaporation residues after fusion reactions from the primary beam, which is suppressed typically by about 10 orders of magnitude. Nevertheless, due to the low cross-section of some μb or less, a detection system is needed behind SHIP which efficiently registers the evaporation residues and separates them from projectiles.

For this purpose, in a recent experiment[1] a detector telescope consisting of a 5 x 7 cm² large double-grid-avalanche counter (DGAC) and a silicon-surface barrier detector has been used. The DGAC delivers the timing, the position in two coordinates and a rough ΔE-signal, whereas the silicon detector gives the time-stop signal and determines the energy. A schematic view of the gas-counter is shown in fig. 1. The detector consists of four electrodes, labelled S, K, A and T. S and T are stretched polypropylen foils (70 μg/cm² thick), evaporated with silver. K and A are grids of 20 μm gold-plated tungsten wires. The counter is operated at 2.5 mb i-butane. The potentials applied to the electrodes are indicated in fig. 1. More details about the detector can be found in ref. 2. The signal from S shows a time-resolution of 200 ps FWHM and T gives the ΔE-signal. In front of the S-electrode there is an additional thin foil as the entrance window, whereas the T-electrode serves as well as the exit-window. Despite the slight bending of this foil due to the gas-pressure, the detector shows a ΔE-resolution of 20 %. The total thickness of the counter is thus only 250 μg/cm². The K- and A-grids determine the position and the read-out is done by the delay-line technique with BELFUSE-delay-line chips (3 ns/tap). The delay-line is read out at both ends, in this way multi-particle hits can clearly be distinguished. The position resolution is 250 μm FWHM (fig. 2).

With this new detector set-up, the performance of SHIP has been greatly improved for this type of experiments. By monitoring the position of the detected particles, the function of SHIP can be controlled. The evaporation residues can be distinguished from scattered projectiles or recoils by determining their mass and their nuclear charge. The pile-up counting rate is greatly reduced, since the DGAC distinguishes particles which are >10 ns apart in time or >2 mm apart in space. This feature is of special importance for symmetric particle-target combinations because pile-up of two projectiles with the velocity selected by SHIP just simulates the signal of an evaporation residue. The detector has a high detection efficiency down to a very low energy of the particle (fig. 3). By means of an anticoincidence condition between the DGAC and the silicon detector it is possible to obtain α-spectra of implanted evaporation residues almost free of background. A pile-up protected energy-TOF spectrum from a first application of the new set-up is shown in fig. 4. The pulses of the evaporation residues are clearly separated from the scattered projectiles.

[1] J.G. Keller et al., this report
[2] H. Stelzer, GSI-82-39

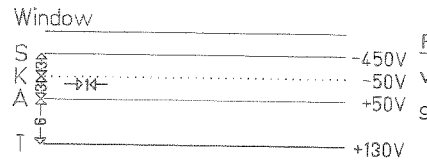


Fig. 1 Schematic view of the gas-counter

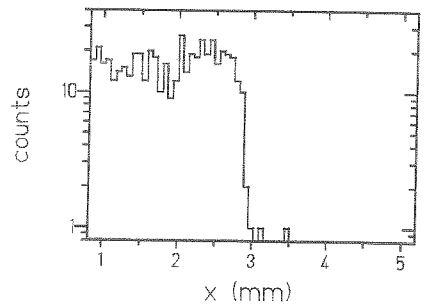


Fig. 2 Position-spectrum of a slit-mask

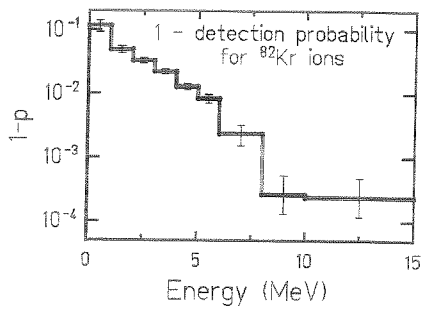


Fig. 3 Inefficiency as a function of the particle energy

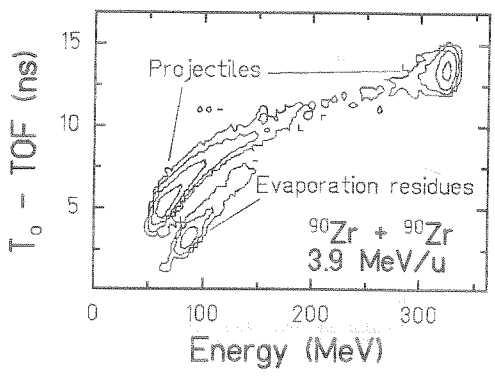


Fig. 4 Energy-TOF-spectrum

Construction and Performance of a Position-Sensitive Particle Detector with Delay Line Readout

B. Liu*, W. Enders, D. Liesen, R. Schulze
GSI Darmstadt

*Permanent Address: Institute of Modern Physics, Academia Sinica, Lanzhou, China

For several reasons the study of inner-shell excitation processes especially in collisions with very small impact parameters has been intensified in the last few years. Since in such collisions besides the scattered primary particles also recoiling target atoms can give a considerable contribution to the scattering intensity under the corresponding lab-angles (typically $\geq 15°$), an unambiguous determination of the kinematics is necessary for a proper determination of the impact parameter. Additionally, a high angular resolution of the particle detector is desirable in order to observe possible structures in the impact parameter dependence of the excitation processes.

Both conditions can be fulfilled by a position-sensitive parallel plate detector similar to that one developed by P. Fuchs et al.[1]. The detector consists of a 2 µ thick metalized Hostaphan foil and an especially designed delay line (for a schematic view see[2]). The delay line is built up from 54 concentric circles of 1 mm width and 1 mm distance from each other and its upper compared to its lower part is shifted by half a period. Both the foil and the delay line are cut into two halves so that the two corresponding regions of the total azimuth are independently covered. The total delay for each half amounts to 180 nsec which corresponds to a specific propagation time of about 140 psec/cm. Without any change of the total delay time and thus with the same resolution also 4 quarters of the whole azimuth can be measured separately, namely just by turning the foil 90° with respect to the delay line. The distance between foil and delay line is 5 mm and the whole assembly is separated from the vacuum by an additional 2 µ Hostaphan foil (25 mm in front of the detector foil) which is supported by a Ni grid.

After first tests with 5.5 MeV α particles from an Am source, several measurements have been performed in the Stripperhalle. It turned out during these experiments that for x-ray-scattered particle coincidences an optimal performance could be reached using Isobuthylen gas at 12 Torr pressure and applying -800 V to the foil and 0 V to the delay line. Fig. 1 shows the energy signals of 1.4 MeV/N U projectiles taken at the detector foil and at the delay line. The pulses from the preamplifier were almost equal in height ($\sim$ 300 mV) with a rise time of about 8 nsec. A change of the sign of the high voltage at the foil resulted in a drastic decrease of the height of the delay line pulses. Fig. 2 gives the time spectrum (which corresponds to the angular dependence of the scattering intensity) which was obtained also with 1.4 MeV/N U projectiles. Both curves (the upper was taken without and the lower with coincidence condition) show the same characteristic features corresponding to the ring structure of the delay line and showing a rather good angular resolution. However, the orgin of this structure is not yet fully understood.

[1] P. Fuchs et al., GSI Scientific report 1977, p. 195
[2] I. Giese et al., this report, p. ..

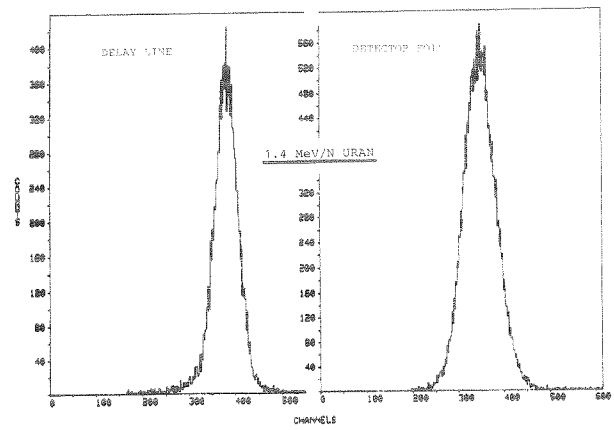


Fig. 1

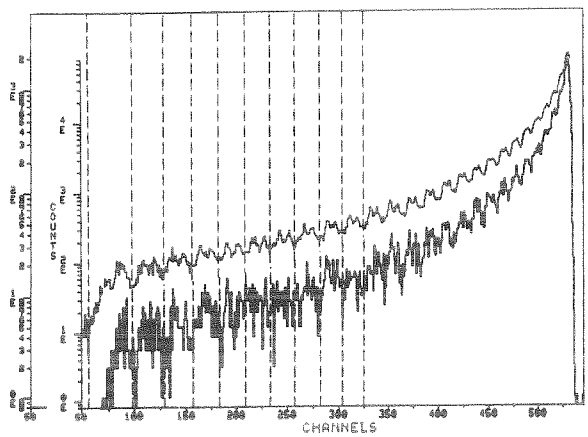


Fig. 2

Luminescence Processes in Heavy Ion Excited Scintillation Gases

P. Grimm, F.-J. Hambsch, M. Mutterer, Chr. Preuss and J.P. Theobald
Institut für Kernphysik, Technische Hochschule Darmstadt

Previous experiments[1] on rare-gas luminescence following excitation by charged particle impact have revealed a rather complicated time structure of scintillation decay, with several components which vary with gas composition and pressure, the specific energy loss of the absorbed ions, and the property of the wave length-shifter material applied to match the emitted VUV light to the spectral response of the light sensor. At present, only the main features of the time evolution of light emission are known in detail for pure noble gases; i.e. recombination luminescence and radiative molecular de-excitation via low-lying excimer states. Only weak information is available on fast structures and on the decay of binary noble-gas mixtures and noble gases doped with molecular gases, e.g. nitrogene.

We have performed a series of decay-time measurements on fast components in low-pressure Ar and Ar-N_2 and He-Xe mixtures using 97-Mo ions of 1.4 MeV/amu and applying single photon techniques: a TAC is started by fast signals from a SB detector defining the interaction time and stopped by single photons measured by a small PM with cooled cathode coupled to the scintillator via a glass-fibre light guide.

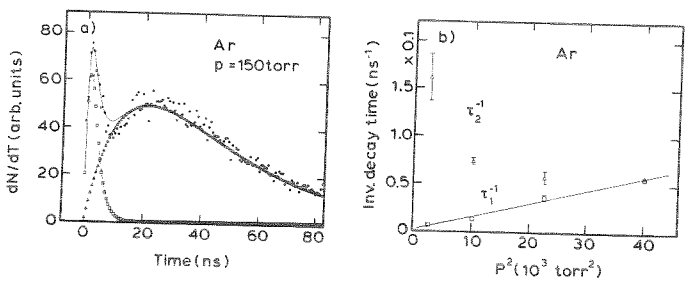


Fig. 1

Figure 1a shows, as example, the fast decay structure in pure Ar, with a prompt component below 1.8 ns and a somewhat delayed structure which represents a sequential decay, with τ_1^{-1} being proportional to the square of pressure characteristic for a three body collisional process and τ_2 being approximately constant (Fig. 1b). In the framework of an accepted model[2], the experimental results can be explained by the formation and decay of higher excited excimer states emitting the so-called third VUV continuum.

In N_2 doped Ar two delayed components are observed (Fig. 2). By varying both pressure and N_2 concentration it is possible to single out different energy transfer processes which lead to excited Ar_2 and N_2 molecular states, respectively, on different levels of excitation. The reaction rates, pictured in Fig. 3, show the importance of atomic energy transfer to N_2 (curve 3) compared

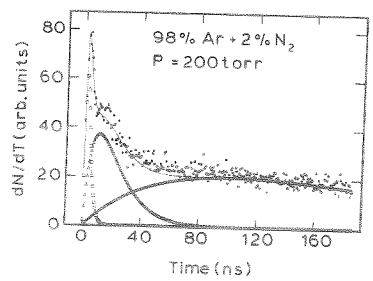


Fig. 2

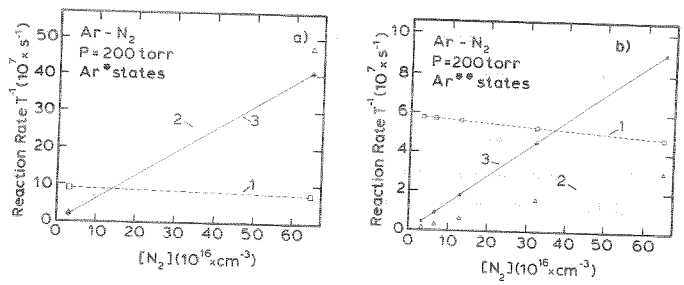


Fig. 3

to the Ar_2 formation processes (curve1 and 2). This explains that N_2 admixtures above ~2 % shift the original VUV spectrum to the line spectrum of N_2 emitted in the visible region[3] which can be detected by standard photo-tubes.

For He doped with Xe, a highly efficient energy transfer from He to Xe is observed. With this gas mixture low energetic heavy ions are, due to the low Z number of He, absorbed with a small contribution of nuclear collisions while scintillation light is emitted preferably by Xe, at relatively long wave lengths which fit to high-purity quartz-window photo tubes. This gas mixture can probably be used with profit for the detection of fission fragments.

References

1. M. Mutterer et.al., IEEE NS-26 (1979) 382
2. M. Salete S.L.P. Leite, Portugal, Phys. 11 (1980) 53
3. T. Takahashi et.al., Rep. RUP 81-16 (1981)

B G

Liquid-scintillator detectors for neutron time-of-flight measurements

H.-A. Bösser, B. Kohlmeyer, D. Bangert, H.-J. Keim, H. Stege and F. Pühlhofer
Fachbereich Physik der Philipps-Universität Marburg
W.F.W. Schneider
GSI Darmstadt

In order to investigate preequilibrium phenomena in heavy-ion induced fusion reactions in the energy range between 10 and 20 MeV/u a multidetector system for light particles has been tested at the UNILAC accelerator. The set-up consists of ten solid-state Si-NE104 telescopes for charged light particles[1] operated in coincidence with three HI-telescopes used for detecting evaporation residues. In particular the heavy ions are identified by one time-of-flight ΔE-E-telescope consisting of two transmission-time detectors at a distance of 170 cm and by two time-of-flight E-telescopes for flight-pathes of 40 cm using the beam pulse as start signal.

This set-up has been complemented by several liquid-scintillator detectors[2] to be mounted outside the scattering chamber in order to measure neutron spectra in coincidence with the heavy fragments. Closed organic liquid-scintillator NE213 cells of Pyrex glass with a diameter of 50 mm were built. On the outside they were covered with a special reflecting paint. Due to the expected wide range of neutron energies detectors with different thicknesses between 25 and 75 mm were chosen. They are mounted on photomultiplier tubes RCA 8575 with ORTEC 265 bases. A method to purify the liquid-scintillator[3] was used in order to obtain optimum pulse shape discrimination (PSD) and time resolution. The detectors show excellent discrimination characteristics which allow nearly complete separation of neutron and gamma ray events using the PSD circuit CANBERRA 2160 D (Fig.1). To determine the absolute neutron efficiency as a function of energy we have started to measure n-γ coincidences in the reaction $^{9}Be(\alpha,n)^{12}C$ (neutron source) for lower energies and n-^{3}He coincidences in the reaction $^{2}H(d,n)^{3}He$ (Marburg Van de Graaff accelerator) for the higher energy range.

In a first test we used the 11.6 MeV/u ^{58}Ni beam of the UNILAC facility to bombard a ^{27}Al target. With a time resolution of 200 ps for the micro beam pulse measured with a Si-detector the flight-path between target and neutron detectors was chosen to be 80 cm in order to obtain adequate energy resolution without ambiguity due to the 37 ns pulse distance. Neutron time-of-flight spectra taken during a few minutes in a test run with a 50 mm detector at $\Theta_L = +26^{o}$ using an external Faraday cup are shown in Fig. 2. In the upper part the free spectrum without PSD-γ separation is plotted. From the γ-peak the detector time resolution is estimated to be much better than 1 ns. The coincidence with the fusion evaporation residues, mass identified by a 300 mm^2 time-of-flight E-telescope at $\Theta_L = -6^{o}$ and served as a fast 200 ns trigger, leads to the spectrum in the lower part. Due to the large center-of-mass motion in the reaction ^{58}Ni+^{27}Al the energies of the evaporated neutrons range up to 40 MeV. From true HI-γ coincident events the prompt γ-peak in the spectrum results.

1 B. Kohlmeyer et al., GSI Scientific Report 1981,p.222
2 H.-A. Bösser, Diplomarbeit, Marburg 1983
3 U. Arlt et al., GSI Scientific Report 1980, p.201

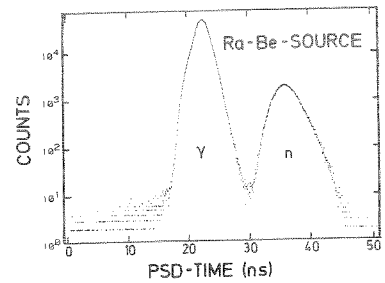


Fig. 1: PSD spectrum from a Ra-Be source for a 50 mm ∅ x 50 mm NE213 detector (peak-to valley 200:1, neutron energy threshold 1 MeV)

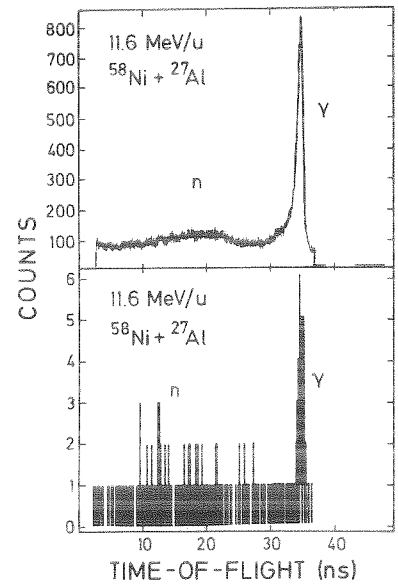


Fig. 2: Free and coincident neutron and gamma ray time-of-flight spectrum taken in a few minutes run from the fusion reaction 11.6 MeV/u ^{58}Ni+^{27}Al at $\Theta_L = +26^{o}$.

Automatic track measurement on streamer chamber pictures with high multiplicity events G

D. Schall, H. Ströbele, K. Tittel
Institut für Hochenergiephysik, Universität Heidelberg

At the Institut für Hochenergiephysik in Heidelberg a facility to measure streamer chamber pictures has been set up. It consists of a PEPR (Precision Encoding and Pattern Recognition) device controlled by a PDP-10 computer. The system is highly interactive and allows the operator to take complete control over the measurement process.

The operator environment consists of the following devices:

1) 2 TV monitors showing the whole and an enlarged section of the streamer chamber picture.
2) a computer display for visualization of track measurements and program control indicators
3) a keybord/printer for program flow control and messages to the operator
4) a speedball for manual positioning fo a cross hair on the TV-picture.

Each track is measured in all 3 views and subsequently reconstructed in space. Details of the measurement procedure are given in the flow chart (fig. 1). The actual digitizations are done either automatically by the flying spot of PEPR or manually by means of a crosshair positioned by the operator. The high level of feedback and guidance provided by the online computer results in a low reject rate. Only short and straight tracks in the vicinity of the target are affected by measuring and reconstruction inefficiencies.

The reconstruction efficiency and measuring time of the system are 95 % and 3h/1 event (~ 50 tracks). Most of this time is needed to find the correct assignment of the track images on the 3 views to one space curve. The operator can match tracks in regions with low track density fast and easily. Program developments are under way to resolve the remaining difficult match ambiguities by simple permutations. We expect this to reduce the measuring time to 1h/event.

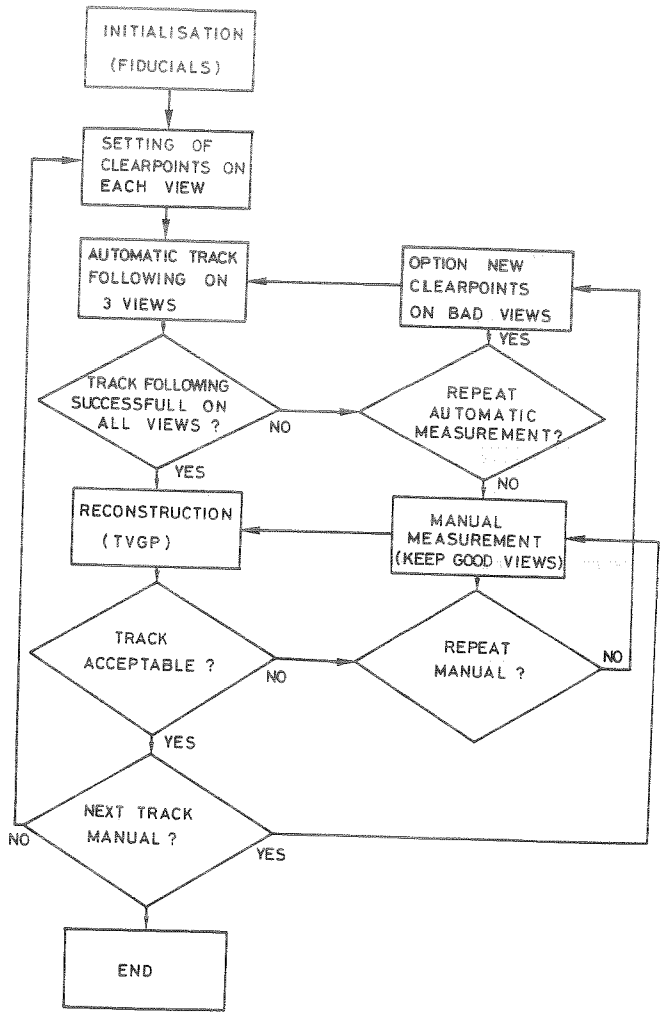


Fig. 1: Flow chart of the measuring process.

Charge measurement by a photometric method G

A.Laschek, W.Weidner, E.Ganßauge, U.Bieschke, N.Klein, R.Kretschmer
FB Physik, University of Marburg, AG Exp.High Energy Physics

In nuclear track emulsion fast nuclei like heavy ions from the Berkeley Bevalac show up as so called tracks, the structure of which depends entirely on the charge and the energy of the particle. To determine the charge Z, in the case of relativistic particles the most important quantity, there exist three different methods:

1) Gap counting (see next contribution) $1 \leq Z \leq 6$
2) δ-ray counting valid for $5 \leq Z \leq 26$
3) Photometrical method valid for $6 \leq Z \leq 26$

In contrast to methods 1) and 2) the last one does not depend on any individual capacity like quality of eyes of the scanning person, it really is an objective method. It works as follows: A small slit moves perpendicularily over the track. Physically this slit is lying in the image plan of a microscope, illuminated from beneath. It is driven by a step motor with step size 0.2 μm at a total number of 120 steps. The light behind the slit is measured by means of a photomultiplier resulting in an absorption profile of the track (see fig.2). At 100× magnification in the objektiv plan the measure of the slit is 0.28 μm * 0.50 μm. At the beginning of the measurement the computer having taken the coordinates of the track segment in question, controlles the step motor to move the slit across the track. At each step the PM measures the amount of light going through the slit and shows the corresponding value at the DVM. This value is taken by the computer which immediately gives the next impuls via the control system SMS-01 to the step motor.

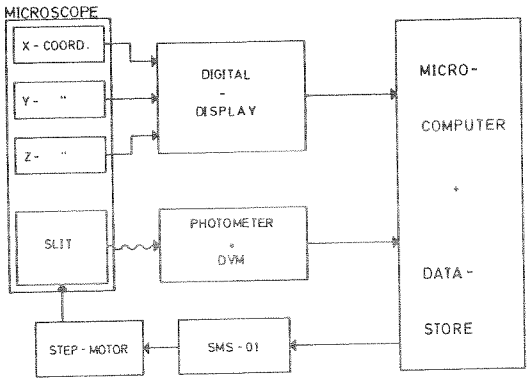


fig.1: Block diagram of the photometric device

The measured profile is divided into three parts, two background and one central part: B1, B2, C. (fig.2)

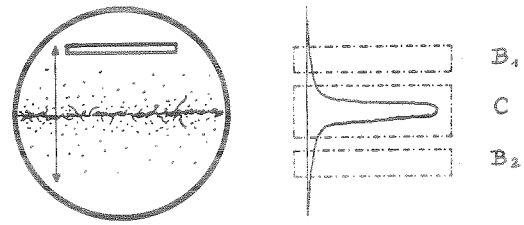


Fig.2: Measurement of the track profile. One field of view is shown with the slit moving across the track (see text).

For each part the mean value of absorption is calculated. The ratio

$$\emptyset = 1000\ (B-C)/B;\ B=(B1+B2)/2$$

is used as a measure of opacity[1]. Out of 50 values of $\emptyset$ the mean W is calculated. The standard deviation of which corresponds to

$$\Delta Z = 0.4\ e.$$

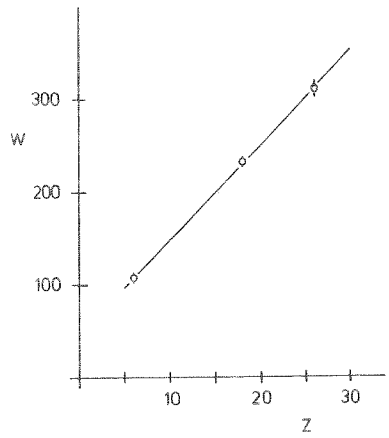


Fig.3 shows the W(Z) dependence. It seems to be linear.

We are just beginning to built up the measuring device and hope to be able not only to extend this method to charges $Z \leq 6$ but also to find an optimum for the width of the slit and also for the step size.

(1) L.Larsson, R.Andersson and O.Mathiesen
Nuclear Instruments and Methods 114 ('74) 35-39.

Charge measurement of projectile fragments with $2 \leq Z \leq 6$ in nuclear track emulsion B C

R.Kretschmer, E.Ganßauge, U.Bieschke, F.Killinger, N.Klein, A.Laschek and W.Weidner
FB Physik, Philipps-University, AG Exp.High Energy Physics
D-3550 Marburg, Federal Republic of Germany

To determine the charge of light projectile fragments ($2 \leq Z \leq 6$) the method of lacunarity measurements was used. Based on 1.88 GeV/u beam energy and considering the Bethe-Bloch formula one can derive an expression

$$\tilde{Z}^2 = \varkappa \cdot \ln L \qquad (1)$$

Z : real charge ; $\tilde{Z}$: measured charge
$\varkappa$: sensitivity factor
L : lacunarity

The sensitivity factor $\varkappa$ depends objectively on the emulsion, subjectively on the personality of the scanning person.

The quality of all charge measurements is closely connected with the homogeneity of the emulsion. Measuring the individual blob-and gap lengths of an α -track through various plates we do not find any systematic variation of L with the depth h (see fig.1).

The measured charge distribution is shown in fig.2. The expected proportionality of $\ln L$ and Z^2 has not been found, the density of the blobs instead seems to squeeze together more and more with rising charge. That means the measured charge $\tilde{Z}$ systematically deviates from the true charge Z for $Z \geq 3$. (The reason is not yet quite clear). As a consequence it is not possible to resolve charges above Z = 6 by this method.

To find the position of the true charges in the L(Z)-plot one can use so called "white" stars, i.e. stars without target fragments, but clearly characterised by the number of Z=1 and Z=2 fragments in the projectile space. The error of this charge measuring method is rather small:

$$\sigma_{\tilde{Z}} \leq 0.05$$

Therefore it should be possible to find for $Z \neq 3$ even fractional charges if they exist. Till now we have not seen any.

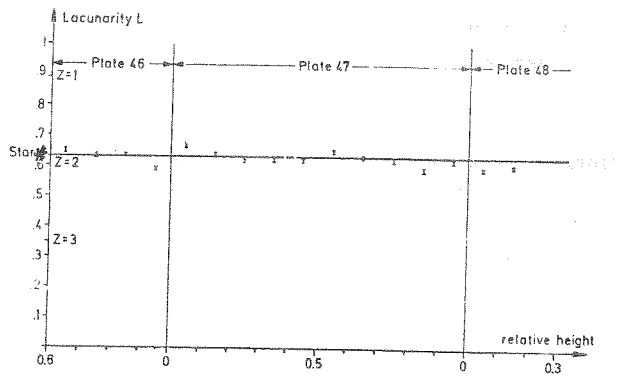


fig. 1: Research on homogeneity of the emulsion, L(h).

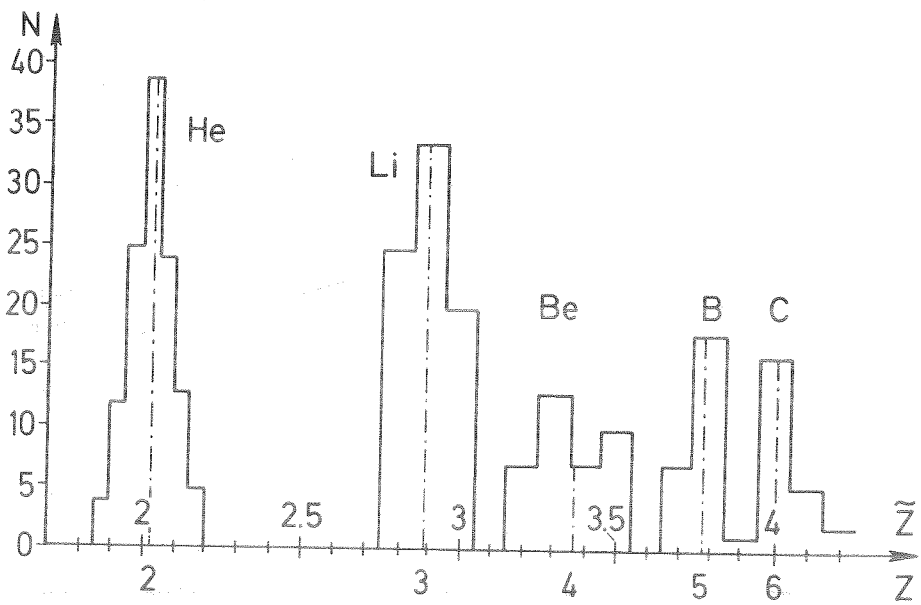


Fig.2:
Charge distribution as measured with the lacunarity-method.
Z : real charge
$\tilde{Z}$: measured charge (eq. 1)
N : number of measured tracks with charge $\tilde{Z}$

Experimental Electronics Department (Elektronik/Experimente)

R. Albrecht, J. Dengler, G. Eidmann, A. Fehres, H. Hammal, H. Hardel,
J. Hoffmann, H. P. Liebold, H.-G. Martens, W. Meufels, K. Mömerzheim,
K. Poppensieker, A. Przybyla, D. Quis, M. Richter, H.-G. Schmidt, G. Schneider,
R. Schulze, K. Senft, H. Spieler*, E. Sturm

GSI Darmstadt

Jiao D., Zhou Yun-yan
Institute of Modern Physics, Academia Sinica, Lanzhou, PR China

T. Batsch
Institute of Experimental Physics, University of Warsaw, Poland

The Experimental Electronics Department is involved in development and maintenance of electronic systems and equipment used for data processing and control in experiments at the UNILAC as well as at outsite experiments of GSI groups (e. g. LBL, Berkeley or CERN). The activities of the department include analog and digital signal processing, the digital online computer systems (hardware and software), control systems, and the assistance of experimentalists.

Detectors and Signal Processing

In 1982, about 250 NIM modules, 570 photomultiplier bases, and 20 special preamplifiers were built. In addition to these about 100 NIM modules and 32 NIM crates were bought. These modules were added either to the GSI NIM-pool or had completed the equipment of large experiments. Nearly 100 km of different coaxial cables were assembled in length between 1 and 70 m. These cables are used for signal transmission as well as for delay purposes.

The following list of new modules were added to the GSI NIM-pool in 1982:

- The Logic Fan-In-Fan-Out, LF4000, which contains 4 channels with 4 fast NIM inputs and 6 fast NIM outputs each, normal and inverted. The propagation delay is approximately 6 ns.

- The low cost Level Adapter, LA8000, which converts Fast NIM to TTL and vice versa. The module has a Fast NIM 50 Ω terminated input and a TTL 1 kΩ terminated input (0-4V). It has normal and inverted Fast NIM and TTL outputs capable for driving 50 Ω cables.

- The new octal Constant Fraction discriminator, CF8000, developed by M. R. Maier, GSI, contains 8 channels in one single 1/12 NIM module. It has separate thresholds for each channel. The deadtime and the output signal width can be adjusted via front pannel screwdriver potentiometers within a range of 20 to 400 ns. One deadtime output, two signal outputs (Fast NIM), one ECL differential line output, and an AC-coupled linear output is available for each of the eight channels. The walk adjust comes automatically by a gated baseline restorer. Internal hybrid delay lines on sockets allow delays from 2 to 50 ns. The fraction is 0.2 and may be changed via a special resistor network. Common to all eight channels, the module contains an inhibit input, an OR-output, and an analog output for the multiplicity and the sum.

The following modules were designed in 1982 and will be available in 1983:

- The hybrid preamplifiers, VT130. A fast preamplifier for energy and time was designed and built in using the hybrid technology introduced by the GSI detector laboratory. It allows the readout of single wires of the 0° detector used by the GSI/LBL/University of Marburg colaboration at LBL, Berkeley. The preamplifier (5 x 2 cm²) has a voltage gain of over 200, an output risetime of 3.5 ns, and a maximum signal output of -3 V at 50 Ω. A high input impedance version for small detector capacities as well as low impedance version for C > 20 pF are available. The preamplifier is noninverting, but a signal inversion may be reached by smaller changes. The noise charge of

* Now at Lawrence Berkeley Laboratory, University of California, Berkeley

the low impedance version was measured to be 3500 electrons RMS. About 600 of these devices will be built in 1983.

- The octal variable nanosecond Delay unit, DV8000. This module is intended to be a compact alternative to the usual 1/12 NIM switchable single cable delays. The module is able to delay 8 independent channels of Fast NIM pulses for a continuously adjustable time between 16 and 66 ns. It contains a NIM-to-ECL level converter, a variable hybrid delay line, line receivers and NIM output drivers for two normal and one inverted Fast NIM output for each channel. Time shifts with temperature change are less than with cable delays.

- The octal Logic Delay unit, DL8000. In most experiments information has to be stored about 150 to 300 ns until a trigger decision is made. This is usualy done by using a large amount of coaxial delay cables. The DL8000 has 8 channels of 170 or 380 ns delay for Fast NIM signals in a 1/12 NIM module. Although still more expensive than delay cables, it saves a lot of space in the experimental setup. The device contains a NIM-to-ECL level converter, a chain of three to seven 50 ns hybrid delays each followed by a line receiver and a NIM output driver for two normal and one inverted Fast NIM output. The temperature stability of the time delay is better than the one of delay cables, due to temperature compensation circuits.

- The 16-fold ECL-NIM-ECL Converter, EC1600. ECL differential line interconnections using twisted pair flat cables begin to be used more and more. The connectors are less expensive and the output drivers have less power consumption compared to conventional Fast NIM cabling. The 16 fold ECL-NIM-ECL converter will have ECL and Fast NIM inputs as well as ECL and Fast NIM outputs for 16 channels.

- The 8x8 Coincidence logic unit, CO8000. This module is a revised version of the older K8000. It handles 8 input and 8 output channels and allows coincidences or anticoincidences between any combination of input signals. The device has a strobe input, LEDs for each input and output, and Fast NIM inputs and outputs.

- The 8 channel Trigger Box, TB8000. Experiments need usualy more than one condition to trigger the electronic devices. The Trigger Box allows the inhibitation of 8 channels by a computer deadtime and the reduction of the data rate for each channel individually (selectable between 1 and 2^{16}). It delivers an OR-output and several ECL outputs for the use of CAMAC scalers.

Online Computer and Control Systems

In 1982, again over 80% of all experiments at GSI used a computer for the online data acquisition of their experimental data. More than 90% of them used the standard GSI online data acquisition system GOLDA, which had been developed by the department and which is under its support.

In 1982, the main hardware activities were concentrated on completing the DULINK, a fast data link between PDP-11 and IBM/30XX computers. It became the standard coupling hardware in experiments. The DULINK replaced the older coupling hardware and improves the reliability and maintainability of the computer coupling.

The development of the new sorting and readout CAMAC module TADEX was continued. It is a general purpose nuclear data acquisition system based on an auxiliary crate controller. For data acquisition, CAMAC dataway control is transferred to the TADEX module which transmits data directly from the CAMAC dataway through direct memory access (DMA) to the DEC VAX, PDP-11, or LSI-11 host computer. The DMA interface to the UNIBUS or Q-BUS TADMA-U and TADMA-Q was also developed. Layout versions for all modules were produced and are under test. These devices will become the 'second generation' standard readout system at GSI within 1983.

The GOLDA software running on the PDP-11 computers is used for accumulating experimental data, raw analysis, and monitoring. The system is part of the general EDAS system which also includes the IBM system SATAN. In 1982, the GOLDA subsystem was expanded to the following features:

- several new commands were included which are connected with the GOLDA-SATAN coupled mode,

- a new GOLDA version MA with much better user communication for the GOLDA-SATAN coupled mode and including the use of the new DULINK hardware was created,

- a new order of commands on the teletype commander box assists the use of the coupled mode.

For small data acquisition systems in laboratories and for some experimental setups a subset of the GOLDA program system, GOLDAX, was generated under RSX-11M V4.0, a standard realtime operating system from DEC for PDP-11 computers. Using the GOLDAX system one may generate, display, save, and fetch histogramming spectra together with the CAMAC memories NE9082 (16k by 24 bits) and the ADC router MR1000. The GOLDAX system will be extended in 1983 by a list mode, using the TADEX-TADMA modules.

A small PDP-11/23 system is used for controlling the magnetic and electrostatic elements of the velocity filter SHIP. In 1982, this system was improved in hardware and software.

A control system for the experimental setup of the applied heavy ion research group will also be based on a PDP-11/23 with a single CAMAC crate and RSX-11M operating system. In 1982, the experimental setup was improved including an INTEL 8085 controlled sample changer, beam stopper, and diagnostic elements. The computer control for all devices of this setup was designed and will be realized in 1983.

For small applications in experiment control (vacuum control, target position control etc.) a single board computer SBC-11 (DEC Falcon) was used instead of fixed hardware solutions. Working with the SBC-11, the change of the needs may be adapted easily without changing the hardware. The use of a PDP-11 family computer allows to use any PDP-11 or VAX system at GSI for development and test of the software.

The PDP-11/45 computers used for data acquisition in experiments have reached their capacities. The memory limitations and the small computing power defeat the expansion of programs and data storage. Therefore considerations begun in 1982 to replace the PDP-11 computers by new 32-bit supermini computers. The plan is to start the software development for these systems in 1983. Within about 3 to 5 years the new system should be available for experimentalists.

A Flexible Graphic Package for Plotting Experimental and Theoretical Data

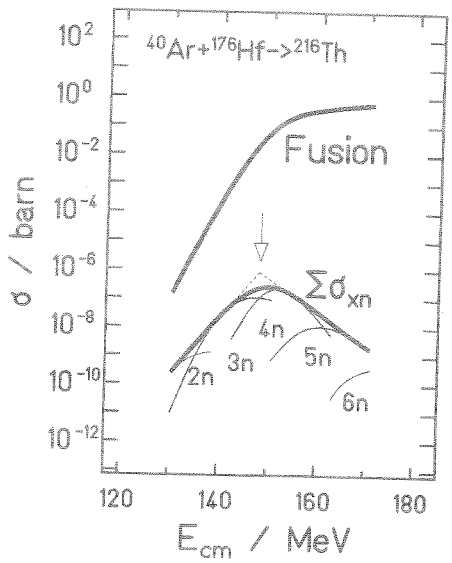
K.-H. Schmidt
GSI Darmstadt

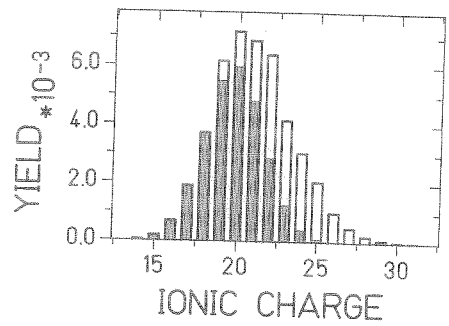
Experimental analyses or theoretical calculations often give a great amount of data in form of tables which are available in the computer. These results can be judged comprehensively in most cases in a graphic representation. Especially when the influence of parameter variations or other modifications is to be controlled, a direct, uncomplicated but flexible graphic output of data is needed.

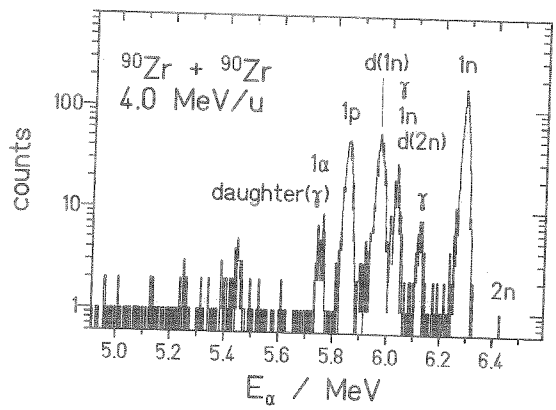
In the framework of the SATAN data evaluation system a new graphic package was developed to perform this task. It is able to plot quickly a few data points which have been entered with the editor (SPF) on a dataset as well as an extensive result from a computer program. The representation mode is automatically determined to show the data in a simple figure. However, several modifications may be specified to achieve the quality which is necessary for using the plots for a publication.

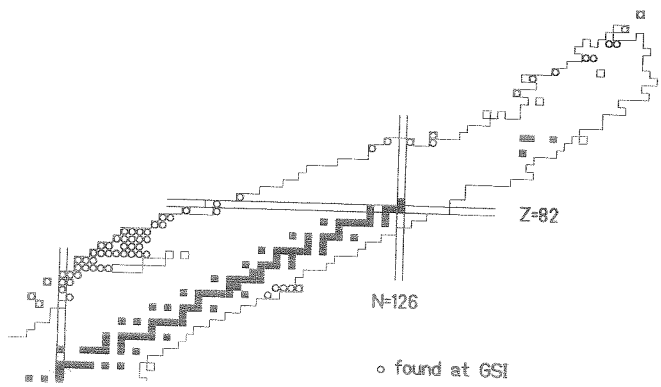
Similar as the desired figure, the dataset is structured in different parts: the title, the text on the abscissa and on the ordinate, several data groups and eventually additional text or special geometrical figures. The datasymbols as well as interconnecting lines can be chosen. Several representations are possible, e.g. also a histogram or columns. Two-dimensional data in a cluster- or a contour-plot may be combined with one-dimensional data on the same plot, enabling to show e.g. a trajectory on a potential surface. Data of a SATAN analyzer may be handled or combined with some additional information (e.g. text, calibration, theoretical curves). For this purpose the analyzer data can be read in a dataset and handled with the editor. The representation mode, e.g. the definition of a window, the scaling and line-widths of the figure can be varied by additional parameters of the plot commands. A detailed description of the graphic package is available[1].

The quality of the figures as well as the flexibility of the package is demonstrated by some examples from different applications.









[1] K.-H. Schmidt, Description of the SATAN Graphic Package, GSI 1983

Global Analysis with Plastic Ball Data [G]

H.H. Gutbrod, M. Löhner, A.M. Poskanzer, T. Renner, H. Riedesel,
H.G. Ritter, A. Warwick, F. Weik, H. Wieman
GSI Darmstadt, LBL Berkeley, and Universität Marburg

The global analysis methods (sphericity, thrust) were developed as a tool to detect and distinguish predicted two jet events at high energy e^+e^- storage rings from events with spherically symmetric emission patterns.[1] patterns. Both methods define a jet axis, the sphericity by minimizing $\sum_i p_{i\perp}^2$ and the thrust by maximizing $\sum |p_{i\parallel}|$ relative to this axis. The sphericity is calculated analytically by diagonalizing the sphericity tensor. One obtains the orientation of the sphericity axis, e.g. relative to the beam direction and three eigenvalues which define an ellipsoid that describes the shape of the event. The thrust analysis yields in addition to the orientation only the magnitude of the thrust, a quantitative measure distinguishing between isotropic and back-to-back emission.

The use of global methods to analyze the more complex events from heavy ion collisions was proposed by several authors.[2,3] Sphericity ($p_\perp^2$) overweights leading particles and gives two nucleons a different weight from a deuteron with the same energy per nucleon. Corrections for these shortcomings have been proposed, e.g. the flow analysis.[4] Since a global analysis has to be performed for each event, statistical fluctuations due to finite number effects and to limited experimental acceptance and efficiency are expected. Experimental data have to be compared with results from an analysis of theoretically calculated events, which have been filtered for experimental acceptance and efficiency. Most theoretical models have not yet reached the sophistication of the experimental equipment in the sense that they are not able to calculate all the measured quantities. Cascade codes do not include composite particles and hydrodynamical codes do not produce event-to-event fluctuations. This makes the comparison between experiment and theory difficult. Complete events generated with a statistical model calculation by Randrup and Fai[5] will be extremely useful to study the effect of finite number fluctuations and experimental biases. As global analysis allows to determine the shape of the event in phase space and takes into account all the measured correlations, it should be well suited to distinguish between emission patterns as predicted by the hydrodynamical and the cascade model. Figure 1 shows the result of a flow analysis[4] of 400 MeV/u Ca on Ca data. The angle of the main axis of the flow ellipsoid is plotted versus the square of the ratio of the largest to the smallest axis. A comparison of those results with theoretical predictions can be only done after the calculated events have been filtered for the experimental acceptance.

Danielewicz and Gyulassy, however, have proposed a new way to calculate and present the results of a flow analysis with the effect that averaged flow angles and aspect ratios that are independent of statistical fluctuations can be obtained. Analysed with this method, the Ca + Ca results are compatible with a mixture of prolate ellipsoids along the beam axis and spheres.

[1] S. Brandt and H. Dahmen, Z. Physik C1, 61 (1979)
S.L. Wu and G. Zoberning, Z. Physik C2, 107 (1979)
[2] J. Kapusta and D. Strottman, Phys. Lett. 106B, 33 (1981)
[3] J. Knoll, Proceedings 5th High Energy Heavy Ion Study, LBL-12652 (1981)
[4] M. Gyulassy et al., Phys. Lett. 110B, 185 (1982)
[5] J. Randrup and G. Fai, Phys. Lett. 115B, 281 (1982)
[6] P. Danielewicz and M. Gyulassy, to be published

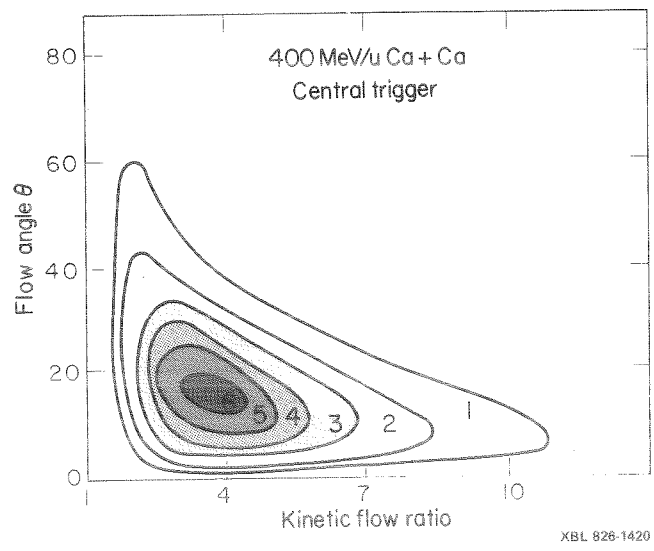


Fig. 1: Flow plot for the reaction 400 MeV/u Ca on Ca.

LISA, an On- and Off-line Data Analysing Program

Burkhard Kolb

GSI Darmstadt and LBL Berkeley

With the installation of the VAX 11/780 at the Bevatron in Berkeley to improve the on- and off-line data analysis for the Plastic Ball and the Streamer Chamber, it was necessary to have adequate software. Before the installation of the VAX the program package MULTI was used on the PDP 11/44, which was coupled through a shared disk to the data-taking PDP 11/50. Now the PDP 11/50 is replaced by the PDP 11/44, which has enough memory to handle the data taking and some on-line analysis. But with an improved data-taking program and the higher bus activity, MULTI analysed just a few percent of the incoming data. The program package LISA, which was developed in Heidelberg and used there for the Crystal Ball experiment, seemed to be a promising alternative to the old MULTI, which was designed for small computers like a PDP 11.

LISA is a FORTRAN program package to evaluate on-line and off-line experimental data of nuclear and particle physics on VAX computers. The design goal of LISA was to provide the user with a flexible, easy to use, safe, and expandable system. The analysis of experiments consists basically of two steps, i.e., reading and sorting events into histograms and the manipulation and graphical or numerical output of the histograms. Accordingly, LISA is divided into a process that deals with events and a large number of processes that act on the accumulated histograms.

All processes share the same common blocks, which are mapped as a global section. While the event-loop process is continuously executing, all other processes are invoked by a command, execute their code (for instance, display a histogram), and then terminate. The user has complete control over his terminal and can run whatever program he likes. While the event-loop is accumulating events, the user can develop completely independent new commands. Even if the user makes a typing mistake or a command process is aborted with an error condition, the event-loop will still work. Little effort is therefore necessary to make everything foolproof. If the event-loop process aborts for any reason, all the accumulated data are still available in the global section and can be saved.

Interactive commands define 1- and 2-dimensional histograms, conditions, and scatter plots. All the spectra can be filled automatically with or without conditions, or the user can supply a special routine with more sophisticated calculations. LISA can read events from a disk file or can access the on-line data through a shared disk from the data-taking front-end computer. For complicated experiments the user has to provide an unpacking routine to pick events from the input buffer and put the information in the one-event buffer. The one-event buffer is an array where the position in the array denotes a unique quantity like the ADC value of a detector. For experiments with large arrays of similar detectors, the more efficient approach of storing the value together with its detector number in a queue-like structure was used. This facilitates the automatic incrementing of histograms (all similar quantities in one 1-dimensional histogram or in a 2-dimensional histogram with the detector number as the Y-axis).

The code for the event-loop is optimized for speed of execution and contains only few modules of straight code. The code for all the command processes is highly modular and consists of some hundred subroutines contained in a library.

The graphic display of data is based on an expanded version of PLOT10. Graphic output exists in the form of histograms, contour plots, pointdensity plots, and scatter plots. The spectra can be fitted with gaussians, polynomials, and exponential functions, and the result can be displayed in the histograms.

In the last experiment LISA was already used for off-line analysis. Compared to the old MULTI system, running on the PDP 11/44, the LISA package on the VAX 11/780 was 200 times faster with exactly the same analysis. The hardware for the shared disk link from the PDP to the VAX was installed in December 1982; the software will be available for the next experiment in February 1983.

Computing Center

(H.Egger, S.Glückert, H.Hultzsch, J.Lowsky, O.Siart)

Installation Activities

Similar to recent years, the computing power needed to perform the GSI specific tasks in experiment data analysis, nuclear theory, and applied areas, has increased by about 40 % with respect to central processing power. In order to supply these resources to the user population, a series of changes and additions were required, allowing for good or acceptable performance conditions, especially in interactive operations. The major installation modifications were the following:

- integration of Memorex 1270 Telecommunications Controller into the GSI computer network,
- addition of IBM 3274-S3D Terminal Controller driving up to 32 display stations, including colour graphics,
- upgrade of one IBM 3274-B01 Terminal Controller to a capacity of 32 lines,
- installation of two IBM 3279 colour graphics displays running under GDDM (Graphics Data Display Monitor) allowing for experiment data analysis graphics as well as for standard graphics,
- addition of four Tektronix graphics displays (4014, 4016 and 4114) for experiment data analysis as well as for the development of graphics documents,
- replacement of the IBM 3032-006 main processor by an IBM 3081-D16 computer,
- installation of an FPS-164 Attached Processor for large scale simulation computing, allowing for processing speed up to 12 MFLOPS,
- addition of 16 disk drives Memorex 3652 with a capacity of 10.2 GBytes, increasing the total DASD storage to 25 GBytes, besides 169 GBytes within the Mass Storage System,
- installation of two frame plotters Benson 9436 and 9211,
- integration of the IDI-facility (Intelligent Dual Interface) into the two string arrays of Memorex 3650 disks, allowing for up to 40 % higher performance in heavy duty operations,
- addition of 24 alphanumeric displays (23 x Memorex 2078, 1 x IBM 3276),
- addition of a second IBM 6670 low speed laser printer for document printing,
- retrenchement of all punch card equipment including IBM 2501 and several IBM 0029 key punch devices,
- retrenchement of one IBM 1403/2821 printer.

The major goal of these installation modifications was allowing for increased utilisation of computing resources, as required to achieve the research and development objectives of GSI. A combination of highest possible quality of services in interactive operations, especially in experiment analysis tasks, with a high availability of all service functions to the computer user have been the conceptional aims. As in the years past, two loosely coupled computers, one of them including two tightly coupled processors, both operating under the same software MVS-SP1.3.0 with TSO/SPF, are coordinated by the Job Entry System JES3, allowing for the desired uniform user image with minimum manpower requirements for operations and system support. A general overview configuration plan (status December 1982) is shown in figure 1, while a more detailed description of the installation, including data paths and adresses, is displayed in figure 2 (next page).

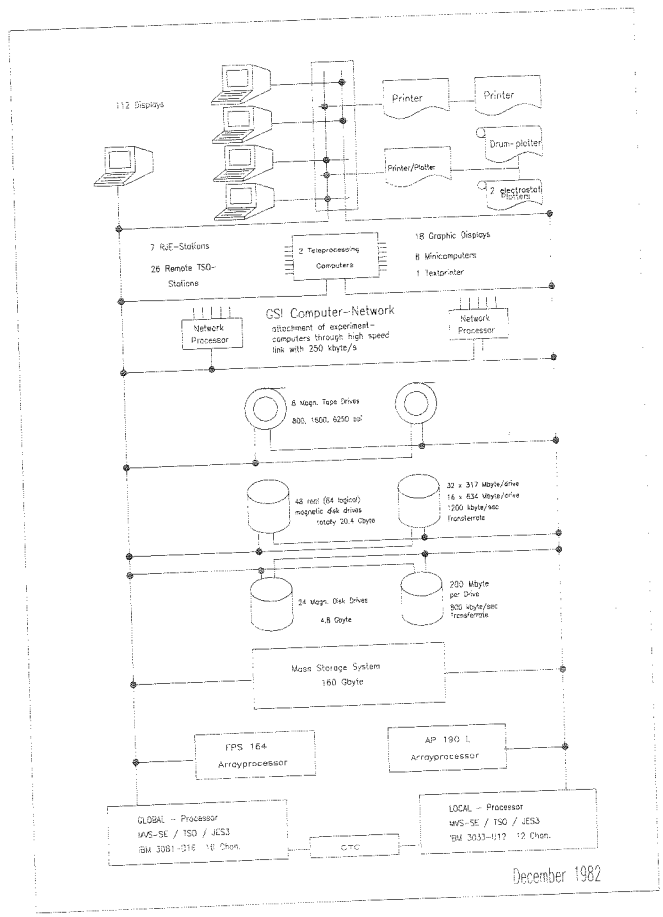


Figure 1: General overview configuration plan.

In order to allow for maximum availabilty and highest performance conditions, devices essential for system functions such as magnetic disks, teleprocessing equipment and tape drives can be accessed via two independent, dynamically interswitchable data paths from each of the

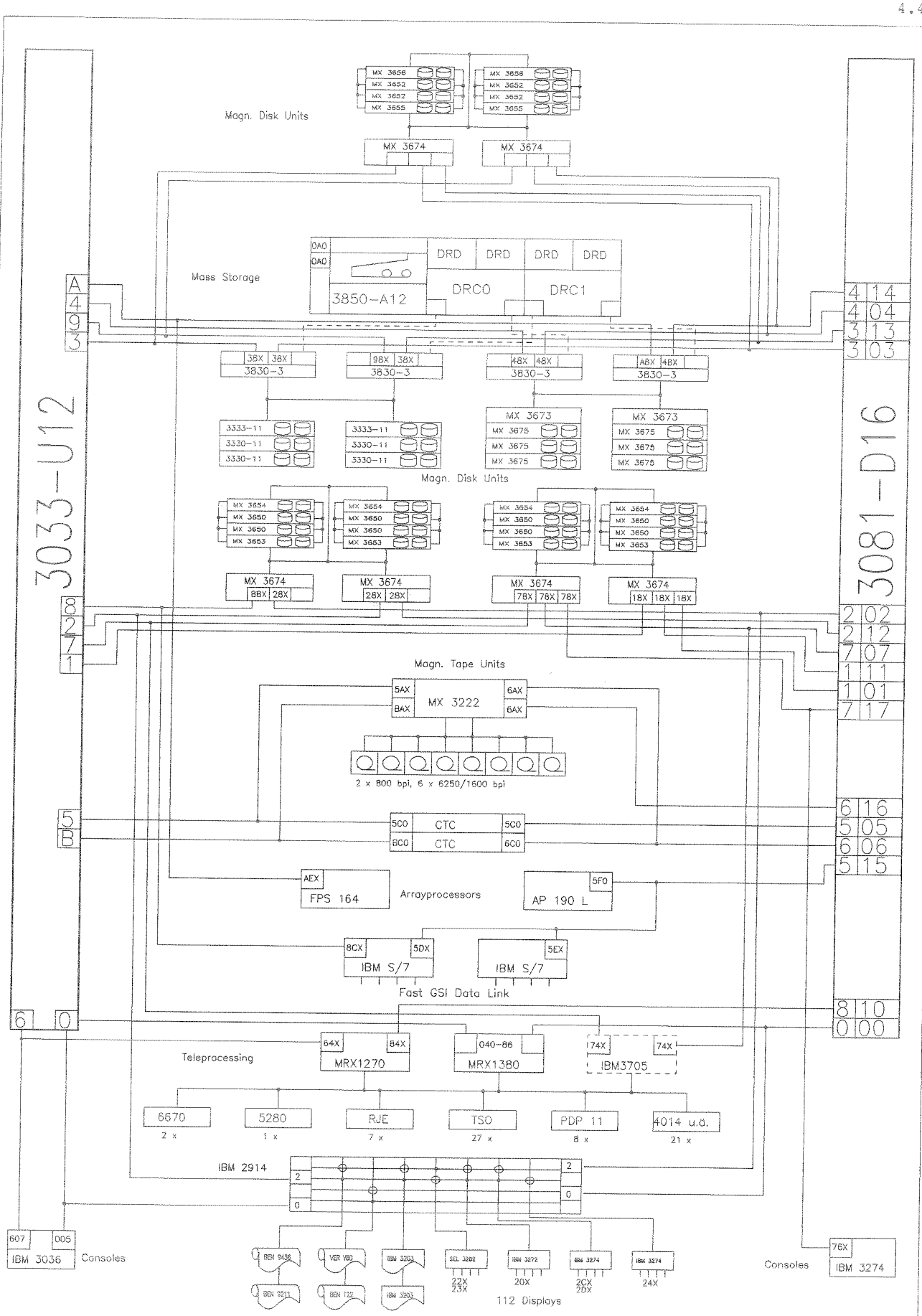


Figure 2: Detailed configuration description with data paths and adressing scheme.

three available processors within the two computers, while other equipment such as printers, plotters and display terminal controllers can be manually switched to different channels of the complex. In case of malfunction or emergency maintenance activities on one installation element, the total computer availability usually is not affected, because automatic system reconfiguration will use the operative elements to perform the system work.

Operations and Services

Computer services are usually scheduled 24 hours a day throughout the week, weekends and holidays included. Most maintenance activities are performed without interruption of user-services, with the exception of occasional electric power supply or air- and water-conditioning checkout. In addition, interactive services usually are interrupted for less than one hour during work days at 7.30 a.m. for data saving operations, but services for active experiments are normally continuously available.

The overall availability has significantly increased after the reasons for the unacceptable power failures throughout the year 1982 have been identified and rectified. But major software instabilities occured during the first weeks after the installation of the IBM 3081-D computer since the software manufacturer did not appropriately verify the operating system and other software components for multiprocessor operations before delivery. But computer consumption increased by the equivalent amount of computing power as supplied to the user population throughout the year 1979 in total. A major part of the increase was devoted to experiment data analysis operations. This is also becoming evident by the increase of tape mounts which average now to 250 per working day compared to 40 tape mounts four years ago.

Computer usage is displayed in four diagrams. Figure 3 shows the user CPU-time in units of IBM 3032 claimed from 1975 to 1982. The CPU-time on the processor 3033 and on

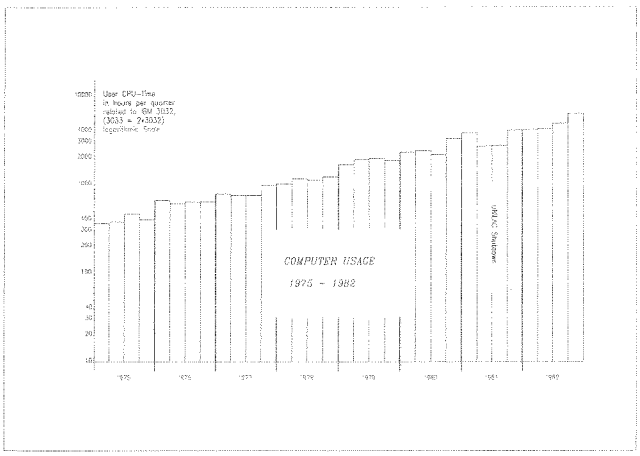


Figure 3: User-CPU-time from 1975 to 1982 per quarter of a year.

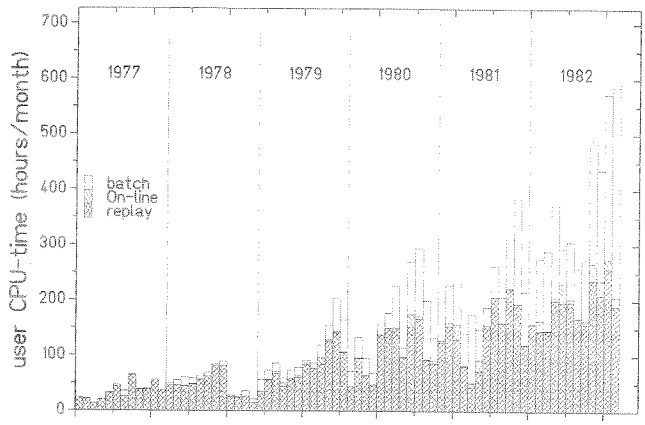


Figure 4: User-CPU-time for experiment data acquisition and analysis tasks running under EDAS from 1977 to 1982 per month in batch, on-line and replay modes.

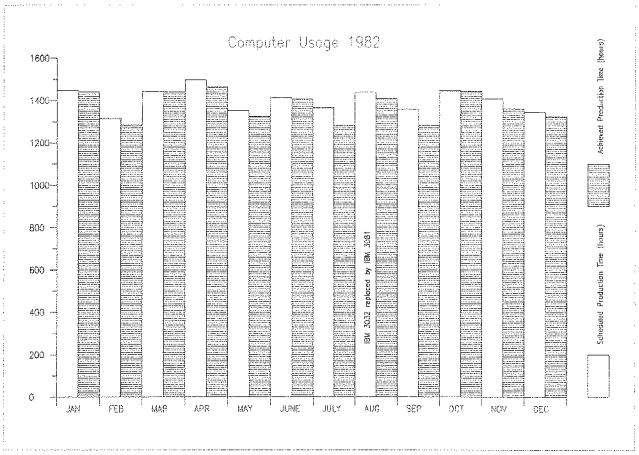


Figure 5: Scheduled and achieved production time in 1982.

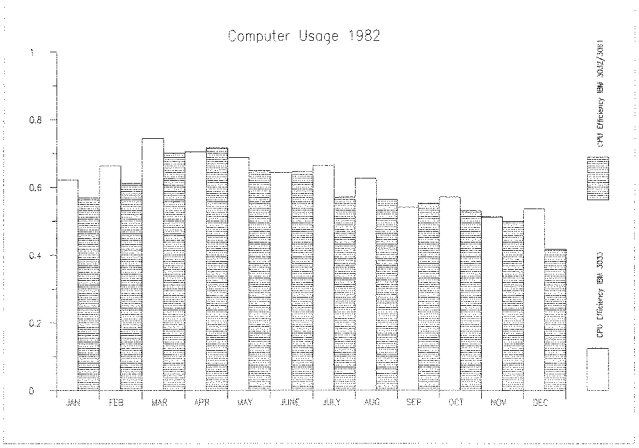


Figure 6: CPU-efficiency of the processors 3032, 3033 and 3081 in 1982. CPU-efficiency is CPU-time in problem status divided by the achieved production time.

both processors of the 3081 computer are multiplied by a factor of two representing the average speed difference between the processors. The user CPU-time consumed within the GSI-developed data acquisition and analysis system EDAS is displayed in figure 4. Scheduled versus

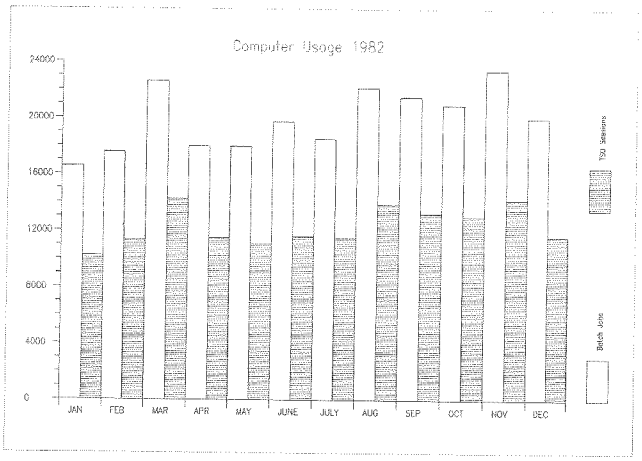


Figure 7: The number of batch jobs and TSO-sessions on a monthly basis in 1982.

achieved production times are displayed in figure 5, while figure 6 shows the CPU-efficiency for the computers 3033 and 3032 as well as 3081 for the time periods January to August and August to December respectively. In total 238.892 batch jobs were run in 1982 and 147.649 TSO-sessions were initiated. The monthly distribution is displayed in figure 7. By the end of the year about 62.000 individual dataset, VSAM and members of partitioned datasets not included, have been kept on-line in the system. The GSI-developed Migration and Back-up system MAKUP guarantees that those dataset are stored on real disk-volumes which are most frequent accessed while dataset larger than 1 MByte in size or less frequent accessed are kept on Mass Storage System Volumes (94 %). Due to the increased amount of data stored in the system, only 50% of the DASD accesses could be directed to real volumes resulting in MSS cartridge mount rates of more than 5000 per day. By the end of the year more real disk space has been added (USER07, USER08) reducing the MSS-load temporarily. Since maintenance and development activities at MAKUP require continuous manpower efforts, it is now considered to replace MAKUP by the software package Hierarchical Storage Manager (HSM) in 1983/84.

User support, user education and assistance are regarded as a set of major tasks which unfortunately can be covered only with limited personal resources. But more and more interactive support facilities such as the Help commands in TSO, SATAN and GNOM are developed for immediate problem determination and recovery. Even though the limited services create user's dissatisfaction when he is faced with weaker support than he is accustomed to from other sites. In order to allow for improved interactive training facilities, the introduction of the Interactive Instruction Programming System (IIPS) is scheduled for the later part of the year 1983.

Besides the two GSI developed software packages EDAS (Experiment Data Acquisition and Analysis System) and GNOM (Graphic and Numeric Operation Method), the following program packages have been supplied to the users of the GSI computers:

FORTRAN-G Compiler	PL/I Optimizing Compiler
FORTRAN-H Compiler	PL/I Checkout Compiler
FORTRAN H Opt. Enhanc.	PL/I FORMAC Translator
FORTRAN Interactive Debug	PASCAL Compiler (THD)
FORTRAN-PL/I Translator	PL-11 Compiler
WATFIV FORTRAN Compiler	SPEAKEASY Interpreter
SFORTRAN Makroprocessor	VS-COBOL
FORTRAN Mult.Prec.Arithm.	VS-ASSEMBLER
SPITBOL Compiler	SYNPLOT Syntaxgraphs
RUNOFF Textformatting	SOAP Parsergenerator
SCRIPT/DCF Textformatting	SLDGL Differ. Equ. Sol.
SCRIPT-6670 Textformatting	SSP Scient. Subr. Pack.
FORMAC Alg. Man. Lang.	PLMATH Scientific Subr.
REDUCE Alg. Man. Lang.	CPC Program Library
SCHOONSCHIP Alg.Man.Lang.	CERN Program Library
TSO Command Package	DESY Program Library
SPF Struct. Progr. Facility	EISPACK Eigenvalue Subr.
PCF Access Control	LDTS Local Display Simul.
RACF Data Security	GDDM Graph. Data Display
Westinghouse Fast Dump/Rest.	CALCOMP Graphics Softw.
MSI Multiple Syst. Int. Fac.	AGF Plotfile Interpreter
CA-Sort	ACF-TCAM Telec. Access.
OMEGAMON Monitor	SAM/E Sequ. Access Meth.
Information/System	MVS Module Packer
Mass Storage System Aids	SPICE for FPS-164
FPS-164 Compiler & Libraries	

System Software

Data and Telecommunication access within the operating system MVS-SP (Multiple Virtual Storage-System Products) Version 1.1 have been significantly enhanced by upgrading to DF/DS, DF/EF, and ACF/TCAM 1.3 (DF/DS = Data Facility/Device Support; DF/EF = Data Facility/Extended Function; ACF/TCAM = Advanced Communication Facility/Telecommunication Access Method). DF/DS allows for enhanced data access methods reducing operations up to about 20 % of the time required by earlier mechanisms, while DF/EF works with a new catalogue structure with better reliability and performance.

Throughout the year, MVS-SP has been upgraded to version 1.3, PUT 8202 and selectively higher. The performance improvements of the version 1.3 result from extended use of microcode, shorter path length within the system, enhanced algorithms for the queue management as well as less paging and swapping overhead.

The upgraded version of the System Productivity Facility (SPF) allowed for major improvements with respect to menu-operated interactive computer usage. It includes the Dialogue Management Services establishing significant functions for the development, test, and execution of interactive applications.

Besides the new software-tools described, major improvements were needed in order to achieve the performance goal, when accessing data stored on data sets, which were kept either on magnetic disks or within the Mass Storage System (MSS):

- more real disk space both for standard user data sets as well as for VSAM data sets
- migration of data sets and temporary experiment data analysis data sets from MSS to real magnetic disks
- implementing the "window staging" for the access to very large MSS data sets allowing for improved MSS performance in heavy duty operations
- development of a high speed data compression and decompression program

In addition to these techniques, several utilities have been developed in order to allow for easier systems management and performance. The major components are:

- Allocation of Virtual IO-data sets larger than 4 MBytes is automatically translated to an allocation of a real data set, thus achieving better total systems performance by offloading the total paging activities.
- A "soft-stop" operation modus of ACF/TCAM prevents from undesirable logon activities during special operations such as system dumps or software tests.
- A fast release of unused but allocated space on magnetic disks allowing for speedy interactive recovery from bottleneck situations during peakload operations.

In order to allow for remote operating during unattended night, weekend, and holiday shifts, the currently used Telecommunications and Interactive Program Components have been modified, and additional software has been developed. After final verification and tests, JES3-operations will run from a special userid under TSO from terminals connected through dial-up telephone lines. In case of system problems, the operator on call may analyse a problem situation from his typewriter, connected through his home telephone, whenever it is needed. A major increase in availability is expected to result from this facility, whenever system failure situations occur during unattended shifts.

Experiment data processing considerations

In 1982, the data acquisition and analysis system EDAS was used by 20 experiments for 93 days in online coupled mode (73 days for experiments and 20 days for calibration and testing). The requirements of future experiments at the UNILAC and other accelerators are growing with repect to complexity as well as computing power. With the existing experiment computers (DEC-PDP11) the demands for fast execution speed, large address space, and standard operating system for sensor oriented or time critical tasks may not be fulfilled. On the other hand it is not reasonable to use a large mainframe for experiment calibration and testing, as it is currently necessary in many situations.

Together with experimentalists involved and the experiment electronics group, the software and hardware requirements were specified. Several alternatives for future experiment computers, which may be interfaced to the central data processing facilities, were studied.

The investigation of currently available computers resulted in a concept for the future structure of computing systems at GSI, designed to meet all needs specific to experiments in Heavy Ion Physics.

Array Processor

H.-J. Lustig
GSI Darmstadt

FPS 164

At the end of April 1982, our new attached processor, the FPS 164, was delivered. The FPS 164 is Floating Point Systems' first attached processor with 64 bits long data words. It is the successor of the AP 190L which has been used at GSI for more than two years now. The AP 190L's data words are 38 bits long, only; so, the accuracy of floating point operations is more than doubled in the new model. There are other important differences: First, the AP 190L segments its data memory into pages of 64 thousand words; each page must be selected with a special command (not directly supported in AP-FORTRAN) before it can be addressed; second, there is a separate program memory in the AP 190L that is too small for large FORTRAN programs so that overlays have to be organized. Both restrictions do not exist anymore with the FPS 164. It can address up to 16 million words which are used for both data and programs. Our model is equipped with 120 thousand words main data which are equivalent to one million bytes of IBM main storage.

Late in May the first test users were able to try running jobs on the FPS 164. We noticed at once that the new FORTRAN cross compiler APFTN64 runs much faster and produces more efficient code than its predecessor APFTN. To give an example: APFTN needs 3.1 seconds CPU time on an IBM 3032 to compile a short program to normalize a vector; APFTN64 consumes only 1.3 seconds; in one of the loops, it replaces the division through a constant by a multiplication by its inverse, thus producing a more efficient code. These times can be compared to 0.7 seconds that FORTRAN H Extended needs to produce code for the IBM (without replacing the division by a multiplication).

One of the first programs to be converted was Prof. Cusson's 3-D TDHF code. Due to the larger storage area available to APFTN64 (APFTN addresses only one page of 64 kW AP 190L main data) more code could be transferred to the FPS 164 resulting in a decrease of IBM 3033 CPU time from about 10 % to 3 % of the total calculation time.

After several minor problems were solved and after the FPS 164 was fully integrated in the new version of our operation system (MVS/SP 1.3), the FPS 164 could be turned over to the general users at the end of August. One serious problem remaind open until the end of the year, namely, that APFTN64 overwrote the data control block of the output dataset. This meant that all users had to take care not to place APFTN64 objects into the same libraries as the objects created by FORTRAN or PL/I, because otherwise those members could not be read any more.

To facilitate using the attached processor's FORTRAN cross compiler APFTN64, the procedures APC, APG, and APCG were implemented. From the outside, these procedures look almost the same as those used at GSI to compile and run FORTRAN or PL/I programs (i. e. FHC, POCG, etc.). For the user, the major difference lies in the fact that he must specify two input datasets, one containing the APFTN64 code and another with those FORTRAN statements that are to be executed on the host. The cross compiler input is given under the DD-name APC.SYSIN, the host FORTRAN code under C.SYSIN.

The general acceptance was good; those who had used the AP 190L agreed that it is much easier to convert a program to the FPS 164 than it was to the AP 190L. As was to be expected, there were several problems, however. For example: even though APFTN64 is a FORTRAN77 compiler, it does not accept IF-THEN-ELSE-ENDIF structures. APLINK64 which binds several APFTN64 object moduls together and resolves external references by scanning system and user libraries causes problems if it must read out of concatenated datasets. A severe problem turned up towards the end of November when we found out that there are certain cases when APFTN64 does not handle multi-dimensional arrays properly.

Those programs that run error free can expect execution speeds between 50 and 100 % the speed of an IBM 3033; for some test programs it was even possible to reach about twice the speed of an IBM 3033.

AP 190L

The 'old' array processor AP 190L was used throughout the year with an average allocation time of about 40 hours per week with peaks of more than 140 hours in certain weeks. Software and hardware ran without major problems and even the switch of host computers from the IBM 3032 to the IBM 3081 did not cause problems.

Experiment Data Processing

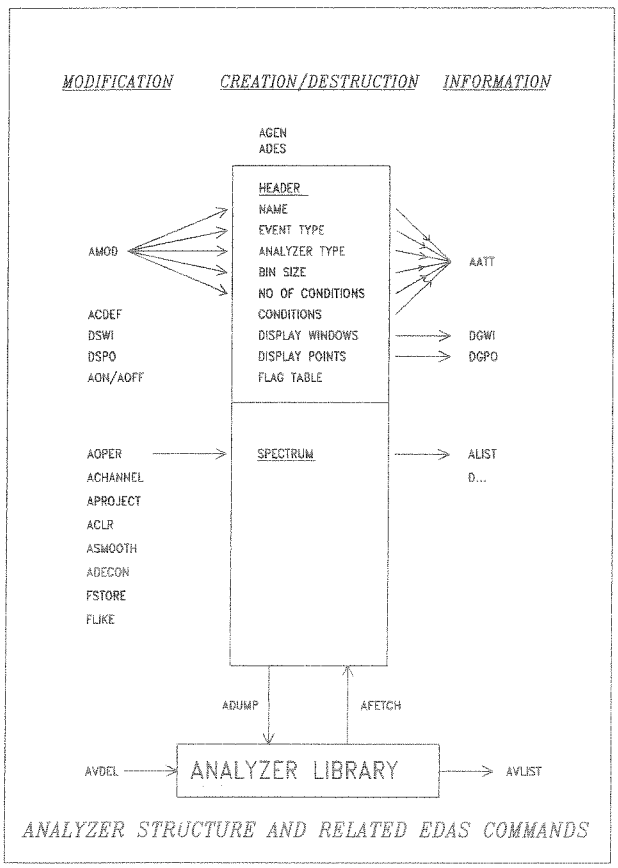
F. Busch, H. Göringer, V. Hartmann, J. Lowsky, D. Marinescu, D. Pissowotzki,
K. Winkelmann, G. Zaidman
GSI Darmstadt

The System to Analyze Tremendous Amounts of Nuclear Data (SATAN), developed as part of the Experimental Data Acquisition and Analysis System (EDAS) of the GSI, has been improved further to match the growing refinement and complexity of experiments and the requirements of on-line operations.

The interactive spectrum evaluation was improved by introducing a variety of new commands supporting the following functions:

- Arithmetic calculations with spectra or parts of them. Spectra or scalars may operate on spectra.
- Automatic Peak Search. This algorithm allows fitting of Gaussian or Lorentzian Peaks without specifying their position.
- Analyzers may be fetched or listed according to the period of time they were created.

The Analyzer structure and available commands for information and modification of contents are summarized in the following figure:



ANALYZER STRUCTURE AND RELATED EDAS COMMANDS

The general concept of fitting mathematical models to physical data with SATAN was extended and improved. With this package a variety of fit functions (Polynomials, Exponentials, Legendre Polynomials, Gaussian- and Lorentzian functions) are supported and the additional possibility of user defined fit functions with an unlimited number of parameters is available.

The graphics capabilities of SATAN have been extended by the implementation of the GSI Graphics Interpreter (see special report). In addition to the existing graphic devices, three different raster plotter types and the IBM Graphics screens (GDDM) are supported. Furthermore, virtual devices and datasets are available for temporary storage of graphic displays. Vectors and text can be drawn during a SATAN session with interface programs, where the coordinates can be specified in a presentation independent way. The SATAN graphics package to produce graphical representations of data for publications which is based on the Calcomp interface, is a good example of user written subsystems offered with SATAN (see special report).

Due to increasing complexity of Analysis Programs the compilation time as well as the execution time were growing, too. Programs with up to 10000 lines of PL1 code were produced. For these programs, creation of in-line code is a compile and run time consuming approach. For this reason, different analysis programs were studied in view of compilation and execution time optimization. The results of this study is presented in a separate report.
The Input/Output handling in SATAN is now performed with two commands INPUT and IOUTPUT, which provide a comprehensive way to direct the data flow in online as well as in replay mode from and to any device available.

The support of floating point arithmetics in GOLDA and SATAN has been unified. New macros have been created expanding basic arithmetics written with PL/1 syntax to the corresponding PL11 code, which is used for analysis programs running with the EDAS subsystem GOLDA.

The EDAS system functions are continously extended. Therefore it was nessesary to introduce an interactive help facility for topical informations, which is available during the SATAN session. This facility is imbedded into a new help concept and allows any user to have the availability of an online help or the printout of actual versions of the SATAN manual (see special report).

Temporary data sets as well as the analyzer library reside now on real disks. As a result, the access to the temporary storage and to SATAN analyzers is reduced significantly.

The integration of front end computers for experiment control and the central computers for data analysis and large scale data processing was developed further (see special report).

EDAS Documentation and interactive HELP

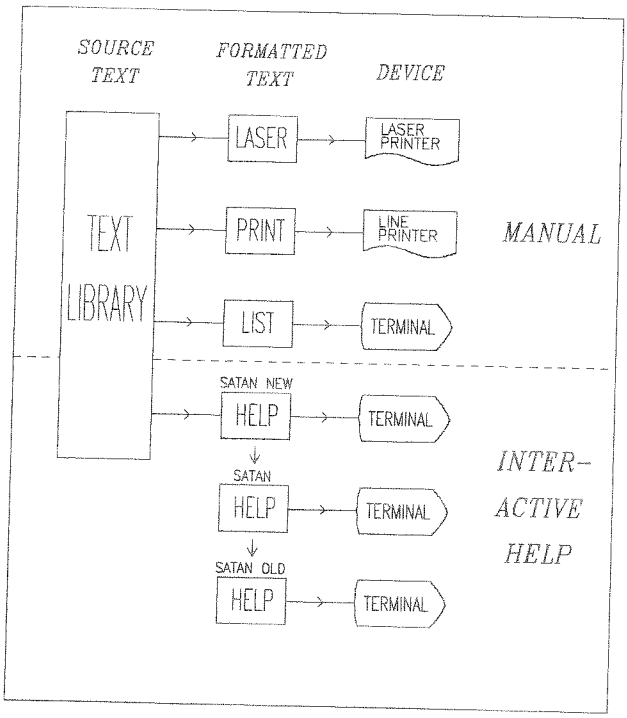
H. Göringer
GSI Darmstadt

The variety and complexity of functions available in the Experiment Data Acquisition System (EDAS) increased considerably in the last years. As a result the different versions of EDAS differ significantly from each other. To facilitate the use of EDAS, and to supply the user with updated information about each version of EDAS, a new documentation system including an interactive HELP facility has been implemented.

The system uses the IBM text processing program SCRIPT/VS. The main objectives are:

- easy updates of text sources simultaneously for the EDAS manuals and for the interactive HELP,
- easy access to all documentation facilities for all users of SATAN (System to Analyze Tremendous Amounts of Nuclear data).

A standard tool for the documentation of user defined commands, including his own interactive HELP facility, is offered to the users by the TSO-Command $SCRI. It has been designed to format easily either single descriptions of a command, macro, or procedure, or single text chapters, or even the whole EDAS documentation including all volumes. The formatted output text, which may be produced optionally with index and table of contents, can be directed to the terminal, the line printer, or the laser printer (see fig).



EDAS Documentation Concept

To format pages for the manual, a number of SCRIPT macros has been created, especially for the description of the commands, macros, and procedures, which have a characteristic periodical text structure. As far as possible, two ideas were followed:

- Writing a documentation, the author should not care about formatting.
- All definitions concerning layout and formatting are performed at one central place.

The first aim is largely realized with the aid of a 'mask' containing the names of the SCRIPT macros needed for formatting. Writing new pages, the author essentially only has to fill up this 'mask' with text.

Following the second principle, future modifications and further developments are facilitated considerably. So, the layout of all pages can easily be changed by just modifying some macro definitions or parameter values. The same holds, correspondingly, for entries in the index, for headings, figure names, and footnotes, or for text passages that may vary in the course of time (e.g. the current computer names). They are named (and defined) in central members of the SCRIPT library, and are referred to within the text by only using their symbolic names. This prevents not only from scanning the whole manual if an often used expression must be changed, but it also makes the use of cross references quite easy.

In order to give the scientists the possibility of online access to information without reading thick manuals, the command 'HELP' has been implemented in SATAN. It provides within a SATAN session several levels of information:

- a list of the existing groups of EDAS commands (e.g. analyzer commands, display commands, or fit commands),
- sections from the table of contents,
- complete descriptions of EDAS commands or user defined commands,
- informations about the parameters of the commands defined within the current SATAN session, and
- the differences between the static 'normal' and the dynamic 'new' version of SATAN.

Improvements in EDAS Coupled Mode

F.Busch, D.C. Marinescu, and M.Richter
GSI Darmstadt

During the past year, the capabilities of SATAN were made available on all DEC PDP-11 Front-End computers, and the software support was improved significantly. As a result, twenty experiments were performed in coupled mode.

The new version of the GOLDA subsystem with enhanced control functions for the coupled mode was constantly used and easily accepted since it provides a comprehensive environment. On the SATAN side, the functions related to data output to external devices have been reviewed and new features have been implemented. It is now possible to write the experimental data directly to a real or virtual disk. The advantages are:

- elimination of the dead time required for mounting of a new tape
- data can be accessed immediately for offline data analysis
- the post experiment data analysis is easier because the data sets are catalogued

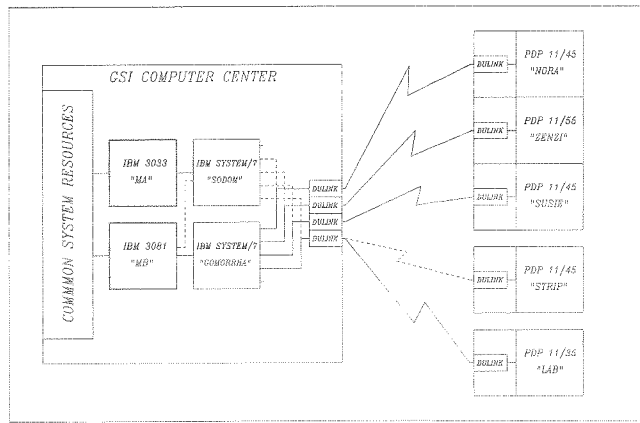
To further facilitate the online mode, a number of users' suggestions were implemented. Among them, we note an improved version of the 'commander box' which allows push-button execution of the most frequently used commands. A number of user defined commands both for SATAN and for GOLDA are available now.

The development of the new DULINK and of the related software succeeded in 1982. At the end of the year, all three DEC PDP-11 Front-End computers in the "Messstation" and a test one in the laboratory of the Experiment Electronics group could be supplied with a fast data link connection to the IBM 3033/3081 main frames. The link line to the "Stripperhalle" will be installed in February 1983. The layout of the present configuration is shown in the figure. On the main computer site, open back-up connections are available.

The installation of the DULINKs and the corresponding change of the link software led to a significant improvement in reliability, transmission speed, and overall stability. Because of the enhanced inter-link protocol, the hardware driver software modules in the DEC PDP-11 and the IBM SYSTEM/7, which is the Front-End processor on the main computer site, are much smaller, simpler, and faster now.

DULINK was developed in-house by the Experiment Electronics group. Data transfer between PDP-11s and the IBM SYSTEM/7 is performed by pairs of DULINK modules. The PDP-11 attached DULINK performs a cycle-steal (DMA) read of data from PDP-11 memory and transfers them to the DULINK on the IBM SYSTEM/7 site which in turn does a cycle-steal write to IBM SYSTEM/7 memory and vice versa. This technique and the new internal link hardware protocol, which performs automatic retries after parity errors, allows for better use of both CPUs. Only the initialisation of a transfer and the acknowledge of its termination requires short actions of the processors.

The maximal cumulative transmission speed of a single line or several lines in parallel, including software overhead in the DEC PDP-11, IBM SYSTEM/7 and the IBM 3033/3081 main frames, has been measured to be 450 KBytes/sec which is the speed limit of the interface between IBM SYSTEM/7 and DULINK. In an experimental set-up the rate of a single new line is now limited by the speed of the CAMAC interface (250 KBytes/sec). The interrupt rate on the SYSTEM/7 and PDP-11 processors amounts to 125 per sec in this case. The old RXL-11 hard- and software, which was formerly used for the fast data link to the PDP-11 "SUSIE", was capable of about 180 KBytes/sec with an interrupt rate of 180 per sec.



A CROSS MEMORY APPROACH TO EXPERIMENTAL DATA PROCESSING

D.C.Marinescu GSI, Darmstadt

The SATAN subsystem of EDAS has a wide spectrum of functions needed for the analysis of experimental data. Among its nice features should be mentioned: the user command language, the analyzer handling, the graphic capabilities, and, most notably, the live display facilities, etc. SATAN provides an interactive environment in which the user written analysis procedure can be controlled.

As for any other user subsystem, the SATAN development should reflect, on one side, the new user requirements and, on the other side, the enhanced hardware and software capabilities of newer computing systems available. Changes in the subsystem's basic control information flow are necessary for two reasons:

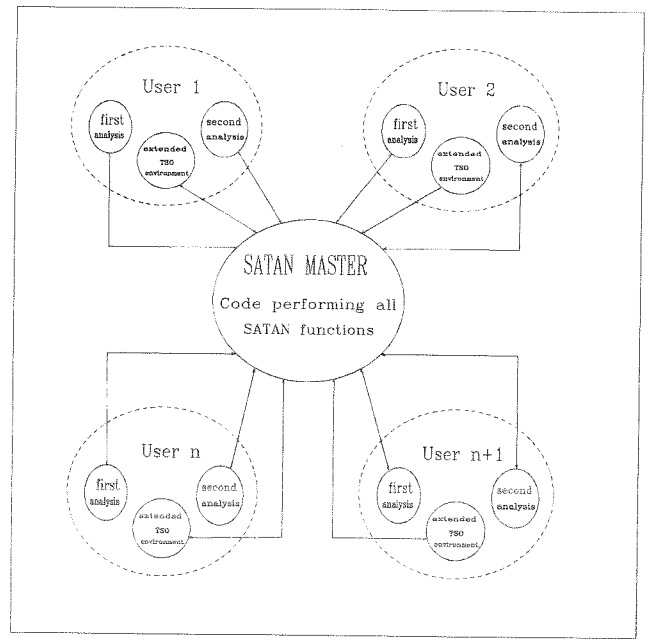
- There are new features and functions which cannot be built in the frame of the present SATAN structure. An example is the protection of the SATAN system code from being overwritten by the user written analysis procedure; another one is the support of more than one user analysis procedure and the dynamic control of all such procedures. Running a number of analysis procedures in parallel under interactive control could speed-up data analysis for experiments with many parameters per event.
- The hardware and the software support of the SATAN host computer is continuously upgraded. Examples are: the 2 Gbytes address space size offered by MVS/XA and the support offered by the Cross Memory Services. In the framework of present SATAN structure it is rather difficult to benefit from these new facilities.

Cross Memory Service is a tool designed for system use to allow cooperation among different address spaces; it allows programm sharing, data sharing, and data movement between different address spaces. The 'late binding technique' provides an efficient way to call procedures which are not linked together with the load module which is currently executing; this is especially convenient for program development and for dynamical change of modules in error. Since the call is performed by a new machine instruction it is quite efficient as our recent tests confirmed.

Currently, each user has his own copy of the SATAN subsystem linked together with his unique analysis procedure. The parallel activities are carried out by different tasks running in the user's address space. Since each user has a copy of the code providing SATAN functions, the system is heavily loaded and has a high paging activity.

The SATAN subsystem can be redesigned using Cross Memory Services so that a permanent, nonswappable address space is the host for the code implementing the functions. Each user may initiate from his address space one or more attached address spaces, each performing one analysis procedure by using the services provided by the SATAN-MASTER. From his extended TSO environment, the user may control the execution of each of his attached analysis procedures by sending commands via the SATAN-MASTER. The main advantages and disadvantages of such a solution are:

- New functions can be built-in without the penalty of a more complex control logic; synchronisation among different parallel activities will be carried out mostly by the standard system functions.
- The duplication of code will be avoided and the SATAN system code will be protected.
- Since Cross Memory was conceived as a tool for operating system design, its Services do not have a simple user interface.
- The SATAN modules must be restructured to take into account the CMS restrictions.



The experimental data processing system structure. Code sharing and inter address space communication supported by MVS with Cross Memory Services.

Optimizing the Data Analysis in SATAN

Klaus Winkelmann
GSI Darmstadt

At least a quarter of the CPU time provided by the Computing Center is used by SATAN, the mainframe part of EDAS. Most of this time is spent in the analysis part, in which events are classified, selected and accumulated. This program is written by the user, though for frequently used pieces of code a set of macros is provided. They are expanded by a compiler written in SPITBOL in executable inline PL/1 code.

In the past, this concept of creation of inline code was sufficient in all cases. But with time the number of parameters per event has increased (3 to about 100), also the number of analyzers (10 to 300) and with that the complexity and size of the analysis programs. In big programs several drawbacks of the current concept have shown up:

- The compile time became too long for working interactively (order of minutes of CPU time).
- Because of too many elements in the program (e.g. more than 1600 variables) the PL/1 Optimizing Compiler is no longer capable to optimize the code.
- The size of the expanded code has increased considerably and could lead to more operating system overhead due to paging and thus to a diminished throughput.

Therefore we decided to try a different way: frequently executed inline code was replaced by calls to subroutines written in Assembler. The optimization was done in two steps:

- a) inline code, which resets all analyzer flags before the next event is analyzed, and
- b) in addition inline code which deals with accumulating data and setting condition codes (macro $ANAL)

were replaced by calls to Assembler subroutines.

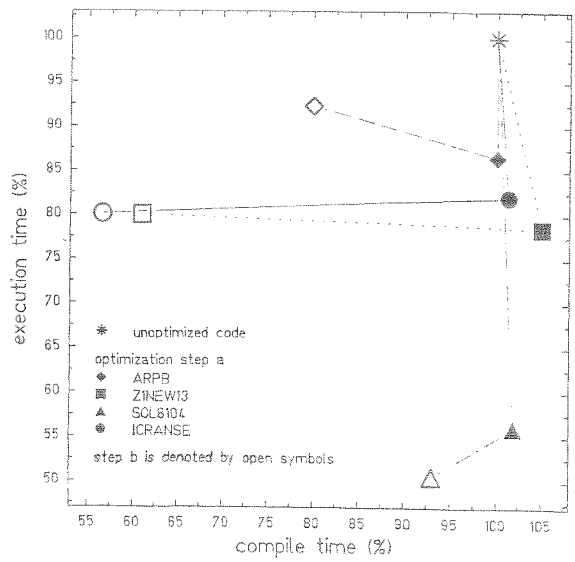
A set of analysis programs were run in SATAN to test this concept. The properties of four examples [1] are summarized in the table. The programs were compiled applying the optimization steps a) and b) described above, then loaded and executed under SATAN (normal) evaluating typical data. All measurements have been carried out on the processor IBM 3033.

Properties of measured programs

	ARPB	Z1NEW13	SOL8104	ICRANSE
parameters/event	6	14	< 37	< 513
no of analyzers	31	31	131	246
avg no of cnds/anal.	0.06	1.63	2.77	0.36
no of $ANALs	11	36	123	>165
compile time (sec)				
unoptimized version	10	18	45	76

In the figure compile and execution time for the various programs and for the steps a) and b) are compared.

The times are normalized to the time spent by the unoptimized programs. It shows that step a) saves up to 45% execution time while b) helps in decreasing the compile time, for big programs also the execution time.



These advantages are due to the facts

- that code is reduced by using calls instead of inline code,
- that in Assembler better use can be made of the register set, most probable data sizes and types are considered, and the underlying hardware structure is exploited [2],
- that a lot of local variables could be abandonned (step b)

Step a) is more successful in saving execution time because the work which has to be done per call is always bigger than in b). Thus overhead due to the call can be overcompensated for by coding in Assembler, whereas in b) the small or less complex programs suffer from the calls. We note that when applying a) and b) the size of the static storage of the analysis program will be decreased to a size of about 70% in all programs.

Since step a is always a gain it will become the default. Usage of step b is offered as an option for the SATAN compilation command PLOB.

References

[1] following programs have been used: ARPB (V.Hartmann, GSI), Z1NEW13 (D.Schuell, GSI), SOL8104 (M.Kraemer, TH Darmstadt), ICRANSE (S.Gralla, GSI).
[2] James W. Rymarczyk: 'Coding Guidelines for Pipelined Processors', IBM Technical Report TR00.3107, 1981; 'MVS/SP Tuning Cookbook', IBM Manual GG24-1516-01, 1981

Graphics and Numeric Operating Method (GNOM)

I. Giese, W. Kynast, M. Feyerabend, M. Steitz
GSI Darmstadt

The Graphics and Numeric Operating Method GNOM, is an interactive procedure oriented programming language for graphics and numeric applications, which has been designed with special attention to high software reliability. The system has been developed at the computing center of GSI in cooperation with KFA/Jülich (ZAM) and is offered in a simple version since 1981. In March 1982 the new version 1.2 of GNOM was offered to the user. This version allows the user to define and change procedures. Within these procedures all GNOM commands are callable to define and change data and pictures, controlled by parameters and using powerful control structures.

The presentation of GNOM at the Hannover fair was a success; it proves that both, industrie and research need a flexible and powerful graphics system with a graphics language as GNOM.

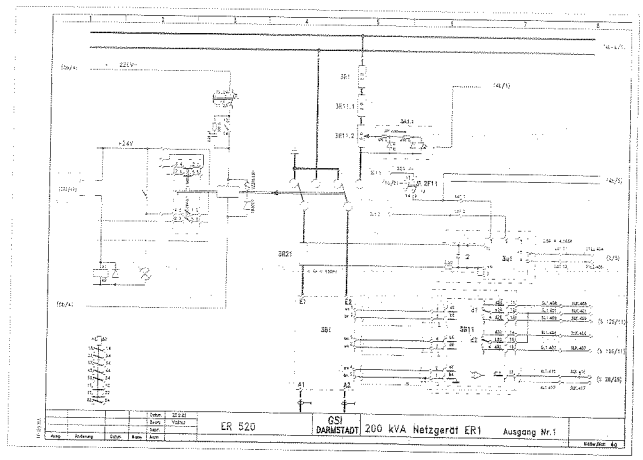
Based on experiences with this version in many applications in GSI and KFA, the current GNOM-Version 2.0 was offered to GSI users in december 1982 with the following new features:

- automatic reformating of procedure and object text.
- interpretation of GNOM commands from sequential or partitioned datasets.
- free selectable output units
- interface to SPF and TSO
- improved error diagnosis and error messages
- improved software reliability
- support of GNOM procedure- and object libraries

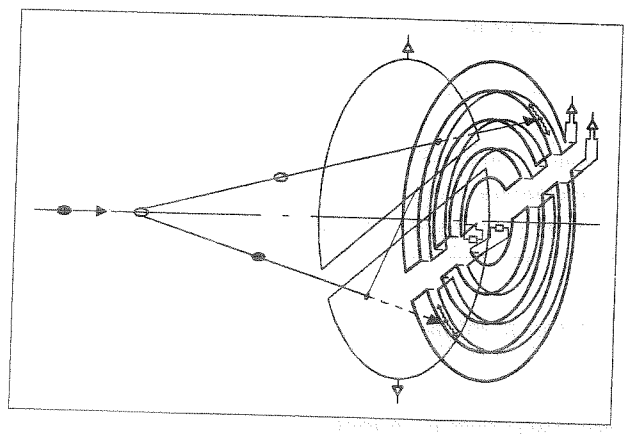
The GNOM system description has been published. Part of this, a short write up into the GNOM system is available in English and German language.

The wide range of different GNOM applications at GSI is extended continuously. The main applications are:

- General documentation, overviews and diagrams
- creation of foils and pictures for publications
- Electric circuit design and documentation. The example below is one of several electronic circuits, which differ only slightly. All these plans are created by one GNOM procedure.



The scheme of a particle detector, which was created with a relatively simple GNOM procedure, (see: Construction and Performance of the Position-Sensitive Particle Detector with Delay Line Readout; B. Liu, W. Enders, D. Liesen, R. Schulze) is a good example for GNOM applications, where graphics work may be done faster by the usage of GNOM procedures.



One step in the direction of integrating the graphics produced with GNOM and text produced with SCRIPT was done: For the postprocessor of SCRIPT an interface to GNOM has been included to define pages of text as GNOM objects. These objects can be displayed on any graphics device or changed according to the wishes of the user. In this way, graphics informations and formatted text may be merged and plotted together.

GSI Plotfile Interpreter

I. Giese, K. Schwinn, G. Zaidman
GSI Darmstadt

Graphics in GSI is produced with usage of CALCOMP interface programs. With simple subprogram calls, a device independent interface was offered for Tektronix displays and a drum plotter. With increasing number of supported graphics devices and in view of graphics standardization, it was neccessary to develop a more general device independent graphics interpreter. This program interprets graphic primitives, point, vector, line, text, area, and graphic attributes (color, linestyle, linewidth, marker and textform). Pictures may be stored on datasets or they may be displayed on any graphic device available in GSI.

The graphics interpreter is based on a device independent graphics metafile (AGF-plotfile). This file structure was originally defined in 1978 by a group of the AGF (Arbeitsgemeinschaft der Großforschungseinrichtungen) as one of the first general graphics metafiles (see Reference). The principle of this structure is now part of the GKS (Graphisches Kernsystem), which is accepted meanwhile by ANSI and ISO.

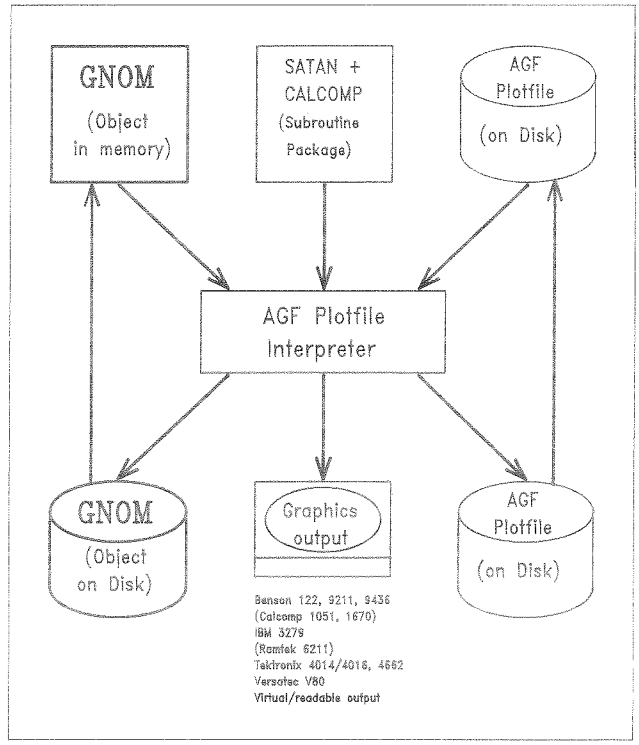
The interpreter, developed in GSI, is independent of other graphics programs and offers one basic interface to GNOM and SATAN and to CALCOMP oriented subprograms written in FORTRAN or PL/1. Additionally, the graphic interpreter program may be started stand-alone to interprete files on datasets, created by batch sessions or distributed from another installation, for output on any graphics device.

The new graphics output devices are three electrostatic raster plotters (Benson 9436 and 9211, Versatec V80) and the graphics terminal IBM 3279 with GDDM (Graphical Data Display Manager). This terminal supporting the full screen mode for editing (SPF) as well as graphics has been proved to be good for developing programs with interactive graphics.

The interpreter offers the following new functions integrating device specific abilities:

- Besides the device specific hardware characters, seven different software character fonts are supported.
- Thick lines are drawn with different methods. Examples are found in many places of this scientific report.

Besides the AGF-plotfile format the GNOM format is part of the supported graphics representations. From the figure below, it may be deduced, that a picture created with SATAN or with the CALCOMP interface or existing in the AGF-plotfile format, can be transformed to a GNOM object. With GNOM, the picture may be corrected, extended, or prepared for publication. With this interface, GNOM is the editor for SATAN and CALCOMP pictures. The typical functions are: Creating a picture consisting of two or more individual pictures and adding titles in a special character font or change parts of this new figure.



Reference: The AGF Plotfile - towards a Standardization for Storage and Transportation of Graphics Information, G.Enderle, I.Giese, M.Krause, H.P.Meinzer; GMD/IGS Bonn, 1979

Engineering and Technology

E. Malwitz, K. Blasche, W. Bleuel, H. Gaiser, C. Hoffmann, K. Illert,
H.-R. Kiesewetter, U. Kopf, W. Schmidt
GSI Darmstadt

Engineering Department

Fig. 1 shows the distribution of engineering effort in 1982. With the end of the UNILAC improvement program the related activities decreased, while activities for SIS have now increased. Design work for the SIS has included studies for the beam transfer line and the ring tunnel, as well as for the various machine components including the ring magnets.

More time became available for experiments after completion of the UNILAC improvements.

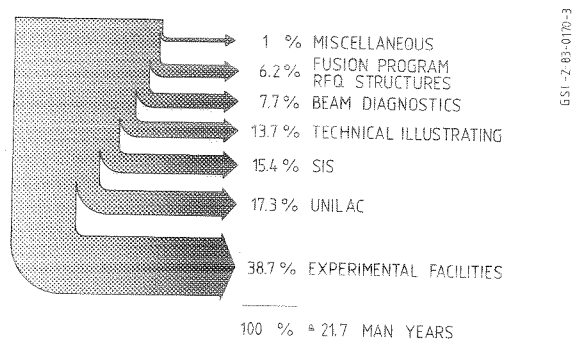


Fig. 1: Distribution of engineering effort in 1982

Production Engineering

As shown in Fig. 2, altogether 1209 orders were passed into GSI workshops and 207 orders were filled in external companies. In addition the production engineers have written 26 of the more complicated programs for the NC milling machine, while 38 simpler programs were prepared by the machine operator. A report of all parts fabricated in 1981 on the NC milling machine has been prepared. In 1983 it is planned, to install an additional NC lathe. In order to further extend this facility it is envisaged to prepare punched tape programs for the two NC machines on a small, independent computer system with a grahics system. Tenders have been called for this system in 1982. In addition a comparison is being made of various CAE program systems.

Workshop

The mechanical workshop handled 646 jobs, the heavy workshop 466, and the technological laboratory 67. About 15 % of the workshop capacity was again required for small tasks that had to be handled immediately.

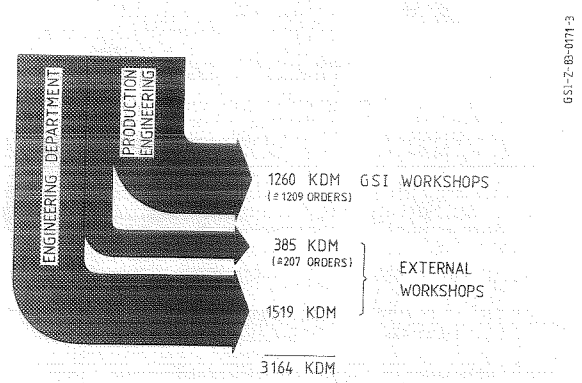
The heavy ion workshop has been improved with more working space and the installation of new cutting machines.

UNILAC

Following the success of the new end plates in the Alvarez tanks III and IV, this design has also been adopted for tanks I and II. This will result in more inter-tank space and improved thermal properties. The rf power lines for the three spiral resonators and the rebuncher in the middle of the Alvarez tank II have been replaced by improved lines that can be pressurised.

Beam Transfer Line from UNILAC to SIS

A study was made of the beam transfer line from UNILAC to SIS for various magnet configurations. The beam is deflected into the cellar of the experiment hall by two 8.75° magnets. The design of this transfer line is complete and tenders will now be called for.



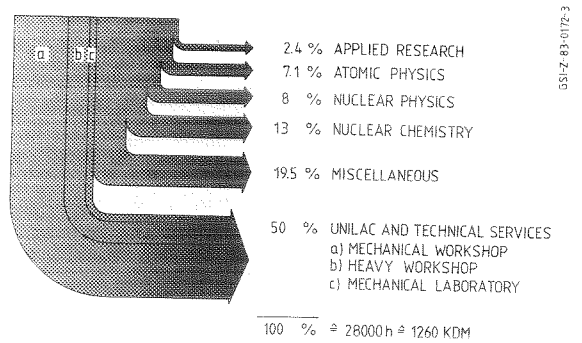


Fig. 2: Distribution of internal and external orders handled by the technical department in 1982 (left) and distribution of workload for the central workshop in 1982 (right).

SIS

The design of the dipole, quadrupole and sextupole magnets has been completed. All magnets are constructed from a stack of 1.5 mm sheets. Instead of holding the stack together with massive end plates, a small number of the end sheets are glued together. This technique has been tested by measuring the modulus of elasticity (1.4×10^4 kp/mm²) and maximum load (5 kp/mm²) of a 30 mm thick test stack and comparing this with massive material. As a further check a finite element program is used to calculate the maximum load within the glued section of the magnet taking as a basis the measured value for the modulus of elasticity. For the sextupole magnets a special winding technique will be used (Fig. 3).

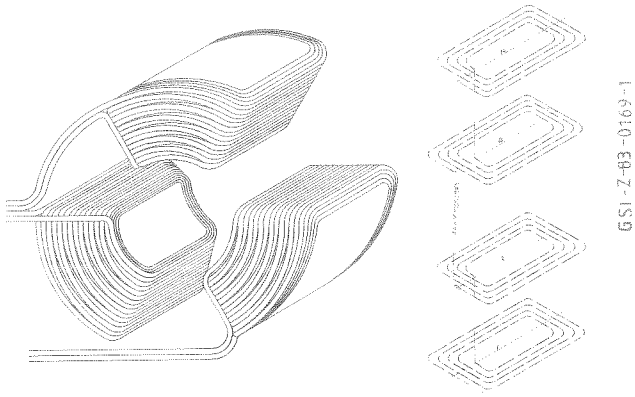


Fig. 3: Winding technique for the SIS sextupole coils

Fusion

As part of the heavy ion fusion program various high-current ion sources (HORDIS I and II, CORDIS), as well a hollow beam test facility (Fig. 4), were constructed and tested. Calculations were made of temperature distributions within the ion sources to give additional knowledge as to where condensation of metal vapours is likely to occur and whether components such as o-rings are adequately cooled.

RFQ Linear Accelerator

The RFQ components were delivered in 1982 and copper plated at GSI. The unusual configuration of these components required some special techniques to be developed for the copper plating. The electrode holders were cast from a special copper alloy containing 0.8 % chromium so that they could be better machined on the NC milling machine. The vacuum outgassing rate of the finished components was measured to be 2×10^{-11} Torr×ℓ×s^{-1}×cm^{-2}.

Experiment facilities

A target wheel holding four targets was built for the eight-crystal X-ray spectrometer. The target can be selected and shifted by up to 600 mm under high vacuum (see Fig. 5).

The design of the mass separator was completed in 1982. Meanwhile all components were delivered. A target wheel wobbler with an amplitude of 5 mm in both x- and y-directions was developed to enable targets to be uniformly irradiated. The analysing magnet was fitted with a new correction coil made on a printed circuit board to accomodate the special geometry. The board was further electroplated to increase the current carrying capacity of the conductors.



Fig. 4: Hollow beam test facility

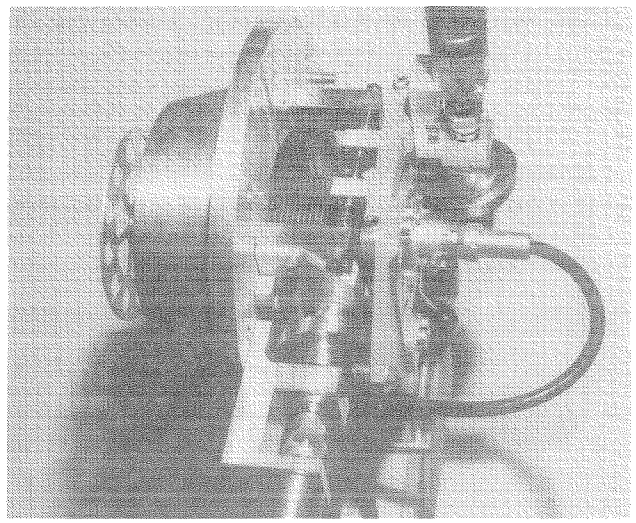


Fig. 5: Target wheel for the eight-crystal X-ray spectrometer

5. Accelerator

		PAGE
5.1	UNILAC Performance and Ameliorations	264
5.2	Accelerator Projects	275

N. Angert, J. Klabunde, M. Müller,
P. Strehl, D. Wilms - GSI Darmstadt

The upgraded Unilac has started operation for experiments as scheduled at the beginning of the year. In January beam properties and energies could be provided comparable to the ones before the upgrading. Already at the end of February previous maximum energies have been exceeded reaching 15 MeV/u krypton. Besides the installation of the two new Alvarez tanks, during the upgrading shut-down modifications have also been made at the injector, the computer control, the cabling of the 40 rf-amplifiers, and the beam switchyard at the end of the Unilac. Therefore, additional shut-down times were needed for minor improvements and developments during the first months. This resulted in a 20 % lower total operation time compared to 1980, the last year with full operation. Table 1 shows the distribution of the operation times in 1982. The fraction of target time was only 52 % compared to 60 % in 1981. The target time was distributed among many different isotopes as indicated by table 2.

The 17 single gap cavity resonators were put into operation again during the first half of 1982. Figure 1 shows the distribution of ion energies used for experiments, comparing 1981/82 graphes. The maximum energies have been 20 MeV/u with argon, 19 MeV/u with krypton, and 17 MeV/u with uranium. The high energies now also offer the possibility of experiments with highly-charged heavy ions. Stripping krypton e.g. at 19 MeV/u in a foil yields about 10 % of hydrogen-like ions and about 1 % of fully-stripped ones respectively.

While the four Alvarez tanks have been operated up to peak power levels, as required for gas stripped uranium, which means some 1.4 MW for U^{28+}, the 17 single-gap cavity resonators need some additional improvements of their final rf amplifiers and their rf coupling loops to the tanks to reach their design fields, which would allow for 18.5 MeV/u with uranium. Due to the large number of resonators and amplifiers these modifications will not be completed before the middle of 1983.

The operation of the Unilac has been greatly advanced by the modifications of the injector beam optics. This, together with PIG-source improvements, resulted in an intensity gain of about one order of magnitude. This helps especially at the highest energies where a second stripper is needed and, of course, when beams of isotopes with low natural abundance are wanted. While remarkable progress can be stated on the above mentioned fields, on the beam optics, and especially on the computer control, the stability and reproducibility of µ-structure of the beam need still further improvements.

Beam on target	2.815 h	
Parasitic beam on target		727 h
Acc. development	338 h	
Tuning (exp. area incl.)	977 h	
Breakdown	1.039 h	
Maintenance	287 h	
Total operation time	5.456 h	

Table 1: Unilac operation times in 1982.

^{14}N	75 h	^{90}Zr	68 h
^{20}Ne	19 h	^{92}Mo	53 h
^{40}Ar	59 h	^{93}Nb	30 h
^{40}Ca	32 h	^{98}Mo	67 h
^{48}Ca	8 h	^{104}Ru	47 h
^{50}Ti	141 h	^{120}Sn	73 h
^{58}Ni	196 h	^{129}Xe	22 h
^{58}Fe	254 h	^{132}Xe	91 h
^{76}Ge	31 h	^{134}Xe	90 h
^{82}Kr	53 h	^{136}Xe	48 h
^{84}Kr	61 h	^{142}Nd	83 h
^{86}Kr	278 h	^{208}Pb	381 h
	^{238}U 551 h		

Table 2: List of accelerated isotopes and corresponding target hours in 1982.

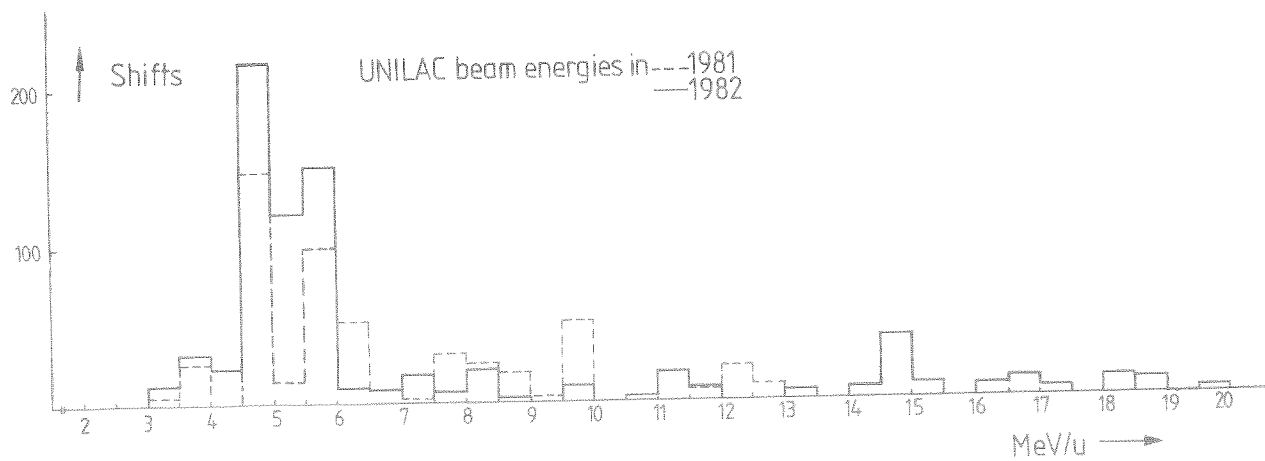


Fig. 1: Statistics of Unilac ion energies

UNILAC INJECTOR

M. Müller, W. Jacoby, M.M. Khaouli, H. Schulte,
J. Bossler, H. Emig, N. Hofmann, M. Stork,
H.-P. Kurz, H. Krichbaum, K. Schneider, R. Rulfs,
K.-D. Leible, G. Jöst - GSI Darmstadt

In 1982 the ion beams for Unilac routine operation have been produced exclusively by the southern injector. Injector north was mainly used for ion source experiments and beam transport tests. Last year's upgrading activities proved to be very successful regarding the injector reliability ion source lifetime and ion beam intensity gain. Unfortunately the geometry changes of the faraday rooms led to a bad high voltage behavior at higher voltage levels (beyond 260 kV), however, this disadvantage does not seriously affect the accelerator operating because the heavier ion species of lead or uranium e.g. are run now in the 9^+ resp. 10^+ charge states with sufficient intensities. A test run delivered 34 electrical microamperes of uranium 10^+ beam to the prestripper entrance. An example illustrating good ion source performance is given in fig.1 showing charge state distributions of lead and uranium beams recorded at the acceleration column high energy end.

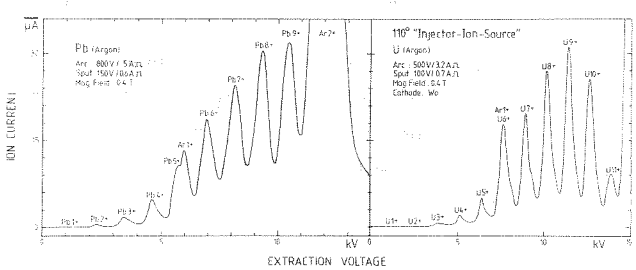


Fig. 1: Charge state distributions of ion beams from Unilac injector PIG ion source.

Breakdowns of the injector system came from defects in the light link data transfer units, the power tubes of the high voltage power supply and the "bouncer" where parts had to be repaired and/or changed several times during the year.

Another point of interest was the production of high intensity beams of the isotopes 48Ca, 50Ti and 58Fe. Some efforts to produce an intensive $48Ca3^+$ beam using natural calcium as sputter electrode in the ion source, culminated in a 20pnA $48Ca11^+$ beam at poststripper energy. Attempts to raise the intensity failed due to severe difficulties with ion extraction (secondary electrons) from the ion source. The sputter electrodes for the above mentioned isotopes were fabricated using metal mixtures and alloy technics.[1] The main purpose for this modification of the sputter electrode preparation was to get a good recycling efficiency for the isotopic pure or highly enriched substances. For the $58Fe4^+$ beam an effective amount of 4.5 grams 58Fe was diluted in gold.

With this metal mixture 16 sputter electrodes were fabricated delivering about 250 hours of beam at an average intensity of 1.25×10^{12} particles/s to the target at the accelerator's high energy end. Most of the sputtered material condensed at the inner wall of the anode insert of the ion source and was easyly conserved for later recycling. Data and results, also for the other isotopes, are listed in the table.

Isotope	Natural abundance %	Mixture basis	Enrichment atom %	Ion source: Charge state/ Ion current µA c.w.	Poststripper: Charge state/ Ion current µA c.w.	Particles/s
^{48}Ca	0.178	gold	0.746	3+/ 5	11+/0.38	2.16×10^{11}
^{50}Ti	5.34	silver	12.58	4+/50	12+/6	3.12×10^{12}
^{58}Fe	0.34	gold	8.32	4+/37	14+/5	2.23×10^{12}

Table: Metal mixture sputter electrodes for intensive ion beams of rare isotopes.

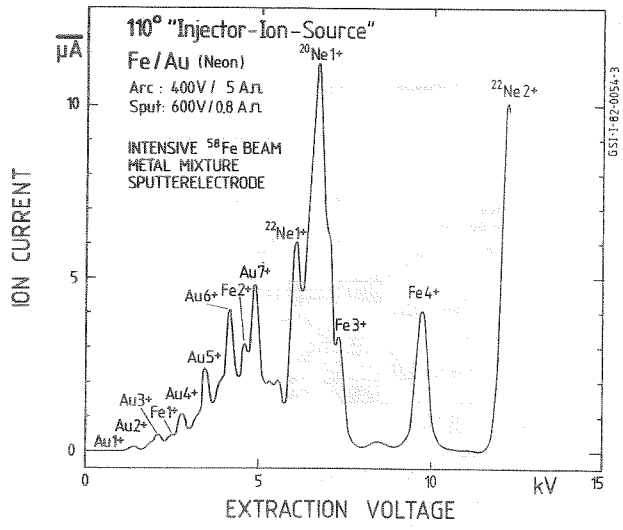


Fig. 2: Charge state distribution of ion beams out of PIG dicharge in neon using iron/gold mixture as sputter electrode.

[1] M. Müller et al., GSI-Report-11/82.

THE "COMPACT-PIG-SOURCE"[1]

Michael Müller, GSI - Darmstadt
Zhao Weijiang, University of Beijing, P.R.C.

Total current measurements of the ion beam in the 110° injector ion source setup revealed a serious disadvantage in the combination of ion source magnetic field and separator field: in the extraction voltage range beyond 6 kV, the ion current yield, measured at the nearest point behind the extractor, in a well shielded faraday cup, was always higher for lower magnetic field values. For better extraction optics the trend is to lower the magnetic field and simultaneously raise the extraction voltage, which is quite opposite to the demands of the field combination arrangement in the 110° injector ion source facility. These difficulties can be bypassed with the "compact-PIG-source" concept.

The principle of charge state preseparation in the ion source magnetic field is abandoned. The ion source discharge geometry remains unchanged and is placed into the field of a small diameter (70 mm), large gap (154 mm) magnet (weight: 0.12 tons) with integrated vacuum chamber, pumped through its extractor port (see fig.1). For ion extraction, magnet and ion source are raised together to high positive potential vs ground. Thus the extraction voltage can now be adjusted independently from source magnetic field, according to plasma density and proper beam focusing, disregarding small steering effects from fringing field.

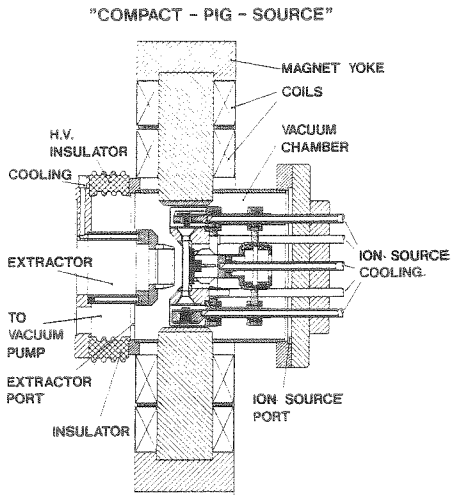


Fig. 1: Sectional view of "compact-PIG-source" assembly.

On the test stand (fig.2), the discharge conditions were investigated by measuring the total extracted ion current versus extraction voltage as displayed in fig.3. From these curves a pulse ion current density of 70 mA/cm² • A could be derived, which is more than twice the value measured for the 110° ion source arrangement. Despite the inhomogeneous axial field distribution (average gradient 0.02 T/cm), there was no trouble with plasma instabilities even for high arc power (10 kW/pulse) which is in favour of the weakly radial decreasing (≤ 1 %) magnetic field within a cylinder of 10 mm diameter around the discharge axis.

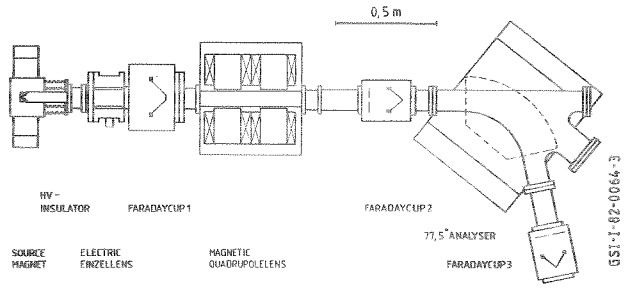


Fig. 2: "Compact-PIG-Source" test stand, showing beam transport system and magnetic analyzer.

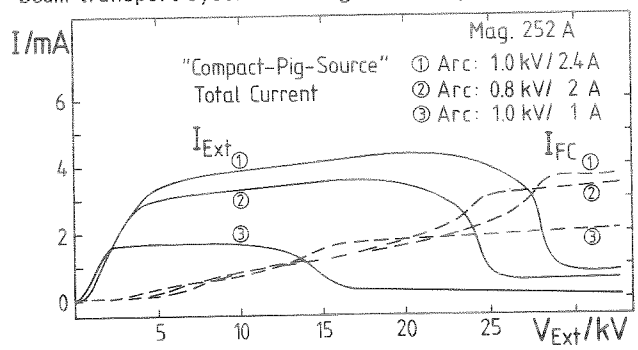


Fig. 3: Total current vs extraction voltage for three different plasma densities of an argon discharge. Arc data for pulsed operation: 50/s, 2 ms. I_{Ext}: average current on the extractor electrode, I_{FC}: average current in faraday cup 1 (fig.2).

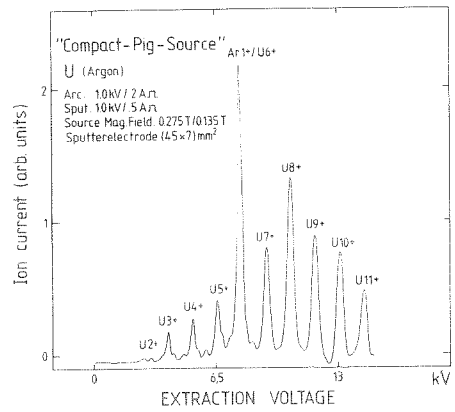


Fig. 4: Uranium charge states of compact-PIG-source ion beam.

The magnetic analyzer allows a qualitative analysis of the charge state composition of the ion beam. For a direct comparison with the 110° injector ion source the charge state spectra were recorded with a fixed magnetic field and the extraction voltage as independent parameter. Fig.4 shows the charge state distribution of an uranium beam produced under moderate discharge conditions which proofs that the magnetic field modification in strength and shape does not disturb the typical PIG source characteristics. Near future work is directed on the improvement of the ion extraction optics and a quantitative ion beam analysis.

[1] M. Müller and Zhao Weijiang, Int. Rep., GSI Darmstadt

ECR SOURCE DEVELOPMENT

H. Schulte, B. Wolf, K.-D. Leible - GSI Darmstadt

Work on the ECR test source (s. GSI Rep. 1980 and 1981) has been continued mainly with the aim to use this existing device for parameter studies for a new ECR source design. Major improvements were no longer intended on this source since the compact construction did not give room for principal changes.

To learn about the action of the permanent magnet hexapole we tried another composition of magnet bars (possible within design limitations). This 18-pole structure (which did show good results of plasma containment in the GSI high current source), did not give significant changes in ECR discharge characteristics or ion output of the test source. Furthermore, since this multipole was too weak to obtain a closed resonance surface, the design aim seemed ineffective in the test source. The next step was the total omission of the multipole with very similar results. The only conclusion to be drawn from these experiments was that the original hexapole were possibly not strong enough to be effective.

Another series of experiments concerned the influence of the axial field. Variations of the field shape, attainable with the original set of coils now separately powered, were small due to the effect of the iron yoke, and did merely show a slight optimum, already known for the case of series connection of both coils. Larger variations in field shape and mirror ratio became possible with the insertion of a third coil, and it was a certain surprise to us that the increase of mirror ratio obviously deteriorated the charge spectrum and that hitherto the best results were obtained with a very low mirror ratio and resonance field strength near the source aperture.

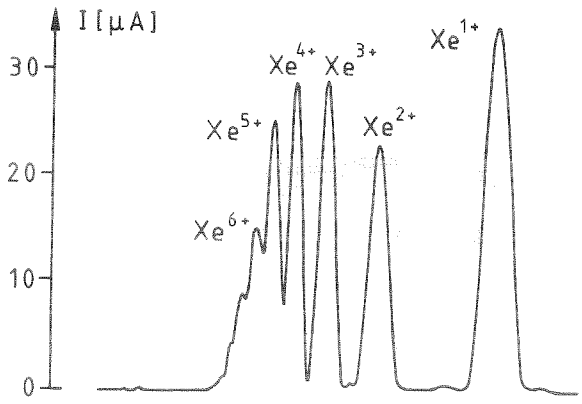


Figure: Charge state distribution of xenon from ECR discharge.

Optimum high charge state yield in this configuration (without hexapole) was approx. 10 μA of Xe^{6+}. Charge states up to Xe^{8+} can be identified in the spectrum.

With the experiences gained from the test source work a new design has been started around the mid of the year 1982. The main differences of the new source compared to the test source will be:

1. The omission of iron from the magnetic circuit (iron mirror plates may later be added if necessary),
2. the use of more coils (7) of larger inner diameter, all powered separately to vary the axial field freely in strength and shape,
3. a stronger two-layer permanent magnet hexapole of the same inner diameter as for the test source to improve plasma containment and shift the resonance zones farther from the cavity walls,
4. increase of the length of the resonance volume by approx. a factor of 6,
5. axial pumping of the cavity,
6. a new integrated "first stage" for primary plasma generation,
7. a new variable gap extractor for easier matching of ion optics.

We further hope that the availability of a new computer code[1] will greatly facilitate the design of electrode geometries for the extraction from a strong axial magnetic field. Improvements on the magnetic spectrometer to obtain a better resolution of the charge spectrum are going on in parallel.

The price to pay for the operation of the new, more versatile source, was mainly that the electric power for the generation of the magnetic field has more than doubled, which required a major upgrading of the test facility, too.

At the end of the year the main source body had been completed and work on the test stand was in progress. First runs with the new source are expected for march 1983.

[1] N. Schmitt and P. Spädtke, GSI Sci. Rep. 1982

OPERATING MODES OF THE ALVAREZ TANKS AT THE UNILAC

J. Klabunde - GSI Darmstadt

The beam energy obtained with the separately excited Alvarez tank is normally determined within narrow limits by the design energy of the synchronous particle. After the upgrading the Unilac poststripper linac consists of 5 Alvarez tanks. By turning off later tanks 5 discrete design energies (3.6, 4.8, 5.9, 8.6, 11.4 MeV/u) can be simply provided. By proper adjusting of rf phase and amplitude of the 17 single cell resonators the energy can be varied continuously from 2 to the maximum energy (with good time structure and energy spread at full beam intensity).

For simplicity and reliability of a linac with variable energy capability it is desired to reduce the number of separately excited cavities. At the Super-Hilac in Berkeley the linac was divided into short separated cavities by fixed rf diaphrams. The length of each section was chosen so that the energy increment can be varied continuously from zero to maximum corresponding to the synchronous value. In order to achieve this flexibility the number of cells in each tank should not exceed 10 - 15. But the efficiency of the accelerator decreases considerably by the large number of separating walls.

At the Unilac the Alvarez sections contain much more cells, e.g. Alvarez tank 3 has 37 cells, tank 4 contains 32 cells. Therefore continuous energy variation at good beam quality is impossible. Nevertheless at certain rf levels below the synchronous value partial energies can be adjusted.

The nonsynchronous behavior of Alvarez tank 3 and 4 is shown in Fig.1. At different rf levels the output energy is plotted as function of the input phase angle of the particle at the design input energy. It can be seen, that only for particular rf levels the output energy does not change so much for a wide range of the input phase, at the 80 %-level the energy of 7.1 MeV/u will be achieved, at the 70 %-level 6.6 MeV/u for tank 3 and 9.5 MeV/u for tank 4.

The development of the time structure at the 80 %-rf level within Alvarez tank 3 is demonstrated in Fig. 2. A phase intervall from - 20° to + 25° is injected. The single particle behavior of the nonsynchronous mode can be seen, if we follow the input particle with $\Delta\phi = \Delta W = 0$ (particle-no. 2). Initially the energy gain is linear, the particle is starting in phase with the accelerating rf field. As the particle slips out of phase with the rf (about after cell 20), the energy gain decreases, later the gain may be negative or positiv, the energy then oscillates about a mean value. After cell 25 the time structure starts to deteriorate. But if the injected pulse width is small (≤ 800 ps), the beam quality at the intermediate energy fits the requirements from the users of the beam or is suitable for further energy variation by the single gap cavities. The calculations were experimentally confirmed. So additional Alvarez energies (6.6, 7.1 MeV/u for Alvarez tank 3, 9.5 MeV/u for Alvarez tank 4) are available at the upgraded Unilac.

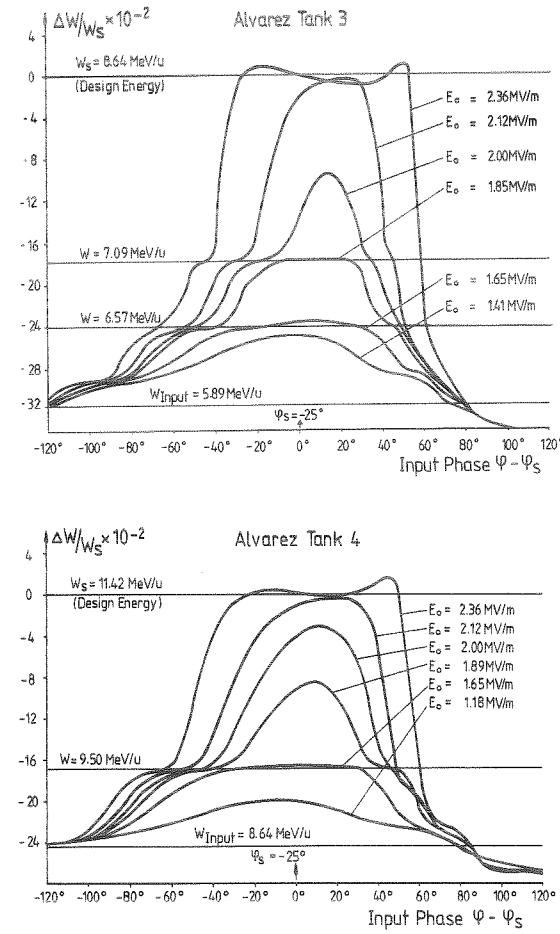


Fig. 1: Output energy at different rf levels as function of particle input phase.

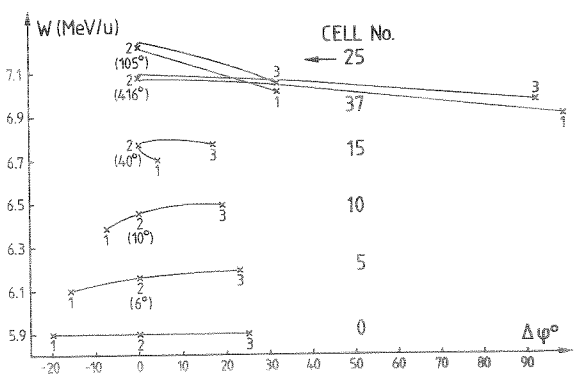


Fig. 2: Development of the time structure at the 80 % rf level for tank 3 (phase slip of reference-particle 2, in brackets).

RECENT DEVELOPMENTS AT THE UNILAC RF

G. Hutter, W. Hartmann, A. Morhardt, W. Vinzenz
GSI - Darmstadt

In 1982 the upgraded four 600 kW/27 MHz amplifiers, including the rf hardware, the new c-mos control and also the microprocessor controller showed very good performance after some normal commissioning problems.
The 1.6 MW/108 MHz amplifiers of the GSI-type[1] had shown in short tests on a prototype in 1981 their ability to deliver the nominal power to a waterload, when sufficient damping of parasitic modes is provided.[2] In 1982, all the five amplifiers were equipped with ferrite absorbers. In addition, the three amplifiers connected to an undivided Alvarez type cavity received new input circuitry for the conversion from the Thomson CSF tube TH518 to the Siemens tube RS2074SK. The TH518 remained in the amplifiers AIIa and AIIb of the divided Alvarez cavity A2, where they have to deliver only about half of the rf power of the others.

In this configuration the amplifiers had still to show their ability to drive a cavity under full power instead of a water load. This was not possible at the beginning of 1982 because of different cavity problems[3,4]. The first full power operation is also too risky to be done during beam operation of the machine, as for instance, a damage of a coupling loop can lead to a longer unplanned shut-down. Therefore the rf power on the cavities was raised very carefully over several months.
As the prototype experiments were based on only one tube and since the cavities did not allow tests of further new tubes with full power, a water load was connected with a coaxial switch to the amplifiers Ala (GSI-type) and Alb (Herfurth-type)[5]. This enabled high power tube tests to be made during shut-downs again.
One of several tested TH518 succeeded in holding 1.6 MW over a long time. In a second test some weeks later, the cathode of this tube was poisened by a bad vacuum, caused by a microleakage. All the tested tubes RS2074SK showed - at least after some conditioning - the capability of delivering 1.6 MW to the dummy load. In a short test the limitation of the voltage capability of this tube and also of the amplifier's plate circuit were found at 2 MW with 25 % duty cycle!

Preparation and execution of these tests during shut-downs required a large amount of manpower. Since this detracted from the routine service, the tests were stopped as soon as we were sure that the power capability of this tube and amplifier combination would not limit the Unilac operation.
Further work with raising the rf on the cavities showed that the ferrite absorber is also sufficient for full power on a resonant load. The power was brought to the design value in several steps and in december 1982 the first gas stripped uranium beam was accelerated by all the Alvarez cavities. The limitation in the duty cycle of 10 % was given by the available conditioning time of about 12 hours. The thermal limitations of the common power supply of amplifier A3 and A4 and of the common water cooling of cavity 3 and 4 were not yet reached.
Some tests on parasitic resonances, damping devices and temperature behaviour were also made with the Herfurth-type amplifier fitted with an Eimac tube 8973, since this is not in Unilac operation. In addition, GSI arranged a cooperation with Siemens AG and Herfurth GmbH to build and test an adapting set for the use of the Siemens tube RS2074SK in this amplifier cavity. This work was mechanically performed at the end of 1982 and electrical tests will follow in 1983.
The divided Alvarez cavity A2 has a rebuncher cell in its middle. This rebuncher is only used when both the Alvarez cavity A2a and A2b are not operating. Its power consumption is satisfied by a 180 kW amplifier. In order to free the single amplifier for another purpose, the driver of the amplifier A2b is now used to supply the rebuncher cell with rf. This was realized with a power coaxial switch plus additional changes to regulation-, measurement- and interlock signals such that the change of the load works fully automatically with a key switch. The work on the 180 kW amplifiers is reported in a separate paper in this report.

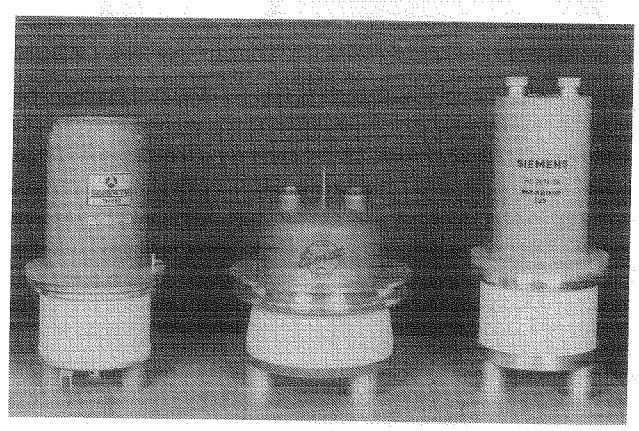


Fig. 1: Tested high power tubes.

[1] G. Hutter, N. Angert, IEEE Trans. Nucl. Sci. Vol.28, 1981, p. 3012.
[2] G. Hutter, GSI scientific report 1981, p. 291.
[3] N. Angert, GSI Nachrichten 2-82, p.2; 3-82, p. 2.
[4] G. Hutter, GSI Nachrichten 4-82, p. 6-8.
[5] K.H. Knobbe, D. Böhne, IEEE Trans. Nucl. Sci. Vol.28, 1981, p. 3010.

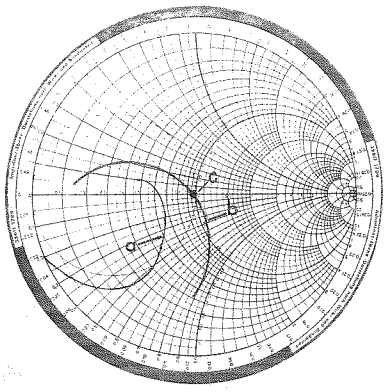
IMPROVEMENTS TO THE 180 KW/108 MHZ AMPLIFIERS

G. Hutter, G. Kube, W. Vinzenz, GSI - Darmstadt

In 1982 the maximum development effort in the rf system was directed at the 29 amplifiers for 108 MHz and 180 kW peak power, which are used for 17 single gap cavities, several rebunchers and driving the 1,6 MW final amplifiers.

Under-rated input circuits and bad impedance matching of both the 180 kW final stage and the 22 kW driver stage limited the output power below the nominal level and produced frequent disconnections.

The problems with the commercial Rhode & Schwarz drivers were mainly caused by its electron tube RS2024 CW. The capacitance between g1 and g2 of this tube was changed by the manufacturer as a result of an improvement in its voltage capability. This change led to an unacceptable mismatch of the driver's input (fig.1a), which disconnected the solid state 300 W preamplifiers at lower than nominal levels. As the improved voltage capability of the tube should be retained it was necessary, to adapt the stripline input circuits of all the drivers. This was possible by adding striplines and short circuits on the printed boards. A general service including several other improvements was made at the same time.



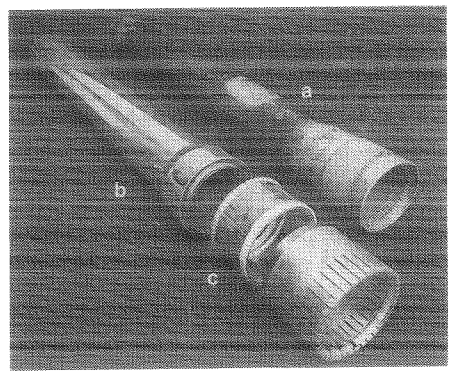
Smith Chart
Z = 50 Ω
a - old circuit
b - new circuit
c - 50 Ω, desired value

Fig. 1)

Tuning range of the R&S driver's input impedance.

Many faults have been caused by a ceramic capacitor which decouples the dc voltage of the g1 in the input of the final 180 kW amplifiers, since the improved frequency tuning system[1] of the accelerating cavities allows full power on the resonant loads. These capacitors are hard to mount and rather expensive. They were damaged very often by flashes as well as by mechanical and thermal stress, as they were poorly centered and badly cooled. A coaxial capton capacitor[2] was used in a completely new input circuit (fig.2).

The new circuit should also enable the input matching to be improved. With the old input circuitry, it was as bad as the driver's in fig.1a, although calculations did not show such a big fault.



a - new

b - old input circuit

c - capton capacitive

Fig. 2)

To measure the proper input impedance of a g1-g2 grounded amplifier, the nominal cathode current has to flow as it loads the input circuitry. Changes cannot be done quickly in a fully mounted amplifier so it is best done in the laboratory. Therefore a dummy was built out of an old tube from which grids and cathode have been removed, simulating the capacitance of the g1-cathode region by 8 small tunable capacitors and the cathode current by 8 resistors of 100 Ω each. That corresponds to the nominal real part of the impedance of the active tube's system at the maximum rf current of about 65 A. Connecting one resistor after the other gives an input impedance curve of decreasing resistance or increasing cathode current and output power. With this simulation, the failure of the old Siemens input circuitry could easily be found: a serial inductance was built in such a way, that its parasitic capacitance was much too high. A changed shape of this inductance resulted in very good matching and good agreement between calculations, simulation (fig.3) and operation (fig.4).

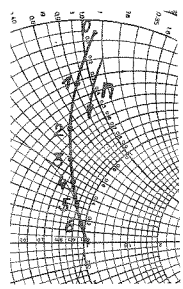


Fig.3)

Simulated input impedance
n = number of connected resistors

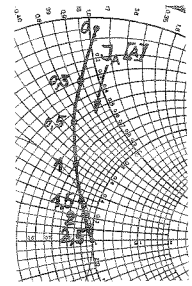


Fig.4)

input impedance with increasing dc anode current

The started work on new test stands, reduction of rf radiation and tests of other tube-types will be reported in a later paper.

[1] M. Emmerling, GSI scientific report 1980, p.244.
[2] K. Heinz et al., application for a patent.

Presently, Unilac beams can be geometrically divided by septa magnets into two or three fractions and be directed separately to different experiment setups. In the future use of the Unilac as an injector for SIS it will be essential to provide on a low repetition rate an ion beam differing in species and energy from that used in Unilac experiments. This capability might as well be used to run an experiment and simultaneously tune another beam (see also Unilac-Nachrichten 4-82). It could be accomplished by setting the parameters of all accelerating and focussing divices to design values for the desired beam within 15 ms between beam pulses. This is easily achieved with the RF-structures but not with the large number of quadrupole magnets in the drifttubes. The effects of this restriction on the operational performance of the Unilac poststripper have been studied. (The final prestripper configuration is as yet undecided.)

The focussing magnets being set for a specific reference ion and the RF systems being adjusted on a pulse-to-pulse basis, allows acceleration of ions in a wide band of rigidities. Fig.1 shows the acceptances of the accelerator cavities over beam rigidity in accelerating (solid lines) and transporting mode (broken lines). The base lines of the curves are set to the maximum beam emittances expected ($\varepsilon\beta_s$ = 1 π mm mrad). The acceptances are larger by a factor of up to 20.

It can be seen that time-shared acceleration of any ions in the range Ne to U is possible to nearly any energy. Production of light soft ions may be inhibited; so should gas stripped Ne be accelerated to at least 8.6 MeV/amu if U is to be delivered at the same time. The figure assumes the focussing magnets to be adjusted for Kr^{17}-ions at a phase advance of 45° per period; scaling the acceptance curves to another reference ion may accomodate specific operating conditions.

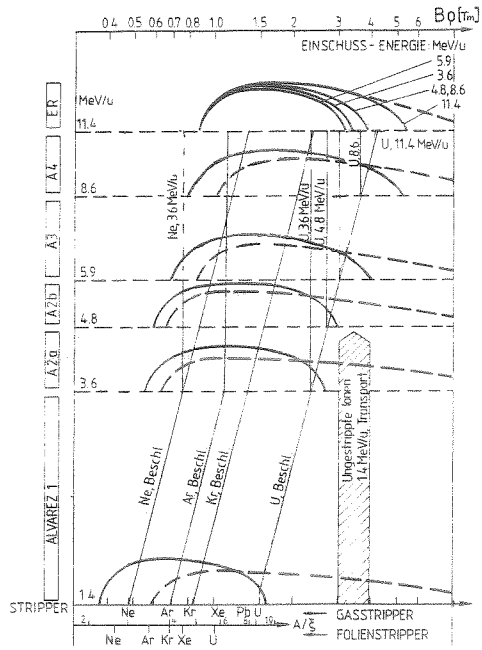


Fig. 1: Ion acceleration schedule for the Unilac poststripper. Acceptance bands are shown over beam rigidity. Some ion paths are shown; sloped lines correspond to acceleration, vertical lines to transport.

Beam emittance geometries at RF-structure bounderies are heavily dependent on particle rigidity and are related to the acceptance figures. It has been determined that beam matching between RF-structures may be performed by a symmetric system of 3 lenses of alternating polarity if their gradients are adjusted to the beams in a pulsed fashion. The excitation curves over beam rigidity (fig.2, relative to the reference particle) are complicated functions of the accelerator parameters and had to be determined pointwise by numerical fitting procedures. The construction of adequate quadrupole magnets and power supplies poses no technical problems.

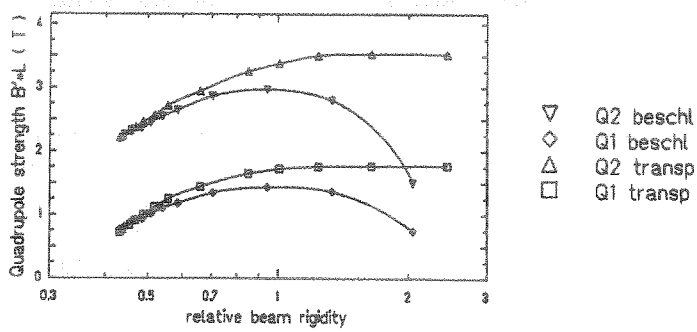


Fig. 2: Typical quadrupole excitation over rigidity in a symmetric 3-lens matching section between Alvarez-cavities. Central lens (upper curve) has inverted polarity.

The homogeneous Alvarez-structure is interrupted if a structure does not accelerate, and at the boundary to the single resonator structures. Here the three-lens matching systems are not appropriate and require larger acceptances. In other terms, an increased beam emittance area is to be assumed at the accelerator exit in order to accomodate the unknown orientation of the actual beam. In Fig. 3 some of these data are shown. Generally, the acceptances remain large compared to the increased emittances; they are at least 50 π mm mrad in the cases shown. The possibilities of matching the accelerator exit beam to the experiment beam lines have not yet been investigated.

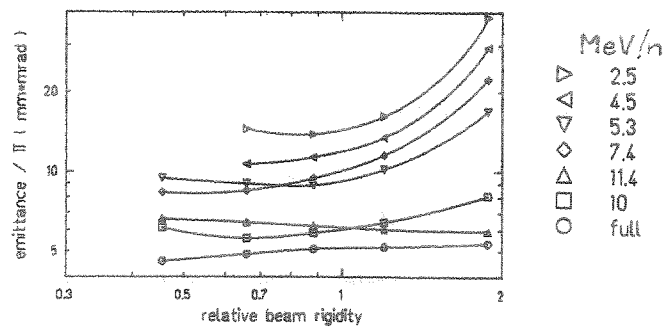


Fig. 3: Minimum acceptances at the Unilac exit required due to imperfect beam matching and emittance shrinking with energy. Assumed normalized true beam emittance is 1 π mm mrad.

Two Kicker Magnets for the UNILAC Beam Sharing System and the Beam Transfer Line to SIS

W. Bourgeois, K. Küper, B. Langenbeck,
G. Moritz, G. Sobainsky, K. Zweig
GSI Darmstadt

A 0.5-degree and a 5.0-degree kicker magnet were built. The first one will allow separation of successive UNILAC macropulses of different energies and their distribution to the target positions in the experiment hall. The second one selects pulses for the beam transfer to SIS. The transfer line will also be used for UNILAC beam diagnostic, which is difficult to do in the now shorter section between the linac and the beam splitting system since the 1982 upgrading.

Main parameters of the two magnets are given in table 1. Cross-sections are shown in figures 1 and 2. Both magnets have window frame structure, the small magnet has a C-shaped yoke. The cores and the coil of the 0.5-degree magnet were made in our laboratories. The 1.5 mm thick 1%-silicium steel sheets were glued together using an epoxy impregnated polyester fleece [1]. The coil was vacuum impregnated with araldit CY205 and hardener HY905 [2].

	+- 0.5-degree	5.0-degree
gap height / mm	51.5	50
gap width / mm	96	120
core length / mm	250	850
overall length / mm	332	930
magnetic length / mm	297.8	n.y.meas.
bending radius / m	34.15	9.9 aprox
flux density / T	0.145	0.50
ramping rate / T/s	20	35
current / A	220 (+-)	1000
resistance / mOhm	30	14
inductance / mH	0.70	1.45
voltage / V	30	110
copper conductor width / mm	5	7
copper conductor height / mm	5	11
number of conductor rows	9	4
number of conductor collums	3	5
flux line length / mm	260	460
vacuum chamber width / mm	74	100
wall thickness / mm	1	1

Tab.1: Main parameters of the two kicker magnets.

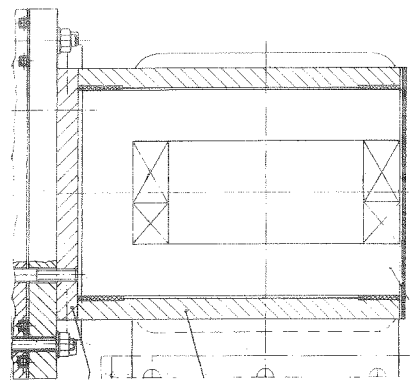


Fig.1 Cross-section of 0.5-degree kicker magnet.

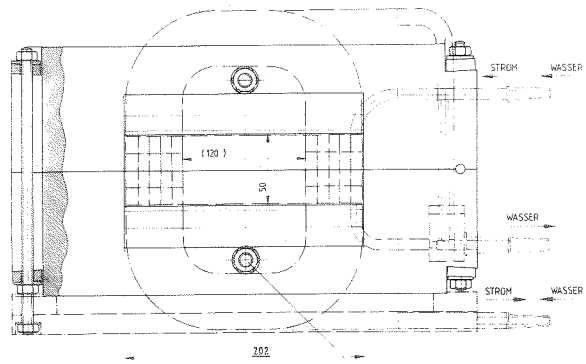


Fig.2 Cross-section of 5.0-degree kicker magnet.

In spite of the fast repetition rate (25 cps maximum for the small magnet and 10 cps maximum for the large one) stainless steel vacuum chambers can be used. We estimated the damping time for eddy currents in the chambers and also in the steel sheets and in the conductors by

$$\tau = \frac{\mu_0 b^2 a}{\pi^2 \rho g}$$

μ_o is the vacuum permeability, g the gap height and ρ the resistivity of the material (Si-steel 2.E-7, stainless steel 7.3E-7, copper 1.7E-8 Ohm*m). The meaning of the parameters a and b is given in table 2 together with the calculated time constants. A measurement of dB/dt as a function of time, which could already be done in the small magnet is in good agreement with the estimate (figure 3). Only the effect of the vacuum chamber can be seen; eddy current field distortions due to the conductors are limited to the near neighbourhood of the coil. Within 0.1 ms after reaching of the flat top eddy currents will vanish and consequently no field distortions in the aperture are present. Eddy current heating is moderate, 8 Watt for the small and 70 Watt for the large chamber.

	b/m	a/m	0.5-dgr magnet	5.0-dgr magnet
sheet[3]	sheet thickness	length of a flux line in the core	7µs	13µs
conductor	conductor width	conductor height x number of rows	160µs	320µs
chamber	horizontal aperture	2x wall thickness	37µs	70µs

Tab.2: Characteristic parameters for eddy current damping times and calculated values for the two kicker magnets.

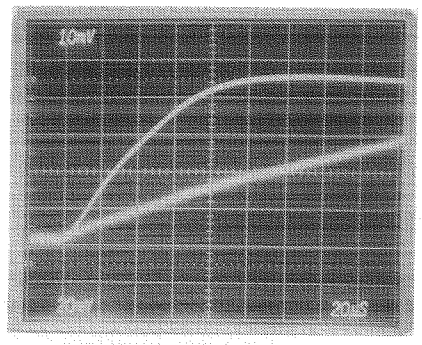


Fig.3: Current (lower curve) and change of flux density (upper curve) as a function of time, measured in the 0.5-degree kicker with a shunt and a wire loop.

References

[1] Isovolta AG, Wiener Neudorf, Austria

[2] CIBA AG, Basel, Swiss

[3] G. Brianti et al., Behavior of the Magnetic Induction B in Solid Steel Cores Submitted to an Exitation Variable with Time, SI/Int. DL/71-3, CERN

300 KV ACCELERATOR

P. Spädtke, D. Vogt, B.H. Wolf
GSI - Darmstadt

A new high current facility was installed at the GSI 300 kV accelerator besides the old beam line.[1] This new beam line can provide high current (≤ 20 mA) beams up to $\beta = 2 \cdot 10^{-3}$ both for transport experiments in a 10 m long quadrupole transport channel[2] and for the MAXILAC RFQ-test resonator[3].

Two different accelerating column geometries were studied: first a low gradient multi gap design (100 mm ∅) with a magnetic quadrupole lens (aperture 45 mm ∅) for beam matching between source and gap on high potential (fig.1a), and secondly a high gradient single gap (100 mm ∅) column without additional matching lens (fig.1b). Both systems were studied with argon ion beams extracted from the GSI high current source ELSIRE[4] with a single aperture system (6 mm ∅, ~ 0.3 cm²). With the first column geometry about 15 mA were extracted with 40 kV from the source, 10 mA could be measured at the entrance of the accelerating column and only 5 mA after 250 kV acceleration (faraday cups 30 mm ∅). The best results led to a parallel beam with large diameter (ca. 60 mm ∅) but only 1 mA could be transported through the 10 m long test beam line (aperture 40 mm ∅). Better beam matching should be possible with enlarged distances between ion source, lens and accelerating column as one can conclude from computer calculations (fig.2a). With the second geometry we got about 15 mA after 40 kV and 250 kV acceleration but also a large beam diameter and therefore only 3 mA at the end of the beam line. Then we changed the high voltage electrode from 100 mm ∅ to 30 mm ∅ and the ground electrode to 50 mm ∅ and got a well focussed beam (~ 15 mm ∅) of 8 mA in an emittance area of 100 mm mrad or 5 mA in 30 mm mrad, which has been transported to the end of the 10 m long beam line. The ion source was always optimized for max. cup-current. Computer calculations of the ion beam in the high gradient column are shown in fig.2b. The emittance measured after the accelerating column shows strong aberrations (fig.3a) which could be confirmed by computer calculations too, if aberrations from the ion source extraction system are taken into account. The given values are valid for the single aperture five electrode extraction system. First experiments with a multi-aperture system (7 x 4 mm ∅ ~ 0.9 cm²) resulted in an increased ion current by a factor of 1.5 (extraction area 3 times larger) with less favorable emittance according to the larger diameter of the joint beams.

[1] B.H. Wolf: reports GSI-J-1-78, p.152 and GSI 82-1, p.296.
[2] J. Klabunde: this report and GSI 82-1, p.311.
[3] R.W. Müller: this report and GSI 82-1, p.312.
[4] R. Keller: report GSI 80-3, p.212 and Nucl. Instr. Meth. 189 97 (1981).

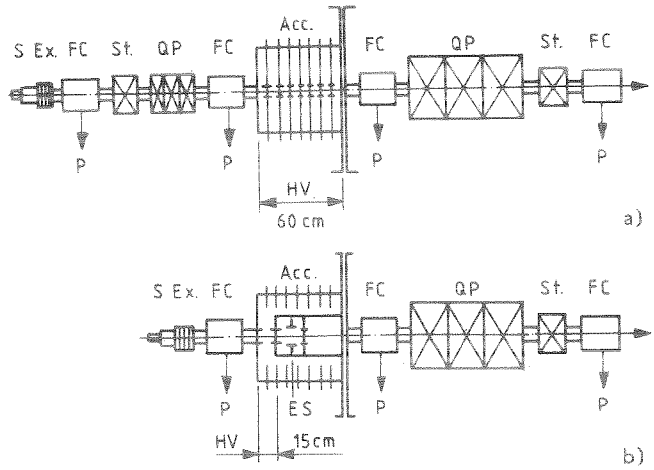


Fig. 1: Accelerating column geometries.
a) Multi-gap column, b) Single-gap column.
S: ion source; Ex: extraction; FC: faraday cup; P:vacuum-pump; St: steerer; QP: quadrupol; Acc: accelerating column; ES: electron suppressor.

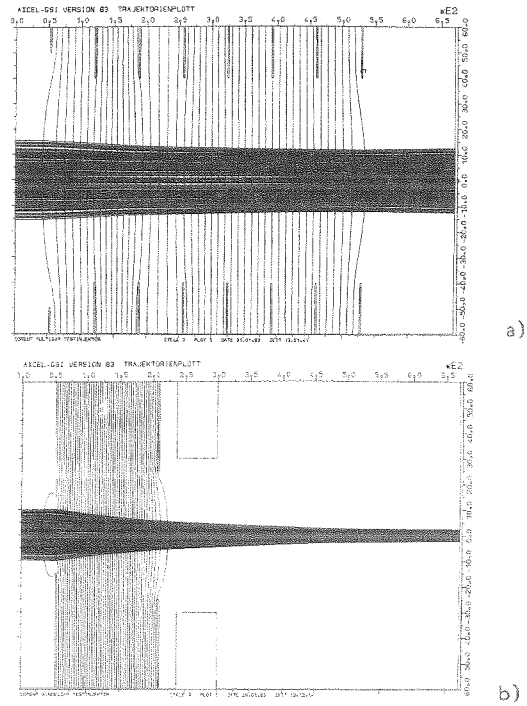


Fig. 2: a) Multi-gap, b) Single-gap; both with input emittance of 50 mm mrad with the ellipse parameter:
a) $\beta = 5$, $\alpha = 0.5$. b) $\beta = 2$, $\alpha = -1.6$.

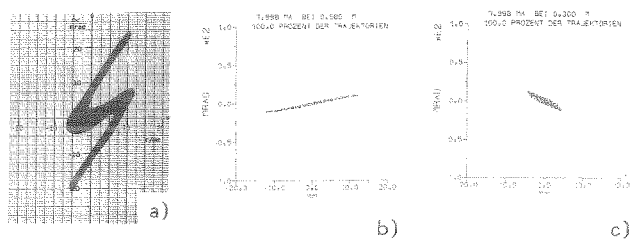


Fig. 3: Output emittance (measured directly behind the gap). Measured: a) single gap; calculated: b) multi gap, c) single gap.

SIS - The Two-Stage Synchrotron Facility For Heavy Ions

K. Blasche, D. Böhne, B. Franzke,
H. Prange, R. Steiner
GSI Darmstadt

In 1982 the SIS-two-stage synchrotron facility has passed final recommendation by the "Gutachterausschuß Kernphysik und Schwerionenforschung". In this expert report it was urged to build the first stage SIS 12/18 without any delay and to realize the second stage very soon.

A very fast construction of the first stage SIS 12/18 had been already envisaged in the time schedule that was proposed in 1981. It had been assumed that construction of the buildings and placing of the orders for the main machine components should start in 1983. Finally, test operation of the SIS 12/18 with ion beams was scheduled for the first half of 1987. With respect to this very tight time schedule the detailed design of machine components and buildings was completed in 1982.

At first the lattice design of the 1981 proposal was revised . The new regular lattice with 12 magnet periods will provide improved conditions for the acceleration of high current heavy ion beams. The only disadvantage of the new lattice is the low transition energy at $\gamma_t = 5.4$ which could complicate the acceleration of high current proton beams to energies from 3.5 to 4.5 GeV. However, with a dynamic change-over from the regular lattice with the superperiodicity S = 12 to the lower periodicity S = 6 the transition energy can be raised to $\gamma_t = \infty$, so that for protons it is also possible to avoid passing through the transition energy. The new lattice design was dicussed thoroughly in a meeting with experts from CERN, and finally adopted for the SIS 12/18 layout.

After the decision on the lattice the detailed layout of the machine as shown in Fig. 1 was completed. The lattice magnets - 24 dipole magnets, 36 quadrupole magnets, and 12 sextupole magnets were designed and all technical specifications written. The tender had to be postponed into 1983 after the GSI board meeting of December.

The main power supplies with a peak power of 30 MW were designed for direct coupling to the electric-

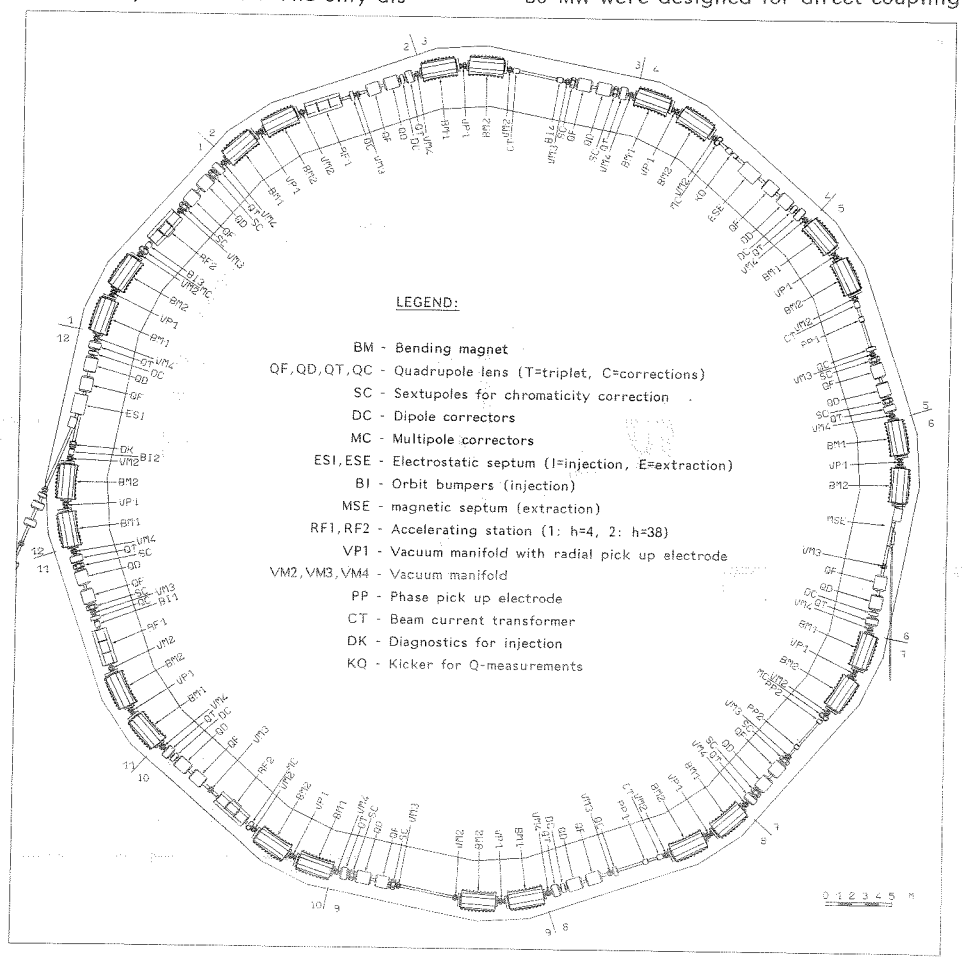


Fig. 1: Layout of the SIS 12/18

ity network. Discussions with the electricity companies have shown that such a solution is feasible. Meanwhile a pulsed 1 MW pulsed power supply was delivered which will be used to test the operation of the SIS magnets and the different control systems of the main power supply.

The prototype rf accelerating cavity was studied thoroughly at low and high rf levels. Spurius resonances turned out to be one of the main problems. These resonances are now under control and operation of the cavity at the design level of 16 kV will be possible as soon as high power blocking capacitors are available. Within the given limitations on the amplitude, the test of the closed-loop control systems for cavity tuning and rf amplitude were fully satisfactory.

The beam injection line from the UNILAC to the SIS 12/18 was designed. Its main part is the transfer line that comprises pulse deflection after the Unilac, matching in the longitudinal phase space and clipping of the 5 ms pulses to the pulse length for multiturn injection. The 25 m long section in front of the SIS 12/18 will be used as an inflection line which contains transverse beam matching, the transition from the UNILAC high vacuum to the SIS ultrahigh vacuum, and the inflector components. These critical components, the inflector magnet and the electrostatic inflector septum have been designed.

The concept for slow beam extraction has been revised, since the free space for deflecting the beam out of the ring has been reduced from 10 to about 5.5 m in the new symmetric lattice.

For the control-system, prototype-work is being done with 16 bit-multimicrosystems, a local area network LAN, a process-control bus and process interfacing equipment including 8 bit micros. Software-specification of LAN transport layer according to ISO-model and ECMA standard, and a feasibility-study for an interpreter written in a high-level implementation language have been started.

In Fig. 2 site layout and buildings are shown. The first stage SIS 12/18 will be installed in a 60 m diameter tunnel north east of the UNILAC experiment hall. The high energy experiment area is situated 150 m south of the synchrotron, with a long beam transport channel for beam splitting, beam sharing, etc. In addition, the distance of the SIS 12/18 from the experiment area provides adequate space for an optional ring. This ring could be used for beam cooling, in-ring experiments, beam storing or beam stretching, and with superconducting magnets to boost the maximum energies to 6 GeV/u (U^{92+}) and 8 GeV/u (Ne^{10+}) respectively. On the northern side of the SIS 12/18 the fast extraction channel into the main stage SIS 100 can be installed. The equipment buildings for the SIS 12/18 lie east of the machine next to the UNILAC power and cooling installation. All the drawings and documents that will be needed to apply for the building permit have been completed.

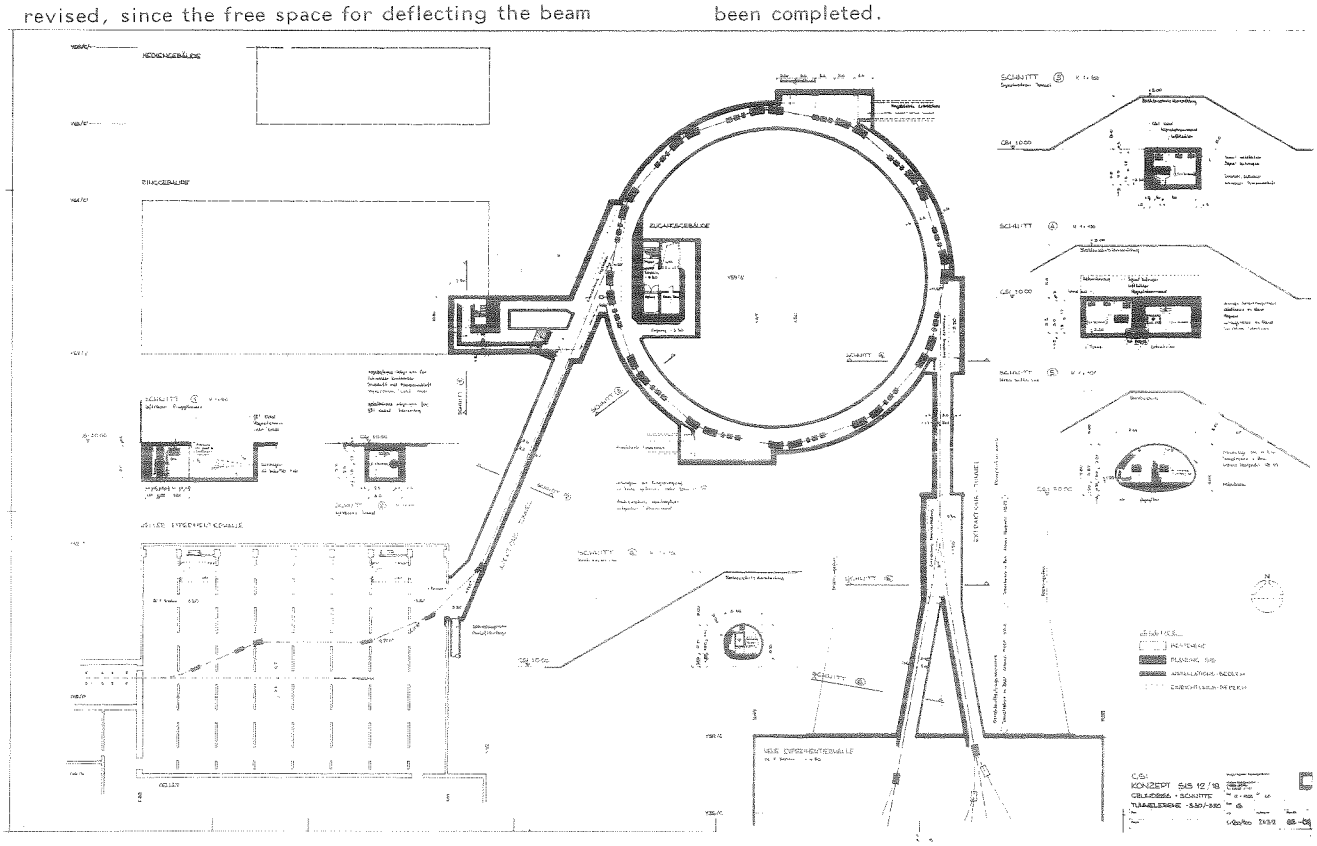


Fig. 2: Site layout and building concept of the SIS 12/18 ring including transfer lines from the Unilac and to the experiment hall

Improved SIS12 Lattice with Variable Optic

B. Franczak
GSI Darmstadt

During the last year the lattice of SIS12 was examined thoroughly and some major changes in the design took place:

- There will be no superperiodicity, all 12 normal periods have the same ion optical properties.
- γ_t can be shifted from 5.4 to infinity just by modulating the main quadrupole currents.
- A dynamic change from triplet to doublet focussing is foreseen to combine the advantages of both.

The main advantage of a periodic lattice without superperiods is, that there are large areas in the (Q_H, Q_V)-diagram free of systematic resonances. Thus a relatively large space-charge tune shift at injection can be tolerated. Additionally the dispersion function α_p is considerably smaller than in the previous design which gives reduced aperture requirements.

The 4 long straight sections are now replaced by 12 short ones, but this is still acceptable for rf, injection, and extraction. Fig.1 shows a part of the resonance chart with the working area for SIS12.

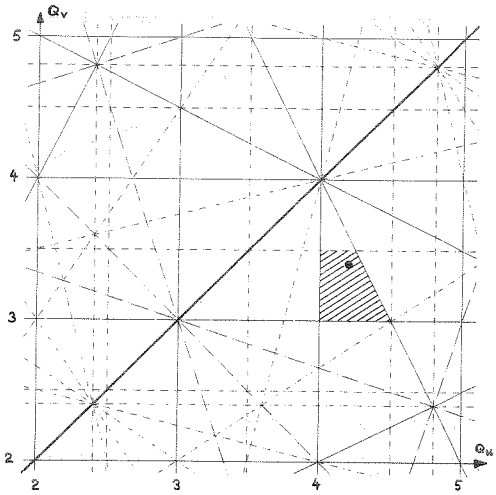


Fig.1: Working area foreseen for SIS12 (////) and systematic resonances up to order 5 for machines with 12 normal periods. Tune is Q_H= 4.2 and Q_V= 3.4 and indicated by •.

On the other hand γ_t in a periodic lattice is too low for protons at maximum energy. This can be overcome by changing the settings of every other doublet dynamically during acceleration at constant tune. It means the generation of a 6th harmonic in focussing, which does not cause problems, since the tune spread shrinks with $\beta\gamma^2$. Fig.2 shows the beam envelopes and dispersion function during this process.

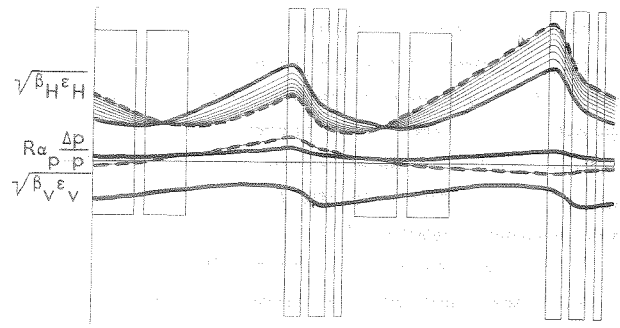


Fig.2: Raising γ_t from 5.4 to infinity by introducing a 6th harmonic in focussing. Envelopes and dispersion function are shown for $\Delta p/p$ = 0.5%, $\pi\varepsilon_H$ = 160π and $\pi\varepsilon_V$ = 40π mm×mrad for normal doublet focussing (———) and with 6th harmonic (– – –).

Though triplet focussing has the advantage of good acceptance, one has to pay with large quadrupole fields and bad conditions for correction elements due to nearly equal β-functions in both planes. Therefore the 3rd lense will be kept at injection field thus providing a dynamic change from triplet to doublet focussing during acceleration, which is illustrated in fig.3.

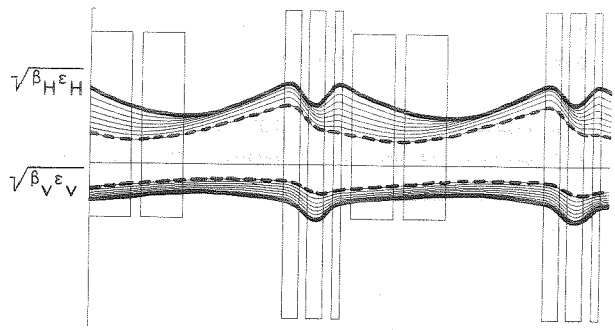


Fig.3: Dynamic change from triplet to doublet focussing. Beam envelopes during acceleration from injection (———) with $\pi\varepsilon_H$ = 200π and $\pi\varepsilon_V$ = 50π mm×mrad to 3.3 times higher $B\rho$ (– – –). Third lens remains at injection field.

Some parameters of SIS12 at $B\rho$=18Tm are listed below:

		TRIPLET	DOUBLET	
β_H	max/min	13.4 / 4.8 m	28.1 / 3.8 m	
β_V	max/min	22.8 / 6.9 m	21.2 / 6.4m	
$R\alpha_p$	max	2.5 m	3.1 m	
Quadrupole strengths:		S=12:	S=12:	S=6:
F-Quad.		6.1/6.4 T	7.3 T	8.7/6.6 T
D-Quad.		10.5 T	6.5 T	7.1/6.1 T
Gamma transition (γ_t)		4.7	5.4	∞

Variable Transition Energy in SIS12

B. Franczak
GSI Darmstadt

In a synchrotron particles with higher momentum usually circulate on a longer path but at a higher velocity than the reference particle. Since relative velocity deviations decrease with energy, while path lengths remain constant, there is one energy, the transition energy γ_t, at which both effects cancel and the revolution time becomes independent on momentum.

It ist not desirable to extract the close to γ_t or to cross it with high particle currents. A strictly periodic machine unavoidably has a γ_t, which is somewhat above the horizontal tune Q_H. In SIS12 with 12 periods and Q_H= 4.2 γ_t is 5.4, but γ for protons at $B\rho$ = 18Tm will be 5.8. So it is necessary to modify the periodicity of the machine, since the choice of tune values depends on other, more stringent considerations.

It can be shown[1], that the introduction of a harmonic somewhat above Q_H in the azimutal distribution of dipoles increases γ_t considerably. For SIS12 this is the 6th harmonic. The azimutal coordinate is the betatron phase advance, which depends on geometrical angle over β-function, rather than the angle itself, so there are two principal ways to introduce this harmonic:

- Rearranging the dipoles with periodic β-functions.
- Strictly periodic dipole pattern, but exitation of the desired harmonic by modulating the β-functions.

Low injection energy and high currents demand for a high symmetry of the SIS12 lattice. This excludes any other dipole pattern than the 12-fold symmetry. Therefore the second possibility had to be chosen[2].

It is done by exiting every other doublet in a different way dynamically during acceleration. So 6 superperiods consisting of 2 normal periods each are formed. During this procedure three things happen:

- γ_t grows, as desired, to infinity.
- The horizontal β-function increases by a factor of 2 in 6 of the 12 F-quadrupoles.
- A systematic stopband is created at 2Q = 6, which is far from Q_H= 4.2, but close to Q_V= 3.4.

Since the increase of β-function occurs, when the emittance has shrunk due to acceleration, this effect will not cause problems with the aperture. But it is not trivial, that the vertical motion remains stable under these conditions. Fortunately one has 4 free parameters, i.e. quadrupoles, and needs only 3 of them to achieve sufficient γ_t and the right tunes in both planes. The fourth one can be used to adjust the vertical β-function so, that the envelopes remain practically unchanged compared with their normal values.

Fig.1 shows the different development of quadrupole strengths in the 2 doublets of a superperiod during the creation of the 6th harmonic.

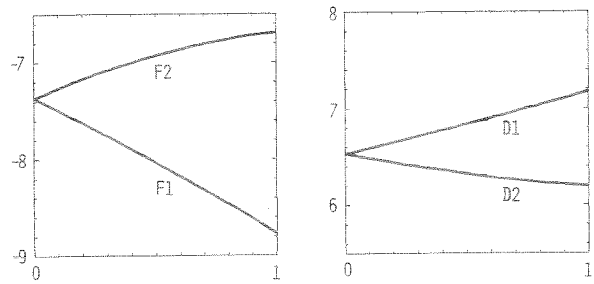


Fig.1: Strengths of quadrupoles QF1,QF2 (left) and QD1,QD2 (right) of the 2 doublets forming 1 of the 6 superperiods, $B\rho$ = 18 Tm, abscissa is the strength of the 6th harmonic: 0 corresponds to normal mode, 1 to nearly unfinite γ_t.

Fig.2 shows the values of γ_t and the momentum compaction factor α for the quadrupole settings plotted in fig.1.

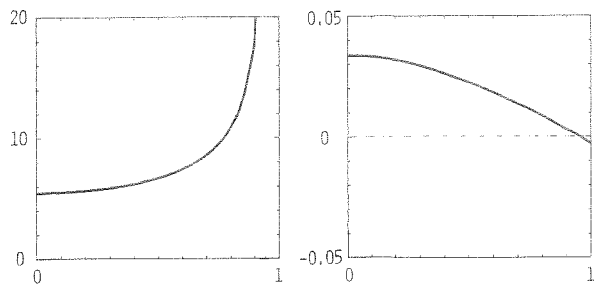


Fig.2: γ_t (left) and momentum compaction factor α (defined as $\alpha = 1/\gamma_t^2$) as a function of the strength of the 6th harmonic: 1 corresponds to nearly unfinite γ_t.

The time scale for the whole process is not critical: one has to start, when the emittance is small enough to compensate the growing β-function, and at any time γ of the particles must be significantly below the instantaneous γ_t.

References:

[1] E.D.Courant, H.S.Snyder, Theory of the Alternating-Gradient Synchroton, Ann. of Phys., 3(1958), p.42

[2] B.Franczak, K.Blasche, K.H.Reich, A Variable Transition Energy Lattice for SIS12/18, Proc. Part. Accel. Conf. 1983, Santa Fe, NM, USA

Triplet / Doublet Focussing in SIS12

B. Franczak
GSI Darmstadt

The amplitude functions β_H and β_V in a synchrotron, which describe the beam width for a given emittance, are mainly dependent on the focussing scheme, i.e. triplet, doublet, or FODO. There are several contradictory requirements on these functions:

- low β means low apertures for the magnets saving money, especially in the dipoles, or provides for given magnets high acceptance and a high space charge limit. Triplet focussing would be adequate to achieve low β-functions.
- high β on the other hand makes kicker magnets, septa, and correcting elements more effective. Thus the correction of chromaticity and extraction become easier. Doublet or FODO gives high β at moderate required focussing strength.

But these requirements are contradictory only at first sight: the emittances decrease with $\beta\gamma$ and the space charge limit increases with $\beta^2\gamma^3$ and therefore low β-functions with high acceptance are important only at injection and the very first part of the machine cycle. A similar consideration is valid for the second argument: only at maximum magnetic rigidity the effectivness of kickers and correcting elements has influence on design and costs. At medium and low energies these elements will be strong enough even at worse conditions.

Thus at different times different optical properties are necessary. Instead of finding a static compromise (triplets or doublets or FODO), for SIS12 a dynamic change over from triplet to doublet focussing during the cycle is foreseen. With triplets instead of doublets the gain of acceptance limited by QF horizontally and dipole vertically is 100% and 50% respectively. Fig.1 shows how the strengths B'L of the three quadrupoles (QF, QD, QT) depend on the type of focussing.

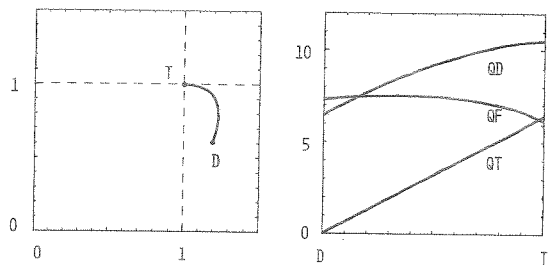


Fig.1: Quadrupole strengths between doublet (D) and triplet (T) mode of focussing at constant tune Q_H= 4.2, Q_V= 3.4. Left: relative B'L of QD versus QF normalized to triplet mode, right: absolute B'L of all three quads at $B\rho$ = 18Tm.

The only restriction on the time scale for this change is, that the increase of β-function must not exceed the decrease of emittance at any time. Calculations have shown, that the most elegant way is to keep the field of the third lens (QT) constant at injection level. Thus the focussing strength decreases with acceleration and an almost pure doublet mode remains at extraction level.

However, the time variation in the magnetic fields of QF and QD becomes more complicated than usual. One has not only to follow the field rise of the dipoles, but also to take into account the dependance on QT as indicated in fig.1 to keep the tune constant. Since this dependance can hardly be expressed analytically, numerical calculations for QF and QD at about 10 values of QT have to be performed. For the regions between them simple quadratic interpolation gives an accuracy in the tune of $<10^{-4}$ compared with the exact values, which is much better than the practical needs. The first part of the magnet programs for QF and QD is shown on fig.2 with the values for pure doublet mode and triplet mode with DC powered QT.

It should be mentioned, that the change from triplet to doublet focussing also causes a change in machine chromaticity. Its dependance on sextupoles is also modified due to the variable β-functions. Therefore the programs for the correcting sextupoles have to include all these effects.

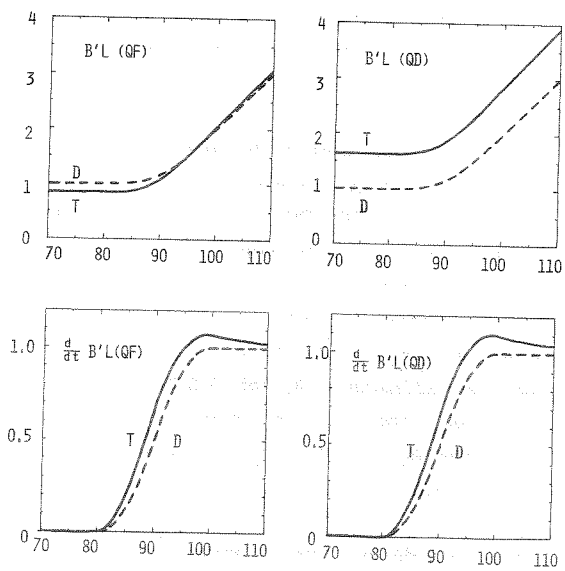


Fig.2: Top: strength of quadrupoles QF (left) and QD (right), bottom: time derivative in arbitrary units as a function of time (ms) during the first part of the machine cycle for QT turned off (D) and DC powered (T).

Beam Injection Line to SIS 12

H. Eickhoff, B. Franzke
GSI Darmstadt

In 1982 the parameters of the beam transport from UNILAC to SIS 12 have been preliminarily determined. The main part of beam preparation and suitable diagnostics as for instance compensation of dispersion, bunch transformation and fast chopping will be performed in the first long section being designed and constructed by the UNILAC-group (transfer line).

The nearly 25 m long remaining section between the so-called handling-over point and the injection septum contains the elements for transversal beam matching to SIS 12 and the inflection elements, a 9° inflector magnet and the electrostatic wire septum which deflects the beam by 2.25° In addition, the transition from the UNILAC high vacuum ($\geq 10^{-7}$ mbar) to the SIS 12 UHV (10^{-10} - 10^{-11} mbar) must be realized in this part called "inflection line".

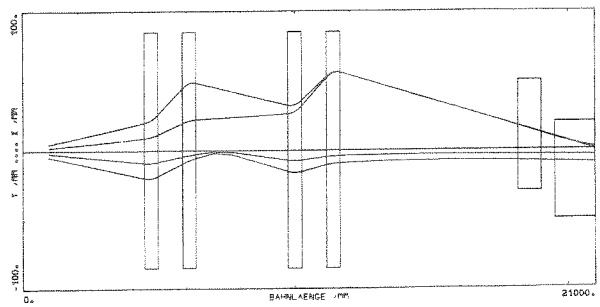


Fig. 1a Envelope functions in the SIS inflection line for two different emittance values: 2 and 10 π mm mrad

The optical concept for the inflection line may be derived from Figs. 1a and 1b. By means of four quadrupole lenses (FQ, DQ) the horizontal and the vertical beam envelopes can be adjusted to the requirement of both phase planes: on one side small beam diameter at given divergence in the horizontal plane, and on the other side a vertical envelope ellipse matched to the vertical acceptance A_V of SIS 12. For high current operation, the beam has to be distributed adequately over the A_V-area by means of a vertically deflecting dipole magnet (VD).

It will probably be desirable to optimize this distribution during the injection process which lasts between 40 µs and 500 µs. For this reason, the VD-design will be similar to the injection orbit bumpers in the ring, but with less power consumption.

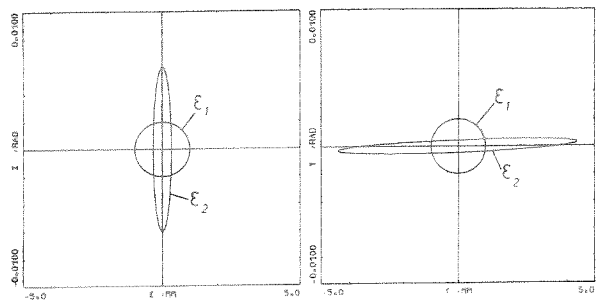


Fig. 1b Envelope ellipses in the x,x' plane (horizontal) and the y,y'-plane (vertical)
ε_1: at the entrance point of the inflection line
ε_2: at the end of the electrostatic septum

The time dependent closed orbit distortion in the ring is done by a set of four bump kicker magnets each with a length of 0.4 m and a maximal deflection angle of about 6 mrad. The required value of dB/dt during the multiturn injection is between 100 and 1000 T/sec. depending on the number turns to be injected.

We are also thinking about a dynamical matching of the beam during injection, mainly in order to reduce the beam losses in the ring. At this time, the technical implications are not elaborated.

All magnetic elements of both the transfer and the injection line will be designed for pulsed operation, though cost reasons will probably compel to start with d.c. power supplies.

Revised Layout for Slow Beam Extraction at SIS 12

H. Eickhoff, B. Franzke
GSI Darmstadt

With regard of important changes in magnetic structure and parameter set of SIS 12 (see respective articles in this report) the concept for slow beam extraction had to be revised:

- The free space between dipole and quadrupole magnets has been reduced from 10.0 m to nearly 5.50 m. Hence, one has to apply stronger magnetic fields to deflect the beam out of the ring, and consequently the total deflection angle increases. In the present design a deflection angle of 11.25° is obtained by three magnets (MSI, MSII, MSIII) with increasing field strengths (0.5, 1.0, and 1.5 T) and septum thicknesses (10, 40 and 60 mm).

- The horizontal betatron tune Q_H has been raised from 3.2 to 4.2 (Q_V = 3.4 unchanged) in order to reduce coupling effects between horizontal and vertical phase spaces. For the slow beam extraction, Q_H has to be shifted toward 4 1/3, a third order resonance (13th harmonic) which may be excited by two sextupoles of reverse polarity and in opposite positions in the ring. It is planned to use two of the 12 chromaticity sextupoles for extraction. The additional sextupole strength is nearly half of the value needed for chromaticity corrections.

- At Q_H = 4 1/3 the horizontal betatron phase advance per focussing period is ϕ_p = 130°. Therefore the optimal transformation of a kick at the electrostatic extraction septum into a horizontal separation between circulating beam and extracted beamlet is obtained over a distance of two focusing periods (ϕ = 260°).

The electrostatic septum will be installed at the inner side of the ring and give a kick of 2-2.5 mrad to the particles to be extracted. Due to this deflection a separation of 12-20 mm is obtained at the entrance of the first septum magnet (MSI), which - at this state of design - will be the only one installed inside the ultrahigh vacuum system.

The parameters of the electrostatic septum are similar to those for the injection septum; because of the small deflection angle, however, it is not necessary to curve the electrodes. Due to the similar design it is sufficient to perform high voltage- and vacuum tests only for one septum. The anodes of the electrostatic septa consist of tungsten wires perpendicular to the beam; preliminary manufacturing tests of such a wire electrode are in progress.

Fig. 1 shows two envelopes with a horizontal emittance of 3 π mm mrad; one that is not affected by the electrostatic septum (1), and another one that is deflected by the electrostatic septum and led into the extraction line with the magnetic septa (2).

Besides the conventinal third integer resonant extraction the possibility of stochastic extraction for very long spills is also taken into consideration.

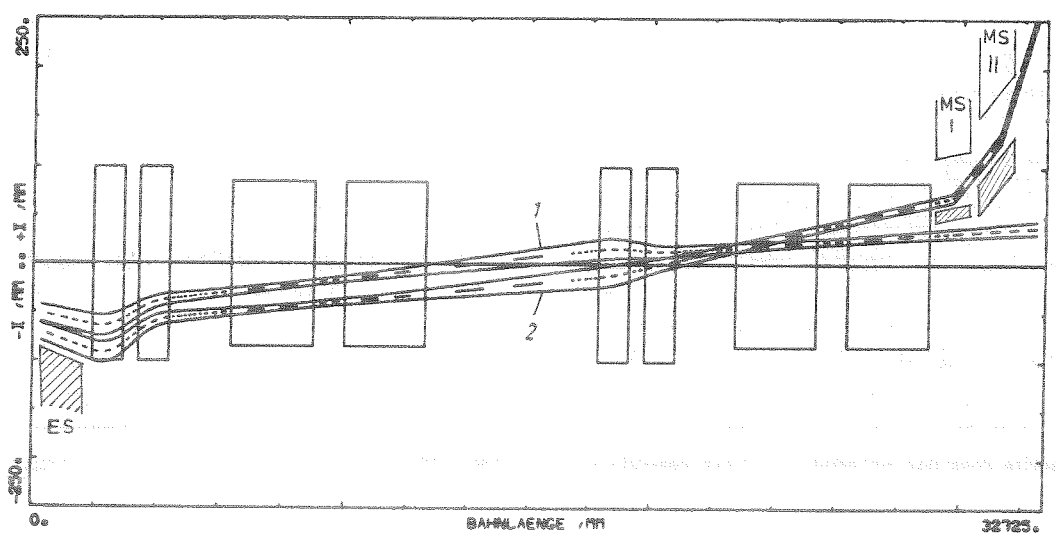


Fig. 1 Envelope functions for the deflected beam (2) and the non-deflected beam (1)

Measurements on the SIS Prototype Accelerating Station

M. Emmerling, K. Kaspar, K. Sato, A. Gasper
GSI Darmstadt

The prototype accelerating station has been described earlier (1). As expected from the very beginning, spurious resonances in the cavity turned out as one of the main problems.

When the six figure-of-eight dc bias-windings are capacitively grounded at the input ends (and no where else) spurious resonances appear at the gap at about 1.0, 3.4, 6.0 MHz and at higher frequencies. The lowest resonances are relatively sharp and make closed-loop frequency tuning impossible. There is also the risk that some resonances produce unexpected overvoltages and damages on various components. Part of the resonances depend strongly of the gap capacity. Surprisingly, the lowest three and several higher resonances do not move in frequency when the cavity is tuned over the whole frequency range. The following steps were undertaken to understand and reduce the resonance effects:

1) Variation of the number of dc-windings from 1 to 6,

2) Measurements with different blocking capacitor types installed in different places of the cavity,

3) Investigation of complex equivalent circuits,

4) Change from 6 figure-of-eight windings to a more symmetrical configuration of 6 windings,

5) Complete redesign of the connection between the power amplifier and the cavity,

6) Studies on different schemes to couple the rf into the cavity (inductively, capacitively, both),

7) Simulation of driving the cavity in push-pull mode.

The results can be summarized as follows. Resonances on the dc-windings are possible when the electric length of the piece of the dc-line between two blocking capacitors is equal to an integer multiple of lambda/2. In some of these cases, the rf magnetic fields around the dc-lines can be such, that they cancel each other when the lines pass through the ferrite stacks. Accordingly, the ferrite bias has no effect on these resonance modes. It seems clear that the 3.4 and 6.0 MHz resonances are of this kind. When each of the six dc-windings is individually grounded by a capacitor, the lowest fixed frequency resonance (except the one at 1 MHz) is at about 16 MHz. This one is probably due to a lamda/2-mode of the single dc-windings. The resonance at about 1 MHz could be identified as a parallel resonance of the anode cable passing through one ferrite stack, the blocking capacitors at its ground end, the coupling capacitors from the anode to the gap, and finally the beam tube. In this case, the currents on the anode cable and on the beam tube have opposite signs and make this mode independent of the ferrite tuning. This resonance can be shifted sufficiently below the operating frequency range by means of additional capacitors.

Another problem showed up, when the cavity was run up to the nominal gap-voltage of 16 kV peak. Several of the ceramic insulators supporting the dc-windings were overheated and damaged. So, for a long time, the cavity could be run at low rf levels only. After replacing the critical insulators by better ones, a new difficulty turned out: the blocking capacitors used until then did not stand the rf currents appearing at full power. As there is space enough to install larger and more powerful capacitors, this problem seems easily solvable.

The closed-loop control systems for cavity tuning and rf amplitude (2) were studied at the prototype in parallel to the above questions. Within the given limitations on the amplitude, tests including cable lengths of 150 m between the cavity and the control units were fully satisfying. Further tests and improvements are required to reach the specified performance of the system at higher rf levels, better frequency response of the gap voltage probes, etc. All other components for programmed frequency generation are under development.

(1) K. Kaspar, M. Emmerling, A. Gasper, Prototype of a Synchrotron Accelerating Cavity, GSI Annual Report 1979

(2) M. Emmerling, K. Kaspar, Amplitude and Phase Control for the SIS Accelerating Cavities, GSI Annual Rep. 1980

Status of the Design of SIS Magnet System

W. Bleuel, H. Gaiser, G. Grösch, B. Langenbeck
GSI Darmstadt

The material for the tender requests of the systems was further completed. Computer programs were written to facilitate parameter determination and to simulate the behavior of the magnets under varying conditions. Attention was given to possible production procedures.

Two computer programs, BLDMGN and SIMMAGN, were written to facilitate evaluation of magnet parameters and to simulate magnet behavior under varying operational conditions. A problem analysis showed that up to fourty primary parameters have to be fixed to determine the structure of the SIS magnets completely. These parameters include assumptions concerning the flux density distribution in the gap. In a first step a guess is made, which must be refined by calculations using well known field computation programs e.g. POISSON and MAGNET taking the preliminary evaluated magnet cross-section. A second step then gives the final design and operational parameters of cores and coils.

The fast ramping rate of SIS made it necessary to estimate eddy currents in cores, coils and vacuum chambers and their influence on field distribution and magnet operation. These effects are also simulated by the two programs using formulas developed at CERN[1]. To keep the resulting relative field errors in SIS small and constant in time, a good solution is a small ramping rate when beginning acceleration but the rate may be increased in an exponential way until reaching its maximum value.

With the aid of programs BLDMGN and SIMMGN the design of the SIS 15-degree window frame bending magnet, the long and short SIS quadrupole lenses and the SIS chromaticity sextupole has been optimized. A design has been done for the quadrupole lenses, the 22.5-degree H-magnets and the 8.75-degree septum magnets for the beam transfer line from UNILAC to SIS. Parameter lists were also provided for the eight types of pulsed quadrupoles in the UNILAC intra- and inter-tank beam transport, which will be needed for the projected multi-ion and multi-energy operation.

Attention was also given to possible production processes of the SIS magnet cores and coils. The fast ramping rate will bring no complications for the coil fabrication using well known and proved methods. After vacuum impregnation the coils will be surrounded by a kapton foil to improve ground insulation.

On the other hand eddy currents do not allow the use of thick end plates to clamp the welded lamination stacks, which is a common method to assemble the cores. We intend therefore to glue the sheets of the short quadrupole and the sextupole. Glueing of short stacks is a well proved production way, but glueing of long ones may be difficult, because a possible twist of the cores can hardly be corrected after manufacturing. (A stack of 850 mm length glued at GSI for a kicker magnet described elsewhere in this report has in total a twist of 2.4 mrad which is accceptable for that magnet[2]). Twist correction in the case of welded cores is usually done by peening the welds. We therefore propose to glue stacks of approximately .3 m length and to use them instead of thick end plates. We estimate the maximum shear strength τ/(pond/m**2) to the glued areas by

$$\tau = \frac{3\ PL^2}{8(1+\mu)a^3b}$$

P/pond is the load, L/m the width, b/m the height of a sheet, a/m the length of the glued piece. μ means the POISSON number. Using a suitable length a of the glued stack it is always possible to get a large safety factor with respect to the adhesive properties of the glue. A small sample has been made which will be submitted to load tests and compared with a solid body of equal dimensions. In addition forces tending to expand the welded cores and giving the main strain to the end pieces will be counteracted by tie rods across the center of the cores.

Assembling of the cores will be done on a support, which allows stacking of straight and curved magnets using demountable guide pieces. The usable support area is 1600 mm x 3500 mm. To have a stacking force of 120 Mp maximum three hydraulic cylinders are mounted; they are in an arrangement to permit an good alignment of the end pieces. The cores will be weighed together with the support. Weighing is done using three extensometers, whose signals are electronicaly added and displayed. An accuracy of 1 kp at a total weight of 14 Mp is guaranted by the manufacturer[3]. The weight of a half core can therefore be well determined within the range of the weight of one sheet (5 kp). The spezified stacking factor (96% or better) is so adjustable within 0.04%.

References:

[1] A. Asner et al., SI/Int. DL/69-2, CERN
G. Brianti et al., SI/Int. DL/71-3, CERN

[2] W. Bourgeois et al., Kicker Magn.for the UNILAC Beam Sharing Syst. and Beam Transf. to SIS, this Rep.,GSI

[3] Hottinger Baldwin Messtechnik GmbH, Darmstadt

Longitudinal Space Charge Limit of SIS 12 Operating in the Micro-pulse Mode with RF-System II

K. Beckert, R.W. Müller
GSI Darmstadt

The question was how many particles per bunch may be injected, longitudinally stabilized and accelerated in SIS 12 under resonable conditions for the rf-voltage amplitude and the bunch length, which is mainly determined by the possibilities for necessary debunching and rebunching processes. The estimated number of particles is less than the limit given by the 1/4-tune-shift condition and reduces therefore the final intensity considerably.

For calculating the space charge induced electrical field strength a parabolic distribution in z was assumed for λ which is the number of ions per unit length. As a result we used a formulation of L. Smith[1]:

$$e \cdot U_o \quad \left(\frac{eV}{turn} \right) = \pm \frac{2\pi \cdot A \cdot m_o c^2 \cdot R^2}{q \cdot h} \left(\frac{\beta^2 \cdot \varepsilon^2}{r_p \cdot Z_m^4} + \frac{3}{2} \cdot \frac{q^2}{A} \cdot \frac{g}{\gamma^2} \cdot \frac{N_B \cdot r_p}{Z_m^3} \right)$$

with $r_p = 1.5347 \times 10^{-18}$ m (class. proton radius), $2 Z_m$(m) = total bunch length, h = harmonic number, $N_B = \frac{\text{number of particles}}{\text{bunch}}$, U_o is the amplitude (per turn) of a vectorial voltage component with $\phi_s = -\frac{\pi}{2}$, acting against the space charge forces within the bunch. The beam tube-beam shape factor g is about 2. The product $(\Delta p/p) \times Z_m = \varepsilon$ represents the longitudinal emittance.

During acceleration the amplitude of the total voltage has to be $U = - U_o/\sin\phi_s$. For estimating the allowed number of particles it has been assumed that every bucket is equally filled by particles. In the equation quoted above two terms appear: the emittance term U_1 and the space charge term U_2. The ratio U_2/U_1 may be interpreted as a space charge parameter. The bigger its value is the bigger is the number of particles to be stored. The limit is reached if Z_m becomes a too large fraction of half of the bucket length, $\beta \times \lambda/2$. The reference length is that which can be reached by a debuncher after the UNILAC without producing too strong nonlinear distortions. This leads to a bunch half length of 4.3 ns. The best value of the longitudinal emittance of the UNILAC is $\varepsilon = 1.2 \times 10^{5}$ m.

To deliver an average current of 1 nAp to the experiment, the space charge parameter has to be fairly large. For multiturn injection no difficulties are expected; the bunching voltages have to be increased during injection from turn to turn to avoid mismatch. A similar method, with decreasing voltage, is applied during slow extraction to produce a high quality beam. In any case, a rebuncher between the SIS exit and the experiment is necessary to get bunches with a length below 1 ns[2].

Equipartitioning is not reached. Coupling terms as well as nonlinear resonances may occur. Therefore an increase of the longitudinal emittance is expected. But, however, the total number of synchotron periods per second is low (only some 100) and therefore the growth rate will probably be small. The exact growth rate can only be determined experimentally.

Additionally, there are a couple of other disturbing effects as bunch oscillations, bunch-bunch mode coupling, turbulent bunch lengthening, the head-tail effect and the interaction of the beam with kickers and cavities. Because of the low currents the influence of these effects on the beam quality should be negligible.

The results of the calculations are given in the following table. Recently, other ways of producing a similarly good time structure of the extracted beam are under discussion. The results will be reported later.

TABELLE 1

Synchronous Capture in SIS-Calculation of $U_o(N_B)$

1) Injection

Parameters: A = 20, R = 31.25 m, β = 0.15436, $2Z_m$ = 0.4m
h = 38, γ = 1.01213, $\Delta p/p = \pm\ 0.6 \times 10^{-4}$
g = 2, $\varepsilon = 1.2 \times 10^{-5}$

	q = 4+		q = 7+		q = 10+	
N_B	U_2/U_1	U_o/KV	U_2/U_1	U_o/KV	U_2/U_1	U_o/KV
4.65×10^7					61.65	39.93
6.6×10^7			42.88	39.95		
1.14×10^8	24.18	40.13				

2) Extraction

β = 0.6113	β = 0.804	β = 0.88
γ = 1.2640	γ = 1.681	γ = 2.175
$\varepsilon = 2.42 \times 10^{-6}$ m	$\varepsilon = 1.38 \times 10^{-6}$ m	$\varepsilon = 9.70 \times 10^{-7}$ m
$2Z_m$ = 0.345m	$2Z_m$ = 0.285m	$2Z_m$ = 0.24m
$\Delta p/p = 1.40 \times 10^{-5}$	$\Delta p/p = 9.68 \times 10^{-6}$	$\Delta p/p = 8.08 \times 10^{-6}$

N_B	U_2/U_1	U_o/KV	U_2/U_1	U_o/KV	U_2/U_1	U_o/KV
4.65×10^7					79.69	39.89
6.6×10^7			51.27	39.89		
1.14×10^8	26.18	39.98				

References:

[1] L. Smith; ERDA Summer Study, LBL/5543, p.77, Dec. 1976.

[2] K. Blasche, B. Franczak; SIS-Notiz vom 9.7.82.

6. Inertial Confinement Fusion

System Studies for Heavy-Ion Inertial Confinement Fusion [B]

R.W. Müller, K. Beckert
GSI Darmstadt

In 1981 the 'HIBALL' (heavy ion beam and lithium lead) design study was brought to a close, and the results were published[1]. In March 1982 the reference design of the HIBALL study formed the central theme of the Symposium on Accelerator Aspects of Heavy Ion Fusion[2] held at GSI.

Many questions and challenges still remain open in the HIBALL development, coming largely from the following design boundary conditions: loss-free injection under the influence of space charge into the rings; technology of the kicker; superconducting rings; aberrations of transverse and longitudinal lenses; more exact knowledge of stripping cross-sections.

The most critical single problem is the production of parasitic microwaves in the storage rings. With the present technology, the circulating current and/or the containment time in the rings is approximately 2 orders of magnitude too high, and it is not anticipated that advances in storage-ring technology will be able to bridge this gap.

Similar instabilities could also occur in the final (fast) compression with the linear induction scheme, caused by its ferrites. The higher costs of this linear scheme have already suggested the alternative use of rings for the fast bunching, but difficulties are already met within the preceding adiabatic bunching in the storage rings. It thus became clear during the symposium that for these reasons it is necessary to return to a concept using the heaviest possible, lowest charge-state ion, e.g. Bi^{+}.

In the summer of 1982 we developed, together with a group from the IPP Garching, a new concept that was consistent in these important points. Here again the beam in the storage rings is not stable, but the storage time is now only 1 ms. This requires that the linac delivers a peak current of 640 mA, or a beam power of 6.4 GW, during 1 ms, with some short gaps within this pulse for the purpose of beam manipulation. Under such conditions stability of the beam transport under the influence of space charge is possible, but extremely expensive. The linac would require an installed amplifier capacity of 10 GW, even though it would only be used with a duty cycle of 1 ms/50 ms = 2%. This concept increases the cost of the linac by a factor of 3 over the HIBALL estimate, increasing the total cost (including power stations and pellet factory) by 23%.

We would hesitate to present such a plan as the 'new HIBALL'; the trend should be reversed towards lower costs. On the other hand we see at least two options that are both promising and would lead to a considerable reduction in cost:

1. Electron-beam cooling, which would permit the ion beam energy to be 'diluted' in a relatively small number of storage rings and to store the beam for a longer time but to first 'cool' the beam to a high brightness only shortly before shooting it onto the target.
2. Non-concentric irradiation of the pellet. Similar proposals to those outlined in the last annual report using hollow beams and grazing incidence beams in the ablator[3] have been made by other groups. All these schemes have the advantage of employing a higher beam energy so that a lower total charge and possibly a somewhat lighter ion-species could be used.

Work has now begun, among others, on scenarios using beam cooling.

In spite of the considerable amount of on-going development work, and even though many criticisms and questions remain unanswered, the HIBALL scenario still stands as the most fully developed proposal for an inertial-confinement fusion reactor, and so wil remain in circulation until there is some considerably better scenario proposed.

In conjunction with the present research into accelerator development and into the hydro- and thermodynamics of the pellets, very high priority must be given to beginning high-intensity target experiments with heavy ions.

[1] HIBALL - A Conceptional Heavy Ion Beam Driven Fusion Reactor Study, KfK 3202 (2 Vol.).

[2] Proc. of the Symposium of Accelerator Aspects of Heavy Ion Fusion, GSI-82-8.

[3] R.W. Müller, in GSI-82-1, p. 324. Similar ideas have also been developed by R. Arnold.

SIS for High-Intensity Target Experiments - A Study Report

B

R.W. Müller
GSI Darmstadt

Target experiments in which high temperature plasmas of high density are generated by ion beams become relevant, among others, for inertial confinement if the mass-related power density in the target is above 10^{-2} TW/mg; this figure is more significant than the energy density which should be above 10^{-1} kJ/mg. With these beams, plasma (ion) temperatures of 10 eV or more at solid density can be expected. This is an unknown and very interesting area of state of matter, and interest in experiments like this is growing in the plasma physics community. The prospects are discussed in more detail elsewhere in this annual report.

To reach this goal in the next years, one should look into the capabilities of existing or scheduled machines. Except for high-power diode machines, there is no existing machine which could be used without major changes being made to it. The next generation of heavy-ion synchrotrons, however, will be able to be used as tool for these experiments if they are equipped with high-current, or more exactly speaking, with high-brillance injector linacs. Besides the Japanese Numatron, SIS 12/18 planned by GSI is one of these machines.

A preliminary report on our ideas was given at the Symposium on Accelerator Aspects of HIF[1]. At that time we considered a set of distributed beam lines from the ring to the target in order to bring three or more bunches to it simultaneously.

We feel, however, that the long and wide-spread tunnels needed, with a total length of more than SIS itself, would be an obstacle to the realization of these plans, since these works would surmount the financial and manpower capacities of GSI if they are to be executed at the same time with SIS. As a rule, additional concrete work is to be avoided.

Therefore, we studied how the SIS bunches can be united into one bunch within the ring, and whether the longitudinal emittance would then be small enough to achieve adequate compression in the bunches together with a sufficiently low momentum spread. Our conclusion is positive.

The procedure is as follows:

From a powerful RFQ linac (maybe a twofold linac plus a funneling device), Unilac is fed with a Bi^{8+} beam. In Unilac, Wideröe, Tank I is used as a static transport line only. The beam is stripped into the Bi^{25+} state at 1.4 MeV, and a 32 mA beam is sent into SIS after further acceleration in the Alvarez and ER sections.

The one- or twofold RFQ linac is of exactly the type now under construction as a 1.5 m long prototype. Though 30 m long, it it does not need a new building, but only an elevated platform in the existing injector hall (BH).

To conserve beam brillance, SIS is filled by single-turn injection. The quarter-tune-shift limit (so-called Laslett limit) is hit after adiabatic bunching, and the coasting beam is slightly sensitive to microwave generation (longitudinal instability), with a growth rate of 0.3 ... 1 ms^{-1}. After bunching it becomes stable again. Since we can tolerate a longitudinal emittance blow-up by a factor of 1.5-2, we are confident that the beam will survive this critical phase. After acceleration the beam is insensitive to any instability.

After acceleration to 18 Tm, the stored beam energy is 200 Joules. This will be sufficient if we are able to concentrate this energy into a target focus of 150 µm radius within an effective time interval of 12 ns. The first of these figures demands single- turn injection so that the beam emittance does not surpass 1.5×10^{-6} m x rad.

During acceleration, four bunches are present in the SIS ring. This figure is set by the frequency span of the standard rf system. We re-unite the four bunches into one after acceleration by a very simple bunch-merging procedure which still uses the standard rf system. The alternative, namely producing a coasting beam and rebunching it into the fundamental mode, would be far more sensitive to the longitudinal instability than the coasting beam which exists at injection.

The new bunch length is 280 ns, still by more than a factor of ten too long. Fast compression is thereby called for which requires a set of high-voltage, fixed-frequency rf cavities in the ring, whose voltage, as seen by the beam, has to be raised from zero to 700 kV at 1.74 MHz within a few microseconds. The fast rise can be achieved by short-circuiting one of two counter-phased, fully excited cavities. Both fast bunchers and RFQ accelerators are part of many HIF scenarios, and therefore are important areas of technological development.

Furthermore, SIS has to have a fast extraction device, the same device which is needed for transferring the beam into a future SIS 100. The target experiments can take place in the piece of SIS 18 - SIS 100 transfer tunnel which is already included in the plans.

More detailed figures will be given in a later report.

This scheme has been worked out in close cooperation with Dr. Ingo Hofmann of IPP Garching.

[1] R.W. Müller, in GSI-82-8, p. 448.

High-Current Ion Sources Development [B]

R. Keller, F. Nöhmayer, P. Spädtke, GSI Darmstadt
M.-H. Schönenberg, Fachhochschule Wiesbaden

The GSI high-current ion source test-stand [1] was again modified, to increase its acceptance. Now high-current ion beams are first measured behind the 80 mm wide magnetic quadrupole triplet, about 2 m distant from the source.

The source for gases, CORDIS [2], see Fig. 1, was further tested on this stand, using single- and multi-aperture extraction systems to produce singly charged argon and xenon ion beams. As compared to the older source type ELSIRE, CORDIS not only needs much less discharge power, but also keeps the plasma density more uniform in time, which results in nearly constant transported ion beam currents for a pulse duration of 0.3 ms at least. CORDIS can also be operated in the d.c. mode without difficulties; only the extraction-plate holders have to be cooled more efficiently than for the pulsed mode.

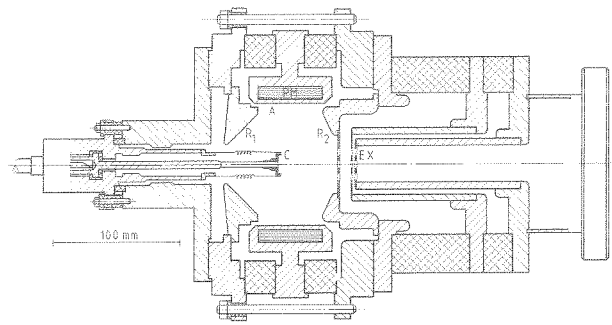


Fig. 1: CORDIS (cold version of a multipole/reflex-discharge high-current ion source). A: Anode. C: Cathode. R_1, R_2: Reflector electrodes. EX: Standard accel/decel multiaperture extraction system. PM: Permanent magnets, tangentially oriented.

For a special application [3], a hollow beam of about 50 mA Ar^+ ions was generated, using an accel/decel extraction system with three curved slit-apertures. Another study concerned a two-gap (pentode) extraction system for CORDIS, basing on experiences made with an analogous system for ELSIRE [4]. Also here, optimum extraction-electrode geometries were looked for in computer simulations followed by experimental tests. The results with the former system were by far exceeded, regarding ion-current values, overall system reliability, and useful pulse-length (now over 0.3 ms, compared to 0.05 ms before).

For the generation of metal-ion beams a new source version, HORDIS II, was constructed, taking the oven and other technical details from HORDIS [5], but with the discharge geometry of CORDIS. The same benefits as with CORDIS were found; the lower gas pressure within the cold source corresponds to lower oven temperatures of HORDIS II, as compared to HORDIS. 37 mA ion current were reached for Bi^+, see Tab. 1, fulfilling the actual Heavy Ion Fusion requirement for the HIBALL scenario [6].

When producing metal-ion beams no auxiliary gas is needed. Then with the very low background-pressure within the beam-line, effects of space-charge compensation can easily be explored. Fig. 2 a illustrates that the build-up time of a well compensated beam (onset of the flat part of the Faraday-cup signal) amounts to 1.7 ms if the beam-line pressure is kept at the minimum value, about $1.2*10^{-7}$ mbar. With a pressure of $1.5*10^{-5}$ mbar, however, the beam-formation time is only 0.7 ms, see Fig. 2 b. In both cases the beam was transported over 4.5 m, focused by triplet and analyzing magnet; the source- and extraction-parameters were identical.

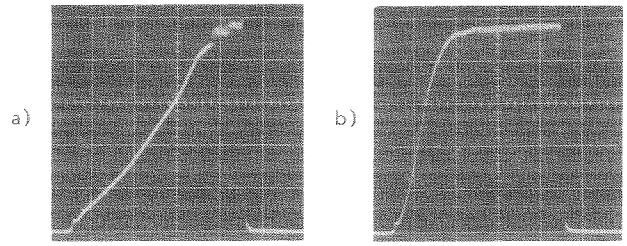


Fig. 2 a, b: Current signals of Bi ions, 1 mA/Div and 0.5 ms/Div.

Ion	I_i	B_{vn}	U_b	ε_n	n_A	F_A	d_{FC}
Ar^+	41.5	5.7	50	0.085	1	1.33	2.7
	120	0.93	50	0.36	7	1.98	1.6
Xe^+	18	5	50	0.06	1	1.33	1.9
	71	>1.1	50	<0.25	7	1.98	1.6
Bi^+	37	>1.4	36	<0.16	7	1.98	2.7

Table 1: Ion beams obtained by CORDIS and HORDIS II. I_i (mA): Ion current. B_{vn} (A/(mm mrad)^2): Velocity-normalized brightness. U_B (kV): Beam voltage. ε_n (mm mrad): Normalized emittance. n_A: Number of extraction holes. F_A (cm^2): Total area of extraction holes. d_{FC} (m): Distance source / Faraday-cup.

References

[1] R.Keller: GSI 81-2, 263 (1981)
[2] R.Keller: Nucl. Instr. Meth. 189, 97 (1981)
[3] P.Krejcik, R.Keller: this annual report
[4] R.Keller, P.Spädtke, K.Hofmann: 4th Int. Conf. on Ion Implantation, Berchtesgaden (1982)
[5] R.Keller, F.Nöhmayer, P.Spädtke: 4th Int. Conf on Ion Implantation, Berchtesgaden (1982)
[6] R.W.Müller: SIT-Arbeitsnotiz 030582, GSI (1982)

Heavy Ion RFQ Status Report B

R.W. Müller, U. Kopf, L.W. Funk*)
GSI Darmstadt

The basic task and design of the heavy ion RFQ prototype, or the first module of "MAXILAC", has been described in the preceding annual report[1]. A time schedule made at the end of 1980 predicted RF power in the tank in autumn of 1982, and first beam through it in early 1983. This is actually the history during 1981 and 1982:

1981, Jan. Start of mechanical design work.

Aug. Order for manufacture of the steel construction, at R+A, Jülich. Copper-plating prototype of an inner conductor beam.

Sept. Material sample (Cu+Cr) for the pole holders (cross-bars) is bought.

Nov. A slight change in the profile of the shaper section is made according to a smoother design; the first and 36th $\beta\lambda/2$ electrode remain fixed, only intermediate elements are shifted by up to 2 mm, the injection energy is lowered from 2.4 to 2.3 keV/amu. Name of new profile is B'.

Dec. Prototype pole holder ready.

1982, Jan. 100 kW amplifier, 6-28 MHz, ordered from Herfurth GmbH, Hamburg. A study for a 1 MW final amplifier for a long MAXILAC (5 modules) was started by Herfurth some months earlier. The ordered amplifier can be the driver of the larger system. RF power cable, RF material and measurement equipment are bought.

Apr. First high-intensity Ar^+ beam from injector.

June Steel resonator tank and inner conductor beams delivered.

Aug. RF amplifier delivered, and 2 weeks later in operation. First attempt to copper-plate the inner conductor beams proves unsatisfactory though copper-plating had been tried on a model (see Aug. 1981).

Sept. Copper-plating of steel tank and lids. Manufacture of pole holders and pole rods completed.

Oct. Second copper-plating of the inner conductor beams, now successful.

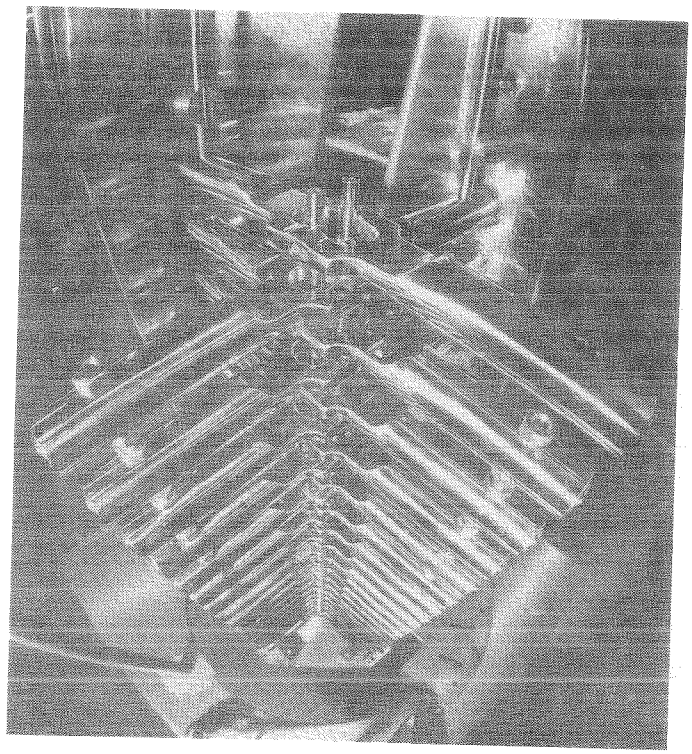
Nov. First assembly of the inner conductor system does not achieve necessary alignment. Water cooling supply system completed. Maintenance period on UNILAC and breakdown repairs prevent RFQ work (not the first time).

Dec. Second assembly of the inner conductor system using an earlier proposed method, proves successful, finished Jan. 4, 1983.

Data are ready for the design of modules 2 through 5 ; 1:4 scale models have been made modules 2 and 4. Nevertheless, the construction shall not be started until we are sure that the design voltage of 150 kV can be held in the first module after careful conditioning.
An RFQ elementary formulary[2] was compiled to show the basis of our RFQ design codes.

*) Visiting scientist from AECL, Chalk River, until June 1982.

[1] R.W. Müller, L.W. Funk, U. Kopf, GSI-82-1, p. 312.
[2] L.W. Funk, R.W. Müller, GSI-82-7.



HIGH CURRENT TRANSPORT EXPERIMENTS AT GSI

J. Klabunde, M. Reiser*, A. Schönlein,
P. Spädtke, J. Struckmeier - GSI Darmstadt

The high current beam transport project at GSI was described in previous reports[1,2]. The periodic transport channel was assembled during the first six months of 1982. A view of the beam line is shown in Fig. 1. The six focusing periods, each period containing one focusing and one defocusing magnetic quadrupole lens, were installed at the 300 kV-dc injector. The GSI high current ion source ELSIRE[3] is used. A large aperture magnetic triplet serves to match the beam to the FODO-channel. Furthermore, a collimating system defining the input emittance is located on the downstream side of a quadrupole triplet. Different beam diagnostic elements are positioned along the line. The emittance measurement can be carried out at the input and output end of the periodic channel. Beam profiles and ion current can be measured behind each section. Turbomolecular pumps provide for a good vacuum of 5 x 10^{-7} torr. Clearing electrodes were installed at different positions of the channel. Negative or positive voltages can be applied in order to study beam neutralization effects.

During the first phase of beam experiments the beam transport from the ion source and the dc-high voltage injector to the input of the FODO-channel was studied (see also ref.4). Ar^+ ions were accelerated up to 200 keV. The achieved maximum current of ca. 8 mA and an emittance of 30 - 60 mm mrad are highly sufficient for beam transport studies. Reduction of current and emittance is possible by variation of the ion source parameters and by use of collimators with variable aperture. Hence the tune depression can be varied over a wide range. This is shown by an example in Fig.2, the channel is adjusted to zero-current phase advance of 90°. The diagram illustrates the variation of tune depression as function of emittance and current.

Experimental observations indicate that the ion beam is partially neutralized by electrons due to residual gas ionization (the pulse length is 2 ms) or secondary electron emission from the walls.[5] The space charge potential of the beam was measured by Langmuir probes, free-space beam envelope expansion and by measurement of the energy of residual gas ions diffusing out of the beam.[7]

Preliminary studies of the transport of such partially neutralized beam were made. In particular, we measured the emittance growth rates in the FODO-channel at different settings for the magnetic field gradient corresponding to different values of the zero-current phase advance. For the high brightness beam, emittance growth rates up to a factor of 6 were measured; for very low current operation, on the other hand no emittance growth occured. Since theoretical studies[6] of instabilities etc. assume unneutralized beams, we have as yet no satisfactory explanation of these measurements. The studies of a partial neutralized beam have also to include the effects of mismatching and spherical aberrations by the external quadrupole field. Further experiments will be carried out with short beam pulses in order to minimize the neutralization effects. Therefore, the use of a chopper system is planned.

[1] J. Klabunde, GSI-82-6, 1982.
[2] J. Klabunde et al., GSI-Nachrichten 11-82.
[3] R. Keller, GSI-report 82-8.
[4] P. Spädtke et al., this report.
[5] A. Schönlein et al., this report.
[6] J. Struckmeier et al., this report.
[7] P. Kreisler et al., this report and GSI-82-6, 1982.

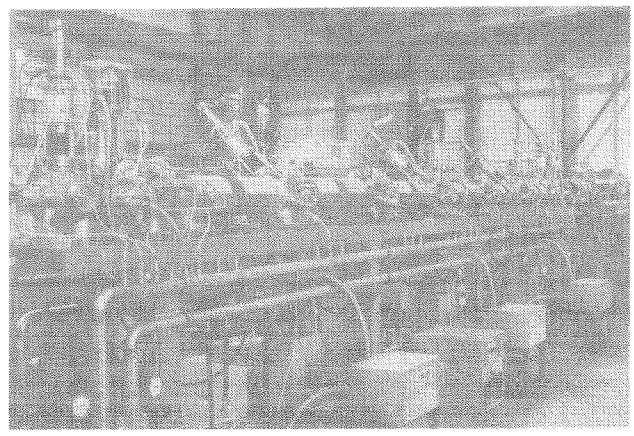


Fig. 1: View of the FODO-Channel.

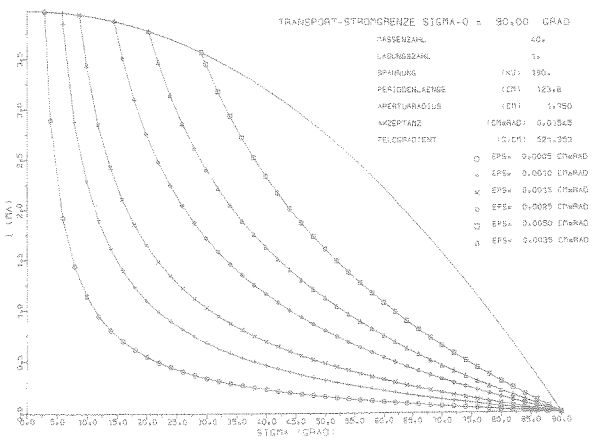


Fig. 2: Dependence of tune depression from ion current and emittance at $\sigma_o = 90°$.

* On sabbatical leave from University of Maryland

B

ASPECTS OF SPACE CHARGE COMPENSATION IN ION BEAMS

A. Schönlein, J. Klabunde, M. Reiser*

GSI - Darmstadt

The maximum current transported through a FODO-channel is restricted by the strong space charge forces and further by theoretically predicted space charge instabilities. In all theoretical models it is assumed that no neutralising charges of opposite sign are in the beam. To compare experiments and theory the partial or total neutralisation must be avoided.

There are two mechanism wich are in the main responsible for the space charge compensation:

1. gas neutralisation
2. secondary electron emission.

In the first case the electrons inside the beam are created by ionisation of residual gas atoms. Electrons are 'trapped' by the ion beam space charge and thereby cause partial neutralisation. The produced slow ions are repelled radially outward of the beam. The number of electrons produced by ionisation is proportional to the gas density, the ion flux and the total ionisation cross section appropriate to the ion energy and gas species.

Secondary electrons are produced on the metallic walls. These electrons are accelereted across the beam and cause partial neutralisation.

Simple theoretical models show that the ionisation of the gas is the mean reason for the space charge neutralisation in our present transport experiment at GSI [1].

The neutralisation by secondary electron emission from the walls is restricted (in the absence of magnetic fields) by the space charge limited electron current from the walls. A simple one-dimensional model considers an ion beam of uniform density bounded by a pair of plane parallel conducting plates [2].

The space charge limited current of a cylindrical beam in a circular pipe is lower then the limited current in the one-dimensional case [3]. Fig.1 shows both the potential distribution relativ to the beam centre for the one-dimensional case and for the more realistic cylindrical geometry. As one can see, it is impossible to compensate an ion beam completely by secondary electron emission from the metallic walls. Because of the lower limited electron current the degree of neutralisation for the cylindrical geometry is much more lower then the one-dimensional case.

Numerical calculations are done to study the motion of electrons inside the magnetic quadrupole lenses in the presence of electric fields produced by the non- neutralized ion beam passing through the quadrupole lenses. The electron orbits in such fields may be extremly complicated. The results show that electrons produced by ionisation inside the beam are 'trapped' and therefore cannot escape radially even if outward forces from clearing electrodes at positive potentials are present. Similar behaviour is found for electrons outside of the beam. Only in a certain region close to the pole tip of the quadrupoles electrons can be 'trapped' inside of the beam. This is also valid for secondary electrons. Fig.2 shows an orbit of an electron which is liberated from the wall close to the pole tip. This electron is 'trapped' inside the beam and contribute to neutralisation. The regions in which this effect may occur are restricted to about 10% of each quadrant of the quadrupole lenses. So only about 10% of the secondary electrons are 'trapped'.

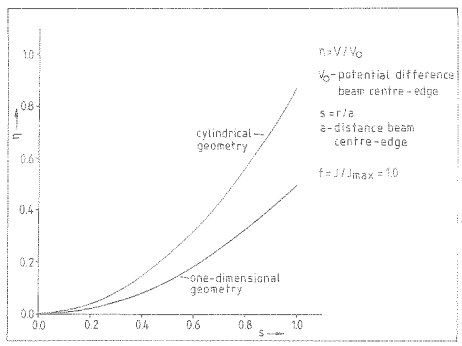


Fig.1: Potential distribution with compensation by secondary electrons.
η - normalized potential difference relativ to the beam centre
s - normalized distance to the beam centre

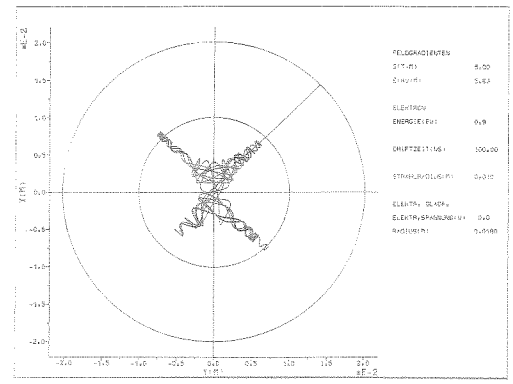


Fig.2: Electron liberated close to the pole tip are 'trapped' inside the beam.

* On sabbatical leave from University of Maryland

References

[1] J. Klabunde et al., this report
[2] Evans a. Warner, CERN/MPS/LIN.71-2(1971)
[3] M.v.Ardenne, Tab. zur Angew. Physik (1962)

ENVELOPE INSTABILITIES IN FODO - CHANNELS

J. Struckmeier , J. Klabunde , M. Reiser*
GSI - Darmstadt

The envelope functions X(s) and Y(s) for a "Kapchinskij-Vladimirskij" particle distribution (leading to linear space charge forces) in a FODO channel are determined by the two coupled differential equations (known as "KV-equations") :

$$X'' + k(s)\,X - 2K/(X+Y) - \varepsilon^2/X^3 = 0 \qquad (1a)$$

$$Y'' - k(s)\,Y - 2K/(X+Y) - \varepsilon^2/Y^3 = 0 \qquad (1b)$$

If the envelope functions X(s) and Y(s) have the periodicity of the FODO lattice, we speak of a "matched" beam. Our purpose now is to investigate the stability of such a matched envelope against small perturbations. We define the two functions:

$$X(s) = X_0(s) + x(s) \,, \quad x(s) \ll X_0(s)$$

$$Y(s) = Y_0(s) + y(s) \,, \quad y(s) \ll Y_0(s)$$

where X_0 and Y_0 denote the matched envelope functions and x(s) and y(s) the small perturbations, respectively. Substituting these functions into the KV - differential equations (1) leads to a set of four first order, coupled, homogeneous, linear differential equations with periodic coefficients. For $z=(x,x',y,y')$ we may write:

$$z' = A(s)\,z \,, \quad A(s+S) = A(s) \qquad (2)$$

where S is the length of one FODO period and A(s) the 4×4 matrix with S-periodic coefficients a_i:

$$A(s) = \begin{pmatrix} 0 & 1 & 0 & 0 \\ -a_1(s) & 0 & -a_3(s) & 0 \\ 0 & 0 & 0 & 1 \\ -a_3(s) & 0 & -a_2(s) & 0 \end{pmatrix}$$

If Z(s) is the 4×4 matrix of linear independent solution vectors of system (2) with Z(0) = E (unit matrix), the solution over n periods is given by:

$$Z(s+nS) = Z(s) \cdot Z(S)^n$$

That means, we only have to examine the solution matrix of (2) obtained by integration through one focusing period. Instability is present if the eigenvalues of the solution matrix Z(S) are not unity. Since Z(S) is symplectic and real, the eigenvalues will occur both as complex-conjugate and as reciprocal pairs. The eigenvalues λ may be written as

$$\lambda = |\lambda| \cdot e^{i\phi}$$

where $|\lambda|$ denotes the growth rate in the presence of instability and φ the phase shift of the appropriate perturbation mode through one FODO period. If we use the "smooth approximation" to calculate envelope perturbations, we get a linear system with constant coefficients which can be solved analytically. From there we obtain the phase shifts for the basic modes of envelope perturbations (parallel and anti-parallel) :

$$\phi_1 = \sqrt{\sigma_0^2 + 3\,\sigma^2} \,, \quad \phi_2 = \sqrt{2\,\sigma_0^2 + 2\,\sigma^2}$$

where σ and σ_0 are the usual particle tune shifts with and without space charge forces. Below $\sigma_0=90°$, where no envelope instabilities occur, these results agree remarkably with the exact solutions of (2) obtained by numerical integration and eigenvalue analysis. Above 90° we get eigenvalues which do not lie on the unit circle in the complex plane. In fig. 1 the phase angles ϕ_1, ϕ_2 and in fig. 2 the appropriate $|\lambda_{1/2}|$-values for $\sigma_0=110°$ are plotted versus descending σ, i.e. increasing beam current. The types of instabilities can be seen as a resonance due to either equal frequencies of both envelope modes ("confluent resonance") or due to one envelope frequency being in half integer resonance with the focusing structure ("parametric resonance"). Fig. 3 shows a slightly mismatched beam in the unstable region ($\sigma_0=110°$, $\sigma=66°$) leading to a remarkable growth in envelope radius.

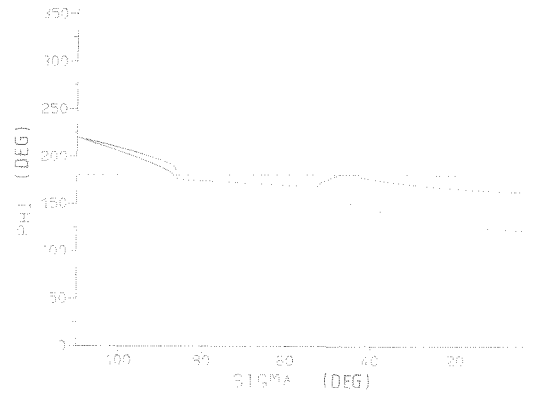


Fig. 1 : Phase shifts of both envelope perturbation modes versus σ for $\sigma_0=110°$

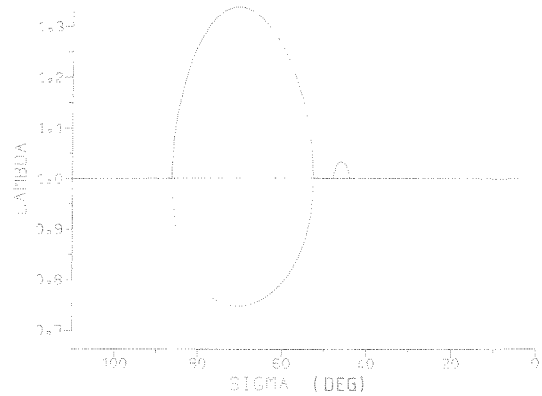


Fig. 2 : Growth rates versus σ for $\sigma_0=110°$

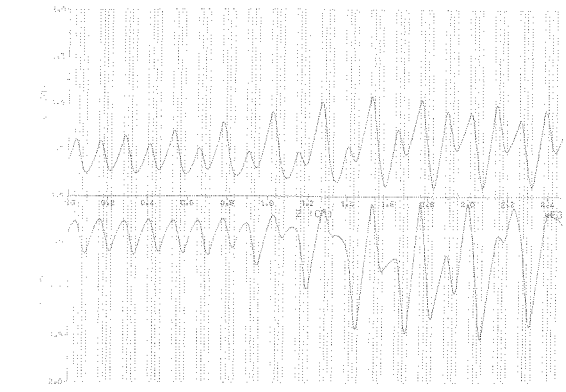


Fig. 3 : Mismatched beam in the unstable region

* On sabbatical leave from University of Maryland

THIRD AND HIGHER ORDER INSTABILITIES IN FODO-CHANNELS FOR DIFFERENT TYPES OF DISTRIBUTION FUNCTIONS

J. Struckmeier , J. Klabunde , M. Reiser*
GSI - Darmstadt

From numerical simulations [1,2] and analytic treatment [3,4] it is known, that the KV-distribution leads to instabilities arising from perturbations of the strictly linear self fields. These perturbations can be classified by the order of the additional terms of the space charge potential, which represent the deviation from the ideal case given by a quadratic potential function. For example, the third order potential perturbation term is:

$$V^{3rd} = Ax^3 + Bx^2y + Cxy^2 + Dy^3$$

In order to investigate these perturbations one has to linearize the Vlasov equation and apply the appropriate perturbation about the stationary solution, yielding a linear system of first order differential equations with periodic coefficients. Integrating through one FODO period and evaluating the eigenvalues of the solution matrix (which is symplectic and real), one obtains "unstable zones" depending on σ and σ_0, indicated by eigenvalues which do not lie on the unit circle in the complex plane. This method is valid if the perturbations are assumed to be small, and this is the crucial point in the whole analysis since this is not true for a realistic density distribution which is of a gaussian type. Fig. 1 shows the results of computer simulation of an initial KV-distribution (with 5000 macroparticles representing the beam). The instability expected from the obove mentioned perturbation theory is evident in the 3 tails of the phase space plots. The transverse rms-emittance grows by a factor of 2.3 in 100 periods.
A similar behavior was found using a waterbag distribution (i. e. constant particle density in the four dimensional transverse phase space). The effective growth rates applying to the appropriate instability however were found to be smaller compared to the KV-distribution, which results in a smaller slope in emittance growth. For parabolic and conical density distributions, these growth rates further decrease. For a gaussian density distribution, the growth in transverse emittance nearly vanishes after about 5 structure periods. This initial growth is due to the matching of the density distribution generated by the PARMILA program to the FODO lattice, yielding a nearly homogenous density distribution in real space surounded by a halo. The emittance growth for the gaussian distribution is not due to third-order instabilities, rather it may be attributed to two effects, as shown in fig. 2 :

a) sperical aberrations due to nonlinear space charge forces which are more pronounced for this type of particle distribution than in the other cases;
b) changes of the distribution towards a uniform density profile.

As a result of our calculations it can be stated that for a realistic particle distribution the danger of resonances are not as great as aspected from simulations with KV- and waterbag distributions.

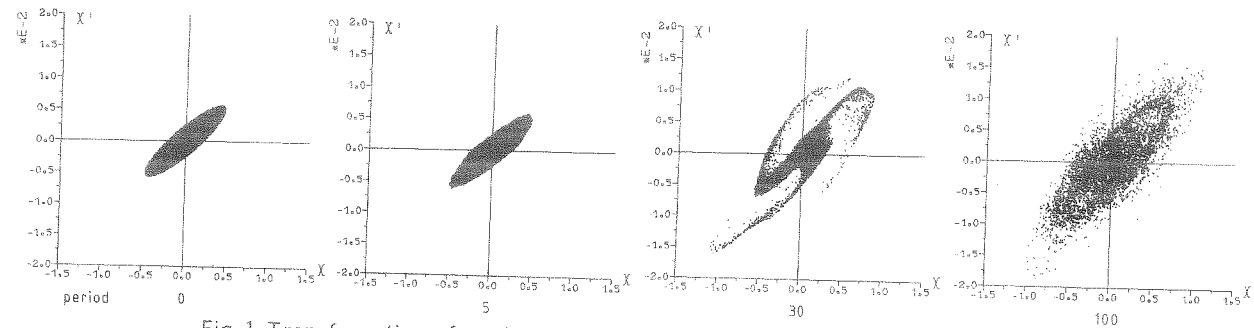


Fig.1 Transformation of an initial KV-distribution for $\sigma_0 = 90°$ and $\sigma = 41°$

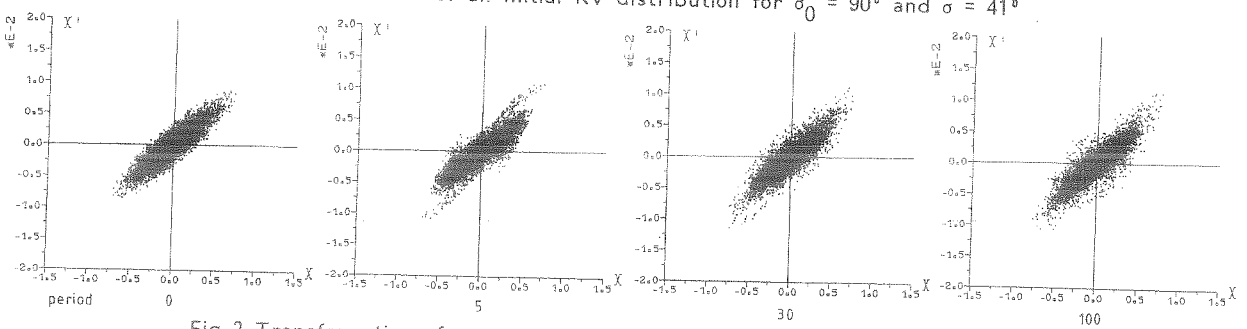


Fig.2 Transformation of an equivalent initial gaussian distribution ($\sigma_0 = 90°$, $\sigma = 41°$)

References:

[1] I. Haber et al. , Phys.Rev.Lett. 42, (1979)
[2] I. Hofmann , Nucl.Inst.Meth. 187, (1981)
[3] L. Smith , HIFAN-13 , LBL
[4] S. Chattopadhyay , HIFAN-14 , LBL

* On sabbatical leave from University of Maryland

KOBRA3 A 3D-COMPUTER CODE SOLVING VLASOV'S EQUATION [B]

N.Schmitt, FH Wiesbaden; P.Spädtke, GSI Darmstadt

A new FORTRAN program, named KOBRA3[1] (Kode zur Berechnung raumladungsbehafteter Teilchenbahnen im 3D Raum), has been generated which simulates ion beams under arbitrary boundary conditions, in order to optimize ion extraction and transport systems and to improve the understanding of ion beams physics. The program contains a three dimensional POISSON solver, raytracing and space charge calculation. Furthermore magnetic fields, computed analytically, or taken from tables, can be included in the orbit calculation. Because of the new POISSON solver, which uses the 'alternating direction implicid method' (ADI), fast convergence is achieved compared to standard algorithms such as the finite difference method, using successive overrelaxation. So the program needs about 50 seconds CPU time only for a given potential problem within the maximum size of 100 * 30 * 30 grid points and a working space of four megabyte. Up to 1000 particles, produced by a monte carlo generator can be run through the calculated potential field, creating there a charge distribution. The number of particles is great enough to yield a smooth distribution. POISSON's equation is then solved again and so on, until its solution converges to that of VLASOV'S equation. Typically we need 4 to 6 main iterations to achieve convergence.

For technical exactness the calculation is carried out with real*4 variables,but a double precision version exists, too.

The output of the program can be distinguished into two main parts;output on the line printer and on the plotter or the graphic display.

The line printer starts with a copy of the input datadeck and prints the following matrices: potential, space charge,components of magnetic flux density and the table with the starting conditions of the particles.

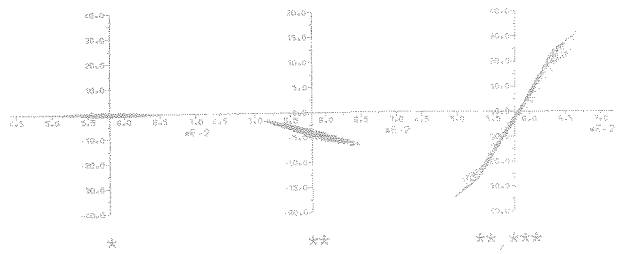
For the graphic output one can choose between a two-dimensional representation of the equipotential lines and a three-dimensional display of the potential distribution, in any plane parallel to the cartesian system, as can be seen in figs.2 and 3.

The starting conditions of the particles are shown by their emittance figure,while the tracks of the particles are displayed either in a three-dimensional cartesian system, or there projection into one of the coordinate planes, or emittance plots. All these pictures can be replotted with changed parameters without needing a rerun of the whole program. If space charge is not negligible this output can be chosen after every iteration step.

Up to now several tests were successfully completed,regarding:

- -Extraction of a beam from a plasma ion source.
- -A magnetic spectrometer
- -Potential caused by an drifting ion beam within a tube.

One example may show the capabilities of the program: Assuming a 10 mA,50 keV Ar^+ ion beam, injected into a drift tube with a misaligned einzel lense. The beam runs parallel to the axis (zero emittance). The diameter of the beam tube is 100 mm, the diameter and length of the einzel lense is 60 mm. Fig.1a shows the horizontal emittance without space charge and with grounded lense. In fig.1b the einzel lense is put on 10 kV, and in fig.1c space charge is included. The potential distribution is shown in figs.2 and 3. The computed value of the beam potential on the axis and the position of the cross-over agree well with the ones obtained by analytical calculations.



* ** **,***

Fig.1: Emittance of the beam (mrad vs. meter)

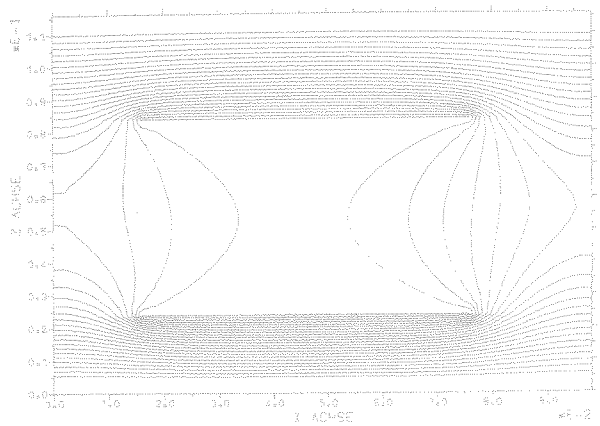
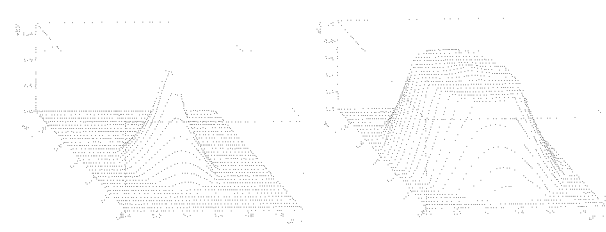


Fig.2: Equipotential lines parallel to the axis distances in meter; NEUMANN boundary condition



*** **,***

Fig.3: Beam potential distribution on a plane perpendicular to the axis (volts vs. meter*meter)
* lense grounded, without space charge
** with einzel lense, *** with space charge

[1] N.Schmitt, Diplomarbeit FH Wiesbaden (1983)

A High-Current Test Facility for Hollow Beams B

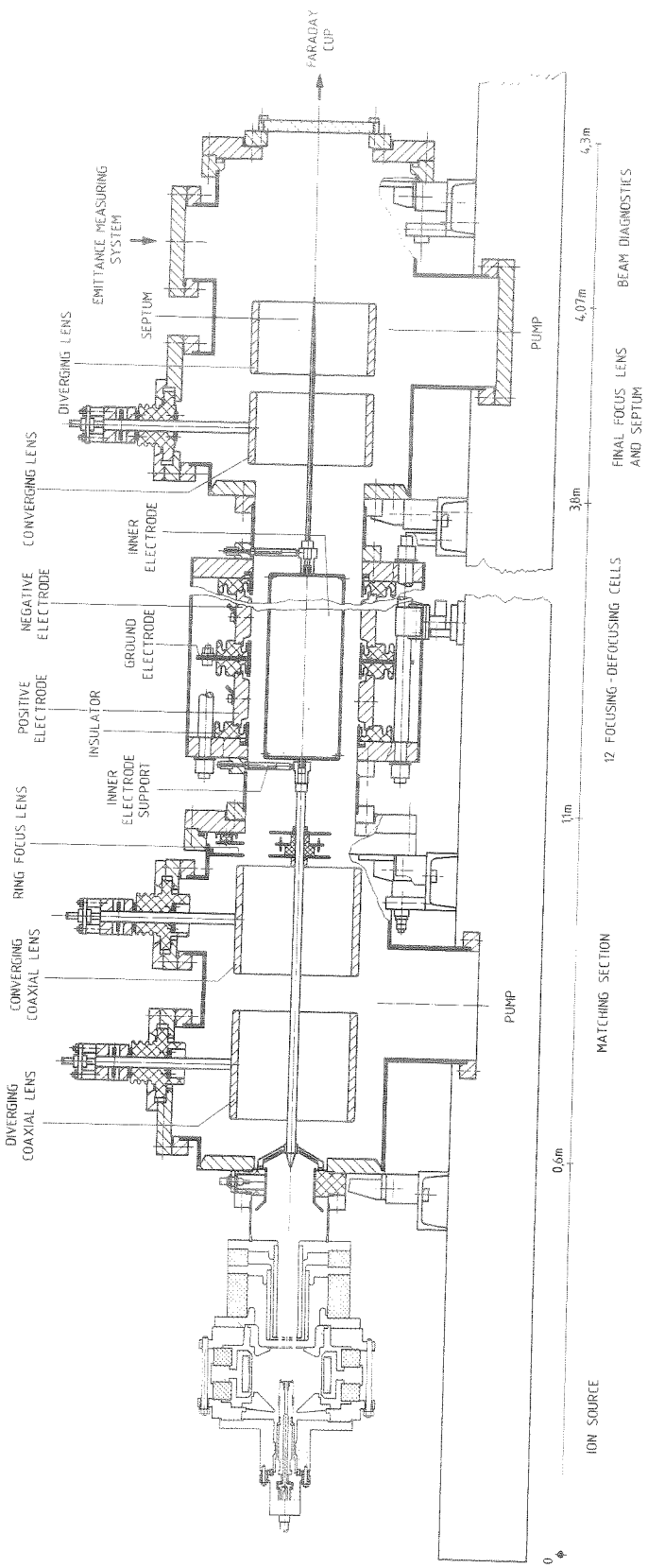
P. Krejcik
GSI Darmstadt

A beam transport line for hollow beams, proposed in last year's annual report[1], has now been constructed. The facility has been designed to test the theory that strong-focusing, electrostatic-coaxial, hollow-beam channels can transport more current than normal, axial transport systems. Operating experience with this new system is described in an accompanying article in this report[2].

The transport channel, shown adjacently, consists of 12 focusing-defocusing periods. The channel has a common inner electrode at ground potential and the outer lens cylinders are formed by dividing the vacuum pipe into short insulated segments, thus avoiding the need for HV leadthroughs. A prototype cell was first built to test this construction principle, and several insulator materials were tested for HV and vacuum properties before the final version was built. The final transport column of 12 cells sandwiched together by long bolts proved to be mechanically stable and easily aligned to within the desired tolerances. To minimise any disturbance to the beam, the inner electrode is suspended at each end from molybdenum, knife-edge supports. The system is turbo-molecularly pumped at both ends through the chambers containing the initial and final focus lenses.

The experiment was conceived to use the existing GSI high current ion source CORDIS[3], which, with a newly built extraction system can provide hollow beams of 35mm diameter. A matching doublet in the first chamber expands the beam to a diameter of 125mm. This doublet, together with a ring-focus einzel lens, also matches the ion source emittance to the acceptance of the periodic channel. Operating experince has shown that some of these matching elements must now be water cooled.

Beam diagnostics can be made in the end chamber, where a final focus doublet can also bring the beam to a point focus for beam emittance measurements.



References

[1] P.Krejcik GSI 82-1,321(1982).

[2] P.Krejcik and R.Keller "Beam Forming Experiments at the Hollow-Beam Test Stand", this annual report.

[3] R.Keller, F.Nöhmayer, P.Spädtke "High-Current Ion Sources Development", this annual report.

Beam-Forming Experiments at the Hollow-Beam Test Stand B

P. Krejcik and R. Keller
GSI Darmstadt

The first hollow beam was produced late in 1982 at the hollow beam test stand[1]. The first investigations concentrated on optimising the ion source CORDIS[2] since this was the first time that a hollow beam extraction system had been tried with a high-current source. The next step was to gain experience with handling the very high beam currents this system is capable of producing, and a variety of components had to be either strengthened or better cooled before beam measurements could begin. The performance of the first lens doublet proved to be successful and the conditions for matching the beam from this section to the periodic channel have now been fully characterized. In this section beam currents of typically 50mA of Ar^+ were transported and much was also learnt of the importance of space charge decompensation processes in the beam.

Three versions of extractor systems have been tested for producing hollow beams from the CORDIS source. The first system used the already tried multi-aperture extraction geometry with 9 small holes arranged in a circle on the extraction plates to form the hollow beam. The holders for the extractor plates, however, were unable to conduct the additional heat from the higher beam currents sufficiently well away with the result that the system deformed itself. Adequate alignment of the many small extraction holes was also difficult to attain so the beam divergence was not optimum. In the second system built, circular slits were machined with great precision on a microprocessor-controlled milling machine and simultaneously a precision jig was made for aligning the sets of slits. New holders for the extraction plates were also fabricated from massive copper to improve the cooling. The precision slits produced a better defined beam than the multi-apertures, but overheating still occured when the clamp system for mounting the extractor plates expanded and lost contact with the cooled copper holders. In the final system, the extractor plates have been machined from solid molybdenum and are firmly fastened to the cooper holders with 12 screws which are also well shielded from the strong electric field region.

With the first operation of the lens doublet in the matching section it was realised that the inner electrode near the ion source must be very well centered with respect to the beam in order to avoid deflecting the beam. If the beam is deflected it can strike one of the lens elements, overheating it and further worsening the alignment. The problem only arises, though, because a small diameter beam is extracted in this test experiment. Once the beam is expanded to a large diameter by the first lens a misalignment of, for example, 1mm produces only a relatively small error.

A simple technique of allowing the beam to strike a metal foil causing it to incandesce, allowed us to check the symmetry of the focused beam and measure its diameter and width as a function of the lens voltages. Measuring this in two places allows us to calculate the matching conditions for the periodic transport section. This can be calculated for any energy by linearly extrapolating the results in fig. 1.

In the short distance between the ion source and the matching section the beam is fully space-charge neutralised, but since our focusing elements are electrostatic the maximum currents we measure are the true space charge limited currents of the channel. The abundant electrons from the compensated ion source beam have caused some problems by producing excessive electron currents in the positive lenses so we are now experimenting with clearing electrodes operating at lower potentials.

Although we have learnt some difficult lessons during the commissioning of this test stand, the results have increased our optimism for transporting higher currents with this technique.

References

[1] P.Krejcik "A High-Current Test Facility for Hollow Beams" this annual report.

[2] R.Keller, F.Nöhmayer, P.Spädtke this annual report.

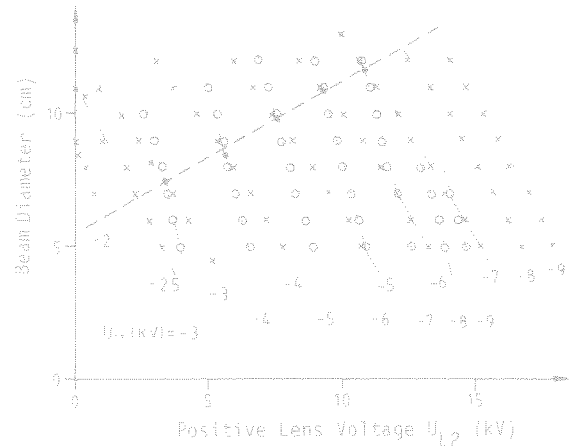


Fig. 1: Beam diameter measured at two axial locations as function of doublet voltages at a beam energy of 35 keV (x: 82.5cm from source; o: 116 cm from source). Conditions for a parallel beam are shown by the dashed line.

Beam Dynamics in the RF Coaxial Accelerator

B

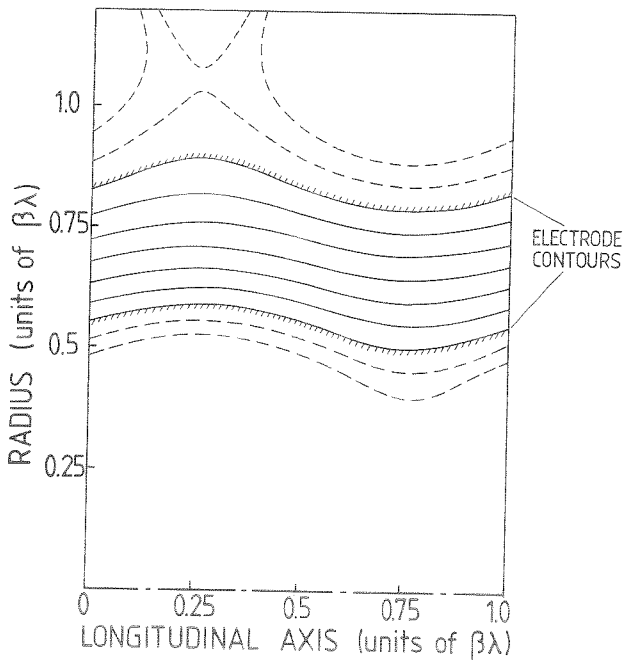
P. Krejcik
GSI Darmstadt

The rf coaxial accelerator for hollow beams, described in last year's annual report[1], has ben further studied as an injector accelerator for high-current beams[2]. The rf coaxial principle uses modulated coaxial cylinders to form a continuous focusing structure that accelerates a beam of annular cross section. The continuous, strong focusing in the structure allows the acceleration profile to be designed for adiabatic bunching of the beam. Thus structures with a high transmission efficiency for high-current beams can be designed.

The potential distribution between the cylinders has the analytic form

$$U(z,r) = [\, EI_o(kr) + FK_o(kr) \,] \sin(kz) + C \ln r + D$$

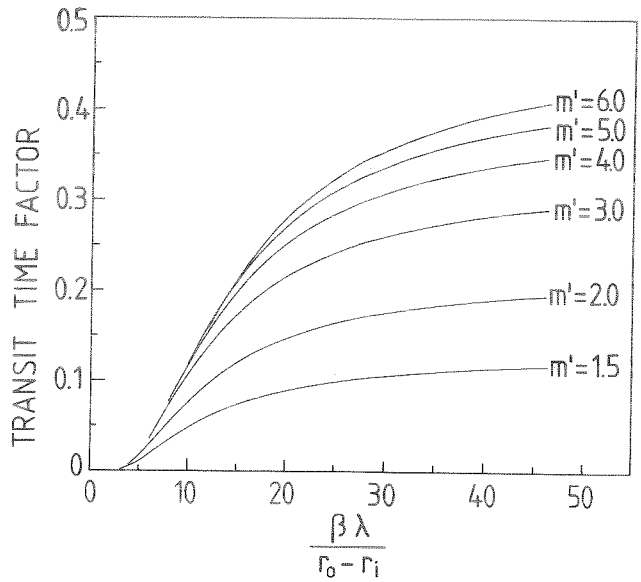
The potential distribution in one $\beta\lambda$ cell is shown in the cross sectional view below.



The acceleration efficiency of the structure can be directly deduced from the potential function, and is given by the transit time factor

$$T = \frac{\pi}{4} [\, EI_o(kr) + FK_o(kr) \,]$$

which is a function of the amplitude, m', of the modulations on the coaxial electrodes. The increase in acceleration efficiency with m' is shown in the following figure:



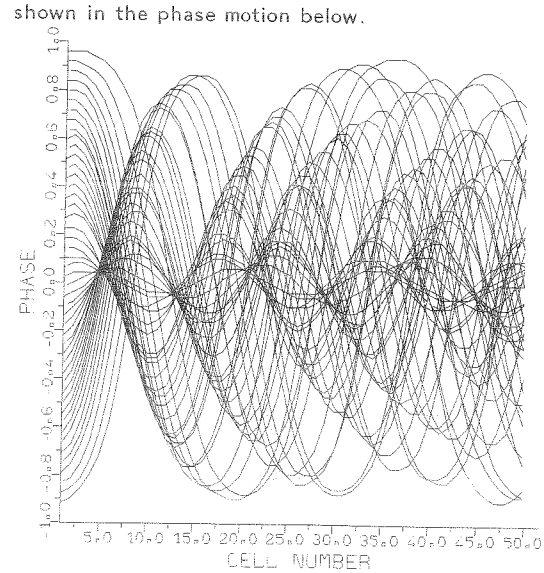
The expression for the transit time factor leads to a formulation for the longitudinal focusing frequency

$$\sigma_{oz} = \left(\frac{2\pi q TV \sin\phi_s}{m_o c^2 \beta^2 \gamma}\right)^{\frac{1}{2}}$$

The transverse focusing frequency can also be deduced from the potential distribution to be

$$\sigma_{oo} = \frac{qV\lambda^2}{2\pi\sqrt{2}\, m_o c^2 R^2 \ln mr_o/r_i}$$

These two focusing frequencies characterize the stable operating space of the structure and can be used to predict the space-charge limited current in each cell. In a hypothetical "worst case" structure where the synchronous phase angle is held constant at -90°, the particle remains stable over a wide range of phase, as shown in the phase motion below.



References

[1] P. Krejcik GSI-82-1, (1982) 322.

[2] P. Krejcik GSI-82-8, (1982) 255-274.

Experimental Electron Loss Cross Sections for Lowly Charged Ne-Ions in H_2 and N_2 at 1.4 MeV/u.

B. Franzke
GSI Darmstadt

The use of powerful heavy ion beams as igniters for inertial confinement fusion pellets has come under world-wide discussion. Severe space charge effects on high current ion beam acceleration and transport require ionic charge states as low as possible. In the Hiball[1]-concept, for instance, a beam of 160 mA Bi^{2+}-ions is accelerated to about 50 MeV/u, and then compressed transversely as well as longitudinally in intermediate storage rings and extended beam transport systems. The beam losses in this compression system are determined by charge changing interactions between fast ions and residual gas molecules on the one side, and between ions in the beam on the other side.

The experiment reported here is concerned with the first type of charge changing processes, by which the vacuum requirements for the beam compression system will be governed. For the initial charge states being of interest in this context ($1 \leq q_i \leq 4$) the maximally available at the UNILAC with respect to mass number and specific energy are Ne-ions at 1.4 MeV/u. H_2 and N_2 were used as targets because these gases are the predominant fractions of residual gas in ultra-high vacuum. A description of the experimental set-up is given in a previous report[2].

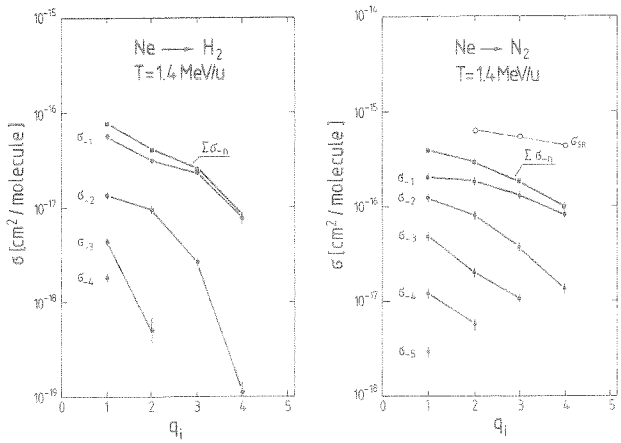


Fig. 1: Electron loss cross sections σ_{-n} for Ne-ions at 1.4 MeV/u vs. initial charge state q_i. n =1 denotes single electron loss, n > 1 multiple loss. $\Sigma\sigma_{-n}$ is the total loss cross section.
a) hydrogen target
b) nitrogen target (For explanation of σ_{sr} see text)

The results of measurements are shown in Fig. 1. Only electron loss processes were observed. The total loss cross section - the sum over all c.s. for single and multiple electron loss - for Ne^{1+} in hydrogen was found to be 7.8×10^{-17} cm²/molecule. The corresponding value for Ne^{1+} in nitrogen is higher by a factor 5. This difference is caused mainly by higher c.s. for single loss, though also a higher fraction of multiple loss is observed with N_2-target.

In Fig. 1b the experimental data for Ne in N_2 (q_i = 2,3,4) are compared with so-called 'sum-rule' cross sections, σ_{sr}, calculated by Y.-K. Kim[3] on the base of Born approximation including electron transitions into both excited and ionized states of ions[4]. It is, therefore, not unexpected that the theoretical values exceed markedly the experimental. In addition, the σ_{sr} fall less strongly with increasing q_i than the experimental stripping c.s. $\Sigma\sigma_{-n}$. This may be explained by an increased contribution of ionic excitation to the σ_{sr}. Due to the obviously large fraction of excitation the comparison of theoretical σ_{sr} with experimental $\Sigma\sigma_{-n}$ is somewhat problematic.

The dependence of stripping cross sections on both the atomic number and the velocity of ions has to be investigated by additional measurements at higher energies. At the UNILAC up to 11.5 MeV/u could be reached only for charge to mass ratios $q_i/A \geq 0.1$, i.e. for neon with $q_i \geq 2$, argon with $q_i \geq 4$ etc.. The first experimental goal will be to prove wether the stripping c.s. are proportional to β^{-2} as predicted for σ_{sr}.

Acknowledgement
The author is indebted to Dr. Y.-K. Kim for his relevant calculations and encouraging consultions during his stay at GSI.

References

[1] Hiball-Study, B. Badger et al., KfK-3202/1 (1981)
[2] B. Franzke, Ann. of Isr. Phys. Soc. 4, 111 (1981)
[3] Y.K.Kim, Argonne Nat.Lab./USA, priv.comm. (1982)
[4] G.H. Gillespie, Y.K. Kim, and K.T. Cheng, Phys. Rev. A17, 1284 (1978)

Soft X-Ray Emission in 1.4 MeV/u Pb-Noble Gas Atom Collisions

B

H. Wahl, H.F. Beyer, P.H. Mokler
GSI Darmstadt

During the slowing down process part of the energy deposited in a target is transferred into photon energies. In order to evaluate the contribution of radiation losses during beam-target interaction it is necessary to know the relevant atomic x-ray emission cross sections. The smaller photon energies carried by soft x rays is more than compensated by the steep rise[1] in the absolute value of the photon emission cross section towards low photon energies.

Here we summarize experimental results for collisions of 1.4 MeV/N Pb ions on rare gases (Ne,Ar,Kr,Xe). A collimated Pb beam with an incoming charge state of q=36 was transmitted through a low-pressure ($\lesssim 10^{-2}$ mbar), differentially pumped gas cell. Both a Si(Li) x-ray detector and a proportional counter were viewing the target region at observation angles of 90 degrees with respect to the ion-beam direction. The energy range covered by both detectors is mainly determined by the transmission of the windows. The Si(Li) detector was a closed one with a 12.5 µm thick Be-window and we used literature values for the transmission. Photons with energies beyond 0.8 keV could be detected. The proportional counter was closed with a 1 µm thick polypropylene window. Its transmission as a function of the photon energy was measured using a crystal spectrometer. Here, we restricted our measurement to photons with energies between 0.4 and 1 keV.

In Fig. 1 the measured photon emission cross sections are given as a function of the atomic number Z_2 of the target gas. With the Si(Li) detector target and projectile radiation could be separated (for matching cases a factor of 1/2 was applied, see data points in brackets). The data points taken by the proportional counter comprises both the radiation from the target and the projectile. For a comparison solid-target data for the Pb-M radiation[1] are shown in the figure. For heavy target atoms the Pb-M radiation from gaseous targets seems to overwhelm that one from solid targets for the projectile charge state used. (It should be mentioned that for a variation of the projectile charges states drastic variations in x-ray emission have been observed)[2].

In Fig. 2 the "photon-energy-flux" cross sections (cm² keV) are plotted as function of the photon energy. Most of the radiation energy is emitted in the soft x-ray region; beyond 1 keV the energy flux decreases rapidly. A comparison of the soft x-ray flux cross sections with stopping cross sections[3] yields that roughly 2 % of the deposited energy are lost by soft x-ray radiation, see Table.

Cross Sections (10^{-16} keV cm²)	Ne	Ar	Kr	Xe
Stopping 1.0 MeV/N	27	46	62	88
Soft x-rays 1.4 MeV/N	0.5	0.8	1.2	1.5

[1] GSI-Report 82-6, p. ..
[2] W.A. Schönfeldt, GSI Report 81-7
[3] H. Geissel, GSI Report 82-12

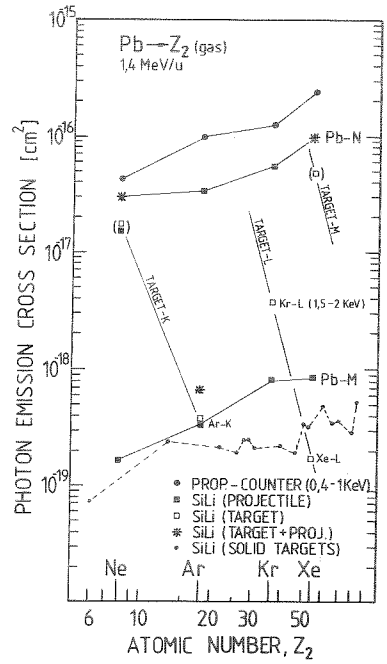


Fig. 1

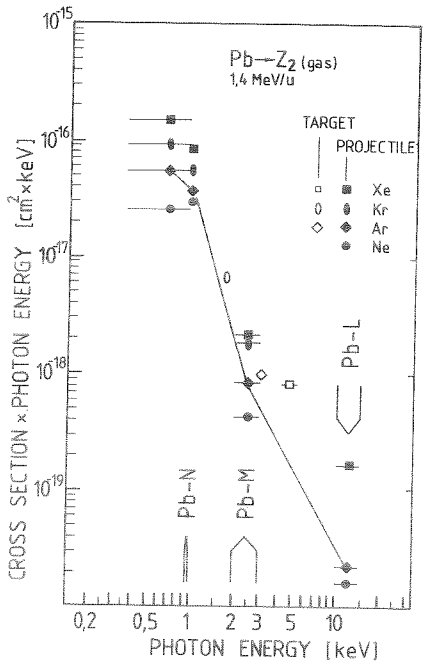


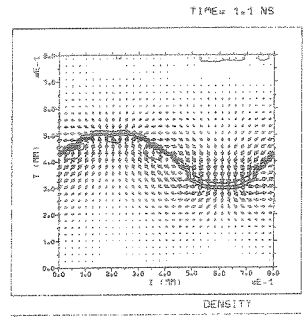
Fig. 2

B

Studies of Rayleigh-Taylor Instabilities - I. Perturbed surfaces

G. Buchwald, G. Graebner, J.A. Maruhn, and W. Greiner
Institut für Theoretische Physik der Universität Frankfurt
J. Theis
GSI Darmstadt
H. Kruse
Nat. Supercond. Cycl. Lab., East Lansing, Michigan, USA

One important problem with inertial confinement fusion (ICF) targets is the sensitivity of the pellet to distortions in accelerated boundary layers. Especially when accelerating the dense PbLi-pusher by the heated outher layer, irregularities in the geometry of the contact zone may lead to Rayleigh-Taylor instabilities. In a two-dimensional compressible fluid dynamical model we can simulate these Rayleigh-Taylor instabilities (RTI). As a first approach we consider a fluid with density ϱ_1 above another with density $\varrho_2 = \frac{1}{4}\varrho_1$ subject to a uniform acceleration. This configuration is stabilized hydrostatically by introducing a temperature distribution such that pressure is constant throughout. The interface between the two fluids is perturbed sinusoidally . Fig. 1 shows the situation after 0,6 ns, when the system just starts to move. The arrows indicating the velocity flow show vortices around the nodes of the perturbation. The contour lines separate the upper (ϱ_1) and lower (ϱ_2) density regions. In figs. 2 and 3 the growth of the instability within the next ns can be seen. The downward distortion grows much more strongly than the upward one because of the nonlinear growth and the excitation of higher order modes.



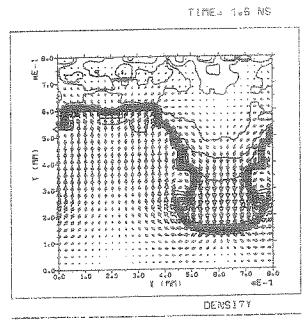
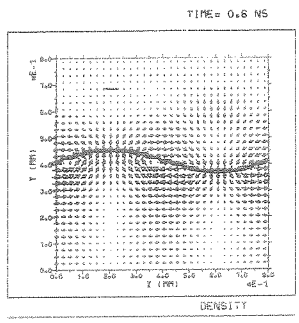


Fig. 1-3: Time sequence of the growth of a Rayleigh-Taylor instability at a density interface. Arrows indicate the flow velocity, density is represented by contour lines.



Studies of Rayleigh-Taylor Instabilities - II. Growth Rates [B]

G. Buchwald, G. Graebner, J.A. Maruhn, and W. Greiner
Institut für Theoretische Physik der Universität Frankfurt
J. Theis
GSI Darmstadt
H. Kruse
Nat. Supercond. Cycl. Lab., East Lansing, Michigan, USA

The growth rate of Rayleigh Taylor instabilities (RTI) is sensitive to the wave length of the initial disturbance. Fig. 1-3 show the time sequence of a developing RTI for the system presented in I but with two sinusoidal disturbances in the calculational grid (N=2 mode). The initial phase of the growth in II particular is somewhat faster than in I. The growth of the RTI-peaks is plotted in fig. 4. In both cases considered, the peak initially grows exponentially in time, but after 1,2 - 1,4 ns the growth rate is definitely slower than exponential. The N=2 mode grows faster than the fundamental (N=1) mode.
Looking at this quantitatively the initial growth rates n estimated from fig. 4 are n_1= .96 ns^{-1} and n_2=1,34 ns^{-1}. These differ by a factor of $\sqrt{2}$ as expected from linear Rayleigh Taylor theory[1].

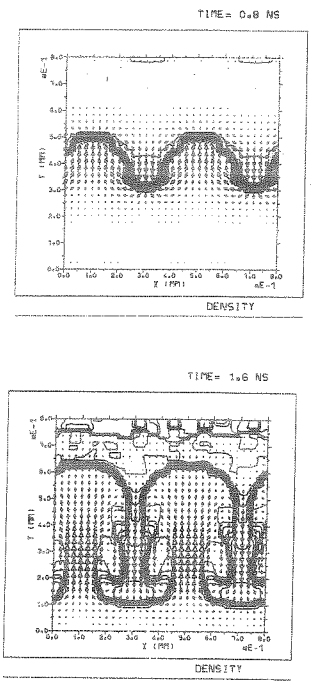
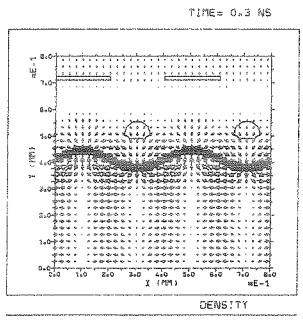


Fig. 1-3: Time sequence of the growth of a RTI between two different densities ϱ_1 and ϱ_2. The interface is perturbed by two wavelengths of a sinusoidal wave



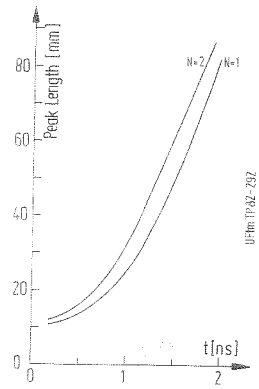


Fig. 4: The time development of the RTI-peak length. High frequency disturtions grow faster than low frequency ones.

[1] Lord Rayleigh, Theory of Sound (Dover Publ., Inc. New York 1894), 2nd ed., Vol. 2
G.B. Taylor, Proc.Roy.Soc. (London) A201, 192 (1950)

Studies of Rayleigh-Taylor Instabilities - III. Pertubed Foils [B]

G. Buchwald, G. Graebner, J.A. Maruhn, and W. Greiner
Institut für Theoretische Physik der Universität Frankfurt
J. Theis
GSI Darmstadt
H. Kruse
Nat. Supercond. Cycl. Lab., East Lansing, Michigan, USA

Recent calculations have started to simulate the RTI for the special case of an ICF target. A small sector of the pusher layer in a pellet can be idealized as a planar foil. Small disturbences in this foil may lead to RTI's. In figs. 1-3 a distorted foil with density ϱ_1 is accelerated against a density ϱ_2 only 1/4 as large . Fig. 2 shows that after 1.09 ns the classical form of the RTI is evident in the lower interface. The upper surface of the foil, on the other hand, is disturbed very little because a lighter material is pushing on denser matter.
The growth of the instability leads to an induced deformation of the upper interface which is clearly visible in fig. 3. This ultimately leads to a perforation and destruction of the foil. The mushroom shaped spike is characteristic of the later statge of an RTI and may sepperate as a drop of denser material.
Thus it seems necessary to do further detailed studies in order to determine the consequences for a realistic pellet geometry.

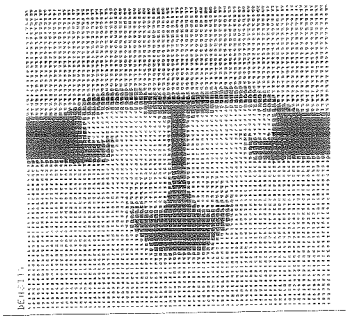
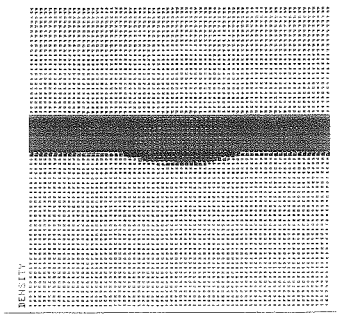
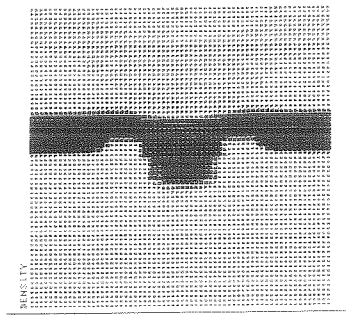


Fig. 1-3:
The time development of a distorted foil pushed against a fluid with 1/4 its density. The degree of shading is proportional to the density of the material.





Quantification of the Pellet Irradiation Asymmetry [BG]

J.A. Maruhn, J. Theis, G. Buchwald, G. Graebner, and W. Greiner
Institut für Theoretische Physik der Universität Frankfurt

Recently presented numerical calculations on the geometrical stability of ICF Targets[1] had the short coming of being 2-dimensional with cylindrical symmetry. To gain some understanding of the differences to the real spherical pellet, we have performed[2] a simple analysis of the magnitude of asymmetry present in the irradiation geometry. For this purpose we assume beams with an arbitrary profile f(s), giving the intensity of the beam at a distance s from its axis (which is assumed to be aligned with the center of the pellet). The deposition is still taken to be uniform, but we shall make the additional assumption of small penetration depth. We assume that the irradiation still is of cylindrical symmetry (the HIBALL design, e.g., has twenty beams distributed at the same polar angle).

The strength of irradiation at a point is $D(\theta)=f(r\sqrt{1-\varepsilon^2})$ with $\varepsilon = \vec{e}_\theta \cdot \vec{e}_b \sin(\theta_b)\cos(\phi) + \sin(\theta)\sin(\theta_b)$ and the penetration depth to first order $\Lambda(\theta)=\max|\lambda\varepsilon,\sigma|$

The total deposition on the radius $(\theta,\phi=0)$ will be $D(\theta)\sim\lambda\int\varepsilon f(r\sqrt{1-\varepsilon^2})d\phi$ where the integration extends over all beams that contribute on the radius. The limiting angle ϕ_0 is determined from the condition that ε, and thus the penetration depth, become zero.

The results of the calculations are shown for different Gaussian-profile beams in figs. 2,3. The cylindrical group of beams at θ_b, $0\le\phi\le180^0$ is supplemented by the lower beams at $-\theta_b$, $0\le\phi\le180^0$. The effect of beam width is quite apparent: for broad beams the asymmetry in irradiation arises mostly from the overlap of beams, while too narrow beams lead to a quite strongly peaked distribution. To define a single quantity characterizing the symmetry of the irradiation is more difficult. The standard mean value definition on the surface of the sphere $D(\theta) = \int D(\theta)d\Omega$ may underestimate the effects, since complete symmetry is assumed in the ϕ-coordinate and this method of averaging weighs all solid angle elements evenly. The alternative formula $D(\theta) = \int D(\theta)d\theta$ ("constant weight") is really appropriate for cylindrical symmetry, but may overemphasize the poles in the average. To give a fair estimate we present results for both methods of averaging in fig. 4. The plotted quantity is Λ, the average relative deviation from symmetry. Apparently both formulas give nearly the same result for the optimum angle of irradiation. Closer investigation of this vicinity leads to optimum values of beam width $\sigma\sim1.3$ and beam angle $\theta_b\sim57^0$ corresponding to 33^0 above the equatorial plane.

[1] GSI Scientific report 1981
[2] G. Buchwald, H. Kruse, J. Theis, J.A. Maruhn, submitted to Nuclear Fusion

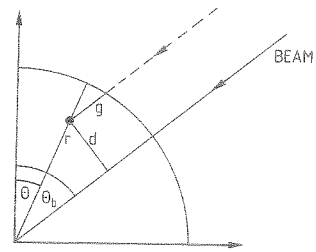


Fig. 1

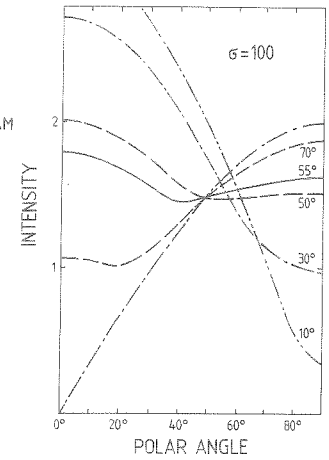


Fig. 3

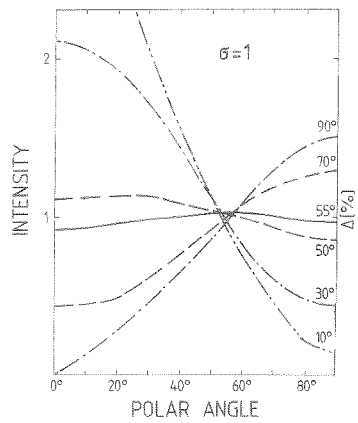


Fig. 2

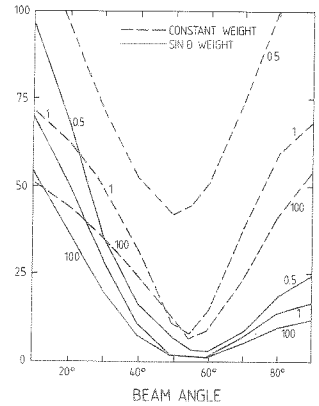


Fig. 4

7. Annex

		PAGE
7.1	Scientific Activities outside GSI	
7.1.1	Publications	306
7.1.2	Conference Contributions	318
7.1.3	Seminars at other Institutes	334
7.1.4	Lectures and Courses	344
7.2	Scientific Activities within GSI	
7.2.1	Conferences and Seminars on Research Proposals	345
7.2.2	Seminars at GSI	346
7.2.3	GSI-Preprints 1982	349
7.2.4	GSI-Reports 1982	351
7.2.5	Visiting Groups at GSI	352
7.3	Scientific Committees, Directorate and Personnel	353
7.4	Scientific Cooperation	356
7.5	Author Index	360

7.1.1 Publications

Albrecht, D., Armbruster, P., Roth, M., Spohr, R.
Small Angle Neutron Scattering Observations from Oriented Latent Nuclear Tracks
Supplement No. 3 to the Journal Nuclear Tracks, p. 55 (1982)

Albrecht, D., Armbruster, P., Roth, M., Spohr, R.
Small Angle Neutron Scattering Observations from Oriented Latent Nuclear Tracks
Radiation Effects, Vol. 65, p. 145 (1982)

Amundsen, P.A., Jakubaßa-Amundsen, D.H.
Charge Transfer at Large Scattering Angles in Asymmetric Ion-Atom Collisions
Physica Scripta 26, 155 (1982)

Angert, N., Bialkowska, H., Bock, R., Gutbrod, H.H., Harris, J.W., Maier, M.R., Poskanzer, A.M., Pühlhofer, F., Pugh, H.G., Renfordt, R.E., Ritter, H.G., Sandoval, A., Schroeder, L.S., Skrypczak, E., Stock, R., Ströbele, H., Szwed, R., Warwick, A., Weik, F., Wieman, H., Wolf, K.L.
Quark Matter Formation and Heavy Ion Collisions, Study of Relativistic Nucleus-Nucleus Reactions Induced by ^{16}O Beams of 9-13 GeV per Nucleon at the CERN PS
World Scientific Publishers, p. 557 (1982)

Arnold, E., Kühl, T., Otten, E.-W., von Reisky, L.
Collinear Laser Spectroscopy of the Balmer-α-Line
Phys. Lett. A90, 399 (1982)

Ayik, S., Nörenberg, W.
Time-Dependent Shell-model Theory of Dissipative Heavy Ion Collisions
Z. Phys. A309, 121 (1982)

Baden, A., Gutbrod, H.H., Löhner, H., Maier, M.R., Poskanzer, A.M., Renner, T., Riedesel, H., Ritter, H.G., Spieler, H., Warwick, A.I., Weik, F., Wieman, H.
The Plastic Ball Spectrometer: an Electronic 4π Detector with Particle Identification
Nucl. Instr. Methods 203, 189 (1982)

Benton, E.V., Gruhn, T., Tran, M., Spohr, R.
Effect of Oxygen on Track Etching in CR-39
Supplement No. 3 to the Journal Nuclear Tracks, p. 155 (1982)

Berdichevsky, D., Mosel U.
Detailed Study of Nuclear Charge and Mass Densities (I): Surface and Asymptotic Properties
Nucl. Phys. A388, 205 (1982)

Berry, S.D., Sellin, I.A., Andersen, L.H., Breining, M., Elston, S.B., Groeneveld, K.O., Hofmann, D.
Shape and Yield of Electron Capture to the Continuum (ECC) Spectra for 15.4 a.u. and 16.6 a.u. Bare Oxygen Nuclei Transversing Helium Gas
Proceedings, VIIIth International Conference on Atomic Physics 1982, p. B51

Beyer, H.F., Mann, R., Folkmann, F., Mokler, P.H.
Röntgen- und Augerübergänge in hochionisierten Argonrückstoßionen
Arbeitsbericht "Energiereiche Atomare Stöße", B. Fricke et al. eds., GH Kassel 1982, S. 23

Beyer, H.F., Mann, R., Folkmann, F., Mokler, P.H.
Röntgen- und Augerübergänge in Hochionisierten Argonrückstoßionen
J. Phys. B15, 3853 (1982)

Beyer, H.F., Mann, R., Folkmann, F.
Electron Capture by Slow Ne^{8+} Recoil Ions
J. Phys. B15, 1083 (1982)

Beyer, H.F., Mann, R., Folkmann, F.
X-Rays and Auger Electrons from Few-Electron Recoil Ions
American Institute of Physics, B. Crasemann ed., New York 1982, p. 253

Beyer, H.F., Folkmann, F., Mann, R.
Spectroscopy of Few Electron Slow Recoil Ions
Nucl. Instr. Methods 202, 177 (1982)

Birkelund, J.R., Freiesleben, H., Huizenga, J.R., Schröder, W.U., Wilcke, W.W., Wolf, K.L., Unik, J.P., Viola, V.E., Jr.
Mechanisms of Heavy Ion Dissipative Collisions: the $^{209}Bi + ^{84}Kr$ Reaction at E_{lab} = 712 MeV
Phys. Rev. C26, 1984 (1982)

Blin, A., Bohrmann, S., Knoll, J.
Energetic Particles Emitted from Energetic Nuclear Reactions
Z. Phys. A306, 177 (1982)

Bock, R., Chu, Y.T., Dakowski, M., Gobbi, A., Grosse, E., Olmi, A., Sann, H., Schwalm, D., Lynen, U., Müller, W., Bjornholm, S., Esbensen, H., Wölfli, W., Morenzoni, E.
Dynamics of the Fusion Process
Nucl. Phys. A388, 334 (1982)

Bock, R.
The German HIF Program
Proceedings, Symposium on Accelerator Aspects of Heavy Ion Fusion, GSI Darmstadt 1982, p. 50

Brosa, U., Cassing, W.
Numerical Studies on the Phase-Space Evolution of Relative Motion of Two Heavy Ions
Z. Phys. A307, 167 (1982)

Brown, B., Devenski, P., Gronemeyer, S., Haggerty, H., Malamud, E., Rapp, P., Abrams, R., Goldberg, H., Halliwell, C., Lopez, F., Margulies, S., Ströbele, H., Ahn, S., Watt, T.
Production of High-Transverse-Energy Events in p-p Collisions
Phys. Rev. Lett. 49, 711 (1982)

Brüchle, W., Herrmann, G.
Decay Properties of Neutron-Rich Silver Isotopes
Radiochim. Acta 30, 1 (1982)

Buchwald, G., Graebner,G., Subramanian, P.R., Csernai, J., Theis, J., Maruhn, J.A., Greiner, W., Stöcker, H.
Cluster Production in Relativistic Heavy Ion Reactions
Proceedings, XX. International Winter Meeting on Nuclear Physics 1982, I. Iori ed., p. 734

Buchwald, G., Kruse, H., Theis, J., Maruhn, J.A., Stöcker, H.
Importance of the Beam Geometry for the Dynamical Stability of Inertial Confinement Fusion Targets
Proceedings, Symposium on Accelerator Aspects of Heavy Ion Fusion, GSI Darmstadt 1982, p. 585

v. Busch, F., Hormes, J., Liesen, D.
A Study of Low Energy Differential Ion-Atom Scattering: I Experiment: Li^+ + Ne
J. Phys. B15, 3695 (1982)

Cassing, W., Stingl, M., Weiguny, A.
Scattering with Absorptive Interaction I
Phys. Rev. C26, 22 (1982)

Cassing, W.,
Quantal Phenomena in Deep Inelastic Heavy Ion Collisions; Heavy Ions and Nuclear Structure
Proceedings, XIVth Mikolajki Summer School on Nuclear Physics, Nuclear Physics Laboratory, Warsaw University 1982, p. 76

Cassing, W., Nörenberg, W.
Diabatic Dynamical Approach to Large Amplitude Collective Nuclear Motion; Heavy Ions and Nuclear Structure
Proceedings, XIVth Mikolajki Summer School on Nuclear Physics, Nuclear Physics Laboratory, Warsaw University 1982, p. 57

Chao, W.Q., Pirner, H.J.
A Model for Multiplicity Distributions in Hadron-Nucleon- and α-α Interactions at Very High Energies
Z. Phys. C14, 165 (1982)

Chao, W.Q., Hegab, M.K., Hüfner, J.
Multiparticle Production in Hadron-Nucleus Collisions Around 100 GeV
Nucl. Phys. A395, 482 (1982)

Christensen, P.R., Hansen, Ole, Nathan, O., Videbaek, F., Freiesleben, H., Britt, H.C., van der Werf, S.Y.
Bombarding Energy Dependence of Angular Momentum Transfer in Deep Inelastic Collisions
Nucl. Phys. A390, 336 (1982)

Clerc, H.-G., Keller, J.G., Sahm, C.-C., Vermeulen, D., Schmidt, K.-H., Armbruster, P., Reisdorf, W.
The Influence of Shell Effects on the Survival Probability of Heavy Nuclei in Fusion Reactions
Lecture Notes in Physics Bd. 158: "Dynamics of Nuclear Fission and Related Collective Phenomena", P. David ed., Springer Verlag, p. 145 (1982)

Collins, M.T., Sandorf, A.M., Hoffmann, D.H.H., Salomaa, M.K.
Evidence for Giant Dipole Resonances on the Excited Prolate Band of ^{28}Si
Phys. Rev. Lett. 49, 1553 (1982)

Csernai, L.P., Greiner, W., Stöcker, H., Tanihata, I., Nagamiya, S., Knoll, J.
Macroscopic Nucleon-Nucleon Correlations Caused by the Bounce-Off Process in Energetic Collisions of Heavy Nuclei
Phys. Rev. C25, 2482 (1982)

Csernai, L.P., Lovas, I., Maruhn, J.A., Rosenhauer, A., Zimanyi, J., Greiner, W.
Three Component Fluid Dynamics for the Description of Energetic Heavy-Ion Reactions
Phys. Rev. C26, 149 (1982)

Csernai, L.P., Stöcker, H.
Comment on "Exactly Central Heavy-Ion Collisions by Nuclear Hydrodynamics"
Phys. Rev. C25, 3208 (1982)

Cugnon, J., Knoll, J., Riedel, C., Yariv, Y.
Event by Event Emission-Pattern Analysis of the Intra-Nuclear Cascade
Phys. Lett. 109B, 167 (1982)

Dahlinger, M., Vermeulen, D., Schmidt, K.-H.
Empirical Saddle-Point and Ground-State Masses as a Probe of the Droplet Model
Nucl. Phys. A376, 94 (1982)

Dakowski, M., Gobbi, A., Nörenberg, W.
Influence of Single-Particle Shell Structure on the Energy Dissipation in Heavy Ion Collisions
Nucl. Phys. A378, 189 (1982)

DeFrenne, D., Thierens, H., Proot, B., Jacobs, E., DeGelder, P., DeClercq, A., Westmeier, W.
Charge Distributions for the Photofission of ^{235}U and ^{238}U with 12-30 MeV Bremsstrahlung
Phys. Rev. C26, 1356 (1982)

Dickhoff, W.H., Fäßler, A., Müther, H.
How Strong is the Rho Exchange in the NN Interaction?
Phys. Rev. Lett. 49, 1902 (1982)

Diebel, M., Mosel, U.
g-Factors as a Sensitive Test for the Influence of Rotation on Nuclear Structure
Proceedings, International Symposium on Dynamics of Nuclear Collective Motion, Mt. Fuji, Japan, 1982, INS Tokyo, p. 249

Dohmann, H.D., Mann, R., Pfeng, E.
Lebensdauern der $^3P_2$ und $^4P^0_{5/2}$ Zustände in He- und Li-ähnlichem Titan
Arbeitsbericht "Energiereiche Atomare Stöße", B. Fricke et al. eds., GH Kassel 1982, S. 23

Dohmann, H.D., Mann, R., Pfeng, E.
Lifetime Measurements of the $^3P_2$ and $^4P^0_{5/2}$ States in He- and Li-Like Titanium and Chromium
Z. Phys. A309, 101 (1982)

Esterlund, R.A., Westmeier, W., Rajagopalan, M., Patzelt, P.
Fusion Near the Barrier in the System $^{132}Xe + ^{nat}Fe$
Lecture Notes in Physics: Dynamics of Nuclear Fission and Related Collective Phenomena, P. David, T. Mayer-Kuckuk, A. van der Woude eds., Springer Verlag Berlin-Heidelberg-New York 1982, p. 377

Fäßler, A., Rikus, L., Sartor, R.
Double-Folding Computation of the Complex Heavy Ion Potential
Nucl. Phys. A376, 263 (1982)

Fan, W., Gäggeler, H.
Thermochromatography of Carrier-Free Lead in Quartz Columns with Hydrogen and Argon as Carrier Gases
Radiochimica Acta 31, 95 (1982)

Ferber, H., Wolf, G.K.
Aqueous Corrosion of Ion Implanted Iron
Ion Implantation into Metals, V. Ashworth et al. ed., Pergamon Press, Oxford 1982, p. 1

Fiedler, G., Haag, R., Crombach, P., Breitbach, G., Gottschalk, P.A., Vater, P., Kahn, E.U., Beckmann, R., Brandt, R.
Application of SSNTDs to Heavy Ion-Reaction-Studies
Proceedings, XIth International Conference SSNTD, Pergamon Press 1982, p. 779

Fischer, B.E., Spohr, R.
Werkzeuge im Mikrokosmos - Schwerionenstrahlen ermöglichen die Abbildung und Schaffung feinster Strukturen
Umschau Nr. 17, S. 514 (1982)

Fischer, B.E., Albrecht, D., Spohr, R.
Preparation of Superinsulating Surfaces by the Nuclear Track Technique
Radiation Effects, Vol. 65, p. 143 (1982)

Fowler, G.N., Raha, S., Stelte, N., Weiner, R.M.
Solitons in Nucleus-Nucleus Collision Near the Speed of Sound
Phys. Lett. 115B, 286 (1982)

Fowler, G.N., Friedländer, E.M., Weiner, R.M.
Centauros as a Superfluorescence Phenomenon
Phys. Lett. 116B, 203 (1982)

Frischkorn, H.J., Groeneveld, K.O., Koschar, P., Latz, R., Schader, J.
Observation of Heavy-Ion-Induced Wake-Potential Interference Effects
Phys. Rev. Lett. 49, 1671 (1982)

Frischkorn, H.J., Koschar, P., Latz, R., Pfennig, J., Schader, J. Szabo, G., Groeneveld, K.O.,
Auger Electron Spectrometry of Beam-Foil Excited Molecular Heavy Ions
Nucl. Instr. Methods 194, 311 (1982)

Frischkorn, H.J., Groeneveld, K.O.
Heavy Ion Induced Electron Emission from Solid Surfaces
Proceedings, IVth International Conference on Inelastic Ion-Surfaces Collision 1982, p. 13

Gäggeler, H. Brüchle, W., Kratz, J.V., Schädel, M., Sümmerer, K., Wirth, G., Sikkeland, T.
Production of Cold ^{246}Fm Compound Nuclei by Different Entrance Channels
Proceedings, Xth International Workshop on Gross Properties of Nuclei and Nuclear Excitations 1982, p.40

Geissel, H., Laichter, Y., Schneider, W.F.W., Armbruster, P.
Stopping Powers and Ranges of (0.1-2.4) GeV Uranium Ions in Solids
Proceedings, Symposium on Accelerator Aspects of Heavy Ion Fusion, GSI Darmstadt 1982, p. 578

Glässel, P., v. Harrach, D., Grodzins, L., Specht, H.J.
Direct Observation of Nonequilibrium Effects in Sequential Fission
Phys. Rev. Lett. 48, 1089 (1982)

Greenberg, J.S., Greiner, W.
Search for the Sparking of the Vacuum
Physics Today, Vol. 35, No. 8, p. 24 (1982)

Groeneveld, K.O.
Coulomb Explosion of High-Energy (MeV) Molecular Heavy Ions
High Energy Ion Atom Collision, Nuclear Methods Monograph Series 2, D. Berenyi, G. Hock eds., Elsevier Scient. Publ. Comp., Amsterdam 1982, p. 157

Groh, W., Schlachter, A., Müller, A., Salzborn, E.
Transfer Ionization in Slow Collisions of He^{2+} Ions in Rare Gases
J. Phys. B15, L207 (1982)

Grosse, E.
Shapes and Moments of Nuclei at High Angular Momentum
Proceedings, International Symposium on Dynamics of Nuclear Collective Motion, Mt. Fuji, Japan, 1982, p.134

Grosse, E.
Shapes and Moments of Nuclei at High Angular Momentum
Proceedings, XXth International Winter Meeting on Nuclear Physics, Bormio, Italy 1982, p. 773

Grün, N., Mühlhans, A., Scheid, W.
Numerical Treatment of the Time-Dependent Schrödinger Equation in Rotating Coordinates
J. Phys. B15, 4043 (1982)

Güttner, F., Koenig, W., Martin, B., Povh, B., Skapa, H., Soltani, J., Bosch, F., Kozhuharov, C.
Study of High Energetic Electrons Emitted during Heavy Ion Collisions
Z. Phys. A304, 207 (1982)

Gutbrod, H.H., Warwick, A.I., Wieman, H.
Nuclear Disintegration in Relativistic Heavy Ion Collisions
Nucl. Phys. A387, 177c (1982)

Häusser, O., Gräf, H., Grodzins, L., Jaeschke, E., Metag, V., Habs, D., Pelte, D., Emling, H., Grosse, E., Kulessa, R., Schwalm, D., Simon, R.S., Keinonen, J.
The g-Factors of High-Spin Yrast States in ^{232}Th and ^{238}U
Phys.Rev.Lett. 48, 383 (1982)

Hagedorn, R., Rafelski, J.
Analytic Structure and Explicit Solution of an Important Implicit Equation
Commun. Math. Phys. 83, 563 (1982)

v. Harrach, D., Glässel, P., Grodzins, L., Kapoor, S.S., Specht, H.J.
Direct Observation of Proximity Effects in Ternary Heavy Ion Reactions
Phys. Rev. Lett. 48, 1093 (1982)

Hartung, H., Fricke, B., Lenz, H., Sepp, W.-D.
Influence of the Electronic Shell Structure on the Elastic Scattering of Heavy Ions
Phys. Lett. 91A, 160 (1982)

Hegab, M.K., Hüfner, J.
The Distribution of Grey Particles in Very High-Energy Hadron-Nucleus Collisions
Nucl. Phys. A384, 353 (1982)

Herrmann, G.
Gibt es superschwere Atomkerne? Ein Kapitel moderner Alchemie.
Universität im Rathaus, Universität Mainz 1982, Bd. 1, S. 118

Herrmann, G.
Nuclear Part, in Actinides in Perspective
Proceedings, Actinides Conference '81, Pacific Grove, N. Edelstein ed., Pergamon Oxford 1982, p. 581

Herrmann, G., Trautmann, N.
Rapid Chemical Methods for Identification and Study of Short-Lived Nuclides
Ann. Rev. Nucl. Part. Sci. 32, 117 (1982)

Hess, P.O., Moshinsky, M., Greiner, E., Schmidt, G.
Relativistic Collective Variables for Many-Body Systems
J. Phys. G8, L179 (1982)

Hingmann, R., Clerc, H.-G., Sahm, C.-C., Vermeulen, D., Schmidt, K.-H., Keller, J.G.
Alpha Decay Properties of ^{199}Rn and ^{199}Rn^{m}
Z. Phys. A309, 27 (1982)

Hofmann, J., Greiner, W.
Hochenergiephysik mit Schweren Ionen
Physik in unserer Zeit, S. 111 (Juli 1982)

Hofmann, S., Reisdorf, W., Münzenberg, G., Heßberger, F.P., Schneider, J.R.H., Armbruster, P.
Proton Radioactivity of ^{151}Lu
Z. Phys. A305, 111-123 (1982)

Jakubaßa-Amundsen, D.H.
Angular Distribution of δ-Electrons Emitted in Slow, Asymmetric Heavy Ion Collisions
Physica Scripta 26, 319 (1982)

Johnston, M.G., Grant, I.S., Misaelides, P., Nolan, P.J., Peuser, P., Kirchner, R., Klepper, O., Roeckl, E., Tidemand-Petersson, P.
The Decay Scheme of ^{109}Sb
J. Phys. G8, 1405 (1982)

Jungclas, H., Danigel, H., Schmidt, L.
Quantitative ^{252}Cf Plasma Desorption Mass Spectrometry for Pharmaceuticals; A New Approach to Coupling Liquid Cromatography with Mass Spectrometry
Org. Mass Spectrom. 17, 86 (1982)

Jungclas, H., Danigel, H., Schmidt, L., Dellbrügge, J.
Combined Liquid Chromatography Time-of-Flight Mass Spectrometry; an Application of ^{252}Cf Fission Fragment Induced Desorption Mass Spectrometry
Org. Mass Spectrom. 17, 499 (1982)

Kaufman, S.B., Freedman, M.S., Henderson, D.J., Steinberg, E.P., Wilkins, B.D., Baden, A., Gutbrod, H.H., Maier, M.R., Peter, J., Ritter, H.G., Stelzer, H., Warwick, A.I., Wieman, H., Weik, F.
Momentum Transfer to the Target in Peripheral Collisions of Relativistic Heavy Ions
Phys. Rev. C26, 2694 (1982)

Keinonen, J., Lieb, K.P., Hellmeister, H.P., Bokisch, A., Emling, H.
Coulomb Excitation and Lifetime Measurements of the 2_1^+ States in $^{76/82/84}$Kr
Nucl.Phys. A376, 246 (1982)

Khan, H.A., Spohr, R.
Scanning Electron Microscopic Studies of Etched Track Profiles
Supplement No. 3 to the Journal Nuclear Tracks, p. 349 (1982)

Kiefer, J.
Biologische Wirkungen der Bestrahlung mit schweren Ionen
Naturwissenschaften 69, 260 (1982)

Kiefer, J., Rase, S., Schneider, E., Straaten, H., Kraft, G., Liesem, H.
Heavy Ion Effects on Yeast Cells: Induction of Canavanine Resistant Mutants
Int. J. Radiat. Biol. 42, 591 (1982)

Kiesewetter, H.
Neue rheologische Techniken und ihre Anwendung in Modellversuchen zur Simulation von Hypoperfusionszuständen bei pathologisch veränderten Bluten
Habilitationsschrift an der RWTH Aachen (1982)

Kirchner, R., Klepper, O., Kurcewicz, W., Roeckl, E., Zganjar, E.F., Runte, E., Schmidt-Ott, W.-D., Tidemand-Petersson, P., Kaffrell, N., Peuser, P., Rykaczewski, K.
New Neutron-Rich ^{179}Yb and $^{181/182}$Lu Isotopes Produced in Reactions of 9 MeV/u ^{136}Xe Ions on Tantalum and Tungsten Targets
Nucl. Phys. A378, 549 (1982)

Klabunde, J.
GSI-Wideröe Experiments
Proceedings, Symposium on Accelerator Aspects of Heavy Ion Fusion, GSI Darmstadt 1982, p. 116

Kleber, M.
The Variational Approach to Atomic Collisions and its Relation to Perturbation Theory
"Physics of Electronic and Atomic Collisions" S. Datz ed., p. 503, North Holland (1982)

Klein, H., Daehne, M., Deitunghoff, H., Gerhard, A., Halfmann, K.D., Junior, P., Langbein, K., Müller, R.W., Müller, J., Neumann, W., Schempp, A., Schönlein, A.
RFQ Development at Frankfurt
Proceedings, Symposium on Accelerator Aspects of Heavy Ion Fusion, GSI Darmstadt 1982, p. 150

Klepper, O., Batsch, T., Hofmann, S., Kirchner, R., Kurcewicz, W., Reisdorf, W., Roeckl, E., Schardt, D., Nyman, G.
Direct and Beta-delayed Proton Decay of very Neutron-Deficient Rare-Earth Isotopes Produced in the Reaction $^{58}Ni + ^{92}Mo$
Z. Phys. A305, 125 (1982)

Knoll, J., Münchow, L., Röpke, G., Schulz, H.
Deuteron Production - an Entropy Puzzle?
Phys. Lett. 112B, 13 (1982)

Knoll, J.
The Dynamics of Heavy Ion Reactions of Relativistic Energies
Proceedings, Workshop on Quark Matter Formation and Heavy Ion Collisions 1982, M. Jacob, H. Satz eds., World Scientific Publishing Co 1982, p. 95

Könnecke, R., Greiner, W., Scheid, W.
A Consistent Imaginary Potential Treatment in the Nuclear Molecular Channel Picture
J. Phys. G8, L11 (1982)

Könnecke, R., Guirguis, J., Greiner, W., Scheid, W.
Second-Order Transitions in $^{12}C - ^{12}C$ Scattering in an Adiabatic Coupling Model
J. Phys. G8, 535 (1982)

Kolb, D., Johnson, W.R., Shorer, Ph.
Electric and Magnetic Susceptibilities and Shielding Factors for Closed Shell Atoms and Ions of High Nuclear Charge
Phys. Rev. A26, 19 (1982)

Kozhuharov, C.
Spectroscopy of High Energy δ-Rays Emitted in Collisions of Very Heavy Ions
Physics of Electronic and Atomic Collisions, S. Datz ed., North-Holland 1982, p. 179

Kraft, G., Kraft-Weyrather, W., Meister, H., Miltenburger, H.G., Roots, R., Wulf, H.
The Influence of Radiation Quality of Biological Effectiveness of Heavy Charged Particles
Proceedings, VIIIth Symposium on Microdosymetry, European Community, Brussels 1982, p. 743

Krejcik, P.
The Hollow Beam Concept for Producing Intense Beams
Proceedings, Symposium on Accelerator Aspects of Heavy Ion Fusion, GSI Darmstadt 1982, p. 255

Kruse, H., Pinkston, W.T., Greiner, W.
A Note on Phase Transitions and Shock Waves in Nuclei
J. Phys. G8, 567 (1982)

Kurcewicz, W., Zganjar, E.F., Kirchner, R., Klepper, O., Roeckl, E., Komninos, P., Nolte, E., Schardt, D., Tidemand-Petersson, P.
Investigations of Very Neutron-Deficient Isotopes Below ^{100}Sn in ^{40}Ca-Induced Reactions
Z. Phys. A308, 21 (1982)

Kurcewicz, W., Szerypo, J., Hornshoj, P., Rud, N., Zelasny, Z., Reisdorf, W.
Fission of ^{232}Th Induced by 4-11 MeV Protons
Z. Phys. A306, 99 (1982)

Kuti, J., Polonyi, J.
Some Applications of a New Stochastic Method in Lattice Theories
Proceedings, John Hoyking Meeting of Theoretical Particle Physics, Maryland 1982, GSI-82-22

Latz, R., Schader, J., Frischkorn, H.J., Groeneveld, K.O., Hofmann, D., Koschar, P.
Strong Dwell-Time Dependence of Convoy Electrons from Atomic and Molecular Projectile Ions in Thin Carbon Foils
Z. Phys. 303, 367 (1982)

Latz, R., Schader, J., Frischkorn, H.J., Groeneveld, K.O., Hofmann, D., Koschar, P.
Strong Dwell-Time Dependence of Convoy Electrons from Atomic and Molecular Projectile Ions in Thin Foils
Z. Phys. A304, 467 (1982)

Latz, R., Astner, G., Frischkorn, H.J., Koschar, P., Pfennig, J., Schader, J., Groeneveld, K.O.
Strong Molecular Effects in Zero Degree Electron Emission from Molecular Ions after Solid Foil Interaction
Nucl. Instr. Methods 194, 315 (1982)

Liesen, D.
What Do We Know About Superheavy Quasiatoms?
Comments at. Mol. Phys. 12, 39 (1982)

Liesen, D., Armbruster, P., Bosch, F., Maor, D., Mokler, P.H., Schmidt-Böcking, H., Schuch, R.
Inner-Schalen-Anregungswahrscheinlichkeiten in Adiabatischen Xe + Au und Pb + U Stößen
Arbeitsbericht "Energiereiche Atomare Stöße", B. Fricke et al. eds., GH Kassel 1982, S. 23

Liesen, D., Zinoviev, A.N., Saris, F.W.
Oszillationen in MO Auger Elektronen Spektren in 450 keV Kr^{+4} + Kr Stößen
Arbeitsbericht "Energiereiche Atomare Stöße", B. Fricke et al. eds., GH Kassel 1982, S. 23

Lougheed, R.W., Hulet, E.K., Landingham, R.L., Nitschke, J.M., Folger, H., Kratz, J.V., Brüchle, W., Gäggeler, H.
The Preparation of Curium Metal Tagets for the Synthesis of Superheavy Elements
Nucl. Instr. Methods 200, 71 (1982)

Lukasiak, A., Cassing, W., Nörenberg, W.
Microscopic Calculation of Diabatic Single Particle Levels
Proceedings, International Workshop on Gross Properties of Nuclei and Nuclear Excitations 1982, p. 80

Lund, T., Molzahn, D., Bergersen, B., Hagebo, E., Haldorsen, I.R., Richard-Serre, C., the ISOLDE Collaboration
Yields and Recoil Properties of Products from the Reaction between Natural Copper and 86 MeV/A ^{12}C Ions
Z. Phys. A306, 43 (1982)

Lund, T., Molzahn, D., Bergersen, B., Bjornstadt, T., Hagebo, E., Haldorsen, I.R., Richard-Serre, C., the ISOLDE Collaboration
Momentum Transfer and Product Kinetic Energies in the Interaction of Silver with 86 MeV/A ^{12}C.
Phys. Lett. 116B, 325 (1982)

Lynen, U., Ho, H., Kühn, W., Pelte, D., Winkler, U., Müller, W.F.J., Chu, Y.T., Doll, P., Gobbi, A., Hildenbrand, K.D., Olmi, A., Sann, H., Stelzer, H., Bock, R., Löhner, H., Glasow, R., Santo, R.
Reactions Between ^{12}C and Heavy Target Nuclei at 84 MeV/u
Nucl. Phys. A387, 129c (1982)

Mann, M., Mokler, P., Fricke, B., Sepp, W.-D., Schönfeldt, W.A., Hartung, H.
Evidence for an Additional Coupling of the Innermost Shells in Very Heavy Quasi-Molecular Ion-Atom Collisions
J. Phys. B15, 4199 (1982)

Mann, R., Beyer, H.F.
Spectroscopy of Few Electron Slow Recoil Ions
Comments At. Mol. Phys. 12, 149 (1982)

Mann, R., Beyer, H.F., Folkmann, F.
Excited States Formed By Electron Capture in Highly Charged Recoil Ions
Physics of Electronic and Atomic Collisions, North Holland Publ. Comp., p. 683 (1982)

Mann, R., Cocke, C.L., Schlachter, A.S., Prior, M., Marrus, R.
Selective Final-State Population in Electron Capture by Low-Energy Highly Charged Projectiles Studied by Energy-Gain Spectroscopy
Phys. Rev. Lett. 49, 1329 (1982)

Maor, D., Mokler, P.H., Schüll, D., Stachura, Z.
Projectile Charge State Distributions in Close, Fast Heavy Ion-Atom Collisions: Dependence on Target Thickness and Inner Shell Vacancy Production
Nucl. Instr. Methods 194, 377 (1982)

Maruhn, J.A., Buchwald, G., Kruse, H., Theis, J.
Application of Flux-Corrected Transport Algorithms
Dynamical Problems in Mathematical Physics, B. Brosowski, E. Martensen eds., Peter Lang Verlag Frankfurt/Bern, 26, 31 (1982)

Merchant, A.C., Nörenberg, W.
Microscopic Transport Theory of Heavy Ion Collisions: V. Transfer of Neutrons and Protons
Z. Phys. A308, 315 (1982)

Mokler, P.H., Maor, D., Meyerhof, W.E., Schönfeld, W.A., Stachura, Z.
Atomare Stöße mit hochgeladenen, abgebremsten schweren Ionen
Arbeitsbericht "Energiereiche Atomare Stöße", B. Fricke et al. eds., GH Kassel 1982, S. 23

Morovic, T., Sepp, W.-D., Frike, B.
$2p_\pi$ - $2p_\sigma$ Crossing in Heavy Symmetric Ion-Atom Collisions I. Level Structure
Z. Phys. A304, 79 (1982)

Mosel, U., Tanimura, O., Wolf, R.
Nuclear Molecular States
Heavy Ion Collisions, G. Madurga et al. ed., Lecture Notes in Physics, Springer Verlag, Vol. 168, 328 (1982)

Müller, B., Rafelski, J.
Self-Consistent Gluon Screening of a Strong SU(2) Source
Phys. Rev. D25, 566 (1982)

Müller, B., Rafelski, J.
Role of Internal Symmetry in $p\bar{p}$-Annihilation
Phys. Lett 116B, 274 (1982)

Müller, E.M., Mühlhans, K., Neergard, K., Mosel, U.
Generalized Pair Field in Fast Rotating Nuclei
Nucl. Phys. A383, 233 (1982)

Müller, R.W.
A Remark on Coupled Motion and Equipartitioning
Proceedings, Symposium on Accelerator Aspects of Heavy Ion Fusion, GSI Darmstadt 1982, p. 241

Müller, R.W.
Use of a Heavy-Ion Synchrotron Facility for ICF Studies
Proceedings, Symposium on Accelerator Aspects of Heavy Ion Fusion, GSI Darmstadt 1982, p. 448

Müller, U., Aboul-el-Naga, N., Reinhardt, J., de Reus, T., Schlüter, P., Seiwert, M., Soff, G., Wietschorke, K.-H., Müller, B., Greiner, W.
Spectroscopy of Superheavy Quasimolecules and Quasiatoms
Proceedings, International Summer School, La Rabida, Huelva, Spain, 1982, Lecture Notes in Physics 168, 1982, "Heavy-Ion Collisions", eds. G. Madurga and M. Lozano, Springer-Verlag, Berlin 1982, p. 388

Müller, U., Reinhardt, J., de Reus, T., Schlüter, P., Soff, G., Wietschorke, K.-H., Müller, B., Greiner, W.
Theory of Positron Creation in Supercritical Quasimolecules
Proceedings, NATO Advanced Study Institutes Programme, Lahnstein/Rhein, June 1981, Plenum, New York 1982, p. 195

Münchow, M., Hahn, D., Scheid, W.
Heavy-Ion Potentials for Ellipsoidally Deformed Nuclei and Application to the System $^{238}U + ^{238}U$
Nucl. Phys. A388, 381 (1982)

Münzenberg, G., Armbruster, P., Heßberger, F.P., Hofmann, S., Poppensieker, K., Reisdorf, W., Schneider, J.H.R., Schneider, W.F.W., Schmidt, K.-H., Sahm, C.-C., Vermeulen, D.
Observation of One Correlated α-Decay in the Reaction ^{58}Fe on $^{209}Bi \rightarrow ^{267}109$
Z. Phys. A309, 89 (1982)

Münzenberg, G., Armbruster, P., Faust, W., Güttner, K., Heßberger, F.P., Hofmann, S., Reisdorf, W., Sahm, C.C., Schmidt, K.-H., Schött, H.J., Thuma, B., Vermeulen, D.
Isotope Identification in the Transfermium Region by α-α Correlation after In-Flight-Separation
ACTINIDES IN PERSPECTIVE, N.M. Edelstein ed., Pergamon Press 1982, p. 223

Münzenberg, G., Hofmann, S., Heßberger, F.P., Reisdorf, W., Schmidt, K.-H., Faust, W., Schött, H.J., Armbruster, P., Güttner, K., Thuma, B., Vermeulen, D. Sahm, C.C.,
Erzeugung und Nachweis von Kernen der Elemente Fm bis 107 aus Schwerionen-Fusionsreaktionen
Atomkernenergie-Kerntechnik 40, 1 (1982)

Mustafa, M.G., Baisden, P.A., Chandra, H.
Equilibrium Shapes and Fission Barriers of Rotating Nuclei with a Macroscopic Two-Center-Model
Phys. Rev. C25, 2524 (1982)

Mutterer, M.
Gas Scintillation Nuclear Particle Detectors
Nucl. Instr. Methods 196, 73 (1982)

Neergard, K.
The Isovector Dipole Mode in Heated Rotating Nuclei
Phys. Lett. 110B, 7 (1982)

Nickel, F.
The Influence of Temperature on Stripper Foil Lifetimes
Nucl. Instr. Methods 195, 457 (1982)

Nörenberg, W.
Statistical and Dynamical Aspects of Heavy Ion Collisions
Nucl. Phys. C.H. Dasso, R.A. Broglia, A. Winther eds., North-Holland, Amsterdam 1982, p. 543

Odenweller, T., Noll, H., Sapotta, K., Renfordt, R.E., Bass, R.
A Gridless Position Sensitive Time-Zero Detector for Heavy Ions
Nucl. Instr. Methods 198, 263 (1982)

Ower, H., Elze, Th.W., Idzko, J., Stelzer, K., Grosse, E., Emling, H., Fuchs, P., Schwalm, D., Wollersheim, H.J., Kaffrell, N., Trautmann, N.
Structure of High Spin States in ^{232}Th, ^{234}U and ^{236}U
Nucl.Phys. A388, 421 (1982)

Park, J.Y., Scheid, W., Greiner, W.
Molecular Single-Particle Excitations in Heavy-Ion Reactions Involving Deformed Light Nuclei
Phys. Rev. C25, 1902 (1982)

Pelte, D., Schwalm, D.
In-Beam γ-Ray Spectroscopy with Heavy Ions
in "Heavy Ion Collisions" (ed. R. Bock, North-Holland Publ. Comp, 1982) vol 3, p. 1

Plochocki, A., Zylicz, J., Kirchner, R., Klepper, O., Roeckl, E., Tidemand-Petersson, P., Grant, I.S., Misaelides, P.
Masses of Very Neutron-Deficient Isotopes in the Cadmium-to- Cesium Region
Nucl. Phys. A388, 91 (1982)

zu Putlitz, G., Körner, H.J.
Die Wege der Schwerionenforschung
Umschau 23, 716 (1982)

Quade, U., Rudolph, K., Armbruster, P., Clerc, H.-G., Lang, W., Mutterer, M., Pannicke, J., Schmitt, C., Theobald, J.P., Gönnewein, F., Schrader, H.
Cold Fragmentation of ^{234}U and ^{236}U
Lecture Notes in Physics 158, 40 (1982)

Rafelski, J.
Extreme States of Nuclear Matter
Nucl. Phys. A347, 489c (1982)

Rafelski, J., Müller, B.
Strangeness Production in the Quark-Gluon Plasma
Phys. Rev. Lett. 48, 1066 (1982)

Rafelski, J.
Formation and Observation of the Quark-Gluon Plasma
Phys. Rep. 88, 331 (1982)

Rashid, K., Fricke, B.
Shifts and Electronic K X-Rays in Muonic Atoms
Z. Phys. A304, 193 (1982)

de Reus, T., Müller, U., Reinhardt, J., Schlüter, P., Soff, G., Wietschorke, K.-H., Müller, B., Greiner, W., Soff, G.
Spectroscopy of Superheavy Quasimolecules

Proceedings, NATO Advanced Study Institutes Programme, Plenum, New York 1982, p. 233

Reus, U., Westmeier, W., Warnecke, I.
Gamma-Ray Catalog
IAEA-Report INDC(NDS)-130/G+P 137, (1982)

Ring, P., Hagashi, A., Hara, K., Emling, H., Grosse, E.
Electromagnetic Moments and Transition Rates from Cranking Model Wave Functions
Phys.Lett. 110B, 423 (1982)

Rinn, K., Müller, A., Eichenauer, H., Salzborn, E.
Development of Single-Particle Detectors for keV-Ions
Rev. Sci. Instr. 53, 829 (1982)

Roggenkamp, H.G., Kiesewetter, H., Schmeink, T., Hollweg, H.G.
Ein neues Verfahren zur Quantifizierung der Verformbarkeit von Erythrozyten
Biomed. Tech. 27, 162-166 (1982)

Rohozinski, S.G., Gajda, M., Greiner, W.
Towards a Unified Collective Model for the Nuclear Quadrupole and Octupole Modes
J. Phys. G8, 787 (1982)

Rosenhauer, A., Csernai, L.P., Maruhn, J.A., Greiner, W.
Momentum Distribution of Nuclear Matter in Energetic Heavy-Ion Collisions
Nuovo Cim. 71A, 215 (1982)

Ruchowska, E., Kurcewicz, W., Kaffrell, N., Bjornstad, T., Nyman, G.
The Decay Scheme of ^{228}Fr and K=0 Bands in ^{228}Ra
Nucl. Phys. A383, 1 (1982)

Rudolf, G., Adloff, J.C., Dischier, D., Rauch, V., Scheibling, F., Dakowski, M., Gobbi, A., Hildenbrand, K.D., Müller, W.F.J., Olmi, A.
Influence of Shells on the Driving Potential in Dissipative Collisions
Phys. Lett. 118B, 315 (1982)

Sahm, C.-C., Clerc, H.-G., Vermeulen, D., Schmidt, K.-H., Armbruster, P., Heßberger, F., Keller, J.G., Münzenberg, G., Reisdorf, W.
The Influence of the N = 126 Neutron Shell on the Survival Probability of Neutron Deficient Th-Isotopes
Proceedings, International Workshop on Gross Properties of Nuclei and Nuclear Excitation, H. Feldmeier ed., p. 48 (1982)

Schädel, M., Brüchle, W., Gäggeler, H., Kratz, J.V., Sümmerer, K., Wirth, G., Herrmann, G., Stakemann, R., Tittel, G., Trautmann, N., Nitschke, J.M., Hulet, E.K., Lougheed, R.W., Hahn, R.L., Fergusson, R.L.,
Actinide Production in Collisions of ^{238}U with ^{248}Cm
Phys. Rev. Lett. 48, 852 (1982)

Schaupert, K., Keiner, K., Fiedler, G., Spohr, R.
SSNTDs for High Energetic Heavy Ions
Proceedings, XIth International Conference SSNTD, Pergamon Press 1982, p. 119

Schießl, Ch., Wagner, W., Hartel, K., Kienle, P., Körner, H.J., Mayer, Waltraud, Rehm, K.E.
A Bragg-Curve-Spectroscopy-Detector
Nucl. Instr. Methods 192, 291 (1982)

Schlachter, A.S., Groh, W., Müller, A., Beyer, H.F., Mann, R., Olson, R.E.
Production of Highly Charged Rare-Gas Recoil Ions by 1.4 MeV/amu U^{44+}
Phys. Rev. A26, 1373 (1982)

Schlüter, P., Soff, G., Greiner, W.
Der Einfluß nuklearer EO-Übergänge auf das Delta-Elektronen-Spektrum im Stoß sehr schwerer Ionen
Arbeitsbericht "Energiereiche Atomare Stöße", B. Fricke et al. eds., GH Kassel 1982, S. 23

Schlüter, P., Soff, G., Müller, B., Greiner, W.
Selbstenergiekorrektur für Elektronen in sehr schweren Ionen
Arbeitsbericht "Energiereiche Atomare Stöße", B. Fricke et al. eds., GH Kassel 1982, S. 23

Schmidt, L., Danigel, H., Jungclas H.
Combined Liquid Chromatography - Mass Spectrometry for Trace Analysis of Pharmaceuticals
Nucl. Instr. Methods 198, 165 (1982)

Schöpfer, F., Schneider, E., Rase, S., Kiefer, J., Kraft, G.
Heavy Ion Effects of Yeast Cells: Survival and Recovery in Vegetative Cells of Different Sensitivity
Radiat. Res. 92, 30 (1982)

Shanker, R., Warke, C.S., Greiner, W., Müller, B.
Cylindrically Deformed Quark Bags
J. Phys. G8, L33 (1982)

Shyam, R., Nagarajan, M.A., Shotter, A.C., Bice, A.N., Cerny, J.
Inelastic Scattering of ^{12}C from ^{208}Pb to the second O^+-State of ^{12}C
Phys. Lett. 116B, 99 (1982)

Siegert, G.
Fünf Jahre Forschung mit schweren Ionen
Atomwirtschaft 1, 46 (1982)

Siegert, G.
Schwerionenforschung bei der GSI in Darmstadt
Chemie für Labor und Betrieb 1, 18 (1982)

Siegert, G.
Element 109 entdeckt
Chemie für Labor und Betrieb 12, 537 (1982)

Siegert, G.
Schwerionenforschung
Enzyklopädie Naturwissenschaft und Technik, Jahresband 1982, Verlag Moderne Industrie, p. 452

Siegert, G.
Überraschungen sind nicht auszuschließen
Umschau 17, 517 (1982)

Siekmann, H., Gebauer, B., Bohlen, H.G., Kluge, H., von Oertzen, W., Fröbrich, P., Strack, B., Hildenbrand, K.D., Sann, H., Lynen, U.
Proton Transfer in Quasi-Elastic and Deep-Inelastic Reactions in the Systems ^{86}Kr on ^{88}Sr, ^{90}Zr and ^{92}Mo at Energies Close to the Coulomb Barrier
Z. Phys. A307, 113 (1982)

Simon, R.S., DeVito, R.P., Emling, H., Kulessa, R., Briancon, Ch., Lefebvre, A.
Rotational Band Crossings in ^{232}Th
Phys.Lett. 108B, 87 (1982)

Simon, R.S., Albrecht, R., Habs, D., Helmer, K., v. Helmolt, U. Heyng, H.W., Kolb, B., Pelte, D., Schwalm, D., Metag, V., Gräf, H., Hennerici, W., Hennrich, H.J., Jaeschke, E., Repnow, R., Wahl, W.
First Result from the Darmstadt - Heidelberg Crystal Ball
Proceedings, International Symposium on Dynamics of Nuclear Collective Motion, Mt. Fuji, Japan, 1982, p. 35

Soff, G., de Reus, T., Müller, B., Greiner, W.
δ-Electron Production Rates in the Superheavy System Br + Pb
Phys. Lett. 88A, 398 (1982)

Soff, G., Schlüter, P., Müller, B., Greiner, W.
Self-Energy of Electrons in Critical Fields
Phys. Rev. Lett. 48, 1465 (1982)

Soff, G., Greiner, W.
Electronic Transition Times in Supercritical Compound Systems
J. Phys. B15, L681 (1982)

Soff, G., de Reus, T., Müller, U., Reinhardt, J., Müller, B., Greiner, W.
Delta-Elektronen-Erzeugungswahrscheinlichkeiten im superschweren Quasimolekül J + Pb
Arbeitsbericht "Energiereiche Atomare Stöße", B. Fricke et al. eds., GH Kassel 1982, S. 23

Soffel, M., Müller, B., Greiner, W.
Stability and Decay of the Dirac Vacuum in External Gauge Fields
Phys. Rep. 85, 51 (1982)

Stachel, J., Kaffrell, N., Grosse, E., Emling, H., Folger, H., Kulessa R., Schwalm, D.
Triaxiality and its Dynamics in ^{104}Ru Investigated by Multiple Coulomb Excitation
Nucl. Phys. A383, 429 (1982)

Stachura, Z., Bosch, F., Maor, D., Mokler, P.H., Schönfeldt, W.A.
L_3-Unterschalenalignment bei Schwerionenbeschuß
Arbeitsbericht "Energiereiche Atomare Stöße", B. Fricke et al. eds., GH Kassel 1982, S. 23

Stakemann, R., Herrmann, G., Heimann, R., Tittel, G., Trautmann, N.
Search for Superheavy Elements in Monazites Using Chemical Enrichment
Nature 297, 136 (1982)

Stelte, N., Weström, M., Weiner, R.M.
Drifting Hot Spots
Nucl. Phys. A384, 190 (1982)

Stock, R., Bock, R., Brockmann, R., Dacal, A., Harris, J.W., Maier, M., Ortiz, M.E., Pugh, H.G., Renfordt, R.E., Sandoval, A., Schroeder, L.S., Ströbele, H., Wolf, K.L.
"Compression Effects in Relativistic Nucleus-Nucleus Collisions"
Phys. Rev. Lett. 49, 1236 (1982)

Stock, R.
Kollisionen schwerer Kerne bei relativistischen Energien
Physikalische Blätter 38, 115 (1982)

Stöcker, H., Buchwald, G., Csernai, L.P., Graebner, G., Maruhn, J.A., Greiner, W.
Dynamics of High Energy Heavy Ion Collisions - Nuclear Matter at High Density and Temperature
Nucl. Phys. A387, 205c (1982)

Stöcker, H., Buchwald, G., Csernai, L.P., Graebner, G., Subramanian, P.R., Theis, J., Maruhn, J.A., Greiner, W.
Microscopic and Macroscopic Models for Nuclear Collisions at Medium and High Energies
Proceedings, XX. International Winter Meeting on Nuclear Physics, January 1982, Bormio, Italy, ed. I. Iori, p. 716

Stöcker, H., Csernai, L.P., Graebner, G., Buchwald, G., Kruse, H., Cusson, R.Y., Maruhn, J.A., Greiner, W.
Jets of Nuclear Matter from High Energy Heavy Ion Collisions
Phys. Rev. C25, 1873 (1982)

Tanimura, O., Mosel, U.
Comparison of Predictions for Alignment in Inelastic Scattering of ^{12}C + ^{12}C
Phys. Lett. 114B, 7 (1982)

Terlecki, G., Grün, N., Scheid, W.
Solution of the Time-Dependent Schrödinger Equation with a Trajectory Method and Application to H^+-H Scattering
Phys. Lett. 88A, 33-36 (1982)

Teubner, E., Grün, N., Scheid, W.
Application of the Relativistic Trajectory Monte Carlo Method to the K Vacancy Production with ^{12}C Projectiles at 250 MeV/u
J. Phys. B15, 1269 (1982)

Theis, J., Kruse, H., Buchwald, G., Graebner, G., Warke, C.S., Maruhn, J.A., Greiner, W., Stöcker, H.
Generalized Nuclear Fluid Dynamics
Proceedings, XX. International Winter Meeting on Nuclear Physics, January 1982, Bormio, Italy, ed. I. Iori, p. 734

Tidemand-Petersson, P., Plochocki, A.,
Resonance Structure in the Beta-Strength Function Indicated by Beta-Delayed Particle Emission from $^{110/112}$I, ^{113}Xe, $^{114/116}$Cs, and ^{117}Ba.
Phys. Lett. 118B, 278 (1982)

Trautmann, N.
Status of Superheavy Element Research
Actinides in Perspective, N.M. Edelstein ed., Pergamon Press, Oxford and New York 1982, p. 267

Tress, G., Ellinger, M., Khan, E.U., Khan, H.A., Vater, P., Brand, R., Kadner, M.
Mica Track Microfilters Applied in a Cascade Particle Fractionator at an Industrial Plant
Nucl. Tracks 6, 87 (1982)

Tress, G., Vater, P., Khan, E.U., Khan, H.A., Brand, R., Kadner, M., Spohr, R.
Applications of Mica Track Microfilters: Surveillance of Hot Contaminated Air at an Industrial Plant
Supplement No. 3 to the Journal Nuclear Tracks, p. 723 (1982)

Tripathi, R.K., Fäßler, A.
Effect of Isobars at Finite Temperature in Pion Condensation in ^{16}O
Phys. Lett. 120B, 54 (1982)

Tserruya, I., Breskin, A., Chechik, R., Fraenkel, Z., Wald, S., Zwang, N., Bock, R., Dakowski, M., Gobbi, A., Sann, H., Bass, R., Kreyling, G., Renfordt, R., Stelzer, K., Arlt, U.
Preequilibrium Neutron Emission in Deep Inelastic Collisions of ^{86}Kr on ^{166}Er at 11.9 MeV/nucleon
Phys. Rev. C26, 2509 (1982)

Unterseer, K., Kleber, M.
Dynamics of Inner-Shell Electrons in Ion-Atom Collisions
Nucl. Instr. Methods 192, 35 (1982)

Warke, C.S., Greiner, W.
Theory of a Relativistic Nuclear Fluid Coupled to Classical Fields
J. Phys. G8, L27 (1982)

Warwick, A.I., Baden, A., Gutbrod, H.H., Maier, M.R., Peter, J., Ritter, H.G., Stelzer, H., Wieman, H., Weik, F., Freedman, M., Henderson, D.J., Kaufman, S.B., Steinberg, E.P., Wilkins, B.D.
Fission and Deep Spallation Characteristics in Relativistic Nuclear Collisions
Phys. Rev. Lett. 48, 1719 (1982)

Westmeier, W., Esterlund, R.A., Rox, A., Patzelt, P.
Further Evidence for "Extra Push"
Phys. Lett 117B, 163-166 (1982)

Wolf, G.K.
Chemical and Catalytic Effects of Ion Implantation
Radiation Effects 65, 107 (1982)

Wolf, G.K.
Metallvergütung durch Ionenbestrahlung
wt-Z. ind.Fertig. 72, 701 (1982)

Wolf, K.L., Gutbrod, H.H., Meyer, W.G., Poskanzer, A.M., Sandoval, A., Stock, R., Gosset, J., Jourdain, J.C., King, C.H., King, G., Nguyen Van Sen, Westfall, G.D.
"Pion Production and Charged-Particle Multiplicity Selection in Relativistic Nuclear Collisions"
Phys. Rev. C26, 2572 (1982)

Wolf, R., Tanimura, O., Mosel, U., Satchler, G.R.
Influence of Strongly Coupled Inelastic Excitations on the Optical Potential for $^{12}C + ^{12}C$
Z. Phys. A305, 179 (1982)

Wollersheim, H.J., Wilcke, W.W., Birkelund, J.R., Huizenga, J.R.
Influence of the Impact Parameter on Element Distributions in Dissipative Heavy-Ion Collisions
Phys.Rev. C25, 338 (1982)

Xu, G.O., Wang, S.J.
The Interacting Boson Approximation in Nuclei with a Few Valence Nucleons
Nucl. Phys. A380, 529 (1982)

Yadav, H.L., Nörenberg, W.
Effects of Local Equilibration in Dissipative Heavy-Ion Collisions
Phys. Lett. 115B, 179 (1982)

Yannouleas, C., Dworzecka, M., Griffin, J.J.
Nuclear Dissipation as Damping of Collective Motion in the Time-Dependent RPA. I: The Microscopic Model
Nucl. Phys. A379, 256 (1982)

Ziegenhain, K.H., Pinkston, W.T., Oberacker, V.E.
On the Schrödinger Equation with a Time Dependent Mass Parameter: Nuclear Fragmentation Theory
Z. Phys. A304, 201 (1982)

7.1.2 Conference Contributions

Amsterdam, The Netherlands: International Conference on Nuclear Structure, 30.08. - 03.09. 1982

R. Beckmann, S. Raha, N. Stelte, R. M. Weiner
Limiting Fragmentation and Transparency in High Energy Heavy Ion Collisions

W. Hennerici, V. Metag, H.J. Hennrich, R. Repnow, W. Wahl, D. Habs, K. Helmer, U. v. Helmolt, H.W. Heyng, B. Kolb, D. Pelte, D. Schwalm, R.S. Simon, R. Albrecht
Spin Dependence and Angular Correlation of Giant Resonances Studied in (HI,xn) Reactions

J. Kunz, U. Mosel, A. Schuh
Flow Patterns of Rotating and Vibrating Nuclei

K. Mühlhans, U. Mosel, M. Diebel, K. Neergard
On the Relationship between Shell Structure and Multipole Pairing

D. Schwalm
Electromagnetic Properties of High Spin States

E. Wüst, U. Mosel
E2-Transition-Probabilities with Angular-Momentum-Projected Cranking Wavefunctions

Banff, Alberta, Canada: Maria Heavy Ion Workshop, 22.02. - 26.02. 1982

H.H. Gutbrod, A.I. Warwick, H. Wieman
The target Nucleus in Relativistic Nuclear Collisions

H.H. Gutbrod, A. Baden, H. Löhner, M.R. Maier, A.M. Poskanzer, T. Renner, H. Riedesel, H.G. Ritter, H. Spieler, A.I. Warwick, F. Weik, H. Wieman
First Experiments with the Plastic Ball

Berchtesgaden, Germany: IVth International Conference on Ion Implantation: Equipment and Techniques, 13.09. - 17.09. 1982

R. Keller, P. Spädke, K. Hofmann
Optimization of a Single Aperture Extraction System for High Current Ion Sources

R. Keller, F. Nöhmayer, P. Spädke,
Development of a High Current Ion Source for Non-Volatile Elements

R. Keller
A High Brightness Duoplasmatron Ion Source

Bergen, Norway: IVth Bergen Workshop in Nuclear Physics, 22.03. - 24.03. 1982

P. Armbruster
Shipping the Shores of Nuclear Stability

Berlin, Germany: Hans Geiger-Symposium on Detectors in Heavy-Ion Reactions, 06.10. - 08.10. 1982

H.H. Gutbrod, H. Löhner, A.M. Poskanzer, T. Renner, H. Riedesel, H.G. Ritter, A. Warwick, F. Weik, H. Wieman
4π Physics with the Plastic Ball

O. Klepper, E. Roecki
Fast On-Line Spectroscopy of Exotic Nuclei

V. Metag, D. Habs, K. Helmer, U. v. Helmolt, H.W. Heyng, B. Kolb, D. Pelte, D. Schwalm, W. Hennerici, H.J. Hennrich, G. Himmele, E. Jaeschke, R. Repnow, W. Wahl, R.S. Simon, R. Albrecht
The Darmstadt-Heidelberg Crystal Ball

D. Schüll
The GSI Magnetic Spectrometer

D. Schwalm
Collective Properties of Nuclei at High Spins from B(E2) Values

H. Stelzer
Gas Filled Heavy Ion Detectors

Bielefeld, Germany: Workshop on "Quark Matter Formation and Heavy Ion Collisions", 10.05. - 15.05. 1982

G.N. Fowler, S. Raha, R.M. Weiner
What Could the Anomalons Be?

H.H. Gutbrod
The GSI-LBL-Heidelberg-Marburg-Warsaw Proposal for Heavy Ions at the CERN PS

U. Heinz
Towards a Classical Dynamical Description of the Quark-Gluon Plasma in Heavy-Ion Collisions

S. Nagamiya, H.J. Specht
Inclusive Measurements and Particle Identification

Bielefeld, Germany: 15. Diskussionstagung der Arbeitsgemeinschaft Massenspektrometrie, 02.06. - 04.06. 1982

H. Danigel, H. Jungclas, L. Schmidt
LC/MS für Arzneimittel mit der Spaltfragment-induzierten Flugzeit-Massenspektroskopie

Bologna, Italy: Xth International Conference - Aerosols in Science, Medicine and Technology, 14.09. - 17.09. 1982

R. Brandt, G. Tress, H.A. Khan, P. Vater, M. Kadner
Investigations with a New Kind of Mica Nuclear Filter Having Rounded-off Entrance Channels

H.A. Khan, R. Brandt, D. Hirdes, G. Tress, G. Dersch, K. Jamil
Use of Mica Nuclear Filter in the Development of a Background-Free-Radon-Personell Dosimeter

Bormio, Italy: XXth International Winter Meeting on Nuclear Physics, 25.01. - 30.01. 1982

G. Buchwald, G. Graebner, P.R. Subramanian, L.P. Csernai, J. Theis, J.A. Maruhn, W. Greiner, H. Stöcker
Cluster Production in Relativistic Heavy Ion Reactions

M. Diebel
Is it the Yrastline, which is Populated when the Actinide Nuclei are Coulomb-Excited?

E. Grosse
Shapes and Moments of Nuclei at High Angular Momentum

W. von Oertzen
Enhancement of Two-Neutron Transfer in the Reaction ^{120}Sn on ^{112}Sn

A. Olmi
Collisions Between Heavy Ions at Intermediate Energies

J. Stachel
Evidence for Triaxiality in ^{104}Ru

H. Stöcker, G. Buchwald, L.P. Csernai, G. Graebner, P.R. Subramanian, J. Theis, J.A. Maruhn, W. Greiner,
Microscopic and Macroscopic Models for Nuclear Collisions at Medium and High Energies

J. Theis, H. Kruse, G. Buchwald, G. Graebner, C.S. Warke, J.A. Maruhn, W. Greiner, H. Stöcker,
Generalized Nuclear Fluid Dynamics

Caen, France: Colloque National de Physique Non Nucleaire au G.A.N.I.L., 24.05. - 25.05. 1982

R. Spohr
Nuclear Track Formation and Track Applications at GSI Darmstadt

Cambridge, UK: The Neutron and Its Applications, 13.09. - 17.09. 1982

P. Armbruster
Heavy Ion Fusion and Exotic Nuclei Studies at SHIP

Cargese, France: Summer School on "Atomic Physics of Highly Ionized Atoms", June 1982

G. Soff, U. Müller, T. de Reus, P. Schlüter, A. Schäfer, J. Reinhardt, B. Müller, W. Greiner
Electron Excitation Processes and Quantum Electrodynamics in High-Z Systems

Darmstadt, Germany: Symposium on Accelerator Aspects of Heavy Ion Fusion, GSI, 29.03. - 02.04. 1982

R. Bock
The German HIF (Heavy Ion Fusion) Program

G. Buchwald, H. Kruse, J. Theis, J.A. Maruhn, H. Stöcker
Importance of the Beam Geometry for the Dynamical Stability of Inertial Confinement Fusion Targets

H. Geissel, Y. Laichter, W.F.W. Schneider, P. Armbruster
Stopping Powers and Ranges (0.1-2.4) GeV Uranium Ions in Solids

R. Keller
Ion Sources and Low Energy Beam Transport

J. Klabunde
GSI-Wideröe Experiments

H. Klein, M. Daehne, H. Deitinghoff, A. Gerhard, K.D. Halfmann, P. Junior, K. Langbein, R.W. Müller, J. Müller, W. Neumann, A. Schempp, A. Schönlein
RFQ Development at Frankfurt

P. Krejcik
The Hollow Beam Concept for Producing Intense Beams

R.W. Müller
A Remark on Coupled Motion and Equipartitioning

R.W. Müller
Use of a Heavy-Ion Synchrotron Facility for ICF Studies

Deidesheim, Germany: First Gentner-Symposium (4th Minerva Symposium) on Physics, 10.10. - 15.10. 1982

H. Emling
Collective Motion and High-Spin States: Discrete γ-Rays

P. Glässel
A New Type of Non-Equlibrium Fission Observed in Ternary Heavy Ion Reactions

K.D. Hildenbrand
Reactions Induced by ^{12}C at 84 MeV/u

P. Kienle
Experiments on Positron Production

Denton, Texas, USA: VIIth Conference on the Application of Accelerators in Research and Industry, 08.11. - 10.11. 1982

H. Folger, J. Klemm, M. Müller
Preparation of Nuclear Accelerator Targets by Focused Ion-Beam Sputter Deposition

M. Müller
Application of Multiply Charged Ions to Small Accelerators

A.S. Schlachter, W. Groh, A. Müller, E. Salzborn
Transfer Ionization in Slow Multiply Charged Ion-Atom Collisions

Dogashima, Japan: 1982 INS Kikuchi Summer School, 02.07. - 05.07. 1982

R.S. Simon
Coulomb Excitation with Heavy Ions

Dronten, The Netherlands: Int. Summer School on Nuclear Structure, 16.08. - 27.08. 1982

D. Schwalm
Modern Trends in Coulomb Scattering

Dubna, USSR: International Conference on Nucleus-Nucleus Collisions and Nuclear Excitations, 29.06. - 02.07. 1982

R.S. Simon, R. Albrecht, D. Habs, K. Helmer, U. v. Helmolt, H.W. Heyng, B. Kolb, D. Pelte, D. Schwalm, V. Metag, H. Gräf, W. Hennerici, H.J. Hennrich, E. Jaeschke, R. Repnow, W. Wahl
The Darmstadt-Heidelberg NaI Crystal Ball

East Lansing, Michigan, USA: International Conference on Nucleus-Nucleus Collisions 26.09. - 01.10. 1982

D. Bangert, F. Busch, B. Kohlmeyer, F. Pühlhofer, H. Freiesleben, B. Heusch, K.D. Hildenbrand, W.F.W. Schneider, D. Schüll
Dissipative Collisions with a Fission-Like Exit Channel in the $^{132}Xe + ^{56}Fe$ System

J. de Boer, Ch. Schandera, Ch. Lauterbach, W. Dünnweber, W. Trautmann
The Relative Contributions of Positive and Negative Angle Scattering in ^{86}Kr-Induced Reactions

W. Cassing, A. Lukasiak, W. Nörenberg
On the Energy Distribution of Diabatically Emitted Neutrons in Heavy Ion Collisions

H.H. Gutbrod, H. Löhner, A.M. Poskanzer, T. Renner, H. Riedesel, H.G. Ritter, A. Warwick, F. Weik, H. Wieman
4π Physics with the Plastic Ball

D. Hahn, W. Scheid and Jae Y. Park
Theory of Heavy Ion Scattering on the Basis of the Two-Center Shell Model

A. Lukasiak, W. Cassing, W. Nörenberg
A Microscopically Determined Diabatic Potential for Heavy Ion Collisions

A. Lukasiak, W. Cassing, W. Nörenberg
Mass Parameters for Collective Nuclear Motion Based on a Diabatic Single-Particle Basis

A. Lukasiak, W. Cassing, W. Nörenberg
The Influence of Symmetries and Nondiabatic Coupling on the Diabatic Potential for Two Colliding Heavy Ions

E. Roeckl
Exotic Nuclei in Deep-Inelastic and Fusion Reactions

A. Sandoval
Streamer Chamber Experiments

H.J. Specht
Nucleus-Nucleus Collisions: Observations and Expectations

A.I. Warwick, H.H. Gutbrod, M.R. Maier, H.G. Ritter, H. Stelzer, F. Weik, H. Wieman, S.B. Kaufman, B.D. Wilkins, E.P. Steinberg, J. Peter
The Breakup of Spectator Residues in Relativistic Nuclear Collisions

W. Westmeier, R.A. Esterlund, A. Rox, P. Patzelt
Further Evidence for "Extra Push"

Erice, Italy: Workshop on Physics at LEAR, May 1982

J. Rafelski, B. Müller
Role of Isospin in $p\bar{p}$-annihilation

Eugene, Oregon, USA: International Conference on X-Ray and Atomic Inner-Shell Physics, 23.08. - 27.08. 1982

H.F. Beyer, R. Mann, F. Folkmann
X-Rays and Auger Electrons from Few Electron Recoil Ions

A. Müller, W. Groh, U. Kneissl, H. Ströher, R. Heil, E. Salborn
Multiple Ionization of Noble Gas Atoms by Relativistic Electrons

U. Müller, J. Reinhardt, T. de Reus, P. Schlüter, G. Soff, W. Greiner, B. Müller
Theory of Positron Creation in Heavy-Ion Collisions

Fuglso, Denmark: Nordic Meeting on Nuclear Physics, 16.08. - 20.08. 1982

T. Dossing, K. Neergard
The Isovector Dipole Mode in Excited Nuclei

D. Habs, U. v. Helmolt, H.W. Heyng, R. Kroth, B. Kolb, D. Pelte, D. Schwalm, H.J. Specht, W. Hennerici, H.J. Hennrich, G. Himmele, R. Repnow, W. Wahl, R.S. Simon, R. Albrecht, V. Metag
First Results on γ-Ray Spectroscopy in the Second Minimum of ^{238}U and ^{240}Pu

K. Neergard
"Non-Rotating" Yrast States

R. Stock
Compression of Nuclear Matter

Gaußig/Dresden, DDR: XIIth International Symposium on Nuclear Physics, November 1982

K.D. Hildenbrand
Fast Processes in Heavy Ion Reactions at Incident Energies of 15 MeV/u

Geneve (CERN), Switzerland: SPS-Workshop-Nuclear Beams and Target, 06.12. 1982

H.H. Gutbrod
The Plastic Ball Spectrometer and the PS-Proposal

R. Stock
PS and SPS Physics with ^{16}O Nuclear Beams

Gothenburg, Sweden: VIII International Conference on Atomic Physics, 02.08. - 06.08. 1982

S.D. Berry, I.A. Sellin, L.H. Andersen, M. Breining, S.B. Elston, K.O. Groeneveld, D. Hofmann
Shape and Yield of Electron Capture to the Continuum (ECC) Spectra for 15.4 a.u. and 16.6 a.u. Bare Oxygen Nuclei Transversing Helium Gas

B. Fricke
Level Structure of the $2p\pi$ - $2p\sigma$ Crossing for all Z

D. Kolb, W.R. Johnson
Electric and Magnetic Susceptibilities and Shielding Factors from Relativistic Coupled Hartree-Fock Calculations

R. Latz, J. Schader, H.J. Frischkorn, P. Koschar, M. Burkhard, I.A. Sellin, K.O. Groeneveld
Isotope Effects in Electron Yield Light and Clustered Projectile Ion Impact on Carbon

D. Liesen, A.N. Zinoviev, F.W. Saris
Oscillations in Coincident Molecular-Orbital Auger Spectra Emitted in 450 keV Kr^{4+}+Kr Collisons

D. Liesen, P. Armbruster, F. Bosch, D. Maor, P.H. Mokler, H. Schmidt-Böcking, R. Schuch
Excitation Probability of Inner-Shell Vacancies in Adiabatic Xe+Au and Pb+U Collisions

P.H. Mokler, D. Maor, W.A. Schönfeldt, Z. Stachura, W.E. Meyerhof
Atomic Collisions with Highly Charged, but Decelerated Heavy Ions

Granlibakken, Tahoe City, California, USA: Workshop on Nuclear Dynamics, 22.02. - 26.02. 1982

H.G. Ritter, A. Baden, H.H. Gutbrod, H. Löhner, M.R. Maier, A.M. Poskanzer, T. Renner, H. Riedesel, H. Spieler, A.I. Warwick, F. Weik, H. Wieman
First Experiments with the Plastic Ball Spectrometer

H. Sann
The Dynamics of the Fusion Process

A.I. Warwick, H.H. Gutbrod, M.R. Maier, H.G. Ritter, H. Stelzer, F. Weik, H. Wieman, S.B. Kaufman, B.D. Wilkins, E.P. Steinberg, J. Peter
Target Fragment Production Mechanism in Relativistic Nuclear Collisions

H. Wieman, A. Baden, M. Freedman, H.H. Gutbrod, D.J. Henderson, S.B. Kaufman, M.R. Maier, J. Peter, H.G. Ritter, E.P. Steinberg, H. Stelzer, A.I. Warwick, F. Weik, B.D. Wilkins
Multiplicities of Slow Target Fragments in Relativistic Heavy Ion Collisions

C. Yannouleas, M. Dworzecka, J.J. Griffin
The Wall Formula for Nuclear Dissipation as Classical Limit of the Damping of Collective Motion in the Time-Dependent RPA

Grenoble, France: International Workshop on ECR Ion Sources and Related Topics, January 1982

E. Salzborn, W. Groh, A. Müller, A.S. Schlachter
Electron Capture by Multiply Charged Ions with Simultaneous Ionization of the Target Atom

Hirschegg, Kleinwalsertal, Austria: Xth International Workshop on Gross Properties of Nuclei and Nuclear Excitations, 18.01. - 23.01. 1982

S. Ayik, W. Nörenberg
Transport Theory of Dissipative Heavy Ion Collisions: Dynamical Treatment of Strong Coupling within a One-Body Theory

H. Gäggeler, W. Brüchle, G. Herrmann, J.V. Kratz, M. Schädel, K. Sümmerer, G. Wirth, T. Sikkeland
Production of Cold ^{246}Fm Compound Nuclei by Complete Fusion in Different Entrance Channels

P. Glässel, D. v. Harrach, L. Grodzins, S.S. Kapoor, H.J. Specht
Observation of fast Fission in Three-Body Processes Induced by 12.5 MeV/u Kr and Xe Projectiles

E. Kankeleit
Deep Inelastic Reactions and Positron Production

A. Lukasiak, W. Cassing, W. Nörenberg
Microscopic Calculation of Diabatic Single-Particle-Levels

J.A. Maruhn
Hydrodynamic Model for Heavy Ion Collisions

W.F.J. Müller, A. Gobbi, K.D. Hildenbrand, A. Olmi, H. Sann, H Stelzer, H. Ho, W. Kühn, U. Lynen, D. Pelte, U. Winkler, R. Glasow, R. Santo
Experiments with 86 MeV/u ^{12}C

C. Yannouleas, M. Dworzecka, J.J. Griffin
Microscopic Nuclear Dissipation Mechanism as Damping of Collective Motion in the Second RPA

Jülich, Germany: VIIIth Symposium on Microdosimetry, 27.09. - 01.10. 1982

J. Kiefer
On the Interpretation of Biological Heavy Ion Action

G. Kraft
The Influence of the Radiation Quality of the Biological Effectiveness of Heavy Charged Particles

M. Schäfer, R. Facius, H. Bücker
On the Role of Secondary Electrons for the Inactivation of Bacillus Subtilis Spores by Very Heavy Ions

H. Straaten, K.J. Weber, J. Kiefer
Radiation Sensitivity of Transcription in Yeast Cells: Influence of Photon Energy

K.J. Weber, J. Kiefer
Radiation Sensitivity of Transcription in Yeast Cells: Influence of Target Size

Karlsruhe, Germany: Frühjahrstagung des Fachausschusses Kernphysik der DPG, 22.03. - 26.03. 1982

U. Arlt, R. Bass, H. Dittmar, V. Hartmann, G. Kreyling, K. Sapotta, K. Stelzer
Neutronen- und Gamma-Emission bei den Reaktionen $^{86}Kr + {}^{64}Ni$, ^{76}Ge (3.8 MeV/u)

U. Arlt, R. Bass, H. Dittmar, N. Georgiadis, M. Körfer, G. Kreyling, R. Merten, K. Stelzer
Entwicklung und Untersuchung von NE213-Detektoren

P. Armbruster, H. Bokemeyer, F. Bosch, H. Emling, J.S. Greenberg, E. Grosse, S. Ito, R. Kulessa, D. Liesen, D. Maor, D. Schwalm, N. Trautmann
Experimentelle Trennung der K-Loch Erzeugung durch nukleare Coulomb-Anregung bzw. durch direkte Ionisation mit Hilfe einer Doppler-Shift Technik - dargestellt am Stoßsystem Pb+Cm

G. Astner, D. Hofmann, W. Meyerhof, K.O. Groeneveld
K-Ionisationswahrscheinlichkeit bei C(p,p)-Kernresonanzstreuung

H. Backe, W. Bonin, E. Kankeleit, R. Köhler, M. Kollatz, M. Krämer, R. Krieg, U. Meyer, V. Metag, P. Senger, N. Trautmann, J.B. Wilhelmy
Positronenerzeugung bei Schwerionenstößen mit Kernkontakt

R. Beckmann, S. Raha, N. Stelte, R.M. Weiner, M. Weström
Preequilibrium Phenomena in Heavy Ion Reactions

G. Beier, J. Friese, K. Hartel, P. Kienle, H.J. Körner, Waltraud Mayer, K.E. Rehm, W. Wagner
^{238}U Induced Transfer Reactions on Medium Weight Nuclei at Bombarding Energies Close to the Coulomb Barrier

E. Berdermann, M. Clemente, P. Kienle, H. Tsertos, W. Wagner, F. Bosch, C. Kozhuharov, W. Koenig
Strukturen im Positronenspektrum im Schwerionen-Atom-Stoß

D. Berdichevsky, U. Mosel, E. Wüst
Analyse der Gestalt und Breite der Kernoberfläche von Kernen im Tal der β-Stabilität

H. Bokemeyer, H. Folger, H. Grein, S. Ito, D. Schwalm, K. Bethge, A. Gruppe, M. Waldschmidt, R. Schule, J.S. Greenberg, J. Schweppe, P. Vincent, N. Trautmann
Search for Spontaneous Positron Production in Heavy-Ion Collisions

P. Braun-Munzinger, K.D. Hildenbrand, D. Schüll, W.F.J. Schneider, H. Stelzer, M. Marinescu, F. Pühlhofer, H. Freiesleben
Inelastische Anregung und Nukleonentransfer bei Reaktionen von 10 MeV/u und 13 MeV/u ^{86}Kr mit ^{208}Pb und ^{197}Au

C. Brendel, J. Carter, G. Delic, A. Richter, G. Schrieder, D. Schüll
Ladungsaustauschreaktionen und Multinukleonentransfer in nichtdissipativen $^{48}Ti + {}^{42}Ca$ Stößen

M. Burkhard, H.J. Frischkorn, D. Hofmann, P. Koschar, K.O. Groeneveld
Augerelektronen von oberflächennahen Festkörperatomen nach Anregung durch molekulare Projektilionen

J. Carter, C. Brendel, H. Feldmeier, A. Richter, G. Schrieder, W. Bohne, K. Grabisch, H. Lehr, H. Morgenstern
Fusion-Fission and Fusion-Evaporation in the $^{40}Ar + {}^{40}Ca$ System at Energies far above the Coulomb Barrier

W. Cassing, A. Lukasiak, W. Nörenberg
Kollektive Bewegung schwerer Kerne aus der Sicht einer diabatischen Einteilchenbasis

H.-G. Clerc, R. Hingmann, C.-C. Sahm, D. Vermeulen, K.-H. Schmidt
Alphazerfallseigenschaften der neutronenarmen Nuklide ^{199}Rn und ^{199m}Rn

H.-G. Clerc, C.-C. Sahm, D. Vermeulen, P. Armbruster, F. Heßberger, J.G. Keller, G. Münzenberg, W. Reisdorf, K.-H. Schmidt
Systematische Untersuchung von Wirkungsquerschnitten für die Bildung neutronenarmer Verdampfungsrestkerne zwischen At und Pa

K. Depta, J. Hahn, J.A. Maruhn, A. Sandulescu, M. Uhlig, K.H. Ziegenhain and W. Greiner
Quantum-mechanical Treatment of Mass and Charge Fragmentation in Heavy-Ion Collisions

M. Diebel, U. Mosel
Kollektive und effektive Trägheitsmomente in Hochspinzuständen

H.Th. Elze, J. Rafelski and W. Greiner
Das Quark-Gluon-Plasma mit Color-Confinement

H. Emling, P. Fuchs, E. Grosse, R. Kulessa, D. Schwalm, H.J. Wollersheim
Spinabhängige Formändernungen in Kernen der seltenen Erden

H.J. Frischkorn, P. Koschar, R. Latz, J. Schader, K.O. Groeneveld, F. Bömmel, G. Saemann-Ischenko, W. Schmidt
Schwerioneninduzierte Elektronenemission aus Festkörperoberflächen

H. Gäggeler, W. Brüchle, G. Herrmann, J.V. Kratz, M. Schädel, K. Sümmerer, G. Wirth, T. Sikkeland
Bildung von ^{246}Fm durch Fusion verschiedener Projektil-Target-Kombinationen

P. Glässel, L. Grodzins, D. v. Harrach, S.S. Kapoor, H.J. Specht
Schnelle Dreikörperzerfälle im System ^{129}Xe + ^{122}Sn bei 12.5 MeV/u

S. Gralla, A. Gobbi, K.D. Hildenbrand, W.F.J. Müller, A. Olmi, M. Petrovici, H. Stelzer, J. Toke, U. Lynen
Emission leichter Teilchen in schnellen Stößen schwerer Kerne

F. Güttner, W. Koenig, B. Martin, H. Skapa, J. Soltani, C. Kozhuharov, M.A. Herath-Banda, A.V. Ramayya
Untersuchung superschwerer Quasiatome (Z_u = 110-171) mittels δ-ELektron, K-X-Ray, Heavy Ion Koinzidenzmessungen

D. Habs, H.W. Heyng, U. v. Helmolt, B. Kolb, D. Pelte, D. Schwalm, W. Wahl, W. Weiter, H. Gräf, E. Jaeschke, O. Häusser, H.J. Hennrich, V. Metag, R. Repnow, R. Albrecht, R.S. Simon
Bericht über den Status des Heidelberg-Darmstädter Kristallkugel-Projekts

O. Häusser, H. Gräf, L. Grodzins, E. Jaeschke, V. Metag, D. Habs, D. Pelte, H. Emling, E. Grosse, R. Kulessa, D. Schwalm, R.S. Simon, J. Keinonen
g-Faktoren von Hochspin-Yrast-Zuständen in ^{232}Th und ^{238}U

F.P. Heßberger, P. Armbruster, K.D. Hildenbrand, S. Hofmann, G. Münzenberg, W. Reisdorf, K.-H. Schmidt, J.R.H. Schneider, W.F.W. Schneider
Ein Flugzeitdetektorsystem zur Untersuchung von Fusionsprodukten aus Schwerionenreaktionen

K.D. Hildenbrand, R. Bock, A. Gobbi, S. Guarino, S. Gralla, W.F.J. Müller, A. Olmi, M. Petrovici, H. Sann, H. Stelzer, J. Toke, U. Lynen
Der Einfluß der Potentialenergiefläche aus Massen- und Ladungstransfer

S. Hofmann
Protonenemitter und Element 107: Neue Kerne an den Grenzen zur Instabilität

G. Ingold, U. Jahnke, D. Hilscher, E. Holub, H. Orf, R. Brandt, G. Feige, E. Kopp, L. Schmidt
Wiederentdeckung der Neutronen-Szintillator-Tanks für Schwerionenexperimente

E. Kankeleit, R. Köhler, M. Kollatz, M. Krämer, R. Krieg, U. Meyer. H. Oeschler, P. Senger
Das Tori-Spektrometer, ein neues Instrument für Positronen- und Elektronenspektroskopie

J. Keinonen, K.P. Lieb, H.P. Hellmeister, A. Bockisch, H. Emling
Zum Abbremsvermögen von Kr Ionen in Al, Zn und Ge

H.A. Khan, P. Vater, T.Lund, R. Brandt
A Study of the Interaction of 1712 MeV- ^{16}O Ions with ^{197}Au Using Threshold-Solid State Nuclear Track Detectors

R. Kirchner, O. Klepper, W. Kurcewicz, E. Roeckl, E.F. Zganjar, E. Runte, W.-D. Schmidt-Ott, P. Peuser, P. Tidemand-Petersson, K. Rykaczewski, N. Kaffrell
New Neutron-Rich Isotopes ^{179}Yb and $^{181/182}$Lu Produced in Reactions of 9 MeV/u ^{136}Xe Ions on Tantalum and Tungsten Targets

O. Klepper, T. Batsch, S. Hofmann, R. Kirchner, W. Kurcewicz, W. Reisdorf, E. Roeckl, D. Schardt
Direct and Beta-Delayed Proton Decay of Very Neutron-Deficient Rare-Earth Isotopes with Mass Number 147

O. Klepper, R. Kirchner, P. Komninos, W. Kurcewicz, E. Nolte, E. Roeckl, D. Schardt, P. Tidemand-Petersson, E.F. Zganjar
Investigation of Very Neutron-Deficient Isotopes Below ^{100}Sn in ^{40}Ca-Induced Reactions

H.-J. Körner
Äquilibrierungsprozesse bei Reaktionen zwischen schweren Atomkernen

B. Kohlmeyer, F. Pühlhofer, H. Lehr, W.F.W. Schneider
Anwendung des Wilczynski-Models auf die Fusion in näherungsweise symmetrischen Systemen

P. Koschar, H.J. Frischkorn, R. Latz, J. Schader, K.O. Groeneveld
Augerelektronen Linienform nach Coulombexplosionen

R. Latz, J. Schader, H.J. Frischkorn, D. Hofmann, P. Koschar, K.O. Groeneveld
Starke Abhängigkeit der Konvoielektronenemission von der Durchflugzeit durch Festkörper

R. Latz, J. Schader, H.J. Frischkorn, D. Hofmann, P. Koschar, K.O. Groeneveld
Targetdickenabhängigkeit der totalen Elektronenemission von Schwerionen-Festkörper-Stößen

Ch. Lauterbach, Ch. Mittag, Ch. Schandera, J. de Boer, Ch. Briancon, A. Lefebvre, C.F. Liang, J.P. Thibaud, R.J. Walen, A. Celler, R. Kulessa, H. Emling, R.S. Simon
Coulombanregung von Hochspinzuständen in ^{230}Th

T. Lund, B. Bergersen, R. Brandt, E. Hagebo, I.R. Haldorsen, D. Molzahn, C. R.-Serre, K. Aleklett, W. Loveland, P. McGaughey, R.H. Kraus jr., Y. Morita, G. Rudstam, G.T. Seaborg, the ISOLDE Collaboration
Nuclear Interactions of 86 Mev/u ^{12}C-Ions, Studied with Radiochemical Methods

C. Michel, H. Emling, E. Grosse, R. Kulessa, D. Schwalm, G. Seiler-Clark, J. Stachel
Deorientation of High Velocity Ions Recoiling into Vacuum

U. Mosel, E. Wüst
Vergleich verschiedener Projektionsmethoden zur Erzeugung von |M>

K. Mühlhans, E.M. Müller, M. Diebel, K. Neergard, U. Mosel
Einfluß von Multipol-Paarfeldern auf Trägheitsmomente

W.F.J. Müller, A. Gobbi, K.D. Hildenbrand, A. Olmi, H. Sann, H. Stelzer, H. Ho, W. Kühn, U. Lynen, D. Pelte, U. Winkler, R. Glasow, R. Santo
Zerfallskanäle von Kernen in Reaktionen mit 86 MeV/u ^{12}C und ^{15}N

M. Münchow, D. Hahn and W. Scheid
Deformationsabhängige Potentiale für Schwerionen-Reaktionen

M. Petrovici, M. Dakowski, A. Gobbi, G. Guarino, S. Gralla, K.D. Hildenbrand, W.F.J. Müller, A. Olmi, H. Sann, H. Stelzer, J. Toke, U. Lynen, D. Pelte
Study of Fast Processes at Large Incident Velocities and Small Energy Losses

M. Plümer, S. Raha, R.M. Weiner
Quark-Gluon Coupling in the Low Density Limit of Quark Matter

M. Rajagopalan, R.A. Esterlund, W. Westmeier, P. Patzelt
Mass- and Charge-Yield Distributions for 600-MeV ^{132}Xe + ^{nat}Fe

T. de Reus, U. Müller, J. Reinhardt, P. Schlüter, G. Soff, K.H. Wietschorke, B. Müller and W. Greiner
Atomic Excitation Processes in Superheavy Quasimolecules

U. Reus, W. Westmeier, R.A. Esterlund, A. Rox, M. Rajagopalan, P. Patzelt
Evolution der Form von Winkelverteilungen im System ^{132}Xe + ^{nat}Fe

E. Runte, W.-D. Schmidt-Ott, P. Tidemand-Petersson, R. Kirchner, O. Klepper, W. Kurcewicz, E. Roeckl, N. Kaffrell, P. Peuser, K. Rykaczewski
Transfer Reactions for Production of New Isotopes ^{62}Mn, and $^{71-73}$Cu

H. Schaaser, J. Rafelski and W. Greiner
The Electrostatic Problem of Two Point-Charges in Nonlinear Electrodynamics

J. Schader, R. Latz, D. Berenyi, H.J. Frischkorn, K.O. Groeneveld, P. Koschar, A. Köver, G. Szabo
Doppelstoßionisation innerer Schalen mit molekularen Schwerionen

Ch. Schandera, J. de Boer, W. Dünnweber, G. Graw, C. Lauterbach, H. Puchta, W. Trautmann
γ-Zirkularpolarisation im System $^{86}Kr + ^{139}La$

P. Schlüter, B. Müller, W. Greiner and G. Soff
Self-Energy Corrections for Electrons in Superheavy Atoms

R. Shanker, C.S. Warke, W. Greiner and B. Müller
Cylindrically deformed Quark Bags

G. Seiler-Clark, D. Pelte. D. Schwalm, A. Balanda, H. Emling, E. Grosse, R. Kulessa, H.J. Wollersheim, M. Hass, G.J. Kumbartzki, K.H. Speidel
Magnetische Momente von Yrastzuständen in ^{158}Dy und ^{156}Dy

M. Seiwert, N. Aboul-El-Naga, V. Oberacker, J.A. Maruhn, and W. Greiner
On the Possibility of Superheavy Nuclear Quasimolecules in U+U Collisions

J. Stachel, N. Kaffrell, H. Emling, H. Folger, E. Grosse, R. Kulessa, D. Schwalm
Zur Struktur von ^{104}Ru

H. Stelzer, P. Braun-Munzinger, C. Brendel, E. Grosse, U. Lynen, C. Michel, W.F.J. Müller, H. Noll, W. Rösch, G. Schrieder
Ein π^0-Spektrometer mit grosser Nachweiswahrscheinlichkeit

K. Sümmerer, W. Brüchle, F. Fan, H. Gäggeler, B. Jacak, J.V. Kratz, T. Sikkeland, G. Wirth, R. Lucas, J. Poitou, M. Weis
Neutronen- und Protonentransfer in der Reaktion von 7.5. MeV/u ^{238}U-Ionen mit ^{197}Au

O. Tanimura, R. Kaps. U. Mosel. R. Wolf
Weak Coupling Model Approach to Molecular Resonance

J. Theis, H. Kruse, M. Uhlig, C.S. Warke, J.A. Maruhn and W. Greiner
Relativistic Nuclear Fluid Coupled to Classical Meson Fields

J. Toke
Excitation Energy Dependence of Nuclear Matter Density, Surface Diffuseness, Level Density Parameter and Fissility

G. Tress, E.U. Khan, H.A. Khan, P. Vater, R. Brandt, M. Kadner, R. Spohr
Filtration heißer, radioaktiver Aerosole in der Industrie mit Kernspurfiltern aus Glimmer in einem "Partikelfraktionator"

W. Westmeier, M. Rajagopalan, P. Patzelt
Analyse eines Experiments vom Ghoshal-Typ im Rahmen des statistischen Modells

W. Westmeier, P. Patzelt
Rechnerische Auswertung von Alpha-Spektren

R. Wolf, O. Tanimura, U. Mosel, S.C. Pieper, M. Rhoades-Brown
Einfluß aller wichtigen Kanalkopplungen im $^{12}C + ^{12}C$ System auf das optische Potential

H.J. Wollersheim, W.W. Wilcke, J.R. Birkelund, J.R. Huizenga, W.U. Schroeder, H. Freiesleben, D. Hilscher
The $^{209}Bi + ^{136}Xe$ Reaction at E_{lab} = 1422 MeV

H.J. Wollersheim, W.W. Wilcke, J.R. Birkelund, J.R. Huizenga
Influence of the Impact Parameter on Element Distributions in Dissipative Heavy-Ion Collisions

Karlsruhe, Germany: Vortragstagung der Fachgruppe Nuklearchemie in der GDCh, 20.09. - 24.09. 1982

W. Brüchle, H. Gäggeler, J.V. Kratz, M. Schädel, G. Wirth, N. Trautmann, P. Peuser, G. Tittel, R. Stakemann, G. Herrmann, E.K. Hulet, R. Lougheed, J.M. Nitschke, R.L. Hahn, R.L. Ferguson
Produktion schwerster Elemente und Suche nach superschweren Elementen in der Reaktion $^{238}U + ^{248}Cm$

M. Brügger, N. Trautmann, A.K. Mazumdar, H. Wagner, W. Walcher
HELIOS - Ein Heliumjet on-line Massenseparator zur Untersuchung kurzlebiger Spaltprodukte

G. Feige, R. Brandt, T. Lund, D. Molzahn, D.C. Hoffman, S.J. de Villiers, A.G. Gancarz, G.W. Knobeloch, R.O. Lawrence, J. Halperin, R.W. Stoughton, B.H. Ketelle
Untersuchungen über Transuranspuren in heißen Salzsolen

H. Jungclas, H. Danigel, L. Schmidt
Kombinierte Flüssigkeitschromatographie - Massenspektrometrie mit Spaltfragment-induzierter Ionisation

M. Lerch, H. Gehmecker, N. Trautmann, G. Herrmann
Chemische Verfahren zur selektiven Abtrennung des Plutoniums aus Umweltproben und zur Bestimmung seiner Wertigkeitsstufen

P. Peuser, J. Bonn, G. Herrmann, M. Lerch, H. Menke, M. Overbeck, H. Rimke, W. Ruster, N. Trautmann, M. Weber
Bestimmung geringster Mengen Plutonium

F.J. Reischmann, B. Rumler, N. Trautmann, G. Herrmann
Chemisches Verhalten von Elementen in extrem geringen Konzentrationen

A. Rox, W. Westmeier, R.A. Esterlund, P. Patzelt
Radiochemische Untersuchungen am Reaktionssystem $^{238}U + ^{nat}Fe$

R. Stakemann, W. Fan, H. Gäggeler, K. Sümmerer
Anregungsfunktionen schwerer Aktiniden aus der Reaktion von $^{238}U + ^{238}U$.

Kreta, Greece: Europhysics Study Conference on Nuclear Structure, 28.06. - 02.07. 1982

D. Schwalm
Electromagnetic Properties of Rotational Bands

Kyoto, Japan: Kyoto Summer Institute on "Microscopic Theories of Nuclear Collective Motion", July 1982

U. Mosel
Vibrational and Rotational Flow in Nuclei

La Rabida, Spain: International Summerschool on Heavy Ion Collisions, 07.06. - 18.06. 1982

A. Gobbi
Different Regimes of Dissipative Collisions

J. Kunz
Nuclear Current Distributions

U. Mosel
Nuclear Molecular States

U. Müller, N. Aboul-El-Naga, J. Reinhardt, T. de Reus, P. Schlüter, M. Seiwert, G. Soff, K.H. Wietschorke, B. Müller, W. Greiner
Spectroscopy of Superheavy Quasimolecules and Quasiatoms

D. Schardt
Direct Proton Decay of ^{147}Tm

Liege, Belgium: European Group for Atomic Spectroscopy, 27.07. - 30.07. 1982

R. Menges, G. Huber, G. Ulm, T. Kühl
Two Photon Spectroscopy of $^{113,115}In$

G. Ulm, G. Huber, H. Lochmann, R. Kirchner, R. Kühl, D. Marx
Collinear Laser Spectroscopy on a Fast Atomic Beam of ^{115}In

J. Eberz, G. Huber, G. Ulm, T. Kühl
Pressure Broadening and Pressure Shift of the (λ = 410 nm) Indium Line

Mainz, Germany: Workshop über Fragen der nuklearen Astrophysik, 13.10. - 15.10. 1982

E. Roeckl
Produktion neutronenreicher Kerne in Schwerionenreaktionen

N. Trautmann
Rapid Chemical Methods for Identification and Study of Exotic Nuclei

Mainz, Germany: Workshop on Photo- and Electroproduction of Pions, 01.11. - 02.11. 1982

E. Grosse
Pion Production from Collisions between Nuclei

Manchester, UK: Winter Meeting, Association for Radiation Research, January 1982

J. Kiefer, E. Schneider, F. Schöpfer, S. Rase
Heavy Ion Effects on Yeast Cells

Maratea, Italy: International Advanced Course on "Fundamental Process in Energetic Atomic Collisions", 20.09. - 01.10. 1982

K.-H. Schartner
Highly Charged Recoil Ions

G. Soff, U. Müller, T. de Reus, P. Schlüter, J. Reinhardt, B. Müller and W. Greiner
Electron Excitation and Positron Emission in Quasimolecular Collisions of Very Heavy Ions

G. Soff
Superheavy Collision Systems

Middelfort, Denmark: IVth International Conference on Inelastic Ion-Surfaces Collision, 21.09. - 24.09. 1982

H.J. Frischkorn, K.O. Groeneveld
Heavy Ion Induced Electron Emission from Solid Surfaces

Montreux, Switzerland: IInd Workshop "Liquid Chromatography Mass Spectrometry (LC/MS) and MS/MS", 21.10. - 22.10. 1982

H. Jungclas, H. Danigel, L. Schmidt
Liquid Chromatography/Mass Spectrometry with ^{252}Cf Fission Fragment Induced Ionization

Mt. Fuji, Japan: Conference on Dynamics of Nuclear Collective Motion, 06.07. - 10.07. 1982

M. Diebel, U. Mosel
Do the Experimental Actinide Spectra Correspond to the Yrastline?

T. Dossing, K. Neergard, H. Sagawa
Deformed Independent Particle Model and the Yrast Spectra in the ^{146}Gd Region

E. Grosse
Shapes and Moments of Nuclei at High Angular Momentum

A. Hagashi, P. Ring, K. Hara, H. Emling, E. Grosse
Dependence of Quadrupole Moments and Transitions on Asymmetry Parameter

U. Mosel
g-Factors as a Sensitive Test for the Influence of Rotation on Nuclear Structure

R.S. Simon, R. Albrecht, D. Habs, K. Helme, U. v. Helmolt, H.W. Heyng, B. Kolb, D. Pelte, D. Schwalm, V. Metag, H. Gräf, W. Hennerici, H.J. Hennrich, E. Jaeschke, R. Repnow, W. Wahl
First Results from the Darmstadt-Heidelberg Crystal Ball

M. Seiwert, J.A. Maruhn, W. Greiner and A.V. Ramayyah
Collective Excited States in Transitional Nuclei

München, Germany: Symposium molekulare und zelluläre Mechanismen der Wirkung ionisierender Strahlen, March 1982

J. Kiefer, E. Schneider, S. Rase, F. Schöpfer, G. Kraft
Zelluläre Wirkungen schwerer Ionen

G. Kraft
Wirkungs-Querschnitte und kritische Targetgröße bei der Inaktivierung von Säugetierzellen durch schwere Ionen

M. Schäfer, R. Facius, H. Bücker
Überleben individueller Sporen von Bazillus Subtilis bei Bestrahlung mit einzelnen Ionen höchsten LET's

K.J. Weber, J. Kiefer, H. Straaten
Wirkung ionisierender Strahlen auf die Funktion transkriptionskontrollierter Prozesse in Hefen

Münster, Germany: Frühjahrstagung des Fachausschusses Metallphysik der DPG, 29.03. - 02.04. 1982

B.H. Wolf
Der 300 KV-Testbeschleuniger der GSI - ein universelles Werkzeug zur Festkörperforschung

Münster, Germany: IInd Workshop "Ion Formation from Organic Solids" 07.09. - 09.09. 1982

H. Jungclas, L. Schmidt, H. Danigel
Problems in Standardization of ^{252}Cf Fission Fragment Induced Desorption Mass Spectrometry

Neunkirchen/Odw., Germany: Pellet-Arbeitstagung, 03.02. - 06.02. 1982

J.A. Maruhn, G. Buchwald, J. Theis and W. Greiner
Zweidimensionale Stabilitätsstudien

New London, New Hampshire, USA: Nuclear Chemistry Gordon Conference, 20.06 - 25.06. 1982

Glässel, P.
Fast Fission in Three-Body Processes Induced by 12.5 MeV/u Kr and Xe Projectiles

A. Olmi
Collisions Between Heavy Nuclei at 10 MeV/A $\leq E_{Lab} \leq$ 20 MeV/A

A.M. Poskanzer
4π Measurements of Relativistic Heavy Ion Reactions

H. Sann
The Dynamics of Fusion in Heavy Ion Reactions

New Orleans, USA: Plasma Physics Meeting, American Physical Society, 01.11. - 05.11. 1982

A.S. Schlachter, W. Graph, A. Müller, E. Salzborn
Electron Capture and Ionization in Slow Multiply Charged Ion-Atom Collisions

Oak Ridge, Tennessee, USA: Conference on High Angular Momentum Properties of Nuclei, 02.11. - 04.11. 1982

J. de Boer, Ch. Lauterbach, Ch. Mittag, Ch. Schandera, Ch. Briancon, A. Lefebvre, L.F. Liang, A. Celler, R. Kulessa, H. Emling, R.S. Simon
Coulomb Excitation of High-Spin States in ^{230}Th

M. Diebel
Bandcrossing for ^{238}U with Quadrupole Pairing

D. Habs, U. v. Helmolt, H.W. Heyng, R. Kroth, B. Kolb, D. Pelte, D. Schwalm, W. Hennerici, H.J. Hennrich, G. Himmele, R. Repnow, W. Wahl, E. Adelberger, A. Lazzarini, R.S. Simon, R. Albrecht, V. Metag
First Results from the Darmstadt-Heidelberg Crystal Ball

R.V.F. Janssens, P. Chowdhury, H. Emling, D. Frekers, T.L. Khoo, W. Kühn, Y.H. Cheng, P.J. Daly, Z.W. Grabowski, M. Korthelahti, J. MacNeil, J.Y. Zhang, G. Leander
Band Structures in ^{186}Hg

D. Schwalm
Collective Properties of Nuclei at High Spins from B(E2) Values

G. Seiler-Clark, D. Pelte, H. Emling, A. Balanda, H. Grein, E. Grosse, R. Kulessa, D. Schwalm, M. Hass, G.J. Kumbartzki, K.H. Speidel
g-Factors of High Spin Yrast States in ^{158}Dy

M. Seiwert, J.A. Maruhn and W.Greiner
The Potential Energy Surface Model of Collective States

Oaxtepex, Mexico: Oaxtepex-Meeting on Nuclear Physics, 02.01. - 08.01. 1982

R. Stock
High Density Nuclear Matter

Oberwolfach, Germany: Symposium über Methoden und Verfahren der mathematischen Physik, 22.02. - 26.02. 1982

J.A. Maruhn, G. Buchwald, H. Kruse and J. Theis
Application of Flux-Corrected Transport Algorithms

Orsay, France: XIIiemes Journees des Actinides, 24.05. - 25.05 1982

F.P. Heßberger, G. Münzenberg, P. Armbruster, W. Faust, S. Hofmann, W. Reisdorf, K.-H. Schmidt, J.R.H. Schneider, H.-J. Schött, C.C. Sahm, D. Vermeulen, K. Güttner B. Thuma
Production and Identification of Isotopes in the Region from Fm to Element 107

N. Trautmann, P. Peuser, W. Ruster, J. Bonn, G. Herrmann
Development of a Laserspectroscopic Detection Method for Trace Amounts of Plutonium

Osaka, Japan: Workshop on Development and Perspectives of Inbeam Particle and γ Spectroscopy, 15.07. - 16.07. 1982

W. Wahl, D. Habs, E. Adelberger, V. Metag, R.S. Simon
Search for Axions in the NaI Crystal Ball

Ottawa, Canada: Meeting of the Committee on Space Research, May/June 1982

R. Facius, M. Schäfer, K. Baltschukat, H. Bücker
Inactivation Probability of Heavy Ion-Irradiated Bacillus Subtilis Spores as a Function of the Radial Distance to the Particle's Trajectory

J. Kiefer, S. Rase, F. Schöpfer, E. Schneider, K. Weber, G. Kraft
Heavy Ion Action on Yeast Cells: Inhibition of Ribosomal RNA-Synthesis, Loss of Colony Forming Ability and Induction of Mutants

Poina Brasov, Romania: International Summer School on Nuclear Collective Dynamics, 26.08. - 08.09. 1982

Ch. Lauterbach, Ch. Schandera, J. de Boer, W. Dünnweber, W. Trautmann
The Circular Polarization of Gamma-Rays Emitted in the $^{86}Kr + ^{139}La$ and $^{86}Kr + ^{166}Er$ Reactions at Incident Energies of 8.2 MeV/u and 10 MeV/u

U. Müller, G. Soff, J. Reinhardt, T. de Reus, B. Müller and W. Greiner
Extreme Superheavy Nuclear Systems with Z=184 and Their Investigation by Positrons from Supercritical Fields

Saclay, France: International Conference on Selected Aspects of Heavy Ion Reactions, 03.05. - 07.05. 1982

R.A. Esterlund, W. Westmeier, A. Rox, P. Patzelt
Further Confirmation of the "Extra Push" Concept

G.N. Fowler, S. Raha, N. Stelte, R.M. Weiner
Heavy Ion Collisions Near the Speed of Sound

H.H. Gutbrod, A.I. Warwick, H. Wieman
Nuclear Desintegration in Relativistic Nuclear Collisions

A. Lukasiak, W. Cassing, W. Nörenberg
Diabaticity In Heavy Ion Collisions and its Role in Non-Equilibrium Neutron Emission

T. Lund, B. Bergersen, S. Engelsen, E. Hagebo, I.R. Haldorsen, D. Molzahn, C. R.-Serre, the ISOLDE Collaboration
Momentum Transfer and Kinetic Energies of Products in the Reaction between V and 86 Mev/A ^{12}C.

M. Münchow and W. Scheid
Nucleus-Nucleus Interaction Potential for Deformed Nuclei

H. Oeschler, M. Kollatz, W. Bohne, K. Grabisch, H. Lehr, H. Freiesleben, K.P. Hildenbrand
Complete Fusion in the Reaction ^{16}O on ^{146}Nd at 10 MeV/u Even for Peripheral Collisions?

M. Petrovici
Fast Processes Induced by Heavy Projectiles at Incident Energies of 10-20 MeV/u

H. Stöcker, G. Buchwald, L.P. Csernai, G. Graebner, J.A. Maruhn and W. Greiner
Dynamics of High Energy Heavy Ion Collisions - Nuclear Matter at High Density and Temperature

S.J. Wang, W. Cassing, W. Nörenberg, G.O. Xu
Comparison of Collective Mass Parameters Given by GCM and the Cranking Model

S.J. Wang, W. Cassing, W. Nörenberg
On the Dynamical Single-Particle Basis in Large Amplitude Collective Motions

G.O. Xu, S. J. Wang
The Inertia Parameter of Nuclear Collective Excitations

Schleching, Germany: Expertentreffen Schleching, 03.03. - 12.03. 1982

P. Armbruster
Experiment am SHIP zur Fusion schwerer Kerne

Schönau/Schwarzwald, Germany: Arbeitstagung: Energiereiche Atomare Stöße, 24.01. - 30.01. 1982

Ch. Achenbach, A. Müller, R. Becker, J. Peschina, H. Klein, E. Salzborn
Elektronenstoßionisation mehrfach geladener Ionen

H.F. Beyer, R. Mann, F. Folkmann, P.H. Mokler
Röntgen- und Augerübergänge in hochionisierten Argonrückstoßionen

H.D. Dohmann, R. Mann, E. Pfeng
Lebensdauern der $^3P_2$ und $^4P^0_{5/2}$ Zustände in He- und Li-ähnlichem Titan

W. Groh, A. Müller, A.S. Schlachter, Ch. Achenbach, E. Salzborn
Transferionisation in Stößen zwischen mehrfach geladenen Ionen und Atomen

M. Kleber
Variationsmethoden in der Schwerionenphysik

D. Liesen, P. Armbruster, F. Bosch, D. Maor, P.H. Mokler, H. Schmidt-Böcking, R. Schuch
Inner-Schalen-Anregungswahrscheinlichkeiten in Adiabatischen Xe + Au und Pb + U Stößen

D. Liesen, A.N. Zinoviev, F.W. Saris
Ozillationen in MO Auger-Elektronenspektren in 450 keV Kr^{4+} + Kr Stößen

P.H. Mokler, D. Maor, W.E. Meyerhof, W.A. Schönfeldt, Z. Stachura
Atomare Stöße mit hochgeladenen, abgebremsten schweren Ionen

U. Müller, T. de Reus, J. Reinhardt, B. Müller and W. Greiner
Die Suche nach langlebigen Schwerionenreaktionen durch Positronenemission

T. de Reus, J.Reinhardt, U. Müller, B. Müller, K.H. Wietschorke, W. Greiner and G. Soff
Abschirmungseffekte auf Loch- und Positronenerzeugungsraten in Schwerionenstößen

E. Salzborn
Hochgeladene Ionen in Fusionsplasmen

P. Schlüter, G. Soff and W. Greiner
Der Einfluß nuklearer EØ-Übergänge auf das δ-Elektronen-Spektrum im Stoß sehr schwerer Ionen

P. Schlüter, G. Soff, B. Müller and W. Greiner
Selbstenergiekorrektur für Elektronen in sehr schweren Ionen

G. Soff, T. de Reus, U. Müller, J. Reinhardt, B. Müller and W. Greiner
δ-Elektronen-Erzeugungswahrscheinlichkeiten im Superschweren Quasimolekül J + Pb

G. Soff
Delta-Elektronen Erzeugung in Superschweren Quasimolekülen

Z. Stachura, F. Bosch, D. Maor, P.H. Mokler, W.A. Schönfeldt
L_3-Unterschalenalignment bei Schwerionenbeschuß

G. Terlecki, N. Grün and W. Scheid
Die H^++H-Streuung im Rahmen einer zeitabhängigen Lösung der Schrödinger-Gleichung mit der Methode klassischer Trajektorien

Seattle, Washington, USA: XIth World Conference of the International Nuclear Target Development Society, 06.10. - 08.10. 1982

H. Folger, J. Klemm, W. Thalheimer
Rotating Target-Substrate Fixture for the Vapor Deposition of Bismuth

H. Folger, N. Trautmann, M. Weber, R. Heimann, D. Gembalies-Datz, W. Hartmann
Actinide Targets Prepared by Molecular Plating Procedures

N. Trautmann, M. Weber, D. Gembalies-Datz, R. Heimann, H. Folger, W. Hartmann
Preparation of Actinide Targets by Molecular Plating for Experiments with Heavy Ions

Stockholm, Sweden: Symposium on Production and Physics of Highly Charged Ions, 01.06. - 06.06. 1982

B. Fricke
Interatomic Potential Structures in Highly Ionized Scattering Systems

E. Salzborn, W. Groh, A. Müller, A.S. Schlachter
Transfer Ionization in Collisions between Multiply Charged Ions and Atoms at keV Energies

A.S. Schlachter, K.H. Berkner, H.F. Beyer, W.G. Graham, W. Groh, R. Mann, A. Müller, R.E. Olson, R.V. Pyle, J.W. Stearns, J.A. Tanis
Collisions of Fast Highly Charged Ions in Gas Targets: Ionization, Recoil-Ion Production and Charge Transfer

Trieste, Italy: Topical Meeting on Nuclear Fluid Dynamics, October 1982

U. Mosel
Current Analysis of Rotating and Vibrating Nuclei

Turku, Finland: Symposium on Relativistic Effects in Quantum Chemistry, 21.06. - 23.06. 1982

B. Fricke
Collision Systems

Varenna, Italy: Third Conference on Nuclear Reaction Mechanism, June 1982

M. Münchow, R.K. Gupta and W. Scheid
Classical Model for Fission Following Deep Inelastic Reactions and Dynamical Effects of the Deformation

H.G. Ritter
Plastic Ball and Streamer Chamber Experiments at the Bevalac

Ch. Schandera, Ch. Lauterbach, J. de Boer, W. Dünnweber, W. Trautmann
Gamma-Ray Circular Polarization in Kr-Induced Reactions

E.P. Steinberg
Nuclear Breakup Mechanism in the Interaction of Relativistic Projectiles with Heavy Targets

Villingen, Germany: Workshop on Radiobiology and Tumor Therapy with Heavy Particles, 27.04. - 30.04. 1982

G. Kraft
The Inactivation of Mammalian Cells by Very Heavy Ions

Washington, DC, USA: Spring Meeting of the American Physical Society, 26.04. - 29.04. 1982

H. Breuer, C.J. Kulessa, G. Lavelle, A.C. Mignerey, J.R. Birkelund, A.D. Hoover, J.R. Huizenga, W.U. Schröder, W.W. Wilcke, H.J. Wollersheim, K. Kwiatkowski, V.E. Viola
Neutron and Proton Exchange in the Reaction ^{238}U + ^{40}Ca

R. Brockmann, J.W. Harris, R.E. Renfordt, A. Sandoval, H. Ströbele, R. Stock, J. Miller, H.G. Pugh, M. Raff, L.S. Schroeder, K. Wolf
Negative Pion Observables in Ar + KCl Collisions

J.W. Harris, R. Brockmann, F. Riess, A. Sandoval, R. Stock, H. Ströbele, H.G. Pugh, L.S. Schroeder, K. Wolf
On the Event Structure of Central Relativistic Heavy Ion Collisions

H. Riedesel, A. Baden, H.H. Gutbrod, H. Löhner, M.R. Maier, A.M. Poskanzer, T. Renner, H.G. Ritter, H. Spieler, A.I. Warwick, F. Weik, H. Wieman
First Results of the Plastic Ball Spectrometer

E. Roeckl
Proton Radioactivity and other Exotic Properties of Nuclei far from the Valley of Stability

H. Wieman, A.I. Warwick, H.H. Gutbrod, S.B. Kaufman, E.P. Steinberg, H. Stelzer, H.G. Ritter, B.D. Wilkins, F. Weik, J. Peter, M. Maier
Multiplicity of Target Fragments in Relativistic Nuclear Collisions

C. Yannouleas, M. Dworzecka, J.J. Griffin
Nuclear Dissipation as Damping of the One-Phonon-Collective State in the Second RPA

C. Yannouleas, M. Dworzecka, J.J. Griffin
Nonlinear Quantal Friction from a Microscopic Model

Wien, Austria: IXth International Mass Spectrometry Conference, 30.08. - 03.09. 1982

H. Jungclas, H. Danigel, L. Schmidt
Liquid Chromatography/Mass Spectrometry with Fission Fragment Induced Ionization

Würzburg, Germany: Frühjahrstagung der Fachausschüsse Atomphysik, Molekülphysik, Kurzzeitphysik und Plasmaphysik, 01.03. - 05.03. 1982

Ch. Achenbach, A. Müller, E. Salzborn, E. Becker, H. Klein, J. Peschina
Elektronenstoßionisation mehrfach geladener Ionen

H.D. Dohmann, R. Mann, E. Pfeng
Messung der Lebensdauern der $(1s2p)^3T_2$- und $(1s2s2p)^4P_{5/2}$- Zustände von He- und Li-ähnlichen Ti- und Cr-Ionen

B. Fricke
Beobachtung und Interpretation eines MO-Zustandes im Kr-Kr Stoß

W. Groh, A. Müller, A.S. Schlachter, Ch. Achenbach, E. Salzborn
Elektroneneinfang mit gleichzeitiger Ionisation des Targets in Stößen zwischen mehrfach geladenen Ionen und Atomen

F. Güttner, W. Koenig, B. Martin, H. Skapa, J. Soltani, C. Kozhuharov, M.A. Herath-Banda, A.V. Ramayya
Untersuchung superschwerer Quasiatome (Z_u = 110-171) mittels δ-Elektron, K-X-Ray, Heavy Ion Koinzidenzmessungen

H. Hartung, H. Lenz
Strukturen in interatomaren Potentialen bei mittleren Energien

D. Kolb, W.R. Johnson
Berechnung atomarer Polarisierbarkeiten und Abschirmfaktoren mittels gekoppeltem, relativistischem Hartree-Fock (RRPA)

P.H. Mokler, D. Maor, W.A. Schönfeldt, Z. Stachura, W.E. Meyerhof
Ladungszustandsabhängige Röntgenemission nach Stößen hochgeladener, abgebremster Ionen mit schweren Atomen

W.A. Schönfeldt, P.H. Mokler
Mehrfach-Anregung Innerer Projektilschalen in 1.4 MeV/u Pb → Z_2 (Gas- und Festkörper-) Stößen

Z. Stachura, F. Bosch, D. Maor, P.H. Mokler
L_3-Shell Alignment by Heavy Ion Impact

W. Wahl, D. Habs, V. Metag, R.S. Simon
Untersuchung von seltenen Zerfallsmoden in der Positronium-Annihilation

7.1.3 Seminars at other Institutes

Achenbach, Ch.
Einfach- und Mehrfachionisation von Xe^{i+} Ionen (i=1,2,3,4) durch Elektronenstoß
Universität Gießen, Germany, 04.11. 1982

Armbruster, P.
Erfolge und Mißerfolge bei der Herstellung der schwersten Elemente über Kernverschmelzungsreaktionen
Hahn-Meitner-Institut Berlin, Germany, 11.01. 1982

Armbruster, P.
Erfolge und Mißerfolge bei der Herstellung der schwersten Elemente über Kernverschmelzungsreaktionen
Technische Hochschule Darmstadt, Germany, 15.01. 1982

Armbruster, P.
Fusion Reaction Studies at SHIP
Dubna, USSR, 18.02. 1982

Armbruster, P.
Cold Fission Studies at LOHENGRIN
Dubna, USSR, 18.02. 1982

Armbruster, P.
Fusion Studies at SHIP
Kopenhagen, Denmark, 26.03. 1982

Armbruster, P.
The Soft Way to Element 107 and Beyond
Lawrence Berkeley Laboratory, USA, 14.06. 1982

Armbruster, P.
Heavy Ion Fusion and Exotic Nuclei Studies at SHIP
Livermore, USA, 21.10. 1982

Armbruster, P.
Die Entdeckung der Elemente 107 und 109
Max Planck Institut Stuttgart, Germany, 16.11. 1982

Armbruster, P.
Die Entdeckung der Elemente 107 und 109
Universität Köln, Germany, 14.12. 1982

Berdichevsky, D.
Systematische Analyse der Ladungs- und Massendichte von Atomkernen
Universität Mainz, Germany, November 1982

de Boer, J.
The Circular Polarization of γ-Rays from Deep-Inelastic Collisions
State University of New York, Stony Brook, USA, 05.10. 1982

de Boer, J.
The Sense of Rotation of Colliding Nuclei
University of Pittsburgh, Pittsburgh, USA, 12.10. 1982

de Boer, J.
The Sense of Rotation of Colliding Nuclei
Kellogg Radiation Laboratory, California Institute of Technology, Pasadena, USA, 15.10. 1982

de Boer, J.
The Circular Polarization of γ-Rays from Deep-Inelastic Collisions
Lawrence Berkeley Laboratory, Berkeley, California, USA, 18.10. 1982

de Boer, J.
The Sense of Rotation of Colliding Nuclei
Los Alamos Scientific Laboratory, Los Alamos, New Mexico, USA, 21.10. 1982

de Boer, J.
The Sense of Rotation of Colliding Nuclei
TUNL Beschleunigerlabor, Durham, North Carolina, USA, 28.10. 1982

Bokemeyer, H.
Search for Spontaneous Positron Emisson - a Challenge to Heavy Ion Physics
Centre de Spectrometrie Nucleaire et de Spectrometrie de Masse, Orsay, France, 27.05. 1982

Bokemeyer, H.
Auf der Suche nach spontaner Positronen-Emission in schwersten quasiatomaren Stoßsystemen
Institut für Strahlen- und Kernphysik, Universität Bonn, Germany, 11.02. 1982

Brandt, R.
Glimmerfilter und ihr Einsatz in der Aerosolforschung
Kernforschungszentrum Karlsruhe, Germany, 08.11. 1982

Cassing, W.
Aspects of Diabatic Single-Particle Motion in Heavy Ion Collisions
Lawrence Berkeley Laboratory, Berkeley, USA, 22.09. 1982

Cassing, W.
Aspects of Diabatic Single-Particle Motion in Heavy Ion Collisions
Centre de Recherches Nucleaires, Strasbourg, France, 04.11. 1982

Cassing, W.
Nichtgleichgewichtsprozesse in niederenergetischen Schwerionenreaktionen

Diebel, M.
Hochspin-Eigenschaften der Aktiniden und Seltenen Erden
Max Planck Institut Heidelberg, Germany, June 1982

Elze, Th.W.
Struktur von Hochspinzuständen in Kernen der Aktiniden
Kernforschungszentrum Karlsruhe, Germany, 26.02. 1982

Emling, H.
Deformation Change at High Spin in Dy Nuclei
Argonne National Laboratory, USA, July 1982

Emling, H.
Messung von Lebensdauern und Feedingzeiten in inversen Schwerionenreaktionen
Universität Köln, Germany, September 1982

Emling, H.
Rotational Alignment in the Actinides
Argonne National Laboratory, USA, November 1982

Feige, G.
A 4π-Neutron Multiplicity Counter for Heavy-Ion Experiments
Los Alamos National Laboratory, USA, 25.11. 1982

Fischer, B.E.
Schwerionenstrahlen - Ein einzigartiges Mikrowerkzeug
Marburg, Germany, 04.10. 1982

Folger, H.
Survey on Recent Experiments and Target Preparations at GSI
IRML, Oak Ridge, USA, 04.11. 1982

Fricke, B.
Wie gut kennen wir eigentlich atomare und molekulare Wellenfunktionen?
II. Physikalisches Institut, Göttingen, Germany, 23.04. 1982

Fricke, B.
Atomic Relativistic Calculations
Göteborg, Sweden, 18.08. 1982

Fricke, B.
Physics of Colliding Ion-Atom-Systems
Göteborg, Sweden, 26.08. 1982

Fricke, B.
Relativistic Calculations of Small Molecules, Clusters and Quasi-Molecules
Aarhus, Denmark, 01.09. 1982

Fricke, B.
Theoretical Description of Atoms anf Small Molecules
Lund, Sweden, 09.09. 1982

Gäggeler, H.
Production of Cold Fermium Compound Nuclei by Different Entrance Channels; a Test for the Limits of Fusion
Joint Institute for Nuclear Research, Dubna, USSR, 18.02. 1982

Gäggeler, H.
On-Line Chemistry at GSI, a Status Report
Joint Institute for Nuclear Research, Dubna, USSR, 19.02. 1982

Gäggeler, H.
Recent Attempts to Produce Superheavy Nuclei by the $^{48}Ca + ^{248}Cm$ Reaction
Lawrence Livermore National Laboratory, USA, 03.11. 1982

Ganßauge, E.
Anomalonen, merkwürdiges Verhalten von schweren Ionen in Emulsion oder neuartige Teilchen?
Universität Mainz, Germany, 27.05. 1982

Ganßauge, E.
New Results on Anomalons
Frascati, Rom, Italy, 05.06. 1982

Ganßauge, E.
Anomalons
DESY, Hamburg, Germany, 02.11. 1982

Ganßauge, E.
Anomalonen, was ist das?
Universität Düsseldorf, Germany, 11.11. 1982

Glässel, P.
Schnelle Drei-Körper-Prozesse - ein Einblick in die Dynamik von Schwerionenstößen
Heidelberg, Germany, May 1982

Glässel, P.
Kr- und Xe-induced Ternary Heavy Ion Processes - an Insight in Nuclear Matter Dynamics
Michigan State University, East Lansing, USA, July 1982

Glässel, P.
Non-Equilibrium Sequential Fission Induced by Heavy-Ion Collisions
Bordeaux, France, July 1982

Glässel, P.
Non-Equilibrium Sequential Fission Induced by Heavy-Ion Collisions
Orsay, France, November 1982

Groh, W.
Elektronen-Einfang mit gleichzeitiger Ionisation des Targets in Stößen zwischen mehrfach geladenen Ionen und Atomen
Universität Gießen, Germnay, 04.02. 1982

Grosse, E.
First Results from Nuclear Reaction Studies at the ^{12}C Beam of the CERN SC
University of Tokyo, Japan, 12.07. 1982

Grosse, E.
Neutral Pion Production from Nucleus Nucleus Collisions
Institut de Physique Nucleaire, Orsay, France, 16.11. 1982

Grosse, E.
Pionproduktion in Kern-Kernstößen unter der Schwelle
Universität Tübingen, Germany, 23.11. 1982

Grosse, E.
Pion Production in Nucleus Nucleus Collisions below the Nucleon Nucleon Threshold
Nils Bohr Institute, Kopenhagen, Denmark, 29.11. 1982

Grosse, E.
Pion Production in Nucleus Nucleus Collisions below the Nucleon Nucleon Threshold
University of Lund, Denmark, 30.11. 1982

Gutbrod, H.H.
Physik mit dem Plastic Ball
Universität Heidelberg, Germany, 26.01. 1982

Gutbrod, H.H.
The Plastic Ball Spectrometer I and II
National Superconducting Cyclotron Laboratory, East Lansing, USA, 01.03. - 02.03. 1982

Gutbrod, H.H.
The Fate of the Target Nucleus in Relativistic Nuclear Collisions
National Superconducting Cyclotron Laboratory, East Lansing, USA, 03.03. 1982

Gutbrod, H.H.
New Results in Relativistic Heavy Ion Physics
Brookhaven National Laboratory, Long Island, USA, 09.11. 1982

Harris, J.W.
Compression versus Transparency in High Energy Nuclear Collisions
Lawrence Berkeley Laboratory, Berkeley, October 1982

Herrmann, G.
Versuche zur Synthese superschwerer Elemente
Universität Hamburg, Germany, January 1982

Herrmann, G.
Production of Very Heavy Nuclei in Strongly Damped Collisions
Joint Institute for Nuclear Research, Dubna, USSR, February 1982

Herrmann, G.
Versuche zur Synthese superschwerer Elemente
Chemische Gesellschaft Karlsruhe, Germany, July 1982

Hoffmann, D.H.H.
Spectroscopy of High Energy Gamma Radiation (1-20 MeV) Induced in Heavy Ion Reactions
Institut Laue Langevin, Grenoble, France, February 1982

Hofmann, S.
Nachweis von Protonenradioaktivität und Element 107 am Geschwindigkeitsfilter SHIP
Universität Bonn, Germany, 28.01. 1982

Kankeleit, E.
Positron- and Electron-Spectroscopy in Deep Inelastic Reactions
Hahn-Meitner-Institut Berlin, Germany, 21.06. 1982

Kankeleit, E.
Quasiatomare Positronen und Kernreaktionszeiten
Universität Duisburg, Germany, 03.05. 1982

Keller, R.
Ionenquellen für Hochfrequenzbeschleuniger
Verein Deutscher Ingenieure, Berlin, Germany, 03.05. 1982

Keller, R.
Plasma Ion Sources
Ecole Polytechnique Federale, Lausanne, Switzerland, 15.11. 1982

Keller, R.
Brillanz von Hochstrom-Ionenquellen
Universität Frankfurt, Germany, 10.12. 1982

Kiefer, J.
Radiation Quality
Ahamadu Bello University, Zaria, Nigeria, 04.03. 1982

Kiefer, J.
Mutant Induction by Heavy Ions
University of Alberta, Edmonton, Canada, 27.05. 1982

Kienle, P.
Positronenerzeugung beim Stoß von Schwerionen mit Atomen
Hochschule der Bundeswehr, München, Germany, 02.02. 1982

Kienle, P.
Paarerzeugung in überkritischen Feldern
Universität Tübingen, Germany, 10.11. 1982

Kienle, P.
Positronenerzeugung im Schwerionenstoß
Universität Gießen, Germany, 22.11. 1982

Kienle, P.
Paarerzeugung im Schwerionenstoß
Universität Bonn, Germany, 16.12. 1982

Kleber, M.
Zur Dynamik der Anregung innerer Schalen
Hahn-Meitner-Institut, Berlin, Germany, 24.05. 1982

Kleber, M.
Optimale Pfade in der Schwerionentheorie
Universität Göttingen, Germany, 23.06. 1982

Knoll, J.
A New Look on Relativistic Heavy Ion Reactions
Max Planck Institut Heidelberg, Germany, 13.01. 1982

Knoll, J.
The Dynamics of Heavy Ion Reactions at Relativistic Energies
Bielefeld, Germany, 14.05. 1982

Knoll, J.
Dynamical Pictures of Relativistic Heavy Ion Reactions
Saclay, France, 27.05 1982

Knoll, J.
Pathintegral Approach to the Solution of Fokker-Planck Equations
Jülich, Germany, 04.06. 1982

Knoll, J.
Dynamische und Statistische Aspekte relativistischer Schwerionenstöße
Marburg, Germany, 14.06. 1982

Knoll, J.
Heavy Ion Reactions at Higher Energies
Fugiso, Denmark, 20.08. 1982

Knoll, J.
Reaktionsmechanismen bei relativistischen Energien I
Technische Hochschule Darmstadt, Germany, 25.11. 1982

Knoll, J.
Reaktionsmechanismen bei relativistischen Energien II
Technische Hochschule Darmstadt, Germany, 16.12. 1982

Kolb, D.
Relativistic Effects in Electric and Magnetic Susceptibilities and Shielding Factors
Göteborg, Sweden, August 1982

Kozhuharov, C.
Spektroskopie von überschweren Qusiatomen mit Hilfe von δ-Strahlen und Positronen
Universität Gießen, Germany, 17.01. 1982

Kraft, G.
Strahlenbiologie mit sehr schweren Ionen
Technische Hochschule Darmstadt, Germany, 11.11. 1982

Kraft, G.
Die biologische Wirkung von Kernwaffen
Technische Hochschule Darmstadt, Germany, 16.12. 1982

Krejcik, P.
The Hollow Beam Concept for Linear Accelerators
TU München, Germany, 09.07. 1982

Kurcewicz, W.
Production of Neutron-Rich Nuclei in Heavy-Ion Collisions
TU München, Garching, Germany, 26.05. 1982

Liesen, D.
Verstehen wir wirklich die Inner-Schalen-Anregung in überschweren Stoßsystemen?
Universität Frankfurt, Germany, 10.05. 1982

Liesen, D.
Interferenzen in atomaren Stößen
Gesamthochschule Kassel, Germany, 25.06. 1982

Lund, T.
Nuclear Interactions of 86 MeV/A ^{12}C-Ions
Los Alamos National Laboratory, USA, 13.05. 1982

Maruhn, J.A.
Hydrodynamic Model for Heavy Ion Collisions
Joint Institute for Nuclear Research, Dubna, USSR, 18.03. 1982

Maruhn, J.A.
Hydrodynamic Model for Heavy Ion Collisions
Universität Mainz, Germany, 05.05. 1982

Maruhn, J.A.
Potential Energy Surface Model of Collective States
Michigan State University, East Lansing, USA, 05.11. 1982

Michel, Ch.
Production of Neutral Pions from Subthreshold Nucleus Nucleus Collisions
Centre d'Etudes Nucleaire, Saclay, France, 17.11. 1982

Mokler, P.H.
Abhängigkeit der Röntgenemission beim Schwerionen-Atom-Stoß vom einkommenden Ladungszustand
Technische Hochschule Darmstadt, Germany, 25.02. 1982

Mosel, U.
Nuclear Molecular States
University of Catania, Italy, September 1982

Mosel, U.
Nuclei at High Spin
University of Catania, Italy, September 1982

Mosel, U.
Wie rotieren die Atomkerne wirklich?
Universität Münster, Germany, December 1982

Müller A.
Significant New Effects in the Ionization of Heavy Atoms by Electrons and Slow, Multicharged Ions
Oak Ridge National Laboratory, Oak Ridge, USA, 05.08. 1982

Müller A.
Electron Impact Ionization of Multiply Charged Ions; Multiple Ionization of Atoms in Slow Multicharged-Ion-Atom Collisions,
Lawrence Berkeley Laboratory, Berkeley, USA, 17.08. 1982

Müller A.
Eine statistische Theorie zur Transfer-Ionisation
Universität Gießen, Germany, 11.11. 1982

Müller, B.
Theory of Positron Creation in Heavy Ion Collisions
Eugene, Oregon, USA, August 1982

Müller, U.
Positron-Emission im Schwerionenstoß - Eine Übersicht zu Theorie und Experiment
Universität Frankfurt, Germany, 08.01. 1982

Müller, U.
Theoretical Survey of Positron Production in Heavy Ion Collisions
Vanderbilt University, Nashville, USA, 08.03. 1982

Münzenberg, G.
Erzeugung und Nachweis von Kernen der Elemente Fm bis 107
Europäisches Institut für Transurane, Karlsruhe, Germany, 21.04. 1982

Münzenberg, G.
Investigations of Isotopes with $Z \geq 100$ Produced in Fusion Reactions
Joint Institute for Nuclear Research, Dubna, USSR, 18.02. 1982

Münzenberg, G.
Ground State Proton Decay of ^{151}Lu and ^{147}Tm
Joint Institute for Nuclear Research, Dubna, USSR, 19.02. 1982

Münzenberg, G.
Erzeugung und Nachweis der Elemente Fm bis 107
Gesamthochschule Kassel, 03.06. 1982

Neergard, K.
The Isovector Dipole Mode in Heated Rotating Nuclei
Riso, Denmark, January 1982

Neergard, K.
The Isovector Dipole Mode in Heated Rotating Nuclei
Max Planck Institut Heidelberg, Germany, May 1982

Neergard, K.
The Isovector Dipole Mode in Heated Rotating Nuclei
Institut Laue-Langevin, Grenoble, France, June 1982

Neergard, K.
"Non-Rotating" Yrast States
Riso, Denmark, August 1982

Nickel, F.
Magnetische und Hochfrequenzmassenspektrometer
Universität Mainz, Germany, 10.11. 1982

Nörenberg, W.
Statistische und dynamische Aspekte in Schwerionenreaktionen
Universität Erlangen, Germany, 26.01. 1982

Nörenberg, W.
Elastic and Dissipative Features of Large-Amplitude Collective Nuclear Motion
Universität Tübingen, Germany, 13.07. 1982

Nörenberg, W.
Statistical and Dynamical Aspects of Heavy Ion Collisions
Universite de Bordeaux, France, 02.04. 1982

Nörenberg, W.
Dissipative Diabatic Dynamics: A Time-Dependent Shell-Model Approach to Large-Amplitude Collective Nuclear Motion
Polytechnicum, Troy, USA, 22.09. 1982

Nörenberg, W.
Coherent and Incoherent Aspects of Heavy Ion Collisions
Institute of Atomic Energy, Beijing, People's Rep. China, 06.10. 1982

Nörenberg, W.
Transport Theory of Heavy Ion Collisions
Institute of Modern Physics, Lanzhou, People's Rep. China, 08.10. 1982

Nörenberg, W.
Dissipative Diabatic Dynamics
University of Lanzhou, People's Rep. China, 09.10. 1982

Nörenberg, W.
Dissipative Diabatic Dynamics
Institute of Nuclear Science, Tokyo, Japan, 15.10. 1982

Nörenberg, W.
Interplay of Coherent and Incoherent Aspects in Large-Amplitude Collective Nuclear Motion
University of Tokyo, Japan, 16.10. 1982

Nörenberg, W.
Six Lectures on Transport Theories of Heavy Ion Collisions
Louvain-la-Neuve, Belgium, 27.-29.10. 1982

von Oertzen, W.
Neutronentransfer zwischen Zinnisotopen
TU München, Germany, 28.05. 1982

Olmi, A.
Collisions between Heavy Ions
University of California, USA, 01.07. 1982

Poskanzer, A.M.
4π Measurements of Relativistic Heavy Ion Reactions
Lawrence Livermore Laboratory, Livermore, USA, 17.06. 1982

zu Putlitz, G.
Atom- und kernphysikalische Experimente mit schweren Ionen bei GSI
Paderborn, Germany, 11.02. 1982

zu Putlitz, G.
Atom- und kernphysikalische Experimente mit schweren Ionen bei GSI
Bielefeld, Germany, 12.02. 1982

zu Putlitz, G.
Atomic and Nuclear Physics Experiments with Heavy Ions at GSI in Darmstadt
JILA, Boulder, Colorado, USA, 24.02. 1982

zu Putlitz, G.
Atomic and Nuclear Physics Experiments with Heavy Ions at GSI in Darmstadt
Argonne National Laboratory, USA, 26.02. 1982

zu Putlitz, G.
Atom- und kernphysikalische Experimente mit schweren Ionen bei GSI
Siemens, Erlangen, Germany, 11.03. 1982

zu Putlitz, G.
The Role of Management in Basic Research
FOM-Institut, Amsterdam, The Netherlands, 23.04. 1982

zu Putlitz, G.
Experimente mit schweren Ionen bei der GSI in Darmstadt
Universität Mainz, Germany, 27.04. 1982

zu Putlitz, G.
SIS - eine Beschleunigeranlage für schwere Ionen hoher Energie
Max Planck Institut Heidelberg, Germany, 03.06. 1982

zu Putlitz, G.
Künstliche Wasserstoffisotope
Universität München, Germany, 22.06. 1982

zu Putlitz, G.
Experiments with Heavy Ions at GSI - the German Heavy Ion Laboratory
University of Bloomington, USA, 29.09. 1982

zu Putlitz, G.
Overview of Science in West Germany - GSI and New Elements
IBM Scientific Center, Palo Alto, USA, 01.10. 1982

zu Putlitz, G.
Atomic and Nuclear Physics with Heavy Ions at GSI
City College, New York, USA, 06.10. 1982

zu Putlitz, G.
SIS - die Beschleunigeranlage für hochenergetische schwere Ionen der GSI
Todtnauberg, Germany, 07.10. 1982

zu Putlitz, G.
Forschungseinrichtungen und Volkswirtschaft: Möglichkeiten und Grenzen des Technologietransfers aus den Großforschungseinrichtungen
BMFT, Bonn, Germany, 14.10. 1982

zu Putlitz, G.
Experimente mit schweren Ionen bei der GSI in Darmstadt
Universität Göttingen, Germany, 22.11. 1982

zu Putlitz, G.
GSI: Overview Nuclear Physics; Outlook on New Accelerators
Institute of Modern Physics, Lanzhou, People's Rep. China, 07.12. 1982

zu Putlitz, G.
GSI: Atomic Physics with Heavy Ions; Application of Heavy Ions in Solid State Physics and Biology
Institute of Modern Physics, Lanzhou, People's Rep. China, 08.12. 1982

zu Putlitz, G.
Recent Advances in Atomic and Solid State Physics with Techniques adopted from Nuclear and Particle Physics
Institute of Modern Physics, Lanzhou, People's Rep. China, 09.12. 1982

zu Putlitz, G.
Recent Advances in Solid State and Nuclear Physics at GSI
Atomic Energy Institute, Peking, People's Rep. China, 11.12. 1982

Riedesel, H.
Cluster Formation Observed with the Plastic Ball and the Question of Entropy Production in High Energy Nuclear Collisions
Lawrence Berkeley Laboratory, Berkeley, USA, 16.11. 1982

Ritter, H.G.
First Experiments with the Plastic Ball
Max Planck Institut für Kernphysik, Heidelberg, Germany, 07.02. 1982

Roeckl, E.
Protonenradioaktivität und andere exotische Eigenschaften neutronenarmer Kerne
Universität Mainz, Germany, 11.05. 1982

Roeckl, E.
Protonenradioaktivität und andere exotische Eigenschaften exotischer Kerne
Universität Göttingen, Germany, 14.05. 1982

Roeckl, E.
Proton Radioactivity and other Exotic Properties of Nuclei far from the Valley of Beta Stability
Chalk River Nuclear Laboratories, Chalk River, Canada, 23.09. 1982

Roeckl, E.
Physikalische Grundlagen der Kernwaffen
Technische Hochschule Darmstadt, Germany, 04.11. 1982

Roeckl, E.
Kernprotonenzerfall und andere exotische Kerneigenschaften weitab von der Betastabilitätslinie
Universität Braunschweig, Germany, 09.11. 1982

Roeckl, E.
Tandembeschleuniger als ultrasensitive Massenspektrometer
Universität Mainz, Germany, 25.11. 1982

Salzborn, E.
Experiments with Multiply Charged Ions: Charge Transfer and Electron Impact Ionization
University of Aarhus, Denmark, 22.03. 1982

Salzborn, E.
Transfer-Ionization in Collisions between Multiply Charged Ions and Atoms
Arifov Institute of Electronics, Taschkent, USSR, 17.09. 1982

Salzborn, E.
Transfer-Ionization in Collisions between Multiply Charged Ions and Atoms
Ioffe Physical-Technical Institute, Leningrad, USSR, 21.09. 1982

Salzborn, E.
Transfer-Ionization in Collisions between Multiply Charged Ions and Atoms
Lebedev Physical Institute, Moskau, USSR, 22.09. 1982

Salzborn, E.
Atomic and Electronic Collisions Involving Low Energy Multiply Charged Ions
Institut de Physique, Universite Louvain la Neuve, Belgium, 06.10. 1982

Salzborn, E.
Electron Capture and Electron Ionization of Multiply Charged Ions
Culham Laboratory, Abingdon, UK, 25.10. 1982

Salzborn, E.
Transfer-Ionization and Electron Impact Ionization Involving Multiply Charged Ions
University College, London, UK, 27.10. 1982

Salzborn, E.
Transfer-Ionization and Electron Impact Ionization Involving Multiply Charged Ions
University of Newcastle upon Tyne, UK, 29.10. 1982

Salzborn, E.
Transfer-Ionisation in Stößen zwischen mehrfach geladenen Ionen und Atomen
Universität Gießen, Germany, 13.12. 1982

Sandoval, A.
Streamer Chamber Experiments
International Conference Nucleus-Nucleus Collisions, East Lansing, USA, September 1982

Sann, H.
MUSIC at HISS
Texas A + M University, College Station, USA, November 1982

Sann, H.
MUSIC at HISS
Oak Ridge National Laboratory, USA, November 1982

Schädel, M.
Formation of Heavy, Neutron-Rich Actinides in Heavy-Ion Reactions
Lawrence Livermore National Laboratory, Livermore, USA, 16.11. 1982

Schartner, K.-H.
Hochauflösende Röntgenspektroskopie bei Schwerionenstößen
Physikalische Technische Bundesanstalt, Braunschweig, Germany, 18.11. 1982

Schwalm, D.
Gegenwart und Zukunft der γ-Spektroskopie
Max Planck Institut für Kernphysik, Heidelberg, Germany, 14.01. 1982

Schwalm, D.
Zur Struktur schnell rotierender Atomkerne
Institut für Strahlenphysik, Stuttgart, Germany, 12.02. 1982

Schwalm, D.
Positronenerzeugung in Schwerionenstößen
Eidgenössische Technische Hochschule, Zürich, Switzerland, 27.04. 1982

Schwalm, D.
Zur Struktur schnell rotierender Atomkerne
Universität Bonn, Germany, 11.06. 1982

Schwalm, D.
Positronen aus Schwerionenstößen
Universität Heidelberg, Germany, 12.07. 1982

Schwalm, D.
Positronenerzeugung in Stößen schwerer Ionen
Technische Universität München, Germany, 21.07. 1982

Schwalm, D.
Electromagnetic Properties of High Spin States
University Pittsburgh, USA, 05.11. 1982

Schwalm, D.
Positronenerzeugung in Schwerionenstößen
Universität Göttingen, Germany, 26.11. 1982

Sepp, W.-D.
Hartree-Fock-Rechnungen in Atomen und atomaren Stoßsystemen
Universität Gießen, Germany, 29.04. 1982

Siegert, G.
Cinq Annees de Recherche avec des Ions Lourds a GSI Darmstadt
Centre d'Etudes Nucleaires de Bordeaux-Gradignan, France, 25.02. 1982

Siegert, G.
Heavy Ion Research at GSI
Institut Laue Langevin, Grenoble, France, 17.11. 1982

Simon, R.S.
Erste Experimente mit der Darmstadt-Heidelberger NaJ Kristallkugel
Universität Mainz, Germany, 27.05. 1982

Simon, R.S.
First Experiments with the Darmstadt-Heidelberg NaI Crystal Ball
Vrije Universiteit Amsterdam, The Netherlands, 21.06. 1982

Simon, R.S.
Search for the Axion Decay of Triplet Positronium
University of Tokyo, Japan, 12.07. 1982

Simon, R.S.
First Results from the Darmstadt-Heidelberg NaI Crystal Ball
Centre de Spectrometry Nucleaire et Spectrometrie de Masse, Orsay, France, 29.10. 1982

Simon, R.S.
γ Ray Spectroscopy with the Darmstadt-Heidelberg Crystal Ball
Nuclear Research Center, Petten, The Netherlands, 15.10. 1982

Soff, G.
Elektronenanregung in superschweren Quasiatomen
Universität Gießen, Germany, 15.04. 1982

Soff, G.
Superschwere Quasiatome
Universität Frankfurt, Germany, 19.05. 1982

Spohr, R.
Herstellung feinster Strukturen in Festkörpern durch Ätzen von Kernspuren
Max Planck Institut für Festkörperforschung, Stuttgart, Germany, 19.05. 1982

Stachel, J.
Triaxialität um A=100 - Was sagen uns elektromagnetische Momente über die Kerngestalt?
Technische Universität und Universität München, Germany, 14.05. 1982

Stachel, J.
Information über die Kernform aus elektromagnetischen Momenten
Technische Hochschule, Darmstadt, Germany, 28.10. 1982

Stachel, J.
Triaxiale Kerndeformation im Massenbereich A=100
Hahn-Meitner-Institut, Berlin, Germany 06.12. 1982

Stachel, J.
Kernstruktur des Übergangskerns ^{104}Ru
Universität Göttingen, Germany, 17.12. 1982

Stelzer, H.
Gas Filled Heavy Ion Detectors
Technische Hochschule Darmstadt, Germany, 06.12. 1982

Stock, R.
Moderne Gasdetektoren
Technische Universität Berlin, Germany, October 1982

Stock, R.
Kernphysik komprimierter Materie
Universität Bochum, Germany, October 1982

Stock, R.
Kernmaterie hoher Dichte
Technische Hochschule Darmstadt, Germany, December 1982

Stock, R.
The Nuclear Matter Equation of State
Lawrence Berkeley Laboratory, Berkeley, USA, April 1982

Ströbele, H.
Exclusive Analysis of Relativistic Heavy Ion Collisions
CERN Colloquium, Geneve, Switzerland, 20.04. 1982

Warwick, A.I.
The Breakup of High Excited Nuclear Residues
Lawrence Berkeley Laboratory, Berkeley, USA, August 1982

Weiner, R.M.
Coherence Phenomena in High Energy Physics
University of California, Irvine, USA, March 1982

Weiner, R.M.
Coherence Phenomena in High Energy Physics
Triumpf, Vancouver, Canada, March 1982

Weiner, R.M.
Centauros as a Superfluorescence Phenomenon
University of Torino, Italy, October 1982

Westmeier, W.
Fusion und tief-inelastische Reaktionen am System $^{132}Xe + ^{nat}Fe$
Universität Stuttgart, Germany, 10.12. 1982

Winkelmann, K.
Investigating Scientific Computations to Aid in the Design of Supercomputers
IBM Palo Alto Scientific Center, Palo Alto, California, USA, 19.05 1982

Winkelmann, K.
The Experiment Data Acquisition and Analysis System at GSI
National Magnetic Fusion Energy Computer Center, Livermore, USA, 21.05. 1982

Wollersheim, H.J.
Einfluß des Stoßparameters auf die Elementverteilung in stark gedämpften Reaktionen
Hahn-Meitner-Institut, Berlin, April 1982

7.1.4 Lectures and Courses

H. Bokemeyer	Einführung in die experimentellen Methoden und Ergebnisse der Schwerionenforschung I und II (Universität Frankfurt)
I. Giese	Rechnergestütztes Konstruieren (CAD) (FH Darmstadt)
S. Glückert	Programmierung wissenschaftlich-technischer Probleme (FH Darmstadt)
S. Glückert	Rechnerarchitektur (FH Darmstadt)
G. Herrmann	Kernchemie I und II (Universität Mainz)
G. Herrmann	Kernchemisches Praktikum I und II (Universität Mainz)
G. Herrmann	Seminar für Kern- und Kosmochemie (Universität Mainz)
G. Herrmann	Chemisches Kolloquium (Universität Mainz)
R. Keller	Seminar über Ionenquellen (FH Wiesbaden-Rüsselsheim)
J. Klabunde	Grundlegende Kapitel der Physik (FH Darmstadt)
D. Liesen	Physik für Informatiker (FH Darmstadt)
D. Liesen	Physikalisches Praktikum für Elektrotechniker (FH Darmstadt)
P. Mokler, A. Richter	Seminar zu speziellen Problemen der Atomphysik (TH Darmstadt)
P. Mokler	Übungen zur Physik I (TH Darmstadt)
G. Soff	Mathematische Methoden in der Theoretischen Physik (Universität Frankfurt)
G. Soff	Numerische Verfahren in der Theoretischen Physik (Universität Frankfurt)
R. Stock	Interdisziplinäre Kernphysik (Universität Marburg)
R. Stock, J. Knoll	Seminar Hochenergie-Kernreaktionen (GSI Darmstadt)
K. Winkelmann	FORTRAN für Fortgeschrittene (FH Darmstadt)

7.2.1 Conferences and Seminars on Research Proposals

03.02. 1982	Research Seminar Biology and Nuclear Track Technology
04.02. 1982	Research Seminar Nuclear and Atomic Physics
16.03.-08.04. 1982	Introduction to Heavy Ion Research for Students
28.03.-03.04. 1982	International Workshop on Heavy Ion Induced Thermo-nuclear Fusion
29.04. 1982	Scientific Meeting on Account of the Starting of the Upgraded UNILAC
30.04. 1982	Research Seminar Nuclear Physics and Applied Heavy Ion Research
07.06.-09.06. 1982	Workshop on Models of the Energy Deposition of Ionizing Radiation and the Biological Response
24.06. 1982	Research Seminar Nuclear and Atomic Physics
30.08.-22.10. 1982	Introduction to Heavy Ion Research for Students
09.09. 1982	Research Seminar Atomic Physics Especially at 1.4 MeV/u and Nuclear Physics
15.11. 1982	Research Seminar Nuclear Physics and Biology
24.11. 1982	Workshop on the Applications of Heavy Ions from a Synchrotron in Science of Medicine

7.2.2 Seminars at GSI

12.01.	W. Essel Heidelberg	Das on-line System "DASSY" am MPI in Heidelberg
12.01.	H.G. Ritter Darmstadt/ Berkeley	Erste Experimente mit dem Plastikball
12.01.	P. Trüol Zürich	Pion-induzierte magnet. Übergänge in Kernen
13.01.	D. Böhne Darmstadt	UNILAC-Betrieb nach dem Umbau
19.01.	H. Orff Darmstadt	Das System IBM 3081
19.01.	S. Hofmann Darmstadt	Proton-Radioaktivität von ^{151}Lu und ^{147}Tm
20.01.	K. Blasche Darmstadt	Projektvorschlag SIS
26.01.	R. Renfordt Darmstadt/ Berkeley	Observation of Pions in Relativistic Ar on KCl Collisions
26.01.	H. Ströbele Darmstadt	Semi Exclusive Analysis of Relativistic Heavy-Ion Reactions
26.01.	H. Faissner Aachen	Evidenz for the Axion
27.01.	A. Ghiorso Berkeley	Heavy-Element Research at Berkeley
02.02.	F. Weik Berkeley	On-line Datenverarbeitung für den Plastik-Ball und die Streamer-Kammer in Berkeley
02.02.	B. Combridge Abington	Heavy Flavor Production
02.02.	H.I. Miettinen Helsinki	Quark Gluon Plasma
09.02.	K. Schwinn Darmstadt	Der AGF-Plot-File und das neue deviceunabhängige Graphikkonzept bei der GSI
09.02.	U. Wambach Darmstadt	Generierung und Benutzung der lokalen Datenbasis in der µP-CAMAC-Kopplung
09.02.	F. Fraenkel Rehovot	Neutron, Proton and α-Emission in Deep Inelastic Collisions of ^{16}O on ^{40,44,48}Ca at 102 MeV and 142 MeV
10.02.	H.L. Yadav Darmstadt	Effects of Local Equilibration on Cross-Sections for Dissipative Heavy-Ion Collisions
10.02.	G. Kraft Darmstadt	Projektvorschlag SIS Biolog. und mediz. Experimente
17.02.	B. Strack Berlin	Fokker-Planck Equation in Deeply Inelastic Collisions
17.02.	M. Suter Zürich	Massenspektrometrie seltener Radioisotope mit Hilfe von Teilchenbeschleunigern
24.02.	K. Aleklett Studsvik	Heavy-Target Fragmentation in Relativistic and Intermediate Energy Heavy-Ion Collisions
11.03.	G. Paul Yorktown Heights	Vectran and Proposed Vector Array Extensions to AINSI FORTRAN
26.03.	B. Jonson Genf	Status of the Electron-Neutrino Mass Experiment at ISOLDE
20.04.	S. Barshay Aachen	Multiplicity Distributions of Charged Particles Produced in Energetic Collisions
20.04.	M. Rho Saclay	Quarks in Nuclei
21.04.	Ch. Toepffer Erlangen	Dämpfung von RPA Schwingungen
27.04.	K. Klingenbeck Erlangen	Pionische Fusion in Kern-Kern Stößen
27.04.	N. Porile Perdue/ Marburg	Fragment Emission in High Energy Nuclear Reactions
28.04.	K. Dietrich München	Heavy-Ion Reactions in the Energy Range of 15 to 800 MeV/u. Review of Existing Theoretical Approaches
04.05.	I. Giese Darmstadt	Der neue GNOM
04.05.	H.R. von Gunten Würenlingen	Produktion von Aktinidenelementen in Reaktionen von Sauerstoff und Neon mit ^{248}Cm und ^{249}Cf
05.05.	M. Bernas Orsay	^{14}C Beam as a Tool for Spectroscopy of Neutron-Rich Nuclei
11.05.	Fr. Pankrath Darmstadt	DF/EF und HSM
11.05.	S. Bashkin Arizona/ Bochum	Beam Foil Interaction Mechanism
12.05.	M. Huyse Leuven	Studies of Neutron-Deficient Isotopes below Tin, using the LISOL on-line Separator at Louvain-La-Neuve
18.05.	H. Jauss Darmstadt	DATEX/P Kommunikations Protokolle
18.05.	R. Brockmann Darmstadt/ Berkeley	π-Observables in Ar*KCl Collisions
18.05.	A. de Rujula Genf	Neutrino Masses
19.05.	W. Nörenberg Darmstadt	Transport Equations for the Initial Energy Dissipation in Heavy-Ion Collisions
19.05.	S. Hübener Rossendorf	Chemische Untersuchungen schwerer Aktiniden
25.05.	J. Knoll Darmstadt	Impressions from the Bielefeld Workshop
25.05.	V. Soergel Hamburg	Neuere Ergebnisse von Petra

26.05.	W. Nörenberg Darmstadt	Transport Equations for the Initial Energy Dissipation in Heavy-Ion Collisions
26.05.	W. Kraft-Weyrather Darmstadt	Ziele des Biologie-Workshops am 7./8.6.82
08.06.	H. Klemens Darmstadt	MVS unter VM
08.06.	H. Baumgart Frankfurt	Untersuchungen zu kollektiven Vorgängen im relat. Kern-Kern Stoß mit Teilchenspurdetektoren
08.06.	C.A. Tobias Berkeley	The Berkeley Experience with Accelerated Heavy-Ions in Cancer Radiobiology and Therapy
09.06.	J. Kuti Santa Barbara/ Budapest	Fermions on the Lattice
14.06.	V. Hughes New Haven	Internal Spin Structure of the Proton
15.06.	A. Remler Willimsburg	Deuteron Production in Relat. Nuclear Collisions
15.06.	V.I. Goldanski Moscow	Quantum Kinetics of Low Temperature Chemical Reactions
16.06.	N. Balasz Stony Brook	Quantum Maps
16.06.	D. Habs Heidelberg	Neueste Ergebnisse von der Darmstadt/Heidelberg Kristallkugel
22.06.	B. Mottelson Copenhagen	Collective and Single-Particle Aspects of Nuclear Rotation
23.06.	U. Smilansky Rehovot	Comments on the Classical Interpretation of the Interacting Boson Model
29.06.	H. Satz Bielefeld	Das Quark-Gluon Plasma in der QCD
14.07.	I.S. Grant Manchester	In-Beam Measurements on Light Tin Isotopes and Plans for Experiments at the Daresbury Tandem
17.08.	K. Winkelmann Darmstadt	DV im IBM Forschungszentrum in Yorktown Heights
28.07.	R. Emmerson England	Präsentation der Erfahrungen im Hard- und Software Entwurf mit dem IAPX 432
25.08.	D. Hartwig Darmstadt	Finanzielle Förderung der Kernphysik in der Bundesrepublik
27.08.	M. Gai New Haven	Moleculare Dipole Bands in ^{8}Be, ^{18}O and ^{218}Ra
31.08.	G. Zaidmann Darmstadt	Implementation of GDDM in the Graphics System at GSI
31.08.	J. Harris Berkeley/ Darmstadt	Pion Production and Compression Effects in Nuclear Collisions
01.09.	K. Winkelmann Darmstadt	Wie macht man große Rechner schneller
08.09.	F.K. Wohn Ames	New Aspects of the Onset of Deformation at N=90
10.09.	A. Menchaca-Rocha Grenoble/ Mexico	Systematics of ^{16}O-induced Reactions at E = 10-20 MeV/u
15.09.	U. Müller GSI	Positronenerzeugung in Stössen mit nuklearem Kontakt
21.09.	D.E. Lang New York	Vector Processors of the Future
22.09.	K.P. Lieb Göttingen	Struktur der Kr- und Ru-Isotope
29.09.	G. Münzenberg H. Geißel Darmstadt	Neues zum Element 109 Experimente zum Energieverlust von schweren Ionen in Materie
06.10.	Y. Gambhir München	Microscopic Interpretation of the Interacting Boson Model
12.10.	H.W. Meuer Mannheim	Zur Auswahl von Universalrechnern
13.10.	D. Hamilton Sussex	Nuclear Spectroscopy of Short Lived Isotopes
19.10.	M. Reiser Maryland/ Darmstadt	Auf der Suche nach neuen Teilchenbeschleunigermethoden
20.10.	T. Tamura Austin/ München	Description of Nuclear Collective Motion in Terms of Boson Expansion Theory
26.10.	M.G. Huber Erlangen	Pionische Fusion: Ein Beispiel einer kohärenten Kernreaktion
27.10.	J. Klabunde Darmstadt	Status und Probleme der UNILAC Strahlführung in der Experimentierhalle
02.11.	I. Giese Darmstadt	Der neue GNOM
02.11.	R. Stock Darmstadt	Kernmaterie bei hoher Dichte und Temperatur
03.11.	J. Vieira Los Alamos	The LAMPF Time-of-Flight Spectrometer for Precision Mass Measurements
09.11.	H.-J. Lustig Darmstadt	Erfahrungen mit dem Vektorprozessor FPS-164 bei der GSI
09.11.	O. Haxel Heidelberg	Hans Geiger und die Physik seiner Zeit
10.11.	H. Hofmann München	Nuclear Collective Coordinates as Quantum Variables and a Self-Consistent Description of Damped Vibrations
10.11.	H. Grawe Berlin	Spektroskopie in ^{96}Pd und das Schalenmodell in der Nähe von ^{100}Sn
16.11.	H. Göringer Darmstadt	Dokumentation und interaktives "HELP" im "SATAN"
16.11.	S. Björnholm Copenhagen	Meilensteine in Schwerionenreaktionen
23.11.	M. Danos Washington	Die Entstehung des Quark-Gluon-Plasmas
23.11.	W. Hillebrandt München	Supernova Explosionen massenreicher Sterne

24.11.	C. Yannouleas Darmstadt	Nuclear Dissipation as Damping of Collective Motion in the Time-Dependent RPA and Extensions of it
24.11.	S.G. Kadmensky Woronesh	Beta-Delayed α-Particles and Protons from Neutron-Deficient Nuclei
30.11.	D.C. Marinescu Darmstadt	Using Cross-Memory for Programm and Data Sharing under MVS
30.11.	L. Camilieri Genf	High p Production in α-α Collision at the ISR
30.11.	K. Maier Stuttgart	Elementarteilchen im Dienste der Festkörperforschung, Pionen als Sonden in Kristallen
01.12.	W. Cassing Darmstadt	Perspectives of Diabatic Single-particle Motion in Heavy-Ion Collision
01.12.	M. Richter Darmstadt	Überlegung zur Experimentdatenverarbeitung bei der GSI
07.12.	R. Kenneson Yorktown Heights	Electronic Mail under MSV/TSO
08.12.	G. Delic Darmstadt	Theory of Charge Exchange in H.I.C.
08.12.	P. Armbruster H. Gäggeler Darmstadt	Neue Versuche sur Synthese superschwerer Elemente mit SASSY am LBL
14.12.	K. Schwinn Darmstadt	Basis Graphik in der GSI
	W. Kynast Darmstadt	Speicherverwaltung im PL1
14.12.	H. Gutbrod Darmstadt	Neue Ergenisse vom Plastik-Ball
14.12.	J.V. Krogh Heidelberg	Interferenz von elektromagn. und schwacher Wechselwirkung in e -e Reaktionen
15.12.	H. Dertinger Karlsruhe	Zellkomunikation und Strahlenempfindlichkeit
21.12.	A. Lukasiak Darmstadt	Diabatic Representation in Heavy-Ion Collisions
22.12.	P. Armbruster H. Gäggeler	Neue Versuche zur Synthese superschwerer Elemente mit SASSY am LBL

7.2.3 GSI-Preprints 1982

82 - 1 O. Klepper, T. Batsch, S. Hofmann, R. Kirchner, W. Kurcewicz, W. Reisdorf, E. Roeckl, D. Schardt, G. Nyman
Direct and Beta-Delayed Proton Decay of Very Neutron-Deficient Rare-Earth Isotopes in the Reaction $^{58}Ni + ^{92}Mo$

82 - 2 J. Knoll, L. Münchow, G. Röpke, H. Schulz
Deuteron Production - an Entropy Puzzle?

82 - 3 A.H. Blin, S. Bohrmann, J. Knoll
Energetic Particles Emitted from Energetic Nuclear Reactions

82 - 4 G. Soff, T. de Reus, B. Müller and W. Greiner
δ-Electron Production Rates in the Superheavy System Br + Pb

82 - 5 P. Armbruster
Cold Rearrangement of Nucleons in Fission and Fusion

82 - 6 D. Liesen
What do we Know About Superheavy Quasiatoms

82 - 6a G. Soff, P. Schlüter, B. Müller, and W. Greiner
The Self-energy of Electrons in Critical Fields

82 - 7 J.V. Kratz
The Search for Superheavy Elements

82 - 8 H. Stöcker, G. Buchwald, L.P. Csernai, G. Gräbner, P.R. Subramanian, J. Theis, J.A. Maruhn, W. Greiner, M. Gyulassy, K. Frankel, K.K. Gudima, V.D. Toneev
Microscopic and Macroscopic Models for Nuclear Collisions at Medium and High Energies

82 - 9 G. Herrmann, N. Trautmann
Rapid Chemical Methods for Identification and Study of Short Lived Nuclides

82 - 10 A. Plochocki, J. Zylicz, R. Kirchner, E. Roeckl, P. Tidemand-Petersson, I.S. Grant, P. Misaelides
Masses of very Neutron-Deficient Isotopes in the Cadmium-to-Cesium Region

82 - 11 J. Stachel, N. Kaffrell, E. Grosse, H. Emling, H. Folger. R. Kulessa, D. Schwalm
Triaxiality and its Dynamics in ^{104}Ru Investigated by Multiple Coulomb Excitation

82 - 12 U. Brosa, W. Cassing
Numerical Studies on the Phase-Space Evolution of Relative Motion of two Heavy Ions

82 - 13 W. Cassing, A. Lukasiak, W. Nörenberg, S.J. Wang, G.O. Xu, and H.L. Yadav
Aspects of Diabatic Single-Particle Motion Motion in Heavy-Ion Reactions

82 - 14 W. Funk
A Report on the Symposium on Accelerator Aspects of Heavy-Ion Fusion at GSI March 29 - April 2, 1982

82 - 15 W. Kurcewicz, E.F. Zganjar, R. Kirchner, O. Klepper, E. Roeckl, P. Komninos, E. Nolte, D. Schardt, and P. Tidemand-Petersson
Investigations of Very Neutron-Deficient Isotopes Below ^{100}Sn in ^{10}Ca-Induced Reactions

82 - 16 M. Petrovici, R. Bock, M. Dakowski, A. Gobbi, G. Guarino, S. Gralla, K.D. Hildebrand, U. Lynen, W.F.J. Müller, A. Olmi, G. Rudolf, H. Sann, H. Stelzer, J. Toke, H.J. Wollersheim,
Fast Processes Induced by Heavy Projectiles at Incident Energies of 10 - 20 MeV/u

82 - 17 G. Soff, U. Müller, T. de Reus, P. Schlüter, A.Schäfer, J. Reinhardt B. Müller, and W. Greiner
Electron Excitation Processes and Quantum Electrodynamics in High-Z Systems

82 - 18 P. Tidemand-Petersson, A. Plochocki
Resonance Structure in the Beta-Strength Function Indicated by Beta-Delayed Particle Emission from $^{110,112}I$, ^{113}Xe, $^{114,116}Cs$ and ^{117}Ba

82 - 19 G. Soff, W. Greiner
Electronic Transition Times in Supercritical Compound Systems

82 - 20 G. Herrmann
Proc. of the Actinides-1981 Conference, Actinides in Perspective Summary: Nuclear Science

82 - 21 M. Gyulassy
Critical Dynamics in Nuclear Collisions

82 - 22 J. Kuti and J. Polonyi
Some Applications of a New Stochastic Method in Lattice Theorie

82 - 23 J. Knoll
The Dynamics of Heavy Ion Reactions at Relativistic Energies

82 - 24 H.F. Beyer, R. Mann, F. Folkmann
X-Rays and Auger Electrons from Few-Electron Recoil Ions

82 - 25 S. Ayik, W. Nörenberg
Time-Dependent Shell-Model Theory of Dissipative Heavy-Ion Collisions

82 - 26 B. Müller, J. Reinhardt, W. Greiner, G. Soff
Critical Remarks on a Scaling Law for Inner- shell Ionization

82 - 27 G. Seiler-Clark, D. Pelte, H. Emling, A. Balanda, H. Grein, E. Grosse, R. Kulessa, D. Schwalm, H.J. Wollersheim M. Hass, G.J. Kumbartzki and K.H. Speidel
Magnetic Moments in the Backbending Region of ^{158}Dy

82 - 28 G. Soff, U. Müller, T.de Reus, P. Schlüter J. Reinhardt, B. Müller, W. Greiner
Electron Excitation and Positron Emission in Quasi-Molecular Collisions of very Heavy Ions

82 - 29 E. Roeckl
Exotic Nuclei in Deep-Inelastic and Fusion Reactions

82 - 30 P. Armbruster
Heavy Ion Fusion and Exotic Nuclei Studies at SHIP

82 - 31 R. Stock, R. Bock, R. Brockmann, A. Dacal, J.W. Harris, M. Maier, M.E. Ortiz, H.G. Pugh, R.E. Renfordt, A. Sandoval, L.S. Schroeder, H. Ströbele, and K.L. Wolf
Compression Effects in Relativistic Nucleus- Nucleus Collisions

82 - 32 H. Ströbele, R. Brockmann, J.W. Harris, F. Riess, A. Sandoval, R. Stock, K.L. Wolf, H.G. Pugh, L.S. Schroeder, K. Tittel, M. Maier
Charged Particle Exclusive Analysis of Central $Ar^{+}KCl$ and $Ar^{+}Pb$ Reactions at 1.8 and 0.8 GeV/u

82 - 33 W. Cassing, W. Nörenberg
On the Role of Memory Effects for Dissipation and Diffusion in Slow Collective Nuclear Motion

82 - 34 E. Runte, W.-D. Schmidt-Ott, P. Tidemand-Petersson, R. Kirchner, O. Klepper, W. Kurcewicz, E. Roeckl, N. Kaffrell, P. Peuser, K. Rykaczewski, M. Bernas, P. Dessagne, and M. Langevin
Decay Studies of Neutron-Rich Products from ^{76}Ge-induced Multinucleon Transfer Reactions Including the new Isotopes ^{62}Mn, ^{63}Fe and $^{71\ 72\ 73}Cu$

82 - 35 D. Schwalm
Electromagnetic Properties of High Spin States

82 - 36 W. Nörenberg
Dissipative Diabatic Dynamics

82 - 37 O. Klepper, E. Roeckl
Fast on-line Spectrometry of Exotic Nuclei

82 - 38 W. Reisdorf, F.P. Heßberger, K.D. Hildenbrand, S. Hofmann, J.V. Kratz, G. Münzenberg, K.H. Schmidt, J.H.R. Schneider, W.F.W. Schneider, K. Sümmerer, G. Wirth
Influence of Collective Surface Motion on the Threshold Behaviour of Nuclear Fusion

82 - 39 H. Stelzer
Gas Filled Heavy Ion Detectors

82 - 40 N. Trautmann, M. Weber, D. Gembalies-Datz, R. Heimann, H. Folger and W. Hartmann
Preparation of Actinide Targets by Molecular Plating

82 - 41 H. Folger, J. Klemm and M. Müller
Preparation of Nuclear Accelerator Targets by Focused Ion Beam Sputter Deposition

7.2.4 GSI-Reports 1982

82 - 1 Scientific Report 1981

82 - 2 SIS Proposal (deutsche Version)

82 - 3 G. Soff
Elektronenanregung in überschweren Quasimolekülen

82 - 4 G. Herrmann
Gibt es superschwere Atomkerne?
Ein Kapitel moderner Alchemie.

82 - 5 A. Baden, H.H. Gutbrod, H. Löhner, M.R. Maier, A.M. Poskanzer, T. Renner H. Riedesel, H.G. Ritter, H. Spieler, A. Warwick, F. Weik, H. Wieman
The Plastic Ball Spectrometer--an Electronic 4π Detector with Particle Identification

82 - 6 Studies on the Feasibility of Heavy-Ion Beams for Inertial Confinement Fusion
Annual Report 1981

82 - 7 L.W. Funk and R.W. Müller
Derivation of an Elementary RFQ Formulary

82 - 8 Proceedings of the Symposium on Accelerator Aspects of Heavy Ion Fusion
GSI, Darmstadt, March 29 to April 2, 1982

82 - 9 P. Zielinski
Nucleus Fragmentation Induced by a High-Energy Hadron
Some Experimental Results
Part III

82 - 10 F + E Programm 1983 - 1985

82 - 11 M. Müller, K.-D. Leible, B.H. Wolf and N. Angert
Special Ion Beam Production by Sputtering of Metal Mixtures and Alloys in the PIG Ion Source

82 - 12 H. Geissel
Untersuchungen zur Abbremsung von Schwerionen in Materie von (0,5-10) MeV/u

82 - 13 P. Zielinski
Nucleus Fragmentation Induced by a High-Energy Hadron
Some Experimental Results
(Reports I, II, III)

82 - 14 K.E. Stiebing, H. Schmidt-Böcking, W. Schardt, K. Bethge, P.H. Mokler, F. Bosch, D. Liesen, P. Vincent, R. Schuch, S. Hagmann
Zur Spektroskopie des 1sσ-Orbitals in superschweren Stoßsystemen. Messung der Emissionswahrscheinlichkeit für die quasimolekulare K-Strahlung am Stoßsystem $^{208}Pb+^{208}Pb$ bei kleinen internuklearen Abständen

82 - 15 Jahresbericht 1981/1982

82 - 16 A. Sandoval, R. Bock, R. Brockmann, A. Dacal, J.W. Harris, M. Maier, M.E. Ortiz, H.G. Pugh, W. Rauch, R.E. Renfordt, F. Riess, L.S. Schroeder, R. Stock, H. Ströbele, and K.L. Wolf
Streamer Chamber Experiments

82 - 17 R. Könnecke
Nukleonen-Transfer am Beispiel der $^{13}C(^{13}C,^{12}C)^{14}C$ - Reaktion

7.2.5 Visiting Groups at GSI

11.01.	Brecht-Schule, Darmstadt	13
21.01.	Studentenprogramm	28
23.01.	Viktoria Gymnasium, Darmstadt	12
25.01.	Konrad Adenauer Stift., Darmstadt	18
25.01.	Physik Studenten, Univ. Kaisersl.	9
26.01.	Main-Taunus-Schule, Hofheim	45
26.01.	Hohe Landesschule, Hanau	12
26.01.	Schülerpraktikanten	5
27.01.	Ärzte, Elisabethenstift, Darmstadt	17
10.02.	Erasmus-Kittler-Schule, Darmstadt	21
24.02.	Berufl. Schule, Gr. Gerau	18
11.03.	Südhessische Gas-und Wasser AG	11
16.03.	Studentenprogramm	19
25.03.	Rotary-Club, Darmstadt	50
26.03.	Erasmus-Kittler-Schule, Darmstadt	23
29.03.	Kommunale Jugendwoche, Darmstadt	25
30.03.	Ministerium für Wiss. und Kult., Bad.-Württemberg	47
30.03.	Kommunale Jugendwoche, Darmstadt	18
01.04.	FH Heerlen, Niederlande	19
03.04.	Fa. Alfred Teves GmbH, Darmstadt	8
15.04.	Rentner	6
23.04.	Englisches Institut, Heidelberg	15
25.04.	Familientreffen	35
28.04.	Robert-Mayer-Gymnasium, Heilbronn	43
28.04.	Neue Mitarbeiter im BMFT, Bonn	15
03.05.	Gymnasium, Wissen	31
04.05.	Fr. vom Stein Schule, Fulda	45
05.05.	Kommunalpol. Grupppe der Volks-hochschule, Darmstadt	13
07.05.	Pestalozzi Schule, Idstein	9
10.05.	Peter-Petersen Gymnasium, Mannheim	7
10.05.	Fachhochschule, Rüsselsheim	19
11.05.	Adolf-Reichwein Gymn., Heusenstamm	11
11.05.	Transuran-Institut, Karlsruhe	25
12.05.	Studenten, Univ. Mainz	60
13.05.	Fachhochschule Wz/Schweinfurt, Informationstechnik	22
15.05.	Ortsverband Mühlhofen	60
18.05.	Abendgymn. II, Frankfurt	6
19.05.	SPD Frauenverband, Darmstadt	21
19.05.	Astronomieverein, Hattersheim	5
21.05.	Franzosen, Exy sur Eure	55
26.05.	Strahlenzentrum, Gießen	35
27.05.	Abendgymn. I, Frankfurt	17
03.06.	Spektrum der Wissenschaften	20
05.06.	Einlad., z. Putlitz, Heidelberg	120
07.06.	Physikstudenten, Univ. Marburg	13
08.06.	Teilnehmer des Bio-Workshops	15
09.06.	Polizei, Darmstadt	29
09.06.	Transuran-Institut, Karlsruhe	20
14.06.	Leistungskurs Physik, Eleonorenschule, Darmstadt	18
25.06.	Studenten der FH, Darmstadt	24
29.06.	Studenten der FH, Friedberg	40
05.07.	MPI für Kernphysik, Heidelberg	8
08.07.	Physikstudenten, Univ. Tübingen	52
09.07.	Studenten der Betriebswirtschaft, Mannheim	18
16.08.	Viktoria Schule, Darmstadt	25
26.08.	Marienschule Limburg	49
30.08.	Erasmus Kittler Schule, Darmstadt	24
31.08.	Studentenprogramm	20
01.09.	Altenbeirat, Erzhausen	37
28.09.	Fachschule des Heeres	22
28.09.	Gustav-Heinemann-Schule, Rüsselsh.	19
29.09.	Universität Kaiserslautern	11
29.09.	Berufsberater für Abiturienten und Hochschüler	22
08.10.	Laiengruppe	4
14.10.	Amt für Wohnungswesen, Darmstadt	12
01.11.	Physikstudenten, München	2
05.11.	FH Rüsselsheim, Nachrichtentechnik	17
05.11.	FH Rüsselsheim	18
08.11.	Main-Taunus-Gymnasium, Hofheim	15
09.11.	Helmholtz-Gymnasium, Frankfurt	18
09.11.	Techn. Ausbildungsleit.,IBM,Mainz	30
10.11.	Berufsschüler, Dillenburg	44
11.11.	Universität Münster	34
12.11.	Gagern-Gymnasium, Frankfurt	21
13.11.	Laiengruppe	20
23.11.	Gymnasiale Oberstufe, Sontra	60
23.11.	Berufsschule, Dillenburg	11
24.11.	Arbeitstreffen Schwerionen in der Medizin	20
25.11.	FH Fachbereich Informatik, Darmstadt	20
30.11.	Bundeswehr, Gerätedepot	17
02.12.	Ricarda-Huch-Schule, Dreieich	34
03.12.	Gesamthochschule Kassel	22
03.12.	Berufl. Gymn., Frankfurt	22
07.12.	Goethegymnasium, Bensheim	40
16.12.	Gymnasium, Groß Gerau	20
17.12.	Gymnasium, Langen	19
17.12.	Universität Mainz,	9
21.12.	Prälat Diehl Schule, Griesheim	22
and 37 guided tours for alltogether		70

125 groups visited the GSI in 1982
totalizing 2195 visitors.

7.3 Scientific Committees, Directorate and Personnel

Scientific Council

Prof. E.W. Otten (Mainz, Chairman), Prof. P. v.Brentano (Köln), Dr. G. Friedlander (Brookhaven), Dr. H.A. Grunder (Berkeley), Prof. F. Gudden (Erlangen), Prof. P. Gütlich (Mainz), Prof. P. Kienle (München), Dr. H.J. Langmann (Darmstadt), Prof. K.H. Lindenberger (Berlin), Prof. U. Mosel (Gießen), Prof. R.H. Siemssen (Groningen), Prof. V. Soergel (Hamburg)

Users Committee

Prof. H.J. Körner (München, Chairman), Prof. P. Armbruster (GSI), Prof. H. Backe (Mainz), Prof. S. Bjornholm (Kopenhagen), Prof. R. Bock (GSI), Prof. R. Brandt (Marburg), Dr. H. Gäggeler (GSI), Prof. D. Gross (Berlin), Prof. B. Müller (Frankfurt), Dr. G. Münzenberg (GSI), Prof. F. Pühlhofer (Marburg), Prof. D. Schwalm (Heidelberg)

Scientific Directorate

Prof. G. zu Putlitz (Chairman, Scientific and Technical Managing Director), H.O. Schuff (Administrative Managing Director), Dr. N. Angert, Prof. P. Armbruster, Prof. W. Nörenberg

Scientific and Technical Division Leaders

Dr. N. Angert, Prof. P. Armbruster, Prof. R. Bock, Dr. D. Böhne, Prof. G. Herrmann, Prof. W. Nörenberg

Scientific Committee

Dr. E. Roeckl (Chairman), Dipl. Chem. H. Ahrens, Prof. R. Bock, Dr. D. Böhne, Dipl. Chem. H. Folger, Dr. E. Grosse, Dipl. Phys. U. Grundinger, Prof. G. Herrmann, Dr. K.D. Hildenbrand, Dr. J. Knoll, Dr. P. Mokler, Prof. G. zu Putlitz (ex officio), Dr. W. Reisdorf, Dr. M. Richter, Ing. N. Schneider, Dr. R. Spohr, Dipl. Phys. R. Steiner, Dr. P. Strehl

Guest Scientists and Consultants

Y.K. Agarwal (India), S. Ayik (Turkey), F. Azgui (Algeria), A. Balanda (Poland), A. Baran (Poland), J. Batsch (Poland), T. Batsch (Poland), M. Clemente (FRG), H. Dabrowski (Poland), G. Dai (People's Rep. China), M. Dakowski (Poland), R. Devito (USA), K. Dietrich (FRG), J. Doernyei (Hungary), B. Eichler (GDR), Y. Eyal (Israel), A. Fässler (FRG), W. Fan (People's Rep. China), H. Feldmeier (FRG), G.-N. Flerov (USSR), H. Freiesleben (FRG), W. Funk (Canada), J. Greenberg (USA), W. Greiner (FRG), G. Guarino (Italy), J. Harris (USA), M. Hass (Israel), S. Hübener (GDR), K. Hulet (USA), S. Ito (Japan), D. Jiao (People's Rep. China), R. Katz (USA), I. Kelson (Israel), Y. Kido (Japan), M. Kleber (FRG), P. Krejcik (Australia), R. Kulessa (Poland), W. Kurcewicz (Poland), J. Kuti (Hungary), V.-B. Kutner (USSR), J. Kuzminski (Poland), P.-O. Larsson (Sweden), Y. Lazarev (USSR), P. Lemmertz (FRG), B. Liu (People's Rep. China), A. Lukasiak (Poland), U. Lynen (FRG), D. Maor (Israel), I. Maor (Israel), D. Marinescu (Rumania), J. Maruhn (FRG), A.C. Merchant (Great Britain), C. Michel (Belgium), U. Mosel (FRG), U. Müller (FRG), A. Plochocki (Poland), S. Polikanov (FRG), J. Polonyi (Hungary), J. Rafelski (FRG), S. Reinsch (USA), M. Reiser (USA), F. Riess (FRG), P. Ring (FRG), K. Rykaczewski (Poland), A. Sandoval (Mexico), K. Sato (Japan), Ch. Schmelzer (FRG), J. Schweppe (USA), V. Shevelko (USSR), R. Shyam (India), J.D. Silver (Great Britain), Z. Stachura (Poland), W. Swiatecki (USA), A. Szentgali (Hungary), G. Ter-Akopian (USSR), J. Theis (FRG), J. Töke (Poland), L. Turko (Poland), P. Vincent (USA), S.J. Wang (People's Rep. China), A. Warczak (Poland), A. Warwick (Great Britain), H. Wieman (USA), J. Wood (Great Britain), H.L. Yadav (India), C. Yannouleas (Greece), J. Yu (People's Rep. China), G. Zaidman (Israel), E. Zganjar (USA), W. Zhao (People's Rep. China), Y. Zhou (People's Rep. China), I.P. Zielinski (Poland), J. Zychor (Poland)

Scientific Personnel

H. Ahrens, J. Ahrens, R. Albrecht, N. Angert, P. Armbruster, K. Beckert, H. Beyer, K. Blasche, R. Bock, D. Böhne, H. Bokemeyer, F. Bosch, I. Bozsik, G. Breitenberger, R. Brockmann, W. Brüchle, F. Busch, W. Cassing, T.E. Cowan, L. Dahl, H. D. Dohmann, H. Egger, H. Eickhoff, H. Emling, M. Emmerling, J. G. Festag, P. Finke, B. Fischer, H. A. Folger, B. Franczak, B. Franzke, P. Fuchs, H. Gäggeler, I. Giese, J. Glatz, S. Glückert, A. Gobbi, H. Göringer, E. Grosse, U. Grundinger, H. H. Gutbrod, T. Györffy, E-M. Heck, G. Herrmann, F. P. Hessberger, K. Hildenbrand, D.H.H. Hoffmann, J. Hoffmann, S. Hofmann, H. Hultzsch, G. Hutter, W. Jacoby, K. Kaspar, H. J. Keller, R. Keller, M. M. Khaouli, R. Kirchner, J. Klabunde, O. Klepper, J. Knoll, C. Kozhuharov, G. Kraft, T. Kühl, B. Langenbeck, H. D. Liesen, J. Lowsky, H. J. Lustig, R. Mann, D. Marx, P. H. Mokler, G. Moritz, M. Müller, R. Müller, W.F.J. Müller, G. Münzenberg, F. Nickel, H. Nienstädt, W. Nörenberg, A. Olmi, K. Poppensieker, H. B. Prange, G. zu Putlitz, J. Rafelski, W. Reisdorf, M. Richter, C. Riedel, H. G. Ritter, E. Roeckl, H. J. Sann, M. Schädel, E. Schaffner, D. Schardt, K. H. Schmidt, W. Schneider, W.-A. Schönfeldt, A. Schönlein D. Schüll, H. Schulte, R. Schulze, D. Schwalm, O. Siart, G. Siegert, R. Simon, R. Spohr, R. Steiner, H. Stelzer, R. Stock, H. Stöcker, P. Strehl, H. Ströbele, J. Struckmeier, K. Sümmerer, U. Wambach, W. Welzel, K. Winkelmann, G. Wirth, B. Wolf, H. I. Wollersheim, V. Zelba

Technical and Administrative Staff

F. Achenbach, K. Adelberger, J. Alt, W. Amann, S. Andresen, T. Archinal, G. Augustinski, E. Babinsky, A. Bach, H. Balonier, S. Bauer, G. Baumann, E. Bayersdorf, H.-J. Beeskow, K-H. Behr, E. Benz, G. P. Benz, H. J. Benz, W. Bergsträsser, L. Bernhardt, C. Besthorn, H. Bingel, H. Blaschke, W. Bleuel, H. Blinn, F. Bock, W. Bock, W. Bock, E. Bohländer, J. Bolle, P. Borisch, I. Bormet, R. Bormet, J. Bossler, W. Bourgeois, G. Braatz, W. Brenger, H. Britz, A. Brünle, S. Brür, M. Brügger, N. Brunner, C. Bruske, D. Bruske, K. Büttner, E. Burger, K. H. Burkhard, H. G. Burkhard, A. Busch, M. Cartharius, R. Christmann, J-P. Clain, H. Dächert, H. Damm, H. W. Daues, J. R. Dengler, V. Deusser, G. Dick, I. M. Diedrich, R. Diehl, H. Döpke, R. Döring, H. Dünkel, R. Dünkel, O. Eberhardt, H. Eckhardt, K. A. Ehrich, M. F. Eick, G. Eidmann, G. Eisold, E. Eitel, H. Emig, W. Enders, G. Englert, U. Ernst, F. Ertan, A. Fehres, M. Feyerabend, H. Fischer, G. Fliss, M. Fradj, O. Frank, P. W. Frank, G. R. Freiwald, P. Freudenberger, E. Fritsch, G. Fröhlich, G. Fröse, R. Gärtner, H. Gaiser, M. Gambietz, K. D. Ganser, A. Gasper, M. Gassner, H. Gebhardt, I. Georg, E. Gerbig, O. Gerhardt, H. Gilbert, W. Gockel, M-G. Göttmann, V-G. Gomez, K. Graf, B. Grasmück, H. Grein, G. Grill, D. Grimm, G. Grimm, H. Grösch, J. Grösser, H. Gross, J. Gross, J.L. Gundlach, W. Gutowski, E. Häcker, B. Häfner, D. Hager, W. Hahn, P. Hahne, P. Hahnel, H. Hammal, E. Hammann, H. Hardel, O. P. Hartmann, R. Hartmann, W. Hartmann, W. Hartmann, M. Hartung, H. Heckwolf, J. Hehner, T. Heinbüchner, K. Heinz, H. Heller, H. Helms, D. Henke, H. Hewig, J. Hey, K .Hill, F. Himmelmann, C. Hoffmann, R-H. Hoffmann, N. Hofmann, G. Holzschuh, L. Horas, H. Horneff, A. Hotop, R. Hotz, W. v.d.Hoya, W. Huber, W. Hüller, G. Ickert, A. Igel, W. Ille, K. Illert, E. Jäger, H. Jakobi, S. Jansen, K. Jobb, I. Jobst, G-K. Jöst, G. Kaiser, R. Kaiser, H. J. Kalawsky, E. Kammer, W. Kappel, F. Keil, H. L. Kempf, H. R. Kiesewetter, C. P Kiesslich, N. Kischnick, A. Kissler, G. Klappich, H. Klecker, H. Klemm, J. Klemm, S. Klemm, K. Klingler, P. Klink, F. P. Klinke, R. Kluber, K-D. Knapp, U. Kniess, W. Köthe, K. Kohl, B. Kolb, U. Kopf, W. Krall, H. Kraus, K-R. Kress, W. Kreuzer, H. Krichbaum, A. Kritzer, C. Kröh, T. Kroll, L. Krüger, G. Kube, K. Kucharczky, H. Kühn, R. Kühn, J. Kühtz, K.K.B. Küper, W. Kunz, H-P. Kurz, E. Labinsky, H. Lameli G. Langer, H. Larem, G. Ledl, K-D. Leible, G. Leidel, E. Leiser, H. Leiser, W. Leiser, G. Lenz, H. Leonhardt, R. Leonhardt, H. P. Liebold, L. Liebschwager, R. Lischetzki, F. List, N. Lohneis, D. Loos, A. Lorenz, I. Lorenz, W. Losert, M. Ludwig, S. Lüdtke, S. Lüttges, H. Mader, K-H. Mader, E. Magnussen, E. Malwitz, I. Malwitz, H. G. Manns, M. Marquardt, H. G. Martens, W. Marx, R. Matheis, K-H. Matthöfer, R. Mayr, H. Meder, H. Meister, M. Melchior, K. Metz, D. Metzger, S. Metzger, W. Meufels, G. Micsa, E. Mitz, K. Möller, K. Mömerzheim, L. Molnar, A. Morhardt, T. Mrugalla, C. H. Mühle, A. Müller, B. Müller, B. Müller, G. Müller, K. Müller, W. Müller, E. Nagel, K-H. Neff, K. Neimanns, W. Neuhäuser, A. Nicklas, G. Niemann, D. Nitsch, R. Norcia, B. Ohmstede, G. Olscha, G. Pabst, J. Palm, W. Panschow, F. Peldzinski, H. Peter, K. Petrich, F. Petrone, E. Pfaff, E-L. Pfaff, K-L. Pfaff, E. Pfeng, P. Pfizenmeier, D. Pissowotzki, D. Pollet, A. Poppe, I. Poppert, M. Poth, G. Pritz, A. Przybyla, W. Quick, D. Quis, M. Rack, E. Rass, W. Rehm, J. Rempe, R. Retzlaff, M. Rhein, T. Riedel-Heine, H. Riesner, D. Rochná, C. Röder, D. Röder, H. Röder, W. Rösch, R. Rulfs, W. Salzer, V. Schaa, H. W. Schäfer, F. Schäffer, J. Schäffer, M. Scheid, H. Schiemann, G. Schill, E. Schimpf, D. Schmalz, G. Schmelig, H-G. Schmidt, W. Schmidt, H. Schmiedler, L. Schmiedler, R. Schmitt K. Schneider, K. Schneider, M. Schneider, N. Schneider, H-J. Schött, M. Schuber, P. Schue, W. Schue, H. Schütz, H.O. Schuff, P. Schulte, K. Schultze, R. Schumann, G. Schunk, W. Schuth, G. Schwarz, R. Schwarz, V. Schwarz, R. Schwedhelm, G. Schweipert, U. Seckert, S. Selent, K. Senft, R-F. Sigmund, H. Sitta, G. Sobainsky, H. Sondershaus, P. Spädtke, H. Spengler, S. Sperling, W. Spiess, H. Spika, A. Spitaler, A. Stagno, K. Stallmann, W. Stampp, E. Stenger, R. Stenner, J. Störmer, M. Stork, U. Stork, W. Stork, B. Strack, I. Strehl, K. Streich, G. Stubenrauch, E. Sturm, A. Suderleith, K. D. Süssbrich, D. Svrcina, W. Thalheimer, R. Thieme, H. Thomas, E. Thurau, C. Vad, H-G. Valter, E. Veith, H. Vilhjalmsson, W. Vinzenz, H. Vogel, U. Vogel, D. Vogt, R. Vrtal, V. Wagner, H. Wahl, K. Waitz, G. Wannemacher, K-H. Wannemacher, I-H. Warsow, R. Weber, W. Weber, E. Weigand, P. W. Weinreuter, L. Weiss, H. Weitzel, D. Wendt, E. Werkmann, H. Wesp, W. Weyrich, G. Wilde, K. Wilhelm, S. Wilhelm, D. Wilms, H. Wirth, W. Wissing, H. Wörner, C. Wolf, G. Wolf, I. Wortmann, R. Zecher, H. Ziegler, A. Ziem, E. Zilch, A. Zschau, K. Zweig,

7.4 Scientific Cooperation

(from contributions to this report)

FEDERAL REPUBLIC OF GERMANY

Technische Hochschule Aachen
F. Jung, H. Kiesewetter, H.G. Roggenkamp

Hahn-Meitner Institut, Berlin
W. Bohne, P. Fröbrich, K. Grabisch, H. Lehr, H. Morgenstern

Universität Bochum
H. Freiesleben, H. Sohlbach

Universität Bonn
Y.K. Agarwal, C. Günther, K. Hardt, P. Schüler

Technische Hochschule Darmstadt
F. Beck, O. Becker, E. Bozek, C. Brendel, P.J. Brülls, P. Buck, J. Carter, H.-G. Clerc, W.F. Feix, H. Feldmeier, U. Gollerthan, P. Grimm, W. Guthier, F.J. Hambsch, E.R. Hilf, R. Hingmann, H.P. Hollenbach, E. Kankeleit, G. Klotz, W. Knippelberg, W. Kraft-Weyrather, M. Krämer, R. Krieg, U. Meyer, H.G.Miltenburger, W.Müller, M.Mutterer, H. Oeschler, J. Pannicke, Chr. Preuss, A. Richter, W. Rösch, W. Rosch, C.-C. Sahm, G. Schrieder, P. Senger, H. Spangenberger, J.P. Theobald, D. Vermeulen, U. Weickert, K. Weingärtner, K. Wien

Battelle Institut, Frankfurt
J. Kirsch

Gesellschaft für Strahlen- und Umweltforschung, Frankfurt
U. Bertsche, G. Iliakis

Universität Frankfurt
N. Abou-el-Naga, U. Arlt, D. Barthel, R. Bass, H. Baumann, K. Bethge, G. Buchwald, M. Burkhard, K. Depta, H. Dittmar, H.-Th. Elze, Th.W. Elze, H.J. Frischkorn, J. Geri, G. Graebner, W. Greiner, K.O. Groeneveld, A. Gruppe, J. Hahn, Th. Happ, R. Herrmann, D. Hofmann, K. Keppler, P. Koch, P. Koschar, T. Kratz, F. Krisztinkovics, R. Latz, B. Lohmüller, J.A. Maruhn, A. Mauthofer, G. Mehler, R. Merten, B. Müller, L. Neise, H. Noll, Th. Odenweller, H. Ower, J. Rafelski, F. Rauch, W. Reeh, J. Reinhardt, T. de Reus, A. Rosenhauer, K. Sapotta, J. Schader, W. Schadt, A. Schäfer, P. Schlüter, H. Schmidt-Böcking, M. Seiwert, R. Shanker, G. Staadt, K. Stelzer, K.E. Stiebing, A. Thiel, M. Uhlig, D. Vasak, K.H. Wietschorke, K.H. Ziegenhain,

Universität Gießen
D. Berdichevsky, M. Diebel, G. Fiedler, R.D. Fischer, W. Groh, N. Grün, R. Kaps, K. Keiner, P.C. Kester, J. Kiefer, W. Kühn, J. Makowka, V. Metag, U. Mosel, K. Mühlhans, R. Mühlhans, A. Müller, E.M. Müller, K. Neergard, U. Post, S. Rase, E. Salzborn, K. Schaupert, W. Scheid, A.S. Schlachter, E. Schneider, F. Schöpfer, B. Schuch, A. Schuh, O. Tanimura, E. Teubner, K.J. Weber, I. Wirkner-Bott, R. Wolf, E. Wüst

Universität Göttingen
S. Brüssermann, K.-L. Gippert, K.P. Lieb, E. Runte, W.D. Schmidt-Ott, P. Sona, P. Tidemand-Petersson

NUKEM, Hanau
M. Kadner

Max Planck Institut für Kernphysik, Heidelberg
E. Adelberger, I. Bock, H. Feldmeier, H. Gräf, S. Gralla, W. Hennerici, H.J. Hennrich, G. Himmele, H. Ho, E. Jaeschke, W. Koenig, O. Koschorrek, W. Kühn, A. Lazzarini, U. Lynen, H.J. Pirner, R. Repnow, W. Wahl, H. Wirth

Universität Heidelberg
W.Q. Chao, J. Dressler, H. Ferber, D. Habs, M.K. Hegab, K. Helmer, U. v. Helmolt, H.W. Heyng, R. Hoffmann, J. Hüfner, E. Justiniano, H. Krieger, R. Kroth, A. Meger, D. Pelte, G. Reiss, R.E. Renfordt, D. Schall, R. Schuch, D. Schwalm, H.J. Specht, H. Ströbele, K. Tittel, U. Winkler, G.K. Wolf, K. Zucholl

Kernforschungszentrum Karlsruhe
H. Albrecht, H. Beer, G. Walter, H. Wild

Universität Kassel
B. Fricke, H. Hartung, D. Kolb, M. Mann, W. Schulze, W. Sengler, W.D. Sepp

Universität Kiel
R. Beaujean, M. Berndt, W. Enge, J. Krause, G. Siegmon

Deutsche Forschungs- und Versuchsanstalt für Luft- und Raumfahrt, Köln
H. Bücker, R. Facius, M. Schäfer

Universität Mainz
H. Backe, R. Barden, M. Begemann, M. Brügger, U. de la Chevallerie, J. Eberz, C. Frink, D. Gembalies-Datz, U. Glatzel, N. Greulich, U. Hickmann, N. Hildebrand, P. Hill, G. Huber, N. Kaffrell, D. Kaplan, Th. Karlewski, W. Kieling, J.V. Kratz, M. Lerch, A. Lewening, H. Lochmann, K. Lützenkirchen, R. Menges, P. Peuser, K. Schlitt, J. Stachel, H. Stuhrmann, N. Trautmann, G. Ulm, S. Zauner

Universität Marburg
M. Baagil, D. Bangert, R. Beckmann, U. Bieschke, H.-A. Bösser, R. Brandt, G. Dersch, R. Dersch, R.A. Esterlund, E. Ganßauge, B. Grabez, B. Jäckel, E.U. Kahn, H.-J. Keim, F. Killinger, N. Klein, B. Kohlmeyer, R. Kretschmer, A. Laschek, H. Löhner, B. Ludewigt, T. Lund, M. Maier, M. Marinescu, A.K. Mazumdar, D. Molzahn, P. Patzelt, F. Pühlhofer, S. Raha, U. Reus, A. Rox, H. Schulte, H. Stege, N. Stelte, G. Tress, P. Vater, H. Wagner, W. Walcher, W. Weidner, R.M. Weiner, W. Westmeier

Universität München
J. de Boer, W. Dünnweber, Ch. Lauterbach, Ch. Mittag, F. Rieß, Ch. Schandera, W. Trautmann

Technische Universität München
P.A. Amundsen, A. Baran, G. Beier, E. Berdermann, M. Clemente, K. Dietrich, W. Elberfeld, J. Friese, D.H. Jakubaßa-Amundsen, P. Kienle, M. Kleber, H.J. Körner, W. Mayer, W.A. Mayer, L. Müller, H. Tsertos, W. Wagner

Universität Münster
M. Brüssermann, B. Cleff, R. Glasow, K.H. Kampert, R. Santo J. Wigger

Fachhochschule Wiesbaden-Rüsselsheim
N. Schmitt, M.-H. Schönenberg

Universität Tübingen
W.H. Dickhoff, A. Faessler, S.B. Khadkikar, H. Müther, L. Rikus, R. Sartor, R.K. Tripathi

Universität Würzburg
A.M. Kellerer, H. Roos, W.-H. Thomas, F. Zilker

CANADA
Chalk River Laboratories
L.W. Funk

DENMARK
University of Aarhus
F. Folkmann

Niels Bohr Institute, Copenhagen
S. Bjornholm

ENGLAND
University of Exeter
G.N. Fowler

Daresbury Laboratory
A.K. Dhar

FRANCE
Universite de Bordeaux
N. Carjan, H. Delagrange, J.P. Dufour, A. Fleury

Institut Laue-Langevin, Grenoble
M. Roth

Institut des Sciences Nucleaires, Grenoble
M. Durand

Centre de Spectrometrie Nucleaire et de Spectrometrie de Masse, Orsay
Ch. Briancon, A. Lefebvre

Universite Paris Sud, Orsay
S. DellaNegra, Y. Le Beyec

Centre de Recherche Nucleaire, Strasbourg
M. Debeauvais, S. Jokic, J. Ralarosy, J. Tripier

HUNGARY
Central Research Institute for Physics, Budapest
L.P. Csernai

INDIA
Tata Institute for Fundamental Research, Bombay
C.S. Warke

ISRAEL
Technion, Haifa
D. Maor

MEXICO
University of Mexico, Mexico City
A. Dacal, M.E. Ortiz

NORWAY
University of Oslo
K. Aashamar, E. Hagebo, I. Haldorsen

PAKISTAN
PINSTECH, Rawalpindi
G. Hussain, K. Jamil, H.A. Khan, N.A. Khan, M.A. Sial

PEOPLE'S REPUBLIC OF CHINA
University of Beijing
W. Zhao

Institute of Modern Physics, Lanzhou
G.-X. Dai, D. Jiao, B. Liu, S.J. Wang, Y.-Y. Zhou

POLAND
University of Cracow
H. Dabrowski, Z. Stachura, A. Warczak

University of Katowice
J. Kuzminski

University of Warsaw
T. Batsch, A. Lukasiak, T. Matulewicz, K. Rykaczewski, J. Toke

ROMANIA
Institute for Physics and Nuclear Engineering, Bucharest
M. Petrovici

SOUTH AFRICA
University of the Witwatersrand, Johannesbourgh
G. Delic, R.H. Lemmer

SWEDEN
University of Technology, Gothenburg
G. Nyman

The Studsvik Science Research Laboratory, Nyköping
K. Aleklett

University of Uppsala
A. Bäcklin, C. Fahlander, L. Hasselgren, V. Mittal, L.E. Swensson

SWITZERLAND
University of Bern
H.R. von Gunten

CERN, Geneva
C.R. Serre

Technische Hochschule Zürich
M. Nessi, Ch. Stoller, W. Wölfli

UNITED STATES OF AMERICA
Argonne National Laboratory
M. Freedman, D.J. Henderson, S.B. Kaufman, E.P. Steinberg, B.D. Wilkins

Lawrence Berkeley Laboratory
F. Bieser, H. Crawford, E.M. Friedländer, A. Ghiorso, D. Greiner, K.E. Gregorich, H.A. Gustafsson, D. Lee, M. Leino, P. Lindstrom, R. Marrus, P. McGaughey, K.J. Moody, W.D. Myers, J.M. Nitschke, M.J. Nurmia, J. Peter, A.M. Poskanzer, M. Prior, H.G. Pugh, T. Renner, H. Riedesel, R. Roots, A.S. Schlachter, L.S. Schroeder, G.T. Seaborg, L.P. Somerville, H. Spieler, C.A. Tobias, R.B. Welch, P. Wilmarth, S. Yashito

University of California, Berkeley
J. Kuti

A&M University, College Station
K. Wolf, K.L. Wolf

State University, Corvallis
W. Loveland

University of California, Davis
P. Brady, B. Christie, J. Romereo, G. Tull

National Superconducting Cyclotron Laboratory, East Lansing
H. Kruse, H. Stöcker

Purdue University, Lafayette
N. Porile

Lawrence Livermore Laboratory
R.J. Dougan, A.D. Hoover, E.K. Hulet, J.H. Landrum, R.W. Lougheed, J.F. Wild

Los Alamos National Laboratory
M. Fowler, D.C. Hoffmann, J. Kunz, M.S. Moore

Kansas State University, Manhattan
C.L. Cocke

University of Maryland
M. Reiser

Vanderbilt University, Nashville
V. Oberacker

Yale University, New Haven
T. Cowan, J.S. Greenberg, J. Schweppe

Oak Ridge National Laboratory
S. Berry, M. Breinig, M.J. Rhoades-Brown,
L.A. Sellin

Stanford University, Palo Alto
W.E. Meyerhof, J.D. Molitoris, E. Morenzoni

University of Rochester
D. Cline, B. Kotlinski

Rutgers University
P. Vincent

State University of New York, Stony Brook
P. Braun-Munzinger

National Bureau of Standards, Washington
M. Danos

7.5 Author Index

Aashamar, K. 177
Abou-el-Naga, N. 83
Adelberger, E. 45
Agarwal, Y.K. 4, 56, 61, 65, 66
Albrecht, D. 202
Albrecht, H. 212
Albrecht, R. 51, 52, 223, 242
Aleklett, K. 43
Amundsen, P.A. 177
Angert, N. 264
Arlt, U. 5
Armbruster, P. 61, 63, 65, 66, 70, 202
Azgui, F. 48, 49, 50, 58, 224
Baagil, M. 44
Backe, H. 230
Bangert, D. 14, 89, 238
Baran, A. 76, 77
Barden, R. 230
Barthel, D. 109, 122
Bass, R. 5, 17
Batsch, T. 60, 242
Baumann, H. 222
Beaujean, R. 204, 208
Beck, F. 15, 85, 87
Becker, O. 165, 166
Beckert, K. 284, 286
Beckmann, R. 25, 30, 43
Beer, H. 62
Begemann, M. 230
Behr, K.H. 218
Beier, G. 16
Berdermann, E. 147
Berdichevsky, D. 74
Berndt, M. 208
Berry, S. 164
Bertsche, U. 201
Bethge, K. 146, 222
Beyer, H.F. 156, 299
Bieschke, U. 44, 240, 241
Bieser, F. 228
Bjoernholm, S. 10
Blasche, K. 261, 275
Bleuel, W. 261, 283
Bock, I. 28, 29
Bock, R. 10, 14, 21, 22, 33
Böhne, D. 275
de Boer, J. 20, 57
Bösser, H.-A. 238
Bohne, W. 84
Bokemeyer, H. 14, 146
Bosch, F. 147, 152, 154
Bossler, J. 265
Bourgeois, W. 272
Bozek, E. 148
Brady, P. 228
Brandt, R. 25, 26, 30, 31, 43, 203, 205, 209, 211, 212
Braun-Munzinger, P. 24, 32, 226
Breinig, M. 164
Brendel, C. 15, 32, 84, 226
Briancon, Ch. 57
Brockmann, R. 33, 34, 35
Bruske, C. 218
Brüchle, W. 7, 8, 13, 69
Brügger, M. 69, 229, 234
Brülls, P.J. 18
Brünle, A. 218
Brüssermann, M. 154
Brüssermann, S. 46, 47
Bäcklin, A. 48
Buchwald, G. 107, 108, 109, 122, 123, 125, 131, 300, 301, 302, 303
Buck, P. 87
Bücker, H. 193
Burkhard, K. 218
Burkhard, M. 164
Busch, F. 89, 254, 256
Carjan, N. 75, 102
Carter, J. 15, 84
Cassing, W. 93, 95, 97, 98, 99, 100
Chao, W.Q. 126, 127
de la Chevallerie, U. 220
Christie, B. 228
Cleff, B. 154
Clemente, M. 147
Clerc, H.-G. 4, 6, 64
Cline, D. 48
Cocke, C.L. 157
Cowan, T. 146
Crawford, H. 228
Csernai, L.P. 120, 121
Dabrowski, H. 32, 226
Dacal, A. 33
Dai, G.-X. 9, 10, 21, 22, 225
Danos, M. 133, 134
Daues, H.W. 18, 225
Debeauvais, M. 27
Delagrange, H. 75
Delic, G. 15
Della Negra, S. 166
Dengler, J. 242
Depta, K. 94
Dersch, G. 43
Dersch, R. 212
Dhar, A.K. 97
Dickhoff, W.H. 115
Diebel, M. 78
Dietrich, K. 76, 77
Dittmar, H. 5
Dohmann, H.D. 149, 150, 155, 231

Dougan, R.J. 67
Dressler, J. 213
Dufour, J.P. 70, 75
Durand, M. 88
Dünnweber, W. 20
Eberz, J. 59, 160
Egger, H. 248
Eickhoff, H. 280, 281
Eidmann, G. 242
Elberfeld, W. 173
Elze, H.-Th. 132
Elze, Th.W. 54, 55
Emig, H. 265
Emling, H. 46, 47, 49, 50, 53, 55, 58, 224
Emmerling, M. 282
Enders, W. 236
Enge, W. 204, 208
Esterlund, R.A. 11, 12
Facius, R. 193
Faessler, A. 114, 115, 117
Fahlander, C. 48
Fan, W. 13
Fehres, A. 242
Feix, W.F. 72
Feldmeier, H. 84, 85, 86, 87
Ferber, H. 213
Feyerabend, M. 259
Fiedler, G. 206
Fischer, B.E. 207, 233
Fischer, R.D. 223
Fleury, A. 75
Folger, H. 146, 214, 216, 217
Folkmann, F. 156
Fowler, G.N. 111, 112, 116, 144
Fowler, M. 69
Franczak, B. 277, 278, 279
Franzke, B. 162, 275, 280, 281, 298
Freedman, M. 40
Freiesleben, H. 14, 24, 89
Fricke, B. 167, 169, 171
Friedländer, E.M. 43, 144
Friese, J. 16
Frink, C. 69, 219
Frischkorn, H.J. 164, 232
Fröbrich, P. 88
Funk, L.W. 289
Gaiser, H. 261, 283
Ganßauge, E. 44, 240, 241
Gasper, A. 282
Gembalies-Datz, D. 220
Gerl, J. 54
Ghiorso, A. 67, 68, 69, 70
Giese, I. 259, 260
Gippert, K.-L. 62
Glasow, R. 28, 29
Glatz, J. 271
Glatzel, U. 216
Glückert, S. 248
Gobbi, A. 9, 10, 18, 21, 22, 23, 28, 29, 90, 102
Gollerthan, U. 148
Grabez, B. 30
Grabisch, K. 84
Graebner, G. 107, 108, 109, 122, 123, 124, 125, 131, 300, 301, 302, 303
Gralla, S. 9, 10, 21, 22, 23, 225
Greenberg, J.S. 146
Gregorich, K.E. 69
Grein, H. 47, 48, 146
Greiner, D. 228
Greiner, W. 83, 94, 103, 105, 106, 107, 108, 109, 120, 121, 122, 123, 124, 125, 129, 130, 131, 132, 136, 137, 138, 139, 140, 143, 174, 175, 176, 179, 180, 181, 182, 183, 184, 185, 186, 187, 188, 300, 301, 302, 303
Greulich, N. 69, 221
Grimm, P. 237
Groeneveld, K.O. 164, 232
Groh, W. 159
Grosse, E. 19, 32, 46, 47, 48, 49, 50, 53, 55, 56, 58, 224, 226
Gräf, H. 223
Gruppe, A. 146
Grösch, G. 283
Grün, N. 172
Gäggeler, H. 7, 8, 13, 69, 234
von Gunten, H.R. 69
Gustafsson, H.A. 42
Gutbrod, H.H. 36, 37, 38, 39, 40, 41, 42, 227, 246
Guthier, W. 166
Göringer, H. 254, 255
Günther, C. 56
Habs, D. 45, 51, 52, 223
Hagebo, E. 31
Hahn, J. 94
Haldorsen, I. 31
Hambsch, F.-J. 237
Hammal, H. 242
Happ, Th. 54
Hardel, H. 242
Hardt, K. 56
Harris, J.W. 33, 34, 35, 118
Hartmann, V. 17, 254
Hartmann, W. 216, 269
Hartung, H. 167, 171
Hasselgren, L. 48
Heßberger, F.P. 2, 3, 4, 61, 63, 65, 66
Heckwolf, H. 32, 226
Hegab, M.K. 126
Helmer, K. 51, 223
v. Helmolt, U. 51, 52, 223
Henderson, D.J. 40
Hennerici, W. 51, 52, 223

Hennrich, H.J. 51, 52, 223
Herrmann, G. 69, 219, 220, 221, 234
Herrmann, R. 94
Heyng, H.W. 51, 52, 223
Hickmann, U. 69
Hildebrand, N. 69, 234
Hildenbrand, K.D. 2, 3, 9, 10, 21, 22, 23, 28, 29
Hilf, E.R. 72
Hill, P. 47, 49
Himmele, G. 51, 52, 223
Hingmann, R. 4, 64
Ho, H. 29
Hoffmann, C. 261
Hoffmann, D.C. 69
Hoffmann, D.H.H. 153, 163
Hoffmann, J. 242
Hoffmann, R. 152
Hofmann, D. 164
Hofmann, N. 265
Hofmann, S. 2, 3, 61, 63, 65, 66, 70
Hollenbach, H.P. 18
Hoover, A.D. 67
Huber, G. 59, 160, 161
Hulet, E.K. 67, 68
Hultzsch, H. 248
Hussain, G. 26, 205
Hutter, G. 269, 270
Hüfner, J. 126
Hüller, W. 218
Iliakis, G. 201
Illert, K. 261
Jacoby, W. 265
Jaeschke, E. 223
Jakubaßa-Amundsen, D.H. 177, 178
Jamil, K. 26, 203, 205, 209
Jiao, D. 242
Jokic, S. 27
Jäckel, B. 12
Jung, F. 210
Justiniano, E. 152
Jöst, G. 265
Kadner, M. 211
Kaffrell, N. 47, 49, 62
Kampert, K.H. 28, 29
Kankeleit, E. 148
Kaplan, D. 59
Kaps, R. 104
Karlewski, Th. 229
Kaspar, K. 282
Kaufman, S.B. 40
Keim, H.-J. 238
Keiner, K. 206
Keller, J.G. 4, 6, 64, 235
Keller, R. 288, 296
Kellerer, A.M. 191
Keppler, K. 54
Kester, P.C. 159
Khadkikar, S.B. 117
Khan, E.U. 25, 211, 212
Khan, H.A. 26, 203, 205, 209, 211
Khan, N.A. 26, 203, 205, 209
Khaouli, M.M. 265
Kido, Y. 146
Kiefer, J. 194, 195, 196
Kieling, W. 220, 234
Kienle, P. 16, 147
Kiesewetter, H. 210
Kiesewetter, H.R. 218, 261
Killinger, F. 44, 241
Kirchner, R. 59, 60, 62, 218
Kirsch, J. 188
Klabunde, J. 264, 268, 290, 291, 292, 293
Kleber, M. 173
Klein, N. 44, 240, 241
Klemm, J. 216
Klepper, O. 32, 59, 60, 226
Klotz, G. 148
Knippelberg, W. 165, 166
Knoll, J. 113, 119
Koch, P. 136, 137
Koenig, W. 147
Kohlmeyer, B. 14, 24, 89, 238
Kolb, B. 36, 37, 38, 39, 42, 51, 52, 223, 227, 247
Kolb, D. 168, 169
Kopf, U. 231, 261, 289
Koschar, P. 164, 232
Koschorrek, O. 223
Kotlinski, B. 48
Kozhuharov, C. 147
Kraft-Weyrather, W. 199, 200
Kraft, G. 190, 192, 194, 197, 198, 199, 200, 201
Kratz, J.V. 2, 3, 7, 8, 13, 69, 220
Kratz, T. 5
Krause, J. 204
Krejcik, P. 295, 296, 297
Kretschmer, R. 44, 240, 241
Krichbaum, H. 265
Krieg, R. 148
Krieger, H. 223
Krisztinkovics, F. 105
Kroth, R. 45, 52, 223
Krämer, M. 148, 190
Kruse, H. 124, 300, 301, 302
Kube, G. 270
Kulessa, R. 48, 56, 58
Kunz, J. 82
Kurcewicz, W. 60, 62
Kurz, H.-P. 265
Kuti, J. 141
Kuzminski, J. 9, 10, 23

Kynast, W. 259
Könnecke, R. 106
Körner, H.J. 16
Kühl, T. 59, 160, 161
Kühn, W. 29, 223
Küper, K. 272
Landrum, J.H. 67, 68
Langenbeck, B. 272, 283
Larsson, M. 192, 198
Larsson, P.O. 59, 60
Laschek, A. 44, 240, 241
Latz, R. 164
Lauterbach, Ch. 20, 57
Lazzarini, A. 52
Le Beyec, Y. 166
Lee, D. 69
Lefebvre, A. 57
Lehr, H. 84
Leible, K.-D. 265, 267
Leino, M. 70
Leiser, W. 218
Lemmer, R.H. 15
Lemmertz, P. 70
Lenz, G. 195
Lerch, M. 13, 220
Lewening, A. 220
Lieb, K.P. 46
Liebold, H.P. 242
Liesen, D. 149, 150, 151, 155, 231, 236
Lindstrom, P. 228
Liu, B. 149, 150, 151, 236
Lochmann, H. 59
Lohmüller, B. 5
Loos, D. 231
Lougheed, R.W. 67, 68
Loveland, W. 43
Lowsky, J. 248, 254
Ludewigt, B. 36, 37, 42
Lukasiak, A. 95, 96, 97
Lund, T. 31, 43
Lustig, H.-J. 253
Lynen, U. 21, 22, 28, 29
Löhner, H. 36, 37, 38, 39, 41, 227, 246
Lützenkirchen, K. 7, 8
Maier, M. 33, 34, 35, 40
Makowka, J. 104
Malwitz, E. 261
Mann, M. 171
Mann, R. 156, 157, 158
Maor, D. 151, 154
Marinescu, D. 254, 256, 257
Marinescu, M. 14, 24, 89
Marrus, R. 157
Martens, H.-G. 242
Marx, D. 59
Matulewicz, T. 90
Mauthofer, A. 55
Mayer, W. 16
Mayer, W.A. 16
Mazumdar, A.K. 229
McGaughey, P. 43
Meger, A. 213
Mehler, G. 187
Meister, H. 199, 200
Menges, R. 161
Merten, R. 146
Metag, V. 45, 51, 52, 223
Meufels, W. 242
Meyer, U. 148
Meyerhof, W.E. 19
Michel, Ch. 19, 32, 47, 48, 49, 50, 53, 58, 224, 226
Miltenburger, H.G. 197, 199, 200
Mittag, Ch. 57
Mittal, V. 48
Mokler, P.H. 151, 152, 153, 154, 163, 171, 299
Maruhn, J.A. 94, 107, 108, 109, 120, 121, 122, 123, 124, 125, 131, 300, 301, 302, 303
Molitoris, J.D. 19
Molnar, L. 218
Molzahn, D. 31
Moody, K.J. 67, 69
Moore, M.S. 58
Morenzoni, E. 19
Morgenstern, H. 84
Morhardt, A. 269
Moritz, G. 272
Mosel, U. 74, 78, 79, 80, 81, 82, 104
Mutterer, M. 18, 58, 237
Myers, W.D. 73
Mömerzheim, K. 242
Mühlhans, K. 78, 81
Mühlhans, R. 223
Müller, A. 159
Müller, B. 105, 128, 139, 143, 179, 180, 181, 182, 183, 184, 185, 186, 187, 188
Müller, E.M. 79, 81
Müller, L. 16
Müller, M. 217, 264, 265, 266
Müller, R.W. 284, 286, 287, 289
Müller, U. 179, 180, 181, 182, 183, 184, 185, 186, 187
Müller, W. 197
Müller, W.F.J. 9, 10, 21, 22, 28, 29, 32, 226
Münzenberg, G. 2, 3, 4, 61, 63, 65, 66, 70
Müther, H. 115
Neergard, K. 79
Neise, L. 94
Nessi, M. 19
Nickel, F. 218
Nitschke, J.M. 68
Noll, H. 17, 32, 226

Nurmia, M.J. 68
Nyman, G. 60
Nöhmayer, F. 288
Nörenberg, W. 92, 93, 95, 96, 97, 98, 99, 100
Oberacker, V. 103
Odenweller, Th. 146
Oeschler, H. 148
Olmi, A. 9, 10, 21, 22, 28, 29
Ortiz, M.E. 33
Ower, H. 54, 55
Pannicke, J. 18
Patzelt, P. 11, 12
Pelte, D. 28, 29, 51, 52, 223
Peter, J. 40
Petrovici, M. 21, 22, 23
Peuser, P. 62
Pfeng, E. 155
Pirner, H.J. 127
Pissowotzki, D. 254
Pollet, D. 198
Polonyi, J. 131, 141, 142
Poppensieker, K. 65, 66, 242
Porile, N. 43
Poskanzer, A.M. 36, 37, 38, 39, 41, 42, 227, 246
Post, U. 80
Prange, H. 275
Preuss, Chr. 237
Prior, M. 157
Przybyla, A. 242
Pugh, H.G. 33, 34, 35
Pühlhofer, F. 14, 24, 89, 238
Quis, D. 242
Rafelski, J. 128, 132, 133, 134, 135, 136, 137, 138, 175
Raha, S. 110, 111, 112, 116
Ralarosy, J. 27
Rase, S. 195
Rauch, F. 222
Reeh, W. 222
Reisdorf, W. 2, 3, 4, 61, 63, 65, 66
Reiser, M. 290, 291, 292, 293
Reinhardt, J. 105, 179, 180, 181, 182, 183, 184, 185, 186, 187
Reiss, G. 213
Renfordt, R.E. 33, 34, 35
Renner, T. 36, 37, 38, 39, 41, 42, 227, 246
Repnow, R. 51, 52, 223
de Reus, T. 179, 180, 181, 182, 183, 184, 185, 186, 187
Reus, U. 11, 12, 71
Rhoades-Brown, M.J. 103
Richter, A. 15, 84
Richter, M. 242, 256
Riedesel, H. 36, 37, 38, 39, 41, 42, 227, 246
Riess, F. 35
Rieß, F. 57
Rikus, L. 117
Ritter, H.G. 36, 37, 38, 39, 40, 41, 42, 227, 246
Roeckl, E. 59, 60, 62, 218
Roggenkamp, H.G. 210
Romereo, J. 228
Roos, H. 191
Roots, R. 192
Rosch, W. 226
Rosenhauer, A. 120, 121
Roth, M. 202
Rox, A. 11, 12
Rulfs, R. 265
Runte, E. 62
Rykaczewski, K. 62
Rösch, W. 32, 231
Sahm, C.-C. 4, 6, 64, 65, 66, 235
Salzborn, E. 159
Sandoval, A. 33, 34, 35
Sann, H. 28, 29, 228
Santo, R. 28, 29
Sapotta, K. 5, 17
Sartor, R. 117
Sato, K. 282
Schader, J. 164
Schadt, W. 152
Schall, D. 34, 35, 239
Schandera, Ch. 20, 57
Schardt, D. 59, 60, 62
Schaupert, K. 202, 206
Scheid, W. 172
Schlachter, A.S. 157, 159
Schlitt, K. 2, 3, 13
Schlüter, P. 174, 176, 187
Schmidt-Böcking, H. 152
Schmidt-Ott, W.-D. 62
Schmidt, H.-G. 242
Schmidt, K.-H. 4, 6, 64, 65, 66, 73, 75, 235, 245
Schmidt, W. 261
Schmitt, N. 294
Schneider, E. 194, 195
Schneider, G. 242
Schneider, J.H.R. 2, 3, 66
Schneider, J.R.H. 61, 63, 65
Schneider, K. 265
Schneider, W.F.W. 2, 3, 14, 24, 65, 66, 238
Schrieder, G. 15, 84
Schroeder, L.S. 33, 34, 35
Schädel, M. 67, 68, 69, 219
Schäfer, A. 143, 175
Schäfer, M. 193
Schuber, M. 199
Schuch, B. 159
Schuch, R. 152
Schuh, A. 82
Schulte, H. (GSI) 265, 267

Schulte, H. (U.Marbg.) 6, 11, 12
Schulze, R. 236, 242
Schulze, W. 167, 168
Schwalm, D. 45, 47, 49, 50, 51, 52, 53, 55, 58, 146, 223
Schweppe, J. 146
Schwinn, K. 260
Schönenberg, M.-H. 288
Schönfeldt, W.A. 152, 153, 154, 163, 171
Schönlein, A. 290, 291
Schöpfer, F. 195
Schött, H.-J. 61, 63, 65, 66
Schüler, P. 56
Schüll, D. 14, 15, 24, 89
Seaborg, G.T. 67, 69
Seiwert, M. 103
Sellin, I.A. 164
Senft, K. 242
Senger, P. 148
Sengler, W. 169
Sepp, W.-D. 167, 170, 171
Serre, C.R. 31
Shanker, R. 139, 140
Shyam, R. 113
Sial, M.A. 26, 203, 205, 209
Siart, O. 248
Siegmon, G. 208
Simon, R.S. 45, 51, 52, 57, 58, 223
Sobainsky, G. 272
Soff, G. 179, 180, 181, 182, 183, 184, 185, 186, 187
Sohlbach, H. 24
Somerville, L.P. 68
Sona, P. 46
Spangenberger, H. 85, 86
Specht, H.J. 45
Spieler, H. 242
Spohr, R. 202, 211
Spreng, W. 48, 49, 56, 58
Spädtke, P. 274, 288, 290, 294
Staadt, G. 138
Stachel, J. 46, 47, 48, 49, 56
Stachura, Z. 151, 152, 153, 154, 163
Stege, H. 238
Steinberg, E.P. 40
Steiner, R. 275
Steitz, M. 259
Stelte, N. 111
Stelzer, H. 21, 22, 28, 29, 32, 40, 225, 226, 235
Stelzer, K. 5, 55
Stiebing, K.E. 146
Stock, R. 33, 34, 35, 118
Stoller, Ch. 19
Stork, M. 265
Strack, B. 88, 119
Strehl, P. 264
Struckmeier, J. 290, 292, 293
Ströbele, H. 33, 34, 35, 239
Stuhrmann, H. 202
Sturm, E. 242
Stöcker, H. 107, 122, 123, 124, 131
Svensson, L.E. 48
Sümmerer, K. 2, 3, 7, 8, 13, 69, 234
Tanimura, O. 104
Teubner, E. 172
Thalheimer, W. 216
Theis, J. 107, 108, 122, 123, 125, 131, 300, 301, 302, 303
Theobald, J.P. 18, 58, 237
Thiel, A. 106
Thomas, W.-H. 191
Tidemand-Petersson, P. 60, 62
Tittel, K. 35, 239
Tobias, C.A. 200
Toke, J. 9, 10, 21, 22, 90, 102, 225
Trautmann, N. 13, 69, 146, 219, 220, 221, 229, 234
Trautmann, W. 20
Tress, G. 211, 212
Tripathi, R.K. 114
Tripier, J. 27
Tsertos, H. 147
Tull, G. 228
Uhlig, M. 94, 122, 129, 130, 131
Ulm, G. 59, 160, 161
Vasak, D. 139, 140
Vater, P. 25, 30, 211, 212
Vermeulen, D. 6, 64, 65, 66, 75
Vincent, P. 146
Vinzenz, W. 269, 270
Vogt, D. 274
Wagner, H. 229
Wagner, W. 16, 147
Wahl, H. 154, 163, 231, 299
Wahl, W. 45, 52, 223
Walcher, W. 229
Walter, G. 62
Wang, S.J. 92, 99, 100, 101
Warczak, A. 149, 150, 153
Warke, C.S. 129, 130, 140
Warwick, A.I. 36, 37, 38, 39, 40, 41, 42, 227, 246
Weber, K.J. 194
Weber, W. 234
Weickert, U. 166
Weidner, W. 44, 240, 241
Weik, F. 36, 37, 38, 39, 40, 227, 246
Weiner, R.M. 43, 110, 111, 112, 116, 144
Weingärtner, K. 18
Welch, R.B. 69
Westmeier, W. 11, 12, 71
Wieman, H. 36, 37, 38, 39, 40, 41, 42, 227, 246
Wien, K. 165, 166
Wietschorke, K.-H. 174, 176, 187

Wigger, J. 154
Wild, H. 212
Wild, J.F. 67
Wilkins, B.D. 40
Wilmarth, P. 69
Wilms, D. 264
Winkelmann, K. 254, 258
Winkler, U. 28, 29
Wirkner-Bott, I. 159
Wirth, G. 2, 3, 7, 8, 13, 69
Wirth, H. 222
Wolf, B. 267, 274
Wolf, G.K. 213, 214
Wolf, K. 34
Wolf, K.L. 33, 35
Wolf, R. 104
Wollersheim, H.J. 21, 22, 47, 48, 49, 50, 53, 54, 55, 56, 58, 224
Wölfli, W. 19
Wüst, E. 80, 82
Yannouleas, C. 91
Yashito, S. 70
Zaidmann, G. 254, 260
Zauner, S. 220
Zhao, W. 266
Zhou, Y.-Y. 242
Ziegenhain, K.H. 94
Zilker, F. 191
Zucholl, K. 214
Zweig, K. 272